



**Computational
Microelectronics**

**Edited by
S. Selberherr**

Peter Pichler

Intrinsic Point Defects,
Impurities, and Their Diffusion
in Silicon

Springer-Verlag Wien GmbH

Dr. techn. Peter Pichler

Fraunhofer Institut für Integrierte Systeme und Bauelementetechnologie (IISB)
Erlangen, Germany

This work is subject to copyright.

All rights are reserved, whether the whole or part of the material is concerned, specifically those of translation, reprinting, re-use of illustrations, broadcasting, reproduction by photocopying machines or similar means, and storage in data banks.

© 2004 Springer-Verlag Wien

Originally published by Springer-Verlag Wien New York 2004

Softcover reprint of the hardcover 1st edition 2004

Product Liability: The publisher can give no guarantee for the information contained in this book. The use of registered names, trademarks, etc., in this publication does not imply, even in the absence of a specific statement, that such names are exempt from the relevant protective laws and regulations and therefore free for general use.

Typesetting: Camera-ready by the author

Printed on acid-free and chlorine-free bleached paper

SPIN: 10975954

With 127 Figures

ISBN 978-3-7091-7204-9
DOI 10.1007/978-3-7091-0597-9

ISBN 978-3-7091-0597-9 (eBook)

CIP data applied for

'The time has come,' the walrus said,
'To talk of many things'
Lewis Carroll, *Through the Looking Glass*

Contents

Preface	xiii
Frequently Used Symbols	xv
Explanation of Frequently Used Abbreviations	xix
1 Fundamental Concepts	1
1.1 Silicon and Its Imperfections	2
1.1.1 Orientations in Crystals: Miller Indices	2
1.1.2 The Silicon Lattice	4
1.1.3 Crystal Defects	5
1.1.4 Symmetries of Defects	8
1.1.5 Selected High-Symmetry Configurations of Point Defects in Silicon	10
1.2 The Electron System	13
1.2.1 Charge Carriers in Solids	13
1.2.2 Dopants	14
1.2.3 Fermi Statistics	15
1.2.4 Boltzmann Statistics	17
1.2.5 High-Concentration Effects	19
1.2.6 Electric Fields and the Electrostatic Potential	20
1.2.7 Physical Parameters	22
1.3 Phenomenological and Atomistic Approaches to Diffusion	25
1.3.1 Fick's Laws	26
1.3.2 Random Walk and the Atomistic View of Diffusion	31
1.3.3 Driving Forces for the Redistribution of Atoms	36
1.3.4 Athermal Diffusion	38
1.4 Thermodynamics	39
1.4.1 Equilibrium Thermodynamics	39
1.4.2 Thermodynamics of Irreversible Processes	42
1.4.3 Stress Effects	44
1.4.4 Thermodiffusion	46
1.5 Reaction Kinetics	47
1.5.1 The Reaction Variable ζ and Equilibrium Thermodynamics	48
1.5.2 Dynamic Theories of Reactions	52
1.5.3 Estimation of Rate Constants for the Kinetic Law of Mass Action	55
1.5.4 Diffusion-Reaction Equations	58
1.6 Exchange of Matter Between Phases	62
Bibliography	66

2 Intrinsic Point Defects	77
2.1 Concentration in Thermal Equilibrium	79
2.2 Diffusion of Intrinsic Point Defects	87
2.3 Self-Diffusion and Tracer Diffusion	90
2.4 Vacancies	103
2.4.1 Experimental Evidence and Suggested Atomic Configurations	103
2.4.2 Concentration in Thermal Equilibrium	107
2.4.3 Diffusion	114
2.4.4 Divacancies	120
2.4.5 Small Vacancy Clusters	127
2.5 Self-Interstitials	131
2.5.1 Experimental Evidence and Suggested Atomic Configurations	132
2.5.2 Concentration in Thermal Equilibrium	136
2.5.3 Diffusion	141
2.5.4 Di-Interstitials	148
2.5.5 Small Clusters of Self-Interstitials	151
2.6 Frenkel Pairs	158
2.7 Bulk Recombination and Bulk Processes	161
2.7.1 Bulk Recombination	161
2.7.2 Indirect Bulk Recombination via Impurities	167
2.7.3 Reactions of Intrinsic Point Defects with Extended Defects	168
2.7.4 Interactions with Traps	171
2.7.5 Influence of Bulk Recombination and Traps on the Point-Defect Diffusivities Observed Experimentally	174
2.7.6 Generation of Point Defects by Chemical Processes in the Bulk	176
2.8 Surface Recombination and Surface Processes	176
2.8.1 Phenomenological Interface and Boundary Conditions	177
2.8.2 Surface Reconstruction	179
2.8.3 Segregation of Self-Interstitials into Oxide Layers	185
2.8.4 Generation of Intrinsic Point Defects by Chemical Reactions at Interfaces	186
2.9 Initial Conditions	188
Bibliography	190
3 Impurity Diffusion in Silicon	229
3.1 Basic Mechanisms	229
3.1.1 Interstitial Diffusion	229
3.1.2 Direct-Exchange Mechanism for Substitutional Impurities	230
3.1.3 Diffusion of Substitutional Atoms via Vacancies	231
3.1.4 Diffusion of Substitutional Impurities as Interstitials or Impurity-Self-Interstitial Pairs	233
3.2 Impurity-Point-Defect Pairs	234
3.2.1 Classification of Pairs	234
3.2.2 Concentration in Thermal Equilibrium	236
3.3 Diffusion of Substitutional Impurities via Mobile Complexes with Intrinsic Point Defects	242
3.3.1 Formation and Diffusion of Mobile Complexes	243
3.3.2 Boundary Conditions for Mobile Impurity Complexes	247
3.3.3 Simplifications	247
3.3.4 Indirect Recombination of Intrinsic Point Defects in Steady State	251

3.4	Pair-Diffusion Models	251
3.4.1	Derivation of the Diffusion Equations	251
3.4.2	The Intrinsic Diffusion Coefficient	253
3.4.3	Estimates of f_I from Experiments	255
3.4.4	The Field Effect	260
3.4.5	Boltzmann-Matano Analysis	261
3.4.6	Isoconcentration Experiments	262
3.4.7	Influence of Dopant Diffusion on the Intrinsic Point Defects	263
3.5	Frank-Turnbull Mechanism	267
3.5.1	Derivation of the Diffusion-Reaction Equations	267
3.5.2	Discussion of Special Cases	268
3.6	Kick-Out Mechanism	272
3.6.1	Derivation of the Diffusion-Reaction Equations	272
3.6.2	Discussion of Special Cases	273
	Bibliography	275
4	Isovalent Impurities	281
4.1	Carbon	281
4.1.1	Basic Atomic Configurations	282
4.1.2	Solubility	284
4.1.3	Diffusion	285
4.1.4	Carbon-Silicon Complexes	289
4.1.5	Complexes with Oxygen	292
4.1.6	Complexes with Dopants	297
4.1.7	Influence on the Concentrations of Intrinsic Point Defects	300
4.2	Germanium	300
4.2.1	Basic Atomic Configurations	301
4.2.2	Solubility	301
4.2.3	Diffusion	302
4.2.4	Complexes	305
4.3	Tin	306
4.3.1	Basic Atomic Configurations	306
4.3.2	Solubility	308
4.3.3	Diffusion	309
4.3.4	Complexes	311
	Bibliography	311
5	Dopants	331
5.1	Dopant Clusters	332
5.2	Ion Pairing	334
5.3	Boron	337
5.3.1	Basic Atomic Configurations	337
5.3.2	Solubility	341
5.3.3	Diffusion	342
5.3.4	Complexes	350
5.4	Aluminum	359
5.4.1	Basic Atomic Configurations	360
5.4.2	Solubility	361
5.4.3	Diffusion	361

5.4.4	Complexes	365
5.5	Gallium	366
5.5.1	Basic Atomic Configurations	366
5.5.2	Solubility	366
5.5.3	Diffusion	367
5.5.4	Complexes	369
5.6	Indium	370
5.6.1	Basic Atomic Configurations	370
5.6.2	Solubility	372
5.6.3	Diffusion	375
5.6.4	Complexes	377
5.7	Nitrogen	378
5.7.1	Basic Atomic Configurations	380
5.7.2	Solubility	383
5.7.3	Diffusion	383
5.7.4	Complexes	385
5.8	Phosphorus	390
5.8.1	Basic Atomic Configurations	390
5.8.2	Solubility	393
5.8.3	Diffusion	395
5.8.4	Complexes	403
5.9	Arsenic	404
5.9.1	Basic Atomic Configurations	404
5.9.2	Solubility	407
5.9.3	Diffusion	408
5.9.4	Complexes	413
5.10	Antimony	416
5.10.1	Basic Atomic Configurations	417
5.10.2	Solubility	418
5.10.3	Diffusion	420
5.10.4	Complexes	424
	Bibliography	425
6	Chalcogens	469
6.1	Oxygen	469
6.1.1	Basic Atomic Configurations	470
6.1.2	Solubility	471
6.1.3	Normal Diffusion	472
6.1.4	Enhanced Diffusion	474
6.1.5	Complexes with Intrinsic Point Defects	475
6.1.6	Oxygen Dimers and Trimers	483
6.2	Sulfur	484
6.2.1	Basic Atomic Configurations	484
6.2.2	Solubility	486
6.2.3	Diffusion	486
6.2.4	Complexes	487
6.3	Selenium	488
6.3.1	Basic Atomic Configurations	488
6.3.2	Solubility	489

6.3.3	Diffusion	489
6.3.4	Complexes	490
6.4	Tellurium	492
6.4.1	Basic Atomic Configurations	492
6.4.2	Solubility	493
6.4.3	Diffusion	494
6.4.4	Complexes	495
	Bibliography	495
7	Halogens	513
7.1	Fluorine	513
7.1.1	Basic Atomic Configurations	514
7.1.2	Diffusion	515
7.1.3	Complexes	517
7.1.4	Influence on Transient Diffusion and Dopant Activation	518
7.1.5	Fluorine and Silicon Oxidation	521
7.2	Chlorine	522
7.2.1	Chlorine in Silicon	522
7.2.2	Addition of Chlorine Compounds during Oxidation	522
7.3	Bromine	525
	Bibliography	526
	List of Tables	537
	List of Figures	539
	Index	543

Preface

When I worked on my diploma in electrical engineering and later on my doctoral thesis at the Technical University of Vienna, I had the pleasure of a close contact to Prof. H. W. Pötzl. In some private hours he used to tell the story of the book¹ he once wrote. After quite some time, when the publisher had become very impatient, Prof. Heywang was asked to join him. But instead of speeding the procedure up, it slowed it down. They needed even more time together for their discussions. While such tales were not really encouraging for writing books, I also had the pleasure of working under direct guidance of Prof. S. Selberherr on my doctoral thesis when he wrote his renowned book on simulation of semiconductor devices.² The writing of this book went, in my estimation, quite smoothly and rapidly. So, it was with much hope that it would be possible to complete my own book on diffusion in silicon in a “short” time when Prof. Selberherr contacted me about it centuries ago in his capacity as editor of the Springer Series in Computational Microelectronics. In retrospect, it seems I rather followed the path of Prof. Pötzl instead.

I recognized soon that my knowledge at that time, and maybe even now, was somewhat limited, that the developent in the area I was writing on went faster than I could write it down, and that the subject had more facets I had imagined. However, I also noticed that — most likely unknown to the authors — concepts were sometimes reinvented or developed against a background of better experimental evidence. After I got hooked on a life as scientific hunter-gatherer, it was my intention to collect as much of the relevant information on point defects and diffusion phenomena in silicon as possible to create a sound basis of knowledge for future scientific generations. In this task, and in my desire to understand things, I profited much from working together with some of the major European scientists, especially in a fruitful cooperation with MEMC Italy and in the projects RAPID and FRENDTECH funded by the European Community, and from participating in the workshops of the ENDEASD network funded likewise by the European Community.

The book is structured as follows: In the first chapter, some fundamental concepts are discussed which form the scientific basis for the remainder of the book. In the second chapter, vacancies and self-interstitials are introduced and their known properties are discussed in detail. The diffusion of impurities is dealt with in third chapter, and the remaining chapters four to seven summarize the properties of isovalent impurities, dopants, chalcogens, and halogens. Unfortunately, it is not possible to present a unified picture of the subject. Too many aspects are not accessible directly to characterization so that ample latitude is available for speculations. When contradictory concepts exist in the literature, except when they are at odds with independent experimental evidence, all of them are discussed impartially and future work may decide about right or wrong. It is my hope that my book is useful to beginners up to experts outside (and maybe sometimes even within) their own field of expertise.

¹W. Heywang and H. W. Pötzl, *Bänderstruktur und Stromtransport, Halbleiter-Elektronik*, vol. 3, Berlin: Springer (1976).

²S. Selberherr, *Analysis and Simulation of Semiconductor Devices*, Vienna: Springer (1984).

Due to limitations in space as well as in time, it was not possible to address all aspects of diffusion in silicon. Especially diffusion in multi-layer systems, macroscopic extended intrinsic and extrinsic defects, metals, hydrogen, and important phenomena like transient effects on diffusion and activation of dopants had to be neglected. It is my declared intention to cover these subjects in a follow-up book. However, having learned from my experiences with this book, one could not expect it to be ready within too short a period.

This book would not have been possible without the support by numerous librarians who did not hesitate to provide me even with the rarest references from the deepest vaults. Mrs. Karin Böhmer, Mrs. Heidrun Escherich, Mrs. Monika Förstel, Mrs. Edeltraud Haagen, and Mrs. Elisabeth Plank of the library of the University Erlangen-Nürnberg and Mrs. Anette Daurer of the library of the Fraunhofer Institute of Integrated Systems and Device Technology in Erlangen were more visible and of direct help to me. However, I am well aware that they are just the tip of the iceberg and I have to apologize to the others for not mentioning. During the years I worked on this book, my understanding was continuously extended by discussions with colleagues with whom I had the pleasure to cooperate at our institute. In particular, I would like to acknowledge Mr. Harald Bauer, Dr. Alexander Burenkov, Dr. Rainer Dürr, Dr. Michael Jacob, Dr. Oliver Krause, Dr. Steffen List, Dr. Christophe Ortiz, Dr. Fabian Quast, Dr. Rainer Schork, Dr. Dorothée Stiebel, and Prof. Horst Zimmermann. Unfortunately, neither my commemorations nor the space available would suffice to give proper reference to all colleagues who enlightened me by discussions at conferences and meetings, or per email. Of particular inspiration were the contacts to Dr. Alain Claverie of CEMES/CNRS and Dr. Filadelfo Cristiano of LAAS/CNRS in Toulouse, Prof. Nick Cowern of the University of Surrey, and Dr. Robert Falster and Prof. Vladimir V. Voronkov of MEMC. I am also very grateful to Prof. Siegfried Selberherr and Prof. Ulrich Gösele for their continued interest in this book. This book would also not have been possible without the support of Prof. Heiner Ryssel and Dr. Jürgen Lorenz at the Fraunhofer Institute of Integrated Systems and Device Technology in Erlangen. Finally, I have to apologize to my wife Juliana, the children Carsten and Friederike, to my mother Theresia, and to my parents in law Dr. h. c. Gerhard and Gudrun Seydel, since this book simply stole too much time I could have spent more happily with them.

Peter Pichler

Frequently Used Symbols

When denoting more than one object, the primary meaning is cited first. The respective units are noted in parentheses.

a^R	Capture radius (m)
a_{Si}	Length of the unit cell of silicon (5.43072 Å)
C	Concentration (m^{-3})
\underline{C}	Number per unit area (m^{-2})
\tilde{C}	Prefactor in the specification of a temperature-dependent concentration in the form $\tilde{C} \cdot \exp(-E_A/kT)$ (m^{-3})
C_I	Concentration of self-interstitials (m^{-3})
C_{Si}	Concentration of silicon atoms, ($5 \cdot 10^{22} \text{ cm}^{-3}$)
C_V	Concentration of vacancies (m^{-3})
C_X	concentration of defects X (m^{-3})
C_X^{eq}	Equilibrium concentration of defects X (m^{-3})
C_X^{sol}	Solubility concentration of impurity X (m^{-3})
C_{X_s}	Concentration of defect X on substitutional sites (m^{-3})
C_{xs}	Concentration of sites for defect X (m^{-3})
D	Diffusion coefficient (m^2/s)
D_0	Prefactor in the specification of a temperature-dependent diffusion coefficient in the form $D_0 \cdot \exp(-E_A/kT)$ or $D_0 \cdot \exp(-H^m/kT)$ (m^2/s)
D_X^i	Intrinsic diffusion coefficient of impurity X (m^2/s)
eV	Electronvolt ($1.60217733(49) \cdot 10^{-19} \text{ J}$)
E	Electric field (V/m)
E_A	Activation energy in the specification of a temperature-dependent concentration or diffusion coefficient (J)
E_c	Energy of the bottom of the conduction band (J)
E_F	Fermi level (J)
E_g	Band gap of silicon (J)
E_v	Energy of the top of the valence band (J)
f^l	Correlation coefficient for the diffusion of silicon tracer atoms via self-interstitials (1)

f_I	Fractional diffusivity of a specific element via self-interstitials (1)
f^V	Correlation coefficient for the diffusion of silicon tracer atoms via vacancies (1)
F	Helmholtz free energy (J)
G	Gibbs free energy (J)
G^B	Binding energy of a defect (J)
G_X^f	Free energy of formation of a defect X (J)
$G_{X^j+e^{-j}}^f$	Free energy of formation of a defect X in charge state j plus j holes (for $j > 0$) or electrons (for $j < 0$) (J)
G^m	Gibbs free energy of migration (J)
h	Planck's constant ($6.6260755(40) \cdot 10^{-34}$ J·s)
H	Enthalpy (J)
H^f	Enthalpy of formation (J)
H^m	Enthalpy of migration (J)
J	Flux, number of atoms passing a unit area per unit time ($\text{m}^{-2}\text{s}^{-1}$)
k	Boltzmann constant ($1.3806(58) \cdot 10^{-23}$ J/K)
$k_{I/V}$	Surface recombination velocity of self-interstitials (I) or vacancies (V) (m/s)
$k_{r\rightarrow}$	Forward reaction constant of reaction r
$k_{r\leftarrow}$	Backward reaction constant of reaction r
L	Phenomenological coefficient within the theory of the thermodynamics of irreversible processes
m	Mass (kg)
m_0	Electron mass ($9.1093897(54) \cdot 10^{-31}$ kg)
m_n^*	Effective mass of electrons (kg)
m_p^*	Effective mass of holes (kg)
m_{Si}	Mass of a silicon atom (^{28}Si : $4.64951256 \cdot 10^{-26}$ kg, ^{29}Si : $4.81556658 \cdot 10^{-26}$ kg, ^{30}Si : $4.9816206 \cdot 10^{-26}$ kg)
n	Electron concentration (m^{-3}); number of moles of a substance (1)
n_i	Intrinsic electron concentration (m^{-3})
n_{ie}	Effective intrinsic electron concentration (m^{-3})
N	Number of atoms, molecules, or defects (1)
N_A	Avogadro constant, number of atoms or molecules in one mole ($6.02213(58) \cdot 10^{23}$ mol $^{-1}$)
N_{X^j}	Number of defects X in charge state j (1)
N_{XS}	Number of sites for defect X (1)
p	Hole concentration (m^{-3})
P	Hydrostatic pressure (Pa)
Q^*	Heat of transfer (J)

s	Mechanical strain, corresponding to a length change relative to the total length (1)
S	Entropy (J/K)
S^f	Entropy of formation (J/K)
S^m	Entropy of migration (J)
t	Time (s)
T	Absolute temperature (K)
U_T	Thermal voltage $k \cdot T/q$ (V)
V	Volume (m^{-3})
\bar{V}	Partial atomic volume (m^{-3})
V_{Si}	Atomic volume associated with one silicon atom, ($20 \text{ \AA}^3 = 2 \cdot 10^{-29} \text{ m}^{-3}$)
x	Space coordinate (m)
x^m	Mole fraction or atomic fraction (1)
x^s	Site fraction (1)
X	X is used in general relationships to represent self-interstitials I or vacancies V
y	Space coordinate (m)
Y	Y is introduced in general relationships in association with X and stands for self-interstitials I when X stands for vacancies V, and <i>vice versa</i>
z	Charge state corresponding to the number of electrons associated (e. g. 2 for doubly negatively charged defects, 0 for neutral ones, and -1 for positively charged defects like ionized donors); Space coordinate (m)
α_{MX}	Partition constant for the direct formation of a specific impurity-point-defect complex MX (1)
γ	Activity coefficient (1)
Γ	Jump frequency (1/s)
Γ_0	Attempt or oscillation frequency (1/s)
δ_{Xj}	Relative concentration of defect X in charge state j under intrinsic conditions with respect to a certain reference charge state of the defect (1)
ΔG	Change in the Gibbs free energy (J)
ϵ	Permittivity constant ($\frac{\text{A}\cdot\text{s}}{\text{V}\cdot\text{m}}$)
ϵ_0	Permittivity constant in vacuum ($8.8542 \cdot 10^{-12} \frac{\text{A}\cdot\text{s}}{\text{V}\cdot\text{m}}$)
ζ	Reaction variable in terms of concentrations of reactants and products (cm^{-3})
Θ	Number of different configurations for a certain defect (1)
Θ^g	Number of geometrically equivalent and distinguishable configurations of a certain defect at a specific site (1)
Θ^i	Number of internal degrees of freedom for a certain geometrical configuration of a defect (1)
λ	Mean path length a defect diffuses before it becomes immobile (m); Lagrange multiplier

μ	Gibbs free energy per atom or molecule, chemical potential (J)
μ^*	Standard value of the chemical potential at the reference state (J)
ξ	Reaction variable in terms of amounts of reactants and products (mol)
π	Ratio of a circle's circumference to its diameter (3.141592653...)
σ	Standard deviation of distribution functions (m); mechanical stress (Pa)
τ	Time constant (s)
ψ	Electrostatic potential (V) Probability amplitude in the Schrödinger equation ($m^{-3/2}$)
Ω	Complexion number (1)

Explanation of Frequently Used Abbreviations

a/c	Relates to an interface between <u>amorphous</u> and <u>crystalline</u> regions
β -NMR	<u>Nuclear magnetic resonance</u> detected in β decay: Characterization technique for the structural properties of magnetic, radioactive nuclei having short half-lives, based on the asymmetries in their β decay relative to the direction of the nuclear polarization.
CMOS	<u>Complementary metal oxide semiconductor</u>
CZ	Denotes <u>Czochralski-grown silicon</u>
DLTS	<u>Deep level transient spectroscopy</u> , also called <u>deep level temperature scan</u> : Method based on the measurement of capacity transients associated with capture and emission of charge carriers at and from deep levels as a function of temperature. ³ Useful to characterize point defects with respect to the position of their electronic levels in the forbidden bandgap and the respective capture cross sections, as well as the concentration of the defects
ENDOR	<u>Electron nuclear double resonance</u> : Spectroscopic method using combined electron-spin and nuclear magnetic resonances
EPR	<u>Electron paramagnetic resonance</u> , also called <u>electron spin resonance (ESR)</u> : Spectroscopic method based on the absorption of microwave-frequency electromagnetic radiation by unpaired electrons in the atomic structure subjected to an appropriately strong stationary magnetic field. An overview of the method and of the centers found until 1983 can be found in the review article of Sieverts. ⁴
ESR	<u>Electron spin resonance</u> : see EPR
EXAFS	<u>Extended X-Ray Absorption Fine Structure</u> : The method probes a particular species of impurity atoms and is able to give information on the number, distance, and chemical identity of the atoms around them.
FTIR	<u>Fourier transform infrared spectroscopy</u> : Variant of the IR spectroscopy
FZ	Denotes <u>float-zone-grown silicon</u>
IED	<u>Implantation enhanced diffusion</u> : Enhanced diffusion of impurities during post-implantation annealing

³D. V. Lang, "Deep-Level Transient Spectroscopy: A New Method to Characterize Traps in Semiconductors," *J. Appl. Phys.*, vol. 45, no. 7, 3023-3032 (1974); G. L. Miller, D. V. Lang, and L. C. Kimerling, "Capacitance Transient Spectroscopy," *Ann. Rev. Mater. Sci.*, vol. 7, 377-448 (1977).

⁴E. G. Sieverts, "Classification of Defects in Silicon after Their g-Values," *phys. stat. sol. (b)*, vol. 120, 11-29 (1983).

IR	<u>Infrared</u> : Spectroscopic method based on the absorption of electromagnetic radiation in the frequency range of infrared light
MBE	<u>Molecular beam epitaxy</u>
MOS	<u>Metal oxide semiconductor</u>
MOSFET	<u>Metal oxide semiconductor field effect transistor</u>
ODMR	<u>Optically Detected Magnetic Resonance</u> : Spectroscopic method based on the detection of magnetic resonances in the frequency range of light and not at the original resonance frequency
OED	<u>Oxidation enhanced diffusion</u> : Enhanced diffusion of impurities during anneals under oxidizing conditions
ORD	<u>Oxidation retarded diffusion</u> : Retarded diffusion of impurities during anneals under oxidizing conditions
OSF	<u>Oxidation stacking fault</u> : Extended self-interstitial aggregate, introducing a stacking fault on a {111} plane
PL	<u>Photoluminescence</u> : Spectroscopic method based on the emission of light induced by the absorption of electromagnetic radiation. An extensive review on PL in silicon was authored by Davies. ⁵
RBS	<u>Rutherford backscattering</u> : Characterization technique based on the nuclear scattering of high-energetic hydrogen or helium atoms at target atoms which, via the electronic energy loss, allows depth profiling of the target composition. In channeling RBS measurements, the incident beam is directed along major crystallographic directions so that backscattering from atoms on regular lattice atoms is avoided to a large extent.
RT	<u>Room temperature</u> , corresponding to about 300 K
RTA	<u>Rapid thermal annealing</u>
RTP	<u>Rapid thermal processing</u>
SANS	<u>Small angle neutron scattering</u> , method to measure the sizes of defects
SIMNI	<u>Separation by implanted nitrogen</u> , method to separate a thin crystalline silicon layer from bulk silicon by implantation of nitrogen in high doses.
SIMOX	<u>Separation by implanted oxygen</u> , method to separate a thin crystalline silicon layer from bulk silicon by implantation of oxygen in high doses.
SIMS	<u>Secondary ion mass spectrometry</u> : Measurement method based on the mass-resolved analysis of the number of charged ions sputtered off from a target by a primary ion beam, usually used to characterize depth profiles of impurities.
SNMS	<u>Secondary neutral mass spectrometry</u> : Measurement method similar to SIMS. But instead of analyzing the charged ions sputtered off the neutral ions sputtered off are ionized and analyzed. Thus, matrix effects are greatly reduced.
SOI	<u>Silicon on insulator</u>
TEM	<u>Transmission electron microscopy</u> : Microscopy method based on the interaction of matter with a penetrating focussed electron beam. Generally used to study crystal defects.
ULSI	<u>Ultra large scale integration</u>

⁵G. Davies, "The Optical Properties of Luminescence Centres in Silicon". *Physics Reports*, vol. 176, no. 3/4, 83-188 (1989).

VLSI	<u>Very large scale integration</u>
XPS	<u>X-ray photoemission spectroscopy</u> : Spectroscopic method reflecting the binding energy of electrons emitted from inner shells of atoms due to their interaction with an X-ray beam

Chapter 1

Fundamental Concepts

A quantitative description of diffusion and activation phenomena requires the application of various phenomenological and atomistic concepts. The goal of this chapter is to introduce them as a basis of more in-depth discussions in the following chapters.

Section 1.1 introduces the silicon lattice and its imperfections. The section starts with a discussion of the system of Miller indices used to characterize orientations of planes and directions in the crystal. Thereafter, the atomic configuration and geometric parameters of the silicon lattice are recapitulated. Most important for the application and processing of silicon devices are deviations from the regular arrangement of atoms, the so-called defects. Many of them are invariant with respect to certain symmetry operations and the respective knowledge is important for their experimental identification. After having discussed the different classes of defects, the Hermann-Mauguin and Schoenflies notations used to characterize the defect symmetries are outlined. Finally, various highly symmetric configurations of point defects are summarized.

Most of the defects in silicon can exist in several charge states. Section 1.2 outlines the concepts of electrons and holes in semiconductors. Both types of charge carriers, either in the conduction or valence-band band, or bound to dopants, determine the Fermi level in the crystal. For low concentrations, Fermi statistics can be approximated by Boltzmann statistics. The parabolic form of the bands leads then to significantly simpler formulations for electron and hole concentrations which can be used in turn to calculate the charge distribution among defects. But already at concentrations above about 10^{18} cm^{-3} , the band structure of silicon will be influenced by a variety of effects. Finally, physical parameters like the carrier concentration under intrinsic conditions and the width of the band gap are summarized.

Redistribution of atoms can be observed in any materials during processing steps carried out at sufficiently high temperatures. There are various phenomenological and atomistic approaches to describe such phenomena quantitatively and the objective of Section 1.3 is to summarize them. Continuum methods are based on an empirical relation between fluxes of defects and the gradient of their concentration. This relation, called Fick's first law, introduces the diffusion coefficient as proportionality constant. Completion by mass conservation gives a partial differential equation describing the change of concentration with time generally called Fick's second law. An alternative to the continuum description of diffusion effects are atomistic concepts based on the concept of "random walk", i. e. atoms performing uncorrelated jumps in random direction. This leads to an identification of the diffusion coefficient of a defect via its mean square displacement from the original position. But concentration gradients are not the only possible causes for the redistribution of atoms. To characterize the influences arising from, e. g. electrostatic fields, gravitational forces, or pressure gradients on atom redistribution, the concept of driving forces was introduced by Manning. Such driving forces are defined as any

influence which makes the jump frequency to depend on the direction of the jump. Finally, besides the thermally agitated jumps of atoms, diffusion can be stimulated by the interaction with charge carriers. Such effects are summarized under the term athermal diffusion.

Additional insights into equilibrium conditions and redistribution processes can be obtained from thermodynamic methods as shown in Section 1.4. Statistical thermodynamics can be used to deduce the conditions in equilibrium. Studies of dynamic processes like diffusion or chemical reactions can be performed within the framework of the thermodynamics of irreversible processes. Near equilibrium, linear relations between fluxes and conjugate generalized forces are postulated to hold. The methodology allows to describe phenomena which would be hardly accessible to kinetic methods alone. As examples, redistribution phenomena due to stress effects and thermal gradients are discussed.

Thermodynamic methods can be applied also to reactions between the species being present in a system. The method of equilibrium thermodynamics, as explained in Section 1.5, results in the law of mass action which establishes a relation between the concentrations of the species involved in the reactions. The evolution of the reaction with time can be described by the dynamic law of mass action or alternative theories like the thermodynamics of irreversible processes or the transition-state theory. For binary reactions, kinetic theories are available to estimate the reaction constants.

Finally, in Section 1.6, redistribution phenomena in adjacent phases are considered. In equilibrium, such processes lead to a distribution of the atoms involved which is inhomogeneous within the system albeit homogeneous within each phase. This effect, called segregation, is characterized by segregation or distribution coefficients. Closely connected to segregation is the concept of solid solubility, identical to the concentration of impurities in a silicon phase in equilibrium with an impurity-related equilibrium phase. The section ends with a discussion of the concepts suggested to describe segregation phenomena dynamically.

1.1 Silicon and Its Imperfections

Defects in crystals are the basis of any technical application and play a dominant role during processing. In the following, the major properties of silicon and the basic concepts of its imperfections are introduced. This includes a discussion of the concepts to characterize crystallographic planes and directions as well as symmetries of point defects.

1.1.1 Orientations in Crystals: Miller Indices

Because of the regular atomic arrangement of the atoms, a crystal can be thought to be subdivided into identical building blocks. The smallest possible one which can no longer be subdivided into other identical blocks is denoted unit cell. In the general case, the unit cell will be a parallelepiped. Except for hexagonal lattices, only translations are necessary to assemble crystals from their unit cells. In such systems, starting from one of the corners of the unit cell as origin, crystallographic axes x , y , and z can be defined conveniently along the edges which meet there. This coordinate system is usually, but not necessarily, orthogonal. The lengths of the edges of the unit cell along the x , y , and z directions will be denoted a , b , and c , respectively.

Based on the definition of the unit cell, crystallographic planes and directions are defined by a system devised in 1839 by the British mineralogist and crystallographer William Hallowes Miller. We will consider now a plane as shown in Figure 1.1 which intersects the x axis at a , the y axis at $b/2$, and the z axis at $c/3$. The so-called Miller indices are then based on the reciprocals of the intercepts measured in lattice units. Enclosing them in parentheses to

indicate that they are the definition of a plane, the Miller indices of our plane would be (123). When reciprocals of intersects come out as fractions, all of them have to be multiplied by the least common multiple of the denominators. As an example, a plane with intersects at $6/7 \cdot a$, $3/4 \cdot b$, and $2/3 \cdot c$ would have Miller indices of (789). If any intersection is found in the negative direction of an axis, this is indicated by a bar over the respective Miller index. Typical examples for planes in cubic crystals can be found in Figure 1.2.

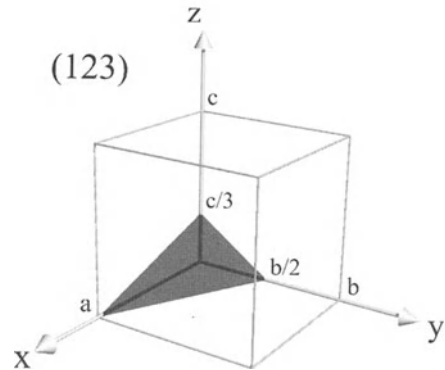


Figure 1.1: Definition of a (123)-oriented crystal plane via Miller indices.

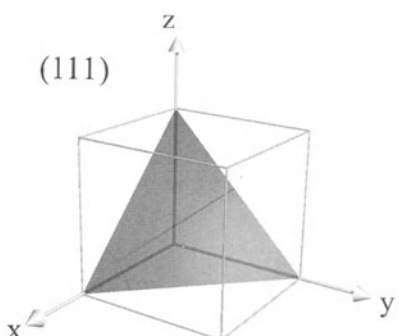
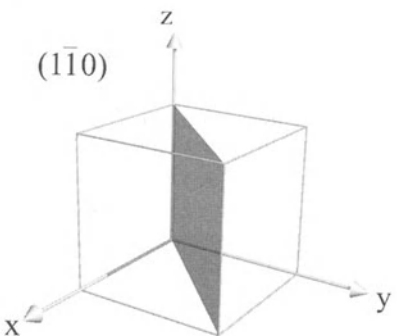
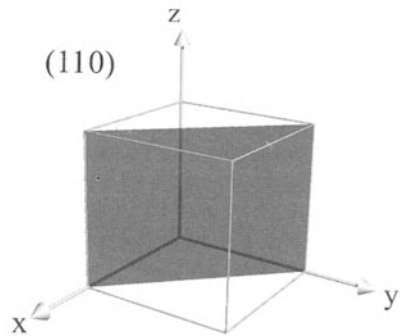
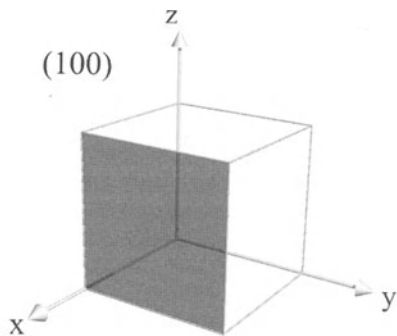


Figure 1.2: Miller indices for typical planes in cubic crystals.

Considering the rules outlined above, it becomes apparent that parallel planes as depicted in Figure 1.3 have the same Miller indices. Thus, the symbol (hkl) stands for all parallel planes with a spacing equal to the distance of the plane with intersects at a/h , b/k , and c/l to the origin. This means that any plane with (hkl) is equivalent to $(\bar{h}\bar{k}\bar{l})$. It also allows us to choose a corner

of another unit cell as origin in order to find the Miller indices of planes which pass through the origin of the coordinate system. Finally, it remains to remark that planes in a hexagonal system are defined via a similar scheme of four Bravais-Miller indices.

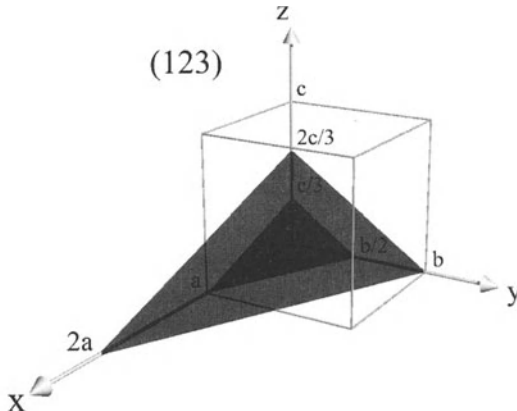


Figure 1.3: Definition of parallel (123)-oriented crystals planes via Miller indices.

In cubic systems, as an example, the planes (100), (010), and (001) are equivalent with respect to the arrangements of atoms and bonds. To express that all equivalent planes in a system are meant, the Miller indices can be enclosed in braces. $\{110\}$, as an example, would include (110), (101), (011), ($\bar{1}10$), ($\bar{1}\bar{1}0$), ($1\bar{0}1$), ($0\bar{1}1$), ($0\bar{1}\bar{1}$), ($\bar{1}\bar{1}\bar{0}$), ($\bar{1}0\bar{1}$), and ($0\bar{1}\bar{1}$) in a cubic system.

Crystallographic directions are specified by integers representing distances in lattice units. If we move, as an example, distances of a in the x direction, $2 \cdot b$ in the y direction, and $3 \cdot c$ in the z direction, the respective crystallographic direction is denoted [123]. The square brackets are used to declare it as a definition of a specific crystallographic direction. In the cubic system, but only there, $[hkl]$ directions are orthonormal to (hkl) planes. To address all equivalent crystallographic directions, angle brackets can be used in the form $\langle hkl \rangle$.

1.1.2 The Silicon Lattice

The atomic arrangement of silicon atoms is shown in Figure 1.4. It corresponds to the diamond structure and can be thought of as the union of a face-centered cubic crystal lattice with another one which is displaced by a quarter of the length of the unit cell in the [100], [010], and [001] directions. Each atom of one sub-lattice is tetrahedrally surrounded by 4 atoms of the other sub-lattice. The silicon-silicon bonds are homopolar covalent bonds formed by sp^3 hybridization with two shared electrons forming each bond. It should be noted that the diamond structure is energetically favored only up to pressures of about 11 GPa. At higher pressures, various other crystal structures were observed [1.1].

The unit cell of silicon, shown in Figure 1.4, has a side length of $a_{Si} = 5.43072 \text{ \AA}$ at 25 °C [1.2] and contains 8 atoms. From this value, the bond length between two silicon atoms follows as $a_{Si} \cdot \sqrt{3}/4 = 2.352 \text{ \AA}$. Similarly, the distance between two second nearest silicon atoms follows as $a_{Si} \cdot \sqrt{2}/2 = 3.84 \text{ \AA}$. Simple calculations show that the volume V_{Si} associated with one silicon atom is close to 20 \AA^3 and the concentration of silicon atoms is $C_{Si} = 5 \cdot 10^{22} \text{ cm}^{-3}$. More precisely, recent measurements by Ohsaka et al. [1.3] indicated that the concentration of silicon atoms decreases linearly from $5.032 \cdot 10^{22} \text{ cm}^{-3}$ at room temperature to $4.955 \cdot 10^{22} \text{ cm}^{-3}$ at the melting point.

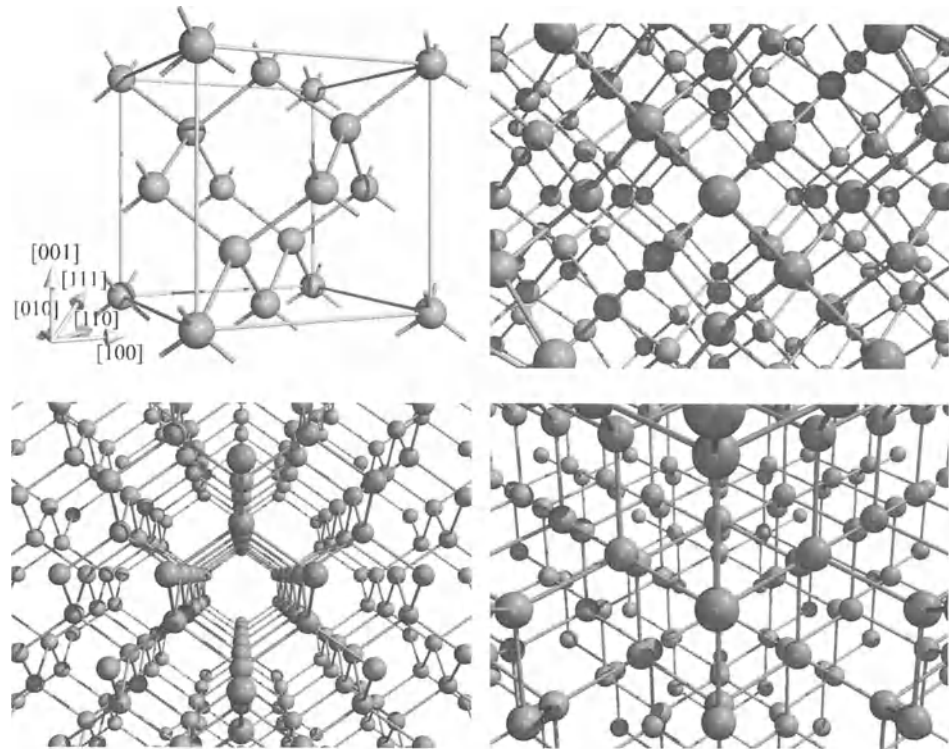


Figure 1.4: Atomic structure of silicon: upper left: silicon unit cell; upper right: view in [100] direction through a silicon crystal of $3 \times 3 \times 3$ unit cells; lower left: view in [110] direction; lower right: view in [111] direction.

The natural abundances of ^{28}Si , ^{29}Si , and ^{30}Si are 92.23%, 4.67%, and 3.1%. The corresponding masses of individual silicon atoms are given by the mass number times the atomic-mass unit (one twelfth of a ^{12}C atom, equivalent to $1.6605402 \cdot 10^{-27}$ kg). This means masses of approximately $4.65 \cdot 10^{-26}$ kg for ^{28}Si , $4.82 \cdot 10^{-26}$ kg for ^{29}Si , and $4.98 \cdot 10^{-26}$ kg for ^{30}Si .

A cut along a {100}-oriented plane may hit 2 atoms per unit cell in an area of a_{Si}^2 which gives an area concentration of $6.78 \cdot 10^{14} \text{ cm}^{-2}$. Along a {110}-oriented plane one might hit up to 4 atoms in an area of $\sqrt{2} \cdot a_{\text{Si}}^2$, corresponding to an area concentration of $9.59 \cdot 10^{14} \text{ cm}^{-2}$. Finally, a cut along a {111}-oriented plane might hit up to 2 atoms in a equilateral triangle with a side length of $\sqrt{2} \cdot a_{\text{Si}}$ which results in a value of $7.83 \cdot 10^{14} \text{ cm}^{-2}$.

1.1.3 Crystal Defects

From the Nernst theorem it is known that a crystal may have a perfect structure only at the absolute zero of temperature. For finite temperatures, crystals necessarily show imperfections. Imperfections involving only atoms which are native to the crystal (e.g. Na or Cl in NaCl crystals) are called “intrinsic” defects. Redistribution of such atoms is termed “self-diffusion.” The eminent significance of intrinsic defects comes from the fact they play a major role in nearly all theories dealing with the diffusion of dopants in silicon. When other atoms such as dopants or metal impurities are involved, the respective defects are called “extrinsic.”

In their simplest form, defects influence only the nearest neighboring atoms of the crystal lattice. They are then called “point defects.” Defects of higher dimensionality are summarized under the term “extended defects”. However, there is no clear-cut borderline between the two concepts. Extended states were even suggested for self-interstitials and vacancies and, depending on the point of view, it might be more convenient to think of agglomerates comprising only a small number of intrinsic point defects and/or impurities as point defects or extended defects.

Defects of the next higher dimensionality introduce local disorder along a line through the crystal. Consequently, such defects are called “line defects.” There are two basic types, edge dislocations and screw dislocations. Edge dislocations bound extra or missing planes. Screw dislocations can be thought of as the result of cutting the crystal along a plane ending at a major crystallographic axis and shifting the atoms at one side of the cut surface by one atomic spacing along the axis at which the cut ended. This leads to a screw dislocation along this axis. Following the planes around the screw dislocation results in a spiral extending from one surface to the other. All complex dislocations can be resolved into their edge and screw components. Line defects are either closed loops or end at the surface.

For any crystallographic direction, parallel planes can be drawn through the atoms. Comparing the atomic arrangements of the atoms on the planes, it becomes apparent that the same patterns are repeated periodically, determining the stacking order of the crystal. Missing or extra planes usually disturb the stacking order and are called “stacking faults.” They are typical examples for two-dimensional defects. Extra planes are usually called “extrinsic” in contrast to missing planes which are termed ‘intrinsic.’ Other typical two-dimensional defects are grain boundaries. They separate crystalline regions of different crystal orientation.

The highest dimensionality of defects are volume defects which constitute of non-native phases in the matrix. Typical examples are spherical oxygen precipitates and octahedral voids.

A schematic representation of the most important point defects can be found in Figure 1.5. In the simplest form, the vacancies shown schematically in Figure 1.5 a) are missing atoms in an otherwise tetrahedrally coordinated network. However, such an atomic arrangement is energetically unfavorable and there will be a relaxation of the surrounding silicon atoms. In addition, more complicated atomic arrangements were suggested as alternatives to simple vacancies. A typical example is the semi-vacancy pair with a silicon atom midway between two vacant lattice sites. The properties of vacancies will be discussed in detail in Section 2.4. In addition to the mono-vacancy, a complex of two vacancies, called divacancy (Figure 1.5 b), as well as larger vacancy clusters were identified. All of them involve only atoms native to the crystal and belong to the intrinsic point defects.

The other class of intrinsic point defects comprise extra silicon atoms. Configurations with just one extra atom are summarized under the term self-interstitials. In the simplest form, self-interstitials are assumed to be extra silicon atoms on well-defined locations (e. g. tetrahedral or hexagonal sites) in the otherwise perfect crystal (Figure 1.5 c). Besides the pure interstitial defect, a configuration in which two silicon atoms share a site has been proposed. This configuration (Figure 1.5 d) is usually called “split interstitial,” “interstitialcy,” or “dumb-bell interstitial” and can be seen as an analog to the semi-vacancy pair. In analogy to the divacancy, a di-interstitial has been proposed in the literature and self-interstitial agglomerates play an important role for transient diffusion phenomena. Self-interstitials in all their possible forms, di-interstitials, and larger self-interstitial agglomerates involve only atoms native to the crystal. Therefore, they are all counted among the intrinsic point defects.

It should be noted that different atomic configurations of vacancies and of self-interstitials may coexist in a crystal. Within the same defect class, a continuous transformation from one configuration into an other can be expected. Some of them will be saddle points for the diffu-

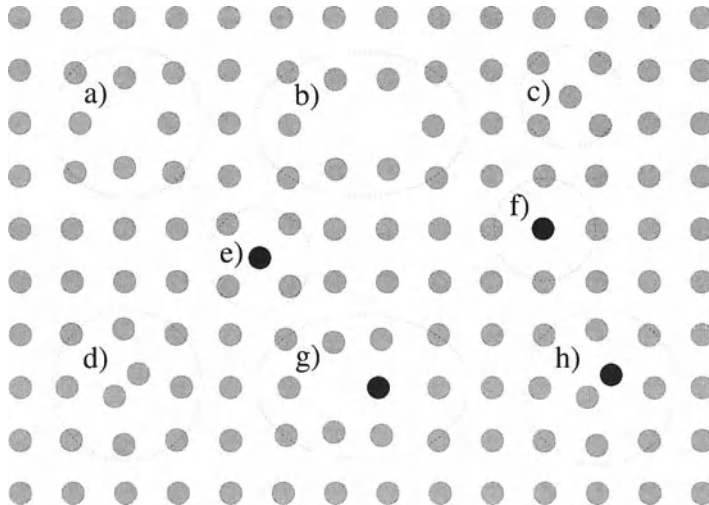


Figure 1.5: Schematic representation of point defects in silicon: a) vacancy, b) divacancy, c) self-interstitial, d) interstitialcy, e) interstitial impurity, f) substitutional impurity, g) impurity-vacancy pair, h) impurity-self-interstitial pair.

sion of energetically more favorable configurations. Averaged with respect to time, the relative concentrations of the coexisting configurations will reflect their energetics.

Because of the very open structure of silicon, many impurities reside predominantly on interstitial positions in the host lattice (Figure 1.5 e). Among them are oxygen and many alkali and heavy metals.

Most important for semiconductors are atoms of the groups III and V of the periodic system which reside predominantly on substitutional lattice sites (Figure 1.5 f). Atoms from group V, the so-called donors, have one positive charge too many for their share of the four valence bonds. The extra electrons neutralizing the positive charges behave much like free electrons. Similarly, atoms from group III, the so-called acceptor impurities, have one positive charge too few for the bonding structure of silicon. In analogy to the electrons, holes are introduced and postulated to behave like positively charged particles in free space. Both types of charge carriers determine the electrical characteristics of devices and the prediction of the spatial distribution of donors and acceptors after processing is one of the main goals of process simulation. Because substitutional impurity atoms are assumed to be immobile in most diffusion theories, an interaction with intrinsic defects has to be taken into consideration. Such an interaction can lead to impurity-vacancy pairs (Figure 1.5 g) and impurity-self-interstitial pairs (Figure 1.5 h).

With interstitial impurity atoms (Figure 1.5 e) and impurity-self-interstitial pairs (Figure 1.5 h), two very similar concepts were introduced for an extrinsic interstitial defect. The important difference between the two is not the atomic arrangement in the energetically most favorable configuration. It is rather the question whether the silicon atom and the impurity involved perform a correlated walk. When they do, the silicon atom may be a tracer atom and the correlated diffusion may accelerate self-diffusion (see Section 2.3). When they do not, as it is certainly the case for interstitial impurity atoms but also when the impurity atom in the pair moves by interacting with continuously changing silicon partners, no direct influence on self-

diffusion is expected. In general, correlated and uncorrelated diffusion of impurities and silicon partners may occur simultaneously, subject to the probability for the respective mechanism. However, as long as the influence on self-diffusion is of minor importance, both forms can be treated alike.

1.1.4 Symmetries of Defects

Some of the techniques used for characterization of crystal defects allow to deduce the symmetry of these defects. The most prominent example is probably EPR, but symmetry information can also be obtained from the application of uniaxial stress and its influence on the measurand. This symmetry information does not allow to identify the defect structure unambiguously, but it narrows the possibilities considerably.

Symmetry Operations

A certain body is called symmetric when it has a shape so that certain operations performed on it bring it into coincidence with itself again. Such operations are called symmetry operations. Besides the trivial identity transformation, they include reflection, rotation, inversion, and rotation-inversion.

A reflection about a mirror plane implies that for each volume element of the body a corresponding volume element exists on the other side of the mirror plane in a direction perpendicular to the mirror plane and in a distance twice that from the volume element to the plane of reflection. The international symbol for a reflection symmetry operation is “ m .”

Rotations about symmetry axes are characterized by an integer n indicating that the body can be transformed into itself by rotating it around the symmetry axis by an angle of $2 \cdot \pi/n$. The international names and symbols for such n -fold rotation symmetry operations are shown in Table 1.1. Evidently, the monad 1 is identical to the trivial identity transformation.

Table 1.1: Rotation and rotoinversion symmetry operations involving rotation by $2 \cdot \pi/n$.

n	Rotation		Rotoinversion		
	n	name	symbols	name	symbols
1	monad	1	1	inversion monad	$\bar{1}$ \circ
2	diad	2	•	inversion diad	$\bar{2}$ \emptyset
3	triad	3	▲	inversion triad	$\bar{3}$ \blacktriangle
4	tetrad	4	◆	inversion tetrad	$\bar{4}$ \blacklozenge
6	hexad	6	●	inversion hexad	$\bar{6}$ \bullet

An inversion about a point implies that for each volume element of the body a corresponding volume element exists in twice the distance in the direction of the inversion point. The international symbol for an inversion symmetry operation is “ \circ ”.

A combination of rotation and inversion elements leads to the rotation-inversion symmetry operations also called rotoinversions. They characterize bodies which can be brought into coincidence by rotating them by an angle of $2 \cdot \pi/n$ and mirroring them about a point on the rotation axis. The international names and symbols for such rotoinversion symmetry operations are shown in Table 1.1. From their definitions it is evident that $\bar{1}$ is identical to the inversion symmetry operation and that $\bar{2}$ is identical to m , a mirror plane normal to the rotation axis of the inversion diad.

Symmetry and Point Groups

Defects may combine any of the symmetry operations described above. Nevertheless, the number of independent combinations is restricted to 32 point groups. These are grouped into the following systems according to the minimum number of symmetries outlined in Table 1.2.

Table 1.2: Definition of symmetry groups.

Symmetry group	Minimum symmetry operations
Cubic	Four 3-fold rotation axes
Tetragonal	One 4-fold rotation (or rotoinversion) axis
Hexagonal	One 6-fold rotation (or rotoinversion) axis
Trigonal	One 3-fold rotation (or rotoinversion) axis
Rhombic	Three perpendicular 2-fold rotation (or rotoinversion) axes
Monoclinic	One 2-fold rotation (or rotoinversion) axis
Triclinic	No rotation axis

In crystals of the diamond structure, only 13 of the 32 point groups exist. None of them belongs to the hexagonal system. To characterize point symmetries, several systems are used in the literature. The two most wide-spread will be discussed shortly in the following.

The Hermann-Mauguin Notation of Point Symmetries

At the beginning of the 20th century several classification schemes for crystal symmetries were in use. Based on the work of Hermann and Mauguin, a unified scheme was finally accepted by an international commission [1.4]. Commented by Hermann [1.5], it was finally published by Mauguin [1.6]. The intention of the new scheme was to present all essential symmetry operations at a glance. The notation for point groups is based on the symbols outlined above: 1, 2, 3, 4, and 6 to represent rotation axes, $\bar{1}$ for an inversion point, $\bar{3}$, $\bar{4}$, and $\bar{6}$ to represent rotoinversion axes, and ‘m’ for mirror planes.

The symmetry of the principal axis is given first and a mirror plane perpendicular to this axis is expressed, e. g. for a triad, in the forms $\frac{3}{m}$ or $3/m$. Thereafter, secondary axes perpendicular to the principal axis and additional symmetry planes parallel to the principal axis are indicated. Two trailing ‘m’s refer to two inequivalent mirror planes. Details on the point groups in silicon can be found in Table 1.3.

The Schoenflies Notation of Point Symmetries

Despite the advantages of the Hermann-Mauguin notation, a classification system suggested by Schoenflies [1.7] before has acquired an extremely wide usage and nearly all publications on defects in silicon are based on this system. The Schoenflies notation of the symbols relevant for the cubic system combines the upper case letters C, D, S, and T standing for the German or Germanized Latin words “cyclisch,” “Dieder,” “Spiegelung” and “Tetraeder” with lower case indices d, h, i, s, and v standing for “diagonal,” “horizontal,” “Inversion,” “Spiegelung,” and “vertical.” The numbers n appearing also in the indices indicate that the system can be brought into coincidence by rotating it by $2 \cdot \pi/n$ around the principal axis of rotation. Those combinations relevant for the cubic system are summarized in Tables 1.3 and 1.4.

At this point it has to be remarked that the symbols listed in Tables 1.3 and 1.4 correspond to those attributed generally to Schoenflies in textbooks. In his original work, Schoenflies used a partly different notation. Instead of on rotoinversion he based his classification system on

Table 1.3: Point groups possible in silicon. A subscript ‘p’ indicates a polar axis.

Symmetry group		Symbols	Symmetry operations	Example figure
	Hermann-Mauguin	Schoenflies		
Triclinic	1 $\bar{1}$	C_1 C_i	\circ	
Monoclinic	2 m $2/m$	C_2 C_s, C_{1h} C_{2h}	\bullet m $\bullet + m$	2.14 1.15, 4.7, 4.8
Rhombic	222 $2mm$	D_2 C_{2v}	$\bullet + \bullet + \bullet$ $\bullet_p + 2m$	
Trigonal	3 3m $\bar{3}m$	C_3 C_{3v} D_{3d}	Δ_p $\Delta_p + 3m$ $\Delta (\equiv \Delta + \circ) + 3(\bullet + m)$	1.13, 1.14, 6.4 1.16, 5.18 1.9, 1.10, 1.11, 1.17
Tetragonal	4 $\bar{4}2m$	C_4 D_{2d}	Δ_p $\Delta + 2\bullet + 2m$	1.12, 6.5
Cubic	$\bar{4}3m$	T_d	$3\Delta + 4\Delta_p + 6m$	1.6, 1.7, 1.8

Table 1.4: Schoenflies notation of point symmetries relevant for the cubic system.

Symbol	Explanation
C_i	Bodies with an inversion point
C_s	Bodies with a mirror plane
C_n	Groups having an n -fold rotation axis
C_{nh}	Groups combining an n -fold rotation axis and a mirror plane perpendicular to it
C_{nv}	Groups combining an n -fold rotation axis with planes of symmetry parallel to it
D_n	Groups with an n -fold principal axis of rotation and at least two two-fold axes perpendicular to the principal axis
D_{nd}	Groups combining an n -fold principal axis of rotation, at least two two-fold axes perpendicular to the principal axis, and diagonal symmetry planes parallel to the principal axis in between the two-fold axes normal to the principal axis
T_d	Tetrahedral bodies having diagonal symmetry planes in addition the 3 3-fold and 3 2-fold symmetry axes of a regular tetrahedron

groups termed S_n for bodies which can be brought into coincidence by rotating them by $2 \cdot \pi/n$ around a principal axis of rotation and by mirroring them about a plane perpendicular to this axis. From this results that the inversion denoted C_i in Table 1.3 appears as S_2 in the original work of Schoenflies, and the mirror symmetry C_{1h} as S . In addition, Schoenflies introduced the symbol V for “Vierergruppe” to denote bodies which have three perpendicular two-fold rotation axes. In the usual notation, V corresponds to D_2 , and V_d to D_{2d} .

1.1.5 Selected High-Symmetry Configurations of Point Defects in Silicon

One of the most simple conceivable point defects in silicon is the vacancy. In the form shown schematically in Figure 1.6, the vacancy is T_d -symmetric. The properties as well as other possible structures of the vacancy are discussed in Section 2.4. Also T_d -symmetric is an impurity atom substituting a silicon atom on a regular lattice site as shown in Figure 1.7.

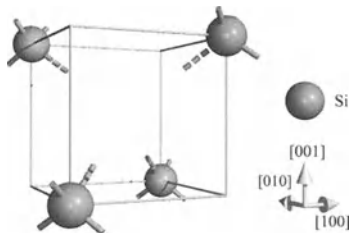


Figure 1.6: Schematic atomic arrangement of atoms around a vacancy.

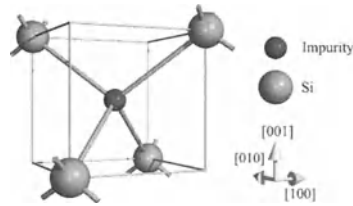


Figure 1.7: Schematic representation of a substitutional impurity atom.

Extra atoms, silicon atoms as well as impurities, may occupy several highly symmetric sites in the silicon lattice. Figures 1.8 to 1.11 show the hexagonal, tetrahedral, bond-centered, and anti-bond interstitial sites in the diamond lattice, respectively. The symmetry of the tetrahedral interstitial is T_d , that of the other three D_{3d} . Atoms at tetrahedral and hexagonal sites are not assumed to bond to neighboring atoms.

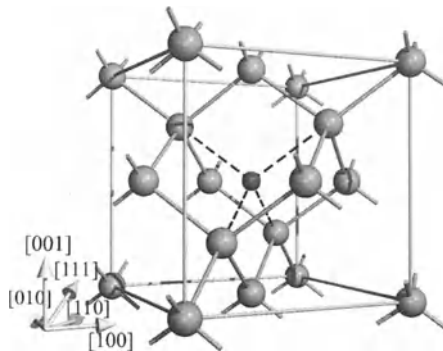


Figure 1.8: Tetrahedral interstitial site in the diamond lattice.

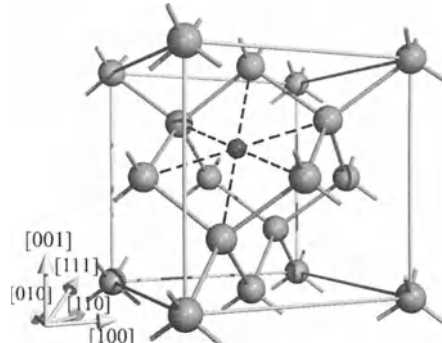


Figure 1.9: Hexagonal interstitial site in the diamond lattice.

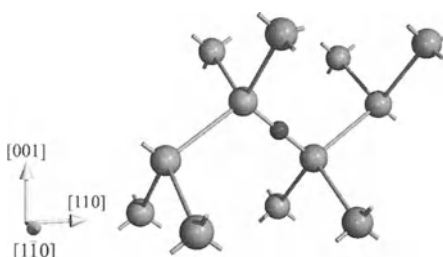


Figure 1.10: Bond-centered interstitial site in the diamond lattice.

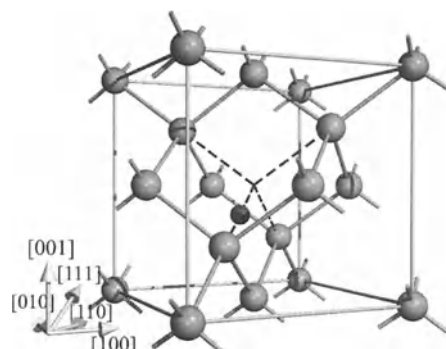


Figure 1.11: Anti-bond interstitial site in the diamond lattice.

The alternative to the true interstitial sites shown above are split interstitials where the extra atom (a silicon atom or an impurity) shares the original lattice site with the silicon atom. Possible configurations of two equivalent atoms are shown schematically in Figures 1.12 and 1.13. Similar arrangements for inequivalent atoms are depicted in Figures 1.14 and 1.15, respectively. The symmetry for the $\langle 001 \rangle$ split interstitial is D_{2d} for inequivalent atoms and lowers to C_{2v} for equivalent atoms. For the $\langle 110 \rangle$ split interstitial, C_{2v} symmetry is reached for equivalent atoms whereas two inequivalent atoms give only C_{1h} symmetry. In addition to these rather common configurations, a split interstitial might be oriented along the $\langle 111 \rangle$ direction. Such defects with equivalent as well as with inequivalent atoms would have C_{3v} symmetry. However, they are only rarely considered to form in the diamond lattice.

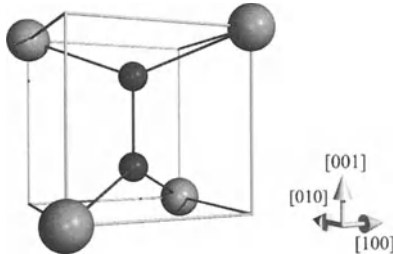


Figure 1.12: Atomic arrangement of a $\langle 001 \rangle$ -oriented split interstitial of equivalent atoms in the diamond lattice (marked by a dumbbell of smaller atoms).

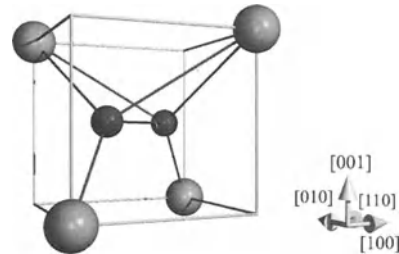


Figure 1.13: Atomic arrangement of a $\langle 110 \rangle$ -oriented split interstitial of equivalent atoms in the diamond lattice (marked by a dumbbell of smaller atoms).

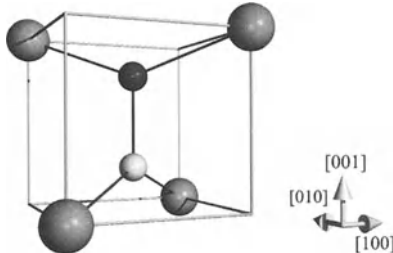


Figure 1.14: Atomic arrangement of a $\langle 001 \rangle$ -oriented split interstitial of inequivalent atoms in the diamond lattice (marked by a dumbbell of smaller atoms).

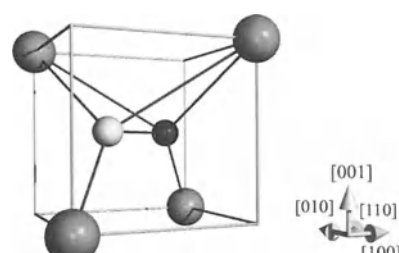


Figure 1.15: Atomic arrangement of a $\langle 110 \rangle$ -oriented split interstitial of inequivalent atoms in the diamond lattice (marked by a dumbbell of smaller atoms).

There are numerous possibilities for pairs between two impurity atoms or between an impurity atom and an interstitial silicon atom. Such of substitutional atoms on nearest neighboring sites are shown in Figures 1.16 and 1.17. The first one represents a C_{3v} -symmetric pair of inequivalent atoms. For two equivalent atoms, the symmetry raises to D_{3d} . Other pairs and atomic configurations of high symmetry will be discussed in the following chapters.

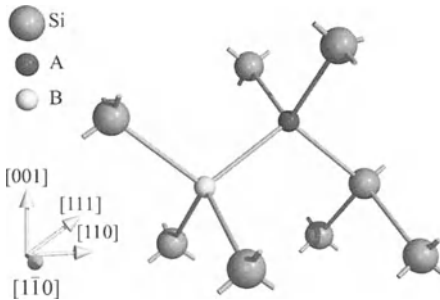


Figure 1.16: Schematic atomic arrangement of a pair of inequivalent substitutional atoms A and B.

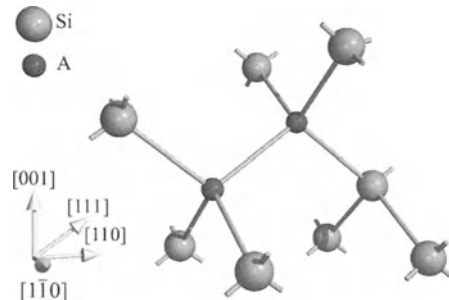


Figure 1.17: Schematic atomic arrangement of a pair of equivalent substitutional atoms A.

1.2 The Electron System

The distribution of the electrons upon the various defects in real semiconductors determines not only the electrical behavior but also the redistribution of the defects at diffusion temperatures. This section summarizes the basic relationships. For a detailed analysis, the interested reader is referred to the literature, especially to the monographs of Shockley [1.8], Sze [1.9], and Selberherr [1.10].

1.2.1 Charge Carriers in Solids

The classical view of an electron is that of a small particle carrying charge and diffusing in analogy to Brownian movement in force fields. This picture fails to account for many effects observed in solids. However, it was possible to explain the respective phenomena by quantum mechanics. In this theory, an electron is a very small particle whose laws of motion are governed by Schrödinger's wave equation. Influenced by forces which can be represented by a potential energy U , the possible energies E and modes of motion of the electron are described by

$$\frac{\hbar^2}{8 \cdot \pi^2 \cdot m} \cdot \text{div grad} \psi + (E - U) \cdot \psi = 0 \quad (1.1)$$

with m standing for the mass of the electron. The wave function ψ is a complex probability amplitude. The square of its absolute value is the probability density of the electron, and the probability to find the electron in the volume dV is given by $|\psi|^2 \cdot dV = \psi^* \cdot \psi \cdot dV$.

In a crystal, the potential in which the electron moves is periodic due to the periodicity of the crystal. Then, solutions of Schrödinger's wave equation are possible only for discrete values of the energy. The wave functions associated have a certain number of wave lengths or half wave lengths in the x , y , and z directions which are naturally arising quantum numbers that can be used to characterize the solution of the wave equation. In addition to the motion in space, the electron rotates about its own axis. This rotation introduces a fourth degree of freedom and a fourth quantum number, the spin, which has only the two permitted values $+\frac{1}{2}$ and $-\frac{1}{2}$. For waves in a crystal, the solutions to Schrödinger's wave equation will be periodic, too. The corresponding wave functions are called Bloch functions.

When several electrons are simultaneously present and exert forces of electrostatic repulsion on each other, it is no longer exact to think of each electron as moving in a constant force field. Consequently, it is not exact to speak of quantum states for individual electrons but instead only of quantum states for the whole system. However, it can be shown that a self-consistent solution

can be obtained by averaging the force fields and the behavior of each electron is described by specifying the quantum state it occupies. In addition, when several electrons are treated, the Pauli exclusion principle has to be considered which states that no two electrons in a system may occupy the same quantum state.

When the atoms of an imaginary crystal are separated so that no overlapping of the wave functions occurs, the atoms can be considered individually. Therefore, wave functions with the same quantum states and the same energy can exist for each of the atoms and the Pauli exclusion principle does not apply. The number of possible quantum states for all atoms is basically the number of possible quantum states for one atom times the number of atoms considered. When the distance between the crystal atoms is reduced in our hypothetical experiment, the influences of the electrons on each other are no longer negligible. The number of quantum states ($> 10^{20}$) will be preserved but the energies associated with the wave functions will differ slightly. As the coupling between the wave functions becomes stronger, the allowed energies will overlap and form bands. The width of the energy band arising from an atomic energy level will be independent of the number of atoms in the crystal and will mainly depend on the lattice constant of the crystal and the energy level from which the band was formed. For the energies between the energy bands, there is no energy level for which a solution of Schrödinger's wave equation exists. These energy intervals are, therefore, called "forbidden energy bands", "band gaps", or "energy gaps".

The electrons in the lowest energy states (1s, 2s, 2p for silicon) show a very weak coupling with the electrons of the surrounding atoms in the real crystal. The spreading of the respective energy bands is then very small and these electrons can be assumed nearly unaffected by their being in the crystal. Of major importance in silicon are the electrons arising from the 3s and 3p quantum states forming the valence-bond band and the conduction band. The valence-bond band and the conduction band are respectively the band with the highest energy levels which is completely filled and the band with the lowest energy levels which is completely empty (semiconductors) or not completely filled (metals) at the absolute zero of temperature. The width of the forbidden band between the bottom of the conduction band and the top of the valence-bond band is called the band gap E_g .

1.2.2 Dopants

Up to this point, the crystal has been considered ideal in the sense that the potential of the crystal is perfectly periodic. However, in reality, as discussed in Section 1.1, defects are present in the crystals. Most important are atoms from the groups III and V of the periodic system, the so-called acceptors and donors.

Atoms from group V have one positive charge too many for their share of the four valence bonds. Therefore, they form a positive charge in the lattice. The defect is accompanied by an extra electron which neutralizes the positive charge but which cannot be a part of the valence-bond structure. The energy states of this extra electron are described by wave functions in the conduction band and, there, behave much like an electron in free space in presence of a positive charge. From this analogy, shallow impurity levels are often denoted "hydrogen-like." However, the effective mass of the electron in the crystal is different from that of a free electron, and the dielectric constant of the crystal is higher than that of free space. The binding energy between the electron and the positive charge is about 0.1 eV which corresponds to the distance in energy of the lowest state in the conduction band to the state of the electron.

Group III acceptor impurities represent negative charges since their atomic cores are insufficiently charged to neutralize the four electrons in their share of the valence bonds. Consequently, they can attract a positive charge. To describe the behavior of this positive charge, the concept of holes in the valence-bond band has been introduced as an abstraction which gives a convenient way of describing the behavior of the electrons. Analogously to the case of donors, holes in the valence-bond band behave much like positively charged particles in free space in the presence of a negative charge. Therefore, a state for holes will be established about 0.1 eV above the valence-bond band.

In addition to the Group V donors and Group III acceptors, defects may exist which introduce significantly deeper states for holes or electrons. In analogy, one speaks of a donor state when the defect is neutral when the electron is bound to it and positively charged when the electron is in the conduction band. When a second electron is bound with an energy less than the band gap to the singly ionized defect, one speaks of a double donor. In analogy, one uses the term acceptor for defects binding one hole, and double acceptors for defects binding two holes with energies less than the band gap. Defects binding electrons and holes with energies less than the band gap are said to be "amphoteric." Besides real donors, so-called "pseudo-donors" were found exist. They are neutral defects with a loosely bound, hydrogen-like electron which can orbit in the Coulomb field of a tightly bound hole. In general, the energy for ionization increases for the second electron or hole. Systems in which this is not the case or in which the ionization level of the donor state is above that of the acceptor state are said to form an Anderson "negative-U" system [1.11]. In the first case, the single charge state is instable. This means that the capture or release of the first charge carrier defect is, with a high probability, followed by the capture or release of a second charge carrier. In analogy, when the donor and acceptor state of an amphoteric defect form a negative-U system, the neutral charge state is instable.

In some charge states, defects in a highly symmetric configuration may be electronically degenerate. Jahn and Teller [1.12] suggested that such a system distorts to a configuration of lower symmetry in which the degeneracy is absent. An extensive review of such "Jahn-Teller distortions" was given by Sturge [1.13].

1.2.3 Fermi Statistics

In general, the deviations from the perfect valence-bond structure will be small. Therefore, it is convenient to deal only with the net excess electrons over the number needed exactly to fill the valence-bond structure. This net excess concentration constitutes of the electrons in the conduction band, the electrons in states bound to a donor, the holes in the valence-bond band, and the holes in states bound to an acceptor with concentrations n , n_D , p , and p_A , respectively. For the sake of simplicity, only one species of donor and acceptor impurities are considered each in the following. An extension to include multiple donor and acceptor impurities as well as double donors and double acceptors is straightforward, see also Section 2.1. Since the crystal has to be electrically neutral in equilibrium, the net excess number of electrons $n + n_D - p - p_A$ has to be equal to the excess of donors over acceptors $C_D - C_A$. This can be expressed in form of the charge-neutrality condition

$$n + n_D - p - p_A = C_D - C_A. \quad (1.2)$$

As long as the number of acceptors and donors are small, it can be assumed that the respective wave functions do not overlap. Each of the states considered below is assumed to be in contact with a reservoir of electrons with the chemical potential μ_n at temperature T . Donor states with energy E_D can be occupied by an electron with spin $\frac{1}{2}$ or $-\frac{1}{2}$ (the donor is then

electrically neutral), or it can be unoccupied (energy = 0, the donor is then positively charged). The concentration of electrons bound to the C_D donors per unit volume is then given by

$$n_D = \frac{C_D}{1 + \frac{1}{2} \cdot \exp\left(\frac{\mu_n - E_D}{k \cdot T}\right)}. \quad (1.3)$$

Each acceptor can accept one electron (energy = E_A) to complete the valence-bond structure (the acceptor is then negatively charged). When the electron is not in the state bound to the acceptor (energy = 0, the acceptor is then electrically neutral), the state is quadruply degenerate due to the doubly degenerate energy level, each of which can accept holes with spin $\frac{1}{2}$ or $-\frac{1}{2}$. Hence, the concentration of holes bound to the C_A acceptors per unit volume can be written as

$$p_A = \frac{C_A}{1 + \frac{1}{4} \cdot \exp\left(\frac{\mu_n - E_A}{k \cdot T}\right)}. \quad (1.4)$$

Similarly, the number of electrons in the conduction band can be obtained by adding the electrons in the respective quantum states. The density of quantum states $\rho_c(E)$ per unit volume in the energy interval E and $E + dE$ in the conduction band near the lowest energy level E_c can be approximated by

$$\rho_c(E) = \frac{4 \cdot \pi \cdot (2 \cdot m_n^*)^{3/2}}{h^3} \cdot \sqrt{E - E_c} \quad (1.5)$$

with m_n^* standing for the effective mass of the electron. In the formulation above, m_n^* already accounts for the spin degeneracies and the six equivalent minima in the conduction band. It has to be remarked, though, that the one-band approximation is valid only for energies E below $E_c + 0.13$ eV. For larger values, as discussed in Appendix 3 of the review of Hu [1.14], other bands begin to contribute considerably to the total density of states. Each of the states can be either occupied (energy = E) or unoccupied (energy = 0). The probability $f_n(E)$ that the state is occupied by an electron, is then given by

$$f_n(E) = \frac{1}{1 + \exp\left(\frac{E - \mu_n}{k \cdot T}\right)}. \quad (1.6)$$

This distribution is usually called “Fermi-distribution.” The energy for which $f_n = \frac{1}{2}$ is called “Fermi level” E_F . From (1.6) follows that the Fermi level corresponds to the chemical potential of the electrons ($E_F = \mu_n$). With (1.5) and (1.6), the concentration of electrons in the conduction band follows as

$$n = \int_{E_c}^{\infty} \rho_c(E) \cdot f_n(E) \cdot dE = N_c \cdot F_{1/2}\left(\frac{E_F - E_c}{k \cdot T}\right). \quad (1.7)$$

The upper boundary of the integration is the highest energy possible in the system. However, since the integrand rapidly converges to zero, the integration can be extended to ∞ with negligible error. N_c denotes the effective density of states in the conduction band

$$N_c = 2 \cdot \left(\frac{2 \cdot \pi \cdot m_n^* \cdot k \cdot T}{h^2} \right)^{3/2}. \quad (1.8)$$

The symbol $F_{1/2}(x)$ denotes the Fermi integral

$$F_n(x) = \frac{1}{\Gamma(n+1)} \cdot \int_0^{\infty} \frac{y^n}{1 + e^{y-x}} \cdot dy \quad (1.9)$$

of order $n = 1/2$. For the important cases $n = -1/2$ and $n = 1/2$, $\Gamma(n+1)$ assumes the values $\sqrt{\pi}$ and $\sqrt{\pi}/2$, respectively.

In analogy to the computation of the number of electrons in the conduction band, the number of holes in the valence-bond band can be calculated by adding the holes in the respective states. The density of quantum states $\rho_v(E)$ per unit volume in the energy interval E and $E + dE$ in the valence-bond band near the highest energy level E_v can be approximated by

$$\rho_v(E) = \frac{4 \cdot \pi \cdot (2 \cdot m_p^*)^{3/2}}{h^3} \cdot \sqrt{E_v - E} \quad (1.10)$$

with m_p^* standing for the effective mass of the hole. Each of the states can either be occupied (energy = E) or unoccupied (energy = 0) by an electron. The probability $f_p(E)$ that the state is occupied by a hole, i. e. not occupied by an electron becomes

$$f_p(E) = \frac{1}{1 + \exp\left(\frac{\mu_n - E}{k \cdot T}\right)} = 1 - f_n(E). \quad (1.11)$$

With (1.10) and (1.11), the concentration of holes in the valence-bond band follows as

$$p = \int_{-\infty}^{E_v} \rho_v(E) \cdot f_p(E) \cdot dE = N_v \cdot F_{1/2}\left(\frac{E_v - E_F}{k \cdot T}\right). \quad (1.12)$$

The lower boundary of the integration can be extended to $-\infty$ since the integrand rapidly converges to zero and the resulting error is negligible. N_v denotes the effective density of states in the valence-bond band

$$N_v = 2 \cdot \left(\frac{2 \cdot \pi \cdot m_p^* \cdot k \cdot T}{h^2} \right)^{3/2} \quad (1.13)$$

The concentrations of the net excess charge carriers are given by (1.3), (1.4), (1.7), and (1.12). All these concentrations depend for given donor and acceptor concentrations only on the Fermi level. Combined by the charge-neutrality equation (1.2), they form a non-linear equation for the Fermi level for which no analytic expression exists.

1.2.4 Boltzmann Statistics

Because of the high computational efforts, only very few reports on process modeling (e. g. [1.15–1.20]) mentioned the application of Fermi statistics. However, it was assumed already above that the concentrations of the impurity atoms are small so that the wave functions of the electrons and holes bound to them do not overlap. In this case, the Fermi level is sufficiently far below the conduction band as well as above the valence-bond band. The shallow donors and acceptors will then be completely ionized, i. e. the concentrations of the electrons bound to the donors (1.3) and of the holes bound to the acceptors (1.4) are negligible compared to the respective concentrations of donors and acceptors. In addition, Boltzmann statistics are a good approximation for Fermi statistics and the probabilities that a state in the conduction band or the valence-bond band is occupied by respectively an electron or a hole can be written as

$$f_n(E) \approx \exp\left(-\frac{E - E_F}{k \cdot T}\right), \quad f_p(E) \approx \exp\left(-\frac{E_F - E}{k \cdot T}\right). \quad (1.14)$$

With these distribution functions, the integrals for the electron (1.7) and hole concentrations (1.12) simplify to

$$n = N_c \cdot \exp\left(\frac{E_F - E_c}{k \cdot T}\right) \quad p = N_v \cdot \exp\left(\frac{E_v - E_F}{k \cdot T}\right). \quad (1.15)$$

The dependence of the electron and hole concentrations (1.15) on the Fermi level is a result of the assumptions made in their derivation. The first assumption was that the form of the conduction band and the valence-band band is parabolic. The second assumption was that Boltzmann statistics can be used instead of Fermi statistics. The product of both charge-carrier concentrations is then independent of the Fermi level and given by

$$n \cdot p = n_i^2 = N_c \cdot N_v \cdot \exp\left(-\frac{E_c - E_v}{k \cdot T}\right). \quad (1.16)$$

The difference $E_c - E_v$ in the exponent is the width of the band gap E_g . In the intrinsic state, when no donors or acceptors are present, the concentrations of holes and electrons are equal and denoted by n_i , the so-called “intrinsic concentration.” The Fermi level has then a value of E_i which is given by

$$E_i = \frac{E_v + E_c}{2} + \frac{k \cdot T}{2} \cdot \ln \frac{N_v}{N_c} \approx \frac{E_v + E_c}{2}. \quad (1.17)$$

The second term at the right-hand side can be estimated as ~ 0.03 eV at 1000°C which is about 4% of the width of the energy gap. Thus, the Fermi energy E_i of an intrinsic semiconductor generally lies very close to the middle of the band gap. Equation (1.17) allows us to rewrite the equations (1.15) in the form

$$n = n_i \cdot \exp\left(\frac{E_F - E_i}{k \cdot T}\right), \quad p = n_i \cdot \exp\left(\frac{E_i - E_F}{k \cdot T}\right). \quad (1.18)$$

One has to consider that E_i as well as E_c and E_v include the energy of the electrons and, therefore, vary with $-q \cdot \psi$ where ψ denotes the electrostatic potential. The origin of the energy scale can be selected so that a value of $\psi = 0$ V represents the intrinsic state. It is then possible to rewrite the equations above into the form commonly used in process simulation

$$\begin{aligned} n &= n_i \cdot \exp\left(\frac{\psi \cdot q}{k \cdot T}\right) = n_i \cdot \exp\left(\frac{\psi}{U_T}\right), \\ p &= n_i \cdot \exp\left(-\frac{\psi \cdot q}{k \cdot T}\right) = n_i \cdot \exp\left(-\frac{\psi}{U_T}\right) \end{aligned} \quad (1.19)$$

with the abbreviation $U_T = k \cdot T / q$. In the following chapters, the gradients of the charge-carrier concentrations will be needed. As long as Boltzmann statistics are valid, they can simply be written as

$$\begin{aligned} \text{grad} \left(\frac{n}{n_i} \right) &= \frac{n}{n_i} \cdot \text{grad} \left(\frac{\psi}{U_T} \right), \\ \text{grad} \left(\frac{p}{n_i} \right) &= -\frac{p}{n_i} \cdot \text{grad} \left(\frac{\psi}{U_T} \right) \end{aligned} \quad (1.20)$$

1.2.5 High-Concentration Effects

The situation becomes more complicated when the concentration of impurities increases above a level of about 10^{18} cm^{-3} . Then, the band structure will be influenced by various effects. In the following, the effects will be quoted only briefly. For a detailed discussion, the reader is referred to the original literature and the references therein as well as to the reviews of Abram et al. [1.21], Lee and Fossum [1.22], and Section 2.4 in the monograph of Selberherr [1.10].

A first class of effects results from many-body effects, i. e. interaction between charge carriers and dopants, and between charge carriers. When the concentration of dopants is sufficiently high, the majority charge carriers will be attracted and will screen the respective dopants. This leads to a reduction of the ionization energy of the dopants [1.22–1.24]. At impurity concentrations of about $3 \cdot 10^{18} \text{ cm}^{-3}$, the ionization energy of shallow impurities becomes zero. Then, the impurity level merges with the respective energy band and the impurities become completely ionized. In fact, it was shown that shallow impurities are basically always ionized, especially at elevated temperatures [1.25]. Interactions between majority charge carriers as well as between majority and minority carriers lead to a reduction of the band gap. The first cause the majority-carrier band to rigidly shift towards the minority-carrier band while the latter induce shifts of the minority-carrier bands towards the majority-carrier band [1.22, 1.24, 1.26].

An important influence on the shape of the band edges results from the inhomogeneous distribution of dopants. The resulting random spatial variation of the electrostatic potential causes a spatial dependence of the local density of states in the bands. The shape of the macroscopic density of states function, which is the average of the local density of states function, will deviate from the parabolic relations (1.5) and (1.10), and band tails will form [1.22, 1.27–1.29].

A further effect of the spatial variation of the electrostatic potential is a statistically averaged variation of the impurity energy level. In addition, the wave functions of the electrons bound to acceptors or donors will overlap. Both effects will lead to the formation of an impurity band [1.22, 1.28, 1.30]. As a consequence, the charge carriers bound to the dopants will find allowed levels to move to in an electric field and may contribute to conduction.

It is evident that a self-consistent solution for the Fermi level taking into account all these effects is very time-consuming and cumbersome to implement. In addition, it is unclear how the concepts developed transform to elevated temperatures around 1000°C . Therefore, in all known commercial programs, Boltzmann statistics are used in spite of the unpredictable errors arising. In retrospect, from a pragmatic point of view, Boltzmann statistics seem to be sufficient to reproduce diffusion phenomena at extrinsic concentrations. Of course, this does not demonstrate the validity of the approach and it can be speculated that its insufficiencies are covered by other phenomena associated with dopant concentrations being present in high concentrations. Moreover, since Boltzmann statistics were used for the parameterization of diffusion effects at extrinsic concentrations, all these experiments would have to be reinterpreted when going to Fermi statistics.

An alternative, pragmatic approach frequently met in bipolar device simulation which accounts qualitatively for most of the effects discussed above is to introduce the so-called effective intrinsic concentration n_{ie} [1.31, 1.32]. It allows to approximate the electron and hole concentrations in analogy to (1.19) by

$$\begin{aligned} n &= n_{ie} \cdot \exp\left(\frac{E_F - E_i}{k \cdot T}\right) = n_{ie} \cdot \exp\left(\frac{\Psi}{U_T}\right), \\ p &= n_{ie} \cdot \exp\left(\frac{E_i - E_F}{k \cdot T}\right) = n_{ie} \cdot \exp\left(-\frac{\Psi}{U_T}\right) \end{aligned} \quad (1.21)$$

with n_{ie} depending on the dopant concentrations. Introducing the effective band-gap narrowing δE , n_{ie} can be written in the form

$$n_{ie} = n_i \cdot \exp\left(\frac{-\delta E_g}{2 \cdot k \cdot T}\right). \quad (1.22)$$

For a recent review of band-gap narrowing, see, e. g. the publication of Van Vliet [1.33]. The inherent problems with the application of an effective band gap narrowing will be addressed in Section 2.1. However, it has to be noted already here that the effective intrinsic concentration of charge carriers determines predominantly the minority-carrier concentration. The concentration of the majority carriers is determined by the charge-neutrality condition in homogeneously doped materials or, as outlined in the next section, by the Poisson equation otherwise.

1.2.6 Electric Fields and the Electrostatic Potential

Electric fields arise from the large differences in diffusion constants of the ionized impurities and the charge carriers associated with them. The charge carriers would ordinarily tend to diffuse away faster than the ions, thus creating a space charge. The electric field originating from this space charge acts on the ions and charge carriers to counteract the separation. When the concentrations of the dopants are not uniform, the charge-neutrality condition (1.2) has to be replaced by the third Maxwell equation

$$\operatorname{div} \vec{D} = \rho. \quad (1.23)$$

The electric displacement vector \vec{D} is related to the electric field vector \vec{E} , and thus the electrostatic potential by

$$\vec{D} = \epsilon_{Si} \cdot \vec{E} = -\epsilon_{Si} \cdot \operatorname{grad} \psi \quad (1.24)$$

with ϵ_{Si} being the permittivity of silicon. The space-charge density ρ at the right-hand side of equation (1.23) can be split into the contributions of the positively charged holes, of the negatively charged electrons, and of all other charged defects. Finally, under the assumption of complete ionization, the Poisson equation takes the form

$$\begin{aligned} \operatorname{div}(\epsilon_{Si} \cdot \operatorname{grad} \psi) &= q \cdot \left(n - p + \sum_i z_i \cdot C_i \right) \\ &= q \cdot \left(2 \cdot n_i \cdot \sinh \frac{\Psi}{U_T} + \sum_i z_i \cdot C_i \right) \end{aligned} \quad (1.25)$$

The symbol z_i denotes the electron charge associated with the defects (+1 for singly ionized acceptors and -1 for singly ionized donors, etc.), C_i their concentration. In the absence of external fields at interfaces to adjacent materials, an appropriate boundary condition would be

$$\epsilon_{Si} \cdot \frac{\partial \psi}{\partial \vec{n}} = Q_{int} \quad (1.26)$$

where Q_{int} represents the charges at the boundary and \vec{n} the direction perpendicular to the interface. The charges at the boundary ($Q_{int} = 0$) are usually neglected so that (1.26) reduces to a Neumann boundary condition for the electrostatic potential. Pinning of the Fermi level by dangling bonds, on the other hand, was suggested by Jung et al. [1.34] to play an important role for post-implantation annealing processes.

It has been shown in various publications (e. g. [1.35–1.38]) that the second derivative of the electrostatic potential with respect to space can be neglected for most applications. Then, one obtains the charge-neutrality condition (1.2) in the form

$$n - p = 2 \cdot n_i \cdot \sinh \frac{\Psi}{U_T} = - \sum_i z_i \cdot C_i. \quad (1.27)$$

This allows to express the electron and hole concentrations explicitly as

$$n, p = \mp \frac{1}{2} \cdot \sum_i z_i \cdot C_i + \sqrt{\left(\frac{1}{2} \cdot \sum_j z_j \cdot C_j \right)^2 + n_i^2} \quad (1.28)$$

with only small errors, provided that changes in the concentrations of the impurity within the Debye length

$$L_D = \sqrt{\frac{\epsilon_{Si}}{q \cdot (n + p)} \cdot \frac{k \cdot T}{q}} \quad (1.29)$$

are sufficiently small. In any case, the charge-neutrality equation (1.27) is a very good initial guess for an iterative solution of the Poisson equation (1.25).

Figure 1.18 shows the electron and hole concentrations as a function of the dopant net concentration and temperature. For net concentrations significantly below the intrinsic concentration, n and p are equal to n_i and one speaks of “intrinsic conditions.” A significant influence of ions on impurity diffusion via the electric field can be expected only when their concentration exceeds the intrinsic concentration of charge carriers. Such conditions are then called “extrinsic.”

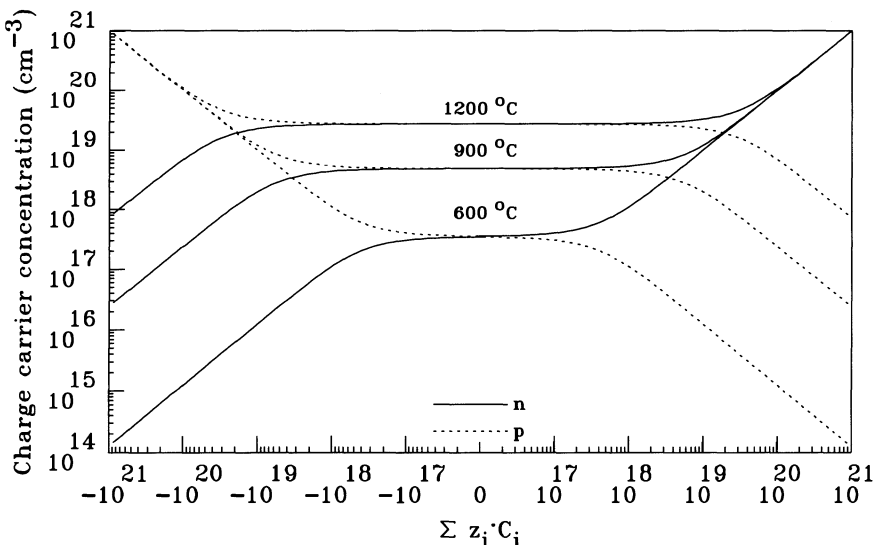


Figure 1.18: Electron and hole concentration as a function of net doping and temperature.

1.2.7 Physical Parameters

A common problem in assigning values to the physical parameters is that reliable measurements exist only up to about 200 °C [1.39]. In lack of any measurements for the temperature range of diffusion processes, values measured below 200 °C are usually extrapolated on the basis of physical models. In such a way, Jain and Van Overstraeten modeled the effective masses of electrons and holes as a function of the width of the indirect band gap E_g [1.17]

$$\begin{aligned} m_n^*(T) &= m_0 \cdot \left(1.1925 \cdot \frac{E_G(300\text{K})}{E_G(T)} \right)^{2/3} \\ m_p^*(T) &= m_0 \cdot \left(0.67818 \cdot \frac{E_G(300\text{K})}{E_G(T)} \right)^{2/3} \end{aligned} \quad (1.30)$$

with $m_0 = 9.1093897(54) \cdot 10^{-31}$ kg standing for the electron mass.

Up to now, the intrinsic carrier concentration n_i has been determined experimentally for elevated temperatures only by Morin and Maita [1.40]. In their experiments, they measured the resistivity of silicon at temperatures up to 837 °C. Together with values for the electron and hole mobility extrapolated from values measured below 130 °C, they obtained the expression

$$n_i^2 = n \cdot p = 1.5 \cdot 10^{33} \cdot T^3 \cdot \exp\left(-\frac{1.21\text{eV}}{k \cdot T}\right) \text{ cm}^{-6} \quad (1.31)$$

for the temperature range up to 430 °C. Above 430 °C, Morin and Maita assumed that the width of the indirect energy gap (the 1.21 eV in (1.31)) depends considerably upon the electrostatic interaction of the charge carriers. They proposed the implicit formulation

$$\begin{aligned} n_i^2 = n \cdot p &= 1.5 \cdot 10^{33} \cdot \left(\frac{T}{K}\right)^3 \cdot \exp\left(-\frac{1.21\text{eV} + \Delta E_g}{k \cdot T}\right) \text{ cm}^{-6} \\ \Delta E_g &= -7.1 \cdot 10^{-10} \cdot \sqrt{\frac{n_i/\text{cm}^{-3}}{T/K}} \text{ eV} \end{aligned} \quad (1.32)$$

The intrinsic carrier concentration so obtained is shown in Figure 1.19. To avoid the implicit definition of (1.32),

$$n_i = 2.16 \cdot 10^{16} \cdot \left(\frac{T}{K}\right)^{3/2} \cdot \exp\left(-\frac{0.592\text{eV} - 5.12 \cdot 10^{-8}\text{eV}/\text{K}^2 \cdot T^2}{k \cdot T}\right) \text{ cm}^{-3} \quad (1.33)$$

can be used with a maximum error of 2% between 500 °C and the melting temperature. From the onset-concentration of the Fermi-level-dependent diffusion of dopants, Barbuscia et al. [1.41] obtained estimates for n_i which were reported to agree well with the model of Morin and Maita. However, it is felt that such experiments are rather ambiguous. Moreover, it has to be accepted that the intrinsic carrier concentration is a non-fundamental parameter which influenced in the form given by Morin and Maita basically all investigations of impurity diffusion at extrinsic concentrations. Even if more precise measurements of the intrinsic carrier concentrations were available for elevated temperatures, this would just mean that all parameters extracted on the basis of Morin and Maita's values would have to be reevaluated.

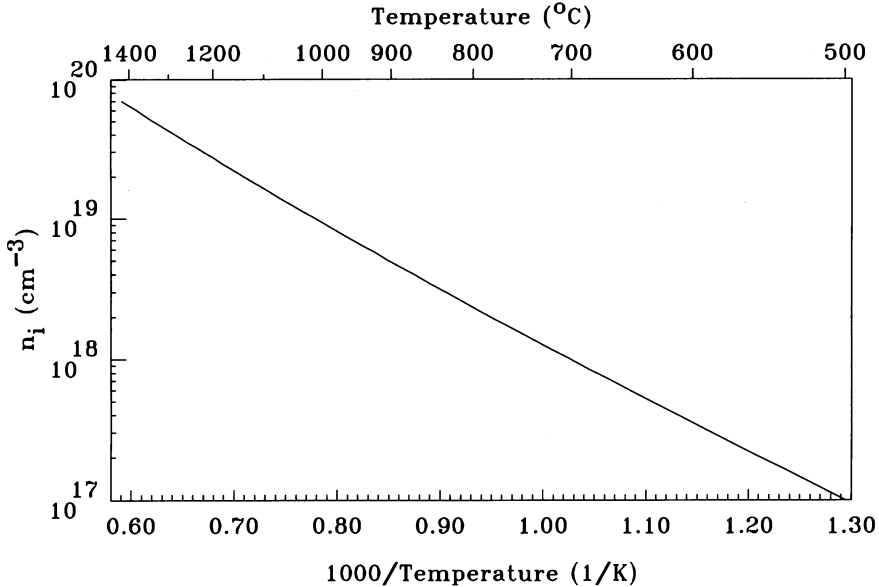


Figure 1.19: Intrinsic carrier concentration after Morin and Maita.

Another important parameter is the width of the band gap $E_g = E_c - E_v$ between conduction band and valence-band band. For undoped crystals, it is a function of temperature and pressure. The temperature dependence of the width of the band gap for intrinsic doping conditions has been determined from optical absorption measurements by Macfarlane et al. [1.42], but only up to about 240 °C. For the temperature range above, no reliable data exist. Therefore, formulas valid for low temperatures were extended to the high-temperature regime. Based on the measurements of Macfarlane et al., the temperature dependence of the width of the band gap has been expressed frequently in the form of a linear relationship

$$E_g(T) = 1.205 \text{ eV} - 2.8 \cdot 10^{-4} \frac{\text{eV}}{\text{K}} \cdot T \quad (1.34)$$

[1.17]. A semi-empirical formula proposed by Varshni [1.43] is based on the assumptions that the energy gap is reduced proportional to T at high temperatures, proportional to T^2 at low temperatures, and that the crossover temperature between the two regimes is at or near to the Debye temperature. It is commonly written in the form below and used with parameters proposed by Thurmond [1.44]

$$E_g = 1.17 \text{ eV} - \frac{4.73 \cdot 10^{-4} \text{ eV} \cdot (T/\text{K})^2}{636 + T/\text{K}}. \quad (1.35)$$

For temperatures around 1000 °C, (1.35) can be approximated by

$$E_g(T) = 1.3 \text{ eV} - 4.21 \cdot 10^{-4} \frac{\text{eV}}{\text{K}} \cdot T. \quad (1.36)$$

As already mentioned above, interactions between charge carriers, which are present in sufficient concentrations at high temperatures, lead to an additional decrease in the width of the energy gap. From their determination of the intrinsic concentration, Morin and Maita [1.40] suggested the relation

$$E_g = 1.21 \text{ eV} - 3.6 \cdot 10^{-4} \frac{\text{eV}}{\text{K}} \cdot T - 7.1 \cdot 10^{-10} \text{ eV} \cdot \sqrt{\frac{n_i/\text{cm}^{-3}}{T/\text{K}}} \quad (1.37)$$

For a graphical representation of the variation of the energy gap with temperature see Figure 1.20. For doped crystals, as discussed in Section 1.2.5, E_g will be reduced further by interactions between the charge carriers. In addition, due to band tailing, the simple definition as distance in energy between the conduction band and the valence-bond band becomes problematic since the band edges are no longer rigid. In device simulation, E_g is frequently used as a mere fitting factor in (1.16) to adjust the value of n_i to the desired value of n_{ie} in (1.21). The resulting value of E_g is then often called “width of the electrical band gap.”

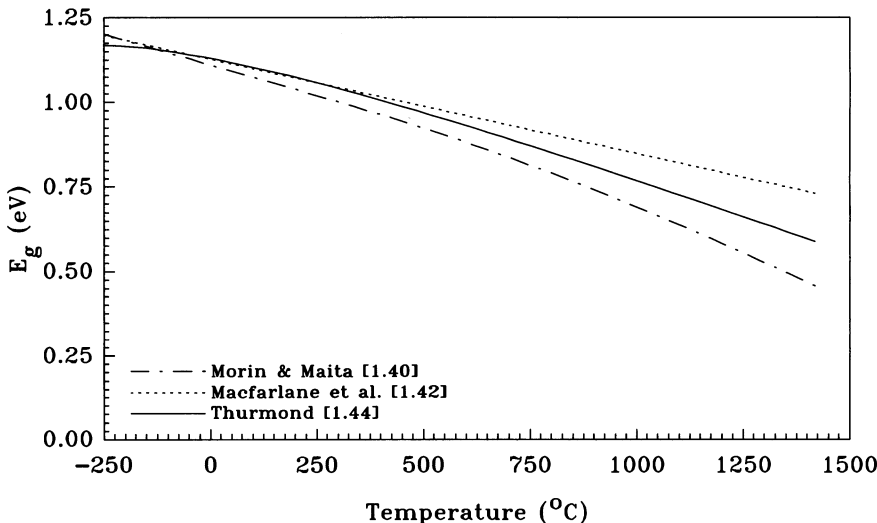


Figure 1.20: Width of the forbidden band gap.

For all materials used for device fabrication, the permittivity ϵ can be treated as a scalar quantity which depends only on the material. Values of the dimension-less relative permittivity constant $\epsilon_r = \epsilon/\epsilon_0$ for important materials are listed in Table 1.5. The symbol ϵ_0 denotes the permittivity constant in vacuum and takes the value $\epsilon_0 \approx 8.8542 \cdot 10^{-12} \frac{\text{A}\cdot\text{s}}{\text{V}\cdot\text{m}}$.

Table 1.5: Relative permittivity constants.

Material	ϵ_r
Si	11.7
SiO ₂	3.9
Si ₃ N ₄	4.2 - 12.7, depending on the deposition method [1.45] 7.0 typically

1.3 Phenomenological and Atomistic Approaches to Diffusion

Atoms in solids occupy well-defined, energetically favorable sites. Above the absolute zero of temperature, thermal agitation will cause them to vibrate around their lattice sites. Eventually, some of them will gain sufficient energy to make a jump to an other energetically favored site.

In equilibrium, in the absence of external forces, all species of atoms are distributed homogeneously within one continuous phase. Fluctuations of atoms caused by their constant thermal motion cancel out on the average. In case of an inhomogeneous distribution, atomic movement will lead to a redistribution of the respective species towards equilibrium conditions. This process is called diffusion.

Historically, the first approaches to deal with such a redistribution of atoms ignored the atomistic nature of solids. Phenomenological equations were used to relate fluxes of atoms to the gradients of their concentrations. They became widely known as Fick's laws and will be discussed in Section 1.3.1. Physically motivated, they are still the basis of the majority of the simulation programs used.

The alternative to continuum approaches are atomistic descriptions of the system considered. In molecular dynamics simulations, the equations of motion are solved iteratively for all atoms in the system. Using *ab-initio* methods to compute the interatomic forces restricts the application to basic defect interactions. Following the work of Car and Parinello [1.46], such approaches are usually referred to as Car-Parinello method. To increase the problem size and the process time which can be simulated, resource-demanding *ab-initio* methods are often replaced by less rigorous methods like tight-binding approaches. Unfortunately, even using empirical potentials for the interatomic forces, molecular dynamics programs are limited to some 10^6 atoms and time scales on the order of nanoseconds. Therefore, such approaches are ideally suited for the simulation of ion-solid interactions and defect reactions [1.47, 1.48] while the simulation of technologically relevant diffusion processes is beyond their scope.

Since most thermal vibrations do not lead to a net movement of atoms, Monte-Carlo approaches came into use for the study of diffusion processes. Kinetic Lattice Monte-Carlo programs¹ consider only processes which actually lead to atomic jumps. Of these, each time, one is select randomly in a manner which reflects the different transition probabilities between possible states. In a further abstraction, the Kinetic Monte-Carlo approach, host atoms are ignored also and only defects, i. e. intrinsic and extrinsic point defects and their agglomerates, are taken into considerations. This allows then to actually simulate technologically relevant processes [1.49–1.51].

Already much earlier, atomistic processes were considered within the framework of the random-walk theories discussed in Section 1.3.2. They result in probabilities for certain atomistic configurations and it will be shown that they are compatible with continuum approaches when the number of jumps is sufficiently high. While the processes addressed up to now consider only the redistribution of atoms in response to spatial inhomogeneities, jumps of atoms can also be induced by forces acting on them. Such effects will be discussed in Section 1.3.3.

Besides surmounting energy barriers between energetically favorable sites by appropriate thermal vibrations, some point defects in silicon were found to be able to use parallel paths and to diffuse much faster by an interaction with charge carriers. Such processes, summarized under the generic term "athermal diffusion," will be discussed in Section 1.3.4.

It should be noted that a conceptually different approach to diffusion processes is based on the thermodynamics of irreversible processes. It will be discussed later in Section 1.4.

¹There is no generally agreed terminology for the variants of diffusion Monte-Carlo approaches in the literature. Lattice Monte-Carlo, as an example, is also used to refer to methods in which lattice atoms are actually not considered explicitly.

1.3.1 Fick's Laws

One of the main approaches to diffusion is to treat diffusing substances as continuous media and to ignore the atomistic nature of the diffusion process. To quantify the distribution of atoms, the concentration is introduced as the number of atoms per unit volume. Often, in a system consisting of several species, only one of them is taken into consideration. A typical example would be the redistribution of an impurity in silicon where the simultaneous redistribution of silicon atoms is of minor importance. The flux or diffusion current J of the species under consideration is defined as the number of respective atoms passing a unit area within a unit time interval. It can be related in a purely phenomenological way to the gradient of their concentration C by

$$J = -D \cdot \text{grad} C. \quad (1.38)$$

The negative sign indicates that the diffusion occurs in the direction of decreasing concentration. Equation (1.38) is generally referred to as Fick's first law of diffusion [1.52] and represents a macroscopic definition for the diffusion coefficient D . In general, the diffusion coefficient is a tensor of second rank. However, because of the high symmetry of cubic crystals and crystals with diamond structure, it reduces to a single scalar quantity in such crystals. Similarly, a scalar quantity is sufficient to characterize the diffusion coefficient in amorphous materials. The product of concentration and diffusion coefficient is known as transport capacity.

In a system with several species, the flux J_i of species i may, in general, depend also on the gradients of the other species

$$J_i = -D_i \cdot \text{grad} C_i - \sum_{j \neq i} T_{i,j} \cdot \text{grad} C_j. \quad (1.39)$$

The transport coefficients $T_{i,j}$ are defined empirically by the flux of species i caused by a gradient of impurity j when all other impurity coefficients vanish. Formally, the diffusion coefficient D_i corresponds to $T_{i,i}$. While diffusion coefficients are never negative, no such restrictions apply to the other transport coefficients.

To calculate the change in the amount of an arbitrary substance in a given volume V , the fluxes via the volume boundary S as well as generation or loss within the volume have to be taken into consideration. This leads to the general continuity equation

$$\frac{\partial}{\partial t} \int_V C \cdot dV = \int_V (G - R) \cdot dV - \oint_S (J \bullet \vec{n}) \cdot dS. \quad (1.40)$$

The symbols G and R stand for the generation and loss rates (often called generation and recombination terms), and $(J \bullet \vec{n})$ is the flux perpendicular to the surface out of the volume. For infinitesimally small volumes, (1.40) can be expressed in the form

$$\frac{\partial C}{\partial t} = -\text{div} J + G - R \quad (1.41)$$

which reduces in the absence of sinks and sources to

$$\frac{\partial C}{\partial t} = -\text{div} J. \quad (1.42)$$

Combining this equation with (1.38) leads to the so-called Fick's second law of diffusion

$$\frac{\partial C}{\partial t} = \text{div}(D \cdot \text{grad} C). \quad (1.43)$$

This form can be used even for a diffusion coefficient which depends on position, e.g. via the concentration [1.53]. When the diffusion coefficient D is independent of position, equation (1.43) reduces to

$$\frac{\partial C}{\partial t} = D \cdot \operatorname{div} \operatorname{grad} C. \quad (1.44)$$

In case of several species to be taken into considerations, a continuity equation in the form of (1.41) applies to each of them.

The relations (1.38) and (1.39) are purely phenomenological definitions for the diffusion and transport coefficients, and the continuity equation (1.42) is universally valid for vanishing generation and loss. However, in general, diffusion coefficients and transport coefficients will depend on temperature and may depend also on the concentrations of all impurities in the system, on the concentrations of charge carriers, crystal defects, and on pressure. The temperature dependence of diffusion coefficients determined from experiments is usually found to obey an Arrhenius relation [1.54]

$$D = D_0 \cdot \exp\left(-\frac{E_A}{k \cdot T}\right) \quad (1.45)$$

characterized by the prefactor D_0 and the activation energy E_A . Activation energies found from experiments vary usually in the range from 0 to about 5 eV. A summary of diffusion coefficients of impurities in silicon is shown in Figure 1.21. There are various other local and non-local influences on diffusion. Influences of the Fermi level and of the concentrations of vacancies and self-interstitials as discussed in Chapter 3 reflect the particular atomic mechanism of diffusion. Effects of stress and stress gradients will be discussed in Section 1.4.3.

For one diffusing species, the evolution of the concentration with time can be found solving (1.43) or (1.44) with appropriate initial conditions and boundary conditions. Initial conditions describe the distribution of the atoms at the beginning of the diffusion process. Boundary conditions establish relations for the profile shape of the atoms at the surfaces of the crystal. There are three basic types of them. Application of “Dirichlet boundary conditions” means that the concentration at the boundary is fixed to a value which may depend on time and position. Alternatively, “Neumann boundary conditions” refer to a vanishing flux of atoms through the surface. Finally, there are boundary conditions which establish a relation between the concentration at the surface and the gradient of the profile perpendicular to the surface.

Equation (1.44) was the basis of nearly all studies of diffusion in silicon at the beginning of silicon processing. In these studies, experimental conditions were usually assumed to correspond to the two basic set-ups described below for which analytical solutions exist. Although especially the assumption of a constant diffusion coefficient is not justified in many cases of impurity diffusion, the analytical solutions given can be used often for first-order estimations. Various other analytical solutions to (1.44) are known for specific assumptions on the initial conditions and boundary conditions [1.55–1.57]. However, their importance has significantly reduced after computer programs became wide-spread and enabled the numerical solution of the diffusion equations.

In experiments in which impurities are present in the ambient gas, their concentration at the surface of the silicon samples is approximately constant with respect to time. Then, the solution to (1.44) is given by

$$C = C_{x=0} + (C_{t=0, x>0} - C_{x=0}) \cdot \operatorname{erf}\left(\frac{x}{\sqrt{4 \cdot D \cdot t}}\right) \quad (1.46)$$

where $\operatorname{erf}(x)$ stands for the error function

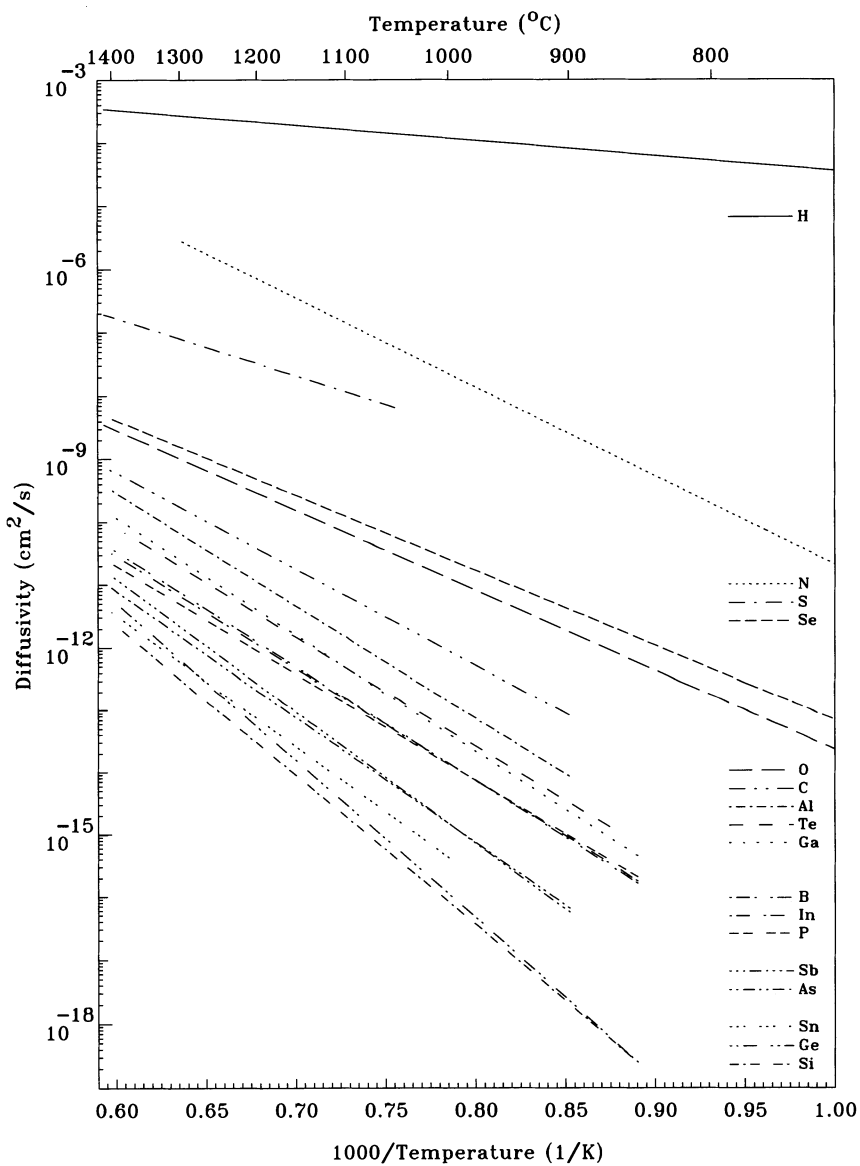


Figure 1.21: Summary of diffusivities in silicon.

$$\operatorname{erf}(x) = \frac{2}{\sqrt{\pi}} \cdot \int_0^x \exp(-\xi^2) \cdot d\xi. \quad (1.47)$$

The case for $C_{x=0} = 0$ and $C_{t=0, x>0} > 0$ corresponds to the out-diffusion of the initial background impurity atoms which are then carried away by the gas flux in the furnace. The technically often more important case of in-diffusion from the ambient gas into a crystal with vanishing initial concentration has the solution

$$C = C_{x=0} \cdot \left(1 - \operatorname{erf} \left(\frac{x}{\sqrt{4 \cdot D \cdot t}} \right) \right) = C_{x=0} \cdot \operatorname{erfc} \left(\frac{x}{\sqrt{4 \cdot D \cdot t}} \right) \quad (1.48)$$

which depends only on the surface concentration and the product of diffusion coefficient and time. The evolution of error-function profiles with time is shown in Figure 1.22. For a given time t , the amount of material N_{\square} having entered the solid is

$$N_{\square} = \int_0^{\infty} C(x, t) \cdot dx = \int_0^t J(\tau) \cdot d\tau = C_{x=0} \cdot \sqrt{\frac{4 \cdot D \cdot t}{\pi}}. \quad (1.49)$$

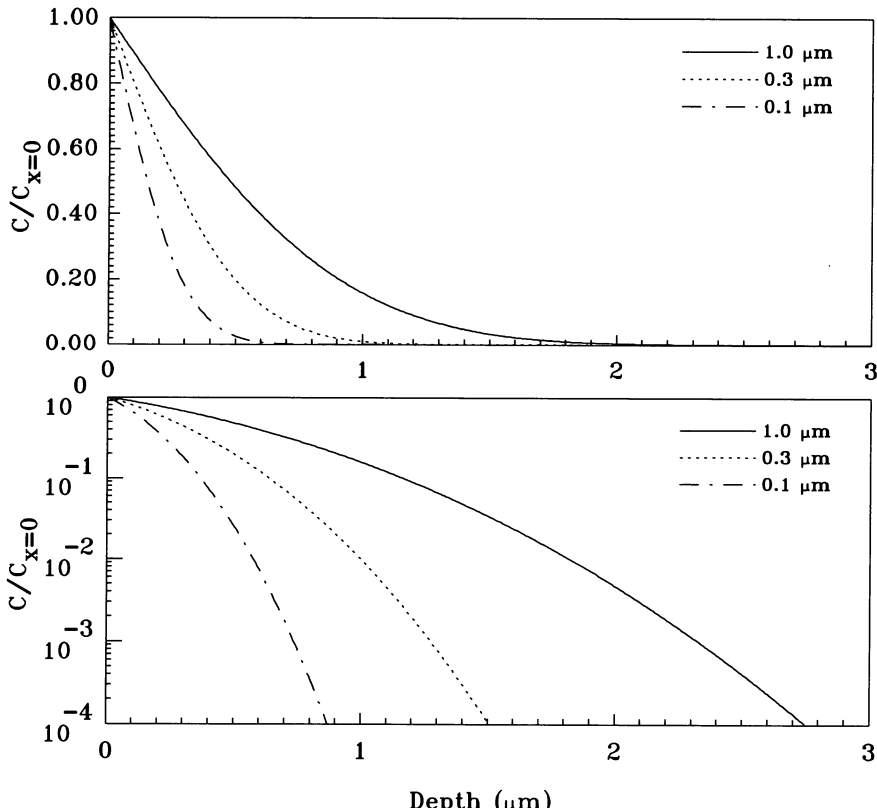


Figure 1.22: Error function profiles for various values of $\sqrt{4 \cdot D \cdot t}$.

The second technically important case is when the initial distribution of atoms at $t=0$ can be represented by a delta function at the surface ($x=0$), and when the flux of atoms through the surface is inhibited. Then, the solution to (1.44),

$$C = \frac{N_{\square}}{\sqrt{\pi \cdot D \cdot t}} \cdot \exp\left(-\frac{x^2}{4 \cdot D \cdot t}\right), \quad (1.50)$$

is a Gaussian distribution which depends on the amount of material N_{\square} in the simulation area and the product of diffusion coefficient and time. The change in the distribution with time is depicted in Figure 1.23. For real applications, it suffices when the standard deviation at the end of the process

$$\sigma(t = t_{end}) = \sqrt{2 \cdot D \cdot t_{end}} \gg \sigma(t = 0) \quad (1.51)$$

is sufficiently larger than that of the initial profile. Since the amount of material does not change with time, the surface concentration in such a system varies with time as

$$C_{x=0} = \frac{N_{\square}}{\sqrt{\pi \cdot D \cdot t}}. \quad (1.52)$$

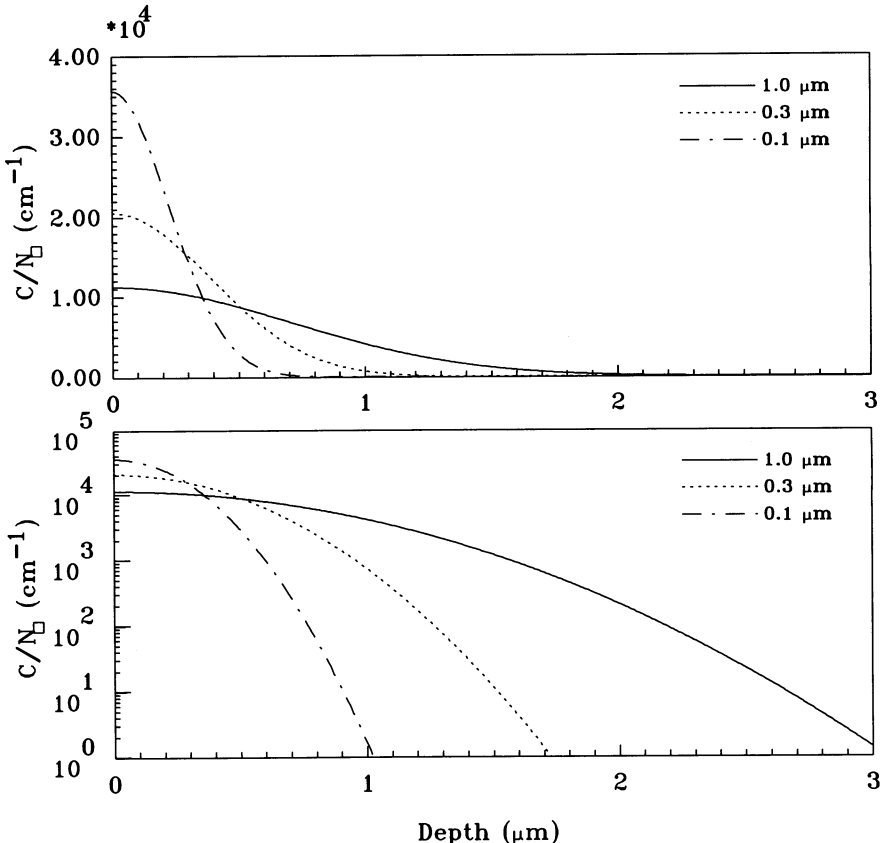


Figure 1.23: Gaussian profiles for various values of $\sqrt{4 \cdot D \cdot t}$.

1.3.2 Random Walk and the Atomistic View of Diffusion

The other central approach to diffusion besides the empirical description discussed above is to consider the detailed kinetics of atomic motion. In solids, above the absolute zero of temperature, the atoms are in constant motion around energetically favored positions. Time-averaged, most of these oscillations do not lead to a net displacement. To arrive at some global conclusions, only such motions are taken into considerations which actually result in jumps of atoms between energetically favorable sites. It has to be noted, though, that they are generally associated with the concerted movement of the neighboring atoms. The direction of each of these jumps is independent of previous jumps so that they perform a so-called “random walk” or “Brownian movement”. For a rigorous analysis as well as for historical remarks on the problem of random flights see the review by Chandrasekhar [1.58]. Although only atoms are mentioned as diffusing particles, the relations derived are valid also for other point defects like vacancies.

When the number of diffusing atoms is large enough, we can assign the mean properties of the atoms to one representative atom. The questions of interest are then what is the most likely distance of the atom from the origin after N jumps and how large is the probability to find it in the interval (x, y, z) and $(x + \delta x, y + \delta y, z + \delta z)$.

For the sake of clarity, we will consider the problem of random walk in a one-dimensional setup with equal step length L . Before the first step, the atom is at the origin. After the first step, the atom is with equal probability at the positions -1 and 1 (see Table (1.6)). The probability to find an atom at the origin is zero since we have assumed that all atoms perform jumps either to the right or to the left. On the same basis, the probability to find the atom after an odd number of jumps N at an even position K from the origin, and *vice versa*, is zero. The non-zero probabilities have a distribution called binomial or Bernoullian, and are given by

$$W(N, K) = \frac{1}{2^N} \cdot \binom{N}{\frac{N+K}{2}} = \frac{N!}{2^N \cdot (\frac{N+K}{2})! \cdot (\frac{N-K}{2})!}. \quad (1.53)$$

The operator ! stands for the factorial function.

Table 1.6: Probability to find an atom after N steps at a position K .

		Distance K from origin in units of the step length								
		-4	-3	-2	-1	0	1	2	3	4
N	0					1				
	1				1/2	0	1/2			
2				1/4	0	2/4	0	1/2		
	3		1/8	0	3/8	0	3/8	0	1/8	
4	1/16	0	4/16	0	6/16	0	4/16	0	1/16	

The most probable position where the atom can be found is near the origin since jumps in the forward and reverse direction cancel out on the average. But this result just shows that the mean distance is inadequate to measure the continuously increasing separation from the origin. A more convenient measure is the square of the distance D since this value is positive for negative as well as for positive displacements. Its mean value $\langle D_N^2 \rangle$ after N steps corresponds to the square of the standard deviation σ of the probability distribution (1.53) and is given by

$$\langle D_N^2 \rangle = \sigma^2 = \sum_{\substack{K=-N \\ \frac{N+K}{2} \in \mathbb{N}}}^N K^2 \cdot L^2 \cdot \frac{1}{2^N} \cdot \binom{N}{\frac{N+K}{2}} = N \cdot L^2. \quad (1.54)$$

This result, that the mean square distance is equal to the product of the number of steps and the square of the step length, is obtained also in two-dimensional and three-dimensional set-ups. The one-dimensional projection of the square distance in such systems is one half and one third of $N \cdot L^2$, respectively.

To demonstrate the significance of this result let us consider atoms which have travelled a mean distance of $\sigma = 100 \text{ nm}$ from the origin with a step length of $L = 2 \text{ \AA}$. To reach this mean distance from the origin, the atoms must have executed $N = (\sigma/L)^2 = 250000$ steps and the total path length of the atoms is $N \cdot L = 50 \mu\text{m}$. This means that, in order to reach a mean distance of 100 nm from the origin, each atom has to travel 50,000 nm. On the other hand, it means also that a lucky atom might have travelled as far as 50 μm . However, the probability for this case is only 10^{-75257} .

For the important case where N , $N+K$ and $N-K$ are large numbers, (1.53) can be simplified using Sterling's formula

$$\ln n! \approx n \cdot (\ln(n) - 1) + \frac{1}{2} \cdot \ln(n) + \frac{1}{2} \cdot \ln(2 \cdot \pi). \quad (1.55)$$

We then receive

$$\ln W(N, K) \approx \frac{1}{2} \cdot \ln \left(\frac{2}{\pi \cdot N} \right) - \frac{N+K+1}{2} \cdot \ln \left(1 + \frac{K}{N} \right) - \frac{N-K+1}{2} \cdot \ln \left(1 - \frac{K}{N} \right). \quad (1.56)$$

For $K \ll N$, the arguments of the logarithms can be evaluated using the Taylor-series expansion

$$\ln(1+x) \approx x - \frac{x^2}{2} \quad (1.57)$$

and we obtain for the probability to find the atom after N steps at the position K

$$W(N, K) \approx \sqrt{\frac{2}{\pi \cdot N}} \cdot \exp \left(-\frac{K^2}{2} \cdot \frac{N-1}{N^2} \right) \approx \sqrt{\frac{2}{\pi \cdot N}} \cdot \exp \left(-\frac{K^2}{2 \cdot N} \right). \quad (1.58)$$

A numerical comparison between the binomial distribution (1.53) and the approximation (1.58) is made in Figure 1.24 for $N = 100$. It can be seen that the accuracy is excellent even for this small number of steps.

Next, we want to return to the question for the probability to find the atom after N steps in the interval $x = K \cdot L$ and $x + \delta x$. When δx is very much larger than the step width L , but small compared to $\sigma \cdot L$, the probability $W(N, K)$ will change only marginally in the interval. Considering that each second probability value is zero (cf. Table (1.6)), $\delta x/2L$ distinct positions exist in the interval δx with non-zero probabilities $W(N, K)$. The total probability $W(N, x, \delta x)$ results then as

$$W(N, x, \delta x) = W \left(N, \frac{x}{L} \right) \cdot \frac{\delta x}{2 \cdot L} = \frac{1}{\sqrt{2 \cdot \pi \cdot N \cdot L^2}} \cdot \exp \left(-\frac{x^2}{2 \cdot N \cdot L^2} \right) \cdot \delta x. \quad (1.59)$$

The scenario which leads to (1.59) is identical to that which resulted in (1.50) in Section 1.3.1: Atoms located initially at the origin spread with time in an infinite or semi-infinite space. A comparison of the standard deviation of both distributions gives an atomistic interpretation of the diffusion coefficient

$$2 \cdot D \cdot t = \sigma^2 = \langle D_N^2 \rangle = N \cdot L^2 \quad (1.60)$$

which goes back to Einstein [1.59]. Assuming that the atom performs Γ jumps per unit time allows to express the diffusion coefficient as

$$D = \frac{N}{t} \cdot \frac{L^2}{2} = \Gamma \cdot \frac{L^2}{2}. \quad (1.61)$$

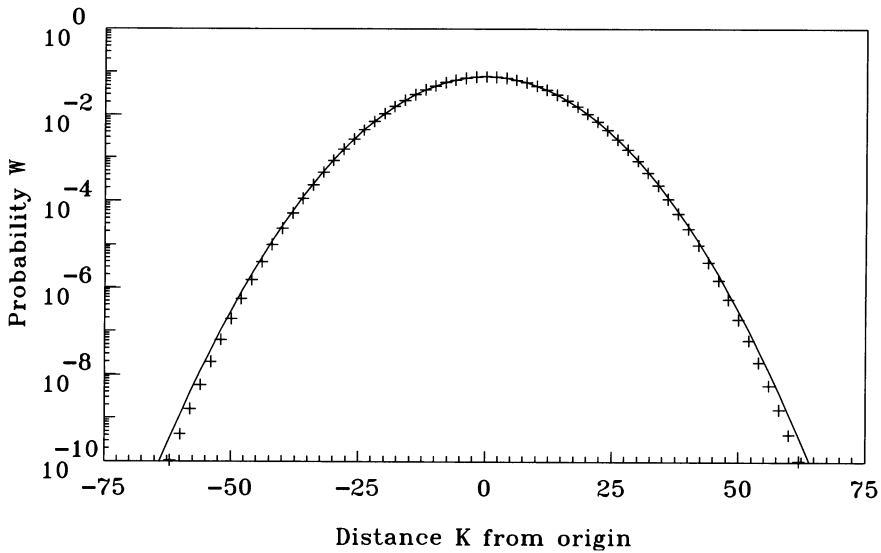


Figure 1.24: Comparison of the binomial distribution and its approximation for $N = 100$ steps.

In a three-dimensional scenario, the mean square distance of a spreading Gaussian function

$$\frac{\int_{-\infty}^{\infty} \int_{-\infty}^{\infty} \int_{-\infty}^{\infty} (x^2 + y^2 + z^2) \cdot \exp\left(-\frac{x^2 + y^2 + z^2}{4 \cdot D \cdot t}\right) \cdot dx \cdot dy \cdot dz}{\int_{-\infty}^{\infty} \int_{-\infty}^{\infty} \int_{-\infty}^{\infty} \exp\left(-\frac{x^2 + y^2 + z^2}{4 \cdot D \cdot t}\right) \cdot dx \cdot dy \cdot dz} = 6 \cdot D \cdot t \quad (1.62)$$

corresponds to $N \cdot L^2$ from which the macroscopic definition

$$D = \frac{N}{t} \cdot \frac{L^2}{6} = \Gamma \cdot \frac{L^2}{6} \quad (1.63)$$

for the diffusion coefficient can be derived. Keeping in mind that $N \cdot L^2$ is the square of the distance a representative atom moves within time t from its original position, (1.63) is used, e. g. in molecular-dynamics simulations to calculate the diffusion coefficient.

An alternative, frequently met approach to derive Fick's laws from random-walk assumptions is to examine the exchange of atoms between adjacent planes of energetically favored sites in the crystal. Following the derivation outlined, e. g. by Manning [1.60], we consider two planes in a one-dimensional set-up as shown in Figure 1.25. At the positions x and $x + \Delta x$, C_x and $C_{x+\Delta x}$ atoms are assumed to be present per unit area, respectively. Some of these atoms will occasionally jump to adjacent planes. The mean jump frequency, i. e. the mean number of jumps per unit time, will be denoted again by Γ . The number of atoms J_x per unit time and area which jump from a site at position x to a site at position $x + \Delta x$ is then given by

$$J_x = \frac{1}{2} \cdot \Gamma \cdot C_x. \quad (1.64)$$

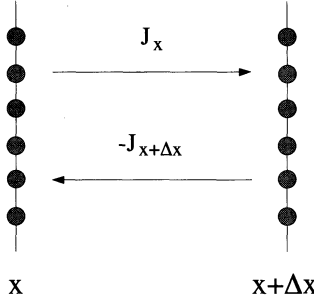


Figure 1.25: Schematic representation of fluxes between adjacent planes.

The factor 1/2 results from the random-walk assumption that jumps occur with equal probability to the sites at positions $x + \Delta x$ and $x - \Delta x$. For the same reason, it would be 1/6 in a three-dimensional analysis. At the same time,

$$-J_{x+\Delta x} = \frac{1}{2} \cdot \Gamma \cdot \underline{C}_{x+\Delta x} \quad (1.65)$$

atoms per unit time and area jump from sites at position $x + \Delta x$ to sites at position x . The net flux $J_x + \Delta x / 2$ results as

$$J_{x+\Delta x/2} = J_x + J_{x+\Delta x} = \frac{1}{2} \cdot \Gamma \cdot (\underline{C}_x - \underline{C}_{x+\Delta x}). \quad (1.66)$$

In the interval $x - \Delta x / 2$ and $x + \Delta x / 2$, the concentration of atoms is defined by $C_x = \underline{C}_x / \Delta x$. This leads to

$$J_{x+\Delta x/2} = -\frac{1}{2} \cdot \Gamma \cdot \Delta x^2 \cdot \frac{\underline{C}_{x+\Delta x} - \underline{C}_x}{\Delta x}. \quad (1.67)$$

Distances between adjacent layers can usually be assumed small against the distances in which the concentration changes considerably. This allows us to replace the differences in (1.67) by the respective derivative and Fick's first law (1.38) is obtained directly with the diffusion coefficient given by (1.61) with $L = \Delta x$. In a three-dimensional set-up where the factor is 1/6 instead of 1/2, the diffusion coefficient is consistently given by (1.63) with $L = \Delta x$.

Due to the fluxes of atoms, their number in the interval $x - \Delta x / 2$ and $x + \Delta x / 2$ changes. Within the time interval Δt ,

$$\Delta \underline{C}_x^- = \Gamma \cdot \underline{C}_x \cdot \Delta t \quad (1.68)$$

atoms per unit area leave the plane at position x and

$$\Delta \underline{C}_x^+ = \frac{1}{2} \cdot \Gamma \cdot (\underline{C}_{x-\Delta x} + \underline{C}_{x+\Delta x}) \cdot \Delta t \quad (1.69)$$

atoms arrive from the adjacent planes. Generation and loss would also have to be taken into consideration, but are ignored here for the sake of simplicity. The total change of atoms is given by the difference between the arriving atoms (1.69) and the leaving atoms (1.68)

$$\begin{aligned} \Delta \underline{C}_x &= \Delta \underline{C}_x^+ - \Delta \underline{C}_x^- = \frac{1}{2} \cdot ((\underline{C}_{x+\Delta x} - \underline{C}_x) + (\underline{C}_{x-\Delta x} - \underline{C}_x)) \cdot \Delta t \\ &= -(J_{x+\Delta x/2} - J_{x-\Delta x/2}) \cdot \Delta t \end{aligned} \quad (1.70)$$

When a large number of jumps occur within the time interval Δt and when the conditions addressed above in the derivation of Fick's first law are met, the differences with respect to time and space can be replaced by the respective derivatives, leading to Fick's second law (1.43).

It remains to discuss the jump frequency Γ . When jumping from one energetically favored site to the other, a moving atom has to overcome an energy barrier as indicated schematically in Figure 1.26. Since such a jump will also involve that other atoms have to move from their equilibrium positions, the barrier will be a Gibbs free energy rather than an enthalpy. In general, only a fraction of the atoms will have the thermal energy to cross the barrier. The most important theories for the jump frequency were presented by Zener [1.61, 1.62], Vineyard [1.63], Rice [1.64], and Flynn [1.65]. Although completely different in the interpretation of the respective parameters, they agree that the jump frequency can be written in the form

$$\Gamma = \Gamma_0 \cdot \exp\left(\frac{S^m}{k}\right) \cdot \exp\left(-\frac{H^m}{k \cdot T}\right) \quad (1.71)$$

for temperatures above the Debye temperature where Γ_0 stands for some weighted mean frequency, often called "attempt frequency," and S^m and H^m are the so-called entropy and enthalpy of migration or entropy and enthalpy of diffusion. At least an order-of-magnitude estimate can be given for Γ_0 for processes involving silicon host atoms by noting that the highest frequency within the Debye model of solids is determined by the Debye temperature. From its value of about 655 K at elevated temperatures [1.66] follows a frequency of $1.36 \cdot 10^{13} \text{ s}^{-1}$. The Gibbs free energy of migration G^m results from $G^m = H^m - T \cdot S^m$.

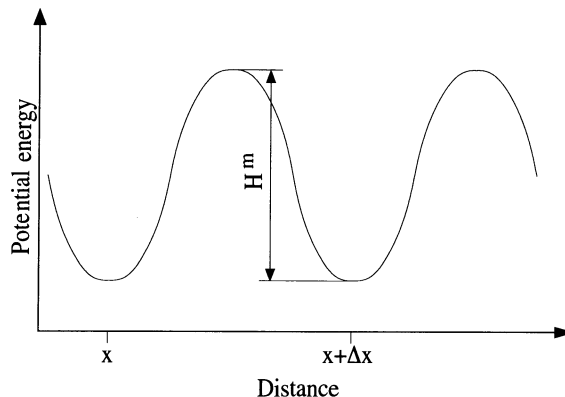


Figure 1.26: Schematic energy-barrier diagram without driving forces.

A comparison of the diffusion coefficient given by (1.61) with the jump frequency (1.71) and the Arrhenius expression (1.45) shows that the migration enthalpy H^m corresponds formally to the activation energy E_a found experimentally, but only when all parameters can be assumed temperature-independent.

A prerequisite of theoretical derivations is usually that the barrier H^m is much larger than $k \cdot T$. This is certainly fulfilled at low temperatures but, e. g. at 1100 °C, $k \cdot T$ is already 0.12 eV and comparable to the migration enthalpy of many point defects. Under such conditions, the probability becomes non-negligible that a defect which has the necessary energy for the first jump may actually perform several consecutive jumps in the same direction. Such processes were actually observed by Car et al. [1.67] in his *ab-initio* molecular-dynamics investigation of the diffusion of vacancies.

The generalization of random walk to include step lengths varying with time was discussed, e. g. in the review of Chandrasekhar [1.58]. For the limiting case of a large number of steps, it was shown that (1.61) and (1.63) remain valid with L^2 replaced by the mean value $\langle L^2 \rangle$ of the square displacement.

1.3.3 Driving Forces for the Redistribution of Atoms

The situation outlined in Section 1.3.2 changes slightly when driving forces act on the point defects. Following the definition of Manning [1.60], a driving force is defined as any influence which makes the jump frequency to depend on the direction of the jump. Typical driving forces are electric fields, gravitational forces, stress gradients, etc.

For a quantitative explanation, one has to examine the influence on the atoms when they pass the energy barriers. The maxima of the energy barriers are, in a first order estimation, in the middle between the planes at $x \pm \Delta x/2$. When moving in the direction of the force, the point defects suffer a loss in potential energy of $\Delta E_p = \Delta x/2 \cdot F$. This loss in potential energy corresponds to a gain in kinetic energy so that the barrier height is effectively reduced by $\Delta H = \Delta x/2 \cdot F$. In the opposite direction, the atoms gain potential energy. This is accompanied by a loss in kinetic energy and, consequently, by an effective increase in the barrier height by ΔH . Figure 1.27 shows a schematic diagram under the assumption that a driving force causes the point defect to jump preferentially to the left.

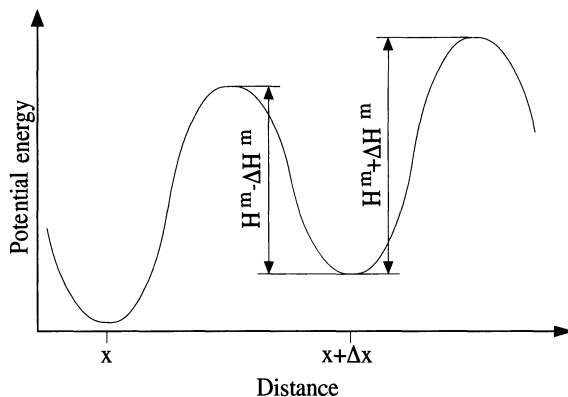


Figure 1.27: Schematic energy-barrier diagram with a driving force.

For a numerical estimation of the order of magnitude of the influence of driving forces on the energy barriers let us assume that the planes of sites are separated by 2 \AA . The gravitational force acting on a point defect is given by the product of its mass m and the gravitational constant g . For a silicon atom, the effective change in barrier height will then be

$$\begin{aligned}\Delta H^m &= m \cdot g \cdot \Delta x/2 = 28.1 \cdot 1.66 \cdot 10^{-27} \text{ kg} \cdot 9.81 \text{ m/s}^2 \cdot 2 \cdot 10^{-10} \text{ m} \cdot 1/2 \\ &= 4.58 \cdot 10^{-35} \text{ kg} \cdot \text{m/s}^2 = 2.86 \cdot 10^{-6} \text{ eV}\end{aligned}$$

The electrostatic force acting on a charged point defect is given by the product of electrostatic field E and its charge. The maximum electrostatic field can be estimated by the breakdown field at room temperature which is $3 \cdot 10^7 \text{ V/m}$. For a singly charged point defect, the charge corresponds to the elementary charge q and the effective change in barrier height will be

$$\Delta H^m = q \cdot E \cdot \Delta x / 2 = 1.6 \cdot 10^{-19} \text{ A} \cdot \text{s} \cdot 3 \cdot 10^7 \text{ V/m} \cdot 2 \cdot 10^{-10} \text{ m} \cdot 1/2 \\ = 4.8 \cdot 10^{-22} \text{ kg} \cdot \text{m/s}^2 = 3 \cdot 10^{-3} \text{ eV}$$

At, e. g. 900 °C, the value of $k \cdot T$ is approximately 0.1 eV. Thus, at least at elevated temperatures, the effective changes in barrier height are much smaller and their effects on the jump frequencies can be estimated by a Taylor-series expansion

$$\Gamma_{\pm} = \Gamma_0 \cdot \exp \left(-\frac{G^m \mp F \cdot \Delta x / 2}{k \cdot T} \right) \approx \Gamma_0 \cdot \exp \left(-\frac{G^m}{k \cdot T} \right) \cdot \left(1 \pm \frac{F \cdot \Delta x}{2 \cdot k \cdot T} \right) \quad (1.72)$$

where Γ_+ and Γ_- denote the jump frequency in the direction and the reverse direction of the driving force F , respectively.

The different jump frequencies for jumps in forward and backward direction lead to a modification of equations (1.64) to (1.66). The number of atoms J_x per unit time and area which jump from sites at position x to sites at position $x + \Delta x$ is now given by

$$J_x = \frac{1}{2} \cdot \Gamma \cdot C_x \cdot \left(1 + \frac{F \cdot \Delta x}{2 \cdot k \cdot T} \right). \quad (1.73)$$

The factor $1/2 \cdot \Gamma$ was kept merely for the sake of consistency with (1.64). It represents here a jump frequency for a specific transition. At the same time,

$$-J_{x+\Delta x} = \frac{1}{2} \cdot \Gamma \cdot C_{x+\Delta x} \cdot \left(1 - \frac{F \cdot \Delta x}{2 \cdot k \cdot T} \right) \quad (1.74)$$

atoms per unit time and area jump from sites at position $x + \Delta x$ to sites at position x . The net flux $J_x + \Delta x / 2$ results as

$$J_{x+\Delta x / 2} = J_x + J_{x+\Delta x} = \frac{1}{2} \cdot \Gamma \cdot (C_x - C_{x+\Delta x}) + \frac{1}{2} \cdot \Gamma \cdot (C_x + C_{x+\Delta x}) \cdot \frac{F \cdot \Delta x}{2 \cdot k \cdot T}. \quad (1.75)$$

Introducing as before the concentration $C_x = C_x / \Delta x$ leads to

$$J_{x+\Delta x / 2} = -\frac{1}{2} \cdot \Gamma \cdot \Delta x^2 \cdot \frac{C_{x+\Delta x} - C_x}{\Delta x} + \frac{1}{2} \cdot \Gamma \cdot \Delta x^2 \cdot \frac{C_x + C_{x+\Delta x}}{2} \cdot \frac{F}{k \cdot T}. \quad (1.76)$$

Distances between planes are usually small compared to the distances in which the concentrations change considerably. The term $(C_x + C_{x+\Delta x})/2$ in (1.76) can then be replaced by the local concentration C , and the difference in concentration can be replaced by the respective derivative. Introducing the diffusion coefficient D from (1.61) with $L = \Delta x$, one obtains a modification of Fick's first law in the form

$$J = -D \cdot \frac{\partial C}{\partial x} + D \cdot C \cdot \frac{F}{k \cdot T}. \quad (1.77)$$

As already mentioned above, the force acting in an electrostatic field E on a charged atom in charge state z (+1 for negatively charged and -1 for positively charged atoms) will be $F = -z \cdot q \cdot E$. This allows to write the flux as

$$J = -D \cdot \frac{\partial C}{\partial x} - z \cdot C \cdot D \cdot \frac{q}{k \cdot T} \cdot E. \quad (1.78)$$

Introducing (1.78) into the continuity equation (1.42) and solving this equation in an infinite space for atoms being initially at the origin takes the form

$$C(x, t) = \frac{N_0}{2 \cdot \sqrt{\pi \cdot D \cdot t}} \cdot \exp \left(-\frac{(x - z \cdot \frac{D \cdot q}{k \cdot T} \cdot E \cdot t)^2}{4 \cdot D \cdot t} \right). \quad (1.79)$$

This solution means that the atoms spread by diffusion as in (1.50) but that their center of mass moves with time. The velocity of this movement is related to the electric field by a macroscopic parameter, the mobility μ . For a singly charged point defect, mobility and diffusion coefficient are related by

$$\mu = \frac{D \cdot q}{k \cdot T}. \quad (1.80)$$

The proportionality of diffusion coefficient and mobility has been shown by Nernst [1.68] and Einstein [1.59] for solutions. Equation (1.80) is, therefore, called Nernst-Einstein relation or Einstein relation. Its general applicability for solids has been shown by Wagner [1.69]. It has to be noted, however, that its applicability is limited to non-degenerate cases. For the degenerate cases, the Nernst-Einstein relation is given by

$$\mu = \frac{D \cdot q}{k \cdot T} \cdot \frac{F_{-1/2} \left(\frac{E_F - E_c}{k \cdot T} \right)}{F_{1/2} \left(\frac{E_F - E_c}{k \cdot T} \right)} \quad (1.81)$$

as a function of the Fermi level E_F [1.19, 1.70, 1.71]. $F_{-1/2}$ and $F_{1/2}$ are the Fermi integrals (1.9) of order -1/2 and 1/2, respectively. For the range of applicability of Boltzmann statistics, the quotient of the Fermi integrals approaches unity and (1.81) reduces to (1.80).

1.3.4 Athermal Diffusion

The standard approach to diffusion is based on the concept that energy barriers between atomic configurations of minimum energy are overcome by defects when the energy associated with their thermally stimulated vibrations exceeds a certain migration barrier. But various investigations indicated that the mobility of the same defects may increase significantly under certain conditions like electron injection or stimulation with light. There were several mechanisms discussed in the literature to explain such phenomena [1.72–1.78]. For a comprehensive discussion, the interested reader is referred to the review article of Bourgoin and Corbett [1.79].

A relatively simple mechanism, suggested first by Watkins for the vacancy [1.80], can be effective when an other charge state of the defect exists and has a lower migration barrier than the dominant charge state. Then, by capturing one of the charge carrier generated, the defect can simply change its charge state and become more mobile.

Probably the most prominent mechanism for athermal diffusion was suggested by Bourgoin and Corbett [1.74, 1.81]. It requires that a point defect can exist in two charge states with the stable atomic configuration A in one charge state corresponding to the saddle point configuration B for migration in the other charge state and *vice versa*. An example would be an interstitial atom assuming predominantly a tetrahedral lattice site in the one charge state and a hexagonal lattice site in the other. Then, by capturing a charge carrier in the stable configuration, say A, the other configuration B becomes energetically. Assuming it means that the point defect moves to the saddle-point for jumps between two A positions. After release of the charge carrier, configuration A becomes energetically more favorable again and the point defect will eventually move to a different A position.

A third possibility for athermal migration is the energy-release mechanism discussed already by Seitz [1.82] and Koehler and McKeighen [1.83]. It is based on the local enhancement of atomic vibrations by the capture of carriers or the non-radiative recombination of electron-hole pairs at a defect site. The local increase in temperature associated with the atomic vibrations may promote the migration of the defect but it will rapidly decrease via the emission of phonons.

1.4 Thermodynamics

Thermodynamics offers an often complementary approach to describe complex relations in a system. Classical thermodynamics, as outlined in Section 1.4.1, can be used to determine the energetically most stable configuration of atoms. This state is called thermal equilibrium. For situations out of equilibrium, classical thermodynamics can only predict that the system is likely to assume an energetically more favorable configuration. To describe such dynamic processes, the concept of classical thermodynamics was extended by the theory of irreversible processes discussed in Section 1.4.2. This theory allows to describe phenomena which would not or not easily be accessible to kinetic approaches alone. As examples, models for the effects of stress and temperature gradients on the redistribution of atoms will be discussed in Sections 1.4.3 and 1.4.4, respectively.

Before going into details, it seems expedient to comment on the precise meaning of the variables and parameters introduced in the following. In the literature, two different approaches are established. In chemistry and physical chemistry, amounts of atoms and molecules n are usually measured in moles.² As a consequence, all quantities relating to unit amounts or the respective derivatives are quantities per mole. In contrast, in statistical physics, amounts N are usually measured as numbers of atoms, molecules, or defects. Except when explicitly indicated, the second system will be used in the following. Thus, although the names and notation of variables are often borrowed from physical chemistry, it has always to be kept in mind that quantities per unit amount of substance refer here to quantities per constituent and not to quantities per mole. To emphasize the different systems of reference, the terms “atomic” and “partial atomic” will be used for quantities denoted “molar” and “partial molar” in physical chemistry. It should be noted that “atomic” is not meant as a restriction to atoms but rather as a generic term for individual constituents of the species considered.

1.4.1 Equilibrium Thermodynamics

The detailed understanding of redistribution processes requires knowledge about the equilibrium concentrations of crystal defects, about the equilibrium concentration of certain configurations of atoms like ion pairs, about the distribution of atoms in coexisting phases, and various other properties of equilibrium states. In addition, their dependence on macroscopic quantities like temperature, pressure, or Fermi level is of primary interest. These informations can be obtained from the application of statistical thermodynamics.

All practical processes in silicon technology where redistribution has to be taken into account take place at constant pressure. In equilibrium, at constant temperature T and pressure, the Gibbs free energy

$$G = H - T \cdot S \quad (1.82)$$

of a crystal is not changed by microscopic, reversible processes and it can be shown that it is at a minimum. Starting with a perfect crystal, both, enthalpy H and entropy S of the system will increase when defects are present. One important contribution to the increase in entropy arises from the number of possible configurations in which the defects can be arranged in the crystal. This number of possible configurations is called complexion number and denoted by

²One mole is define as the quantity that has a weight in grams numerically equal to the molecular weight of the substance. As an example, one mole of O₂ with its molecular weight of 31.9988 equals 31.9988 g of O₂. The number of molecules in a mole is a constant and corresponds to Avogadro's constant $N_A = (6.0221358 \pm 0.0000041) \cdot 10^{23}$.

Ω . The corresponding entropy term which is identical to the entropy of mixing in classical thermodynamics is called configuration entropy and given by

$$\Delta S_c = k \cdot \ln \Omega. \quad (1.83)$$

The enthalpy and the non-configurational part of the entropy rise proportional to the numbers of defects of the various species.

As an example, let us consider that N defects are distributed upon N_S sites. When the internal degree of freedom of a defect at a specific site is denoted by Θ , the complexion number can be derived from combinatorial considerations and is given by

$$\Omega = \binom{N_S}{N} \cdot \Theta^N = \frac{\Theta^N \cdot N_S!}{N! \cdot (N_S - N)!}. \quad (1.84)$$

The operator ! stands for the factorial function. From this, the configuration entropy results as

$$\Delta S_c = k \cdot \ln(N_S!) - k \cdot \ln(N!) - k \cdot \ln((N_S - N)!) + N \cdot k \cdot \ln(\Theta). \quad (1.85)$$

For large numbers, Sterling's formula (1.55) can be used in a form

$$\ln n! \approx n \cdot (\ln(n) - 1) \quad (1.86)$$

in which the comparatively small terms $\frac{1}{2} \cdot \ln n$ and $\frac{1}{2} \cdot \ln(2 \cdot \pi)$ have already been neglected. When each defect introduced at a specific site increases the Gibbs free energy by G^f , the total change in Gibbs free energy is

$$\Delta G = N \cdot G^f - T \cdot \Delta S_c. \quad (1.87)$$

$G^f = H^f - T \cdot S^f$ is usually called the "Gibbs free energy of formation" or, for the sake of brevity, "formation energy" of the defect. It will be discussed in more detail in Section 1.5.1. H^f and S^f are the enthalpy and entropy of formation, respectively. In case of charged defects, charge neutrality has to be included as auxiliary condition via the method of Lagrange multipliers. The minimum in Gibbs free energy is characterized by a vanishing derivative

$$\frac{\partial G}{\partial N} = G^f + k \cdot T \cdot \ln(N) - k \cdot T \cdot \ln(N_S - N) - k \cdot T \cdot \ln(\Theta) = 0 \quad (1.88)$$

of the Gibbs free energy G with respect to the number of defects N . From this condition, the number of defects in thermal equilibrium is obtained as

$$N^{eq} = N_S \cdot \frac{\Theta \cdot \exp\left(-\frac{G^f}{k \cdot T}\right)}{1 + \Theta \cdot \exp\left(-\frac{G^f}{k \cdot T}\right)} \approx \Theta \cdot N_S \cdot \exp\left(-\frac{G^f}{k \cdot T}\right). \quad (1.89)$$

More complete examples for the application of statistical thermodynamics to the calculation of equilibrium concentrations can be found in Sections 2.1 and 3.2.2.

Often, it is advantageous to consider systems subject to other auxiliary conditions. A typical example might be that the total number of silicon atoms existing as self-interstitials or bound to extended defects is conserved. Minimization of the Gibbs free energy of such a system leads to steady state rather than to thermal equilibrium. This is usually indicated by saying that, e. g. "...the self-interstitials are in steady state with the extended defects ..." Such constrained equilibria are used extensively to express the backward rate constants of reactions in terms of the forward rate constants and some thermodynamic parameters (see Section 1.5.3).

An important quantity to characterize the energetic state of a system is the chemical potential μ . It is defined for each component i as the change in the Gibbs free energy of a system when one part of the respective species is added at constant temperature and pressure

$$\mu_i = \left(\frac{\partial G}{\partial N_i} \right)_{P,T}. \quad (1.90)$$

Its dependences on temperature and pressure are described by

$$\begin{aligned} \left(\frac{\partial \mu_i}{\partial T} \right)_P &= \left(\frac{\partial \left(\frac{\partial G}{\partial N_i} \right)_{P,T,N_j \neq i}}{\partial T} \right)_P \\ &= \left(\frac{\partial \left(\frac{\partial G}{\partial T} \right)_P}{\partial N_i} \right)_{P,T,N_j \neq i} = \left(\frac{\partial (-S)}{\partial N_i} \right)_{P,T,N_j \neq i} = -\bar{S}_i. \end{aligned} \quad (1.91)$$

and

$$\begin{aligned} \left(\frac{\partial \mu_i}{\partial P} \right)_T &= \left(\frac{\partial \left(\frac{\partial G}{\partial N_i} \right)_{P,T,N_j \neq i}}{\partial P} \right)_T \\ &= \left(\frac{\partial \left(\frac{\partial G}{\partial P} \right)_T}{\partial N_i} \right)_{P,T,N_j \neq i} = \left(\frac{\partial V}{\partial N_i} \right)_{P,T,N_j \neq i} = \bar{V}_i \end{aligned} \quad (1.92)$$

respectively. Therein, the partial atomic entropy \bar{S}_i stands for the entropy change upon addition of a defect i to the system. Similarly, the partial atomic volume \bar{V}_i corresponds to the volume change associated with its addition. It might be added that the general concept of a partial atomic quantity X as $\partial X / \partial N_i$ lets us identify the chemical potential as partial atomic Gibbs free energy $\mu_i = \bar{G}_i$.

There are several ways in which the dependence of the chemical potential on the concentration of the species can be formulated. The most common ones will be discussed in the following.

In solutions, the dependence of the chemical potential on the concentration C_i can be expressed as

$$\mu_i = \mu_i^* + k \cdot T \cdot \ln \left(\gamma_{C_i} \cdot \frac{C_i}{C^*} \right). \quad (1.93)$$

with the μ_i^* denoting the standard value of the chemical potential at the standard concentration C^* . The activity coefficient γ_{C_i} is used to introduce non-ideal effects and will, in general, depend on local parameters like the concentrations of all species in the system as well as on macroscopic parameters like temperature and pressure. For ideally dilute solutions, the activity coefficient becomes unity and the chemical potential (1.93) simplifies to

$$\mu_i = \mu_i^* + k \cdot T \cdot \ln \frac{C_i}{C^*}. \quad (1.94)$$

In chemistry it is usual to quantify any substance in moles and to define chemical potentials in terms of their mole fraction $x_i^m = n_i / \sum_j n_j$ in the form

$$\mu_i = \frac{\partial G}{\partial n_i} = \mu_i^* + k \cdot T \cdot \ln(\gamma_i \cdot x_i^m). \quad (1.95)$$

At the reference state associated with pure substances ($x_i^m = 1$), the activity coefficient γ_i approaches unity. For ideally dilute solutions, γ_i will be constant, but not unity. It reflects the different binding energies in the pure substance and in ideally dilute solutions. It has to be emphasized that the standard value of the chemical potential μ_i^* in (1.93) is determined by the choice of a particular standard concentration C^* and will be different from the respective value in (1.95) where it stands for the chemical potential in pure substances. Since the number of atoms or molecules in a mole is always equal to Avogadro's constant, x^m corresponds also to the ratio of the respective numbers of atoms or molecules. Thus, x^m will alternatively be addressed as "atomic fraction" in the sense discussed in the introduction to Section 1.4 to indicate that our reference system is based on numbers of atoms and molecules and not on moles of them.

From the definition of the chemical potential (1.90) as the derivative of the Gibbs free energy with respect to the number of defects it follows that it corresponds to (1.88) for the example discussed above. It can thus be written in the form

$$\mu_i = G_i^f + k \cdot T \cdot \ln \left(\frac{N_i}{\Theta_i \cdot (N_S - N_i)} \right). \quad (1.96)$$

The first term therein is the Gibbs free energy of formation of the defect while the second term arises from the configurational entropy. It is usually expected that the number of defects is much smaller than the number of sites. Then, N_i can be neglected in comparison to N_S . Introducing the activity coefficient γ_i to account for non-ideal solution effects which were not taken into considerations in the derivation, the chemical potential results as

$$\mu_i = G_i^f - k \cdot T \cdot \ln(\Theta_i) + k \cdot T \cdot \ln \left(\gamma_i \cdot \frac{N_i}{N_S} \right). \quad (1.97)$$

A comparison with the definitions above shows that the number of sites N_S is a natural choice for the reference concentration in crystalline matter. The parameter corresponding to the mole fraction is here the site fraction $x_i^s = N_i/N_S$. For defects which do not occupy regular lattice sites like interstitial defects, sub-lattices can be defined which comprise the respective sites.

In general, the dependence of the activity coefficients on the state variables and on the concentrations of the impurities are not known. An exception are electrons and holes. Their chemical potentials are E_F and $-E_F$, respectively (cf. Section 1.2.3). For a reference point, undoped material with $C^* = n_i$ and $\mu^* = E_i$ can be taken. It follows then from (1.93) that $\gamma_n \cdot n$ and $\gamma_p \cdot p$ are identical to

$$\gamma_n \cdot n = n_i \cdot \exp \left(\frac{E_F - E_i}{k \cdot T} \right) \quad (1.98)$$

and

$$\gamma_p \cdot p = n_i \cdot \exp \left(\frac{E_i - E_F}{k \cdot T} \right). \quad (1.99)$$

The limit where the activity coefficients γ_n and γ_p are close to unity corresponds to the range where Boltzmann statistics are applicable.

1.4.2 Thermodynamics of Irreversible Processes

Classical thermodynamics and statistical thermodynamics are valuable methods to describe the properties of systems in equilibrium. Within this framework, processes involving chemical reactions or the redistribution of defects cannot be studied directly. Only their net effect can be analyzed from the properties of the initial and the final state. Thermodynamics of irreversible

processes is an extension of the traditional thermodynamic methods to describe quantitatively the time dependence of systems which are not in equilibrium.

Within the theory of the thermodynamics of irreversible processes as discussed, e. g. in the articles of Onsager [1.84, 1.85] and the monographs of De Groot [1.86] and Haase [1.87], all irreversible processes are attributed to generalized forces. These generalized forces or affinities are denoted by the symbol X_j and can be, e. g. temperature gradients, or concentration gradients, potential gradients, or affinities of chemical reactions. They cause irreversible phenomena as, e. g. heat flow, diffusion fluxes, electrical currents, or chemical reactions, denoted by J_i . One postulate of irreversible thermodynamics is that the relations between the fluxes and the generalized forces can be expressed in a linear form

$$J_i = \sum_j L_{ij} \cdot X_j \quad (1.100)$$

for systems near equilibrium. The L_{ij} are called phenomenological coefficients. They may be arbitrary functions of the state variables (temperature, pressure, composition, etc.), but supposedly not of the fluxes and generalized forces. With equal indices, the L_{ii} are related to, e. g. the heat conductivity, diffusion coefficients, or the electrical conductivity. Those phenomenological coefficients with $i \neq j$ describe cross-phenomena like, e. g. matter transport due to a temperature gradient. A second postulate of the thermodynamics of irreversible processes is that thermodynamic methods can be still applied for sufficiently small volumes V so that the Gibbs-Duhem equation for isotropic regions without electric and magnetic polarization

$$S \cdot dT - V \cdot dP + \sum_k N_k \cdot d\mu_k = 0 \quad (1.101)$$

and the Gibbs fundamental equation

$$T \cdot dS - dU - P \cdot dV + \sum_k \mu_k \cdot dN_k = 0 \quad (1.102)$$

remain valid for the processes in question. From (1.102) follows the change in entropy as a function of changes in energy U , volume V , and numbers N_i of species i . The symbol P denotes the hydrostatic pressure, and the μ_i are the chemical potentials of the species i . Enthalpy, energy, pressure and volume are related to each other via

$$H = U + P \cdot V. \quad (1.103)$$

For the volume V , the dissipation function Ψ which is defined as product of temperature and entropy production per unit volume and time can be written in the form

$$\Psi = \frac{T}{V} \cdot \frac{d_i S}{dt} = \sum_i J_i \cdot X_i \geq 0 \quad (1.104)$$

from which the conjugate fluxes and generalized forces can be identified. The subscript i in the derivative of the entropy with respect to time indicates that only entropy changes due to processes inside of the volume under consideration (e. g. chemical reactions) are taken into account whereas entropy changes due to heat or mass transfer into or out of the volume under consideration are neglected. The dissipation function is never negative and is zero only for reversible processes. A third postulate which was proposed by Onsager on the basis of microscopic reversibility is that the phenomenological coefficients L_{ij} are symmetric

$$L_{ij} = L_{ji} \quad (1.105)$$

as long as Coriolis forces and magnetic fields are not involved.

For diffusing defects, the numbers of defects i crossing a unit area per unit time (cf. Section 1.3.1) can be taken as fluxes J_i . The conjugate generalized forces X_i can be written as

$$X_i = F_i - T \cdot \text{grad} \left(\frac{\mu_i}{T} \right) \quad (1.106)$$

where F_i stands for the actual forces acting on the defect (cf. Section 1.3.3). Under isothermal conditions, (1.106) takes the more familiar form

$$X_i = F_i - \text{grad}(\mu_i). \quad (1.107)$$

Ignoring other effects than their concentration gradient and the Newtonian forces F acting on them, the redistribution of ideally dilute, charged defects of one species can be described by combining (1.94), (1.100), and (1.107) to

$$J_1 = \frac{L_{11} \cdot k \cdot T}{C_1} \cdot \left(-\text{grad} C_1 + C_1 \cdot \frac{F}{k \cdot T} \right). \quad (1.108)$$

It corresponds formally to (1.77) and allows us to relate the phenomenological coefficient L_{11} to the diffusion coefficient obtained from rate theories.

For non-ideal solutions, the activity coefficient γ will deviate from unity. When γ can be expressed as a function of the concentration C (and temperature, pressure, etc.), one obtains

$$J_1 = \frac{L_{11} \cdot k \cdot T}{C_1} \cdot \left(- \left(1 + \frac{\partial \ln(\gamma)}{\partial \ln(C_1/C^*)} \right) \cdot \text{grad} C_1 + C_1 \cdot \frac{F}{k \cdot T} \right). \quad (1.109)$$

instead of (1.108). It should be noted that the Nernst-Einstein relation (1.80) is only approximately valid then.

1.4.3 Stress Effects

Processing of silicon devices is generally performed under constant pressure, usually atmospheric pressure. However, this does not mean that the mechanical stress in the wafer is also uniform. Local oxidation of silicon and similar chemical reactions at surfaces and interfaces were recognized early as major sources of stress. In analogy, local stress arises from phase transformations like the precipitation of oxygen or other impurities in the bulk. Formation of extended defects occurs often in response to large stresses and serves to reduce them. Stress can also build up in multilayer structures during heating up or down when the thermal expansion coefficients of neighboring layers are different. Last but not least, stress is introduced by virtually all point defects from intrinsic point defects to impurities.

First reports on the effects of stress on dopant diffusion reach back at least to the work of Todokoro and Teramoto [1.88] who reported an enhanced diffusion of boron which reduced with distance from the edge of an SiO_2 mask. Mechanical stress imposed by the bounding isolation oxide was also made responsible by Hook et al. [1.89] for changes in the boron distribution of p -channel MOSFETs which manifested themselves as a dependence of the electrical channel length on the channel width. Clear evidence came also from various investigations in which hydrostatic pressure or two-dimensionally strained layers were used to study self-diffusion and the diffusion of impurities. These experiments will be discussed in the following chapters.

There are also various direct and indirect influences of strain on devices. Strain, as an example, was found to affect the conduction and valence bands of silicon [1.90] and to influence carrier mobilities [1.91–1.96]. This allows to obtain significantly increased electron and hole mobilities in the channels of MOSFETs. However, strain was also made responsible for degradation of device performance and reliability [1.97–1.101].

There are numerous ways in which dopant diffusion may be influenced by stress. A first, phenomenological approach to pressure effects can be obtained from thermodynamics. With the diffusion coefficient given by (1.63) and (1.71), the pressure dependence of the logarithm of the diffusion coefficient is given by

$$\left(\frac{\partial \ln(D)}{\partial P} \right)_T = -\frac{1}{k \cdot T} \cdot \left(\frac{\partial G^m}{\partial P} \right)_T = -\frac{\Delta V}{k \cdot T} \quad (1.110)$$

when the comparatively small effects of pressure on the jump distance L and on the attempt frequency Γ_0 are ignored. This allows to write the pressure dependence of the diffusion coefficient in the form

$$D(P) = D(P=0) \cdot \exp \left(-\frac{P \cdot \Delta V}{k \cdot T} \right). \quad (1.111)$$

ΔV is referred to as activation volume. It may be positive or negative and its absolute value usually ranges from 1 to 20 Å³, i.e. from 5% of V_{Si} to V_{Si} . Positive numbers mean retarded diffusion under compressive stress and enhanced diffusion under tensile stress. For negative values, the effects are *vice versa*. When individual components of the stress tensor σ_{ii} do not correspond in magnitude to the hydrostatic pressure

$$P = -\frac{\sigma_{xx} + \sigma_{yy} + \sigma_{zz}}{3}, \quad (1.112)$$

the activation volume has to be replaced by a “strain-activation tensor” [1.102]. It should be noted that shear stress does not contribute to the energetics of point defects so that only the main diagonal entries ΔV_{ii} of the strain-activation tensor are non-zero. Then, the stress dependence of diffusion coefficients can be written in the form

$$D \propto \exp \left(- \sum_{i=x,y,z} \frac{\sigma_{ii} \cdot \Delta V_{ii}}{k \cdot T} \right) \quad (1.113)$$

which appears as a generalization of (1.111).

An atomistic interpretation of experimental data is everything but straightforward. Already the effects of pressure on the concentrations of the intrinsic point defects are non-trivial and depend, as discussed at the end of Section 2.1, on non-local properties. The effects of pressure on the diffusion of impurities is further complicated by their interaction with intrinsic point defects. Stress may influence the formation and migration of the mobile impurity-related species, their preferential orientation, and even their preferential diffusion path. Extensions of diffusion theories to include the effects of hydrostatic pressures have been presented on various levels of theoretical treatments, e.g., by Girifalco and Grimes [1.103], Sugino and Oshiyama [1.104], Cowern et al. [1.105], Park et al. [1.106], Mehrer [1.107], Aziz [1.108], and Laudon, Daw, Windl, and coworkers [1.109–1.111]. It is expected that the requirements of future silicon technology will intensify the work on stress effects on diffusion.

Effects of pressure gradients can be taken formally into account via the thermodynamics of irreversible processes. Taking the pressure dependence of the chemical potential (1.92) into account in (1.107), equation (1.108) is modified to

$$J_1 = \frac{L_{11} \cdot k \cdot T}{C_1} \cdot \left(-\text{grad}C_1 - C_1 \cdot \frac{\bar{V}_1}{k \cdot T} \cdot \text{grad}P + C_1 \cdot \frac{F}{k \cdot T} \right). \quad (1.114)$$

While the effects of pressure gradients in semiconductors are usually considered to be of minor importance, they were frequently included to describe redistribution phenomena in metals [1.112–1.114]. When the stress tensor cannot be reduced to a hydrostatic pressure, a tensorial description has to be introduced for the partial atomic volume \bar{V} .

It has to be mentioned here that the introduction of defects is generally associated with local contractions or expansions of the lattice which put the lattice into a state of stress. Consequently, inhomogeneous distributions of defects lead to stress gradients which, in turn, cause the defects to migrate. Larché and Cahn [1.115, 1.116] and Larché [1.117] described such effects in their review and showed that they can be reduced for certain limiting cases to equations similar to Fick's law. Except for some rare exceptions [1.118], they were not taken into consideration in silicon technology. It is important to note that the diffusion coefficients determined empirically lump already redistribution in direct response to concentration gradients and in indirect response to concentration gradients via stress and stress gradients.

1.4.4 Thermodiffusion

In most of the preceding sections, isothermal conditions were assumed implicitly. Major thermal gradients are not expected during the majority of the processes due to the high thermal conductivity of silicon. However, they may be important during crystal growth as well as during processes like laser annealing in which very high temperature ramps are used. Such temperature gradients are known to act as driving forces for a redistribution of matter, usually called thermomigration, Ludwig-Soret effect (after C. Ludwig [1.119] and C. Soret [1.120]), or often simply Soret effect.

Within the framework of the thermodynamics of irreversible processes, the generalized force associated with the heat flux J_q is

$$X_q = -\frac{\text{grad } T}{T}. \quad (1.115)$$

Assuming that the motion of each defect i is associated with the transport of a heat Q_i^* , it follows from Onsager's reciprocity law that a temperature gradient induces corresponding particle fluxes. In a one-component system, as an example, the total flux becomes

$$J_1 = L_{11} \cdot \left(F - T \cdot \text{grad} \left(\frac{\mu_1}{T} \right) - \frac{Q^*}{T} \cdot \text{grad } T \right). \quad (1.116)$$

In silicon, the Q^* for the intrinsic point defects and the impurities are not measurable so that (1.116) is mainly of theoretical interest.

Motivated by the form of (1.116), diffusion in a temperature gradient is conventionally described by

$$J = -D \cdot \text{grad } C - \frac{C \cdot D \cdot Q^*}{k \cdot T^2} \cdot \text{grad } T. \quad (1.117)$$

The parameter Q^* therein is often also called “heat of transfer” but it should be noted that it is of phenomenological nature here and not directly identical to the Q_i^* in (1.116). The latter really stand for the heat transported by each defect i while the former contains also the contributions proportional to $\text{grad } T$ from the expansion of $L_{11} \cdot T \cdot \text{grad}(\mu_1/T)$. Unfortunately, the Q^* are not easily accessible to an experimental determination.

Although Q^* was derived in numerous theoretical investigations from combinations of kinetic and thermodynamic theories [1.121–1.135], agreement was rather limited. When the results were given in terms of the migration enthalpy H^m and/or the formation enthalpy H^f of the defect, values for Q^* were between the two extrema $Q^* = -H^f$ and $Q^* = H^m$. The former limit comes from considerations of the equilibrium concentrations while the latter results from considerations of the effects of a thermal gradient on the jump frequency. Frequently, taking both into account, Q^* was found to equal $Q^* = H^m - H^f$.

The same range of values was used also in simulations of crystal growth. In one of the first quantitative investigations, Voronkov [1.136] assumed that Q^* would be less than the defect-migration enthalpy H^m and used it as argument to ignore thermodiffusion. On the other extreme were Habu et al. [1.137] and Brown et al. [1.138] who based their work on $Q^* = -H^f$. Both approaches were followed in a variety of similar studies afterwards. Treating Q^* for self-interstitials and vacancies as free parameters, Nakamura et al. [1.139] found that they have only a small influence on the results of defect formation during crystal growth.

In a recent analysis, Tan [1.140] suggested from a combination of kinetic and thermodynamic considerations that Q^* takes the form

$$Q^* = G^m - G^f + k \cdot T \cdot \ln \left(\frac{C}{C^{eq}} \right) \quad (1.118)$$

wherein G^m , G^f , and C^{eq} are the Gibbs free energy of migration, the Gibbs free energy of formation, and the equilibrium concentration of the migrating point defect, respectively. However, it can be shown that the last term vanishes when the $T \cdot \text{grad}(\mu/T)$ as in (1.106) is correctly taken as driving force under non-isothermal conditions instead of $\text{grad}(\mu)$ and that the G^m and G^f should correctly be replaced by H^m and H^f , respectively.

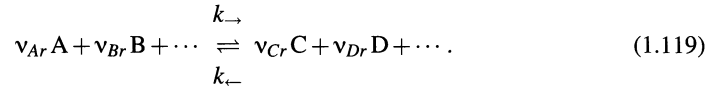
1.5 Reaction Kinetics

Besides redistribution of the defects being present in a system in specific charge states, their generation or loss has to be taken into considerations. Loss of a defect can be the result of its break-up, or of a reaction with other defects or charge carriers. The reverse processes will lead to its creation. Typical examples are ionization of defects, the formation of pairs between intrinsic point defects and impurity atoms, the formation of extended intrinsic defects like stacking faults, or the formation of extended extrinsic defects like impurity clusters or precipitates.

The mathematical description of reactions presented in Section 1.5.1 is based on the theory of irreversible processes outlined in Section 1.4. From this theory, the law of mass action follows as a consequence and, for systems in equilibrium, describes the relation between the concentrations of the species involved in the reaction. For the change of the reaction variable with time, several formulations are known and will be discussed in Section 1.5.2. Most important is the kinetic law of mass action, but alternative equations can be established within the theory of irreversible processes or from the theory of the activated complex. For the first two theories, the parameters determining the velocity of the reactions have to be supplied by kinetic theories. A convenient way is the theory of diffusion-limited reactions presented in Section 1.5.3. Finally, in Section 1.5.4, a standard method for the mathematical formulation of continuum-diffusion models is presented. It considers any elemental point defects like vacancies, self-interstitials, and impurity atoms as well as all composite defects resulting from reactions between them as individual defects. The formation and redistribution of such defects is then described by a set of continuity equations with diffusion terms and generation/recombination terms which reflect the reactions between the species.

1.5.1 The Reaction Variable ζ and Equilibrium Thermodynamics

When we denote the stoichiometric number of species i involved in reaction r by v_{ir} , the R chemical reactions are of the form



By definition, stoichiometric numbers appearing at the left-hand side are negative. The symbols k_{\rightarrow} and k_{\leftarrow} stand for the rate constants in forward and backward direction, respectively. Following De Donder [1.141], a reaction variable can be introduced as a measure of the extent of reaction r . One way is to define a reaction variable ξ in terms of the numbers of constituents of the species involved. This has the advantage that volume changes associated with the reaction are irrelevant. For defect reactions in bulk silicon, no significant volume change is expected for a sample of sufficient dimensions because of the rigidity of the material and it is advantageous to define a reaction variable $\xi_r = \xi_r/V$ as concentration instead of number of constituents. When only one reaction has to be considered, the change in the concentration of species i in a closed, constant volume is then simply given by

$$dC_i = v_{ir} \cdot d\xi_r. \quad (1.120)$$

When several parallel reactions have to be considered, the change in the concentration of any of the species i

$$dC_i = \sum_r v_{ir} \cdot d\xi_r \quad (1.121)$$

is the sum of the changes associated with the particular reactions r . The affinity A_r , a measure of the driving force of the reaction r , is defined as a linear combination of the chemical potentials μ_i of the species participating therein

$$A_r = - \sum_i v_{ir} \cdot \mu_i. \quad (1.122)$$

In equilibrium, changes in the concentrations C_i have to vanish. When the reaction equations are linearly independent, i. e. when the matrix v_{ir} is regular, the reaction variables have to be zero, too. Additionally, the Gibbs free energy of the crystal is at a minimum. Deviations from equilibrium lead to an increase in Gibbs free energy. The change in Gibbs free energy of a system without electric and magnetic polarization can be obtained from the definition of the Gibbs free energy (1.82) with the help of the Gibbs fundamental equation (1.102) and the relation (1.103) between enthalpy and energy. For constant temperature and pressure, the condition for equilibrium results as

$$dG = - \sum_r A_r \cdot d\xi_r = -V \cdot \sum_r A_r \cdot d\xi_r = 0 \quad (1.123)$$

with the second form valid for reactions which are not accompanied by volume changes. When the reaction variables ξ_r (or ζ_r) are independent for the R reactions, all affinities A_r have to vanish in equilibrium. Introducing the chemical potential from (1.93), (1.122) can be written in the form

$$A_r = - \sum_i v_{ir} \cdot \mu_i^* - k \cdot T \cdot \ln \left(\frac{\prod_i (\gamma_i \cdot C_i)^{v_{ir}}}{\prod_i (C_i^*)^{v_{ir}}} \right). \quad (1.124)$$

The standard values of the chemical potential and the standard concentration can be combined to a constant

$$K_r = \prod_i (C_i^*)^{v_{ir}} \cdot \exp\left(-\frac{\sum_i v_{ir} \cdot \mu_i^*}{k \cdot T}\right) \quad (1.125)$$

which depends only on the state variables, but not on concentrations. In equilibrium, where the A_r have to vanish, the concentrations of the various species i are related to each other by

$$\prod_i (\gamma_i \cdot C_i)^{v_{ir}} = \frac{(\gamma_C \cdot C_C)^{v_{Cr}} \cdot (\gamma_D \cdot C_D)^{v_{Dr}} \dots}{(\gamma_A \cdot C_A)^{-v_{Ar}} \cdot (\gamma_B \cdot C_B)^{-v_{Br}} \dots} = K_r \quad (1.126)$$

where we have used again the notation of (1.119). For ideally dilute concentrations, (1.126) reduces to the “law of mass action”

$$\prod_i C_i^{v_{ir}} = \frac{C_C^{v_{Cr}} \cdot C_D^{v_{Dr}} \dots}{C_A^{-v_{Ar}} \cdot C_B^{-v_{Br}} \dots} = K_r. \quad (1.127)$$

For the description of phase transformations, mole fractions are sometimes used in the literature to define the chemical potential via (1.95). This leads to

$$\prod_i (\gamma_i \cdot x_i^m)^{v_{ir}} = \frac{(\gamma_C \cdot x_C^m)^{v_{Cr}} \cdot (\gamma_D \cdot x_D^m)^{v_{Dr}} \dots}{(\gamma_A \cdot x_A^m)^{-v_{Ar}} \cdot (\gamma_B \cdot x_B^m)^{-v_{Br}} \dots} = K_r^m \quad (1.128)$$

with K_r^m being defined in terms of the standard chemical potentials

$$K_r^m = \exp\left(-\frac{\sum_i v_{ir} \cdot \mu_{ir}^*}{k \cdot T}\right) = \exp\left(-\frac{\Delta G_r}{k \cdot T}\right). \quad (1.129)$$

ΔG_r is the molar Gibbs free energy of the reaction. In chemical reactions, the standard values of the chemical potential μ_i^* are commonly related to standard states of the substances where they are zero per definition (for, e. g. silicon in the crystalline phase, gaseous H_2 and O_2 , etc.). The values of the μ_i^* for the reaction products correspond then to the molar free energies of formation ΔG_i^f which are tabulated in all major reference books.

Finally, using the definition of the chemical potential as a function of the site fraction (1.97), one obtains a third version of the law of mass action

$$\prod_i (\gamma_i \cdot x_i^s)^{v_{ir}} = \frac{(\gamma_C \cdot x_C^s)^{v_{Cr}} \cdot (\gamma_D \cdot x_D^s)^{v_{Dr}} \dots}{(\gamma_A \cdot x_A^s)^{-v_{Ar}} \cdot (\gamma_B \cdot x_B^s)^{-v_{Br}} \dots} = K_r^s \quad (1.130)$$

with the equilibrium constant K_r^s given as

$$K_r^s = \prod_i (\Theta_i)^{v_i} \cdot \exp\left(-\frac{\sum_i v_{ir} \cdot G_i^f}{k \cdot T}\right). \quad (1.131)$$

In solids, the energetics of defects is usually discussed in terms of their “formation energy” and “binding energy.” However, it should be noted that there is no general consensus for the usage of these terms in the literature. The definitions used within this book will be discussed in the following.

For elemental intrinsic point defects like vacancies or self-interstitials, the formation energy $G^f = H^f - T \cdot S^f$ is equal to the increase in Gibbs free energy of the system when one of them

is formed at a specific site under conservation of the silicon atoms in the system. They and individual impurity atoms are the elemental point defects from which all other defects can be thought to compose of. For such composite defects, the term formation energy will be used in this book to denote the energy of the system with respect to a certain reference state associated with elemental point defects only. The reference state for intrinsic point defects is usually the undisturbed lattice. But it may be convenient to associate it with already formed, well-separated intrinsic point defects. Impurity atoms in the reference state are also well-separated from the other elemental point defects. For dopants, it is customary to associate the reference state with the ionized, substitutional configuration since it is the energetically most favorable one. For other impurities, it may be more convenient to use, e. g. an interstitial configuration. A further alternative is to assume that host atoms and impurities may be taken from a reservoir, e. g. an equilibrium phase, where they have a specific chemical potential.

In contrast to the definition given, the term formation energy is also used in the literature when the reference state includes a composite defect. Taking a cluster of n impurities as an example, this would mean that the reference system would consist of a cluster of $n - 1$ impurities well-separated from an individual impurity. In the definition used in this book, the reference state would be n well-separated impurities.

The term binding energy G^B is similar to the formation energy but the reference state consists only of existing elemental defects. This relates especially to intrinsic point defects for which the reference point for the formation energy is usually the undisturbed lattice. The more the system energy is lowered upon formation of a composite defect, the more stable will this defect be. Since stability is intuitively associated with a positive binding of the elemental defects involved, positive values for the binding energy will be associated in this book with a lowering of the energy of the system upon formation of the composite defect from its reference state. However, it has to be noted that there are also other definitions customary in the literature which associate a negative value for the binding energy with an energy reduction upon defect formation. It is further customary in the literature to use the term binding energy to describe the change in system energy associated with the reaction of an elemental defect with a composite defect. Such differential binding energies will be referred to in this work by stating that the elemental defect “binds with an energy of ...” to the composite defect. Again, positive values are used to indicate that the reaction leads to a decrease in the system energy.

Important for the methodology of diffusion-reaction equations to be discussed in Section 1.5.4 are binary reactions of the form

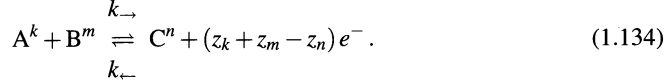


In steady state, for ideally dilute concentrations ($\gamma_A = \gamma_B = \gamma_C = 1$), it follows from (1.130) and (1.131) that the site fractions of the species involved are related to each other by

$$\frac{x_C^s}{x_A^s \cdot x_B^s} = \frac{\Theta_C}{\Theta_A \cdot \Theta_B} \cdot \exp \left(\frac{G_A^f + G_B^f - G_C^f}{k \cdot T} \right) = \frac{\Theta_C}{\Theta_A \cdot \Theta_B} \cdot \exp \left(\frac{G^B}{k \cdot T} \right). \quad (1.133)$$

G^B is the reduction of the Gibbs free energy of the system associated with each reaction of A and B to C. For elemental defects A and B, G^B is the binding energy of the defect C. Otherwise, it is the Gibbs free energy with which the last elemental constituent added binds to the composite defect. It has to be mentioned also that the binding energy is the most important parameter in the equation while the degrees of freedom are all on the order of unity and the numbers of sites for the reactants are all on the order of the number of lattice sites.

The situation becomes slightly more complicated when the species are ionized. Assuming that the species A, B, and C contain k , m , and n electron charges, respectively, the reaction equation (1.132) can be written in the form



Within Fermi statistics, the electrons at the right-hand side of (1.134) are not considered species like A, B, and C. They enter via the charge-neutrality equation (see also Section 2.1) and contribute in the energy balance with their formation energy which corresponds to the Fermi level. Thus, instead of (1.133), one obtains

$$\begin{aligned} \frac{x_{C^n}^s}{x_{A^k}^s \cdot x_{B^m}^s} &= \frac{\Theta_{C^n}}{\Theta_{A^k} \cdot \Theta_{B^m}} \cdot \exp \left(\frac{G_{A^k}^f + G_{B^m}^f - G_{C^n}^f - (z_k + z_m - z_n) \cdot E_F}{k \cdot T} \right) \\ &= \frac{\Theta_C}{\Theta_A \cdot \Theta_B} \cdot \exp \left(\frac{G^B}{k \cdot T} \right) . \end{aligned} \quad (1.135)$$

Here, the binding energy G^B depends in the general case ($z_k + z_m - z_n \neq 0$) on the Fermi level.

To illustrate the formalism, let us consider the simple ionization reaction



of a donor D. Its positive charge state, as discussed in Section 1.2.3, is non-degenerate ($\Theta_{D^+} = 1$) and can be taken as reference energy. The neutral state is doubly degenerate ($\Theta_{D^0} = 2$) and will be higher in energy (E_D). Then, simply ignoring the second reactant, one obtains

$$\frac{C_{D^+}}{C_{D^0}} = \frac{x_{D^+}}{x_{D^0}} = \frac{\Theta_{D^+}}{\Theta_{D^0}} \cdot \exp \left(\frac{G_{D^0}^f - G_{D^+}^f - E_F}{k \cdot T} \right) = \frac{1}{2} \cdot \exp \left(\frac{E_D - E_F}{k \cdot T} \right) . \quad (1.137)$$

Taking into account that the total concentration C_D corresponds to the sum of C_{D^0} and C_{D^+} , one obtains directly the concentration of neutral donors C_{D^0} which corresponds to n_D in (1.3).

When charge is not conserved in a reaction without additional, compensating charge carriers ($z_k + z_m - z_n \neq 0$), the binding energy will depend on the Fermi level, as noted already above. Often, binding energies are then given for the Fermi level at mid-gap (E_i). Denoting them by $G^{B,i}$, (1.135) can be written in the form

$$\frac{x_{C^n}^s}{x_{A^k}^s \cdot x_{B^m}^s} = \frac{\Theta_C}{\Theta_A \cdot \Theta_B} \cdot \exp \left(\frac{G^{B,i}}{k \cdot T} \right) \cdot \exp \left(- \frac{(z_k + z_m - z_n) \cdot (E_F - E_i)}{k \cdot T} \right) . \quad (1.138)$$

The last exponential term can be written via (1.18) as $(n/n_i)^{-(z_k+z_m-z_n)}$ within the range of applicability of Boltzmann statistics so that one obtains

$$\frac{x_{C^n}^s \cdot (n/n_i)^{(z_k+z_m-z_n)}}{x_{A^k}^s \cdot x_{B^m}^s} = \frac{\Theta_C}{\Theta_A \cdot \Theta_B} \cdot \exp \left(\frac{G^{B,i}}{k \cdot T} \right) . \quad (1.139)$$

In this form, the electrons appear as if treated in the reaction as quasi-defects. But instead of the concentration of lattice sites, the intrinsic concentration n_i has to be used as scaling factor for the electron concentration.

1.5.2 Dynamic Theories of Reactions

The velocity of the reaction r is characterized by the reaction rate $d\zeta_r/dt$. The generation and loss terms $G - R$ in the continuity equation for a certain species (1.41) corresponds to the change of its concentration with time associated with the reactions of the respective species only. They follow from (1.121) as

$$G_i - R_i = \left(\frac{dC_i}{dt} \right)_{\text{Reactions}} = \sum_r v_{ir} \cdot \frac{d\zeta_r}{dt}. \quad (1.140)$$

When reactions of the form (1.119) occur without back-reaction, the reaction rates found experimentally in chemical reactions follow usually the relation

$$\frac{d\zeta}{dt} \propto (C_A)^{n_A} \cdot (C_B)^{n_B} \dots \quad (1.141)$$

The reaction is then said to have order n_i with respect to substance i , and $\sum_i n_i$ is referred to as the order of the reaction. The n_i are expected to be integers for elemental reactions.

When both forward and backward reactions contribute significantly to the net reaction, one speaks of an “incomplete reaction”. Various formulations for the reaction rate were derived from different theories to describe this situation. They will be discussed in the following.

Kinetic Law of Mass Action

In virtually all theoretical studies on defect reactions in silicon, the respective reaction rates are assumed to follow the so-called “kinetic” or “dynamic” law of mass action derived by Brönsted [1.142, 1.143] and generalized by Haase [1.144, 1.145]. In the nomenclature of (1.119), it can be written as

$$\begin{aligned} \frac{d\zeta_r}{dt} &= k_{\rightarrow} \cdot \prod_{i, v_{ir} < 0} (\gamma_i \cdot C_i)^{-v_{ir}} - k_{\leftarrow} \cdot \prod_{j, v_{jr} > 0} (\gamma_j \cdot C_j)^{v_{jr}} \\ &= k_{\rightarrow} \cdot (\gamma_A \cdot C_A)^{-v_{Ar}} \cdot (\gamma_B \cdot C_B)^{-v_{Br}} \dots \\ &\quad - k_{\leftarrow} \cdot (\gamma_C \cdot C_C)^{v_{Cr}} \cdot (\gamma_D \cdot C_D)^{v_{Dr}} \dots \end{aligned} \quad (1.142)$$

It is intuitively appealing that the exponents of the concentrations in the kinetic law of mass actions correspond to the absolute values of the stoichiometric numbers. It should also be mentioned that, according to Haase, a valid description is obtained even far from steady state.

The kinetic law of mass action determines just the structure of the equations. The rate constants can be obtained from kinetic theories as discussed in Section 1.5.3.

Theory of Irreversible Thermodynamics

An alternative expression for the reaction rate can be obtained within the theory of thermodynamics of irreversible processes as outlined by De Donder [1.141]. For reactions, the reaction rates $d\zeta_r/dt$ and the respective affinities A_r of the independent reactions form pairs of fluxes and conjugate generalized forces in the sense of (1.104). Phenomenological relations can be established between the reaction rates and the affinities in the form of (1.100) for each of the reactions

$$\frac{d\zeta_r}{dt} = \sum_s L_{rs} \cdot A_s. \quad (1.143)$$

As long as the reactions are linearly independent, all phenomenological coefficients L_{rs} are zero for $r \neq s$. For coupled reactions, the phenomenological coefficients obey Onsager's reciprocity law (1.105). Moreover, since the dissipation function

$$\Psi = \sum_r \sum_s L_{rs} \cdot A_r \cdot A_s > 0 \quad (1.144)$$

has to be positive, the determinants of all submatrices of the matrix L_{rs} have to be positive. For systems of independent reactions, each reaction rate follows from (1.143) and the definition of the affinity (1.124) as

$$\frac{d\zeta_r}{dt} = L_{rr} \cdot k \cdot T \cdot \ln \prod_i \left(\frac{\gamma_i \cdot C_i}{\gamma_i^{eq} \cdot C_i^{eq}} \right)^{v_{ir}}. \quad (1.145)$$

To derive this equation, the standard values of the chemical potentials and the standard concentrations have been combined to the constant K_r defined via (1.125). Then, K_r has been substituted by (1.126) with the activity coefficients and concentrations taken from the situation where the reaction is in equilibrium (indicated by the superscript ' eq '). Since (1.100) is valid only near equilibrium, (1.145) can be developed in a Taylor series leading to an equation with the structure of (1.142). The comparison allows to establish a relation between the phenomenological coefficients and the reaction constants

$$k_{\rightarrow} = \frac{L_{rr} \cdot k \cdot T}{\prod_{i, v_i < 0} (C_i^{eq})^{-v_{ir}}}, \quad k_{\leftarrow} = \frac{L_{rr} \cdot k \cdot T}{\prod_{j, v_j > 0} (C_j^{eq})^{v_{jr}}}. \quad (1.146)$$

Although, as mentioned, its application is restricted to near-equilibrium situations, (1.145) was used, e.g. by Habu et al. [1.146], to model the bulk recombination of vacancies and self-interstitials.

The theory of irreversible thermodynamics is also able to provide important conclusions for parallel reactions. The discussion above has been restricted to independent reactions. This corresponds to case a) in Figure 1.28 which shows possible reactions in a ternary system. When the reactions are not independent, as in case b) in Figure 1.28, one has to be aware that the equilibrium conditions $d\zeta_r = 0$ cannot be deduced from $dC_i = 0$. However, based on the principle of dynamic reversibility, Onsager [1.84] has postulated that, in equilibrium, all individual reactions are in balance, and that the respective reaction rates vanish. This postulate, usually called "principle of detailed balance" or "principle of detailed equilibrium," implies that cyclic processes as shown in Figure 1.28 c) are forbidden.

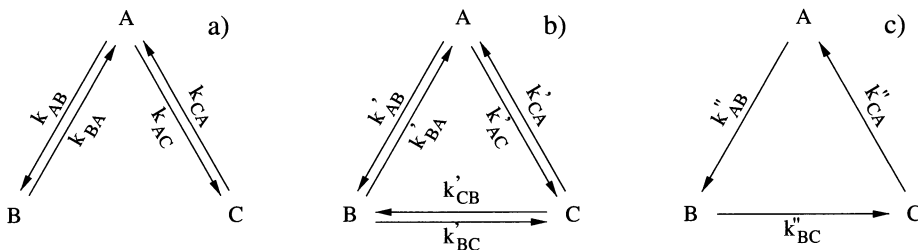


Figure 1.28: Reactions in a ternary system: a) linearly independent reactions, b) linearly dependent reactions, c) cyclic reactions.

Transition-State Theory

A third theory used extensively in chemistry but only rarely to describe defect reactions in silicon was developed by Eyring and his coworkers [1.147] and is known as “transition-state theory”, “theory of absolute reaction rates”, or “activated-complex theory.” It is based on the concept that a reaction starts from some initial configuration and passes by a continuous change of coordinates into a final configuration. Between the initial and the final states, an intermediate configuration exists, the attainment of which is critical for the reaction. This critical configuration is called the “activated complex” M^\ddagger of the reaction. It is characterized, as shown schematically in Figure 1.29, by the highest free energy of the system along the most favorable reaction path with G^\ddagger being the free energy of the barrier to be surmounted. Then, the forward reaction rate is given by

$$\frac{d\zeta_{\rightarrow}}{dt} = \frac{k \cdot T}{h} \cdot C_{M^{\ddagger \rightarrow}}. \quad (1.147)$$

$C_{M^{\ddagger \rightarrow}}$ is the concentration of the activated complexes which are assumed to be in steady state with the reactants according to the reaction



The concentration of the activated complexes can then be computed from concentrations of the reactants by applying the concept of equilibrium thermodynamics as discussed in Section 1.5.1. A relation similar to (1.147) describes the backward reaction and the difference between both the net rate of the reaction. A critical discussion of the application of the transition-state theory to the solid state can be found in chapter III of the monograph of Christian [1.148].

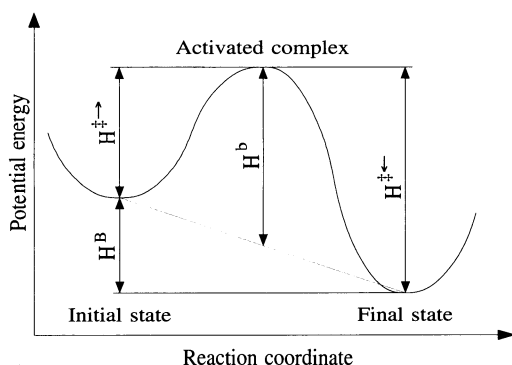


Figure 1.29: Schematic energy-barrier diagram for a reaction according to the transition-state theory.

The transition-state theory leads to the same structure as the kinetic law of mass action but provides in addition a quantitative estimate for the reaction constants. However, in practice, it is desirable to estimate G^\ddagger for the forward and backward reaction from independently determinable parameters like migration energies of reactants or the binding energy of the reaction. The first approach is to associate $G^{\ddagger \rightarrow}$ of the forward reaction in Figure 1.29 with the migration enthalpy G^m of the fastest reactant. $G^{\ddagger \leftarrow}$ of the backward reaction is then the sum of the migration enthalpy and the binding energy. An alternative would be to assume that a barrier H^b as shown in Figure 1.29 has to be overcome during the reaction which may again be associated with the migration enthalpy G^m of the fastest reactant. G^\ddagger can then be expressed approximately as $G^{\ddagger \rightarrow} = G^m - G^B/2$ for the forward reaction and $G^{\ddagger \leftarrow} = G^m + G^B/2$ for the backward reaction. The analogy to diffusion processes suggests also to associate the term $k \cdot T/h$ in (1.147) with the attempt frequency Γ_0 . It is interesting to note that $k \cdot T/h$ is close to, although at diffusion temperatures higher than, the highest frequency within the Debye model of solids.

1.5.3 Estimation of Rate Constants for the Kinetic Law of Mass Action

The kinetic law of mass action (1.142) gives just the structure of the kinetic equations. The parameters, especially the rate constants, have to be obtained from kinetic theories. Already in 1916, von Smoluchowski [1.149] presented a theory for the coagulation in colloidal solutions. According to this theory, the rate of coagulation is determined mainly by the diffusion of the reactants towards each other. As soon as the distance between the reactants is as low as the capture radius a^R , the reaction is assumed to take place immediately.

It is evident that this mechanism will lead predominantly to binary reactions in the form (1.132). Assuming the reaction to be diffusion-limited, the von Smoluchowski approach leads to a rate constant given by

$$k_{\rightarrow} = 4 \cdot \pi \cdot a^R \cdot (D_A + D_B). \quad (1.149)$$

The symbols D_A and D_B stand for the diffusion coefficients of the reacting species. The theory presented by von Smoluchowski contained implicitly limiting statistical assumptions. However, based on a more sound statistical basis, Waite [1.150] came to virtually the same conclusion. The capture or reaction radius a^R for reaction between point defects is usually assumed to be on the order of the distance between two substitutional silicon atoms ($a^R \approx 2.5 \text{ \AA}$). In the work of Bunea et al. [1.151], the reaction radius for the mutual annihilation of self-interstitials and vacancies was investigated by kinetic Monte-Carlo calculations using an empirical potential. For long-ranging interactions between the two point defects, a capture radius of 6.7 \AA was obtained for $900 \text{ }^\circ\text{C}$. A similar result of approximately 7 to 8.3 \AA was reported for $900 \text{ }^\circ\text{C}$ by Beardmore et al. [1.152] who combined *ab-initio* calculations and kinetic Monte-Carlo calculations. For the interaction between self-interstitials and substitutional boron atoms and between vacancies and arsenic or phosphorus atoms, capture radii of 4.6 \AA , 6.9 \AA , and 7.4 \AA were obtained at $900 \text{ }^\circ\text{C}$, respectively. Both investigations reported a decrease of the capture radius for increasing temperature. For reactions between point defects and extended defects, an increased capture radius can be introduced which reflects the geometry of the extended defect.

The treatment of von Smoluchowski and Waite is valid only if, at least, one of the reacting species is electrically neutral. When both reacting species are electrically charged with charge states z_1 and z_2 , Coulombic attraction and repulsion has to be taken into consideration. As demonstrated by Debye [1.153], this leads to a modification of the rate constant in the form

$$k_{\rightarrow} = 4 \cdot \pi \cdot a^R \cdot (D_A + D_B) \cdot \frac{W}{e^W - 1} \quad (1.150)$$

$$W = \frac{z_1 \cdot z_2 \cdot q^2}{4 \cdot \pi \cdot \epsilon_0 \cdot \epsilon_r \cdot k \cdot T \cdot a^R}.$$

The symbols ϵ_0 and ϵ_r stand for the absolute permittivity and the relative permittivity, respectively. There is some uncertainty about the appropriate value of ϵ_r , since the macroscopic value of the relative permittivity (see Section 1.2) is most likely inapplicable. Still, it might be the best guess available. In addition, a “proximity-charging effect” was suggested by Kimerling et al. [1.154]. When two oppositely charged defects approach each other, their respective defect states are perturbed in energy by the Coulombic interaction such that the donor state moves toward the conduction band and the acceptor state moves towards the valence-bond band. As a consequence, the ionization probability of the defects is increased. The shifts in the levels are given by

$$\Delta E = \frac{q^2}{\epsilon_0 \cdot \epsilon_r \cdot r} \quad (1.151)$$

with r denoting the distance between the two defects. Clearly, as discussed by Berezhnov et al. [1.155], reactions may be enhanced or retarded also by local strain fields which may act as driving forces for the diffusion of the reactants to or from each other. Such effects are usually taken into account by an effective capture radius.

The rate constants (1.149) and (1.150) were obtained under the assumption that the reaction takes place immediately when the distance between the reactants becomes as low as the capture radius. This scenario was extended by Waite [1.156] who introduced the probability

$$p \cdot \exp\left(-\frac{\Delta E}{k \cdot T}\right) \quad (1.152)$$

that the reaction really occurs when the reactants meet. He then found that the reaction is still of second order and that the rate constant (1.149) for times exceeding an initial period can be written in the form

$$k_{\rightarrow} = 4 \cdot \pi \cdot a^R \cdot (D_A + D_B) \cdot \frac{a^R \cdot \beta}{a^R \cdot \beta + 1}. \quad (1.153)$$

Therein, β stands for

$$\beta = \frac{\Delta a \cdot \Gamma_0 \cdot p \cdot \exp\left(-\frac{\Delta E}{k \cdot T}\right)}{D_A + D_B}. \quad (1.154)$$

with Γ_0 standing for the attempt frequency and Δa being on the order of the distance between two neighboring atoms. In general, only barriers exceeding the migration enthalpy are taken into considerations and 1.153 is used in the approximate form

$$\begin{aligned} k_{\rightarrow} &= 4 \cdot \pi \cdot a^R \cdot (D_1 + D_2) \cdot \exp\left(-\frac{\Delta G}{k \cdot T}\right) \\ &= 4 \cdot \pi \cdot a^R \cdot (D_1 + D_2) \cdot \exp\left(\frac{\Delta S}{k}\right) \cdot \exp\left(-\frac{\Delta H}{k \cdot T}\right) \end{aligned} \quad (1.155)$$

wherein ΔG stands for the barrier in excess of the Gibbs free energy of diffusion of the fastest reactant. The energy barrier might be an enthalpy barrier or an entropy barrier. The meaning of an entropy barrier is that the entropy of the system is lowered during the reaction. In (1.150), an energy barrier can be introduced analogously.

The situation becomes slightly more complicated when charge states are involved. To start with, let us consider the ionization reaction of an acceptor



For an order-of-magnitude estimate, the electron will be assumed to be a quasi-defect to which Waite's theory can be applied. Then, the change in the concentration of neutral acceptors is given by

$$\frac{dC_{A^0}}{dt} = -k_{\rightarrow} \cdot C_{A^0} \cdot n + k_{\leftarrow} \cdot C_{A^-} = -\frac{C_{A^0}}{\tau} + \dots \quad (1.157)$$

Therein, τ is the characteristic time constant for the charging process. Using Waite's theory, an estimate for τ can be given in the form

$$\tau = \frac{1}{4 \cdot \pi \cdot D_e \cdot a^R \cdot n} . \quad (1.158)$$

The diffusion coefficient of the electrons can be estimated via the Einstein relation (1.80) from the mobility given, e. g. by Sah et al. [1.157]. Assuming a reaction radius of 2 nm and the electron concentration to correspond to the intrinsic concentration leads to time constants of less than one picosecond at temperatures of 500 °C and above. Even allowing for some uncertainties in parameters and method, this means that steady state between the charge states of a defect is established quasi instantaneously in comparison to process times.

When charge states are involved in binary reactions, as in the reaction equation (1.134), additional care has to be exercised in estimating the reaction constants. According to the kinetic reaction theories discussed above, the forward reaction rate depends just on the reactants and corresponds to the total concentration of defects C forming per unit time by this reaction. How many of the defects C form in a particular charge states is not predicted. The most straightforward assumption seems to be that charge is conserved so that the pairs forming have charge state $z_k + z_m$. But this is just as artificial as any other assumption since it is not even guaranteed that such a charge state exists for defect C. On the other hand, at least at elevated temperatures, it can be assumed that steady state between the charge states n of the products C is established more or less instantaneously. Then, the concentration of pairs forming in a specific charge state per unit time is given by the product of the total rate times the Fermi-level dependent probability that the pair exists in this charge state. It is convenient to use only the total concentrations of reactants and products then, but when individual forward reaction constants have to be given explicitly, they can be written in the form

$$k_{\rightarrow}^{kmn} = k_{\rightarrow}^{km} \cdot \frac{C_C^n}{\sum_n C_C^n}. \quad (1.159)$$

The rate constants k_{\rightarrow}^{km} therein can be estimated as discussed above.

Waite's theory in the form (1.149) and its extensions are valid only for a uniform distribution of the reacting species. Such conditions are not expected under conditions of, e. g. electron irradiation or ion implantation where vacancies and self-interstitials may occupy closely correlated sites. Extensions to include spatial correlation effects were discussed, e. g. by Peak and Corbett [1.158].

Having quantified the forward reaction constant k_{\rightarrow} , it needs to quantify also the backward reaction constant k_{\leftarrow} . However, it is often not possible to derive the backward reaction constant from kinetic theories. Instead, one uses the fact that, in steady state, the forward and backward rates have to be equal so that $d\zeta_r/dt$ in (1.142) vanishes. This allows to write the backward reaction constant

$$k_{\leftarrow} = k_{\rightarrow} \cdot \left(\frac{\gamma_A \cdot \gamma_B}{\gamma_C} \cdot \frac{C_A \cdot C_B}{C_C} \right)_{\text{steady state}} \quad (1.160)$$

in terms of the forward reaction constant and the concentrations and activity coefficients in steady state. At least for ideally dilute solutions, the activity coefficients can be assumed to be unity and the fraction of the concentrations can be expressed via (1.133) in terms of thermodynamic and geometric parameters. For the temperature dependence of the backward reaction constant, k_{\leftarrow} will contribute with the enthalpy of diffusion of the faster-migrating reactant plus eventual reaction barriers, and $C_A \cdot C_B / C_C$ with the binding energy. The sum of these contributions, i. e. the barrier which has to be overcome thermally to dissociate the pair is usually called "dissociation energy." However, one has to be very careful with the interpretation of information given in the literature since dissociation energy is used sometimes also as a synonym for binding energy.

1.5.4 Diffusion-Reaction Equations

A totally rigorous physical model for the redistribution of defects in silicon does not exist and would probably be too complicated to be implemented into continuum-based process simulation programs. Among the various simplifications, the so-called methodology of diffusion-reaction equations was shown to be very efficient for the numerical simulation of diffusion phenomena. It was developed by Yoshida et al. [1.159] to describe the diffusion of phosphorus and can be generalized to design a set of coupled partial differential equations from some assumptions about possible reactions between intrinsic point defects and impurities. The intention of this section is that of a cookbook, enabling everybody in the end to create own diffusion models and to implement them into process simulation tools with generalized model interfaces.

A basic assumption of all diffusion-reaction schemes is that interactions between impurities and point defects lead to distinguishable defect configurations. Each of them is characterized by its diffusion coefficient and charge state. Substitutional impurities are generally assumed to be immobile. Interactions are approximated by binary reaction schemes as discussed above. Each possible charge state of a point defect and its possible reactions have to be considered individually at first. Charge states of intrinsic as well as of extrinsic point defects are assumed to result from binary reactions with charge carriers which are assumed to act as quasi-particles.

Development of a model starts with defining the point defects and complexes considered within the model and the possible reactions between them. As an example, the important case of the diffusion of substitutional impurities like dopants will be considered in the following. Basically all interactions between such substitutional impurity atoms M_s , interstitial impurity atoms M_i , vacancies V , and self-interstitials I fall into the three categories of reactions

- An interstitial impurity reacts with a vacancy and becomes substitutional according to the reaction



This so-called “Frank-Turnbull reaction” will be discussed in detail in Section 3.5. The reverse reaction is known also as “dissociative mechanism.”

- A self-interstitial displaces a substitutional impurity atom to an interstitial site according to the reaction



This so-called “kick-out reaction” will be discussed in detail in Section 3.6. The reverse reaction is known as “Watkins replacement mechanism.”

- A vacancy or self-interstitial forms a mobile pair with a substitutional impurity according to the reactions

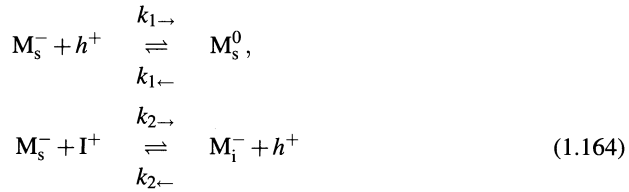


Such pair diffusion reactions will be discussed in detail in Section 3.4. A comparison of the pair reaction with self-interstitials and (1.162) shows that both reaction have the same structure. Since the atomistic form of the mobile complex is only of secondary importance in diffusion-reaction equations, only pair reaction with vacancies presents a complementary third reaction to the Frank-Turnbull reaction and the kick-out reaction.

Since charge has to be conserved in the reactions, electrons or holes may also appear at the right-hand sides of the reaction equations. The forward reaction constants of these equations are given by (1.149) when at least one of the reactants is electrically neutral. Otherwise, (1.150) has to be applied. Barriers in Gibbs free energy opposing recombination may be included as in

(1.155). In addition to reactions between extrinsic and intrinsic point defects, reactions between intrinsic point defects may be considered as outlined in Section 2.7.

As an example to demonstrate the methodology, without the intention to create a new diffusion model, negatively charged and neutral impurities on substitutional sites M_s^- and M_s^0 , negatively charged interstitial impurities M_i^- , and positively charged self-interstitials I^+ will be considered in the following. Their concentrations will be denoted by $C_{M_s^-}$, $C_{M_s^0}$, $C_{M_i^-}$, and C_{I^+} . The holes involved in the reactions will be symbolized by h^+ , their concentration by p . Between these species, following reactions are assumed:



For each of the point defects considered, a continuity equation (1.41) has to be provided. The diffusion current in an electrostatic field $E = -\text{grad}\psi$ results from (1.78). As before, the thermal voltage U_T will be used as abbreviation for $k \cdot T/q$. Reactions between the point defects determine the generation-loss terms of the continuity equations via (1.140). Since only binary reactions are considered, the dynamic law of mass action (1.142) simplifies considerably and the reaction constants can be estimated as discussed in Section 1.5.3. Then, since substitutional impurities are considered immobile, the reactions lead directly to

$$\frac{\partial C_{M_s^0}}{\partial t} = k_{1\rightarrow} \cdot C_{M_s^-} \cdot p - k_{1\leftarrow} \cdot C_{M_s^0} \quad (1.165)$$

$$\begin{aligned} \frac{\partial C_{M_s^-}}{\partial t} &= -k_{1\rightarrow} \cdot C_{M_s^-} \cdot p + k_{1\leftarrow} \cdot C_{M_s^0} \\ &\quad - k_{2\rightarrow} \cdot C_{M_s^-} \cdot C_{I^+} + k_{2\leftarrow} \cdot C_{M_i^-} \cdot p \end{aligned} \quad (1.166)$$

$$\begin{aligned} \frac{\partial C_{M_i^-}}{\partial t} &= \text{div} \left(D_{M_i^-} \cdot \text{grad} C_{M_i^-} - D_{M_i^-} \cdot C_{M_i^-} \cdot \text{grad}(\psi/U_T) \right) \\ &\quad + k_{2\rightarrow} \cdot C_{M_s^-} \cdot C_{I^+} - k_{2\leftarrow} \cdot C_{M_i^-} \cdot p \end{aligned} \quad (1.167)$$

$$\frac{\partial C_{I^+}}{\partial t} = \text{div} (D_{I^+} \cdot \text{grad} C_{I^+} + D_{I^+} \cdot C_{I^+} \cdot \text{grad}(\psi/U_T)) \quad (1.168)$$

$$- k_{2\rightarrow} \cdot C_{M_s^-} \cdot C_{I^+} + k_{2\leftarrow} \cdot C_{M_i^-} \cdot p \quad (1.169)$$

The same methodology will be used in Chapters 2 and 3 for the diffusion and recombination of intrinsic point defects and impurities, respectively. But, as mentioned already above, it should be kept in mind that point-defect-impurity pairs and interstitial impurity atoms considered here as individual point defects are just abstractions for the complicated interactions of intrinsic point defects and impurities. It should be noted that the inclusion of the hole concentration in the product $k_{2\leftarrow} \cdot C_{M_i^-} \cdot p$ is not mandatory. It serves just to keep $k_{2\leftarrow}$ Fermi-level-independent.

The resulting system of coupled partial differential equations can be solved directly with one of the general-purpose process simulation tools which became customary. But, in general, it is often desirable to reduce the numbers of equations, e. g. to understand the macroscopic behavior of the system. Due to the much higher mobility of charge carriers than of atoms, as discussed in the previous section, equilibrium between the charge states of a point defect will be established on a time scale on which concentration changes due to diffusion or reactions are negligible. This allows here to express $C_{M_s^-}$ in the form

$$C_{M_s^-} = \frac{k_{1\leftarrow}}{p \cdot k_{1\rightarrow} + k_{1\leftarrow}} \cdot C_{M_s} \quad (1.170)$$

via the total concentration $C_{M_s} = C_{M_s^0} + C_{M_s^-}$ of substitutional dopant atoms. The usage of p for the hole concentration implicitly restricts the validity of the equation to the applicability range of Boltzmann statistics. Otherwise, the product of activity coefficient and hole concentration $\gamma_p \cdot p$ has to be used which can be expressed in terms of the Fermi level via (1.99). For electrons, the respective product of activity coefficient and electron concentration is given by (1.98). The assumption of local equilibrium between the charge states allows then to combine (1.165) and (1.166) to one continuity equation in the form

$$\frac{\partial C_{M_s}}{\partial t} = \frac{\partial C_{M_s^0} + C_{M_s^-}}{\partial t} = -\frac{k_{1\leftarrow} \cdot k_{2\rightarrow}}{p \cdot k_{1\rightarrow} + k_{1\leftarrow}} \cdot C_{M_s} \cdot C_{I^+} + k_{2\leftarrow} \cdot C_{M_i^-} \cdot p. \quad (1.171)$$

All further simplifications are not straightforward. But a customary assumption valid at least for long diffusion times is that the mobile complexes and the substitutional atoms are also in local equilibrium. This allows to express the concentration of interstitial impurity atoms in the form

$$C_{M_i^-} = \frac{k_{1\leftarrow} \cdot k_{2\rightarrow} \cdot C_I \cdot C_M}{k_{2\leftarrow} \cdot p \cdot (p \cdot k_{1\rightarrow} + k_{1\leftarrow}) + k_{1\leftarrow} \cdot k_{2\rightarrow} \cdot C_I} = f(C_I, p, C_M) \quad (1.172)$$

via the total concentrations of impurities $C_M = C_{M_s} + C_{M_i^-}$ and self-interstitials $C_I = C_I^+$, and to combine (1.167) and (1.171) to a continuity equation in the form

$$\frac{\partial C_M}{\partial t} = \text{div} \left(D_{M_i^-} \cdot \text{grad} f(C_I, p, C_M) - D_{M_i^-} \cdot f(C_I, p, C_M) \cdot \text{grad}(\psi/U_T) \right). \quad (1.173)$$

Finally, all continuity equations for extrinsic point defects were combined to one non-linear diffusion equation for the total concentration. In fact, the physical assumptions contained implicitly in such macroscopic diffusion models and their range of validity can be made clear by comparison with diffusion-reaction models. Typical assumptions for the intrinsic point defects are equilibrium, a time-dependent but depth-independent oversaturation as for oxidation-enhanced diffusion, or even a function of space and time, as for implantation-enhanced diffusion. The last simplification often found in the literature for dopant diffusion is that the concentrations of mobile extrinsic complexes are much smaller than the concentration of substitutional atoms. This leads to a linearization of the function $f(C_I, p, C_M)$. It should be noted that this last simplification leads to a break-down of the resulting equation in all situations where point defects are present in large oversaturation.

The consequences of assuming local equilibrium between substitutional impurities and the corresponding mobile species can be seen in Figure 1.30. For the sake of simplicity, it was assumed that the self-interstitials maintain always their equilibrium value and that the charge-

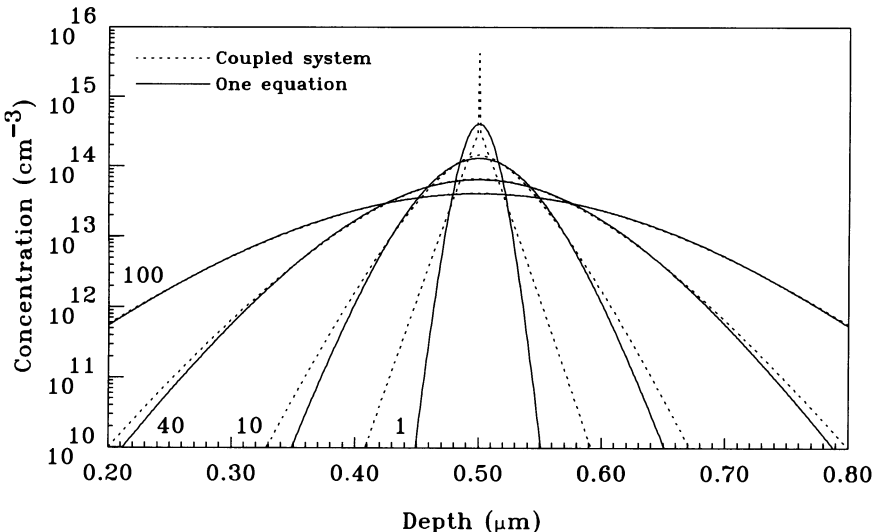


Figure 1.30: Diffusion of impurities from an initially delta-doped layer, simulated by diffusion equations for mobile species and substitutional species and under the assumption of local equilibrium between these species. The running index is the diffusion time in multiples of the time constant τ .

carrier concentrations correspond to the intrinsic concentration n_i . Then, the equations (1.171) and (1.167) can be rewritten in the form

$$\frac{\partial C_{M_s}}{\partial t} = -\frac{1}{\tau} \cdot (C_{M_s} - \alpha \cdot C_{M_i^-}) \quad (1.174)$$

$$\frac{\partial C_{M_i^-}}{\partial t} = \text{div}(D_{M_i^-} \cdot \text{grad}C_{M_i^-}) - \frac{\partial C_{M_s}}{\partial t} \quad (1.175)$$

with the time constant τ given by

$$\tau = \frac{n_i \cdot k_{1\rightarrow} + k_{1\leftarrow}}{k_{1\leftarrow} \cdot k_{2\rightarrow} \cdot C_{I^+}^{eq}}. \quad (1.176)$$

The parameter α was introduced as an abbreviation for the ratio of the concentrations of substitutional impurities and interstitial impurities in equilibrium. For Figure 1.30, a value of $\alpha = 1000$ was assumed and the diffusion coefficient of the interstitial impurities was chosen in a way that the macroscopic projected diffusion length for the time τ equals $\sqrt{2 \cdot D_{M_i^-} \cdot \tau / \alpha} = 10 \text{ nm}$. A detailed analysis given by Cowern et al. [1.160] shows that t/τ is the mean number of diffusion events per atom within the time t , τ/α is the mean time an impurity stays in the mobile state, and $\lambda = \sqrt{D_{M_i^-} \cdot \tau / \alpha}$ the mean projected path length the impurity migrates while it is mobile. Combining the two continuity equations (1.174) and (1.175) under the assumption of local equilibrium leads to Fick's second law (1.43) with the diffusion coefficient corresponding to $D_{M_i^-}/\alpha$. Simulations based on this combined equation give always Gaussian profiles, as discussed in Section 1.3.1. For sufficiently long times, these solutions agree with what is obtained by solving the coupled system (1.174) and (1.175). But for times around τ , the contrast is apparent: The delta-doped layer has not completely dissolved and the impurity profile has typical flanks which decrease exponentially with the distance from the delta-doped layer. As a

résumé, the assumption of local equilibrium is a valuable method to reduce the necessary computer resources for process times well above the respective time constant. But it is inadmissible for short-time processes.

In addition to the simple reactions between intrinsic and extrinsic point defects, reactions between extrinsic point defects have to be considered at high concentrations. Typical examples are the formation of ion pairs, i. e. complexes of a donor and an acceptor impurity at adjacent lattice sites (see Section 5.2), or of clusters of intrinsic point defects or impurities of the same kind (see Sections 2.7.3 and 5.1). Ion pairing and the formation of a cluster of two impurities can be incorporated straightforwardly into the diffusion-reaction approach via binary reactions of e. g. a mobile donor complex and a substitutional acceptor ion in case of the ion pair. Clusters with a higher number of atoms can be included, in principle, by considering the complete chain of cluster sizes up to the largest one. Their evolution with time is then determined by a system of binary reactions. But the expenses in terms of computer resources are considerable and they are usually inadmissible for precipitates which may consist of thousands of intrinsic point defects or impurity atoms. Therefore, the *ad-hoc* formation of extended defects or clusters of a certain size is often assumed and formulated as reaction. While this is certainly a possible simplification, it has to be noted that the absolute values of the forward and backward rate constants can no longer be derived from kinetic considerations. Their ratio, on the other hand, is still determined by the law of mass action.

Diffusion-reaction schemes fail when the impurity concentration exceeds about $2 \cdot 10^{20} \text{ cm}^{-3}$. For such concentrations, sharp increases of the diffusivities of germanium, tin, arsenic, and antimony were reported (see Sections 4.2.3, 4.3.3, 5.9.3, and 5.10.3). Following the suggestion of Mathiot and Pfister [1.161], they are usually interpreted within the percolation theory of Stauffer [1.162] to arise from the proximity of the dopant atoms which reduces the formation and migration enthalpies of vacancies in their vicinity and which leads to an enhanced diffusion of dopants within the percolation cluster.

1.6 Exchange of Matter Between Phases

Although this monograph is devoted to diffusion phenomena in crystalline silicon, it is nevertheless necessary to mention that the crystalline phase coexists in all real devices with other phases. A phase in a general sense is a homogeneous quantity of matter with a specific stoichiometry and structure which differs in any of the properties from matter in neighboring volumes. Impurities and low-dimensional defects are not considered in this definition as long as their concentration is comparatively small. Of the fundamental phases, only the solid and the liquid phase are usually important. They coexist during crystal growth but also during laser annealing with sufficient energy. An other typical example of a phase differing only in structure is the amorphous phase which can be formed by deposition or the implantation of crystalline materials with sufficient doses of heavy ions. Phases involving other elements are commonly used for isolation and interconnects and include silicon dioxide, oxynitrides, high-k or low-k dielectrics, silicides, or metals. Finally, phases related to impurities may also form in single-crystalline silicon when their solid solubility is exceeded.

When a system composes of adjacent phases, the species involved will redistribute in such a way that, in equilibrium, their chemical potentials in both phases are equal. The continuity of the chemical potential may imply discontinuities of the concentration of the respective species at the boundaries between the phases. Such discontinuities are characterized for each species

i by the distribution coefficient $k_{i,\alpha/\beta}$ defined as the ratio of the respective mole fractions (or atomic fractions) in the adjacent phases denoted by the additional subscripts ' α ' and ' β '

$$k_{i,\alpha/\beta} = \frac{x_{i,\alpha}^m}{x_{i,\beta}^m}, \quad (1.177)$$

or by the segregation coefficient $m_{i,\alpha/\beta}$ defined as ratio of the respective concentrations

$$m_{i,\alpha/\beta} = \frac{C_{i,\alpha}}{C_{i,\beta}}. \quad (1.178)$$

This nomenclature is in agreement with the majority of the publications. It has to be mentioned, though, that in some publications, the assignment of terms (distribution and segregation coefficient) can be found also *vice versa*. Both parameters lump properties of the materials involved. In silicon, the species considered may exist in various charge states which introduces an influence of the Fermi level. But, at first, such effects are ignored and only the distribution of electrically neutral species will be discussed.

Closely connected with segregation is the solid solubility of impurities. When impurities are added to silicon at a given temperature, the concentration finally reaches a point where the formation of a second phase is favored energetically. In thermal equilibrium, the interface between the two phases will be flat and the concentration in the silicon saturates at the so-called "solubility concentration" or "solid solubility". All additionally added impurities lead to the growth of the newly formed phase only. Below the eutectic temperature, the newly formed phase is either a silicon-rich silicide or, when a silicide does not exist, a pure impurity phase. Above the eutectic temperature, the newly formed phase will be a liquid impurity phase saturated with silicon. In thermal equilibrium, the concentrations of silicon and of the other impurity in both phases are related to each other by the respective segregation coefficients. Dynamically, the formation of a new phase occurs via nucleation and growth of precipitates.

The concept of thermal equilibrium in a system of electrically neutral species requires that the chemical potential of each species involved is constant in the system, i. e. equal in adjacent phases. Using the relation of classical thermodynamics (1.95) for the chemical potential, one obtains

$$\mu_{i,\alpha}^* + k \cdot T \cdot \ln(\gamma_{i,\alpha} \cdot x_{i,\alpha}^m) = \mu_{i,\beta}^* + k \cdot T \cdot \ln(\gamma_{i,\beta} \cdot x_{i,\beta}^m) \quad (1.179)$$

as condition for thermal equilibrium. The symbols γ , x^m , and μ^* denote the activity coefficients, mole fractions, and standard chemical potentials of the species under consideration in the respective phases. From (1.179), the distribution coefficient can be expressed as

$$k_{i,\alpha/\beta} = \frac{x_{i,\alpha}}{x_{i,\beta}} = \frac{\gamma_{i,\beta}}{\gamma_{i,\alpha}} \cdot \exp\left(\frac{\mu_{i,\beta}^* - \mu_{i,\alpha}^*}{k \cdot T}\right). \quad (1.180)$$

In pure substances ($x_i^m = 1$), as outlined in Section 1.4.1, the respective activity coefficients γ_i approaches unity. For ideally dilute concentrations ($x_i^m \ll 1$), the activity coefficients are expected not to depend on the concentration.

When both phases are solid, the standard chemical potentials are identical, and the distribution coefficient corresponds to the inverse ratio

$$k_{i,\alpha/\beta} = \frac{x_{i,\alpha}}{x_{i,\beta}} = \frac{\gamma_{i,\beta}}{\gamma_{i,\alpha}} \quad (1.181)$$

of the activity coefficients in the phases. To characterize the temperature dependence of activity coefficients, the partial atomic excess enthalpy \bar{H}_i^E and entropy \bar{S}_i^E are usually introduced in the form

$$k \cdot T \cdot \ln(\gamma_i) = \bar{H}_i^E - T \cdot \bar{S}_i^E. \quad (1.182)$$

In principal, the activity coefficients depend also on concentration. But in silicon, the atomic fractions of impurities are always much smaller than unity so that the activity coefficient of silicon atoms is unity and the activity coefficients of impurities are independent of their concentration. In silicide phases, the atomic fractions of impurities and silicon atoms are constant and so are their activity coefficients. Pure impurity phases are characterized by a low equilibrium concentration of silicon so that the activity coefficient of the impurity approaches unity and that of silicon should only weakly depend on concentration. In summary, solid solubility concentrations of impurities in silicon in equilibrium with a solid impurity phase should follow Arrhenius relations closely.

The other important case of a binary system is a solid, single-crystalline silicon phase (additional subscript 's') in equilibrium with a liquid phase (additional subscript 'l'). Evaluation of the distribution coefficients can be based again on (1.180). It has to be reminded, though, that $\mu_{i,l}^* - \mu_{i,s}^*$ is the difference in the standard state of the chemical potentials of species i in its pure liquid and solid phases and will not vanish here. Under the assumption that the heat capacities of the pure liquid and solid phases are nearly identical, this difference can be written in the form [1.163–1.165]

$$\mu_{i,l}^* - \mu_{i,s}^* = \Delta\bar{S}_i^m \cdot (T_i^m - T) = \Delta\bar{H}_i^m - T \cdot \Delta\bar{S}_i^m. \quad (1.183)$$

Therein, $\Delta\bar{H}_i^m = \Delta\bar{S}_i^m \cdot T_i^m$, $\Delta\bar{S}_i^m$, and T_i^m represent the atomic enthalpy of fusion, the atomic entropy of fusion, and the melting point of the pure species i , respectively. For silicon, the atomic enthalpy and entropy of fusion, and the melting point are 0.525 eV, 3.63 · k , and 1683 K, respectively. The activity coefficient in the solid phase can be expressed again in terms of the partial atomic excess enthalpy and entropy (1.182). Variations of the activity coefficient in the liquid phase are generally assumed to arise predominantly from their composition dependence. Following the work of Buff and Schindler [1.166], Thurmond and Kowalchik [1.167] suggested that the activity coefficient $\gamma_{Si,l}$ of silicon atoms in the liquid can be approximated sufficiently well in the form

$$k \cdot T \cdot \ln(\gamma_{Si,l}) = (a - b \cdot T) \cdot (1 - x_{Si,l}^m)^2. \quad (1.184)$$

The parameters a and b depend on the second species in the system and were tabulated by Thurmond and Kowalchik [1.167] and Weber [1.165] for various impurities. In the silicon crystal, the atomic fraction of silicon atoms and their activity coefficient is basically unity ($x_{Si,s}^m \approx 1$, $\gamma_{Si,s}^m \approx 1$). With this information and (1.184), the liquidus curve, i. e. the atomic fraction $x_{Si,l}^m$ of silicon atoms in the melt follows from (1.180) with the difference in standard chemical potentials given by (1.183). Assuming that the relation applies at all temperatures and compositions, the Gibbs-Duhem relationship (1.101) can be integrated at constant temperature and pressure [1.168, 1.169] to obtain the activity coefficient of the second component i in the liquid phase as

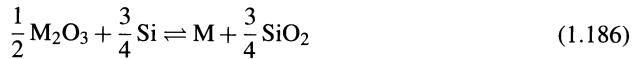
$$k \cdot T \cdot \ln(\gamma_{i,l}) = (a - b \cdot T) \cdot (1 - x_{i,l}^m)^2 \quad (1.185)$$

with the same values of a and b as in (1.184). Given the atomic fraction of the impurity i in the melt $x_{i,l}^m = 1 - x_{Si,l}^m$, the solid solubility of the impurity in the silicon follows from a combination of the equations (1.180), (1.182), (1.183), and (1.185).

Up to now, the discussion was restricted to neutral impurities. The effects of ionized impurities being present has been investigated in detail by Reiss [1.170] and Thurmond [1.171].

Ionization can be included in the previous considerations by noting that, in equilibrium, the ionized impurities have to be in equilibrium with the neutral ones which, in turn, are in equilibrium with the neutral impurities in the other phase. Thus, the discussion of charge effects can be carried out individually for each phase. In phases without band gap or with a large band gap, charged impurities are generally assumed not to play an important role. In a crystalline silicon phase, the ratio of the atomic fractions of neutral and total impurities $x_{i(0)}^m/x_{i(T)}^m$ can be obtained from (1.3) and (1.4) for donors and acceptors, respectively. Then, the distribution coefficient depends on the Fermi level E_F which itself depends implicitly on the concentration of ionized impurities in the silicon (cf. Section 1.2). A direct consequence is the observation of Reiss and Fuller [1.172] that the solubility of the donor lithium in germanium was increased in the presence of the acceptor boron and decreased in presence of the donor arsenic. Similar effects were observed by Kuhlmann et al. [1.173] for aluminum in silicon. They found that its solubility is reduced in a boron background and increased in a phosphorus background. In a system with donors and acceptors being present at the same time, the formation of ion pairs has eventually to be taken into consideration, too.

Technologically important is the distribution of impurities between silicon and oxide glass layers. Thurmond [1.171] argued that impurities (M) will dissolve as oxides in the silicon dioxide films. Except of phosphorus (P_2O_5) and antimony (SbO_2), these oxides were assumed to be of the form M_2O_3 for group III and V impurities. The exchange of impurities M between the silicon dioxide phase and the single-crystalline silicon phase was proposed to be represented by following reaction



occurring at the interface. From this reaction, the distribution coefficient can be obtained as

$$k_{M,s/gl} = \frac{x_{M,s}^m}{x_{MO_{1.5},gl}^m} = \frac{\gamma_{MO_{1.5},gl}}{\gamma_{M,s}} \cdot \exp\left(-\frac{\frac{3}{4} \cdot \bar{G}_{SiO_2}^f - \frac{1}{2} \cdot \bar{G}_{M_2O_3}^f}{k \cdot T}\right). \quad (1.187)$$

The symbols $\gamma_{MO_{1.5},gl}$ and $\gamma_{M,s}$ stand for the activity coefficients of M in the SiO_2 and in crystalline silicon, respectively. $\bar{G}_{SiO_2}^f$ and $\bar{G}_{M_2O_3}^f$ denote the formation energies of SiO_2 and M_2O_3 , i. e. the changes in the Gibbs free energy upon formation of one molecule of respectively SiO_2 or M_2O_3 from the standard states. Qualitative estimations by Thurmond [1.171] and Fair and Tsai [1.174] resulted in values very much smaller than unity for aluminum, around unity for boron, and very much larger than unity for gallium, indium, phosphorus, arsenic, and antimony.

Up to now, the conditions discussed related to thermal equilibrium. However, diffusion of many impurities in solids is so slow that thermal equilibrium is basically never attained. Therefore, dynamical models were developed to describe segregation effects locally at phase boundaries in the form of interface conditions for the diffusion equations describing redistribution within the phases. After sufficiently long times, predictions of these dynamical models obviously have to coincide with models based on thermal equilibrium.

The most simple form of an interface condition for the diffusion equations in the adjacent phases α and β was introduced by Grove et al. [1.175]. It assumes that the concentrations at both sides of an interface are locally always in equilibrium. This equilibrium is characterized by the segregation coefficient $m_{\alpha/\beta}$ defined by (1.178). Although such an interface condition can be implemented numerically in a straightforward way, one has to make sure that mass conservation is obeyed in all situations in which the segregation coefficient changes. This applies, e. g. to the onset of diffusion when the initial condition does not satisfy (1.178) as well as during ramping steps where the segregation coefficient changes with temperature and, consequently, time.

The next higher level of sophistication is represented by a first-order kinetic model as introduced by Antoniadis et al. [1.176]. In this model, the segregation flux of impurities from phase α to phase β via the interface is described by

$$J_s = h_{\alpha \rightarrow \beta} \cdot (C^\alpha - C^\beta \cdot m_{\alpha/\beta}). \quad (1.188)$$

For the sake of simplicity, in this and the remaining formulae in this chapter, the subindex i for the species has been omitted. Please note further that the transport coefficient $h_{\alpha \rightarrow \beta}$ depends on the association of α and β with the respective phases. Thus, the mass transport coefficient $h_{\alpha \rightarrow \beta}$ from phase α to phase β and $h_{\beta \rightarrow \alpha}$ from phase β to phase α correspond only for $m_{\alpha/\beta} = 1$.

A third model suggested in the literature is inspired by experimental observations that impurities accumulate at interfaces. At grain boundaries, such phenomena were known since long. But Johannessen et al. [1.177] and Schwarz et al. [1.178] reported also that phosphorus piles up within 5 nm of the interface between silicon and silicon dioxide with a peak concentration exceeding the bulk concentration by one order of magnitude. This pile-up was observed even after anneals in inert atmosphere so that it has to be seen as an equilibrium property of the interface. Such phenomena will be referred to as “interface segregation” in the following in contrast to “bulk segregation” which will be used to denote concentration differences from one interior of a phase to the interior of an adjacent phase. To include interface segregation in the system polysilicon/silicon, Lau, Orlowski and coworkers [1.179, 1.180] introduced an interface layer at which atoms may be trapped and emitted into one of the two adjacent phases. A current drawback of the three-phase model is that experimentally determined parameters for the absorption and emission coefficients were not reported together with the model or in any other publication.

Finally, You et al. [1.181] suggested a model in which adjacent phases are no longer treated separately. Instead, a reference concentration $C_{ref}(x)$ is defined which reflects the distribution of impurities in thermal equilibrium. On the basis of the theory of irreversible thermodynamics, the authors derived a so-called “diffusion-segregation equation” in the form

$$J = -D \cdot C_{ref} \cdot \text{grad} \frac{C}{C_{ref}} = -D \cdot \left(\text{grad}C - \frac{C}{C_{ref}} \cdot \text{grad}C_{ref} \right) \quad (1.189)$$

as a generalization of Fick’s first law (1.38). Comparing their model to earlier segregation models, Tan et al. [1.182] claimed that the mass transport coefficient h in the flux-limited segregation model (1.188) and the emission and absorption rates in the three-phase boundary model have no physical meaning and depend on computational grid size. But this statement results from overrating a mathematical formalism and ignores clearly the atomistic nature of solids.

Bibliography

- [1.1] J. Z. Hu, L. D. Merkle, C. S. Menoni, and I. L. Spain, “Crystal Data for High-Pressure Phases of Silicon,” *Phys. Rev. B*, vol. 34, no. 7, 4679–4684 (1987).
- [1.2] A. Smakula and J. Kalnajs, “Precision Determination of Lattice Constants with a Geiger-Counter X-Ray Diffractometer,” *Phys. Rev.*, vol. 99, no. 6, 1737–1743 (1955).
- [1.3] K. Ohsaka, S. K. Chung, W. K. Rhim, and J. C. Holzer, “Densities of Si Determined by an Image Digitizing Technique in Combination with an Electrostatic Levitator,” *Appl. Phys. Lett.*, vol. 70, no. 4, 423–425 (1997).
- [1.4] P. P. Ewald, “Tagung des erweiterten Tabellenkomitees in Zürich, 28.-31. Juli 1930,” *Z. Kristallogr.*, vol. 75, 159–160 (1930).
- [1.5] C. Hermann, “Zur systematischen Strukturtheorie. IV. Untergruppen,” *Z. Kristallogr.*, vol. 69, 533–555 (1929).

- [1.6] C. Mauguin, “Sur le symbolisme des groupes de répétition ou de symétrie des assemblages cristallins,” *Z. Kristallogr.*, vol. 76, 542–558 (1931).
- [1.7] A. Schoenflies, *Krystallsysteme und Krystallstructur*, Leipzig: Teubner (1891).
- [1.8] W. Shockley, *Electrons and Holes in Semiconductors*, New York: Van Nostrand (1951).
- [1.9] S. M. Sze, *Physics of Semiconductor Devices*, John Wiley & Sons, second ed. (1981).
- [1.10] S. Selberherr, *Analysis and Simulation of Semiconductor Devices*, Vienna: Springer (1984).
- [1.11] P. W. Anderson, “Model for the Electronic Structure of Amorphous Semiconductors,” *Phys. Rev. Lett.*, vol. 34, no. 15, 953–955 (1975).
- [1.12] H. A. Jahn and E. Teller, “Stability of Polyatomic Molecules in Degenerate Electronic States. I — Orbital Degeneracy,” *Proc. Roy. Soc. Lond. A*, vol. 161, 220–235 (1937).
- [1.13] M. D. Sturge, “The Jahn-Teller Effect in Solids,” *Solid State Physics*, vol. 20, 91–211 (1967).
- [1.14] S. M. Hu, “Diffusion in Silicon and Germanium,” in: *Atomic Diffusion in Semiconductors*, edited by D. Shaw, London: Plenum Press, 217–350 (1973).
- [1.15] A. F. W. Willoughby, “Anomalous Diffusion Effects in Silicon (A Review),” *Journal of Materials Science*, vol. 3, 89–98 (1968).
- [1.16] W. Nuyts and R. Van Overstraeten, “Computer Calculations of Impurity Profiles in Silicon (I),” *phys. stat. sol. (a)*, vol. 15, 329–341 (1973).
- [1.17] R. K. Jain and R. J. Van Overstraeten, “Theoretical Calculations of the Fermi Level and of Other Parameters in Phosphorus Doped Silicon at Diffusion Temperatures,” *IEEE Trans. Electron Devices*, vol. ED-21, no. 2, 155–165 (1974).
- [1.18] R. K. Jain and R. J. Van Overstraeten, “Accurate Theoretical Arsenic Diffusion Profiles in Silicon from Processing Data,” *J. Electrochem. Soc.*, vol. 122, no. 4, 552–557 (1975).
- [1.19] P. T. Landsberg and S. A. Hope, “Diffusion Currents in Semiconductors,” *Solid-State Electronics*, vol. 19, 173–174 (1976).
- [1.20] R. Shrivastava and A. H. Marshak, “A Model for Diffusion of Arsenic in Degenerate Silicon,” *J. Appl. Phys.*, vol. 51, no. 6, 3222–3229 (1980).
- [1.21] R. A. Abram, G. J. Rees, and B. L. H. Wilson, “Heavily Doped Semiconductors and Devices,” *Advances in Physics*, vol. 27, no. 6, 799–892 (1978).
- [1.22] D. S. Lee and J. G. Fossum, “Energy-Band Distortion in Highly Doped Silicon,” *IEEE Trans. Electron Devices*, vol. ED-30, no. 6, 626–634 (1983).
- [1.23] H. P. D. Lanyon and R. A. Tuft, “Bandgap Narrowing in Moderately to Heavily Doped Silicon,” *IEEE Trans. Electron Devices*, vol. ED-26, no. 7, 1014–1018 (1979).
- [1.24] G. D. Mahan, “Energy Gap in Si and Ge: Impurity Dependence,” *J. Appl. Phys.*, vol. 51, no. 5, 2634–2646 (1980).
- [1.25] W. Kuzmicz, “Ionization of Impurities in Silicon,” *Solid-State Electronics*, vol. 29, no. 12, 1223–1227 (1986).
- [1.26] A. Schenk, “Finite-Temperature Full Random-Phase Approximation Model of Band Gap Narrowing for Silicon Device Simulation,” *J. Appl. Phys.*, vol. 84, no. 7, 3684–3695 (1998).
- [1.27] E. O. Kane, “Thomas-Fermi Approach to Impure Semiconductor Band Structure,” *Phys. Rev.*, vol. 131, no. 1, 79–88 (1963).
- [1.28] T. F. Lee, R. D. Pashley, T. C. McGill, and J. W. Mayer, “Investigation of Tellurium-Implanted Silicon,” *J. Appl. Phys.*, vol. 46, no. 1, 381–388 (1975).
- [1.29] P. Van Mieghem, S. Decoutere, G. Borghs, and R. Mertens, “Influence of Majority Carrier Bandtails on the Performance of Semiconductor Devices,” *Solid-State Electronics*, vol. 35, no. 5, 699–704 (1992).
- [1.30] T. N. Morgan, “Broadening of Impurity Bands in Heavily Doped Semiconductors,” *Phys. Rev.*, vol. 139, no. 1A, A343–A348 (1965).
- [1.31] J. W. Slotboom and H. C. de Graaff, “Measurements of Bandgap Narrowing in Silicon Bipolar Transistors,” *Solid-State Electronics*, vol. 19, 857–862 (1976).

- [1.32] D. B. M. Klaassen, J. W. Slotboom, and H. C. de Graaff, “Unified Apparent Bandgap Narrowing in *n*- and *p*-Type Silicon,” *Solid-State Electronics*, vol. 35, no. 2, 125–129 (1992).
- [1.33] C. M. Van Vliet, “Bandgap Narrowing and Emitter Efficiency in Heavily Doped Emitter Structures Revisited,” *IEEE Trans. Electron Devices*, vol. 40, no. 6, 1140–1147 (1993).
- [1.34] M. Y. L. Jung, R. Gunawan, R. D. Braatz, and E. G. Seebauer, “New Physics for Modeling Transient Enhanced Diffusion in RTP,” in: *Rapid Thermal and Other Short-Time Processing Technologies*, edited by F. Roozeboom, M. C. Öztürk, J. C. Gelpey, K. G. Reid, and D.-L. Kwong, *Electrochem. Soc. Proc.*, vol. 2000-9, 15–20 (2000).
- [1.35] R. Shrivastava and A. H. Marshak, “Charge Neutrality and the Internal Electric Field Produced by Impurity Diffusion,” *Solid-State Electronics*, vol. 23, 73–74 (1980).
- [1.36] W. Jüngling, P. Pichler, S. Selberherr, E. Guerrero, and H. W. Pötzl, “Simulation of Critical IC Fabrication Processes Using Advanced Physical and Numerical Methods,” *IEEE Trans. Electron Devices*, vol. ED-32, no. 2, 156–167 (1985).
- [1.37] P. Pichler, W. Jüngling, S. Selberherr, and H. Pötzl, “Two-Dimensional Coupled Diffusion Modeling,” in: *Solid State Devices 1984*, edited by J. P. Noblanc and J. Zimmermann, *Phyica*, vol. 129B, 187–191 (1985).
- [1.38] A. Buonomo and C. Di Bello, “Some Remarks About the Use of the Charge-Neutrality Approximation in the Simulation of Diffusion Processes,” *IEEE Trans. Electron Devices*, vol. 40, no. 5, 885–889 (1993).
- [1.39] M. A. Green, “Intrinsic Concentration, Effective Densities of State, and Effective Mass in Silicon,” *J. Appl. Phys.*, vol. 67, no. 6, 2944–2954 (1990).
- [1.40] F. J. Morin and J. P. Maita, “Electrical Properties of Silicon Containing Arsenic and Boron,” *Phys. Rev.*, vol. 96, no. 1, 28–35 (1954).
- [1.41] G. P. Barbuscia, G. Chin, R. W. Dutton, T. Alvarez, and L. Arledge, “Modeling of Polysilicon Dopant Diffusion for Shallow-Junction Bipolar Transistors,” in: *Technical Digest of the 1984 International Electron Devices Meeting (IEDM)*, New York: IEEE, 757–760 (1984).
- [1.42] G. G. Macfarlane, T. P. McLean, J. E. Quarrington, and V. Roberts, “Fine Structure in the Absorption-Edge Spectrum of Si,” *Phys. Rev.*, vol. 111, no. 5, 1245–1254 (1958).
- [1.43] Y. P. Varshni, “Temperature Dependence of the Energy Gap in Semiconductors,” *Physica*, vol. 34, 149–154 (1967).
- [1.44] C. D. Thurmond, “The Standard Thermodynamic Functions for the Formation of Electrons and Holes in Ge, Si, GaAs, and GaP,” *J. Electrochem. Soc.*, vol. 122, no. 8, 1133–1141 (1975).
- [1.45] J. T. Milek, *Silicon Nitride for Microelectronics Applications, Handbook of Electronic Materials*, vol. 3, New York: IFI/Plenum (1971).
- [1.46] R. Car and M. Parrinello, “Unified Approach for Molecular Dynamics and Density-Functional Theory,” *Phys. Rev. Lett.*, vol. 55, no. 22, 2471–2474 (1985).
- [1.47] G. H. Gilmer, T. Diaz de la Rubia, D. M. Stock, and M. Jaraiz, “Diffusion and Interactions of Point Defects in Silicon: Molecular Dynamics Simulations,” in: *Computer Simulation of Radiation Effects in Solids*, edited by T. Diaz de la Rubia, G. H. Gilmer, and M.-J. Caturla, *Nuclear Instruments and Methods in Physics Research B*, vol. 102, 247–255 (1995).
- [1.48] T. Diaz de la Rubia, “Irradiation-Induced Defect Production in Elemental Metals and Semiconductors: A Review of Recent Molecular Dynamics Studies,” *Ann. Rev. Mater. Sci.*, vol. 26, 613–649 (1996).
- [1.49] M. M. Bunea and S. T. Dunham, “3D Atomistic Simulations of Submicron Device Fabrication,” in: *Semiconductor Process and Device Performance Modelling*, edited by S. T. Dunham and J. S. Nelson, *Mat. Res. Soc. Symp. Proc.*, vol. 490, 3–8 (1998).
- [1.50] M. Jaraiz, P. Castrillo, R. Pinacho, L. Pelaz, J. Barbolla, G. H. Gilmer, and C. S. Rafferty, “Atomistic Modeling of Complex Silicon Processing Scenarios,” in: *Si Front-End Processing — Physics and Technology of Dopant-Defect Interactions II*, edited by A. Agarwal, L. Pelaz, H.-H. Vuong, P. Packan, and M. Kase, *Mat. Res. Soc. Symp. Proc.*, vol. 610, B11.1.1–B11.1.7 (2000).

- [1.51] M. Hane, T. Ikezawa, K. Takeuchi, and G. H. Gilmer, “Monte Carlo Impurity Diffusion Simulation Considering Charged Species for Low Thermal Budget Sub-50nm CMOS Process Modeling,” in: *Technical Digest of the 2001 International Electron Devices Meeting (IEDM)*, Piscataway: IEEE, 843–846 (2001).
- [1.52] A. Fick, “Über Diffusion,” *Annalen der Physik und Chemie von Poggendorff*, vol. 94(170), 59–86 (1855).
- [1.53] L. Boltzmann, “Zur Integration der Diffusionsgleichung bei variablen Diffusionscoefficienten,” *Annalen der Physik und Chemie*, vol. 53, 959–964 (1894).
- [1.54] S. Arrhenius, “Über die Reaktionsgeschwindigkeit bei der Inversion von Rohrzucker durch Säuren,” *Z. Phys. Chem.*, vol. 4, 226–248 (1889).
- [1.55] H. S. Carslaw and J. C. Jaeger, *Conduction of Heat in Solids*, Oxford: Clarendon Press (1959).
- [1.56] A. M. Smith, “Diffusion,” in: *Fundamentals of Silicon Integrated Device Technology, Vol. I, Section II*, edited by R. M. Burger and R. P. Donovan, Englewood Cliffs: Prentice-Hall, 183–345 (1967).
- [1.57] J. Crank, *The Mathematics of Diffusion*, Oxford: Clarendon Press (1975).
- [1.58] S. Chandrasekhar, “Stochastic Problems in Physics and Astronomy,” *Reviews of Modern Physics*, vol. 15, no. 1, 1–89 (1943).
- [1.59] A. Einstein, “Über die von der molekularkinetischen Theorie der Wärme geforderte Bewegung von in ruhenden Flüssigkeiten suspendierten Teilchen,” *Annalen der Physik*, vol. 17, 549–560 (1905).
- [1.60] J. R. Manning, *Diffusion Kinetics for Atoms in Crystals*, Princeton: Van Nostrand (1968).
- [1.61] C. Zener, “Theory of Diffusion,” in: *Imperfections in Nearly Perfect Crystals*, edited by W. Shockley, J. H. Hollomon, R. Maurer, and F. Seitz, New York: John Wiley & Sons, 289–314 (1952).
- [1.62] C. Zener, “Theory of D_0 for Atomic Diffusion in Metals,” *J. Appl. Phys.*, vol. 22, no. 4, 372–375 (1951).
- [1.63] G. H. Vineyard, “Frequency Factors and Isotope Effects in Solid State Rate Processes,” *J. Phys. Chem. Solids*, vol. 3, 121–127 (1957).
- [1.64] S. A. Rice, “Dynamic Theory of Diffusion in Crystals,” *Phys. Rev.*, vol. 112, no. 3, 804–811 (1958).
- [1.65] C. P. Flynn, “Atomic Migration in Monatomic Crystals,” *Phys. Rev.*, vol. 171, no. 3, 682–698 (1968).
- [1.66] H.-M. Kagaya, T. Soma, and M. R. Brozel, “Specific Heats of c-Si and Molten Si,” in: *Properties of Crystalline Silicon*, edited by R. Hull, *EMIS Datareviews Series*, no. 20, London: INSPEC, 151–152 (1999).
- [1.67] R. Car, P. Blöchl, and E. Smargiassi, “Ab-Initio Molecular Dynamics of Semiconductor Defects,” in: *Defects in Semiconductors 16*, edited by G. Davies, G. G. DeLeo, and M. Stavola, *Materials Science Forum*, vol. 83–87, 433–446 (1992).
- [1.68] W. Nernst, “Zur Kinetik der in Lösung befindlichen Körper,” *Z. Phys. Chem.*, vol. 2, 613–637 (1888).
- [1.69] C. Wagner, “Über den Zusammenhang zwischen Ionenbeweglichkeit und Diffusionsgeschwindigkeit in festen Salzen,” *Z. Phys. Chem. B*, vol. 11, 139–151 (1931).
- [1.70] P. T. Landsberg, “On the Diffusion Theory of Rectification,” *Proc. Roy. Soc. Lond. A*, vol. 213, 226–237 (1952).
- [1.71] K. M. van Vliet and A. H. Marshak, “Conduction Current and Generalized Einstein Relations for Degenerate Semiconductors and Metals,” *phys. stat. sol. (b)*, vol. 78, 501–517 (1976).
- [1.72] J. C. Bourgoin, J. W. Corbett, and H. L. Frisch, “Ionization Enhanced Diffusion,” *J. Chem. Phys.*, vol. 59, no. 8, 4042–4046 (1973).
- [1.73] J. D. Weeks, J. C. Tully, and L. C. Kimerling, “Theory of Recombination-Enhanced Defect Reactions in Semiconductors,” *Phys. Rev. B*, vol. 12, no. 8, 3286–3292 (1975).

- [1.74] J. Bourgoin and J. W. Corbett, “Ionization Effects on Impurity and Defect Migration in Semiconductors,” in: *Lattice Defects in Semiconductors, 1974, Inst. Phys. Conf. Ser.*, no. 23, 149–163 (1975).
- [1.75] P. J. Dean and W. J. Choyke, “Recombination-Enhanced Defect Reactions — Strong New Evidence for an Old Concept in Semiconductors,” *Advances in Physics*, vol. 26, no. 1, 1–30 (1977).
- [1.76] A. M. Stoneham, “Non-Radiative Processes in Insulators and Semiconductors,” *Phil. Mag.*, vol. 36, no. 4, 983–997 (1977).
- [1.77] L. C. Kimerling, “Recombination Enhanced Defect Reactions,” *Solid-State Electronics*, vol. 21, 1391–1401 (1978).
- [1.78] H. Sumi, “Carrier-Density Dependence of Dynamic Multiphonon Nonradiative Recombination through Deep Levels in Semiconductors,” in: *Proceedings of the 12th International Conference on Defects in Semiconductors*, edited by C. A. J. Ammerlaan, *Physica*, vol. 116B, 39–44 (1983).
- [1.79] J. C. Bourgoin and J. W. Corbett, “Enhanced Diffusion Mechanisms,” *Radiation Effects*, vol. 36, 157–188 (1978).
- [1.80] G. D. Watkins, “The Interaction of Irradiation-Produced Defects with Impurities and Other Defects in Semiconductors EPR Studies in Silicon,” in: *Colloque international sur l'action des rayonnements sur les composants à semiconducteurs*, edited by F. Cambou, C. Fert, and J. Lagasse, A1/1–13 (1967).
- [1.81] J. C. Bourgoin and J. W. Corbett, “A New Mechanism for Interstitial Migration,” *Phys. Lett.*, vol. 38A, no. 2, 135–137 (1972).
- [1.82] F. Seitz, “Generation of F Centers at Low Temperature,” *Phys. Rev.*, vol. 89, no. 6, 1299 (1953).
- [1.83] J. S. Koehler and R. E. McKeighen, “Athermal Migration of Defects in Electron Irradiated Semiconductors,” *Bull. Am. Phys. Soc., Series II*, vol. 16, no. 3, 396–397 (1971).
- [1.84] L. Onsager, “Reciprocal Relations in Irreversible Processes. I.” *Phys. Rev.*, vol. 37, 405–426 (1931).
- [1.85] L. Onsager, “Reciprocal Relations in Irreversible Processes. II.” *Phys. Rev.*, vol. 38, 2265–2279 (1931).
- [1.86] S. R. De Groot, *Thermodynamics of Irreversible Processes*, Amsterdam: North-Holland (1952).
- [1.87] R. Haase, *Thermodynamics of Irreversible Processes*, Reading: Addison-Wesley (1969).
- [1.88] Y. Todokoro and I. Teramoto, “The Stress-Enhanced Diffusion of Boron in Silicon,” *J. Appl. Phys.*, vol. 49, no. 6, 3527–3529 (1978).
- [1.89] T. Hook, S. Biesemans, and J. Slinkman, “The Dependence of Channel Length on Channel Width in Narrow-Channel CMOS Devices for 0.35-0-13 μm Technologies,” *IEEE Trans. Electron Devices*, vol. 21, no. 2, 85–87 (2000).
- [1.90] I. Goroff and L. Kleinman, “Deformation Potentials in Silicon. III. Effect of a General Strain on Conduction and Valence Levels,” *Phys. Rev.*, vol. 132, no. 3, 1080–1084 (1963).
- [1.91] B.-Y. Tsaur, J. C. C. Fan, and M. W. Geis, “Stress-Enhanced Carrier Mobility in Zone Melting Recrystallized Polycrystalline Si Films on SiO₂-Coated Substrates,” *Appl. Phys. Lett.*, vol. 40, 322–324 (1982).
- [1.92] J. Welser, J. L. Hoyt, and J. F. Gibbons, “NMOS and PMOS Transistors Fabricated in Strained Silicon/Relaxed Silicon-Germanium Structures,” in: *Technical Digest of the 1992 International Electron Devices Meeting (IEDM)*, New York: IEEE, 1000–1002 (1992).
- [1.93] D. K. Nayak, J. C. S. Woo, J. S. Park, K. L. Wang, and K. P. MacWilliams, “High-Mobility p-Channel Metal-Oxide-Semiconductor Field-Effect Transistor on Strained Si,” *Appl. Phys. Lett.*, vol. 62, no. 22, 2853–2855 (1993).
- [1.94] J. E. Dijkstra and W. T. Wenckebach, “Hole Transport in Strained Si,” *J. Appl. Phys.*, vol. 81, no. 3, 1259–1263 (1997).
- [1.95] M. T. Currie, C. W. Leitz, T. A. Langdo, G. Taraschi, E. A. Fitzgerald, and D. A. Antoniadis, “Carrier Mobilities and Process Stability of Strained Si n- and p-MOSFETs on SiGe Virtual Substrates,” *J. Vac. Sci. Technol. B*, vol. 19, no. 6, 2268–2279 (2001).

- [1.96] J. L. Hoyt, H. M. Nayfeh, S. Eguchi, I. Aberg, G. Xia, T. Drake, E. A. Fitzgerald, and D. A. Antoniadis, "Strained Silicon MOSFET Technology," in: *Technical Digest of the 2002 International Electron Devices Meeting (IEDM)*, Piscataway: IEEE, 23–26 (2002).
- [1.97] A. Hamada, T. Furusawa, N. Saito, and E. Takeda, "A New Aspect of Mechanical Stress Effects in Scaled MOS Devices," *IEEE Trans. Electron Devices*, vol. 38, no. 4, 895–900 (1991).
- [1.98] P. Smeys, P. B. Griffin, and K. C. Saraswat, "Influence of Post-Oxidation Cooling Rate on Residual Stress and pn-Junction Leakage Current in LOCOS Isolated Structures," *IEEE Trans. Electron Devices*, vol. 43, no. 11, 1989–1993 (1996).
- [1.99] B. Maiti, P. J. Tobin, C. Hobbs, R. I. Hedge, F. Huang, D. L. O'Meara, D. Jovanovich, M. Mendicino, J. Chen, D. Connelly, O. Adetutu, J. Mogab, J. Candelaria, and L. B. La, "PVD TiN Metal Gate MOSFETs on Bulk Silicon and Fully Depleted Silicon-on-Insulator (FDSOI) Substrates for Deep Sub-Quarter Micron CMOS Technology," in: *Technical Digest of the 1998 International Electron Devices Meeting (IEDM)*, Piscataway: IEEE, 781–784 (1998).
- [1.100] P. Smeys, P. B. Griffin, Z. U. Rek, I. De Wolf, and K. Saraswat, "Influence of Process-Induced Stress on Device Characteristics and Its Impact on Scaled Device Performance," *IEEE Trans. Electron Devices*, vol. 46, no. 6, 1245–1252 (1999).
- [1.101] G. Scott, J. Lutze, M. Rubin, F. Nouri, and M. Manley, "NMOS Drive Current Reduction Caused by Transistor Layout and Trench Isolation Induced Stress," in: *Technical Digest of the 1999 International Electron Devices Meeting (IEDM)*, Piscataway: IEEE, 827–830 (1999).
- [1.102] M. J. Aziz, P. C. Sabin, and G.-Q. Lu, "The Activation Strain Tensor: Nonhydrostatic Stress Effects on Crystal-Growth Kinetics," *Phys. Rev. B*, vol. 44, no. 18, 9812–9816 (1991).
- [1.103] L. A. Girifalco and H. H. Grimes, *The Theory of Diffusion in Strained Systems*, Technical Note 4408, Washington: National Advisory Committee for Aeronautics (1958).
- [1.104] O. Sugino and A. Oshiyama, "Pressure Dependence of Formation and Migration Enthalpies for Atomic Diffusion in Si: Conjugate Gradient Minimization of Total Energy," in: *Defects in Semiconductors 16*, edited by G. Davies, G. G. DeLeo, and M. Stavola, *Materials Science Forum*, vol. 83–87, 469–474 (1992).
- [1.105] N. E. B. Cowern, P. C. Zalm, P. van der Sluis, D. J. Gravestijn, and W. B. de Boer, "Diffusion in Strained Si(Ge)," *Phys. Rev. Lett.*, vol. 72, no. 16, 2585–2588 (1994).
- [1.106] H. Park, K. S. Jones, J. A. Slinkman, and M. E. Law, "Effects of Hydrostatic Pressure on Dopant Diffusion in Silicon," *J. Appl. Phys.*, vol. 78, no. 6, 3664–3670 (1995).
- [1.107] H. Mehrer, "The Effect of Pressure on Diffusion," in: *Diffusion and Stresses*, edited by D. L. Beke and I. A. Szabó, *Defect and Diffusion Forum*, vol. 129–130, 57–74 (1996).
- [1.108] M. J. Aziz, "Stress Effects on Defects and Dopant Diffusion in Si," *Materials Science in Semiconductor Processing*, vol. 4, 397–403 (2001).
- [1.109] M. Laudon, N. N. Carlson, M. P. Masquelier, M. S. Daw, and W. Windl, "Multiscale Modeling of Stress-Mediated Diffusion in Silicon: Ab Initio to Continuum," *Appl. Phys. Lett.*, vol. 78, no. 2, 201–203 (2001).
- [1.110] W. Windl, M. S. Daw, N. N. Carlson, and M. Laudon, "Multiscale Modeling of Stress-Mediated Diffusion in Silicon — Volume Tensors," in: *Advances in Materials Theory and Modeling — Bridging over Multiple-Length and Time Scales*, edited by V. Bulov, F. Cleri, L. Colombo, L. Lewis, and N. Mousseau, *Mat. Res. Soc. Symp. Proc.*, vol. 677, AA9.4.1–AA9.4.6 (2001).
- [1.111] M. S. Daw, W. Windl, N. N. Carlson, M. Laudon, and M. P. Masquelier, "Effect of Stress on Dopant and Defect Diffusion in Si: A General Treatment," *Phys. Rev. B*, vol. 64, 045205 (2001).
- [1.112] J. W. Harrison, "A Simulation Model for Electromigration in Fine Line Metallization of Integrated Circuits Due to Repetitive Pulsed Currents," *IEEE Trans. Electron Devices*, vol. 35, no. 12, 2170–2179 (1988).
- [1.113] R. Kirchheim, "Stress and Electromigration in Al-Lines of Integrated Circuits," *Acta metall. mater.*, vol. 40, no. 2, 309–323 (1992).

- [1.114] R. Kirchheim, “Modelling Electromigration and Induced Stresses in Aluminum Lines,” in: *Materials Reliability in Microelectronics III*, edited by K. Rodbell, B. Filter, H. Frost, and P. Ho, *Mat. Res. Soc. Symp. Proc.*, vol. 309, 101–110 (1993).
- [1.115] F. C. Larché and J. W. Cahn, “The Effect of Self-Stress on Diffusion in Solids,” *Acta Metallurgica*, vol. 30, 1835–1845 (1982).
- [1.116] F. C. Larché and J. W. Cahn, “The Interactions of Composition and Stress in Crystalline Solids,” *Acta Metallurgica*, vol. 33, no. 3, 331–357 (1985).
- [1.117] F. C. Larché, “The Appearance of Stresses and Their Effects in Diffusion-Reaction Processes in Solids,” in: *Reactive Phase Formation at Interfaces and Diffusion Processes*, edited by Y. Limoge and J. L. Boucquet, *Materials Science Forum*, vol. 155–156, 267–277 (1994).
- [1.118] O. I. Velichki and A. K. Fedotov, “Simulation of Point Defect Diffusion in Semiconductors,” in: *Gettering and Defect Engineering in Semiconductor Technology GADEST’99*, edited by H. G. Grimmeiss, L. Ask, M. Kleverman, M. Kittler, and H. Richter, *Solid State Phenomena*, vol. 69–70, 513–518 (1999).
- [1.119] C. Ludwig, “Diffusion zwischen ungleich erwärmten Orten gleich zusammengesetzter Lösungen,” *Sitzungsberichte der Akademie der Wissenschaften, Wien, Mathematisch-Naturwissenschaftliche Klasse*, vol. 20, 539 (1856).
- [1.120] C. Soret, “Sur l’état d’équilibre que prend, au point de vue de sa concentration, une dissolution saline promitivement homogène dont deux parties sont portées à des températures différentes,” *Arch. Sci. Phys. Nat. Genève*, vol. 2, 48–61 (1879).
- [1.121] K. Wirtz, “Zur kinetischen Theorie der Thermodiffusion im Kristallgitter,” *Physikalische Zeitschrift*, vol. 44, no. 11, 221–231 (1943).
- [1.122] K. Wirtz and J. W. Hiby, “Kinetische Theorie der Thermodiffusion in Flüssigkeiten,” *Physikalische Zeitschrift*, vol. 44, no. 18, 369–382 (1943).
- [1.123] S. Prager and H. Eyring, “Thermal Diffusion in Binary Systems,” *J. Chem. Phys.*, vol. 21, no. 8, 1347–1350 (1953).
- [1.124] A. D. LeClaire, “Some Predicted Effects of Temperature Gradients on Diffusion in Crystals,” *Phys. Rev.*, vol. 93, no. 2, 344 (1954).
- [1.125] J. A. Brinkman, “The Effect of Temperature Gradients on Diffusion in Crystals,” *Phys. Rev.*, vol. 93, no. 2, 345 (1954).
- [1.126] R. E. Howard, “Soret Effect in Doped Ionic Crystals,” *J. Chem. Phys.*, vol. 27, no. 6, 1377–1381 (1957).
- [1.127] P. Shewmon, “Thermal Diffusion of Vacancies in Zinc,” *J. Chem. Phys.*, vol. 29, no. 5, 1032–1036 (1958).
- [1.128] A. R. Allnatt and S. A. Rice, “On the Dynamical Theory of Diffusion in Crystals. V. Random-Walk Treatment of the Heat of Transport,” *J. Chem. Phys.*, vol. 33, no. 2, 573–578 (1960).
- [1.129] P. Shewmon, “The Thermal Diffusion of Carbon in α and γ Iron,” *Acta Metallurgica*, vol. 8, 605–611 (1960).
- [1.130] W. G. Brammer, “Self-Diffusion of Alpha-Iron in a Large Temperature Gradient,” *Acta Metallurgica*, vol. 8, 630–636 (1960).
- [1.131] A. R. Allnatt and A. V. Chadwick, “Thermal Diffusion in Crystalline Solids,” *Chem. Rev.*, vol. 67, no. 6, 681–705 (1967).
- [1.132] H. B. Huntington, “Driving Forces for Thermal Mass Transport,” *J. Phys. Chem. Solids*, vol. 29, 1641–1651 (1968).
- [1.133] R. A. Oriani, “Thermomigration in Solid Metals,” *J. Phys. Chem. Solids*, vol. 30, 339–351 (1969).
- [1.134] L. A. Girifalco, “Diffusion in Non-Uniform Crystals,” *Materials Science and Engineering*, vol. 9, 61–79 (1972).
- [1.135] C. Jones, P. J. Grout, and A. B. Lidiard, “The Heat of Transport of Vacancies in Solid Argon,” *Phil. Mag. Lett.*, vol. 74, no. 3, 217–223 (1996).

- [1.136] V. V. Voronkov, "The Mechanism of Swirl Defects Formation in Silicon," *J. Crystal Growth*, vol. 59, 625–643 (1982).
- [1.137] R. Habu, I. Yunoki, T. Saito, and A. Tomiura, "Diffusion of Point Defects in Silicon Crystals during Melt Growth. I Uphill Diffusion," *Jpn. J. Appl. Phys.*, vol. 32, no. 4, 1740–1746 (1993).
- [1.138] R. A. Brown, D. Maroudas, and T. Sinno, "Modelling Point Defect Dynamics in the Crystal Growth of Silicon," *J. Crystal Growth*, vol. 137, 12–25 (1994).
- [1.139] K. Nakamura, T. Saishoji, and J. Tomioka, "Simulation of the Point Defect Diffusion and Growth Condition for Defect Free Cz Silicon Crystal," in: *Semiconductor Silicon 2002*, edited by H. R. Huff, L. Fabry, and S. Kishino, *Electrochem. Soc. Proc.*, vol. 2002-2, 554–566 (2002).
- [1.140] T. Y. Tan, "Mass Transport Equations Unifying Descriptions of Isothermal Diffusion, Thermomigration, Segregation, and Position-Dependent Diffusivity," *Appl. Phys. Lett.*, vol. 73, no. 18, 2678–2680 (1998).
- [1.141] T. De Donder, "Sur la vitesse reactionelle," *Bulletins de la Classe des Sciences, Academie royale de Belgique*, vol. 24, 15–18 (1938).
- [1.142] J. N. Brönsted, "Zur Theorie der chemischen Reaktionsgeschwindigkeit," *Z. Phys. Chem.*, vol. 102, no. 2, 169–207 (1922).
- [1.143] J. N. Brönsted, "Zur Theorie der chemischen Reaktionsgeschwindigkeit. II." *Z. Phys. Chem.*, vol. 115, no. 5/6, 337–364 (1925).
- [1.144] R. Haase, "Reaction Rate, Activities, and Affinity," *Z. Phys. Chem. Neue Folge*, vol. 128, 225–228 (1981).
- [1.145] R. Haase, "Reaction Rate in Non-Ideal Systems," *Z. Phys. Chem. Neue Folge*, vol. 153, 217–219 (1987).
- [1.146] R. Habu, K. Kojima, H. Harada, and A. Tomiura, "Diffusion of Point Defects in Silicon Crystals during Melt Growth. III Two Diffusor Model," *Jpn. J. Appl. Phys.*, vol. 32, no. 4, 1754–1758 (1993).
- [1.147] S. Glasstone, K. J. Laidler, and H. Eyring, *The Theory of Rate Processes*, New York: McGraw-Hill (1941).
- [1.148] J. W. Christian, *The Theory of Transformations in Metals and Alloys*, Oxford: Pergamon Press (1965).
- [1.149] M. von Smoluchowski, "Versuch einer mathematischen Theorie der Koagulationskinetik kolloider Lösungen," *Z. Phys. Chem.*, vol. 92, no. 2, 129–168 (1917).
- [1.150] T. R. Waite, "Theoretical Treatment of the Kinetics of Diffusion-Limited Reactions," *Phys. Rev.*, vol. 107, no. 2, 463–470 (1957).
- [1.151] M. M. Bunea, P. Fastenko, and S. T. Dunham, "Atomistic Simulations of Damage Evolution in Silicon," in: *Si Front-End Processing — Physics and Technology of Dopant-Defect Interactions*, edited by H.-J. L. Gossmann, T. E. Haynes, M. E. Law, A. Nylandsted Larsen, and S. Odanaka, *Mat. Res. Soc. Symp. Proc.*, vol. 568, 135–140 (1999).
- [1.152] K. M. Beardmore, W. Windl, B. P. Haley, and N. Grønbech-Jensen, "Diffusion Mechanisms and Capture Radii in Silicon," in: *Computational Nanoscience and Nanotechnology 2002*, Cambridge: Applied Computational Research Society, 251–254 (2002).
- [1.153] P. Debye, "Reaction Rates in Ionic Solutions," *Transactions of the Electrochemical Society*, vol. 82, 265–272 (1942).
- [1.154] L. C. Kimerling, M. T. Asom, J. L. Benton, P. J. Drevinsky, and C. E. Caefter, "Interstitial Defect Reaction in Silicon," in: *Defects in Semiconductors 15*, edited by G. Ferenczi, *Materials Science Forum*, vol. 38-41, 141–150 (1989).
- [1.155] N. I. Berezhnov, A. R. Chelyadinskii, M. Jadon, and Y. R. Suprun-Belevich, "On the Problems of Watkins Substitution and Migration of Silicon Atoms in Silicon," *Nuclear Instruments and Methods in Physics Research B*, vol. 73, 357–361 (1993).
- [1.156] T. R. Waite, "General Theory of Bimolecular Reaction Rates in Solids and Liquids," *J. Chem. Phys.*, vol. 28, no. 1, 103–106 (1958).

- [1.157] C. T. Sah, P. C. H. Chan, C.-K. Wang, R. L.-Y. Sah, K. A. Yamakawa, and R. Lutwack, “Effect of Zinc Impurity on Silicon Solar-Cell Efficiency,” *IEEE Trans. Electron Devices*, vol. ED-28, no. 3, 304–313 (1981).
- [1.158] D. Peak and J. W. Corbett, “Diffusion-Controlled Reaction Kinetics,” *Phys. Rev. B*, vol. 5, no. 4, 1226–1238 (1972).
- [1.159] M. Yoshida, E. Arai, H. Nakamura, and Y. Terunuma, “Excess Vacancy Generation Mechanisms at Phosphorus Diffusion into Silicon,” *J. Appl. Phys.*, vol. 45, no. 4, 1498–1506 (1974).
- [1.160] N. E. B. Cowern, K. T. F. Janssen, G. F. A. van de Walle, and K. J. Gravesteijn, “Impurity Diffusion via an Intermediate Species: The B-Si System,” *Phys. Rev. Lett.*, vol. 65, no. 19, 2434–2437 (1990).
- [1.161] D. Mathiot and J. C. Pfister, “Dopant Redistribution in Heavily Doped Silicon: Confirmation of the Validity of the Vacancy-Percolation Model,” *J. Appl. Phys.*, vol. 66, no. 2, 970–972 (1989).
- [1.162] D. Stauffer, “Scaling Theory of Percolation Clusters,” *Physics Reports*, vol. 54, 1–74 (1979).
- [1.163] C. D. Thurmond and J. D. Struthers, “Equilibrium Thermochemistry of Solid and Liquid Alloys of Germanium and of Silicon. II. The Retrograde Solid Solubilities of Sb in Ge, Cu in Ge, and Cu in Si,” *J. Phys. Chem.*, vol. 57, 831–835 (1953).
- [1.164] R. C. Dorward and J. S. Kirkaldy, “Thermodynamic Properties of Copper and Gold in Silicon and Germanium,” *Trans. Metall. Soc. AIME*, vol. 242, 2055–2061 (1968).
- [1.165] E. R. Weber, “Transition Metals in Silicon,” *Appl. Phys. A*, vol. 30, 1–22 (1983).
- [1.166] F. P. Buff and F. M. Schindler, “Small Perturbations in Solution Theory,” *J. Chem. Phys.*, vol. 29, no. 5, 1075–1081 (1958).
- [1.167] C. D. Thurmond and M. Kowalchik, “Germanium and Silicon Liquidus Curves,” *Bell Syst. Techn. J.*, vol. 39, no. 1, 169–204 (1960).
- [1.168] K. Weiser, “Theoretical Calculations of Distribution Coefficients of Impurities in Germanium and Silicon, Heats of Solid Solutions,” *J. Phys. Chem. Solids*, vol. 7, 118–126 (1958).
- [1.169] F. A. Trumbore, C. R. Isenberg, and E. M. Porbansky, “On the Temperature-Dependence of the Distribution Coefficient,” *J. Phys. Chem. Solids*, vol. 9, 60–69 (1958).
- [1.170] H. Reiss, “Chemical Effects Due to Ionization of Impurities in Semiconductors,” *J. Chem. Phys.*, vol. 21, no. 7, 1209–1217 (1953).
- [1.171] C. D. Thurmond, “Distribution Coefficients of Impurities Distributed between Ge or Si Crystals and Ternary Alloys or Surface Oxides,” in: *Properties of Elemental and Compound Semiconductors*, edited by H. C. Gatos, New York: Interscience, 121–140 (1960).
- [1.172] H. Reiss and C. S. Fuller, “Influence of Holes and Electrons on the Solubility of Lithium in Boron-Doped Silicon,” *J. Metals*, vol. 8, 276–282 (1956).
- [1.173] U. Kuhlmann, D. Nagel, and R. Sittig, “Short-Time Diffusion of Aluminium in Silicon and Co-Diffusion with Phosphorus and Boron,” in: *Diffusion in Materials*, edited by H. Mehrer, C. Herzig, N. A. Stolwijk, and H. Bracht, *Defect and Diffusion Forum*, vol. 143-147, 1009–1014 (1997).
- [1.174] R. B. Fair and J. C. C. Tsai, “Theory and Direct Measurement of Boron Segregation in SiO_2 during Dry, Near Dry, and Wet O_2 Oxidation,” *J. Electrochem. Soc.*, vol. 125, no. 12, 2050–2058 (1978).
- [1.175] A. S. Grove, O. Leistikow, Jr., and C. T. Sah, “Redistribution of Acceptor and Donor Impurities during Thermal Oxidation of Silicon,” *J. Appl. Phys.*, vol. 35, no. 9, 2695–2701 (1964).
- [1.176] D. A. Antoniadis, M. Rodoni, and R. W. Dutton, “Impurity Redistribution in SiO_2 -Si during Oxidation: A Numerical Solution Including Interfacial Fluxes,” *J. Electrochem. Soc.*, vol. 126, no. 11, 1939–1945 (1979).
- [1.177] J. S. Johannessen, W. E. Spicer, J. F. Gibbons, J. D. Plummer, and N. J. Taylor, “Observation of Phosphorus Pile-Up at the SiO_2 -Si Interface,” *J. Appl. Phys.*, vol. 49, no. 8, 4453–4458 (1978).
- [1.178] S. A. Schwarz, R. W. Barton, C. P. Ho, and C. R. Helms, “Studies of Phosphorus Pile-Up at the $\text{Si}-\text{SiO}_2$ Interface Using Auger Sputtering Profiling,” *J. Electrochem. Soc.*, vol. 128, no. 5, 1101–1106 (1981).

- [1.179] F. Lau, L. Mader, C. Mazure, C. Werner, and M. Orlowski, "A Model for Phosphorus Segregation at the Silicon-Silicon Dioxide Interface," *Appl. Phys. A*, vol. 49, 671–675 (1989).
- [1.180] M. Orlowski, "New Model for Dopant Redistribution at Interfaces," *Appl. Phys. Lett.*, vol. 55, no. 17, 1762–1764 (1989).
- [1.181] H.-M. You, U. M. Gösele, and T. Y. Tan, "Simulation of the Transient Indiffusion-Segregation Process of Triply Negatively Charged Ga Vacancies in GaAs and AlAs/GaAs Superlattices," *J. Appl. Phys.*, vol. 74, no. 4, 2461–2470 (1993).
- [1.182] T. Y. Tan, R. Gafitanu, and U. M. Gösele, "Diffusion-Segregation Equation and Simulation of the Diffusion-Segregation Phenomena," in: *Semiconductor Silicon*, edited by H. R. Huff, W. Bergholz, and K. Sumino, *Electrochem. Soc. Proc.*, vol. 94-10, 920–930 (1994).

Chapter 2

Intrinsic Point Defects

One of the most remarkable phenomena in the early days of silicon technology was the “emitter-push” effect which causes an enhanced diffusion of dopants below regions with high phosphorus concentrations (see Section 5.8.3). To explain it, it was soon concluded that some sort of far-ranging “interaction particle” is needed. Since other impurities as well as extended defects could be excluded, this role was equally soon attributed to the intrinsic point defects introduced in Section 1.1.3. Indeed, intrinsic point defects play important roles in nearly all theories of impurity diffusion in silicon. Therefore, before proceeding with the latter in the next chapters, the properties of intrinsic point defects will be reviewed in the following.

From the vast experience with metals, vacancies were the prime candidates for “diffusion vehicles” at the beginning. However, in contrast to metals for which the Simmons-Baluffi experiment [2.1] led to a generally recognized determination of the vacancy concentration, no unambiguous result was achieved for silicon. Neither was it possible for the self-interstitials which were postulated by Seeger and coworkers [2.2, 2.3] to have a main influence on self-diffusion and dopant diffusion. Although vacancies and, with significantly less certainty, self-interstitials were identified at low temperatures, no direct evidence is available at the high temperatures typical for technological processes. Therefore, much of the information presented in this chapter was obtained indirectly, mainly from the diffusion of dopant atoms and metals, but also from the dynamics of extended defects. Accordingly, a significant scatter can be observed in parameters like the equilibrium concentrations or the diffusion coefficients suggested in the literature. But this does not mean that the concept of intrinsic point defects and their interaction with dopants stands at disposition. It merely means that most experiments are sensitive only to certain combinations of point-defect-related parameters like the product of the point-defect concentration in equilibrium and the respective diffusion coefficient, as the most prominent example.

One of the key parameters of intrinsic point defects is their concentration in thermal equilibrium. It can be obtained in principle from thermodynamics as outlined in Section 2.1. An important conclusion from thermodynamics is that the equilibrium concentration of neutral intrinsic point defects does not depend on the position of the Fermi level. But they interact also with charge carriers so that various charge states of intrinsic point defects have to be considered. The results obtained from thermodynamics cannot be used directly for kinetic simulations. But it will be shown that an alternative approach based on reaction kinetics leads to results compatible to that of statistical thermodynamics.

A second key parameter is the diffusion coefficient of point defects. At cryogenic temperatures, intrinsic point defects with different charge states can be considered individually. On the other hand, at elevated temperatures, reactions with charge carrier will occur on a time scale much shorter than the time scales associated with diffusive broadening or reactions with

other defects. Then, as discussed in Section 2.2, the diffusion of intrinsic point defects can be described with an effective, Fermi-level-dependent diffusion coefficient with a field term characterized by a likewise effective, Fermi-level-dependent charge state.

Experimentally, the best-studied process associated directly with intrinsic point defects is tracer diffusion, i. e. the diffusion of labelled silicon atoms in the matrix. These experiments will be summarized in Section 2.3. Unfortunately, the stable silicon isotopes have all a high abundance and the only radioactive silicon isotope has a half-life time of few hours. The situation changed recently when isotope-pure quantum-well structures became available and the tracer diffusion coefficient in intrinsic silicon is now pretty well known. Less well known are the Fermi-level dependence and the relative contributions of self-interstitials, vacancies, and direct mechanisms to tracer diffusion.

In Sections 2.4 and 2.5, the properties of respectively vacancies and self-interstitials, and of their clusters, are recapitulated. At least vacancies were identified unambiguously at low temperatures and their donor energy levels could be established. Unfortunately, there are major differences with respect to the acceptor levels of the vacancies and to the levels of self-interstitials. Concerning the diffusivities and equilibrium concentrations, variations of up to ten orders of magnitude exist between experimentally determined values. The apparent reason is that most experiments are not sensitive to individual point-defect related parameters but, as in the case of tracer diffusion, to certain combinations. Considering the large discrepancies, results from *ab initio* calculations may provide valuable complementary information and the results reported in the literature are included in the discussion. Divacancies are among the major defects in irradiation studies and clusters comprising higher numbers of vacancies were identified after irradiation with neutrons and other high-energetic particles. Clusters of self-interstitials, beginning with di-interstitials, play major roles in post-implantation annealing processes. Again, as for single defects, complementary information was provided by theoretical investigations.

A particular defect comprising a self-interstitial next to a vacancy is the so-called Frenkel pair. Frenkel pairs, as noted in Section 2.6, are assumed to play an important role in irradiation experiments. Later, a related defect was identified in theoretical investigations which consists of two four-fold coordinated atoms which are displaced towards each other from their equilibrium sites. This defect was suggested to be a building block for amorphization.

Important for the global redistribution behavior of vacancies and self-interstitials are their recombination as well as their individual reactions with other point defects and extended defects. Section 2.7 explains the basics of such processes. In addition to the mutual annihilation of self-interstitials and vacancies, their indirect recombination has to be taken into considerations. Indirect recombination means that a vacancy or self-interstitial forms a complex with an impurity first, consecutively followed by the reaction with a self-interstitial or vacancy, respectively. Important points are also reactions of intrinsic point defects with extended defects and so-called traps. The former have a main influence on transient-enhanced diffusion after ion implantation, the latter may lead to a reduced point-defect diffusivity and were introduced to explain systematic errors in the determination of self-interstitial diffusion coefficients. Finally, it has to be mentioned that intrinsic point defects are generated or consumed by chemical reactions in the bulk such as the precipitation of oxygen or dopants.

Intrinsic point defects may also interact with surfaces and interfaces and the objective of Section 2.8 is to summarize such effects. Individual self-interstitials may diffuse to kinks at the surface and attach there to become part of the regular silicon lattice. *Vice versa*, silicon atoms may break free from kinks at the surface to become self-interstitials. Analogously, such reactions are conceivable for vacancies. All of them are required to establish the individual equilibrium concentrations of the intrinsic point defects in the bulk since bulk recombination

and generation removes and generates vacancies and self-interstitials only in equal number. Mathematically, interactions with surfaces can be formulated as boundary conditions for the continuity equations. In addition to individually recombining at the surface, self-interstitials were found to segregate into adjacent oxide layers. Finally, the section summarizes the various chemical reactions at interfaces and surfaces which lead to a deviation of the concentrations of intrinsic point defects from equilibrium concentrations.

Section 2.9 finally is devoted to a discussion of the initial conditions for the intrinsic point defects. They correspond basically to the state after the end of the previous process step. In as-grown wafers, they are established by the crystal-pulling technique. Depending on the ratio of pull rate and thermal gradient at the interface, crystals can be grown vacancy-rich and self-interstitial-rich. Near the surface (within a depth range sufficient for most investigations), except during post-implantation annealing, the concentrations of the intrinsic point defects are determined primarily by the respective boundary conditions. This justifies somewhat the frequently found ignorance of the true initial conditions in process simulation. But initial conditions of intrinsic point defects are important for various bulk processes like oxygen precipitation where the distribution of vacancies influences the nucleation and, thus, the spatial distribution of precipitates.

2.1 Concentration in Thermal Equilibrium

Intrinsic point defects, especially self-interstitials and vacancies, play a major role in nearly all diffusion theories of dopant impurities in silicon. Their concentrations in equilibrium were shown by Schottky [2.4] to be intrinsic properties of the crystal and can be computed from statistical thermodynamics as outlined in Section 1.4. The method discussed below follows the work of Lannoo and Bourgoin [2.5] and Guerrero [2.6]. An alternative approach to calculate the equilibrium concentration of charged intrinsic point defects is to consider reactions with charge carriers. Finally, the effects of stress on the concentrations of the intrinsic point defects will be discussed.

Derivation from Thermodynamics

Starting with a perfect crystal, the introduction of intrinsic point defects increases the enthalpy H of the system as well as its entropy S . The energetically most favorable state is reached when the Gibbs free energy $G = H - T \cdot S$ is at a minimum. To create a vacancy, a host atom is moved from its lattice site to a kink at the surface. Similarly, a self-interstitial is generated by moving a host atom from a surface kink to an interstitial site in the lattice. Both processes conserve the number of silicon atoms. In a first-order approximation, the surface area and kink density remain unchanged by such processes so that the introduction of intrinsic point defects does not affect the Gibbs free energy associated with the surface. A more extensive reasoning can be found in Section 2.1 of the review of Van Vechten [2.7]. As already mentioned in Section 1.5, ionization of intrinsic point defects can be interpreted as reactions between the intrinsic point defects and charge carriers. This allows us to calculate the fraction of charged point defects by an alternative approach to statistical thermodynamics.

By introducing one intrinsic point defect of type X in charge state j , the enthalpy of the system is increased by the enthalpy of formation H_{Xj}^f of the respective point defect. X can stand for self-interstitials I or vacancies V. Any of them may be in several charge states indicated by the superscript j . The numbers of electrons associated with each charge state are denoted by the symbol z_j . Interactions of point defects are ignored at first since they lead to the formation

of complexes which are counted separately (see, e. g. Section 1.5.4). Then, the total increase in enthalpy due to N_{X^j} point defects is $N_{X^j} \cdot H_{X^j}^f$. The increase in the entropy is attributed in part to lattice vibrations. The respective contribution $N_{X^j} \cdot S_{X^j}^f$ increases linearly with the number of the respective point defect, with $S_{X^j}^f$ being the entropy of formation at a specific site. In addition, the configurational or mixing entropy ΔS_c has to be taken into account. $H_{X^j}^f$ and $S_{X^j}^f$ include already the contributions from electrons and holes bound to the defects. But one has to take the contributions ΔG^n from the electrons in the conduction band and ΔG^p from the holes in the valence-bond band into account. The total change in the Gibbs free energy is then given by

$$\begin{aligned}\Delta G &= \Delta H - T \cdot \Delta S \\ &= \sum_j N_{X^j} \cdot (H_{X^j}^f - T \cdot S_{X^j}^f) + \Delta G^n + \Delta G^p - T \cdot \Delta S_c\end{aligned}\quad (2.1)$$

In addition, the crystal has to be electrically neutral which can be formulated as an auxiliary condition in the form

$$F = V \cdot (n - p) + \sum_j z_j \cdot N_{X^j} = 0. \quad (2.2)$$

Therein, V is the volume of the crystal and $V \cdot n$ and $V \cdot p$ are the numbers of electrons in the conduction band and holes in the valence band within the volume, respectively.

The auxiliary condition of electrical neutrality has to be taken into account by the method of Lagrange so that instead of equation (2.1), the function $\Delta G + \lambda \cdot F$ has to be minimized with respect to the numbers of each of the point defects, the electron and hole concentrations, and the Lagrange multiplier λ . Its derivative with respect to λ results in equation (2.2), and the derivatives with respect to the numbers of defects lead to equations of the form

$$\frac{\partial(\Delta G + \lambda \cdot F)}{\partial N_{X^j}} = H_{X^j}^f - T \cdot S_{X^j}^f - T \cdot \frac{\partial \Delta S_c}{\partial N_{X^j}} + \lambda \cdot z_j = 0 \quad (2.3)$$

A possible dependence of ΔG^n and ΔG^p on the numbers of point defects comes from the fact that donor and acceptor states remove quantum states from the conduction and valence-bond bands, respectively. However, the numbers of quantum states there are so large in comparison to the numbers of removed states that ΔG^n and ΔG^p are attributed predominantly to changes of the Fermi-level. Therefore, the explicit derivatives of ΔG^n and ΔG^p with respect to the number of defects were ignored in (2.3). The derivative with respect to the number of electrons

$$\frac{\partial(\Delta G + \lambda \cdot F)}{\partial(V \cdot n)} = \frac{\partial \Delta G^n}{\partial(V \cdot n)} + \lambda = \mu_n + \lambda = E_F + \lambda = 0 \quad (2.4)$$

gives a relation for λ . Therein, the definition of the chemical potential of the electrons as derivative of the Gibbs free energy with respect to the number of electrons was used. On the other hand, it has been shown in Section 1.2.3 that the chemical potential of the electrons is identical to the Fermi level in Fermi-Dirac statistics.

The configurational entropy can be calculated from the complexion number Ω , i. e. the number of distinct configurations, by (1.83). The number of possible configurations can be calculated assuming that N_{X^+} defects are distributed upon N_{X^+} possible sites, N_{X^-} defects on the remaining sites, etc. A defect may have several internal degrees of freedom due to, e. g., spin degeneracy or equivalent geometric configurations at the same site. As a consequence, the number of possible configurations is increased by Θ_{X^j} to the power of N_{X^j} where Θ_{X^j} denotes

the number of internal degrees of freedom of the defect at a specific lattice site. The complexion number is then given by

$$\begin{aligned}\Omega &= \binom{N_{XS}}{N_{X^=}} \cdot \binom{N_{XS} - N_{X^=}}{N_{X^-}} \cdot \dots \cdot \binom{N_{XS} - \sum_{j,j \neq ++} N_{X^j}}{N_{X^{++}}} \cdot \prod_j \Theta_{X^j}^{N_{X^j}} \\ &= \frac{(N_{XS})!}{\left(N_{XS} - \sum_j N_{X^j}\right)! \cdot \prod_j (N_{X^j})!} \cdot \prod_j \Theta_{X^j}^{N_{X^j}}\end{aligned}\quad (2.5)$$

Since the number of defects N_X as well as the number of possible sites for the defects N_{XS} are large, Sterling's formula can be used in the simplified version (1.86). We then obtain for the configurational entropy

$$\begin{aligned}\Delta S_c &= k \cdot N_{XS} \cdot (\ln N_{XS} - 1) - k \cdot \sum_j N_{X^j} \cdot (\ln N_{X^j} - \ln \Theta_{X^j} - 1) \\ &\quad - k \cdot \left(N_{XS} - \sum_j N_{X^j} \right) \cdot \left(\ln \left(N_{XS} - \sum_j N_{X^j} \right) - 1 \right)\end{aligned}\quad (2.6)$$

The derivatives of the configurational entropy with respect to the N_{X^j} are given by

$$\frac{\partial \Delta S_c}{\partial N_{X^j}} = k \cdot \left(\frac{\partial N_{XS}}{\partial N_{X^j}} \cdot \ln \frac{N_{XS}}{N_{XS} - \sum_i N_{X^i}} - \ln \frac{N_{X^j}}{N_{XS} - \sum_i N_{X^i}} + \ln \Theta_{X^j} \right) \quad (2.7)$$

which reduces to

$$\frac{\partial \Delta S_c}{\partial N_{X^j}} = -k \cdot \ln \frac{N_{X^j}}{\Theta_{X^j} \cdot N_{XS}} \quad (2.8)$$

when the numbers of the point defects are significantly lower than the number of sites.

Combining equations (2.3), (2.4), and (2.8) gives the numbers of point defects in thermal equilibrium (indicated by the superscript ' eq '). Their concentrations, i. e. their numbers per unit volume, can be written as

$$\begin{aligned}C_{X^j}^{eq} &= \Theta_{X^j} \cdot C_{XS} \cdot \exp \left(-\frac{H_{X^j}^f - T \cdot S_{X^j}^f - z_j \cdot E_F}{k \cdot T} \right) \\ &= \Theta_{X^j} \cdot C_{XS} \cdot \exp \left(-\frac{G_{X^j}^f - z_j \cdot E_F}{k \cdot T} \right)\end{aligned}\quad (2.9)$$

for the various charge states. Considering that the charge state of neutral point defects z_0 is zero, one notices that the equilibrium concentration of neutral point defects does not depend on the Fermi-level. It is given by

$$C_{X^0}^{eq} = \Theta_{X^0} \cdot C_{XS} \cdot \exp \left(\frac{S_{X^0}^f}{k} \right) \cdot \exp \left(-\frac{H_{X^0}^f}{k \cdot T} \right). \quad (2.10)$$

This independence on the Fermi level was derived already by Shockley and Moll [2.8] who considered diffusion of neutral defects across a p-n junction. However, they admitted that it neglects second-order effects such as a change in the lattice constant with doping level or polarization. In our derivation, such effects may also influence the Gibbs free energy of formation of a neutral point defect but a quantitative analysis of such effects is not known.

At this point it is necessary to discuss the term formation energy and the relations between the formation energies of charged species in more detail. In general, the formation energy of a defect will be different for each charge state. The differences correspond to the ionization energies. For negatively charged defects,

$$E_{X^-} = G_{X^-}^f - G_{X^0}^f \quad \text{and} \quad E_{X^=} = G_{X^=}^f - G_{X^0}^f \quad (2.11)$$

correspond to the energies of negative ionization of a neutral and a singly ionized defect, respectively. This means that the respective levels can be found at $E_c - E_{X^-}$ and $E_c - E_{X^=}$. For positively charged defects,

$$E_{X^+} = G_{X^0}^f - G_{X^+}^f \quad \text{and} \quad E_{X^{++}} = G_{X^+}^f - G_{X^{++}}^f \quad (2.12)$$

are the corresponding negative energies of positive ionization. The levels associated are at $E_v + E_{X^+}$ and $E_v + E_{X^{++}}$. All these formation energies $G_{X^j}^f$ are independent of the Fermi level. Electrical neutrality, on the other hand, requires that for each ionized defect an appropriate number of charge carriers (holes for negatively charged defects and electrons for positively charged defects) are generated. The formation energy for the defect and the compensating charge carriers

$$G_{X^j+e^{-j}}^f = G_{X^j}^f - z_j \cdot E_F \quad (2.13)$$

consists of the formation energy of the defect and the formation energy of the free charge carriers. Although not absolutely correct, $G_{X^j+e^{-j}}^f$ is generally addressed as formation energy of defect X, too. The difference is subtle, but $G_{X^j+e^{-j}}^f$ will vary for ionized defects with the Fermi level. Any specification refers to a specific reference state E_F^{ref} . From the differences

$$G_{X^=+2h^+}^f(E_F^{ref}) - G_{X^-+h^+}^f(E_F^{ref}) = E_{X^=} - E_F^{ref}, \quad (2.14)$$

$$G_{X^-+h^+}^f(E_F^{ref}) - G_{X^0}^f = E_{X^-} - E_F^{ref}, \quad (2.15)$$

$$G_{X^0}^f - G_{X^++e^-}^f(E_F^{ref}) = E_{X^+} - E_F^{ref}, \quad (2.16)$$

$$G_{X^++e^-}^f(E_F^{ref}) - G_{X^{++}+2e^-}^f(E_F^{ref}) = E_{X^{++}} - E_F^{ref}, \quad (2.17)$$

the positions of the levels of the defect with respect to the reference state follow directly.

It has to be mentioned also that the procedure outlined until now is correct only when the electronic transitions are associated with negligible atomic rearrangements since the levels of a defect will, in general, depend on its atomic configuration. If this is not case as for meta-stable defects, all atomic configurations would have to be taken into considerations individually with their charge states, to be correct. But such a procedure would exceed current process-simulation approaches by far.

Since the concentration of neutral point defects is, to first order, a function of temperature only, it is customary to take it as a reference concentration for the concentrations of the charged point defects in the following form

$$\begin{aligned} \frac{C_{X^=}^{eq}}{C_{X^0}^{eq}} &= \frac{\Theta_{X^=}}{\Theta_{X^0}} \cdot \exp\left(-\frac{G_{X^=}^f - G_{X^0}^f - 2 \cdot E_F}{k \cdot T}\right) \\ &= \frac{\Theta_{X^=}}{\Theta_{X^0}} \cdot \exp\left(-\frac{E_{X^=} + E_{X^-} - 2 \cdot E_F}{k \cdot T}\right), \end{aligned} \quad (2.18)$$

$$\frac{C_{X^-}^{eq}}{C_{X^0}^{eq}} = \frac{\Theta_{X^-}}{\Theta_{X^0}} \cdot \exp\left(-\frac{G_{X^-}^f - G_{X^0}^f - E_F}{k \cdot T}\right) = \frac{\Theta_{X^-}}{\Theta_{X^0}} \cdot \exp\left(-\frac{E_{X^-} - E_F}{k \cdot T}\right), \quad (2.19)$$

$$\frac{C_{X^+}^{eq}}{C_{X^0}^{eq}} = \frac{\Theta_{X^+}}{\Theta_{X^0}} \cdot \exp\left(-\frac{G_{X^+}^f - G_{X^0}^f + E_F}{k \cdot T}\right) = \frac{\Theta_{X^+}}{\Theta_{X^0}} \cdot \exp\left(-\frac{E_F - E_{X^+}}{k \cdot T}\right), \quad (2.20)$$

$$\begin{aligned} \frac{C_{X^{++}}^{eq}}{C_{X^0}^{eq}} &= \frac{\Theta_{X^{++}}}{\Theta_{X^0}} \cdot \exp\left(-\frac{G_{X^{++}}^f - G_{X^0}^f + 2 \cdot E_F}{k \cdot T}\right) \\ &= \frac{\Theta_{X^{++}}}{\Theta_{X^0}} \cdot \exp\left(-\frac{2 \cdot E_F - E_{X^{++}} - E_{X^+}}{k \cdot T}\right). \end{aligned} \quad (2.21)$$

This result is identical to the findings of Longini and Greene [2.9], Valenta and Ramasastri [2.10], and Shockley and Last [2.11], the generalization of which has been discussed by Fahey [2.12] in his PhD thesis.

In the following splitting of the equations, the concentrations of electrons and holes (1.18) will be introduced as obtained from Boltzmann statistics. In addition, as discussed in Section 1.2.4, it will be assumed that the Fermi-level in the intrinsic state is very close to the middle of the band gap $E_g = E_c - E_v$ (1.17).

$$\begin{aligned} \frac{C_{X^=}^{eq}}{C_{X^0}^{eq}} &= \frac{\Theta_{X^=}}{\Theta_{X^0}} \cdot \exp\left(\frac{E_c - E_{X^=}}{k \cdot T}\right) \cdot \exp\left(\frac{E_c - E_{X^-}}{k \cdot T}\right) \\ &\quad \cdot \exp\left(\frac{2 \cdot (E_F - E_i)}{k \cdot T}\right) \cdot \exp\left(-\frac{2 \cdot (E_c - E_i)}{k \cdot T}\right) \\ &= \frac{\Theta_{X^=}}{\Theta_{X^0}} \cdot \exp\left(\frac{E_c - E_{X^=}}{k \cdot T}\right) \cdot \exp\left(\frac{E_c - E_{X^-}}{k \cdot T}\right) \cdot \left(\frac{n}{n_i}\right)^2 \cdot \exp\left(-\frac{E_g}{k \cdot T}\right) \\ &= \delta_{X^=} \cdot \left(\frac{n}{n_i}\right)^2 \end{aligned} \quad (2.22)$$

$$\begin{aligned} \frac{C_{X^-}^{eq}}{C_{X^0}^{eq}} &= \frac{\Theta_{X^-}}{\Theta_{X^0}} \cdot \exp\left(\frac{E_c - E_{X^-}}{k \cdot T}\right) \cdot \exp\left(\frac{E_F - E_i}{k \cdot T}\right) \cdot \exp\left(-\frac{E_c - E_i}{k \cdot T}\right) \\ &= \frac{\Theta_{X^-}}{\Theta_{X^0}} \cdot \exp\left(\frac{E_c - E_{X^-}}{k \cdot T}\right) \cdot \frac{n}{n_i} \cdot \exp\left(-\frac{E_g}{2 \cdot k \cdot T}\right) = \delta_{X^-} \cdot \frac{n}{n_i} \end{aligned} \quad (2.23)$$

$$\begin{aligned} \frac{C_{X^+}^{eq}}{C_{X^0}^{eq}} &= \frac{\Theta_{X^+}}{\Theta_{X^0}} \cdot \exp\left(\frac{E_{X^+} - E_v}{k \cdot T}\right) \cdot \exp\left(\frac{E_i - E_F}{k \cdot T}\right) \cdot \exp\left(-\frac{E_i - E_v}{k \cdot T}\right) \\ &= \frac{\Theta_{X^+}}{\Theta_{X^0}} \cdot \exp\left(\frac{E_{X^+} - E_v}{k \cdot T}\right) \cdot \frac{p}{n_i} \cdot \exp\left(-\frac{E_g}{2 \cdot k \cdot T}\right) = \delta_{X^+} \cdot \frac{p}{n_i} \end{aligned} \quad (2.24)$$

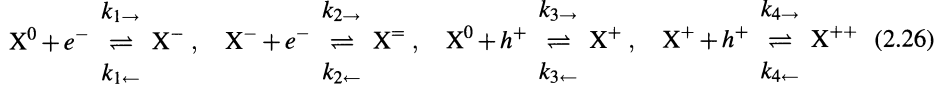
$$\begin{aligned}
\frac{C_{X^{++}}^{eq}}{C_{X^0}^{eq}} &= \frac{\Theta_{X^{++}}}{\Theta_{X^0}} \cdot \exp\left(\frac{E_{X^{++}} - E_v}{k \cdot T}\right) \cdot \exp\left(\frac{E_{X^+} - E_v}{k \cdot T}\right) \\
&\quad \cdot \exp\left(\frac{2 \cdot (E_i - E_F)}{k \cdot T}\right) \cdot \exp\left(-\frac{2 \cdot (E_i - E_v)}{k \cdot T}\right) \\
&= \frac{\Theta_{X^{++}}}{\Theta_{X^0}} \cdot \exp\left(\frac{E_{X^{++}} - E_v}{k \cdot T}\right) \cdot \exp\left(\frac{E_{X^+} - E_v}{k \cdot T}\right) \cdot \left(\frac{p}{n_i}\right)^2 \cdot \exp\left(-\frac{E_g}{k \cdot T}\right) \\
&= \delta_{X^{++}} \cdot \left(\frac{p}{n_i}\right)^2
\end{aligned} \tag{2.25}$$

The parameters δ_{X^j} in the equations (2.22) to (2.25) correspond to the relative concentrations of defects X in charge state j under intrinsic conditions with respect to the concentration in the neutral state. Formally, δ_{X^0} is equal to unity. For low dopant concentrations, the δ_{X^j} will be a function of temperature only. There may be deviations from an ideal Arrhenius law, though, since the ionization energies as well as the band gap will depend on temperature. The reduction of the band gap with temperature was discussed already in Section 1.2.7. The influence of temperature on the ionization levels is not known in general but there were some suggestions in the literature. For vacancies, Van Vechten and Thurmond [2.13] proposed that the distances in energy between the edge of the conduction band and the levels E_{V^-} and E_{V^0} remains constant with respect to temperature. Similarly, the distances in energy between the edge of the valence-bond band and the levels E_{V^+} and $E_{V^{++}}$ were suggested to be temperature-independent. This is the main reason for a splitting in the form of (2.22) to (2.25). On the other hand, considering that the vacancy was postulated to change from a localized state at low temperatures to an extended state at elevated temperatures, an influence of the temperature on its ionization level can probably not be excluded. Therefore, one has to be very careful when extending the significance of measured levels to other temperatures. An alternative approach was used, e.g. by Mathiot and Pfister [2.14] who assumed that the distances in energy scale with the band gap so that the relative positions of the levels in the band gap remain temperature-independent. Reported values for the positions of the ionization levels are discussed in Sections 2.4 and 2.5 for vacancies and self-interstitials, respectively.

In addition to temperature effects, influences of the dopant concentration on band gap and ionization levels are expected. As discussed in Section 1.2.5, they are known to occur at room temperature already at moderate doping levels around and above 10^{18} cm^{-3} . The concentration-dependent changes in the width of the forbidden band gap δE_g can, in principle, be separated from the δ_{X^j} and combined with n_i to an effective intrinsic carrier concentration n_e as in (1.22). In process simulation, such an extension has been introduced by Fair [2.15] to explain the measured reduction of the diffusion coefficient of phosphorus at concentrations above $4 \cdot 10^{20} \text{ cm}^{-3}$. The discussion in Section VI.D of the review of Fahey et al. [2.16] has shown that such an approach is problematic, though. A main point is that a reduced band gap has only a negligible effect on the majority carriers in extrinsically doped silicon. It is merely the concentration of the minority carriers which will be affected. In consequence, Fahey et al. suggested that an effective band-gap narrowing can be a convenient form to mimic high-concentration effects since it allows to keep the favorable structure of the equations (2.22) to (2.25). However, there should be no physical meaning attached to δE_g .

Reaction of Intrinsic Point Defects with Charge Carriers

A second approach to calculate the concentrations of ionized point defects results from reaction kinetics and is frequently used in the literature. We assume that the charged defects X^j result from reactions with electrons e^- and holes h^+ in the form



The concentrations of the electrons and holes will be denoted by n and p , respectively. Because of their high mobility, as discussed in Section 1.5.3, capturing of charge carriers at defects will be very fast in comparison to the time constants of other processes like diffusion of the respective point defects or their reactions with other point defects or extended defects. The dynamics of the ionization reactions can then be ignored and, since forward reaction rates and backward reaction rates have to cancel, one obtains

$$C_{X^-} = \frac{k_{1\rightarrow}}{k_{1\leftarrow}} \cdot C_{X^0} \cdot n \quad (2.27)$$

$$C_{X^=} = \frac{k_{2\rightarrow}}{k_{2\leftarrow}} \cdot C_{X^-} \cdot n = \frac{k_{1\rightarrow}}{k_{1\leftarrow}} \cdot \frac{k_{2\rightarrow}}{k_{2\leftarrow}} \cdot C_{X^0} \cdot n^2 \quad (2.28)$$

$$C_{X^+} = \frac{k_{3\rightarrow}}{k_{3\leftarrow}} \cdot C_{X^0} \cdot p \quad (2.29)$$

$$C_{X^{++}} = \frac{k_{4\rightarrow}}{k_{4\leftarrow}} \cdot C_{X^+} \cdot p = \frac{k_{3\rightarrow}}{k_{3\leftarrow}} \cdot \frac{k_{4\rightarrow}}{k_{4\leftarrow}} \cdot C_{X^0} \cdot p^2 \quad (2.30)$$

as relations between the concentrations of the defects in the different charge states. The usage of the electron and hole concentrations n and p limits the applicability to the range of validity of Boltzmann statistics. Otherwise, the concentrations n and p have to be replaced by the respective activities $\gamma_n \cdot n$ and $\gamma_p \cdot p$ which can be expressed in terms of the Fermi-level by (1.98) and (1.99). The equations (2.27) to (2.30) are not restricted to thermal equilibrium. In thermal equilibrium, they correspond to the equations (2.22) to (2.25), and the parameters δ_{X^j} can be related to the reaction constants $k_{1\rightarrow}$ to $k_{4\leftarrow}$ via

$$\delta_{X^-} = \frac{k_{1\rightarrow}}{k_{1\leftarrow}} \cdot n_i, \quad \delta_{X^=} = \frac{k_{2\rightarrow}}{k_{2\leftarrow}} \cdot n_i \cdot \delta_{X^-}, \quad \delta_{X^+} = \frac{k_{3\rightarrow}}{k_{3\leftarrow}} \cdot n_i, \quad \delta_{X^{++}} = \frac{k_{4\rightarrow}}{k_{4\leftarrow}} \cdot n_i \cdot \delta_{X^+}. \quad (2.31)$$

The total concentration of point defects X is given by the sum of the concentrations in the various charge states. In the syntax adopted in (2.22) to (2.25), it evaluates as

$$C_X = \sum_j C_{X^j} = C_{X^0} \cdot \sum_j \delta_{X^j} \cdot \left(\frac{n}{n_i} \right)^{z_j}. \quad (2.32)$$

Similarly, the total concentration in thermal equilibrium is given by

$$C_X^{eq} = \sum_j C_{X^j}^{eq} = C_{X^0}^{eq} \cdot \sum_j \delta_{X^j} \cdot \left(\frac{n}{n_i} \right)^{z_j}. \quad (2.33)$$

Reported values for the equilibrium concentrations of intrinsic point defects under intrinsic conditions are commonly given in the form of an Arrhenius law

$$C_X^{eq} = \tilde{C}_X \cdot \exp\left(-\frac{H_X^f}{k \cdot T}\right) \quad (2.34)$$

with the prefactor \tilde{C}_X combining all terms in (2.33) which do not depend explicitly on temperature. For vacancies and self-interstitials, the reported values are discussed in Sections 2.4 and 2.5, respectively. As a superposition of temperature-dependent values, the equilibrium concentrations can be assumed to obey an Arrhenius law even under intrinsic conditions only when one of the charge states dominates for all temperatures or when the activation energies of the relative concentrations δ_{Xj} are nearly equal. But experimental evidence is currently far from allowing a verification.

Stress Effects

In the most simple experimental set-up, hydrostatic pressure is exerted on the sample. Generating a vacancy means that a silicon atom is brought from the interior to a surface kink while a silicon atom is transferred from a surface kink into the silicon bulk to create a self-interstitial. The extra work done against or by the hydrostatic pressure has to be taken into considerations for the total change in the Gibbs free energy. Considering that the pressure dependence of the chemical potential $\partial G/\partial N$ in (1.88) is dominated by far by the pressure dependence of G^f , the activation volume given by

$$\Delta V^f = \frac{\partial \left(-k \cdot T \cdot \ln \left(\frac{N^{eq}}{\Theta \cdot N_S} \right) \right)}{\partial P} = \frac{\partial G^f}{\partial P} = \bar{V} \quad (2.35)$$

can be identified, as in (1.92), as the atomic volume change \bar{V} of the system associated with one of the defects being introduced. This allows to write the equilibrium concentration of intrinsic point defects in samples under hydrostatic pressure in the form

$$C_{V,I}^{eq}(P) = C_{V,I}^{eq}(P=0) \cdot \exp\left(-\frac{P \cdot \Delta V^f}{k \cdot T}\right). \quad (2.36)$$

Vacancies will increase the volume of the sample by the volume V_{Si} of the silicon atom brought from the bulk to the surface while relaxation of the crystal will tend to decrease the volume. As a consequence, when the volume change $\Delta V^r < 0$ due to relaxation does not exceed V_{Si} in magnitude, the total volume change $\Delta V^f = V_{Si} + \Delta V^r$ will be positive and the equilibrium concentration of vacancy defects will decrease under compressive pressure and increase under tensile pressure. For self-interstitials, it is *vice versa*. They decrease the volume by the volume of the silicon atom V_{Si} taken from the surface while relaxations of the crystal will tend to increase the volume again. As a consequence, when the volume change $\Delta V^r > 0$ due to relaxation does not exceed $-V_{Si}$, the total volume change $\Delta V^f = -V_{Si} + \Delta V^r$ will be negative and the concentration of self-interstitials is expected to increase under compressive pressure and to decrease under tensile pressure.

The situation becomes more complicated when internal forces, e. g. exerted by dislocations, have to be taken into considerations. In the derivation given by Hirth and Lothe in Section 14-4 of their monograph on dislocations [2.17], work at the site to which the associated silicon atom is transferred to is again done against or by the hydrostatic pressure with the volume change

given by V_{Si} for vacancies and $-V_{Si}$ for self-interstitials. On the other hand, at the site where the point defect is generated, work is assumed to be done against or by the sum of the external hydrostatic pressure P and an internal pressure P^{int} . With the associated volume change ΔV^r , the dependence of the equilibrium concentration on the external and internal pressures is given by

$$\begin{aligned} C_{V,I}^{eq}(P, P^{int}) &= C_{V,I}^{eq}(P = 0, P^{int} = 0) \cdot \exp\left(\mp \frac{P \cdot V_{Si}}{k \cdot T}\right) \cdot \exp\left(-\frac{(P + P^{int}) \cdot \Delta V^r}{k \cdot T}\right) \\ &= C_{V,I}^{eq}(P, P^{int} = 0) \cdot \exp\left(-\frac{P^{int} \cdot \Delta V^r}{k \cdot T}\right). \end{aligned} \quad (2.37)$$

Since, as mentioned above, ΔV^r is expected to be negative for vacancies and positive for self-interstitials, internal compressive pressures are expected to lead to an increase in the equilibrium concentration of vacancies while internal tensile pressures are expected to cause a decrease. For self-interstitials, the situation is *vice versa*. These relationships were found to play important roles for the modeling of the growth of dislocation loops [2.18–2.20], crystal growth [2.21], and the formation of voids [2.22].

Comparing the effects of internal and external pressures, one is faced by the paradox that the local pressure does not suffice to know whether the equilibrium (or rather steady-state) concentration of intrinsic point defects will increase or decrease. It is rather necessary to know where the silicon atom associated with the intrinsic point defects goes to or comes from and what the energetic conditions are at that point.

2.2 Diffusion of Intrinsic Point Defects

Intrinsic point defects in silicon are assumed to be mobile *per se*, migrating by uncorrelated jumps similar to Brownian movement as discussed in Section 1.3.2. For an independently migrating point defect, the diffusion coefficient is given by (1.61) and can be written in the form

$$D = g \cdot \Gamma \cdot a_{Si}^2 \quad (2.38)$$

where g denotes a geometrical factor and a_{Si} the lattice parameter of silicon. For vacancies, Γ stands for the jump frequency of an atom adjacent to the vacancy into the vacancy and the geometrical factor g takes the value 1/8 [2.3].¹ For self-interstitials in the form of a ⟨100⟩-oriented split interstitial, Seeger et al. [2.23] suggested g to be 1/12. The jump frequency Γ is given by (1.71), and the attempt frequency Γ_0 has been estimated for the jump of a surrounding atom into a vacancy [2.2] as well as for self-interstitials [2.23] to be

$$\Gamma_0 = \sqrt{\frac{8 \cdot H^m}{3 \cdot m_{Si} \cdot a_{Si}^2}} \quad (2.39)$$

with m_{Si} denoting the atomic mass of silicon, and H^m the enthalpy of migration of the respective point defect. It evaluates as $\Gamma_0 = 2.5 \cdot 10^{12} \text{ s}^{-1}$ for a migration enthalpy of 0.2 eV which is one order of magnitude smaller than the highest frequency within the Debye model of solids (see Section 1.3.2). Customarily, the parameters without explicit temperature dependence are combined to a prefactor D_0 and the diffusion coefficient is written in the form of (1.45) with

¹In some publications, Γ is associated with the jump frequency of the vacancy which is four times as high as the jump frequency of one of its surrounding atoms. The geometrical factor g is then 1/32.

the activation energy E_A . This activation energy corresponds then formally to the enthalpy of migration H^m discussed in Section 1.3.2 as long as the latter does not vary with temperature.

At least at cryogenic temperatures, such a diffusion coefficient can be assigned to each of the charge states of a point defect. Besides uncorrelated diffusion, migration of charged point defects in an electric field $E = -\text{grad}\psi$ has to be taken into account via (1.78) which can be written for charge state j in the form

$$J_{X^j} = -D_{X^j} \cdot \text{grad}C_{X^j} + z_j \cdot D_{X^j} \cdot C_{X^j} \cdot \text{grad}(\psi/U_T). \quad (2.40)$$

In the continuity equations, in addition to the currents, the reactions with charge carriers (2.26) have to be taken into account by the kinetic law of mass action as outlined in Section 1.5. Other recombination and generation mechanisms are ignored at the moment and will be discussed later in Section 2.7. For ideally dilute solutions within the range of applicability of Boltzmann statistics, one obtains the following set of coupled partial differential equations describing the redistribution of point defect X in its various charge states

$$\begin{aligned} \frac{\partial C_{X^0}}{\partial t} &= \text{div}(D_{X^0} \cdot \text{grad}C_{X^0}) \\ &- k_{1\rightarrow} \cdot C_{X^0} \cdot n + k_{1\leftarrow} \cdot C_{X^-} - k_{3\rightarrow} \cdot C_{X^0} \cdot p + k_{3\leftarrow} \cdot C_{X^+} \end{aligned} \quad (2.41)$$

$$\begin{aligned} \frac{\partial C_{X^-}}{\partial t} &= \text{div}(D_{X^-} \cdot \text{grad}C_{X^-} - D_{X^-} \cdot C_{X^-} \cdot \text{grad}(\psi/U_T)) \\ &+ k_{1\rightarrow} \cdot C_{X^0} \cdot n - k_{1\leftarrow} \cdot C_{X^-} - k_{2\rightarrow} \cdot C_{X^-} \cdot n + k_{2\leftarrow} \cdot C_{X^=} \end{aligned} \quad (2.42)$$

$$\begin{aligned} \frac{\partial C_{X^=}}{\partial t} &= \text{div}(D_{X^=} \cdot \text{grad}C_{X^=} - 2 \cdot D_{X^=} \cdot C_{X^=} \cdot \text{grad}(\psi/U_T)) \\ &+ k_{2\rightarrow} \cdot C_{X^-} \cdot n - k_{2\leftarrow} \cdot C_{X^=} \end{aligned} \quad (2.43)$$

$$\begin{aligned} \frac{\partial C_{X^+}}{\partial t} &= \text{div}(D_{X^+} \cdot \text{grad}C_{X^+} + D_{X^+} \cdot C_{X^+} \cdot \text{grad}(\psi/U_T)) \\ &+ k_{3\rightarrow} \cdot C_{X^0} \cdot p - k_{3\leftarrow} \cdot C_{X^+} - k_{4\rightarrow} \cdot C_{X^+} \cdot p + k_{4\leftarrow} \cdot C_{X^{++}} \end{aligned} \quad (2.44)$$

$$\begin{aligned} \frac{\partial C_{X^{++}}}{\partial t} &= \text{div}(D_{X^{++}} \cdot \text{grad}C_{X^{++}} + 2 \cdot D_{X^{++}} \cdot C_{X^{++}} \cdot \text{grad}(\psi/U_T)) \\ &+ k_{4\rightarrow} \cdot C_{X^+} \cdot p - k_{4\leftarrow} \cdot C_{X^{++}} \end{aligned} \quad (2.45)$$

As discussed in Section 1.5.3, it can be assumed that the reactions with charge carriers occur at elevated temperatures on a much shorter time scale than diffusive broadening or reactions with other point defects or extended defects. The relative concentrations of the charged point defects are then given by (2.22) to (2.25) with the parameters δ_{X^j} related to the reaction constants by (2.31). This allows to express the gradients of the concentrations of the charged point defects in terms of the gradients of the concentration of the neutral defects and the gradient of the electrostatic potential as

$$\text{grad} C_{X^-} = \delta_{X^-} \cdot n/n_i \cdot (\text{grad} C_{X^0} + C_{X^0} \cdot \text{grad}(\psi/U_T)) \quad (2.46)$$

$$\text{grad} C_{X^=} = \delta_{X^=} \cdot (n/n_i)^2 \cdot (\text{grad} C_{X^0} + 2 \cdot C_{X^0} \cdot \text{grad}(\psi/U_T)) \quad (2.47)$$

$$\text{grad} C_{X^+} = \delta_{X^+} \cdot p/n_i \cdot (\text{grad} C_{X^0} - C_{X^0} \cdot \text{grad}(\psi/U_T)) \quad (2.48)$$

$$\text{grad} C_{X^{++}} = \delta_{X^{++}} \cdot (p/n_i)^2 \cdot (\text{grad} C_{X^0} - 2 \cdot C_{X^0} \cdot \text{grad}(\psi/U_T)) \quad (2.49)$$

Inserting these relationships into (2.42) to (2.45) shows that the contributions of the gradient of the electrostatic potential cancel out. By adding the equations (2.41) to (2.45), the reaction rates are eliminated, resulting in

$$\frac{\partial C_X}{\partial t} = \sum_j \frac{\partial C_{X^j}}{\partial t} = \text{div}(D_X^0 \cdot \text{grad} C_{X^0}) \quad (2.50)$$

with D_X^0 given by

$$D_X^0 = \sum_j \delta_{X^j} \cdot D_{X^j} \cdot (n/n_i)^{z_j}. \quad (2.51)$$

When the gradient of the total concentration C_X is used instead of the gradient of the concentration of the electrically neutral defects C_{X^0} , a field term is introduced again by the derivatives of the charge-carrier concentrations resulting in [2.24]

$$\frac{\partial C_X}{\partial t} = \sum_j \frac{\partial C_{X^j}}{\partial t} = -\text{div} J_X \quad (2.52)$$

with J_X standing for the total current of defect X

$$J_X = \sum_j J_{X^j} = -D_X \cdot \text{grad} C_X + z_X \cdot D_X \cdot C_X \cdot \text{grad}(\psi/U_T). \quad (2.53)$$

Therein, the symbols D_X and z_X denote the Fermi-level-dependent effective diffusion coefficient

$$D_X = \frac{\sum_j D_{X^j} \cdot \delta_{X^j} \cdot (n/n_i)^{z_j}}{\sum_j \delta_{X^j} \cdot (n/n_i)^{z_j}} \quad (2.54)$$

and the Fermi-level-dependent effective charge state

$$z_X = \frac{\sum_j z_j \cdot \delta_{X^j} \cdot (n/n_i)^{z_j}}{\sum_j \delta_{X^j} \cdot (n/n_i)^{z_j}}. \quad (2.55)$$

Often, it is assumed that the diffusion coefficients of the various charge states of a point defect are on the same order of magnitude or even equal [2.25, 2.26]. Then, the effective diffusion coefficient (2.54) becomes independent of the Fermi-level. Otherwise, as superposition of the diffusion coefficients in the different charge states, D_X can be described by one activation energy only when it is dominated by one of the charge states or when the activation energies of the diffusion coefficients as well as of the relative concentrations δ_{X^j} are very similar. This is certainly not the case for vacancies at cryogenic temperatures. At elevated temperatures, the current uncertainties in the experimental determination allow no verification of this subject.

When the application of Boltzmann statistics is not justified, the concentrations n and p have to be replaced by the respective activities $\gamma_n \cdot n$ and $\gamma_p \cdot p$ which can be expressed in terms of the Fermi-level by (1.98) and (1.99). Introducing an effective value for the intrinsic concentration via (1.21) shows that (2.50) to (2.55) remain valid with n_i replaced by n_{ie} only as long as the gradients of the δ_{X^j} can be neglected. However, as discussed in Section 2.1, at high concentrations, the δ_{X^j} may depend on the doping concentration and, consequently, on space. Here, it would not even help to use different values for n_{ie} for each charge state since then, the equations (1.20), on which the derivation of (2.46) to (2.49) was based, are no longer valid.

In the intrinsic regime, the quotient of electron concentration and intrinsic carrier concentration is equal to unity, and (2.52) and (2.53) can be combined to

$$\frac{\partial C_X}{\partial t} = \text{div} (D_X^i \cdot \text{grad} C_X) \quad (2.56)$$

with the intrinsic diffusion coefficient of point defect X given by

$$D_X^i = \frac{\sum_j D_{X^j} \cdot \delta_{X^j}}{\sum_j \delta_{X^j}}. \quad (2.57)$$

Despite the problems with the superposition of individual diffusion coefficients, the diffusivity of intrinsic point defects is usually given in the form of (1.45) with the activation energy E_A corresponding to the enthalpy of migration H^m (cf. Section 1.3.2). For self-interstitials and vacancies, the reported values are discussed in Sections 2.4 and 2.5.

2.3 Self-Diffusion and Tracer Diffusion

Even at vanishing gradients of their spatial distributions, point defects perform random walks in the crystal. Each jump of a vacancy implies the jump of a silicon atom in the reverse direction. Likewise, the migration of a self-interstitial implies the transport of silicon atoms. This “self-diffusion” of the silicon atoms is one of the few directly measurable properties related to point defects in silicon.

The most direct method to measure the self-diffusion coefficient of silicon is to use one of the isotopes of silicon as a tracer. In the early investigations, the usage of the stable isotopes ^{29}Si and ^{30}Si had a drawback from the high isotope abundances of 4.67% and 3.1%, respectively. Only recently, isotopically enriched ^{28}Si became available and enabled reliable experiments. Before, as an alternative, the unstable isotope ^{31}Si was used in several investigations. But it has a half-life time of 2.62 h only which, together with the small self-diffusion coefficient, limited its application to temperatures above 1050 °C.

Contributions to Self-Diffusion and Tracer Diffusion

Silicon atoms at substitutional sites surrounded by lattice atoms at all coordination sites are generally assumed to be immobile. In order to jump via a vacancy mechanism, a vacancy has to be at one of the four nearest neighbouring sites. The respective probability is given by four times the quotient of the number of vacancies and the number of lattice sites in the volume of interest. But for each of the vacancies, the probability that it exchanges sites with our tracer atom is one fourth of its total jump probability. Thus, the so-called “self-diffusion coefficient via vacancies” in the various charge states is given by

$$D_{Si}^V = \sum_j D_{V^j} \cdot \frac{C_{V^j}}{C_{Si}} \quad (2.58)$$

with C_{Si} denoting the number of lattice sites per unit volume. Similarly, migration via an interstitial mechanism implies that the atom under consideration is at an interstitial site in any charge state k where it can perform a random walk with the respective diffusion coefficient. The probability for a silicon atom to be at an interstitial site is given by the quotient of the number of interstitials and the total number of silicon atoms (basically the number of lattice sites) in the volume of interest. The “self-diffusion coefficient via self-interstitials” in the various charge states evaluates then as

$$D_{Si}^I = \sum_k D_{Ik} \cdot \frac{C_{Ik}}{C_{Si}}. \quad (2.59)$$

When we assume that tracer atoms may diffuse via either vacancies or self-interstitials, the tracer diffusion coefficient can be related to the self-diffusion coefficients via

$$D_T = f^I \cdot D_{Si}^I + f^V \cdot D_{Si}^V = f^I \cdot D_I \cdot \frac{C_I^{eq}}{C_{Si}} + f^V \cdot D_V \cdot \frac{C_V^{eq}}{C_{Si}} \quad (2.60)$$

[2.3, 2.27, 2.28]. The symbols f , D , and C^{eq} denote the diffusion correlation factors, the diffusion coefficients, and the equilibrium concentrations of silicon self-interstitials (super/subscript ‘ I ’) and vacancies (super/subscript ‘ V ’), respectively. The correlation factors take into account that, although the intrinsic point defects migrate randomly, successive jumps of a tracer atom due to interactions with intrinsic point defects are correlated². For diffusion via vacancies, the tracer correlation coefficient takes the value $f^V = 0.5$ [2.3, 2.29–2.31], and $f^I = 0.7273$ for tracer diffusion via the interstitialcy mechanism [2.32]. Alternatively, invoking the thermodynamics of irreversible processes, Hu [2.33] claimed that the tracer diffusion coefficient via vacancies has to be written in the form

$$D_T = (1 + f^V) \cdot D_V \cdot \frac{C_V^{eq}}{C_{Si}}. \quad (2.61)$$

This formulation was cited and even extended to self-interstitials in several publications (e. g. in the review of Fahey et al. [2.16]), but apparently dropped in Hu’s most recent review [2.34].

In addition to self-diffusion via vacancies and self-interstitials, other contributions were suggested in the literature to affect self-diffusion and tracer diffusion, leading to additional terms in (2.60). From the high prefactor of his tracer-diffusion coefficient, Peart [2.35] suggested the possibility of a non-negligible contribution of divacancies. Reviewing the limited information on self-diffusion and theoretical predictions of point-defect properties available at that time, Ghoshtagore [2.36] and Kendall and De Vries [2.37] concluded self-diffusion to be even dominated by divacancies. Similarly, based in part on not reproduced positron-annihilation experiments of Dannefaer et al. [2.38] (see Section 2.4), Van Vechten [2.39] suggested that divacancies could account for a significant fraction of self-diffusion. The general consensus nowadays, based especially on refined theoretical methods, is that no compelling arguments remain for a significant contribution of divacancies to self-diffusion and tracer diffusion.

A further mechanism frequently taken into considerations is the concerted-exchange mechanism suggested by Pandey [2.40]. The activation energy obtained from their *ab-initio* calculations was 4.3 eV which would be consistent with self-diffusion. Thus, the contribution of concerted exchange to self-diffusion depends on the entropy factors. Using an improved Ter-soff potential, Heggie [2.41] found that the concerted-exchange mechanism involves an entropy penalty of $-4.6 \cdot k$ which would make it extremely unlikely. Based on the transition-rate theory, Pandey and Kaxiras [2.42] calculated an entropy of $3.3 \cdot k$. This value, as noted by Blöchl et

²To make the meaning of this statement more clear: For the first exchange of a tracer atom with a vacancy, the probability that a vacancy is at a nearest neighboring site is $4 \cdot C_V/C_{Si}$. After a first jump has occurred, this probability is unity and the probability is 1/4 that tracer atom and vacancy exchange sites again.

al. [2.43], would make the concerted-exchange mechanism also negligible. In a subsequent study, Kaxiras and Pandey [2.44] corrected their estimate for the entropy to $6.3 \cdot k$. This would leave the contribution of concerted exchange to about 2% at the melting temperature. Finally, Antonelli et al. [2.45] estimated entropy factors around $8 \cdot k$ from their Monte-Carlo simulations. Thus, the concerted-exchange mechanism could account for about 13% of self-diffusion at the melting temperature, and for about 35% at 900 °C. The concerted-exchange mechanism was studied also by Leung et al. [2.46]. Their calculations resulted in activation energies of 4.45 and 4.8 eV based on the local density approximation and the generalized gradient approximation, respectively. Slightly higher values of 4.58 and 4.93 eV were reported by Needs [2.47]. While these activation energies would be consistent with experimental values for the activation energies reported for tracer diffusion, Leung et al. [2.46] and Needs [2.47] remarked that the sum of formation and activation energy they got for self-interstitials was significantly lower so that they would expect self-diffusion via self-interstitials to dominate. Considering the large uncertainties in such analyses one can conclude at least that the concerted-exchange mechanism cannot be excluded *a priori*. In this sense, Ural et al. [2.48] estimated the contributions of concerted exchange to self-diffusion from his experiments to be $\leq 11\%$ and $\leq 14\%$ for 1000 and 1100 °C, respectively. In a more conservative estimate, Ural et al. [2.49] gave bounds of $\leq 27\%$ at 1000 °C and $\leq 62\%$ at 1100 °C.

Additional contributions to self-diffusion and tracer diffusion may arise from the diffusion of impurities. Some of the atomistic mechanisms to be discussed in Chapter 3 involve also the motion of host atoms. The respective contributions to self-diffusion and tracer diffusion have to be taken into consideration by correlation coefficients which reflect the particularities of the mechanism [2.50].

Tracer Diffusion Experiments at Intrinsic Concentrations

The various values reported in the literature for the tracer diffusion coefficient are summarized in Table 2.1. For a graphical representation see Figure 2.1. The regression line

$$D_T^i = 323 \cdot \exp\left(-\frac{4.705 \text{ eV}}{k \cdot T}\right) \text{ cm}^2/\text{s} \quad (2.62)$$

also shown is based on the published diffusivity measurements in isotopically enriched silicon crystals [2.49, 2.51–2.55]. The activation energy ranges with a confidence level of 90% from 4.6 to 4.8 eV. The 90% confidence interval for the diffusion coefficient is about +8.6/-7.9% of the regression curve at 1020 °C and increases to +24/-19% at the melting point and +17/-14% at 850 °C. Additional measurements are expected with 90% confidence within a range of +60/-38% of the regression curve at 1020 °C which increases slightly to +67/-40% at the melting point and +63/-39% at 850 °C.

Various reasons were given in the literature for the obvious disagreement between some of the values reported. In the tracer diffusion experiment of Peart [2.35], the isotope source was an evaporated layer of radioactive silicon. Shaw [2.31] argued that the tracer could migrate in the evaporated layer via short-circuit paths so that Peart's data probably overestimated the tracer diffusion coefficient. Shaw [2.31] and Van Vechten [2.25] pointed out that oxidation effects during heat treatment could have a non-negligible influence on the self-diffusion experiments of Peart [2.35], Ghoshtagore [2.56], and Fairfield and Masters [2.57]. The experiments of Ghoshtagore [2.56] have been criticized also by Hu [2.27]. He could show that the peak concentration in Ghoshtagore's experiment carried through at 1178 °C was only a factor of two above

³The self-diffusion coefficient given by Peart, as noted already by Kendall and De Vries [2.37], does not fit his experimental values. A better approximation for them would be $D^T = 2.516 \cdot 10^3 \cdot \exp(-4.887 \text{ eV}/kT) \text{ cm}^2/\text{s}$

Table 2.1: Prefactors and activation energies E_A reported for tracer diffusion. A trailing star indicates the usage of a layer in which this isotope is enriched.

	D_0 (cm 2 /s)	E_A (eV)	Tracer	Temperature range (°C)	Ref.
Pearl ³	$1.8 \cdot 10^3$	4.774	^{31}Si	1200–1400	[2.35]
Ghoshtagore	$1.2 \cdot 10^3$	4.73	^{30}Si	1278–1300	[2.56]
Fairfield & Masters	$9 \cdot 10^3$	5.13	^{31}Si	1100–1300	[2.57]
Mayer et al.	$1.46 \cdot 10^3$	5.02	^{31}Si	1047–1387	[2.58]
Hirvonen & Anttila	8.0	4.1	^{30}Si	900–1100	[2.59]
Kalinowski & Seguin	154	4.648	^{30}Si	855–1175	[2.60, 2.61]
Demond et al.	20	4.4	^{30}Si	830–1200	[2.62]
Bracht et al.	530	4.75	$^{28}\text{Si}^*$	855–1388	[2.51]
Bracht et al.	560	4.76	$^{28}\text{Si}^*$	855–1388	[2.52]
Ural et al.	570	4.77	$^{28}\text{Si}^*$	900–1100	[2.48]

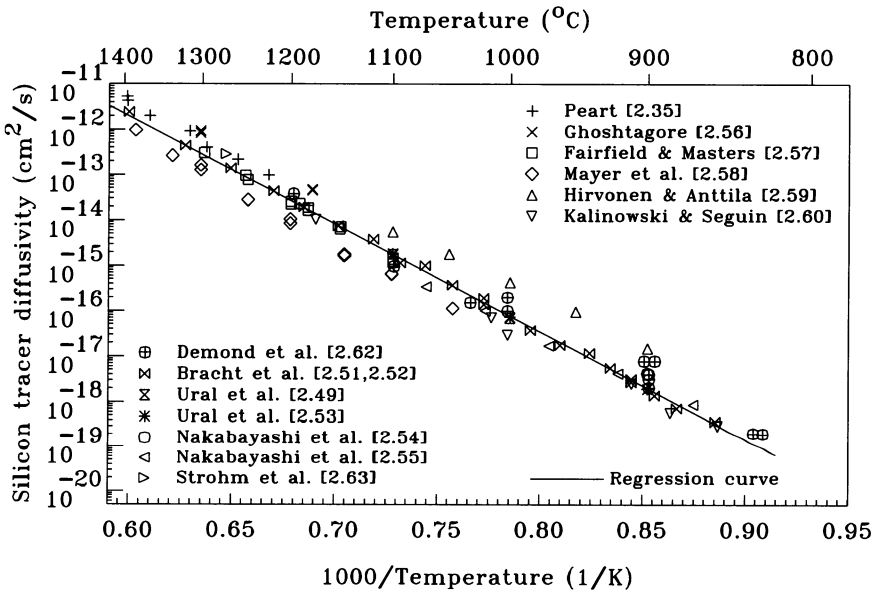


Figure 2.1: Tracer diffusion coefficient in silicon.

the natural abundance of ^{30}Si in contradiction to Ghoshtagore's picture showing data covering more than one decade. In the work of Hirvonen and Anttila [2.59] as well as in the work of Demond et al. [2.62], isotopes were introduced by ion implantation. The damage produced by the implantation process can be expected to enhance tracer diffusion in analogy to the enhanced diffusion of dopants observed during post-implantation annealing.

Recently, the growth of highly isotope-enriched epitaxial silicon layers became possible [2.48, 2.49, 2.51–2.55] and helped to avoid most of the problems mentioned above. Experimental results obtained this way agreed well with the reports of Fairfield and Masters [2.57],

Kalinowski and Seguin [2.60, 2.61], and Demond et al. [2.62]. But they are significantly lower than those of Peart [2.35], Ghoshtagore [2.56], Hirvonen and Anttila [2.59], and Strohm et al. [2.63], and they are, by a factor of 2, larger than those of Mayer et al. [2.58] considered the most reliable experiments before. The experiments with isotope-enriched layers also show that tracer diffusion can be described within a wide temperature range with a single activation energy. This contradicts the early result of Tan and Gösele [2.64] which was used in a large number of investigations since then until today. They had, on the basis of the limited number of experiments available then, postulated a marked cross-over of the activation energy of self-diffusion from 4.8 eV at high temperatures to 4.03 eV at low temperatures which they interpreted in terms of a change in the dominant diffusion mechanism.

When self-diffusion in silicon was compared to self-diffusion in metals with a similar melting point, two significant differences were noted and discussed in length in the literature, notably by Seeger and coworkers [2.2, 2.3]. On the one hand, self-diffusion in silicon is much slower than in metals. On the other hand, the pre-exponential factors are much higher in silicon. The first observation can be explained by high formation energies of the intrinsic point defects and was resolved consistently by recent theoretical investigations. The second observation, addressed often as “entropy dilemma,” implies that the sum of formation entropy and migration entropy is about $S^f + S^m \approx (12 - 15) \cdot k$. To explain such large entropies, various concepts were developed. Some authors, as discussed above, postulated that self-diffusion in silicon would be governed by a divacancy mechanism. An alternative concept, developed by Seeger and coworkers, postulated that the intrinsic point defects assume an extended state at elevated temperatures. Extended states of the intrinsic point defects and other concepts will be discussed in Sections 2.4 and 2.5. However, it has to be mentioned that no complete agreement has been achieved up to now, especially with respect to the entropies of migration of the intrinsic point defects.

Pressure Effects

The effect of hydrostatic pressure on self-diffusion was investigated by Aziz et al. [2.65]. These measurements clearly indicated a negative activation volume but, as remarked later by Aziz [2.66], considerable uncertainties were introduced into the results by the experimental technique used.

Tracer Diffusion Experiments at Extrinsic Concentration

Diffusion of tracers in doped silicon has been studied under isoconcentration conditions by Ghoshtagore [2.56], Fairfield and Masters [2.57], Hettich et al. [2.67],⁴ Nakabayashi et al. [2.54, 2.55], Ural et al. [2.68], and Osman et al. [2.69]. Their results are shown in Figure 2.2. To account for systematic differences between the reported diffusivities, the data sets of Ghoshtagore and Nakabayashi et al., were multiplied each by a constant so that the scaled values corresponded for intrinsic conditions to (2.62). The full lines were obtained by a numerical optimization based on the data points used for the regression curve in Figure 2.1 in addition to data from tracer diffusion experiments in intrinsic silicon [2.49, 2.51–2.55, 2.57, 2.60–2.62]. They are described by

⁴The values of Hettich et al. [2.67], have not been included in the analysis. Their silicon tracer experiments were carried out in boron-doped samples with a concentration of about 10^{19} cm^{-3} . Within the temperature range of the experiment from 1050 to 1250 °C, p/n_i drops from 1.47 to 1.15. Thus, it is felt that the experiments are rather typical for intrinsically doped silicon and that the remaining variations reflect statistical errors. The diffusion coefficients reported are indeed in agreement with recent tracer-diffusion studies in isotopically enriched silicon.

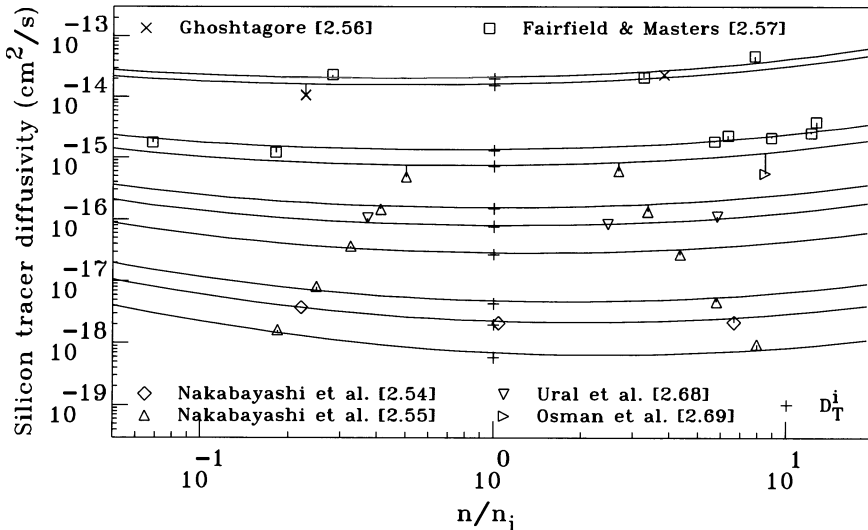


Figure 2.2: Tracer diffusion coefficient as a function of the normalized electron concentration. The full lines correspond, from top to bottom, to temperatures of 1190, 1180, 1090, 1070, 1020, 1000, 970, 920, 900, and 870 °C.

$$\begin{aligned}
 D_T = & 394 \cdot \exp\left(-\frac{4.741 \text{ eV}}{k \cdot T}\right) \text{ cm}^2/\text{s} + \frac{n}{n_i} \cdot 508 \cdot \exp\left(-\frac{5.034 \text{ eV}}{k \cdot T}\right) \text{ cm}^2/\text{s} \\
 & + \frac{n_i}{n} \cdot 7.63 \cdot 10^{-4} \cdot \exp\left(-\frac{3.55 \text{ eV}}{k \cdot T}\right) \text{ cm}^2/\text{s}. \tag{2.63}
 \end{aligned}$$

For values of $n/n_i > 10$, Osman et al. [2.69] found a quadratic increase of the tracer diffusion coefficient. This increase is probably similar to phenomena observed for tin, arsenic, and antimony. They were explained by the proximity of impurities which reduces the formation and migration enthalpies of vacancies in their vicinity and leads to an enhanced diffusion.

It has to be repeated that the old tracer experiments of Ghoshtagore [2.56] suffered from the high abundance of the isotope ^{30}Si used while the experiments of Fairfield and Masters [2.57], were limited by the short-lived tracer ^{31}Si . It is thus clear that one cannot hope for a too high significance of the parameters. However, it is also clear that Fermi-level effects, especially at the higher temperatures, play a minor role in self-diffusion when compared to dopant diffusion.

Complementary information about the diffusion of intrinsic point defects at extrinsic concentrations came from the carefully designed tracer-diffusion experiments of Silvestri et al. [2.70] and Sharp et al. [2.50] in which dopants were diffused at high concentrations into a structure of isotopically enriched marker layers. From the values reported by Silvestri et al. [2.70], the tracer diffusion coefficient results in the form

$$\begin{aligned}
 D_T = & 3.23 \cdot \exp\left(-\frac{4.32 \text{ eV}}{k \cdot T}\right) \text{ cm}^2/\text{s} + \frac{p}{n_i} \cdot 129 \cdot \exp\left(-\frac{4.74 \text{ eV}}{k \cdot T}\right) \text{ cm}^2/\text{s} \\
 & + \frac{n}{n_i} \cdot 4.85 \cdot 10^3 \cdot \exp\left(-\frac{5.18 \text{ eV}}{k \cdot T}\right) \text{ cm}^2/\text{s} \tag{2.64}
 \end{aligned}$$

for the temperature range of about 900 to 1100 °C. This relation gives a stronger dependence on the Fermi level than (2.63), especially when extrapolated to the highest temperatures shown in Figure 2.2.

Alternative Experimental Techniques

Because suitable diffusion experiments with silicon tracer atoms were not possible until recently, isovalent tracer atoms like germanium were often used for basic investigations of diffusion mechanisms in silicon. It was suggested that the activation energies characterizing the diffusion of germanium and silicon tracers in silicon should be very similar because both atoms have nearly the same covalent radius in silicon [2.71]. Measured data of germanium diffusion in silicon can be found in Section 4.2.

Alternative estimates of the self-diffusion coefficients via self-interstitials and vacancies were based on the diffusion of impurities assuming certain interactions between them and the intrinsic point defects. In any case, a non-equilibrium situation is required. Such conditions can be achieved by chemical reactions at the boundaries of the silicon sample (oxidation or nitridation) or the diffusion of impurities, dopants as well as metals, with a higher transport capacity than the intrinsic point defects.

The primary method to estimate especially values of the self-diffusion coefficient via self-interstitials is based on the diffusion of metals like gold, platinum, or zinc. They diffuse via interstitial sites and assume in equilibrium predominantly substitutional sites. The transition from interstitial sites to substitutional sites requires an interaction with intrinsic point defects. The Frank-Turnbull mechanism (see Section 3.5) envisions that interstitial metal atoms occupy vacancies to become substitutional. But simulations based on this assumption could not explain the respective diffusion profiles. They were reproduced for the first time by the kick-out mechanism (see Section 3.6) which assumes interstitial metal atoms to become substitutional by dislocating silicon atoms from substitutional sites to interstitial sites. In the following, self-interstitial properties were extracted from fitting kick-out diffusion profiles to metal diffusion profiles. But already Morehead et al. [2.72] and Kitagawa and Yoshida [2.73] showed quite clearly that there is no real distinction to be expected between the two mechanisms when bulk recombination is effective. Since there is no compelling evidence for an efficient barrier against bulk recombination (see Section 2.7), attempts to distinguish between self-diffusion via self-interstitials and vacancies from metal-diffusion experiments can be possible only for short-time processes. A flavor of the opposite opinions on this topic can be obtained from the discussion of Bracht and Haller [2.74] and Ural et al. [2.75]. But the non-uniqueness of values for the self-diffusion coefficient via self-interstitials extracted from metal diffusion was noted already before even for short-time processes. Reinterpreting zinc-diffusion experiments of Bracht et al. [2.76], Gossmann et al. [2.77] found that a parameter set with a 50% larger self-diffusion coefficient via self-interstitial than in the original work fitted the experiments equally well. Moreover, the present author could show that diffusion profiles of gold [2.78] and zinc [2.79] could be reproduced by self-diffusion coefficients exceeding experimental values by far.

Hardly more reliable are individual self-diffusion coefficients extracted from dopant diffusion. Models for high-concentration dopant diffusion where non-equilibrium effects can be expected do not lack *a-priori* assumptions. As an example, several of the respective investigations assumed the diffusion of phosphorus and boron to be governed by a vacancy mechanism. This assumption is at least at low dopant concentrations at variance with more recent oxidation/nitridation studies.

A summary of the reported self-diffusion coefficients via vacancies and self-interstitials is given in Tables 2.2 and 2.3. The parameters attributed to Mathiot and Pfister [2.14] and Mathiot [2.80] were calculated from the respective self-diffusion coefficients of neutral point defects as proposed in [2.81]. Graphical representations can be found in Figures 2.3 and 2.4, respectively. The upper limits from tracer diffusion also shown were derived from (2.62) divided by the respective tracer correlation coefficient. Summarizing the results one can conclude that the individual self-diffusion coefficients are not more accurately known than within about one order of magnitude.

Table 2.2: Prefactors D_0 and activation energies E_A reported for self-diffusion via vacancies.

	D_0 (cm ² /s)	E_A (eV)	Temperature range (°C)	Experimental technique	Ref.
Yoshida & Saito	30	4.5	950–1200	Nickel diffusion	[2.82]
Voronkov	$9.94 \cdot 10^{-13}$		1412	Swirl defect formation	[2.83]
Morehead et al.	$6.3 \cdot 10^{-17}$		1000	Gold diffusion	[2.72]
Gösele & Tan	0.57	4.03	700–1100	Collection of data	[2.28]
Mathiot & Pfister	$4.69 \cdot 10^{-2}$	3.92	850–1100	Dopant diffusion	[2.14]
Wada & Inoue	44	4.4	1080–1170	Stacking fault growth	[2.84]
Mathiot	4.6	4.43	820–1160	Dopant diffusion	[2.80]
Budil et al.	$8.12 \cdot 10^{-16}$		1100	OED	[2.85]
Brabec et al.	$8.18 \cdot 10^{-16}$		1100	Dopant diffusion	[2.86]
Griffin	700	5.01	950–1100	Dopant diffusion	[2.87]
Zimmermann et al.	0.4	4.01	700–950	Platinum diffusion	[2.88]
Law	0.6	4.021	900–1100	Dopant diffusion	[2.89]
Dunham	$5.76 \cdot 10^{-17}$		1000	Phosphorus diffusion	[2.90]
Park & Law	0.6	4	800–1100	Dopant diffusion	[2.91]
Okino	$9.66 \cdot 10^{-16}$		1100	OED/ORD	[2.92]
Habu et al.	$7 \cdot 10^5$	4.45		Crystal growth	[2.93]
Okino & Onishi	$9.24 \cdot 10^{-16}$		1100	OED/ORD	[2.94]
Ghaderi et al.	$8.7 \cdot 10^7$	6.228	900–1100	Gold diffusion	[2.95]
Bracht et al.	$8.4 \cdot 10^{-2}$	3.8	870–942	Zinc diffusion	[2.76]
Habu & Tomiura	128	4.2		Crystal growth	[2.96]
Knowlton et al.	$3.7 \cdot 10^{-18}$ $5.9 \cdot 10^{-18}$		950	Li drift after P diffusion	[2.97]
Sinno et al.	$D_0 = 2.46 \cdot 10^{-5} \text{ cm}^2/\text{s}$ $\cdot \exp(3.85 \cdot 10^{-3} \cdot T/\text{K})$ $E_A/\text{eV} = 2.94 + 2.33 \cdot 10^{-4} \cdot T/\text{K}$			Computed values fitted to crystal-growth experiments	[2.98]
Chakravarthi & Dunham	0.139	3.88	870–1208	Zinc diffusion	[2.99]
Nakamura et al.	$3.99 \cdot 10^5$	5.54		Crystal growth and defect formation	[2.100]
Walton et al.	$3.29 \cdot 10^{-24}$		950	Li drift after P diffusion	[2.101]
Sinno et al.	$D_0 = 2.46 \cdot 10^{-5} \text{ cm}^2/\text{s}$ $\cdot \exp(3.53 \cdot 10^{-3} \cdot T/\text{K})$ $E_A/\text{eV} = 2.94 + 2.33 \cdot 10^{-4} \cdot T/\text{K}$			Computed values fitted to crystal-growth experiments	[2.102]
Giese et al.	$5.5 \cdot 10^{-16}$ $9.2 \cdot 10^{-16}$		1107 1154	Zinc outdiffusion	[2.103]

	D_0 (cm ² /s)	E_A (eV)	Temperature range (°C)	Experimental technique	Ref.
Bracht et al.	0.92	4.14	855–1388	Self-diffusion & metal diffusion	[2.51]
Bracht et al.	0.71	4.11	855–1388	Self-diffusion & metal diffusion	[2.52]
Dornberger et al.	$D_0 = 3.19 \cdot 10^{-5} \text{ cm}^2/\text{s}$ $\cdot \exp(3.53 \cdot 10^{-3} \cdot T/\text{K})$			Computed values fitted to crystal-growth experiments	[2.104]
Voronkov & Falster	64.4	4.75	1070–1412	Nucleation and growth of voids, and generation of A-centers	[2.105]
Ural et al.	149	4.68	800–1100	Self-diffusion & oxidation	[2.53]
Falster et al.	$8.64 \cdot 10^{-13}$ 449	4.85	1412 1150–1280	Crystal growth Vacancy profiles	[2.106]
Mori et al.	11.2	4.257		Crystal growth	[2.107]
Akatsuka et al.	$1.8 \cdot 10^7$	6.032	1000–1280	Effect of RTP on oxygen precipitation	[2.108]
Pichler	$(5.9\text{--}22) \cdot 10^{-14}$		1277	Formation of Si- <i>E</i> centers	[2.109]
Okui & Nishimoto	$4.21 \cdot 10^6$	5.817		Crystal growth	[2.110]

Table 2.3: Prefactors D_0 and activation energies E_A reported for self-diffusion via self-interstitials.

	D_0 (cm ² /s)	E_A (eV)	Temperature range (°C)	Experimental technique	Ref.
Sanders & Dobson	5.8	4.1	970–1070	Shrinkage of stacking faults	[2.111]
Wada & Inoue	1390	5.01	850–1200	Stacking fault growth	[2.112]
Voronkov	$1.3 \cdot 10^{-12}$		1412	Swirl defect formation	[2.83]
Morehead et al.	$6.3 \cdot 10^{-17}$		1000	Gold diffusion	[2.72]
Stolwijk et al.	914	4.84	800–1400	Gold & tracer diffusion	[2.113]
Taniguchi et al.	421.8	4.7	1100–1200	OSF growth	[2.114]
Mantovani et al.		5.01	658–850	Platinum diffusion	[2.115]
Mathiot & Pfister	14.4	4.46	850–1100	Dopant diffusion	[2.14]
Stolwijk et al.	600	4.8	800–1400	Gold & tracer diffusion	[2.116]
Bronner & Plummer	945	4.84	800–1000	Gettering	[2.117]
Tan & Gösele	1000	4.8	900 (–1410)	Collection of data	[2.64]
Hauber et al.	640	4.8	800–1400	Gold diffusion	[2.118]
Mantovani et al.	1400	5.01	700–1400	Gold & Platinum diffusion	[2.119]
Mathiot	36.1	4.56	820–1160	Dopant diffusion	[2.80]
Budil et al.	$3.08 \cdot 10^{-14}$		1100	OED	[2.85]
Brabec et al.	$2.39 \cdot 10^{-15}$		1100	Dopant diffusion	[2.86]
Bronner & Plummer	600	4.8	700–800	Gold & Phosphorus diffusion	[2.120]

	D_0 (cm ² /s)	E_A (eV)	Temperature range (°C)	Experimental technique	Ref.
Morehead	4000	5	700–1250	Gold & Platinum diffusion	[2.121]
Coffa et al.	$6 \cdot 10^{-3}$	3.3	800–1200	Gold diffusion	[2.122]
Griffin	700	5.01	900–1100	Dopant diffusion	[2.87]
Jäger et al.	1.26	4.24	900–1100	Phosphorus diffusion	[2.123]
Hauber	2000	4.94	700–1400	Gold & platinum diffusion	[2.124]
Perret et al.	$2.1 \cdot 10^{-17}$		989	Zinc diffusion	[2.125]
Boit et al.	641	4.8	800–1200	Gold diffusion	[2.126]
Giles	360	4.8	700–1050	IED of phosphorus	[2.127]
Grünebaum et al.	600	4.79	900–1200	Zinc and gold diffusion	[2.128]
Dunham	$5.98 \cdot 10^{-17}$		1000	Phosphorus diffusion	[2.90]
Huang & Dutton	$1.72 \cdot 10^{-18}$		900	OED and loop growth	[2.129]
Okino	$1.56 \cdot 10^{-15}$		1100	OED/ORD	[2.92]
Habu et al.	$1.2 \cdot 10^3$	7.2		Crystal growth	[2.93]
Okino & Onishi	$1.58 \cdot 10^{-15}$		1100	OED/ORD	[2.94]
Ghaderi et al.	$5.94 \cdot 10^6$	5.813	900–1100	Gold diffusion	[2.95]
Bracht et al.	3000	4.95	870–1208	Zinc diffusion	[2.76]
Habu & Tomiura	$7.75 \cdot 10^4$	5.36		Crystal growth	[2.96]
Knowlton et al.	$2.2 \cdot 10^{-18}$ $2.4 \cdot 10^{-18}$		950	Li drift after P diffusion	[2.97]
Sinno et al.	$D_0 = 5.83 \text{ cm}^2/\text{s}$ $\cdot \exp(3.85 \cdot 10^{-3} \cdot T/\text{K})$ $E_A/\text{eV} = 4.4 + 3.08 \cdot 10^{-4} \cdot T/\text{K}$			Computed values fitted to crystal-growth experiments	[2.102]
Chakravarthi & Dunham	$1.02 \cdot 10^4$	5.1	870–1208	Zinc diffusion	[2.99]
Nakamura et al.	$3.11 \cdot 10^3$	5.05		Crystal growth and defect formation	[2.100]
Walton et al.	$8.3 \cdot 10^{-21}$		950	Li drift after P diffusion	[2.101]
Lerch & Stolwijk	$4.07 \cdot 10^{-16}$ $4.02 \cdot 10^{-15}$		1050 1119	Gold diffusion	[2.130]
Ural et al.	636	4.86	800–1100	Self-diffusion & oxidation	[2.53]
Cowern et al.	$1.06 \cdot 10^{-25}$ $6.3 \cdot 10^{-23}$ $1.7 \cdot 10^{-20}$		600 700 800	Kinetics of self-interstitial clusters	[2.131]
Falster et al.	$5.98 \cdot 10^{-12}$ $2.49 \cdot 10^3$	4.95	1412 1150–1280	Crystal growth Vacancy profiles	[2.106]
Mori et al.	$D_0 = 4.17 \cdot 10^3 \text{ cm}^2/\text{s}$ $E_A/\text{eV} = 4.4 + 3.08 \cdot 10^{-4} \cdot T/\text{K}$			Crystal growth	[2.107]
Akatsuka et al.	$1.64 \cdot 10^7$	5.86	1000–1280	Effect of RTP on oxygen precipitation	[2.108]
Meyer & Dunham	1000	4.86	700–1000	IED	[2.132]
Okui & Nishimoto	$3.92 \cdot 10^6$	5.71		Crystal growth	[2.110]

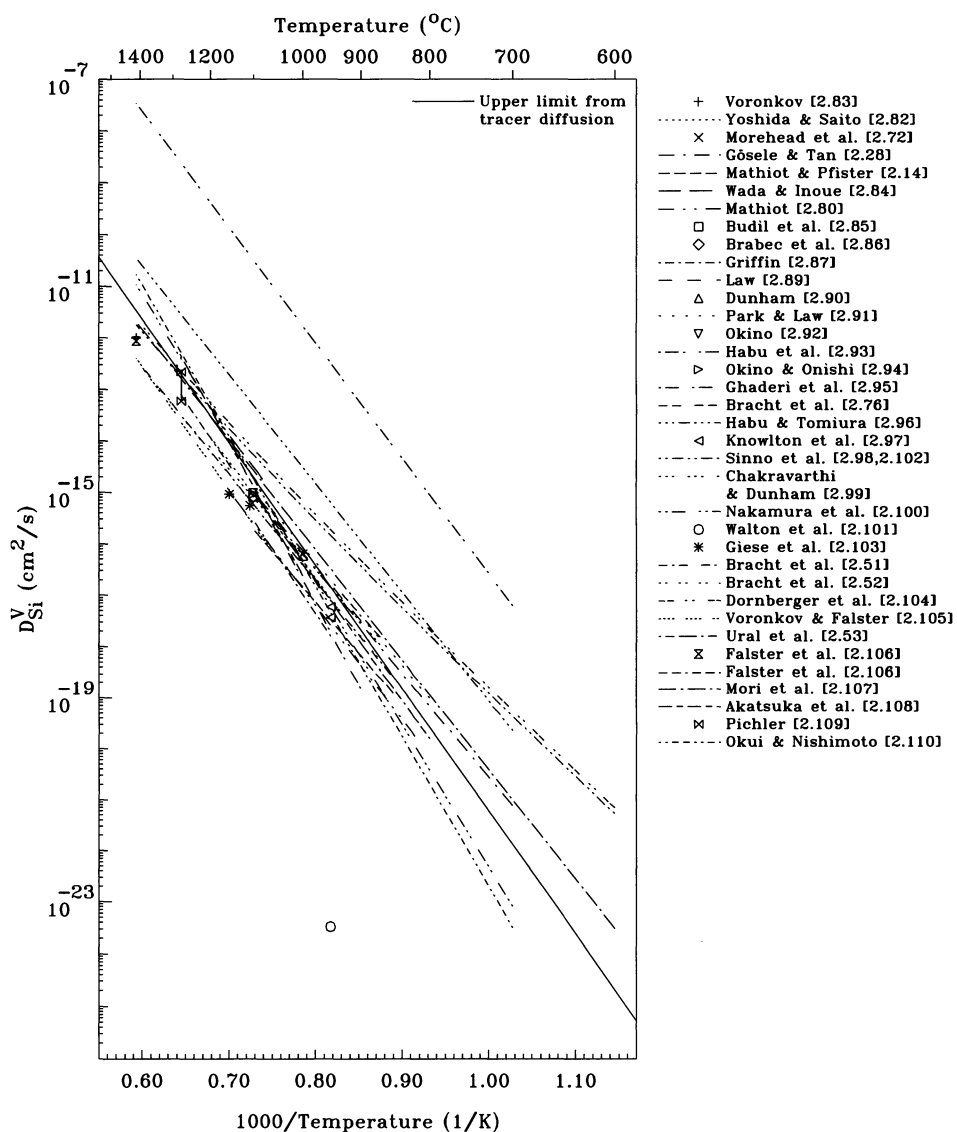


Figure 2.3: Self-diffusion coefficients via vacancies.

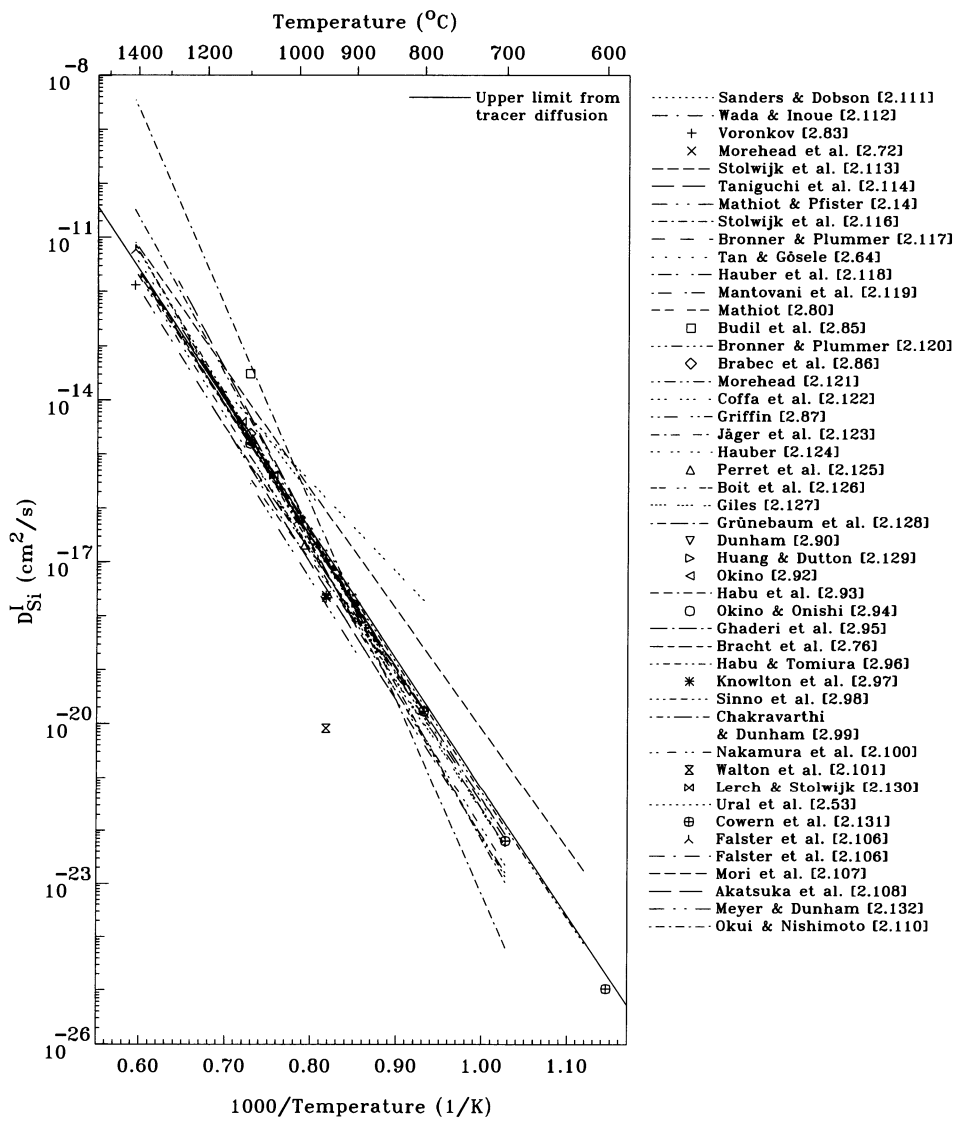


Figure 2.4: Self-diffusion coefficients via self-interstitials.

Splitting of Self-Diffusion into Individual Contributions

From crystal growth, as discussed in more detail in Section 2.9, it is known that the self-diffusion coefficient of self-interstitials has to exceed that of the vacancies at the melting point [2.83]. In several of the investigations summarized in Tables 2.2 and 2.3, self-diffusion coefficients via vacancies as well as via self-interstitials were determined. From them, the fractional contribution f_I^{Si} of diffusion via self-interstitials to self-diffusion can be obtained. The results are compared graphically in Figure 2.5 together with the more direct estimates of Ural et al. [2.48, 2.49, 2.53] from the comparison of tracer and dopant diffusion under non-equilibrium conditions. In addition to the original data set of Silvestri et al. [2.70], one with exchanged contributions of V^- and I^0 was included since, as they noted, their experiment did not allow to distinguish between vacancy and self-interstitial contribution for the influence of arsenic on self-diffusion. Accordingly, the two cases can be seen as limits only. Most of the other experimental

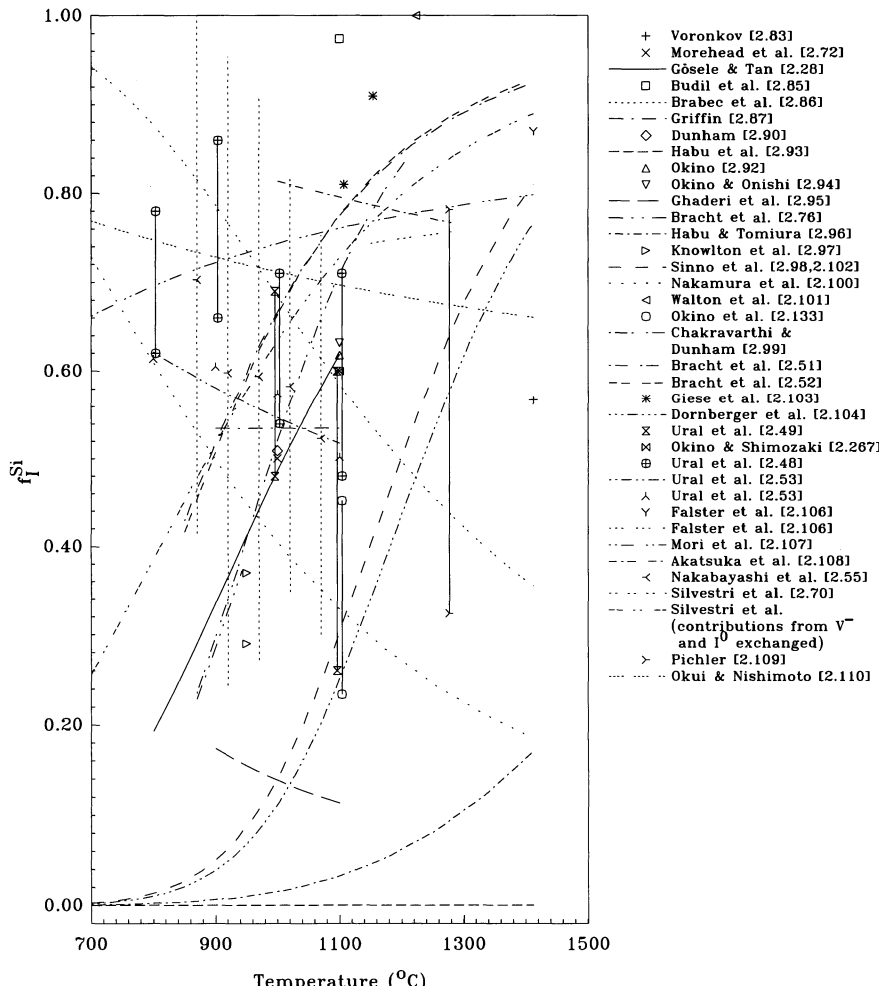


Figure 2.5: Fractional contribution of self-interstitials to self-diffusion. Vertical full and dashed lines are error bars.

results come from metal diffusion and predict, as suggested already by Seeger and Chik [2.3], that self-diffusion is dominated at high temperatures by the contribution of self-interstitials. In addition, an estimate of Okino et al. [2.133] from the growth of oxidation stacking faults was included. Also included were estimates from Nakabayashi et al. [2.55] derived from the enhancement of tracer diffusion in extrinsically doped samples although the analysis contains various very restrictive assumptions, in particular about the level structures of the intrinsic point defects. It is apparent that the agreement between the various investigations is rather limited, resulting predominantly from above mentioned uncertainties in the self-diffusion coefficients via vacancies and self-interstitials.

Besides self-diffusion via self-interstitials and vacancies, Ural et al. [2.48, 2.49] considered contributions from concerted exchange as discussed above. For 1000 and 1100 °C, these contributions were estimated to be respectively $\leq 11\%$ and $\leq 14\%$ in [2.48] while more conservative estimates of respectively $\leq 27\%$ and $\leq 62\%$ were given in [2.49].

An investigation of self-diffusion under oxidizing and extrinsic conditions was performed by Nakabayashi et al. [2.26]. They found that boron doping enhances the oxidation-enhanced diffusion of tracer atoms further while arsenic doping retards it. From this, it was concluded that self-diffusion in silicon doped extrinsically with boron and arsenic is dominated by singly positively charged self-interstitials and singly negatively charged vacancies, respectively.

2.4 Vacancies

The vacancy is certainly the most simple intrinsic point defect in silicon. Its basic form is just a missing silicon atom in an otherwise tetrahedrally coordinated network. A further advantage for the vacancy was an early identification by EPR which enabled to study its properties. However, such studies were restricted to cryogenic temperatures and a direct association with phenomena at elevated temperatures was and is not straightforward. Section 2.4.1 reviews properties like structure and energy levels deduced from experiments. In Section 2.4.2, the equilibrium concentration of vacancies is discussed with respect to experiments as well as to theoretical work. The same is done for the diffusivity of vacancies in Section 2.4.3. Vacancies in supersaturation are expected to agglomerate. The most simple form is the divacancy introduced in Section 2.4.4. Larger agglomerates were also identified by spectroscopic methods, complemented by theoretical work. Section 2.4.5 presents an overview of the structures found, including their energetics.

2.4.1 Experimental Evidence and Suggested Atomic Configurations

Much of our knowledge of the structure and properties of vacancies is based on the EPR investigations of Watkins and his coworkers. The vacancy spectrum he reported first [2.134] was labelled later Si-G1 and assigned to the positive charge state of the vacancy [2.135]. A second one, labelled Si-G2, was associated with its negative charge state [2.135]. Because of Jahn-Teller relaxations, the symmetries of V^- and V^+ were found to be lowered to D_{2d} and C_{2v} , respectively. These and later investigations [2.136, 2.137] established many of the properties of vacancies like electronic structure, the Jahn-Teller relaxations of vacancies not observable by EPR, characteristic time constants, and activation energies for reorientation and diffusion. The picture of the vacancy in its negative charge state was completed by the ENDOR investigations of Sprenger and coworkers [2.138, 2.139].

From the fact that the positive and the negative charge states of the vacancies could be observed by EPR only after illumination, Watkins [2.135] suggested that the vacancy may exist in a doubly negative charge state and suspected the position of E_{V^+} below $E_V + 0.05$ eV. This

assignment remained unquestioned until transient-capacitance techniques and DLTS became available. Based on such techniques, hole traps 0.08 eV [2.140], 0.11 eV [2.141], and 0.14 eV [2.142] above the valence band were associated with the vacancy. Reviewing the temperature dependence of the respective hole emission rates and combining them with own data, Watkins et al. [2.137] confirmed the assignments and estimated the level to be more precisely at $E_v + 0.13$ eV. Evidence for the assignment of the level to the vacancy came especially from the close agreement in its annealing kinetics to the EPR data. Further extensive investigations by Watkins and Troxell [2.143] and Newton et al. [2.144] established that the level at $E_v + 0.13$ eV is actually the second donor level $E_{V^{++}}$ while the first donor level E_{V^+} is, with an ionization energy of 0.05 eV, nearer to the valence band. This means that, upon capture of the first hole, the energy barrier of the vacancy for capturing a second hole is lowered instead of raised. As a consequence, the positive charge state of the vacancy is not stable. In such a system, the charge states V^0 , V^+ and V^{++} are said to form an Anderson “negative-U” system [2.145] as already predicted by Baraff et al. [2.146–2.148]. Levels determined by DLTS and similar techniques, as emphasized by Baraff et al. [2.148], are not necessarily the levels E_{V^+} and $E_{V^{++}}$ needed for the calculation of the concentrations of vacancies as a function of the Fermi level in (2.18) to (2.21). Significant differences can be expected when there are strong lattice relaxations associated with the capture or release of charge carriers as they are known for the vacancy. In order to determine E_{V^+} and $E_{V^{++}}$ and the equilibrium occupancy level $(E_{V^+} + E_{V^{++}})/2$, Mukashev et al. [2.149] used Hall-effect and electrical measurements of electron-irradiated samples. This interpretation became doubtful after Hoffmann [2.150] showed that the experimental data is better explained by a system which doesn’t have negative-U properties. Emtsev et al. [2.151] found also other inconsistencies in the analysis of Mukashev et al. Their own Hall-effect measurements on gamma-irradiated samples resulted in values of 0.028 and 0.128 eV for the distances of the first and second donor levels from the valence band, respectively [2.151, 2.152].

While the donor levels of the vacancy seem to be pretty well established, no agreement was achieved with respect to the acceptor levels. Popular are especially the ionization energies suggested by Van Vechten [2.153] although it is not clear how they were derived. The comments given by Van Vechten in [2.39] indicate that the acceptor values suggested by him later were taken from a schematic drawing of Watkins [2.136] who claimed that “... with the exception of the donor levels being very close to the valence band, nothing is known about the position of the levels.” Based on the negative results of DLTS investigations, Troxell and Watkins [2.154] concluded that the acceptor levels are more than about 0.17 eV below the conduction band which excludes several suggestions of shallower levels. In positron-annihilation studies of electron irradiated, high-purity samples, Mäkinen et al. [2.155] found the positron-trapping rate to be consistent with expectations for V^- . They located the Fermi level at mid band gap and concluded that the acceptor level of the vacancy has to be somewhere below, but above the double donor level at $E_v + 0.13$ eV. Simulating experimental data of Kimerling et al. [2.156] for the two-stage annealing of Si- E centers in low-resistivity n -type silicon after electron irradiation, Boyarkina [2.157] found that the experiments can be much better explained by a system in which the acceptor and double acceptor levels of the vacancy form a negative-U. Accordingly, the acceptor and double acceptor levels were suggested to be at $E_c - 0.09$ eV and $E_c - 0.39$ eV, respectively. From investigations of the Fermi-level dependence of the introduction rates of radiation defects in electron-irradiated samples with charge-dependent selective traps, Lukjanitsa [2.158] concluded that levels at $E_c - 0.28$ eV and $E_c - 0.65$ eV belong to vacancies. The values reported in the literature are listed in Table 2.4. For the sake of completeness, the suggested donor levels were included.

Table 2.4: Energy levels proposed for vacancies. A “*” behind the ionization energy indicates that it was originally given with respect to the other band edge and converted assuming a band gap of 1.12 eV.

		Level and position (eV)	Applied method	Ref.
Van Vechten Kimerling	$E_c - E_{V^=}$	0.12* 0.09	Unspecified Kinetics after electron irradiation measured by DLTS	[2.153] [2.141]
Fair		0.11	Unspecified	[2.159]
Troxell & Watkins		$\gtrsim 0.17$	DLTS	[2.154]
Kimerling et al.		0.09	Kinetics after electron irradiation measured by DLTS	[2.142]
Gubskaya et al.		0.24	Defect introduction by electron irradiation	[2.160]
Van Vechten		0.24*	From a schematic drawing of Watkins [2.136]	[2.39]
Emtsev et al.		0.24	Defect formation during gamma irradiation	[2.161]
Boyarkina Matsui & Hasiguti	$E_c - E_{V^-}$	0.39 0.92*	Annealing of Si-E centers Defect formation during gamma irradiation	[2.157] [2.162]
Fairfield & Masters		0.34	Tracer diffusion under extrinsic conditions	[2.57]
Naber et al.		0.39	Carrier removal after electron irradiation	[2.163]
Van Vechten Fair		0.57* 0.44	Unspecified Unspecified	[2.153] [2.159]
Troxell & Watkins		$\gtrsim 0.17$	DLTS	[2.154]
Gubskaya et al.		0.93*	Defect introduction by electron irradiation	[2.160]
Van Vechten		0.7*	From a schematic drawing of Watkins [2.136]	[2.39]
Lugakov & Lukashevich Mäkinen et al.		0.47–0.54 $\geq 0.56,$ $\leq 0.99^*$	Formation of radiation defects Observation of V^- by positron annihilation	[2.164] [2.155]
Boyarkina Naber et al.	$E_{V^+} - E_v$	0.09 0.44	Annealing of Si-E centers Carrier removal after electron irradiation	[2.157] [2.163]
Van Vechten Kimerling		0.37* 0.11	Unspecified Kinetics after electron irradiation measured by DLTS	[2.153] [2.141]
Brabant et al.		0.12	Kinetics after electron irradiation measured by junction capacitance techniques	[2.165]
Fair Kimerling et al.		0.35 0.14	Unspecified Kinetics after electron irradiation measured by DLTS	[2.159] [2.142]
Watkins & Troxell		0.05	EPR	[2.143]

	Level and position (eV)	Applied method	Ref.
Newton et al.	0.05	EPR	[2.144]
Mukashev et al.	0.0567	Hall effect	[2.149]
Emtsev et al.	0.028	Hall effect	[2.151, 2.152]
Watkins & Troxell	$E_{V^{++}} - E_v$	DLTS	[2.143]
Newton et al.	0.13	DLTS	[2.144]
Mukashev et al.	0.112	Hall effect	[2.149]
Emtsev et al.	0.128	Hall effect	[2.151, 2.152]
Zangenberg et al.	0.118	DLTS	[2.166]

For negatively and positively charged vacancies, Van Vechten [2.7] suggested a two-fold spin-degeneracy $\Theta_{V^-} = \Theta_{V^+} = 2$ while a non-degenerate state ($\Theta_{V^0} = 1$) was mentioned for the neutral vacancy. These factors do probably not contain degeneracies introduced by the Jahn-Teller distortions and Al-Mushadani and Needs [2.167] suggested V_0 to be triply degenerate ($\Theta_{V^0} = 3$). However, it is felt that degeneracies contribute only factors on the order of unity which is certainly negligible in comparison to the other uncertainties.

In positron-annihilation studies after electron irradiation, positron lifetimes of 247 to 273 ps were associated with vacancies [2.38, 2.155, 2.168–2.173]. These values agree well with predictions from theoretical investigations which indicated lifetimes of 248 to 279 ps [2.174–2.180].

Around a vacancy, lattice relaxations are expected. Such conserving the symmetry are usually called “breathing-mode” relaxations. In addition, symmetry-breaking lattice relaxations can occur. The most prominent of them is the Jahn-Teller effect which causes a T_d -symmetric vacancy in an electronically degenerate state to change to a configuration of lower symmetry in which the degeneracy is absent. While the first theoretical investigations indicated an expansion of the lattice around a vacancy [2.181–2.183], a contraction was predicted by the later, more refined, calculations [2.184–2.197]. The comparison of Kelly and Car [2.186] has shown that outward relaxation can be the result of an insufficient cluster size. When charge states were taken into consideration, the neighboring atoms were usually found to relax more outwardly when holes are captured.

The *ab-initio* simulations of Antonelli et al. [2.194] indicated that the neutral vacancy may exist in two different atomic configurations. Both configurations were found to have nearly the same formation energy at zero pressure but different formation volumes. This result was corroborated by the experimental investigation of Zangenberg et al. [2.166]. They found that the annealing of a defect with a DLTS level at $E_v + 0.2$ eV at approximately 140 K led to an increase in the concentration of another defect with a level at $E_v + 0.12$ eV. Both levels were associated with the vacancy and the process observed was argued to arise from the conversion of the less stable vacancy configuration to the more stable one.

In early investigations, the properties of vacancies determined at low temperatures were often suggested to disagree with those estimated at elevated temperatures from self-diffusion data, impurity diffusion, and theoretical estimates. To explain similar discrepancies in metals, Nachtrieb and Handler [2.198] had proposed that vacancies may exist in an “extended” state. The term extended means for the vacancy that one atom in an amorphous region, overall tetrahedrally coordinated and consisting of about 12–16 atoms, is missing in comparison to a perfect crystalline network of such a volume. A similar concept was considered by Seeger and Chik [2.3] and Van Vechten [2.199] for silicon. Alternatively, Masters [2.200] suggested

a semi-vacancy pair with a silicon atom midway between two vacant lattice sites. The large formation enthalpies obtained from the theoretical investigations mentioned above reconcile low-temperature and high-temperature experiments at least in part. To explain large entropies of formation and migration, Lannoo and Bourgoin [2.201] considered the relaxation of the neighboring silicon atoms around a vacancy. Assuming a 10% elongation of the bonds in the vicinity of a vacancy, an entropy of about $12.5 \cdot k$ was obtained from the softening of the force constants. In addition, Pantelides [2.202] suggested that the migration path may change with temperature, giving rise to a curvature in the apparent diffusion coefficient. This phenomenon would also contribute to the high entropy observed in high-temperature self-diffusion. On the other hand, the notion of an extended vacancy was supported also by the *ab-initio* molecular-dynamics investigation of Car et al. [2.203] discussed in more detail below and by the work of Bracht et al. [2.204]. The latter derived from their investigations of radiation-enhanced self-diffusion around $800\text{ }^{\circ}\text{C}$ a migration enthalpy of 1.8 eV and concluded from the significantly smaller values at cryogenic temperatures that the vacancy assumes an extended state at the process temperature.

2.4.2 Concentration in Thermal Equilibrium

The equilibrium concentration of vacancies is among the most controversially discussed parameters for silicon. One reason is certainly that the detection limits of the more direct methods like thermal expansion measurements and positron annihilation are limited. Indirect determinations as from metal diffusion experiments, on the other hand, give often ambiguous results.

The most direct method to determine the equilibrium concentration of vacancies was developed by Simmons and Balluffi [2.1] for metals. It uses the fact that intrinsic point defects give rise to a difference between macroscopic linear thermal expansion and the thermal expansion of the lattice parameter. Since vacancies and self-interstitials have opposite effects, only their difference can be determined. In one such experiment, Okada [2.205] determined $C_V - C_I$ to be about $(3.9 \pm 3) \cdot 10^{15} \text{ cm}^{-3}$ at $727\text{ }^{\circ}\text{C}$, $(1.8 \pm 1.2) \cdot 10^{16}$ at $1027\text{ }^{\circ}\text{C}$, and $3.6 \cdot 10^{16} \text{ cm}^{-3}$ at the melting point. Neglecting possible contributions from self-interstitials, these data would imply an entropy of formation which has to be smaller than $-8.8 \cdot k$. It was also remarked by Hu [2.34] that the absolute value of $C_V - C_I$ around 500 K as estimated from their Figure 1 would be about the same as at 1300 K while one would expect immeasurably small concentrations of self-interstitials and vacancies at such low temperatures.

A second method which gave direct and reliable results for the equilibrium concentration of vacancies in many materials is quenching. It has often been argued (e. g. [2.206]) that the diffusivity of vacancies would be too high to allow their quenching. This is entirely true for isolated vacancies. But vacancies will agglomerate and interact with impurities like oxygen and nitrogen during quenching. Such “preserving” reactions immobilize them and prevent them from diffusing to surfaces and interfaces where they would be annihilated. Clearly, the effectiveness of quenching processes increases with sample size. Thus, crystal-growth experiments with their enormous “sample” volume should be suited best. The main problem, especially in the early experiments, was to identify the quenched vacancy-related defects unambiguously and to quantify them. It should also be mentioned that reactions between vacancies and self-interstitials may occur during quenching. Thus, the concentration of vacancy complexes measured after the quench is rather somewhere between the net difference of the equilibrium concentrations of vacancies and self-interstitials and the equilibrium concentration of vacancies.

In early quenching experiments, Elstner and Kamprath [2.207] found deep donors characterized by an ionization level at $E_v + 0.37$ eV and suggested them to be clusters of about 4 to 6 vacancies. These levels were associated already by Collins and Carlson [2.208] with iron. By similar quenching experiments, Lee et al. [2.209] could show that the defect is indeed interstitial iron rather than a vacancy agglomerate. Moreover, from their inability to find impurity-vacancy complexes after quenches by EPR, the authors suggested an upper limit of 10^{14} cm $^{-3}$ for the equilibrium concentration of vacancies at 1200 °C. The association of iron with a level at about $E_v + 0.37$ eV to $E_v + 0.4$ eV was suggested also in various other investigations [2.210, 2.211]. In the work of Boltaks and Budarina [2.212], density measurements and resistivity measurements were combined to estimate the formation enthalpy of vacancies. Both methods agreed closely and gave a value of about 2.8 eV for undoped silicon. From the density measurements, a vacancy concentration of about $4 \cdot 10^{18}$ cm $^{-3}$ was found after quenching from 1200 °C which, extrapolated to the melting point of silicon, gives a concentration of about $7 \cdot 10^{19}$ cm $^{-3}$. This value exceeds all other estimates by at least two orders of magnitude and can hardly be associated with vacancies. In the work of Chantre et al. [2.213–2.215], on the other hand, phosphorus-vacancy pairs and aluminum-vacancy pairs were identified by DLTS after quenching from 1280 °C. These experiments were suggested to provide strong evidence that the equilibrium concentration of vacancies exceeds that of self-interstitials at this temperature. A detailed analysis of Pichler [2.109] showed that the result is basically independent of self-interstitial parameters due to the short processing time. It was also shown that such experiments allow the independent determination of equilibrium concentration and diffusion coefficient of vacancies within a narrow range. A further way to characterize the concentration of vacancy-related defects is the platinum diffusion technique discussed in Section 3.5.2. Using this method, Falster et al. [2.106] showed that an excess of vacancies remains in wafers RTP-treated in argon at temperatures from 1150 to 1280 °C. In the work of Fukata et al. [2.216], the samples were quenched in water after annealing in a hydrogen atmosphere. The authors assumed that the vacancies would form complexes with the hydrogen upon quenching and determined a formation enthalpy of 4.0 eV for vacancies.

From positron-annihilation experiments, Dannefaer et al. [2.38] reported the observation of vacancies at temperatures of 1050 °C and higher. This would mean a concentration of at least $5 \cdot 10^{15}$ cm $^{-3}$. This result was used in a number of publications to support theories about vacancies. However, it was not reproduced in subsequent similar investigations. Würschum et al. [2.170] and Throwe et al. [2.217], found no clear indication of vacancies up to the melting point of silicon. From this, the latter deduced an upper limit of $2.5 \cdot 10^{16}$ cm $^{-3}$ for the equilibrium concentration of vacancies at the melting point and a lower limit of 3.6 eV for the formation enthalpy of neutral vacancies. Possible problems associated with the experimental set-up used by Dannefaer et al. and their interpretation of results were discussed by Würschum et al. [2.170], Throwe et al. [2.217], and Hautojärvi et al. [2.218].

Since the more direct methods discussed so far had limited success, indirect methods were used extensively. Such methods are based on non-equilibrium situations caused by chemical reactions (e. g. oxidation) or the diffusion of impurities with a higher transport capacity than the intrinsic point defects.

Clear evidence about the relative concentration of self-interstitials and vacancies comes from crystal growth. Depending on the growth conditions, interstitial-rich or vacancy-rich crystals can be grown. Such phenomena are explained by the theory of Voronkov [2.83] discussed later in more detail in Section 2.9. To obtain the observed vacancy-rich crystals at high pull rates, the equilibrium concentration of vacancies has to exceed that of self-interstitials at the melting point. Similar evidence at lower temperatures comes from the influence of rapid ther-

mal annealing on the precipitation of oxygen. Investigations like that of Falster et al. [2.106] and Akatsuka et al. [2.108] made clear that annealings in inert atmosphere at temperatures in the range from 1180 to 1280 °C, followed by a rapid cooling-down, led to an increase in the nucleation of oxygen precipitates during subsequent heat treatments. Oxygen precipitation is known to need free volume to accommodate the volume increase associated and it is known that the nucleation of oxygen precipitates is hampered in self-interstitial rich wafers. Thus, it is evident that the increased nucleation is the result of an increased concentration of vacancy complexes. This requires in turn that the equilibrium concentration of vacancies exceeds the equilibrium concentration of self-interstitials at the process temperature of the rapid-thermal annealing step.

The most influential work was published by Tan and Gösele [2.64] in 1985. They reviewed the diffusion data available then and gave an estimate for the self-diffusion coefficient of vacancies. The splitting into diffusion coefficient and equilibrium concentration was based on measurements of an effective diffusion coefficient of self-interstitials from back-side oxidation experiments. These measurements indicated a rather low diffusion coefficient of self-interstitials and Tan and Gösele interpreted it as an effective value resulting from the recombination with slowly diffusing vacancies with a high equilibrium concentration. Biased by this result, basically all investigations in the following $1\frac{1}{2}$ decades led to estimates for the equilibrium concentration of vacancies which are, e. g. at a temperature of 900 °C, all above 10^{14} cm^{-3} . It remains to remark that current diffusion theories explain a low effective diffusion coefficient of self-interstitials qualitatively by an interaction with traps, most likely carbon, so that the assumption of a high equilibrium concentration of vacancies is no longer required. On the other hand, an unambiguous quantitative interpretation of the back-side oxidation experiments and an identification of the traps being eventually responsible are still missing.

An often used method to estimate diffusion coefficient and equilibrium concentration of vacancies is based on the diffusion of metals like gold, platinum, or zinc. The limitations of this method were already discussed in Section 2.3. They are even more severe here since the splitting of a self-diffusion coefficient into diffusion coefficient and equilibrium concentration requires a second-order analysis at a point where the reliability of the first-order estimate of the self-diffusion coefficient is not always clear. In addition, influenced by the work of Tan and Gösele [2.64] discussed above, researchers apparently looked only for the upper range of vacancy equilibrium concentrations and almost unanimously suggested rather high values. Reinterpreting zinc-diffusion experiments, Chakravarthi and Dunham [2.99] could explain the profiles by an equilibrium concentration of vacancies which was orders of magnitude below the value extracted in the original work. An error analysis demonstrated the uniqueness of the extracted diffusion coefficients and equilibrium concentrations. Somewhat in contrast, reinterpreting gold-diffusion experiments [2.78] and zinc out-diffusion experiments [2.79], the present author concluded that almost any value for the equilibrium concentration of vacancies suffices to reproduce the experiments as long as the diffusion coefficient is adjusted accordingly. Similar problematic as parameters extracted from metal diffusion are parameters from dopant diffusion. Important points for all investigations are the influences of bulk recombination and of reactions with impurities like carbon or with other “traps” which will be discussed in Section 2.7.5. Unfortunately, they were ignored in the majority of the cases. As a result of the experimental uncertainties and the different *a-priori* assumptions, the estimates listed in Table 2.5 and shown graphically in Figure 2.6 differ considerably. It has also to be noted that several of the prefactors suggested are significantly lower than the number of lattice sites ($5 \cdot 10^{22} \text{ cm}^{-3}$). This would imply a negative entropy of formation which is rather unlikely. However, they can often be understood to reflect the limited temperature range of the investigations.

Table 2.5: Prefactors \tilde{C} and formation enthalpies H^f reported for the equilibrium concentration of vacancies under intrinsic conditions.

	\tilde{C} (cm $^{-3}$)	H^f (eV)	Temperature range (°C)	Experimental technique	Ref.
Fairfield & Masters	$5 \cdot 10^{25}$	3.4	1000–1400	Tracer diffusion	[2.57]
Yoshida & Saito	$2 \cdot 10^{28}$	4.17	950–1200	Nickel diffusion & literature data	[2.82]
Masters & Gorey	$5 \cdot 10^{25}$	3.66	600–900	Radiation-enhanced dopant diffusion	[2.219]
Lee et al.	$\leq 10^{14}$		1200	Impurity-vacancy pairs after quenching	[2.209]
Voronkov	$1.4 \cdot 10^{14}$		1412	Swirl defect formation	[2.83]
Tan & Gösele	$2 \cdot 10^{23}$	2	900–1200	Collection of data	[2.64]
Wada & Inoue	$8.56 \cdot 10^{21}$	1.56	1080–1170	Stacking fault growth	[2.84]
Budil et al.	$1.4 \cdot 10^{16}$		1100	OED	[2.85]
Brabec et al.	$9.09 \cdot 10^{14}$		1100	Dopant diffusion	[2.86]
Griffin	$4.92 \cdot 10^{20}$	1.24	950–1100	Dopant diffusion	[2.87]
Zimmermann et al.	$3.68 \cdot 10^{16}$	0.618	770–950	Platinum diffusion	[2.88]
Okada	$3.9 \cdot 10^{15}$		727	Thermal expansion	[2.205]
	$1.8 \cdot 10^{16}$		1027		
	$3.6 \cdot 10^{16}$		1412		
Budil et al.	$9.1 \cdot 10^{15}$		1100	OED	[2.220]
Zimmermann	$1.83 \cdot 10^{19}$	1.162	700–950	Platinum & Gold diffusion	[2.221]
Law	$4.77 \cdot 10^{18}$	0.731	900–1100	Dopant diffusion	[2.89]
Zimmermann & Ryssel	$4.4 \cdot 10^{13}$		770	Platinum diffusion	[2.222]
Zimmermann	$4.1 \cdot 10^{13}$		800	Platinum diffusion	[2.223]
Dunham	$2.4 \cdot 10^{15}$		1000	Phosphorus diffusion	[2.90]
Park & Law	$2.31 \cdot 10^{21}$	1.08	800–1100	Dopant diffusion	[2.91]
Okino	$2.1 \cdot 10^{17}$		1100	OED/ORD	[2.92]
Gossmann et al.		1.4	750–900	Enhanced Sb diffusion in epi-Si	[2.224]
Habu et al.	$8.02 \cdot 10^{29}$	4.0		Crystal growth	[2.93]
Okino & Onishi	$2.2 \cdot 10^{17}$		1100	OED/ORD	[2.94]
Ghaderi et al.	$1.64 \cdot 10^{24}$	2.226	900–1100	Gold diffusion	[2.95]
Bracht et al.	$1.4 \cdot 10^{23}$	2	870–942	Zinc diffusion	[2.76]
Habu & Tomiura	$5.75 \cdot 10^{22}$	2.6		Crystal growth	[2.96]
Knowlton et al.	$5.4 \cdot 10^{12}$		950	Li drift after P diffusion	[2.97]
	$3.5 \cdot 10^{12}$				
Tan et al.		≥ 3.0		Formation of voids	[2.225]
Sinno et al.		$\tilde{C} = 1.23 \cdot 10^{21} \text{ cm}^{-3}$ $\cdot \exp(3.85 \cdot 10^{-3} \cdot T / \text{K})$ $H^f / \text{eV} = 2.48 + 2.33 \cdot 10^{-4} \cdot T / \text{K}$		Computed values fitted to crystal-growth experiments	[2.98]
Chakravarthi & Dunham	$1.2 \cdot 10^{19}$	2	870–1208	Zinc diffusion	[2.99]
Nakamura et al.	$4.92 \cdot 10^{26}$	3.9		Crystal growth and defect formation	[2.100]
Walton et al.	$1.77 \cdot 10^9$		950	Li drift after P diffusion	[2.101]

	\tilde{C} (cm $^{-3}$)	H^f (eV)	Temperature range (°C)	Experimental technique	Ref.
Sinno et al.	$\tilde{C} = 1.23 \cdot 10^{21} \text{ cm}^{-3}$ $\cdot \exp(3.53 \cdot 10^{-3} \cdot T/\text{K})$ $H^f/\text{eV} = 2.48 + 2.33 \cdot 10^{-4} \cdot T/\text{K}$			Computed values fitted to crystal-growth experiments	[2.102]
Giese et al.	$1.1 \cdot 10^{15}$ $4.7 \cdot 10^{14}$		1107 1154	Zinc outdiffusion	[2.103]
Jacob et al.	$\leq 5 \cdot 10^{13}$		1180	Platinum diffusion in nitrided samples	[2.226]
Voronkov & Falster	$1.45 \cdot 10^{28}$	4.4	1070–1412	Nucleation and growth of voids	[2.105]
Scholz et al.	$2 \cdot 10^{14}$		900	Carbon diffusion	[2.227]
Okino & Shimozaki	$5 \cdot 10^{22}$	1.13		Self-diffusion and OED	[2.228]
Pichler	$\lesssim 10^{15}$		1107	Outdiffusion of zinc	[2.79]
Falster et al.	$1.08 \cdot 10^{15}$ $2.88 \cdot 10^{28}$		1412 1150–1280	Crystal growth Vacancy profiles	[2.106]
Mori et al.	$2.81 \cdot 10^{26}$	3.8		Crystal growth	[2.107]
Akatsuka et al.	$1.01 \cdot 10^{27}$	3.9	1000–1280	Effect of RTP on oxygen precipitation	[2.108]
Fukata et al.		4.0	1200–1390	Quenching	[2.216]
Nakamura et al.	$(3.9\text{--}4.6) \cdot 10^{26}$ $(5.4\text{--}6) \cdot 10^{25}$	3.94 3.64		Formation of voids during crystal growth	[2.229]
Pichler	$(3.1\text{--}8.3) \cdot 10^{14}$		1277	Formation of Si- <i>E</i> centers	[2.109]
Okui & Nishimoto	$1.12 \cdot 10^{27}$	3.9		Crystal growth	[2.110]
Bracht et al.	$2.25 \cdot 10^{22}$	2.1	780–872	Radiation-enhanced self-diffusion	[2.204]

After powerful theoretical methods were developed to compute properties of point defects in silicon, they were applied in several investigations to calculate the formation enthalpy of vacancies. The results of these calculations are listed in Table 2.6.

The values for $H_{V^j+e^{-j}}^f$ refer to the formation of vacancies and the appropriate number of compensating charge carriers in intrinsic silicon. When other reference points were assumed in the original publications, they were converted assuming a band gap of 1.12 eV. The differences between the results can be explained by different problem sizes and pseudopotentials used, as well as by different relaxations of the atomic structure around the defect [2.193, 2.197]. In all investigations in which the formation energies of the neutral, positive, and doubly positive charge states were computed, the metastability of the positive charge state was confirmed. The computations of Puska et al. [2.193] also indicated that the negative charge state would not be stable. This was not reproduced in the work of Mueller et al. [2.230] but the authors predicted that quadruply negatively charged vacancies become energetically most favorable for Fermi levels above $E_v + 0.66$ eV (0.87 eV corrected for the band-gap error). The triply negative charge state, on the other hand, was found to be instable.

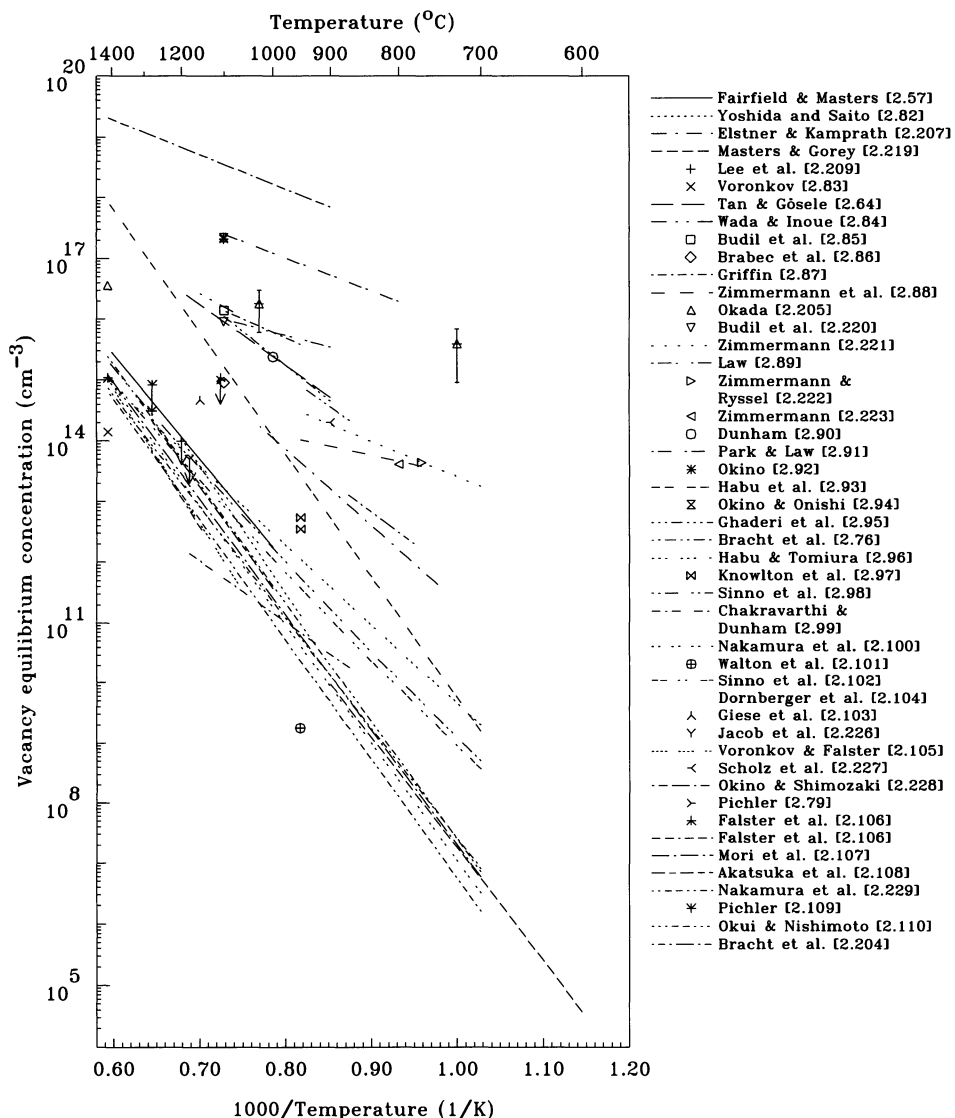


Figure 2.6: Equilibrium concentration of vacancies under intrinsic condition.

Table 2.6: Formation enthalpies and entropies of vacancies in intrinsic silicon obtained from *ab-initio* calculations.

	Charge state	$H_{V^j+e^-}^f$ (eV)	S_V^f/k	Ref.
Car et al.	-	5.49		[2.231]
	0	5		
	+	5.47		
	++	5.85		
Bar-Yam & Joannopoulos	0	3.6		[2.232]
	+	4.1		
	++	4.6		
Car et al.	-	4.25		[2.233]
	0	3.8		
	+	4.24		
	++	4.68		
Kelly et al.	0	3.92		[2.184]
	++	4.55		
Nichols et al.	0	3.5		[2.234]
Blöchl et al.		3.3	5.0	[2.235]
Antonelli & Bernholc	0	4.42		[2.185]
Kelly & Car	0	3.3		[2.186]
	++	4.52		
Car et al.	0	4.1	5.0	[2.203]
Blöchl et al.	0	4.1	5.0	[2.43]
Zhu et al.	0	3.7		[2.188]
Seong & Lewis	0	3.29		[2.190]
Hastings et al.	0	4.15		[2.236]
Zywietz et al.	0	3.37–3.68		[2.237]
Zhu	0	3.65		[2.238]
Mercer et al.	0	3.6		[2.192]
Puska et al.	=	3.17		[2.193]
	-	3.32		
	0	3.31		
	+	3.76		
	++	4.13		
Nelson et al.	0	3.69		[2.239]
Antonelli et al.	0	3.49		[2.194]
Xie & Chen	0	3.6		[2.240]
Coutinho et al.	0	3.61		[2.241]
Liu et al.	0	3.69		[2.242]
Probert & Payne	0	3.17		[2.197]
Mueller et al.	=	3.62		[2.230]
	-	3.60		
	0	3.66		
	+	4.16		
Al-Mushadani & Needs	++	4.49		
	0	3.53	11.9	[2.167]

2.4.3 Diffusion

The diffusivity of vacancies was characterized by various methods. In the low-temperature regime, vacancies were identified directly by EPR and their diffusivities in various charge states were deduced from their reactions with impurities. At the usual processing temperatures, no direct observation of vacancies is possible. Moreover, they will recombine with self-interstitials or form complexes with other vacancies or impurities like oxygen and nitrogen so that only an effective diffusion coefficient can be expected. In the absence of direct results, indirect determinations of vacancy diffusivities via the diffusion of dopants or metals were attempted. Such methods were discussed already above and it was concluded that unique results cannot be expected from the majority of them.

After electron irradiation of *p*-type CZ silicon samples, Watkins [2.134] found the EPR vacancy signal to decay exponentially with time. The decay was associated with the trapping of vacancies at oxygen atoms and from its characteristic time constant, a value of 0.33 ± 0.03 eV was estimated for the migration enthalpy of the vacancy. Moreover, from the known number of oxygen atoms, the jump frequency of the vacancy was obtained. The prefactor of the jump frequency so obtained agreed with a value of $2 \cdot 10^{12} \text{ s}^{-1}$ closely to the oscillation frequency estimated via (2.39). Initially, the activation energy was attributed to the vacancy in its neutral charge state. After the level structure became more clear, it was reassigned to the doubly positive charge state. Including DLTS measurements, Watkins et al. [2.137] corrected the activation energy later to 0.32 eV. Using the same values for the concentration of oxygen atoms and the capture radius of the vacancies as Watkins [2.134], the diffusion coefficient follows as

$$D_{V^{++}} = 9.6 \cdot 10^{-5} \cdot \exp\left(-\frac{0.32 \text{ eV}}{k \cdot T}\right) \text{ cm}^2/\text{s} \quad (2.65)$$

for the temperature range from 150 to 180 K. In *n*-type silicon, samples Watkins [2.243] found the diffusion of vacancies to be characterized by an even smaller activation energy of 0.18 ± 0.02 eV attributed to the migration enthalpy of the doubly negatively charged vacancy. Using the same capture radius of 2.35 Å as above and assuming an oxygen concentration of about 10^{18} cm^{-3} , the characteristic time constant for diffusion of vacancies to oxygen reported by Watkins [2.136] leads to a diffusion coefficient of

$$D_{V^-} = 0.015 \cdot \exp\left(-\frac{0.18 \text{ eV}}{k \cdot T}\right) \text{ cm}^2/\text{s} \quad (2.66)$$

for the temperature range from 70 to 85 K. Finally, information about the diffusivity of the vacancy in a third charge state was obtained by Watkins et al. [2.137] from measurements of the annealing kinetics of a hole trap at $E_V + 0.13$ eV. Annealing in *p*-type FZ silicon under zero-bias conditions followed closely the kinetics known from the previous EPR investigations [2.134]. Under reverse bias conditions, on the other hand, the vacancies annealed with a typical time constant governed by an activation energy of 0.45 eV. Watkins [2.206] suggested that this activation energy should be assigned to V^0 since he found by correlative EPR measurement that this charge state has a higher stability. From a comparison of the kinetics measured under zero-bias conditions and the EPR investigations, a trap density of about $8 \cdot 10^{16} \text{ cm}^{-3}$ followed for the FZ samples. Then, assuming again a capture radius of 2.35 Å, the diffusion coefficient of neutral vacancies can be estimated as

$$D_{V^0} = 1.3 \cdot 10^{-3} \cdot \exp\left(-\frac{0.45 \text{ eV}}{k \cdot T}\right) \text{ cm}^2/\text{s} \quad (2.67)$$

for the temperature range from 190 to 235 K.

Similar values for the migration enthalpies were reported also by other investigators from the low-temperature recovery kinetics of the minority-carrier lifetime in solar cells or transistors after the introduction of radiation damage. From such experiments using neutron irradiation, Gregory and Sander [2.244] estimated an activation energy of 0.17 eV for *n*-type silicon and 0.3 to 0.4 eV for *p*-type silicon. In a similar experimental set-up, Stein and Vook [2.245] and Binder et al. [2.246] estimated somewhat smaller activation energies of 0.3 and 0.28 ± 0.02 eV, respectively, for *p*-type silicon. The value of 0.32 eV reported by Srour [2.247] from electron-irradiation studies using *p*-type silicon is again nearer to the value of the migration enthalpy of vacancies in *p*-type silicon. Based on the Fermi-level dependence of the annealing kinetics of the photo-stimulated electron emission after defect generation, Ershov et al. [2.248] suggested migration energies of 0.48, 0.33, and 0.18 eV for positively charged, neutral, and negatively charged vacancies, respectively. Later, Panteleev et al. [2.249] associated V^- with a migration energy of 0.25 eV and V^+ with the migration energy of 0.18 eV. An activation energy near the 0.45 eV was also suggested by Partyka et al. [2.250] from *in-situ* Huang diffuse X-ray scattering characterization of the annealing of defects produced by He irradiation.

Diffusion of vacancies at and above room temperature was deduced indirectly from various experiments. In the investigation of Panteleev et al. [2.251], point defects were generated by ion implantation at one side of the samples while their arrival at the other side was detected by photostimulated electron emission. Two types of point defects were found to arrive. Their diffusion coefficients were estimated to be characterized by a prefactor of $2.2 \cdot 10^{-4}$ cm²/s and an activation energy of 0.3 ± 0.04 eV for the one defect, and by a prefactor of $1.1 \cdot 10^{-6}$ cm²/s and an activation energy of 0.12 ± 0.04 eV for the other. Based on the similarities of the values with the EPR experiments of Watkins, the former was tentatively associated with vacancies while latter was associated with self-interstitials. In an electron-irradiation study, Wang et al. [2.252] observed that the distribution of defects, notably of VO complexes, decreased towards the surface. The authors suggested that this decrease reflects the steady-state distribution of vacancies during irradiation and determined the vacancy-diffusion length to be between about 3 to 6 μ m. From their capture at oxygen atoms, vacancy diffusion coefficient between about $3.4 \cdot 10^{-9}$ to $1.4 \cdot 10^{-8}$ cm²/s were estimated. Details of the analysis were, unfortunately, not given. An additional conclusion from the distribution of impurity interstitials was that self-interstitials diffuse faster than vacancies. Formation of VO complexes was also used by Voronkov and Falster [2.105] to estimate a value of $3 \cdot 10^{-10}$ cm²/s for the diffusion coefficient of vacancies at room temperature. Priolo et al. [2.253] suggested from the dependence of vacancy-related defect profiles generated by MeV He implantation on the dopant background concentration that it reflects trap-limited vacancy diffusion. From the profile broadening in epitaxial material, a lower limit of $3 \cdot 10^{-12}$ cm²/s was deduced for the diffusivity of vacancies at room temperature. After room-temperature ion implantation with MeV energies, Hallén et al. [2.254] observed that the concentration of VO and V₂ complexes decreased with the dose rate. The effects could be reproduced quantitatively assuming a vacancy diffusion coefficient of $4.2 \cdot 10^{-9}$ cm²/s. To exclude athermal diffusion effects, Coffa and Libertino [2.255] monitored *in-situ* the leakage current of a diode during and after MeV helium implantation. Defect identification was performed *ex situ* by DLTS and the leakage current was suggested to be caused by divacancies and vacancy-phosphorus complexes. For the vacancy diffusivity a value of $3 \cdot 10^{-13}$ cm²/s was obtained from numerical simulations of the measurements. In their subsequent work, Libertino and Coffa [2.256] reported a value of $4 \cdot 10^{-13}$ cm²/s. Remarkably, these values are about two orders of magnitude larger than the diffusion coefficient of self-interstitials obtained also from the simulations. Nylandsted Larsen et al. [2.257] studied the deactivation of dopants caused by a shallow germanium implantation. In contrast to the interpretation of Kyllesbech Larsen

et al. [2.258] discussed in Section 2.5.3, the deactivation was found by DLTS to arise from the formation of vacancy-phosphorus pairs. From the respective profile a lower limit of $4 \cdot 10^{-11} \text{ cm}^2/\text{s}$ was deduced for the diffusivity of doubly negatively charged vacancies.

At elevated temperatures, various indirect methods were applied to estimate the diffusivity of vacancies. Most of them were based on the diffusion of metals and dopants. Their insufficiencies were commented already in Section 2.4.2. Only few investigations resulted in more direct estimates. The analysis of Pichler [2.109] of the formation of phosphorus-vacancy pairs during laser annealing as measured by Chantre et al. [2.213, 2.214] showed that such experiments allow in principle to determine the equilibrium concentration and the diffusion coefficient of vacancies independently. A rather direct estimate of the migration enthalpy was derived by Bracht et al. [2.204]. They found a value of 1.8 eV from the radiation-enhanced diffusion of silicon tracers around 800 °C and concluded from a comparison to the values found at cryogenic temperatures that the vacancies were in an extended state. The results are summarized in Table 2.7 and shown graphically in Figure 2.7. The high-temperature data is depicted in more detail in Figure 2.8.

Table 2.7: Prefactors D_0 and enthalpies of migration H^m reported for the diffusion coefficient of vacancies under intrinsic conditions.

	D_0 (cm^2/s)	H^m (eV)	Temperature range ($^\circ\text{C}$)	Experimental technique	Ref.
Fairfield & Masters	9	1.7	1000–1400	Tracer diffusion	[2.57]
Hu		0.5		Dopant diffusion	[2.259]
Panteleev et al.	$2.2 \cdot 10^{-4}$	0.3	100–350	Arrival of point defects at surfaces after ion implantation	[2.251]
Masters & Gorey	10	1.47	600–900	Radiation-enhanced dopant diffusion	[2.219]
Wang et al.	$(3.4\text{--}14) \cdot 10^{-9}$		RT	Defect production by electron irradiation	[2.252]
Voronkov	$3.55 \cdot 10^{-4}$		1412	Swirl defect formation	[2.83]
Chantre et al.	$4 \cdot 10^{-5}$		1277	Formation of Si- <i>E</i> centers	[2.213]
Tan & Gösele	0.1	2	900–1200	Collection of data	[2.64]
Wada & Inoue	257	2.84	1080–1270	Stacking fault growth	[2.84]
Budil et al.	$2.9 \cdot 10^{-9}$		1100	OED	[2.85]
Fedina & Aseev		< 0.2	20–600	Growth of extended defects due to electron irradiation	[2.260]
Brabec et al.	$4.5 \cdot 10^{-8}$		1100	Dopant diffusion	[2.86]
Griffin	$7.12 \cdot 10^4$	3.77	950–1100	Dopant diffusion	[2.87]
Zimmermann et al.	$5.43 \cdot 10^5$	3.392	770–950	Platinum diffusion	[2.88]
Budil et al.	$5.3 \cdot 10^{-9}$		1100	OED	[2.220]
Griffin et al.	$2 \cdot 10^{-11} \text{ to } 10^{-9}$		950 1100	Lateral dopant diffusion	[2.261]
Zimmermann	$1.09 \cdot 10^3$	2.838	700–950	Platinum & gold diffusion	[2.221]
Law	$6.34 \cdot 10^3$	3.29	900–1100	Dopant diffusion	[2.89]
Dunham	$1.2 \cdot 10^{-9}$		1000	Phosphorus diffusion	[2.90]
Park & Law	13	2.92	800–1000	Dopant diffusion	[2.91]

	D_0 (cm ² /s)	H^m (eV)	Temperature range (°C)	Experimental technique	Ref.
Okino	$2.3 \cdot 10^{-10}$		1100	OED/ORD	[2.92]
Okino	$2.1 \cdot 10^{-10}$		1100	OED/ORD	[2.262]
Gossmann et al.	$2.5 \cdot 10^{-13}$		850	Dopant diffusion	[2.224]
Habu et al.	0.0437	0.45		Crystal growth	[2.93]
Okino & Onishi	$2.1 \cdot 10^{-10}$		1100	OED/ORD	[2.94]
Ghaderi et al.	$2.64 \cdot 10^6$	4.002	900–1100	Gold diffusion	[2.95]
Shimizu et al.	$4.1 \cdot 10^{-9}$		1000	Dopant diffusion	[2.263]
Eidenzon & Puzanov	$(3\text{--}5) \cdot 10^{-5}$		1050	Crystal growth	[2.264]
Bracht et al.	$3 \cdot 10^{-2}$	1.8	870–942	Zinc diffusion	[2.76]
Habu & Tomiura	111	1.6		Crystal growth	[2.96]
Mogi et al.	$7.9 \cdot 10^{-14}$		810	Nitridation- enhanced diffusion	[2.265]
	$1.2 \cdot 10^{-12}$		860		
	$2.1 \cdot 10^{-11}$		910		
Knowlton et al.	$3.4 \cdot 10^{-8}$		950	Li drift after P diffusion	[2.97]
	$8.3 \cdot 10^{-8}$				
Sinno et al.	10^{-3}	0.457		Computed values fitted to crystal-growth experiments	[2.102]
Puzanov et al.		1.3		Crystal-growth simulations	[2.266]
Priolo et al.	$\geq 3 \cdot 10^{-12}$		RT	Defect profiles after He implants	[2.253]
Chakravarthi & Dunham	579	1.88	870–1208	Zinc diffusion	[2.99]
Nakamura et al.	40.5	1.64		Crystal growth and defect formation	[2.100]
Walton et al.	$9.27 \cdot 10^{-11}$		950	Li drift after P diffusion	[2.101]
Giese et al.	$2.5 \cdot 10^{-8}$		1107	Zinc outdiffusion	[2.103]
	$9.8 \cdot 10^{-8}$		1154		
Dornberger et al.	$1.3 \cdot 10^{-3}$	0.457		Computed values fitted to crystal-growth experiments	[2.104]
Hallén et al.	$4.2 \cdot 10^{-9}$		RT	Defect production by MeV ion implantation	[2.254]
Voronkov & Falster	$1.1 \cdot 10^{-5}$		1070	Nucleation and growth of voids	[2.105]
	$3 \cdot 10^{-10}$		RT	Generation of A-centers	
Coffa and Libertino	$2.23 \cdot 10^{-4}$	0.35	RT–1412	Combination of both	
	$3 \cdot 10^{-13}$		RT	MeV-He- implantation- induced diode leakage current	[2.255]
Scholz et al.	$3.86 \cdot 10^{-10}$		900	Carbon diffusion	[2.227]
Okino & Shimozaki	$1.6 \cdot 10^{-11}$		1100	Self-diffusion and OED	[2.267]
Okino & Shimozaki	0.6	2.9		Self-diffusion and OED	[2.228]

	D_0 (cm ² /s)	H^m (eV)	Temperature range (°C)	Experimental technique	Ref.
Nylandsted Larsen et al.	$\geq 4 \cdot 10^{-11}$		RT	Dopant deactivation	[2.257]
Falster et al.	$4.5 \cdot 10^{-4}$	0.35	RT–1412	Nucleation of voids and generation of A-centers	[2.106]
Mori et al.	$7.8 \cdot 10^{-4}$	0.35	1150–1280	Vacancy profiles	
Akatsuka et al.	$2.0 \cdot 10^{-3}$	0.457		Crystal growth	[2.107]
	886	2.132	1000–1280	Effect of RTP on oxygen precipitation	[2.108]
Ngau et al.	$1.88 \cdot 10^{-12}$		750	Transient diffusion of boron and carbon	[2.268]
Nakamura et al.	$(3.0\text{--}3.6) \cdot 10^{-4}$	0.3		Formation of voids during crystal growth	[2.229]
	$(2.3\text{--}2.6) \cdot 10^{-3}$	0.6			
Libertino & Coffa	$4 \cdot 10^{-13}$		RT	Implantation-induced diode leakage current	[2.256]
Pichler	$(4.9\text{--}26) \cdot 10^{-6}$		1277	Formation of Si-E centers	[2.109]
Okui & Nishimoto	188	1.917		Crystal growth	[2.110]
Bracht et al.		1.8 ± 0.5	780–872	Radiation-enhanced self-diffusion	[2.204]

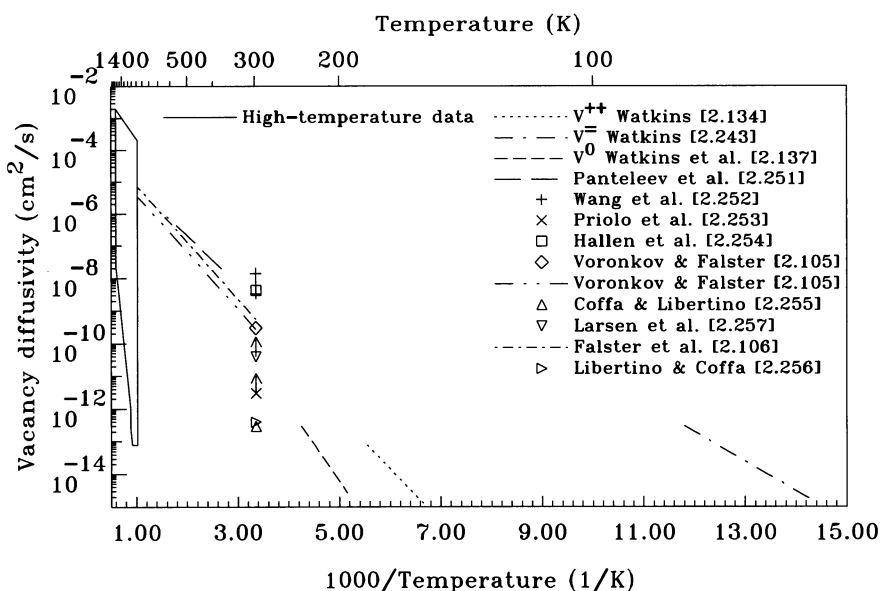


Figure 2.7: Intrinsic diffusion coefficient of vacancies.

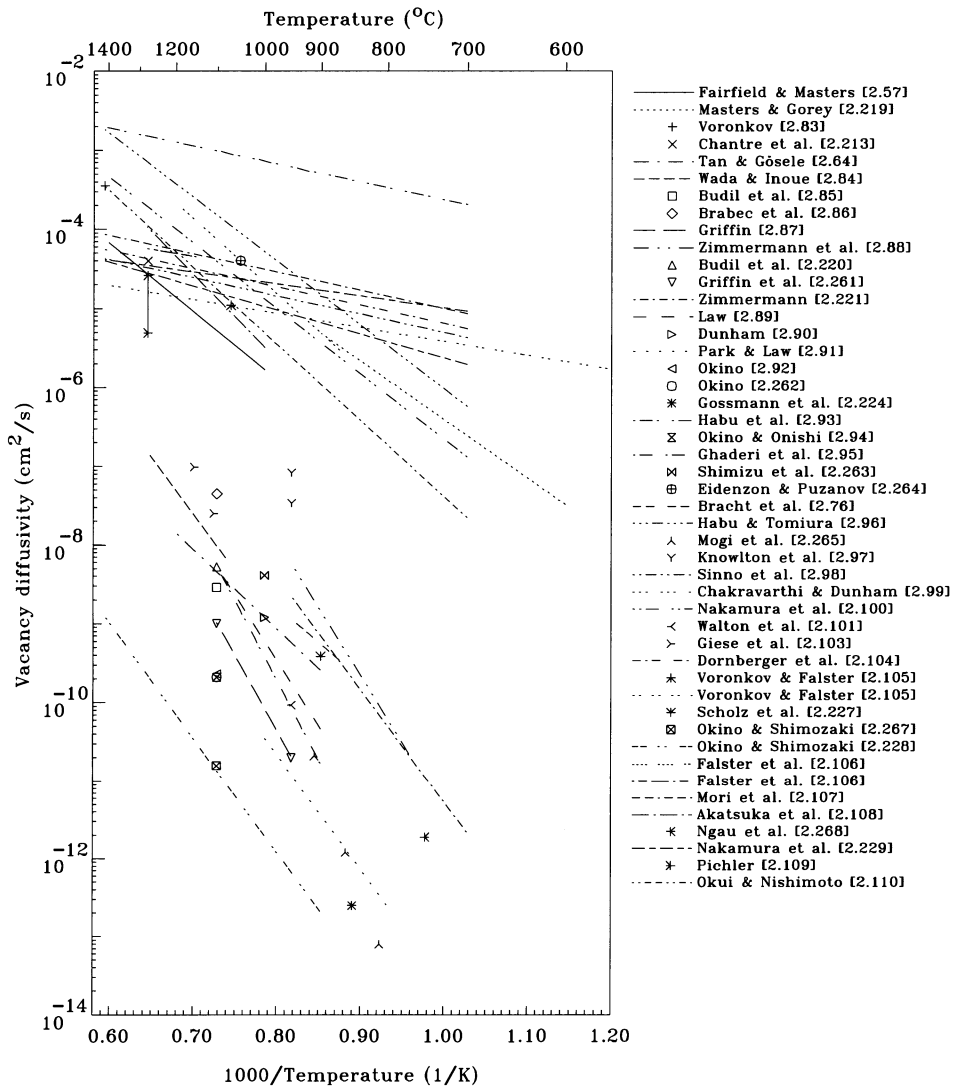


Figure 2.8: Intrinsic diffusion coefficient of vacancies at elevated temperatures.

After powerful theoretical methods were developed to compute properties of point defects in silicon, they were applied in several investigations to calculate the migration enthalpy of vacancies. The results of these calculations are listed in Table 2.8.

Remarkable with respect to the diffusion behavior of vacancies were especially the *ab-initio* molecular-dynamics investigation of Car et al. [2.203]. They indicated that vacancies do not necessarily perform a random walk at elevated temperatures but may perform several jumps in succession before changing their direction. At temperatures above 1300 °C also second- and third-neighbour jumps were observed and the diffusion behavior was suggested to be in agreement with the concept of an extended vacancy mentioned above. It has to be noted, however, that correlated, consecutive jumps are expected alone because $k \cdot T$ is comparable to the migration enthalpy.

Table 2.8: Migration enthalpies of vacancies obtained from *ab-initio* calculations.

	Charge state	H^m (eV)	Ref.
Kelly et al.	0	0.27	[2.184]
	++	0.42	
Car et al.	0	0.3	[2.203]
Sugino & Oshiyama	-	0.1	[2.269]
	++	0.4	
Nichols et al.	0	0.3	[2.234]
Zhu	0	0.3	[2.238]
Xie & Chen	0	0.31	[2.240]
Xie and Chen	0	0.3	[2.195]

Besides normal diffusion, evidence was given in the literature that vacancies may diffuse athermally. Watkins [2.136] noted an unexpectedly high rate of formation of oxygen-vacancy complexes and germanium-vacancy pairs which indicated that vacancies diffused already at 20.4 K. More detailed studies of this phenomenon [2.137] indicated that athermal vacancy diffusion can be stimulated by two processes: the generation of electron-hole pairs by laser illumination and the injection of electrons during DLTS studies. To reconcile his estimates of vacancy-migration enthalpies estimated at elevated temperatures with the much smaller ones observed at cryogenic temperatures, Van Vechten [2.270] suggested that the latter are the result of the recombination of thermally generated electrons and holes at vacancies which cause an athermal diffusion even without illumination or injection of electrons.

2.4.4 Divacancies

In irradiation studies, the silicon divacancy is one of the major defects. It forms after electron irradiation as soon as vacancies become mobile or already in the collision cascade in case of higher-energetic particles. Due to its rather high migration energy, the divacancy is immobile at room temperature which made its properties accessible to a variety of characterization methods. Although most investigations were concerned with scientific aspects of divacancies, there are technical applications as well. Divacancies, generated e. g. by low-mass MeV ion implantation, were found to determine the Shockley-Read-Hall carrier lifetime at low injection levels [2.271, 2.272]. A possible application is life-time control in power semiconductors. In detectors for highly energetic particles, on the other hand, detrimental effects were associated with the formation of V_2 [2.273, 2.274].

The divacancy was identified by Corbett and Watkins [2.275] and Bemski et al. [2.276] via two associated EPR spectra, the Si-C and the Si-J centers (relabelled later to Si-G7 and Si-G6, respectively [2.135]). They were interpreted as arising from the singly ionized acceptor state and the singly ionized donor state. The atomic arrangement suggested and the bonds between the atoms are shown schematically in Figure 2.9. In addition, the neutral charge state of the divacancy was associated by Brosious [2.277] with a nearly $\langle 111 \rangle$ -axially symmetric EPR spectrum labelled Si-I1. It has to be noted, though, that the reexamination by Sieverts and Corbett [2.278] indicated that Si-I1 is identical to the V_2O -related Si-A14 EPR center. At low temperatures, Watkins and Corbett [2.279] observed a lowering of the symmetry of the divacancy in its singly positive and singly negative charge states from D_{3d} to C_{2h} . This was attributed to Jahn-Teller distortions which increased the number of distinguishable orientations to three along the axis between the two lattice sites, and to 12 in total for the four possible main directions. Between about 40 and 110 K, changes in the spectra were observed and attributed to motional averaging due to thermally activated reorientations between the three equivalent C_{2h} -symmetric configurations per main orientation. Complementary ENDOR investigations by de Wit et al. [2.280] and Sieverts et al. [2.281] confirmed that the motional averaging lifts the symmetry effectively again to D_{3d} . For the doubly negative charge state, a static (not motionally averaged) D_{3d} symmetry was deduced by Dobaczewski et al. [2.282] from an extensive analysis based on Laplace-DLTS investigations under uniaxial stress. The Jahn-Teller distortions of the divacancy in its negative and neutral charge state were observed also by Nagai et al. [2.283] using the two-dimensional angular-correlation of positron annihilation radiation (2D-ACAR) technique.

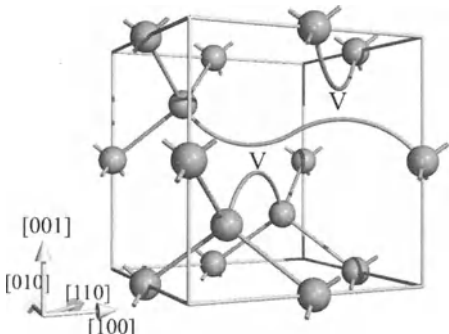


Figure 2.9: Schematic arrangement of atoms around a divacancy. The “V”’s indicate the vacant lattice sites.

The fingerprint of a divacancy with spatially separated vacancies was identified by Sieverts and Corbett [2.278]. Discussed at first in terms of a simple divacancy, the Si-NL11 EPR center was rejected as such [2.284]. Including calculations based on the extended-Hückel theory in their reasoning, the center was finally attributed to two vacancies at third-nearest neighboring sites of each other. As in the “sponge” defect suggested earlier by Hornstra (unpublished except for the discussion in the review of Corbett et al. [2.285]), the two silicon atoms in between are expected to relax from their lattice sites and to form double bonds.

From a detailed IR investigation, including a correlation of the annealing behavior to EPR measurements, Cheng et al. [2.286] concluded that absorption bands at $1.8 \mu\text{m}$ ($\approx 5560 \text{ cm}^{-1}$, RT), $3.3 \mu\text{m}$ ($\approx 3027 \text{ cm}^{-1}$, RT), and $3.9 \mu\text{m}$ ($\approx 2560 \text{ cm}^{-1}$, RT) are associated with the divacancy. The occurrence of these absorption bands was known already before to depend on the position of the Fermi level. Comparing the data of Fan and Ramdas [2.287] with the level scheme of the divacancy, Cheng et al. [2.286] suggested tentatively that the absorption bands at 1.8 , 3.3 , and $3.9 \mu\text{m}$ are associated with the neutral, doubly negative, and positive charge

states of the divacancy, respectively. The association of the $1.8 \mu\text{m}$ band with the neutral divacancy alone has been corroborated by Cheng and Vadja [2.288] but questioned by Svensson et al. [2.289, 2.290]. A band at $3.9 \mu\text{m}$ was found also by Cheng [2.291] by photoconductivity measurements. A detailed comparison to the EPR and IR experiments allowed him to corroborate the association of the respective IR and photoconductivity bands with the positively charged divacancy. Further support for this identification was given by Kalma and Corelli [2.292]. At low temperatures, the broad $3.3 \mu\text{m}$ band was found to contain two distinguishable sub-bands at $3.46 \mu\text{m}$ ($\approx 2890 \text{ cm}^{-1}$, 4.2 K) and $3.62 \mu\text{m}$ ($\approx 2766 \text{ cm}^{-1}$, 4.2 K) [2.287, 2.288, 2.293]. However, based on various pieces of evidence, Chen and Corelli [2.293] questioned the association of the bands with the doubly negative charge state of the divacancy. Their tentative association with the singly negative charge state of the divacancy was substantiated by Carton-Merlet et al. [2.294] and Svensson et al. [2.289].

Being one of the best-studied defects in silicon, numerous investigations were carried through to establish the ionization levels of the divacancy. It is remarkable, though, that some inconsistencies remained. A summary of all values suggested in the literature can be found below in Table 2.9.

Basically all DLTS measurements agree that the single and double acceptor levels can be found around $E_c - (0.39\text{--}0.43) \text{ eV}$ and $E_c - (0.21\text{--}0.23) \text{ eV}$, respectively. The only potential inconsistency in these investigations is that the capture cross section for electrons at the single acceptor level is several orders of magnitude higher than expected for a repulsive, ionized defect [2.141, 2.295, 2.296]. On the other hand, evidence from EPR, photoconductivity, and IR absorption measurements, supported by the positron-annihilation studies of Kauppinen et al. [2.297, 2.298], indicated that these levels can be found at about $E_c - 0.54 \text{ eV}$ and $E_c - 0.4 \text{ eV}$, respectively. A reasonable explanation for this discrepancy was suggested by Svensson et al. [2.299]. They noted that the EPR and photoconductivity measurements were performed at very low temperatures ($< 20 \text{ K}$) where the divacancy is frozen in its C_{2h} -symmetric configuration resulting from Jahn-Teller distortions. In contrast, DLTS measurements are performed at significantly higher temperatures where the time constant for charge-carrier emission is orders of magnitude higher than the time constant for reorientation between the low-symmetric configurations. As a consequence, the DLTS measurements relate to the divacancy in its motionally averaged D_{3d} -symmetric configuration. While this would explain the results from the EPR, photoconductivity, and IR absorption measurements, it cannot be applied directly to explain the evidence from the positron-annihilation studies since the latter were performed at room temperature. In addition, there are other discrepancies yet to be explained in the low-temperature regime. One of them is that Svensson et al. [2.289] observed the $3.61 \mu\text{m}$ absorption band associated with V_2^- in an IR investigation at 9 K in samples in which the Fermi level was above $E_c - 0.17 \text{ eV}$. Similarly, Svensson et al. [2.299] noted that Sieverts et al. [2.284] observed simultaneously the V_2^- -related Si-*G7* and the (V-O)⁻-related Si-*B1* EPR centers in an irradiation study. Since the latter is observed only when the Fermi level is above $E_c - 0.17 \text{ eV}$, the single and double acceptor levels were suggested to be at low temperatures at $E_c - (0.41\text{--}0.48) \text{ eV}$ and $E_c - (0.07\text{--}0.13) \text{ eV}$, respectively. This assignment is in clear contrast to the position of the double acceptor level at $E_c - 0.4 \text{ eV}$ assigned by Watkins and Corbett [2.279] on the basis of a study of the production rate of the V_2^- -related Si-*G7* EPR spectrum in *n*-type silicon.

The association of the DLTS levels at $E_c - 0.23 \text{ eV}$ and $E_c - 0.42 \text{ eV}$ to the same defect was corroborated by the observation that both levels have perfectly correlated introduction rates during irradiation with electrons and γ rays [2.141, 2.295, 2.300, 2.301]. This one-to-one proportionality was neither observed in irradiation studies with protons and alpha particles [2.302], nor when neutrons [2.303, 2.304] or ions in the MeV range were implanted [2.299, 2.305, 2.306]. In

these investigations, the concentration associated with the single acceptor level at $E_c - 0.42$ eV was found to exceed that of the concentration associated with the double acceptor level at $E_c - 0.23$ eV significantly around the maximum of the damage. This was explained by Vasil'ev et al. [2.304] by a bending of the energy bands near disordered regions resulting from the collision cascade which inhibits the observation of the level at $E_c - 0.23$ eV there. The $E_c - 0.23$ eV signal corresponds then only to the divacancies in the undisturbed matrix remote from the cores of the disordered regions while the level at $E_c - 0.42$ eV accounts for the total concentration. An alternative explanation offered initially by Hallén, Svensson, Lalita, and coworkers [2.299, 2.302, 2.305] involves that lattice strain in the peak region prevents, to a large extent, the motional averaging of the divacancy and affects the state of the second, less tightly bound electron. Later, Monakhov et al. [2.306] suggested a local compensation of the charge-carrier concentration in highly disordered regions within the collision cascade. Somewhat in contrast, Evans-Freeman et al. [2.296] concluded from their Laplace-DLTS measurements that the differences observed are associated with the presence of other defects with levels around the single acceptor level of the divacancy. This result is in agreement with the work of Giri and coworkers reviewed in [2.307]. As discussed in more detail in Section 2.5.5, they found a metastable defect with negative-U properties, presumably a self-interstitial cluster, to form after argon implantation with one level overlapping with the divacancy level at $E_c - 0.42$ eV. Problems with the correlation of the concentrations of the divacancy in its single and double acceptor state were also reported in investigations in which they were characterized via the temperature dependence of the electron concentration [2.308, 2.309]. Some of the discrepancies were explained by Vasil'ev et al. [2.310] who noted that the level at $E_c - 0.23$ eV was simply not visible in some experiments because of the experimental conditions chosen. In addition, it was shown by Korshunov et al. [2.311], that the reliable determination of the concentration of defects with closely spaced levels is a severe problem in such experiments.

The donor level of the divacancy is usually reported around 0.18 to 0.23 eV above the valence-band edge. Among other evidence, it was found by Kuchinskii and Lomako [2.300] to have introduction rates during irradiation with electrons and γ rays which are perfectly correlated with those of the acceptor values. However, Londos [2.312] noted that the values reported for the donor level appear to be inconsistent and cluster around 0.19 eV and 0.23 eV. As an explanation, he speculated that his level at $E_v + 0.19$ arises from a divacancy modified by a near-by silicon self-interstitial. Alternatively, Trauwaert et al. [2.313] suggested that the level at $E_v + 0.23$ eV is associated with a V_2O complex. Comparing the literature data, most of the recent investigations confirm the donor level at $E_v + 0.19$ eV rather than at higher values.

Table 2.9: Energy levels proposed for divacancies. A '*' behind the distance value indicates that it was defined with respect to the other band edge and converted assuming a band gap of 1.12 eV.

	Level and position (eV)	Applied method	Ref.
Watkins & Corbett	$E_c - E_{V_2^=}$	0.4	EPR study [2.279]
Kalma & Corelli		0.39	Photoconductivity [2.292]
Konozenko et al.		0.2	Hall-effect measurements [2.314]
Lappo & Tkachev		0.42	Photoconductivity and IR absorption [2.315]
Evvaraye & Sun		0.23	DLTS [2.295]
Kimerling		0.23	DLTS [2.141]
Tokuda et al.		0.21	DLTS [2.303]
Krynicki et al.		0.23	DLTS [2.316]

	Level and position (eV)	Applied method	Ref.
Carton-Merlet et al.	0.28 ± 0.05	Illumination-dependent IR absorption	[2.294]
Meese et al.	0.24	DLTS	[2.317]
Bortherton and Bradly	0.23	DLTS	[2.318]
Vasil'ev et al.	0.23	DLTS	[2.304]
Kuchinskii & Lomako	0.23	DLTS	[2.300]
Svensson & Willander	0.23	DLTS	[2.301]
Hallén et al.	0.225	DLTS	[2.271]
Trauwaert et al.	0.23	DLTS	[2.313]
Kauppinen et al.	0.37*	Positron annihilation	[2.298]
Hazdra & Vobecký	0.229	DLTS	[2.319]
Evans-Freeman et al.	0.23	Laplace DLTS	[2.296]
Monakhov et al.	0.237	DLTS	[2.320]
Zangenbergs et al.	0.24	Laplace DLTS	[2.166]
Kalma & Corelli	$E_c - E_{V_2}$	Photoconductivity	[2.292]
Lappo & Tkachev	0.57	Photoconductivity and IR absorption	[2.315]
Evvarayye and Sun	0.41	DLTS	[2.295]
Kimerling	0.39	DLTS	[2.141]
Kimerling et al.	0.41	DLTS	[2.142]
Tokuda et al.	0.39	DLTS	[2.303]
Krynicki et al.	0.39	DLTS	[2.316]
Carton-Merlet et al.	0.36 ± 0.05	Illumination-dependent IR absorption	[2.294]
Meese et al.	0.45	DLTS	[2.317]
Bortherton and Bradly	0.413	DLTS	[2.318]
Vasil'ev et al.	0.39	DLTS	[2.304]
Kuchinskii & Lomako	0.39	DLTS	[2.300]
Svensson & Willander	0.41	DLTS	[2.301]
Svensson et al.	0.41	IR absorption study	[2.289]
Hallén et al.	0.421	DLTS	[2.271]
Trauwaert et al.	0.42	DLTS	[2.313]
Kauppinen et al.	0.56	Positron annihilation	[2.298]
Hazdra & Vobecký	0.421	DLTS	[2.319]
Evans-Freeman et al.	0.43	Laplace DLTS	[2.296]
Monakhov et al.	0.43	DLTS	[2.320]
Zangenbergs et al.	0.435	Laplace DLTS	[2.166]
Watkins & Corbett	$E_{V_2^+} - E_V$	Photo-EPR	[2.279]
Konozenko et al.	0.27	Hall-effect measurements	[2.314]
Lappo & Tkachev	0.32	Photoconductivity and IR absorption	[2.315]
Brabant et al.	0.115	Thermally stimulated capacitance	[2.140]
Kimerling	0.21	DLTS	[2.141]
Mooney et al.	0.23	DLTS	[2.321]
Kimerling et al.	0.21	DLTS	[2.142]
Lee et al.	0.23	DLTS	[2.322]
Meese et al.	0.18	DLTS	[2.317]
Stavola & Kimerling	0.21	Stress alignment and photocapacitance	[2.323]
Londos	0.19	DLTS	[2.312]
Kuchinskii & Lomako	0.21	DLTS	[2.300]

	Level and position (eV)	Applied method	Ref.
Svensson et al.	0.28	Fermi-level-dependent IR investigations	[2.290]
Asghar et al.	0.21	DLTS	[2.324]
Trauwaert et al.	0.19	DLTS	[2.313]
Hallén et al.	0.194	DLTS	[2.271]
Khan et al.	0.18	DLTS	[2.325]
Zangenberg et al.	0.191	Laplace DLTS	[2.166]

Positron-annihilation investigations of electron-irradiated samples indicated positron lifetimes of 260 to 327 ps to be associated with the divacancy [2.168–2.171, 2.297, 2.326–2.331]. The large range of values can be explained in part by the experimental ovservation that the positron lifetime depends on the charge state of the divacancy and on the sample temperature [2.329]. Other potential reasons for these dependences were given by Krause-Rehberg and Leipner [2.332] and relate to the divacancy concentration being at the lower detection limit and to a possible influence of impurity-vacancy pairs. Theoretical investigations gave values of 299 to 309 ps [2.175, 2.176, 2.178–2.180].

At low temperatures, as mentioned, the divacancy in its singly positive and singly negative charge states may assume three equivalent configurations along the axis between the two vacant lattice sites. Reorientations between them were found experimentally by Watkins and Corbett [2.279] to be characterized by an activation energy of 0.056 eV for V_2^- and 0.073 eV for V_2^+ .

In stress studies after electron irradiation, Watkins and Corbett [2.279] found the atomic reorientation of the divacancy to be governed by an activation energy of 1.3 eV. This value reflects the energy barrier of the limiting process, the separation of the divacancy by one coordination site. Annealing studies in FZ silicon resulted in a lower limit of 1.95 eV for the energy needed to dissociate the divacancy completely. From this, a lower limit of 1.6 eV was suggested for the binding energy of the divacancy. From the similarities in the annealing of Si-G6 and Si-G7, it was suggested tentatively that the properties refer to the divacancy in its neutral charge state. Activation energies from 1.2 to 1.3 eV were also found to govern realignment and defect annealing of divacancies in various other studies [2.286, 2.292, 2.323, 2.328, 2.333, 2.334]. In positron-annihilation studies, Dannefaer et al. [2.168] observed that divacancies dissolve above 340 °C with first-order kinetics. The activation energy of about 1.7 eV should again correspond to the energy of complete dissociation of V_2 . Annealing of neutral divacancies was found by Svensson et al. [2.290] to be characterized by an apparent activation energy of 1.4 to 1.5 eV. A similar value of 1.47 eV was reported already before by Ewvaraye and Sun [2.295]. However, taking diffusion and dissociation processes into account in a more detailed analysis, Svensson et al. [2.290] estimated activation energies of 1.275 and 1.71 eV for the two processes, respectively. Following their own concept that the level at $E_c - 0.42$ eV corresponds in neutron-irradiated samples to the total concentration of divacancies while the level at $E_c - 0.23$ eV gives only the concentration of divacancies off from the cores of disordered regions, Vasil'ev et al. [2.335] found the annealing of divacancies to be characterized by different annealing mechanisms with activation energies of 1.1, 1.3, and 1.47 eV. Refining this analysis, Antonova et al. [2.336] extracted an activation energy of 1.5 eV for divacancies in the undisturbed crystal matrix while divacancies near the dislocation cores were suggested to anneal with an activation energy of 1.0 eV. The latter mechanism was suggested to involve an interaction with self-interstitials liberated from interstitial complexes.

Complementary experimental evidence was obtained from calorimetry measurements and their correlation to IR absorption measurements. In such studies, Roorda [2.337] found significant heat releases around 150 and 250 °C from electron-irradiated samples which correlated

to the annealing of divacancies. In a subsequent investigation, Poirier et al. [2.338] determined activation energies of approximately 1.2 and 1.5 eV, respectively, for these heat releases. The two values were associated tentatively with migration and dissociation of divacancies.

Complementary information about the structure and energetics of divacancies came from theoretical work, especially *ab-initio* calculations. In one of the first in which structural relaxation was fully taken into account, Saito and Oshiyama [2.189, 2.339] suggested an outward Jahn-Teller distortion with “resonant bonds” across the divacancy. This claim was discussed controversially by Watkins [2.340] and Saito and Oshiyama [2.341]. It was found by Seong and Lewis [2.190] also for the neutral charge state. Using a larger cell and a different approximation to the exchange-correlation potential, Pesola et al. [2.342] found mixed structures of pairing and resonant bonds for the singly negative and neutral charge states of the divacancy. In contrast to Seong and Lewis, the pairing structures were found to dominate for the neutral charge state while the predominance of resonant bonds was confirmed for the singly negative one. Finally, the vacancy in its doubly negative charge state was found to be D_{3d} -symmetric. In subsequent investigations, Coomer et al. [2.343] and Öğüt and Chelikowsky [2.196] found that resonant-bond structures in silicon are unstable for any charge state and suggested that their appearance might be associated with insufficiencies of the respective calculations. The absence of Jahn-Teller distortions for the doubly negative charge state of the divacancy was confirmed also by Öğüt and Chelikowsky. It remains to remark that the two-dimensional angular-correlation measurements of positron annihilation radiation (2D-ACAR) performed by Nagai et al. [2.283] confirmed the existence of pairing Jahn-Teller distortions for the neutral divacancy while resonant bonds were rejected. In addition to Jahn-Teller distortions, breathing-mode distortions around a divacancy are expected. Inward relaxation was indicated in several of the *ab-initio* calculations. Qualitatively, Seong and Lewis [2.190] reported a volume decrease of 17%.

In their *ab-initio* calculations, Seong and Lewis [2.190] calculated a binding energy of 1.95 eV for two neutral vacancies at neighboring sites. For two neutral vacancies on next-nearest neighboring sites, the binding energy was found to reduce to 0.68 eV. Using similar methods, Pesola et al. [2.342], Xie and Chen [2.195], Akiyama et al. [2.344], Hwang and Goddard III [2.345], and Mueller et al. [2.230] reported binding energies of 1.6, 1.84, 1.77–2.02, 1.74, and 1.86 eV, respectively, for two neutral vacancies to V_2^0 . In this context, it should be noted that the concentration of sites for divacancies $C_{V_2S} = 2 \cdot C_{Si}$ is equal to the number of bonds between neighboring silicon atoms and, therefore, twice the number of lattice sites.

Diffusion and dissociation of neutral divacancies was investigated in the work of Hwang and Goddard III [2.345] by *ab-initio* methods. Diffusion via dissociation and association was found to require surmounting a barrier of 1.36 eV. Since no metastability was found for the intermediate state, it was suggested that the break-up of a divacancy requires the simultaneous movement of two neighboring silicon atoms into the divacancy. For this process, an activation energy of 1.89 eV was calculated while a barrier of 0.49 eV was found to stabilize the resulting structure with the two vacancies on third-nearest neighboring sites against returning into the divacancy configuration. A significantly more complex picture arises from the molecular-dynamics simulations of Prasad and Sinno [2.346] which were based on an empirical potential. In their energy diagram, several configurations of metastability are apparent. The divacancy diffusion coefficient reported by them is characterized by a prefactor of $0.15 \text{ cm}^2/\text{s}$ and an activation energy of 1.45 eV for the temperature interval from about 1000 to 1400 °C. However, they indicated that the activation decreases from about 2.0 eV at the higher temperature to 1.3 eV at the lower temperature, indicating different diffusion mechanisms.

Based on *ab-initio* calculations of the electronic levels of divacancies, Estreicher et al. [2.347] suggested tentatively that they give rise to the zero-phonon 1.018 eV photoluminescence line labelled I_1 or W . However, in the experiments of Giri et al. [2.348], no correlation was found between divacancies and the I_1/W -line. It should be noted that this line was assigned to various other defects, too. It is discussed in more detail in Section 2.5.5.

2.4.5 Small Vacancy Clusters

Much of our knowledge of vacancy clusters is based on the structural identification of defects after electron or neutron irradiation. Certainly one of the most prominent defects in such studies is the divacancy discussed in Section 2.4.4. It forms already at temperatures below 100 K because of the high mobility of vacancies. Larger vacancy agglomerates were observed especially after irradiation with neutrons or particles of higher mass to form already in the collision cascade [2.317]. Some of them could be identified structurally by elaborate spectroscopic analyses. Other centers like several DLTS peaks associated tentatively with vacancy clusters [2.349, 2.350] still require a definite assignment. Most other open-volume defects can be detected probably only in positron-annihilation measurements. In the absence of more detailed experimental evidence, important complementary information came especially from calculations of the structure and energetics of vacancy agglomerates by the approximate solution of the Schrödinger equation or by using empirical potentials. One general finding obtained by Prasad and Sinno [2.346] from molecular-dynamics simulations based on an empirical potential is that many vacancy clusters are mobile.

Trivacancies

In a neutron-irradiation study, Lee et al. [2.351] found an EPR spectrum which they labelled Si-A4. It was introduced around 150 °C and annealed out around 270 °C. From its symmetry, Lee and Corbett [2.352] concluded that it arises from an odd number of vacancies in a chain along the $\langle 1\bar{1}0 \rangle$ direction in the $\{110\}$ plane. Tentatively, the defect was suggested to comprise three vacancies, but a linear pentavacancy could not be excluded.

In the molecular-dynamics simulations of Prasad and Sinno [2.346] based on an empirical potential, trivacancies were found to be mobile with a diffusion coefficient of $2.2 \cdot 10^{-6}$ cm²/s at 1330 °C. Diffusion was discussed to occur by elementary transitions between seven atomic configurations of the trivacancy.

Tetravacancies

A straight chain of 4 vacancies aligned approximately along the $\langle 1\bar{1}0 \rangle$ direction in the $\{110\}$ plane was identified by Brower [2.353] to give rise to the Si-P3 EPR center originally reported as (II, III) EPR center by Jung and Newell [2.354]. This assignment was confirmed later by the investigations of Lee and Corbett [2.352]. From a correlation of the kinetics of defects characterized by DLTS and EPR, Meese et al. [2.317] suggested tentatively that the planar tetravacancy should give rise to a level at $E_v + 0.35$ eV.

Around 170 °C where the Si-P3 center was observed to anneal out in neutron-irradiated silicon samples [2.354], Lee et al. [2.351] found that an other EPR spectrum, labelled Si-A3, is introduced. This spectrum was associated by Lee and Corbett [2.352] with a tetravacancy in a C_{3v}-symmetric configuration along the $\langle 111 \rangle$ direction in which three vacancies are arranged at nearest-neighboring positions of a fourth one. In their annealing study, Lee et al. [2.351] found the defect to disappear again around 300 °C.

Pentavacancies

In neutron-irradiated samples annealed at temperatures of 170 °C and above, Nisenoff and Fan [2.355] found a dominant EPR spectrum which they labelled Si-*N* and which they associated tentatively with a vacancy cluster. It was relabelled later to Si-*P1* [2.135] and identified by Lee and Corbett [2.352, 2.356] to arise from a non-planar five-vacancy cluster in its negative charge state. In the structural model suggested, three vacancies are aligned in a row along the $\langle 110 \rangle$ axis with two additional vacancies arranged at both sides of the vacancy at the end of the chain. In this form, the complex is C_s -symmetric with a $\{110\}$ -oriented mirror plane. It is interesting to note that the same defect was found in plastically deformed silicon [2.357].

From a correlation of the kinetics of defects characterized by DLTS and EPR, Meese et al. [2.317] suggested tentatively that the non-planar pentavacancy should give rise to a level at $E_c - 0.34$ eV.

Based on its apparent impurity-independence and a similar introduction and annealing kinetics as the Si-*P1* EPR center, Kirkpatrick et al. [2.358] and Tkachev and Mudryi [2.359] suggested tentatively that the zero-phonon 1.018 photoluminescence line labelled *I*₁ or *W* arises from a pentavacancy. However, the defect was found later to have C_{3v} symmetry which excludes at least the configuration responsible for the Si-*P1* EPR center. It should be noted that the *I*₁/*W*-line was assigned to various other defects, too. It is discussed in more detail in Section 2.5.5.

It has to be mentioned also that the Si-*A4* EPR spectrum, discussed above to arise from a trivacancy, might arise from a planar pentavacancy, too.

Hexavacancies

In one of the first theoretical investigations on vacancy clusters, Chadi and Chang [2.360] estimated on the basis of the number of dangling bonds that a ring-like V₆ cluster would be among the most stable vacancy agglomerates. This expectation, as discussed below, was confirmed by basically all subsequent theoretical investigations. The only exception is probably the work of van Veen et al. [2.361] who suggested hexavacancies from molecular-dynamics calculations based on the Stillinger-Weber potential to be among the least stable vacancy agglomerates.

From *ab-initio* studies of hydrogen-decorated hexavacancies, Hourahine et al. [2.362] suggested that V₆ complexes should be optically active. Based on an extensive reasoning, they were suggested to give rise to a PL line at 1.108 eV which shows C_{3v} symmetry and was labelled *J* by Jones et al. [2.363] and *B*₈₀⁴ by Kaminskii et al. [2.364]⁵. Its properties, reviewed by Sauer and Weber [2.365], include a trigonal symmetry. It has to be mentioned also that hexavacancies at the cores of dislocations were suggested tentatively by Jones et al. [2.366] to give rise to the PL lines at 0.812, 0.875, 0.934, and 1.0 eV, labelled *D1* to *D4*, which are usually observed in samples containing dislocations [2.367].

Vacancy Clusters in Positron-Annihilation Studies

In positron-annihilation experiments, measured lifetimes were usually correlated to the kinetics of defects identified by EPR. These studies resulted in the values summarized in Table 2.10 together with the results of theoretical investigations. Especially large clusters require very large

⁵Actually, the PL line was labelled *X*₈₀⁴ while *B*₈₀⁴ referred to the defect giving rise to the PL line. This distinction was dropped in later references and shall not be stressed further here.

simulation cells which makes it impossible to use the computationally demanding local-density and generalized-gradient approaches. A further problem, especially for the larger clusters, was certainly to find the minimum-energy configuration for each cluster size.

Table 2.10: Positron lifetimes in ps associated with vacancy clusters.

	V ₃	V ₄	V ₅	V ₆	V ₈	V ₁₀	Ref.
Experimental results							
Dannefaer et al.		435					[2.168]
Dannefaer et al.				520			[2.368]
Dannefaer et al.			505				[2.369]
Würschum et al.			320–350				[2.170]
Motoko Kwete et al.		350	390				[2.327]
Kulkarni et al.		346					[2.370]
Kawasuso et al.		350		400		500	[2.371]
Theoretical results							
Puska and Corbel		354	376		399		[2.175]
Saito & Oshiyama	320	325–337	345	348		386	[2.178]
Hakala et al.	321	330	355				[2.179]
Staab et al.	329	343	353	375	389	420	[2.180]

Energetic Properties from Experiments and Theory

Experimental investigations sensitive to the properties of vacancy clusters are rare. From an experiment in which vacancies were generated by high-energy ion implantation into an SOI structure, Venezia et al. [2.372] estimated that the binding energy of vacancies to vacancy clusters is only 0.34 ± 0.3 eV smaller than the formation energy of a vacancy. Using similar experiments, Kalyanaraman et al. [2.373] estimated binding energies of 2.6 ± 0.6 eV and 3.2 ± 0.2 eV from vacancy concentrations in different depth regions.

While an evaluation of experimental data with necessarily simple models cannot be expected to yield more than mean values for the binding energy of vacancies to vacancy clusters, significantly more detailed information about the dependence of the energetics of clusters on their size can be expected from theory. In one of the first theoretical investigations on vacancy clusters, Chadi and Chang [2.360] estimated on the basis of the number of dangling bonds that a ring-like V₆ cluster and an “adamantine cage” V₁₀ cluster would be among the most stable vacancy agglomerates. These expectations were confirmed in a variety of simulations summarized in Table 2.11 and Figure 2.10 for vacancy agglomerates with “magic numbers” like V₆ and V₁₀, but also for some other sizes. Also shown in Figure 2.10 is a frequently-used continuous expression in the form $3.65 - 5.15 \cdot (n^{2/3} - (n-1)^{2/3})$ eV suggested by Jaraiz et al. [2.379] from a fit to the data of Gilmer et al. [2.374].

Problems in the calculations are on the one hand that very large cell sizes are needed to allow the relaxation of large clusters. This restricts the application of the local-density and generalized gradient approaches to rather small vacancy clusters. Simulations based on empirical potentials like Stillinger-Weber and Tersoff were shown by Colombo et al. [2.375] to predict binding energies of vacancies to vacancy clusters which are qualitatively different from such calculated by *ab-initio* methods. On the other hand, an other potential named “environment-dependent interatomic potential” (EDIP) was shown by Prasad and Sinno [2.378] to give reasonable results. A second problem is to find the minimum-energy configuration for each vacancy cluster of a certain size. This is most likely the reason why the investigations agree qualitatively at least

Table 2.11: Reduction of the system energy due to the formation of a vacancy agglomerate of size n from an agglomerate of size $n - 1$ and a well-separated vacancy. The abbreviations EP, GGA, HF, LDA, and TB refer to empirical potential, generalized gradient approximation, Hartree-Fock, local-density approximation, and tight-binding methods.

$n =$	3	4	5	6	7	8	9	Method	Ref.
Oshiyama et al.	1.84	1.83	2.02	3.09	1.68	1.66	3.74	LDA	[2.189]
Gilmer et al.	0.62	0.59	1.39	1.37				EP	[2.374]
Colombo et al.	1.45	1.26	2.37	3.33	1.04	3.10	1.88	TB	[2.375]
Hastings et al.	2.08	1.92	3.05	3.76	1.3			TB	[2.236]
	2.12	4.65	5.07	6.50	-0.77			HF	
Bongiorno et al.	1.46	1.19	2.08	2.72	1.07	3.04	2.77	TB	[2.376]
Akiyama et al.	2.05	2.78	3.09	3.32	1.83	3.58	3.40	TB	[2.377]
Akiyama et al.	1.66	1.46	2.28	2.83	1.03	2.08		LDA (64)	[2.344]
Akiyama et al.	1.88	1.60	2.33	3.06	1.37	2.31		LDA (64)	[2.344]
Akiyama et al.					1.10	2.09	2.84	GGA (216)	[2.344]
Staab et al.	1.6	2.4	3.1	3.5	1.4	2.2	3.5	TB	[2.180]
Prasad & Sinno	1.61	1.67	1.54	2.00	2.72	1.59		EP	[2.378]

$n =$	10	11	12	13	14	15	16	Method	Ref.
Oshiyama et al.	3.33							LDA	[2.189]
Colombo et al.	3.39	1.07	3.11	2.74	2.59	0.93	3.11	TB	[2.375]
Bongiorno et al.	2.55	1.15	2.98	2.81	2.66	0.99	3.00	TB	[2.376]
Akiyama et al.	3.72	2.34	1.94	2.93	3.26	2.57	3.20	TB	[2.377]
Akiyama et al.	3.04	2.28						GGA (216)	[2.344]
Staab et al.	3.4	0.8	2.5	2.8	3.1	2.2	2.6	TB	[2.180]

$n =$	17	18	19	20	21	22	23	Method	Ref.
Colombo et al.	2.74	2.61						TB	[2.375]
Bongiorno et al.	2.80	2.66	1.93	2.37	2.81	1.96	1.91	TB	[2.376]
Akiyama et al.	3.59	2.82	2.73					TB	[2.377]
Staab et al.	2.7	3.3						TB	[2.180]

$n =$	24	25	26	27	28	29	30	Method	Ref.
Bongiorno et al.	3.21	3.39	3.07	3.06	3.27	3.04	2.60	TB	[2.376]

$n =$	31	32	33	34	35	Method	Ref.
Bongiorno et al.	2.62	2.63	2.63	2.63	3.32	TB	[2.376]

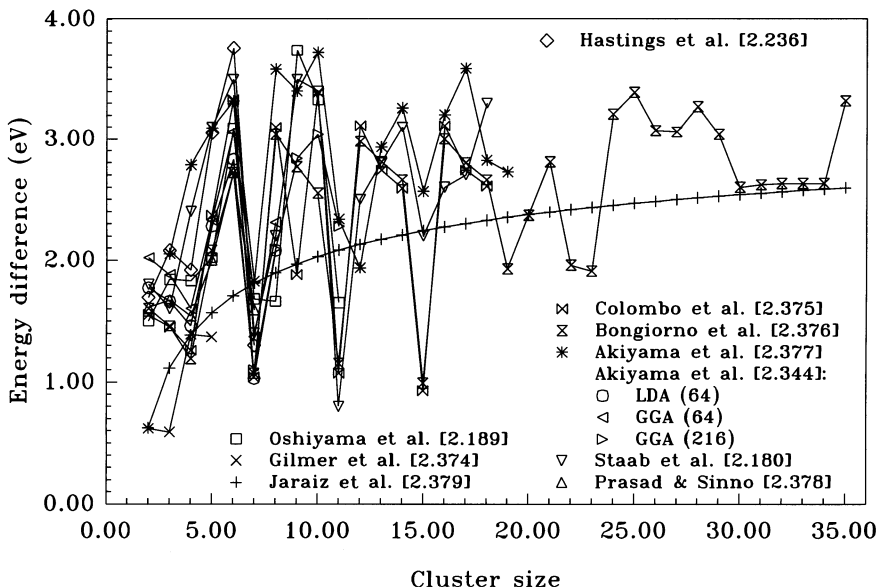


Figure 2.10: Reduction of the system energy due to the formation of a vacancy agglomerate of size n from an agglomerate of size $n - 1$ and a well-separated vacancy. The lines are just to guide the eye.

until $n = 8$ while the increasing discrepancies observed for larger sizes can probably be related to different atomic configurations. Thus, with respect to both problems, the energies reported have to be taken *cum grano salis*.

Comparing clusters constructed by removing atoms from six-membered rings to clusters constructed by removing atoms from successive shells, Bongiorno et al. [2.376], found the former to be energetically favorable until a size of $n = 24$. For larger sizes, the trend is reversed until the formation energies become equal for both and the former become energetically more favorable again around $n = 35$. In Figure 2.10 and Table 2.11, only the binding energies of vacancies in the energetically most favorable clusters have been included. Based on these values, Chakravarthi and Dunham [2.380] reported the successful simulation of the evolution of vacancy clusters in samples implanted with silicon atoms at MeV energies.

2.5 Self-Interstitials

Self-interstitials in silicon are the natural counterpart of the vacancies. However, they are an elusive species and the majority of our knowledge about their properties was obtained from indirect evidence. These experiments are discussed in Section 2.5.1. Due to the lacking direct evidence, considerable uncertainties exist with respect to the properties of self-interstitials. This concerns their level scheme, but also their equilibrium concentration and the diffusion coefficient reviewed in Sections 2.5.2 and 2.5.3, respectively. Their agglomerates play important roles in situations like post-implantation annealing processes in which a high supersaturation of self-interstitials exists. The di-interstitial discussed in Section 2.5.4 is the counterpart of the divacancy and several EPR centers were associated with it. With respect to the small clusters of self-interstitials reviewed in Section 2.5.5, only meager experimental information is available and most identifications or suggestions of particular structures rely on theoretical investigations.

2.5.1 Experimental Evidence and Suggested Atomic Configurations

In analogy to their dominance in metals, vacancies have long been believed to be exclusively responsible for self-diffusion and impurity diffusion in silicon. Seeger and Swanson [2.2] introduced the idea that self-diffusion near the melting temperature occurs via an interstitial mechanism. At least at low temperatures, self-interstitials are assumed to be extra silicon atoms on well-defined locations in the otherwise perfect crystal. Early pictures of self-interstitials considered especially the tetrahedral and hexagonal lattice sites. Based on a tight-binding approximation, Blount [2.381] suggested that self-interstitials in the diamond lattice should be amphoteric with an acceptor level in the upper half of the band gap and a donor level in the lower half. Diffusion was assumed either to occur by jumps from one site to the other or via the interstitialcy mechanism suggested by Seitz [2.382]. The latter assumes that self-interstitials move by pushing one of the neighboring atoms to an interstitial position while they occupy the substitutional position themselves. As an alternative to a silicon atom at an interstitial site, a configuration in which two silicon atoms share a site has been proposed by Huntington and Seitz [2.383]. This configuration is usually called “split interstitial” and can be seen as an analogy to the semi-vacancy pair. Later, also the bond-centered interstitial site was taken into consideration. At high temperatures, in order to explain seeming discrepancies between early theories and self-diffusion data, an “extended” state of self-interstitials has been postulated by Seeger and coworkers [2.2,2.3] in analogy to the extended vacancy. To reconcile low-temperature and high-temperature experiments, Frank [2.384] suggested that self-interstitials gradually loose their atomic configuration with increasing temperature and finally become spread out over several atomic volumes. It should be mentioned here that the large formation enthalpies obtained from the theoretical investigations mentioned below reconcile low-temperature and high-temperature experiments in part. On the other hand, the few *ab-initio* molecular-dynamics simulations available do not allow to decide conclusively whether self-interstitials are extended or not at elevated temperatures.

Although it is clear that self-interstitials and vacancies are formed in pairs during electron irradiation, only the vacancies were found in the early EPR investigations [2.135]. Instead of self-interstitials, interstitial group III atoms were found in *p*-type silicon in approximately equal number as vacancies. To explain this, Watkins [2.135] suggested that self-interstitials are able to perform long-range diffusion already at temperatures of 4.2 K. Complementary experiments performed by Gwozdz and Koehler [2.385] indicated that self-interstitials are mobile even at 0.5 K.

In *n*-type silicon, the fate of the self-interstitials created during electron irradiation was less clear. The appearance of interstitial-oxygen complexes at 130 K [2.386] and of carbon interstitials at about 150 to 170 K [2.142, 2.387] were first indications of long-range diffusion of silicon self-interstitials. Similar conclusions were drawn from samples irradiated by protons or alpha particles [2.388] and helium or argon [2.250]. From a migration temperature of 150 K, Partyka et al. [2.250] estimated an activation energy of about 0.3 eV. At lower temperatures, Watkins [2.243] found the majority of the vacancies in divacancies which were perturbed by the strain field of a nearby defect and which did not reorient when external stress was applied. Dissolution of this complex occurred at about 140 K and it was suggested that the nearby defect might be a self-interstitial. Similar observations and conclusions were reported by Stein and Vook [2.389], and Massarani and Brelot [2.390] reported an annealing stage of divacancies at 130 K which they associated with the capture of self-interstitials being mobile at this temperature. In approximately the same temperature range, Watkins [2.136, 2.243] found the Si-G25 center to anneal out and speculated that it might be associated with a self-interstitial. In a subsequent study, Harris and Watkins [2.387] showed that the non-reorientable divacancies,

the EPR Si-*G*25 center, and a newly found EPR center Si-*L*1 contain indeed self-interstitials. From kinetic studies they concluded that the defects near the non-reorientable divacancies are di-interstitials and that both recombine directly without release of vacancies or self-interstitials. Annealing of the two EPR centers, on the other hand, was found to be correlated with increases in the concentration of interstitial carbon requiring long-range diffusion of self-interstitials. For the $\langle 100 \rangle$ -axially symmetric Si-*L*1 center, annealing occurs around 150 K. The Si-*G*25 center has also axial symmetry around a $\langle 100 \rangle$ axis and an electrical level at about $E_c - 0.35$ eV. Its annealing around 175 K was characterized by a time constant with an activation energy of 0.57 eV and a prefactor which indicated the break-up of a complex rather than long-range migration.

In high-resistivity silicon, Bech Nielsen and Andersen [2.391] investigated the damage created by implantation with low-energy deuterium at 30 K by an ion-beam technique. Thermal annealing showed two annealing stages at about 110 and 190 K. The former was attributed to the migration of V^- while the latter was ascribed to the diffusion of self-interstitials. Analyzing the angular dependence of the backscattering yield allowed to identify a small interstitial component. Its atomic arrangement was concluded to be consistent with split interstitials oriented along $\langle 110 \rangle$ or $\langle 111 \rangle$ directions with the silicon atoms displaced by 1.2 ± 0.5 Å. On the other hand, $\langle 100 \rangle$ -oriented split interstitials and self-interstitials on tetrahedral sites were inconsistent with the analysis.

The picture in *p*-type silicon changed after electron irradiation was complemented by irradiation with alpha particles and protons. In such studies, Abdullin et al. [2.392, 2.393] found two levels at $E_c - 0.26$ eV and $E_c - 0.39$ eV by DLTS which formed irrespective of the kind of acceptor impurity and of the presence of oxygen. Athermal annealing of the defects could be stimulated optically and by electron injection, and led to the generation of carbon and aluminum interstitials as well as pairs of interstitial oxygen and self-interstitials. Annealing at 180 K led to a dissolution of IO_i pairs and to a partial recovery of the level at $E_c - 0.26$ eV. Without electron injection, temperatures around room temperature were required for the carbon and aluminum interstitials to appear. Considering also other details of their experimental results, Abdullin et al. [2.392] tentatively associated the levels at $E_c - 0.26$ eV and $E_c - 0.39$ eV with the donor and double donor levels of a self-interstitial, respectively. Later, Abdullin et al. [2.393] reversed their order and assigned the level at $E_c - 0.39$ eV to the donor transition and the level at $E_c - 0.25$ eV to the double-donor transition. They then form an Anderson “negative-U” system [2.145] in agreement with the theoretical predictions discussed below. Complementary thermally-stimulated capacitance measurements performed by Abdullin and Mukashev [2.394] confirmed that the level around $E_c - 0.36$ eV is associated with the capture of electrons at a positively charged defect. In an EPR investigation, Abdullin et al. [2.395] found a T_d -symmetric EPR center which they labelled Si-AA12. From its observation in irradiated high-purity silicon, it was concluded that it arises from an intrinsic defect. The (presumably positive [2.388]) charge state from which Si-AA12 arises was found to be unstable at 160 K and from the kinetics of the recharging process by light the position of the energy level was deduced to be 0.4 eV below the conduction band or above the valence band. Annealing of the Si-AA12 spectrum was observed in the temperature range from 280 to 350 K but could be stimulated at much lower temperatures by irradiation with light. Detailed comparisons to the DLTS investigations finally led to the conclusion that the Si-AA12 spectrum arises from the same self-interstitial defect as the DLTS level at $E_c - 0.39$ eV [2.388, 2.395]. The identification of the Si-AA12 as self-interstitials was also supported by Eberlein et al. [2.396] on the basis of *ab-initio* investigations. From investigations of the Fermi-level dependence of the introduction rates of radiation defects in electron-irradiated samples with charge-dependent selective traps, Lukjanitsa [2.158] concluded that levels at $E_c -$

0.44 eV, E_c - 0.86 eV, and presumably E_c - 0.67 eV belong to self-interstitials. A summary of the levels suggested for self-interstitials can be found in Table 2.12.

Table 2.12: Levels proposed for self-interstitials. A “*” behind the ionization energy indicates that it was originally given with respect to the other band edge and converted assuming a band gap of 1.12 eV.

	Level and position (eV)	Applied method	Ref.
Roth & Plummer	$E_c - E_{I^=}$ 0.3	OED	[2.397]
Chik	$E_c - E_{I^-}$ 0.425*	Self-diffusion	[2.398]
Seeger & Frank	0.45		[2.399]
Frank	0.4		[2.400]
Lefèvre	0.49	DLTS	[2.401]
Giles	0.09	OED at 1000 °C	[2.402]
Giles	0.09	IED at 800 °C	[2.403]
John & Law	0.11	OED	[2.404]
Roth & Plummer	0.4	OED	[2.397]
Chik	$E_{I^+} - E_v$ 0.316*	Self-diffusion	[2.398]
Seeger & Frank	0.4		[2.399]
Tsoukalas & Chenevier	0.33	OED at 1000 °C	[2.405]
Lugakov & Lukashevich	0.43–0.45	Formation of radiation defects	[2.164]
Giles	0.34	OED at 1000 °C	[2.402]
Giles	0.39	IED at 900 °C	[2.403]
Abdullin et al.	0.87*	DLTS	[2.392]
Abdullin et al.	0.73*	DLTS	[2.393]
John & Law	0.17	OED	[2.404]
Roth & Plummer	0.5	OED	[2.397]
Abdullin et al.	$E_{I^{++}} - E_v$ 0.73*	DLTS	[2.392]
Abdullin et al.	0.87*	DLTS	[2.393]

For neutral hexagonal self-interstitials, Al-Mushadani and Needs [2.167] suggested a two-fold degeneracy while a six-fold degeneracy was found for the neutral ⟨110⟩-oriented split interstitial.

To complement irradiation experiments, point-defect properties were deduced from measurements on quenched specimen. In the investigations of Bemski and Dias [2.406], Elstner and Kamprath [2.207], and Swanson [2.407], a defect was found which introduces a level at about $E_v + 0.4$ eV. After the paradigm change from vacancy-dominated to self-interstitial-dominated diffusion in silicon, this defect was associated by Seeger and Frank [2.399] with the self-interstitial. From the concentration of quenched defects reported by Elstner and Kamprath [2.207], it was then concluded that the neutral self-interstitial has a migration enthalpy of 1.5 eV or more, and the migration enthalpy of 0.81 eV reported by Swanson [2.407] was assigned to the positive charge state of the self-interstitial. As noted in Section 2.4.2, the defect responsible for the level at $E_v + 0.4$ eV was finally identified by Lee et al. [2.209] as interstitial iron. As also discussed in that section, it is fairly established that the equilibrium concentration of vacancies exceeds that of self-interstitials at high temperatures so that self-interstitials can hardly be expected to survive after quenching. In summary, it appears that the assignments made as well as the various conclusions based on them are questionable.

From an interpretation of internal-friction studies, Tan et al. [2.408] and Frank [2.409] suggested the neutral self-interstitial to assume a configuration in the form of a ⟨100⟩-oriented split interstitial while a ⟨110⟩-oriented split interstitial was assigned to the positive charge state. From the annealing kinetics of the observed peaks, migration enthalpies of about 1.5

and 0.85 eV were deduced for these charge states. Frank [2.409] emphasized the closeness of these values to the estimates of Seeger and Frank [2.399] from quenching experiments discussed above. Unfortunately, there are serious doubts about the identity of the associated defects which apply *vice versa* here to the assignment of friction peaks to self-interstitials. It should also be noted that $\langle 100 \rangle$ -oriented split interstitials were excluded as energetically favorable configuration by all recent theoretical investigations as discussed below.

Because of the inconclusive information from experiments, various theoretical methods were used to predict equilibrium configuration, formation and migration enthalpies, and possible diffusion paths. One class of them, usually considered the most reliable, is based on the approximate solution of the Schrödinger equation. The various approaches differ by the choice of the Hamiltonian and by the choice of the numerical technique. Besides self-consistent Hamiltonians based on the local-density approximation or the generalized-gradient approximation, various semi-empirical Hamiltonians were used. Numerical solutions were obtained by Green's-function approaches, cluster calculations, or supercell methods.

In early theoretical studies, especially the tetrahedral and hexagonal interstitial configurations were considered. Applying extended-Hückel-theory cluster calculations to self-interstitials in the diamond lattice, Watkins et al. [2.410] and Weigel et al. [2.411] suggested the $\langle 100 \rangle$ -oriented split interstitial to be the energetically most favorable configuration in the neutral, singly negative, and singly positive charge states. The investigations also indicated that the bond-centered configuration would be energetically favored for the doubly positive charge state so that an athermal diffusion via the Bourgoin-Corbett mechanism would be possible.

In contrast, based on *ab-initio* simulations using the Green's-function method, Pantelides et al. [2.412] favored again the tetrahedral position as the most likely site for a doubly positively charged self-interstitial. They also suggested migration along the low-electron-density channel connecting tetragonal and hexagonal lattice sites. Other *ab-initio* investigations confirmed the tetrahedral position as the energetically most favored site for the doubly positive charge state [2.186, 2.231–2.233, 2.238, 2.396, 2.413–2.417]. Although the tetrahedral site was sometimes also found to be energetically favorable for the neutral and the singly positive charge states of the self-interstitial [2.396], other minimum-energy configurations were reported, too. Depending on the charge state and the actual sites taken into considerations, a minimum of the formation energy was reported for the hexagonal site [2.186, 2.238, 2.413, 2.414, 2.416], the bond-centered configuration [2.231, 2.233], and a $\langle 110 \rangle$ -oriented split interstitial [2.46, 2.47, 2.167, 2.203, 2.232, 2.415, 2.417–2.421]. Especially for the neutral charge state, the $\langle 110 \rangle$ -oriented split interstitial was found in nearly all investigations to be energetically most favorable in which this configuration was included in the calculations. At this point, it has to be mentioned that the structure of the $\langle 110 \rangle$ -oriented split interstitial obtained from *ab-initio* calculations is not identical to that of the extended $\langle 110 \rangle$ -oriented split interstitial obtained by using the empirical Stillinger-Weber potential [2.422, 2.423] frequently used in molecular-dynamics studies. Later, Clark and Ackland [2.421] found a split-interstitial configuration with low symmetry which showed remarkable stability and which they named “caged” interstitial. It was found by Leung et al. [2.46] and Needs [2.47] to be instable and to relax towards the $\langle 110 \rangle$ -oriented split interstitial. This configuration was also found to be the configuration of minimum energy for the negative [2.396, 2.417] and doubly negative [2.417] charge states of the self-interstitials. In addition to the perfectly symmetric hexagonal interstitial site, Al-Mushadani and Needs [2.167] found a similar configuration in which the self-interstitial is displaced by 0.48 Å out of the hexagonal ring which was slightly more stable in the neutral charge state than the hexagonal configuration. The dependence of the minimum-energy configuration on the charge state found in nearly all studies supports the possibility of athermal migration by capture and release of

charge carriers. Similarly, several of the studies [2.186, 2.231–2.233, 2.238, 2.417] indicated that the positive charge state is only metastable so that the positive and doubly positive charge states of the self-interstitial form an Anderson “negative-U” system. In other investigations, also the neutral charge state was found to be unstable [2.417]. Finally, in the work of Needs [2.47], no localized electron states were found for hexagonal and $\langle 110 \rangle$ -oriented split interstitials.

2.5.2 Concentration in Thermal Equilibrium

Since self-interstitials were never detected directly in equilibrium situations, only indirect methods were invoked to estimate their equilibrium concentration.

After *A*-swirls were identified as self-interstitial agglomerates, Seeger et al. [2.23] estimated from their density and size a minimum self-interstitial concentration at the melting point of $\gtrapprox 10^{15} \text{ cm}^{-3}$. Including *B*-swirls in their considerations, an upper limit of 10^{17} cm^{-3} was estimated. Interpreting quenching experiments in which a high concentration of interstitial iron was found, Frank et al. [2.424] suggested that their concentration reflects the concentration of self-interstitials before the quench. This theory was rejected by Lee et al. [2.209] who found that self-interstitials generated by electron irradiation do not cause substitutional iron to move into interstitial sites. They reported also that no aluminum or carbon interstitials were observed after quenching of samples doped with these impurities. From this, they suggested an upper limit of 10^{13} cm^{-3} for the equilibrium concentration of self-interstitials at 1200 °C. This interpretation was in turn criticized by Seeger et al. [2.425] who argued in favor of the original interpretation of Frank et al.

Information about the relative equilibrium concentrations of self-interstitials and vacancies can be obtained from crystal growth and from the influence of rapid thermal annealing on the nucleation of oxygen precipitates. These experiments, as discussed already in Section 2.4.2, led to the conclusion that the equilibrium concentration of vacancies exceeds that of self-interstitials at the melting point and at temperatures from 1150 to 1280 °C.

An often used method to estimate diffusion coefficient and equilibrium concentration of self-interstitials is based on the diffusion of metals like gold, platinum, or zinc. The limitations of this method were discussed already in Section 2.3. They are even more severe here since the splitting of a self-diffusion coefficient into diffusion coefficient and equilibrium concentration requires a second-order analysis at a point where the first-order estimate of the self-diffusion coefficient is sometimes already unreliable. In addition, most researchers contented themselves with giving one parameter set without considering that similar results might be obtainable by other parameter combinations. An exception to that rule was the work of Gossman et al. [2.77]. Reinterpreting zinc-diffusion experiments of Bracht et al. [2.76], they showed that equally good fits can be obtained for a self-interstitial diffusion coefficient which was one order of magnitude smaller than that in the original work as long as the equilibrium concentration was adjusted appropriately. It has also to be noted that the parameter set of Gossmann et al. meant a self-diffusion coefficient via self-interstitials which is 50% larger than that of Bracht et al. Introducing traps for self-interstitials as discussed in Section 2.7.4, Gossmann et al. could show that an increasingly faster diffusion of self-interstitials and lower equilibrium coefficients are necessary to reproduce the experiments when the trap concentration exceeds values of about 10^{15} cm^{-3} . In contrast, based the same zinc-diffusion experiments of Bracht et al. [2.76], Chakravarthi and Dunham [2.99] concluded the uniqueness of their parameters from an error analysis. In our own investigations reinterpreting gold-diffusion experiments [2.78] and on platinum diffusion at low temperatures [2.426], no particular influence of the equilibrium concentration of self-interstitials was found as long as the diffusion coefficient was adjusted accordingly. The same reservations as about parameters from metal diffusion apply to param-

ters extracted from dopant-diffusion experiments under non-equilibrium conditions. Important points for all investigations are the influences of bulk recombination with vacancies and of reactions with impurities like carbon or with other “traps” which will be discussed in Sections 2.7.4 and 2.7.5. They can reduce the apparent diffusion coefficients of intrinsic point defects and the respective measured values were reported correctly as effective diffusion coefficients in several investigations. Unfortunately, even in most of these investigations, a characterization of the traps and their properties was beyond the experimental possibilities.

As a result of the experimental ambiguities and the different *a-priori* assumptions, the estimates listed in Table 2.13 and shown graphically in Figure 2.11 differ considerably. Since the number of sites for self-interstitials per unit volume would hardly be lower than about $5 \cdot 10^{22} \text{ cm}^{-3}$, it can be concluded that all prefactors which are significantly lower would imply rather unlikely negative entropies of formation. However, such values can often be understood to reflect the limited temperature range of the investigations.

Table 2.13: Prefactors \tilde{C} and formation enthalpies H^f reported for the equilibrium concentration of self-interstitials under intrinsic conditions.

	\tilde{C} (cm^{-3})	H^f (eV)	Temperature range ($^\circ\text{C}$)	Experimental technique	Ref.
Seeger et al.	$10^{15}\text{--}10^{17}$			Self-interstitials in swirls	[2.23]
Seeger et al.	$\tilde{C} = 4.08 \cdot 10^{23} \text{ cm}^{-3} \cdot (T/570\text{K})^{4.79}$			Tracer diffusion	[2.23]
	$H^f/\text{eV} = 2.35 + 4.13 \cdot 10^{-4} \cdot T/\text{K}$				
Frank et al.	$3.3 \cdot 10^{25}$	2.8	847–1047	Interstitial iron after quenching	[2.424]
Lee et al.	$\leq 10^{13}$		1200	Interstitial aluminum and carbon after quenching	[2.209]
Leroy	$4.76 \cdot 10^{25}$	3.02		Collection of data	[2.427]
Wada & Inoue	$1.52 \cdot 10^{18}$	0.35	850–1200	Stacking fault growth	[2.112]
Voronkov	$1.3 \cdot 10^{14}$		1412	Swirl defect formation	[2.83]
Taniguchi et al.	$2.4 \cdot 10^{19}$	0.7	1100–1200	OSF growth	[2.114]
Bronner & Plummer	$1.26 \cdot 10^{34}$	4.71	800–1000	Gettering	[2.117]
Tan & Gösele	$5 \cdot 10^{30}$	4.4	900 (-1410)	Collection of data	[2.64]
Mantovani et al.	$4.3 \cdot 10^8$ $3.5 \cdot 10^{10}$		700 850	Platinum diffusion	[2.119]
Budil et al.	$1.4 \cdot 10^{16}$		1100	OED	[2.85]
Bronner & Plummer	$5 \cdot 10^{22}$	2.36	700–800	Gold & phosphorus diffusion	[2.120]
Brabec et al.	$4.57 \cdot 10^{16}$		1100	Dopant diffusion	[2.86]
Morehead	10^{27}	3.8	700–1250	Gold & platinum diffusion	[2.121]
Griffin	$8.09 \cdot 10^{20}$	1.35	900–1100	Dopant diffusion	[2.87]
Jäger et al.	$3.08 \cdot 10^{26}$	2.52	900–1100	Phosphorus diffusion	[2.123]
Boit et al.	$3.11 \cdot 10^{19}$	1.58	800–1200	Gold diffusion	[2.126]
Budil et al.	$1.3 \cdot 10^{16}$		1100	OED	[2.220]
Okada et al.	$1.7 \cdot 10^{13}$ $3.5 \cdot 10^{14}$		750 850	Emitter-push effect	[2.428]
Rogers & Massoud	$2 \cdot 10^{15}$		1125	Oxygen-precipitation-enhanced diffusion	[2.429]

	\bar{C} (cm $^{-3}$)	H^f (eV)	Temperature range (°C)	Experimental technique	Ref.
Hu	$1.8 \cdot 10^{16}$		1200	OSF growth during oxygen precipitation	[2.430]
Bracht et al.	$7 \cdot 10^{13}$		1208	Zinc diffusion	[2.431]
Zimmermann et al.	$1.94 \cdot 10^{27}$	3.835	770–950	Platinum diffusion	[2.221]
Wijaranakula	$2.18 \cdot 10^{26}$	3.1	900–1400	Collection of data	[2.432]
Dunham	$2.3 \cdot 10^{13}$		1000	Phosphorus diffusion	[2.90]
Hu	$3 \cdot 10^{16}$		1200	Oxygen precipitation	[2.433]
Okino	$3.4 \cdot 10^{16}$		1100	OED/ORD	[2.92]
Habu et al.	$1.244 \cdot 10^{30}$	4.4		Crystal growth	[2.93]
Okino & Onishi	$3.3 \cdot 10^{16}$		1100	OED/ORD	[2.94]
Ghaderi et al.	$1.13 \cdot 10^{18}$	1.377	900–1100	Gold diffusion	[2.95]
Satoh et al.	10^{12}		1000	Depth dependence of oxygen precipitation	[2.434]
Gossmann et al.	$2.7 \cdot 10^9 - 9.6 \cdot 10^{11}$		1115	Zinc diffusion	[2.77]
Bracht et al.	$2.9 \cdot 10^{24}$	3.18	870–1208	Zinc diffusion	[2.76]
Habu & Tomiura	$1.9 \cdot 10^{28}$	4.49		Crystal growth	[2.96]
Chao et al.	$7.7 \cdot 10^{11}$		750	IED	[2.435]
Knowlton et al.	$2.4 \cdot 10^{12}$ $1.5 \cdot 10^{12}$		950	Li drift after P diffusion	[2.97]
Sinno et al.	$\bar{C} = 1.2 \cdot 10^{24} \text{ cm}^{-3}$ $\cdot \exp(3.85 \cdot 10^{-3} \cdot T / \text{K})$ $H^f / \text{eV} = 3.46 + 3.08 \cdot 10^{-4} \cdot T / \text{K}$			Computed values fitted to crystal-growth experiments	[2.98]
Okino et al.	$5 \cdot 10^{22}$	2.02		OSF growth	[2.133]
Chakravarthi & Dunham	$1.6 \cdot 10^{19}$	2	870–1208	Zinc diffusion	[2.99]
Nakamura et al.	$2.35 \cdot 10^{28}$	4.5		Crystal growth and defect formation	[2.100]
Walton et al.	$4.71 \cdot 10^9$		950	Li drift after P diffusion	[2.101]
Bharatan et al.	$5.6 \cdot 10^{12}$		685	IED and counting of self-interstitials in loops	[2.436]
	$1.0 \cdot 10^{14}$ $2.8 \cdot 10^{14}$		750 815		
Okino & Shimozaki	$5 \cdot 10^{22}$	1.44		Self-diffusion and OED	[2.228]
Falster et al.	$8.3 \cdot 10^{14}$ $8.79 \cdot 10^{28}$	4.7	1412 1150–1280	Crystal growth Vacancy profiles	[2.106]
Mori et al.	$\bar{C} = 8.01 \cdot 10^{26} \text{ cm}^{-3}$ $H^f / \text{eV} = 3.46 + 3.08 \cdot 10^{-4} \cdot T / \text{K}$			Crystal growth	[2.107]
Akatsuka et al.	$7.04 \cdot 10^{26}$	3.86	1000–1280	Effect of RTP on oxygen precipitation	[2.108]
Ngau et al.	$1.67 \cdot 10^9$		750	Transient diffusion of boron and carbon	[2.268]
Nakamura et al.	$4.96 \cdot 10^{27}$ $6.28 \cdot 10^{26}$	4.35 4.05		Formation of voids during crystal growth	[2.229]
Okui & Nishimoto	$2.52 \cdot 10^{26}$	3.71		Crystal growth	[2.110]

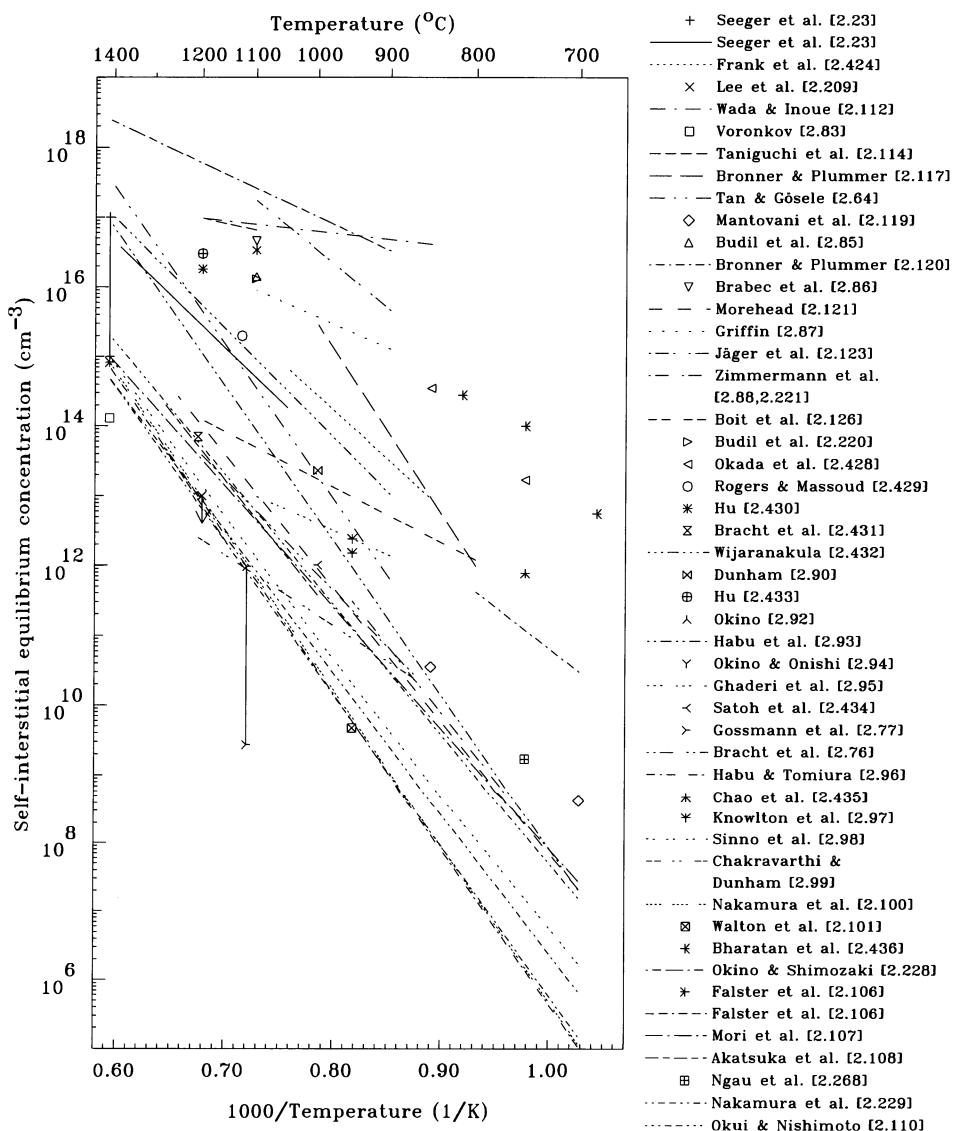


Figure 2.11: Equilibrium concentration of self-interstitials under intrinsic conditions.

After powerful theoretical methods were developed to compute properties of point defects in silicon, they were applied in several investigations to calculate the formation enthalpy of self-interstitials. The results are listed in Table 2.14. The values given therein for H_{j+e-j}^f refer to the formation of self-interstitials in charge state j and the compensating charge carriers in intrinsic silicon. When other reference points were assumed in the original publications, they were converted assuming a band gap of 1.12 eV. A comparison of different theoretical methods based on pseudopotentials by Leung et al. [2.46] indicated that the formation energies calculated using the generalized gradient approximation to the density functional theory are about 0.5 eV higher than those calculated using the local density approximation. A fixed-node diffusion quantum Monte Carlo calculation resulted in values which were even 1.5 eV higher.

Table 2.14: Formation enthalpies and entropies of self-interstitials in intrinsic silicon obtained from *ab-initio* calculations. The energetically most favorable configuration of several investigated is underlined. Abbreviations for sites: T: Tetrahedral, H: Hexagonal, B: Bond-centered, S110: ⟨110⟩-oriented split interstitial. The abbreviations LDA and GGA refer to local density approximation and generalized gradient approximation methods.

	Charge state	H_{j+e-j}^f (eV) or H_{j+e-j}^f (eV) / S_I^f/k				Ref.
		T	H	B	S110	
Car et al.	0	7.21	6.31	<u>6.11</u>		[2.231]
	+	<u>6.59</u>	6.62	<u>6.23</u>		
	++	<u>6.0</u>	7.18	6.59		
Baraff & Schlüter	++	4.7				[2.416]
Bar-Yam & Joannopoulos	0			3.6		[2.232]
	+			4.4		
	++	4.0				
Car et al.	0	6.11	5.18	<u>4.98</u>		[2.233]
	+	5.51	5.52	<u>5.12</u>		
	++	<u>4.87</u>	6.08	5.46		
Antonelli & Bernholc	0	4.31				[2.185]
Kelly & Car	++	<u>3.59</u>				[2.186]
	0	4.74	<u>4.41</u>			
	+	<u>4.51</u>	4.97			
Blöchl et al.	++	<u>4.3</u>	5.53			[2.43]
Zhu et al.	0			3.3/6.0		
Van de Walle & Neugebauer	0			3.25		
Zhu et al.	0			3.33		[2.188]
Clark & Ackland	0		2.45	<u>2.16</u>		
0	4.6					
Lee et al.	=	5.28	5.09	<u>4.78</u>		[2.420]
	-	4.68	4.5	<u>4.3</u>		
	0	4.32	4.28	<u>4.15</u>		
	+	<u>4.04</u>	4.5	4.63		
	++	<u>3.72</u>	4.87	5.04		
Leung et al. (LDA)	0	3.43	<u>3.31</u>	<u>3.31</u>		[2.46, 2.47]
Leung et al. (GGA)	0	4.07	<u>3.8</u>	3.84		[2.46, 2.47]
Hakala et al.	0			3.3		[2.437]
	++	3.18				
Eberlein et al.	0	<u>3.36</u>	3.52	3.41		[2.396]
Al-Mushadani & Needs	0		3.42/5.4	<u>3.40/5.4</u>		[2.167]

2.5.3 Diffusion

Self-interstitials are thought to stand behind many diffusion phenomena in silicon. On the other hand, direct information about their properties is largely missing. Much of our experimental knowledge about diffusion properties of the self-interstitial comes from investigations in which they were generated by irradiation of silicon with electrons, protons, or alpha particles. The indirect evidence obtained this way has been discussed largely already in Section 2.5.1 and will only be outlined shortly here.

From electron-irradiation studies of *p*-type silicon Watkins [2.135] concluded self-interstitials to be able to perform long-range migration already at a temperature as low as 4.2 K. Although the mechanism was not clarified experimentally, it was soon speculated to be athermal [2.410, 2.438, 2.439]. Athermal diffusion via the Bourgoin-Corbett mechanism was supported as possibility by basically all the theoretical investigations summarized above. After electron irradiation was complemented by irradiation with protons and alpha particles, impurity interstitials needed thermal anneals around room temperature to appear. Similarly, in high-resistivity silicon, interstitial migration was observed to start at 190 K, and impurity interstitials were found to form in *n*-type silicon only after thermal annealings at 150 K and above. These temperatures are considerably higher than the annealing temperatures of vacancies. Investigations of the annealing kinetics of the EPR Si-G25 center associated by Harris and Watkins [2.387] with a self-interstitial-related complex if not a self-interstitial indicated an activation energy of 0.57 eV. However, their analysis of the frequency factor indicated also that the activation energy would be characteristic for the break-up of a defect rather than for long-range diffusion. As a consequence, the activation enthalpy for the diffusion of self-interstitials might be significantly smaller. On the same basis it can be speculated that the appearance of carbon interstitials at 77 K observed by Kimerling et al. [2.142] upon electron-injection is not necessarily evidence for athermal diffusion of silicon self-interstitials but probably for an athermal break-up of the defects to which the self-interstitials are bound. The same considerations apply to irradiation of *p*-type silicon with protons or alpha-particles where it is not sure whether the appearance of interstitial impurities is indicative of the slow migration of self-interstitials or of the break-up of a complex by which the self-interstitials are finally released.

Diffusion of self-interstitials at room temperature and above was deduced indirectly from various experiments in which a large number of point defects was generated usually by ion implantation or irradiation. In the investigation of Panteleev et al. [2.251], point defects were generated by ion implantation at one side of the samples while their arrival at the other side was detected by photostimulated electron emission. Two types of point defects were found to arrive. Their diffusion coefficients were estimated to be characterized by a prefactor of $2.2 \cdot 10^{-4} \text{ cm}^2/\text{s}$ and an activation energy of $0.3 \pm 0.04 \text{ eV}$ for the one defect, and by a prefactor of $1.1 \cdot 10^{-6} \text{ cm}^2/\text{s}$ and an activation energy of $0.12 \pm 0.04 \text{ eV}$ for the other. Based on the similarities of the values with the EPR experiments of Watkins, the former was tentatively associated with vacancies while the latter was associated with self-interstitials. Annihilation of vacancy defects by self-interstitials from contiguous collision cascades was suggested by Hallén et al. [2.440], Svensson et al. [2.305], and Lévéque et al. [2.441] to explain dose-rate effects on the generation of defects during proton irradiation and implantation with heavy ions. To investigate the diffusion of self-interstitials at room temperature quantitatively, two experimental methods were introduced by Privitera and his coworkers. In the work started by Kyllesbech Larsen et al. [2.258], shallow implants with silicon or heavier ions were shown to cause dopant deactivation in depths significantly deeper than the penetration depth of the implanted ions. This deactivation was finally ascribed to the formation of dopant-self-interstitial complexes which allowed to estimate lower limits for the diffusivity of self-interstitials ranging from $3 \cdot 10^{-11}$ to

10^{-10} cm²/s [2.258, 2.442]. Dopant deactivation was also investigated by Privitera et al. [2.442] in a two-dimensional set-up. In these experiments it was found that the extent of the region of deactivated dopants spreads much farther in samples with an epi-layer than in FZ wafers. This effect was suggested to reflect the higher purity of the epi material and was taken as an evidence for trap-limited diffusion of self-interstitials. It has to be mentioned, however, that Nylandsted Larsen et al. [2.257] found in similar experiments by DLTS that the dopant deactivation was caused by the formation of phosphorus-vacancy pairs. In a second procedure reported first by Privitera et al. [2.443], low-dose MeV helium implants were used to generate divacancies in depths of several microns from the surface. These divacancies were used in a subsequent step to monitor the appearance of self-interstitials generated by a shallow silicon implant. The method led to very similar lower bounds for the self-interstitial diffusivity ranging from $2 \cdot 10^{-11}$ to 10^{-10} cm²/s [2.253, 2.443]. In the experiments of Buzynin et al. [2.444], the deactivation of boron atoms and the associated formation of a p-n junction was observed as the result of a low-energy argon implant. Assuming that the deactivation is associated with the diffusion of self-interstitials generated by the argon implant, they deduced a lower limit of 10^{-7} cm²/s for the diffusion coefficient of self-interstitials at the irradiation temperature (< 100 °C). From the largely linear variation of the depth of the p-n junction with the irradiation time it can be concluded that the handling times after irradiation had most likely a negligible influence on the result. The dopant-deactivation procedure was improved considerably by Cowern et al. [2.445] who measured the deactivation of a buried boron layer *in situ* and deduced a lower limit of 10^{-7} cm²/s for the diffusion coefficient of self-interstitials. After room-temperature ion implantation with MeV energies, Hallén et al. [2.254] observed that the concentration of VO and V₂ complexes decreased with the dose rate. The effects could be reproduced quantitatively assuming a self-interstitial diffusion coefficient of $3.2 \cdot 10^{-4}$ cm²/s. To definitely exclude athermal diffusion effects, Coffa and Libertino [2.255] monitored *in situ* the leakage current of a diode during and after MeV helium implantation. Defect identification was performed *ex situ* by DLTS and the leakage current was suggested to be caused by divacancies and vacancy-phosphorus complexes. For the self-interstitial diffusivity, a value of $1.5 \cdot 10^{-15}$ cm²/s was obtained from numerical simulations of the measurements. In their subsequent work, Libertino and Coffa [2.256] reported a value of $2 \cdot 10^{-15}$ cm²/s. Remarkably, these values are about two orders of magnitude smaller than the diffusion coefficient of vacancies obtained also from the simulations.

In the regime of elevated temperatures, diffusion coefficients of self-interstitials were extracted largely from the diffusion of metals like gold, platinum, or zinc, or from the diffusion of dopants under non-equilibrium conditions. These methods were already commented in Section 2.5.2 and resulted, as above, in values which differ by orders of magnitude for a certain temperature. The values reported are summarized in Table 2.15 and shown graphically in Figure 2.12. The high-temperature data is depicted in more detail in Figure 2.13.

Table 2.15: Prefactors D_0 and enthalpies of migration H^m reported for the diffusion coefficient of self-interstitials under intrinsic conditions.

	D_0 (cm ² /s)	H^m (eV)	Temperature range (°C)	Experimental technique	Ref.
Panteleev et al.	$1.1 \cdot 10^{-6}$	0.12	100–350	Detection at wafer back-side after ion implantation	[2.251]
Seeger et al.	$D_0 = \sqrt{17.1 + 6.68 \cdot 10^{-3} \cdot T/K} \cdot 10^{-3} \cdot (T/570\text{K})^{5.57}$ cm ² /s			Tracer diffusion	[2.23]
Leroy	2.13	2		Collection of data	[2.427]

	D_0 (cm ² /s)	H^m (eV)	Temperature range (°C)	Experimental technique	Ref.
Wada & Inoue	$4.57 \cdot 10^7$	4.66	850–1200	Stacking fault growth	[2.112]
Hill et al.	$\geq 3 \cdot 10^{-7}$		845	Gold diffusion	[2.446]
Voronkov	$5 \cdot 10^{-4}$		1412	Swirl defect formation	[2.83]
Taniguchi et al.	$8.6 \cdot 10^5$	4	1100–1200	OSF growth	[2.114]
Bronner & Plummer	$3.75 \cdot 10^{-9}$	0.13	800–1000	Gettering	[2.117]
Griffin et al.	$> 9 \cdot 10^{-9}$		950	OED	[2.447]
	$> 3 \cdot 10^{-8}$		1100		
	$> 3 \cdot 10^{-7}$		1200		
Tan & Gösele	10^{-5}	0.4	900 (-1400)	Collection of data	[2.64]
Scheid & Chenevier	$2 \cdot 10^{-9}$		1100	OED	[2.448]
Abe et al.	$6 \cdot 10^{-8}$		900	Defect annihilation	[2.449]
	$2 \cdot 10^{-6}$		1000		
Griffin & Plummer	$3.5 \cdot 10^4$	3.5	1000–1100	OED	[2.450]
Budil et al.	$1.1 \cdot 10^{-7}$		1100	OED	[2.85]
Griffin & Plummer	$5 \cdot 10^{-9}$		1100	OED	[2.451]
Griffin & Plummer	$4.89 \cdot 10^{-11}$		900	OED	[2.452]
	$1.05 \cdot 10^{-10}$		1000		
	$5.13 \cdot 10^{-10}$		1100		
Rogers et al.	10^{-9}		1125	Back-side oxidation	[2.453]
Bronner & Plummer	600	2.44	700–800	Gold & phosphorus diffusion	[2.120]
Ahn et al.	$9 \cdot 10^{-10}$		1100	Dopant diffusion	[2.454]
Brabec et al.	$2.62 \cdot 10^{-9}$		1100	Dopant diffusion	[2.86]
Kump & Dutton	$3.65 \cdot 10^{-4}$	1.58	900–1100	Dopant diffusion	[2.455]
Morehead	0.2	1.2	700–1250	Gold & platinum diffusion	[2.121]
Griffin	$4.33 \cdot 10^4$	3.66	900–1100	Dopant diffusion	[2.87]
Ahn et al.	$9 \cdot 10^{-10}$		1100	Back-side oxidation	[2.456]
Jäger et al.	$2.04 \cdot 10^{-4}$	1.72	900–1100	Phosphorus diffusion	[2.123]
Zimmermann et al.	$2.58 \cdot 10^{-2}$	0.965	770–950	Platinum diffusion	[2.221]
Kawakami et al.	10^{-6}		1100	Stacking-fault growth	[2.457]
Boit et al.	$1.03 \cdot 10^6$	3.22	800–1200	Gold diffusion	[2.126]
Wijaranakula	0.335	1.86	460–1200	Collection of data	[2.458]
Yamanaka et al.	$> 5 \cdot 10^{-7}$		1000	Oxygen precipitation	[2.459]
Dunham et al.	$\approx 10^{-9}$		1100	Lateral dopant diffusion	[2.460]
Budil et al.	$6 \cdot 10^{-9}$		1100	OED	[2.220]
Griffin et al.	10^{-11}		900	Lateral dopant diffusion	[2.261]
	10^{-10}		1000		
	$2 \cdot 10^{-9}$		1100		
Okada et al.	$3.3 \cdot 10^{-11}$		750	Emitter-push effect	[2.428]
	$2.7 \cdot 10^{-10}$		850		
Dunham et al.	$\sim 10^{-9}$		1100	OED	[2.461]
Rogers & Massoud	$4 \cdot 10^{-9}$		1125	Back-side oxidation	[2.462]
Rogers & Massoud	$3 \cdot 10^{-7}$		1125	Oxygen precipitation	[2.429]
Bracht et al.	$8 \cdot 10^{-5}$		1208	Zinc diffusion	[2.431]
Dunham	$1.3 \cdot 10^{-7}$		1000	Phosphorus diffusion	[2.90]
Gossmann et al.	100	3.1	750–900	Boron OED	[2.463]
Okino	$2.3 \cdot 10^{-9}$		1100	OED/ORD	[2.92]

	D_0 (cm ² /s)	H^m (eV)	Temperature range (°C)	Experimental technique	Ref.
Agarwal & Dunham	$4.1 \cdot 10^{-8}$		1100	OED	[2.464]
Okino	$4.2 \cdot 10^{-10}$		1100	OED/ORD	[2.262]
Habu et al.	$4.84 \cdot 10^5$	2.8		Crystal growth	[2.93]
Yamanaka & Aoki	$5.9 \cdot 10^{-6}$		1000	Growth of bulk-micro-defects	[2.465]
Okino & Onishi	$2.4 \cdot 10^{-9}$		1100	OED/ORD	[2.94]
Stolk et al.	$6.4 \cdot 10^{-15}$		570	IED of boron marker layers	[2.466]
	$1.1 \cdot 10^{-13}$		730		
	$1.3 \cdot 10^{-12}$		790		
Ghaderi et al.	$2.63 \cdot 10^{11}$	4.436	900–1100	Gold diffusion	[2.95]
Bracht et al.	51	1.77	870–1208	Zinc diffusion	[2.76]
Habu & Tomiura	0.204	0.87		Crystal growth	[2.96]
Gossmann et al.	$1.43 \cdot 10^{-12}$		810	OED	[2.467]
Satoh et al.	$7.34 \cdot 10^{-7}$		850	Depth dependence	[2.434]
	$1.97 \cdot 10^{-6}$		900	of oxygen precipitation	
	$4.52 \cdot 10^{-6}$		950		
Stolk et al.	$1.3 \cdot 10^{-12}$		790	IED	[2.468]
Gossmann et al.	$2.9 \cdot 10^{-4}$ – $6.7 \cdot 10^{-2}$		1115	Zinc diffusion	[2.77]
Kyllesbech Larsen et al.	$\geq 3 \cdot 10^{-11}$		RT	Dopant deactivation	[2.258]
Chao et al.	$1.4 \cdot 10^{-10}$		750	IED	[2.435]
Privitera et al.	$\geq 2 \cdot 10^{-11}$		RT	Annihilation of divacancies	[2.443]
Huizing et al.	$\geq 2 \cdot 10^{-10}$		700	IED caused by Si implantation	[2.469]
Priolo et al.	$\geq 6 \cdot 10^{-11}$		RT	Annihilation of divacancies	[2.253]
Knowlton et al.	$4.6 \cdot 10^{-8}$ $7.9 \cdot 10^{-8}$		950	Li drift after P diffusion	[2.97]
Sinno et al.	0.242	0.937		Computed values fitted to crystal-growth experiments	[2.98]
Puzanov et al.		1.3		Crystal-growth simulations	[2.266]
Okino et al.	914	2.82		OSF growth	[2.133]
Chakravarthi & Dunham	$3.19 \cdot 10^7$	3.1	870–1208	Zinc diffusion	[2.99]
Nakamura et al.	$6.63 \cdot 10^{-3}$	0.55		Crystal growth and defect formation	[2.100]
Walton et al.	$8.81 \cdot 10^{-8}$		950	Li drift after P diffusion	[2.101]
Knowlton et al.	$\geq 3.5 \cdot 10^{-6}$		950	D-defect annihilation by self-interstitial injection	[2.470]
Privitera et al.	$\geq 10^{-10}$		RT	Dopant deactivation	[2.442]
Cowern et al.	$\geq 10^{-7}$		RT	Dopant deactivation	[2.445]
Hallén et al.	$3.2 \cdot 10^{-4}$		RT	Defect production by MeV ion implantation	[2.254]

	D_0 (cm ² /s)	H^m (eV)	Temperature range (°C)	Experimental technique	Ref.
Coffa & Libertino	$1.5 \cdot 10^{-15}$		RT	MeV-He-implantation-induced diode leakage current	[2.255]
Okino & Shimozaki	914	3.4		Self-diffusion and OED	[2.228]
Falster et al.	$3.6 \cdot 10^{-4}$		1412	Crystal growth	[2.106]
	$1.68 \cdot 10^{-3}$	0.25	1150–1280	Vacancy profiles	
Mori et al.	0.26	0.937		Crystal growth	[2.107]
Akatsuka et al.	$1.17 \cdot 10^3$	2.0	1000–1280	Effect of RTP on oxygen precipitation	[2.108]
Ngau et al.	$3.81 \cdot 10^{-8}$		750	Transient diffusion of boron and carbon	[2.268]
Shauly et al.	$1.06 \cdot 10^{-4}$	1.32	850–950	OED	[2.471]
Partyka et al.		0.3	150	X-ray measurements after irradiation with He and Ar	[2.250]
Nakamura et al.	$3.12 \cdot 10^{-2}$	0.6		Formation of voids during crystal growth	[2.229]
	0.246	0.9			
Libertino & Coffa	$2 \cdot 10^{-15}$		RT	Implantation-induced diode leakage current	[2.256]
Buzynin et al.	$\geq 10^{-7}$		≈ 100	Deactivation of boron	[2.444]
Okui & Nishimoto	777	2.0		Crystal growth	[2.110]

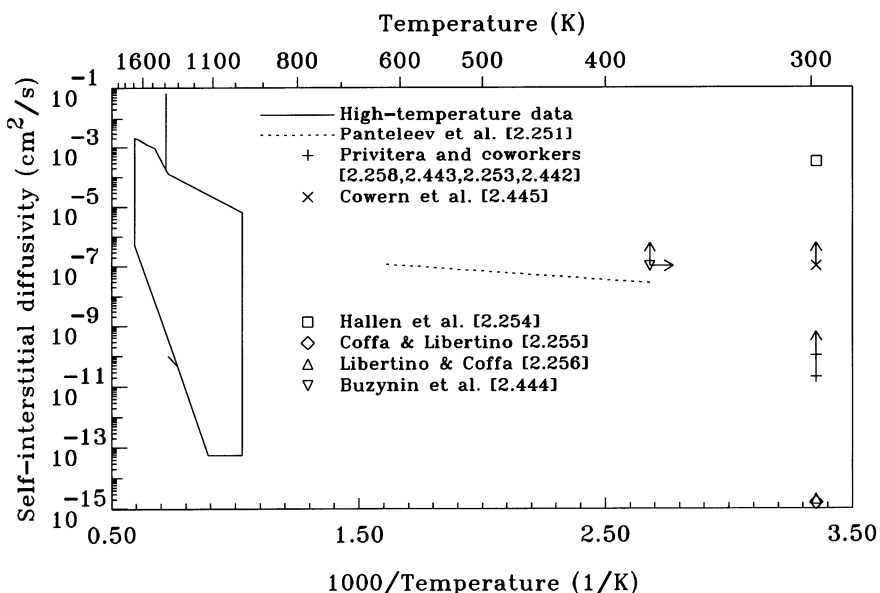


Figure 2.12: Intrinsic diffusion coefficient of self-interstitials.

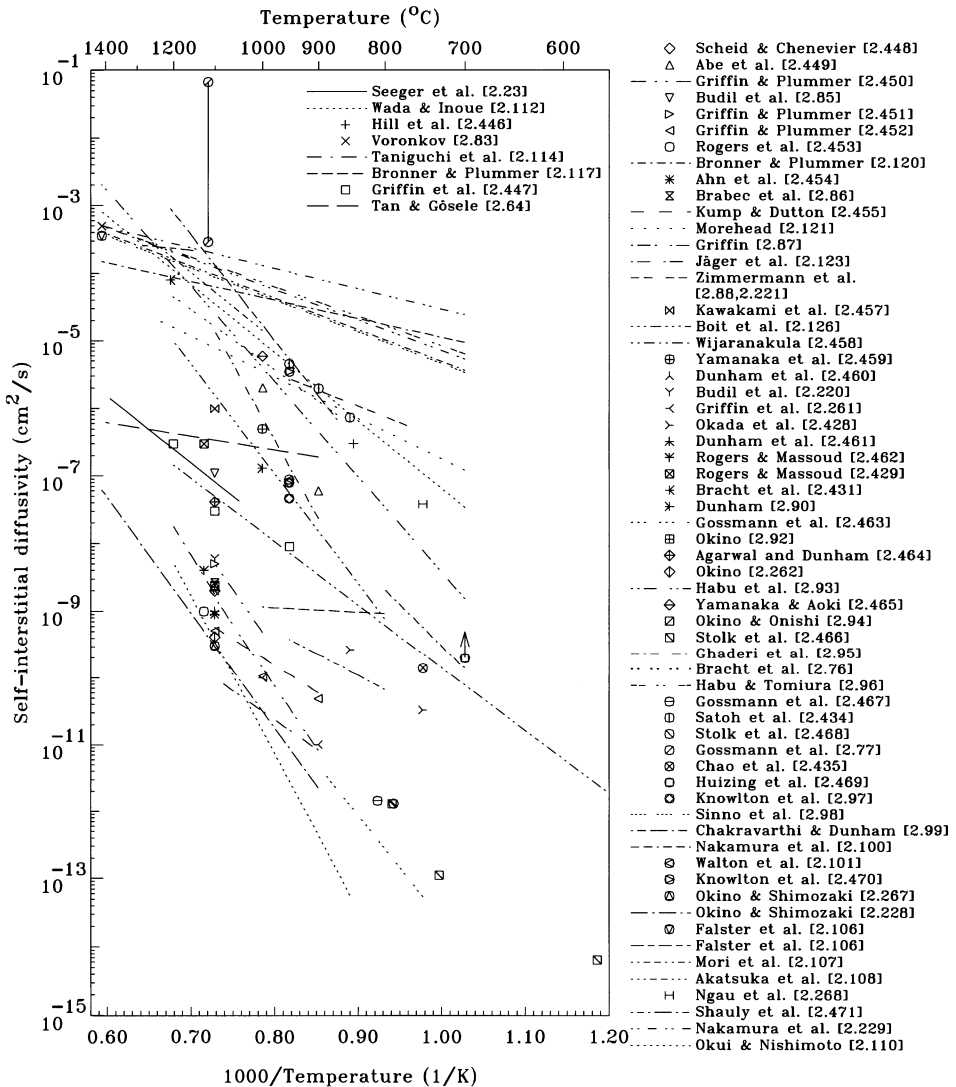


Figure 2.13: Intrinsic diffusion coefficient of self-interstitials at elevated temperatures.

After powerful theoretical methods were developed to compute properties of point defects in silicon, they were applied to the migration of self-interstitials. The results are listed in Table 2.16. The differences between the various investigations reflect the development of more adequate pseudopotentials and the usage of larger ensembles to account for lattice relaxations. Various investigations also indicated that the migration enthalpy can be lowered by the capture and release of charge carriers on the way from one stable configuration to the next one. Remarkable are also the results of the *ab-initio* molecular-dynamics simulation of Clark and Ackland [2.421]. They suggested that self-interstitials do not necessarily perform random walks. Instead, they were found to perform series of moves between long periods of immobility.

Table 2.16: Migration enthalpies of self-interstitials in intrinsic silicon obtained from *ab-initio* calculations. Abbreviations for the path: T: Tetrahedral, H: Hexagonal, B: Bond-centered, S100: $\langle 100 \rangle$ -oriented split interstitial, S110: $\langle 110 \rangle$ -oriented split interstitial.

	Charge state	Path	H^m (eV)	Ref.
Bar-Yam & Joannopoulos	0	H-T-H	1.0 ± 0.3	[2.413]
	++	T-H-T	1.4 ± 0.2	
Bar-Yam & Joannopoulos	0	H-T-H	1.2 ± 0.3	[2.414]
	++	T-H-T	1.2 ± 0.2	
Bar-Yam & Jannopoulos	0	S110-H-S110	0.4 ± 0.4	[2.415]
		S110-T-S110	1.7 ± 0.4	
		B-T-B	1.3 ± 0.4	
		H-T-H	1.3 ± 0.4	
	++	T-H-T	1.1 ± 0.3	
		T-S100-T	1.9 ± 0.4	
		T-B-T	0.8 ± 0.4	
		T-S110-T	1.1 ± 0.3	
	0	H-T-H	1.6 ± 0.5	[2.416]
Baraff & Schlüter	++	T-H-T	0.4 ± 0.5	
	0	H-T-H	0.327	[2.186]
Kelly and Car	+	T-H-T	0.463	
	++	T-H-T	0.122	
	0	S110-H-S110	0.3	[2.232]
Bar-Yam & Joannopoulos	+	S110-H-S110	0.2	
		S110-B-S110	0.1	
	++	T-H-T	1.1	
		T-B-T	0.8	
		T-S110-T	1.1	
	0	S110-T-S110	1.4	[2.238]
Zhu	0	S100-T ⁺ -S110	0.9	
	0	S110-T-S110	0.18	[2.417]
Lee et al.		S110-H-S110	0.15	
	+	T-H-T	0.47	
		T-S110-T	0.59	
	++	T-H-T	1.15	
		T-S110-T	1.32	
	0	S110-H-S100	0.15	[2.46, 2.47]
Leung et al. (LDA)		H-H	0.03	
	0	H-S110-H	0.2	[2.46, 2.47]
Leung et al. (GGA)		H-H	0.18	
	0	T-H-T	< 0.2	[2.396]
Eberlein et al.	++	T-H-T	1.00	

2.5.4 Di-Interstitials

Compared with the divacancy, very few is known about its counterpart, the di-interstitial. Basically all the experimental evidence comes from some EPR measurements which were interpreted in favor of di-interstitials. Based on similarities to their annealing kinetics, electronic levels were suggested. Complementary evidence came from theoretical work which showed di-interstitial to be highly mobile species.

In silicon irradiated at room temperature, Lee et al. [2.351] found an EPR spectrum which they labelled Si-A5 and which was found to anneal out at 150 °C. A detailed investigation showed that it is axially symmetric along the $\langle 100 \rangle$ direction and arises from two dipoles separated by about 9 Å. The atomic configuration suggested tentatively consists of two aligned $\langle 100 \rangle$ -oriented split interstitials at fifth-nearest lattice sites.

An alternative configuration for an I₂ complex was proposed by Lee et al. [2.472]. Their study of the Si-P6 EPR spectrum (originally reported by Jung and Newell [2.354] who labelled it IX center) showed a very unusual symmetry. The configuration of the defect suggested to explain the data is shown in Figure 2.14 a). In its low-temperature configuration, the defect has C₂ symmetry which is lifted to D₂ at higher temperatures due to motional averaging. The recovery kinetics after stress alignment was found to be activated with a barrier of 0.6 ± 0.2 eV. Si-P6 was found by Lee et al. [2.351] to anneal around 150 °C, similar to Si-A5. After a reexamination of his data, Lee [2.473] claimed D_{2d} symmetry instead of D₂ for the motionally averaged state, withdrew the original interpretation, and suggested the atomic configuration shown in Figure 2.14 b). The two silicon interstitials are in a (001) plane and their connection line is only 17° off from the [100] direction. The defect has C₂ symmetry which was suggested to be lifted to D_{2d} due to motional averaging at room temperature.

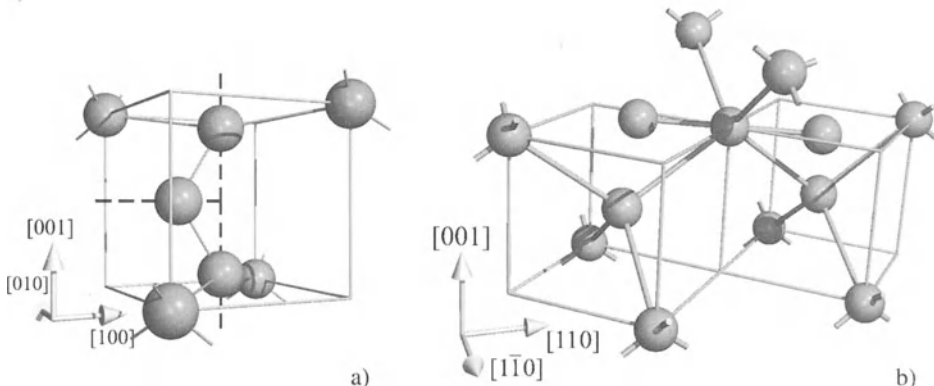


Figure 2.14: Schematic atomic configurations of di-interstitials derived from the Si-P6 EPR center. a) Configuration suggested by Lee et al. [2.472]; b) Configuration suggested by Lee [2.473].

A third EPR spectrum associated with a di-interstitial was originally reported as Si-B3 by Daly [2.474]. It was found to form in neutron-irradiated samples by annealing around 170 °C when Si-A5 and Si-P6 anneal out. In the subsequently analysis by Brower [2.475], the defect was found to have a D_{2d} symmetry which does not arise from motional averaging, and to be centered either around a lattice site or a tetrahedral interstitial site. It was suggested tentatively to arise from a $\langle 100 \rangle$ -oriented pair of silicon atoms at a tetragonal interstitial site. A $\langle 100 \rangle$ -oriented self-interstitial configuration around a lattice site would also explain the symmetry but was rejected because self-interstitials are assumed to be mobile already at much lower tem-

peratures. Finally, a third possibility would be a configuration similar to that in Figure 2.14 a) with the three silicon atoms in the cell in line and the middle silicon atom at a substitutional site. At temperatures above about 400 °C, the defect was found to undergo thermally activated atomic reorientations with an activation energy around 2.3 eV. Isochronal annealing experiments showed that the defect is stable up to about 500 °C. An alternative identification was suggested by Coomer et al. [2.476]. They found from *ab-initio* simulations of its properties that the I₄ cluster discussed later in Section 2.5.5 is a better-suited candidate for the Si-*B3* EPR center than a di-interstitial. This identification was supported by the subsequent EPR investigation of Pierreux and Stesmans [2.477]. Comparing the properties of the EPR Si-*B3* center to an EPR center labelled Si-*NL51* which they found in hydrogen-implanted silicon, Stallinga et al. [2.478] indicated that Si-*NL51* might arise from the neutral charge state of the same defect giving rise to Si-*B3* in its positive charge state.

For the sake of completeness, it has to be noted that there is a further EPR signal which is sometimes classed as belonging to the di-interstitials [2.479]. It was reported originally by Murakami et al. [2.480] without giving it a label. In succession of their nomenclature, it entered the literature as Si-*O2* [2.285]. It was described as an interstitial-related center with ⟨100⟩ symmetry which was introduced in phosphorus-implanted samples after annealing at 300 °C and annealed out between 450 and 600 °C.

Some indications about possible levels of di-interstitials came from comparisons of the respective annealing kinetics to EPR data. Based on a correlation to the Si-*P6* spectrum, Meese et al. [2.317] suggested tentatively that the defect responsible should give rise to a level at $E_v + 0.39$ eV which they found in neutron-transmutation-doped silicon. This interpretation has been adopted by Maekawa et al. [2.481] who also observed a level at $E_v + 0.4$ eV in neutron-transmutation-doped samples. However, some reservations seem appropriate since the level was reported to be stable up to 560 °C. Including also the annealing characteristics of Si-*P6* in his considerations, Lefèvre [2.482] associated tentatively two levels at $E_c - 0.07$ eV and $E_c - 0.49$ eV, found in wafers with grown-in A-swirls, with di-interstitials. In samples implanted with carbon, Mukashev et al. [2.483] noted that a level at $E_v + 0.29$ eV shows similar kinetics of introduction and annealing as the Si-*B3* EPR line. In this work, the level at $E_v + 0.4$ eV was also found to anneal out when the level at $E_v + 0.29$ eV is introduced. However, it was tentatively associated with an interstitial-carbon-related defect.

Important complementary information about di-interstitials came from theoretical investigations. Using molecular-dynamics calculations based on the Stillinger-Weber potential, Gilmer et al. [2.374] estimated a binding energy of 1.6 eV for neutral self-interstitials in an I₂ complex. The same technique was used by Rasband et al. [2.484] who found a configuration energetically most favorable in which three atoms in an equilateral triangle in a {111} plane share a lattice site. It is shown in Figure 2.15 a). Other structures, one with the triangle in a {110} plane and a Z-shaped di-interstitial in the ⟨110⟩ chain were slightly higher in their formation energy. The structure shown in Figure 2.15 a) was confirmed by the *ab-initio* calculations of Kim et al. [2.487]. They computed a binding energy of 1.36 eV within the generalized gradient approximation, and a barrier of 0.5 eV against reorientation. The symmetry of the defect in its low-symmetry state was found to be C_{1h}. This would be compatible to the Si-*P6* EPR center which was predicted from the EPR measurements to arise from a defect with monoclinic (C_{1h} or C₂) symmetry [2.472]. At its saddle point, being most likely close to the configuration with the triangle in the {110} plane in the work of Rasband et al. [2.484], the defect has C_{2v} symmetry which could account for the high-temperature data reported for Si-*P6*. The configuration was reproduced by the tight-binding molecular-dynamics simulations of Colombo [2.485] and Hane et al. [2.488], and the *ab-initio* calculations of Chichkine and De Souza [2.489]. The binding

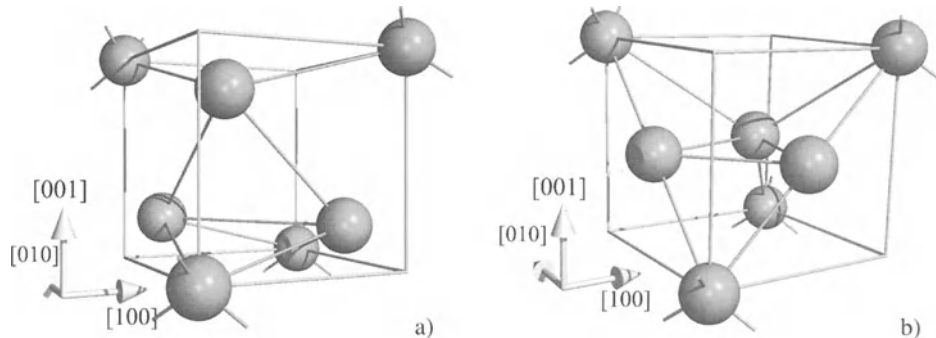


Figure 2.15: Schematic atomic configurations of di-interstitials predicted from theoretical investigations. a) Configuration suggested by Rasband et al. [2.484]; b) Configuration suggested by Colombo [2.485] and Coomer [2.486].

energies reported were 1.41, 2.2, and 1.68 eV, respectively. Hane et al. [2.488] computed also the barrier against reorientation and found it to be 0.96 eV. An alternative di-interstitial configuration, shown in Figure 2.15 b), was found by Colombo [2.485] and Coomer [2.486]. The atoms of the di-interstitial form again a triangle around a substitutional site. But here, the silicon atoms are arranged in a $\{100\}$ plane. Finally, from a comparison of the stress tensor calculated and measured for the motionally averaged configuration, Eberlein et al. [2.396] concluded that the Si-P6 EPR center does not arise from I_2 . As an alternative, Jones et al. suggested that it is associated with a larger defect with a structure close to that of I_4 . Finally, it has to be mentioned that the studies of Richie et al. [2.490] revealed two additional structures which were found to be about 0.4 eV higher in energy than the structure in Figure 2.15 a). In the one, two silicon dimers form a C_{1h} -symmetric chair-like structure in the $[110]$ plane, the other is a likewise C_{1h} -symmetric structure, similar to that in Figure 2.15 a) but with one atom strongly displaced from a lattice site along the $\langle 111 \rangle$ direction.

With respect to the electronic structure, Kim et al. [2.487] suggested from their *ab-initio* simulations that the C_{1h} -symmetric di-interstitial has a donor level at $E_v + 0.1$ eV and an acceptor level at $E_v + 0.6$ eV. For the motionally averaged state, both states were found around $E_v + 0.4$ eV. In the work of Eberlein et al. [2.396], a donor level of the low-symmetric configuration was calculated to be at $E_v + 0.3$ eV.

An important result of several theoretical investigations is that di-interstitials are highly mobile. This is of particular importance for all processes like post-implantation anneals in which a large supersaturation of self-interstitials is present. In the work of Gilmer et al. [2.374], the diffusion of di-interstitials was investigated by molecular-dynamics simulations based on the Stillinger-Weber potential. The regression line for the diffusion coefficient shown is characterized by a prefactor of $6.8 \cdot 10^{-5}$ cm²/s and an activation energy of 0.18 eV. A significantly larger value of 0.7 ± 0.1 eV was reported for the activation energy by Kim et al. [2.487] from their tight-binding molecular-dynamics study. By similar simulations, Hane et al. [2.488] found that di-interstitials have to surmount an energy of 0.96 eV to come into a state in which they may move with a barrier of less than 0.1 eV. Molecular-dynamics simulations of the diffusion process in the temperature range from 1200 to 1400 °C led to effective diffusion coefficients which can be described by a prefactor of 0.38 cm²/s and an activation energy of 1.52 eV. Hane et al. also suggested that the recombination of di-interstitials at the surface is able to account for different surface-recombination constants to model transient-enhanced diffusion during post-implantation treatments and oxidation enhanced diffusion. A high mobility of I_2 was mentioned

by Estreicher et al. [2.491], too, but no details of the kinetics were reported. The *ab-initio* calculations of Eberlein et al. [2.396] indicated a migration barrier of about 0.5 eV for I₂. A similar value of 0.52 eV was obtained by Richie et al. [2.492] from tight-binding molecular-dynamics simulations.

Independent experimental evidence for mobile di-interstitials is rather scarce. They were included in the kinetic Monte-Carlo simulations of Martin-Bragado et al. [2.493]. While the migration enthalpy was assumed to be 1.0 eV, it was found that the results are sensitive to the binding energy of I₂. For the latter, a value of 1.8 eV was obtained which is in good agreement with the results from theoretical work.

2.5.5 Small Clusters of Self-Interstitials

Information about small self-interstitial clusters is scarce and contradictory. Nevertheless, they are important defects which determine the supersaturation of self-interstitials, e.g. during the initial phase of post-implantation annealing. Except for some old work on photoluminescence lines, nearly all experimental and theoretical contributions discussed in this section were published within the last four years. This demonstrates the continual interest but it means also that part of the information presented will be antiquated soon.

Tri-Interstitials

One of the first structural suggestions of a tri-interstitial in silicon was given by Colombo [2.485]. In the form shown in Figure 2.16 a) it contains four silicon atoms in the form of a tetrahedral cage arranged T_d-symmetrically around an empty lattice site. It was confirmed by the tight-binding molecular-dynamics simulations of Richie et al. [2.492] as the energetically most stable structure of an I₃ cluster. An alternative structure was suggested by Coomer et al. [2.486] and is shown in Figure 2.16 b). It is C_{3v}-symmetric and all atoms are four-fold coordinated which is generally understood as an indication of high stability. Their *ab-initio* calculations also indicated a donor level close to the valence-band edge ($\approx E_v + 0.1$ eV). The stability of this structure was confirmed by the tight-binding molecular-dynamics simulations of Gharaibeh et al. [2.494]. But these authors also found an other C_{3v}-symmetric structure, shown in Figure 2.16 c), to be competitive if not energetically more favorable. This structure is similar to the tetrahedral cage suggested already by Colombo [2.485], but twisted by 60° around the [111] direction and shifted towards the bond-centered site. *Ab-initio* calculations performed thereafter by Estreicher et al. [2.491] indicated that it is 1.7 eV lower in energy than the structure suggested by Coomer et al. Similarly, Chichkine and De Souza [2.489] found by *ab-initio* calculations that the structure suggested by Coomer et al. is 1.5 eV higher in energy while the other two configurations are, with a binding energy of 1.24 eV per self-interstitial, energetically about equally favorable. The *ab-initio* simulations of Lopez and Fiorentini [2.495] confirmed that the structure of Coomer et al. has an 1.4 eV higher formation energy than the structure of Colombo et al. An energetically even more stable configuration (by 0.21 eV) was reported by Richie et al. [2.490]. It has an extended nature with C₂ symmetry involving six additional atoms which are significantly displaced from their lattice positions. All atoms were found to be four-fold coordinated with bond lengths which are within 5% of that of crystalline silicon. In addition, a C₃-symmetric configuration with a complex geometry was found to be similar in energy as the structure in Figure 2.16 a).

From their *ab-initio* simulations, Coomer et al. [2.486] suggested that the calculated properties of their I₃ model shown in Figure 2.16 b) agree well with those of the I₁/W photoluminescence line discussed in more detail below. This suggestion was supported by Giri et al. [2.348].

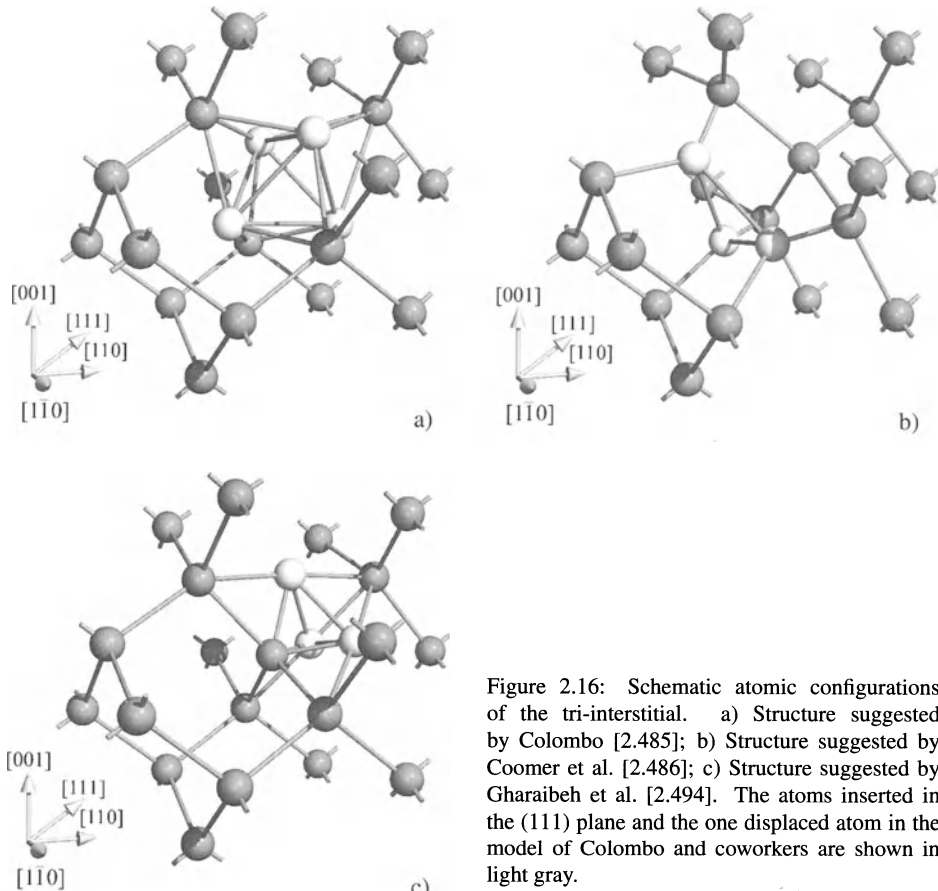


Figure 2.16: Schematic atomic configurations of the tri-interstitial. a) Structure suggested by Colombo [2.485]; b) Structure suggested by Coomer et al. [2.486]; c) Structure suggested by Gharaibeh et al. [2.494]. The atoms inserted in the (111) plane and the one displaced atom in the model of Colombo and coworkers are shown in light gray.

The tentative identification was corroborated by the work of Coomer et al. [2.476] who associated the I_3/X photoluminescence line with an I_4 cluster and argued on the basis that the I_3/X line grows on the expense of the I_1/W line that the latter has to comprise less self-interstitials. The *ab-initio* simulations of Lopez and Fiorentini [2.495] confirmed that the structure of Coomer et al. has a vibrational mode in the right energy range. They pointed out, however, that the significantly higher formation energy makes an identification problematic.

A further association of I_3 was suggested by Giri [2.307]. As discussed in detail further below, a deep metastable defect with negative-U properties was found by Giri and coworkers from a detailed analysis of spectra from DLTS and time-analyzed transient-spectroscopy measurements after argon implantation [2.307]. This defect was associated tentatively with self-interstitial clusters and in particular to I_3 .

Already in the work of Gharaibeh et al. [2.494], the possibility of a diffusion of an I_3 cluster was mentioned. This was confirmed by Estreicher et al. [2.491] who estimated a migration enthalpy of less than 0.23 eV for the structure in Figure 2.16 c). In the work of Richie et al. [2.492], a value of 0.48 eV was obtained from tight-binding molecular-dynamics simulations.

Tetra-Interstitials

In one of the first theoretical investigations on self-interstitial clusters, Arai et al. [2.496] suggested the structure shown in Figure 2.17 b) for the tetra-interstitial. It has D_{2d} symmetry, contains no dangling bonds, and all bond lengths and angles are close to the values for bulk silicon. The structure was suggested before by Humble [2.497] as a building block of a platelet defect in diamond. For silicon, it was supported by the *ab-initio* simulations of Coomer et al. [2.486] and Kohyama and Takeda [2.498], the tight-binding molecular-dynamics study of Gharaibeh et al. [2.494], and the empirical-potential-based molecular-dynamics simulations of Birner et al. [2.499].

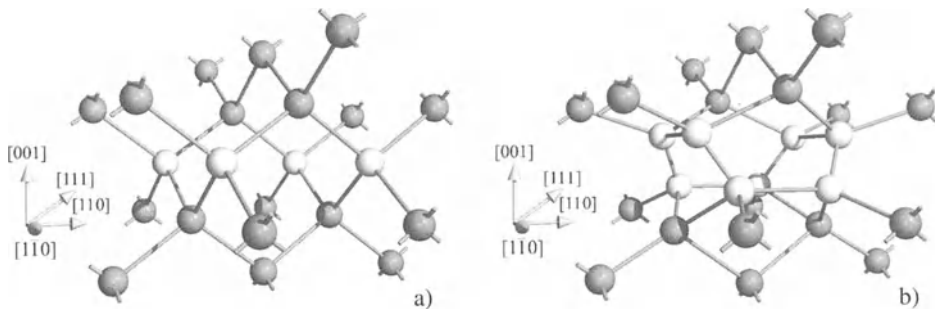


Figure 2.17: Schematic atomic configuration of the tetra-interstitial. a) Section of the ideal lattice. The four silicon atoms in light gray will be replaced by atom pairs; b) Tetra-interstitial with the atoms replaced. The four atom pairs are again shown in light gray.

Alternative structures for tetra-interstitials were obtained from simulations based on the empirical Ackland potential. In the work of De Souza et al. [2.500], four silicon atoms forming the tetra-interstitial were suggested to form a rhombus with $\langle 110 \rangle$ -oriented sides connecting bond-centered sites in the $\{111\}$ plane. The formation energy was with 1.4 eV per self-interstitial only slightly higher than that of the structure in Figure 2.17 b). Two other structures were obtained in the work of Chichkine et al. [2.501]. Adding silicon atoms to a face of an I_3 cluster resulted in a double-pyramid with a triangular basis. Energetically even more favorable was a structure which arose from joining two di-interstitials. It has the form of a prism with a triangular basis. Both appear to be C_{3v} -symmetric about a $\langle 111 \rangle$ axis.

The expected high stability of the I_4 cluster shown in Figure 2.17 b) was confirmed by a formation energy of 2.46 eV per self-interstitial calculated by Arai et al. [2.496] in their tight-binding study. In the *ab-initio* studies of Kohyama and Takeda [2.498] and Coomer et al. [2.476], formation energies of 1.49 and 2.18 eV per self-interstitial were calculated, respectively. All these values are significantly less than the formation energy of self-interstitials. For the binding energy, Coomer et al. [2.476] reported a value of 1.73 eV per self-interstitial in the cluster.

With respect to the electronic structure of I_4 , divergent results were reported. Coomer et al. [2.486] found from his *ab-initio* calculations an acceptor and a donor state which lie within approximately 0.1 eV of the conduction-band edge and the valence-band edge, respectively. In the subsequent work of Coomer et al. [2.476], the determination of the donor level was refined by a comparison to the known level of the carbon interstitial, leading to an estimate of $E_v + (0.16\text{--}0.27)$ eV. In contrast, using also an *ab-initio* approach, Kohyama and Takeda [2.498] reported the absence of states in the band gap.

Based on an extensive comparison of *ab-initio* calculations to the properties of the Si-*B3* EPR center, Coomer et al. [2.476] concluded that this center should be associated with the I_4 cluster rather than with a di-interstitial (see Section 2.5.4). This suggestion was supported by the subsequent EPR investigation of Pierreux and Stesmans [2.477]. An identification of the tetra-interstitial with the Si-*B3* EPR center includes the level at $E_v + 0.29$ eV reported by Mukashev et al. [2.483] and probably the Si-*NL51* EPR center found by Stallinga et al. [2.478]. Both were from the beginning associated with the Si-*B3* EPR center on the basis of their introduction and annealing kinetics. A further tentative suggestion of Coomer et al. [2.476] was that the I_4 cluster gives rise to the 1.0398 eV photoluminescence line labelled I_3 by Kirkpatrick et al. [2.358] and X by Tkachev and Mudryi [2.359]. The limited information available [2.359, 2.502–2.505] indicates that the defect responsible is introduced at the expense of the I_1/W photoluminescence line after neutron irradiation or ion implantation by heat treatments around 200 °C, that it is stable up to 550 °C, has tetragonal symmetry, and that there is no apparent dependence on the impurities being present in the samples or being implanted. It has to be noted, though, that the defect was associated previously with a vacancy cluster [2.502] due to its high response to stress. The association of the EPR spectra Si-*B3* and Si-*NL51* as well as of the PL I_1/W -line with I_4 was further substantiated by the EPR investigations of Mchedlidze and Suezawa [2.506].

Penta-interstitials

In the work of Colombo [2.485], the penta-interstitial found from tight-binding molecular-dynamics simulations consists of an octahedron arranged symmetrically around an empty lattice site with two adjacent atoms along the $\langle 110 \rangle$ chain displaced to anti-bond interstitial sites. The symmetry of the complex should be C_{2v} .

An alternative found by Gharaibeh et al. [2.494] and Birner et al. [2.499] consists of the I_4 structure with an adjacent $\langle 110 \rangle$ -oriented split interstitial.

A further alternative was suggested by Chichkine et al. [2.501] from their simulations based on the empirical Ackland potential. They found that the lowest-energy configuration is a capped prism with a triangular basis arranged around two empty lattice sites. With a symmetry close to C_{3v} and a higher calculated stability than I_3 , it was suggested as a candidate for the I_1/W photoluminescence line discussed in more detail below.

Hexa-Interstitials

In their *ab-initio* study, Gharaibeh et al. [2.507] suggested that the energetically most favorable configuration of a hexa-interstitial results from the reaction of two tri-interstitials with an energy gain of 2.5 eV. The six silicon atoms from which it composes are arranged in two parallel triangles in $\{111\}$ planes, twisted with respect to each other by 60° and centered around a bond-centered interstitial site. A further reaction with a tri-interstitial to I_9 was calculated to be associated with an energy reduction of at least 3.0 eV.

Alternative structures for I_6 were found from simulations using the empirical Ackland potential. In the work of De Souza et al. [2.500], a hexagonal, fully coordinated ring of silicon atoms, inserted in the $\{111\}$ plane around a bond-centered interstitial site, was found to have a formation energy of 1.53 eV per self-interstitial. The structure suggested by Chichkine et al. [2.501] has the form of a bi-capped prism with a trigonal basis, arranged C_{3v} -symmetrically around two lattice sites.

Octo-Interstitials

Investigating the formation of I_8 complexes, Gharaibeh et al. [2.507] found that the reaction of a hexa-interstitial with a di-interstitial is accompanied by a reduction of the system energy by at least 3.2 eV. This indicates that I_8 could be particularly stable as suggested by Cowern et al. [2.131] from their experimental investigations (see below). Based on simulations with the empirical Ackland potential, De Souza et al. [2.500], suggested that the self-interstitials form eight-membered rings with a formation energy slightly higher per self-interstitial than that of the I_4 cluster in Figure 2.17 b).

The 1.018 eV I_1/W Photoluminescence Line

One of the most controversially discussed photoluminescence centers is the zero-phonon photoluminescence line at 1.018 eV labelled I_1 by Noonan et al. [2.508] and W by Tkachev and Mudryi [2.359]. It was found to be introduced after irradiation, especially with neutrons and ions, and annealing above between about 50 and 200 °C, and to anneal out between about 300 and 450 °C [2.358, 2.359, 2.503, 2.509, 2.510]. Detailed investigations indicated that the formation is thermally activated with an energy of approximately 0.85 eV [2.348, 2.509].

Since the introduction and annealing behavior was found to be independent of the impurities being present in the sample (particularly oxygen) or implanted into it (except carbon, see below) [2.348, 2.358, 2.359, 2.509–2.513], and because the line is always sharp, it is generally assumed to arise from an intrinsic defect. The only argument against such an association is the observation that the introduction rate shows a saturation [2.503] which might indicate the exhaustion of an impurity in the material. Measurements under uniaxial stress established the spectrum to arise from a defect with trigonal C_{3v} symmetry [2.503, 2.511, 2.514]. In addition, it was concluded from a detailed investigation of its vibronic properties that the defect should be extrinsic, i. e. related to self-interstitials rather than to vacancies [2.503]. An other indication in favor of a self-interstitial complex came from the implantation of carbon into CZ silicon [2.512]. As a rare exception to the rule mentioned above, it led to a decrease of the PL-line intensity. This effect was explained consistently by the consumption of silicon self-interstitials by competing reactions and it has to be remarked that implanted carbon is generally found to reduce the concentration of self-interstitials during post-implantation anneals (see Section 4.1.7). From the dose dependence of the PL signal, Nakamura [2.510] concluded that the formation reaction is of second order.

The association with self-interstitial agglomerates makes the defect responsible for the I_1/W line a highly interesting object since such clusters known to control transient diffusion effects during post-implantation annealing. A further point of relevance is that the defect was found to correlate with the radiation-induced negative charge in the depletion region of radiation detectors for high-energy physics experiments [2.515] which limits their period of use.

Tentative identifications of the defect responsible for the I_1/W photoluminescence line include divacancies [2.347], non-planar tetravacancies [2.514], pentavacancies [2.358, 2.359], $\langle 111 \rangle$ -oriented split interstitials [2.510, 2.514, 2.516, 2.517], di-interstitials [2.517], tri-interstitials [2.348, 2.486], penta-interstitials [2.501], and extended {113} defects [2.518].

Other Self-Interstitial-Cluster-Related Experimental Observations

Self-interstitial clusters and their role in the transient-enhanced diffusion made them an important target for dedicated investigations. The DLTS investigations of Benton, Libertino, and coworkers [2.519–2.521], Giri and Mohapatra [2.522], and Schmidt et al. [2.523], and the complementary photoluminescence measurements of Libertino et al. [2.521], Schmidt et al. [2.523],

and Nakamura and Murakami [2.524] gave indications of the evolution of self-interstitial clusters and helped to elucidate the transition towards extended defects. Depending on the implantation and annealing conditions as well as on the impurities being present, different defect signatures were observed. Although it is obvious that the respective defects comprise self-interstitials, no clear assignment was achievable up to now.

In experiments involving electron irradiation or low-dose silicon implantation (10^9 to 10^{11} cm $^{-2}$), the defects forming at room temperature and upon annealing up to about 600 °C were all explained as divacancies and impurity-point-defect complexes [2.519]. After annealing at temperatures above 350 °C, only the self-interstitial-related defects were found in the silicon-implanted samples. A quantitative analysis up to a silicon dose of 10^{11} cm $^{-2}$ indicated that about three silicon self-interstitials per implanted silicon atom survive in clusters [2.519].

Implantation of MeV argon ions with doses around 10^{14} cm $^{-2}$ or MeV gold atoms with a dose of $5 \cdot 10^9$ cm $^{-2}$ into *n*-type silicon, followed eventually by annealing at 160 °C, was found by Giri and Mohapatra [2.522] to introduce a deep level compensating the background dopants. Complementary time-analyzed transient-spectroscopy investigations indicated that the level varies within E_c - (0.49–0.56), decreasing with increasing dose and increasing with annealing at 160 °C. These dependences were suggested tentatively to reflect the evolution of the defects responsible. Moreover, detailed investigations of the spectra indicated that the defect responsible is metastable and has levels forming an Anderson “negative-U” system [2.307]. The metastable configuration of the defect was found to have a level in DLTS which overlaps with the divacancy level at E_c - 0.42 eV. As the most likely candidate, a tri-interstitial complex in two configurations was suggested [2.307].

After implantation of silicon atoms with a dose of about 10^{12} to 10^{13} cm $^{-2}$ and annealing from about 550 to 700 °C, the formation of two new levels at $E_v + (0.29\text{--}0.36)$ eV and $E_v + (0.48\text{--}0.53)$ eV was observed in *p*-type material [2.519–2.521]. From experiments at lower doses, it was known that only self-interstitial complexes survive the annealing. Oxygen, carbon, and boron were excluded as main constituents [2.520]. In addition, it was concluded from an analysis of the width and the capture cross sections of the peaks that they are related to small clusters rather than to point-like defects or extended defects [2.521]. The identification as self-interstitial clusters was corroborated by the observation that the concentration of the respective levels reduces drastically when extended {113} defects form upon implantation of silicon with doses exceeding $5 \cdot 10^{13}$ cm $^{-2}$ and annealing at 680 °C and above for one hour [2.519, 2.521]. Annealing of the self-interstitial-cluster-related levels was found to be characterized by an activation energy of about 2.3 eV and to correlate with transient-enhanced diffusion in the absence of extended defects [2.521]. Correlated with the two DLTS levels found in *p*-type material were an acceptor level at E_c - (0.29–0.33) eV and a donor level at E_c - 0.5 eV [2.520, 2.523] observed in *n*-type silicon. They were suggested to arise from the identical or similar self-interstitial clusters.

Under similar implant and annealing conditions under which the self-interstitial-cluster-related DLTS levels were observed, broad photoluminescence features at 0.885 and 0.94 eV were also found together with a number of well-resolved PL lines [2.521, 2.523, 2.524]. An association with self-interstitial-related defects seems obvious, though no consensus on their size or structure is currently foreseeable.

Energetic Properties from Experiments and Theory

Our experimental knowledge about the energetics of self-interstitial clusters originates primarily from the experiments of Cowern et al. [2.131]. They investigated the oversaturation of self-interstitials in the bulk, after a surface-near silicon implantation, via the diffusion of buried

marker layers. A reproduction of the time evolution of the self-interstitial oversaturation required some stringent assumptions about the energetics of small self-interstitial clusters. In particular, it was shown that two self-interstitial clusters with sizes of $n = 4$ and $n = 8$ should be particularly stable. The absolute values of the energies extracted are probably known only within certain limits. They depend on the particular choice of the size-dependent capture radii of the self-interstitials at the clusters, and at least for one set of data, the assumption of only one very stable cluster with a size of $n = 8$ was found to suffice [2.525]. An experimental corroboration of the exceptional stability of octo-interstitials was reported by Schietekatte et al. [2.526]. They investigated the formation of extended defects in dependence on the implanted dose and found that their area density increases with the eight power. The enhanced stability of clusters consisting of at least eight interstitial atoms was deduced from a probabilistic interpretation of the nucleation process. In the work of Martin-Bragado et al. [2.493], the experiments of Cowern et al. [2.131] were reviewed including mobile di-interstitials.

In addition to the experimental findings, complementary information came from theoretical work. The binding energies found are summarized together with the experimentally derived values in Table 2.17 and Figure 2.18. The data attributed to Cowern et al. [2.131] were derived by assuming a formation energy of 3.8 eV for self-interstitials. Smaller values result in a decrease of the binding energy, higher ones in an increase. Also shown in Figure 2.18 is a frequently-used continuous expression in the form $2.1 - 1.45 \cdot (\sqrt{n} - \sqrt{n-1})$ eV suggested by Jaraiz et al. [2.379] from a fit to the data of Gilmer et al. [2.374].

Table 2.17: Reduction of the system energy due to the formation of a self-interstitial agglomerate of size n from an agglomerate of size $n - 1$ and a well-separated self-interstitial. The abbreviations EP, Exp, and TB refer to empirical potential, experimental, and tight-binding methods.

$n =$	3	4	5	6	7	8	9	Method	Ref.
Gilmer et al.	1.6	2.25	0.93	1.5				EP	[2.374]
Kim et al. ($\{113\}$ plane)	2.2	1.4	2.5	2.1				TB	[2.527]
Kim et al. ($\{100\}$ plane)	3.5	0.9	2.6	1.6				TB	[2.527]
Cowern et al. ⁶	2.64	2.77	2.67	2.48	2.46	3.24	2.40	Exp	[2.131]
Colombo	2.09	1.15	2.2	0.58	2.29	0.68	2.88	TB	[2.485]
Gharabeih et al.	2.54	2.09	1.73					TB	[2.494]
Chichkine et al.	2.49	0.88	2.33	1.67	1.37	1.98	1.47	EP	[2.501]
Martin-Bragado et al.	2.22	2.35	2.45	1.60	1.60	2.86	2.40	Exp	[2.493]

$n =$	10	11	12	13	14	15	16	Method	Ref.
Cowern et al. ⁶	2.69	2.73	2.92	3.00	3.06			Exp	[2.131]
Colombo	-0.05	2.95						TB	[2.485]
Chichkine et al.	2.16							EP	[2.501]
Martin-Bragado et al.	2.36	2.61	2.71	2.68	2.67	2.68		Exp	[2.493]

⁶A value of 3.8 eV was assumed for the formation energy of self-interstitials. Smaller values result in a decrease of the binding energy, higher ones in an increase.

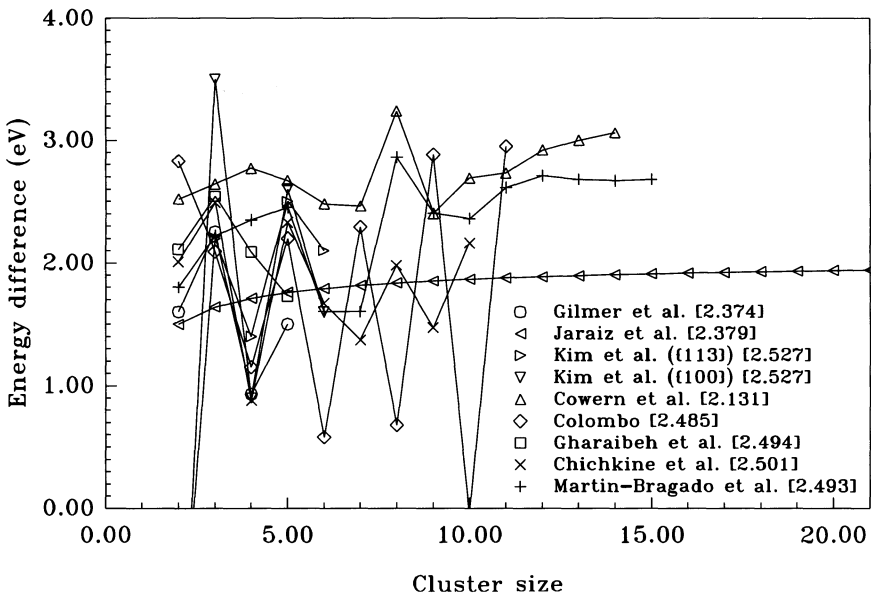


Figure 2.18: Reduction of the system energy due to the formation of a self-interstitial agglomerate of size n from an agglomerate of size $n - 1$ and a well-separated self-interstitial. The lines are just to guide the eye.

Problems in the calculations of cluster properties are on the one hand that very large cell sizes are needed to allow the relaxation of large clusters. This restricts the application of the local-density and generalized gradient approaches to rather small self-interstitial clusters. A further problem is to find the minimum-energy configuration for each self-interstitial cluster of a certain size. This is for self-interstitials and their many possible configurations an even more challenging task than for vacancy clusters. With respect to both problems, the energies reported have to be taken *cum grano salis*.

2.6 Frenkel Pairs

A Frenkel pair [2.528] consists of a self-interstitial next to a vacancy. In this configuration, the two point defects are but one step away from mutual annihilation or from dissociation. Thus, to survive for some time as an entity, a long-ranging attractive interaction is needed to prevent dissociation and a short-ranging reaction barrier to prevent annihilation. There are, as outlined below, indications that both prerequisites may be fulfilled in silicon under certain conditions. Frenkel pairs as an intermediate state are also of high interest for the introduction of defects during irradiation, for the bulk recombination process discussed in the next section, and for amorphization during ion implantation.

The first indications for the existence of metastable Frenkel pairs in silicon came from the observation that the damage-production rate decreases significantly when the temperature is lowered during electron irradiation with an energy around 1 MeV [2.529–2.532]. In contrast, for electron energies of 5 MeV and above, no such temperature dependence was observed [2.243, 2.533, 2.534]. To explain such effects in silicon and germanium, Wertheim [2.530] and MacKay and Klontz [2.535] suggested a model in which metastable Frenkel pairs are produced

preferentially by the low-energy electron irradiation. Figure 2.19 shows a schematic energy diagram of the system after the creation of a Frenkel pair. Due to thermal motions, the vacancy and the self-interstitial may anneal by surmounting a recombination barrier G^r or break up by overcoming a liberation barrier G^l . At high irradiation energies, the energy transferred suffices to separate self-interstitial and vacancy further so that less metastable Frenkel pairs are produced. In a first estimate, Wertheim [2.530] determined the liberation barrier to be smaller than or equal to 0.3 eV and the recombination barrier to be smaller than the liberation barrier by 0.04 eV. From similar analyses Whan and Vook [2.536] estimated $G^l - G^r$ to be about 0.05 eV, Stein and Vook [2.532] reported values between 0.055 and 0.071 eV, and Vook and Stein [2.537] obtained 0.064 eV. The simple model was extended by MacKay and Klontz [2.535, 2.538] to account for the dependence of the defect-introduction rate on the concentration and charge state of the substrate doping observed experimentally. They suggested that the recombination barrier might depend on the charge state of the Frenkel pair and, for silicon, that there is no recombination barrier for neutral Frenkel pairs. Following this idea, Vook and Stein [2.537] assumed that all neutral Frenkel pairs recombine while all positively charged pairs dissociate. An analysis based on this model indicated that Frenkel pairs might have a donor level at $E_c - 0.07$ eV. Gregory and Barnes [2.539] found that the data could be equally well described by a parameter set with the donor level at $E_c - 0.063$ eV.

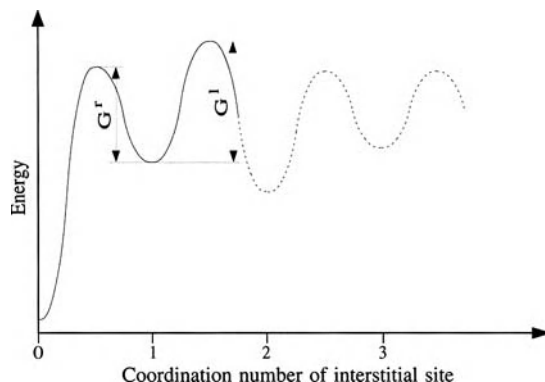


Figure 2.19: Schematic representation of the energy-barrier diagram for a self-interstitial in the vicinity of a vacancy.

In a later analysis of radiation damage, Emtsev et al. [2.540] found that additional acceptors were introduced by gamma irradiation at 4 to 6.5 K. They attributed them to Frenkel pairs and suggested that the level at about $E_c - 0.07$ eV found in the previous investigations would be their acceptor level rather than a donor level. Negatively charged Frenkel pairs were further suggested to be stable up to about 70 K. In a subsequent review, Emtsev et al. [2.161] suggested Frenkel pairs to have a double acceptor level at about $E_c - 0.07$ eV to reproduce the temperature-dependence of defect production in *n*-type silicon. However, Frenkel pairs were no longer claimed to be directly observable at any temperature.

In most of the irradiation experiments, information about Frenkel pairs was obtained indirectly from the rate of introduction of self-interstitials and vacancies and their reactions. In contrast, Bausch, Ehrhart and, Zillgen [2.541, 2.542] concluded from their X-ray measurements that stable Frenkel pairs form in large numbers during high-dose electron irradiation at a temperature of 4 K. The non-linear dependence of the scattering cross section of the Huang diffuse

X-ray scattering at the highest irradiation doses was interpreted in terms of the slow growth of small defect agglomerates. Despite the large number of Frenkel pairs, no significant change of the lattice parameter was observed. This was explained by displacement fields around the vacancy and the self-interstitial which cancel approximately. A detailed analysis of the measurements led to the conclusion that the vacancy and the self-interstitial are separated by one to two coordination sites. This was included schematically in Figure 2.19 by assuming the energy at the second interstitial site from the vacancy to be lower than at the neighboring interstitial sites. Such an energetically favored site was already suggested by Wertheim [2.530] although it was no crucial part of his model. The work was completed by the *in-situ* Huang diffuse X-ray scattering measurements of Partyka et al. [2.250] who used irradiation with helium, argon, and gallium in addition to electron irradiation. Simulations of the measured scattering intensities indicated that the separation of self-interstitials and vacancies in pairs generated by low-energy recoil events is about 1 nm while it is about twice that value for defects produced in cascades.

Using proton and α -particle irradiation at 77 K instead of irradiation with electrons, Abdullin and Mukashev [2.394] observed the formation of a defect which gave rise to a DLTS level at $E_v + 0.2$ eV and was labeled *H4*. Its relatively large half-width of $\gtrsim 20$ K was taken as an indication that the level arises from a group of defects with similar energy levels. During heat treatment around 140 K, *H4* showed a complex annealing behavior characterized by an activation energy of about 0.48 eV during which vacancies were liberated. Athermal annealing at significantly lower temperatures could be stimulated by electron injection. On the basis of this evidence, *H4* was suggested to arise from Frenkel pairs or higher vacancy-self-interstitial complexes. The *H4* level was observed also in electron-irradiated samples and Londos [2.312] associated it tentatively with a divacancy-self-interstitial complex. Based on its properties and on the annealing kinetics, Mukashev et al. [2.543] identified the EPR spectrum of a C_{1h} -symmetric defect, labeled Si-AA19, to arise from a vacancy distorted by an interstitial.

The first *ab-initio* investigations of Frenkel pairs were reported by Dal Pino et al. [2.544]. They found that moving a silicon atom from a substitutional site to the next tetrahedral site increases the energy of the system by about 3.6 eV and that there is no barrier against recombination. In contrast, the presence of oxygen was found to stabilize the silicon atom in a position 0.56 Å from its lattice site towards the tetrahedral interstitial site. In this configuration, the system energy was calculated to be increased by about 1.2 eV with a barrier of about 0.08 eV against recombination. In contrast, using tight-binding molecular-dynamics simulations, Tang et al. [2.545] found that vacancies diffuse towards near self-interstitials and form the complex depicted in Figure 2.20 instead of recombining. Besides “I-V complex”, the configuration was called “bond defect” in the literature. Reconstruction of an undisturbed lattice was estimated

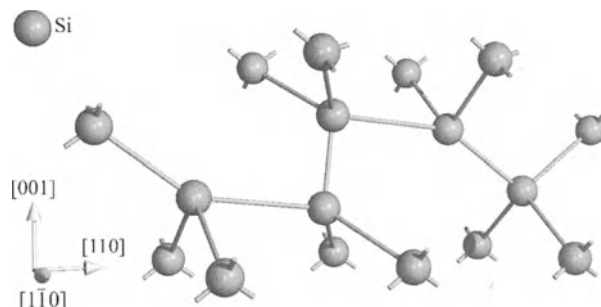


Figure 2.20: Schematic representation of the atomic arrangement of the bond defect.

to require overcoming an energy barrier of 1.13 eV. The defect was described already before by Heggie [2.41] in his investigation of the concerted-exchange mechanism. In his calculations based on an improved Tersoff potential, such a configuration was found to be metastable with a formation energy of about 2.3 eV and a barrier of about 1.2 eV against reconstruction of the perfect lattice. In a subsequent analysis by Cargnoni et al. [2.546], the structure of the bond defect was confirmed by tight-binding molecular-dynamics simulations as well as by *ab-initio* calculations. For the barrier against recombination, a value of 1.24 eV was estimated from the tight-binding molecular-dynamics simulations. The *ab-initio* calculations gave values of 1.32 and 2.05 eV for restrained and relaxed clusters. Such energy barriers against recombination of self-interstitials and vacancies are, as discussed in the next section, hardly possible. Thus, it may be concluded that the bond defect, if it exists and has such large barriers against recombination, is not a mandatory step in the recombination process. This expectation was confirmed by the tight-binding molecular-dynamics simulations of Zawadzki et al. [2.547] who reported that the formation of bond defects occurred in some but not in all cases. But also the recombination barriers estimated remained not undisputed. Using a Tersoff potential in their molecular dynamics simulations and a different strategy for its extraction, Marqués et al. [2.548] estimated a value of 0.43 eV for the barrier against recombination of a bond defect. The bond defect was also found in the *ab-initio* calculations of Goedecker et al. [2.549] who called it fourfold coordinated defect (FFCD) and determined a value of 2.39 eV for its formation energy. Since clusters of such defects were found to be energetically favorable in comparison to separated defects, bond defects were suggested as building blocks for amorphization. In a subsequent *ab-initio* analysis of Al-Mushadani and Needs [2.167], a formation energy of 2.80 eV, a formation entropy of about $3.9 \cdot k$ around 1000 °C, and a six-fold degeneracy were found for the neutral bond defect.

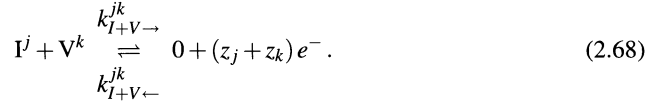
2.7 Bulk Recombination and Bulk Processes

Vacancies and self-interstitials may react in the bulk without leaving more than an undisturbed lattice site. This mechanism is discussed in detail in Section 2.7.1. Competing with bulk recombination is an indirect process for the mutual annihilation of self-interstitials and vacancies which involves impurities. It becomes, as outlined in Section 2.7.2, the more effective the higher their concentration. But the intrinsic point defects may also interact individually with extended defects and traps. These processes are reviewed in Sections 2.7.3 and 2.7.4, respectively. Bulk recombination of self-interstitials and vacancies, and their reactions with traps were suggested in the literature to affect their effective diffusivity and to explain inconsistencies in experimental determinations. Approximate quantitative descriptions of such effects are derived and discussed in Section 2.7.5. Finally, intrinsic point defects may be generated by chemical reactions in the bulk. An overview of such processes is given in Section 2.7.6.

2.7.1 Bulk Recombination

The reaction of a self-interstitial and a vacancy leads to their mutual annihilation, leaving behind an undisturbed lattice site. In analogy to the recombination of electrons and holes, this process is usually termed bulk recombination. The reverse process of bulk recombination is the thermal generation of a Frenkel pair consisting of a vacancy and a self-interstitial separated spatially. Equilibrium always has to be understood as a balance between generation and recombination processes.

Vacancies and self-interstitials can exist in various charge states and it will be assumed again that steady state between the charge states is established rapidly in comparison to the time constants of all other processes. For a complete description of bulk recombination, all individual reactions between self-interstitials in charge state j and vacancies in charge state k have to be considered. The numbers of electron charges attributed to these vacancies and self-interstitials will be denoted by z_j and z_k , their concentrations by C_{Ij} and C_{V^k} , respectively. Each of the reactions can be written as



The symbols 0 and e^- at the right-hand side stand for the undisturbed lattice and a remaining electron, respectively.

In a system with electrically neutral self-interstitials and vacancies only, bulk recombination would lead to the continuity equations

$$\frac{\partial C_I}{\partial t} = \frac{\partial C_V}{\partial t} = -k_{I+V\rightarrow} \cdot C_I \cdot C_V - k_{I+V\leftarrow} \quad (2.69)$$

when the point defects are homogeneously distributed. Including all charge states of the self-interstitials and vacancies, the continuity equation for the total concentration of self-interstitials $C_I = \sum_j C_{Ij}$ and for the total concentration of vacancies $C_V = \sum_k C_{V^k}$ follows in the form

$$\begin{aligned} \frac{\partial C_I}{\partial t} = \frac{\partial C_V}{\partial t} &= - \frac{C_I}{\sum_j \delta_{Ij} \cdot \left(\frac{n}{n_i}\right)^{z_j}} \cdot \frac{C_V}{\sum_k \delta_{V^k} \cdot \left(\frac{n}{n_i}\right)^{z_k}} \\ &\cdot \sum_{j,k} k_{I+V\rightarrow}^{jk} \cdot \delta_{Ij} \cdot \delta_{V^k} \cdot \left(\frac{n}{n_i}\right)^{z_j+z_k} + \sum_{j,k} k_{I+V\leftarrow}^{jk} \cdot n^{z_j+z_k} \end{aligned} \quad (2.70)$$

As before, differently charged point defects were assumed to be in equilibrium so that their concentrations can be expressed in terms of the neutral ones via (2.22) to (2.25). In case of inhomogeneously distributed point defects, the right-hand side of (2.70) can be identified as a generation-recombination term (1.140) in the continuity equations of the intrinsic point defects. For diffusion-limited reactions, the forward reaction constants $k_{I+V\rightarrow}^{jk}$ are given by (1.149) when at least one of the reactants is electrically neutral, and by (1.150) when both are ionized. The backward reaction constants $k_{I+V\leftarrow}^{jk}$ will be deduced from equilibrium conditions.

From the principle of detailed balance follows that, in equilibrium, all reaction equations in (2.68) are related to each other by

$$\frac{k_{I+V\rightarrow}^{jk}}{k_{I+V\leftarrow}^{jk}} = \frac{k_{I+V\rightarrow}^{00}}{k_{I+V\leftarrow}^{00}} \cdot \frac{n_i^{z_j+z_k}}{\delta_{Ij} \cdot \delta_{V^k}} \quad (2.71)$$

so that (2.70) can be rewritten in the form

$$\begin{aligned} \frac{\partial C_I}{\partial t} = \frac{\partial C_V}{\partial t} &= \left(\frac{k_{I+V\leftarrow}^{00}}{k_{I+V\rightarrow}^{00}} - \frac{C_I}{\sum_j \delta_{Ij} \cdot \left(\frac{n}{n_i}\right)^{z_j}} \cdot \frac{C_V}{\sum_k \delta_{V^k} \cdot \left(\frac{n}{n_i}\right)^{z_k}} \right) \\ &\cdot \sum_{j,k} k_{I+V\rightarrow}^{jk} \cdot \delta_{Ij} \cdot \delta_{V^k} \cdot \left(\frac{n}{n_i}\right)^{z_j+z_k} \end{aligned} \quad (2.72)$$

In equilibrium, the derivatives of the point-defect concentrations with respect to time vanish and the point-defect concentrations correspond to their equilibrium values. This allows to express the backward reaction constants $k_{I+V\leftarrow}^{jk}$ in terms of the forward reaction constant $k_{I+V\rightarrow}^{jk}$ and the equilibrium concentrations as

$$k_{I+V\leftarrow}^{jk} = k_{I+V\rightarrow}^{jk} \cdot \frac{C_I^{eq}}{\sum_j \delta_{Ij} \cdot \left(\frac{n}{n_i}\right)^{z_j}} \cdot \frac{C_V^{eq}}{\sum_k \delta_{V^k} \cdot \left(\frac{n}{n_i}\right)^{z_k}} \cdot \frac{\delta_{Ij} \cdot \delta_{V^k}}{n_i^{z_j+z_k}} \quad (2.73)$$

so that (2.72) can be written in the well-known form

$$\frac{\partial C_I}{\partial t} = \frac{\partial C_V}{\partial t} = k_B \cdot (C_I^{eq} \cdot C_V^{eq} - C_I \cdot C_V) \quad (2.74)$$

with the bulk-recombination constant k_B related to the reaction constants in (2.72) by

$$k_B = \frac{\sum_{j,k} k_{I+V\rightarrow}^{jk} \cdot \delta_{Ij} \cdot \delta_{V^k} \cdot \left(\frac{n}{n_i}\right)^{z_j+z_k}}{\sum_j \delta_{Ij} \cdot \left(\frac{n}{n_i}\right)^{z_j} \cdot \sum_k \delta_{V^k} \cdot \left(\frac{n}{n_i}\right)^{z_k}}. \quad (2.75)$$

The bulk-recombination constant k_B can be seen as an effective forward reaction constant. Although it results from a superposition of reaction constants between self-interstitials and vacancies in various charge states, it is usually used in the form of (1.149) with an effective recombination radius a_{IV}^R . For diffusion-limited recombination of neutral point defects, one would expect a recombination radius on the order of the distance between two silicon atoms, i. e. 2 to 3 Å. For the recombination of singly charged self-interstitials and vacancies in opposite charge states, (1.150) predicts the recombination radius to increase by a factor of 3 to 4 at elevated temperatures. *Vice versa*, the reaction constant for the recombination of equally charged defects is expected to be decreased by such a factor.

In the literature exist also alternative formulations of the bulk-recombination rate. Habu and coworkers [2.93, 2.96, 2.550] used in their studies a bulk-recombination term in the form

$$\frac{\partial C_I}{\partial t} = \frac{\partial C_V}{\partial t} = -4 \cdot \pi \cdot (D_I + D_V) \cdot a_{IV}^R \cdot \exp\left(-\frac{\Delta G}{k \cdot T}\right) \cdot \frac{k \cdot T}{\Delta E_{FP}} \cdot C_I \cdot C_V \cdot \ln\left(\frac{C_I \cdot C_V}{C_I^{eq} \cdot C_V^{eq}}\right) \quad (2.76)$$

with ΔE_{FP} denoting the energy released by the annihilation of a pair. The general form of (2.76) results from the theory of the thermodynamics of irreversible processes and is, as discussed in Section 1.5, valid only near equilibrium. In this limit, the last term corresponds to

$$C_I \cdot C_V \cdot \ln\left(\frac{C_I \cdot C_V}{C_I^{eq} \cdot C_V^{eq}}\right) \approx C_I \cdot C_V - C_I^{eq} \cdot C_V^{eq}. \quad (2.77)$$

A comparison of (2.74) and (2.76) with k_B taken from (1.155) shows that only the term $k \cdot T / \Delta E_{FP}$ has no correspondence in (2.74). It has to be remarked, though, that the $k \cdot T$ originates from the theory of irreversible processes while the term ΔE_{FP} in its denominator was probably introduced only to keep the dimensions constant. Intuitively, one would expect ΔE_{FP} to correspond to the sum of the formation enthalpies of self-interstitials and vacancies, but the numbers given were 2.58 eV larger.

Studies of the generation of intrinsic point defects by irradiation led to the picture of Frenkel pairs discussed in Section 2.6 which probably have a slightly higher barrier against dissociation than against recombination. However, all estimates for barriers were on the order of tenths of an

eV and probably imperceptible at elevated temperatures. An opposite view was held in the early papers especially by Hu [2.551] who suggested that the energy barrier against recombination can be computed approximately as the difference between the displacement threshold of about 13.0 eV and the formation energies for a vacancy and a self-interstitial. This estimate would lead to an energy barrier of several eV. It has to be remarked, though, that this number can only be considered an upper limit. For thermally activated processes, a possible barrier against recombination is expected to be reduced by the cooperative motion of neighboring host atoms while such effects are not or only to a significantly smaller degree expected for the generation of electron-vacancy pairs by collision processes. Equally ambiguous and contradicting were the conclusions drawn from a variety of other experiments. The main contributions will be discussed in the following.

Important informations on the recombination of intrinsic point defects came from experiments in which one intrinsic point defect is introduced or depleted and in which the concentration of the other intrinsic point defect is monitored via its effect on dopant diffusion. The first such experiment was reported by Antoniadis and Moskowitz [2.552]. They observed that the diffusion of antimony during oxidation became retarded only after some delay. To explain this result, they postulated an energy barrier of 1.4 eV for bulk recombination. Gösele et al. [2.553] suggested that this barrier against recombination should be interpreted as an entropy barrier. This allowed to reconcile the experiments of Antoniadis and Moskowitz with early irradiation experiments and indicated also that self-interstitials might exist in an extended state at elevated temperatures. In the work of Sinno et al. [2.102] and Dornberger et al. [2.104], the bulk-recombination rate reading correctly

$$k_B = 1.2 \cdot 10^{-6} \cdot (D_I + D_V) \cdot \exp\left(-\frac{0.61 \text{ eV}}{k \cdot T}\right) \cdot \exp\left(2.3 - 7.38 \cdot 10^{-3} \cdot \frac{T}{K}\right) \quad (2.78)$$

[2.554] was based on the experiments of Antoniadis and Moskowitz, too. But it was also found that the recombination barrier is not overly important for the simulation of the dynamics of oxidation-stacking-fault rings in grown crystals as long as recombination is sufficiently rapid [2.554]. Simulating similar experiments, Mori et al. [2.107] suggested an entropy barrier of $8.54 \cdot k$, and Okui and Nishimoto [2.110] an energy barrier of 1.8 eV. In both investigations, a recombination radius of one nm was used.

The postulation of a recombination barrier by Antoniadis and Moskowitz [2.552] became questionable after the experiments of Moynagh and Rosser [2.555], Guerrero et al. [2.556], and Packan [2.557] led to results controversial to those of Antoniadis and Moskowitz and gave no evidence for a recombination barrier. Similarly, from the oxidation-retarded diffusion of antimony under extrinsic conditions, Perozziello et al. [2.558] estimated an upper boundary of 0.22 eV for an energy barrier opposing recombination of self-interstitials and vacancies. Because of the low diffusivity of antimony, such investigations based on ion implantation and annealing were restricted to temperatures of 1100 °C and above. Investigations at significantly lower temperatures became possible when delta-doped layers came into use. In one such a study, Gossman et al. [2.224] investigated the diffusion of boron and antimony spikes during vacuum anneals. They found the diffusion of boron to be retarded and that of antimony to be enhanced. The enhancement of antimony was interpreted to arise from grown-in vacancy defects while the retardation of boron was assumed to reflect the recombination of self-interstitials and vacancies. Based on this model, they estimated the barrier against bulk recombination to be about 0.2 eV at 800 °C. In a subsequent study, Gossman et al. [2.559] found the retarded boron diffusion to be caused by a drain of self-interstitials at the surface during vacuum anneal-

ing and concluded that bulk recombination should be significantly less effective than estimated in their previous investigation. At significantly higher temperatures, Falster et al. [2.106] found that bulk recombination has to be very efficient to explain their vacancy profiles measured after annealing at high temperatures followed by a fast quench. Simulating similar experiments, Akatsuka et al. [2.108] assumed a reaction barrier of 1.0 eV.

In various other experiments, bulk recombination was found to play an important role, too. From their study of radiation-enhanced diffusion of boron, Loualiche et al. [2.560] estimated a rather large value of $a_{IV}^R = 4 \cdot a_{Si} = 21.7 \text{ \AA}$. To explain boron profiles after implantation at temperatures from 800 to 1000 °C quantitatively, Pichler et al. [2.561] identified the product $k_B \cdot C_I^{eq} \cdot C_V^{eq}$ as the parameter of supreme influence. It was estimated for temperatures below 957 °C to be $5.26 \cdot 10^{36} \cdot \exp(-6.19 \text{ eV}/kT) \text{ cm}^{-3}\text{s}^{-1}$, and $2.24 \cdot 10^{41} \cdot \exp(-7.32 \text{ eV}/kT) \text{ cm}^{-3}\text{s}^{-1}$ above. Most of the implicit assumptions could, as shown by Pichler and Schork [2.562], be justified. However, the analysis was based on point-defect parameters characterized by a much larger equilibrium concentration of vacancies than of self-interstitials. As a consequence, the discontinuity of the point-defect-creation process did not lead to significant non-linearities in the bulk-recombination term since the vacancy concentration remained basically in steady state. The consequences of this assumption are not as clear as considered since recent results indicate that the equilibrium concentrations of the intrinsic point defects should be on the same order of magnitude. To reproduce important features of their lithium-ion-drift experiments after high-concentration phosphorus diffusion, Knowlton et al. [2.97] reported a bulk-recombination rate which, depending on the parameter set used, means effective recombination radii of $3.6 \cdot 10^{-2}$ and $7 \cdot 10^{-3} \text{ \AA}$. For the 950 °C of their investigation, this could mean an enthalpy barrier of 0.47 to 0.64 eV or an entropy barrier of $4.4 \cdot k$ to $6.1 \cdot k$. It has to be commented, however, that the simulation of the interaction between the injected self-interstitials and the grown-in defects as recombination between self-interstitials and vacancies is probably oversimplified.

Besides in the rather dedicated experiments discussed above, bulk-recombination rates were extracted within general studies of point-defect parameters. Zimmermann and Ryssel [2.221] suggested from studies of platinum diffusion in silicon that bulk recombination cannot be effective. The bulk-recombination constant given implies a barrier of 3.95 eV associated with an entropy increase of $35.6 \cdot k$. However, it is felt that these conclusions are influenced by the assumption that the equilibrium concentrations of vacancies is orders of magnitude larger than that of self-interstitials. The ambiguities of such investigations were shown clearly in the work of Law [2.89]. Law re-examined various studies of dopant diffusion under non-equilibrium conditions and, in [2.89], extracted two complete sets of point-defect diffusion parameters based on the self-interstitial diffusion parameters proposed by Bronner and Plummer [2.120] and Boit et al. [2.126]. Both parameter sets fitted the experimental data equally well, but the parameter set based on the self-interstitial diffusion coefficient of Bronner and Plummer had a bulk-recombination constant with a negative activation energy. This would indicate a negative recombination barrier of -3.4 eV together with a recombination radius of 10^{-14} \AA . The physical meaning of such parameters is questionable and reflects, as indicated by Law, the other assumptions of the analysis. Based on the self-interstitial diffusion coefficient of Boit et al., the analysis led to a recombination barrier of 0.77 eV and a recombination radius of 10.8 \AA . From a similar study, including also high-concentration diffusion, Baccus et al. [2.563] concluded that a barrier of 0.5 eV opposes bulk recombination. In contrast, modeling the diffusion of phosphorus at high concentrations, Dunham [2.90, 2.564] found the best agreement for a little or no barrier to recombination. Finally, in the work of Ghaderi et al. [2.95], a recombination barrier of 0.3 eV was found from the simulation of gold-diffusion experiments. This value resulted from the assumption of a recombination radius of 5 Å.

Bulk recombination was investigated theoretically by Nichols et al. [2.234]. Their *ab-initio* simulations indicated a recombination barrier of about 1.0 eV. Even higher recombination barriers could be expected when the bond defect discussed in Section 2.6 is a mandatory step in the recombination process. Recombination between self-interstitials and vacancies was also investigated in the kinetic Monte-Carlo simulations of Bunea et al. [2.565] and Beardmore et al. [2.566] who used empirical potentials and potentials from *ab-initio* simulations, respectively. Despite the different potentials, both investigations indicated a vanishing barrier and a capture radius of about 7 to 8 Å at 900 °C which decreases slightly with increasing temperature.

When bulk recombination is very efficient in comparison to individual annihilation of point defects in the bulk and at the surface, local equilibrium ($C_I \cdot C_V = C_I^{eq} \cdot C_V^{eq}$) can be assumed for sufficiently long process times as suggested, e. g. by Sirtl [2.567], Baruch [2.568], and Mizuo and Higuchi [2.569]. In such a system, it is always interesting to ask for the time constant with which small perturbations from steady state $C_I^* + \Delta C$ and $C_V^* + \Delta C$ of the point-defect concentrations relax. Provided that $C_I^* \cdot C_V^* = C_I^{eq} \cdot C_V^{eq}$ and $\Delta C \ll C_I^* + C_V^*$, the following differential equation results from a small signal analysis of (2.74)

$$\frac{d\Delta C}{\Delta C} = -k_B \cdot (C_I^* + C_V^*) \cdot dt \quad (2.79)$$

from which the time constant

$$\tau_B = \frac{1}{k_B \cdot (C_I^* + C_V^*)} \quad (2.80)$$

for the relaxation of the point defects can be identified. Modeling the bulk-recombination rate in the form (1.149), one obtains

$$\tau_B = \frac{1}{4 \cdot \pi \cdot a_B \cdot (D_I + D_V) \cdot (C_I^* + C_V^*)} \quad (2.81)$$

with a_B denoting the capture radius for bulk recombination (usually assumed to be on the order of the bond length between two neighboring silicon atoms). When we assume only vacancies and self-interstitials to contribute to tracer diffusion via (2.60), the bulk relaxation time constant can be expressed near equilibrium in the form

$$\tau_B = \frac{f^I \cdot \frac{D_I}{D_V} \cdot \frac{C_I^{eq}}{C_V^{eq}} + f^V}{4 \cdot \pi \cdot a_B \cdot C_{Si} \cdot D_T \cdot \left(1 + \frac{D_I}{D_V}\right) \cdot \left(1 + \frac{C_I^{eq}}{C_V^{eq}}\right)}. \quad (2.82)$$

This relation has maxima for $D_I/D_V \rightarrow \infty$, $C_I^{eq}/C_V^{eq} \rightarrow \infty$ and $D_I/D_V \rightarrow 0$, $C_I^{eq}/C_V^{eq} \rightarrow 0$ which allows to estimate an upper limit for τ_B in the form

$$\tau_B < \frac{1}{4 \cdot \pi \cdot a_B \cdot D_T \cdot C_{Si}} \quad (2.83)$$

for diffusion-limited bulk recombination.

In several investigations, bulk-recombination rates and equilibrium concentrations of point defects were given explicitly [2.89, 2.93, 2.95, 2.96, 2.106, 2.221, 2.563]. The resulting values for the relaxation time constant τ_B are shown in Figure 2.21. Also shown is the upper limit for diffusion-limited reactions (2.83) and estimates according to (2.81) from investigations in which equilibrium concentrations and diffusion coefficients of self-interstitials and vacancies were determined. All these values have been derived assuming a bulk-recombination radius of 3 Å. The value given by Gossmann et al. [2.224] is a direct estimate of the bulk relaxation time from the non-equilibrium diffusion of boron and antimony marker layers.

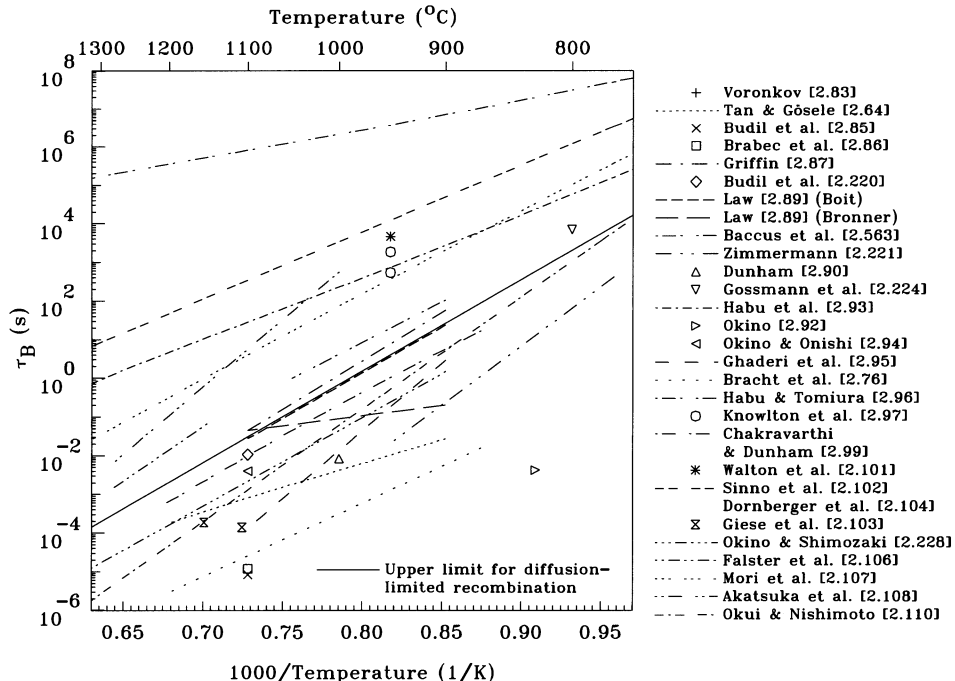


Figure 2.21: Relaxation time constant for bulk recombination.

The apparent disagreement between the various investigations can be related in part to ambiguities in the determination of diffusion coefficients and equilibrium concentrations of the intrinsic point defects addressed already above as well as to an insensitivity of the respective experiments to bulk recombination. Several of them were influenced by the investigation of Antoniadis and Moskowitz [2.552] and adopted their notion of a recombination barrier. The values resulting from the analyses of Habu et al. [2.93] and Habu and Tomiura [2.96] are difficult to interpret. The factor $k \cdot T / \Delta E_{FP}$ in their bulk-recombination term does not appear to be well-founded and increases τ_B by roughly 2 orders of magnitude. But the main influence comes from the recombination barrier which, according to Habu and Tomiura [2.96], increases τ_B by a factor of $3 \cdot 10^4$ at 700 °C to a factor of $5 \cdot 10^9$ at the melting point⁷.

2.7.2 Indirect Bulk Recombination via Impurities

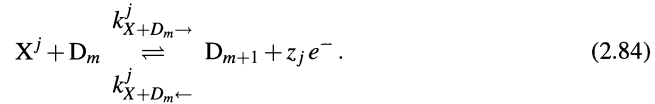
Direct recombination between self-interstitials and vacancies is not the only process in the bulk able to remove them in pairs. In Section 3.3, the formation of mobile complexes between point defects and dopants will be discussed. The concentration of such complexes can be considerably higher than the concentration of the respective point defects. The probability for, e. g., a self-interstitial to recombine with a dopant-vacancy pair to a substitutional dopant may then be higher than the probability to recombine with a vacancy. In analogy to direct recombination, such a mechanism can be considered an indirect bulk-recombination mechanism between self-interstitials and vacancies.

⁷The logarithm of a negative number in equation (6.e) of the work of Habu and Tomiura [2.96] is assumed to be a typo and the recombination barrier is taken to vary as $\Delta G = R \cdot T \cdot (2.0 + 22.0 \cdot \ln(T/670 \text{ K}))$ with temperature.

Such reactions can be included within the framework of diffusion-reaction equations as outlined in Section 1.5.4. The analysis in Section 3.3.4 shows that indirect recombination leads in steady state also to a term which is proportional to $C_I^{eq} \cdot C_V^{eq} - C_I \cdot C_V$. The indirect-bulk-recombination constant which can be defined in analogy to (2.74) is proportional to the concentration of substitutional impurities and depends in the general case also on the concentrations of the intrinsic point defects.

2.7.3 Reactions of Intrinsic Point Defects with Extended Defects

Besides mutual annihilation of self-interstitials and vacancies, point defects may react individually with extended defects like stacking faults, dislocation loops, or voids being present in the bulk of a silicon wafer. When we assume that charge will not be accumulated in these defects, the charge carriers are released in the reaction process. Then, one has to consider individual reactions for each charge state j of point defect X with extended defects D in the form



The subscripts m and $m + 1$ indicate the number of point defects X the extended defect comprises before and after the reaction. Clearly, such reactions have to be assumed for any size m of a specific class of extended defects (e. g. small clusters, {113} defects, faulted dislocation loops, and perfect dislocation loops) and for all these classes of coexisting extended defects.

In a system of homogeneously distributed neutral defects only, (2.84) would lead to the continuity equation

$$\frac{\partial C_X}{\partial t} = -C_X \cdot \sum_m k_{X+D_m \rightarrow} \cdot C_{D_m} + \sum_m k_{X+D_m \leftarrow} \cdot C_{D_{m+1}} \quad (2.85)$$

for the defects X. The sums arise from the interaction of point defects with extended defects in their various sizes. Including also charge states in analogy to (2.26), the respective contributions have to be summed up, too. For homogeneously distributed point defects and extended defects, one then obtains a continuity equation for the total concentration $C_X = \sum_j C_{X^j}$ of point defects X in the form

$$\begin{aligned} \frac{\partial C_X}{\partial t} &= -\frac{C_X}{\sum_j \delta_{X^j} \cdot \left(\frac{n}{n_i}\right)^{z_j}} \cdot \sum_m C_{D_m} \cdot \sum_j k_{X+D_m \rightarrow}^j \cdot \delta_{X^j} \cdot \left(\frac{n}{n_i}\right)^{z_j} \\ &\quad + \sum_m C_{D_{m+1}} \cdot \sum_j k_{X+D_m \leftarrow}^j \cdot n^{z_j} . \end{aligned} \quad (2.86)$$

For the sake of simplicity, the coexistence of different classes of extended defects was ignored but could be included straight-forwardly.

From the principle of detailed balance follows that all reaction constants are related to each other by

$$\frac{k_{X+D_m \rightarrow}^j}{k_{X+D_m \leftarrow}^j} = \frac{k_{X+D_m \rightarrow}^0}{k_{X+D_m \leftarrow}^0} \cdot \frac{n_i^{z_j}}{\delta_{X^j}}, \quad (2.87)$$

similar to (2.71), so that (2.86) can be rewritten as

$$\begin{aligned} \frac{\partial C_X}{\partial t} = & \sum_m \left(C_{D_{m+1}} \cdot \frac{k_{X+D_m \leftarrow}^0}{k_{X+D_m \rightarrow}^0} - \frac{C_X}{\sum_j \delta_{X^j} \cdot \left(\frac{n}{n_i}\right)^{z_j}} \cdot C_{D_m} \right) \\ & \cdot \sum_j k_{X+D_m \rightarrow}^j \cdot \delta_{X^j} \cdot \left(\frac{n}{n_i}\right)^{z_j}. \end{aligned} \quad (2.88)$$

Since the extended defects were assumed to be electrically neutral, one can expect that the capture radii of the intrinsic point defects at the extended defects reflect primarily the size of the extended defect and do not depend much on the charge state of the former. The dependence of the forward reaction constants $k_{X+D_m \rightarrow}^j$ on the charge state is then related to the respective diffusion coefficients of the intrinsic point defects which was discussed in Section 2.2. The ratio $k_{X+D_m \rightarrow}^0/k_{X+D_m \leftarrow}^0$ in (2.87), on the other hand, reflects the energetics of the reaction of a neutral intrinsic point defect X^0 with an extended defect of size m . It can be obtained as discussed at the end of Section 1.5.3. Assuming that the number of sites and degeneracies are equal for extended defects of size m and $m+1$, the ratio of the reaction constants can be expressed in the form

$$\frac{k_{X+D_m \rightarrow}^0}{k_{X+D_m \leftarrow}^0} = \frac{1}{\Theta_{X^0} \cdot C_{XS}} \cdot \exp\left(\frac{\Delta G_{X^0+D_m}}{k \cdot T}\right) \quad (2.89)$$

with $\Delta G_{X^0+D_m}$ standing for the reduction in the Gibbs free energy of the system associated with the reaction.

In addition to the equation (2.88) for the intrinsic point defects, a system of continuity equations results from (2.84) for each of the different sizes m of the extended defects (and, in a strict sense, for all coexisting classes of extended defects). For a system with neutral point defects only, the continuity equation is given by

$$\frac{\partial C_{D_m}}{\partial t} = C_{D_{m-1}} \cdot k_{X+D_{m-1} \rightarrow} \cdot C_X - C_{D_m} \cdot (k_{X+D_{m-1} \leftarrow} + k_{X+D_m \rightarrow} \cdot C_X) + C_{D_{m+1}} \cdot k_{X+D_m \leftarrow} \quad (2.90)$$

for homogeneously distributed defects. Including all charge states of the intrinsic point defect X , the continuity equation takes the somewhat more complicated form

$$\begin{aligned} \frac{\partial C_{D_m}}{\partial t} = & C_{D_{m-1}} \cdot \frac{C_X}{\sum_j \delta_{X^j} \cdot \left(\frac{n}{n_i}\right)^{z_j}} \cdot \sum_j k_{X+D_{m-1} \rightarrow}^j \cdot \delta_{X^j} \cdot \left(\frac{n}{n_i}\right)^{z_j} \\ & - C_{D_m} \cdot \left(\frac{k_{X+D_{m-1} \leftarrow}^0}{k_{X+D_{m-1} \rightarrow}^0} \cdot \sum_j k_{X+D_{m-1} \rightarrow}^j \cdot \delta_{X^j} \cdot \left(\frac{n}{n_i}\right)^{z_j} \right. \\ & \left. + \frac{C_X}{\sum_j \delta_{X^j} \cdot \left(\frac{n}{n_i}\right)^{z_j}} \cdot \sum_j k_{X+D_m \rightarrow}^j \cdot \delta_{X^j} \cdot \left(\frac{n}{n_i}\right)^{z_j} \right) \\ & + C_{D_{m+1}} \cdot \frac{k_{X+D_m \leftarrow}^0}{k_{X+D_m \rightarrow}^0} \cdot \sum_j k_{X+D_m \rightarrow}^j \cdot \delta_{X^j} \cdot \left(\frac{n}{n_i}\right)^{z_j}. \end{aligned} \quad (2.91)$$

Especially the simulation of transient effects on diffusion and activation of dopants requires that extended defects of various sizes are taken into consideration and their evolution with respect to time is simulated. Exchange of point defects between the extended defects leads to the growth of the energetically more favorable larger extended defects on the expense of the energetically less favorable smaller defects. This process is called coarsening or Ostwald ripening.

For special conditions, simplifications may be admissible. One such condition is when extended defects are nucleated within a short time compared to the total process time. Then, all extended defects will have approximately the same size. Growth and shrinkage of them are determined by the balance of capture and release of intrinsic point defects. Their effects on the concentration of defects X can then be written in the form

$$\frac{\partial C_X}{\partial t} = k_{BX} \cdot (C_X^* - C_X) \quad (2.92)$$

with the sink-rate constant k_{BX} given by

$$k_{BX} = C_D \cdot \frac{\sum_j k_{X+D_m \rightarrow}^j \cdot \delta_{X^j} \cdot \left(\frac{n}{n_i}\right)^{z_j}}{\sum_j \delta_{X^j} \cdot \left(\frac{n}{n_i}\right)^{z_j}}. \quad (2.93)$$

In general, k_{BX} will depend on type and size of the extended defect. The concentration

$$C_X^* = C_X^{eq} \cdot \exp\left(\frac{\Delta G}{k \cdot T}\right) \quad (2.94)$$

corresponds to that concentration of X at which capture and release processes cancel for an extended defect. $\Delta G = G_X^f - \Delta G_{X+D_m}$ is the Gibbs free energy needed to create a point defect and to transfer it to the extended defects. It will, in general, depend on type and size of the respective extended defect.

Small extended defects, as they are often found after annealing of non-amorphizing implants, are energetically unfavorable and C_X^* may exceed C_X^{eq} by orders of magnitude. In the limit of infinitely large extended defects, perfect dislocation loops are the energetically most favorable extended defects with C_X^* approaching C_X^{eq} . Highly dislocated samples are used, e. g. in metal-diffusion experiments to keep the concentrations of the intrinsic point defects near their equilibrium values [2.128, 2.570–2.573]. For a moderate density of dislocations acting as sinks for self-interstitials along their entire length, Seeger and Frank [2.574] suggested that k_{BI} takes the form

$$k_{BI} = \gamma \cdot C_D \cdot D_I \quad (2.95)$$

with C_D being the number of dislocation lines per unit area. The sink efficiency γ should be theoretically close to unity. Experimental values were obtained from the diffusion of gold in moderately dislocated silicon samples. In single-crystalline silicon, Stolwijk and Hölzl [2.570] thus obtained a value of $\gamma = 1.4$, and the data of Stolwijk et al. [2.575] indicated a value of $\gamma = 1.15$. Analyzing data of Kästner and Hesse [2.576] obtained from diffusing gold into dislocated crystalline silicon, Yang et al. [2.577] found a sink efficiency of less than 1% which improved towards unity by pre-annealing at 1200 °C for 24 hours. The analysis of their own gold-diffusion experiments in polycrystalline material resulted in a sink efficiency of $\gamma > 10\%$. Again in single-crystalline silicon, Pichaud et al. [2.578] reported values of γ between 0.7 and 0.8 for (111)-oriented FZ silicon samples and between 0.3 and 0.4 for (100)-oriented FZ samples. In CZ silicon, a significantly lower value was obtained and tentatively explained by a generation of

self-interstitials caused by the precipitation of oxygen during gold diffusion. After a thermal pre-treatment of 2 h at 1150 °C, values of γ between 0.3 and 0.4 were found again.

Since C_X^* exceeds C_X^{eq} , two important consequences follow. The first is that the concentration of the respective point defects in presence of extended intrinsic defects exceeds the equilibrium concentration. This supersaturation invokes a flux of point defects to near surfaces and into the bulk. To maintain the increased point-defect concentration, point defects are continuously transferred from the extended defects to the adjacent bulk area which causes at least the energetically less favorable extended defects to dissolve. From the dissolution of the extended defects follows the other consequence, that intrinsic extended defects are not stable. However, a complete dissolution of extended defects may exceed typical process times by far.

It is evident that the possible reactions are not restricted to self-interstitials interacting with self-interstitial agglomerates and vacancies with vacancy agglomerates. Stiebel and Pichler [2.579] have shown that reactions between vacancies and self-interstitial agglomerates and between self-interstitials and vacancy agglomerates may contribute significantly more to the removal of self-interstitials and vacancies from the system than bulk recombination. On the other hand, from the growth of self-interstitial agglomerates during electron irradiation, Fedina and Aseev [2.260] concluded that the interaction of vacancies with such defects is negligible below 960 °C.

Finally, it has to be noted that the divacancies discussed in Section 2.4.4 and many of the small self-interstitial clusters presented in Section 2.5.5 were found to be mobile. Their interactions with extended defects would have to be included by reactions complementary to (2.84).

2.7.4 Interactions with Traps

The concept of traps which are able to immobilize intrinsic point defects has been introduced by Griffin et al. [2.580] to explain the discrepancies between the various experimental determinations of the diffusion coefficient of self-interstitials. It was later generalized by Cowern [2.581] to include mobile traps.

The nature of the postulated traps is not identified unambiguously. As the most likely candidate for self-interstitials, carbon was suggested in the literature [2.77, 2.582–2.585]. It has a smaller covalent radius than silicon and provides some free volume which may be occupied by self-interstitials. However, its interaction with silicon atoms, discussed in Section 4.1, is significantly more complex than implied by the simple concept of immobile traps and trapped intrinsic point defects. And there are indications that unphysically high carbon concentrations might be needed to explain self-interstitial diffusivities obtained from OED experiments in bulk wafers consistently. A similar candidate would be boron and Jäger [2.586] suggested that the apparent depth dependence of enhanced diffusion in superlattice layers can be explained by the interaction of silicon self-interstitials with the boron in the spikes. On the other hand, by varying the peak concentration and spacing of the spikes in their superlattice layers, Gossman et al. [2.467] showed that neither the boron nor an other impurity in the spikes can be responsible for the trapping of self-interstitials. In addition, the effect was found to be independent of the growth temperature of the superlattice layers. This statement did not remain unchallenged. Johnson et al. [2.585] simulated the experiments of Gossman et al. by a kinetic Monte-Carlo approach and found that the interaction between boron spikes and self-interstitials should lead to a reduced diffusivity for the spikes with the higher boron concentrations. Such a reduction was not observed experimentally but Johnson et al. noted that the spikes with the higher boron concentration are clearly extrinsic so that Fermi-level effects might be able to compensate for the reduction due to the trapping of the self-interstitials.

Although most trapping models were proposed for self-interstitials, a similar mechanism could influence vacancy diffusion. Trapping of vacancies, most likely from an interaction with antimony, was suggested, e. g. by Mogi et al. [2.265] from the observation of a time-dependent nitridation-enhanced diffusion of antimony superlattice layers. Trapping of vacancies at interstitial oxygen was investigated by Casali et al. [2.587] as a possible reason to explain the low diffusivities of vacancies reported in some investigations. However, they found that oxygen concentrations in excess of 10^{20} cm^{-3} would be necessary to reconcile the data with theoretical investigations.

In terms of the general reaction (2.84), the concentration C_{D_m} corresponds to the concentration of free traps C_T , and the concentration $C_{D_{m+1}}$ to that of the trapped point defects C_{XT} . One then obtains differential equations for the point defects, for the traps, and for the trapped point defects. In a system of homogeneously distributed, neutral defects only, the trapping reaction would lead to the continuity equations

$$\frac{\partial C_T}{\partial t} = \frac{\partial C_X}{\partial t} = -\frac{\partial C_{XT}}{\partial t} = k_{X+T \rightarrow} \cdot C_X \cdot C_T - k_{X+T \leftarrow} \cdot C_{XT}. \quad (2.96)$$

Apart from the sign, all three equations have identical right-hand sides since the trapping of an intrinsic point defect removes also a trap but increases the number of trapped point defects. Including the charge states of the intrinsic point defects leads to

$$\begin{aligned} \frac{\partial C_T}{\partial t} &= \frac{\partial C_X}{\partial t} = -\frac{\partial C_{XT}}{\partial t} \\ &= \left(C_{XT} \cdot \frac{k_{X+T \leftarrow}^0}{k_{X+T \rightarrow}^0} - \frac{C_X}{\sum_j \delta_{X^j} \cdot \left(\frac{n}{n_i}\right)^{z_j}} \cdot C_T \right) \cdot \sum_j k_{X+T \rightarrow}^j \cdot \delta_{X^j} \cdot \left(\frac{n}{n_i}\right)^{z_j}. \end{aligned} \quad (2.97)$$

In addition to this equation, the conservation of traps has to be fulfilled resulting in

$$C_T + C_{XT} = C_T^{tot} \quad (2.98)$$

where C_T^{tot} corresponds to the total concentration of traps. This allows to eliminate the concentration of trapped point defects in (2.97) and one arrives at

$$\begin{aligned} \frac{\partial C_T}{\partial t} &= \frac{\partial C_X}{\partial t} = -\frac{\partial C_{XT}}{\partial t} \\ &= \left(C_T^{tot} \cdot \frac{k_{X+T \leftarrow}^0}{k_{X+T \rightarrow}^0} - \left(\frac{k_{X+T \leftarrow}^0}{k_{X+T \rightarrow}^0} + \frac{C_X}{\sum_j \delta_{X^j} \cdot \left(\frac{n}{n_i}\right)^{z_j}} \right) \cdot C_T \right) \\ &\quad \cdot \sum_j k_{X+T \rightarrow}^j \cdot \delta_{X^j} \cdot \left(\frac{n}{n_i}\right)^{z_j} \end{aligned} \quad (2.99)$$

In steady state, the derivatives have to vanish and the concentration of trapped point defects can be expressed as

$$C_{XT} = \frac{k_{X+T \rightarrow}^0}{k_{X+T \leftarrow}^0} \cdot \frac{C_X}{\sum_j \delta_{X^j} \cdot \left(\frac{n}{n_i}\right)^{z_j}} \cdot C_T, \quad (2.100)$$

and the concentration of trapped point defects can be obtained from (1.133). It can be expressed in the form

$$C_{XT} = \frac{\Theta_{XT}}{\Theta_{X^0} \cdot \Theta_T} \cdot \frac{C_X}{\sum_j \delta_{X^j} \cdot \left(\frac{n}{n_i}\right)^{z_j}} \cdot \frac{C_T}{C_{Si}} \cdot \exp\left(\frac{G_{XT}^B}{k \cdot T}\right) \quad (2.101)$$

with the Θ s standing again for the numbers of internal degrees of freedom of the respective defects. G_{XT}^B is the binding energy between a neutral defect X^0 and a trap T defined as the reduction in Gibbs free energy due to the trapping process. A combination of the two equations allows to express the ratio of the reaction constants as a function of the binding energy

$$\frac{k_{X+T \rightarrow}^0}{k_{X+T \leftarrow}^0} = \frac{\Theta_{XT}}{\Theta_{X^0} \cdot \Theta_T} \cdot \frac{1}{C_{Si}} \cdot \exp\left(\frac{G_{XT}^B}{k \cdot T}\right). \quad (2.102)$$

It follows from (2.101) that $(C_T^{tot} - C_T)/C_T$ can be assumed to be thermally activated in equilibrium. Unfortunately, in some analyses (e. g. [2.89]), C_T was instead assumed to be thermally activated in equilibrium. As a consequence, the fitting parameters reported do not reflect physically meaningful parameters like pair-binding energies.

For the sake of simplicity and because the state of the art did not go further, only neutral traps and trapped defects have been considered. An extension to include charge states for traps and trapped point defects leads to a replacement of C_{XT} and C_T in (2.99) by $C_{XT}/\sum_k \delta_{XT^k} \cdot (n/n_i)^{z_k}$ and $C_T/\sum_l \delta_{T^l} \cdot (n/n_i)^{z_l}$. The parameters δ_{XT^k} reflect in analogy to the similar case of the formation of mobile point-defect-impurity pairs discussed in Section 3.2.2 the binding energies of the various charge states of the trapped point defects. In addition, terms have to be added to the sum with the forward reaction constants to reflect the additional reactions between charged traps and intrinsic point defects.

For FZ material, Griffin et al. [2.580] assumed a trap concentration 100 times the equilibrium concentration of self-interstitials and postulated an even higher concentration of traps for CZ material and a very low density for epitaxially grown material. Their model also assumed implicitly that a liberation of trapped point defects is impossible. In the analysis of Law [2.89], various diffusion experiments were reviewed and two different sets of point-defect parameters were shown to describe them equally well. The total concentrations of traps obtained for the two parameter sets were 10^{18} cm^{-3} and $2 \cdot 10^{18} \text{ cm}^{-3}$. In layers grown epitaxially at low temperatures, trap concentrations of $3 \cdot 10^{16}$, $2.2 \cdot 10^{16}$, $(2.4 \pm 0.5) \cdot 10^{16}$, and $(1.7 \pm 0.4) \cdot 10^{16} \text{ cm}^{-3}$ were estimated by Cowern [2.588], Vuong et al. [2.589], Vuong et al. [2.590], and Giannazzo et al. [2.591], respectively. From the depth dependence of the implantation-enhanced diffusion of marker layers, Stolk et al. [2.466] estimated the concentration of traps to be on the order of $1.5 \cdot 10^{15} \text{ cm}^{-3}$ in their epitaxially grown material. The binding energy was estimated to be in the range from 2 to 2.3 eV. Based on the same concentration of traps, Stolk et al. [2.468] reported that a binding energy of 2.3 ± 0.3 eV is needed to reconcile their marker-layer experiments with self-interstitial data obtained from metal-diffusion investigations. Finally, reviewing their previous marker-layer experiments, Gossmann et al. [2.582] and Stolk et al. [2.583] suggested that binding energies of 2.2 to 2.5 eV are needed for a typical carbon concentration of about 10^{18} cm^{-3} to reconcile self-diffusion coefficients obtained from dopant diffusion under non-equilibrium conditions with such from metal-diffusion experiments.

2.7.5 Influence of Bulk Recombination and Traps on the Point-Defect Diffusivities Observed Experimentally

After having discussed the concepts of bulk recombination and traps, it remains to discuss their influence on the estimates of the diffusivities of the intrinsic point defects derived from experiments.

In the following, a system will be analyzed consisting of continuity equations for vacancies C_V and self-interstitials C_I (cf. Section 2.2) as well as for traps for vacancies C_{T_V} and self-interstitials C_{T_I} (cf. Section 2.7). The point-defect continuity equations are coupled by generation-loss terms resulting from bulk recombination (cf. Section 2.7). The resulting system of coupled partial differential equations can be written in the form

$$\begin{aligned} \frac{\partial C_V}{\partial t} &= \text{div} \left(D_V \cdot \text{grad} C_V - z_V \cdot D_V \cdot C_V \cdot \text{grad} \left(\frac{\Psi}{U_T} \right) \right) \\ &\quad - k_B \cdot (C_I \cdot C_V - C_I^{eq} \cdot C_V^{eq}) \\ &\quad - (k_{T_V \rightarrow} \cdot C_V + k_{T_V \leftarrow}) \cdot C_{T_V} + k_{T_V \leftarrow} \cdot C_{T_V}^{tot} \end{aligned} \quad (2.103)$$

$$\begin{aligned} \frac{\partial C_I}{\partial t} &= \text{div} \left(D_I \cdot \text{grad} C_I - z_I \cdot D_I \cdot C_I \cdot \text{grad} \left(\frac{\Psi}{U_T} \right) \right) \\ &\quad - k_B \cdot (C_I \cdot C_V - C_I^{eq} \cdot C_V^{eq}) \\ &\quad - (k_{T_I \rightarrow} \cdot C_I + k_{T_I \leftarrow}) \cdot C_{T_I} + k_{T_I \leftarrow} \cdot C_{T_I}^{tot} \end{aligned} \quad (2.104)$$

$$\frac{\partial C_{T_V}}{\partial t} = - (k_{T_V \rightarrow} \cdot C_V + k_{T_V \leftarrow}) \cdot C_{T_V} + k_{T_V \leftarrow} \cdot C_{T_V}^{tot} \quad (2.105)$$

$$\frac{\partial C_{T_I}}{\partial t} = - (k_{T_I \rightarrow} \cdot C_I + k_{T_I \leftarrow}) \cdot C_{T_I} + k_{T_I \leftarrow} \cdot C_{T_I}^{tot} \quad (2.106)$$

An analysis of this system for conditions far from equilibrium can be done only numerically. However, it can be reduced for the important case of local equilibrium for the various reactions and for point-defect concentrations showing only small deviations from equilibrium ($C_X = C_X^{eq} + \delta C_X$, $\delta C_X \ll C_X^{eq}$). Then, the concentrations C_V , C_{T_V} , and C_{T_I} can be expressed in terms of the concentration C_I of self-interstitials. Likewise, their derivatives with respect to time or space can be related to the respective derivatives via

$$\partial C_V = - \frac{C_V^{eq}}{C_I^{eq}} \cdot \partial C_I \quad (2.107)$$

$$\partial C_{T_I} = - \frac{k_{T_I \rightarrow} \cdot k_{T_I \leftarrow} \cdot C_{T_I}^{tot}}{(k_{T_I \rightarrow} \cdot C_I^{eq} + k_{T_I \leftarrow})^2} \cdot \partial C_I \quad (2.108)$$

$$\partial C_{T_V} = \frac{C_V^{eq}}{C_I^{eq}} \cdot \frac{k_{T_V \rightarrow} \cdot k_{T_V \leftarrow} \cdot C_{T_V}^{tot}}{(k_{T_V \rightarrow} \cdot C_V^{eq} + k_{T_V \leftarrow})^2} \cdot \partial C_I \quad (2.109)$$

Combining the continuity equations in (2.103) to (2.109) to $\partial(C_I - C_V - C_{T_I} + C_{T_V})/\partial t$ and substituting the derivatives of the concentrations C_V , C_{T_I} , and C_{T_V} from equations (2.107) to (2.109) results in a single continuity equation for the self-interstitial concentration

$$\frac{\partial C_I}{\partial t} = \text{div} \left(D_\delta \cdot \text{grad} C_I - z_\delta \cdot D_\delta \cdot C_I \cdot \text{grad} \left(\frac{\Psi}{U_T} \right) \right) \quad (2.110)$$

with the abbreviations

$$D_\delta = \frac{D_I \cdot C_I^{eq} + D_V \cdot C_V^{eq}}{C_I^{eq} + C_V^{eq} + \frac{k_{T_V \rightarrow} \cdot k_{T_V \leftarrow} \cdot C_V^{eq} \cdot C_I^{tot}}{(k_{T_V \rightarrow} \cdot C_V^{eq} + k_{T_V \leftarrow})^2} + \frac{k_{T_I \rightarrow} \cdot k_{T_I \leftarrow} \cdot C_I^{eq} \cdot C_I^{tot}}{(k_{T_I \rightarrow} \cdot C_I^{eq} + k_{T_I \leftarrow})^2}} \quad (2.111)$$

$$z_\delta = \frac{z_I \cdot D_I \cdot C_I^{eq} - z_V \cdot D_V \cdot C_V^{eq}}{D_I \cdot C_I^{eq} + D_V \cdot C_V^{eq}}. \quad (2.112)$$

Similarly, a continuity equation can be derived for the vacancies in the form

$$\frac{\partial C_V}{\partial t} = \text{div} \left(D_\delta \cdot \text{grad} C_V + z_\delta \cdot D_\delta \cdot C_V \cdot \text{grad} \left(\frac{\psi}{U_T} \right) \right) \quad (2.113)$$

which has the same effective diffusion coefficient but a negative effective charge state in comparison to the continuity equation (2.110) of the self-interstitials.

The concept that bulk recombination between self-interstitials and vacancies may effectively reduce the diffusion coefficient of the former has been introduced by Tan and Gösele [2.64] to explain the slow effective diffusion coefficient observed in backside-oxidation experiments. The concept requires that the equilibrium concentration of vacancies exceeds that of the self-interstitials by far. Ignoring traps for the moment and calling into mind that the self-diffusion coefficients are on the same order of magnitude at elevated temperatures, the effective diffusion coefficient of the self-interstitials D_δ will then be on the order of the diffusion coefficient of the vacancies $D_\delta \approx D_V$ and independent of the diffusion coefficient of the self-interstitials. Similarly, it was suggested in other analyses that such a mechanism may explain the low diffusion coefficients of self-interstitials obtained generally from dopant diffusion under non-equilibrium conditions [2.261, 2.592]. It should be noted, however, that the *ab-initio* calculations of point-defect properties and evidence from crystal growth agree that the equilibrium concentration of the vacancies should exceed that of the self-interstitials only slightly. Thus, low effective diffusivities of self-interstitials can hardly be expected to result from their recombination with vacancies.

Traps, as introduced by Griffin et al. [2.580], may additionally reduce the effective diffusion coefficient. The nature of possible traps is not entirely clear. Carbon, as discussed in Sections 2.7.4 and 4.1, has the ability to trap self-interstitials and may be a candidate. However, it has not been demonstrated that the slow effective self-interstitial diffusivity extracted from backside-oxidation experiments can be really explained on the basis of such a model.

It follows as an important conclusion that experiments under near-equilibrium conditions may lead to artificially small estimates of point-defect diffusion coefficients. Such situations are typical for oxidation-enhanced diffusion, especially backside-oxidation experiments.

The situation changes when the self-interstitials are in extreme supersaturation. Then, assuming again local equilibrium between the various reactions, equations (2.107) to (2.109) have to be replaced by

$$\partial C_V = -\frac{C_I^{eq} \cdot C_V^{eq}}{C_I^2} \cdot \partial C_I \quad (2.114)$$

$$\partial C_{T_I} = -\frac{k_{T_I \rightarrow} \cdot k_{T_I \leftarrow} \cdot C_{T_I}^{tot}}{(k_{T_I \rightarrow} \cdot C_I + k_{T_I \leftarrow})^2} \cdot \partial C_I \quad (2.115)$$

$$\partial C_{T_V} = \frac{C_I^{eq} \cdot C_V^{eq}}{C_I^2} \cdot \frac{k_{T_V \rightarrow} \cdot k_{T_V \leftarrow} \cdot C_{T_V}^{tot}}{\left(k_{T_V \rightarrow} \cdot \frac{C_I^{eq} \cdot C_V^{eq}}{C_I^2} + k_{T_V \leftarrow} \right)^2} \cdot \partial C_I \quad (2.116)$$

In analogy to (2.110), the system behavior condenses to a diffusion equation for the self-interstitials in the form

$$\begin{aligned} & \left(1 + \frac{C_I^{eq} \cdot C_V^{eq}}{C_I^2} + \frac{k_{T_I \rightarrow} \cdot k_{T_I \leftarrow} \cdot C_{T_I}^{tot}}{(k_{T_I \rightarrow} \cdot C_I + k_{T_I \leftarrow})^2} + \frac{C_I^{eq} \cdot C_V^{eq}}{C_I^2} \cdot \frac{k_{T_V \rightarrow} \cdot k_{T_V \leftarrow} \cdot C_{T_V}^{tot}}{\left(k_{T_V \rightarrow} \cdot \frac{C_I^{eq} \cdot C_V^{eq}}{C_I^2} + k_{T_V \leftarrow} \right)^2} \right) \cdot \frac{\partial C_I}{\partial t} \\ &= \text{div} \left(\left(D_I + D_V \cdot \frac{C_I^{eq} \cdot C_V^{eq}}{C_I^2} \right) \cdot \text{grad} C_I \right. \\ &\quad \left. - \left(z_I \cdot D_I \cdot C_I - z_V \cdot D_V \cdot C_I^{eq} \cdot \frac{C_V^{eq}}{C_I^2} \right) \cdot \text{grad} \left(\frac{\psi}{U_T} \right) \right) \end{aligned} \quad (2.117)$$

For a sufficiently high oversaturation of self-interstitials, all terms with C_I in the denominator can be neglected and (2.117) reduces to

$$\frac{\partial C_I}{\partial t} = \text{div} \left(D_I \cdot \text{grad} C_I - z_I \cdot D_I \cdot C_I \cdot \text{grad} \left(\frac{\psi}{U_T} \right) \right). \quad (2.118)$$

Evidently, in a set-up with a high supersaturation of self-interstitials, the diffusion coefficient of the self-interstitials could be determined. In real experiments, the extracted effective diffusion coefficient can be expected to be in the interval given by D_δ from equation (2.111) and the real value of the diffusion coefficient of the self-interstitials D_I . This dependence on the experimental technique might be the reason for the large scatter in the experimentally determined values for the equilibrium concentration and the diffusion coefficient of self-interstitials (see Sections 2.5.2 and 2.5.3). Similar considerations hold for vacancies.

2.7.6 Generation of Point Defects by Chemical Processes in the Bulk

An important source of point defects are chemical reactions, especially phase transformations, in the bulk. Many of them are associated with an increase in molar volume which has to be accommodated either by the absorption of vacancies or by the emission of self-interstitials into the adjacent silicon lattice. The best-studied system of this kind is the precipitation of oxygen in silicon. Already early reports indicated that interstitial-type extended defects grow during thermal treatment of CZ wafers [2.593, 2.594]. The phenomenon was explained quantitatively by Hu [2.595] and oxygen precipitation as a source of self-interstitials was used in the studies of Ahn et al. [2.596] and Rogers and Massoud [2.429]. Similar to oxygen, Bourret and Schröter [2.597] found that the precipitation of phosphorus is an efficient source of self-interstitials. The generation of self-interstitials associated with the clustering of arsenic will be discussed in Section 5.9.4. Precipitation of carbon, on the other hand, is an example for a phase transformation associated with a decrease in molar volume. In consequence, it is associated with an absorption of self-interstitials and eventually the emission of vacancies.

2.8 Surface Recombination and Surface Processes

Although the equilibrium concentration of intrinsic point defects is a bulk property, it requires the diffusion of vacancies and self-interstitial to kinks at the surface to establish it. Attachment of intrinsic point defects at surface kinks, called surface recombination, is of special importance when the point-defect concentrations in the bulk are out of equilibrium, e. g. during annealing

processes after ion implantation. The mathematical description of such processes is usually based on some phenomenological models. They and some common simplifications are outlined in Section 2.8.1. The process itself and our knowledge from experiments is discussed in Section 2.8.2. In addition, the segregation of self-interstitials into capping silicon-dioxide layers may be of importance. The respective concepts are presented in Section 2.8.3. Finally, in Section 2.8.4, surface processes are summarized which cause the concentrations of the intrinsic point defects to deviate from their equilibrium values.

2.8.1 Phenomenological Interface and Boundary Conditions

Apart from recombination in the bulk, point defects can be annihilated individually at the surfaces of crystalline silicon or at its interfaces to covering layers, e.g. silicon dioxide. This recombination could be described by assuming that the point defects react within a finite layer at the surface according to (2.92). From the mathematical as well as from the physical point of view, a description in the form of an interface or boundary condition for the diffusion equations introduced in Section 2.2 seems more expedient. Even when recombination within a definite layer is assumed, boundary conditions for the diffusion equations are required. Of course, interface and boundary conditions have to be provided for each of the diffusion equations for the various charge states (2.41) to (2.45).

The most frequently used interface or boundary condition results from the assumption that the point-defect concentrations at the boundary or interface correspond to their equilibrium values

$$C_{X^j} = C_{X^j}^{eq}. \quad (2.119)$$

Since the total concentration is given as the sum of the concentrations of the various charge states, a condition for the total concentration at the boundary results in the form

$$C_X = \sum_j C_{X^j} = \sum_j C_{X^j}^{eq} = C_X^{eq}. \quad (2.120)$$

Such a boundary condition is usually called Dirichlet boundary condition. It is assumed to represent the idealization of a free surface or the interface between silicon and silicon dioxide [2.28].

A second frequently met interface or boundary condition comes from the assumption that there is no current of the respective species through the boundary

$$J_{X^j} \bullet \vec{n} = 0. \quad (2.121)$$

Here, J_{X^j} denotes the current of point defects X in charge state j according to (2.40). The dot between J_{X^j} and the normal vector \vec{n} indicates the scalar (dot, inner) product of the two vectors. The normal vector \vec{n} is perpendicular to the surface with the positive direction pointing out of the volume under consideration. The boundary condition for the total current (2.53) is similarly given by

$$J_X \bullet \vec{n} = 0 \quad (2.122)$$

since (2.121) holds for each of the individual currents. A boundary condition like that is usually referred to as Neumann boundary condition. In various investigations, it was found that an oversaturation of self-interstitials caused by oxygen precipitation, backside oxidation, or se-

lective oxidation in a spatially separated region causes an increased growth of stacking faults [2.429, 2.462, 2.595, 2.598], increased diffusion enhancement of phosphorus and boron [2.599], and increased diffusion retardation of antimony [2.600] below nitride-covered surfaces in comparison to oxide-covered surfaces. Such observations were taken as an indication that a silicon/silicon nitride interface is a less effective sink for point defects than a silicon/silicon dioxide interface with a Neumann boundary condition as its idealization. It should be remarked at this point that this assumption is very problematic even as an idealization. Experimental evidence discussed below in Section 2.8.4 indicates that nitride layers grown or deposited on bare silicon lead actively to an enhancement of the vacancy concentration.

A more realistic description can be obtained by a first-order model assuming that the current flowing perpendicular to the interface is a homogeneous function of the excess of the respective point defects

$$J_{X^j} \bullet \vec{n} = k_{X^j} \cdot (C_{X^j} - C_{X^j}^{eq}) . \quad (2.123)$$

The parameter k_{X^j} in this generalized boundary condition has the units of a velocity and is, therefore, customarily called surface recombination velocity. A boundary condition for the total current (2.53) is obtained with the help of (2.27) to (2.32) in the form

$$J_X \bullet \vec{n} = k_X \cdot (C_X - C_X^{eq}) \quad (2.124)$$

with the Fermi-level-dependent effective surface recombination velocity

$$k_X = \frac{\sum_j k_{X^j} \cdot \delta_{X^j} \cdot (n/n_i)^{z_j}}{\sum_j \delta_{X^j} \cdot (n/n_i)^{z_j}} . \quad (2.125)$$

Introducing the current of defects X from (2.53) results in a boundary condition for the oversaturation of point defects C_X/C_X^{eq} determined by only one parameter k_X/D_X

$$\text{grad} \left(\frac{C_X}{C_X^{eq}} \right) \bullet \vec{n} - z_X \cdot \frac{C_X}{C_X^{eq}} \cdot \text{grad} \left(\frac{\Psi}{U_T} \right) \bullet \vec{n} = - \frac{k_X}{D_X} \cdot \left(\frac{C_X}{C_X^{eq}} - 1 \right) . \quad (2.126)$$

It will be shown in Section 3.4 that the diffusivity of impurities increases with the oversaturation of the point defects. Equation (2.126) determines their value near the boundary. Thus, when parameters are estimated from dopant diffusion, physical significance should be attributed to k_X/D_X rather than to k_X , especially since the diffusion coefficients of vacancies and self-interstitials adopted may differ by orders of magnitude from investigation to investigation.

In a one-dimensional, intrinsic system, the term k_X/D_X , or rather its inverse, can be interpreted in a simple way when one keeps in mind that the extrapolation of the concentration of intrinsic point defects with a concentration $C_X(x=0)$ at the surface and a gradient of

$$\frac{\partial C_X}{\partial x} = \frac{k_X}{D_X} \cdot (C_X(x=0) - C_X^{eq}) \quad (2.127)$$

to negative values of x assumes a value of $C_X = C_X^{eq}$ at a depth of $x = -D_X/k_X$. Thus, it appears as if the Dirichlet boundary condition (2.120) would be applied at a distance D_X/k_X before the interface.

2.8.2 Surface Reconstruction

Pair-wise generation of self-interstitials and vacancies, as discussed in Section 2.7.1, is not able to establish equilibrium conditions in a crystal. The process generally considered to be required is usually called “surface reconstruction” or “surface recombination” and implies that intrinsic point defects are transferred to kinks at the “free surface.” In reality, except probably during annealing in hydrogen, the free surface of silicon is an abstraction. Because of its high reactivity, interfacial oxide layers form even at room temperature. The presence of layers may significantly influence the recombination behavior of the intrinsic point defects and, as in the case of nitride layers, even the concentrations of the intrinsic point defects in steady state. Nevertheless, mainly because a free surface is not feasible, oxide-covered surfaces are usually taken as a reference point and assumed to be close in their properties to a free surface.

Assuming a diffusion-limited annihilation of self-interstitials at kinks, Hu [2.601] derived the expression

$$k_I = \pi \cdot a^R \cdot \rho_s \cdot D_I \quad (2.128)$$

for the surface recombination velocity of self-interstitials. Assuming the recombination radius a^R to be approximately 3.85 Å and the density of surface kinks ρ_s to be about 10^{12} cm^{-2} , Hu estimated k_I/D_I to be on the order of 10^5 cm^{-1} . Similarly, taking $a^R \sim 3 \text{ Å}$ and $\rho_s \sim 10^{13} \text{ cm}^{-2}$, Hamasaki [2.602] estimated k_I/D_I to be on the order of 10^6 cm^{-1} . Both values are comparable to the largest values obtained from experiments.

Since trapping of vacancies can be assumed to occur also at kinks, (2.128) should hold for vacancies, too. A comparison of the k/D values for vacancies and self-interstitials arises from the work of Aseev and coworkers [2.603, 2.604]. They observed by *in-situ* electron-microscopy investigations that self-interstitial clusters form in narrow regions below the surface. This effect was explained by an orders of magnitude higher recombination efficiency of vacancies than of self-interstitials at Si/SiO₂ interfaces. It has to be mentioned, though, that there is no compelling evidence from independent experiments that self-interstitials should recombine less effectively at Si/SiO₂ interfaces than vacancies.

As a superposition of the contributions of various charge states, k_X will depend on the Fermi level. This leads to the already mentioned problems in assigning an activation energy. However, in a first-order model, one can assume that no Coulombic attraction or repulsion exists so that the recombination radius in (2.128) is independent of the charge state of the respective defects. Then, after substituting (2.128) into (2.125), the factors $\pi \cdot a^R \cdot \rho_s$ can be written before the sum so that the resulting quotient of the sums is identical to the diffusion coefficient as given in (2.54). The effective surface-recombination constant of defects X has then the same structure as (2.128) and k_X/D_X should be at most a weak function of the Fermi level.

From oxidation and nitridation experiments in intrinsic silicon, various values were obtained for k_V , k_V/D_V , k_I , and k_I/D_I at silicon/silicon dioxide interfaces and reported in the literature. In addition, some estimates for k_I and k_I/D_I at silicon/silicon nitride and silicon/gold interfaces are available. For both, it was concluded that interface recombination is less effective than at a silicon/silicon dioxide interface. All these values are summarized in Table 2.18 for the recombination of vacancies, and in Table 2.19 for the recombination of self-interstitials. For graphical representations, see Figures 2.22 to 2.25.

Table 2.18: Parameters reported for the recombination of vacancies at Si/SiO₂ interfaces.

	k_V Prefactor (cm/s)	E_A (eV)	k_V/D_V Prefactor (cm ⁻¹)	E_A (eV)	Temperature range (°C)	Ref.
Shin & Kim ⁸			1.3·10 ⁴		1000	[2.605]
Brabec et al.	8·10 ⁻⁸		1.78		1100	[2.86]
Griffin	1.25·10 ⁴	3.11	0.176	-0.66	950–1100	[2.87]
Law	1.37·10 ³	2.19	1.37·10 ⁴	0.19	900–1100	[2.89]
Law	1.12·10 ⁴	2.48	1.77	-0.81	900–1100	[2.89]
Park & Law	418	2.47	32.2	-0.45	800–1100	[2.91]
Shimizu et al.	8.9·10 ⁻¹⁰		0.217		1000	[2.263]
Crowder et al.	1.68·10 ⁻⁷	0.682	2.65·10 ⁻¹¹	-2.61	950–1100	[2.606]
Rücker et al.			1.43·10 ⁵		900	[2.607]

Table 2.19: Parameters reported for the recombination of self-interstitials at Si/SiO₂, Si/Si₃N₄, and Si/Au interfaces.

	k_I Prefactor (cm/s)	E_A (eV)	k_I/D_I Prefactor (cm ⁻¹)	E_A (eV)	Temperature range (°C)	Ref.
Si/SiO ₂ interfaces						
Hill et al.	1.25·10 ⁻⁴ – 1.25·10 ⁻³				1245	[2.446]
Taniguchi et al.	460 ⁹	2.4	5.35·10 ⁻⁴	-1.6	1100–1200	[2.114]
Shin & Kim			7000 ± 3000		900–1100	[2.608]
Scheid & Chenevier	2.5·10 ⁻⁶		1250		1100	[2.448]
Collard & Taniguchi	0.86	1.8	10 ⁻⁶	-2.2	892–992	[2.609]
Rafferty et al.	2·10 ⁻³		4000		1100	[2.610]
Griffin & Plummer	2·10 ⁻⁶		400		1100	[2.451]
Ahn et al.	3·10 ⁻⁷		300		1100	[2.454]
Griffin & Plummer	2.2·10 ⁻⁷ 2.0·10 ⁻⁷ 6.0·10 ⁻⁸		4500 1900 117		900 1000 1100	[2.452]
Brabec et al.	3.6·10 ⁻⁷		137		1100	[2.86]
Kump & Dutton	6.01·10 ⁻¹³	-1.58	1.65·10 ⁻⁹	-3.16	892–1092	[2.455]
Griffin	2.87·10 ⁶	3.45	66.3	-0.21	900–1100	[2.87]
Giles	10 ⁻³		5·10 ⁵		800	[2.611]
Rogers & Massoud	2·10 ⁻⁶		447		1125	[2.462]
Rogers & Massoud	3·10 ⁻⁴		974		1125	[2.429]
Law	2.89·10 ⁻²	0.834	4.82·10 ⁻⁵	-1.606	900–1100	[2.89]
Law	1.204·10 ⁻³	0.44	1.17·10 ⁻⁹	-2.78	900–1100	[2.89]
Shibata et al.	2.4·10 ⁻⁶ 2.7·10 ⁻⁵ 2.5·10 ⁻⁴		4.9·10 ³ 1.5·10 ⁴ 4.3·10 ⁴		1050 1100 1150	[2.612]

⁸The experiment was based on the enhanced diffusion of phosphorus under intrinsic conditions caused by high-concentration phosphorus diffusion. Contemporary models for phosphorus diffusion in the regime of high concentrations predict a generation of self-interstitials. Then, the value of k_V/D_V reported by Shin & Kim should be attributed rather to self-interstitials

⁹In the original work of Taniguchi, the prefactor has the value 0.046. According to reference 30 in the paper of Ahn et al. [2.454], this value should read 460.

	k_I Prefactor (cm/s)	E_A (eV)	k_I/D_I Prefactor (cm $^{-1}$)	E_A (eV)	Temperature range (°C)	Ref.
Park & Law	$4.65 \cdot 10^5$	2.35	775	-0.09	800–1100	[2.91]
Jacobs et al.	$2 \cdot 10^{-4}$		$1.32 \cdot 10^4$		900	[2.613]
van Dort et al.	$7 \cdot 10^{-4}$				900	[2.614]
Crowder et al.			$8.18 \cdot 10^4$		850	[2.615]
			$6.89 \cdot 10^4$		950	
Agarwal & Dunham	$2.3 \cdot 10^{-4}$		343		1100	[2.616]
	$4.9 \cdot 10^{-4}$		730			
van Dort et al.			$6 \cdot 10^4$		900	[2.617]
Crowder et al.			$2.4 \cdot 10^{-3}$	-1.45	750–850	[2.618]
			$4.73 \cdot 10^{-3}$	-1.34	750–1200	
van Dort et al.			$6 \cdot 10^4$		900	[2.619]
Lim et al.			10^5		880	[2.620]
Agarwal & Dunham	$4.2 \cdot 10^4$	1.9	824	0.13	900–1100	[2.592]
Chao et al.	$2 \cdot 10^{-3}$		$1.43 \cdot 10^7$		750	[2.435]
Agarwal et al.			$> 10^6$		810, 950, 1050	[2.621]
Colombeau et al.			$3.3 \cdot 10^6$		950	[2.622]
Colombeau et al.			$5 \cdot 10^5$		815	[2.623]
Shauly et al.	$-1.26 \cdot 10^{-11}$	1.65	$1.19 \cdot 10^{-7}$	-2.97	800–950	[2.471]
Mirabella et al.			$5 \cdot 10^5 (> 2.5 \cdot 10^5)$		800	[2.624]
Giannazzo et al.			$1.67 \cdot 10^6$		800	[2.591]
Si/Si ₃ N ₄ interfaces						
Rafferty et al.	$6 \cdot 10^{-4}$		1200		1100	[2.610]
Griffin & Plummer	$6 \cdot 10^{-7}$		120		1100	[2.451]
Rogers & Massoud	$7 \cdot 10^{-7}$		187		1125	[2.462]
Rogers & Massoud	$6 \cdot 10^{-5}$		190		1125	[2.429]
Si/Au interfaces						
Hill et al.	$8.3 \cdot 10^{-6} - 8.3 \cdot 10^{-5}$		83		[2.446]	
Stolwijk et al.	0.0195		$1.72 \cdot 10^3$		1050	[2.625]
	0.0658		$4.19 \cdot 10^3$		1119	

It is evident that the agreement is neither good for the values of k_X nor for the values of k_X/D_X reported in the literature. This may be explained in part by inherent uncertainties of such analyses. A typical example is the work of Law [2.89] who found two completely different data sets to fit a large number of experimental data equally well. Relatively reliable should be the estimates of k_I/D_I from the kinetics of extended defects [2.621–2.623] since the depths of the extended defects studied is on the same order of magnitude as D_I/k_I . In addition, as suggested by Boussey-Said et al. [2.626], Crowder et al. [2.627], and Pindl et al. [2.628] from their study of stacking-fault growth and OED in SOI structures, surface recombination may depend strongly on the morphology of silicon/silicon dioxide interfaces. But there are also competing processes which might be mistakenly interpreted in terms of a recombination of single point defects. These are especially the bimolecular annihilation discussed below, and the segregation of self-interstitials into oxides discussed in the next section.

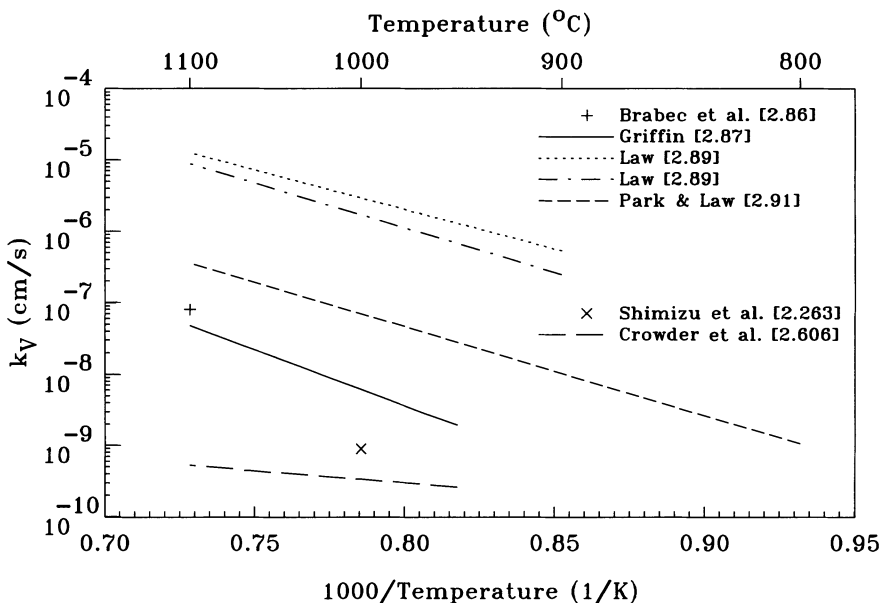


Figure 2.22: Recombination constant for vacancies at a silicon/silicon dioxide interface.

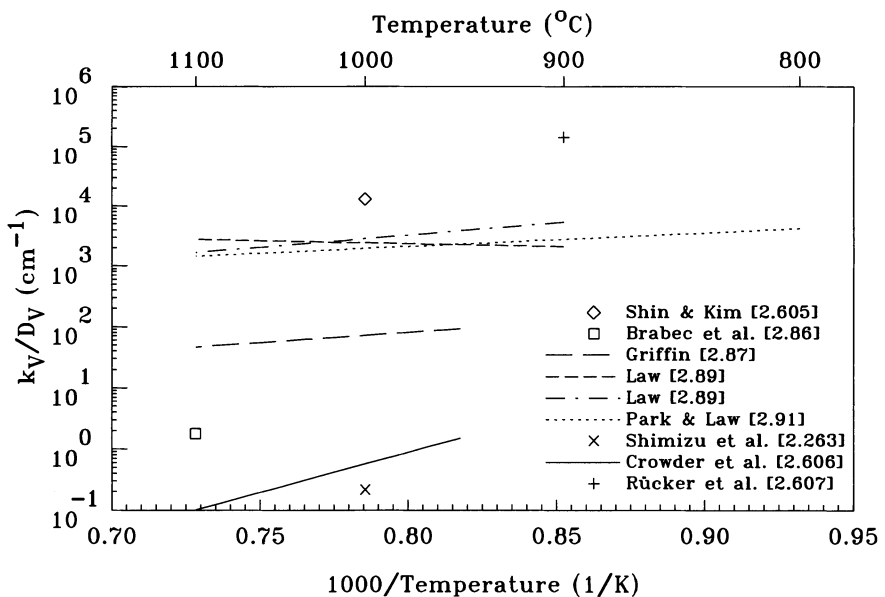


Figure 2.23: Quotient of surface-recombination constant and diffusion coefficient for vacancies at a silicon/silicon dioxide interface.

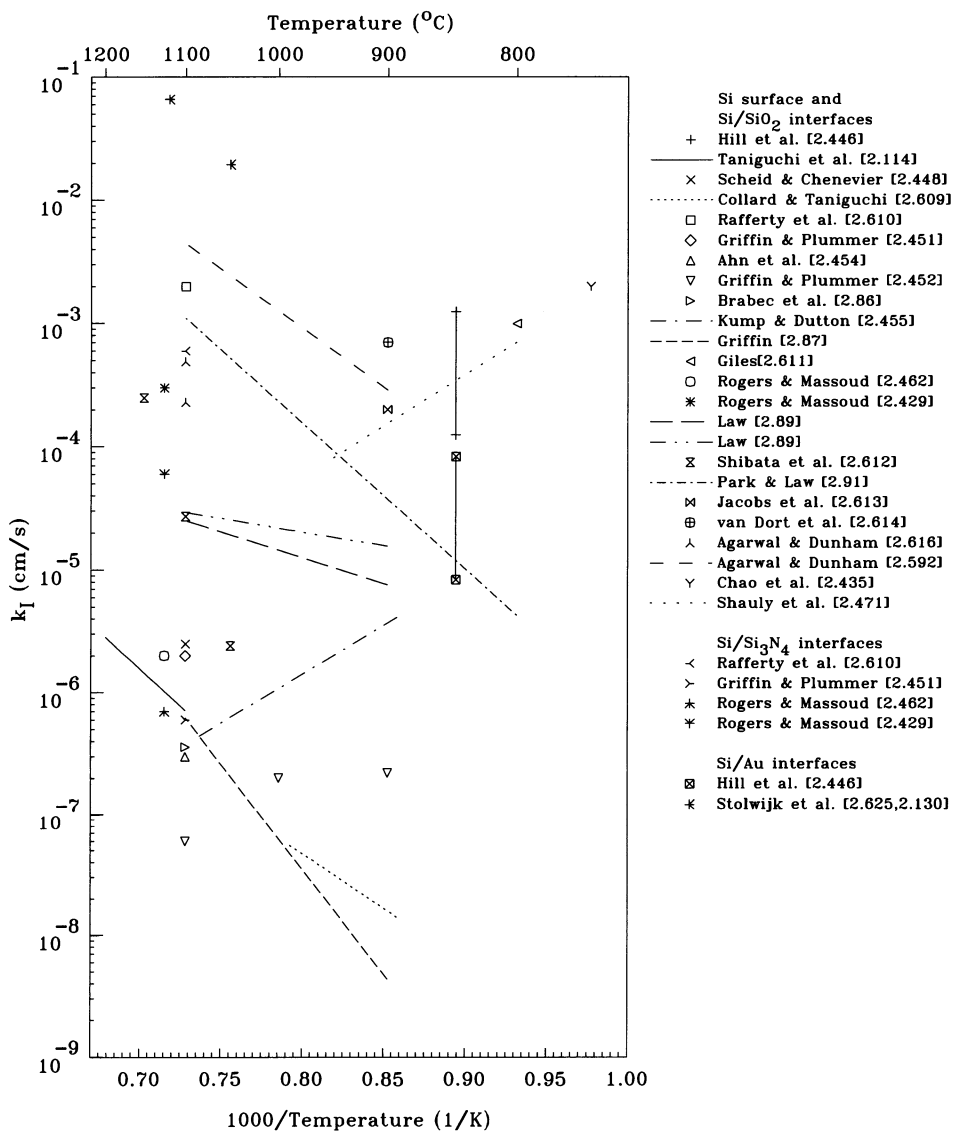


Figure 2.24: Recombination constant for self-interstitials at silicon/silicon dioxide, silicon/silicon nitride, and silicon/gold interfaces.

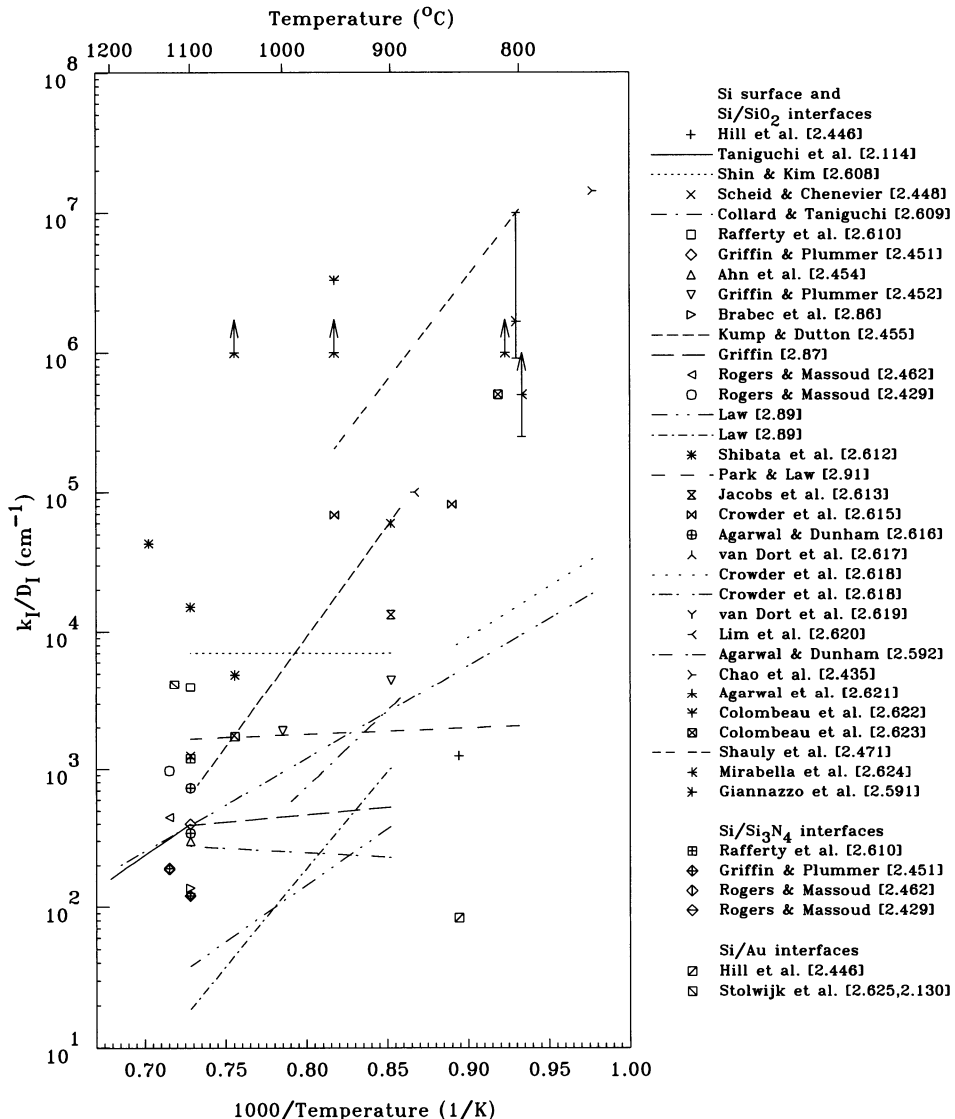


Figure 2.25: Quotient of surface-recombination constant and diffusion coefficient for self-interstitials at silicon/silicon dioxide, silicon/silicon nitride, and silicon/gold interfaces.

As an alternative to surface recombination of self-interstitials via (2.124), Hu [2.629] suggested that the structure of the {100} silicon surface favors the annihilation of self-interstitials in pairs. This leads to a complementary recombination term proportional to the square of the point-defect concentrations

$$J_X \bullet \vec{n} \propto \left(C_X^2 - C_X^{eq2} \right). \quad (2.129)$$

The same functional relationship was obtained by Law et al. [2.630] who suggested the surface recombination of di-interstitials which they assumed to be in equilibrium with the self-interstitials. The application of this model allowed them to consistently explain apparently different surface-recombination constants needed to model transient-enhanced diffusion during oxidation enhanced diffusion and post-implantation treatments. With the same intension, Hane et al. [2.488] suggested the annihilation of highly mobile di-interstitials at the surface as an explanation. On the other hand, based on kinetic Monte-Carlo simulations, Martin-Bragado et al. [2.493] found that a dominant recombination of di-interstitials is incompatible with other experimental and theoretical constraints. The molecular-dynamics simulations reported also indicated that self-interstitials and di-interstitials react both without problems with a free surface, in contrast to the initial concept of Hu [2.629].

In various investigations, beginning with the work of Ahn et al. [2.454], Griffin and Plummer [2.631], and Law [2.89], it was assumed that the recombination of point defects is more effective at oxidizing interfaces than at stationary ones. While this is not impossible, it has to be mentioned that effects like segregation of self-interstitials into the growing oxide layers or other competing mechanism were not taken into consideration in these investigations so that conclusive evidence is still lacking.

2.8.3 Segregation of Self-Interstitials into Oxide Layers

Inspired by the large volume increase associated with the oxidation of silicon, Tiller [2.632] suggested that it is mediated in part by an injection of silicon atoms into the oxide and, as self-interstitials, into the silicon. The supersaturation of self-interstitials in the silicon is then determined by their segregation coefficient between silicon and silicon dioxide. This idea was further developed by Lin et al. [2.633] but, in order to explain the orientation dependence of OED, an anisotropic segregation coefficient had to be introduced in contradiction to the expectations from thermodynamics. Segregation of silicon atoms into the oxide is also an important element of the OED models of Dunham and Plummer [2.634–2.636], Budil et al. [2.85], and Taniguchi and coworkers [2.637, 2.638].

Based on the experience with oxidizing interfaces, the segregation of self-interstitials across the interface into silicon dioxide was also assumed at non-oxidizing interfaces by Ahn et al. [2.639], Dunham [2.640], Guillemot et al. [2.641], Tsamis et al. [2.642, 2.643], Agarwal and Dunham [2.592, 2.616], and Hane et al. [2.644] to explain a variety of diffusion effects. Among them are the retarded diffusion during annealing in inert ambients, time-dependent surface recombination velocities, and apparent differences between surface recombination velocities needed to simulate OED and post-implantation anneals. The question whether silicon diffuses in the oxide as atomic silicon or as SiO has been addressed but seems of minor significance. A core element of all models is that the segregation coefficient $m_{SiO_2/Si}$ is very large so that the concentration of mobile silicon atoms in the oxide exceeds the concentration of self-interstitials in the silicon by orders of magnitude. Diffusion of the silicon atoms in the oxide, on the other hand, is very slow and characterized by an activation energy which exceeds 4.0 eV. Therefore, it was suggested that the importance of segregation of self-interstitials into oxide layers increases with temperature.

Clear experimental evidence for segregation of self-interstitials into an oxide layer and diffusion through it was reported by Tsoukalas et al. [2.645]. They used a structure in which a layer with oxidation stacking faults (OSF) was separated from the bulk by a thick SIMOX layer, and from a silicon layer on top by an oxide of 10 nm thickness. During oxidation of the top silicon layer, in contrast to not oxidized control samples, the OSFs in the buried oxide layer were found to grow, giving evidence of self-interstitials originating from the surface oxidation which penetrated the 10 nm oxide layer.

2.8.4 Generation of Intrinsic Point Defects by Chemical Reactions at Interfaces

During processes at elevated temperatures, non-inert gas molecules may react with silicon wafers or with other layers covering them. The most typical process of this kind is the thermal oxidation of silicon. Already early it was found that such processes may have a significant influence on the concentrations of the intrinsic point defects in silicon and, via them, on dopant diffusion. In case of ambient gases like nitrogen and argon, or vacuum anneals, no such influences are expected intuitively. However, it will be shown that even these ambients may cause diffusion phenomena which are not in accord with equilibrium conditions, especially when bare silicon surfaces or silicon surfaces covered only with thin oxides are involved.

The first reports on the influence of chemical reactions on dopant diffusion date back to the time when (100)-oriented wafers were investigated as replacement for the then customary (111)-oriented ones. In such studies, diffusion was found to be anisotropic [2.646–2.651]. In some of these investigations the usually oxygen-containing atmosphere was replaced by an inert gas and it was found that the diffusion coefficients agreed in wafers of both orientations [2.647, 2.649, 2.650]. What was actually observed for the first time was the enhanced diffusion of dopants during annealing in an oxidizing atmosphere, termed later oxidation-enhanced diffusion. Years later, under the same conditions under which the diffusion of boron and phosphorus was found to be enhanced, retarded diffusion of antimony was reported by Mizuo and Higuchi [2.569] and Antoniadis and Moskowitz [2.552]. The current understanding of oxidation-enhanced and oxidation-retarded diffusion is based on the suggestions of Dobson [2.652] and Hu [2.601] that, during oxidation, to accommodate the volume increase of the oxidized silicon atoms at the interface, a small fraction of unoxidized silicon atoms enter the bulk as self-interstitials. The injection of self-interstitials during oxidation was confirmed experimentally by the observed growth of stacking faults [2.653–2.658] which were identified to be of extrinsic nature, i.e. agglomerates of self-interstitials [2.655, 2.656, 2.658, 2.659].

While most kinetically motivated models for the effects of oxide growth on the intrinsic point defects assume an injection of point defects proportional to the growth rate of the oxide in association with surface reconstruction or diffusion of silicon atoms into the oxide, discrepancies still exist with respect to the boundary or interface conditions for the vacancies. In early publications, Antoniadis [2.660] assumed that the oxidation process would consume vacancies so that the point-defect concentrations would conform to $C_I \cdot C_V < C_I^{eq} \cdot C_V^{eq}$. Later, in their analysis of the diffusion of antimony under oxidizing conditions, Antoniadis and Moskowitz [2.552] suggested that the surface would act as a source of vacancies and balance bulk recombination. In contrast, Hu [2.661] argued that individual recombination and generation of vacancies at oxidized interfaces would be unaffected by the oxidation. He suggested a mixed boundary condition similar to (2.126) for the vacancies and showed that $C_I \cdot C_V > C_I^{eq} \cdot C_V^{eq}$ has then to be expected. Boundary conditions of this kind are used in virtually all two-dimensional numerical process-simulation programs with recombination velocities which are either constants or which depend on the oxidation rate. Based on thermodynamic considerations, Budil et al. [2.85]

suggested that the equilibrium concentrations of self-interstitials and vacancies change due to the oxidation process. They used mixed boundary conditions similar to (2.126) with a time-dependent value for $C_I^{eq}(t)$, and $C_V^{eq}(t)$ given by $C_V^{eq}(t) = C_F^2 / C_I^{eq}(t)$ with C_F^2 given by the product $C_F^2 = C_I^{eq} \cdot C_V^{eq}$ of the equilibrium concentrations of the intrinsic point defects under non-oxidizing conditions.

But not only an injection of self-interstitials was observed during oxidation. For long oxidation times at high temperatures, retarded diffusion of the interstitial-diffusers boron, phosphorus, aluminum, and gallium was observed in (111)-oriented wafers [2.662–2.665]. Under similar conditions, the diffusion of antimony was found to be enhanced [2.666]. These effects may be associated with the segregation of self-interstitials into the oxide as it was suggested in the models of Taniguchi et al. [2.637] and Dunham and Jeng [2.667]. As discussed in Section 2.8.3 and below, segregation of self-interstitials into silicon dioxide was observed also during annealing in inert ambient.

Similar effects as during oxidation were observed during nitridation of oxides in NH_3 . Such processes resulted in the growth of stacking faults [2.668, 2.669], in enhanced diffusion of phosphorus and boron [2.669–2.672], and in the retarded diffusion of antimony [2.669, 2.670]. Based on the observation of an oxygen-rich layer at the interface between the nitrided oxide and the silicon bulk it was concluded that an injection of self-interstitials originates from the re-oxidation of the silicon/silicon dioxide interface by oxygen liberated in the bulk of the nitrided oxide by a slow nitridation reaction [2.673, 2.674].

Nitridation of bare silicon surfaces, on the other hand, was found to increase the shrinkage rate of stacking faults [2.668, 2.669], to decrease the diffusion of boron and phosphorus [2.669, 2.670, 2.675], and to enhance the diffusion of antimony [2.669, 2.670, 2.675]. The mechanism associated with this apparent introduction of vacancies is not obvious. At least, it is not associated with the growth of the nitride layer since nitride growth decreases rapidly and almost stops after minutes at usual process temperatures with a thickness of 3 to 5 nm while the effects on dopant diffusion last for hours. In addition, it was shown by Mizuo et al. [2.669], Ahn et al. [2.676], and Osada et al. [2.677] that even deposited silicon-nitride films lead to similar diffusion effects as thermally grown ones.

In contrast to oxygen-containing ambients and NH_3 , N_2 is usually considered inert. But there are reports of nitrides observed to form on the silicon surface at temperatures above 1000 °C [2.678–2.681]. This nitride growth gives rise to expectations that there might be an influence on the concentrations of the intrinsic point defects associated. Indeed, a retarded diffusion of boron and phosphorus and an enhanced diffusion of antimony under such conditions were observed by Mizuo et al. [2.669] and Kook and Jaccodine [2.682] at 1100 °C. Direct evidence for an introduction of vacancies was obtained also by Jacob et al. [2.683] who observed by platinum diffusion at low temperatures that the vacancy concentrations after annealing at 1200 and 1250 °C has a slightly U-shaped form and increases, within the experimental error of the analysis, continuously with time. Despite the fact that the observed diffusion effects are correlated with the formation of a nitride layer, the mechanism is not clear and it may well be that the mechanism described in the next paragraph is also involved.

The mechanism of vacancy introduction into silicon during annealing in N_2 is not clear despite the analogy to NH_3 (where it is not clear either). But a retarded diffusion of phosphorus, enhanced diffusion of antimony, and enhanced shrinkage of extended stacking faults were found by Ahn et al. [2.639] even during annealing of silicon covered by thin oxides in argon. This effect was found to decrease at 1100 °C rapidly with the thickness of the covering oxide characterized by a length scale of about 45 nm. To explain this phenomenon, the authors assumed that volatile SiO forms at the interface between the oxide and the bulk silicon according to the re-

action $\text{Si} + \text{SiO}_2 \rightarrow 2 \text{SiO}$ and that this reaction is associated with the introduction of vacancies into the silicon bulk. Using boron and antimony superlattice layers as point-defect detectors, Gossmann et al. [2.559] found that annealing of samples with nominally bare surfaces at 810 °C leads to a depletion of silicon self-interstitials while it leaves the vacancy concentration virtually unaffected. Based on this observation, it was suggested that the experiments of Ahn et al. similarly result from a depletion of self-interstitials rather than from an injection of vacancies by the SiO formation and that the supersaturation of vacancies is caused by bulk recombination. It has to be noted that the segregation of self-interstitials into covering oxide layers is more in line with the concepts discussed in Section 2.8.3, too.

A final process associated with the introduction of vacancies into the silicon bulk is the growth of silicides. In one of the first publications, Wittmer and Tu [2.684] reported an effective diffusion coefficient at 250 °C which was more than 15 orders of magnitude higher than what is expected from an extrapolation of high-temperature diffusion data. Later, Wittmer et al. [2.685] investigated the diffusion of dopant marker layers during palladium silicidation at 200 °C. They found asymmetric profiles, partly with kink and tail towards the surface. The effect was later found to be spurious and Wittmer et al. [2.686] discussed and confirmed that at least some of the asymmetric profiles might be the results of SIMS artifacts. However, clear evidence for asymmetric profiles was given by Honeycutt and Rozgonyi [2.687] after cobalt silicidation at 700 °C. To avoid possible SIMS artifacts, they used junction delineation in addition. Clear evidence for an introduction of vacancies was also given in a number of reports on dopant diffusion during the growth of refractory silicides [2.687–2.689]. Complementary evidence came from the observation of an enhanced shrinkage of extrinsic extended defects during silicide growth [2.690–2.694]. But not only the injection of vacancies is possible. Erlesand et al. [2.695] and Kringshøj [2.696] concluded from their experiments that self-interstitials rather than vacancies are injected during rhodium and palladium silicidation, respectively. In addition, Chen et al. [2.697] found that the injection of vacancies decreases and finally changes to an injection of self-interstitials when the oxygen content in the titanium layer is increased to more than 25%.

2.9 Initial Conditions

Initial conditions for the intrinsic point defects are usually the poor cousins of process modeling. They describe the state of the wafer at the beginning of a simulated high-temperature process step. Evidently, these initial conditions correspond to the state at the end of the preceding process step, with the first process step being the pulling of the crystal. Similar information is required about all agglomerates of intrinsic point defects.

In process-simulation programs, except for simulating post-implantation processes, it is often assumed that the initial concentrations of the intrinsic point defects prior to a diffusion step at a certain temperature correspond to the equilibrium concentrations at this temperature. Such an assumption implies that a near-by surface establishes equilibrium conditions on a short time scale. While it may be admissible for surface-near regions, it is certainly wrong for processes like short-time metal diffusion or nucleation of oxygen precipitates which are influenced by the concentrations of the intrinsic point defects in the bulk, far away from the surfaces. In addition, one has to remember that self-interstitials as well as vacancies are mobile already well below room temperature. Thus, because of their inferior equilibrium concentrations at room temperature, one cannot expect a significant concentration of free intrinsic point defects to exist under such conditions. They will be either in extended defects or in stable complexes with

impurities. However, since heating of the wafers to elevated temperatures leads to a dissociation of these complexes and to a liberation of the intrinsic point defects, it may be an acceptable abstraction under certain conditions to assume the intrinsic point defects to be actually free.

According to the overview of silicon pulling techniques given by Zulehner [2.698], about 95% of all silicon single crystals were grown in 2000 by the Czochralski (CZ) technique, and the rest by the float zone (FZ) technique. In the CZ method, a single-crystalline seed is dipped into molten silicon contained in a quartz crucible and the crystal is then pulled under opposite rotation of crystal and crucible. Since oxygen from the crucible dissolves into the silicon melt, typical oxygen concentrations in pulled crystals range from $6 \cdot 10^{17}$ to 10^{18} cm^{-3} . Induced by proper processing steps, the oxygen will form precipitates in the bulk of the crystals which are then used to getter undesired impurities like metals. For power semiconductors, oxygen precipitates in the bulk would be detrimental. The FZ method used generally to grow such crystals of high purity uses a short melt zone which is passed along a polysilicon rod placed on top of a seed crystal to achieve monocrystalline growth. During this process, undesired impurities will segregate predominantly to the molten zone so that, by repeating the process, their concentration in the grown crystal can be reduced sufficiently.

Extended defects resulting from the agglomeration of intrinsic point defects were detected early in FZ and CZ crystals. Because of their distribution in wafers cut perpendicular to the growth direction, they were referred to as "swirl defects." In the nomenclature of de Kock [2.699], the larger ones were denoted A-swirls, and the smaller ones B-swirls. The A-swirls were finally identified by Föll and Kolbesen [2.700] as extrinsic dislocation loops, i.e. agglomerates of self-interstitials. For the B-swirls patterns, agglomerates of carbon and silicon self-interstitials were suggested to be responsible by Föll et al. [2.701]. Varying the crystal-growth rate, Roksnoer and van den Boom [2.702] found that A-swirls and B-swirls vanish above a certain growth rate. Increasing the growth rate further beyond a certain limit within which defect-free crystals were obtained, a new type of defects, called D-defects was found to form. They were associated with vacancy agglomerates and, depending on the mode of detection, also referred to as voids, crystal-originated particles or pits (COPs), flow-pattern defects, light-scattering-tomography defects, and gate-oxide-integrity defects (GOI defects) in the literature.

The first theory able to predict the transition from a self-interstitial-dominated growth regime to a vacancy-dominated growth regime was presented by Voronkov [2.83] in 1982. Considering the continuous introduction of intrinsic point defects at the interface to the melt, their transport in the temperature gradient along the crystal axis, and recombination, he could show that type and concentration of the point defects prevailing in a crystal depend primarily on the quotient $\xi = V/G$ of the growth rate V and the thermal gradient G at the interface. For large values of this parameters, those point defects are expected to remain after recombination for which the equilibrium concentration is larger at the melting point. On the other hand, for low values of ξ , transport of intrinsic point defects by diffusion from the melt interface becomes more important and those intrinsic point defects will dominate finally for which the transport capacity is larger. From the experimentally observed transition from self-interstitial agglomerates to vacancy agglomerates with increasing ξ , it follows that the equilibrium concentration of vacancies exceeds at the melting temperature the equilibrium concentration of self-interstitials while the transport capacity is larger for self-interstitials. The critical value of ξ for which a defect-free crystal results is about $1.3 \cdot 10^{-3} \text{ cm}^2 \text{min}^{-1} \text{K}^{-1}$ [2.703] for low-doped crystals. However, it was also found that the critical value of ξ depends on the impurities present [2.704–2.706]. When the temperature is further reduced, i.e. in regions more remote from the interface to the melt, the point defects remaining in the crystal will eventually agglomerate to the extrinsic defects ob-

served when their supersaturation is large enough. In CZ crystals, at intermediate supersaturations of vacancies, small oxide particles were found to form instead of D-defects [2.105, 2.707].

While the growth rate during crystal pulling is everywhere the same, the thermal gradient at the interface to the melt will vary radially. As a consequence, vacancy-dominated and interstitial-dominated regions may be observed on the same wafer. In particular, Hasabe et al. [2.708], Yamauchi et al. [2.709], and Shimizu et al. [2.710] reported observations of a ring-like feature at which stacking faults form upon oxidation at high temperatures. This oxidation-induced stacking-fault (OSF) ring separates a vacancy-rich inner region from a defect-free and largely self-interstitial-dominated outer region. After the OSFs were shown to nucleate at the oxygen precipitates discussed above [2.105, 2.707], it is clear that the OSF ring marks the border of the D-defect region rather than directly the transition from the interstitial-rich to the vacancy-rich growth regime.

Experimental data about the state of defects in as-grown, swirl-free silicon came especially from platinum-diffusion experiments [2.426]. Using this technique, the concentration of vacancies in FZ wafers was usually found to be on the order of 10^{14} cm^{-3} . In contrast, in CZ wafers, significantly lower concentrations were found which were usually even below the detection limit of about 10^{11} cm^{-3} . Using *in-situ* doping of FZ crystals with rhodium during their growth, Riemann and Lüdge [2.711] found a vacancy concentration of about 10^{14} cm^{-3} at large pull rates which reduced rapidly when ξ approached its critical value. These values were confirmed by the positron-annihilation studies of Gebauer et al. [2.712] who reported vacancy concentrations of 10^{14} to $4 \cdot 10^{14} \text{ cm}^{-3}$ in FZ silicon. For CZ samples, no measurable concentration of vacancies was found. A vacancy concentration of $3 \cdot 10^{16} \text{ cm}^{-3}$ as it was reported in the positron-annihilation study of Dannefaer et al. [2.713] for as-grown CZ wafers seems highly unlikely and similar discrepancies between positron-annihilation experiments of Dannefaer et al. and others were already discussed in Section 2.4.2. The reason for the significantly smaller concentration of vacancies (or rather vacancy-nitrogen and vacancy-oxygen complexes as noted above) in CZ silicon is that they were either pulled self-interstitial rich or that the vacancies agglomerated. Similarly, in FZ crystals not intentionally doped with nitrogen, a vacancy concentration of only $4 \cdot 10^{11} \text{ cm}^{-3}$ was found and attributed to the formation of voids [2.714]. An estimate of Hourai et al. [2.715] of the vacancies in voids in CZ wafers corresponded again to $(0.98\text{--}3.5) \cdot 10^{14} \text{ cm}^{-3}$.

Bibliography

- [2.1] R. O. Simmons and R. W. Balluffi, “Measurement of Equilibrium Vacancy Concentration in Aluminium,” *Phys. Rev.*, vol. 117, no. 1, 52–61 (1960).
- [2.2] A. Seeger and M. L. Swanson, “Vacancies and Diffusion Mechanisms in Diamond-Structure Semiconductors,” in: *Lattice Defects in Semiconductors*, edited by R. R. Hasiguti, Tokyo: University of Tokyo Press, 93–130 (1968).
- [2.3] A. Seeger and K. P. Chik, “Diffusion Mechanism and Point Defects in Silicon and Germanium,” *phys. stat. sol.*, vol. 29, 455–542 (1968).
- [2.4] W. Schottky, “Über den Mechanismus der Ionenbewegung in festen Elektrolyten,” *Z. Phys. Chem. B*, vol. 29, 335–355 (1935).
- [2.5] M. Lannoo and J. Bourgoin, *Point Defects in Semiconductors I, Springer Series in Solid-State Sciences*, vol. 22, Berlin: Springer (1981).
- [2.6] E. Guerrero, *Verteilung von Dotierungsatomen in Silicium-Einkristallen*, Ph.D. thesis, Technical University of Vienna (1984).

- [2.7] J. A. Van Vechten, "A Simple Man's View of the Thermochemistry of Semiconductors," in: *Materials, Properties and Preparations*, edited by S. P. Keller, *Handbook on Semiconductors*, vol. 3, Amsterdam: North-Holland, 1–111 (1980).
- [2.8] W. Shockley and J. L. Moll, "Solubility of Flaws in Heavily-Doped Semiconductors," *Phys. Rev.*, vol. 119, no. 5, 1480–1482 (1960).
- [2.9] R. L. Longini and R. F. Greene, "Ionization Interaction between Impurities in Semiconductors and Insulators," *Phys. Rev.*, vol. 102, no. 4, 992–999 (1956).
- [2.10] M. W. Valenta and C. Ramasastry, "Effects of Heavy Doping on the Self-Diffusion of Germanium," *Phys. Rev.*, vol. 106, no. 1, 73–75 (1957).
- [2.11] W. Shockley and J. T. Last, "Statistics of the Charge Distribution for a Localized Flaw in a Semiconductor," *Phys. Rev.*, vol. 107, no. 2, 392–396 (1957).
- [2.12] P. M. Fahey, *Point Defects and Dopant Diffusion in Silicon*, Ph.D. thesis, Integrated Circuits Laboratory, Department of Electrical Engineering, Stanford University (1985).
- [2.13] J. A. Van Vechten and C. D. Thurmond, "Entropy of Ionization and Temperature Variation of Ionization Levels of Defects in Semiconductors," *Phys. Rev. B*, vol. 14, no. 8, 3539–3550 (1976).
- [2.14] D. Mathiot and J. C. Pfister, "Dopant Diffusion in Silicon: A Consistent View Involving Nonequilibrium Defects," *J. Appl. Phys.*, vol. 55, no. 10, 3518–3530 (1984).
- [2.15] R. B. Fair, "The Effect of Strain-Induced Band-Gap Narrowing on High Concentration Phosphorus Diffusion in Silicon," *J. Appl. Phys.*, vol. 50, no. 2, 860–868 (1979).
- [2.16] P. M. Fahey, P. B. Griffin, and J. D. Plummer, "Point Defects and Dopant Diffusion in Silicon," *Reviews of Modern Physics*, vol. 61, no. 2, 289–384 (1989).
- [2.17] J. P. Hirth and J. Lothe, *Theory of Dislocations*, New York: McGraw-Hill (1968).
- [2.18] L. Borucki, "Modeling the Growth and Annealing of Dislocation Loops," in: *Proceedings NUPAD IV*, New York: IEEE, 27–32 (1992).
- [2.19] H. Park, K. S. Jones, and M. E. Law, "A Point Defect Based Two-Dimensional Model of the Evolution of Dislocation Loops in Silicon during Oxidation," *J. Electrochem. Soc.*, vol. 141, no. 3, 759–765 (1994).
- [2.20] I. V. Peidous and K. V. Loiko, "Screening of Dislocations in Silicon by Point Defects," in: *High Purity Silicon VI*, edited by C. L. Claeys, P. Rai-Choudhury, M. Watanabe, P. Stallhofer, and H. J. Dawson, *Electrochem. Soc. Proc.*, vol. 2000-17, 145–155 (2000).
- [2.21] K. Tanahashi and N. Inoue, "Non-Equilibrium Thermodynamic Analysis on the Behaviour of Point Defects in Growing Silicon Crystals: Effects of Stress," *Journal of Materials Science: Materials in Electronics*, vol. 10, 359–363 (1999).
- [2.22] K. V. Loiko, I. V. Peidous, T. E. Harrington, and W. R. Frensley, "Stress-Induced Redistribution of Point Defects in Silicon Device Structures," in: *Gettering and Defect Engineering in Semiconductor Technology GADEST 2001*, edited by V. Raineri, F. Priolo, M. Kittler, and H. Richter, *Solid State Phenomena*, vol. 82-84, 225–230 (2002).
- [2.23] A. Seeger, H. Föll, and W. Frank, "Self-Interstitials, Vacancies and Their Clusters in Silicon and Germanium," in: *Radiation Effects in Semiconductors, 1976*, edited by N. B. Urli and J. W. Corbett, *Inst. Phys. Conf. Ser.*, no. 31, 12–29 (1977).
- [2.24] M. Budil, H. Pötzl, G. Stingereder, M. Grasserbauer, and K. Goser, "A New Model of Anomalous Phosphorus Diffusion in Silicon," in: *Defects in Semiconductors 15*, edited by G. Ferenczi, *Materials Science Forum*, vol. 38-41, 719–724 (1989).
- [2.25] J. A. Van Vechten, "Enthalpy of Vacancy Migration in Si and Ge," *Phys. Rev. B*, vol. 10, no. 4, 1482–1506 (1974).
- [2.26] Y. Nakabayashi, H. I. Osman, K. Yokota, K. Toyonaga, S. Matsumoto, J. Murota, K. Wada, and T. Abe, "Type and Charge States of Point Defects in Heavily As- and B-Doped Silicon," *Materials Science in Semiconductor Processing*, vol. 6, 15–19 (2003).
- [2.27] S. M. Hu, "Diffusion in Silicon and Germanium," in: *Atomic Diffusion in Semiconductors*, edited by D. Shaw, London: Plenum Press, 217–350 (1973).

- [2.28] U. Gösele and T. Y. Tan, “The Nature of Point Defects and Their Influence on Diffusion Processes in Silicon at High Temperatures,” in: *Defects in Semiconductors II*, edited by S. Mahajan and J. W. Corbett, *Mat. Res. Soc. Symp. Proc.*, vol. 14, 45–59 (1983).
- [2.29] K. Compaan and Y. Haven, “Correlation Factors for Diffusion in Solids,” *Trans. Faraday Soc.*, vol. 52, 786–801 (1956).
- [2.30] M. Yoshida, “Diffusion of Group V Impurity in Silicon,” *Jpn. J. Appl. Phys.*, vol. 10, no. 6, 702–713 (1971).
- [2.31] D. Shaw, “Self- and Impurity Diffusion in Ge and Si,” *phys. stat. sol. (b)*, vol. 72, 11–39 (1975).
- [2.32] K. Compaan and Y. Haven, “Correlation Factors for Diffusion in Solids. Part 2 — Indirect Interstitial Mechanism,” *Trans. Faraday Soc.*, vol. 54, 1498–1508 (1958).
- [2.33] S. M. Hu, “Modeling Diffusion in Silicon: Accomplishments and Challenges,” in: *VLSI Science and Technology/1985*, edited by W. M. Bullis and S. Broydo, *Electrochem. Soc. Proc.*, vol. 85-5, 465–506 (1985).
- [2.34] S. M. Hu, “Nonequilibrium Point Defects and Diffusion in Silicon,” *Materials Science and Engineering*, vol. R13, 105–192 (1994).
- [2.35] R. F. Peart, “Self Diffusion in Intrinsic Silicon,” *phys. stat. sol.*, vol. 15, K119–K122 (1966).
- [2.36] R. N. Ghoshtagore, “On the Mechanism of Substitutional Diffusion in Silicon,” *phys. stat. sol.*, vol. 20, K89–K94 (1967).
- [2.37] D. L. Kendall and D. B. De Vries, “Diffusion in Silicon,” in: *Semiconductor Silicon*, edited by R. R. Haberecht and E. L. Kerns, *Electrochem. Soc. Proc.*, 358–421 (1969).
- [2.38] S. Dannefaer, P. Mascher, and D. Kerr, “Monovacancy Formation Enthalpy in Silicon,” *Phys. Rev. Lett.*, vol. 56, no. 20, 2195–2198 (1986).
- [2.39] J. A. Van Vechten, “Divacancy Binding Enthalpy and Contribution of Divacancies to Self-Diffusion in Si,” *Phys. Rev. B*, vol. 33, no. 4, 2674–2689 (1986).
- [2.40] K. C. Pandey, “Diffusion without Vacancies or Interstitials: A New Concerted Exchange Mechanism,” *Phys. Rev. Lett.*, vol. 57, no. 18, 2287–2290 (1986).
- [2.41] M. I. Heggie, “Self-Diffusion, Deformation and Melting in Silicon — A Microscopic Link,” *Phil. Mag. Lett.*, vol. 58, no. 2, 75–80 (1988).
- [2.42] K. C. Pandey and E. Kaxiras, “Entropy Calculation beyond the Harmonic Approximation: Application to Diffusion by Concerted Exchange in Si,” *Phys. Rev. Lett.*, vol. 66, no. 7, 915–918 (1991).
- [2.43] P. E. Blöchl, E. Smargiassi, R. Car, D. B. Laks, W. Andreoni, and S. T. Pantelides, “First-Principles Calculation of Self-Diffusion Constants in Silicon,” *Phys. Rev. Lett.*, vol. 70, no. 16, 2435–2438 (1993).
- [2.44] E. Kaxiras and K. C. Pandey, “Contribution of Concerted Exchange to the Entropy of Self-Diffusion in Si,” *Phys. Rev. B*, vol. 47, no. 3, 1659–1662 (1993).
- [2.45] A. Antonelli, S. Ismail-Beigi, E. Kaxiras, and K. C. Pandey, “Free Energy of the Concerted-Exchange Mechanism for Self-Diffusions in Silicon,” *Phys. Rev. B*, vol. 53, no. 3, 1310–1314 (1996).
- [2.46] W.-K. Leung, R. J. Needs, G. Rajagopal, S. Itoh, and S. Ihara, “Calculations of Silicon Self-Interstitial Defects,” *Phys. Rev. Lett.*, vol. 83, no. 12, 2351–2354 (1999).
- [2.47] R. J. Needs, “First-Principles Calculations of Self-Interstitial Defect Structures and Diffusion Paths in Silicon,” *J. Phys.: Condens. Matter*, vol. 11, 10437–10450 (1999).
- [2.48] A. Ural, P. B. Griffin, and J. D. Plummer, “Experimental Study of Self-Diffusion in Silicon Using Isotopically Enriched Structures,” in: *Si Front-End Processing — Physics and Technology of Dopant-Defect Interactions*, edited by H.-J. L. Gossmann, T. E. Haynes, M. E. Law, A. Nylandsted Larsen, and S. Odanaka, *Mat. Res. Soc. Symp. Proc.*, vol. 568, 97–102 (1999).
- [2.49] A. Ural, P. B. Griffin, and J. D. Plummer, “Fractional Contributions of Microscopic Diffusion Mechanisms for Common Dopants and Self-Diffusion in Silicon,” *J. Appl. Phys.*, vol. 85, no. 9, 6440–6446 (1999).

- [2.50] I. D. Sharp, H. A. Bracht, H. H. Silvestri, S. P. Nicols, J. W. Beeman, J. L. Hansen, A. Nylandsted Larsen, and E. E. Haller, "Self- and Dopant Diffusion in Extrinsic Boron Doped Isotopically Controlled Silicon Multilayer Structures," in: *Defect and Impurity Engineered Semiconductors and Devices III*, edited by S. Ashok, J. Chevalier, N. M. Johnson, B. L. Sopori, and H. Okushi, *Mat. Res. Soc. Symp. Proc.*, vol. 719, F13.11.1–F13.11.6 (2002).
- [2.51] H. Bracht, E. E. Haller, and R. Clark-Phelps, "Silicon Self-Diffusion in Isotope Heterostructures," *Phys. Rev. Lett.*, vol. 81, no. 2, 393 (1998).
- [2.52] H. Bracht, E. E. Haller, K. Eberl, M. Cardona, and R. Clark-Phelps, "Self-Diffusion in Isotopically Controlled Heterostructures of Elemental and Compound Semiconductors," in: *Diffusion Mechanisms in Crystalline Materials*, edited by Y. Mishin, G. Vogl, N. Cowern, R. Catlow, and D. Farkas, *Mat. Res. Soc. Symp. Proc.*, vol. 527, 335–346 (1998).
- [2.53] A. Ural, P. B. Griffin, and J. D. Plummer, "Self-Diffusion in Silicon: Similarity between the Properties of Native Point Defects," *Phys. Rev. Lett.*, vol. 83, no. 17, 3454–3457 (1999).
- [2.54] Y. Nakabayashi, H. I. Osman, T. Segawa, K. Saito, S. Matsumoto, J. Murota, K. Wada, and T. Abe, "Self-Diffusion in Extrinsic Silicon Using Isotopically Enriched ^{30}Si Layer," *Jpn. J. Appl. Phys., Part 2*, vol. 40, no. 3A, L181–L182 (2001).
- [2.55] Y. Nakabayashi, H. I. Osman, K. Toyonaga, K. Yokota, S. Matsumoto, J. Murota, K. Wada, and T. Abe, "Self-Diffusion in Intrinsic and Extrinsic Silicon Using Isotopically Pure ^{30}Si /Natural Silicon Heterostructures," *Jpn. J. Appl. Phys., Part 1*, vol. 42, no. 6A, 3304–3310 (2003).
- [2.56] R. N. Ghoshtagore, "Method for Determining Silicon Diffusion Coefficients in Silicon and in Some Silicon Compounds," *Phys. Rev. Lett.*, vol. 16, no. 20, 890–892 (1966).
- [2.57] J. M. Fairfield and B. J. Masters, "Self-Diffusion in Intrinsic and Extrinsic Silicon," *J. Appl. Phys.*, vol. 38, no. 8, 3148–3154 (1967).
- [2.58] H. J. Mayer, H. Mehrer, and K. Maier, "Self-Diffusion in Silicon between 1320 K and 1660 K," in: *Radiation Effects in Semiconductors, 1976*, edited by N. B. Urli and J. W. Corbett, *Inst. Phys. Conf. Ser.*, no. 31, 186–193 (1977).
- [2.59] J. Hirvonen and A. Anttila, "Self-Diffusion in Silicon As Probed by the (P, γ) Resonance Broadening Method," *Appl. Phys. Lett.*, vol. 35, no. 9, 703–705 (1979).
- [2.60] L. Kalinowski and R. Seguin, "Self-Diffusion in Intrinsic Silicon," *Appl. Phys. Lett.*, vol. 35, no. 3, 211–212 (1979).
- [2.61] L. Kalinowski and R. Seguin, "Erratum: Self-Diffusion in Intrinsic Silicon [Appl. Phys. Lett. 35, 211 (1979)]," *Appl. Phys. Lett.*, vol. 36, no. 2, 171 (1980).
- [2.62] F. J. Demond, S. Kalbitzer, H. Mannsperger, and H. Damjantschitsch, "Study of Self-Diffusion by Nuclear Techniques," *Physics Letters*, vol. 93A, no. 9, 503–506 (1983).
- [2.63] A. Strohm, T. Voss, W. Frank, P. Laitinen, and J. Räisänen, "Self-Diffusion of ^{71}Ge and ^{31}Si in Si-Ge Alloys," *Z. Metallkd.*, vol. 93, no. 7, 737–744 (2002).
- [2.64] T. Y. Tan and U. Gösele, "Point Defects, Diffusion Processes, and Swirl Defect Formation in Silicon," *Appl. Phys. A*, vol. 37, 1–17 (1985).
- [2.65] M. J. Aziz, E. Nygren, W. H. Christie, C. W. White, and D. Turnbull, "Effect of Pressure on Self Diffusion in Crystalline Silicon," in: *Impurity Diffusion and Gettering in Silicon*, edited by R. B. Fair, C. Pearce, and J. Washburn, *Mat. Res. Soc. Symp. Proc.*, vol. 36, 101–104 (1985).
- [2.66] M. J. Aziz, "Stress Effects on Defects and Dopant Diffusion in Si," *Materials Science in Semiconductor Processing*, vol. 4, 397–403 (2001).
- [2.67] G. Hettich, H. Mehrer, and K. Maier, "Tracer Diffusion of ^{71}Ge and ^{31}Si in Intrinsic and Doped Silicon," in: *Defects and Radiation Effects in Semiconductors, 1978*, edited by J. H. Albany, *Inst. Phys. Conf. Ser.*, no. 46, 500–507 (1979).
- [2.68] A. Ural, P. B. Griffin, and J. D. Plummer, "Silicon Self-Diffusion under Extrinsic Conditions," *Appl. Phys. Lett.*, vol. 79, no. 26, 4328–4330 (2001).

- [2.69] H. I. Osman, Y. Nakabayashi, S. Tomohisa, K. Toyonaga, S. Matsumoto, J. Murota, K. Wada, and T. Abe, “Effect of Vacancy Double Acceptor Level on Si Self-Diffusion under Heavy Doping Conditions,” in: *Semiconductor Silicon 2002*, edited by H. R. Huff, L. Fabry, and S. Kishino, *Electrochem. Soc. Proc.*, vol. 2002-2, 248–253 (2002).
- [2.70] H. H. Silvestri, I. D. Sharp, H. A. Bracht, S. P. Nicols, J. W. Beeman, J. Hansen, A. Nylandsted-Larsen, and E. E. Haller, “Dopant and Self-Diffusion in Extrinsic n-Type Silicon Isotopically Controlled Heterostructures,” in: *Defect and Impurity Engineered Semiconductors and Devices III*, edited by S. Ashok, J. Chevallier, N. M. Johnson, B. L. Sopori, and H. Okushi, *Mat. Res. Soc. Symp. Proc.*, vol. 719, F13.10.1–F13.10.6 (2002).
- [2.71] G. L. McVay and A. R. DuCharme, “The Diffusion of Germanium in Silicon,” *J. Appl. Phys.*, vol. 44, no. 3, 1409–1410 (1973).
- [2.72] F. Morehead, N. A. Stolwijk, W. Meyberg, and U. Gösele, “Self-Interstitial and Vacancy Contribution to Silicon Self-Diffusion Determined from the Diffusion of Gold in Silicon,” *Appl. Phys. Lett.*, vol. 42, no. 8, 690–692 (1983).
- [2.73] H. Kitagawa and M. Yoshida, “On the Distinction between the Dissociative and Kick-Out Mechanisms for Site Exchange in Silicon,” *Jpn. J. Appl. Phys., Part 1*, vol. 31, no. 9A, 2859–2963 (1992).
- [2.74] H. Bracht and E. E. Haller, “Comment on ‘Self-Diffusion in Silicon: Similarity between the Properties of Native Point Defects’,” *Phys. Rev. Lett.*, vol. 85, no. 22, 4835 (2000).
- [2.75] A. Ural, P. B. Griffin, and J. D. Plummer, “Reply: Ural, Griffin, and Plummer,” *Phys. Rev. Lett.*, vol. 85, no. 22, 4836 (2000).
- [2.76] H. Bracht, N. A. Stolwijk, and H. Mehrer, “Properties of Intrinsic Point Defects in Silicon Determined by Zinc Diffusion Experiments under Nonequilibrium Conditions,” *Phys. Rev. B*, vol. 52, no. 23, 16542–16560 (1995).
- [2.77] H.-J. Gossmann, P. A. Stolk, D. J. Eaglesham, C. S. Rafferty, and J. M. Poate, “Fast Metal Diffusers in Si in the Presence of Si Self-Interstitial Traps,” *Appl. Phys. Lett.*, vol. 67, no. 21, 3135–3137 (1995).
- [2.78] P. Pichler, “A Reinterpretation of Platinum-Diffusion Experiments,” in: *ESSDERC'98*, edited by A. Touboul, Y. Danto, J. P. Klein, and H. Grünbacher, Paris: Edition Frontières, 348–351 (1998).
- [2.79] P. Pichler, “Extraction of Vacancy Parameters from Outdiffusion of Zinc from Silicon,” in: *Gettering and Defect Engineering in Semiconductor Technology GADEST'99*, edited by H. G. Grimmeiss, L. Ask, M. Kleverman, M. Kittler, and H. Richter, *Solid State Phenomena*, vol. 69-70, 455–460 (1999).
- [2.80] D. Mathiot, “Diffusion Modeling from a Fundamental Viewpoint,” in: *Semiconductor Silicon*, edited by H. R. Huff, T. Abe, and B. Kolbesen, *Electrochem. Soc. Proc.*, vol. 86-4, 556–570 (1986).
- [2.81] D. Mathiot, “Gold, Self-, and Dopant Diffusion in Silicon,” *Phys. Rev. B*, vol. 45, no. 23, 13345–13355 (1992).
- [2.82] M. Yoshida and K. Saito, “Dissociative Diffusion of Nickel in Silicon and Self-Diffusion of Silicon,” *Jpn. J. Appl. Phys.*, vol. 6, no. 5, 573–581 (1967).
- [2.83] V. V. Voronkov, “The Mechanism of Swirl Defects Formation in Silicon,” *J. Crystal Growth*, vol. 59, 625–643 (1982).
- [2.84] K. Wada and N. Inoue, “Depth Profile of Bulk Stacking Fault Radius in Czochralski Silicon,” *J. Appl. Phys.*, vol. 58, no. 3, 1183–1186 (1985).
- [2.85] M. Budil, E. Guerrero, T. Brabec, S. Selberherr, and H. Pötzl, “A New Model for the Determination of Point Defect Equilibrium Concentrations in Silicon,” in: *NUMOS I*, edited by J. J. H. Miller, Dún Laoghaire: Boole Press, 37–44 (1986).
- [2.86] T. Brabec, E. Guerrero, M. Budil, and H. W. Pötzl, “Simulation of Retarded Diffusion of Antimony and Enhanced Diffusion of Phosphorus in Silicon,” *Z. Phys. B*, vol. 67, 415–420 (1987).

- [2.87] P. B. Griffin, *Physics and Modeling of Two-Dimensional Diffusion in SUPREM-IV*, Ph.D. thesis, Integrated Circuits Laboratory, Department of Electrical Engineering, Stanford University (1989).
- [2.88] H. Zimmermann, A. Strauß, and H. Ryssel, "The Modeling of Platinum Diffusion in Silicon," in: *Process Physics and Modeling in Semiconductor Technology*, edited by G. R. Srinivasan, J. D. Plummer, and S. T. Pantelides, *Electrochem. Soc. Proc.*, vol. 91-4, 337–344 (1991).
- [2.89] M. E. Law, "Parameters for Point-Defect Diffusion and Recombination," *IEEE Trans. Computer-Aided Design*, vol. 10, no. 9, 1125–1131 (1991).
- [2.90] S. T. Dunham, "A Quantitative Model for the Coupled Diffusion of Phosphorus and Point Defects in Silicon," *J. Electrochem. Soc.*, vol. 139, no. 9, 2628–2636 (1992).
- [2.91] H. Park and M. E. Law, "Point Defect Based Modeling of Low Dose Silicon Implant Damage and Oxidation Effects on Phosphorus and Boron Diffusion in Silicon," *J. Appl. Phys.*, vol. 72, no. 8, 3431–3439 (1992).
- [2.92] T. Okino, "Diffusivity of Self-Interstitials and Vacancies in Silicon," *Jpn. J. Appl. Phys., Part 2*, vol. 32, no. 6B, L856–L858 (1993).
- [2.93] R. Habu, T. Iwasaki, H. Harada, and A. Tomiura, "Diffusion Behavior of Point Defects in Si Crystal during Melt Growth IV: Numerical Analysis," *Jpn. J. Appl. Phys., Part 1*, vol. 33, no. 3A, 1234–1242 (1994).
- [2.94] T. Okino and M. Onishi, "Analysis of P and Sb Diffusion during Thermal Oxidation in Silicon," *Jpn. J. Appl. Phys., Part 1*, vol. 33, no. 6A, 3362–3367 (1994).
- [2.95] K. Ghaderi, G. Hobler, M. Budil, L. Mader, and H. J. Schulze, "Determination of Silicon Point Defect Parameters and Reaction Barrier Energies from Gold Diffusion Experiments," *J. Appl. Phys.*, vol. 77, no. 3, 1320–1322 (1995).
- [2.96] R. Habu and A. Tomiura, "Distribution of Grown-in Crystal Defects in Silicon Crystals Formed by Point Defect Diffusion during Melt-Growth: Disappearance of the Oxidation Induced Stacking Faults-Ring," *Jpn. J. Appl. Phys., Part 1*, vol. 35, no. 1A, 1–9 (1996).
- [2.97] W. B. Knowlton, J. T. Walton, J. S. Lee, D. Lewak, Y. K. Wong, and E. E. Haller, "Properties of Silicon Point Defects As Revealed by Lithium Ion Drift," in: *Process Physics and Modeling in Semiconductor Technology*, edited by G. R. Srinivasan, C. S. Murthy, and S. T. Dunham, *Electrochem. Soc. Proc.*, vol. 96-4, 324–336 (1996).
- [2.98] T. Sinno, R. A. Brown, W. von Ammon, and E. Dornberger, "On the Dynamics of the Oxidation-Induced Stacking-Fault Ring in As-Grown Czochralski Silicon Crystals," *Appl. Phys. Lett.*, vol. 70, no. 17, 2250–2252 (1997).
- [2.99] S. Chakravarthi and S. T. Dunham, "Point Defect Properties from Metal Diffusion Experiments — What Does the Data Really Tell Us?" in: *Defects and Diffusion in Silicon Processing*, edited by T. Diaz de la Rubia, S. Coffa, P. A. Stolk, and C. S. Rafferty, *Mat. Res. Soc. Symp. Proc.*, vol. 469, 47–52 (1997).
- [2.100] K. Nakamura, T. Saishoji, T. Kubota, T. Iida, Y. Shimanuki, T. Kotooka, and J. Tomioka, "Formation Process of Grown-in Defects in Czochralski Grown Silicon Crystals," *J. Crystal Growth*, vol. 180, 61–72 (1997).
- [2.101] J. T. Walton, E. E. Haller, W. B. Knowlton, Y. K. Wong, W. von Ammon, and W. Zulehner, "Lithium-Ion Drifting: Application to the Study of Point Defects in Floating-Zone Silicon," in: *Diagnostic Techniques for Semiconductor Materials and Devices*, edited by P. Rai-Choudhury, J. L. Benton, D. K. Schroder, and T. J. Shaffner, *Electrochem. Soc. Proc.*, vol. 97-12, 400–411 (1997).
- [2.102] T. Sinno, R. A. Brown, W. von Ammon, and E. Dornberger, "Point Defect Dynamics and the Oxidation-Induced Stacking-Fault Ring in Czochralski-Grown Silicon Crystals," *J. Electrochem. Soc.*, vol. 145, no. 1, 302–318 (1998).
- [2.103] A. Giese, H. Bracht, J. T. Walton, and N. A. Stolwijk, "Properties of Vacancies in Silicon Determined by Out-Diffusion of Zinc from Silicon," in: *Diffusion Mechanisms in Crystalline Materials*, edited by Y. Mishin, G. Vogl, N. Cowern, R. Catlow, and D. Farkas, *Mat. Res. Soc. Symp. Proc.*, vol. 527, 395–400 (1998).

- [2.104] E. Dornberger, T. Sinno, J. Esfandyari, J. Vanhellemont, R. A. Brown, and W. von Ammon, “Determination of Intrinsic Point Defect Properties in Silicon by Analyzing OSF Ring Dynamics and Void Formation,” in: *High Purity Silicon V*, edited by C. L. Claeys, P. Rai-Choudhury, M. Watanabe, P. Stallhofer, and J. J. Dawson, *Electrochem. Soc. Proc.*, vol. 98-13, 170–187 (1998).
- [2.105] V. V. Voronkov and R. Falster, “Vacancy-Type Microdefect Formation in Czochralski Silicon,” *J. Crystal Growth*, vol. 194, 76–88 (1998).
- [2.106] R. Falster, V. V. Voronkov, and F. Quast, “On the Properties of the Intrinsic Point Defects in Silicon: A Perspective from Crystal Growth and Wafer Processing,” *phys. stat. sol. (b)*, vol. 222, 219–244 (2000).
- [2.107] T. Mori, Z. Wang, and R. A. Brown, “Transient Simulation of Grown-in Defect Dynamics in Czochralski Crystal Growth of Silicon,” in: *High Purity Silicon VI*, edited by C. L. Claeys, P. Rai-Choudhury, M. Watanabe, P. Stallhofer, and H. J. Dawson, *Electrochem. Soc. Proc.*, vol. 2000-17, 118–128 (2000).
- [2.108] M. Akatsuka, M. Okui, N. Morimoto, and K. Sueoka, “Effect of Rapid Thermal Annealing on Oxygen Precipitation Behavior in Silicon Wafers,” *Jpn. J. Appl. Phys., Part 1*, vol. 40, no. 5A, 3055–3062 (2001).
- [2.109] P. Pichler, “Properties of Vacancies in Silicon Determined from Laser-Annealing Experiments,” in: *ESSDERC 2002*, edited by G. Baccarani, E. Gnani, and M. Rudan, Bologna: University of Bologna, 335–338 (2002).
- [2.110] M. Okui and M. Nishimoto, “Effect of the Axial Temperature Gradient on the Formation of Grown-in Defect Regions in Czochralski Silicon Crystals; Reversion of the Defect Regions between the Inside and Outside of the Ring-OSF,” *J. Crystal Growth*, vol. 237-239, 1651–1656 (2002).
- [2.111] I. R. Sanders and P. S. Dobson, “The Application of the Loop Annealing Technique to Self Diffusion Studies in Silicon,” *Journal of Materials Science*, vol. 9, 1987–1993 (1974).
- [2.112] K. Wada and N. Inoue, “Diffusion Coefficient of Self-Interstitials Determined by Bulk Stacking Fault Growth in CZ Silicon,” in: *Defects and Radiation Effects in Semiconductors, 1980*, edited by R. R. Hasiguti, *Inst. Phys. Conf. Ser.*, no. 59, 461–466 (1981).
- [2.113] N. A. Stolwijk, B. Schuster, J. Hözl, H. Mehrer, and W. Frank, “Diffusion and Solubility of Gold in Silicon,” in: *Proceedings of the 12th International Conference on Defects in Semiconductors*, edited by C. A. J. Ammerlaan, *Physica*, vol. 116B, 335–342 (1983).
- [2.114] K. Taniguchi, D. A. Antoniadis, and Y. Matsushita, “Kinetics of Self-Interstitials Generated at the Si/SiO₂ Interface,” *Appl. Phys. Lett.*, vol. 42, no. 11, 961–963 (1983).
- [2.115] S. Mantovani, F. Nava, and C. Nobili, “Thermal Diffusion of Pt in Silicon from PtSi,” *Appl. Phys. Lett.*, vol. 44, no. 3, 328–330 (1984).
- [2.116] N. A. Stolwijk, B. Schuster, and J. Hözl, “Diffusion of Gold in Silicon Studied by Means of Neutron-Activation Analysis and Spreading-Resistance Measurements,” *Appl. Phys. A*, vol. 33, 133–140 (1984).
- [2.117] G. B. Bronner and J. D. Plummer, “Physical Modeling of Backside Gettering,” in: *Impurity Diffusion and Gettering in Semiconductors*, edited by R. B. Fair, C. W. Pearce, and J. Washburn, *Mat. Res. Soc. Symp. Proc.*, vol. 36, 49–54 (1985).
- [2.118] J. Hauber, N. A. Stolwijk, L. Tapfer, H. Mehrer, and W. Frank, “U- and W-Shaped Diffusion Profiles of Gold in Silicon,” *J. Phys. C*, vol. 19, 5817–5836 (1986).
- [2.119] S. Mantovani, F. Nava, C. Nobili, and G. Ottaviani, “In-Diffusion of Pt from the PtSi/Si Interface,” *Phys. Rev. B*, vol. 33, no. 8, 5536–5544 (1986).
- [2.120] G. B. Bronner and J. D. Plummer, “Gettering of Gold in Silicon: A Tool for Understanding the Properties of Silicon Interstitials,” *J. Appl. Phys.*, vol. 61, no. 12, 5286–5298 (1987).
- [2.121] F. F. Morehead, “The Diffusivity of Self-Interstitials in Silicon,” in: *Defects in Electronic Materials*, edited by M. Stavola, S. J. Pearton, and G. Davies, *Mat. Res. Soc. Symp. Proc.*, vol. 104, 99–104 (1988).

- [2.122] S. Coffa, L. Calcagno, S. U. Campisano, G. Calleri, and G. Ferla, "Diffusion of Ion-Implanted Gold in p-Type Silicon," *J. Appl. Phys.*, vol. 64, no. 11, 6291–6295 (1988).
- [2.123] H. U. Jäger, T. Feudel, and S. Ulbricht, "Modeling of Defect-Phosphorus Pair Diffusion in Phosphorus-Implanted Silicon," *phys. stat. sol. (a)*, vol. 116, 571–581 (1989).
- [2.124] J. Hauber, W. Frank, and N. A. Stolwijk, "Diffusion and Solubility of Platinum in Silicon," in: *Defects in Semiconductors 15*, edited by G. Ferenczi, *Materials Science Forum*, vol. 38-41, 707–712 (1989).
- [2.125] M. Perret, N. A. Stolwijk, and L. Coshausz, "Kick-Out Diffusion of Zinc in Silicon at 1262 K," *J. Phys.: Condens. Matter*, vol. 1, 6347–6361 (1989).
- [2.126] C. Boit, F. Lau, and R. Sittig, "Gold Diffusion in Silicon by Rapid Optical Annealing," *Appl. Phys. A*, vol. 50, 197–205 (1990).
- [2.127] M. D. Giles, "Transient Phosphorus Diffusion below the Amorphization Threshold," *J. Electrochem. Soc.*, vol. 138, no. 4, 1160–1165 (1991).
- [2.128] D. Grünebaum, T. Czekalla, N. A. Stolwijk, H. Mehrer, I. Yonenaga, and K. Sumino, "Diffusion and Solubility of Zinc in Dislocation-Free and Plastically Deformed Silicon Crystals," *Appl. Phys. A*, vol. 53, 65–74 (1991).
- [2.129] R. Y. S. Huang and R. W. Dutton, "Experimental Investigation and Modeling of the Role of Extended Defects during Thermal Oxidation," *J. Appl. Phys.*, vol. 74, no. 9, 5821–5827 (1993).
- [2.130] W. Lerch and N. A. Stolwijk, "Diffusion of Gold in Silicon during Rapid Thermal Annealing: Effectiveness of the Surface As a Sink for Self-Interstitials," *J. Appl. Phys.*, vol. 83, no. 3, 1312–1320 (1998).
- [2.131] N. E. B. Cowern, G. Mannino, P. A. Stolk, F. Roozeboom, H. G. A. Huizing, J. G. M. van Berkum, F. Cristiano, A. Claverie, and M. Jaraiz, "Cluster Ripening and Transient Enhanced Diffusion in Silicon," *Materials Science in Semiconductor Processing*, vol. 2, 369–376 (1999).
- [2.132] H. Meyer and S. T. Dunham, "Modeling of TED and Point Defect Parameter Extraction," in: *Silicon Front-End Junction Formation Technologies*, edited by D. F. Downey, M. E. Law, A. P. Claverie, and M. J. Rendon, *Mat. Res. Soc. Symp. Proc.*, vol. 717, C4.8.1–C4.8.6 (2002).
- [2.133] T. Okino, T. Shimosaki, and R. Takaue, "Self-Interstitials in Silicon," *Jpn. J. Appl. Phys., Part I*, vol. 36, no. 11, 6591–6594 (1997).
- [2.134] G. D. Watkins, "An EPR Study of the Lattice Vacancy in Silicon," in: *Proceedings of the International Conference on Crystal Lattice Defects, 1962*, *J. Phys. Soc. Japan*, vol. 18, Supplement II, 22–27 (1963).
- [2.135] G. D. Watkins, "A Review of EPR Studies in Irradiated Silicon," in: *Radiation Damage in Semiconductors*, Paris: Dunod, 97–113 (1964).
- [2.136] G. D. Watkins, "EPR Studies of the Lattice Vacancy and Low-Temperature Damage Processes in Silicon," in: *Lattice Defects in Semiconductors, 1974*, *Inst. Phys. Conf. Ser.*, no. 23, 1–22 (1975).
- [2.137] G. D. Watkins, J. R. Troxell, and A. P. Chatterjee, "Vacancies and Interstitials in Silicon," in: *Defects and Radiation Effects in Semiconductors, 1978*, edited by J. H. Albany, *Inst. Phys. Conf. Ser.*, no. 46, 16–30 (1979).
- [2.138] M. Sprenger, S. H. Muller, and C. A. J. Ammerlaan, "The Negatively Charged Vacancy in Silicon: Hyperfine Interactions from ENDOR Measurement," in: *Proceedings of the 12th International Conference on Defects in Semiconductors*, edited by C. A. J. Ammerlaan, *Physica*, vol. 116B, 224–229 (1983).
- [2.139] M. Sprenger, S. H. Muller, E. G. Sieverts, and C. A. J. Ammerlaan, "Vacancy in Silicon: Hyperfine Interactions from Electron-Nuclear Double Resonance Measurements," *Phys. Rev. B*, vol. 35, no. 4, 1566–1581 (1987).
- [2.140] J. C. Brabant, M. Pugnet, J. Barbolla, and M. Brousseau, "Studies of Defects Introduced by Electron Irradiation at 4.2 K in p-Silicon by Thermally Stimulated Capacitance Technique," *J. Appl. Phys.*, vol. 47, no. 11, 4809–4813 (1976).

- [2.141] L. C. Kimerling, “Defect States in Electron-Bombarded Silicon: Capacitance Transient Analyses,” in: *Radiation Effects in Semiconductors, 1976*, edited by N. B. Urli and J. W. Corbett, *Inst. Phys. Conf. Ser.*, no. 31, 221–230 (1977).
- [2.142] L. C. Kimerling, P. Blood, and W. M. Gibson, “Defect States in Proton-Bombarded Silicon at $T < 300$ K,” in: *Defects and Radiation Effects in Semiconductors, 1978*, edited by J. H. Albany, *Inst. Phys. Conf. Ser.*, no. 46, 273–280 (1979).
- [2.143] G. D. Watkins and J. R. Troxell, “Negative-U Properties for Point Defects in Silicon,” *Phys. Rev. Lett.*, vol. 44, no. 9, 593–596 (1980).
- [2.144] J. L. Newton, A. P. Chatterjee, R. D. Harris, and G. D. Watkins, “Negative-U Properties of the Lattice Vacancy in Silicon,” in: *Proceedings of the 12th International Conference on Defects in Semiconductors*, edited by C. A. J. Ammerlaan, *Physica*, vol. 116B, 219–223 (1983).
- [2.145] P. W. Anderson, “Model for the Electronic Structure of Amorphous Semiconductors,” *Phys. Rev. Lett.*, vol. 34, no. 15, 953–955 (1975).
- [2.146] G. A. Baraff, E. O. Kane, and M. Schlüter, “Silicon Vacancy: A Possible ‘Anderson Negative-U’ System,” *Phys. Rev. Lett.*, vol. 43, no. 13, 956–959 (1979).
- [2.147] G. A. Baraff, E. O. Kane, and M. Schlüter, “Simple Parameterized Model for Jahn-Teller Systems: Vacancy in p-Type Silicon,” *Phys. Rev. B*, vol. 21, no. 8, 3563–3570 (1980).
- [2.148] G. A. Baraff, E. O. Kane, and M. Schlüter, “Theory of the Silicon Vacancy: An Anderson Negative-U System,” *Phys. Rev. B*, vol. 21, no. 12, 5662–5686 (1980).
- [2.149] B. N. Mukashev, V. V. Frolov, and L. G. Koldin, “Determination of the Electrical Level of Vacancy in Electron Irradiated p-Type Silicon,” *Phys. Lett.*, vol. 91A, no. 7, 358–360 (1982).
- [2.150] H. J. Hoffmann, “Negative-U Properties of the Vacancy in Si and Experimental p(1/T) Characteristics,” *Phys. Lett.*, vol. 98A, no. 8/9, 444–446 (1983).
- [2.151] V. V. Emtsev, T. V. Mashovets, and A. V. Dabagyan, “Equilibrium Occupancy Level of Vacancies in Silicon,” *Sov. Phys. Semicond.*, vol. 21, no. 10, 1143–1146 (1987).
- [2.152] V. V. Emtsev, M. A. Margaryan, and T. V. Mashovets, “Determination of the Energy Characteristics of a Vacancy in Silicon As a Center with a Negative Correlation Energy,” *Sov. Phys. Semicond.*, vol. 18, no. 8, 950–951 (1984).
- [2.153] J. A. Van Vechten, “The Entropy of Neutral and Ionized Vacancies in Si and Ge,” in: *Lattice Defects in Semiconductors, 1974*, *Inst. Phys. Conf. Ser.*, no. 23, 212–220 (1975).
- [2.154] J. R. Troxell and G. D. Watkins, “DLTS Studies of the Isolated Vacancy in Silicon,” *Bull. Am. Phys. Soc., Series II*, vol. 24, no. 1, 18 (1979).
- [2.155] J. Mäkinen, C. Corbel, P. Hautojärvi, P. Moser, and F. Pierre, “Positron Trapping at Vacancies in Electron-Irradiated Si at Low Temperatures,” *Phys. Rev. B*, vol. 39, no. 14, 10162–10173 (1989).
- [2.156] L. C. Kimerling, H. M. De Angelis, and C. P. Carnes, “Annealing of Electron-Irradiated n-Type Silicon. I. Donor Concentration Dependence,” *Phys. Rev.*, vol. 3, no. 2, 427–433 (1971).
- [2.157] N. I. Boyarkina, “Participation of the Electron Subsystem of a Crystal in the Reactions of Defect-Complex Decomposition in Semiconductors,” *Semiconductors*, vol. 34, no. 4, 410–414 (2000).
- [2.158] V. V. Lukjanitsa, “Energy Levels of Vacancies and Interstitial Atoms in the Band Gap of Silicon,” *Sov. Phys. Semicond.*, vol. 37, no. 4, 404–413 (2003).
- [2.159] R. B. Fair, “Recent Advances in Implementation and Diffusion Modeling for the Design and Process Control of Bipolar ICs,” in: *Semiconductor Silicon 1977*, edited by H. R. Huff and E. Sirtl, *Electrochem. Soc. Proc.*, vol. 77-2, 968–987 (1977).
- [2.160] V. I. Gubskaya, P. V. Kuchinskii, and V. M. Lomako, “The Effect of the Vacancy Charge State on the Radiation Defect Formation in Silicon,” *phys. stat. sol. (a)*, vol. 85, 585–590 (1984).
- [2.161] V. V. Emtsev, T. V. Mashovets, V. V. Mikhnovich, and N. A. Vitovskii, “Frenkel Pairs in Silicon and Germanium,” *Radiation Effects*, vol. 111&112, no. 1-2, 99–118 (1989).
- [2.162] K. Matsui and R. R. Hasiguti, “Gamma-Irradiation of High Purity p-Type Silicon with Special Reference to Single Vacancy,” *J. Phys. Soc. Japan*, vol. 20, no. 4, 487–490 (1965).

- [2.163] J. A. Naber, C. E. Mallon, and R. E. Leadon, "Charge State Dependence of Defects Produced in Electron-Irradiated Silicon," in: *Radiation Damage and Defects in Semiconductors, Inst. Phys. Conf. Ser.*, no. 16, 26–33 (1973).
- [2.164] P. F. Lugakov and T. A. Lukashevich, "Characteristic of Formation of Radiation Defects in High-Resistivity Silicon," *Sov. Phys. Semicond.*, vol. 23, no. 3, 365 (1989).
- [2.165] J. C. Brabant, M. Pugnet, J. Barbolla, and M. Brousseau, "Study by Thermally Stimulated Capacitance Techniques of Defects Introduced at Low Temperature by Electron Irradiation in p-Silicon," in: *Radiation Effects in Semiconductors, 1976*, edited by N. B. Urli and J. W. Corbett, *Inst. Phys. Conf. Ser.*, no. 31, 200–206 (1977).
- [2.166] N. Zangenberg, J.-J. Goubet, and A. Nylandsted Larsen, "On-Line DLTS Investigations of the Mono- and Di-Vacancy in p-Type Silicon after Low Temperature Electron Irradiation," *Nuclear Instruments and Methods in Physics Research B*, vol. 186, 71–77 (2002).
- [2.167] O. K. Al-Mushadani and R. J. Needs, "Free-Energy Calculations of Intrinsic Point Defects in Silicon," *Phys. Rev. B*, vol. 68, 235205 (2003).
- [2.168] S. Dannefaer, G. W. Dean, D. P. Kerr, and B. G. Hogg, "Influence of Defects and Temperature on the Annihilation of Positrons in Neutron-Irradiated Silicon," *Phys. Rev. B*, vol. 14, no. 7, 2709–2714 (1976).
- [2.169] W. Fuhs, U. Holzhauer, S. Mantl, F. W. Richter, and R. Sturm, "Annihilation of Positron in Electron-Irradiated Silicon Crystals," *phys. stat. sol. (b)*, vol. 89, 69–75 (1978).
- [2.170] R. Würschum, W. Bauer, K. Maier, A. Seeger, and H.-E. Schaefer, "Defects in Semiconductors after Electron Irradiation or in High-Temperature Thermal Equilibrium, As Studied by Positron Annihilation," *J. Phys.: Condens. Matter*, vol. 1, SA33–SA48 (1989).
- [2.171] P. Mascher, S. Dannefaer, and D. Kerr, "Positron Trapping Rates and Their Temperature Dependencies in Electron-Irradiated Silicon," *Phys. Rev. B*, vol. 40, no. 17, 11764–11771 (1989).
- [2.172] S. Mäkinen, H. Rajainmäki, and S. Linderoth, "Low-Temperature Positron-Lifetime Studies of Proton-Irradiated Silicon," *Phys. Rev. B*, vol. 42, no. 17, 11166–11173 (1990).
- [2.173] K. Saarinen, J. Nissilä, H. Kauppinen, M. Hakala, M. J. Puska, P. Hautojärvi, and C. Corbel, "Identification of Vacancy-Impurity Complexes in Highly n-Type Si," *Phys. Rev. Lett.*, vol. 82, no. 9, 1883–1886 (1999).
- [2.174] M. J. Puska, O. Jepsen, O. Gunnarsson, and R. M. Nieminen, "Electronic Structure and Positron States at Vacancies in Si and GaAs," *Phys. Rev. B*, vol. 34, no. 4, 2695–2705 (1986).
- [2.175] M. J. Puska and C. Corbel, "Positron States in Si and GaAs," *Phys. Rev. B*, vol. 38, 9874–9880 (1988).
- [2.176] M. J. Puska, S. Mäkinen, M. Manninen, and R. M. Nieminen, "Screening of Positrons in Semiconductors and Insulators," *Phys. Rev. B*, vol. 39, no. 11, 7666–7679 (1989).
- [2.177] M. J. Puska, "Theory of Positron Annihilation and Trapping in Semiconductors," in: *Positron Annihilation*, edited by Z. Kajcsos and C. Szeles, *Materials Science Forum*, vol. 105–110, 419–430 (1992).
- [2.178] M. Saito and A. Oshiyama, "Lifetimes of Positrons Trapped at Si Vacancies," *Phys. Rev. B*, vol. 53, no. 12, 7810–7814 (1996).
- [2.179] M. Hakala, M. J. Puska, and R. M. Nieminen, "Momentum Distributions of Electron-Positron Pairs Annihilating at Vacancy Clusters in Si," *Phys. Rev. B*, vol. 57, no. 13, 7621–7627 (1998).
- [2.180] T. E. M. Staab, A. Sieck, M. Haugk, M. J. Puska, T. Frauenheim, and H. S. Leipner, "Stability of Large Vacancy Clusters in Silicon," *Phys. Rev. B*, vol. 65, 115210 (2002).
- [2.181] U. Lindefelt, "Symmetric Lattice Distortions around Deep-Level Impurities in Semiconductors: Vacancy and Substitutional Cu in Silicon," *Phys. Rev. B*, vol. 28, no. 8, 4510–4518 (1983).
- [2.182] M. Scheffler, J. P. Vigneron, and G. B. Bachelet, "Total-Energy Gradients and Lattice Distortions at Point Defects in Semiconductors," *Phys. Rev. B*, vol. 31, no. 10, 6541–6551 (1985).
- [2.183] G. A. Samara, "Breathing-Mode Lattice Relaxation Associated with the Vacancy and Phosphorus-Vacancy-Pair (E-Center) Defect in Silicon," *Phys. Rev. B*, vol. 37, no. 14, 8523–8526 (1988).

- [2.184] P. J. Kelly, R. Car, and S. T. Pantelides, “Theoretical Determination of the Vacancy Migration Energy in Silicon,” in: *Defects in Semiconductors 14*, edited by H. J. von Bardeleben, *Materials Science Forum*, vol. 10-12, 115–120 (1986).
- [2.185] A. Antonelli and J. Bernholc, “Pressure Effects on Self-Diffusion in Silicon,” *Phys. Rev. B*, vol. 40, no. 15, 10643–10646 (1989).
- [2.186] P. J. Kelly and R. Car, “Green’s-Matrix Calculation of Total Energies of Point Defects in Silicon,” *Phys. Rev. B*, vol. 45, no. 12, 6543–6563 (1992).
- [2.187] O. Sugino and A. Oshiyama, “Vacancy in Si: Successful Description within the Local-Density Approximation,” *Phys. Rev. Lett.*, vol. 68, no. 12, 1858–1861 (1992).
- [2.188] J. Zhu, L. H. Yang, C. Mailhiot, T. D. de la Rubia, and G. H. Gilmer, “Ab Initio Pseudopotential Calculations of Point Defects and Boron Impurity in Silicon,” in: *Computer Simulation of Radiation Effects in Solids*, edited by T. Diaz de la Rubia, G. H. Gilmer, and M.-J. Caturla, *Nuclear Instruments and Methods in Physics Research B*, vol. 102, 29–32 (1995).
- [2.189] A. Oshiyama, M. Saito, and O. Sugino, “Covalency, Elasticity and Electron Correlation in Si Vacancies,” *Applied Surface Science*, vol. 85, 239–245 (1995).
- [2.190] H. Seong and L. J. Lewis, “First-Principles Study of the Structure and Energetics of Neutral Divacancies in Silicon,” *Phys. Rev. B*, vol. 53, no. 15, 9791–9796 (1996).
- [2.191] S. Öğüt, H. Kim, and J. R. Chelikowsky, “Ab Initio Cluster Calculations for Vacancies in Bulk Si,” *Phys. Rev. B*, vol. 56, no. 18, R11353–R11356 (1997).
- [2.192] J. L. Mercer, J. S. Nelson, A. F. Wright, and E. B. Stechel, “Ab Initio Calculations of the Energetics of the Neutral Si Vacancy Defect,” *Modelling Simul. Mater. Sci. Eng.*, vol. 6, 1–8 (1998).
- [2.193] M. J. Puska, S. Pöykkö, M. Pesola, and R. M. Nieminen, “Convergence of Supercell Calculations for Point Defects in Semiconductors: Vacancy in Silicon,” *Phys. Rev. B*, vol. 58, no. 3, 1318–1325 (1998).
- [2.194] A. Antonelli, E. Kaxiras, and D. J. Chadi, “Vacancy in Silicon Revisited: Structure and Pressure Effects,” *Phys. Rev. Lett.*, vol. 81, no. 10, 2088–2091 (1998).
- [2.195] J. Xie and S. P. Chen, “Interaction Potentials for Vacancy-Assisted As Diffusion in Silicon,” *J. Phys.: Condens. Matter*, vol. 11, no. 38, 7219–7226 (1999).
- [2.196] S. Öğüt and J. R. Chelikowsky, “Ab Initio Investigation of Point Defects in Bulk Si and Ge Using a Cluster Method,” *Phys. Rev. B*, vol. 64, 245206 (2001).
- [2.197] M. I. J. Probert and M. C. Payne, “Improving the Convergence of Defect Calculations in Supercells: An *Ab Initio* Study of the Neutral Silicon Vacancy,” *Phys. Rev. B*, vol. 67, 075204 (2003).
- [2.198] N. H. Nachtrieb and G. S. Handler, “A Relaxed Vacancy Model for Diffusion in Crystalline Metals,” *Acta Metallurgica*, vol. 2, 797–802 (1954).
- [2.199] J. A. Van Vechten, “Extended Amorphous Vacancies, an Alternative to the Self-Interstitial in Si,” in: *Thirteenth International Conference on Defects in Semiconductors*, edited by L. C. Kimerling and J. M. Parsey, Jr., The Metallurgical Society of AIME, 293–299 (1985).
- [2.200] B. J. Masters, “Semivacancy Pair in Crystalline Silicon,” *Solid State Communications*, vol. 9, 283–286 (1971).
- [2.201] M. Lannoo and J. C. Bourgoin, “On the Self Diffusion Entropy in Silicon,” *Solid State Communications*, vol. 32, 913–917 (1979).
- [2.202] S. T. Pantelides, “Temperature Effects in Atomic Diffusion in Silicon,” *Phys. Rev. B*, vol. 36, no. 6, 3462–3464 (1987).
- [2.203] R. Car, P. Blöchl, and E. Smargiassi, “Ab-Initio Molecular Dynamics of Semiconductor Defects,” in: *Defects in Semiconductors 16*, edited by G. Davies, G. G. DeLeo, and M. Stavola, *Materials Science Forum*, vol. 83-87, 433–446 (1992).
- [2.204] H. Bracht, J. Fage Pedersen, N. Zangenberg, A. Nylandsted Larsen, E. E. Haller, G. Lulli, and M. Posselt, “Radiation Enhanced Silicon Self-Diffusion and the Silicon Vacancy at High Temperatures,” *Phys. Rev. Lett.*, vol. 91, 245502 (2003).

- [2.205] Y. Okada, "Concentration of Native Point Defects in Si Single Crystals at High Temperatures," *Phys. Rev. B*, vol. 41, no. 15, 10741–10743 (1990).
- [2.206] G. D. Watkins, "The Lattice Vacancy in Silicon," in: *Deep Centers in Semiconductors*, edited by S. T. Pantelides, New York: Gordon and Breach Science Publishers, 147–181 (1986).
- [2.207] L. Elstner and W. Kamprath, "Quenched-in Levels in p-Type Silicon," *phys. stat. sol.*, vol. 22, 541–547 (1967).
- [2.208] C. B. Collins and R. O. Carlson, "Properties of Silicon Doped with Iron or Copper," *Phys. Rev.*, vol. 108, no. 6, 1409–1414 (1957).
- [2.209] Y. H. Lee, R. L. Kleinhenz, and J. W. Corbett, "EPR Studies on Quenched-in Defects in Silicon," in: *Defects and Radiation Effects in Semiconductors, 1978*, edited by J. H. Albany, *Inst. Phys. Conf. Ser.*, no. 46, 521–527 (1979).
- [2.210] H. Feichtinger, J. Waltl, and A. Gschwandtner, "Localization of the Fe₀-Level in Silicon," *Solid State Communications*, vol. 27, 867–871 (1978).
- [2.211] K. Graff and H. Pieper, "The Properties of Iron in Silicon," *J. Electrochem. Soc.*, vol. 128, no. 3, 669–674 (1981).
- [2.212] B. I. Boltaks and S. I. Budarina, "Thermal Defects in Silicon," *Sov. Phys. Solid State*, vol. 11, no. 2, 330–333 (1969).
- [2.213] A. Chantre, M. Kechouane, and D. Bois, "Vacancy-Diffusion Model for Quenched-in E-Centers in CW Laser Annealed Virgin Silicon," in: *Proceedings of the 12th International Conference on Defects in Semiconductors*, edited by C. A. J. Ammerlaan, *Physica*, vol. 116B, 547–552 (1983).
- [2.214] A. Chantre, M. Kechouane, G. Auvert, and D. Bois, "Influence of Scan Speed on Deep Level Defects in CW Laser Annealed Silicon," *Appl. Phys. Lett.*, vol. 43, no. 1, 98–100 (1983).
- [2.215] A. Chantre, "Defects in Ultrafast Quenched Aluminum-Doped Silicon," *Appl. Phys. Lett.*, vol. 46, no. 3, 263–265 (1985).
- [2.216] N. Fukata, A. Kasuya, and M. Suezawa, "Vacancy Formation Energy of Silicon Determined by a New Quenching Method," *Jpn. J. Appl. Phys., Part 2*, vol. 40, no. 8B, L854–L856 (2001).
- [2.217] J. Throwe, T. C. Leung, B. Nielsen, H. Huomo, and K. G. Lynn, "Search for Thermally Generated Monovacancies in Silicon Using Monoenergetic Positrons," *Phys. Rev. B*, vol. 40, no. 17, 12037–12040 (1989).
- [2.218] P. Hautajarvi, K. Saarinen, J. Mäkinen, and C. Corbel, "Vacancies and Vacancy Defects in Si Observed by Positron Annihilation," in: *Diffusion in Silicon*, edited by D. J. Fisher, *Defect and Diffusion Forum*, vol. 153–155, 97–110 (1998).
- [2.219] B. J. Masters and E. F. Gorey, "Proton-Enhanced Diffusion and Vacancy Migration in Silicon," *J. Appl. Phys.*, vol. 49, no. 5, 2717–2724 (1978).
- [2.220] M. Budil, M. Heinrich, M. Schrems, and H. Pötzl, "Determination of the Physical Properties of Point Defects in Silicon from Back-Side Oxidation Experiments," *J. Electrochem. Soc.*, vol. 137, no. 12, 3931–3934 (1990).
- [2.221] H. Zimmermann and H. Ryssel, "Gold and Platinum Diffusion: The Key to the Understanding of Intrinsic Point Defect Behavior in Silicon," *Appl. Phys. A*, vol. 55, 121–134 (1992).
- [2.222] H. Zimmermann and H. Ryssel, "Direct Determination of Point-Defect Equilibrium Concentrations," *Phys. Rev. B*, vol. 44, no. 16, 9064–9067 (1991).
- [2.223] H. Zimmermann, "Accurate Measurement of the Vacancy Equilibrium Concentration in Silicon," *Appl. Phys. Lett.*, vol. 59, no. 24, 3133–3135 (1991).
- [2.224] H.-J. Gossman, C. S. Rafferty, A. M. Vredenberg, H. S. Luftman, F. C. Unterwald, D. J. Eaglesham, D. C. Jacobson, T. Boone, and J. M. Poate, "Time Dependence of Dopant Diffusion in Delta-Doped Si Films and Properties of Si Point Defects," *Appl. Phys. Lett.*, vol. 64, no. 3, 312–314 (1994).
- [2.225] T. Y. Tan, P. Plekhanov, and U. M. Gösele, "Nucleation Barrier of Voids and Dislocation Loops in Silicon," *Appl. Phys. Lett.*, vol. 70, no. 13, 1715–1717 (1997).

- [2.226] M. Jacob, P. Pichler, M. Wohs, H. Ryssel, and R. Falster, “Influence of RTP on Vacancy Concentrations,” in: *Semiconductor Process and Device Performance Modelling*, edited by S. T. Dunham and J. S. Nelson, *Mat. Res. Soc. Symp. Proc.*, vol. 490, 129–134 (1998).
- [2.227] R. F. Scholz, P. Werner, U. Gösele, and T. Y. Tan, “The Contribution of Vacancies to Carbon Out-Diffusion in Silicon,” *Appl. Phys. Lett.*, vol. 74, no. 3, 392–394 (1999).
- [2.228] T. Okino and T. Shimozaki, “Thermal Equilibrium Concentrations and Diffusivities of Intrinsic Point Defects in Silicon,” in: *20th International Conference on Defects in Semiconductors*, edited by C. Van de Walle and W. Walukiewicz, *Physica B*, vol. 273–274, 509–511 (1999).
- [2.229] K. Nakamura, T. Saishoji, and J. Tomioka, “Simulation of the Point Defect Diffusion and Growth Condition for Defect Free Cz Silicon Crystal,” in: *Semiconductor Silicon 2002*, edited by H. R. Huff, L. Fabry, and S. Kishino, *Electrochem. Soc. Proc.*, vol. 2002-2, 554–566 (2002).
- [2.230] D. C. Mueller, E. Alonso, and W. Fichtner, “Arsenic Deactivation in Si: Electronic Structure and Charge States of Vacancy-Impurity Clusters,” *Phys. Rev. B*, vol. 68, 045208 (2003).
- [2.231] R. Car, P. J. Kelly, A. Oshiyama, and S. T. Pantelides, “Microscopic Theory of Atomic Diffusion Mechanisms in Silicon,” *Phys. Rev. Lett.*, vol. 52, no. 20, 1814–1817 (1984).
- [2.232] Y. Bar-Yam and J. D. Joannopoulos, “Intrinsic Defects in Silicon: Formation and Migration Barriers,” in: *17th International Conference on the Physics of Semiconductors*, edited by J. D. Chadi and W. A. Harrison, New York: Springer-Verlag, 721–724 (1985).
- [2.233] R. Car, P. J. Kelly, A. Oshiyama, and S. T. Pantelides, “Microscopic Theory of Self-Diffusion and Impurity Diffusion in Silicon,” in: *Thirteenth International Conference on Defects in Semiconductors*, edited by L. C. Kimerling and J. M. Parsey, Jr., The Metallurgical Society of AIME, 269–275 (1985).
- [2.234] C. S. Nichols, C. G. van de Walle, and S. T. Pantelides, “Mechanisms of Dopant Impurity Diffusion in Silicon,” *Phys. Rev. B*, vol. 40, no. 8, 5484–5496 (1989).
- [2.235] P. E. Blöchl, D. B. Laks, S. T. Pantelides, E. Smargiassi, R. Car, W. Andreoni, and M. Parrinello, “First-Principles Calculations of Self-Diffusion Coefficients in Silicon,” in: *20th International Conference on the Physics of Semiconductors*, edited by E. M. Anastassakis and J. D. Joannopoulos, Singapore: World Scientific, 533–536 (1990).
- [2.236] J. L. Hastings, S. K. Estreicher, and P. A. Fedders, “Vacancy Aggregates in Silicon,” *Phys. Rev. B*, vol. 56, no. 16, 10215–10220 (1997).
- [2.237] A. Zywiertz, J. Furthmüller, and F. Bechstedt, “The Jahn-Teller Effect and the Structure of Monovacancies in Si, SiC and C,” in: *Defects in Semiconductors 19*, edited by G. Davies and M. H. Nazaré, *Materials Science Forum*, vol. 258–263, 653–658 (1997).
- [2.238] J. Zhu, “Ab Initio Pseudopotential Calculations of Dopant Diffusion in Si,” *Comput. Mater. Sci.*, vol. 12, 309–318 (1998).
- [2.239] J. S. Nelson, P. A. Schultz, and A. F. Wright, “Valence and Atomic Size Dependent Exchange Barriers in Vacancy-Mediated Dopant Diffusion,” *Appl. Phys. Lett.*, vol. 73, no. 2, 247–249 (1998).
- [2.240] J. Xie and S. P. Chen, “Ab Initio Calculations of Point Defects in Silicon,” in: *Multiscale Modeling of Materials*, edited by V. V. Bulatov, T. Diaz de la Rubia, R. Phillips, E. Kaxiras, and N. Ghoniem, *Mat. Res. Soc. Symp. Proc.*, vol. 538, 389–394 (1999).
- [2.241] J. Coutinho, R. Jones, P. R. Briddon, and S. Öberg, “Oxygen and Dioxygen Centers in Si and Ge: Density-Functional Calculations,” *Phys. Rev. B*, vol. 62, no. 16, 10824–10840 (2000).
- [2.242] X.-Y. Liu, W. Windl, K. M. Beardmore, and M. P. Masquelier, “First-Principles Study of Phosphorus Diffusion in Silicon: Interstitial and Vacancy-Mediated Diffusion Mechanisms,” *Appl. Phys. Lett.*, vol. 82, no. 12, 1839–1841 (2003).
- [2.243] G. D. Watkins, “The Interaction of Irradiation-Produced Defects with Impurities and Other Defects in Semiconductors EPR Studies in Silicon,” in: *Colloque international sur l'action des rayonnements sur les composants à semiconducteurs*, edited by F. Cambou, C. Fert, and J. Lagasse, A1/1–13 (1967).
- [2.244] B. L. Gregory and H. H. Sander, “Injection Dependence of Transient Annealing in Neutron-Irradiated Silicon Devices,” *IEEE Trans. Nuclear Science*, vol. 14, no. 6, 116–126 (1967).

- [2.245] H. J. Stein and F. L. Vook, "Transient Radiation Defects," in: *Colloque international sur l'action des rayonnements sur les composants à semiconducteurs*, edited by F. Cambou, C. Fert, and J. Lagasse, A3/1–21 (1967).
- [2.246] D. Binder, D. T. Butcher, J. R. Crepps, and E. L. Hammer, "Rapid Annealing in Silicon Transistors," *IEEE Trans. Nuclear Science*, vol. NS-15, no. 6, 84–87 (1968).
- [2.247] J. R. Srour, "Short-Term Annealing in Electron-Irradiated p-Type Silicon," *IEEE Trans. Nuclear Science*, vol. NS-17, no. 6, 118–122 (1970).
- [2.248] S. N. Ershov, V. V. Panteleev, S. N. Nagornyykh, and V. V. Chernyakhovskii, "Migration Energy of Intrinsic Point Defects in Different Charge States in Silicon and Germanium," *Sov. Phys. Solid State*, vol. 19, no. 1, 187 (1977).
- [2.249] V. A. Panteleev, S. N. Ershov, and Y. L. Kalinkin, "Investigation of the Migration of Primary Radiation Defects in Silicon in the Temperature Range from 200 to 400 °C (russ.)," in: *Radiation Physics of Semiconductors and Related Materials, 1979*, edited by G. P. Kekelidze and V. I. Shakhovtsov, Tbilisi: Tbilisi State University Press, 497–500 (1980).
- [2.250] P. Partyka, Y. Zhong, K. Nordlund, R. S. Averback, I. M. Robinson, and P. Ehrhart, "Grazing Incidence Diffuse X-Ray Scattering Investigation of the Properties of Irradiation-Induced Point Defects in Silicon," *Phys. Rev. B*, vol. 64, 235207 (2001).
- [2.251] V. A. Panteleev, S. N. Ershov, V. V. Chernyakhovskii, and S. N. Nabornyykh, "Determination of the Migration Energy of Vacancies and of Intrinsic Interstitial Atoms in Silicon in the Temperature Interval 400–600 °K," *JETP Lett.*, vol. 23, no. 12, 633–635 (1976).
- [2.252] K. L. Wang, Y. H. Lee, and J. W. Corbett, "Defect Distribution near the Surface of Electron-Irradiated Silicon," *Appl. Phys. Lett.*, vol. 33, no. 6, 547–548 (1978).
- [2.253] F. Priolo, V. Privitera, S. Coffa, and S. Libertino, "Ion Beam Injected Point Defects in Crystalline Silicon: Migration, Interaction and Trapping Phenomena," in: *Materials Modification and Synthesis by Ion Beam Processing*, edited by D. E. Alexander, N. W. Cheung, B. Park, and W. Skorupa, *Mat. Res. Soc. Symp. Proc.*, vol. 438, 53–64 (1997).
- [2.254] A. Hallén, N. Keskitalo, and B. G. Svensson, "Diffusion and Reaction Kinetics of Fast-Ion-Induced Point Defects Studied by Deep Level Transient Spectroscopy," in: *Diffusion in Silicon*, edited by D. J. Fisher, *Defect and Diffusion Forum*, vol. 153–155, 193–204 (1998).
- [2.255] S. Coffa and S. Libertino, "Room Temperature Diffusivity of Self-Interstitials and Vacancies in Ion-Implanted Si Probed by In-Situ Measurements," *Appl. Phys. Lett.*, vol. 73, no. 23, 3369–3371 (1998).
- [2.256] S. Libertino and S. Coffa, "Room Temperature Point Defect Migration in Crystalline Si," in: *Gettering and Defect Engineering in Semiconductor Technology GADEST 2001*, edited by V. Rainieri, F. Priolo, M. Kittler, and H. Richter, *Solid State Phenomena*, vol. 82–84, 207–212 (2002).
- [2.257] A. Nylandsted Larsen, C. Christensen, and J. Wulff Petersen, "Room-Temperature Vacancy Migration in Crystalline Si from an Ion-Implanted Surface Layer," *J. Appl. Phys.*, vol. 86, no. 9, 4861–4864 (1999).
- [2.258] K. Kyllsbech Larsen, V. Privitera, S. Coffa, F. Priolo, S. U. Campisano, and A. Carnera, "Trap-Limited Migration of Si Self-Interstitials at Room Temperature," *Phys. Rev. Lett.*, vol. 76, no. 9, 1493–1496 (1996).
- [2.259] S. M. Hu, "On Interaction Potential, Correlation Factor, Vacancy Mobility, and Activation Energy of Impurity Diffusion in Diamond Lattice," *phys. stat. sol. (b)*, vol. 60, 595–603 (1973).
- [2.260] L. I. Fedina and A. L. Aseev, "Study of Interaction of Point Defects with Dislocations in Silicon by Means of Irradiation in an Electron Microscope," *phys. stat. sol. (a)*, vol. 95, 517–529 (1986).
- [2.261] P. B. Griffin, P. A. Packan, and J. D. Plummer, "Consistent Models for Point Defects in Silicon," in: *1991 International Workshop on VLSI Process and Device Modeling (1991 VPAD)*, Japan Society of Applied Physics, 4–7 (1991).

- [2.262] T. Okino, “Behavior of Self-Interstitials and Vacancies in Silicon,” in: *Diffusion in Materials DIMAT-92*, edited by M. Koiwa, K. Hirano, H. Nakajima, and T. Okada, *Defect and Diffusion Forum*, vol. 95-98, 961–966 (1993).
- [2.263] T. Shimizu, Y. Zatisu, S. Matsumoto, E. Arai, M. Yoshida, and T. Abe, “Determination of Vacancy Diffusivity in Silicon for Process Simulation,” in: *Simulation of Semiconductor Devices and Processes, Vol. 6*, edited by H. Ryssel and P. Pichler, Vienna: Springer-Verlag, 444–447 (1995).
- [2.264] A. M. Eidenzon and N. I. Puzanov, “Native Point Defects in Silicon at High Temperatures,” *Inorganic Materials*, vol. 31, no. 9, 1043–1048 (1995).
- [2.265] T. K. Mogi, M. O. Thompson, H.-J. Gossmann, J. M. Poate, and H. S. Luftman, “Thermal Nitridation Enhanced Diffusion of Sb and Si(100) Doping Superlattices,” *Appl. Phys. Lett.*, vol. 69, no. 9, 1273–1275 (1996).
- [2.266] N. I. Puzanov, A. E. Eidenzon, and D. N. Puzanov, “Modelling Microdefect Distribution in Dislocation-Free Si Crystals Grown from the Melt,” *J. Crystal Growth*, vol. 178, 468–478 (1997).
- [2.267] T. Okino and T. Shimozaki, “Analysis of Dopant Diffusion in Si with Stacking Faults,” *Materials Transactions, JIM*, vol. 40, no. 6, 474–478 (1999).
- [2.268] J. L. Ngau, P. B. Griffin, and J. D. Plummer, “Modeling the Suppression of Boron Transient Enhanced Diffusion in Silicon by Substitutional Carbon Incorporation,” *J. Appl. Phys.*, vol. 90, no. 4, 1768–1778 (2001).
- [2.269] O. Sugino and A. Oshiyama, “Pressure Dependence of Formation and Migration Enthalpies for Atomic Diffusion in Si: Conjugate Gradient Minimization of Total Energy,” in: *Defects in Semiconductors 16*, edited by G. Davies, G. G. DeLeo, and M. Stavola, *Materials Science Forum*, vol. 83-87, 469–474 (1992).
- [2.270] J. A. Van Vechten, “Activation Enthalpy of Recombination-Enhanced Vacancy Migration in Si,” *Phys. Rev. B*, vol. 38, no. 14, 9913–9919 (1988).
- [2.271] A. Hallén, N. Keskitalo, F. Masszi, and V. Nágli, “Lifetime in Proton Irradiated Silicon,” *J. Appl. Phys.*, vol. 79, no. 8, 3906–3014 (1996).
- [2.272] H. Bleichner, P. Jonsson, N. Keskitalo, and E. Nordlander, “Temperature and Injection Dependence of the Shockley-Read-Hall Lifetime in Electron Irradiated n-Type Silicon,” *J. Appl. Phys.*, vol. 79, no. 12, 9142–9148 (1996).
- [2.273] S. J. Watts, J. Matheson, I. H. Hopkins-Bond, A. Holmes-Siedle, A. Mohammadzadeh, and R. Pace, “A New Model for Generation-Recombination in Silicon Depletion Regions after Neutron Irradiation,” *IEEE Trans. Nuclear Science*, vol. 43, no. 6, 2587–2594 (1996).
- [2.274] B. MacEvoy, K. Gill, and G. Hall, “Defect-Engineering Rad-Hard Detectors for the CERN LHC,” in: *Defects in Semiconductors 19*, edited by G. Davies and M. H. Nazaré, *Materials Science Forum*, vol. 258–263, 671–676 (1997).
- [2.275] J. W. Corbett and G. D. Watkins, “Silicon Divacancy and Its Direct Production by Electron Irradiation,” *Phys. Rev. Lett.*, vol. 7, no. 8, 314–316 (1961).
- [2.276] G. Bemski, B. Szymanski, and K. Wright, “A New Paramagnetic Center in Electron Irradiated Silicon,” *J. Phys. Chem. Solids*, vol. 24, 1–6 (1963).
- [2.277] P. R. Brosious, “EPR of a Spin-1 Two-Vacancy Defect in Electron-Irradiated Silicon,” in: *Defects and Radiation Effects in Semiconductors, 1978*, edited by J. H. Albany, *Inst. Phys. Conf. Ser.*, no. 46, 248–257 (1979).
- [2.278] E. G. Sieverts and J. W. Corbett, “The Neutral Divacancy in Silicon,” *Solid State Communications*, vol. 43, no. 1, 41–46 (1982).
- [2.279] G. D. Watkins and J. W. Corbett, “Defects in Irradiated Silicon: Electron Paramagnetic Resonance of the Divacancy,” *Phys. Rev.*, vol. 138, no. 2A, A543–A555 (1965).
- [2.280] J. G. de Wit, E. G. Sieverts, and C. A. J. Ammerlaan, “Divacancy in Silicon: Hyperfine Interactions from Electron-Nuclear Double Resonance Measurements,” *Phys. Rev. B*, vol. 14, no. 8, 3494–3503 (1976).

- [2.281] E. G. Sieverts, S. H. Muller, and C. A. J. Ammerlaan, "Divacancy in Silicon: Hyperfine Interactions from Electron-Nuclear Double-Resonance Measurements. II," *Phys. Rev. B*, vol. 18, no. 12, 6834–6848 (1978).
- [2.282] L. Dobaczewski, K. Gościński, Z. R. . Ztykiewicz, K. Bonde Nielsen, L. Rubaldo, O. Andersen, and A. R. Peaker, "Piezoscopic Deep-Level Transient Spectroscopy Studies of the Silicon Divacancy," *Phys. Rev. B*, vol. 65, 113203 (2002).
- [2.283] Y. Nagai, K. Inoue, Z. Tang, I. Yonenaga, T. Chiba, M. Saito, and M. Hasegawa, "Jahn-Teller Distortion of Neutral Divacancy in Si Studied by Positron Annihilation Spectroscopy," in: *Proceedings of the 22nd International Conference on Defects in Semiconductors*, edited by K. Bonde Nielsen, A. Nylandsted Larsen, and G. Weyer, *Physica B*, vol. 340-342, 518–522 (2003).
- [2.284] E. G. Sieverts, S. H. Muller, and C. A. J. Ammerlaan, "On the Production of Paramagnetic Defects in Silicon by Electron Irradiation," *Solid State Communications*, vol. 28, 221–225 (1978).
- [2.285] J. W. Corbett, J. P. Karins, and T. Y. Tan, "Ion-Induced Defects in Semiconductors," *Nuclear Instruments and Methods in Physics Research*, vol. 182/183, 457–476 (1981).
- [2.286] L. J. Cheng, J. C. Corelli, J. W. Corbett, and G. D. Watkins, "1.8-, 3.3-, and 3.9- μ Bands in Irradiated Silicon: Correlations with the Divacancy," *Phys. Rev.*, vol. 152, no. 2, 761–774 (1966).
- [2.287] H. Y. Fan and A. K. Ramdas, "Infrared Absorption and Photoconductivity in Irradiated Silicon," *J. Appl. Phys.*, vol. 30, no. 8, 1127–1134 (1959).
- [2.288] L. J. Cheng and P. Vadja, "Effect of Polarized Light on the 1.8-, 3.3-, and 3.9- μ Radiation-Induced Absorption Bands in Silicon," *Phys. Rev.*, vol. 186, no. 3, 816–823 (1969).
- [2.289] J. H. Svensson, B. G. Svensson, and B. Monemar, "Infrared Absorption Studies of the Divacancy in Silicon: New Properties of the Singly Negative Charge State," *Phys. Rev. B*, vol. 38, no. 6, 4192–4197 (1988).
- [2.290] B. G. Svensson, K. Johnsson, D.-X. Xu, J. H. Svensson, and J. L. Lindström, "Annealing of Divacancy-Related Infrared Absorption Bands in Boron-Doped Silicon," *Radiation Effects and Defects in Solids*, vol. 111/112, no. 1-2, 439–447 (1989).
- [2.291] L. J. Cheng, "3.9 μ Photoconductivity Band in Neutron-Irradiated p-Type Silicon," *Phys. Lett. A*, vol. 24, no. 13, 729–731 (1967).
- [2.292] A. H. Kalma and J. C. Corelli, "Photoconductivity Studies of Defects in Silicon: Divacancy-Associated Energy Levels," *Phys. Rev.*, vol. 173, no. 3, 734–745 (1968).
- [2.293] C. S. Chen and J. C. Corelli, "Infrared Spectroscopy of Divacancy-Associated Radiation-Induced Absorption Bands in Silicon," *Phys. Rev. B*, vol. 5, no. 4, 1505–1517 (1972).
- [2.294] F. Carton-Merlet, B. Pajot, and P. Vajda, "Detection of the Photopopulation and Photoionisation of Intrinsic Point Defects in Irradiated Silicon by IR Absorption," in: *Defects and Radiation Effects in Semiconductors, 1978*, edited by J. H. Albany, *Inst. Phys. Conf. Ser.*, no. 46, 311–316 (1979).
- [2.295] A. O. Evwaraye and E. Sun, "Electron-Irradiation-Induced Divacancy in Lightly Doped Silicon," *J. Appl. Phys.*, vol. 47, no. 9, 3776–3780 (1976).
- [2.296] J. H. Evans-Freeman, A. R. Peaker, I. D. Hawkins, P. Y. Y. Kan, J. Terry, L. Rubaldo, M. Ahmed, S. Watts, and L. Dobaczewski, "High-Resolution DLTS Studies of Vacancy-Related Defects in Irradiated and in Ion-Implanted n-Type Silicon," *Materials Science in Semiconductor Processing*, vol. 3, 237–241 (2000).
- [2.297] H. Kauppinen, C. Corbel, K. Skog, K. Saarinen, T. Laine, P. Hautojäautrvi, P. Desgardin, and E. Ntsoenzok, "Divacancy and Resistivity Profiles in n-Type Si Implanted with 1.15-MeV Protons," *Phys. Rev. B*, vol. 55, no. 15, 9598–9608 (1997).
- [2.298] H. Kauppinen, C. Corbel, J. Nissilä, K. Saarinen, and P. Hautojärvi, "Photoionization of the Silicon Divacancy Studied by Positron-Annihilation Spectroscopy," *Phys. Rev. B*, vol. 57, no. 20, 12911–12922 (1998).
- [2.299] B. G. Svensson, B. Mohadjeri, A. Hallén, J. H. Svensson, and J. W. Corbett, "Divacancy Acceptor Levels in Ion-Irradiated Silicon," *Phys. Rev. B*, vol. 43, no. 3, 2292–2298 (1991).

- [2.300] P. V. Kuchinskii and V. M. Lomako, “On the Mechanism of Primary Radiation Defect Annihilation in Si,” *phys. stat. sol. (a)*, vol. 102, 653–658 (1987).
- [2.301] B. G. Svensson and M. Willander, “Generation of Divacancies in Silicon Irradiated by 2-MeV Electrons: Depth and Dose Dependence,” *J. Appl. Phys.*, vol. 62, no. 7, 2758–2762 (1987).
- [2.302] A. Hallén, B. U. R. Sundqvist, Z. Paska, B. G. Svensson, M. Rosling, and J. Tirén, “Deep Level Transient Spectroscopy Analysis of Fast Ion Tracks in Silicon,” *J. Appl. Phys.*, vol. 67, no. 3, 1266–1271 (1990).
- [2.303] Y. Tokuda, N. Shimizu, and A. Usami, “Studies of Neutron-Produced Defects in Silicon by Deep-Level Transient Spectroscopy,” *Jpn. J. Appl. Phys.*, vol. 18, no. 2, 309–315 (1979).
- [2.304] A. V. Vasil’ev, S. A. Smagulova, and S. S. Shaĭmeev, “Capacitance Spectroscopy Investigation of Defects Formed in *n*-Type Silicon by Neutron Irradiation,” *Sov. Phys. Semicond.*, vol. 16, no. 11, 1279–1281 (1982).
- [2.305] B. G. Svensson, C. Jagadish, A. Hallén, and J. Lalita, “Generation of Vacancy-Type Point Defects in Single Collision Cascades during Swift-Ion Bombardment of Silicon,” *Phys. Rev. B*, vol. 55, 10498–10507 (1997).
- [2.306] E. V. Monakhov, J. Wong-Leung, A. Y. Kuznetsov, C. Jagadish, and B. G. Svensson, “Ion Mass Effect on Vacancy-Related Deep Levels in Si Induced by Ion Implantation,” *Phys. Rev. B*, vol. 65, 245201 (2002).
- [2.307] P. K. Giri, “Metastability of Interstitial Clusters in Ion-Damaged Silicon Studied by Isothermal Capacitance Transient Spectroscopy,” *Defect and Diffusion Forum*, vol. 210-212, 1–13 (2002).
- [2.308] B. V. Shemaev, “Positions of Acceptor Levels of a Divacancy in the Band Gap of *n*-Type Silicon Irradiated with 6.3 MeV Protons,” *Sov. Phys. Semicond.*, vol. 17, no. 11, 1254–1255 (1983).
- [2.309] L. A. Kazakevich, V. I. Kuznetsov, and P. F. Lugakov, “On the Nature of the Radiation Defects with Level E_c - 0.22 eV in *n*-Type Silicon,” *Radiation Effects Letters*, vol. 87, 147–154 (1986).
- [2.310] A. V. Vasil’ev, L. S. Smirnov, and S. S. Shaĭmeev, “Divacancy Levels in the Band Gap of Silicon,” *Sov. Phys. Semicond.*, vol. 20, no. 4, 465–467 (1986).
- [2.311] F. P. Korshunov, V. P. Markevich, I. F. Medvedeva, and L. I. Murin, “Acceptor Levels of a Divacancy in Silicon,” *Sov. Phys. Semicond.*, vol. 26, no. 11, 1129–1131 (1992).
- [2.312] C. A. Londos, “Divacancy Production in Low-Temperature Electron-Irradiated Silicon,” *Phys. Rev. B*, vol. 35, no. 14, 7511–7514 (1987).
- [2.313] M.-A. Trauwaert, J. Vanhellemont, H. E. Maes, A.-M. Van Bavel, G. Langouche, A. Stesmans, and P. Clauws, “Influence of Oxygen and Carbon on the Generation and Annihilation of Radiation Defects in Silicon,” *Materials Science and Engineering B*, vol. 36, 196–199 (1996).
- [2.314] I. D. Kononenko, A. K. Semenyuk, and V. I. Khivrich, “Radiation Defects Created by Co^{60} γ -Rays in *p*- and *n*-Type Si of High Purity,” *phys. stat. sol.*, vol. 35, 1043–1052 (1969).
- [2.315] M. T. Lappo and V. D. Tkachev, “Divacancies in Silicon Irradiated with Fast Neutrons,” *Sov. Phys. Semicond.*, vol. 4, no. 11, 1882–1884 (1971).
- [2.316] J. Krynicki, J. C. Bourgoin, and G. Vassal, “Energy Dependence of Defect Energy Levels in Electron Irradiated Silicon,” *Revue Phys. Appl.*, vol. 14, 481–484 (1979).
- [2.317] J. M. Meese, M. Chandrasekhar, D. L. Cowan, S. L. Chang, H. Yousif, H. R. Chandrasekhar, and P. McGrail, “Defect Production during Neutron Doping of Si,” in: *Neutron-Transmutation-Doped Silicon*, edited by J. M. Meese, New York: Plenum Press, 101–140 (1981).
- [2.318] S. D. Brotherton and P. Bradley, “Defect Production and Lifetime Control in Electron and gamma-Irradiated Silicon,” *J. Appl. Phys.*, vol. 53, no. 8, 5720–5732 (1982).
- [2.319] P. Hazdra and J. Vobecký, “Nondestructive Defect Characterization and Engineering in Contemporary Silicon Power Devices,” in: *Gettering and Defect Engineering in Semiconductor Technology GADEST'99*, edited by H. G. Grimmeiss, L. Ask, M. Kleverman, M. Kittler, and H. Richter, *Solid State Phenomena*, vol. 69-70, 545–550 (1999).
- [2.320] E. V. Monakhov, B. S. Avset, A. Hallén, and B. G. Svensson, “Formation of a Double Acceptor Center during Divacancy Annealing in Low-Doped High-Purity Oxygenated Si,” *Phys. Rev. B*, vol. 65, 233207 (2002).

- [2.321] P. M. Mooney, L. J. Cheng, M. Süli, J. D. Gerson, and J. W. Corbett, "Defect Energy Levels in Boron-Doped Silicon Irradiated with 1-MeV Electrons," *Phys. Rev. B*, vol. 15, no. 8, 3836–3843 (1977).
- [2.322] Y. H. Lee, K. L. Wang, A. Jaworoski, P. M. Mooney, L. J. Cheng, and J. W. Corbett, "A Transient Capacitance Study of Radiation-Induced Defects in Aluminum-Doped Silicon," *phys. stat. sol. (a)*, vol. 57, 697–704 (1980).
- [2.323] M. Stavola and L. C. Kimerling, "Symmetry Determination for Deep States in Semiconductors from Stress-Induced Dichroism of Photocapacitance," *J. Appl. Phys.*, vol. 54, no. 7, 3897–3901 (1983).
- [2.324] M. Asghar, M. Zafar Iqbal, and N. Zafar, "Study of Alpha-Radiation-Induced Deep Levels in p-Type Silicon," *J. Appl. Phys.*, vol. 73, no. 9, 4240–4247 (1993).
- [2.325] A. Khan, M. Yamaguchi, S. J. Taylor, T. Hisamatsu, and S. Matsuda, "Effects of Annealing on Type Converted Si and Space Solar Cells Irradiated with Heavy Fluence 1 MeV Electrons," *Jpn. J. Appl. Phys., Part 1*, vol. 38, no. 5A, 2679–2685 (1999).
- [2.326] M. Shimotomai, Y. Ohgino, H. Fukushima, Y. Nagayasu, T. Mihara, K. Inoue, and M. Doyama, "The Utility of Positrons for Studies of Vacancy-Type Defects in Semiconductors," in: *Defects and Radiation Effects in Semiconductors, 1980*, edited by R. R. Hasiguti, *Inst. Phys. Conf. Ser.*, no. 59, 241–246 (1981).
- [2.327] Motoko Kwete, D. Segers, M. Dorikens, L. Dorikens-Vanpraet, and P. Clauws, "Positron Annihilation Study of Defects Created in Silicon Irradiated with Electrons of High Energy," *phys. stat. sol. (a)*, vol. 122, 129–138 (1990).
- [2.328] A. Kawasuso, M. Hawegawa, M. Suezawa, S. Yamauchi, and K. Sumino, "An Annealing Study of Defects Induced by Electron Irradiation of Czochralski-Grown Si Using a Positron Lifetime Technique," *Applied Surface Science*, vol. 85, 280–286 (1995).
- [2.329] M. Hasegawa, A. Kawasuso, T. Chiba, T. Akahane, M. Suezawa, S. Yamaguchi, and K. Sumino, "Positron Lifetime and 2D-ACAR Studies of Divacancies in Silicon," *Appl. Phys. A*, vol. 61, 65–70 (1995).
- [2.330] V. Avalos and S. Dannefaer, "Positron-Annihilation Investigation of Vacancy Agglomeration in Electron-Irradiated Float-Zone Silicon," *Phys. Rev. B*, vol. 54, no. 3, 1724–1728 (1996).
- [2.331] A. Polity, F. Börner, S. Huth, S. Eichler, and R. Krause-Rehberg, "Defects in Electron-Irradiated Si Studied by Positron-Lifetime Spectroscopy," *Phys. Rev. B*, vol. 58, no. 16, 10363–10377 (1998).
- [2.332] R. Krause-Rehberg and H. S. Leipner, "Defect Characterization in Elemental Semiconductors: Silicon," in: *Positron Annihilation in Semiconductors, Solid-State Sciences*, vol. 127, Section 4.1, Berlin: Springer, 127–182 (1999).
- [2.333] H. J. Stein, J. A. Knapp, and P. S. Peercy, "Divacancy Annealing in Crystalline Silicon Using E-Beam and Pulsed Ruby Laser Excitation," in: *Laser and Electron-Beam Interactions with Solids*, edited by B. R. Appleton and G. K. Celler, *Mat. Res. Soc. Symp. Proc.*, vol. 4, 319–324 (1982).
- [2.334] P. Pellegrino, P. Lévêque, J. Lalita, A. Hallén, C. Jagadish, and B. G. Svensson, "Annealing Kinetics of Vacancy-Related Defects in Low-Dose MeV Self-Ion-Implanted n-Type Silicon," *Phys. Rev. B*, vol. 64, 195211 (2001).
- [2.335] A. V. Vasil'ev, S. A. Smagulova, and L. S. Smirnov, "Annealing of Divacancies in Silicon Irradiated with Fast Neutrons," *Sov. Phys. Semicond.*, vol. 20, 354 (1986).
- [2.336] I. V. Antonova, A. V. Vasil'ev, V. I. Panov, and S. S. Shaimeev, "Characteristics of Annealing of Divacancies in Silicon Containing Disordered Regions," *Sov. Phys. Semicond.*, vol. 23, no. 6, 671–673 (1989).
- [2.337] S. Roorda, "Divacancy Annealing in Silicon Monitored by Differential Calorimetry and Infrared Absorption Spectroscopy," in: *Materials Synthesis and Processing Using Ion Beams*, edited by R. J. Culbertson, O. W. Holland, K. S. Jones, and K. Maex, *Mat. Res. Soc. Symp. Proc.*, vol. 316, 159–165 (1994).

- [2.338] R. Poirier, S. Roorda, F. Schiettekatte, M. Lalancette, and J. Zikovsky, “Divacancies in Proton Irradiated Silicon: Characterization and Annealing Mechanisms,” *Physica B*, vol. 308–310, 462–464 (2001).
- [2.339] M. Saito and A. Oshiyama, “Resonant Bonds in Symmetry-Lowering Distortion around a Si Divacancy,” *Phys. Rev. Lett.*, vol. 73, no. 6, 866–869 (1994).
- [2.340] G. D. Watkins, “Comment on ‘Resonant Bonds in Symmetry-Lowering Distortion around a Si Divacancy’ [Phys. Rev. Lett. 73, 866 (1994)],” *Phys. Rev. Lett.*, vol. 74, no. 21, 4353 (1995).
- [2.341] M. Saito and A. Oshiyama, “Response to ‘Comment on ‘Resonant Bonds in Symmetry-Lowering Distortion around a Si Divacancy’ ’ [Phys. Rev. Lett. 73, 866 (1994)],” *Phys. Rev. Lett.*, vol. 74, no. 21, 4354 (1995).
- [2.342] M. Pesola, J. von Boehm, S. Pöykkö, and R. M. Nieminen, “Spin-Density Study of the Silicon Divacancy,” *Phys. Rev. B*, vol. 58, no. 3, 1106–1109 (1998).
- [2.343] B. J. Coomer, A. Resende, J. P. Goss, R. Jones, S. Öberg, and P. R. Briddon, “The Divacancy in Silicon and Diamond,” in: *20th International Conference on Defects in Semiconductors*, edited by C. Van de Walle and W. Walukiewicz, *Physica B*, vol. 273–274, 520–523 (1999).
- [2.344] T. Akiyama, Y. Okamoto, M. Saito, and A. Oshiyama, “Multivacancy and Its Hydrogen Decoration in Crystalline Si,” *Jpn. J. Appl. Phys., Part 2*, vol. 38, no. 12A, L1363–L1365 (1999).
- [2.345] G. S. Hwang and W. A. Goddard III, “Diffusion and Dissociation of Neutral Divacancies in Crystalline Silicon,” *Phys. Rev. B*, vol. 65, 233205 (2002).
- [2.346] M. Prasad and T. Sinno, “Internally Consistent Approach for Modeling Solid-State Aggregation. I. Atomistic Calculations of Vacancy Clustering in Silicon,” *Phys. Rev. B*, vol. 68, 045206 (2003).
- [2.347] S. K. Estreicher, J. Weber, A. Derecskei-Kovacs, and D. S. Marynick, “Noble-Gas-Related Defects in Si and the Origin of the 1018 meV Photoluminescence Line,” *Phys. Rev. B*, vol. 55, no. 8, 5037–5044 (1997).
- [2.348] P. K. Giri, S. Coffa, and E. Rimini, “Evidence for Small Interstitial Clusters As the Origin of Photoluminescence W Band in Ion-Implanted Silicon,” *Appl. Phys. Lett.*, vol. 78, no. 3, 291–293 (2001).
- [2.349] J. Lalita, B. G. Svensson, and C. Jagadish, “Point Defects Observed in Crystalline Silicon Implanted by MeV Si Ions at Elevated Temperatures,” *Nuclear Instruments and Methods in Physics Research B*, vol. 96, 210–214 (1995).
- [2.350] Y. Nakano, M. Ishiko, and H. Tadano, “Deep Level Centers in Silicon Introduced by High-Energy He Irradiation and Subsequent Annealing,” *J. Vac. Sci. Technol. B*, vol. 20, no. 1, 379–381 (2002).
- [2.351] Y. H. Lee, Y. M. Kim, and J. W. Corbett, “New EPR Spectra in Neutron-Irradiated Silicon,” *Radiation Effects*, vol. 15, 77–84 (1972).
- [2.352] Y.-H. Lee and J. W. Corbett, “EPR Study of Defects in Neutron-Irradiated Silicon: Quenched-in Alignment under ⟨110⟩-Uniaxial Stress,” *Phys. Rev. B*, vol. 9, no. 10, 4351–4361 (1974).
- [2.353] K. L. Brower, “Structure of Multiple-Vacancy (Oxygen) Centers in Irradiated Silicon,” *Radiation Effects*, vol. 8, 213–219 (1971).
- [2.354] W. Jung and G. S. Newell, “Spin-1 Centers in Neutron-Irradiated Silicon,” *Phys. Rev.*, vol. 132, no. 2, 648–662 (1963).
- [2.355] M. Nisenoff and H. Y. Fan, “Electron Spin Resonance in Neutron-Irradiated Silicon,” *Phys. Rev.*, vol. 128, no. 4, 1605–1613 (1962).
- [2.356] Y. H. Lee and J. W. Corbett, “EPR Studies in Neutron-Irradiated Silicon: A Negative Charge State of a Nonplanar Five-Vacancy Cluster (V_5^-),” *Phys. Rev. B*, vol. 8, no. 6, 2810–2826 (1973).
- [2.357] M. Brohl, C. Kisielowski-Kemmerich, and H. Alexander, “Pentavacancies in Plastically Deformed Silicon,” *Appl. Phys. Lett.*, vol. 50, no. 24, 1733–1735 (1987).
- [2.358] C. G. Kirkpatrick, J. R. Noonan, and B. G. Streetman, “Recombination Luminescence from Ion Implanted Silicon,” *Radiation Effects*, vol. 30, 97–106 (1976).

- [2.359] V. D. Tkachev and A. V. Mudryi, "Radiative Recombination Centres in Silicon Irradiated by Fast Neutrons and Ions," in: *Radiation Effects in Semiconductors, 1976*, edited by N. B. Urli and J. W. Corbett, *Inst. Phys. Conf. Ser.*, no. 31, 231–243 (1977).
- [2.360] D. J. Chadi and K. J. Chang, "Magic Numbers for Vacancy Aggregation in Crystalline Si," *Phys. Rev. B*, vol. 38, no. 2, 1523–1525 (1988).
- [2.361] A. van Veen, H. Schut, A. Rivera, and A. V. Fedorov, "Growth of Vacancy Clusters during Post-Irradiation Annealing of Ion Implanted Silicon," in: *Ion-Solid Interactions for Materials Modification and Processing*, edited by D. B. Poker, D. Ila, Y.-T. Cheng, L. R. Harriott, and T. W. Sigmon, *Mat. Res. Soc. Symp. Proc.*, vol. 396, 155–160 (1996).
- [2.362] B. Hourahine, R. Jones, A. N. Safonov, S. Öberg, P. R. Briddon, and S. K. Streicher, "Identification of the Hexavacancy in Silicon with the B_{80}^4 Optical Center," *Phys. Rev. B*, vol. 61, no. 19, 12594–12597 (2000).
- [2.363] C. E. Jones, E. S. Johnson, W. D. Compton, J. R. Noonan, and F. B. Streetman, "Temperature, Stress, and Annealing Effects on the Luminescence from Electron-Irradiated Silicon," *J. Appl. Phys.*, vol. 44, no. 12, 5402–5410 (1973).
- [2.364] A. S. Kaminski, B. M. Leiferov, and A. N. Safonov, "Excitons Bound to Defect Complexes in Silicon," *Sov. Phys. Solid State*, vol. 29, no. 4, 551–556 (1987).
- [2.365] R. Sauer and J. Weber, "Photoluminescence Characterization of Deep Defects in Silicon," in: *Proceedings of the 12th International Conference on Defects in Semiconductors*, edited by C. A. J. Ammerlaan, *Physica*, vol. 116B, 195–209 (1983).
- [2.366] R. Jones, B. J. Coomer, J. P. Goss, S. Öberg, and P. R. Briddon, "Intrinsic Defects and the D1 to D4 Optical Bands Detected in Plastically Deformed Si," *phys. stat. sol. (b)*, vol. 222, 133–140 (2000).
- [2.367] R. Sauer, J. Weber, J. Stoltz, E. R. Weber, K.-H. Küsters, and H. Alexander, "Dislocation-Related Photoluminescence in Silicon," *Appl. Phys. A*, vol. 36, 1–13 (1985).
- [2.368] S. Dannefaer, N. Fruensgaard, S. Kupca, B. Hogg, and D. Kerr, "A Positron Study of Plastic Deformation of Silicon," *Can. J. Phys.*, vol. 61, 451–459 (1983).
- [2.369] S. Dannefaer, D. Kerr, and B. G. Hogg, "A Study of Defects in Amorphous Silicon Films," *J. Appl. Phys.*, vol. 54, no. 1, 155–160 (1983).
- [2.370] N. M. Kulkarni, R. Kulkarni, and A. D. Shaligram, "Defect Recovery Study of e-Irradiated Silicon during Rapid Thermal Annealing," *phys. stat. sol. (a)*, vol. 133, 283–289 (1992).
- [2.371] A. Kawasuso, M. Hasegawa, M. Suezawa, S. Yamaguchi, and K. Sumino, "Annealing Processes of Vacancies in Silicon Induced by Electron Irradiation: Analysis Using Positron Lifetime," in: *Positron Annihilation*, edited by Y.-J. He, B.-S. Cao, and Y. C. Jean, *Materials Science Forum*, vol. 175–178, 423–426 (1995).
- [2.372] V. C. Venezia, L. Pelaz, H.-J. L. Goosmann, T. E. Haynes, and C. S. Rafferty, "Binding Energy of Vacancy Clusters Generated by High-Energy Ion Implantation and Annealing of Silicon," *Appl. Phys. Lett.*, vol. 79, no. 9, 1273–1275 (2001).
- [2.373] R. Kalyanaraman, T. E. Haynes, O. W. Holland, H.-J. L. Goosmann, C. S. Rafferty, and G. H. Gilmer, "Binding Energy of Vacancies to Clusters Formed in Si by High-Energy Ion Implantation," *Appl. Phys. Lett.*, vol. 79, no. 13, 1983–1985 (2001).
- [2.374] G. H. Gilmer, T. Diaz de la Rubia, D. M. Stock, and M. Jaraiz, "Diffusion and Interactions of Point Defects in Silicon: Molecular Dynamics Simulations," in: *Computer Simulation of Radiation Effects in Solids*, edited by T. Diaz de la Rubia, G. H. Gilmer, and M.-J. Caturla, *Nuclear Instruments and Methods in Physics Research B*, vol. 102, 247–255 (1995).
- [2.375] L. Colombo, A. Bongiorno, and T. Diaz de la Rubia, "Formation and Binding Energies of Vacancy Clusters in Silicon," in: *Defects and Diffusion in Silicon Processing*, edited by T. Diaz de la Rubia, S. Coffa, P. A. Stolk, and C. S. Rafferty, *Mat. Res. Soc. Symp. Proc.*, vol. 469, 205–210 (1997).
- [2.376] A. Bongiorno, L. Colombo, and T. Diaz De la Rubia, "Structural and Binding Properties of Vacancy Clusters in Silicon," *Europhysics Letters*, vol. 43, no. 6, 695–700 (1998).

- [2.377] T. Akiyama, A. Oshiyama, and O. Sugino, “Magic Numbers of Multivacancy in Crystalline Si: Tight-Binding Studies for the Stability of the Multivacancy,” *J. Phys. Soc. Japan*, vol. 67, no. 12, 4110–4116 (1998).
- [2.378] M. Prasad and T. Sinno, “Atomistic-to-Continuum Description of Vacancy Cluster Properties in Crystalline Silicon,” *Appl. Phys. Lett.*, vol. 80, no. 11, 1951–1953 (2002).
- [2.379] M. Jaraiz, G. H. Gilmer, J. M. Poate, and T. D. de la Rubia, “Atomistic Calculations of Ion Implantation in Si: Point Defect and Transient Enhanced Diffusion Phenomena,” *Appl. Phys. Lett.*, vol. 68, no. 3, 409–441 (1996).
- [2.380] S. Chakravarthi and S. T. Dunham, “Modeling of Vacancy Cluster Formation in Ion Implanted Silicon,” *J. Appl. Phys.*, vol. 89, no. 9, 4758–4765 (2001).
- [2.381] E. I. Blount, “Energy Levels in Irradiated Germanium,” *J. Appl. Phys.*, vol. 30, no. 8, 1218–1221 (1959).
- [2.382] F. Seitz, “On the Theory of Diffusion in Metals,” *Acta Cryst.*, vol. 3, 355–363 (1950).
- [2.383] H. B. Huntington and F. Seitz, “Mechanism for Self-Diffusion in Metallic Copper,” *Phys. Rev.*, vol. 61, 315–325 (1942).
- [2.384] W. Frank, “Self-Interstitials and Vacancies in Elemental Semiconductors between Absolute Zero and the Temperature of Melting,” *Festkörperprobleme*, vol. 21, 221–242 (1981).
- [2.385] P. S. Gwozdz and J. S. Koehler, “Changes in AC Conductivity of Silicon with Electron Irradiation at 0.5 K,” *Phys. Rev. B*, vol. 6, no. 12, 4571–4574 (1972).
- [2.386] A. Brelot, “Selective Trapping of Vacancies,” in: *Radiation Damage and Defects in Semiconductors, Inst. Phys. Conf. Ser.*, no. 16, 191–201 (1973).
- [2.387] R. D. Harris and G. D. Watkins, “Interstitial Related Defects in n-Type Silicon,” in: *Thirteenth International Conference on Defects in Semiconductors*, edited by L. C. Kimerling and J. M. Parsey, Jr., The Metallurgical Society of AIME, 799–805 (1985).
- [2.388] B. N. Mukashev, K. A. Abdullin, Y. V. Gorelkinski, and S. Z. Tokmoldin, “Self-Interstitial Related Reactions in Silicon Irradiated by Light Ions,” *Materials Science and Engineering B*, vol. 58, 171–178 (1999).
- [2.389] H. J. Stein and F. L. Vook, “Characteristics of Electron-Induced Defects in n-Type Silicon,” in: *Radiation Effects in Semiconductors*, edited by F. L. Vook, New York: Plenum Press, 115–123 (1968).
- [2.390] B. Massarani and A. Breton, “Evidence of 130 K Annealing Stage of Divacancy in Electron-Irradiated Silicon,” in: *Radiation Damage and Defects in Semiconductors*, edited by J. E. Whitehouse, *Inst. Phys. Conf. Ser.*, no. 16, 269–277 (1973).
- [2.391] B. Bech Nielsen and J. U. Andersen, “Beam-Induced Annealing of Defects in Silicon after Light-Ion Implantation at 30 K,” *Phys. Rev. B*, vol. 35, no. 6, 2732–2739 (1987).
- [2.392] K. A. Abdullin, B. N. Mukashev, M. F. Tamendarov, and T. B. Tashenov, “Electronic Levels and Properties of the Selfinterstitials in Irradiated Silicon,” *Physics Letters A*, vol. 166, 40–42 (1992).
- [2.393] K. A. Abdullin, B. N. Mukashev, M. F. Tamendarov, and T. B. Tashenov, “Electronic Levels and Properties of the Selfinterstitials in Irradiated Silicon,” in: *Defect Engineering in Semiconductor Growth, Processing and Device Technology*, edited by S. Ashok, J. Chevallier, K. Sumino, and E. Weber, *Mat. Res. Soc. Symp. Proc.*, vol. 262, 1109–1113 (1992).
- [2.394] K. A. Abdullin and B. N. Mukashev, “Defects in p-Si Bombarded at 77 K: Energy Spectrum and Annealing Kinetics,” *Semiconductors*, vol. 28, no. 10, 1012–1017 (1994).
- [2.395] K. A. Abdullin, B. N. Mukashev, and Y. V. Gorelkinskii, “Metastable Oxygen-Silicon Interstitial Complex in Crystalline Silicon,” *Semicond. Sci. Technol.*, vol. 11, 1696–1703 (1996).
- [2.396] T. A. G. Eberlein, N. Pinho, R. Jones, B. J. Coomer, J. P. Goss, P. R. Briddon, and S. Öberg, “Self-Interstitial Clusters in Silicon,” *Physica B*, vol. 308–310, 454–457 (2001).
- [2.397] D. J. Roth and J. D. Plummer, “Oxidation-Enhanced Diffusion of Boron and Phosphorus in Heavily Doped Layers in Silicon,” *J. Electrochem. Soc.*, vol. 141, no. 4, 1074–1081 (1994).

- [2.398] K. P. Chik, "Doping Effects on Diffusion and Diffusion Mechanisms in Ge and Si," *Radiation Effects*, vol. 4, 33–37 (1970).
- [2.399] A. Seeger and W. Frank, "Self-Interstitials in Silicon and Germanium," in: *Radiation Damage and Defects in Semiconductors, Inst. Phys. Conf. Ser.*, no. 16, 262–268 (1973).
- [2.400] W. Frank, "The Nature of Interstitials in Silicon and Germanium," in: *Lattice Defects in Semiconductors, 1974, Inst. Phys. Conf. Ser.*, no. 23, 23–43 (1975).
- [2.401] H. Lefèvre, "Trap-Centers of Self-Interstitials in Silicon," *Appl. Phys.*, vol. 22, 15–22 (1980).
- [2.402] M. D. Giles, "Defect-Coupled Diffusion at High Concentrations," *IEEE Trans. Computer-Aided Design*, vol. 8, no. 5, 460–467 (1989).
- [2.403] M. D. Giles, "Extrinsic Transient Diffusion in Silicon," *Appl. Phys. Lett.*, vol. 58, no. 21, 2399–2401 (1991).
- [2.404] J. P. John and M. E. Law, "Oxidation Enhanced Diffusion of Phosphorus in Silicon in Heavily Doped Background Concentrations," *J. Electrochem. Soc.*, vol. 140, no. 5, 1489–1491 (1993).
- [2.405] D. Tsoukalas and P. Chenevier, "Boron Diffusion in Silicon in Inert and Oxidizing Ambient and Extrinsic Conditions," *phys. stat. sol. (a)*, vol. 100, 461–465 (1987).
- [2.406] G. Bemski and C. A. Dias, "Quenched-in Defects in p-Type Silicon," *J. Appl. Phys.*, vol. 35, no. 10, 2983–2985 (1964).
- [2.407] M. L. Swanson, "Defects in Quenched Silicon," *phys. stat. sol.*, vol. 33, 721–730 (1969).
- [2.408] S. I. Tan, B. S. Berry, and W. F. J. Frank, "Internal Friction Study of Point Defects in Boron-Implanted Silicon," in: *Ion Implantation in Semiconductors and Other Materials*, edited by B. Crowder, New York: Plenum Press, 19–30 (1973).
- [2.409] W. Frank, "Interstitial Properties Deduced from Internal Friction Measurements on Boron-Implanted Silicon," *Radiation Effects*, vol. 21, 119–133 (1974).
- [2.410] G. D. Watkins, R. P. Messmer, C. Weigel, D. Peak, and J. W. Corbett, "Properties of the Interstitial in the Diamond-Type Lattice," *Phys. Rev. Lett.*, vol. 27, no. 23, 1573–1575 (1971).
- [2.411] C. Weigel, D. Peak, J. W. Corbett, G. D. Watkins, and R. P. Messmer, "Carbon Interstitial in the Diamond Lattice," *Phys. Rev. B*, vol. 8, no. 6, 2906–2915 (1973).
- [2.412] S. T. Pantelides, I. Ivanov, M. Scheffler, and J. P. Vigneron, "Multivacancies, Interstitials, and Self-Interstitial Migration in Silicon," in: *Proceedings of the 12th International Conference on Defects in Semiconductors*, edited by C. A. J. Ammerlaan, *Physica*, vol. 116B, 18–27 (1983).
- [2.413] Y. Bar-Yam and J. D. Joannopoulos, "Barrier to Migration of the Silicon Self-Interstitial," *Phys. Rev. Lett.*, vol. 52, no. 13, 1129–1132 (1984).
- [2.414] Y. Bar-Yam and J. D. Joannopoulos, "Electronic Structure and Total-Energy Migration Barriers of Silicon Self-Interstitials," *Phys. Rev. B*, vol. 30, no. 4, 1844–1852 (1984).
- [2.415] Y. Bar-Yam and J. D. Joannopoulos, "Silicon Self-Interstitial Migration: Multiple Paths and Charge States," *Phys. Rev. B*, vol. 30, no. 4, 2216–2218 (1984).
- [2.416] G. A. Baraff and M. Schlüter, "Migration of Interstitials in Silicon," *Phys. Rev. B*, vol. 30, no. 6, 3460–3469 (1984).
- [2.417] W.-C. Lee, S.-G. Lee, and K. J. Chang, "First-Principles Study of the Self-Interstitial Diffusion Mechanism in Silicon," *J. Phys.: Condens. Matter*, vol. 10, 995–1002 (1998).
- [2.418] D. J. Chadi, "Self-Interstitial Bonding Configurations in GaAs and Si," *Phys. Rev. B*, vol. 46, no. 15, 9400–9407 (1992).
- [2.419] C. G. Van de Walle and J. Neugebauer, "Hydrogen Interactions with Self-Interstitials in Silicon," *Phys. Rev. B*, vol. 52, no. 20, R14320–R14323 (1995).
- [2.420] J. Zhu, T. Diaz de la Rubia, L. H. Yang, C. Maillhot, and G. H. Gilmer, "Ab Initio Pseudopotential Calculations of B Diffusion and Pairing in Si," *Phys. Rev. B*, vol. 54, no. 7, 4741–4747 (1996).
- [2.421] S. J. Clark and G. J. Ackland, "Ab Initio Calculations of the Self-Interstitial in Silicon," *Phys. Rev. B*, vol. 56, no. 1, 47–50 (1997).
- [2.422] H. R. Schober, "Extended Interstitials in Silicon and Germanium," *Phys. Rev. B*, vol. 39, no. 17, 13013–13015 (1989).

- [2.423] D. Maroudas and R. A. Brown, “Calculation of Thermodynamic and Transport Properties of Intrinsic Point Defects in Silicon,” *Phys. Rev. B*, vol. 47, no. 23, 15562–15577 (1993).
- [2.424] W. Frank, U. Gösele, and A. Seeger, “Foreign Interstitial Atoms and Their Relation to Thermal Intrinsic Defects in Silicon,” in: *Defects and Radiation Effects in Semiconductors, 1978*, edited by J. H. Albany, *Inst. Phys. Conf. Ser.*, no. 46, 514–520 (1979).
- [2.425] A. Seeger, W. Frank, and U. Gösele, “Diffusion in Elemental Semiconductors: New Developments,” in: *Defects and Radiation Effects in Semiconductors, 1978*, edited by J. H. Albany, *Inst. Phys. Conf. Ser.*, no. 46, 148–149 (1979).
- [2.426] M. Jacob, P. Pichler, H. Ryssel, and R. Falster, “Determination of Vacancy Concentrations in the Bulk of Silicon Wafers by Platinum Diffusion Experiments,” *J. Appl. Phys.*, vol. 82, no. 1, 182–191 (1997).
- [2.427] B. Leroy, “Kinetics of Growth of the Oxidation Stacking Faults,” *J. Appl. Phys.*, vol. 50, no. 12, 7996–8005 (1979).
- [2.428] T. K. Okada, H. Kawaguchi, S. Onaga, and K. Yamabe, “Non-Equilibrium Diffusion Process Modeling Based on Three-Dimensional Simulator and Regulated Point Defect Injection Experiments,” in: *1991 International Workshop on VLSI Process and Device Modeling (1991 VPAD)*, Japan Society of Applied Physics, 8–9 (1991).
- [2.429] W. B. Rogers and H. Z. Massoud, “Determination of the Kinetic Coefficients of Silicon Self-Interstitials from Oxygen Precipitation/Front-Surface Stacking-Fault Growth Experiments,” *J. Electrochem. Soc.*, vol. 138, no. 11, 3492–3498 (1991).
- [2.430] S. M. Hu, “Vacancies and Self-Interstitials in Silicon,” in: *Defects in Silicon II*, edited by W. M. Bullis, U. Gösele, and F. Shimura, *Electrochem. Soc. Proc.*, vol. 91-9, 211–236 (1991).
- [2.431] H. Bracht, N. A. Stolwijk, H. Mehrer, and I. Yonenaga, “Short-Time Diffusion of Zinc in Silicon for the Study of Intrinsic Point Defects,” *Appl. Phys. Lett.*, vol. 59, no. 27, 3559–3561 (1991).
- [2.432] W. Wijaranakula, “Numerical Modeling of the Point Defect Aggregation during the Czochralski Silicon Crystal Growth,” *J. Electrochem. Soc.*, vol. 139, no. 2, 604–616 (1992).
- [2.433] S. M. Hu, “Vacancies and Self-Interstitials in Silicon: Generation and Interaction in Diffusion,” *J. Electrochem. Soc.*, vol. 139, no. 7, 2066–2075 (1992).
- [2.434] Y. Satoh, H. Furuya, M. Kadoi, and Y. Shimanuki, “Anomalous Depth Distributions of Bulk Microdefects in Heat-Treated Czochralski Silicon Wafers Due to Nonequilibrium Self-Interstitials,” *J. Appl. Phys.*, vol. 77, no. 8, 3710–3724 (1995).
- [2.435] H. S. Chao, S. W. Crowder, P. B. Griffin, and J. D. Plummer, “Species and Dose Dependence of Ion Implantation Damage Induced Transient Enhanced Diffusion,” *J. Appl. Phys.*, vol. 79, no. 5, 2352–2363 (1996).
- [2.436] S. Bharatan, Y. M. Haddara, M. E. Law, and K. S. Jones, “Determining the Enthalpy of Formation of a Si Interstitial Using Quantitative TEM and SIMS,” in: *Silicon Front-End Technology — Materials Processing and Modelling*, edited by N. E. B. Cowern, D. C. Jacobson, P. B. Griffin, P. A. Packan, and R. P. Webb, *Mat. Res. Soc. Symp. Proc.*, vol. 532, 111–118 (1998).
- [2.437] M. Hakala, M. J. Puska, and R. M. Nieminen, “First-Principles Calculations of Interstitial Boron in Silicon,” *Phys. Rev. B*, vol. 61, no. 12, 8155–8161 (2000).
- [2.438] R. E. McKeighen and J. S. Koehler, “Electron-Irradiation Effects in Silicon at Liquid-Helium Temperatures Using AC Hopping Conductivity,” *Phys. Rev. B*, vol. 4, no. 2, 462–478 (1971).
- [2.439] J. C. Bourgoin and J. W. Corbett, “A New Mechanism for Interstitial Migration,” *Phys. Lett.*, vol. 38A, no. 2, 135–137 (1972).
- [2.440] A. Hallén, D. Fenyö, B. U. R. Sundqvist, R. E. Johnson, and B. G. Svensson, “The Influence of Ion Flux on Defect Production in MeV Proton-Irradiated Silicon,” *J. Appl. Phys.*, vol. 70, no. 6, 3025–3030 (1991).
- [2.441] P. Lévéque, A. Hallén, P. Pellegrino, B. G. Svensson, and V. Privitera, “Dose-Rate Influence on the Defect Production in MeV Proton-Implanted Float-Zone and Epitaxial n-Type Silicon,” *Nuclear Instruments and Methods in Physics Research B*, vol. 186, 375–379 (2002).

- [2.442] V. Privitera, S. Coffa, K. Kyllesbech Larsen, S. Libertino, G. Mannino, and F. Priolo, "Point Defects Migration in Si at Room Temperature: The Role of Surface and Impurity Content," in: *Defects and Diffusion in Silicon Processing*, edited by T. Diaz de la Rubia, S. Coffa, P. A. Stolk, and C. S. Rafferty, *Mat. Res. Soc. Symp. Proc.*, vol. 469, 163–173 (1997).
- [2.443] V. Privitera, S. Coffa, F. Priolo, K. Kyllesbech Larsen, and G. Mannino, "Room-Temperature Migration and Interaction of Ion Beam Generated Defects in Crystalline Silicon," *Appl. Phys. Lett.*, vol. 68, no. 24, 3422–3424 (1996).
- [2.444] A. N. Buzynin, A. E. Luk'yanov, V. V. Osiko, and V. V. Voronkov, "Non-Equilibrium Impurity Redistribution in Si," *Nuclear Instruments and Methods in Physics Research B*, vol. 186, 366–370 (2002).
- [2.445] N. E. B. Cowern, E. J. H. Collart, J. Politiek, P. H. L. Bancken, J. G. M. van Berkum, K. Kyllesbech Larsen, P. A. Stolk, H. G. A. Huitzing, P. Pichler, A. Burenkov, and D. J. Gravensteijn, "Low Energy Implantation and Transient Enhanced Diffusion: Physical Mechanisms and Technology Implications," in: *Defects and Diffusion in Silicon Processing*, edited by T. Diaz de la Rubia, S. Coffa, P. A. Stolk, and C. S. Rafferty, *Mat. Res. Soc. Symp. Proc.*, vol. 469, 265–276 (1997).
- [2.446] M. Hill, M. Lietz, and R. Sittig, "Diffusion of Gold in Silicon," *J. Electrochem. Soc.*, vol. 129, no. 7, 1579–1587 (1982).
- [2.447] P. B. Griffin, P. M. Fahey, J. D. Plummer, and R. W. Dutton, "Measurement of Silicon Interstitial Diffusivity," *Appl. Phys. Lett.*, vol. 47, no. 3, 319–321 (1985).
- [2.448] E. Scheid and P. Chenevier, "Determination des paramètres de distribution des auto-interstitiels silicium en vue de la modélisation 2-D des processus technologiques. Discussion sur la validité physique," *Revue Phys. Appl.*, vol. 20, no. 7, 483–491 (1985).
- [2.449] T. Abe, H. Harada, N. Ozawa, and K. Adomi, "Deep Level Generation-Annihilation in Nitrogen Doped FZ Crystals," in: *Oxygen, Carbon, Hydrogen, and Nitrogen in Crystalline Silicon*, edited by J. C. Mikkelsen, Jr., S. J. Pearton, J. W. Corbett, and S. J. Pennycook, *Mat. Res. Soc. Symp. Proc.*, vol. 59, 537–544 (1986).
- [2.450] P. B. Griffin and J. D. Plummer, "Point Defect Models for Two-Dimensional Diffusion Kinetics," *Electrochem. Soc. Extended Abstracts*, vol. 86-2, 818–819 (1986).
- [2.451] P. B. Griffin and J. D. Plummer, "The Influence of Point Defects on Two Dimensional Diffusion Kinetics," in: *Materials Issues in Silicon Integrated Circuit Processing*, edited by M. Wittmer, J. Stimmell, and M. Strathman, *Mat. Res. Soc. Symp. Proc.*, vol. 71, 75–80 (1986).
- [2.452] P. B. Griffin and J. D. Plummer, "Point Defect Models for Two Dimensional Diffusion Kinetics," in: *Proc. Process Physics and Modeling in Semiconductor Technology*, edited by G. R. Srinivasan, J. Plummer, and D. Antoniadis, *Electrochem. Soc. Proc.*, vol. 88-16, 53–65 (1988).
- [2.453] W. B. Rogers, H. Z. Massoud, R. B. Fair, U. M. Gösele, R. Shaw, H. Korb, and M. Guse, "Point Defect Kinetics during Backside Oxidation Measured by Frontside Stacking-Fault Growth," *Electrochem. Soc. Extended Abstracts*, vol. 87-1, no. 264, 384–385 (1987).
- [2.454] S. T. Ahn, P. B. Griffin, J. D. Shott, J. D. Plummer, and W. A. Tiller, "A Study of Silicon Interstitial Kinetics Using Silicon Membranes: Applications to 2D Dopant Diffusion," *J. Appl. Phys.*, vol. 62, no. 12, 4745–4755 (1987).
- [2.455] M. R. Kump and R. W. Dutton, "The Efficient Simulation of Coupled Point Defect and Impurity Diffusion," *IEEE Trans. Computer-Aided Design*, vol. 7, no. 2, 191–204 (1988).
- [2.456] S. T. Ahn, J. D. Shott, and W. A. Tiller, "Determination of Modeling Parameters for Silicon Interstitial Diffusion Using Silicon Membranes," in: *Proc. Process Physics and Modeling in Semiconductor Technology*, edited by G. R. Srinivasan, J. Plummer, and D. Antoniadis, *Electrochem. Soc. Proc.*, vol. 88-16, 66–75 (1988).
- [2.457] K. Kawakami, M. Hasebe, and S. Shinoyama, "Growth Model of Ring-Likely Distributed Stacking Faults," in: *Extended Abstracts of the 37th Spring Meeting Japan. Soc. Appl. Phys. and Related Societies*, 221 (1990).
- [2.458] W. Wijaranakula, "An Experimental Estimation of Silicon Interstitial Diffusivity," *J. Appl. Phys.*, vol. 67, no. 12, 7624–7626 (1990).

- [2.459] H. Yamanaka, Y. Aoki, and T. Samizo, “Role of Silicon Self-Interstitials Injected by Thermal Oxidation in Oxygen Precipitation in Czochralski Silicon,” *Jpn. J. Appl. Phys.*, vol. 29, no. 11, 2450–2455 (1990).
- [2.460] S. T. Dunham, A. M. Agarwal, and N. Jeng, “Measurements of Enhanced Diffusion of Buried Layers in Silicon Membrane Structures during Oxidation,” in: *Impurities, Defects and Diffusion in Semiconductors: Bulk and Layered Structures*, edited by D. J. Wolford, J. Bernholc, and E. E. Haller, *Mat. Res. Soc. Symp. Proc.*, vol. 163, 543–548 (1990).
- [2.461] S. T. Dunham, A. M. Agarwal, and N. Jeng, “Determination of Silicon Point Defect Properties Using Buried Layer and Membranes,” in: *Process Physics and Modeling in Semiconductor Technology*, edited by G. R. Srinivasan, J. D. Plummer, and S. T. Pantelides, *Electrochem. Soc. Proc.*, vol. 91-4, 516–528 (1991).
- [2.462] W. B. Rogers and H. Z. Massoud, “Determination of the Kinetic Coefficients of Silicon Self-Interstitials from Back-Side Oxidation/Front-Surface Stacking-Fault Growth Experiments,” *J. Electrochem. Soc.*, vol. 138, no. 11, 3483–3491 (1991).
- [2.463] H.-J. Gossmann, C. S. Rafferty, H. S. Luftman, F. C. Unterwald, T. Boone, and J. M. Poate, “Oxidation Enhanced Diffusion in Si B-Doping Superlattices and Si Self-Interstitial Diffusivities,” *Appl. Phys. Lett.*, vol. 63, no. 5, 639–641 (1993).
- [2.464] A. M. Agarwal and S. T. Dunham, “Determination of Silicon Point Defect Properties from Oxidation Enhanced Diffusion of Buried Layers,” *Appl. Phys. Lett.*, vol. 63, no. 6, 800–802 (1993).
- [2.465] H. Yamanaka and Y. Aoki, “Crude Estimates of Diffusivity and Supersaturation of Silicon Self-Interstitials Injected by Thermal Oxidation of Czochralski Silicon,” *Jpn. J. Appl. Phys., Part 2*, vol. 33, no. 4B, L559–L562 (1994).
- [2.466] P. A. Stolk, H.-J. Gossmann, D. J. Eaglesham, D. C. Jacobson, J. M. Poate, and H. S. Luftman, “Trap-Limited Interstitial Diffusivity and Enhanced Boron Clustering in Silicon,” *Appl. Phys. Lett.*, vol. 66, no. 5, 568–570 (1995).
- [2.467] H.-J. Gossmann, G. H. Gilmer, C. S. Rafferty, F. C. Unterwald, T. Boone, J. M. Poate, H. S. Luftman, and W. Frank, “Determination of Si Self-Interstitial Diffusivities from the Oxidation-Enhanced Diffusion in B Doping-Superlattices: The Influence of the Marker Layers,” *J. Appl. Phys.*, vol. 77, no. 5, 1948–1951 (1995).
- [2.468] P. A. Stolk, H.-J. Gossmann, D. J. Eaglesham, and J. M. Poate, “Implantation and Transient Boron Diffusion: The Role of the Silicon Self-Interstitial,” in: *Ion Implantation Technology—94*, edited by S. Coffa, G. Ferla, F. Priolo, and E. Rimini, *Nuclear Instruments and Methods in Physics Research B*, vol. 96, Amsterdam: Elsevier, 187–195 (1995).
- [2.469] H. G. A. Huizing, C. C. G. Visser, N. E. B. Cowern, P. A. Stolk, and R. C. M. de Kruif, “Ultrafast Interstitial Injection during Transient Enhanced Diffusion of Boron in Silicon,” *Appl. Phys. Lett.*, vol. 69, no. 9, 1211–1213 (1996).
- [2.470] W. B. Knowlton, J. T. Walton, Y. K. Wong, I. A. Mason, and E. E. Haller, “High Silicon Self-Interstitial Diffusivity As Revealed by Lithium Ion Drift,” in: *Defects and Diffusion in Silicon Processing*, edited by T. Diaz de la Rubia, S. Coffa, P. A. Stolk, and C. S. Rafferty, *Mat. Res. Soc. Symp. Proc.*, vol. 469, 77–82 (1997).
- [2.471] E. N. Shauly, R. Ghez, and Y. Komem, “Two-Dimensional Diffusion Characterization of Boron in Silicon Using Reverse Modeling,” in: *Simulation of Semiconductor Processes and Devices 2001*, edited by D. Tsoukalas and C. Tsamis, Vienna: Springer-Verlag, 384–387 (2001).
- [2.472] Y.-H. Lee, N. N. Gerasimenko, and J. W. Corbett, “EPR Study of Neutron-Irradiated Silicon: A Positive Charge State of the ⟨100⟩ Split Di-Interstitial,” *Phys. Rev. B*, vol. 14, no. 10, 4506–4520 (1976).
- [2.473] Y. H. Lee, “Silicon Di-Interstitial in Ion-Implanted Silicon,” *Appl. Phys. Lett.*, vol. 73, no. 8, 1119–1121 (1998).
- [2.474] D. F. Daly, “New EPR Spectra in Irradiated Silicon,” *J. Appl. Phys.*, vol. 42, no. 2, 864–865 (1971).

- [2.475] K. L. Brower, "EPR of a $\langle 001 \rangle$ Si Interstitial Complex in Irradiated Silicon," *Phys. Rev. B*, vol. 14, no. 3, 872–883 (1976).
- [2.476] B. J. Coomer, J. P. Goss, R. Jones, S. Öberg, and P. R. Briddon, "Identification of the Tetra-Interstitial in Silicon," *J. Phys.: Condens. Matter*, vol. 13, no. 1, L1–L7 (2001).
- [2.477] D. Pierreux and A. Stesmans, "Atomic Structure of the B3 Defect in Neutron-Irradiated Silicon," *Phys. Rev. B*, vol. 68, 193208 (2003).
- [2.478] P. Stallinga, T. Gregorkiewicz, C. A. J. Ammerlaan, and Y. V. Gorelkinskii, "Electron Paramagnetic Resonance Study of the NL51 Spectrum in Hydrogen-Implanted Silicon," *Solid State Communications*, vol. 90, no. 6, 401–404 (1994).
- [2.479] A. R. Chelyadinskii and V. A. Burenkov, "Model of the Pair Phosphorus Atom-Interstitial Silicon Atom," *Physics of the Solid State*, vol. 40, no. 11, 1806–1808 (1998).
- [2.480] K. Murakami, K. Masuda, K. Gamo, and S. Namba, "ESR Studies on Annealing Behavior of Heavily Damaged Silicon," in: *Ion Implantation in Semiconductors*, edited by S. Namba, New York: Plenum Press, 533–538 (1975).
- [2.481] T. Maekawa, S. Inone, and A. Usami, "Hole Trap Annealing in Neutron-Transmutation-Doped Silicon with Different Initial Resistivities," *Semicond. Sci. Technol.*, vol. 5, 663–668 (1990).
- [2.482] H. Lefèvre, "Annealing Behavior of Trap-Centers in Silicon Containing A-Swirl Defects," *Applied Physics A*, vol. 29, 105–111 (1982).
- [2.483] B. N. Mukashev, A. V. Spitsyn, N. Fukuoka, and H. Saito, "Defects in Carbon-Implanted Silicon," *Jpn. J. Appl. Phys.*, vol. 21, no. 2, 399–400 (1982).
- [2.484] P. B. Rasband, P. Clancy, and M. O. Thompson, "Equilibrium Concentrations of Defects in Pure and B-Doped Silicon," *J. Appl. Phys.*, vol. 79, no. 12, 8998–9011 (1996).
- [2.485] L. Colombo, "Native Defects and Their Interactions in Silicon," in: *20th International Conference on Defects in Semiconductors*, edited by C. Van de Walle and W. Walukiewicz, *Physica B*, vol. 273–274, 458–462 (1999).
- [2.486] B. J. Coomer, J. P. Goss, R. Jones, S. Öberg, and P. R. Briddon, "Interstitial Aggregates and a New Model for the I₁/W Optical Centre in Silicon," in: *Proceedings of the 20th International Conference on Defects in Semiconductors*, edited by C. G. Van de Walle and W. Walukiewicz, *Physica B*, vol. 274, 505–508 (1999).
- [2.487] J. Kim, F. Kirchhoff, W. G. Aulbur, J. W. Wilkins, F. S. Khan, and G. Kresse, "Thermally Activated Reorientation of Di-Interstitial Defects in Silicon," *Phys. Rev. Lett.*, vol. 83, no. 10, 1990–1993 (1999).
- [2.488] M. Hane, T. Ikezawa, and G. H. Gilmer, "Di-Interstitial Diffusivity and Migration Path Calculations Based on Tight-Binding Hamiltonian Molecular Dynamics," in: *2000 International Conference on Simulation of Semiconductor Processes and Devices*, Piscataway: IEEE, 119–122 (2000).
- [2.489] M. P. Chichkine and M. M. De Souza, "Dynamics of Self-Interstitial Cluster Formation in Silicon," *Phys. Rev. B*, vol. 66, 045205 (2002).
- [2.490] D. A. Richie, J. Kim, S. A. Barr, K. R. A. Hazzard, R. Hennig, and J. W. Wilkins, "Complexity of Small Silicon Self-Interstitial Defects," *Phys. Rev. Lett.*, vol. 92, 045501 (2004).
- [2.491] S. K. Estreicher, M. Gharaibeh, P. A. Fedders, and P. Ordejón, "Unexpected Dynamics for Self-Interstitial Clusters in Silicon," *Phys. Rev. Lett.*, vol. 86, no. 7, 1247–1250 (2001).
- [2.492] D. A. Richie, J. Kim, R. Hennig, K. Hazzard, S. Barr, and J. W. Wilkins, "Large-Scale Molecular Dynamics Simulations of Interstitial Defect Diffusion in Silicon," in: *Modeling and Numerical Simulation of Materials Behavior and Evolution*, edited by V. Tikare, E. A. Olevsky, and A. Zavalaniagos, *Mat. Res. Soc. Symp. Proc.*, vol. 731, W9.10.1–W9.10.5 (2002).
- [2.493] I. Martin-Bragado, M. Jaraiz, P. Castrillo, R. Pinacho, J. Barbolla, and M. M. De Souza, "Mobile Silicon Di-Interstitial: Surface, Self-Interstitial Clustering, and Transient Enhanced Diffusion Phenomena," *Phys. Rev. B*, vol. 68, 195204 (2003).
- [2.494] M. Gharaibeh, S. K. Estreicher, and P. A. Fedders, "Molecular-Dynamics Studies of Self-Interstitial Aggregates in Si," in: *20th International Conference on Defects in Semiconductors*, edited by C. Van de Walle and W. Walukiewicz, *Physica B*, vol. 273–274, 532–534 (1999).

- [2.495] G. M. Lopez and V. Fiorentini, “Vibrational Modes of Three-Membered Self-Interstitial Clusters in Silicon,” *J. Phys.: Condens. Matter*, vol. 15, 7851–7857 (2003).
- [2.496] N. Arai, S. Takeda, and M. Kohyama, “Self-Interstitial Clustering in Crystalline Silicon,” *Phys. Rev. Lett.*, vol. 78, no. 22, 4265–4268 (1997).
- [2.497] P. Humble, “The Structure and Mechanism of Formation of Platelets in Natural Type Ia Diamond,” *Proc. Roy. Soc. Lond. A*, vol. 381, 65–81 (1982).
- [2.498] M. Kohyama and S. Takeda, “First-Principles Calculations of the Self-Interstitial Cluster I4 in Si,” *Phys. Rev. B*, vol. 60, no. 11, 8075–8080 (1999).
- [2.499] S. Birner, J. Kim, D. A. Richie, J. W. Wilkins, A. F. Voter, and T. Lenosky, “Accelerated Dynamics Simulations of Interstitial-Cluster Growth,” *Solid State Communications*, vol. 120, 279–282 (2001).
- [2.500] M. M. De Souza, M. P. Chichkine, and E. M. Sankara Narayanan, “A Study of Fully Coordinated Precursors in Silicon Using the Ackland Potential,” *Physica B*, vol. 304, 483–488 (2001).
- [2.501] M. P. Chichkine, M. M. De Souza, and E. M. Sankara Narayanan, “Growth of Precursors in Silicon Using Pseudopotential Calculations,” *Phys. Rev. Lett.*, vol. 88, no. 8, 085501 (2002).
- [2.502] Z. Ciechanowska, G. Davies, and E. C. Lightowers, “Uniaxial Stress Measurements on the 1039.8 meV Zero-Phonon Line in Irradiated Silicon,” *Solid State Communications*, vol. 49, no. 5, 427–431 (1984).
- [2.503] G. Davies, E. C. Lightowers, and Z. E. Ciechanowska, “The 1018 meV (W or I₁) Vibronic Band in Silicon,” *J. Phys. C*, vol. 20, 191–205 (1987).
- [2.504] K. Terashima, T. Ikarashi, M. Watanabe, and T. Kitano, “Luminescence Centers in High-Energy Ion-Implanted Silicon,” in: *Defects in Semiconductors 19*, edited by G. Davies and M. H. Nazaré, *Materials Science Forum*, vol. 258–263, 587–592 (1997).
- [2.505] O. O. Awadelkarim, “Photoluminescence Study of Radiative Channels in Ion-Implanted Silicon,” *Phys. Rev. B*, vol. 42, no. 9, 5635–5640 (1990).
- [2.506] T. Mchedlidze and M. Suezawa, “Properties of Tetra-Interstitial Agglomerate in Silicon: an ESR Study,” in: *Proceedings of the 22nd International Conference on Defects in Semiconductors*, edited by K. Bonde Nielsen, A. Nylandsted Larsen, and G. Weyer, *Physica B*, vol. 340–342, 682–686 (2003).
- [2.507] M. Gharaibeh, S. K. Estreicher, and P. A. Fedders, “Dynamics of Si Self-Interstitial Clustering Using the Fast-Diffusing I₃ Cluster,” *Physica B*, vol. 308–310, 510–512 (2001).
- [2.508] J. R. Noonan, C. G. Kirkpatrick, and B. G. Streetman, “Low-Temperature Photoluminescence from Boron Ion Implanted Si,” *Radiation Effects*, vol. 21, 225–228 (1974).
- [2.509] P. J. Schultz, T. D. Thompson, and R. G. Elliman, “Activation Energy for the Photoluminescence W Center in Silicon,” *Appl. Phys. Lett.*, vol. 60, no. 1, 59–61 (1992).
- [2.510] M. Nakamura, “Order of the Formation Reaction and the Origin of the Photoluminescence W Center in Silicon Crystal,” *Jpn. J. Appl. Phys., Part 2*, vol. 40, no. 10A, L1000–L1002 (2001).
- [2.511] N. Bürger, K. Thonke, R. Sauer, and G. Pensl, “New Class of Related Optical Defects in Silicon Implanted with the Noble Gases He, Ne, Ar, Kr, and Xe,” *Phys. Rev. Lett.*, vol. 52, no. 18, 1645–1648 (1984).
- [2.512] M. Nakamura, S. Nagai, Y. Aoki, and H. Naramoto, “Oxygen Participation in the Formation of the Photoluminescence W Center and the Center’s Origin in Ion-Implanted Silicon Crystals,” *Appl. Phys. Lett.*, vol. 72, no. 11, 1347–1349 (1998).
- [2.513] H. Feick and E. R. Weber, “Annealing of the Photoluminescence W-Center in Proton-Irradiated Silicon,” in: *20th International Conference on Defects in Semiconductors*, edited by C. Van de Walle and W. Walukiewicz, *Physica B*, vol. 273–274, 497–500 (1999).
- [2.514] N. S. Minaev, A. V. Mudrii, and V. D. Tkachev, “Symmetry and Nature of the 1.0186 eV Luminescence Centre in Neutron-Irradiated Silicon,” *phys. stat. sol. (b)*, vol. 108, K89–K94 (1981).

- [2.515] B. C. MacEvoy and S. J. Watts, "Defect Engineering Radiation Tolerant Silicon Detectors," in: *Gettering and Defect Engineering in Semiconductor Technology GADEST'97*, edited by C. Claeys, J. Vanhellemont, H. Richter, and M. Kittler, *Solid State Phenomena*, vol. 57-58, 221–231 (1997).
- [2.516] R. J. Davis, H.-U. Habermeier, and J. Weber, "Photoluminescence of Low-Energy Ion Bombarded Silicon," *Appl. Phys. Lett.*, vol. 47, no. 12, 1295–1297 (1985).
- [2.517] M. Nakamura and S. Nagai, "Influence of High-Energy Electron Irradiation on the Formation and Annihilation of the Photoluminescence W Center and the Center's Origin in a Proton-Implanted Silicon Crystal," *Phys. Rev. B*, vol. 66, 155204 (2002).
- [2.518] S. J. Watts, "Irradiation Induced Defects in Silicon Detectors," in: *Crystalline Defects and Contamination: Their Impact and Control in Device Manufacturing II*, edited by B. O. Kolbesen, C. Claeys, P. Stallhofer, and F. Tardif, *Electrochem. Soc. Proc.*, vol. 97-22, 116–131 (1997).
- [2.519] J. L. Benton, S. Libertino, P. Kringsøj, D. J. Eaglesham, J. M. Poate, and S. Coffa, "Evolution from Point to Extended Defects in Ion Implanted Silicon," *J. Appl. Phys.*, vol. 82, no. 1, 120–125 (1997).
- [2.520] J. L. Benton, K. Halliburton, S. Libertino, D. J. Eaglesham, and S. Coffa, "Electrical Signatures and Thermal Stability of Interstitial Clusters in Ion Implanted Si," *J. Appl. Phys.*, vol. 84, no. 9, 4749–4756 (1998).
- [2.521] S. Libertino, S. Coffa, and J. L. Benton, "Formation, Evolution, and Annihilation of Interstitial Clusters in Ion-Implanted Si," *Phys. Rev. B*, vol. 63, 195206 (2001).
- [2.522] P. K. Giri and Y. N. Mohapatra, "Electrical Characterization of MeV Heavy-Ion-Induced Damage in Silicon: Evidence for Defect Migration and Clustering," *J. Appl. Phys.*, vol. 84, no. 4, 1901–1912 (1998).
- [2.523] D. C. Schmidt, B. G. Svensson, M. Seibt, C. Jagadish, and G. Davies, "Photoluminescence, Deep Level Transient Spectroscopy and Transmission Electron Microscopy Measurements on MeV Self-Ion Implanted and Annealed *n*-Type Silicon," *J. Appl. Phys.*, vol. 88, no. 5, 2309–2317 (2000).
- [2.524] M. Nakamura and S. Murakami, "Evolution of Photoluminescence Defect Clusters in Proton- and Copper-Implanted Silicon Crystals during Annealing," *J. Appl. Phys.*, vol. 94, no. 5, 3075–3081 (2003).
- [2.525] D. Stiebel and P. Pichler, "Transient-Diffusion Effects," *Appl. Phys. A*, vol. 76, 1041–1048 (2003).
- [2.526] F. Schietekatte, S. Roorda, R. Poirier, M. O. Fortin, S. Chazal, and R. Héliou, "Direct Evidence for 8-Interstitial-Controlled Nucleation of Extended Defects in c-Si," *Appl. Phys. Lett.*, vol. 77, no. 26, 4322–4324 (2000).
- [2.527] J. Kim, J. W. Wilkins, F. S. Khan, and A. Canning, "Extended Si {311} Defects," *Phys. Rev. B*, vol. 55, no. 24, 16186–16197 (1997).
- [2.528] J. Frenkel, "Über die Wärmebewegung in festen und flüssigen Körpern," *Z. Physik*, vol. 35, 652–669 (1926).
- [2.529] D. E. Hill, "Electron Bombardment of Silicon," *Phys. Rev.*, vol. 114, no. 6, 1414–1420 (1959).
- [2.530] G. K. Wertheim, "Temperature-Dependent Defect Production in Bombardment of Semiconductors," *Phys. Rev.*, vol. 115, no. 3, 568–569 (1959).
- [2.531] G. D. Watkins, J. W. Corbett, and R. M. Walker, "Spin Resonance in Electron Irradiated Silicon," *J. Appl. Phys.*, vol. 30, no. 8, 1198–1203 (1959).
- [2.532] H. J. Stein and F. L. Vook, "Electrical Studies of Electron-Irradiated n-Type Si: Impurity and Irradiation-Temperature Dependence," *Phys. Rev.*, vol. 163, no. 3, 790–800 (1967).
- [2.533] E. G. Wikner and D. P. Snowden, "Temperature Dependence of the Production of the Si-B1 Center by High-Energy Electrons," *Bull. Am. Phys. Soc., Series II*, vol. 9, no. 7, 706 (1964).
- [2.534] L. J. Cheng and J. C. Correlli, "Recovery of Electrical Properties in 45-MeV-Electron-Irradiated n-Type Si from 80 to 350°K," *Phys. Rev.*, vol. 140, no. 6A, A2130–A2135 (1965).

- [2.535] J. W. MacKay and E. E. Klontz, "Low-Temperature Annealing Studies in Ge," *J. Appl. Phys.*, vol. 30, no. 8, 1269–1274 (1959).
- [2.536] R. E. Whan and F. L. Vook, "Infrared Studies of Defect Production in n-Type Si: Irradiation-Temperature Dependence," *Phys. Rev.*, vol. 153, no. 3, 814–822 (1967).
- [2.537] F. L. Vook and H. J. Stein, "Production of Defects in n-Type Silicon," in: *Radiation Effects in Semiconductors*, edited by F. L. Vook, New York: Plenum Press, 99–114 (1968).
- [2.538] J. W. MacKay and E. E. Klontz, "Effects of Defect Charge State on Radiation Damage in Semiconductors," in: *Radiation Effects in Semiconductors*, edited by F. L. Vook, New York: Plenum Press, 175–185 (1968).
- [2.539] B. L. Gregory and C. E. Barnes, "Defect Reordering at Low Temperatures in Gamma Irradiated n-Type Silicon," in: *Radiation Effects in Semiconductors*, edited by F. L. Vook, New York: Plenum Press, 124–135 (1968).
- [2.540] V. V. Emtsev, T. V. Mashovets, and E. K. Nazaryan, "Metastable Frenkel Pairs in Silicon," *Sov. Phys. Semicond.*, vol. 16, no. 4, 440–443 (1982).
- [2.541] S. Bausch, H. Zillgen, and P. Ehrhart, "Frenkel Defects in Low Temperature e(-)-Irradiated Ge and Si Investigated by X-Ray Diffraction," in: *Defects in Semiconductors 18*, edited by M. Suezawa and H. Katayama-Yoshida, *Materials Science Forum*, vol. 196–201, 1141–1145 (1995).
- [2.542] P. Ehrhart and H. Zillgen, "Bound Vacancy Interstitial Pairs in Irradiated Silicon," *Nuclear Instruments and Methods in Physics Research B*, vol. 127/128, 27–31 (1997).
- [2.543] B. N. Mukashev, K. A. Abdullin, and Y. V. Gorelkinskii, "Interactions of Primary Defects with Impurities in Silicon," *Nuclear Instruments and Methods in Physics Research B*, vol. 186, 83–87 (2002).
- [2.544] A. Dal Pino, Jr., M. Needels, and J. D. Joannopoulos, "Oxygen-Induced Broken-Bond Defect in Silicon," *Phys. Rev. B*, vol. 45, no. 7, 3304–3308 (1992).
- [2.545] M. Tang, L. Colombo, J. Zhou, and T. Diaz de la Rubia, "Intrinsic Point Defects in Crystalline Silicon: Tight-Binding Molecular Dynamics Studies of Self-Diffusion, Interstitial-Vacancy Recombination, and Formation Volumes," *Phys. Rev. B*, vol. 55, no. 21, 14279–14289 (1997).
- [2.546] F. Cagnoni, C. Gatti, and L. Colombo, "Formation and Annihilation of a Bond Defect in Silicon: An Ab Initio Quantum-Mechanical Characterization," *Phys. Rev. B*, vol. 57, no. 1, 170–177 (1998).
- [2.547] M. T. Zawadzki, W. Luo, and P. Clancy, "Tight-Binding Molecular Dynamics Study of Vacancy-Interstitial Annihilation in Silicon," *Phys. Rev. B*, vol. 63, 205205 (2001).
- [2.548] L. A. Marqués, L. Pelaz, J. Hernández, J. Barbolla, and G. H. Gilmer, "Stability of Defects in Crystalline Silicon and Their Role in Amorphization," *Phys. Rev. B*, vol. 64, 045214 (2001).
- [2.549] S. Goedecker, T. Deutsch, and L. Billard, "A Fourfold Coordinated Point Defect in Silicon," *Phys. Rev. Lett.*, vol. 88, no. 23, 235501 (2002).
- [2.550] R. Habu, K. Kojima, H. Harada, and A. Tomiura, "Diffusion of Point Defects in Silicon Crystals during Melt Growth. III Two Diffusor Model," *Jpn. J. Appl. Phys.*, vol. 32, no. 4, 1754–1758 (1993).
- [2.551] S. M. Hu, "Defects in Silicon Substrates," *J. Vac. Sci. Technol.*, vol. 14, no. 1, 17–31 (1977).
- [2.552] D. A. Antoniadis and I. Moskowitz, "Diffusion of Substitutional Impurities in Silicon at Short Oxidation Times: An Insight into Point Defect Kinetics," *J. Appl. Phys.*, vol. 53, no. 10, 6788–6796 (1982).
- [2.553] U. Gösele, W. Frank, and A. Seeger, "An Entropy Barrier Against Vacancy-Interstitial Recombination in Silicon," *Solid State Communications*, vol. 45, no. 1, 31–33 (1983).
- [2.554] T. Sinno, Private communication (2002).
- [2.555] P. B. Moynagh and P. J. Rosser, "Quantification of Diffusion Mechanisms of Boron, Phosphorus, Arsenic, and Antimony in Silicon," in: *ESSDERC'89*, edited by A. Heuberger, H. Ryssel, and P. Lange, Berlin: Springer-Verlag, 291–296 (1989).

- [2.556] E. Guerrero, W. Jüngling, H. Pötzl, U. Gösele, L. Mader, M. Grasserbauer, and G. Stinger, "Determination of the Retarded Diffusion of Antimony by SIMS Measurements and Numerical Simulations," *J. Electrochem. Soc.*, vol. 133, no. 10, 2181–2185 (1986).
- [2.557] P. A. Packan, *Physical Modeling of Transient Diffusion Effects in Silicon Due to Surface Oxidation and Ion-Implantation*, Ph.D. thesis, Integrated Circuits Laboratory, Department of Electrical Engineering, Stanford University (1991).
- [2.558] E. A. Perozziello, P. B. Griffin, and J. D. Plummer, "Retarded Diffusion of Sb in a High Concentration As Background during Silicon Oxidation," *Appl. Phys. Lett.*, vol. 61, no. 3, 303–305 (1992).
- [2.559] H.-J. Gossmann, T. K. Mogi, C. S. Rafferty, P. A. Stolk, D. J. Eaglesham, H. S. Luftman, F. C. Unterwald, T. Boone, M. O. Thompson, and J. M. Poate, "Influence of Vacuum Annealing on Native Si Point Defects," in: *ULSI Science and Technology/1995*, edited by E. M. Middlesworth and H. Massoud, *Electrochem. Soc. Proc.*, vol. 95-5, 177–186 (1995).
- [2.560] S. Loualiche, C. Lucas, P. Baruch, J. P. Gaillard, and J. C. Pfister, "Theoretical Model for Radiation Enhanced Diffusion and Redistribution of Impurities," *phys. stat. sol. (a)*, vol. 69, 663–676 (1982).
- [2.561] P. Pichler, R. Schork, T. Klauser, and H. Ryssel, "Evaluation of the Point Defect Bulk Recombination Rate by Ion Implantation at High Temperatures," *IEICE Trans. Electron.*, vol. E75-C, no. 2, 128–137 (1992).
- [2.562] P. Pichler and R. Schork, "On Modeling of Ion Implantation at High Temperatures," *Radiation Effects and Defects in Solids*, vol. 127, 367–384 (1994).
- [2.563] B. Baccus, T. Wada, N. Shigyo, M. Norishima, H. Nakajima, K. Inoue, T. Iinuma, and H. Iwai, "A Study of Nonequilibrium Diffusion Modeling — Applications to Rapid Thermal Annealing and Advanced Bipolar Technologies," *IEEE Trans. Electron Devices*, vol. 39, no. 3, 648–661 (1992).
- [2.564] S. T. Dunham, "Modeling of Phosphorus Diffusion in Silicon," in: *Process Physics and Modeling in Semiconductor Technology*, edited by G. R. Srinivasan, K. Taniguchi, and C. S. Murthy, *Electrochem. Soc. Proc.*, vol. 93-6, 54–65 (1993).
- [2.565] M. M. Bunea, P. Fastenko, and S. T. Dunham, "Atomistic Simulations of Damage Evolution in Silicon," in: *Si Front-End Processing — Physics and Technology of Dopant-Defect Interactions*, edited by H.-J. L. Gossmann, T. E. Haynes, M. E. Law, A. Nylandsted Larsen, and S. Odanaka, *Mat. Res. Soc. Symp. Proc.*, vol. 568, 135–140 (1999).
- [2.566] K. M. Beardmore, W. Windl, B. P. Haley, and N. Grønbech-Jensen, "Diffusion Mechanisms and Capture Radii in Silicon," in: *Computational Nanoscience and Nanotechnology 2002*, Cambridge: Applied Computational Research Society, 251–254 (2002).
- [2.567] E. Sirtl, "Facts and Trends in Silicon Material Processing," in: *Semiconductor Silicon 1977*, edited by H. R. Huff and E. Sirtl, *Electrochem. Soc. Proc.*, vol. 77-2, 4–17 (1977).
- [2.568] P. Baruch, "Radiation Defects and Impurity Diffusion in Silicon," in: *Radiation Effects in Semiconductors, 1976*, edited by N. B. Urli and J. W. Corbett, *Inst. Phys. Conf. Ser.*, no. 31, 126–143 (1977).
- [2.569] S. Mizuo and H. Higuchi, "Retardation of Sb Diffusion in Si during Thermal Oxidation," *Jpn. J. Appl. Phys.*, vol. 20, no. 4, 739–744 (1981).
- [2.570] N. A. Stolwijk and J. Hözl, "The Influence of Dislocations on the Diffusion Behavior of Gold in Silicon," in: *Impurity Diffusion and Gettering in Semiconductors*, edited by R. B. Fair, C. W. Pearce, and J. Washburn, *Mat. Res. Soc. Symp. Proc.*, vol. 36, 137–142 (1985).
- [2.571] N. A. Stolwijk, J. Hözl, W. Frank, E. R. Weber, and H. Mehrer, "Diffusion of Gold in Dislocation-Free or Highly Dislocated Silicon Measured by the Spreading-Resistance Technique," *Appl. Phys. A*, vol. 39, 37–48 (1986).
- [2.572] H. Bracht, N. A. Stolwijk, I. Yonenaga, and H. Mehrer, "Interstitial-Substitutional Diffusion Kinetics and Dislocation-Induced Trapping of Zinc in Plastically Deformed Silicon," *phys. stat. sol. (a)*, vol. 137, 499–514 (1993).

- [2.573] W. Lerch, N. A. Stolwijk, H. Mehrer, and C. Poisson, “Diffusion of Platinum into Dislocated and Non-Dislocated Silicon,” *Semicond. Sci. Technol.*, vol. 10, 1257–1263 (1995).
- [2.574] A. Seeger and W. Frank, “On the Theory of the Diffusion of Gold into Dislocated Silicon Wafers,” *Appl. Phys. A*, vol. 27, 171–176 (1982).
- [2.575] N. A. Stolwijk, J. Hözl, W. Frank, J. Hauber, and H. Mehrer, “Decoration of Defects in Silicon with Gold, and Related Subjects,” *phys. stat. sol. (a)*, vol. 104, 225–245 (1987).
- [2.576] S. Kästner and J. Hesse, “The Influence of Dislocations on the Diffusion of Gold in Silicon,” *phys. stat. sol. (a)*, vol. 25, 261–267 (1974).
- [2.577] W.-S. Yang, W. J. Taylor, B. P. R. Marioton, and U. Gösele, “The Efficiency of Dislocations As Sinks for Silicon Self-Interstitials in Ribbon-Grown Polycrystalline Silicon,” in: *Polycrystalline Semiconductors II*, edited by J. H. Werner and H. P. Strunk, *Springer Proceedings in Physics*, vol. 54, 236–241 (1991).
- [2.578] B. Pichaud, G. Mariani, W. J. Taylor, and W.-S. Yang, “Dislocation-Gold Interactions in FZ and CZ Silicon: The Role of Self-Interstitials,” in: *Dislocations '93*, edited by J. Rabier, A. George, Y. Bréchet, and L. Kubin, *Solid State Phenomena*, vol. 35–36, 491–496 (1994).
- [2.579] D. Stiebel and P. Pichler, “Recombination of Point Defects via Extended Defects and Its Influence on Dopant Diffusion,” in: *Simulation of Semiconductor Processes and Devices 1998*, edited by K. De Meyer and S. Biesemans, Vienna: Springer-Verlag, 360–363 (1998).
- [2.580] P. B. Griffin, S. T. Ahn, W. A. Tiller, and J. D. Plummer, “Model for Bulk Effects on Si Interstitial Diffusivity in Silicon,” *Appl. Phys. Lett.*, vol. 51, no. 2, 115–117 (1987).
- [2.581] N. E. B. Cowern, “Analytical Description for the Diffusion and Recombination of Point Defects in Silicon,” *Appl. Phys. Lett.*, vol. 54, no. 15, 1415–1417 (1989).
- [2.582] H.-J. Gossmann, C. S. Rafferty, P. A. Stolk, D. J. Eaglesham, G. H. Gilmer, J. M. Poate, H.-H. Vuong, T. K. Mogi, and M. O. Thompson, “Properties of Point-Defects in Si for Process Modeling,” in: *Modeling and Simulation of Thin-Film Processing*, edited by D. J. Srolovitz, C. A. Volkert, M. J. Fluss, and R. J. Kee, *Mat. Res. Soc. Symp. Proc.*, vol. 389, 3–14 (1995).
- [2.583] P. A. Stolk, H.-J. Gossmann, D. J. Eaglesham, and J. M. Poate, “The Effect of Carbon on Diffusion in Silicon,” *Materials Science and Engineering B*, vol. 36, 275–281 (1996).
- [2.584] U. Gösele, A. Plößl, and T. Y. Tan, “The Influence of Carbon on the Effective Diffusivities of Intrinsic Point Defects in Silicon,” in: *Process Physics and Modeling in Semiconductor Technology*, edited by G. R. Srinivasan, C. S. Murthy, and S. T. Dunham, *Electrochem. Soc. Proc.*, vol. 96-4, 309–323 (1996).
- [2.585] M. D. Johnson, M.-J. Caturla, and T. Diaz de la Rubia, “A Kinetic Monte-Carlo Study of the Effective Diffusivity of the Silicon Self-Interstitial in the Presence of Carbon and Boron,” *J. Appl. Phys.*, vol. 84, no. 4, 1963–1967 (1998).
- [2.586] H. U. Jäger, “An Explanation of Trap-Limited Self-Interstitial Diffusion and Enhanced Boron Clustering in Boron Doped Silicon Superlattices,” in: *Process Physics and Modeling in Semiconductor Technology*, edited by G. R. Srinivasan, C. S. Murthy, and S. T. Dunham, *Electrochem. Soc. Proc.*, vol. 96-4, 210–215 (1996).
- [2.587] R. A. Casali, H. Rücker, and M. Methfessel, “Interaction of Vacancies with Interstitial Oxygen in Silicon,” *Appl. Phys. Lett.*, vol. 78, no. 7, 913–915 (2001).
- [2.588] N. E. B. Cowern, “Interstitial Traps and Diffusion in Epitaxial Silicon Films,” *Appl. Phys. Lett.*, vol. 64, no. 20, 2646–2648 (1994).
- [2.589] H.-H. Vuong, H.-J. Gossmann, C. S. Rafferty, H. S. Luftman, F. C. Unterwald, D. C. Jacobson, R. E. Ahrens, and T. Boone, “Influence of Fluorine Implant on the Transient Enhanced Diffusion of Boron: Determination of Process Modeling Parameters,” *Electrochem. Soc. Extended Abstracts*, vol. 95-1, 442–443 (1995).
- [2.590] H.-H. Vuong, H.-J. Gossmann, C. S. Rafferty, H. S. Luftman, F. C. Unterwald, D. C. Jacobson, R. E. Ahrens, T. Boone, and P. M. Zeitzoff, “Influence of Fluorine Implant on Boron Diffusion: Determination of Process Modeling Parameters,” *J. Appl. Phys.*, vol. 77, no. 7, 3056–3060 (1995).

- [2.591] F. Giannazzo, S. Mirabella, D. De Salvador, E. Napolitani, V. Raineri, A. Carnera, A. V. Drigo, A. Terrasi, and F. Priolo, "Direct Observation of Two-Dimensional Diffusion of the Self-Interstitials in Crystalline Si," *Phys. Rev. B*, vol. 66, 161310 (2002).
- [2.592] A. M. Agarwal and S. T. Dunham, "Consistent Quantitative Model for the Spatial Extent of Point Defect Interactions in Silicon," *J. Appl. Phys.*, vol. 78, no. 9, 5313–5319 (1995).
- [2.593] D. M. Maher, A. Staudinger, and J. R. Patel, "Characterization of Structural Defects in Annealed Silicon Containing Oxygen," *J. Appl. Phys.*, vol. 47, no. 9, 3813–3825 (1976).
- [2.594] T. Y. Tan and W. K. Tice, "Oxygen Precipitation and the Generation of Dislocations in Silicon," *Phil. Mag.*, vol. 34, no. 4, 615–631 (1976).
- [2.595] S. M. Hu, "The Shrinkage and Growth of Oxidation Stacking Faults in Silicon and the Influence of Bulk Oxygen," *J. Appl. Phys.*, vol. 51, no. 7, 3666–3671 (1980).
- [2.596] S. T. Ahn, H. W. Kennel, J. D. Plummer, W. A. Tiller, Z. U. Rek, and S. R. Stock, "Effect of Oxygen Precipitation on Phosphorus Diffusion in Czochralski Silicon," *Appl. Phys. Lett.*, vol. 53, no. 1, 34–36 (1988).
- [2.597] A. Bourret and W. Schröter, "HREM of SiP Precipitates at the (111) Silicon Surface during Phosphorus Predeposition," *Ultramicroscopy*, vol. 14, 97–106 (1984).
- [2.598] S. Mizuo and H. Higuchi, "Effects of Backside Oxidation on the Size of Oxidation Induced Stacking Faults at the Front Surface of FZ Si Wafers," *Jpn. J. Appl. Phys.*, vol. 21, no. 11, 1547–1553 (1982).
- [2.599] S. Mizuo and H. Higuchi, "Anomalous Diffusion of B and P in Si Directly Masked with Si₃N₄," *Jpn. J. Appl. Phys.*, vol. 21, no. 2, 281–286 (1982).
- [2.600] S. Mizuo and H. Higuchi, "Effects of Back-Side Oxidation of Si Substrates on Sb Diffusion at Front Side," *J. Electrochem. Soc.*, vol. 130, no. 9, 1942–1947 (1983).
- [2.601] S. M. Hu, "Formation of Stacking Faults and Enhanced Diffusion in the Oxidation of Silicon," *J. Appl. Phys.*, vol. 45, no. 4, 1567–1573 (1974).
- [2.602] M. Hamasaki, "On an Analytical Solution for Two-Dimensional Diffusion of Silicon Self-Interstitials during Oxidation of Silicon," *Solid-State Electronics*, vol. 25, no. 1, 1–4 (1982).
- [2.603] A. L. Aseev and V. M. Astakhov, "Interaction of Point Defects with the Surface of Silicon Crystals Irradiated in High-Voltage Electron Microscope," *Sov. Phys. Solid State*, vol. 24, no. 7, 1163–1166 (1982).
- [2.604] A. L. Aseev, S. G. Denisenko, and L. I. Fedina, "Influence of the Processes of Point Defect Annihilation on the Growth of Interstitial Atom Clusters during Irradiation of Si and Ge Crystals with Electrons in a High-Voltage Electron Microscope," *Sov. Phys. Semicond.*, vol. 25, no. 4, 352–355 (1991).
- [2.605] Y.-S. Shin and C.-K. Kim, "The Effect of Si-SiO₂ Interface on the Excess Point Defect Distribution in Silicon," in: *Semiconductor Processing*, edited by D. C. Gupta, *ASTM Special Technical Publication*, vol. 850, 283–293 (1984).
- [2.606] S. W. Crowder, P. B. Griffin, and J. D. Plummer, "Nitridation Enhanced Diffusion of Antimony in Bulk and Silicon-on-Insulator Material," in: *Process Physics and Modeling in Semiconductor Technology*, edited by G. R. Srinivasan, C. S. Murthy, and S. T. Dunham, *Electrochem. Soc. Proc.*, vol. 96-4, 54–63 (1996).
- [2.607] H. Rücker, B. Heinemann, and R. Kurps, "Nonequilibrium Point Defects and Dopant Diffusion in Carbon-Rich Silicon," *Phys. Rev. B*, vol. 64, 073202 (2001).
- [2.608] Y. Shin and C. Kim, "A Two-Dimensional Model for the Excess Interstitial Distribution in Silicon during Thermal Oxidation," *IEEE Trans. Electron Devices*, vol. ED-31, no. 6, 797–800 (1984).
- [2.609] D. Collard and K. Taniguchi, "IMPACT — A Point-Defect-Based Two-Dimensional Process Simulator: Modeling the Lateral Oxidation-Enhanced Diffusion of Dopants in Silicon," *IEEE Trans. Electron Devices*, vol. ED-33, no. 10, 1454–1462 (1986).
- [2.610] C. S. Rafferty, M. E. Law, P. B. Griffin, J. D. Shott, R. W. Dutton, and J. D. Plummer, "Modeling LOCOS Effects on Diffusion," in: *Semiconductor Silicon*, edited by H. R. Huff, T. Abe, and B. Kolbesen, *Electrochem. Soc. Proc.*, vol. 86-4, 426–436 (1986).

- [2.611] M. D. Giles, "Transient Phosphorus Diffusion below the Amorphization Threshold," *Electrochem. Soc. Extended Abstracts*, vol. 90-1, 369–370 (1990).
- [2.612] Y. Shibata, K. Taniguchi, and C. Hamaguchi, "Stripe Width Dependence of Oxidation-Enhanced Diffusion in Submicron Local Oxidation of Silicon Structures," *J. Appl. Phys.*, vol. 70, no. 9, 4846–4851 (1991).
- [2.613] H. Jacobs, A. von Schwerin, D. Scharfetter, and F. Lau, "MOSFET Reverse Short Channel Effect Due to Silicon Interstitial Capture in Gate Oxide," in: *Technical Digest of the 1993 International Electron Devices Meeting (IEDM)*, Piscataway: IEEE, 307–310 (1993).
- [2.614] J. J. van Dort, H. Lifka, P. C. Zalm, R. C. M. de Kruif, W. B. de Boer, P. H. Woerlee, C. A. H. Juffermans, A. J. Walker, J. W. Slotboom, and N. E. B. Cowern, "A High-Resolution Study of Two-Dimensional Oxidation-Enhanced Diffusion in Silicon," in: *Technical Digest of the 1993 International Electron Devices Meeting (IEDM)*, Piscataway: IEEE, 299–302 (1993).
- [2.615] S. W. Crowder, P. B. Griffin, and J. D. Plummer, "Oxidation Enhanced Dopant Diffusion in Thin SOI Films," in: *Process Physics and Modeling in Semiconductor Technology*, edited by G. R. Srinivasan, K. Taniguchi, and C. S. Murthy, *Electrochem. Soc. Proc.*, vol. 93-6, 108–119 (1993).
- [2.616] A. M. Agarwal and S. T. Dunham, "Models for the Physical Extent of Point Defect Interactions in Silicon," in: *Process Physics and Modeling in Semiconductor Technology*, edited by G. R. Srinivasan, K. Taniguchi, and C. S. Murthy, *Electrochem. Soc. Proc.*, vol. 93-6, 149–158 (1993).
- [2.617] M. J. van Dort, H. Lifka, P. C. Zalm, W. B. de Boer, P. H. Woerlee, J. W. Slotboom, and N. E. B. Cowern, "New Technique for Measuring Two-Dimensional Oxidation-Enhanced Diffusion in Silicon at Low Temperatures," *Appl. Phys. Lett.*, vol. 64, no. 16, 2130–2132 (1994).
- [2.618] S. W. Crowder, C. J. Hsieh, P. B. Griffin, and J. D. Plummer, "Effect of Buried Si-SiO₂ Interfaces on Oxidation and Implant-Enhanced Dopant Diffusion in Thin Silicon-on-Insulator Films," *J. Appl. Phys.*, vol. 76, no. 5, 2756–2764 (1994).
- [2.619] M. J. van Dort, W. van der Wel, J. W. Slotboom, N. E. B. Cowern, M. P. G. Knuvers, J. Lifka, and P. C. Zalm, "Two-Dimensional Transient Enhanced Diffusion and Its Impact on Bipolar Transistors," in: *Technical Digest of the 1994 International Electron Devices Meeting (IEDM)*, Piscataway: IEEE, 865–868 (1994).
- [2.620] D. R. Lim, C. S. Rafferty, and F. P. Klemens, "The Role of the Surface in Transient Enhanced Diffusion," *Appl. Phys. Lett.*, vol. 67, no. 16, 2302–2304 (1995).
- [2.621] A. Agarwal, H.-J. Gossmann, D. J. Eaglesham, L. Pelaz, D. C. Jacobson, T. E. Haynes, and Y. E. Erokhin, "Reduction of Transient Diffusion from 1-5 keV Si⁺ Ion Implantation Due to Surface Annihilation of Interstitials," *Appl. Phys. Lett.*, vol. 71, no. 21, 3141–3143 (1997).
- [2.622] B. Colombeau, F. Cristiano, G. Ben Assayag, A. Altibelli, and A. Claverie, "Energetics of Interstitial Defects and TED in Ultra Low Energy Implants," in: *Ion Implantation Technology — 2000*, edited by H. Ryssel, L. Frey, J. Gyulai, and H. Glawischnig, Piscataway: IEEE, 107–110 (2000).
- [2.623] B. Colombeau, F. Cristiano, A. Altibelli, C. Bonafos, G. Ben Assayag, and A. Claverie, "Atomistic Simulations of Extrinsic Defects Evolution and Transient Enhanced Diffusion in Silicon," *Appl. Phys. Lett.*, vol. 78, no. 7, 940–942 (2001).
- [2.624] S. Mirabella, A. Coati, D. De Salvador, E. Napolitani, A. Mattoni, G. Bisognin, M. Berti, A. Carnera, A. V. Drigo, S. Scalese, S. Pulvirenti, A. Terrasi, and F. Priolo, "Interaction between Self-Interstitials and Substitutional C in Silicon: Interstitial Trapping and C Clustering Mechanism," *Phys. Rev. B*, vol. 65, 045209 (2002).
- [2.625] N. A. Stolwijk, W. Lerch, and A. Giese, "Modeling of the Surface Annihilation of Excess Self-Interstitials Generated by Gold Diffusion into Silicon," in: *Semiconductor Process and Device Performance Modelling*, edited by S. T. Dunham and J. S. Nelson, *Mat. Res. Soc. Symp. Proc.*, vol. 490, 111–116 (1998).

- [2.626] J. Boussey-Said, N. Guillemot, and J. Stoemenos, "Recombination of Oxidation-Induced Silicon Interstitials at Si/SiO₂ Interfaces in SOI Structures," in: *1992 IEEE International SOI Conference*, New York: IEEE, 70–71 (1992).
- [2.627] S. W. Crowder, P. B. Griffin, C. J. Hsieh, G. Y. Wei, J. D. Plummer, and L. P. Allen, "Oxidation Enhanced Dopant Diffusion in Separation by Implantation by Oxygen Silicon-on-Insulator Material," *Appl. Phys. Lett.*, vol. 64, no. 24, 3264–3265 (1994).
- [2.628] S. Pindl, M. Biebl, E. Hammer, H. Schäfer, and H. v. Philipsborn, "Oxidation Enhanced Diffusion of Boron in Silicon-on-Insulator Substrates," in: *ULSI Science and Technology/1997*, edited by H. Z. Massoud, H. Iwai, C. Claeys, and R. B. Fair, *Electrochem. Soc. Proc.*, vol. 97-3, 623–631 (1997).
- [2.629] S. M. Hu, "Kinetics of Interstitial Supersaturation during Oxidation of Silicon," *Appl. Phys. Lett.*, vol. 43, no. 5, 449–451 (1983).
- [2.630] M. E. Law, Y. M. Haddara, and K. S. Jones, "Effect of the Silicon/Oxide Interface on Interstitials: Di-Interstitial Recombination," *J. Appl. Phys.*, vol. 84, no. 7, 3555–3560 (1998).
- [2.631] P. B. Griffin and J. D. Plummer, "Implications of Oxidation Models on the Point Defect Behavior in the Silicon Substrate," in: *The Physics and Chemistry of SiO₂ and the Si-SiO₂ Interface*, edited by C. R. Helms and B. E. Deal, New York: Plenum Press, 469–476 (1988).
- [2.632] W. A. Tiller, "On the Kinetics of the Thermal Oxidation of Silicon. III. Coupling with Other Key Phenomena," *J. Electrochem. Soc.*, vol. 128, no. 3, 689–697 (1981).
- [2.633] A. M. Lin, R. W. Dutton, D. A. Antoniadis, and W. A. Tiller, "The Growth of Oxidation Stacking Faults and the Point Defect Generation at Si-SiO Interface during Thermal Oxidation of Silicon," *J. Electrochem. Soc.*, vol. 128, no. 5, 1121–1130 (1981).
- [2.634] S. T. Dunham and J. D. Plummer, "Point-Defect Generation during Oxidation of Silicon in Dry Oxygen. I. Theory," *J. Appl. Phys.*, vol. 59, no. 7, 2541–2550 (1986).
- [2.635] S. T. Dunham and J. D. Plummer, "Point-Defect Generation during Oxidation of Silicon in Dry Oxygen. II. Comparison to Experiment," *J. Appl. Phys.*, vol. 59, no. 7, 2551–2561 (1986).
- [2.636] S. T. Dunham, "Interstitial Kinetics near Oxidizing Silicon Interfaces," *J. Electrochem. Soc.*, vol. 136, no. 1, 250–254 (1989).
- [2.637] K. Taniguchi, Y. Shibata, and C. Hamaguchi, "Theoretical Model for Self-Interstitial Generation at the Si/SiO₂ Interface during Thermal Oxidation of Silicon," *J. Appl. Phys.*, vol. 65, no. 7, 2723–2727 (1989).
- [2.638] Y. Shibata, S. Hashimoto, K. Taniguchi, and C. Hamaguchi, "Oxidation Enhanced Diffusion of Phosphorus over a Wide Range of Oxidation Rates," *J. Electrochem. Soc.*, vol. 139, no. 1, 231–237 (1992).
- [2.639] S. T. Ahn, H. W. Kennel, W. A. Tiller, and J. D. Plummer, "Vacancy Supersaturation in Si under SiO₂ by SiO Formation during Annealing in Ar," *J. Appl. Phys.*, vol. 65, no. 8, 2957 (1989).
- [2.640] S. T. Dunham, "Interaction of Silicon Point Defects with SiO₂ Films," *J. Appl. Phys.*, vol. 71, no. 2, 685–696 (1992).
- [2.641] N. Guillemot, D. Tsoukalas, C. Tsamis, J. Margail, A. M. Papon, and J. Stoemenos, "Suppression Mechanisms for Oxidation Stacking Faults in Silicon on Insulator," *J. Appl. Phys.*, vol. 71, no. 4, 1713–1720 (1992).
- [2.642] C. Tsamis, D. Tsoukalas, and J. Stoemenos, "Comparison between the Growth and Shrinkage of Oxidation Stacking Faults in Silicon and Silicon on Insulator," *J. Appl. Phys.*, vol. 73, no. 7, 3246–3249 (1993).
- [2.643] C. Tsamis and D. Tsoukalas, "Model for the Recombination Velocity of Silicon Interstitials at Nonoxidizing Interfaces," *J. Appl. Phys.*, vol. 84, no. 12, 6650–6658 (1998).
- [2.644] M. Hane, T. Ikezawa, M. Hiroi, and M. Matsumoto, "Dopant Diffusion Model Refinement and Its Impact on the Calculation of Reverse Short Channel Effect," in: *Technical Digest of the 1996 International Electron Devices Meeting (IEDM)*, Piscataway: IEEE, 803–806 (1996).
- [2.645] D. Tsoukalas, C. Tsamis, and J. Stoemenos, "Investigation of Silicon Interstitial Reactions with Insulating Films Using the Silicon Wafer Bonding Technique," *Appl. Phys. Lett.*, vol. 63, no. 23, 3167–3169 (1993).

- [2.646] J. F. Shepard, R. J. Dendall, and P. Balk, "Study of a Liquid Source Boron Diffusion Process for Silicon," *Electrochem. Soc. Extended Abstracts*, vol. 66-2, no. 196, 87–90 (1966).
- [2.647] G. N. Wills, "The Orientation Dependent Diffusion of Boron in Silicon under Oxidizing Conditions," *Solid-State Electronics*, vol. 12, 133–134 (1969).
- [2.648] K. E. Bean and P. S. Gleim, "The Influence of Crystal Orientation on Silicon Semiconductor Processing," *Proc. IEEE*, vol. 57, no. 9, 1469–1476 (1969).
- [2.649] R. A. Kovalev, V. B. Bernikov, Y. I. Pashintsev, and V. A. Marasanov, "Boron Diffusion in Silicon along Different Crystallographic Orientations," *Sov. Phys. Solid State*, vol. 11, no. 7, 1571–1573 (1970).
- [2.650] M. Okamura, "The Orientation Dependence of Boron Diffusion," *Jpn. J. Appl. Phys.*, vol. 9, 848–849 (1970).
- [2.651] T. C. Chan and C. C. Mai, "Diffusion of Boron, Phosphorus, Arsenic, and Antimony into (100) and (111) Silicon Slices," *Proc. IEEE*, vol. 58, no. 4, 588–589 (1970).
- [2.652] P. S. Dobson, "The Effect of Oxidation on Anomalous Diffusion in Silicon," *Phil. Mag.*, vol. 24, 567–576 (1971).
- [2.653] D. J. D. Thomas, "Surface Damage and Copper Precipitation in Silicon," *phys. stat. sol.*, vol. 3, 2261 (1963).
- [2.654] H. J. Queisser and P. G. G. van Loon, "Growth of Lattice Defects in Silicon during Oxidation," *J. Appl. Phys.*, vol. 35, 3066–3067 (1964).
- [2.655] G. R. Booker and W. J. Tunstall, "Diffraction Contrast Analysis of Two-Dimensional Defects Present in Silicon after Annealing," *Phil. Mag.*, vol. 13, 71–83 (1966).
- [2.656] R. J. Jaccodine and C. M. Drum, "Extrinsic Stacking Faults in Silicon after Heating in Wet Oxygen," *Appl. Phys. Lett.*, vol. 8, no. 1, 29–30 (1966).
- [2.657] A. W. Fisher and J. A. Amick, "Defect Structure on Silicon Surfaces after Thermal Oxidation," *J. Electrochem. Soc.*, vol. 113, no. 10, 1054–1060 (1966).
- [2.658] M. L. Joshi, "Stacking Faults in Steam-Oxidized Silicon," *Acta Metallurgica*, vol. 14, 1157–1172 (1966).
- [2.659] O. L. Krivanek and D. M. Maher, "The Core Structure of Extrinsic Stacking Faults in Silicon," *Appl. Phys. Lett.*, vol. 32, no. 8, 451–453 (1978).
- [2.660] D. A. Antoniadis, "Oxidation-Induced Point Defects in Silicon," *J. Electrochem. Soc.*, vol. 129, no. 5, 1093–1097 (1982).
- [2.661] S. M. Hu, "Interstitial and Vacancy Concentrations in the Presence of Interstitial Injection," *J. Appl. Phys.*, vol. 57, no. 4, 1069–1075 (1985).
- [2.662] R. Francis and P. S. Dobson, "The Effect of Oxidation on the Diffusion of Phosphorus in Silicon," *J. Appl. Phys.*, vol. 50, no. 1, 280–284 (1979).
- [2.663] C. Hill, "Measurements of Local Diffusion Coefficients in Planar Device Structures," in: *Semiconductor Silicon*, edited by H. R. Huff, R. J. Kriegler, and Y. Takeishi, *Electrochem. Soc. Proc.*, vol. 81-5, 988–1006 (1981).
- [2.664] S. Mizuo and H. Higuchi, "Effects of Oxidation on Aluminium Diffusion in Silicon," *Jpn. J. Appl. Phys.*, vol. 21, no. 1, 56–60 (1982).
- [2.665] S. Mizuo and H. Higuchi, "Oxidation Effects on Gallium Diffusion in Silicon," *Denki Kagaku*, vol. 50, no. 4, 338–343 (1982).
- [2.666] T. Y. Tan and B. J. Ginsberg, "Observation of Oxidation-Enhanced and -Retarded Diffusion of Antimony in Silicon: The Behavior of (111) Wafers," in: *Defects in Semiconductors II*, edited by S. Mahajan and J. W. Corbett, *Mat. Res. Soc. Symp. Proc.*, vol. 14, 141–145 (1983).
- [2.667] S. T. Dunham and N. Jeng, "Dopant Diffusion during High-Temperature Oxidation of Silicon," *Appl. Phys. Lett.*, vol. 59, no. 16, 2016–2018 (1991).
- [2.668] Y. Hayafuji, K. Kajiwara, and S. Usui, "Shrinkage and Growth of Oxidation Stacking Faults during Thermal Nitridation of Silicon and Oxidized Silicon," *J. Appl. Phys.*, vol. 53, no. 12, 8639–8646 (1982).

- [2.669] S. Mizuo, T. Kusaka, A. Shintani, M. Nanba, and H. Higuchi, "Effect of Si and SiO₂ Thermal Nitridation on Impurity Diffusion and Oxidation Induced Stacking Fault Size in Si," *J. Appl. Phys.*, vol. 54, no. 7, 3860–3866 (1983).
- [2.670] P. Fahey, G. Barbuscia, M. Moslehi, and R. W. Dutton, "Kinetics of Thermal Nitridation Processes in the Study of Dopant Diffusion Mechanisms in Silicon," *Appl. Phys. Lett.*, vol. 46, no. 8, 784–786 (1985).
- [2.671] S. S. Wong and T. W. Ekstedt, "CMOS Well Drive-in in NH₃ for Reduced Lateral Diffusion and Heat Cycle," *IEEE Electron Device Letters*, vol. EDL-6, no. 12, 659–661 (1985).
- [2.672] N. K. Chen and C. Lee, "Oxynitridation-Enhanced Diffusion of Boron in ⟨100⟩ Silicon," *J. Electrochem. Soc.*, vol. 140, no. 8, 2390–2394 (1993).
- [2.673] M. M. Moslehi, C. J. Han, K. C. Saraswat, C. R. Helms, and S. Shatas, "Compositional Studies of Thermally Nitrided Silicon Dioxide (Nitroxide)," *J. Electrochem. Soc.*, vol. 132, no. 9, 2189–2197 (1985).
- [2.674] C. J. Han, M. M. Moslehi, C. R. Helms, and K. C. Saraswat, "Time-Dependent Compositional Variation in SiO₂ Films Nitrided in Ammonia," *Appl. Phys. Lett.*, vol. 46, no. 7, 641–643 (1995).
- [2.675] T. K. Mogi, M. O. Thompson, H.-J. Goosmann, D. J. Eaglesham, C. S. Rafferty, J. S. Luftman, F. C. Unterwald, T. Boone, and J. M. Poate, "Dopant Diffusion in Si(100) Delta-Doping Superlattice during Thermal Nitridation and Native Si Point Defect Properties," *Electrochem. Soc. Extended Abstracts*, vol. 95-1, 473–474 (1995).
- [2.676] S. T. Ahn, H. W. Kennel, J. D. Plummer, and W. A. Tiller, "Film Stress-Related Vacancy Supersaturation in Silicon under Low-Pressure Chemical Vapor Deposited Silicon Nitride Films," *J. Appl. Phys.*, vol. 64, no. 10, 4914–4919 (1988).
- [2.677] K. Osada, S. Matsumoto, M. Yoshida, and E. Arai, "Effect of Stress in the Deposited Silicon Nitride Films on Boron Diffusion in Silicon," in: *Process Physics and Modeling in Semiconductor Technology*, edited by G. R. Srinivasan, K. Taniguchi, and C. S. Murthy, *Electrochem. Soc. Proc.*, vol. 93-6, 98–107 (1993).
- [2.678] S. M. Hu, "Properties of Amorphous Silicon Nitride Films," *J. Electrochem. Soc.*, vol. 113, no. 7, 693–698 (1966).
- [2.679] R. G. Frieser, "Direct Nitridation of Silicon Substrates," *J. Electrochem. Soc.*, vol. 115, no. 10, 1092–1094 (1968).
- [2.680] T. Ito, S. Hijiya, T. Nozaki, H. Arakawa, M. Shinoda, and Y. Fukukawa, "Very Thin Silicon Nitride Films Grown by Direct Thermal Reaction with Nitrogen," *J. Electrochem. Soc.*, vol. 125, no. 3, 448–452 (1978).
- [2.681] R. V. Giridhar and K. Rose, "Low Pressure Direct Thermal Nitridation of Si in Nitrogen," in: *Silicon Nitride Thin Insulating Films*, edited by V. J. Kapoor and H. J. Stein, *Electrochem. Soc. Proc.*, vol. 83-8, 312–323 (1983).
- [2.682] T. Kook and R. J. Jaccodine, "Diffusion of Sb in (111) Silicon during N₂ Heat-Treatment," *J. Electrochem. Soc.*, vol. 132, no. 4, 989–990 (1985).
- [2.683] M. Jacob, P. Pichler, H. Ryssel, R. Falster, M. Cornara, D. Gambaro, M. Olmo, and M. Paganini, "Observation of Vacancy Enhancement during Rapid Thermal Annealing in Nitrogen," in: *Gettering and Defect Engineering in Semiconductor Technology GADEST'97*, edited by C. Claeys, J. Vanhellemont, H. Richter, and M. Kittler, *Solid State Phenomena*, vol. 57-58, 349–354 (1997).
- [2.684] M. Wittmer and K. N. Tu, "Low-Temperature Diffusion of Dopant Atoms in Silicon during Interfacial Silicide Formation," *Phys. Rev. B*, vol. 29, no. 4, 2010–2020 (1984).
- [2.685] M. Wittmer, P. Fahey, G. J. Scilla, and S. S. Iyer, "Novel Diffusion Phenomenon of Dopants in Silicon at Low Temperatures," *Phys. Rev. Lett.*, vol. 66, no. 5, 632–635 (1991).
- [2.686] M. Wittmer, P. Fahey, J. Cotte, S. S. Iyer, and G. J. Scilla, "Silicide Formation and Dopant Diffusion," *Phys. Rev. B*, vol. 45, no. 19, 11383–11386 (1992).
- [2.687] J. W. Honeycutt and G. A. Rozgonyi, "Enhanced Diffusion of Sb-Doped Layers during Co and Ti Reactions with Si," *Appl. Phys. Lett.*, vol. 58, no. 12, 1302–1304 (1991).

- [2.688] S. M. Hu, "Point Defect Generation and Enhanced Diffusion in Silicon Due to Tantalum Silicide Overlay," *Appl. Phys. Lett.*, vol. 51, no. 5, 308–310 (1987).
- [2.689] A. G. Italyantsev and A. Y. Kuznetsov, "Excess Vacancy Generation in Silicon during Surface Silicide Formation," *Applied Surface Science*, vol. 73, 203–208 (1993).
- [2.690] I. Ohdomari, K. Konuma, M. Takano, T. Chikyow, H. Kawarada, J. Nakanishi, and T. Ueno, "Dopant Redistribution during Silicide Formation," in: *Thin Films — Interfaces and Phenomena*, edited by R. J. Nemanich, P. S. Ho, and S. S. Lau, *Mat. Res. Soc. Symp. Proc.*, vol. 54, 63–72 (1986).
- [2.691] K. Maex, R. D. Keersmaecker, C. Claeys, J. Vanhellemont, and P. F. A. Alkemade, "The Kinetics of Silicide Formation Using Rapid Thermal Processing and Related Defect Behavior," in: *Semiconductor Silicon*, edited by H. R. Huff, T. Abe, and B. Kolbesen, *Electrochem. Soc. Proc.*, vol. 86-4, 346–357 (1986).
- [2.692] D. S. Wen, P. L. Smith, C. M. Osburn, and G. A. Rozgonyi, "Defect Annihilation in Shallow p⁺ Junctions Using Titanium Silicide," *Appl. Phys. Lett.*, vol. 51, no. 15, 1182–1184 (1987).
- [2.693] W. Lur, J. Y. Cheng, C. H. Chu, M. H. Wang, T. C. Lee, Y. J. Wann, W. Y. Chao, and L. J. Chen, "Effects of Silicide Formation on the Removal of End-of-Range Ion Implantation Damage in Silicon," in: *Ion Beam Modification of Materials*, edited by S. Namba, N. Itoh, and M. Iwaki, *Nuclear Instruments and Methods in Physics Research B*, vol. 39, 297–301 (1989).
- [2.694] J. Chen, H. G. Robinson, S. B. Herner, and K. S. Jones, "Effect of Oxygen on Point Defect Injection during Silicidation of Titanium," in: *Semiconductor Silicon*, edited by H. R. Huff, W. Bergholz, and K. Sumino, *Electrochem. Soc. Proc.*, vol. 94-10, 1029–1040 (1994).
- [2.695] U. Erlesand, M. Östling, B. G. Svensson, and P. Gas, "Point Defect Generation during Silicide Formation," *Applied Surface Science*, vol. 53, 224–229 (1991).
- [2.696] P. Kringshøj, "Silicon Interstitials: Injection during Palladium Silicide Formation and Trapping by Ion Implantation Damage," *Appl. Phys. Lett.*, vol. 68, no. 2, 247–249 (1996).
- [2.697] J. Chen, H. G. Robinson, and K. S. Jones, "Effect of Oxygen on Point Defect Injection during Silicidation of Titanium," *Electrochem. Soc. Extended Abstracts*, vol. 94-1, 788 (1994).
- [2.698] W. Zulehner, "Historical Overview of Silicon Crystal Pulling Development," *Materials Science and Engineering B*, vol. 73, 7–15 (2000).
- [2.699] A. J. R. de Kock, "Microdefects in Dislocation-Free Silicon Crystals," *Philips Res. Repts Suppl.*, vol. 28, no. 1, 1–105 (1973).
- [2.700] H. Föll and B. O. Kolbesen, "Formation and Nature of Swirl Defects in Silicon," *Appl. Phys.*, vol. 8, 319–331 (1975).
- [2.701] H. Föll, U. Gösele, and B. O. Kolbesen, "Swirl-Defects in Silicon," in: *Semiconductor Silicon 1977*, edited by H. R. Huff and E. Sirtl, *Electrochem. Soc. Proc.*, vol. 77-2, 565–574 (1977).
- [2.702] P. J. Roksnoer and M. M. B. van den Boom, "Microdefects in a Non-Striated Distribution in Floating-Zone Silicon Crystals," *J. Crystal Growth*, vol. 53, 563–573 (1981).
- [2.703] W. von Ammon, E. Dornberger, H. Oelkrug, and H. Weidner, "The Dependence of Bulk Defects on the Axial Temperature Gradient of Silicon Crystals during Czochralski Growth," *J. Crystal Growth*, vol. 151, 273–277 (1995).
- [2.704] E. Dornberger, D. Graf, and M. Suhren, "Influence of Boron on the Oxidation-Induced Stacking Fault Ring in Czochralski Silicon Crystals," *J. Crystal Growth*, vol. 180, 343–352 (1997).
- [2.705] V. V. Voronkov and R. Falster, "Dopant Effect on Point Defect Incorporation into Growing Silicon Crystal," *J. Appl. Phys.*, vol. 87, no. 9, 4126–4129 (2000).
- [2.706] V. V. Voronkov and R. Falster, "Intrinsic Growth and Impurities in Silicon Crystal Growth," *J. Electrochem. Soc.*, vol. 149, no. 3, G167–G174 (2002).
- [2.707] K. Harada, H. Tanaka, T. Watanabe, and H. Furuya, "Defects in the Oxidation-Induced Stacking Fault Ring Region in Czochralski Silicon Crystal," *Jpn. J. Appl. Phys., Part 1*, vol. 37, no. 6A, 3194–3199 (1998).

- [2.708] M. Hasabe, Y. Takeoka, S. Shinoyama, and S. Naito, "Formation Process of Stacking Faults with Ringlike Distribution in CZ-Si Wafers," *Jpn. J. Appl. Phys.*, vol. 28, no. 11, L1999–L2002 (1989).
- [2.709] T. Yamauchi, Y. Tsumori, T. Nakashizu, H. Esaka, S. Takao, and S. Shinoyama, "Application of Copper-Decoration Method to Characterize as-Grown Czochralski-Silicon," *Jpn. J. Appl. Phys., Part 2*, vol. 31, no. 4B, L439–L442 (1992).
- [2.710] H. Shimizu, C. Munakata, N. Honma, S. Aoki, and Y. Kosaka, "Observation of Ring-Distributed Microdefects in Czochralski-Grown Silicon Wafers with a Scanning Photon Microscope and Its Diagnostic Application to Device Processing," *Jpn. J. Appl. Phys., Part 1*, vol. 31, no. 6A, 1817–1822 (1992).
- [2.711] H. Riemann and A. Lüdge, "Intrinsic Defects in FZ Silicon and Their Impact on X-Ray PIN Sensor Parameters," in: *High Purity Silicon VI*, edited by C. L. Claeys, P. Rai-Choudhury, M. Watanabe, P. Stallhofer, and H. J. Dawson, *Electrochem. Soc. Proc.*, vol. 2000-17, 509–515 (2000).
- [2.712] J. Gebauer, F. Rudolf, A. Polity, R. Krause-Rehberg, J. Martin, and P. Becker, "On the Sensitivity Limit of Positron Annihilation: Detection of Vacancies in As-Grown Silicon," *Appl. Phys. A*, vol. 68, 411–416 (1999).
- [2.713] S. Dannefaer, T. Bretagnon, K. Abdurahman, D. Kerr, and S. Hahn, "Heat-Treatment Induced Defects in CZ-Silicon," in: *Defect Engineering in Semiconductor Growth, Processing and Device Technology*, edited by S. Ashok, J. Chevallier, K. Sumino, and E. Weber, *Mat. Res. Soc. Symp. Proc.*, vol. 262, 671–676 (1992).
- [2.714] F. Quast, P. Pichler, H. Ryssel, and R. Falster, "Vacancy-Nitrogen Complexes in Float-Zone Silicon," in: *High Purity Silicon VI*, edited by C. L. Claeys, P. Rai-Choudhury, M. Watanabe, P. Stallhofer, and H. J. Dawson, *Electrochem. Soc. Proc.*, vol. 2000-17, 156–163 (2000).
- [2.715] M. Hourai, T. Ono, S. Umeno, and T. Tanaka, "Control of Grown-in Defects in Nitrogen-Doped CZ Silicon Crystals for New Generation Devices," in: *Crystalline Defects and Contamination: Their Impact and Control in Device Manufacturing III—DECON 2001*, edited by B. O. Kolbesen, C. Claeys, P. Stallhofer, and F. Tardif, *Electrochem. Soc. Proc.*, vol. 2001-29, 19–34 (2001).

Chapter 3

Impurity Diffusion in Silicon

The general discussion of diffusion in Section 1.3 did not take into account the particular structure of silicon. The intention of this chapter is to discuss the atomistic processes associated with the diffusion of impurities and their interaction with intrinsic point defects in more detail. In Section 3.1, the various mechanisms for diffusion of impurities in silicon are introduced and discussed. Most important for impurities residing predominantly on substitutional sites are mechanisms in which they form mobile pairs with intrinsic point defects. The energetics of such pairs is discussed in detail in Section 3.2. Diffusion of mobile complexes can be described within the method of diffusion-reaction equations. The derivation of the basic equations and of special cases will be explained in Section 3.3. The most important special cases, pair diffusion, diffusion via the Frank-Turnbull mechanism, and diffusion via the kick-out mechanism are discussed in detail in the Sections 3.4 to 3.6.

3.1 Basic Mechanisms

Impurities may reside on various sites in the crystal lattice and even more diverse are their diffusion paths. Some impurities dissolve predominantly on interstitial sites. Their diffusion, as outlined in Section 3.1.1, does then not involve intrinsic point defects and can be described simply by Fick's laws. Most other impurities prefer substitutional sites. The most direct way for their diffusion, discussed briefly in Section 3.1.2, would be to directly exchange sites with neighboring atoms. Such processes are usually not considered energetically favorable and the vast bulk of the diffusion theories are based on an interaction of the impurities with intrinsic point defects. Historically, interactions with vacancies were considered first. The respective concepts are summarized in Section 3.1.3. The alternative, diffusion via interactions with self-interstitials, will be touched on in Section 3.1.4. Mechanisms involving interactions with vacancies and self-interstitials will be discussed in detail in the remaining sections of this chapter.

3.1.1 Interstitial Diffusion

Because of the very open nature of the silicon crystal many atoms dissolve on interstitial sites, i. e. on tetrahedral, hexagonal, or bond-centered positions between the lattice atoms, and diffuse likewise. These include most alkali and heavy metals like copper, iron, and nickel, but also hydrogen and oxygen.

Because of the low concentration of atoms on such interstitial sites, all interstitial sites neighboring to an occupied interstitial site will, in general, be free. Interstitial diffusion does not involve direct interaction with intrinsic point defects. As a consequence, such atoms perform

a random walk as outlined in Section 1.3.2, characterized by a diffusion coefficient which is a function of temperature only. These diffusion coefficients are usually orders of magnitude larger than that of self-diffusion and of the group III and V dopants. Early theoretical approaches to the diffusion of intrinsic impurities were derived by Wert and Zener [3.1] for metals, and by Weiser [3.2] and Swalin [3.3] for crystals with a diamond structure. When sufficient computer resources became available, various studies based on molecular dynamics or *ab-initio* methods were published which show that an estimate of the barrier height opposing the migration of interstitial impurities may require to account for the concerted motion of various atoms in their vicinity and is everything but trivial.

Experiments performed at low temperatures have shown that interstitially dissolved atoms may exist in several charge states characterized potentially by different diffusion coefficients. However, it was discussed in Section 1.5.3 that steady state between these charge states is established very rapidly at the high temperatures of usual thermal processes so that the diffusion current for the total concentration of the atoms can be described in analogy to (2.52) with an effective diffusion coefficient.

Interstitial atoms, as mentioned, do not need an interaction with intrinsic point defects for diffusion. This does not mean that such interactions are not possible or likely. Similarly, reactions with other impurities or even atoms of the same species are quite common and kept scientists busy with the identification and characterization of the resulting defects. Some of the results, where appropriate, are addressed in the following chapters. Most of the reactions immobilize the interstitial impurities. A typical example is the formation of pairs between interstitial metals and substitutional dopants. But there are also cases, e. g. oxygen forming complexes with hydrogen or carbon, which lead to a considerable enhancement of the effective diffusivity of the interstitial diffuser.

The maximum concentration of impurities on interstitial sites is limited by a rather low solubility concentration. When this solubility concentration is exceeded, e. g. during the ramping-down phase of diffusion processes, the impurities may form precipitates. Because of the high diffusivity of interstitial diffusers, precipitation can occur even at moderate temperatures as during chemical-layer deposition in back-end processes. Forming in active device areas, such precipitates can reduce drastically device performance and yield. Therefore, it is desirable to get rid of detrimental interstitial diffusers in areas where they do not cause harm. There are various methods by which this can be achieved. All of them have in common that either sites are provided at which nucleation and precipitation of the interstitial diffusers is energetically more favorable than in the active device areas, that impurities are provided which act as potential reaction partners for the interstitial diffusers, or that layers are deposited on silicon to which the impurities segregate preferentially. In the continuity equations of the interstitial diffusers, precipitation and the first two gettering concepts can be included by appropriate generation and loss terms. Segregation to adjacent layers can be described by appropriate boundary conditions.

3.1.2 Direct-Exchange Mechanism for Substitutional Impurities

Most important for semiconductors are atoms of the groups III and V of the periodic system. They reside predominantly in ionized form on substitutional sites and have a comparatively low macroscopic diffusion coefficient. But there are also various other impurities known to prefer substitutional sites. Among them are the isovalent impurities and metals like gold, platinum, and zinc.

The most simple diffusion mechanism for substitutional impurities as well as for silicon lattice atoms would be to exchange places with adjacent atoms. Such a mechanism has been investigated by Huntington and Seitz [3.4, 3.5] for the self-diffusion of copper. But the results indicated that a direct-exchange mechanism can be ruled out at least for this process. As an alternative, Zener [3.6] pointed out that the cooperative motion of a ring of four atoms can reduce the activation energy in comparison to an exchange of only two atoms. As a further variant, Millea [3.7] suggested an indirect interchange mechanism. In his model, a lattice atom leaves first its substitutional site, one of the neighboring atoms moves into the vacancy left behind, and the first atom moves from the interstitial position into the vacancy left behind by the second atom. These mechanisms were discussed by Hu [3.8] and found to be unlikely because of energetic considerations. Decades later, Pandey [3.9] proposed a concerted mechanism for the exchange of two substitutional atoms. For the case of self-diffusion in silicon, he estimated an activation energy of 4.3 eV, a value close to the activation energy of self-diffusion determined experimentally. For dopant atoms, the possibility of a direct exchange with neighboring silicon atoms was indicated but taken into consideration only in a minority of the investigations on dopant diffusion. All these diffusion mechanisms have in common that they do not require interactions with intrinsic point defects so that the diffusion coefficient associated should be a function of temperature only.

3.1.3 Diffusion of Substitutional Atoms via Vacancies

In general, the diffusion of substitutional atoms is assumed to proceed with the help of intrinsic point defects. One possible mechanism is that substitutional atoms exchange position with adjacent vacancies. It was proposed first by Steigman et al. [3.10] for diffusion in metals. They already noted that the pre-exponential factors and activation energies for diffusion are highest for self-diffusion and lower for impurity diffusion. This experimental finding which was not predicted by their theory was explained by Johnson [3.11] assuming a binding energy between the impurity atoms and vacancies. This impurity-vacancy binding leads to a series of migration steps of the impurity atom and the vacancy without dissociation. List and Ryssel [3.12] later found that a non-attractive interaction can also lead to the experimentally observed reduction of the activation energy of impurity diffusion in comparison to self-diffusion. However, such an interaction was never reproduced by *ab-initio* calculations.

Diffusion of a substitutional impurity and a vacancy as a pair was shown by Bardeen [3.13] and LeClaire and Lidiard [3.14] to involve correlation effects arising from the atomistic nature of the migration process. Obviously, for diffusion via vacancies, the probability for the first jump of a substitutional impurity atom is proportional to the probability that an adjacent lattice site is vacant. But when such a first jump has occurred, the probability that a lattice site adjacent to the impurity atom is vacant increases to unity and it is likely that impurity atom and vacancy exchange sites again. Such successive exchanges of position do not lead to an effective migration. Diffusion as a pair implies that the vacancy dissociates from the impurity to return at another nearest neighboring site. In such a process, the jump frequency of a vacancy will depend on its distance to adjacent impurity atoms. For dilute concentrations, only the distance to the nearest impurity atom is important. This situation was analyzed by Manning [3.15], Hu [3.16], and Koiwa and Ishioka [3.17] based on a model considering impurity-vacancy interaction ending at the second coordination site. But in silicon, to perform a random walk as a pair, a vacancy has to pass a third coordination site and Mehrer [3.18], Yoshida [3.19], Hu [3.20], and Dunham and Wu [3.21] later included long-ranging interactions between vacancies and doping atoms.

Important for many applications is the influence of vacancy gradients on the diffusion of dopants and *vice versa*. The first considerations in this direction go back to Seitz [3.22] who

came to the conclusion that impurity atoms which diffuse faster than the lattice atoms cause a “chemical pump” effect which drives a vacancy flux in the opposite direction. In the reverse situation, called “vacancy wind,” a vacancy flux would induce a flux of impurities in the opposite direction. The deficiencies of this theory were discussed by Hu [3.23] who criticized especially that the atomic nature of the processes was ignored. Pair-diffusion theories as outlined in Section 3.4 assume that pairs form proportional to the product of vacancy concentration and dopant concentration. When the concentration of vacancies increases with depth, the concentration of pairs forming in samples with homogeneously distributed dopants will also increase with depth. Their migration leads to a flux of dopants and of vacancies towards the surface. In contrast, ignoring pair-binding and correlation effects, Uskow and Vas’kin [3.24] and Kurata et al. [3.25] developed a “non-Fickian” diffusion model in which dopants and vacancies move in opposite directions. This means a flux of dopants from the surface into the bulk and a flux of vacancies towards the surface for the example above. This model was applied and extended later by Morikawa et al. [3.26], Kozlovskii et al. [3.27], Aleksandrov et al. [3.28], and Maser [3.29]. Both models can be generalized in the form

$$-J_M = D_M \cdot \frac{C_V}{C_V^{eq}} \cdot \text{grad}(C_M) + T_M \cdot C_M \cdot \text{grad} \left(\frac{C_V}{C_V^{eq}} \right) \quad (3.1)$$

with $D_M/T_M = 1$ for pair diffusion theories and $D_M/T_M = -1$ for the “non-Fickian” diffusion mechanism. Both are clearly simplifications. But the theoretical investigations of List and Ryssel [3.12] based on model potentials clearly showed that $T_M/D_M = 1$ can be considered the limit to which all interaction potentials converge when the extent and range of the vacancy-impurity interaction is extended. The value $T_M/D_M = -1$, on the other hand, can be expected only for very special interaction potentials and has no general validity. For cases without interaction between impurity and vacancy, the ratio of diffusion and transport coefficient takes the value $T_M/D_M = -2$. The concepts of List and Ryssel were confirmed by the Lattice-Monte-Carlo investigations of Dunham and Wu [3.30] who estimated $T_M/D_M \approx 1/3$ for a model potential assumed for the interaction of vacancies and arsenic. Based on dopant-impurity binding energies from *ab-initio* calculations, Bunea and Dunham [3.31] found the ratio T_M/D_M to decrease for arsenic from about 0.8 at 900 °C to about 0.4 at 1300 °C. In contrast, for phosphorus, they found that T_M/D_M converges to 1, independent of temperature. The Lattice-Monte-Carlo investigations of Pankratov et al. [3.32] based also on binding energies obtained from *ab-initio* simulations finally indicated that arsenic diffusion is dominated in the temperature range from 427 to 1023 °C by pair diffusion. In a later publication, based also on the *ab-initio* simulations of Pankratov et al. [3.32], Bunea and Dunham [3.33] reported improved results with respect to their previous work which indicated that T_M/D_M drops for arsenic from 0.85 at 700 °C to 0.29 at 1300 °C. For phosphorus, a less significant reduction from 0.92 at 700 °C to 0.69 at 1300 °C was calculated from the binding energies reported by Nelson et al. [3.34]. But not only theoretical results are available. Redistribution of initially homogeneously distributed boron [3.35], antimony [3.36, 3.37], and phosphorus [3.38] in situations involving large gradients of intrinsic point defects show that point-defect migration and dopant migration goes in the same direction. Especially the experiments in which protons and boron atoms were implanted into an initially constant background of antimony [3.36, 3.37] gave a clear evidence in favor of diffusion of antimony via vacancy-dopant pairs since antimony, in contrast to the other dopants, is known to diffuse nearly entirely via vacancies.

3.1.4 Diffusion of Substitutional Impurities as Interstitials or Impurity-Self-Interstitial Pairs

Some metals, as mentioned above, reside predominantly on substitutional sites. Their diffusion, on the other hand, was found to proceed via interstitial metal atoms. One possible way for an impurity to change from an interstitial site to a substitutional site has been proposed by Frank and Turnbull [3.39] to describe the diffusion of copper in germanium. In their model, generally termed “Frank-Turnbull mechanism,” an interstitial metal atom may react with a vacancy to become substitutional. The same mechanism was suggested by Longini [3.40] for the diffusion of zinc in gallium arsenide. At least in the silicon community, reference to their work is not customary but “dissociative mechanism” is frequently used as a synonym for the Frank-Turnbull process. It has its name from the backward reaction which can be seen as a dissociation process in which the impurity atom leaves a vacancy behind when it assumes an interstitial position. An extended discussion of the equations describing the mechanism as well as of the profile shapes to be expected can be found in Section 3.5.

As an alternative to a vacancy mechanism, Seitz [3.22] proposed that host atoms and impurity atoms can diffuse in metals via an interstitialcy mechanism. It assumes that an interstitial atom (impurity or self-interstitial) displaces an atom (impurity or host atom) on an adjacent lattice site to an interstitial site to become substitutional. The displaced interstitial atom is then expected to displace an other substitutional atom in its vicinity. While the mechanism was considered unlikely for metals, Seeger and Chik [3.41] suggested it to be a viable alternative for the diffusion of substitutional impurities in silicon. When the self-interstitial is bound, e. g. by Coulombic attraction, to the impurity atom, both can diffuse as a pair. To perform a random walk as a pair, the silicon atom has to pass only a second-nearest interstitial site [3.20] whereas a vacancy has to pass a third coordination site. Diffusion as a pair does not necessarily imply that the self-interstitial remains the same atom. There may be mechanisms, on the other hand, in which this is the case. Since this would imply the transport of labelled atoms, there would be a significant influence on self-diffusion as discussed in Section 2.3.

The dislocation of a substitutional impurity by a self-interstitial to a metastable interstitial site was suggested first by Watkins [3.42]. In his electron-irradiation studies using aluminum-doped samples, he found no trace of the self-interstitials which were expected to be present in the same concentration as the vacancies he found. Instead, there were interstitial aluminum atoms in about the same concentration as the vacancies and it was concluded that they resulted from the above mentioned reaction. Once, a substitutional impurity is dislocated to an interstitial site, it may perform a random walk in the interstitial sub-lattice before it displaces again a substitutional atom. The reverse mechanism of the so-called “Watkins replacement mechanism” is that an interstitial impurity dislocates a silicon atom to an interstitial site to become substitutional. It has been proposed by Gösele et al. [3.43] and given the name “kick-out mechanism.” Based on this assumption, as discussed in Section 3.6, it was possible to reproduce the shape of gold profiles in silicon.

Although the differences between the interstitialcy mechanism and the kick-out mechanism might be important from a scientific point of view, both appear as different sides of the same coin for dopant diffusion and can be described by the pair-diffusion theory outlined in Section 3.4. Accordingly, both are usually addressed by the generic term “interstitial mechanism.” A main influence on the shape of the resulting profile comes from the transport capacity of the impurities. U-shaped profiles after predeposition are expected only for impurities with higher transport capacities than that of self-diffusion. For impurities with lower transport coefficients, conventional error-function shapes can be expected.

Within a campaign against self-interstitials, Schmid et al. [3.44] claimed that the kick-out mechanism would not be able to reproduce the U-shaped metal profiles observed experimentally. The main evidence was based on kinetic-Monte-Carlo studies. Already Mathiot [3.45] criticized that the limitations of computational resources did not allow to simulate the whole process so that the conclusion is influenced by the use of effective parameters and scaling rules. It was also not shown that metal-diffusion profiles can be reproduced assuming an interaction of metal interstitials with vacancies only. As nearly always in such cases, a further discussion [3.46] did not lead to a convergence but rather to a hardening of attitudes.

As in the case of diffusion via vacancies, effects of dopant diffusion on the concentrations of the intrinsic point defects and *vice versa* were discussed controversially in the literature. In the first of such considerations, Seitz [3.22] suggested that impurity atoms which diffuse faster than lattice atoms cause an interstitialcy flux in the same direction. In the reverse situation, called “interstitial wind,” an interstitialcy flux causes a dopant flux in the same direction. Hu [3.47] discussed several shortcomings of this theory and concluded that it would not be able to predict fluxes in real situations. In analogy to the case of vacancies, the pair-diffusion theory outlined in Section 3.4 predicts that pairs form proportional to the product of self-interstitial concentration and dopant concentration. When the concentration of self-interstitials increases with depth, the concentration of pairs forming in samples with homogeneously distributed dopants will also increase with depth. Their migration leads to a flux of dopants and of self-interstitials towards the surface. In contrast, Maser [3.29] extended his vacancy model formally to self-interstitials and suggested that the dopant flux would be in the other direction. As in the case of vacancy gradients and their effects on dopant diffusion discussed in the previous section, pair diffusion can be seen as a limiting assumption for a strong binding between impurity and self-interstitial. More realistic macroscopic models were, most likely because of the complicated interactions of self-interstitials and impurity atoms, not discussed in the literature.

3.2 Impurity-Point-Defect Pairs

The dominant mechanism considered for the diffusion of substitutional impurities via vacancies includes the formation of mobile impurity-vacancy pairs. These pairs are postulated to perform a series of uncorrelated random steps before dissociation. Experimental observations and theoretical investigations are in agreement with an attractive interaction between impurity and vacancy, but there were other concepts considered in the literature as well.

Mobile pairs of impurities with self-interstitials were introduced initially as an analogy to pairs with vacancies and there are indications from experiments and from theoretical investigations that such pairs exist. It should be noted, however, that mobile impurity interstitials are viable alternatives to bound or virtual pairs of impurities and self-interstitials performing a random walk together.

In the following, the concepts of pairs will be described in more detail and the concentrations of bound pairs in a constrained equilibrium will be derived. Finally, the atomistic processes associated with the diffusion of bound point-defect-impurity pairs will be discussed.

3.2.1 Classification of Pairs

Historically, at first, only pairs with vacancies were assumed. The barrier diagram in Figure 3.1 reflects the information obtained from the EPR investigations and from theoretical investigations discussed in more detail in the following chapters. It suggests that the crystal energy is lowered when a vacancy approaches an impurity atom. To perform a random walk as a

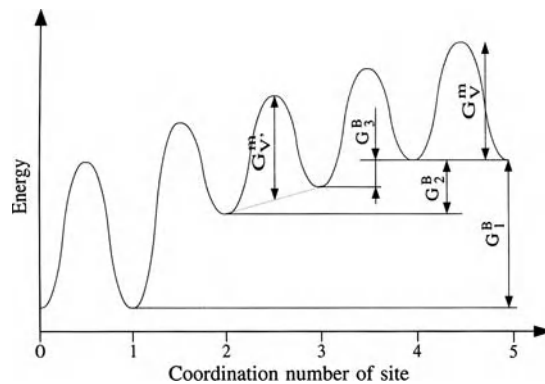


Figure 3.1: Schematic representation of the vacancy potential as a function of the distance to an impurity with an attractive interaction extending to the 3rd coordination site.

pair, the vacancy has to move without dissociating from one nearest neighboring site of the impurity atom to an other, at times exchanging sites with the impurity atom. Manning [3.15], Hu [3.16], and Koiwa and Ishioka [3.17] analyzed correlation effects resulting from pair binding, but considered only interactions ending at the second coordination site. In silicon, when moving from one nearest neighboring site to the other, the vacancy has to pass at least one of the third coordination sites. At such third coordination sites, when the interaction ends at the second coordination site, the pair is already dissociated. Diffusion as a pair is possible only when a vacancy at a third neighboring site of an impurity is still bound to it. Later, Mehrer [3.18], Yoshida [3.19], Hu [3.20], and Dunham and Wu [3.21] presented analyses with far-ranging interactions between vacancies and dopants.

In addition to attractive dopant-vacancy interactions, List and Ryssel [3.12] investigated non-attractive interactions as shown in Figure 3.2. In the vicinity of a dopant atom, the jump frequency of the vacancy is enhanced. But since there is no attractive interaction between vacancy and impurity atom, one can speak at most of a “virtual” pair. List and Ryssel could show

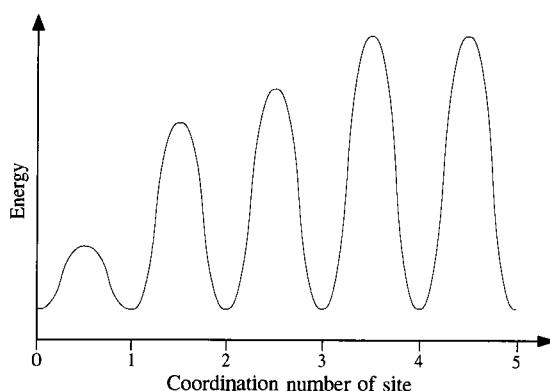


Figure 3.2: Schematic representation of the vacancy potential as a function of the distance to an impurity with a non-attractive interaction extending to the 3rd coordination site.

that the experimentally observed lower activation energy of dopant diffusion in comparison to self-diffusion would result also from such a non-attractive interaction. However, it has to be mentioned that the experimental evidence and the results from theoretical investigations discussed in the following chapters favor attractive interactions resulting from Coulomb attraction and/or lattice relaxations.

An alternative to the vacancy as “diffusion vehicle” was proposed by Seeger and Chik [3.41]. In their interstitial mechanism, a self-interstitial adjacent to an impurity atom displaces the impurity atom to an interstitial position, occupying the lattice site itself. The interstitial impurity atom subsequently displaces one of the neighboring silicon atoms to an interstitial position and takes up its substitutional position again. When an attractive interaction exists between the self-interstitial and the doping atom, the two can perform a random walk. To perform a random walk as a pair, as pointed out by Hu [3.20], the silicon atom has to pass only a second-nearest interstitial site whereas a vacancy would have to pass a third coordination site. Here, it has to be mentioned that the formation of a mobile pair of a self-interstitial and a substitutional impurity is just one possibility for the diffusion of impurities via self-interstitials. Another possibility, very similar to the kick-out mechanism discussed in more detail in Section 3.6, is that a silicon atom mobilizes a substitutional impurity by dislocating it to an instable interstitial configuration or by forming an instable split-interstitial with it. Within the formalism discussed in Section 3.3, there is no difference between these mechanisms and the notion of a bound impurity-self-interstitial complex will be adopted in analogy. It should be mentioned also that the results remain the same when a substitutional impurity atom is assumed to be displaced by the self-interstitial to a metastable interstitial site where it may perform a random walk until it becomes substitutional again by displacing a silicon lattice atom to an interstitial site.

3.2.2 Concentration in Thermal Equilibrium

The equilibrium concentration of the pairs can be computed from statistical thermodynamics as outlined in Section 1.4. In this way, Lidiard [3.48] derived the concentration of vacancy-impurity pairs under the assumption that the vacancies in the pairs occupy only nearest neighboring site to the impurities. Hu [3.23] extended this treatment and included partial ionization of impurities, and vacancies in different charge states. But diffusion as a pair, as already noted above, involves a long-ranging association of intrinsic point defects and substitutional impurities beyond the nearest neighboring site. The energy needed to introduce an intrinsic point defect X (either vacancy V or self-interstitial I) will depend on the distance to the substitutional impurities in the crystal. For sufficiently low impurity concentrations, only the distance to the nearest impurity has to be considered. Such a simplification fails potentially for high concentrations.

Within the association range of one of the N_M substitutional impurities, various different configurations of a pair with an intrinsic point defect X have to be considered. Each of these configurations j is characterized by a specific arrangement of the impurity and the intrinsic point defect in the lattice, comprises a number of geometrically equivalent orientations, and may be in charge state k . In the following, only the single acceptor and donor states of pairs, if existent, are taken into considerations. An extension to higher degrees of ionization is straightforward. The change in Gibbs free energy of the crystal upon introducing one of $N_{MX_j^k}$ of such point defects is denoted by $G_{MX_j^k}^f = H_{MX_j^k}^f - T \cdot S_{MX_j^k}^f$ and is a function of the distance between impurity and intrinsic point defect as well as of the charge state of the pair. Unlike in the analysis of Hu [3.23], it will not be distinguished here whether the charge is attributed to the impurity or to the intrinsic point defect. This is an as-well abstraction and consistent with the methodology of

diffusion-reaction equations outlined below where pairs are considered individual point defects and attributed parameters like charge states or diffusion coefficients. In analogy to (2.11) and (2.12), the differences between the formation energies

$$E_{MX_j^-} = G_{MX_j^-}^f - G_{MX_j^0}^f \quad \text{and} \quad E_{MX_j^+} = G_{MX_j^0}^f - G_{MX_j^+}^f \quad (3.2)$$

correspond to the energy of negative ionization and the negative energy of positive ionization of a neutral pair in configuration j , respectively. The electronic levels associated with these transitions can be found at $E_c - E_{MX_j^-}$ and $E_v + E_{MX_j^+}$, respectively.

Outside of the association range, the change in Gibbs free energy of the crystal upon introduction of one of N_{X^i} point defects X in charge state i is independent of the presence of substitutional impurities and, as in (2.1), denoted by $G_{X^i}^f = H_{X^i}^f - T \cdot S_{X^i}^f$. Taking the ionized impurity as a reference point (zero formation energy), it is convenient to define the difference in the Gibbs free energy between an unassociated point defect and a point defect associated with an ionized impurity as its binding energy to the impurity

$$G_{MX_j^k}^B = G_{X^{k-M}}^f - G_{MX_j^k}^f \quad (3.3)$$

indicated in Figure 3.1. The charge state $i \equiv k - M$ of point defect X indicates that a point defect in charge state i leads to a pair within the association range the charge state of which corresponds to $z_k = z_i + z_M$ electron charges. For each configuration, the binding energy in a specific charge state can be expressed in terms of the binding energy of an other charge state, the ionization energies (3.2) of the pairs, and the ionization energies (2.11) and (2.12) of the intrinsic point defects. As an example, it follows for pairs with acceptors ($M = 1$) from the binding energy of neutral pairs $G_{MX^0}^B = G_{X^+}^f - G_{MX^0}^f$ that the binding energy of negatively charged pairs is given by $G_{MX^-}^B = G_{X^0}^f - G_{MX^-}^f = E_{X^+} + G_{X^+}^f - E_{MX^-} - G_{MX^0}^f = G_{MX^0}^B + E_{X^+} - E_{MX^-}$.

Within the system, the number of silicon atoms and impurities is conserved. Their contribution to the free energy of the system less the configurational entropy can be taken as a reference point. But substitutional impurities may exist in several charge states (usually in an ionized state and in an electrically neutral state). It will be assumed in the following that each of the N_{M^0} electrically neutral substitutional impurities requires an energy E_M in excess to ionized impurities. In total, the change in free energy of the crystal upon introducing the associated and unassociated intrinsic point defects is given by

$$\begin{aligned} \Delta G &= \sum_{X=V,I} \sum_j \sum_k N_{MX_j^k} \cdot \left(H_{MX_j^k}^f - T \cdot S_{MX_j^k}^f \right) \\ &\quad + \sum_{X=V,I} \sum_i N_{X^i} \cdot \left(H_{X^i}^f - T \cdot S_{X^i}^f \right) \\ &\quad + N_{M^0} \cdot E_M + \Delta G^n + \Delta G^p - T \cdot \Delta S_c \end{aligned} \quad (3.4)$$

As in Section 2.1, ΔG^n and ΔG^p stand for the contributions from electrons in the conduction band and holes in the valence-bond band to the increase in Gibbs free energy, and ΔS_c for the configurational entropy. Charge neutrality demands that the function F defined by

$$\begin{aligned}
F &= V \cdot (n - p) + \sum_{X=V,I} \left(\sum_i z_i \cdot N_{Xi} + \sum_j \sum_k z_k \cdot N_{MX_j^k} \right) \\
&\quad + z_M \cdot \left(N_M - \sum_{X=V,I} \sum_j \sum_k N_{MX_j^k} - N_{M^0} \right) = 0
\end{aligned} \tag{3.5}$$

is zero in equilibrium. V is the volume of the crystal and $V \cdot n$ and $V \cdot p$ are the numbers of electrons and holes in the volume. As before, this auxiliary condition has to be taken into account by the method of Lagrange.

The configurational entropy ΔS_c results via (1.83) from the complexion number Ω , i. e. the number of possible ways in which the defects can be arranged on the respective sites. This requires to take all possible configurations into account. Depending on the particular way the complexion number is derived, slightly different results may be obtained which agree when the site concentration is much larger than the defect concentration.

The most simple pairs are probably pairs of impurities and vacancies since both species occupy only regular lattice sites. Arranging them in the lattice means always that the impurity has to be at one of the N_{MS} sites available for them. Around the impurity, the vacancy may be arranged in a number of geometrically equivalent and distinguishable main orientations for which the parameter $\Theta_{MV_j}^g$ is introduced. For nearest-neighboring vacancy-impurity pairs, as an example, vacancies on the $\Theta_{MV_1}^g = 4$ nearest neighboring sites are geometrically equivalent since they have the same distance of $a_{Si} \cdot \sqrt{3}/4$ from the impurity. The same is true for the $\Theta_{MV_2}^g = 12$ second coordination sites which are all in a distance of $a_{Si}/\sqrt{2}$ from the impurity. The scheme becomes more complicated for sites further apart since already the third coordination sites can be found in two different distances (12 each with $a_{Si} \cdot \sqrt{11}/4$ and $a_{Si} \cdot \sqrt{19}/4$) from the substitutional impurity. In addition to the main orientation, possible structural relaxations about the main orientation as well as electronic degeneracies have to be taken into considerations. They will be summarized as internal degrees of freedom for which the parameter $\Theta_{MX_j^k}^i$ is introduced.

For pairs with self-interstitials, the situation is similarly complex. Pairs of substitutional impurities with adjacent, bound self-interstitials can be treated in analogy to impurity-vacancy pairs. Again, parameters $\Theta_{MI_j}^g$ are introduced to characterize the number of possible geometrically equivalent and distinguishable main configurations of self-interstitials around a substitutional atom. An alternative to such pairs are self-interstitial-impurity pairs arranged in split configurations around a regular lattice site. The number of possible geometrically equivalent configurations for such pairs will depend on the geometry of the split configuration. As an example, Θ_{MI}^g is 6 for the $\langle 001 \rangle$ -oriented split configuration shown in Figure 1.14, and 8 for the $\langle 110 \rangle$ -oriented split configuration shown in Figure 1.15. Impurities on well-defined interstitial sites (bond-centered, hexagonal, tetrahedral, ...) are not considered in the classical theory of impurity-point-defect pairs but can be included in analogy. For them, Θ_{MI}^g is unity for each site and there exist no “further separated” configurations. But it has to be taken into considerations that the numbers of possible sites for such defects may be larger than N_{MS} . In principle, all these configurations may coexist and would have to be taken into considerations with their specific formation energies. However, such a procedure would exceed current process-simulation approaches by far.

Without intrinsic point defects, the number of possible sites N_{MS} for a substitutional impurity is equal to the number of silicon atoms N_{Si} plus the number of substitutional impurities N_M . Vacancies increase the number of sites and self-interstitials decrease them by the respective number of intrinsic point defects, independent of whether they are in pairs or not. An important point, and a distinguished source of apparent differences, is the question by how much the

number of possible sites is reduced due to the introduction of a specific pair. Since all sites for pairs are correlated to the N_{MS} , it will be assumed that each defect MX_j reduces the number of lattice sites available for other pairs by Λ_{MX_j} . Then, the complexion number, i. e. the number of ways to distribute impurity-point defect pairs upon the lattice sites, is given by

$$\Omega_{MX} = \prod_j \prod_k \left(\begin{array}{c} \left(N_{MS} - \sum_{l,l < j} \sum_{m,m < k} \Lambda_{MX_l} \cdot N_{MX_l^m} \right) \\ N_{MX_j^k} \end{array} \right) \cdot \left(\Theta_{MX_j}^g \cdot \Theta_{MX_j}^i \right)^{N_{MX_j^k}}. \quad (3.6)$$

After the pairs have been arranged, the number of sites available for substitutional impurity atoms corresponds to $N'_{MS} = N_{MS} - \sum_{X=I,V} \sum_j \sum_k \Lambda_{MX_j} \cdot N_{MX_j^k}$. Upon them, N_{M^0} electrically neutral and the remaining $N_M - \sum_{X=I,V} \sum_j \sum_k N_{MX_j^k} - N_{M^0}$ ionized impurities are distributed. The respective complexion number is

$$\Omega_M = \begin{pmatrix} N'_{MS} \\ N_{M^0} \end{pmatrix} \cdot \Theta_{M^0}^{N_{M^0}} \cdot \begin{pmatrix} N'_{MS} - N_{M^0} \\ N_M - \sum_{X=V,I} \sum_j \sum_k N_{MX_j^k} - N_{M^0} \end{pmatrix}. \quad (3.7)$$

wherein a Θ_{M^0} times degenerated neutral charge state of the impurities was assumed (see Section 1.2).

The sites remaining after placement of pairs and isolated impurities are partly available for unassociated intrinsic point defects. Partly, because no unassociated intrinsic point defect X may be at one of the Λ_X^{max} sites within the association range of an impurity atom. Thus, the number of available sites is simply $N_{XS} - N_M \cdot \Lambda_X^{max}$ in comparison to N_{XS} in (2.5). It follows that the respective complexion number, i. e. the number of possible ways to arrange the point defects X^i in charge state i upon the respective sites, is given by (2.5) with N_{XS} replaced by the reduced number of sites

$$\Omega_X = \prod_i \left[\begin{pmatrix} N_{XS} - N_M \cdot \Lambda_X^{max} - \sum_{k,k < i} N_{X^k} \\ N_{X^i} \end{pmatrix} \cdot (\Theta_{X^i})^{N_{X^i}} \right]. \quad (3.8)$$

The total number of ways to arrange the various point defects on the respective sites finally results as $\Omega = \Omega_{MV} \cdot \Omega_{MI} \cdot \Omega_M \cdot \Omega_V \cdot \Omega_I$.

In thermal equilibrium, the Gibbs free energy is at a minimum and the numbers of defects N_{Xi} , the number of pairs $N_{MX_j^k}$, and the number of electrically neutral impurities N_{M^0} can be calculated from minimizing $\Delta G + \lambda \cdot F$ with respect to the numbers of interest. The minimum of $\Delta G + \lambda \cdot F$ with respect to the electron concentration results in (2.4) and shows that the Lagrange multiplier is again equal to $\lambda = -E_F$. Similarly, the number of electrically neutral impurities N_{M^0} is obtained in the form

$$N_{M^0} = \frac{N_M - \sum_{X=I,V} \sum_j \sum_k N_{MX_j^k}^{eq}}{1 + \frac{1}{\Theta_{M^0}} \cdot \exp \left(\frac{E_M + z_M \cdot E_F}{k \cdot T} \right)} \quad (3.9)$$

which compares directly to (1.3) and (1.4) with the total concentration of impurities C_T replaced here by the number of unassociated impurity atoms $N_M - \sum_X \sum_j \sum_k N_{MX_j^k}^{eq}$ per unit volume.

Minimization of $\Delta G + \lambda \cdot F$ with respect to the concentrations of unassociated intrinsic defects results in (2.9) with the concentration of sites C_{XS} replaced by $C_{XS} - C_M \cdot \Lambda_X^{max}$. With other words, the equilibrium concentration of unassociated point defects is not a constant, but decreases for high dopant concentrations. Within the methodology of diffusion-reaction equations discussed below, the existence of unassociated point defects is mandatory. For vacancies, as an example, the number of possible sites equals $N_{VS} = N_{Si} - N_M \cdot \Lambda_X^{max}$. Assuming an association range up to the 12 nearest of the 24 third coordination sites (the minimum association range for pair diffusion), the number of vacancy sites is reduced by 28 sites per impurity. An important consequence is that above an impurity concentration of about $2 \cdot 10^{21} \text{ cm}^{-3}$ no sites for unassociated vacancies will remain and all point defects are associated with dopant atoms. Effects attributed to the proximity of impurities were observed experimentally for germanium, tin, arsenic, and antimony already at concentrations around $2 \cdot 10^{20} \text{ cm}^{-3}$ and will be discussed in the respective sections. At this concentration more than 85% of the sites would still be available. So, one might be tempted to assume that the concentration of neutral, free vacancies is nearly unchanged, in comparison to intrinsic conditions, when proximity effects set in. But for a farther-ranging association, the possible sites vanish at even lower concentrations (in the extreme case of a Coulomb-type interaction one can never speak of unassociated point defects in a strict sense). The physical significance of an association of point defects and impurities depends on the type of association. In case of a decreased free energy of formation within the association range, as in Figure 3.1, the total concentration of point defects will increase with increasing impurity concentration. When the association results from a reduced free energy of migration within the association range, as indicated in Figure 3.2, the total number of point defects is independent of the number of dopants, but the effective diffusion coefficient will increase with the dopant concentration.

From the condition of minimal free energy one obtains the equilibrium number of pairs in the form

$$\begin{aligned} N_{MX_j^k}^{eq} &= \Theta_{MX_j}^g \cdot \Theta_{MX_j^k}^i \cdot \left(N_M - \sum_{X=V,I} \sum_j \sum_k N_{MX_j^k}^{eq} - N_{M0} \right) \\ &\cdot \frac{N_{Si} + N_M}{N_{Si}} \cdot \exp \left(- \frac{G_{MX_j^k}^f + E_F \cdot (z_M - z_k)}{k \cdot T} \right) \end{aligned} \quad (3.10)$$

for pairs with vacancies as well as with self-interstitials, despite the differences in the respective complexion numbers. It is a consequence of the already noted assumption that the associated and unassociated numbers of intrinsic point defects are negligible with respect to the number of silicon atoms. Due to their limited solubility, the number of impurities will be significantly smaller than the number of silicon atoms. Consequently, the fraction $(N_{Si} + N_M)/N_{Si}$ is nearly identical to unity and will be omitted in the following. $N_M - \sum_X \sum_j \sum_k N_{MX_j^k}^{eq} - N_{M0}$ represents the number of ionized, unpaired, substitutional impurities. This choice of a reference point is motivated by the usually nearly total ionization of substitutional dopant atoms. Taking, e.g. the neutral substitutional impurity atoms as a reference point would have no effect on the final results. Within the methodology of diffusion-reaction equations described below, the concentration of ionized, unpaired, substitutional impurities will be represented by an own variable. Thus, it is not necessary to resolve the implicit definition of $N_{MX_j^k}^{eq}$ in (3.10). The total concentration $N_{MX^k}^{eq}$ of associated point defects X in charge state k follows from (3.10) as

$$\begin{aligned}
N_{MX^k}^{eq} &= \sum_j N_{MX_j^k}^{eq} \\
&= \left(N_M - \sum_{X \in V, I} \sum_k N_{MX^k}^{eq} - N_{M^0} \right) \cdot \exp \left(-\frac{E_F \cdot (z_M - z_k)}{k \cdot T} \right) \\
&\quad \cdot \sum_j \Theta_{MX_j}^g \cdot \Theta_{MX_j^k}^i \cdot \exp \left(-\frac{G_{MX_j^k}^f}{k \cdot T} \right)
\end{aligned} \tag{3.11}$$

In general, the formation energy will increase with distance from the impurity. Coulombic attraction alone implies that the formation energy of a vacancy in the vicinity of an oppositely charged impurity increases by 0.2 eV when going from a nearest to a second-nearest neighboring site. As a consequence of the increasing formation energy, the total number of associated point defects in a particular charge state will be dominated by pairs on nearest sites. For a first-order estimate, all contributions from farther separated pairs can be ignored and the index j for the configurations is dropped. Keeping the equations general would be straightforward but would neither add to clarity nor would it allow to point out general relationships.

When looking for a reference point, similar to the concentration of neutral point defects (2.10) for the other charge states (2.9), it is clear that only the concentration of pairs C_{MX^M} in charge state M

$$N_{MX^M}^{eq} = \left(N_M - \sum_{X \in V, I} \sum_k N_{MX^k}^{eq} - N_{M^0} \right) \cdot \Theta_{MX}^g \cdot \Theta_{MX^M}^i \cdot \exp \left(-\frac{G_{MX^M}^f}{k \cdot T} \right) \tag{3.12}$$

is largely independent of the Fermi level. The relative concentrations of the other charge states k can then be written in analogy to the relative concentrations of the intrinsic point defects (2.22) to (2.25) in the form

$$\begin{aligned}
\frac{N_{MX^k}}{N_{MX^M}} &= \frac{\Theta_{MX^k}^i}{\Theta_{MX^M}^i} \cdot \exp \left(-\frac{G_{MX^k}^f - G_{MX^M}^f + E_F \cdot (z_M - z_k)}{k \cdot T} \right) \\
&= \delta_{MX^k} \cdot \left(\frac{n}{n_i} \right)^{z_k - z_M}
\end{aligned} \tag{3.13}$$

with δ_{MX^M} being formally identical to unity. For the other charge states, the δ_{MX^k} are

$$\delta_{MX^0} = \frac{\Theta_{MX^0}^i}{\Theta_{MX^-}^i} \cdot \exp \left(-\frac{E_c - E_{MX^-}}{k \cdot T} \right) \cdot \exp \left(\frac{E_g}{2 \cdot k \cdot T} \right) \tag{3.14}$$

$$\delta_{MX^+} = \delta_{MX^+} \frac{\Theta_{MX^+}^i}{\Theta_{MX^-}^i} \cdot \exp \left(-\frac{E_c - E_{MX^-}}{k \cdot T} \right) \cdot \exp \left(\frac{E_{MX^+} - E_v}{k \cdot T} \right) \tag{3.15}$$

for acceptors and

$$\delta_{MX^0} = \frac{\Theta_{MX^0}^i}{\Theta_{MX^+}^i} \cdot \exp \left(-\frac{E_{MX^+} - E_v}{k \cdot T} \right) \cdot \exp \left(\frac{E_g}{2 \cdot k \cdot T} \right) \tag{3.16}$$

$$\delta_{MX^-} = \frac{\Theta_{MX^-}^i}{\Theta_{MX^+}^i} \cdot \exp \left(-\frac{E_{MX^+} - E_v}{k \cdot T} \right) \cdot \exp \left(\frac{E_c - E_{MX^-}}{k \cdot T} \right) \tag{3.17}$$

for donors.

The relation (3.13) is clearly not restricted to equilibrium situations but describes the relative concentrations of charged pairs under the condition that steady state between the charge states is established. As in Section 2.1, Boltzmann statistics were introduced to characterize the position of the Fermi level via the electron concentration.

As an alternative to (3.11), the number of point defects MX^k in charge state k can be expressed in terms of the binding energy (3.3) and the number of unassociated point defects via (2.9) in the form

$$\begin{aligned} N_{\text{MX}^k}^{eq} &= \frac{N_X^{eq}}{N_{XS} - N_M \cdot \Lambda_X^{max}} \cdot \left(N_M - \sum_{X=V,I} \sum_k N_{\text{MX}^k}^{eq} - N_{M^0} \right) \\ &\quad \cdot \frac{\Theta_{MX}^g \cdot \Theta_{\text{MX}^k}^i}{\Theta_{X^{k-M}}} \exp \left(\frac{G_{\text{MX}^k}^B}{k \cdot T} \right), \end{aligned} \quad (3.18)$$

independent of the Fermi level. With the help of (2.22) to (2.25) and (3.13), the total concentration of pairs MX in equilibrium can be written as

$$\begin{aligned} N_{\text{MX}}^{eq} &= \sum_k N_{\text{MX}^k}^{eq} \\ &= \frac{N_X^{eq}}{N_{XS} - N_M \cdot \Lambda_X^{max}} \cdot \left(N_M - \sum_{X=V,I} N_{\text{MX}}^{eq} - N_{M^0} \right) \\ &\quad \cdot \frac{\sum_k \delta_{\text{MX}^k} \cdot \left(\frac{n}{n_i} \right)^{z_k}}{\sum_j \delta_{X^j} \cdot \left(\frac{n}{n_i} \right)^{z_j}} \cdot \frac{\Theta_{MX}^g \cdot \Theta_{\text{MX}^M}^i}{\Theta_{X^0}} \cdot \left(\frac{n}{n_i} \right)^{-z_M} \cdot \exp \left(\frac{G_{\text{MX}^M}^B}{k \cdot T} \right). \end{aligned} \quad (3.19)$$

Considering a situation in which the number of point defects X is not free to assume its value under equilibrium conditions but in which a total number N_X^{tot} is given. Then, N_{MX}^{eq} and N_X^{eq} in (3.19) are replaced by N_{MX} and $N_X^{tot} - N_{\text{MX}}$, respectively.

3.3 Diffusion of Substitutional Impurities via Mobile Complexes with Intrinsic Point Defects

From statistical thermodynamics, only information about numbers and concentrations of species in equilibrium can be obtained. For a description of the influence of pair formation or formation of mobile impurity-point-defect complexes in general on the redistribution of impurities and intrinsic point defects, kinetic approaches have to be used. The application of diffusion-reaction-equation schemes goes back to the work of Yoshida et al. [3.49]. The basics of this methodology were discussed in Section 1.5.4.

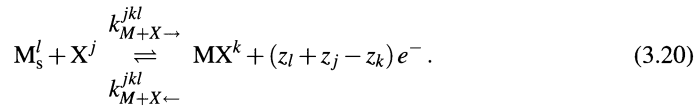
Mobile impurity-point-defect pairs may form via two different mechanisms. The first one is the direct formation of pairs by the reaction of a substitutional impurity with an intrinsic point defect. Alternatively, impurity-vacancy pairs or impurity-self-interstitial pairs may form by leaving respectively a self-interstitial or a vacancy behind. Based on these mechanisms, continuity equations for all point defects involved are developed in Section 3.3.1. Problems with assigning boundary conditions for mobile pairs are summarized in Section 3.3.1. An important point for the application to process simulation and for an estimation of the global system

behavior are suitable simplifications. A thorough discussion of such issues can be found in Section 3.3.3. Finally, as outlined in Section 3.3.4, direct and indirect formation of pairs forms a parallel path to bulk recombination.

3.3.1 Formation and Diffusion of Mobile Complexes

In general, diffusion theories assume reactions of unassociated, substitutional impurity atoms M_s with intrinsic point defects (vacancies V and self-interstitials I) to mobile complexes MX (MV and MI, respectively). Complexes with vacancies will be pairs as outlined above while complexes with self-interstitials may be pairs, split interstitials, or impurity interstitials. The important point is that the mobile complexes have to be able to perform a random walk before the complex dissociates again into a substitutional impurity atom and the respective point defect.

All these point defects may exist in more than one charge state. For the sake of consistency with Sections 2.1 and 3.2.2, the symbols j and k will be used for the charge states of the intrinsic point defects and the pairs, respectively. For the charge states of the substitutional impurities, the symbol l will be used. The corresponding numbers of electron charges are z_j , z_k , and z_l , and the respective concentrations will be denoted by C_{X^j} , C_{MX^k} , and $C_{M_s^l}$. Each of the reactions between them can be written in the form



It should be noted that several mobile complexes of impurities and self-interstitials may exist in parallel. An example would be bound impurity-self-interstitial complexes and impurity interstitials. An extension of the procedure to include such competing reactions is straightforward but was omitted because it would just increase the complexity of the equations without giving significantly more insight. The symbol e^- on the right-hand side of (3.20) stands for the electrons remaining from the reaction. In general, only two charge states (neutral and ionized) will exist for dopants.

The total number of impurities N_M , per unit volume, corresponds to the sum of the concentrations of these charge states plus the concentrations of the impurities in the complexes

$$C_M = \sum_l C_{M_s^l} + \sum_{X=V,I} \sum_k C_{MX^k} . \quad (3.21)$$

Based on the formalism of diffusion-reaction equations outlined in Section 1.5.4, the continuity equations result nearly automatically from (3.20). However, the resulting equations are rather complex and unwieldy. To make the structure of the equations clear, a system with only neutral defects will be considered in parallel whenever appropriate.

Some researchers, especially Richardson and Mulvaney [3.50], presented systems of equations in which reactions of point defects and charge carriers are accounted for by individual continuity equations for the various charge states. But, as argued in Section 1.5.3, charge states can be assumed to be in steady state on a time scale much shorter than those of the other phenomena involved. The relative concentrations of the charged intrinsic point defects and of the mobile complexes are then given by (2.22) to (2.25) and (3.13), respectively. For the substitutional impurities, a similar relationship can be obtained from a generalization of (3.9) in the form

$$\frac{C_{M_s^l}}{C_{M_s^M}} = \delta_{M_s^l} \cdot \left(\frac{n}{n_i} \right)^{z_l - z_M} . \quad (3.22)$$

For all species, the concentration of a specific charge state can be written in terms of the total concentrations as

$$\frac{C_{M_s^l}}{C_{M_s}} = \frac{\delta_{M_s^l} \cdot \left(\frac{n}{n_i}\right)^{z_l}}{\sum_l \delta_{M_s^l} \cdot \left(\frac{n}{n_i}\right)^{z_l}}, \quad \frac{C_{X^j}}{C_X} = \frac{\delta_{X^j} \cdot \left(\frac{n}{n_i}\right)^{z_j}}{\sum_j \delta_{X^j} \cdot \left(\frac{n}{n_i}\right)^{z_j}}, \quad \frac{C_{MX^k}}{C_{MX}} = \frac{\delta_{MX^k} \cdot \left(\frac{n}{n_i}\right)^{z_k}}{\sum_k \delta_{MX^k} \cdot \left(\frac{n}{n_i}\right)^{z_k}} \quad (3.23)$$

with $\delta_{M_s^M}$, δ_{X^0} , and δ_{MX^M} being formally identical to unity.

Combining the continuity equations for the various charge states, the continuity equation for the total concentration $C_{M_s} = \sum_l C_{M_s^l}$ results in

$$\frac{\partial C_{M_s}}{\partial t} = R_{M+V} + R_{M+I} + \text{div} (D_M^{CE} \cdot \text{grad} C_{M_s}). \quad (3.24)$$

The last term on the right-hand side accounts for diffusion via direct exchange or, more likely, concerted exchange.

For a system with neutral defects only, the rates R_{M+X} are given by

$$R_{M+X} = k_{M+X \leftarrow} \cdot C_{MX} - k_{M+X \rightarrow} \cdot C_X \cdot C_{M_s}. \quad (3.25)$$

Taking all charge states into account, the rates take the considerably more complicated form

$$\begin{aligned} R_{M+X} &= \frac{C_{MX}}{\sum_k \delta_{MX^k} \cdot \left(\frac{n}{n_i}\right)^{z_k}} \cdot \sum_{j,k,l} k_{M+X \leftarrow}^{jkl} \cdot \delta_{MX^k} \cdot \frac{n^{z_j+z_l}}{n_i^{z_k}} \\ &\quad - \frac{C_X}{\sum_j \delta_{X^j} \cdot \left(\frac{n}{n_i}\right)^{z_j}} \cdot \frac{C_{M_s}}{\sum_l \delta_{M_s^l} \cdot \left(\frac{n}{n_i}\right)^{z_l}} \cdot \sum_{j,k,l} k_{M+X \rightarrow}^{jkl} \cdot \delta_{X^j} \cdot \delta_{M_s^l} \cdot \left(\frac{n}{n_i}\right)^{z_j+z_l} \end{aligned} \quad (3.26)$$

with X standing for vacancies V or self-interstitials I. It has to be mentioned here that the reaction constants are related to each other by

$$\frac{k_{M+X \rightarrow}^{jkl}}{k_{M+X \leftarrow}^{jkl}} = \frac{k_{M+X \rightarrow}^{0MM}}{k_{M+X \leftarrow}^{0MM}} \cdot \frac{\delta_{MX^k}}{\delta_{M_s^l} \cdot \delta_{X^j}} \cdot n_i^{z_j-z_k+z_l} \quad (3.27)$$

since, in equilibrium, all individual reactions (3.20) have to be in balance. As a consequence, (3.26) can be written in the form

$$\begin{aligned} R_{M+X} &= \left(\frac{C_{MX}}{\sum_k \delta_{MX^k} \cdot \left(\frac{n}{n_i}\right)^{z_k}} \cdot \frac{k_{M+X \leftarrow}^{0MM}}{k_{M+X \rightarrow}^{0MM}} - \frac{C_X}{\sum_j \delta_{X^j} \cdot \left(\frac{n}{n_i}\right)^{z_j}} \cdot \frac{C_{M_s}}{\sum_l \delta_{M_s^l} \cdot \left(\frac{n}{n_i}\right)^{z_l}} \right) \\ &\quad \cdot \sum_{j,k,l} k_{M+X \rightarrow}^{jkl} \cdot \delta_{X^j} \cdot \delta_{M_s^l} \cdot \left(\frac{n}{n_i}\right)^{z_j+z_l} \end{aligned} \quad (3.28)$$

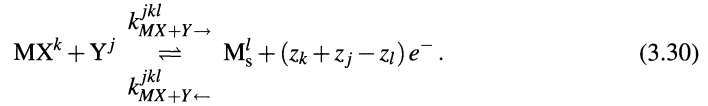
In equilibrium, the reaction rate has to vanish and the concentration of pairs obtained from (3.28) can be compared to the expression (3.19) obtained from thermodynamics. Taking into account that $N_M - \sum N_{MX} - N_{M^0}$ therein corresponds to the number of substitutional, ionized

metal ions, the ratio of the reaction constants can be expressed in terms of the pair-binding energies as

$$\frac{k_{M+X \rightarrow}^{0MM}}{k_{M+X \leftarrow}^{0MM}} = \frac{\Theta_{MX}^g \cdot \Theta_{MX^M}^i}{\Theta_{X^0}} \cdot \frac{1}{C_{XS} - C_M \cdot \Lambda_X^{max}} \cdot \exp \left(\frac{G_{MX^M}^B}{k \cdot T} \right). \quad (3.29)$$

This result compares directly to (1.160) and (1.133) when one considers that the number of sites for pairs and substitutional impurities are equal here and that the ionized impurity state is non-degenerate.

Additional terms have to be included when reactions between dopant-vacancy pairs and self-interstitials or dopant-self-interstitial complexes and vacancies are taken into consideration. In a generalized form, reactions between mobile complexes MX in charge state k with intrinsic point defects Y (Y has to be I when X is V, and *vice versa*) in charge state i to substitutional impurities M_s in charge state l can be written as



Including these reactions in the continuity equation for the total concentration, (3.24) can be written in the form

$$\frac{\partial C_{M_s}}{\partial t} = R_{M+V} + R_{M+I} + R_{MI+V} + R_{MV+I} + \text{div} (D_M^{CE} \cdot \text{grad} C_{M_s}). \quad (3.31)$$

For a system of neutral defects only, the additional reaction rates R_{MX+Y} are given by

$$R_{MX+Y} = k_{MX+Y \rightarrow} \cdot C_{MX} \cdot C_Y - k_{MX+Y \leftarrow} \cdot C_{M_s}. \quad (3.32)$$

Including all the charge states, the rates take the considerably more complicated form

$$\begin{aligned} R_{MX+Y} &= \frac{C_{MX}}{\sum_k \delta_{MX^k} \cdot \left(\frac{n}{n_i}\right)^{z_k}} \cdot \frac{C_Y}{\sum_j \delta_{Y^j} \cdot \left(\frac{n}{n_i}\right)^{z_j}} \cdot \sum_{j,k,l} k_{MX+Y \rightarrow}^{jkl} \cdot \delta_{MX^k} \cdot \delta_{Y^j} \cdot \left(\frac{n}{n_i}\right)^{z_k+z_j} \\ &\quad - \frac{C_{M_s}}{\sum_l \delta_{M_s^l} \cdot \left(\frac{n}{n_i}\right)^{z_l}} \cdot \sum_{j,k,l} k_{MX+Y \leftarrow}^{jkl} \cdot \delta_{M_s^l} \cdot \frac{n^{z_k+z_j}}{n_i^{z_l}} \end{aligned} \quad (3.33)$$

with Y standing for I when X is replaced by V and *vice versa*. As above, it has to be mentioned that the reaction constants are related to each other by

$$\frac{k_{MX+Y \rightarrow}^{jkl}}{k_{MX+Y \leftarrow}^{jkl}} = \frac{k_{MX+Y \rightarrow}^{0MM}}{k_{MX+Y \leftarrow}^{0MM}} \cdot \frac{\delta_{M_s^l}}{\delta_{Y^j} \cdot \delta_{MX^k}} \cdot n_i^{z_j+z_k-z_l} \quad (3.34)$$

since, in equilibrium, all individual reactions (3.30) have to be in balance. In addition, since the condition holds for both sets of reactions (3.20) and (3.30), their reaction constants have to obey the condition

$$\frac{k_{M+X \rightarrow}^{0MM}}{k_{M+X \leftarrow}^{0MM}} \cdot \frac{k_{MX+Y \rightarrow}^{0MM}}{k_{MX+Y \leftarrow}^{0MM}} \cdot \frac{C_X^{eq}}{\sum_j \delta_{X^j} \cdot \left(\frac{n}{n_i}\right)^{z_j}} \cdot \frac{C_Y^{eq}}{\sum_j \delta_{Y^j} \cdot \left(\frac{n}{n_i}\right)^{z_j}} = 1. \quad (3.35)$$

As a consequence, (3.33) can be written alternatively in the form

$$\begin{aligned}
 R_{MX+Y} = & \left(\frac{C_{MX}}{\sum_k \delta_{MX^k} \cdot \left(\frac{n}{n_i}\right)^{z_k}} \cdot \frac{C_Y}{\sum_j \delta_{Y^j} \cdot \left(\frac{n}{n_i}\right)^{z_j}} \right. \\
 & - \frac{C_{M_s}}{\sum_l \delta_{M_s^l} \cdot \left(\frac{n}{n_i}\right)^{z_l}} \cdot \frac{k_{M+X \rightarrow}^{0MM}}{k_{M+X \leftarrow}^{0MM}} \cdot \frac{C_X^{eq}}{\sum_j \delta_{X^j} \cdot \left(\frac{n}{n_i}\right)^{z_j}} \cdot \frac{C_Y^{eq}}{\sum_j \delta_{Y^j} \cdot \left(\frac{n}{n_i}\right)^{z_j}} \\
 & \left. \cdot \sum_{j,k,l} k_{MX+Y \rightarrow}^{jkl} \cdot \delta_{MX^k} \cdot \delta_{Y^j} \cdot \left(\frac{n}{n_i}\right)^{z_k+z_j} \right) \\
 & \cdot \sum_{j,k,l} k_{MX+Y \rightarrow}^{jkl} \cdot \delta_{MX^k} \cdot \delta_{Y^j} \cdot \left(\frac{n}{n_i}\right)^{z_k+z_j}. \tag{3.36}
 \end{aligned}$$

In the continuity equations for the total concentrations of mobile complexes MX, their diffusion has to be taken into consideration, in addition to recombination. Expressed in terms of the individual concentrations of mobile complexes, the continuity equations take the form

$$\begin{aligned}
 \frac{\partial C_{MX}}{\partial t} = & \text{div} \left(\sum_k D_{MX^k} \cdot \text{grad} C_{MX^k} - z_k \cdot D_{MX^k} \cdot C_{MX^k} \cdot \text{grad} (\psi/U_T) \right) \\
 & - R_{M+X} - R_{MX+Y} \tag{3.37}
 \end{aligned}$$

which can be rewritten via (3.13) as a function of the gradient of the total concentration of mobile complexes

$$\begin{aligned}
 \frac{\partial C_{MX}}{\partial t} = & \text{div} \left(\sum_k \left(\delta_{MX^k} \cdot D_{MX^k} \cdot \left(\frac{n}{n_i}\right)^{z_k} \right) \cdot \text{grad} \left(\frac{C_{MX}}{\sum_k \delta_{MX^k} \cdot \left(\frac{n}{n_i}\right)^{z_k}} \right) \right) \\
 & - R_{M+X} - R_{MX+Y} \tag{3.38}
 \end{aligned}$$

It should be noted that the gradient of the factor $C_{MX} / \sum_k \delta_{MX^k} \cdot (n/n_i)^{z_k}$ can, as in (2.53) for the intrinsic point defects, be split into a concentration gradient and a gradient of the electrostatic potential with an effective charge state.

In addition to the reactions between substitutional impurities, intrinsic point defects, and mobile complexes (3.20) and (3.30), bulk recombination of the intrinsic point defects and their reactions with extended defects have to be taken into account. Introducing the effective point-defect diffusion coefficient via (2.54), the effective charge state via (2.55), bulk recombination in the form (2.74), and reactions with sinks from (2.92) leads to continuity equations for the total concentrations of the intrinsic point defects $C_X = \sum_j C_{X^j}$

$$\begin{aligned}
 \frac{\partial C_V}{\partial t} = & \text{div} (D_V \cdot (\text{grad} C_V - z_V \cdot C_V \cdot \text{grad} (\psi/U_T))) + R_{M+V} - R_{MI+V} \\
 & - k_{BV} \cdot (C_V - C_V^*) - k_B \cdot (C_I \cdot C_V - C_I^{eq} \cdot C_V^{eq}), \tag{3.39}
 \end{aligned}$$

$$\begin{aligned}
 \frac{\partial C_I}{\partial t} = & \text{div} (D_I \cdot (\text{grad} C_I - z_I \cdot C_I \cdot \text{grad} (\psi/U_T))) + R_{M+I} - R_{MV+I} \\
 & - k_{BI} \cdot (C_I - C_I^*) - k_B \cdot (C_I \cdot C_V - C_I^{eq} \cdot C_V^{eq}). \tag{3.40}
 \end{aligned}$$

When several impurity species are present, a term $R_{M+X} - R_{MY+X}$ has to be added to the continuity equations for the vacancies and self-interstitials for each of them.

Each dopant introduces three equations, one for the substitutional impurities (3.24) and two for the mobile complexes with self-interstitials and vacancies (3.38). With the two additional equations for the intrinsic point defects (3.39) and (3.40), the model consists of five equations for one dopant and is commonly referred to as “five-stream model.” To reduce the computational efforts, various additional simplifying assumptions are generally made. They will be discussed in Section 3.3.3.

3.3.2 Boundary Conditions for Mobile Impurity Complexes

It is evident that boundary conditions are required for a numerical solution of the continuity equations (3.38) for the mobile impurity complexes. However, a physically consistent definition of such boundary conditions is far from being trivial and depends on the type of the defect. To illustrate this point, let us consider possible scenarios of the interaction of mobile impurity complexes with surfaces and interfaces.

Interstitial impurity atoms, as the most simple example, will segregate either to the interface, into the adjacent layer, or remain in the silicon layer. The probabilities for these processes result from thermodynamics as discussed in Section 1.6 and, depending on the level of complexity, any of the segregation models discussed therein is applicable.

For impurity-point-defect pairs, on the other hand, no equivalent defect will usually exist in the other phase. When a vacancy-impurity pair or a self-interstitial-impurity pair approaches the interface to an adjacent layer, it may well be that the impurity reaches the interface where it may assume an energetically favored position or segregate to the adjacent bulk phase. The point defect accompanying it is likely to recombine individually at one of the kinks at the interface. Alternatively, it may remain in the silicon or, in the case of a self-interstitial, segregate as silicon atom into the adjacent phase. On the other hand, one has to keep in mind that pair diffusion requires a partial dissociation of the intrinsic point defect from the impurity. Thus, near interfaces, the probability increases that the partially dissociated intrinsic point defect goes to a kink at the interface and recombines there individually or, in the case of a self-interstitial, segregates as silicon atom into the adjacent phase. The impurity would then be trapped on a substitutional site near the surface and it has to be mentioned that there are indeed indications that such a process is operative and important for the simulation of ultrashallow junction formation. While such processes are no problem for atomistic simulations, they were probably never consistently implemented in continuum approaches. The currently predominating approach is to apply standard boundary conditions like Dirichlet or Neumann boundary conditions, or segregation models also for pairs.

3.3.3 Simplifications

Pair-diffusion theories as derived in the previous section are quite complex. For the understanding of the global system behavior as well as for the extraction of parameters from experiments, simpler forms are highly desired. They can be achieved under certain limiting assumptions which have to be justified on a case-to-case basis. In the following, the most usual ones are discussed.

Negligible Concentration of Neutral Impurities

An implicit assumption of nearly all published models is that the concentration of electrically neutral substitutional impurities is negligible with respect to the concentration of the ionized ones. Then, with $\delta_{M'_s} = 0$ for $l \neq M$, $k_{M+X \rightarrow}^{jkl} = 0$ for $l \neq M$, and $k_{MX+Y \rightarrow}^{jkl} = 0$ for $l \neq M$, (3.26) and (3.33) reduce to

$$R_{M+X} = \left(\frac{C_{MX}}{\sum_k \delta_{MX^k} \cdot \left(\frac{n}{n_i}\right)^{z_k}} \cdot \frac{k_{M+X \leftarrow}^{0MM}}{k_{M+X \rightarrow}^{0MM}} - \frac{C_X}{\sum_j \delta_{X^j} \cdot \left(\frac{n}{n_i}\right)^{z_j}} \cdot C_{M_s} \cdot \left(\frac{n}{n_i}\right)^{-z_M} \right) \cdot \sum_{j,k} k_{M+X \rightarrow}^{jKM} \cdot \delta_{X^j} \cdot \left(\frac{n}{n_i}\right)^{z_j+z_l} \quad (3.41)$$

$$R_{MX+Y} = \left(\frac{C_{MX}}{\sum_k \delta_{MX^k} \cdot \left(\frac{n}{n_i}\right)^{z_k}} \cdot \frac{C_Y}{\sum_j \delta_{Y^j} \cdot \left(\frac{n}{n_i}\right)^{z_j}} - C_{M_s} \cdot \left(\frac{n}{n_i}\right)^{-z_M} \cdot \frac{k_{M+X \rightarrow}^{0MM}}{k_{M+X \leftarrow}^{0MM}} \cdot \frac{C_X^{eq}}{\sum_j \delta_{X^j} \cdot \left(\frac{n}{n_i}\right)^{z_j}} \cdot \frac{C_Y^{eq}}{\sum_j \delta_{Y^j} \cdot \left(\frac{n}{n_i}\right)^{z_j}} \right) \cdot \sum_{j,k} k_{MX+Y \rightarrow}^{jKM} \cdot \delta_{MX^k} \cdot \delta_{Y^j} \cdot \left(\frac{n}{n_i}\right)^{z_k+z_j} \quad (3.42)$$

The assumption is well justified for shallow dopants being present in low concentrations but fails potentially in the high-concentration regime. But there, the application of Boltzmann statistics is questionable, too.

Steady State between Pairs and Intrinsic Point Defects

For a further reduction it can be assumed that formation and dissociation of mobile complexes occurs on a much faster time scale than redistribution by diffusion. This is motivated by the usually much higher diffusion coefficients of pairs in comparison to the effective diffusivity associated with the total concentration. Rewriting (3.38) in the form

$$\frac{\partial C_{MX}}{\partial t} = \text{div}(\dots) - \frac{C_{MX}}{\tau_{MX}} + \dots, \quad (3.43)$$

the time constant τ_{MX} characteristic for formation and dissolution of mobile complexes MX can be extracted from the reaction terms depending linearly on C_{MX} . It follows as

$$\begin{aligned} \frac{1}{\tau_{MX}} &= \frac{1}{\sum_k \delta_{MX^k} \cdot \left(\frac{n}{n_i}\right)^{z_k}} \cdot \frac{k_{M+X \leftarrow}^{0MM}}{k_{M+X \rightarrow}^{0MM}} \cdot \sum_{j,k} k_{M+X \rightarrow}^{jKM} \cdot \delta_{X^j} \cdot \left(\frac{n}{n_i}\right)^{z_j+z_l} \\ &+ \frac{1}{\sum_k \delta_{MX^k} \cdot \left(\frac{n}{n_i}\right)^{z_k}} \cdot \frac{C_Y}{\sum_j \delta_{Y^j} \cdot \left(\frac{n}{n_i}\right)^{z_j}} \sum_{j,k} k_{MX+Y \rightarrow}^{jKM} \cdot \delta_{MX^k} \cdot \delta_{Y^j} \cdot \left(\frac{n}{n_i}\right)^{z_k+z_j}. \end{aligned} \quad (3.44)$$

Good approximations, as discussed already in Section 1.5.4, can be expected only for times $t \gg \tau_{MX}$. However, this criterion is not rigorous since we have to keep in mind that there is the formation of mobile complexes with vacancies as well as with self-interstitials to be considered each of which is governed by a different time constant. When both mechanisms contribute in a considerable way, good approximations can be expected only for times exceeding the longer time constant of the two. On the other hand, when one of the two mechanisms is ineffective, good approximations can be expected for times exceeding the time constant of the effective mechanism irrespective of whether this is the longer time constant or not.

In steady state, the concentration of mobile complexes C_{MX} can be written in the form

$$\frac{C_{MX}}{\sum_k \delta_{MX^k} \cdot \left(\frac{n}{n_i}\right)^{z_k}} = \vartheta_{MX} \cdot C_{M_s} \cdot \left(\frac{n}{n_i}\right)^{-z_M} \cdot \frac{C_X/C_X^{eq} + \alpha_{MX}}{1 + \alpha_{MX} \cdot C_Y/C_Y^{eq}} \quad (3.45)$$

with ϑ_{MX} introduced as abbreviation for

$$\vartheta_{MX} = \frac{k_{M+X \rightarrow}^{0MM}}{k_{M+X \leftarrow}^{0MM}} \cdot C_{X^0}^{eq}. \quad (3.46)$$

The partition constant

$$\alpha_{MX} = \frac{k_{M+X \rightarrow}^{0MM}}{k_{M+X \leftarrow}^{0MM}} \cdot C_{Y^0}^{eq} \cdot \frac{\sum_{j,k} k_{MX+Y \rightarrow}^{jkM} \cdot \delta_{MX^k} \cdot \delta_{Y^j} \cdot \left(\frac{n}{n_i}\right)^{z_k+z_j}}{\sum_{j,k} k_{M+X \leftarrow}^{jkM} \cdot \delta_{X^j} \cdot \left(\frac{n}{n_i}\right)^{z_j+z_l}} \quad (3.47)$$

was introduced in analogy to [3.51] as a Fermi-level-dependent measure of the extent to which the formation of mobile complexes occurs via the direct reactions of substitutional impurities with intrinsic point defects (3.20) or via the simultaneous formation of a mobile impurity complex and an intrinsic point defect (3.30). The case $\alpha_{MX} = 0$ corresponds to a situation in which only direct reactions of substitutional impurities are effective while $\alpha_{MX} = \infty$ refers to situations in which the simultaneous formations of mobile impurity complexes and intrinsic point defects is the only important mechanism.

Adding the continuity equations for the substitutional impurities (3.24) and the mobile complexes (3.38) one obtains a continuity equation for the total concentration $C_M = C_{M_s} + C_{MV} + C_{MI}$

$$\begin{aligned} \frac{\partial C_M}{\partial t} &= \sum_{\{X,Y\}} \text{div} \left(\vartheta_{MX} \cdot \sum_k \delta_{MX^k} \cdot D_{MX^k} \cdot \left(\frac{n}{n_i}\right)^{z_k} \right. \\ &\quad \cdot \text{grad} \left(C_{M_s} \cdot \frac{C_X/C_X^{eq} + \alpha_{MX}}{1 + \alpha_{MX} \cdot C_Y/C_Y^{eq}} \cdot \left(\frac{n}{n_i}\right)^{-z_M} \right) \Big) \\ &\quad + \text{div} (D_M^{CE} \cdot \text{grad} C_{M_s}) \end{aligned} \quad (3.48)$$

with $\{X,Y\}$ standing for the combinations $X = V, Y = I$ and $X = I, Y = V$. The concentration of substitutional atoms C_{M_s} appearing in (3.48) is related to the total concentration C_M via

$$C_M = C_{M_s} \cdot \left(1 + \sum_{\{X,Y\}} \vartheta_{MX} \cdot \frac{C_X/C_X^{eq} + \alpha_{MX}}{1 + \alpha_{MX} \cdot C_Y/C_Y^{eq}} \cdot \sum_k \delta_{MX^k} \cdot \left(\frac{n}{n_i}\right)^{z_k-z_M} \right) \quad (3.49)$$

so that an effective diffusion coefficient can be defined as

$$D_M = \frac{\sum_{\{X,Y\}} \vartheta_{MX} \cdot \frac{C_X/C_X^{eq} + \alpha_{MX}}{1 + \alpha_{MX} \cdot C_Y/C_Y^{eq}} \cdot \sum_k \delta_{MX^k} \cdot D_{MX^k} \cdot \left(\frac{n}{n_i}\right)^{z_k - z_M}}{1 + \sum_{\{X,Y\}} \vartheta_{MX} \cdot \frac{C_X/C_X^{eq} + \alpha_{MX}}{1 + \alpha_{MX} \cdot C_Y/C_Y^{eq}} \cdot \sum_k \delta_{MX^k} \cdot \left(\frac{n}{n_i}\right)^{z_k - z_M}} + D_M^{CE}. \quad (3.50)$$

Negligible Concentrations of Pairs

For some dopants like boron and phosphorus it is known that the concentrations of pairs in thermal equilibrium are much lower than the concentration of impurities on substitutional sites. As a consequence, the concentration of substitutional impurities C_{Ms} can be replaced in (3.48) by the total concentration of impurities C_M . In addition, the denominator in (3.50) becomes unity. The effective diffusion coefficient appears then as a linear combination of contributions from diffusion via complexes with vacancies and self-interstitials.

$$D_M = \sum_{\{X,Y\}} \vartheta_{MX} \cdot \frac{C_X/C_X^{eq} + \alpha_{MX}}{1 + \alpha_{MX} \cdot C_Y/C_Y^{eq}} \cdot \sum_k \delta_{MX^k} \cdot D_{MX^k} \cdot \left(\frac{n}{n_i}\right)^{z_k - z_M} + D_M^{CE}. \quad (3.51)$$

Discussion of Special Cases

Pair diffusion models assume in general only the formation of mobile pairs via the direct reactions (3.20). α_{MI} and α_{MV} then become zero and the terms

$$\frac{C_X/C_X^{eq} + \alpha_{MX}}{1 + \alpha_{MX} \cdot C_Y/C_Y^{eq}} = \frac{C_X}{C_X^{eq}} \quad (3.52)$$

assume a simple form which corresponds to the oversaturation of the respective point defects. The resulting diffusion equations will be discussed in detail in Section 3.4. The same simple form, as pointed out already by Marioton et al. [3.52] and Cowern [3.51], results from the assumption of steady state $C_I \cdot C_V = C_I^{eq} \cdot C_V^{eq}$ between the intrinsic point defects. In the general case, however, the concentration of pairs MX and with it the effective diffusion coefficient via such pairs will depend on the concentrations of both vacancies and self-interstitials. They were discussed in detail by Cowern [3.51] and the discussion below follows largely his arguments.

In cases where self-interstitials or vacancies are introduced into the crystal by chemical reactions like oxidation or nitridation of surfaces, or by the growth of precipitates in the bulk, steady state between the intrinsic point defects will be established by bulk recombination. When the intrinsic point defect in supersaturation is denoted by X, the oversaturation of the other intrinsic point defects Y can be expected between $C_X^{eq}/C_X \leq C_Y/C_Y^{eq} \leq 1$. The first of the two limiting cases leads, as discussed above, to (3.52). The second one, $C_Y/C_Y^{eq} = 1$, results in

$$\frac{C_X/C_X^{eq} + \alpha_{MX}}{1 + \alpha_{MX} \cdot C_Y/C_Y^{eq}} = \frac{C_X/C_X^{eq}}{1 + \alpha_{MX}} + \frac{\alpha_{MX}}{1 + \alpha_{MX}} \quad (3.53)$$

which has a term which is, by a factor $1/(1 + \alpha_{MX})$, smaller than the oversaturation C_X/C_X^{eq} , and a term between 0 and 1 which is independent of the concentrations of the intrinsic point defects.

In some cases like during irradiation at elevated temperatures, or after ion implantation, the concentrations of both self-interstitials and vacancies may be present in a high supersaturation. In this case, when $C_X/C_X^{eq} \gg \alpha_{MX}$ and $C_Y/C_Y^{eq} \gg 1/\alpha_{MX}$, the terms

$$\frac{C_X/C_X^{eq} + \alpha_{MX}}{1 + \alpha_{MX} \cdot C_Y/C_Y^{eq}} = \frac{1}{\alpha_{MX}} \cdot \frac{C_X/C_X^{eq}}{C_Y/C_Y^{eq}} \quad (3.54)$$

depend on the ratio of the oversaturations of the intrinsic point defects.

3.3.4 Indirect Recombination of Intrinsic Point Defects in Steady State

Inserting the concentration of mobile impurity pairs in steady state (3.45) into the reaction rates (3.41) and (3.42) leads to

$$R_{M+X} = -R_{MX+Y} = \frac{k_{M+X \rightarrow}^{0MM} \cdot C_I^{eq} \cdot C_V^{eq} \cdot \sum_{j,k} k_{MX+Y \rightarrow}^{jKM} \cdot \delta_{MX^k} \cdot \delta_{Y^j} \cdot \left(\frac{n}{n_i}\right)^{z_k+z_j}}{k_{M+X \leftarrow}^{0MM} \cdot 1 + \alpha_{MX} \cdot C_Y / C_Y^{eq}} \cdot C_{M_s} \cdot \left(\frac{n}{n_i}\right)^{-z_M} \cdot \left(1 - \frac{C_I}{C_I^{eq}} \cdot \frac{C_V}{C_V^{eq}}\right)}. \quad (3.55)$$

The resulting reaction rates which appear as $R_{M+V} - R_{MI+V}$ and $R_{M+I} - R_{MV+I}$ in the continuity equations (3.39) and (3.40) of the intrinsic point defects are equal and proportional to $C_I^{eq} \cdot C_V^{eq} - C_I \cdot C_V$. As a consequence, as already suggested by Loualiche et al. [3.53] and Mathiot and Pfister [3.54], the reactions $M_s + X \rightleftharpoons MX$, $MX + Y \rightleftharpoons M_s$ can be seen to form an alternative path for bulk recombination. The indirect-bulk-recombination constant which can be defined in analogy to (2.74) is proportional to the concentration of substitutional impurities and depends in the general case ($\alpha_{MX} \neq 0$) also on the concentrations of the intrinsic point defects.

3.4 Pair-Diffusion Models

Most diffusion theories assume that mobile pairs of substitutional impurities and intrinsic point defects form exclusively by the direct reactions (3.20). These diffusion theories are summarized under the term pair-diffusion models although the microscopic form of the mobile impurity-self-interstitial complex is unimportant and may be an impurity interstitial as well as a real pair of a substitutional impurity atom and a self-interstitial.

Based on the results of Section 3.3, the diffusion equations resulting from pair-diffusion models are derived in Section 3.4.1. One of the most important parameters, the diffusion coefficient under intrinsic and inert conditions, is discussed in Section 3.4.2 together with possible problems for its experimental determination. A second main parameter is the fractional diffusivity via self-interstitials. Methods for its determination from experiments are outlined in Section 3.4.3. At extrinsic concentrations, various effects are expected. Among them are the effects from electric fields explained in Section 3.4.4. Methods for the estimation of diffusion coefficients from extrinsic diffusion profiles and via isoconcentration experiments are explained in Sections 3.4.5 and 3.4.6, respectively. Finally, in Section 3.4.7, the effects of impurity diffusion on the concentrations of the intrinsic point defects are discussed.

3.4.1 Derivation of the Diffusion Equations

In order to derive a simplified description of the diffusion of impurities which can be used to interpret experiments qualitatively, the various simplifications discussed in Section 3.3.3 are usually applied. In particular, it is generally assumed that contributions from a direct-exchange mechanism or from a concerted-exchange mechanism are negligible and that the concentrations of electrically neutral substitutional impurities and of the mobile pairs are negligible in comparison to the concentration of charged substitutional impurities. When steady state between pairs, substitutional impurities and intrinsic point defects is established after a transient period, (3.48) reduces to

$$\frac{\partial C_M}{\partial t} = \sum_{X=V,I} \text{div} \left(D_{MX} \cdot \text{grad} \left(C_M \cdot \frac{C_X}{C_X^{eq}} \right) - z_M \cdot D_{MX} \cdot \frac{C_X}{C_X^{eq}} \cdot \text{grad} \left(\frac{\Psi}{U_T} \right) \right) \quad (3.56)$$

with

$$D_{MX} = \Theta_{MX} \cdot \sum_k \delta_{MX^k} \cdot D_{MX^k} \cdot \left(\frac{n}{n_i} \right)^{z_k - z_M} \quad (3.57)$$

introduced for the effective, Fermi-level-dependent diffusion coefficients via pairs with point defects X under conditions of thermal equilibrium. In general, pairs are assumed to exist in neutral, singly positive, and singly negative charge states. The diffusion coefficients via the respective pairs contain then a Fermi-level-independent term and terms which vary with p and p^2 for pairs with acceptors ($z_M = 1$), and n and n^2 for pairs with donors ($z_M = -1$).

For a large number of applications, e. g. during diffusion under oxidizing conditions, the gradients of the point defects can be neglected. Models ignoring the effects of these gradients are usually called “dual-diffusion” models when they include diffusion via both vacancies and self-interstitials. They can be written as

$$\frac{\partial C_M}{\partial t} = \text{div} \left(\left(D_{MV} \cdot \frac{C_V}{C_V^{eq}} + D_{MI} \cdot \frac{C_I}{C_I^{eq}} \right) \cdot \left(\text{grad} C_M - z_M \cdot C_M \cdot \text{grad} \left(\frac{\Psi}{U_T} \right) \right) \right). \quad (3.58)$$

Such an equation corresponds again to the macroscopic description of diffusion in electrostatic fields (1.78) and

$$D_M = D_{MV} \cdot \frac{C_V}{C_V^{eq}} + D_{MI} \cdot \frac{C_I}{C_I^{eq}} \quad (3.59)$$

can be seen as a macroscopic diffusion coefficient of the total concentration of impurities. It depends on the local concentrations of the intrinsic point defects and on the Fermi level.

The diffusion coefficient defined by (3.59) composes of two terms which stand for the diffusion via vacancies and self-interstitials, respectively. To differentiate between these contributions, the fractional diffusivity via self-interstitials f_I was introduced in the literature as

$$f_I = \frac{D_{MI}}{D_{MV} + D_{MI}}. \quad (3.60)$$

Under intrinsic conditions the diffusion coefficient can then be written as

$$D = D^i \cdot \left(f_I \cdot \frac{C_I}{C_I^{eq}} + (1 - f_I) \cdot \frac{C_V}{C_V^{eq}} \right) \quad (3.61)$$

with D^i standing for the so-called “intrinsic diffusion coefficient” discussed further in Section 3.4.2. It follows from (3.60) that f_I is not likely described by an Arrhenius law. But when the diffusion coefficients D_{MI} and D_{MV} via self-interstitials and vacancies follow approximately Arrhenius laws, the quantity

$$\frac{1}{f_I} - 1 = \frac{D_{MV}}{D_{MI}} \sim \exp \left(- \frac{E_A}{k \cdot T} \right) \quad (3.62)$$

shows also an approximate Arrhenius behavior. The methods used to estimate f_I from experiments are summarized in Section 3.4.3. The results of such analyses published in the literature can be found in Sections 4.2, 4.3, and 5.3 to 5.10. For antimony, there is general agreement that it diffuses predominantly via vacancies. Boron and phosphorus were suggested in the recent literature to diffuse nearly exclusively via self-interstitials. Discrepancies in the estimates of f_I were noted especially for arsenic [3.55]. Possible origins will be discussed in more detail in Section 3.4.3. Under non-equilibrium conditions, f_I will, in general, depend on the Fermi level. But quantitative models are available only for few impurities.

3.4.2 The Intrinsic Diffusion Coefficient

One of the few parameters which is rather easily accessible to measurements is the so-called “intrinsic diffusion coefficient” D^i . Formally, it is the diffusion coefficient of impurities measured under intrinsic ($n = n_i$) and inert ($C_{I,V} = C_{I,V}^{eq}$) conditions. Even within the simplifications of pair diffusion models, D^i appears as a sum of ideally Arrhenius-like terms. Nevertheless, it is apparent from the data shown in Chapters 4 to 6 that the intrinsic diffusion coefficient of these impurities can usually be described quite accurately by an Arrhenius expression with a single activation energy. This would indicate that either diffusion via one and the same intrinsic point defect in a certain charge state dominates for all temperatures or that the activation energies of the individual contributions are similar.

The intrinsic diffusion coefficient is usually the best-studied parameter for all impurities. However, from dopants like boron and phosphorus for which many experimental determinations are available, it is apparent that individual determinations may differ by factors between two and four for a certain temperature. For the diffusion of aluminum, the differences even amount to more than an order of magnitude for low temperatures. Although the experimental determination of D^i seems straightforward, various deviations from the ideal conditions may have occurred unnoticed or, at least, unreported. Therefore, it seems appropriate to discuss potential pitfalls associated with the determination of intrinsic diffusion coefficients and with diffusion experiments in general.

The requirement of intrinsic conditions was potentially violated in several of the experiments reported in the literature. Especially early investigations were often based on the diffusion of impurities from the gas phase which can result in concentrations exceeding intrinsic concentrations by far. However, the main problem is that the intrinsic point defects have to be in equilibrium. It can be split into two separate problems, the introduction of the dopants and the annealing process.

Impurities are introduced either by diffusion from the gas phase, from doped epitaxially deposited layers or doped oxides, or by ion implantation. Sometimes, “intrinsic” diffusion coefficients were deduced from impurity profiles measured after predeposition from the gas phase. However, in such cases, chemical reactions at the silicon surface are virtually inevitable during the process and may affect the concentrations of the intrinsic point defects. Ion implantation is known to introduce significant lattice damage. Its annealing leads to transient-enhanced diffusion and reliable experimental determinations require pre-annealing steps with sufficient thermal budgets to avoid interferences. Diffusion from epitaxially deposited layers should be quite reliable but it has to be kept in mind that defects may be grown-in during low-temperature epitaxy processes and may affect diffusion at least at low temperatures.

A second major concern, discussed already in Section 2.8.4, is the atmosphere during annealing. The ideal situation would be a free surface in an inert ambient. But this is just an abstraction since a native oxide film grows rapidly on wafers even at room temperature and the formation of volatile SiO is known to affect at least the concentrations of self-interstitials. To avoid the formation of SiO, some percent of oxygen are often added to inert ambients without mentioning which may lead to oxidation-enhanced/retarded diffusion. But even trace amounts of oxygen, e.g. from the back-diffusion of oxygen in horizontal furnaces, may already lead to enhanced diffusion. In the absence of more reliable experiments, the oxidation model of Ling [3.56] and the OED model of Dunham and Plummer [3.57] have been used to estimate the partial pressure of oxygen needed to establish a certain oversaturation of self-interstitials. The result is shown in Figure 3.3 and indicates that trace amounts of oxygen should be significantly more influential at lower temperatures. It has to be noted that the absolute values have to be taken *cum grano salis* since both models had to be used outside the range of parameters

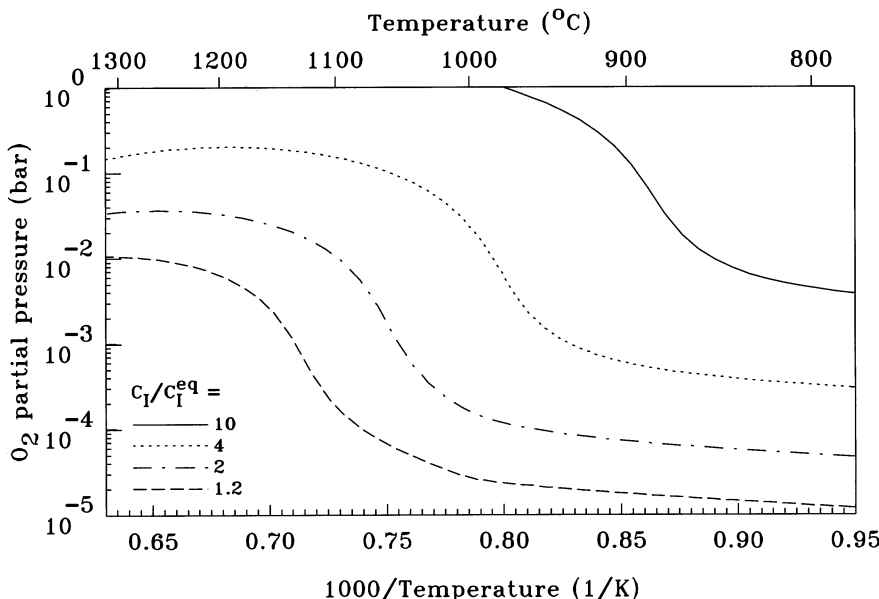


Figure 3.3: Oxygen partial pressure required to establish a certain oversaturation of self-interstitials in a wafer covered by a 2.5 nm thick oxide layer. The values were obtained from simulations based on the oxidation model of Ling [3.56] and the OED model of Dunham and Plummer [3.57].

for which they were calibrated. However, at 1200 °C, the effects predicted are in quantitative agreement with the dependence of the formation of “Magic Denuded Zones¹” on the oxygen partial pressure [3.59] and Lerch et al. [3.60] observed significant OED already at an oxygen partial pressure of 33 ppm for temperatures from 1000 to 1100 °C. To avoid ambient influences, samples were often covered by thick oxide layers or combinations of oxide and nitride layers during annealing. While this should work well at higher temperatures, it might lead to stress effects at low temperatures where no viscous flow of the oxide occurs. As a conclusion, it has to be stated that inert conditions are quite a challenge, especially at low temperatures.

A further point to be addressed concerns the measurement techniques used. Especially the first experiments were based on junction delineation and sheet-resistivity measurements only. These measurements imply considerably more interpretation than depth-resolved measurements. Electrical measurements in general require calibration, their resolution is basically limited by the Debye length, and they rely on the skill of the operator to yield reproducible and reliable results. Methods like RBS or SIMS seem rather straightforward nowadays. But especially the sputtering processes during SIMS or Auger measurements introduces a broadening of the profile which has to be taken into considerations especially for the low thermal-annealing budgets used today.

Last but not least, it remains to mention that the reliability of temperature data is a major concern. In horizontal furnaces, temperature calibration is usually done prior to experiments, and the temperature is controlled during annealing via spike thermocouples outside the tube. In addition, especially due to the gas flow, thermal equilibrium is often not established and wafers may be colder than the nominal temperature. In RTP systems, the wafer temperature

¹“Magic Denuded Zone” is a process to control the depth of zones free from oxygen precipitates by controlling the vacancy profile rather than the oxygen profile, see [3.58]

is usually measured by a pyrometer from the back side of the samples. Since the temperature is then measured past the lamps and through the quartz process chamber, interferences may occur, e. g. when the quartz chamber heats up during processing or calibration. In addition, pyrometer readings are influenced by the state of the back-side of the samples. Nowadays, there is production equipment available which promises measurements of the absolute temperature with an accuracy of some Kelvin. However, because of the considerable costs, it is not expected that it will be used excessively in research.

3.4.3 Estimates of f_I from Experiments

Values for f_I were estimated by various experimental methods. Their basics and advantages will be discussed in the following.

Self-Interstitial Oversaturation from the Growth of Oxidation Stacking Faults

Many of the early investigations were based on oxidation-enhanced diffusion with the oversaturation of self-interstitials estimated from the growth of stacking faults. This method, labeled “OSF” in the f_I tables of Chapters 4 and 5, was the best choice at that time but it appears in retrospect that the uncertainties in the parameters involved were too high for a reliable determination of f_I .

High-Concentration Diffusion

Similarly problematic were estimates based on the fitting of diffusion theories to diffusion profiles of dopants at high-concentration or under other non-equilibrium situations. They will be referred to by “DifModel” in the f_I tables. Evidence from such work is definite only if some *a-priori* assumptions hold which are problematic to check. In addition, the same phenomena have been explained in some investigations by diffusion via vacancies while other researchers explained them by diffusion via self-interstitials.

Retarded Diffusion

A significantly improved method was introduced by Gösele and Tan [3.61]. It is based on the observation of retarded diffusion of dopants and will be denoted by “RD” in the f_I tables. Gösele and Tan assumed that the self-interstitials and vacancies are in local equilibrium and, by rewriting (3.61), obtained a relation between the relative changes in the diffusion coefficient and the concentration of self-interstitials

$$\delta D = \frac{D - D^i}{D^i} = \frac{s_I}{s_I + 1} \cdot (2 \cdot f_I + f_I \cdot s_I - 1) \quad (3.63)$$

with

$$s_I = \frac{C_I - C_I^{eq}}{C_I^{eq}}. \quad (3.64)$$

This relation is shown graphically in Figure 3.4. The curves $\delta D(s_I)$ have a minimum for a self-interstitial oversaturation of $s_I = \sqrt{(1 - f_I)/f_I} - 1$. The associated value of δD at the minimum is $\delta D_{min} = 2 \cdot \sqrt{f_I \cdot (1 - f_I)} - 1$. It assumes a value of 0 for $f_I = 0.5$ and decreases monotonically towards -1 for values of f_I which are larger or smaller. Gösele and Tan considered only observations of retarded diffusion and argued that any experimentally observed retardation $\delta D < 0$

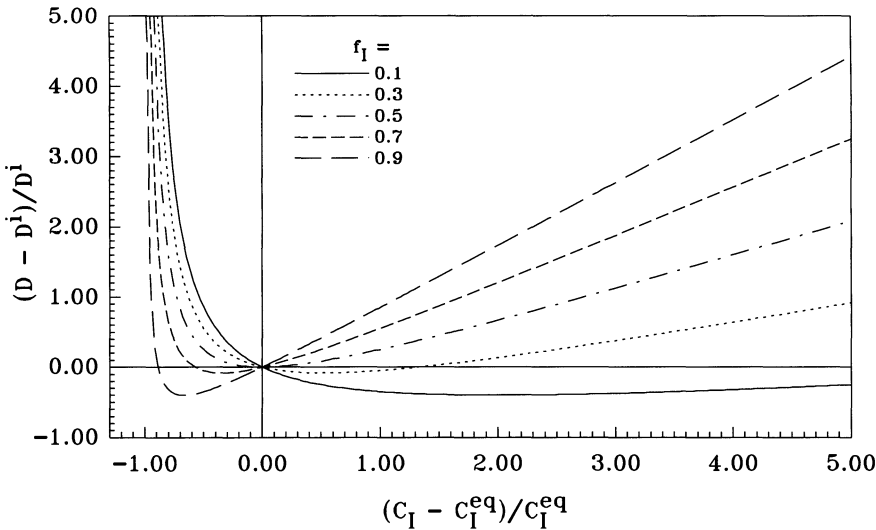


Figure 3.4: Relative diffusion enhancement as a function of the self-interstitial oversaturation.

has to be larger or equal to the minimum value. As a consequence, because of the monotonicity of the relation, a lower or an upper limit for f_I can be estimated in the form

$$f_I \begin{cases} \leq \frac{1}{2} - \frac{1}{2} \cdot \sqrt{1 - (\delta D + 1)^2} & \text{for } s_I > 0 \\ \geq \frac{1}{2} + \frac{1}{2} \cdot \sqrt{1 - (\delta D + 1)^2} & \text{for } s_I < 0 \end{cases} \quad (3.65)$$

from the observation of retarded diffusion. The question which of the two forms applies can be decided on the basis of whether the retarded diffusion is observed during an oversaturation or an undersaturation of self-interstitials.

Comparison of the Diffusivities of Dopants

The last method, referred to by “DifComp” in the following, is based on a comparison of the diffusivities of two or more dopants under non-equilibrium conditions. There were various investigations in the literature in which numerical solutions of the diffusion equations of the dopants were used to extract estimates for their fractional diffusivities via self-interstitials. They sometimes lack rigor and overlap considerably with the estimates from diffusion models discussed above as method.

A more elegant and usually also more rigorous approach was introduced by Fahey et al. [3.55]. Starting from (3.61) for time-averaged quantities (indicated by a bar over the symbol), they rewrote the equation for f_I which is given by

$$f_I = \frac{\bar{D}/D^i - \bar{C}_V/C_V^{eq}}{\bar{C}_I/C_I^{eq} - \bar{C}_V/C_V^{eq}}. \quad (3.66)$$

For an excess of vacancies, the inequalities $0 \leq \bar{C}_I/C_I^{eq} \leq \bar{D}/D^i \leq \bar{D}_{VE}/D_{VE}^i \leq \bar{C}_V/C_V^{eq}$ and $\bar{C}_I/C_I^{eq} < \bar{C}_V/C_V^{eq}$ hold. “VE” denotes the element with the largest value of \bar{D}/D^i for an excess

of vacancies. Usually, this would be antimony. A lower limit for f_I of the elements can then be obtained from

$$f_I = \frac{\overline{C_V}/C_V^{eq} - \overline{D}/D^i}{\overline{C_V}/C_V^{eq} - \overline{C_I}/C_I^{eq}} \geq \frac{\overline{D_{VE}}/D_{VE}^i - \overline{D}/D^i}{\overline{D_{VE}}/D_{VE}^i - \overline{C_I}/C_I^{eq}} \geq \frac{\overline{D_{VE}}/D_{VE}^i - \overline{D}/D^i}{\overline{D_{VE}}/D_{VE}^i}. \quad (3.67)$$

Clearly, for element VE, this estimate would give only the trivial estimate $f_I^{VE} \geq 0$. For an excess of self-interstitials, $0 \leq \overline{C_V}/C_V^{eq} \leq \overline{D}/D^i \leq \overline{D_{IE}}/D_{IE}^i \leq \overline{C_I}/C_I^{eq}$ and $\overline{C_V}/C_V^{eq} < \overline{C_I}/C_I^{eq}$ hold. “IE” denotes the element with the largest value of \overline{D}/D^i for an excess of self-interstitials. Depending on the elements investigated, this would be aluminum, boron, or phosphorus. A lower limit for $1 - f_I$ of the elements can then be obtained from

$$1 - f_I = \frac{\overline{C_I}/C_I^{eq} - \overline{D}/D^i}{\overline{C_I}/C_I^{eq} - \overline{C_V}/C_V^{eq}} \geq \frac{\overline{D_{IE}}/D_{IE}^i - \overline{D}/D^i}{\overline{D_{IE}}/D_{IE}^i - \overline{C_V}/C_V^{eq}} \geq \frac{\overline{D_{IE}}/D_{IE}^i - \overline{D}/D^i}{\overline{D_{IE}}/D_{IE}^i} \quad (3.68)$$

which leads directly to an upper limit for f_I . For element IE, again only the trivial estimate $f_I^{IE} \leq 1$ would be obtained.

An alternative way to estimate f_I from the diffusion enhancements of two or more dopants was suggested by Gossmann et al. [3.62]. They started from (3.61) for two dopants *A* and *B*. From these equations, the oversaturation of vacancies and self-interstitials can be expressed as

$$\frac{C_V}{C_V^{eq}} = \frac{f_I^B \cdot D_A/D_A^i - f_I^A \cdot D_B/D_B^i}{f_I^B - f_I^A}, \quad (3.69)$$

$$\frac{C_I}{C_I^{eq}} = \frac{(1 - f_I^A) \cdot D_B/D_B^i - (1 - f_I^B) \cdot D_A/D_A^i}{f_I^B - f_I^A}. \quad (3.70)$$

wherein f_I^A and f_I^B are not known *a priori*. Assuming *B* to be the dopant with the higher value of f_I , the inequalities

$$f_I^A \leq f_I^B \cdot \frac{D_A/D_A^i}{D_B/D_B^i} \leq \frac{D_A/D_A^i}{D_B/D_B^i} \quad (3.71)$$

and

$$f_I^B \geq 1 - \frac{D_B/D_B^i}{D_A/D_A^i} \cdot (1 - f_I^A) \geq 1 - \frac{D_B/D_B^i}{D_A/D_A^i} \quad (3.72)$$

follow straightforwardly from $C_V/C_V^{eq} \geq 0$ and $C_I/C_I^{eq} \geq 0$. Non-trivial estimates for the dopant with the lower f_I can be expected from (3.71) only when $D_A/D_A^i < D_B/D_B^i$. Such a situation can be realized by the injection of self-interstitials, e.g. by thermal oxidation. Similarly, a meaningful lower limit can be obtained from (3.72) only for $D_A/D_A^i > D_B/D_B^i$. This condition corresponds to an injection of vacancies as it is typically observed during nitridation of bare silicon surfaces.

Sources of Misinterpretations

Estimates of f_I can contain significant errors when certain effects like contributions from concerted exchange, non-negligible pair concentrations, or alternative pair-formation reactions are not taken into account. These pitfalls will be discussed in the following.

Concerted Exchange

The approaches for an estimation of f_I discussed above are all based on (3.59). When direct exchange or concerted exchange contributes significantly to dopant diffusion, the effective diffusion coefficient under non-equilibrium conditions is always smaller than expected from (3.59). As a consequence, f_X is underestimated for $C_X/C_X^{eq} > 1$. Similarly, f_Y is underestimated for $C_X/C_X^{eq} < 1$ which means that $f_X = 1 - f_Y$ is overestimated.

Contributions of concerted exchange to the diffusion of dopants were considered by Cowern [3.51] who used it to explain the apparent inconsistency in the determination of f_I^{As} by Fahey et al. [3.55]. A satisfactory fit was achieved with a 40% contribution from concerted exchange but the result was found to be at variance with other experiments. Interpreting their own experiments, Ural et al. [3.63] estimated that concerted exchange might contribute up to 36% to the diffusion of arsenic at 1000 °C, and up to 61% at 1100 °C.

Alternative Reactions for the Formation of Pairs

Pair-diffusion theories ignore the alternative reactions (3.30) to derive an effective diffusion coefficient (3.59) which can be split into diffusion terms via vacancies and self-interstitials each of which varies linearly with the respective oversaturation of intrinsic point defects. It was shown above that this particular form of the diffusion coefficient is reproduced for the same level of simplifications when the alternative reactions are included and when self-interstitials and vacancies can be assumed to be in steady state ($C_I \cdot C_V = C_I^{eq} \cdot C_V^{eq}$). However, in the general case (3.50), no such simple form is possible even when the concentrations of the pairs are assumed to be negligible in comparison to the concentration of the substitutional impurities.

Values for f_I , as discussed in Section 3.4.3, are usually derived from situations in which one of the intrinsic point defects, say X, is introduced by a chemical reaction at the surface. The concentration of this intrinsic point defect will then be in supersaturation while that of the other, Y, will be reduced by bulk recombination to values below its equilibrium concentration. In general, the normalized concentration of Y can be expected in the limits

$$\frac{C_X^{eq}}{C_X} < \frac{C_Y}{C_Y^{eq}} \leq 1. \quad (3.73)$$

This can be quantified in the form

$$\frac{C_Y}{C_Y^{eq}} = 1 + \chi \cdot \left(\frac{C_X^{eq}}{C_X} - 1 \right) \quad (3.74)$$

with a parameter χ in the limits $0 \leq \chi < 1$. Then, it can be shown that the terms

$$\frac{C_X/C_X^{eq} + \alpha_{MX}}{1 + \alpha_{MX} \cdot C_Y/C_Y^{eq}} = \frac{C_X/C_X^{eq} + \alpha_{MX}}{1 + \alpha_{MX} - \alpha_{MX} \cdot \chi + \alpha_{MX} \cdot \chi \cdot C_X^{eq}/C_X} < \frac{C_X}{C_X^{eq}} \quad (3.75)$$

and

$$\frac{C_Y/C_Y^{eq} + \alpha_{MY}}{1 + \alpha_{MY} \cdot C_X/C_X^{eq}} = \frac{C_X^{eq}/C_X \cdot \chi + 1 - \chi + \alpha_{MY}}{1 + \alpha_{MY} \cdot C_X/C_X^{eq}} < \frac{C_Y}{C_Y^{eq}} \quad (3.76)$$

are all below the oversaturations of the respective point defects. As a consequence, the effective diffusion coefficient is always smaller than expected from (3.59) and f_X is underestimated for $C_X/C_X^{eq} > 1$. Similarly, f_Y is underestimated for $C_X/C_X^{eq} < 1$ which means that $f_X = 1 - f_Y$ is overestimated.

The analysis was presented first by Cowern [3.51] who used it to explain the apparent inconsistency in the determination of f_I^{As} by Fahey et al. [3.55]. Fitting Fahey's data, Cowern et

al. estimated the constant α_{AsI} to be in the range $3 \lesssim \alpha_{AsI} \lesssim 10$. A similar, but more detailed analysis of Fahey's experiments by Vandebossche and Baccus [3.64] led to estimates of $\alpha_{PI} = 0.3$ for phosphorus, $\alpha_{SbV} = 0.01$ for antimony, and $0.01 \leq \alpha_{AsV} \leq 0.02$ and $5 \leq \alpha_{AsI} \leq 7$ for arsenic. It should be noted, however, that the same effect can be explained also by concerted exchange and non-negligible concentrations of pairs as discussed above and below.

Non-Negligible Concentrations of Pairs of Dopants and Intrinsic Point Defects

In the derivation of (3.56), it was assumed that the concentration of dopants in pairs is negligible in comparison to the concentration of substitutional atoms. When one of the intrinsic point defects is in extreme oversaturation, the majority of the dopant atoms will be in pairs with the oversaturated point defects. The macroscopic diffusion coefficient (3.50) is then identical to that of the respective pairs given by

$$D_M = \begin{cases} \frac{\sum_k \delta_{MV^k} \cdot D_{MV^k} \cdot \left(\frac{n}{n_i}\right)^{z_k}}{\sum_k \delta_{MV^k} \cdot \left(\frac{n}{n_i}\right)^{z_k}} & \text{for } C_{MV} \gg C_{M_s}, C_{MV} \gg C_{MI} \\ \frac{\sum_k \delta_{MI^k} \cdot D_{MI^k} \cdot \left(\frac{n}{n_i}\right)^{z_k}}{\sum_k \delta_{MI^k} \cdot \left(\frac{n}{n_i}\right)^{z_k}} & \text{for } C_{MI} \gg C_{M_s}, C_{MI} \gg C_{MV} \end{cases} \quad (3.77)$$

and independent of the concentrations of intrinsic point defects. But even when the point-defect concentrations are in equilibrium, pairs may exist in non-negligible concentrations. Indications for such an effect were reported for arsenic (see Section 5.9).

As an example, the normalized diffusion coefficient of arsenic under intrinsic conditions is depicted in Figure 3.5 as a function of the oversaturation of self-interstitials under the assumptions of dilute pair concentrations according to (3.59), and of non-dilute pair concentrations according to (3.50). The parameters were adjusted according to the models of Heinrich et

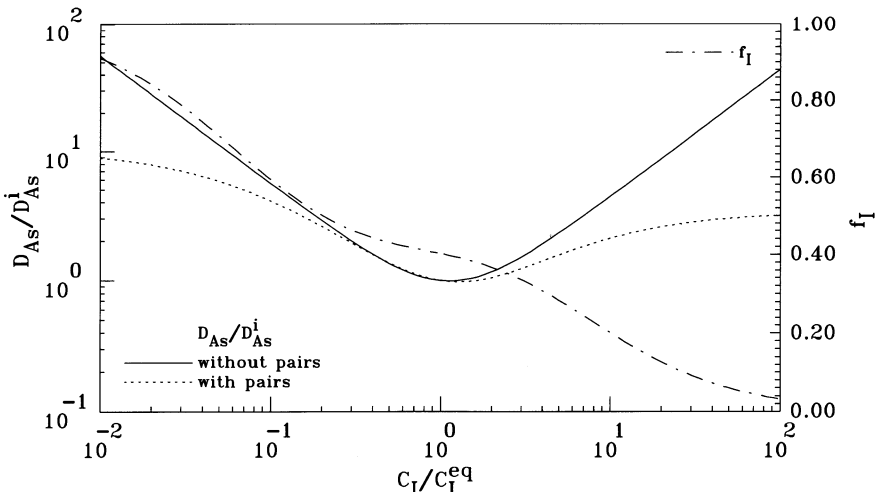


Figure 3.5: Normalized diffusion coefficient and estimate for f_I from measured diffusivities of arsenic under intrinsic conditions as a function of the oversaturation of self-interstitials.

al. [3.65] and Novell and Law [3.66] who explained the apparent inconsistency in the experiments of Fahey et al. [3.55] by non-negligible pair concentrations. It should be noted, however, that the same effects can be explained also by including diffusion via the concerted-exchange mechanism or alternative pair reactions as discussed above.

From Figure 3.5, a markedly reduced effective diffusion coefficient under non-equilibrium conditions is apparent when non-dilute pair concentrations are included in the analysis. Assuming local equilibrium between self-interstitials and vacancies, f_I follows from (3.61) in the form

$$f_I = \frac{D/D^i \cdot C_I/C_I^{eq} - 1}{(C_I/C_I^{eq})^2 - 1}. \quad (3.78)$$

In case of non-dilute pair concentrations, the diffusion coefficient (3.50) will be smaller than expected from (3.61). Thus, f_I , as shown also in Figure 3.5, will be underestimated for $C_I/C_I^{eq} > 1$ while it will be overestimated for $C_I/C_I^{eq} < 1$.

3.4.4 The Field Effect

Dopant concentrations exceeding the intrinsic concentration at process temperature result in an electric field which exerts additional forces on the dopants. The diffusion is then called “extrinsic” in contrast to “intrinsic” diffusion referring to concentrations well below the intrinsic carrier concentration.

For a first-order estimate, the charge neutrality equation (1.27) can be used to describe the electric field. This allows to express the gradient of the electrostatic potential in terms of the dopant concentrations as

$$\text{grad} \left(\frac{\psi}{U_T} \right) = - \frac{\sum_i z_i \cdot \text{grad} C_i}{\sqrt{\left(\sum_j z_j \cdot C_j \right)^2 + 4 \cdot n_i^2}}. \quad (3.79)$$

Then, (3.58) becomes

$$\frac{\partial C_M}{\partial t} = \text{div} \left(D_M \cdot \left(\text{grad} C_M + \frac{z_M \cdot C_M}{\sqrt{\left(\sum_j z_j \cdot C_j \right)^2 + 4 \cdot n_i^2}} \cdot \sum_i z_i \cdot \text{grad} C_i \right) \right). \quad (3.80)$$

For systems with only one dopant being present in the system, Smits [3.67] and Lehovec and Slobodskoy [3.68] showed that the equation reduces further to

$$\frac{\partial C_M}{\partial t} = \text{div} (D_M \cdot f_f \cdot \text{grad} C_M) \quad (3.81)$$

with the field enhancement factor f_f given by

$$f_f = 1 + \frac{C}{\sqrt{C^2 + 4 \cdot n_i^2}}. \quad (3.82)$$

It increases from unity at low concentrations $C \ll n_i$ to two at high concentrations $C \gg n_i$. A doubling of the diffusion coefficient due to electric fields was predicted already before by Bardeen et al. [3.69].

It should be noted that the field enhancement in the form of (3.82) is a result of the application of Boltzmann statistics and limited to non-degenerate concentrations. For conditions where the Fermi level is above the conduction band, Shockley [3.70], Thai [3.71], and Shaw [3.72] derived field enhancement factors which increase unlimited with dopant concentration. Their point of view was opposed by Hu [3.73]. He showed that the field-enhancement factor is fundamentally limited by two, no matter how heavily doped and how the electrostatic potential is modified by the degenerate statistics. To remain consistent, he suggested that the Nernst-Einstein relation has to be used in its generalized form (1.81) instead of in its simple form (1.80).

Much more important than a doubling of the diffusion coefficient may be the effect of an impurity being present at high concentrations on the diffusion of an impurity being present at low concentrations. As an example, the effects of field-coupled diffusion on an initially flat profile are shown in Figure 3.6. The product $4 \cdot D \cdot t$ was $(0.2 \mu\text{m})^2$ for the low-concentration profiles and $(0.06 \mu\text{m})^2$ for the high-concentration profile. Qualitatively, ions with equal charge state as the ions forming the high-concentration profiles are pushed away while ions with opposite charge state are pulled under the high-concentration region. The expected dip in the profile has been found already early experimentally, e. g. by Jones and Willoughby [3.74].

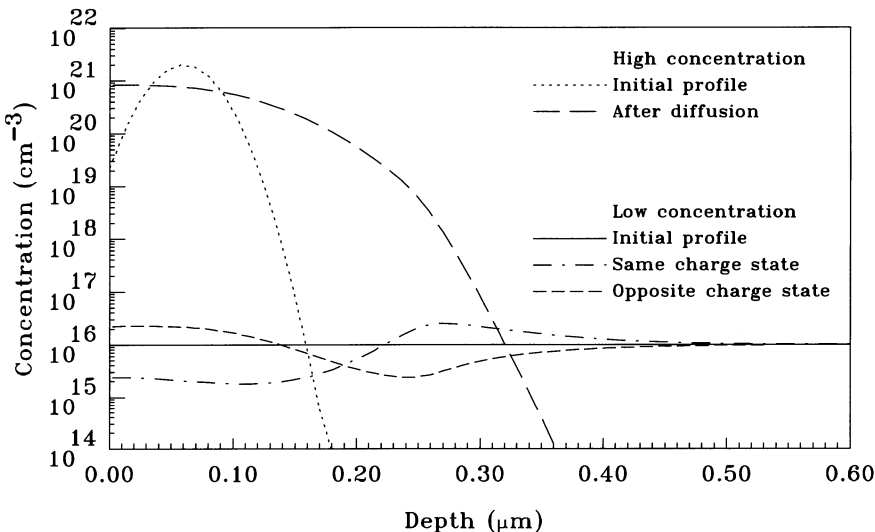


Figure 3.6: Diffusion coupling via the electrostatic field.

3.4.5 Boltzmann-Matano Analysis

For concentrations exceeding the intrinsic carrier concentration at process temperature, the local diffusion coefficients (3.57) via vacancies and self-interstitials will depend on the Fermi level. When only one dopant is present, the Fermi level can be expressed in a good approximation by the charge neutrality equation (1.27) and the diffusion coefficient becomes a local function of the dopant concentration.

Starting from a diffusion equation

$$\frac{\partial C}{\partial t} = \frac{\partial}{\partial x} \left(D(C) \cdot \frac{\partial C}{\partial x} \right) \quad (3.83)$$

with a diffusion coefficient $D(C)$ which may be a function of the local concentration C , Boltzmann [3.75] and Matano [3.76] could show that the coordinate transformation

$$\eta = \frac{x}{2 \cdot \sqrt{t}} \quad (3.84)$$

leads to an ordinary differential equation

$$-2 \cdot \eta \cdot \frac{dC}{d\eta} = \frac{d}{d\eta} \left(D(C) \cdot \frac{d}{d\eta} C \right) \quad (3.85)$$

which can be integrated with respect to η . Reintroducing x and t gives

$$D(C = C_x) = \frac{1}{2 \cdot t} \cdot \left(\frac{dx}{dC} \right)_{C_x} \cdot \int_0^{C_x} x \cdot dC. \quad (3.86)$$

A prerequisite for the application of the Boltzmann-Matano method is clearly that the concentration profile $C(x, t)$ can be written as a function of $C(x/\sqrt{t})$ which includes that the surface concentration has to be constant. It has to be verified for each analysis by varying the process time t . In several applications of the Boltzmann-Matano analysis to the diffusion of phosphorus at high concentrations, this prerequisite was checked and found fulfilled by some authors [3.49, 3.77] while others found disagreements [3.78]. Some elements, as discussed in Section 3.4.7, cause a non-local influence on the concentrations of the intrinsic point defects. When their profiles can be written as a function of $C(x/\sqrt{t})$, this seems to indicate that D is really a local function, but not necessarily a monotonic function of the concentration C . In addition, in such analyses, the diffusion coefficient was found to depend on the surface concentration. However, the situation is far too complicated to justify a general statement. A practical problem in the application of the Boltzmann-Matano method is also the evaluation of the gradient dC/dx which usually involves smoothing of the profiles.

3.4.6 Isoconcentration Experiments

A characterization of the dependence of the diffusion coefficient on the Fermi level in extrinsically doped silicon from the shape of diffusion profiles is sometimes problematic. The application of the Boltzmann-Matano method (see the previous section) is restricted to some limiting cases while a reverse simulation requires *a-priori* assumptions about the models. In particular, an influence of dopant diffusion on the concentrations of the intrinsic point defects, as discussed in the next section, will affect both analyses.

The most elegant way to obtain the Fermi-level dependence of the diffusivity of a dopant is to perform diffusion experiments under isoconcentration conditions, i. e. in a homogeneously and extrinsically doped background either of a different isotope of the same dopant or of a dopant of the same doping type. The majority dopants determine then the Fermi level while, because of the vanishing gradient of the dominant doping, all gradients of the Fermi level vanish and non-equilibrium effects, as described in the next section, can be excluded. Self-diffusion under isoconcentration conditions was mentioned already in Section 2.3. Further examples for impurities can be found in the next two chapters in the descriptions of the diffusion behavior of isovalent impurities and dopants.

It is evident that the diffusion of an acceptor in an extrinsic donor background or *vice versa* can also be investigated. But then, as discussed later in Section 5.2, donor-acceptor pairs will form and one does not get the true Fermi-level dependence of the diffusion coefficient of the minority dopant.

3.4.7 Influence of Dopant Diffusion on the Intrinsic Point Defects

Pair-diffusion models describe the effects of point-defect concentrations and point-defect gradients on dopant diffusion. When a pair finally dissociates, not only the substitutional atom has migrated but also the intrinsic point defect associated. As a consequence, dopant diffusion also influences the distribution of the intrinsic point defects. This influence comes from the pair formation reactions and is included in the continuity equations of the intrinsic point defects (3.39) and (3.40) via the recombination terms R_X and R_{MX+Y} .

The effect is demonstrated in Figure 3.7. It shows a comparison between simulations (courtesy C. Ortiz, FhG-IISB) and an experiment of OrrArienzo et al. [3.79] in which boron diffused from a doped polycrystalline layer into the silicon bulk. During the diffusion process, a constant concentration equivalent to the solubility of boron in silicon was maintained at the interface. The first simulation shown was based on the intrinsic diffusion coefficient and it is apparent that it was too shallow to reproduce the experiment. In a second simulation, the Fermi-level dependence of the diffusion coefficient (5.14) known from isoconcentration diffusion experiments was used together with field enhancement. Still, the simulation underestimates diffusion. Finally, in the third simulation, full coupling with the intrinsic point defects was included with the Fermi-level dependence of their diffusion taken from the work of Sharp et al. [3.80]. The agreement is then excellent with no additional fitting parameters required. Also shown in the figure is the depth dependence of the oversaturation of self-interstitials caused by the high-concentration boron diffusion.

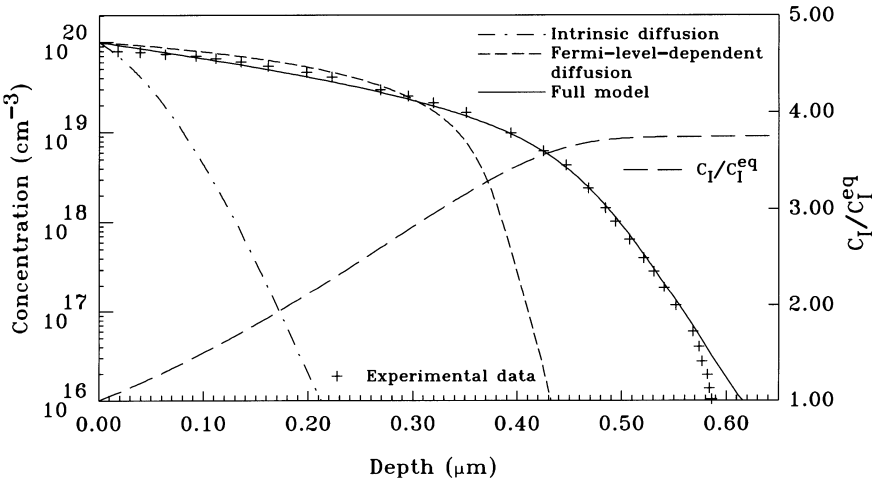


Figure 3.7: Simulation of the diffusion of boron at high concentrations (courtesy C. Ortiz, FhG-IISB) and comparison to the experiment of OrrArienzo et al. [3.79] at 950 °C. A detailed description of the simulations is given in the text.

In practice, numerical simulation of such effects has sometimes to find a trade-off between the computer resources needed and the accuracy obtained. Simplifications of the system of continuity equations are sometimes useful, but have to be justified on a case-to-case basis. The first generally used simplification, as discussed above, is to neglect the concentration of electrically neutral substitutional impurities. A second step is often to assume that steady state between substitutional impurities, intrinsic point defects, and pairs is established rapidly in comparison to the total process time. Finally, one has to take into considerations that the diffusion coef-

ficients of point defects are several orders of magnitude larger than the macroscopic diffusion coefficient of the substitutional impurity atoms. After a transient phase, the point defects will be in a steady state which is determined predominantly by the profile of the dopants. Point-defect models based on steady-state assumptions were used, e. g. by Schaake [3.81], Mathiot and Pfister [3.82], Morehead and Lever [3.83], and Dürr and Pichler [3.84], to simulate high-concentration effects. Evidently, such models fail to reproduce transient effects during post-implantation annealing and similar situations in which point defects and pairs are far from steady state.

Steady state is characterized by negligible derivatives of the concentration of point defects X and pairs MX with respect to time. One then obtains two coupled, elliptic partial differential equations for the oversaturation of self-interstitials and vacancies in the form

$$\begin{aligned} \frac{\partial C_{MX}}{\partial t} + \frac{\partial C_X}{\partial t} &= \operatorname{div} \left(\sum_k \left(\delta_{MX^k} \cdot D_{MX^k} \cdot \vartheta_{MX} \cdot \left(\frac{n}{n_i} \right)^{z_k} \right) \right. \\ &\quad \left. \cdot \operatorname{grad} \left(C_{M_s} \cdot \frac{C_X}{C_X^{eq}} \cdot \left(\frac{n}{n_i} \right)^{-z_M} \right) \right) \\ &\quad + \operatorname{div} \left(D_X \cdot \operatorname{grad} C_X - z_X \cdot D_X \cdot C_X \cdot \operatorname{grad} \left(\frac{\Psi}{U_T} \right) \right) \\ &\quad - k_X \cdot (C_X - C_X^*) - k_B \cdot (C_I \cdot C_V - C_I^{eq} \cdot C_V^{eq}) \\ &= 0 \end{aligned} \quad (3.87)$$

with the concentration of substitutional impurities C_{M_s} related again to the total concentration C_M by (3.49). For the case when the pair concentrations can be neglected, (3.87) reduces to

$$\begin{aligned} \operatorname{div} \left(D_{MX} \cdot \operatorname{grad} \left(C_M \cdot \frac{C_X}{C_X^{eq}} \right) - z_M \cdot D_X \cdot \frac{C_X}{C_X^{eq}} \cdot \operatorname{grad} \left(\frac{\Psi}{U_T} \right) \right) \\ + \operatorname{div} \left(D_X \cdot \operatorname{grad} C_X - z_X \cdot D_X \cdot C_X \cdot \operatorname{grad} \left(\frac{\Psi}{U_T} \right) \right) \\ - k_X \cdot (C_X - C_X^*) - k_B \cdot (C_I \cdot C_V - C_I^{eq} \cdot C_V^{eq}) = 0 \end{aligned} \quad (3.88)$$

A further simplification to one equation is possible when local equilibrium between self-interstitials and vacancies is assumed. Ignoring also possible sources and sinks for point defects, one obtains

$$\begin{aligned} &\left(D_{MI} \cdot C_M + D_I \cdot C_I^{eq} + (D_{MV} \cdot C_M + D_V \cdot C_V^{eq}) \cdot \left(\frac{C_I}{C_I^{eq}} \right)^2 \right) \cdot \operatorname{grad} \left(\frac{C_I}{C_I^{eq}} \right) \\ &+ \left(D_{MI} \cdot \left(\frac{C_I}{C_I^{eq}} \right) - D_{MV} \cdot \left(\frac{C_I^{eq}}{C_I} \right) \right) \cdot \left(\operatorname{grad} C_M - z_M \cdot C_M \cdot \operatorname{grad} \left(\frac{\Psi}{U_T} \right) \right) \\ &- \left(z_I \cdot D_I \cdot C_I^{eq} \cdot \frac{C_I}{C_I^{eq}} - z_V \cdot D_V \cdot C_V^{eq} \cdot \frac{C_V^{eq}}{C_I} \right) \cdot \operatorname{grad} \left(\frac{\Psi}{U_T} \right) = 0 \end{aligned} \quad (3.89)$$

which can be integrated for C_I/C_I^{eq} .

Equation (3.89) allows also to estimate whether dopant diffusion affects the concentrations of the intrinsic point defects. Because of the complexity of (3.89), an analytical analysis can be performed only on the basis of some approximations. At first, the field terms will be ignored since they contribute with a diffusion enhancement of less than two (see Section 3.4.4). At the threshold of an enhanced point-defect concentration in the bulk, C_I/C_I^{eq} will be close to unity. Then, the gradient of the self-interstitial oversaturation for an expected enhancement of the self-interstitial concentration in the bulk will be

$$\text{grad} \left(\frac{C_I}{C_I^{eq}} \right) \approx \frac{(1 - 2 \cdot f_I) \cdot D_M}{D_M \cdot C_M + D_I \cdot C_I^{eq} + D_V \cdot C_V^{eq}} \cdot \text{grad} C_M. \quad (3.90)$$

Ignoring the Fermi-level dependence of the diffusion coefficients, this equation can be integrated from the solubility concentration C^{sol} at the surface to a vanishing impurity concentration

$$\frac{C_I}{C_I^{eq}} \approx 1 + (2 \cdot f_I - 1) \cdot \ln \left(\frac{D_M \cdot C^{sol} + D_I \cdot C_I^{eq} + D_V \cdot C_V^{eq}}{D_I \cdot C_I^{eq} + D_V \cdot C_V^{eq}} \right). \quad (3.91)$$

A significant increase in the oversaturation of self-interstitials can be expected only for $f_I > 0.5$ and $D_M \cdot C^{sol} > 0.1 \cdot (D_I \cdot C_I^{eq} + D_V \cdot C_V^{eq})$. For dopants diffusing predominantly via vacancies, an analogous derivation would have resulted in

$$\frac{C_V}{C_V^{eq}} \approx 1 + (1 - 2 \cdot f_I) \cdot \ln \left(\frac{D_M \cdot C^{sol} + D_I \cdot C_I^{eq} + D_V \cdot C_V^{eq}}{D_I \cdot C_I^{eq} + D_V \cdot C_V^{eq}} \right) \quad (3.92)$$

and a vacancy supersaturation would be expected for $f_I < 0.5$ and a criterion for $D_M \cdot C^{sol}$ which follows in analogy to the interstitial case.

The ratio $D_M \cdot C^{sol}/(D_I \cdot C_I^{eq} + D_V \cdot C_V^{eq})$ is shown graphically in Figure 3.8 for dopant elements and in Figure 3.9 for isovalent impurities and chalcogens at their solubility concentration. According to this simple analysis, an influence on the concentrations of the intrinsic point defects could be expected for phosphorus, arsenic, aluminum, boron, and sulphur. For phosphorus, as outlined in Section 5.8.3, the formation of kink and tail in the diffusion profile as well as an oversaturation of self-interstitials in the bulk were observed and attributed to the influence of phosphorus diffusion on the intrinsic point defects. Similar phenomena, albeit less pronounced, were observed for boron, aluminum, and sulphur (see the discussion of Figure 3.7 above as well as Sections 5.3.3, 5.4.3, and 6.2.3). For arsenic, such effects were never observed experimentally, probably because of its f_I around 0.5. In the case of the completely miscible germanium, the relative transport capacity was calculated for a 10% germanium alloy. It has to be kept in mind, however, that composition and strain effects become already important at such high concentrations and would most likely cover possible influences on the intrinsic point defects. For gallium and selenium, an influence on the concentrations of the intrinsic point defects should be unlikely, and highly unlikely for indium, antimony, tin, carbon, and tellurium. It has to be remarked also that the ratios shown in Figure 3.8 correspond to solid solubility only. Especially after solid-phase epitaxy and after epitaxial deposition of doped layers, impurities may be present in concentrations exceeding solid solubility by far. In such systems, influences of impurity diffusion on the intrinsic point defects can be observed even for systems for which the transport capacity is usually well below that of the intrinsic point defects. Typical examples, discussed in Section 4.1.3, are highly-carbon-doped epitaxially grown layers.

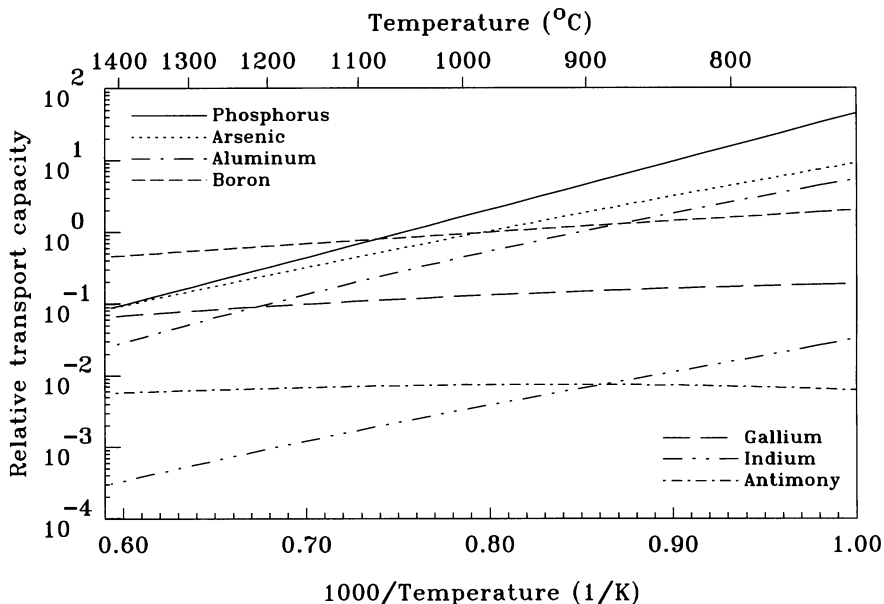


Figure 3.8: Relative transport capacity $D_M \cdot C^{sol} / (D_I \cdot C_I^{eq} + D_V \cdot C_V^{eq})$ of dopants at their solubility concentration.

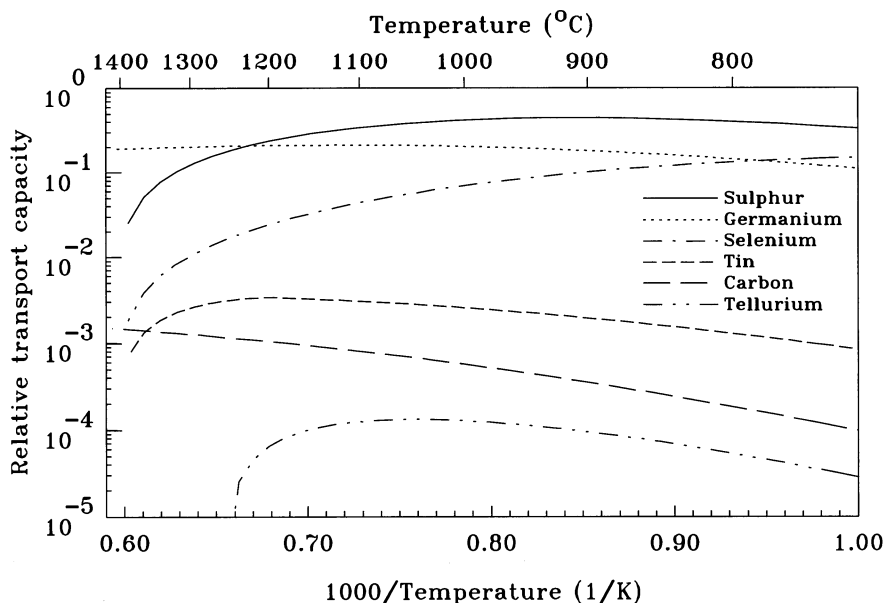


Figure 3.9: Relative transport capacity $D_M \cdot C^{sol} / (D_I \cdot C_I^{eq} + D_V \cdot C_V^{eq})$ of isovalent impurities and chalcogens at their solubility concentration.

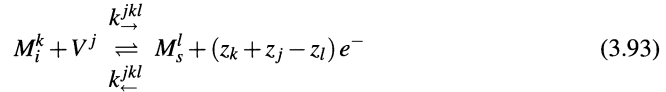
3.5 Frank-Turnbull Mechanism

Some metals diffuse very rapidly as interstitial atoms and reside predominantly on substitutional sites. Frank and Turnbull [3.39] proposed that the interstitial atoms react with vacancies to become substitutional to explain self-diffusion in copper. This model, also called “dissociative mechanism,” was extended by Sturge [3.85]. In silicon, it was used by Wilcox and La Chapelle [3.86] to explain gold diffusion profiles and extended by Huntley and Willoughby [3.87] to include vacancy sources.

3.5.1 Derivation of the Diffusion-Reaction Equations

The Frank-Turnbull or dissociative mechanism assumes an interstitial impurity atom M_i to react with a lattice vacancy V leading to a substitutional impurity atom M_s . This corresponds to the reaction $MX + V \rightarrow M_s$ in (3.30). A difference to dopant diffusion is that the reference state of the substitutional metal is traditionally the electrically neutral state. In addition, for the sake of compatibility with the literature, the mobile complex is denoted here M_i instead MI .

All three point defects can exist in more than one charge state denoted by k , j , and l with the number of electron charges z_k , z_j , and z_l (positive charge states have negative numbers). The respective concentrations will be referred to as $C_{M_i^k}$, $C_{M_s^l}$, and C_{V^j} . Each of the reactions can be written as



with e^- representing the remaining electrons. As usual, the charge states are assumed to be in local equilibrium so that the concentrations of the ionized vacancies can be expressed in terms of the concentration of the neutral ones via (2.22) to (2.25). For the interstitial and substitutional impurities, such a relation can be written in analogy. For all species, the relative concentrations of a particular charge state can be written as

$$\frac{C_{M_i^k}}{C_{M_i}} = \frac{\delta_{M_i^k} \cdot \left(\frac{n}{n_i}\right)^{z_k}}{\sum_k \delta_{M_i^k} \cdot \left(\frac{n}{n_i}\right)^{z_k}}, \quad \frac{C_{M_s^l}}{C_{M_s}} = \frac{\delta_{M_s^l} \cdot \left(\frac{n}{n_i}\right)^{z_l}}{\sum_l \delta_{M_s^l} \cdot \left(\frac{n}{n_i}\right)^{z_l}}, \quad \frac{C_{V^j}}{C_V} = \frac{\delta_{V^j} \cdot \left(\frac{n}{n_i}\right)^{z_j}}{\sum_j \delta_{V^j} \cdot \left(\frac{n}{n_i}\right)^{z_j}} \quad (3.94)$$

with $\delta_{M_i^0}$, $\delta_{M_s^0}$, and δ_{V^0} being formally identical to unity.

In a system with neutral point defects only, the continuity equation for the concentration of impurities at substitutional sites would be

$$\frac{\partial C_{M_s}}{\partial t} = k_{\rightarrow} \cdot C_{M_i} \cdot C_V - k_{\leftarrow} \cdot C_{M_s}. \quad (3.95)$$

Including the charge states, the continuity equation for the total concentration of impurities at substitutional sites $C_{M_s} = \sum_l C_{M_s^l}$ results in the form

$$\begin{aligned} \frac{\partial C_{M_s}}{\partial t} &= \frac{C_{M_i}}{\sum_k \delta_{M_i^k} \cdot \left(\frac{n}{n_i}\right)^{z_k}} \cdot \frac{C_V}{\sum_j \delta_{V^j} \cdot \left(\frac{n}{n_i}\right)^{z_j}} \cdot \sum_{j,k,l} k_{\rightarrow}^{jkl} \cdot \delta_{M_i^k} \cdot \delta_{V^j} \cdot \left(\frac{n}{n_i}\right)^{z_k + z_j} \\ &\quad - \frac{C_{M_s}}{\sum_l \delta_{M_s^l} \cdot \left(\frac{n}{n_i}\right)^{z_l}} \cdot \sum_{j,k,l} k_{\leftarrow}^{jkl} \cdot \delta_{M_s^l} \cdot \frac{n^{z_k + z_j}}{n_i^{z_l}}. \end{aligned} \quad (3.96)$$

Similarly, the continuity equation for the interstitial impurity atoms is

$$\frac{\partial C_{M_i}}{\partial t} = \text{div} (D_{M_i} \cdot \text{grad} C_{M_i}) - \frac{\partial C_{M_s}}{\partial t} \quad (3.97)$$

for a system of neutral impurities only. Including charge states, the total concentration of interstitial impurity atoms $C_{M_i} = \sum_k C_{M_i^k}$ is given by

$$\frac{\partial C_{M_i}}{\partial t} = \text{div} \left(\sum_k \left(\delta_{M_i^k} \cdot D_{M_i^k} \cdot \left(\frac{n}{n_i} \right)^{z_k} \right) \cdot \text{grad} \left(\frac{C_{M_i}}{\sum_k \delta_{M_i^k} \cdot \left(\frac{n}{n_i} \right)^{z_k}} \right) \right) - \frac{\partial C_{M_s}}{\partial t}. \quad (3.98)$$

In addition to the Frank-Turnbull reaction (3.93), bulk recombination and reactions of the vacancies with extended defects (cf. Section 2.7) have to be included. Introducing the effective vacancy diffusion coefficient via (2.54), the effective charge state via (2.55), bulk recombination in the form (2.74), and reactions with sinks from (2.92) leads to a continuity equation for the total vacancy concentration $C_V = \sum_j C_{Vj}$

$$\begin{aligned} \frac{\partial C_V}{\partial t} &= \text{div} (D_V \cdot (\text{grad} C_V - z_V \cdot C_V \cdot \text{grad}(\psi/U_T))) \\ &\quad - \frac{\partial C_{M_s}}{\partial t} - k_B \cdot (C_I \cdot C_V - C_I^{eq} \cdot C_V^{eq}) - k_{BV} \cdot (C_V - C_V^*). \end{aligned} \quad (3.99)$$

The continuity equation for vacancies has to be complemented by a similar continuity equation for self-interstitials, but without the time derivative of the substitutional impurity atoms. This term results solely from the Frank-Turnbull reaction and appears with different signs also in the continuity equations of the interstitial metal ions and the vacancies since, when the number of interstitial impurity atoms increases by one, the number of vacancies increases also by one while the number of substitutional impurity atom reduces by one.

3.5.2 Discussion of Special Cases

Since metal-diffusion experiments are nearly exclusively carried out in intrinsically doped wafers, the discussion of diffusion phenomena will be restricted in the following to intrinsic conditions. The set of equations above can be simplified for some special assumptions to demonstrate the general diffusion behavior [3.43]. After an initial, transient phase, the Frank-Turnbull reaction can be considered to be in steady state. This leads to

$$\frac{C_{M_i} \cdot C_V}{C_{M_s}} = \frac{C_{M_i}^{eq} \cdot C_V^{eq}}{C_{M_s}^{eq}} = \frac{\sum_k \delta_{M_i^k} \cdot \sum_j \delta_{Vj} \cdot \sum_{j,k,l} k_{\leftarrow}^{jkl} \cdot \delta_{M_i^l} \cdot n_i^{z_k + z_j - z_l}}{\sum_l \delta_{M_i^l} \cdot \sum_{j,k,l} k_{\rightarrow}^{jkl} \cdot \delta_{M_i^k} \cdot \delta_{Vj}}. \quad (3.100)$$

When the density of vacancy sources is very high, the concentration of vacancies can be assumed to correspond to C_V^* which should be near the equilibrium value of vacancies. Adding (3.96) and (3.98), and substituting the concentration of interstitial impurity atoms from (3.100) leads to

$$\frac{\partial C_M}{\partial t} = \frac{\partial C_{M_i} + C_{M_s}}{\partial t} = \text{div} \left(\frac{\sum_k \delta_{M_i^k} \cdot D_{M_i^k}}{\sum_k \delta_{M_i^k}} \cdot \frac{C_{M_i}^{eq}}{C_M^{eq}} \cdot \text{grad} C_M \right). \quad (3.101)$$

This diffusion equation is characterized by a concentration-independent effective diffusion coefficient. The fraction of the two sums is the effective diffusion coefficient of the interstitial impurities. The second term is the relative concentration of interstitial impurities with respect to the total concentration. It should be noted that from such experiments only the product can be extracted.

In samples in which the vacancy sources are not sufficient to maintain the vacancy concentration at a constant value, the interstitial impurity atoms will rapidly penetrate the sample because of their much higher transport capacity in comparison to vacancies. Their concentration can then be considered constant within the sample and equal to the equilibrium concentration $C_{M_i}^{eq}$. An important special case results then from the assumption that bulk recombination of vacancies can be neglected. This situation results in a continuity equation for the substitutional metal impurities in the form

$$\frac{\partial C_{M_s}}{\partial t} = \text{div} \left(\frac{D_V \cdot C_V^{eq}}{C_{M_s}^{eq} + C_V^{eq}} \cdot \text{grad } C_{M_s} \right) - k_{BV} \cdot \frac{C_V^{eq}}{C_{M_s}^{eq} + C_V^{eq}} \cdot (C_{M_s} - C_{M_s}^*) . \quad (3.102)$$

It can be seen that the apparent diffusion coefficient is proportional to the self-diffusion coefficient of vacancies. Therefore, gold and platinum experiments have been used to determine self-diffusion coefficients via vacancies. The concentration of substitutional impurity atoms in steady state $C_{M_s}^*$ does not directly correspond to the equilibrium concentration $C_{M_s}^{eq}$ since, as discussed in Section 2.7, the vacancy concentration in local equilibrium with recombination centers corresponds to C_V^* rather than to the vacancy equilibrium concentration. For sufficiently large extended defects like dislocation networks, on the other hand, C_V^* will be very close to the equilibrium concentration and only insignificant differences between $C_{M_s}^*$ and $C_{M_s}^{eq}$ are expected.

Of special importance for an identification of the diffusion mechanism of gold, platinum, or similarly diffusing impurities is the increase of the substitutional concentration in the middle of the wafer. Based on the finding that experimental profiles show a plateau in this area ($\partial^2 C_{M_s} / \partial x^2 \approx 0$), Gösele et al. [3.43] suggested a reduction of (3.102) to the ordinary differential equation

$$\frac{\partial C_{M_s}}{\partial t} = -k_{BV} \cdot \frac{C_V^{eq}}{C_{M_s}^{eq} + C_V^{eq}} \cdot (C_{M_s} - C_{M_s}^*) \quad (3.103)$$

with the solution

$$C_{M_s} = C_{M_s}^* + (C_{M_s}^0 - C_{M_s}^*) \cdot \exp \left(-\frac{k_{BV} \cdot C_V^{eq}}{C_{M_s}^{eq} + C_V^{eq}} \cdot t \right) . \quad (3.104)$$

The initial condition for (3.102) and (3.103) results from the initial concentration of the vacancies. In a wafer, prior to gold or platinum diffusion, the concentration of impurity atoms on substitutional sites is zero, the concentration of vacancies is denoted by C_V^0 . As mentioned, the interstitial impurity atoms are assumed to diffuse so rapidly that their concentration is soon close to their equilibrium concentration. According to the Frank-Turnbull reaction, the number of vacancies is reduced by $C_{M_s}^0$ when $C_{M_s}^0$ interstitial impurity atoms are placed on substitutional sites. This placement on substitutional sites continues until (3.100) is satisfied. Any further changes in the concentration of substitutional impurity atoms results from the much slower transport of vacancies from the surface to the bulk. Thus, the point of time at which steady state is established is the origin of the time scale for the equations (3.102) and (3.103) which assume steady state to be established from the beginning. The initial condition for the substitutional impurity atoms is, therefore, given by

$$C_{M_s}^0 = C_V^0 \cdot \frac{C_{M_s}^{eq}}{C_{M_s}^{eq} + C_V^{eq}} \approx C_V^0 . \quad (3.105)$$

This situation is depicted in Figure 3.10. It represents a full simulation of the Frank-Turnbull mechanism (3.96)-(3.99) for an initial vacancy concentration of 10^{11} cm^{-3} and a temperature of 730°C . The parameters were taken from the publication of Jacob et al. [3.88] with k_B and k_{BV} assumed to be zero. After about 10 seconds, the concentration in the middle of the wafer is already more than 85% of the vacancy concentration. For longer diffusion times, the platinum profile can be described well by error functions.

Based on (3.105), Zimmermann and Ryssel [3.89] proposed a method to measure the initial concentration of vacancies as well as to determine their equilibrium concentration. A combination with lifetime measurements allowed later even a mapping of the distribution of vacancies in a whole wafer. An extensive review of the method was published by Zimmermann [3.90]. The characterization of vacancies via the diffusion of platinum was optimized then by Jacob et al. [3.88] who applied it to as-grown and processed silicon wafers (see also Section 2.9). A variant of the method is the “gold labeling technique” developed by Venezia et al. [3.91] to characterize the concentration of vacancies in the surface-near part of implanted samples.

A third important case results from the assumption that the recombination of vacancies with self-interstitials is also fast in comparison to concentration changes caused by the diffusion of the two so that they are in local equilibrium. Combining the respective equations leads to

$$\begin{aligned}
 \frac{\partial(C_V + C_{M_s} - C_I)}{\partial t} &= \left(1 + \frac{C_V^{eq}}{C_{M_s}^{eq}} + \frac{C_I^{eq} \cdot C_{M_s}^{eq}}{C_{M_s}^2}\right) \cdot \frac{\partial C_{M_s}}{\partial t} \\
 &= \operatorname{div}(D_V \cdot \operatorname{grad} C_V - D_I \cdot \operatorname{grad} C_I) \\
 &\quad - k_{BV} \cdot (C_V - C_V^*) + k_{BI} \cdot (C_I - C_I^*) \\
 &= \operatorname{div} \left(\frac{D_V \cdot C_V^{eq}}{C_{M_s}^{eq}} + \frac{C_{M_s}^{eq} \cdot D_I \cdot C_I^{eq}}{C_{M_s}^2} \right) \cdot \operatorname{grad} C_{M_s} \\
 &\quad - \left(k_{BV} \cdot \frac{C_V^{eq}}{C_{M_s}^{eq}} + k_{BI} \cdot \frac{C_I^{eq} \cdot C_{M_s}^{eq}}{C_{M_s} \cdot C_{M_s}^*} \right) \cdot (C_{M_s} - C_{M_s}^*) \quad (3.106)
 \end{aligned}$$

This diffusion equation is identical to that obtained later for the kick-out mechanism under analogue assumptions (cf. Section 3.6). This means that it cannot be distinguished in this situation whether steady state between the interstitial and substitutional impurity atoms is established by the Frank-Turnbull or the kick-out reaction [3.92, 3.93]. Differentiating between the two mechanisms makes only sense and is only possible for sufficiently low temperatures and short process times for which the recombination between self-interstitials and vacancies is not effective. Figure 3.11 shows a comparison of simulations of the diffusion of gold at 900°C for 1 h under various assumptions on the diffusion mechanism. The diffusion coefficients and equilibrium concentrations for these simulations were taken from the work of Zimmermann and Ryssel [3.94] and the reaction constants from the theory of diffusion-limited reactions (1.149) with a reaction radius of 2 nm. The efficient bulk recombination, when taken into consideration, leads, as expected, to virtually the same profiles, independent of the mechanism. The differences between simulations assuming the kick-out mechanism alone and including bulk recombination result from the initial concentration of the vacancies which was set to $2 \cdot 10^{14} \text{ cm}^{-3}$. With a vanishing value, the curves overlap.

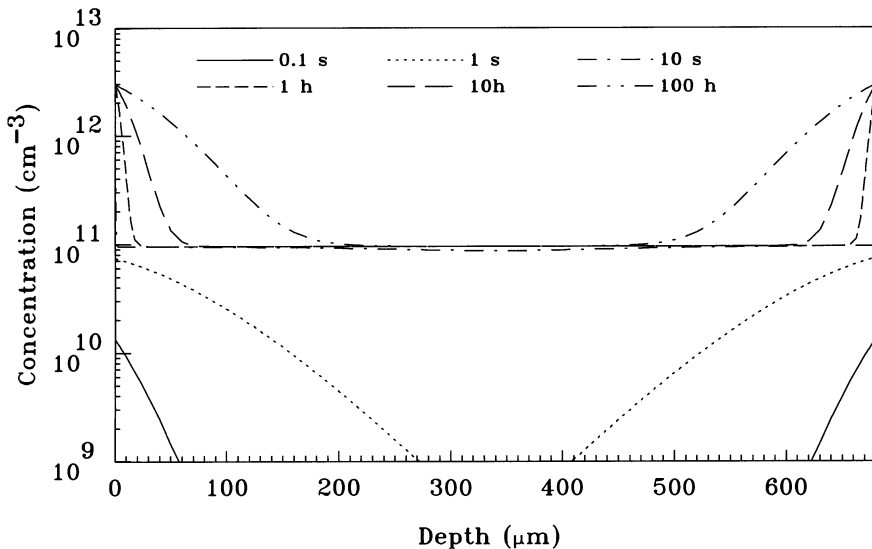


Figure 3.10: Diffusion of platinum via the Frank-Turnbull mechanism at 730 °C computed for an initial vacancy concentration of 10^{11} cm^{-3} .

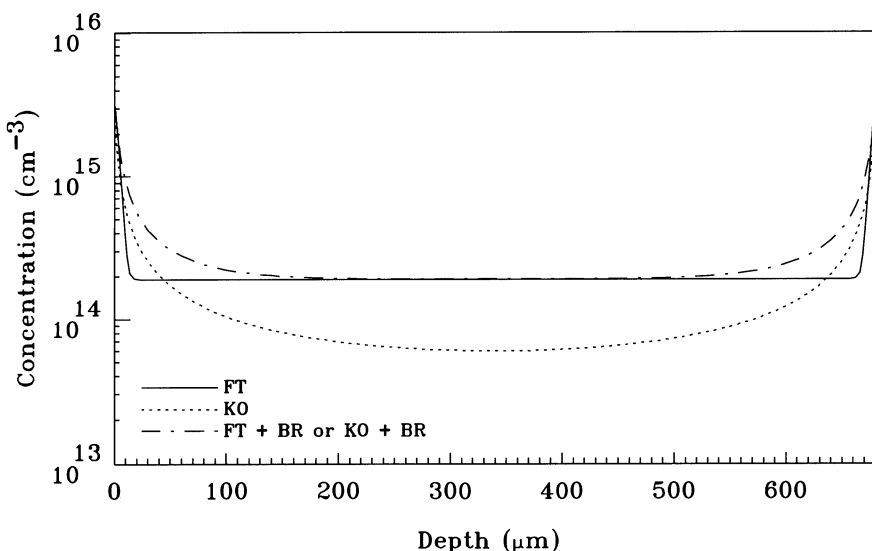


Figure 3.11: Simulation of the diffusion of gold at 900 °C for 1 h with an initial vacancy concentration of $2 \cdot 10^{14} \text{ cm}^{-3}$. Compared are simulations of diffusion via the Frank-Turnbull mechanism (FT), the kick-out mechanism (KO), and of the two mechanisms in combination with bulk recombination (BR).

When bulk recombination is sufficiently rapid, also the initial conditions (3.105) are affected. Starting from a vanishing concentration of substitutional impurities and point-defect concentrations C_V^0 and C_I^0 , for each impurity atom on substitutional sites either the concentration of self-interstitials increases or the vacancy concentration decreases. When both, the Frank-Turnbull reaction and the bulk recombination process are in equilibrium, the substitutional concentration of impurity atoms is given by

$$C_{M_s}^0 = \frac{1}{2} \cdot C_{M_s}^{eq} \cdot \frac{C_V^0 - C_I^0 + \sqrt{(C_V^0 - C_I^0)^2 + 4 \cdot C_I^{eq} \cdot (C_V^{eq} + C_{M_s}^{eq})}}{C_V^{eq} + C_{M_s}^{eq}}. \quad (3.107)$$

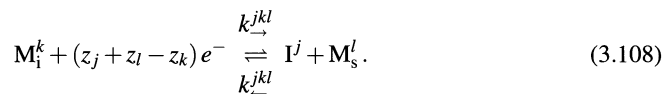
In the limit of very high initial vacancy concentrations, one obtains again (3.105) whereas in case of very high concentrations of self-interstitials, the initial concentration of substitutional platinum atoms will approach zero.

3.6 Kick-Out Mechanism

Because the typical U-shaped diffusion profiles of gold in silicon (see Figure 3.11) could not be explained sufficiently well by the Frank-Turnbull mechanism alone, Gösele et al. [3.43] proposed an alternative way for an interstitial atom to become substitutional. The model assumes that an interstitial impurity atom M_i generates a self-interstitial I in the course of occupying a substitutional site M_s . This corresponds to the backward reaction of the pair-formation reaction with a self-interstitial in (3.20). Following the traditional notation of metal diffusion in silicon, the mobile complex is denoted M_i and the reaction $M_i \rightarrow M_s + I$ is considered here the forward reaction. In addition, in contrast to impurity diffusion, the reference point for substitutional metals is here the neutral charge state.

3.6.1 Derivation of the Diffusion-Reaction Equations

All three point defects M_i , I , and M_s can exist in several charge states denoted by k , j , and l with z_k , z_j , and z_l standing for the numbers of electron charges associated. Each of the reactions can be written as



The symbol e^- stands for the electrons involved in the reaction. In this form, the backward reaction constant can be estimated from diffusion-limited reaction kinetics. Therefore, the electrons needed for charge conservation during the reaction were written at the left-hand side. As in the previous section, the charge states of the defects are assumed to be in local equilibrium. The concentrations of charged species can then be written in analogy to (3.94) with V replaced by I .

In a system of neutral point defects only, the continuity equation of the concentration of substitutional impurities reads simply

$$\frac{\partial C_{M_s}}{\partial t} = k_{\rightarrow} \cdot C_{M_i} - k_{\leftarrow} \cdot C_I \cdot C_{M_s}. \quad (3.109)$$

Including charge states, the continuity equation of the total concentration of impurities at substitutional sites $C_{M_s} = \sum_l C_{M_s}^l$ takes the somewhat more complicated form

$$\begin{aligned}\frac{\partial C_{M_s}}{\partial t} &= \frac{C_{M_i}}{\sum_k \delta_{M_i^k} \cdot \left(\frac{n}{n_i}\right)^{z_k}} \cdot \sum_{j,k,l} k_{\rightarrow}^{jkl} \cdot \delta_{M_i^k} \cdot \frac{n_i^{z_j+z_l}}{n_i^{z_k}} \\ &\quad - \frac{C_I}{\sum_j \delta_{I^{ij}} \cdot \left(\frac{n}{n_i}\right)^{z_j}} \cdot \frac{C_{M_s}}{\sum_l \delta_{M_s^l} \cdot \left(\frac{n}{n_i}\right)^{z_l}} \cdot \sum_{j,k,l} k_{\leftarrow}^{jkl} \cdot \delta_{I^{ij}} \cdot \delta_{M_s^l} \cdot \left(\frac{n}{n_i}\right)^{z_j+z_l}. \quad (3.110)\end{aligned}$$

In analogy, the continuity equation for the total concentration of interstitial impurity atoms $C_{M_i} = \sum_k C_{M_i^k}$ can be derived by adding all contributions from the various reactions. It takes again the form (3.98) already derived for the Frank-Turnbull process. The last continuity equation to be derived is that of the self-interstitials. As in case of the Frank-Turnbull mechanism, bulk recombination of vacancies and self-interstitials and reactions of self-interstitials with extended defects (cf. Section 2.7) have to be included. Introducing the effective self-interstitial diffusion coefficient via (2.54), the effective charge state via (2.55), bulk recombination in the form (2.74), and reactions with sinks from (2.92), the continuity equation for the total concentration of the self-interstitials $C_I = \sum_j C_{I^{ij}}$ results as

$$\begin{aligned}\frac{\partial C_I}{\partial t} &= \text{div}(D_I \cdot (\text{grad}C_I - z_I \cdot C_I \cdot \text{grad}(\psi/U_T))) \\ &\quad + \frac{\partial C_{M_s}}{\partial t} - k_B \cdot (C_I \cdot C_V - C_I^{eq} \cdot C_V^{eq}) - k_{BI} \cdot (C_I - C_I^*) \quad (3.111)\end{aligned}$$

In addition, to complete the system, a continuity equation for the vacancies has to be provided. It is of the same structure as the continuity equation for the self-interstitials, but without the time derivative of the substitutional impurity concentration.

3.6.2 Discussion of Special Cases

As in the discussion of the Frank-Turnbull mechanism in Section 3.5.2, intrinsic conditions will be assumed since metal-diffusion experiments were carried out nearly exclusively in intrinsically doped samples. To demonstrate the general behavior of the system, the system of coupled partial differential equation has to be simplified. A first assumption [3.43] is that the reactions involving interstitial and substitutional impurity atoms and self-interstitials are fast compared to their diffusion. Then, local equilibrium between the concentration of interstitial impurity atoms, substitutional impurity atoms, and the total concentration of self-interstitials can be assumed to result in

$$\frac{C_{M_i}}{C_I \cdot C_{M_s}} = \frac{C_{M_i}^{eq}}{C_I^{eq} \cdot C_{M_s}^{eq}} = \frac{\sum_k \delta_{M_i^k} \cdot \sum_{j,k,l} k_{\leftarrow}^{jkl} \cdot \delta_{I^{ij}} \cdot \delta_{M_s^l}}{\sum_j \delta_{I^{ij}} \cdot \sum_l \delta_{M_s^l} \cdot \sum_{j,k,l} k_{\rightarrow}^{jkl} \cdot \delta_{M_i^k} \cdot n_i^{z_j+z_l-z_k}}. \quad (3.112)$$

When the density of interstitial sources is very high, the concentration of self-interstitials can be assumed to be equal to C_I^* which should be close to the equilibrium value. By adding (3.110) and (3.98), and by substituting the interstitial impurity concentration from (3.112) with $C_I = C_I^{eq}$, one obtains again (3.101). The diffusion behavior in materials with a high defect density is, therefore, identical to that obtained from the Frank-Turnbull mechanism for similar conditions (cf. Section 3.5).

An other important case follows from the assumption that the concentration of sinks for self-interstitials is not high enough to maintain the concentration of self-interstitials at a constant value, that recombination between self-interstitials and vacancies is negligible, and that the diffusion of interstitial metal atoms is very fast in comparison to the diffusion of self-interstitials. The concentration of interstitial impurity atoms can then be considered constant and equal to its equilibrium value C_I^{eq} . In addition, Gösele et al. [3.43] have shown that the concentration of substitutional impurity atoms for all cases of interest is higher than $C_{M_s} \gg \sqrt{C_I^{eq} \cdot C_{M_s}^{eq}}$. One obtains then a continuity equation for the substitutional metal-impurities from (3.111) in the form

$$\frac{\partial C_{M_s}}{\partial t} = \text{div} \left(\frac{C_{M_s}^{eq} \cdot D_I \cdot C_I^{eq}}{C_{M_s}^2} \cdot \text{grad} C_{M_s} \right) + k_{BI} \cdot C_I^{eq} \cdot \left(\frac{C_{M_s}^{eq}}{C_{M_s}} - \frac{C_I^*}{C_I^{eq}} \right) \quad (3.113)$$

in which the apparent diffusion coefficient is proportional to the self-diffusion coefficient of the self-interstitials. Accordingly, metal diffusion experiments have been used frequently to extract self-diffusion coefficients via self-interstitials.

To identify the mechanism responsible for the change of an interstitial impurity to a substitutional site, the increase in the middle of the wafer is usually taken as a criterion. In case of the Frank-Turnbull process, an exponential increase with time is expected from (3.104). Based on the observation that experimental profiles show a plateau in the middle of the wafer ($\partial^2 C_{M_s} / \partial x^2 \approx 0$) and on the assumption $C_I^* \approx C_I^{eq}$, Gösele et al. [3.43] suggested a reduction of (3.113) to the ordinary differential equation

$$\frac{\partial C_{M_s}}{\partial t} = k_{BI} \cdot C_I^{eq} \cdot \left(\frac{C_{M_s}^{eq}}{C_{M_s}} - 1 \right) \quad (3.114)$$

for the concentration of the plateau. It has the solution

$$C_{M_s}^{eq} \cdot \ln \left(\frac{C_{M_s}^{eq} - C_{M_s}}{C_{M_s}^{eq} - C_{M_s}^0} \right) + C_{M_s} - C_{M_s}^0 + k_{BI} \cdot C_I^{eq} \cdot t = 0 \quad (3.115)$$

with $C_{M_s}^0$ standing for the initial concentration of substitutional metal atoms. For short times where $C_{M_s} \ll C_{M_s}^{eq}$, the solution can be approximated by the more convenient form

$$C_{M_s} = \sqrt{(C_{M_s}^0)^2 + 2 \cdot k_{BI} \cdot C_{M_s}^{eq} \cdot C_I^{eq} \cdot t}. \quad (3.116)$$

Given a sink-rate constant in the form (2.95), the concentration of substitutional atoms is expected to increase with the square root of the number of dislocations per unit area C_D . This behavior was indeed found experimentally [3.95].

The initial condition for (3.113) and (3.116) results from the initial concentration of self-interstitials. Prior to metal diffusion, the substitutional concentration of impurities is virtually zero while the interstitial impurity atoms are assumed to diffuse so rapidly that they are in equilibrium on a shorter time scale than the other phenomena. By the kick-out reaction (3.108), the number of self-interstitials is increased by $C_{M_s}^0$ when $C_{M_s}^0$ interstitial impurity atoms are placed on substitutional sites. Incorporation of metal atoms on substitutional sites continues until local equilibrium according to (3.112) is satisfied. This point of time is then the origin of the time scale for (3.113) and (3.116) which assume equilibrium to be established already from the beginning. The initial condition for the substitutional impurity atoms is then given by

$$C_{M_s}^0 = \sqrt{(C_I^0/2)^2 + C_{M_s}^{eq} \cdot C_I^{eq}} - C_I^0/2. \quad (3.117)$$

Based on this relation, Zimmermann and Ryssel [3.89] proposed a method to evaluate the concentration of self-interstitials prior to metal diffusion as well as their equilibrium concentration. But to put the concept into practice seems to be much more complicated here than in case of the Frank-Turnbull mechanism.

When the concentration of sinks for self-interstitials is very low, as it can be expected for commercial wafers, the increase of the metal concentration in a depth of the half wafer thickness d_w with time is determined by the diffusion of the self-interstitials. The respective diffusion equation can be solved approximately and Gösele et al. [3.43] have shown that this approximate solution increases for negligible initial concentration again with the square root of time

$$C_{M_s} \approx \frac{2}{d_w} \cdot \sqrt{\pi \cdot C_{M_s}^{eq} \cdot D_I \cdot C_I^{eq} \cdot t}. \quad (3.118)$$

When bulk recombination between self-interstitials and vacancies is assumed to be fast compared to the diffusion processes, local equilibrium between self-interstitials and vacancies can be assumed. Combining the continuity equations for substitutional impurity atoms, self-interstitials, and vacancies leads again to (3.106). As already stated, a differentiation between the two mechanisms makes only sense and is only possible for temperatures and process times for which the recombination between self-interstitials and vacancies is not effective.

Bibliography

- [3.1] C. Wert and C. Zener, "Interstitial Atomic Diffusion Coefficients," *Phys. Rev.*, vol. 76, no. 8, 1169–1175 (1949).
- [3.2] K. Weiser, "Theory of Diffusion and Equilibrium Position of Interstitial Impurities in the Diamond Lattice," *Phys. Rev.*, vol. 126, no. 4, 1427–1436 (1962).
- [3.3] R. A. Swalin, "Diffusion of Interstitial Impurities in Germanium and Silicon," *J. Phys. Chem. Solids*, vol. 23, 154–155 (1962).
- [3.4] H. B. Huntington and F. Seitz, "Mechanism for Self-Diffusion in Metallic Copper," *Phys. Rev.*, vol. 61, 315–325 (1942).
- [3.5] H. B. Huntington and F. Seitz, "Energy for Diffusion by Direct Interchange," *Phys. Rev.*, vol. 76, no. 11, 1728 (1949).
- [3.6] C. Zener, "Ring Diffusion in Metals," *Acta Cryst.*, vol. 3, 346–354 (1950).
- [3.7] M. F. Millea, "The Effect of Heavy Doping on the Diffusion of Impurities in Silicon," *J. Phys. Chem. Solids*, vol. 27, 315–325 (1966).
- [3.8] S. M. Hu, "Diffusion in Silicon and Germanium," in: *Atomic Diffusion in Semiconductors*, edited by D. Shaw, London: Plenum Press, 217–350 (1973).
- [3.9] K. C. Pandey, "Diffusion without Vacancies or Interstitials: A New Concerted Exchange Mechanism," *Phys. Rev. Lett.*, vol. 57, no. 18, 2287–2290 (1986).
- [3.10] J. Steigman, W. Shockley, and F. C. Nix, "The Self-Diffusion of Copper," *Phys. Rev.*, vol. 56, 13–21 (1939).
- [3.11] R. P. Johnson, "A Note on the Hole Theory of Diffusion," *Phys. Rev.*, vol. 56, 814–818 (1939).
- [3.12] S. List and H. Ryssel, "Atomistic Analysis of the Vacancy Mechanism of Impurity Diffusion in Silicon," *J. Appl. Phys.*, vol. 83, no. 12, 7585–7594 (1998).
- [3.13] J. Bardeen, "Diffusion in Binary Alloys," *Phys. Rev.*, vol. 76, no. 9, 1403–1405 (1949).
- [3.14] A. D. LeClaire and A. B. Lidiard, "Correlation Effects in Diffusion in Crystals," *Phil. Mag.*, vol. 1, 518–527 (1956).
- [3.15] J. R. Manning, "Correlation Factors for Impurity Diffusion. bcc, Diamond, and fcc Structures," *Phys. Rev.*, vol. 136, no. 6A, A1758–A1766 (1964).

- [3.16] S. M. Hu, "Correlation Factor of Impurity Diffusion in Diamond Lattice," *Phys. Rev.*, vol. 177, no. 3, 1334–1340 (1969).
- [3.17] M. Koiwa and S. Ishioka, "Integral Methods in the Calculation of Correlation Factors for Impurity Diffusion," *Phil. Mag. A*, vol. 47, no. 6, 927–938 (1983).
- [3.18] H. Mehrer, "Correlation Factor for the Diffusion of Charged Impurities in the Diamond Structure," *Z. Naturforsch.*, vol. 26a, 308–316 (1971).
- [3.19] M. Yoshida, "Diffusion of Group V Impurity in Silicon," *Jpn. J. Appl. Phys.*, vol. 10, no. 6, 702–713 (1971).
- [3.20] S. M. Hu, "On Interaction Potential, Correlation Factor, Vacancy Mobility, and Activation Energy of Impurity Diffusion in Diamond Lattice," *phys. stat. sol. (b)*, vol. 60, 595–603 (1973).
- [3.21] S. T. Dunham and C. D. Wu, "Atomistic Models of Vacancy-Mediated Diffusion in Silicon," *J. Appl. Phys.*, vol. 78, no. 4, 2362–2366 (1995).
- [3.22] F. Seitz, "On the Theory of Diffusion in Metals," *Acta Cryst.*, vol. 3, 355–363 (1950).
- [3.23] S. M. Hu, "General Theory of Impurity Diffusion in Semiconductors via the Vacancy Mechanism," *Phys. Rev.*, vol. 180, no. 3, 773–784 (1969).
- [3.24] V. A. Uskov and V. V. Vas'kin, "Effect of Nonuniform Vacancy Distribution on Diffusion of Impurities in Semiconductors," *Inorganic Materials*, vol. 8, no. 10, 1617–1618 (1972).
- [3.25] M. Kurata, Y. Morikawa, K. Nagami, and H. Kuroda, "Remarks on the Vacancy Mechanisms in Ion Implantation," *Jpn. J. Appl. Phys.*, vol. 12, no. 3, 472–473 (1973).
- [3.26] Y. Morikawa, K. Yamamoto, and K. Nagami, "Uphill Diffusion Mechanism in Proton-Irradiated Silicon," *Appl. Phys. Lett.*, vol. 36, no. 12, 997–999 (1980).
- [3.27] V. V. Kozlovskii, V. N. Lomasov, and N. V. Marushchak, "Diffusion of a Substitutional Impurity in a Crystal Irradiated with Ions," *Sov. Phys. Tech. Phys.*, vol. 30, no. 11, 1283–1285 (1985).
- [3.28] O. V. Aleksandrov, V. V. Kozlovskii, V. V. Popov, and B. E. Samorukov, "Diffusion of Impurities from Implanted Silicon Layers by Rapid Thermal Annealing," *phys. stat. sol. (a)*, vol. 110, K61–K65 (1988).
- [3.29] K. Maser, "Die Rolle der Überkreuz-Komponenten beim Dotandentransport im Festkörper," *Experimentelle Technik der Physik*, vol. 39, no. 2, 169–180 (1991).
- [3.30] S. T. Dunham and C. D. Wu, "Lattice Monte-Carlo Simulations of Vacancy-Mediated Diffusion and Implications for Continuum Models of Coupled Diffusion," in: *Simulation of Semiconductor Devices and Processes, Vol. 6*, edited by H. Ryssel and P. Pichler, Vienna: Springer-Verlag, 476–479 (1995).
- [3.31] M. M. Bunea and S. T. Dunham, "Lattice Monte Carlo Simulations of Vacancy-Mediated Diffusion and Aggregation Using Ab-Initio Parameters," in: *Defects and Diffusion in Silicon Processing*, edited by T. Diaz de la Rubia, S. Coffa, P. A. Stolk, and C. S. Rafferty, *Mat. Res. Soc. Symp. Proc.*, vol. 469, 353–358 (1997).
- [3.32] O. Pankratov, H. Huang, T. Diaz de la Rubia, and C. Mailhot, "As-Vacancy Interaction and Ring Mechanism of Diffusion in Si," *Phys. Rev. B*, vol. 56, no. 20, 13172–13176 (1997).
- [3.33] M. M. Bunea and S. T. Dunham, "Monte Carlo Study of Vacancy-Mediated Impurity Diffusion in Silicon," *Phys. Rev. B*, vol. 61, no. 4, R2397–R2400 (2000).
- [3.34] J. S. Nelson, P. A. Schultz, and A. F. Wright, "Valence and Atomic Size Dependent Exchange Barriers in Vacancy-Mediated Dopant Diffusion," *Appl. Phys. Lett.*, vol. 73, no. 2, 247–249 (1998).
- [3.35] P. Baruch, "Radiation Defects and Impurity Diffusion in Silicon," in: *Radiation Effects in Semiconductors, 1976*, edited by N. B. Urli and J. W. Corbett, *Inst. Phys. Conf. Ser.*, no. 31, 126–143 (1977).
- [3.36] V. V. Kozlovskii, V. N. Lomasov, G. M. Gur'yanov, and A. P. Kovarskii, "Proton-Stimulated Diffusion of Antimony in Silicon," *Sov. Phys. Semicond.*, vol. 18, no. 5, 598–599 (1984).
- [3.37] P. Pichler, R. Schork, T. Klauser, and H. Ryssel, "Direct Experimental Evidence for Diffusion of Dopants via Pairs with Intrinsic Point Defects," *Appl. Phys. Lett.*, vol. 60, no. 8, 953–955 (1992).

- [3.38] M. D. Giles, "Transient Phosphorus Diffusion from Silicon and Argon Implantation Damage," *Appl. Phys. Lett.*, vol. 62, no. 16, 1940–1942 (1993).
- [3.39] F. C. Frank and D. Turnbull, "Mechanism of Diffusion of Copper in Germanium," *Phys. Rev.*, vol. 104, no. 3, 617–618 (1956).
- [3.40] R. L. Longini, "Rapid Zinc Diffusion in Gallium Arsenide," *Solid-State Electronics*, vol. 5, 127–130 (1962).
- [3.41] A. Seeger and K. P. Chik, "Diffusion Mechanism and Point Defects in Silicon and Germanium," *phys. stat. sol.*, vol. 29, 455–542 (1968).
- [3.42] G. D. Watkins, "A Review of EPR Studies in Irradiated Silicon," in: *Radiation Damage in Semiconductors*, Paris: Dunod, 97–113 (1964).
- [3.43] U. Gösele, W. Frank, and A. Seeger, "Mechanism and Kinetics of the Diffusion of Gold in Silicon," *Appl. Phys.*, vol. 23, 361–368 (1980).
- [3.44] U. Schmid, J. A. Van Vechten, N. C. Myers, and U. Koch, "Failure of the "Kick-Out" Model for the Diffusion of Au into Si When Tested by Monte-Carlo Simulation," in: *Impurities, Defects and Diffusion in Semiconductors: Bulk and Layered Structures*, edited by D. J. Wolford, J. Bernholc, and E. E. Haller, *Mat. Res. Soc. Symp. Proc.*, vol. 163, 609–614 (1990).
- [3.45] D. Mathiot, "Gold, Self-, and Dopant Diffusion in Silicon," *Phys. Rev. B*, vol. 45, no. 23, 13345–13355 (1992).
- [3.46] T. K. Monson, J. A. Van Vechten, Q. S. Zhang, and R. K. Graupner, "Comment on "Gold, Self-, and Dopant Diffusion in Silicon"," *Phys. Rev. B*, vol. 49, no. 4, 2972–2976 (1994).
- [3.47] S. M. Hu, "Vacancies and Self-Interstitials in Silicon," in: *Defects in Silicon II*, edited by W. M. Bullis, U. Gösele, and F. Shimura, *Electrochem. Soc. Proc.*, vol. 91-9, 211–236 (1991).
- [3.48] A. B. Lidiard, "The Influence of Solutes on Self-Diffusion in Metals," *Phil. Mag.*, vol. 5, no. 59, 1171–1180 (1960).
- [3.49] M. Yoshida, E. Arai, H. Nakamura, and Y. Terunuma, "Excess Vacancy Generation Mechanisms at Phosphorus Diffusion into Silicon," *J. Appl. Phys.*, vol. 45, no. 4, 1498–1506 (1974).
- [3.50] W. B. Richardson and B. J. Mulvaney, "Nonequilibrium Behaviour of Charged Point Defects during Phosphorus Diffusion in Silicon," *J. Appl. Phys.*, vol. 65, no. 6, 2243–2247 (1989).
- [3.51] N. E. B. Cowern, "General Model for Intrinsic Dopant Diffusion in Silicon under Nonequilibrium Point-Defect Conditions," *J. Appl. Phys.*, vol. 64, no. 9, 4484–4490 (1988).
- [3.52] B. P. R. Marioton, U. Gösele, and T. Y. Tan, "Are Self-Interstitials Required to Explain Non-Equilibrium Diffusion Phenomena in Silicon?" *Chemtronics*, vol. 1, 156–160 (1986).
- [3.53] S. Loualiche, C. Lucas, P. Baruch, J. P. Gailliard, and J. C. Pfister, "Theoretical Model for Radiation Enhanced Diffusion and Redistribution of Impurities," *phys. stat. sol. (a)*, vol. 69, 663–676 (1982).
- [3.54] D. Mathiot and J. C. Pfister, "Dopant Diffusion in Silicon: A Consistent View Involving Nonequilibrium Defects," *J. Appl. Phys.*, vol. 55, no. 10, 3518–3530 (1984).
- [3.55] P. Fahey, G. Barbucia, M. Moslehi, and R. W. Dutton, "Kinetics of Thermal Nitridation Processes in the Study of Dopant Diffusion Mechanisms in Silicon," *Appl. Phys. Lett.*, vol. 46, no. 8, 784–786 (1985).
- [3.56] Z. M. Ling, *Silicon Oxidation: Modelling, Characterization and Strategic Considerations*, Ph.D. thesis, Katholieke Universiteit Leuven (1989).
- [3.57] S. T. Dunham and J. D. Plummer, "Point-Defect Generation during Oxidation of Silicon in Dry Oxygen. II. Comparison to Experiment," *J. Appl. Phys.*, vol. 59, no. 7, 2551–2561 (1986).
- [3.58] R. Falster and V. V. Voronkov, "Intrinsic Point Defects and Their Control in Silicon Crystal Growth and Wafer Processing," *MRS Bulletin*, vol. 25, no. 6, 28–32 (2000).
- [3.59] R. Falster, Private communication (2003).
- [3.60] W. Lerch, M. Glück, N. A. Stolwijk, H. Walk, M. Schäfer, S. D. Marcus, D. F. Downey, and J. W. Chow, "Boron Ultrashallow Junction Formation in Silicon by Low-Energy Implantation and Rapid Thermal Annealing in Inert and Oxidizing Ambient," *J. Electrochem. Soc.*, vol. 146, no. 7, 2670–2678 (1999).

- [3.61] U. Gösele and T. Y. Tan, “The Nature of Point Defects and Their Influence on Diffusion Processes in Silicon at High Temperatures,” in: *Defects in Semiconductors II*, edited by S. Mahajan and J. W. Corbett, *Mat. Res. Soc. Symp. Proc.*, vol. 14, 45–59 (1983).
- [3.62] H.-J. Gossmann, T. E. Haynes, P. A. Stolk, D. C. Jacobson, G. H. Gilmer, J. M. Poate, H. S. Luftman, T. K. Mogi, and M. O. Thompson, “The Interstitial Fraction of Diffusivity of Common Dopants in Si,” *Appl. Phys. Lett.*, vol. 71, no. 26, 3862–3864 (1997).
- [3.63] A. Ural, P. B. Griffin, and J. D. Plummer, “Fractional Contributions of Microscopic Diffusion Mechanisms for Common Dopants and Self-Diffusion in Silicon,” *J. Appl. Phys.*, vol. 85, no. 9, 6440–6446 (1999).
- [3.64] E. Vandebosch and B. Baccus, “Interactions between Dopants and Point Defects during Nitridation Processes,” *J. Appl. Phys.*, vol. 72, no. 2, 447–453 (1992).
- [3.65] M. Heinrich, M. Budil, and H. W. Pötzl, “Determination of Diffusion Parameters for Arsenic,” in: *Impurities, Defects and Diffusion in Semiconductors: Bulk and Layered Structures*, edited by D. J. Wolford, J. Bernholc, and E. E. Haller, *Mat. Res. Soc. Symp. Proc.*, vol. 163, 535–541 (1990).
- [3.66] P. Novell and M. E. Law, “The Effect of Nondilute Dopant-Defect Pair Concentrations on Arsenic Diffusion,” in: *Proceedings NUPAD IV*, New York: IEEE, 41–44 (1992).
- [3.67] F. M. Smits, “Formation of Junction Structures by Solid-State Diffusion,” *Proc. IRE*, vol. 46, 1049–1061 (1958).
- [3.68] K. Lehovec and A. Slobodskoy, “Diffusion of Charged Particles into a Semiconductor under Consideration of the Built-in Field,” *Solid-State Electronics*, vol. 3, 45–50 (1961).
- [3.69] J. Bardeen, W. H. Brattain, and W. Shockley, “Investigation of Oxidation of Copper by Use of Radioactive Cu Tracers,” *J. Chem. Phys.*, vol. 14, no. 12, 714–721 (1946).
- [3.70] W. Shockley, “Field-Enhanced Donor Diffusion in Degenerate Semiconductor Layers,” *J. Appl. Phys.*, vol. 32, no. 7, 1402–1403 (1961).
- [3.71] N. D. Thai, “Concentration-Dependent Diffusion of Boron and Phosphorus in Silicon,” *J. Appl. Phys.*, vol. 41, no. 7, 2859–2866 (1970).
- [3.72] D. Shaw, “General Features of Diffusion in Semiconductors,” in: *Atomic Diffusion in Semiconductors*, edited by D. Shaw, London: Plenum Press, 1–63 (1973).
- [3.73] S. M. Hu, “Modeling Diffusion in Silicon: Accomplishments and Challenges,” in: *VLSI Science and Technology/1985*, edited by W. M. Bullis and S. Broydo, *Electrochem. Soc. Proc.*, vol. 85-5, 465–506 (1985).
- [3.74] C. L. Jones and A. F. W. Willoughby, “The Complete Base Profile Shape in a Push-Out Diffused Transistor Analyzed by Radiotracer Methods,” *Appl. Phys. Lett.*, vol. 25, no. 2, 114–116 (1974).
- [3.75] L. Boltzmann, “Zur Integration der Diffusionsgleichung bei variablen Diffusionscoefficienten,” *Annalen der Physik und Chemie*, vol. 53, 959–964 (1894).
- [3.76] C. Matano, “On the Relation between the Diffusion-Coefficients and Concentrations of Solid Metals (The Nickel-Copper System),” *Jpn. J. Phys.*, vol. 8, no. 3, 109–113 (1933).
- [3.77] R. B. Fair and J. C. C. Tsai, “A Quantitative Model for the Diffusion of Phosphorus in Silicon and the Emitter Dip Effect,” *J. Electrochem. Soc.*, vol. 124, no. 7, 1107–1117 (1977).
- [3.78] S. M. Hu, P. Fahey, and R. W. Dutton, “On Models of Phosphorus Diffusion in Silicon,” *J. Appl. Phys.*, vol. 54, no. 12, 6912–6922 (1983).
- [3.79] W. A. OrrArienzo, R. Glang, R. F. Lever, R. K. Lewis, and F. F. Morehead, “Boron Diffusion in Silicon at High Concentrations,” *J. Appl. Phys.*, vol. 63, no. 1, 116–120 (1988).
- [3.80] I. D. Sharp, H. A. Bracht, H. H. Silvestri, S. P. Nicols, J. W. Beaman, J. L. Hansen, A. Nylandsted Larsen, and E. E. Haller, “Self- and Dopant Diffusion in Extrinsic Boron Doped Isotopically Controlled Silicon Multilayer Structures,” in: *Defect and Impurity Engineered Semiconductors and Devices III*, edited by S. Ashok, J. Chevallier, N. M. Johnson, B. L. Sopori, and H. Okushi, *Mat. Res. Soc. Symp. Proc.*, vol. 719, F13.11.1–F13.11.6 (2002).
- [3.81] H. F. Schaake, “The Diffusion of Phosphorus in Silicon from High Surface Concentrations,” *J. Appl. Phys.*, vol. 55, no. 4, 1208–1211 (1984).

- [3.82] D. Mathiot and J. C. Pfister, "Evidences That P Diffusion in Si Is Assisted Mainly by Vacancies," *Appl. Phys. Lett.*, vol. 47, no. 9, 962–964 (1985).
- [3.83] F. F. Morehead and R. F. Lever, "The Steady-State Model for Coupled Defect-Impurity Diffusion in Silicon," *J. Appl. Phys.*, vol. 66, no. 11, 5349–5352 (1989).
- [3.84] R. Dürr and P. Pichler, "A Consistent Pair-Diffusion Based Steady-State Model for Phosphorus Diffusion," in: *ESSDERC'89*, edited by A. Heuberger, H. Ryssel, and P. Lange, Berlin: Springer-Verlag, 297–301 (1989).
- [3.85] M. D. Sturge, "A Note on the Theory of Diffusion of Copper in Germanium," *Proc. Phys. Soc. (London)*, vol. 73, no. 2, 297–306 (1959).
- [3.86] W. R. Wilcox and T. J. La Chapelle, "Mechanisms of Gold Diffusion into Silicon," *J. Appl. Phys.*, vol. 35, no. 1, 240–246 (1964).
- [3.87] F. A. Huntley and A. F. W. Willoughby, "The Diffusion of Gold in Thin Silicon Slices," *Solid-State Electronics*, vol. 13, 1231–1240 (1970).
- [3.88] M. Jacob, P. Pichler, H. Ryssel, and R. Falster, "Determination of Vacancy Concentrations in the Bulk of Silicon Wafers by Platinum Diffusion Experiments," *J. Appl. Phys.*, vol. 82, no. 1, 182–191 (1997).
- [3.89] H. Zimmermann and H. Ryssel, "Direct Determination of Point-Defect Equilibrium Concentrations," *Phys. Rev. B*, vol. 44, no. 16, 9064–9067 (1991).
- [3.90] H. Zimmermann, "Vacancy Distributions in Silicon and Methods for Their Accurate Determination," in: *Diffusion in Silicon*, edited by D. J. Fisher, *Defect and Diffusion Forum*, vol. 153–155, 111–136 (1998).
- [3.91] V. C. Venezia, D. J. Eaglesham, T. E. Haynes, A. Agarwal, D. C. Jacobson, H.-J. Gossman, and F. H. Baumann, "Depth Profiling of Vacancy Clusters in MeV-Implanted Si Using Au Labeling," *Appl. Phys. Lett.*, vol. 73, no. 20, 2980–2982 (1998).
- [3.92] F. Morehead, N. A. Stolwijk, W. Meyberg, and U. Gösele, "Self-Interstitial and Vacancy Contribution to Silicon Self-Diffusion Determined from the Diffusion of Gold in Silicon," *Appl. Phys. Lett.*, vol. 42, no. 8, 690–692 (1983).
- [3.93] H. Kitagawa and M. Yoshida, "On the Distinction between the Dissociative and Kick-Out Mechanisms for Site Exchange in Silicon," *Jpn. J. Appl. Phys., Part 1*, vol. 31, no. 9A, 2859–2963 (1992).
- [3.94] H. Zimmermann and H. Ryssel, "Gold and Platinum Diffusion: The Key to the Understanding of Intrinsic Point Defect Behavior in Silicon," *Appl. Phys. A*, vol. 55, 121–134 (1992).
- [3.95] B. Pichaud, G. Mariani, W. J. Taylor, and W.-S. Yang, "Dislocation-Gold Interactions in FZ and CZ Silicon: The Role of Self-Interstitials," in: *Dislocations '93*, edited by J. Rabier, A. George, Y. Bréchet, and L. Kubin, *Solid State Phenomena*, vol. 35–36, 491–496 (1994).

Chapter 4

Isovalent Impurities

Besides silicon, group IVa of the periodic system contains also the isovalent elements carbon, germanium, tin, and lead. Carbon, the lightest of them, is an omnipresent impurity introduced often unintentionally. On the other hand, as discussed in Section 4.1, it is used for a variety of applications from stress compensation to proximity gettering. The properties of germanium in silicon are summarized in Section 4.2. Unfortunately, the space would not have sufficed for a presentation of silicon-germanium materials in general. Tin, the last isovalent impurity considered here, has already limited technical applications. However, it was studied to investigate basic diffusion processes in silicon. The main results will be presented in Section 4.3.

4.1 Carbon

Carbon is a very common impurity in silicon wafers, introduced either from the polysilicon used in crystal growth, or from contaminations during this process. Typical concentrations in silicon wafers used in VLSI technology are now below 10^{16} cm^{-3} , but can be one or two orders of magnitude higher in solar-grade silicon [4.1] and up to $2 \cdot 10^{18} \text{ cm}^{-3}$ in intentionally doped crystals [4.2]. Epitaxial deposition or solid-phase epitaxial regrowth of carbon-doped layers allows even the incorporation of carbon in a concentration on the order of 10^{21} cm^{-3} into Si and SiGe [4.3–4.7]. In addition, carbon may be introduced intentionally or unintentionally during process steps. Typical examples for the both would be ion implantation of carbon and dry etching, respectively.

Carbon, as outlined below, resides predominantly on substitutional sites in the silicon lattice. Of special importance is the reaction with silicon self-interstitials which displaces substitutional carbon atoms to interstitial sites where they are highly mobile. Carbon interstitials subsequently form a variety of complexes with intrinsic point defects, substitutional carbon, and dopants. Substitutional carbon atoms otherwise remain relatively inert and are only known to form complexes with oxygen atoms.

The formation of carbon interstitials and their reactions with other point defect means effectively the removal of one silicon self-interstitial per carbon atom displaced from its substitutional site. In consequence, substitutional carbon is able to provide the free volume needed for the nucleation of oxygen precipitates [4.8–4.12] and for an enhanced formation of new donors [4.13–4.16]. Probably due to reactions with oxygen, but most likely also because of its influence on the intrinsic point defects, carbon was reported to cause a reduced formation of thermal donors [4.15–4.19]. More important now, the oversaturation of self-interstitials during post-implantation anneals can be reduced significantly by the presence of implanted carbon [4.20–4.24] or carbon incorporated during the epitaxial growth of silicon layers [4.25–4.29].

This results in a drastic reduction of transient-enhanced diffusion during post-implantation annealing. Because of its small covalent radius, the addition of carbon to SiGe layers was investigated as a means to reduce strain in such structures [4.5, 4.6, 4.30–4.35] and provides an additional degree of freedom for band-gap engineering. A side-effect of the carbon doping was a reduced diffusion of boron in carbon-rich layers not only during post-implantation annealing but also during anneals in inert atmospheres. Concepts to explain this phenomenon are discussed at the end of this section.

The formation of carbon-silicon complexes is not restricted to small complexes. But energetic restrictions allow carbon precipitates to form only in the presence of a high supersaturation of self-interstitials, at surfaces and dislocations, or together with oxygen [4.36–4.38]. A typical representative of the first kind are the B-swirls which were found to form during the cooling phase of interstitial-rich-grown crystals [4.39].

Further technical applications of carbon are usually based on the implantation of carbon in high doses. For the “proximity gettering” introduced by Wong et al. [4.40], impurities are implanted to form a buried layer near the active region of devices. Various studies thereafter demonstrated the effectiveness of carbon as gettering agent [4.41–4.43]. Implantations of even higher doses were investigated for the synthesis of silicon carbide [4.44–4.47]. In comparison to oxygen and nitrogen, few investigations were concerned with the formation of buried silicon carbide layers [4.48–4.50]. As a further application, annealed high-dose carbon implants were studied for an application as etch-stop layers [4.51, 4.52].

Complexes resulting from the reaction of point defects with carbon or carbon precipitates may be electrically active and, because of their limited thermal stability, detrimental to device performance and reliability. Most likely due to the formation of such complexes, carbon at high concentrations was found by Akiyama et al. [4.53], Hill and Van Iseghem [4.54], and Abe et al. [4.55] to negatively influence the electrical characteristics of p/n junctions. Detrimental effects of carbon on power devices were summarized by Kolbesen and Mühlbauer [4.56] who also reported that no such effects were observed for carbon concentrations below $5 \cdot 10^{16} \text{ cm}^{-3}$. Detrimental effects on leakage currents, generation lifetimes, and carrier mobilities were observed again more than one decade later in studies stimulated by the ability of carbon to getter undesired impurities and to suppress transient effects during post-implantation anneals [4.57–4.60]. Recovery of advantageous electrical properties was reported after annealing at 1100 °C. Similarly, carbon introduced during epitaxial growth was shown by Osten et al. [4.61] to reduce the carrier lifetime in SiGe structures. But the observed reduction by about one order of magnitude at a carbon concentration around 10^{20} cm^{-3} was still admissible for device functionality.

In the following sections, the basic atomic configurations of carbon in silicon, its solubility, the diffusion behavior, and the formation of complexes are discussed in detail. For a comprehensive review of the various aspects of carbon in crystalline silicon, the interested reader is referred especially to the publications of Kolbesen and Mühlbauer [4.56], Kolbesen [4.62], Gösele [4.63], Davies and Newman [4.64], and Skorupa and Yankov [4.12].

4.1.1 Basic Atomic Configurations

Substitutional Carbon

Already from its rather high activation energy of diffusion, close to that governing the diffusion of dopants, Newman and Wakefield [4.65, 4.66] concluded that carbon resides predominantly on substitutional sites. Further indirect evidence came from the work of Newman and Willis [4.67] and Newman and Smith [4.2] who found that their infrared-absorption measurements were in

close agreement with that of boron and that the dependences on the measurement temperature and isotope effects were as expected from the theory of local vibration modes of substitutional impurities of Dawber and Elliott [4.68, 4.69]. The substitutional character of carbon in silicon was finally demonstrated by the investigations of Baker et al. [4.70] and Windisch and Becker [4.71] who found that the presence of carbon leads to a reduction of the lattice parameter to an extent close to what can be expected from a linear interpolation between pure silicon and β -SiC. Windisch and Becker [4.71] also reported that carbon-rich crystals consist of consecutive layers which are either almost free from carbon or carbon-enriched. Measurement of the carbon concentration is usually based on its local vibrational mode found at room temperature for ^{12}C at 607 cm^{-1} (77 K) [4.67].

Theoretical investigations confirm that carbon assumes predominantly a substitutional, T_{d} -symmetrical position, centered between its four silicon neighbours [4.72–4.74]. These neighbors are relaxed inwardly by about 0.03 nm, reflecting the much smaller tetrahedral covalent radius (0.77 Å) in comparison to silicon (1.17 Å). The strain energy resulting from this deformation was estimated to be 1.76 eV per carbon atom [4.73]. On a substitutional site, the isovalent carbon would be expected to be electrically neutral. However, theoretical investigations indicated that substitutional carbon has a deep antibonding acceptor level around the edge of the conduction band [4.75–4.77]. This state was also suggested to be responsible for the lowering of the band gap at small carbon concentrations found in *ab-initio* simulations [4.76–4.78] instead of the increase expected intuitively from the much higher band gaps of SiC and diamond.

Carbon Interstitials

A second prominent atomic configuration is the carbon interstitial. It results from the reaction of substitutional carbon with a silicon self-interstitial [4.79–4.81] or may be introduced from a CF_4 plasma during processes at low temperatures like reactive ion etching [4.82]. Carbon interstitials were first detected by IR spectroscopy [4.79, 4.83] where ^{12}C has IR local-mode absorption bands at 922 and 932 cm^{-1} (77 K). The structure of carbon interstitials in their positive charge state was identified by Watkins and Brower [4.81] by EPR spectroscopy where they give rise to the Si-G12 center. Isotope shifts and the application of uniaxial stress were found to be in agreement with Figure 4.1 showing a bound carbon-silicon pair centered as interstitialcy along the $\langle 001 \rangle$ direction. Therefore, to describe atomic arrangements of carbon-related defects more clearly, it will also be denoted as $[\text{C-Si}]_s$ pair in the following wherever appropriate. Similarities in the formation and annealing behavior were used to identify a donor level at $E_v + 0.28$ eV and an acceptor level at about $E_c - 0.12$ eV [4.84–4.89]. EPR investigations by Song and Watkins [4.90] served again to identify the atomic structure and it was found that the Si-L6 EPR center corresponds to the negative charge state of the $[\text{C-Si}]_s$ pair shown in Figure 4.1. Structural informations about the neutral charge state of the carbon interstitial were reported

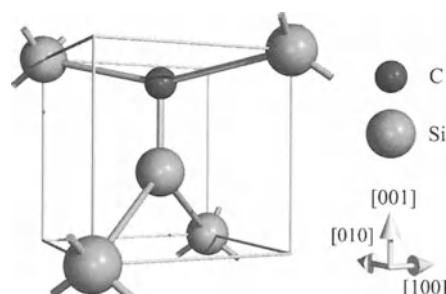


Figure 4.1: Schematic representation of the atomic arrangement of interstitial carbon.

by Zheng et al. [4.91] from stress effects on IR bands. Again, the atomic arrangement shown schematically in Figure 4.1 was suggested. Based on correlations of kinetics and symmetry, Woolley et al. [4.92] assigned the PL line at 0.856 eV to the carbon interstitial. The same conclusion was drawn by Thonke et al. [4.93] who deduced from the PL data a hole-binding energy of 0.25 eV which is in perfect agreement with the donor level determined by DLTS. Quoting otherwise unpublished results of Drevinsky et al., Kimerling et al. [4.94] estimated the capture of self-interstitials at substitutional boron to be seven times as effective as the capture at substitutional carbon. Davies and Newman [4.64] even estimated this ratio to be 50.

Consistent with the experimental results, theoretical investigations agreed that the $\langle 001 \rangle$ -oriented split interstitial is the most stable configuration of a carbon interstitial [4.74, 4.95–4.98] with relaxations which are probably large enough to break some bonds of silicon atoms adjacent to the carbon atom. Estimates for the binding energy of the pair relative to an electrically neutral silicon interstitial well-separated from a substitutional carbon atom gave values of about 1.2 eV [4.98], 1.45 eV [4.74], and 1.75 eV [4.97]. From simulations of diffusion experiments in which carbon was involved, including the diffusion of carbon in superlattice layers, Law et al. [4.99] suggested a binding energy of 2.25 eV for carbon interstitials.

Carbon-Vacancy Pairs

Investigating the EPR Si-G16 center reported already by Watkins and Corbett [4.100] as Si-B center, Dvurechenskii et al. [4.101] found that it is consistent with a vacancy at a second coordination site of an impurity atom which was tentatively assumed to be carbon. Reorientation of the defect was found to be governed by two processes with activation energies of 0.25 and 1.4 eV. After irradiation with alpha particles, Abdullin and Mukashev [4.102] observed a center which they showed to be vacancy-related. Excluding oxygen as a constituent, it was tentatively assigned to a vacancy stabilized by a carbon atom. The two levels observed at $E_c - 0.15$ eV and $E_c - 0.29$ eV correspond to its double acceptor level and its acceptor level, respectively. Annealing of the center was found to be governed by an activation energy of 0.28 eV. From their theoretical investigation, Dal Pino, Jr. et al. [4.103] obtained a binding energy of 0.19 eV for a pair of a vacancy next to a substitutional carbon atom.

4.1.2 Solubility

According to the phase diagram compiled by Olesinski and Abbaschian [4.104], the carbon in the silicon phase is at all temperatures in equilibrium with a SiC phase. Precise data for the solubility of carbon in silicon are rare. Early experiments by Papazian and Wolsky [4.105] indicated carbon concentrations on the order of 10^{19} cm $^{-3}$. Newman and Wakefield [4.65, 4.66] subsequently based their experiments on the diffusion of ^{14}C into CZ silicon. The surface concentration thus obtained should correspond to the solubility. But there was a considerable scatter attributed by the authors to the silicon carbide film at the surface being not an equilibrium phase. In addition, because of carbon-oxygen complexes forming in the oxygen-rich CZ silicon, the total concentration measured can be expected to be larger than the solubility concentration of substitutional carbon. Using a nuclear reaction with a helium beam which converts ^{12}C to unstable ^{11}C , Nozaki et al. [4.106] determined a value of $3.5 \cdot 10^{17}$ cm $^{-3}$ for the solubility of carbon at the melting point. Some of the pitfalls of the experiments of Newman and Wakefield were avoided in the work of Bean and Newman [4.37] in which the concentration of substitutional carbon was measured by IR spectroscopy. Based on the same method, Endo et al. [4.107] obtained somewhat smaller values characterized by a similar activation energy. The solubility values obtained are shown in Figure 4.2.

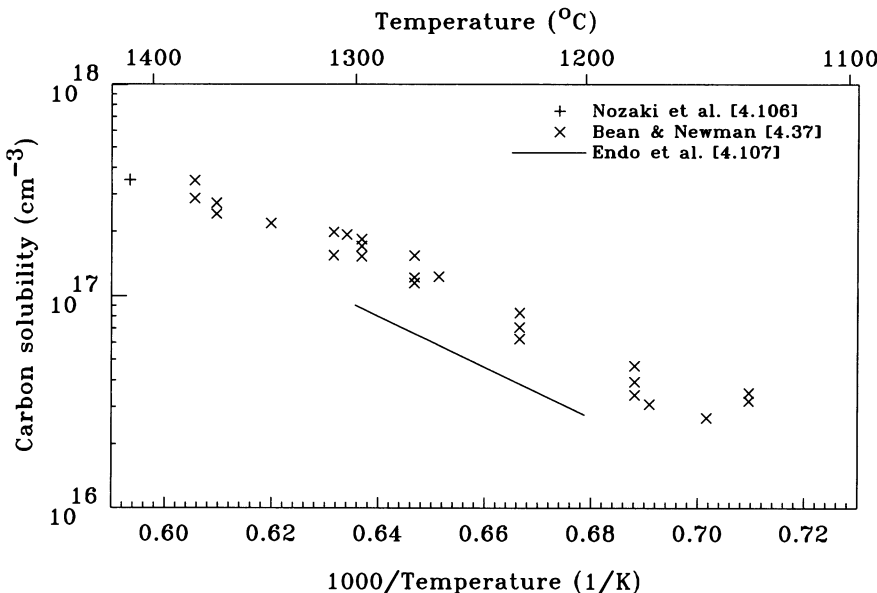


Figure 4.2: Solubility of carbon in silicon.

4.1.3 Diffusion

Intrinsic Diffusion

Diffusivities of carbon were measured by Newman and Wakefield [4.65, 4.66] and Rollert et al. [4.108] via in-diffusion of ¹⁴C isotopes, and by Ladd and Kalejs [4.109] from out-diffusion profiles of supersaturated carbon. The respective experimental data are shown in Figure 4.3 together with the regression curve

$$D_C = 6.11 \cdot \exp\left(-\frac{3.293 \text{ eV}}{k \cdot T}\right) \text{ cm}^2/\text{s} \quad (4.1)$$

derived from these measurements. The activation energy ranges with a confidence level of 90% from 3.21 to 3.37 eV. The 90% confidence interval for the diffusion coefficient is about +7.8/-7.2% of the regression curve at 1165 °C and increases to +13/-11% at the melting point and +26/-20% at 800 °C. Additional measurements are expected with 90% confidence within a range of +79/-44% of the regression curve at 1165 °C which increases slightly to +80/-45% at the melting point and +86/-46% at 800 °C.

Diffusion Mechanism

The diffusion of carbon is generally assumed to proceed via an interstitial mechanism. Evidence for such a mechanism resulted from irradiation experiments where it was observed that the production of vacancy-oxygen pairs and divacancies is increased by the presence of carbon [4.110]. Evidence for a significant fraction of diffusion via self-interstitials comes also from the experiments of Kalejs et al. [4.111] and Ladd and Kalejs [4.109] who observed enhanced carbon diffusion under conditions where the concentration of self-interstitials is enhanced by thermal oxidation or diffusion of phosphorus at high concentrations.

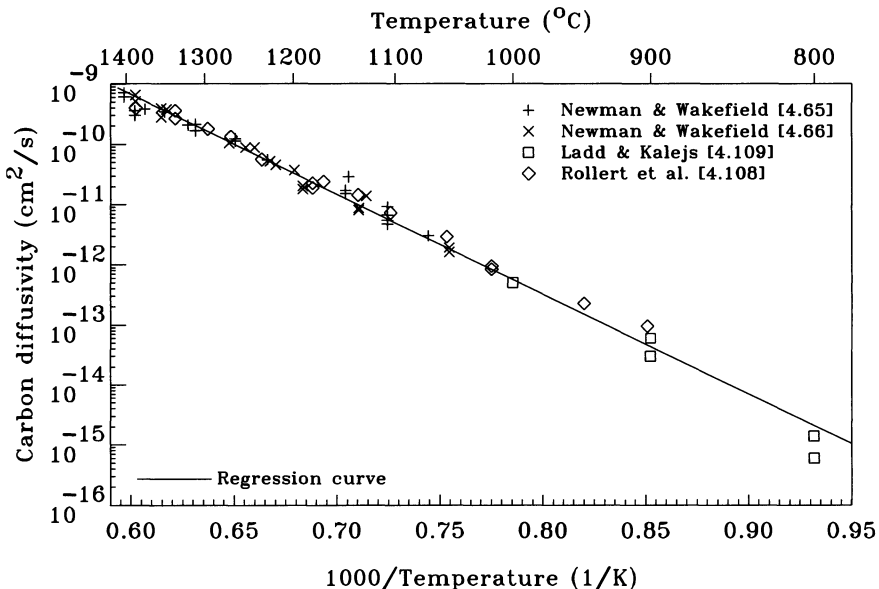


Figure 4.3: Diffusion coefficient of carbon in silicon.

Carbon Interstitials

For carbon interstitials, a diffusivity of

$$D_{C_i} = 4.4 \cdot \exp\left(-\frac{0.88 \text{ eV}}{k \cdot T}\right) \text{ cm}^2/\text{s} \quad (4.2)$$

was derived by Gösele [4.63] from measurements of the reorientation time of the Si-G12 center reported by Watkins and Brower [4.81].¹ Additional data for the reorientation time of the EPR Si-G12 center reported later by Song and Watkins [4.90] were about a factor of 3 lower, indicating a somewhat higher diffusivity. Reorientation times reported for the EPR Si-L6 center were about two orders of magnitude smaller. As an alternative to the EPR measurements, diffusivities were estimated by Tipping and Newman [4.113] from the first-order reaction kinetics of carbon interstitials with substitutional carbon to C_iC_s pairs. Applying their procedure for the extraction of diffusion coefficients also to the similar experiments of Davies et al. [4.114] and Chappell et al. [4.115] gives nearly identical values. They agree also with the result of Lalita et al. [4.116] who extracted their values from the reaction of interstitial carbon with oxygen at room temperature. The experimental data are summarized in Figure 4.4 together with the expression derived by Gösele [4.63]. Unfortunately, Tipping and Newman [4.113] used in their analysis incorrect values for the reorientation time from the work of Watkins and Brower [4.81] (see footnote 1) so that part of their diffusivities were, by a factor of 10, too small. In consequence, the perfect agreement over eight decades reported by them is not reproduced. But this finding should not be rated too high since the diffusivities extracted from reaction kinetics refer to neutral carbon interstitials while the reorientation times of the EPR Si-G12 and Si-L6 centers are associated with their positive and negative charge states, respectively. Comparing the diffusion kinetics of

¹The reorientation times in Figure 3 of the publication of Watkins and Brower [4.81] are, by a factor of 10, too large while the analytical expression $1.1 \cdot 10^{-16} \cdot \exp(0.88 \text{ eV}/kT)$ given also is correct [4.112].

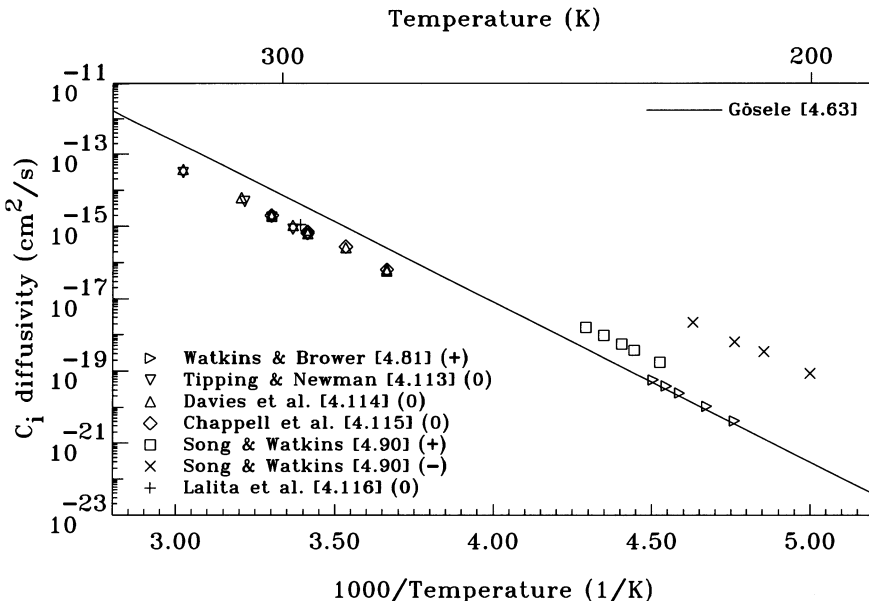


Figure 4.4: Diffusion coefficient of carbon interstitials in silicon computed from published data as suggested by Tipping and Newman [4.113]. The charge state of the carbon interstitials associated with the measurements is indicated in parentheses.

carbon interstitials in several charge states, it was concluded that all of them have approximately the same activation energy [4.85, 4.90, 4.92, 4.113]. The activation energies estimated experimentally range from 0.71 to 0.88 eV [4.81, 4.90, 4.92, 4.113–4.115, 4.117] with most of them above 0.8 eV. Such activation energies were reproduced by theoretical investigations within their accuracy limits [4.74, 4.95, 4.97].

Studying the short-time diffusion behavior of carbon delta-layers from 730 to 900 °C, Pinacho et al. [4.118] concluded that they would not follow a Gaussian distribution and extracted values for the mean path length λ_C a carbon atom migrates while it is mobile (see Section 1.5.4). The values, depicted in Figure 4.5,² did not show the expected temperature behavior and increased with increasing temperature. In addition, the experimentally determined values were significantly smaller than expected by the authors. The discrepancies were finally explained by the trapping of carbon interstitials at substitutional carbon atoms or complexes of two substitutional carbon atoms. In a subsequent study, Cowern et al. [4.119, 4.120] extracted the mean path length at 850 °C from diffusion processes in different atmospheres at one order of magnitude smaller carbon concentrations than in the work of Pinacho et al. It was found that all experiments led to basically the same value for λ_C . In agreement with the arguments of Pinacho et al., they were, by a factor of about two, larger than the former results.

In addition to thermal diffusion, evidence for athermal diffusion (see Section 1.3.4) of carbon interstitials was presented by Asom et al. [4.121], Frederickson et al. [4.122], Benton et al. [4.123], and Frederickson and Karakashian [4.124].

²A factor of $\sqrt{3}$ was used to convert projected mean path lengths to mean path lengths. In [4.118], a factor of $\sqrt{6}$ was used.

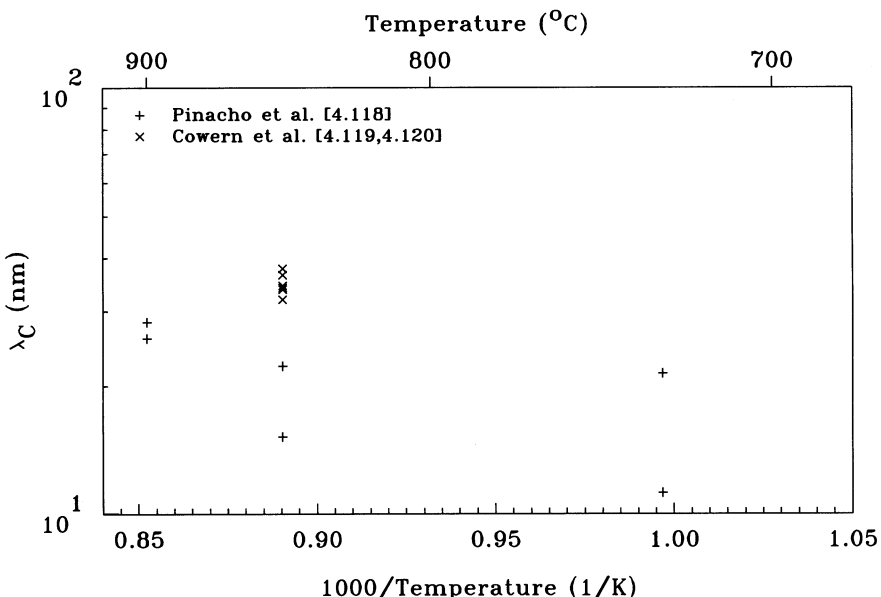


Figure 4.5: Mean path length λ_C a carbon atom migrates while it is mobile.

Diffusion Behavior Well Above Solid Solubility

Despite the fact that all point defects determining the macroscopic diffusion behavior of carbon were reasonably well characterized, no satisfying simulation results were obtained initially when the carbon concentration was well above solid solubility. The simulations of Rücker et al. [4.125], Werner et al. [4.126], and Scholz et al. [4.127] showed quite clearly that a simple system based on the kick-out reaction of self-interstitials with substitutional carbon atoms to carbon interstitials leads to an underestimation of the profile broadening. Complementary information from the diffusion of dopants in carbon-doped layers (see Section 4.1.7) confirmed that the undersaturation of self-interstitials predicted by the simulations exceeded the experimentally found values significantly. To improve the simulations, Rücker et al. [4.125], assumed that carbon interstitials are supplied by dissolving silicon carbide agglomerates. Being far above the solid solubility of carbon, a dissolution of existing agglomerates would probably not be expected. Alternatively, Scholz et al. [4.127] and Rücker et al. [4.128] explained the observed discrepancies by a non-negligible reaction of interstitial carbon with vacancies. The continuum simulations were complemented by the atomistic Monte-Carlo simulations of Pinacho et al. [4.118]. To explain the observed discrepancies, they included the release of self-interstitials via the reactions $C_s + C_i \rightarrow C_{2s} + I$ and $C_{2s} + C_i \rightarrow C_{3s} + I$. In a subsequent publication, Pinacho et al. [4.129] included a chain of reactions leading via the capture and release of carbon interstitials and intrinsic point defects to clusters comprising up to six carbon atoms. Despite the trend to include more and more complicated mechanism, there is good hope that this is not really required. After the erratum of Rücker et al. [4.130] made clear that the carbon concentrations reported in their original article [4.125] were, by a factor of two, too high, Colombeau and Cowern [4.131] found that the previously noted discrepancies between experiments and simulations based on the kick-out mechanism disappear when this is taken into account.

4.1.4 Carbon-Silicon Complexes

Carbon was found in various investigations to form complexes with self-interstitials. The known properties of such complexes are discussed in the following.

$\mathbf{C}_i\mathbf{I}_n$

In the absence of other dopants, carbon interstitials may react only with intrinsic point defects or other carbon atoms. In electron-irradiation experiments, it was observed that the concentration of substitutional carbon atoms decreased continuously with an increasing electron dose while the concentration of interstitial carbon saturated and finally decreased after a maximum [4.132, 4.133]. This behavior was interpreted in favor of a reaction between carbon interstitials and silicon self-interstitials to $\mathbf{C}_i\mathbf{I}$ complexes [4.133, 4.134] with the latter giving rise to absorption bands at 959 and 966 cm^{-1} (77 K). Such defects were associated by Guldberg [4.135] and Lefèvre [4.88] with a level at $E_c - 0.2$ eV. Analyzing the experimental results of Chappell and Newman [4.133] numerically, Davies and Newman [4.64] estimated that the capture radius of self-interstitials at interstitial carbon is five times as large as at substitutional carbon atoms. The reaction of self-interstitials and carbon interstitials was investigated also by Mattoni et al. [4.98]. Their *ab-initio* calculations indicated that such a reaction leads to an energy reduction of 2.0 eV.

Further reactions of $\mathbf{C}_i\mathbf{I}$ complexes with silicon self-interstitials were assumed to lead to the formation of $\mathbf{C}_i\mathbf{I}_n$ complexes although they did not give rise to IR absorption [4.133, 4.134].

\mathbf{C}_{2s}

Using an analytical model for the strain energy in silicon-carbon alloys calibrated by *ab-initio* simulations, Rücker et al. [4.136] found that substitutional carbon atoms on nearest neighboring sites are characterized by a repulsive interaction energy of more than 1.0 eV. On the other hand, a configuration with two substitutional carbon atoms at opposite vertices of the six-membered ring structures in silicon was found to be stable. Experimental evidence for such complexes was found by Raman and IR measurements. Early *ab-initio* studies mentioned in the work of Meléndez-Lira et al. [4.137] confirmed that such a structure should be the energetically most favorable configuration of two substitutional carbon atoms. Similar work by Windl et al. [4.138] confirmed that the D_{3d} -symmetric configuration of two neighboring, substitutional carbon atoms is characterized by a repulsive interaction energy of about 1.8 eV. The energetically most favorable configurations were shown to be substitutional atoms on third-nearest and fourth-nearest neighboring sites although there was no apparent binding between the two carbon atoms.

Using a combination of EPR measurements and theoretical investigations, Byberg et al. [4.139] identified a pair of two substitutional carbon atoms at neighboring lattice sites. Besides the negative charge state found to give rise to the previously unidentified EPR signal known as Si-GGA2 [4.140], a neutral charge state was suggested with a shorter bond length between the carbon atoms. Both charge states have D_{3d} symmetry which would exclude the third-nearest neighboring configuration found in the previous investigations. In addition, a positive charge state was found in the theoretical investigations with an even further separation than $(\mathbf{C}_s-\mathbf{C}_s)^-$. In this configuration, the bond between the carbon atoms is basically broken and the positive charge is localized at one of the carbon atoms. As a consequence, the two carbon atoms are no longer equivalent and the symmetry of the $(\mathbf{C}_s-\mathbf{C}_s)^+$ defect is only C_{3v} . Further investigations by Lavrov et al. [4.141] established the local vibrational modes of the neutral and negatively charged di-carbon complex at 527.4 and 748.7 cm^{-1} (10K), respectively. This assignment was shown to be in agreement with vibration frequencies calculated from *ab-initio* simulations.

Formation of C_s - C_s was suggested to be associated with the trapping of a vacancy at a C_iC_s complex.

In a Laplace-DLTS investigation, Markevich et al. [4.142] found that the disappearance of phosphorus-vacancy pairs was accompanied by a reduction in the concentration of C_iC_s complexes and the formation of a defect with an acceptor level at $E_c - 0.21$ eV. The level was assumed to result from the trapping of a liberated vacancy at a C_iC_s complex and assigned to a pair of substitutional carbon atoms.

From the simulation of the diffusion of superlattice layers, Pinacho et al. [4.118] obtained a value of 1.51 eV for the binding energy of two substitutional carbon atoms on adjacent sites. In a later publication [4.129], a value of 1.2 eV was given.

C_iC_s and C_s -I- C_s

Substitutional carbon atoms, when present in a sufficiently high concentration, appear as a natural reaction partner for interstitial carbon atoms. The first successful identification of such a complex was reported by Brower [4.143, 4.144] who found that the Si-*G*11 EPR center results from the positive charge state of an interstitial carbon-substitutional carbon pair. Years later, the ODMR studies of Lee et al. [4.145] and O'Donnell et al. [4.146] revealed that the zero-phonon 0.969 eV *G*-line, one of the most widely studied PL centers, arises from two substitutional carbon atoms with a silicon self-interstitial in between. A re-examination of the vibronic sidebands of the *G*-line by Davies et al. [4.147] gave indeed indications of a second carbon atom involved. But, unlike in the center studied by ODMR, the two carbon atoms were suggested to be in inequivalent crystal sites. Complementary DLTS investigations found a defect with bistable electrical properties [4.148–4.150] which was initially assumed to be the VO pair, but finally ascribed also to C_iC_s [4.121, 4.151]. A full analysis of the C_iC_s pair was given by Song et al. [4.152], combining results from DLTS, EPR, IR, and ODMR measurements. In summary, the defect was found to be amphoteric and may exist in two configurations shown in Figure 4.6. The positive and negative charge states correspond to the EPR centers Si-*G*11 and Si-*G*17 and share a common stable configuration shown in Figure 4.6 a). For this configuration, the acceptor and donor levels are at $E_c - 0.17$ eV and $E_v + 0.09$ eV, respectively. Its atomic configuration was suggested to consist of a substitutional carbon atom directly adjacent to the silicon atom of the $[C-Si]_s$ pair. In the neutral charge state, a second configuration of the C_iC_s pair shown in Figure 4.6 b) is favored energetically. It gives rise to the EPR Si-*L*7 center and resembles two substitutional carbon atoms with a silicon self-interstitial in between. This configuration was also suggested to be responsible for the EPR spectrum Si-*PT*1 [4.153, 4.154]. Its acceptor level

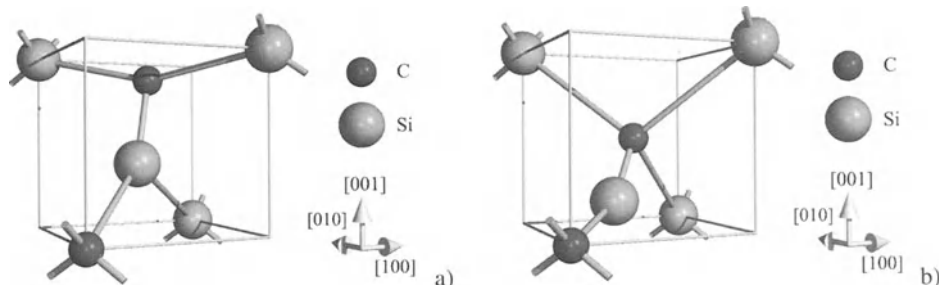


Figure 4.6: Atomic configuration of the C_iC_s pair. a) stable configuration for the negative and positive charge states; b) stable configuration for the electrically neutral charge state.

was found at $E_c - 0.11$ eV but no donor level was identified. In addition to the levels assigned by Song et al., donor levels at $E_v + 0.36$ [4.85] and $E_v + 0.37$ [4.155, 4.156] were suggested to arise from the C_iC_s pair. In the work of Lavrov et al. [4.157], a number of local vibrational modes have been observed in carbon-doped silicon and assigned to the two configurations of the C_iC_s complex. In particular, absorption lines at 594.6, 596.6, 722.4, 872.6, and 953 cm⁻¹ (10 K) were associated with the C_iC_s (A) configuration in its neutral charge state, and absorption lines at 540.4, 543.3, 579.8, 640.6, 730.4, and 842.4 cm⁻¹ (10 K) with the C_s -I- C_s (B) configuration in its neutral charge state. These frequencies were shown to be in agreement with theoretical predictions. An absorption band observed at room temperature at 544 cm⁻¹ was discussed by Londos et al. [4.158] to arise from the bands at 540.4 and 543.3 cm⁻¹ of the C_s -I- C_s (B) configuration when recorded at 10 K. Based on the occurrence of the PL G-line, C_iC_s pairs were also shown to exist in silicon implanted with carbon [4.159].

Comparing the kinetics of carbon interstitials and of C_iC_s pairs, a short delay in the formation of the latter was reported [4.92, 4.114]. To explain such observations, Davies et al. [4.114] and Chappell et al. [4.115] postulated an intermediate stage from which the transformation into a C_iC_s pair requires to surmount an energy barrier of 0.94 eV. Dissociation of the C_iC_s pairs was found to be governed by a time constant for which activation energies of 1.25 [4.160], 1.34 [4.161], and 1.7 eV [4.162] were reported. An extensive analysis of Davies et al. [4.163] revealed that the break-up of the pair into a substitutional and an interstitial carbon atom is associated with an activation energy on the order of 1.7 to 1.9 eV while the lower values can be explained by the reaction with another defect with a migration energy of about 1.25 eV. In the work of Boyarkina et al. [4.164], the binding and dissociation energies of C_iC_s were estimated to be 1.12 and approximately 2.0 eV, respectively. Comparing the capture radii of carbon interstitials at substitutional carbon atoms and oxygen atoms, Davies et al. [4.132] found the former to be 3.1 times higher than the latter.

Basic features of the model proposed by Song et al. [4.152] were reproduced by theoretical investigations [4.74, 4.96, 4.98, 4.165] although other possible configurations were indicated, too. In particular, Liu et al. [4.97] reported that a $[C-C]_s$ split configuration oriented along the $\langle 100 \rangle$ axis would be energetically more favorable than the configurations shown in Figure 4.6. For the binding energy of the energetically most favorable C_iC_s complex with respect to well-separated carbon atoms on interstitial and substitutional sites, values of 0.8 eV [4.98], 1.0 eV [4.74], and 1.39 eV [4.97] were estimated. From the depth dependence of the enhanced diffusion of boron in samples with high carbon concentrations, Chakravarthi and Dunham [4.166] deduced a relation between the concentrations C_s of substitutional carbon and $C_{C_iC_s}$ of C_iC_s pairs in thermal equilibrium in the form

$$\frac{C_s^2}{C_{C_iC_s}} = 1.2 \cdot 10^{43} \cdot \exp\left(-\frac{5 \text{ eV}}{k \cdot T}\right) \text{ cm}^{-3}. \quad (4.3)$$

To reproduce the effects of carbon on the transient diffusion of boron, Ngau et al. [4.167] derived kinetic parameters for the formation and dissolution of a C_iC_s complex which can be interpreted in terms of a binding energy of 2.72 eV. Such values are significantly higher than the values from theoretical investigations and lump probably contributions from the formation of more carbon-rich clusters. In the work of Pinacho et al. [4.118], a binding energy of 0.7 eV was used and further growth to larger carbon-interstitial clusters was taken into consideration. Experimental evidence for the formation of C_iC_s pairs comes also from the work of De Salvador et al. [4.168] and Mirabella et al. [4.169] in which it was reported that self-interstitial injection from a surface-near silicon implantation caused the deactivation and immobilization of about two carbon atoms per self-interstitial in a carbon-rich layer.

C_iC_sI_n

Formation of C_iC_s pairs is one mechanism leading to a reduction of the concentration of self-interstitials in oxygen-lean samples. In addition, it was observed in irradiation experiments that C_iC_s pairs capture self-interstitials and may act as nucleation centers for self-interstitial agglomerates [4.132, 4.133, 4.170–4.172]. The first one in this chain, C_iC_sI, was associated tentatively by Londos et al. [4.158] with absorption bands at 987 and 993 cm⁻¹ (RT). Taking the capture radius of a silicon self-interstitial at a substitutional carbon atom as a reference, the capture radius for a silicon self-interstitial at a C_iC_s pair was estimated to be 7.2 times as high [4.132]. Further reactions of C_iC_sI_n complexes with self-interstitials were suggested to be governed by a similar capture radius being 6.8 times that for the reaction between a silicon self-interstitial and a substitutional carbon atom. The *ab-initio* calculations of Mattoni et al. [4.98] indicated a reduction of the system energy by 1.5 eV upon capture of a self-interstitial at C_iC_s. For the reaction of two carbon interstitials, an energy gain of 1.2 eV was calculated. In the work of Pinacho et al. [4.129], the formation of a complex comprising two carbon atoms and two silicon atoms around two lattice sites was associated with an energy gain of 4.7 eV in comparison to a well-separated self-interstitial and a C_iC_s complex. For its formation from two carbon interstitials, an energy gain of 4.0 eV was reported.

C_i-I-C_i

C_i-I-C_i complexes were assumed by Wijaranakula and Matlock [4.173] to introduce thermally induced donors in silicon with high carbon concentrations. In addition, it was suggested that other carbon interstitials may attach to the complex leading to chains of interstitial silicon and carbon atoms.

C_nI_m

In order to reproduce the diffusion behavior of carbon superlattice layers, Pinacho et al. [4.118] included the reaction of carbon interstitials with complexes of two substitutional carbon atoms on adjacent sites. This reaction was found to be associated with an energy increase of 2.02 eV. In a later publication, Pinacho et al. [4.129] reported an energy increase of 1.0 eV. Release of a self-interstitial was suggested by Pinacho et al. [4.118] to lead to the formation of a defect consisting of three substitutional carbon atoms for which a total binding energy of 0.3 eV was estimated. This means an energy increase of 1.21 eV upon addition of the third substitutional carbon atom to C_{2s} and an energy increase of 0.79 eV upon release of a self-interstitial from C_{2s}C_i. In a later publication, Pinacho et al. [4.129] considered a chain of reactions leading to carbon-interstitial clusters with up to six carbon atoms.

4.1.5 Complexes with Oxygen

In silicon crystals containing carbon and oxygen, various IR and PL bands were found which are not observed in silicon doped with only one of them. In consequence, these bands were ascribed to complexes involving both impurities. For several of them, as outlined below, specific atomic arrangements were suggested.

C_sO_i, C_iO_iV, and C_sO_{2i}

Probably the most simple atomic configuration for a carbon-oxygen complex was suggested by Newman and Smith [4.2]. They found that their IR measurements of lines at 1104 and 1052

cm^{-1} (4.2 K) can be explained by a substitutional carbon atom paired with an interstitial oxygen atom at a second or third nearest neighbor position. This assignment was corroborated by the theoretical investigations of Kaneta et al. [4.174]. Further experimental studies by Shirakawa et al. [4.175] concentrated on absorption lines from 1026 to 1112 cm^{-1} (4.2 K). Correlating their kinetics to oxygen and carbon concentrations, they and Yamada-Kaneta et al. [4.176] confirmed the previous assignment for the line at 1104 cm^{-1} (4.2 K) and identified the others to arise from complexes of carbon with one to three oxygen atoms. Using data from Bean and Newman [4.17], Babitskii et al. [4.177] estimated the binding energy of C_sO_i to be 0.8 eV.

Studying electron-irradiation-induced defects, Davies et al. [4.178] found that an absorption band at 3942 cm^{-1} arises from a defect with C_{1h} or C_2 symmetry. Isotope experiments showed that the defect contains carbon and oxygen and that only one of each contributes to the isotope shift. The reduction of the strength of the line in tin-doped samples indicated that a vacancy is involved in the defect so that the absorption band was tentatively associated with $\text{C}_i\text{O}_i\text{V}$.

From the kinetics of the formation of complexes due to electron irradiation of carbon-rich samples at elevated temperatures, Lindström et al. [4.179] concluded that C_sO_{2i} complexes would form by the reaction of VO_2 with an interstitial carbon atom. The complex was associated with a band at 1099 cm^{-1} (10 K). Using data from Bean and Newman [4.17], Babitskii et al. [4.177] estimated the binding energy of C_sO_{2i} to be 1.0 eV.

C_iO_i

Using IR spectroscopy, Newman and Bean [4.79] observed that the concentration of carbon interstitials created by electron irradiation reduced during annealing at room temperature. At the same time, absorption bands at 865.2 and 1115.5 cm^{-1} (77 K), labelled C(3), appeared and were tentatively ascribed to a pair composed of a carbon interstitial and an oxygen interstitial. Measurements concentrating on the zero-phonon 0.7894 eV C-line in PL spectra showed that the defect associated has C_{1h} symmetry [4.180, 4.181], contains carbon and oxygen [4.182, 4.183], and is an effective-mass-like pseudo-donor [4.184] which binds a hole tightly with 0.3412 eV and an electron loosely with 38.3 meV [4.181]. The work of Davies et al. [4.170] finally showed the close correlation of the PL C-line to the IR C(3) center and, demonstrating that vacancies cannot be involved, corroborated Newman and Bean's assignment of the C(3) center to a C_iO_i complex. Following the suggestion of Jones and Compton [4.185, 4.186], Trombetta and Watkins [4.187] could show that the PL C-line arises from the same defect as the EPR center labelled Si-*G15* by Watkins [4.188] and Si-*K* by Almeleh and Goldstein [4.189]. This identification closed the circle since Lee et al. [4.190] reported the EPR Si-*G15* line to be associated with the above mentioned IR band at 865 cm^{-1} . This EPR center was identified³ to arise from the positive charge state of a $[\text{C-Si}]_s$ pair near to an interstitial oxygen atom as depicted in Figure 4.7 a). In addition, Mukashev et al. [4.192] suggested the formation of metastable C_iO_i complexes similar to that suggested by Trombetta and Watkins but with the oxygen atom next to the silicon atom of the $[\text{C-Si}]_s$ pair. The structure suggested by Trombetta and Watkins remained not undisputed. Jones and Öberg [4.193] and Coutinho et al. [4.194] noted that the vibrational modes observed experimentally are inconsistent with what would be expected from a bond-centered oxygen. As an alternative, they suggested the atomic arrangement shown schematically in Figure 4.7 b). For this structure, the binding energy between the carbon interstitial and the oxygen interstitial was calculated to be 1.7 eV by Coutinho et al. [4.194].

³It should be noted that Lee et al. [4.191] originally assigned the EPR Si-*G15* center to a carbon-oxygen-divacancy defect. This assignment is reflected in various other reports which should correctly be attributed to C_iO_i complexes.

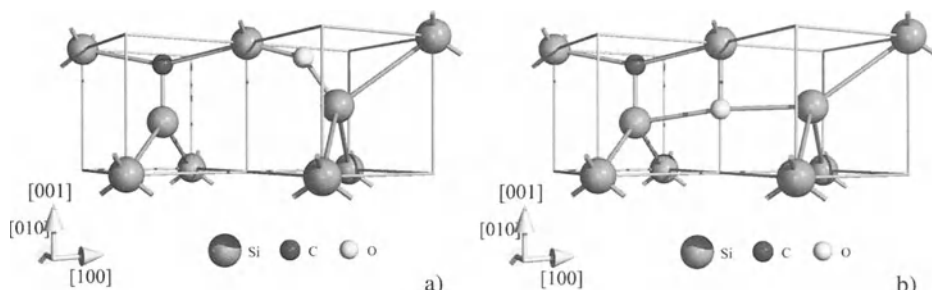


Figure 4.7: Atomic configurations suggested for the C_iO_i complex. a) Structure suggested by Trombetta and Watkins [4.187]; b) Structure suggested by Jones and Öberg [4.193].

Complementary information on ionization levels was obtained by electrical measurements and DLTS. Based usually on a correlation to the EPR Si-G15 center, the donor level was reported to be at $E_v + 0.3$ eV [4.189], $E_v + 0.32$ eV [4.191], $E_v + 0.33$ eV [4.87, 4.195], $E_v + 0.35$ eV [4.196], $E_v + 0.36$ eV [4.197], $E_v + 0.38$ eV [4.198], and $E_v + 0.4$ eV [4.199]. Asom et al. [4.121] found a value of $E_v + 0.36$ eV from a correlation to the PL C-line. This ionization level was attributed to the C_iO_i pair also by Ferenczi et al. [4.155] and Trauwaert et al. [4.156]. But these authors suggested that the level consists of two energetically closely spaced levels one of which has to be attributed to the C_iC_s complex. In contrast, Londos [4.200] suggested that the second defect is also a carbon-oxygen complex, but with a different atomic arrangement than the C_iO_i pair. Based on their study of the degradation of solar cells by electron irradiation, Yamaguchi et al. [4.201] and Khan et al. [4.197] tentatively suggested that C_iO_i gives rise to a minority trap at $E_v + 0.36$ eV. In addition to the donor level, possible acceptor levels were reported. Based on an extensive reasoning, Svensson et al. [4.202] attributed tentatively a DLTS level at $E_c - 0.36$ eV to the acceptor level of the Si-G15 EPR center.

Comparing the capture radii of carbon interstitials at oxygen atoms and substitutional carbon atoms, Davies et al. [4.132] found the former to be by a factor of 3.1 lower than the latter. Quoting otherwise unpublished results of Drevinsky et al., Kimerling et al. [4.94] reported that the reaction probability of oxygen with interstitial carbon is one seventh of that with interstitial boron. Finally, it should be noted that rapidly diffusing C_iO_i complexes were suggested to be responsible for the diffusion enhancement of oxygen observed in carbon-doped silicon [4.203, 4.204].

Annealing of C_iO_i was found to follow a first-order reaction [4.205] characterized by an activation energy of 1.99 eV. The first-order reaction means either dissociation of the pair or the reaction with an other defect like oxygen the concentration of which must not change significantly by the reaction. Interpreting the loss of oxygen interstitials from CZ crystals with high carbon concentrations tentatively as an enhanced out-diffusion via C_iO_i complexes, Babitskii et al. [4.177] derived their diffusion coefficient to be around $2 \cdot 10^{-8}$ cm²/s for the temperature range from 1000 to 1050 °C.

In CZ samples irradiated by α particles, Abdullin et al. [4.206] observed a trap at $E_v + 0.35$ eV which grew when the concentration of carbon interstitials decreased and which finally transformed into C_iO_i . Accordingly, it was associated with a metastable precursor of C_iO_i . In an electron-irradiation study, Shinoda and Ohta [4.207] found an acceptor level at $E_c - 0.06$ eV. From the kinetics of formation and annealing they suggested it likewise to be a metastable

precursor of the Si-G15 EPR center. Indications for metastable precursors were also found in IR spectroscopy investigations. Khirunenko et al. [4.208] found the appearance of the C_iO_i band at 865 cm^{-1} to be correlated with the disappearance of a vibration band at 922 cm^{-1} (10 K) and the appearance and disappearance of a vibration band at 967 cm^{-1} (10 K). Both bands were found from isotope experiments to contain oxygen and were tentatively identified as precursors of C_iO_i .

$C_iO_iI_n$

Based on the dependence of the concentration of C_iO_i pairs on the electron dose, Brozel et al. [4.209] concluded that further reactions with silicon self-interstitials lead to $C_iO_iI_n$ clusters. The first one in this chain, C_iO_iI , was identified by Davies et al. [4.132] to give rise to the C(4) IR line at 1020 cm^{-1} (RT). In a later review, Davies and Newman [4.64] located the absorption bands associated at 940 and 1024 cm^{-1} (RT). From numerical simulations of electron-irradiation experiments, they concluded that the capture radius for self-interstitials at C_iO_i is by a factor of 3.6 larger than the capture radius for self-interstitials at substitutional carbon and 0.5 times that of self-interstitials at C_iC_s pairs. For further reactions of such $C_iO_iI_n$ complexes with silicon self-interstitials, the capture radius was suggested to be even 6.8 times higher than for the capture of a self-interstitial at a substitutional carbon atom.

The Photoluminescence *P*-Line: C_iVO_{2i} or C_iO_{2i}

Investigations of the zero-phonon 0.7673 eV photoluminescence *P*-line indicated a picture similar to the PL *C*-line. The defect responsible was found to increase in intensity with the oxygen concentration [4.210], to contain carbon [4.211], to have C_{1h} symmetry [4.212], and to be an effective-mass-like pseudo-donor [4.184] which binds a hole tightly with 0.368 eV and an electron loosely with 34.3 meV [4.213]. Kürner et al. [4.214] concluded from isotope shifts that the defect has the same carbon-related core as the defect responsible for the *C*-line while the oxygen-related part of the complex is different. The atomic structure suggested composes finally of a $[C\text{-Si}]_s$ pair adjacent to a VO_2 complex as shown in Figure 4.8. The photoluminescence investigations of Fukuoka et al. [4.215] confirmed the involvement of a carbon interstitial and of two or more oxygen atoms and supported the structure suggested by Kürner et al. Alternative structures for the center were proposed by Ewels et al. [4.216] on the basis of their *ab-initio* calculations. They consist of an interstitial carbon atom and two oxygen interstitials as shown in Figure 4.9. The upper one is C_{1h} -symmetric and has a lower energy than the C_{2v} -symmetric lower configuration shown below.

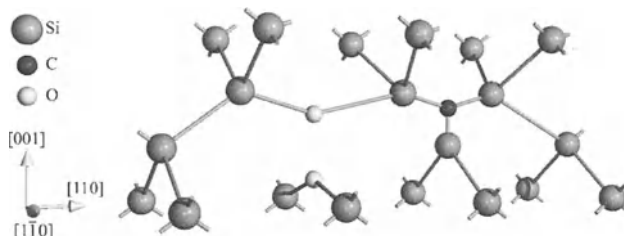


Figure 4.8: Atomic configuration of the C_iVO_2 complex suggested by Kürner et al. [4.214] for the *P*-line defect.

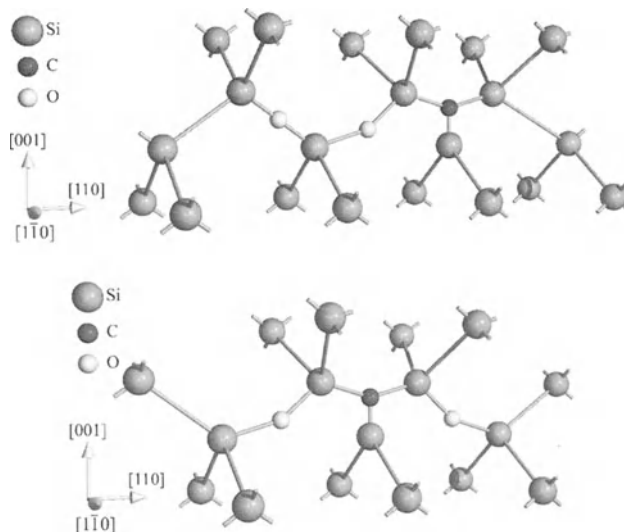


Figure 4.9: Possible atomic configurations of C_iO_{12} complexes suggested by Ewels et al. [4.216] for the *P*-line defect.

For the sake of completeness, it has to be mentioned that a PL line at 0.7667 to 0.767 eV was found also after thermal treatment of CZ wafers for several hours at 450 °C [4.217, 4.218]. The same thermal treatment gives rise to the formation of thermal donors and the generation of both defects was found to correlate. With increasing carbon concentration, the intensity of the PL line was found by Tajima et al. [4.218] to grow on the expense of the thermal donors. Carbon, as mentioned above, is known to reduce the rate of formation and the maximum concentration of thermal donors [4.15–4.19]. The mechanism proposed usually is the competing formation of carbon-oxygen complexes and the investigation of Lindström et al. [4.219] showed that two oxygen atoms are consumed in such complexes per carbon atom. Thus, it seems a likely supposition that the defects observed after thermal treatment of CZ wafers are identical to the PL *P*-line defects observed after electron irradiation. It has to be mentioned, though, that Fukuoka et al. [4.215] found later no correlation between the kinetics of the *P* line and thermal donors during heat treatment of CZ wafers at 450 °C.

$VO_2O_iC_i$

From the kinetics of the formation of complexes due to electron irradiation of carbon-rich samples at elevated temperatures, Lindström et al. [4.179] concluded that $VO_2O_iC_i$ complexes would form by the reaction of VO_2O_i with an interstitial carbon atom which attaches to the interstitial oxygen. The complex was associated with bands at 902, 956, and 1025 cm^{-1} (10 K).

$C_{2s}O_i$

Interpreting the kinetics of a DLTS level at $E_c - 0.2$ eV, Dobrovinskii et al. [4.220] suggested that it might be associated with a highly stable complex composing of two substitutional carbon atoms on adjacent lattice sites with an interstitial oxygen atom in between.

Other Carbon-Oxygen Complexes

From a comparison of the properties of a zero-phonon PL line at 1.0595 eV with those of the PL C-line and from isotope experiments which revealed the presence of carbon and oxygen, Kürner et al. [4.221] concluded that the former PL line arises from a modification of the C_iO_i defect. Its lower symmetry was suggested to arise from the capture of a silicon or carbon interstitial at the C_iO_i core.

4.1.6 Complexes with Dopants

Phosphorus

Fingerprints of one of the most remarkable defects in silicon were found and reported by Chantre and Kimerling [4.222], Song et al. [4.223], and Asom et al. [4.121] in DLTS studies of electron-irradiated silicon. Covered partly by other prominent centers, the defect was suggested to exist in four different configurations with donor levels 0.21, 0.23, 0.29, and 0.3 eV below the conduction band. Based on its correlation with phosphorus and carbon, it was tentatively identified as C_iP_s pair. In a subsequent study, Su et al. [4.224] observed that the conversion from the configuration characterized by the level at $E_c - 0.3$ eV to the configuration with the level at $E_c - 0.21$ eV depends strongly on the sample-fabrication method used. From the correlation with boron introduced during sample fabrication, it was suggested that the latter configuration involves a boron atom trapped near the C_iP_s pair. Su et al. also found that the donor level at $E_c - 0.21$ eV results at least from two overlapping defect levels. Later, based on their previous work, Gürer et al. [4.225] identified a fifth configuration. According to their review, the various configurations of the C_iP_s pair are associated with the ionization levels listed in Table 4.1. In complementary experiments on carbon-enhanced dissolution of thermal donors at 470 °C, Kamiura et al. [4.226] observed a deep level at $E_c - 0.36$ eV. Based on its correlation to carbon and phosphorus, it was tentatively ascribed to a C_iP_s pair, too.

Table 4.1: Ionization levels of the configurations of the C_iP_s pair after Gürer et al. [4.225].

Configuration	E_-	E_+
IA	$E_c - 0.38$ eV	$E_v + 0.48$ eV
IB	$E_c - 0.07$ eV	$E_c - 0.39$ eV
IIA	$E_c - 0.26$ eV	$E_v + 0.57$ eV
IIB		$E_c - 0.32$ eV
III		$E_c - 0.23$ eV

For the stable form IA of the C_iP_s complex, Gürer et al. [4.225] suggested a C_{2v} -symmetric configuration in which a phosphorus atom and a carbon atom, arranged along the $\langle 100 \rangle$ direction, share a lattice site. The neutral charge state of such a configuration was identified by Zhan and Watkins [4.227] as EPR Si-L8 center in phosphorus-doped silicon. Quoting otherwise unpublished results of Drevinsky et al. who found the capture radius for a carbon interstitial at a phosphorus atom to be 2 to 12 times as large as for a carbon interstitial at a substitutional carbon atom, Kimerling et al. [4.94] suggested an electrostatically enhanced reaction between C_i^- and P_s^+ . Based on a model which explains the ionization levels observed by the Coulomb interactions between oppositely charged carbon interstitials and substitutional phosphorus atoms, Gürer et al. [4.225] concluded that the metastable configurations of the C_iP_s pair are characterized by larger separations. It was also found that the thermally induced conversions between configurations are consistent with the motion of the carbon interstitial. Two other EPR centers,

Si-*L*9 and Si-*L*10 were found by Zhan and Watkins [4.228] to arise from the metastable configurations IB and IIA of the C_iP_s pair, respectively. The atomic arrangements suggested compose of a carbon-interstitial pair occupying a substitutional site on a second nearest coordination site of the substitutional phosphorus atom. For Si-*L*9, the carbon atom in the pair is nearer to the phosphorus atom than the silicon atom, and *vice versa* for Si-*L*10.

Arsenic

Investigating electron-irradiation-induced defects in arsenic-doped silicon, Gürer and Benson [4.229] found a multi-configurational defect with acceptor levels 0.12, 0.27, and 0.43 eV below the conduction band. In analogy to the other donor-carbon pairs, donor levels were reported 0.34 and 0.45 eV below the conduction band. One configuration suggested is a C_{2v}-symmetric carbon-arsenic pair oriented in the ⟨001⟩ direction around a lattice site. For a further bistable configuration, a structure of a carbon-silicon pair near a substitutional arsenic atom was supposed with configurations similar to the C_iC_s pair. The neutral charge state of the stable arsenic-carbon pair was suggested by Zhan and Watkins [4.228] to give rise to the EPR Si-*L*11 spectrum. They also concluded from kinetic studies that the dissociation energy of the pair is about 1.3 eV.

Antimony

A similar multi-configurational defect with acceptor levels 0.13, 0.16, 0.27, and 0.39 eV below the conduction band was reported by Benson et al. [4.230] and Gürer and Benson [4.229] in antimony-doped silicon. In addition, donor levels were reported 0.42 and 0.46 eV below the conduction band. The levels were suggested to arise from four different atomic configurations with structures like those of the arsenic-carbon pair. The neutral charge state of the stable antimony-carbon pair was proposed by Zhan and Watkins [4.228] to give rise to the EPR Si-*L*12 spectrum.

Indium

In indium-doped silicon, an acceptor level at $E_v + 0.111 \pm 0.002$ eV was found to correlate with indium [4.231–4.238]. This level, sometimes called Si-X center, is located at about 72% of the indium ionization energy and leads to a deterioration of indium-based infrared detectors. On the other hand, it may advantageously contribute to the electrical activation of indium profiles in VLSI applications [4.239, 4.240]. Baron et al. [4.241] showed that the concentration of this level correlates also with the concentration of carbon. Based on the binding enthalpy of 0.7 ± 0.1 eV determined from the experiments, they suggested that the level arises from an indium-carbon pair at nearest neighbouring substitutional sites. Interpreted in terms of a pair of substitutional atoms, the formation of a pair involves also an entropy reduction of $1.33 \cdot k$. Doubts about the assignment as a pair of substitutional atoms were raised again by Swaminathan et al. [4.242]. They found that the concentration of Si-X centers increases with electron irradiation and suggested it to arise from defects of indium atoms and intrinsic point defects. However, a linear correlation with carbon was found by Jones et al. [4.243], too. Their measurements of the defect concentration confirmed the binding enthalpy of 0.7 eV with a slightly higher entropy reduction of $3.1 \cdot k$ upon pair formation. The identification as a pair of neighboring substitutional atoms was corroborated by an extensive reasoning, including similarities to ⟨111⟩-symmetric complexes in aluminum-doped silicon and a computation of the expected energy levels by an extended-Hückel cluster calculation.

Aluminum

An acceptor level similar to the In_sC_s pair was reported by Scott [4.234] and Jones et al. [4.243] for silicon doped with aluminum. The optical ionization energy of the level was found to be $0.0563 \pm 3 \cdot 10^{-4}$ eV, 82% of the aluminum ionization energy. Interpreted in terms of a pair of substitutional atoms, its formation was found to involve an enthalpy reduction of 0.28 eV and an entropy increase of $4.0 \cdot k$. Uniaxial stress experiments established a trigonal $\langle 111 \rangle$ symmetry as it is expected for a pair of neighboring substitutional atoms.

In silicon doped with aluminum and carbon, Drakeford and Lightowers [4.244] found a PL line at 0.922 eV to form during heat treatment at 450 °C. This line was attributed tentatively to a complex involving aluminum and carbon.

Boron

An acceptor level similar to the In_sC_s pair was reported by Jones et al. [4.243] for silicon doped with boron. The optical ionization energy of the level was found to be 0.0371 eV, 84% of the boron ionization energy. Interpreted in terms of a pair of substitutional atoms, its formation was found to involve an enthalpy reduction of 0.03 eV and an entropy increase of $8.1 \cdot k$. The investigations of Yarykin et al. [4.245], on the other hand, indicated that B_iC_s has no levels detectable by DLTS in *p*-type silicon.

Based on the kinetics of a DLTS level at $E_v + 0.29$ eV during electron irradiation, Drevinsky et al. [4.246] suggested the level to be associated with a B_iC_s complex. Its appearance was found to correlate with the annealing of C_iO_i and not to depend on the oxygen concentration. This assignment was substantiated by the *ab-initio* simulations of Adey et al. [4.247].

Various investigations indicated that boron atoms implanted into carbon-doped silicon show a reduced electrical activation after annealing when compared to similar experiments in carbon-lean samples [4.159, 4.248, 4.249]. In their PL investigations, Irion et al. [4.250] found that the no-phonon photoluminescence *T*-line at 0.9351 eV arises from a C_{2v} -symmetric defect which contains boron and carbon. Although no complete atomic arrangement was given, the boron atom was suggested to be substitutional.

After the irradiation of solar cells with electrons, Roux et al. [4.195] found that cells with low oxygen content are more prone to degradation during illumination than solar cells with a high oxygen concentration. In a subsequent study, Peters et al. [4.251] found the introduction rate of a level at $E_v + 0.47$ eV to correlate with the dopant dependence of the degradation. Based on the same evidence, it was associated with B_iC_s .

The *ab-initio* calculations of Liu et al. [4.97] indicated that the energetically most favorable configuration would be a C_{2v} -symmetric $\langle 100 \rangle$ -oriented split configuration of a boron atom and a carbon atom around a regular lattice site. Its neutral charge state was suggested to be the most stable in intrinsic silicon with the formation energies of the negative and the positive charge states being 0.05 and 0.67 eV higher, respectively. Compared to a neutral substitutional carbon atom and a neutral boron interstitial, a lowering of the system energy by 2.36 eV was suggested to accompany the formation of the complex. A second reaction path in which a neutral carbon interstitial complexes with a neutral substitutional boron atom was found to be characterized by a binding energy of 1.11 eV. Similar work by Adey et al. [4.247] confirmed the configuration found by Liu et al. They reported the reaction of B_s^- and C_i^+ to $(\text{B}_i\text{C}_s)^+$ to be associated with an energy gain of 1.2 eV when the Fermi level is near to the valence-band edge.

Gallium

An acceptor level similar to the In_sC_s pair was reported by Jones et al. [4.243] for silicon doped with gallium. The optical ionization energy of the level was found to be 0.057 eV, 70% of the gallium ionization energy. Interpreted in terms of a pair of substitutional atoms, its formation was found to involve an enthalpy reduction of 0.4 eV. Similar to indium, pair formation with carbon was found to reduce the system entropy by $2.4 \cdot k$.

Nitrogen

Complexes with nitrogen will be discussed in Section 5.7.4.

4.1.7 Influence on the Concentrations of Intrinsic Point Defects

The basic interaction between carbon and intrinsic point defects is certainly the reaction of substitutional carbon atoms with silicon self-interstitials to carbon interstitials. Further reactions of these highly mobile point defects with substitutional carbon, self-interstitials, or other impurities lead to an effective reduction of an oversaturation of self-interstitials.

In addition to the well understood reduction of an oversaturation of self-interstitials by carbon, Lanzerotti et al. [4.252], Rücker et al. [4.125, 4.253], and Carroll et al. [4.28] reported a strongly reduced diffusivity of epitaxially grown boron spikes within a carbon-rich layer. Complementary investigations by Zaumseil and Rücker [4.254] indicated a carbon-induced, enhanced interdiffusion in SiGe superlattices. The effects observed were reproduced qualitatively by the numerical simulations of Scholz et al. [4.127, 4.255] and Rücker et al. [4.125] who explained it by an undersaturation of self-interstitials in the carbon-rich layer which, in turn, is caused by the out-diffusion of carbon interstitials from this layer. Somewhat in contrast, Liu et al. [4.97] deduced a dominating influence of boron-carbon clusters from their kinetic simulations which adds to the undersaturation of self-interstitials also found. In agreement with the predicted undersaturation of self-interstitials, Rücker et al. [4.128, 4.253] found a suppression of the diffusion of phosphorus and an enhancement of the diffusion of arsenic and antimony. The enhanced diffusion of antimony in and below highly carbon-doped layers was observed experimentally also by Lavéant et al. [4.256]. Especially the enhanced diffusion of antimony is a clear indication of an enhanced vacancy concentration and shows that the reduced diffusion of boron observed at first is not caused primarily by the formation of immobile complexes.

4.2 Germanium

Germanium is an isovalent impurity in silicon. Since its covalent radius is only 4% larger than that of silicon, germanium atoms are expected to behave very much like silicon atoms. As a consequence, germanium diffusion in silicon was studied in order to gain insight into self-diffusion in silicon which was considerably more problematic to investigate at that time.

Because of their high mass, germanium atoms are frequently used to amorphize silicon prior to the implantation of dopants. Such layers, in comparison to layers preamorphized with silicon, are characterized by a smoother interface and a much lower density of hairpin dislocations after recrystallization [4.257–4.259].

The technologically most important application comes from the use of thin SiGe layers which can be used either as single layer or as Si/SiGe/Si structure for band-gap engineering and to enhance the electron mobility. Actual applications include resonant tunnelling diodes (RTDs), heterojunction bipolar transistors (HBTs), heterojunction field effect transistors

(HFETs), modulation-doped field effect transistors (MODFETs), SiGe heterostructure CMOS (HCMOS) devices, velocity modulation transistors (VMTs), and optoelectronic devices. The addition of carbon, discussed in Section 4.1, leads to an additional degree of freedom for the design of such devices. Unfortunately, a discussion of silicon-germanium materials would exceed the scope of this book by far and it just remains to refer the interested reader to some review articles in this field [4.260–4.265]. In the following sections, the basic atomic configurations of germanium in silicon, the diffusion behavior, and the formation of complexes will be discussed.

4.2.1 Basic Atomic Configurations

Substitutional Germanium

In agreement with the covalent radius, volume expansions $\Delta V/V_{Si}$ of 3.6% [4.266] and 4% [4.267] were predicted to be associated with a substitutional germanium atom. Investigations of the phonon spectra by Logan et al. [4.268] indicated that the germanium atoms occupy only next-nearest neighboring sites in the diamond lattice rather than forming clusters.

Germanium-Vacancy Pairs

The EPR spectra of the positive and negative charge states of a vacancy at a next neighbor position of a germanium atom were reported by Watkins [4.269] and labelled Si-G26 and Si-G27, respectively [4.270]. To investigate the electrical properties of germanium-vacancy complexes, Emtsev et al. [4.271] irradiated germanium-doped silicon samples with γ rays. The irradiation resulted in acceptor states located at about E_c - (0.05–0.08) eV. Based on a comprehensive reasoning, they were associated with germanium-vacancy pairs. After irradiation of germanium-doped samples with α particles, Abdullin and Mukashev [4.102] observed by DLTS a center which they showed to be vacancy-related and which was not observed in samples not doped with germanium. As a consequence, it was tentatively assigned to a vacancy stabilized by a germanium atom. The two levels observed at E_c - 0.22 eV and E_c - 0.4 eV correspond to its double acceptor level and its acceptor level, respectively. In an electron-irradiation experiment, Budtz-Jørgensen et al. [4.272] identified a level at E_c - 0.29 eV to be associated with the germanium-vacancy pair and argued that it might be the double acceptor level.

In electron-irradiation experiments, Brelot and Charlemagne [4.273] found that virtually no vacancies are trapped by oxygen when germanium is present in a concentration of $3 \cdot 10^{20} \text{ cm}^{-3}$. This effect was explained by a capture of the vacancies generated at the germanium atoms. From a quantitative analysis, the authors concluded that the vacancy-capturing efficiencies of oxygen and germanium are about the same. The vacancy-germanium complexes were found to dissociate between 200 and 280 K, associated with the formation of divacancies and vacancy-oxygen pairs. Germanium, on the other hand, was not found in these studies to interact in a noticeable way with self-interstitials. A more detailed study published by Brelot [4.274] confirmed the very similar vacancy-capture efficiencies of germanium atoms and oxygen atoms. With respect to silicon self-interstitials, he estimated the capture efficiency of germanium at 90 K to be less or equal to $2 \cdot 10^{-3}$ that of oxygen and $7 \cdot 10^{-5}$ that of carbon. Brelot's observation of an efficient trapping of vacancies by germanium atoms was confirmed later by the investigations of Khirunenko et al. [4.275] and Sobolev and Nazaré [4.276].

4.2.2 Solubility

According to the phase diagram of the germanium-silicon system compiled by Olesinski and Abbaschian [4.277], the two elements are completely miscible.

4.2.3 Diffusion

Because suitable diffusion experiments with silicon-tracer atoms were not possible until recently, isovalent tracer atoms like germanium were often used for basic investigations of diffusion mechanisms in silicon. It was suggested that the activation energies characterizing the diffusion of germanium and silicon tracers in silicon should be nearly equal because both atoms have nearly the same covalent radius in the diamond structure [4.278].

Intrinsic Diffusion

Diffusion coefficients of germanium under nominally inert and intrinsic conditions were reported in several studies. In them, germanium was introduced from a deposited germanium layer [4.278–4.282], from an epitaxially grown, germanium-doped layer [4.283–4.286], from a germanium-doped oxide [4.287], or by ion implantation [4.288]. For the characterization of the diffusion profile, depth profiling by radiochemical methods [4.278, 4.279, 4.288], RBS [4.284], or SIMS [4.280–4.283, 4.285–4.287] were used. A summary of the diffusion coefficients reported can be found in Figure 4.10 together with the regression curve

$$D_{Ge}^i = 1.72 \cdot 10^3 \cdot \exp\left(-\frac{4.830 \text{ eV}}{k \cdot T}\right) \text{ cm}^2/\text{s} \quad (4.4)$$

derived from these measurements. The activation energy ranges with a confidence level of 90% from 4.69 to 4.97 eV. The 90% confidence interval for the diffusion coefficient is about +12/-11% of the regression curve at 1074 °C and increases to +30/-23% at the melting point and at 850 °C. Additional measurements are expected with 90% confidence within +209/-68% of the regression curve at 1074 °C which increases slightly to +216/-68% at the melting point and at 850 °C.

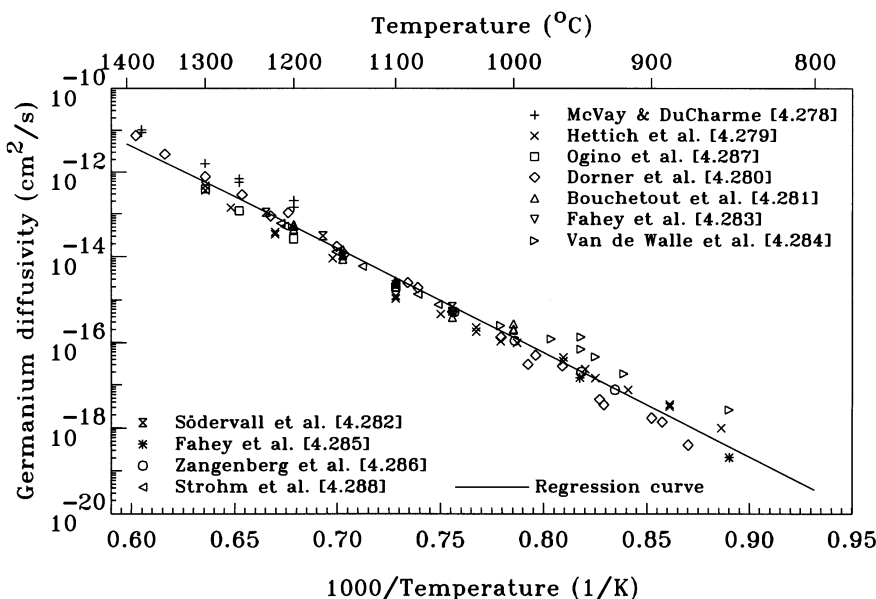


Figure 4.10: Diffusion coefficient of germanium under intrinsic and inert conditions in silicon.

It is evident from Figure 4.10 that the agreement between the investigations is not exceptional and qualitatively different results were reported for the temperature dependence. From the investigations of Hettich et al. [4.279], a kink in the Arrhenius representation of the diffusion coefficient is apparent around 1020 °C. It separates a high-temperature regime with an activation energy of 4.97 eV from a low-temperature regime with a significantly lower activation energy of 3.93 eV. Hettich et al. interpreted this temperature dependence as a change from an interstitial mechanism at high temperatures to a vacancy mechanism at low temperatures and emphasized the similarity to silicon. In the more recent investigations of Dorner et al. [4.280], no such kink can be found. Similarly, in the recent investigations of tracer diffusion in silicon, a large temperature range could be described by a single activation energy. Finally, in the work of Bouchetout et al. [4.281], a kink around 1020 °C appears again, but this observation is supported only by data points at one temperature. A reason for the discrepancies is not apparent but an influence of the hydrogen atmosphere used in the measurements of Hettich et al. cannot be excluded *a posteriori*. A general problem in investigations in which a deposited germanium layer was used as source is that fairly high germanium concentrations are expected in the silicon near to this layer. Since the diffusivity of germanium is known to increase with the germanium concentration, the prerequisite condition of a constant diffusion coefficient was probably not fulfilled in all investigations.

Diffusion Mechanism

In an oxygen-containing ambient, Ogino et al. [4.287] observed enhanced diffusion of germanium. Based on a comparison to the diffusivities of other impurities, Fahey et al. [4.283] estimated the fractional diffusivity of germanium at 1050 °C to be between 0.3 and 0.4. The same range for f_I was found by Fahey et al. [4.285] at 950 °C. Based on a similar same method, Cowern et al. [4.289] estimated f_I^{Ge} to be 0.22 ± 0.04 at 875 °C.

Investigating the diffusion of germanium during post-implantation annealing at a temperature of 400 °C, Perozziello et al. [4.290] found that the resulting profiles can be reproduced best assuming that only a fraction of the implanted germanium atoms become mobile and diffuse a mean distance of 80 nm in the mobile state before they are immobilized again.

Pressure Dependence

Pressure-dependent diffusion studies performed by Södervall et al. [4.282] at 1050, 1170, and 1230 °C resulted in estimates of the activation volume of about -0.52, 0.47, and 0.27 times the silicon volume V_{Si} . Investigating the concentration dependence of the diffusion of germanium in strained and unstrained SiGe layers, Cowern et al. [4.291] found that the diffusivity in compressively strained layers increases exponentially with composition. A numerical evaluation indicated that the apparent activation energy of germanium diffusion changes by $s \cdot (40 \pm 5)$ eV with s denoting the strain in the layer. In the work of Zangenberg et al. [4.286], this relation was found to be characterized by $s \cdot (110\text{--}160)$ eV.

Extrinsic Diffusion

Information about the diffusion of germanium at extrinsic concentrations is available from the isoconcentration diffusion studies of McVay and DuCharme [4.292], Hettich et al. [4.279], Bouchetout et al. [4.281], and Nylandsted Larsen et al. [4.293]. For an isovalent impurity like germanium, ion pairing effects like for dopants are not expected in general. Therefore, it should be possible to use samples doped extrinsically with donors and acceptors to evaluate the

Fermi-level dependence of the diffusion coefficient. However, McVay and DuCharme [4.292], Hettich et al. [4.279], and Bouchetout et al. [4.281] reported significantly enhanced diffusion already for boron background concentrations below or near the intrinsic carrier concentration at that temperature. Such effects cannot be explained by a simple Fermi-level dependence. Boron-germanium complexes are expected to form (see Section 4.2.4) but it is doubtful whether they can explain the effect even when they are mobile. Therefore, for the results shown in Figure 4.11, only the measurements in *n*-type silicon were taken into consideration. The full lines were obtained by a numerical optimization using all data points in Figure 4.10 in addition to those in Figure 4.11, and are described by

$$D_{Ge} = 4.29 \cdot 10^3 \cdot \exp\left(-\frac{4.997 \text{ eV}}{k \cdot T}\right) \text{ cm}^2/\text{s}$$

$$+ \frac{n}{n_i} \cdot 1.81 \cdot 10^3 \cdot \exp\left(-\frac{5.002 \text{ eV}}{k \cdot T}\right) \text{ cm}^2/\text{s}. \quad (4.5)$$

According to these numbers, intrinsic diffusion is dominated by the Fermi-level-independent component. Considering the limited experimental data and the partly gross differences, not too much faith should be put into these values.

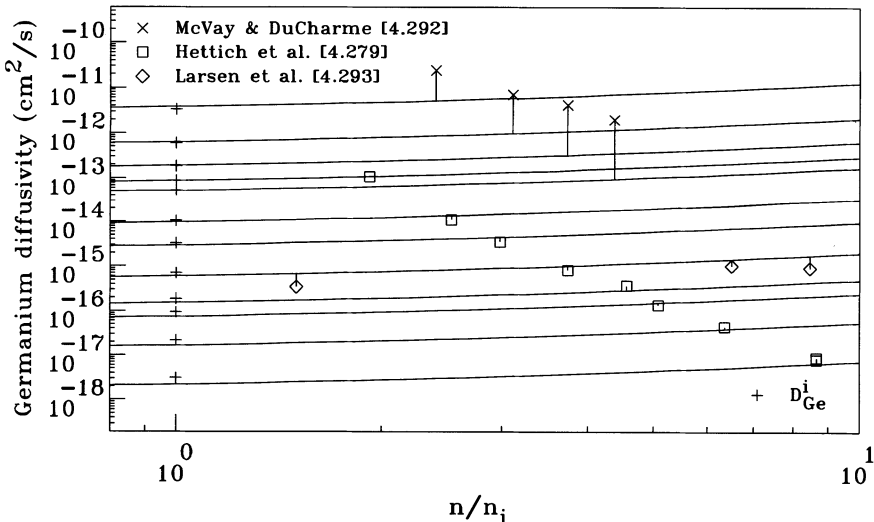


Figure 4.11: Dependence of the normalized diffusion coefficient of germanium in silicon on n/n_i for moderate dopant concentrations with $n/n_i \leq 20$. The full lines correspond, from top to bottom, to temperatures of 1380, 1300, 1250, 1220, 1200, 1140, 1100, 1050, 1010, 990, 950, and 900 °C.

A rapid increase of the germanium diffusivity for donor background concentrations exceeding $2 \cdot 10^{20} \text{ cm}^{-3}$ was not observed in the work of Kyllesbech Larsen et al. [4.294]. Later, Nylandsted Larsen et al. [4.293] reported such an increase proportional to about the fifth power of n/n_i . As for tin, arsenic, and antimony, the phenomenon was suggested tentatively to arise from the proximity of the impurities which reduces the formation and migration enthalpies of vacancies in their vicinity and which leads to an enhanced diffusion.

Diffusion at High Germanium Concentrations

Investigations of the diffusion of germanium in highly-germanium-doped, epitaxially deposited layers indicated that the diffusion coefficient increases considerably with the germanium concentration [4.284, 4.286, 4.292, 4.295]. Comparing the germanium diffusion inside and outside the SiGe layer, Van de Walle et al. [4.284] concluded that the diffusion enhancement is associated primarily with the local germanium concentration. This conclusion was supported by the work of Zangenberg et al. [4.286] who investigated concentration effects and strain effects independently.

4.2.4 Complexes

Using a combination of *ab-initio* calculations and β -NMR measurements, Hattendorf et al. [4.296] reported the identification of a pair of a boron and a germanium atom on neighboring substitutional sites. Already before, in investigations of boron diffusion in $\text{Si}/\text{Si}_{1-x}\text{Ge}_x$ structures, it was found that boron diffuses significantly slower in SiGe layers than in silicon [4.297–4.303]. To explain this phenomenon, an influence of the composition on the band gap and further on the diffusivity [4.297], but especially the formation of immobile pairs of boron and germanium [4.298, 4.299, 4.302] was postulated. This is supported by the finding of Kuo et al. [4.299] and Zangenberg et al. [4.303] that composition has a much more pronounced effect on boron diffusion than strain. However, it has to be noted that in the latest publication of Zangenberg et al. [4.304], no significant retardation of boron was found in germanium-doped silicon.

The concept of pair formation leads to a retardation factor $R_{B:\text{SiGe}}$ defined via

$$\frac{D_{B:\text{SiGe}}}{D_{B:\text{Si}}} = \frac{1}{1 + x_{Ge}^s \cdot R_{B:\text{SiGe}}} \quad (4.6)$$

where $x_{Ge}^s = C_{Ge}/(C_{Si} + C_{Ge})$ stands for the site fraction of germanium in the alloy, and $D_{B:\text{SiGe}}$ and $D_{B:\text{Si}}$ denote the diffusion coefficients of boron in SiGe and Si, respectively. Interpreted in terms of an immobile pair, $R_{B:\text{SiGe}}$ can be written in the form

$$R_{B:\text{SiGe}} = 4 \cdot \exp \left(\frac{G^B}{k \cdot T} \right) \quad (4.7)$$

with G^B standing for the binding energy of the boron-germanium complex. The retardation factors deduced from the experiments are shown in Figure 4.12. Only the one reported by Loechelt et al. [4.298] is against the trend and also against expectations since pair formation always becomes less significant with increasing temperature. The other data points can be interpreted in terms of a binding energy of about 0.15 eV around 850 °C. The regression curve also shown corresponds to

$$R_{B:\text{SiGe}} = 4.55 \cdot 10^{-3} \cdot \exp \left(\frac{0.791 \text{eV}}{k \cdot T} \right). \quad (4.8)$$

which can be interpreted in terms of a lowering of the system enthalpy and entropy by respectively 0.791 eV and $6.78 \cdot k$ upon formation of a germanium-boron pair from well-separated constituents. In the work of Rajendran et al. [4.305], properties of the reaction of boron and germanium to GeB were obtained from simulations of diffusion profiles in layered Si/SiGe structures. In particular, the equilibrium constant was suggested to be independent of temperature while the reaction constants were suggested to be activated with 4.1 eV and to depend non-linearly on the concentrations of germanium and boron.

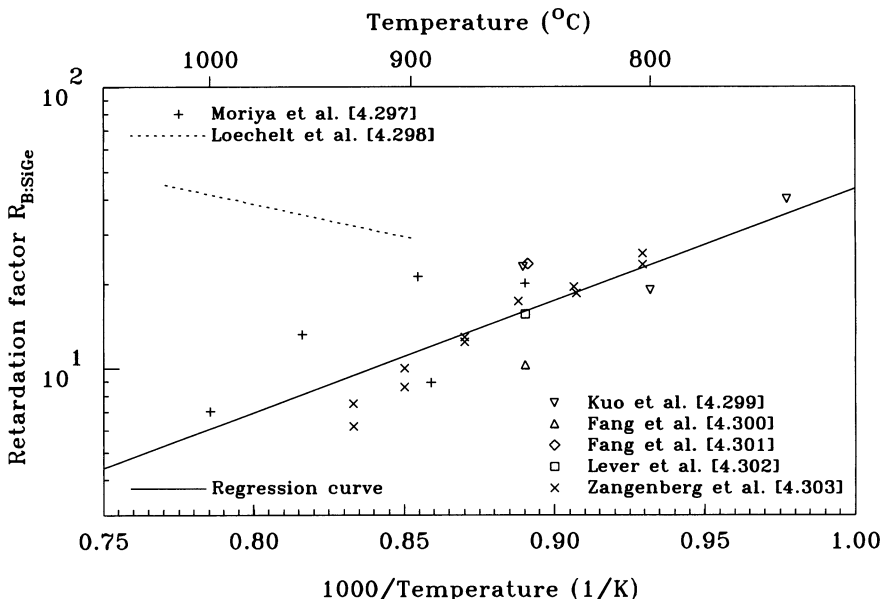


Figure 4.12: Retardation factor for the diffusion of boron in SiGe.

4.3 Tin

The first investigations of tin in silicon were clearly initiated to gain information about basic diffusion phenomena by the usage of an isovalent impurity. Because of its large covalent radius and its electrical neutrality, tin was also investigated as a method to compensate the strain in layers doped with a high concentration of impurities like boron or phosphorus which have smaller covalent radii than silicon [4.306–4.308]. The main application of tin in silicon in the following came from its ability to trap vacancies. Suggested already by Breloet [4.309], doping of silicon with tin was therefore investigated as a means to increase the radiation hardness of silicon solar cells and detectors [4.310–4.313]. These investigations confirmed that the introduction rate of the common radiation-induced point defects and their clusters can be reduced. However, at the same time, new tin-related defects are introduced which introduce levels in the band gap and open new paths for recombination. Successful attempts to use tin for preamorphization [4.314] were not taken up in the following probably because of the success of germanium for such applications. In the following sections, the basic atomic configurations of tin in silicon, its solubility, the diffusion behavior, and the formation of complexes are discussed in detail.

4.3.1 Basic Atomic Configurations

The two basic atomic configurations of tin in silicon are a tin atom on a substitutional site and the tin-vacancy pair. Interactions of tin with self-interstitials were not reported.

Substitutional Tin

In the investigations of Trumbore et al. [4.315], tin was neither found to provide free charge carriers nor to be an effective recombination center for holes and electrons. Studying the lattice location of tin diffused at 1100 and 1200 °C into silicon by RBS, Akasaka et al. [4.316] found

89% to 98% of the tin atoms to occupy substitutional sites. Similarly, Mössbauer-spectroscopy investigations indicated that tin occupies at sufficiently low concentrations predominantly substitutional sites [4.317–4.320].

The Mössbauer-spectroscopy investigations in strongly *n*-doped and *p*-doped silicon reported by de Waard and Kemerink [4.321] gave no indication of a change of the electronic environment with the Fermi level. This confirms that tin has no ionization levels in the band gap as expected from an isovalent impurity.

Because of the larger covalent radius of tin in comparison to silicon, an expansion of the lattice around a substitutional tin atom can be expected. From theoretical investigations, estimates for $\Delta V/V_S$ of 16% [4.266] and 21% [4.267] were given.

Tin-Vacancy Pairs

Indirect evidence for the formation of tin-vacancy pairs was reported by Brelot [4.274, 4.309] who observed that the formation of vacancy-oxygen pairs was suppressed in tin-doped samples. The tin-vacancy pairs were found to dissociate again between 150 and 190 °C, accompanied by the formation of vacancy-oxygen pairs. In contrast, no noticeable interaction was found between tin and silicon self-interstitials. Brelot's observation of an efficient trapping of vacancies by tin atoms was confirmed later by the investigations of Neřmash et al. [4.322], Svensson et al. [4.323], Dobrovinskii et al. [4.324], and Svensson and Lindström [4.325].

A first identification of the tin-vacancy pair was achieved in the Mössbauer-spectroscopy investigations of Matsui et al. [4.326] and it was shown to anneal in the same temperature range as observed by Brelot [4.274]. Different characteristics of the spectra in *n*-type and *p*-type silicon were interpreted to arise from different charge states of the same defect. In tin-doped silicon, Watkins [4.327] found an EPR spectrum which he labeled Si-*G29* and which grew as the vacancy spectrum vanished. Annealing studies showed that the defect was stable up to about 230 °C. In the atomistic model suggested for the neutral charge state of the tin-vacancy pair observed by EPR, the tin atom assumes a D_{3d}-symmetric position halfway between two vacancies on adjacent lattice sites. Watkins' observations were confirmed by the EPR investigations of Fanciulli and Byberg [4.328]. In addition, they identified an EPR center labeled Si-*DK4* to arise from the negative charge state of the vacancy-tin pair. Its structure was suggested to be similar to that of the Si-*G29* center with a small distortion of the D_{3d} symmetry. The Mössbauer-spectroscopy investigations of Damgaard et al. [4.329], on the other hand, led to a rather different result. They found a line with an isomer shift of 2.3 mm/s relative to CaSnO₃ which they associated with a tin-vacancy pair. But they also concluded that the tin atom assumes a substitutional site with a vacancy at a next neighboring position. This assignment was supported by Müller et al. [4.330] who associated the tin-vacancy pair with the tin atom midway between two vacancies tentatively with a line with an isomer shift of 1.22 mm/s. However, in the later publication of Nylandsted Larsen et al. [4.331], it was suggested that the dominating non-substitutional Mössbauer spectrum with the isomer shift of 2.3–2.4 mm/s arises most likely from the structure suggested by Watkins. A confirmation of this tin-split-vacancy configuration in its neutral and negative charge state was obtained by the theoretical investigations of Nylandsted Larsen et al. [4.331]. These calculations also reproduced the ionization-level scheme discussed below. The binding energy of the neutral tin-vacancy complex was found to be 0.9 eV which reduces to 0.6 eV when the vacancy is at a second neighboring site of the tin atom. In the work of Kaukonen et al. [4.332], a binding energy of 1.0 eV was calculated.

Several investigations based on electron-irradiated, tin-doped samples indicated that tin-vacancy pairs introduce levels in the band gap. From illumination during his EPR investigations, Watkins [4.327] found a donor level at approximately $E_v + 0.35$ eV. Watkins and Troxell [4.333]

later reported the identification of two levels at $E_v + 0.07$ eV and $E_v + 0.32$ eV associated with the tin-vacancy pair which were interpreted to correspond to its double- and single-donor level, respectively. The DLTS investigations of Nylandsted Larsen et al. [4.331] led to the identification of two levels at $E_c - 0.214$ eV and $E_c - 0.501$ eV as the double and single acceptor levels of the tin-vacancy pair, respectively. After proton irradiation, Simoen and Claeys [4.313] found two levels by DLTS which were 0.29 and 0.61 eV below the conduction band. They were suggested to arise from double-acceptor and single-acceptor levels of vacancy-tin complexes.

Comparative studies reported by [4.331] showed that tin is a less effective trap for vacancies than germanium.

4.3.2 Solubility

The phase diagram of the binary system silicon-tin was compiled by Olesinski and Abbaschian [4.334]. Below the eutectic temperature of 231.9 °C, the tin in the silicon phase is in equilibrium with a pure βSn phase.

To extract the solubility of tin in silicon, crystal-pulling experiments [4.315], a thermal-gradient crystallization technique [4.315] as well as diffusion from the gas phase [4.335], from a deposited tin layer [4.318, 4.320], and from a doped oxide [4.316] were used. Among the methods applied to determine the concentration values were spectrophotometry [4.315], neutron activation [4.318, 4.320, 4.335], and RBS [4.316]. The solubility values obtained are shown in Figure 4.13.

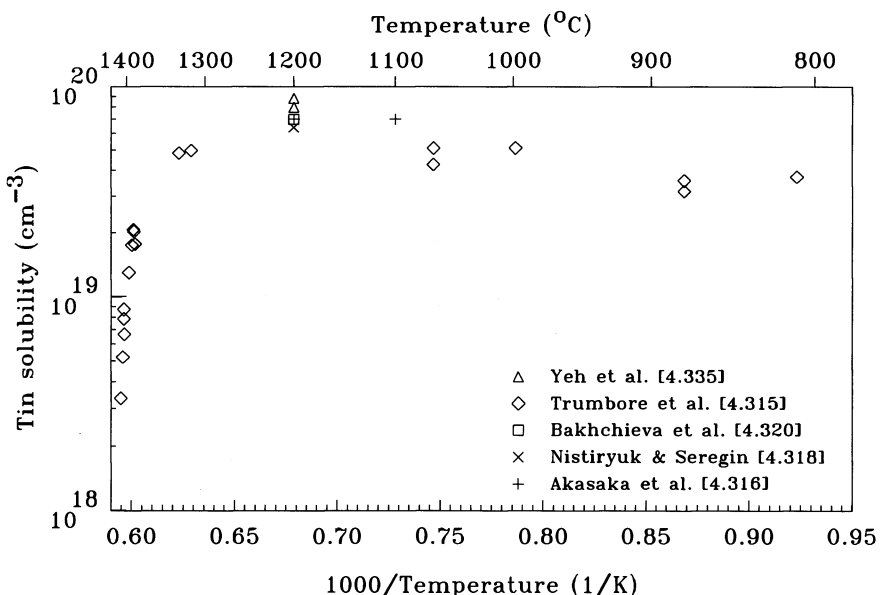


Figure 4.13: Solubility of tin in silicon.

4.3.3 Diffusion

Intrinsic Diffusion

The diffusion of tin under nominally inert and intrinsic conditions was investigated in several studies. In them, tin was introduced from the gas phase [4.335], a deposited tin layer [4.318, 4.320, 4.336], an epitaxially grown, a tin-doped layer [4.337] or a tin-doped oxide layer [4.316], or by ion implantation [4.338]. Depth profiles of the isovalent impurity were studied by neutron activation [4.318, 4.320, 4.335], via a radioactive tin isotope [4.336], by RBS [4.316], or by SIMS [4.337, 4.338]. A summary of the diffusion coefficients reported can be found in Figure 4.14 together with the regression curve

$$D_{Sn}^i = 1300 \cdot \exp\left(-\frac{4.728\text{eV}}{k \cdot T}\right) \text{cm}^2/\text{s} \quad (4.9)$$

derived from these measurements. The activation energy ranges with a confidence level of 90% from 4.52 to 4.94 eV. The 90% confidence interval for the diffusion coefficient is about +14/-12% of the regression curve at 1100 °C and increases to +43/-30% at the melting point and +39/-28% at 900 °C. Additional measurements are expected with 90% confidence within a range of +99/-50% of the regression curve at 1100 °C which increases slightly to +115/-53% at the melting point and +112/-53% at 900 °C.

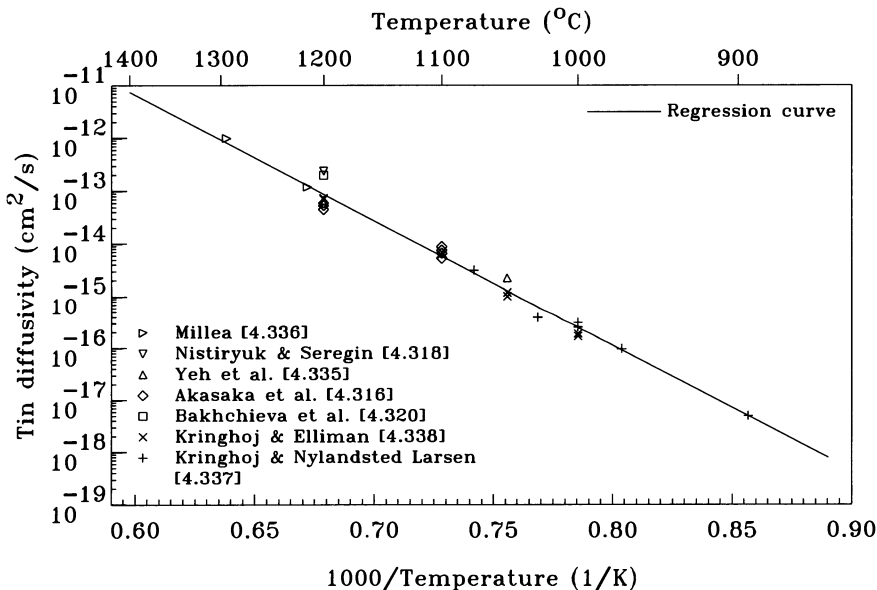


Figure 4.14: Diffusion coefficient of tin under intrinsic and inert conditions in silicon.

Diffusion Mechanism

A comparison of the nitridation-enhanced diffusion of tin and antimony performed by Kringhøj and Nylandsted Larsen [4.337] indicated that the fractional diffusivities of the two impurities are approximately equal, i. e. that tin diffuses nearly entirely via a vacancy mechanism.

Extrinsic Diffusion

Information about the diffusion of tin at extrinsic concentrations is available from the isoconcentration diffusion studies of Millea [4.336], Yeh et al. [4.335], and Nistiryuk and Seregin [4.318]. For an isovalent impurity like tin, ion-pairing effects like for dopants are not expected. Therefore, it should be possible to use samples doped extrinsically with donors and acceptors to evaluate the Fermi-level dependence of the diffusion coefficient. Strangely, a pronounced diffusivity enhancement was reported by Nistiryuk and Seregin already for acceptor and donor background concentrations significantly lower than the intrinsic carrier concentration at that temperature. The results of the other two studies are shown in figure 4.15. The full lines were obtained by a numerical optimization using all data points in Figure 4.14 in addition to those in Figure 4.15, and are described by

$$\begin{aligned} D_{Sn} = & \quad 1.29 \cdot 10^3 \cdot \exp\left(-\frac{4.73\text{eV}}{k \cdot T}\right) \text{cm}^2/\text{s} \\ & + \frac{n}{n_i} \cdot 190 \cdot \exp\left(-\frac{4.594\text{eV}}{k \cdot T}\right) \text{cm}^2/\text{s} \\ & + \frac{n_i}{n} \cdot 98.5 \cdot \exp\left(-\frac{6.572\text{eV}}{k \cdot T}\right) \text{cm}^2/\text{s}. \end{aligned} \quad (4.10)$$

Considering the limited experimental data and the partly gross differences, not too much faith should be put into these parameters.

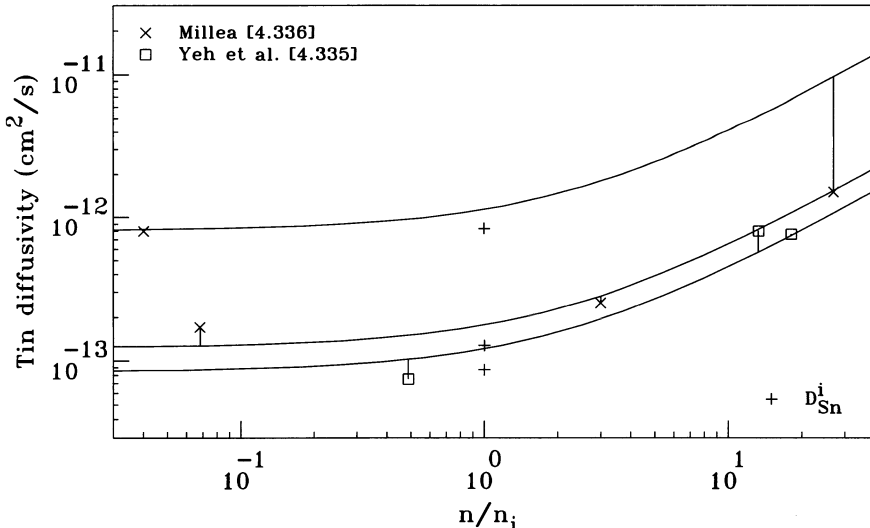


Figure 4.15: Dependence of the normalized diffusion coefficient of tin in silicon on n/n_i . The full lines correspond, from top to bottom, to temperatures of 1290, 1220, and 1200 °C.

A rapid increase of the tin diffusivity for donor background concentrations exceeding about $2 \cdot 10^{20} \text{ cm}^{-3}$ was reported for short-time processes by Nylandsted Larsen and his coworkers [4.293, 4.339]. As for germanium, arsenic, and antimony, the phenomenon was suggested tentatively to arise from the proximity of the impurities which reduces the formation and migration enthalpies of vacancies in their vicinity and which leads to enhanced diffusion.

4.3.4 Complexes

After electron irradiation of tin-doped, *n*-type silicon, Fanciulli and Byberg [4.340] found a triclinic EPR spectrum which they labeled Si-*DK1* and which they identified to arise from a tin-divacancy complex in its negative charge state. In the structure suggested, the tin atom and the divacancy are arranged along a [110] chain in a (110) plane and have C_{1h} symmetry. Annealing above 500 K caused a decay of the Si-*DK1* signal associated with the emergence of two other monoclinic EPR spectra which were labeled Si-*DK2* and Si-*DK3* and which annealed out at 690 K. The C_{2h}-symmetric Si-*DK2* was suggested to be associated with the negative charge state of a divacancy with tin atoms on substitutional sites at either end, all arranged in a (110) plane. Si-*DK3* was likewise assigned to the negative charge state of a Sn₂V₂ complex, but with a C_{1h}-symmetric arrangement in which a central vacancy has two tin atoms and a second vacancy at nearest neighboring sites. To explain the formation of Sn₂V₂ complexes, SnV₂ was suggested to be mobile. Similarly, Sn₂V₂ complexes were assumed mobile. After electron irradiation of tin-doped silicon, Khirunenko et al. [4.341] observed the annealing of V₂ at temperatures between 180 and 210 °C to be accompanied by the appearance of an absorption band at 4100 cm⁻¹ (RT) silicon. The line was found to increase with the tin concentration and to show an annealing behavior similar to the Sn₂V₂ complex identified tentatively by Fanciulli and Byberg [4.340]. At measurement temperatures below 120 K, a series of satellites was found with higher wave numbers separated by 70 cm⁻¹. At the same time, a series of absorption frequencies were found at 2750 cm⁻¹ and above which had a similar spacing and were interpreted to arise from an other charge state of Sn₂V₂. In an *ab-initio* study, Kaukonen et al. [4.332] estimated the energy levels and the formation energies of Sn_{*m*}V_{*n*} complexes. These calculations indicated that the second vacancy binds to an SnV₂ complex with 1.5 eV. Formation of Sn₂V from a substitutional tin atom well-separated from a SnV pair was shown to be associated with an energy gain of 0.4 eV. For the reaction with an additional vacancy to Sn₂V₂, a lowering of the system energy by 2.3 eV was computed.

Annealing of VO centers in electron-irradiated, tin-doped silicon around 290 to 320 °C was found by Khirunenko et al. [4.341] to be accompanied by the appearance of an absorption line at 807 cm⁻¹ (RT). The new absorption line was associated with an SnVO complex.

In their Mössbauer-spectroscopy investigations of samples doped with tin and phosphorus, Müller et al. [4.330] found a line with an isomer shift of 2.66 nm/s. It was finally assigned to a vacancy with a tin atom and a phosphorus atom at nearest neighboring sites.

The formation of tin-carbon pairs was studied by IR spectroscopy and *ab-initio* simulations by Lavrov et al. [4.342]. The absorption lines found at 873.5, 1025, and 6875 cm⁻¹ (10 K) were attributed to a carbon interstitial next to a substitutional tin atom. The calculations indicated also that a substitutional carbon atom next to or near to a substitutional tin atom should lead to an electrically inactive, stable defect. In addition to the previously assigned absorption bands, such as 888.9, 985.3, and 6915 cm⁻¹ (10 K) were assigned by Khirunenko et al. [4.343] to a pair of a substitutional tin atom and an interstitial carbon atom at a next-nearest neighboring site.

Bibliography

- [4.1] J. P. Kalejs and L. A. Ladd, "Influence of High-Temperature Annealing on Performance of Edge-Defined Film-Fed Growth Silicon Ribbon Solar Cells," *Appl. Phys. Lett.*, vol. 45, no. 5, 540–542 (1984).
- [4.2] R. C. Newman and R. S. Smith, "Vibrational Absorption of Carbon and Carbon-Oxygen Complexes in Silicon," *J. Phys. Chem. Solids*, vol. 30, 1493–1505 (1969).

- [4.3] J. B. Posthill, R. A. Rudder, S. V. Hattangady, G. G. Fountain, and R. J. Markunas, “On the Feasibility of Growing Dilute C_xSi_{1-x} Epitaxial Alloys,” *Appl. Phys. Lett.*, vol. 56, no. 8, 734–736 (1990).
- [4.4] S. S. Iyer, K. Eberl, M. S. Goorsky, F. K. Legoues, F. Cardone, and B. A. Ek, “The Synthesis and Stability of $Si_{1-y}C_y$ Alloys and Strained Layer Superlattices,” in: *Silicon Molecular Beam Epitaxy*, edited by J. C. Bean, S. S. Iyer, and K. L. Wang, *Mat. Res. Soc. Symp. Proc.*, vol. 220, 581–588 (1991).
- [4.5] A. R. Powell, K. Eberl, B. A. Ek, and S. S. Iyer, “ $Si_{1-x-y}Ge_xC_y$ Growth and Properties of the Ternary System,” *J. Crystal Growth*, vol. 127, 425–429 (1993).
- [4.6] H. J. Osten, E. Bugiel, and P. Zaumseil, “Growth of an Inverse Tetragonal Distorted SiGe Layer on Si(001) by Adding Small Amounts of Carbon,” *Appl. Phys. Lett.*, vol. 64, no. 25, 3440–3442 (1994).
- [4.7] J. W. Strane, H. J. Stein, S. R. Lee, S. T. Picraux, J. K. Watanabe, and J. W. Mayer, “Carbon Incorporation into Si at High Concentrations by Ion Implantation and Solid Phase Epitaxy,” *J. Appl. Phys.*, vol. 79, no. 2, 637–646 (1996).
- [4.8] R. F. Pinizzotto and F. Marks, “Carbon and the Kinetics of Oxygen Precipitation in Silicon,” in: *Defects in Semiconductors II*, edited by S. Mahajan and J. W. Corbett, *Mat. Res. Soc. Symp. Proc.*, vol. 14, 147–152 (1983).
- [4.9] C. Claeys and J. Vanhellemont, “Advances in the Understanding of Oxygen and Carbon in Silicon,” in: *Gettering and Defect Engineering in the Semiconductor Technology GADEST'89*, edited by M. Kittler, *Solid State Phenomena*, vol. 6/7, 21–32 (1989).
- [4.10] Q. Sun, K. H. Yao, J. Lagowski, and H. C. Gatos, “Effect of Carbon on Oxygen Precipitation in Silicon,” *J. Appl. Phys.*, vol. 67, no. 9, 4313–4319 (1990).
- [4.11] S. Pizzini, S. Binetti, M. Acciarri, and S. Acerboni, “Interactions of Oxygen, Carbon, and Extended Defects in Silicon,” *phys. stat. sol. (a)*, vol. 138, 451–464 (1993).
- [4.12] W. Skorupa and R. A. Yankov, “Carbon-Mediated Effects in Silicon and in Silicon-Related Materials,” *Materials Chemistry and Physics*, vol. 44, 101–143 (1996).
- [4.13] A. Kanamori and M. Kanamori, “Comparison of Two Kinds of Oxygen Donors in Silicon by Resistivity Measurements,” *J. Appl. Phys.*, vol. 50, no. 12, 8095–8101 (1979).
- [4.14] K. Yasutake, M. Umeno, H. Kawabe, H. Nakayama, T. Nishino, and Y. Hamakawa, “Oxygen-Related Donors Generated at 800 °C in CZ-Si,” *Jpn. J. Appl. Phys.*, vol. 19, no. 9, L544–L546 (1980).
- [4.15] M. Tajima, T. Masui, T. Abe, and T. Iizuka, “Photoluminescence Analysis of Silicon Crystals,” in: *Semiconductor Silicon 1981*, edited by H. R. Huff, R. J. Kriegler, and Y. Takeishi, *Electrochem. Soc. Proc.*, vol. 81-5, 72–89 (1981).
- [4.16] J. Leroueille, “Influence of Carbon on Oxygen Behavior in Silicon,” *phys. stat. sol. (a)*, vol. 67, 177–181 (1981).
- [4.17] A. R. Bean and R. C. Newman, “The Effect of Carbon on Thermal Donor Formation in Heat Treated Pulled Silicon Crystals,” *J. Phys. Chem. Solids*, vol. 33, 255–268 (1972).
- [4.18] D. Helmreich and E. Sirtl, “Oxygen in Silicon: A Modern View,” in: *Semiconductor Silicon 1977*, edited by H. R. Huff and E. Sirtl, *Electrochem. Soc. Proc.*, vol. 77-2, 626–636 (1977).
- [4.19] R. C. Newman, M. Claybourn, S. H. Kinder, S. Messoloras, A. S. Oates, and R. J. Stewart, “Precipitation of Oxygen at Low Temperatures,” in: *Semiconductor Silicon*, edited by H. R. Huff, T. Abe, and B. Kolbesen, *Electrochem. Soc. Proc.*, vol. 86-4, 766–777 (1986).
- [4.20] M. Tamura, T. Ando, and K. Ohya, “MeV-Ion-Induced Damage in Si and Its Annealing,” in: *Ion Beam Modification of Materials*, edited by S. P. Withrow and D. B. Poker, *Nuclear Instruments and Methods in Physics Research B*, vol. 59/60, 572–583 (1991).
- [4.21] S. Nishikawa, A. Tanaka, and T. Yamaji, “Reduction of Transient Boron Diffusion in Preamorphized Si by Carbon Implantation,” *Appl. Phys. Lett.*, vol. 60, no. 18, 2270–2272 (1992).
- [4.22] J. R. Loeffing, J. S. Custer, and F. W. Saris, “C Implantation for Suppression of Dislocation Formation,” in: *Phase Formation and Modification by Beam-Solid Interactions*, edited by G. S. Was, L. E. Rehn, and D. M. Follstaedt, *Mat. Res. Soc. Symp. Proc.*, vol. 235, 179–184 (1992).

- [4.23] S. Nishikawa and T. Yamaji, "Elimination of Secondary Defects in Preamorphized Si by C⁺ Implantation," *Appl. Phys. Lett.*, vol. 62, no. 3, 303–305 (1993).
- [4.24] S. Lombardo, F. Priolo, S. U. Campisano, and S. Lagomarsino, "Reduction of Secondary Defect Density by C Implant and B Implant in Ge_xSi_{1-x} Layers Formed by High Dose Ge Implantation in (100) Si," *Appl. Phys. Lett.*, vol. 62, no. 19, 2335–2337 (1993).
- [4.25] P. A. Stolk, D. J. Eaglesham, H.-J. Gossman, and J. M. Poate, "Carbon Incorporation in Silicon for Suppressing Interstitial-Enhanced Boron-Diffusion," *Appl. Phys. Lett.*, vol. 66, no. 11, 1370–1372 (1995).
- [4.26] L. D. Lanzerotti, J. C. Sturm, E. Stach, R. Hull, T. Buyuklimanli, and C. Magee, "Suppression of Boron Outdiffusion in SiGe HBTs by Carbon Incorporation," in: *Technical Digest of the 1996 International Electron Devices Meeting (IEDM)*, Piscataway: IEEE, 249–252 (1996).
- [4.27] H. J. Osten, G. Lippert, D. Knoll, R. Barth, B. Heinemann, H. Rücker, and P. Schley, "The Effect of Carbon Incorporation on SiGe Heterobipolar Transistor Performance and Process Margin," in: *Technical Digest of the 1997 International Electron Devices Meeting (IEDM)*, Piscataway: IEEE, 803–806 (1997).
- [4.28] M. S. Carroll, L. D. Lanzerotti, and J. C. Sturm, "Quantitative Measurement of Reduction of Boron Diffusion by Substitutional Carbon Incorporation," in: *Diffusion Mechanisms in Crystalline Materials*, edited by Y. Mishin, G. Vogl, N. Cowern, R. Catlow, and D. Farkas, *Mat. Res. Soc. Symp. Proc.*, vol. 527, 417–422 (1998).
- [4.29] E. Napolitani, A. Coati, D. De Salvador, A. Carnera, S. Mirabella, S. Scalese, and F. Priolo, "Complete Suppression of the Transient Enhanced Diffusion of B Implanted in Preamorphized Si by Interstitial Trapping in a Spatially Separated C-Rich Layer," *Appl. Phys. Lett.*, vol. 79, no. 25, 4145–4147 (2001).
- [4.30] A. Fukami, K.-i. Shoji, T. Nagano, and C. Y. Yang, "Characterization of SiGe/Si Heterostructures Formed by Ge⁺ and C⁺ Implantation," *Appl. Phys. Lett.*, vol. 57, no. 22, 2345–2347 (1990).
- [4.31] K. Eberl, S. S. Iyer, S. Zollner, J. C. Tsang, and F. K. LeGoues, "Growth and Strain Compensation Effects in the Ternary Si_{1-x-y}Ge_xC_y Alloy System," *Appl. Phys. Lett.*, vol. 60, no. 24, 3033–3035 (1992).
- [4.32] S. Im, J. Washburn, and R. Gronsky, "Optimization of Ge/C Ratio for Compensation of Misfit Strain in Solid Phase Epitaxial Growth of SiGe Layers," *Appl. Phys. Lett.*, vol. 63, no. 19, 2682–2684 (1993).
- [4.33] J. L. Regolini, S. Bodnar, J. C. Oberlin, F. Ferrieu, G. Gauneau, B. Lambert, and P. Boucaud, "Strain Compensated Heterostructures in the Si_{1-x-y}Ge_xC_y Ternary System," *J. Vac. Sci. Technol. A*, vol. 12, no. 4, 1015–1019 (1994).
- [4.34] P. Warren, J. Mi, F. Overney, and M. Dutoit, "Thermal Stability of Si/Si_{1-x-y}Ge_xC_y/Si Heterostructures Grown by Rapid Thermal Chemical Vapor Deposition," *J. Crystal Growth*, vol. 157, 414–419 (1995).
- [4.35] H. J. Osten, "SiGeC Device Applications," in: *Semiconductor Silicon 2002*, edited by H. R. Huff, L. Fabry, and S. Kishino, *Electrochem. Soc. Proc.*, vol. 2002-2, 342–353 (2002).
- [4.36] R. C. Newman, "The Identification of Precipitate Particles in Single Crystals of Silicon by Reflection Electron Diffraction," *Proc. Phys. Soc. (London)*, vol. 76, 993–996 (1960).
- [4.37] A. R. Bean and R. C. Newman, "The Solubility of Carbon in Pulled Silicon Crystals," *J. Phys. Chem. Solids*, vol. 32, 1211–1219 (1971).
- [4.38] W. J. Taylor, T. Y. Tan, and U. Gösele, "Carbon Precipitation in Silicon: Why Is It So Difficult?" *Appl. Phys. Lett.*, vol. 62, no. 25, 3336–3338 (1993).
- [4.39] H. Föll, U. Gösele, and B. O. Kolbesen, "Swirl-Defects in Silicon," in: *Semiconductor Silicon 1977*, edited by H. R. Huff and E. Sirtl, *Electrochem. Soc. Proc.*, vol. 77-2, 565–574 (1977).
- [4.40] H. Wong, N. W. Cheung, P. K. Chu, J. Liu, and J. W. Mayer, "Proximity Gettering with Mega-Electron-Volt Carbon and Oxygen Implantations," *Appl. Phys. Lett.*, vol. 52, no. 12, 1023–1025 (1988).

- [4.41] H. Wong, N. W. Cheung, and P. K. Chu, "Gettering of Gold and Copper with Implanted Carbon in Silicon," *Appl. Phys. Lett.*, vol. 52, no. 11, 889–891 (1988).
- [4.42] T. Ando, S. Isomae, and M. Tamura, "Reduction of p-n Junction Leakage Currents by High-Energy Carbon Ion Implantation," in: *Defects in Silicon II*, edited by W. M. Bullis, U. Gösele, and F. Shimura, *Electrochem. Soc. Proc.*, vol. 91-9, 659–666 (1991).
- [4.43] K. Tsukamoto, S. Komori, T. Kuroi, and Y. Akasaka, "High-Energy Ion Implantation for ULSI," in: *Ion Beam Modification of Materials*, edited by S. P. Withrow and D. B. Poker, *Nuclear Instruments and Methods in Physics Research B*, vol. 59/60, 584–591 (1991).
- [4.44] J. A. Borders, S. T. Picraux, and W. Beezhold, "Formation of SiC in Silicon by Ion Implantation," *Appl. Phys. Lett.*, vol. 18, no. 11, 509–511 (1971).
- [4.45] W. Rothemund and C. R. Fritzsch, "Optical Absorption and Electrical Conductivity of SiC Films Produced by Ion Implantation," *J. Electrochem. Soc.*, vol. 121, no. 4, 586–588 (1974).
- [4.46] F. L. Edelman, O. N. Kuznetsov, L. V. Lezheiko, and E. V. Lubopytova, "Formation of SiC and Si₃N₄ in Silicon by Ion Implantation," *Radiation Effects*, vol. 29, 13–15 (1976).
- [4.47] T. Kimura, S. Kagiyama, and S. Yugo, "Characteristics of the Synthesis of a β-SiC by the Implantation of Carbon Ions into Silicon," *Thin Solid Films*, vol. 94, 191–198 (1982).
- [4.48] I. P. Akimchenko, K. V. Kisileva, V. V. Krasnopol'stsev, A. G. Turyanski, and V. S. Vavilov, "Structure and Optical Properties of Silicon Implanted by High Doses of 70 and 310 keV Carbon Ions," *Radiation Effects*, vol. 48, 7–12 (1980).
- [4.49] I. Golecki, L. Kroko, and H. L. Glass, "Properties of Buried SiC Layers Produced by Carbon Ion Implantation in (100) Bulk Silicon and Silicon-on-Sapphire," *J. Electronic Materials*, vol. 16, no. 5, 315–321 (1987).
- [4.50] N. V. Nguyen and K. Vedam, "Spectroscopic Ellipsometry Studies of Crystalline Silicon Implanted with Carbon Ions," *J. Appl. Phys.*, vol. 67, no. 8, 3555–3559 (1990).
- [4.51] V. Lehmann, K. Mitani, D. Feijóo, and U. Gösele, "Implanted Carbon: An Effective Etch-Stop in Silicon," *J. Electrochem. Soc.*, vol. 138, no. 5, L3–L4 (1991).
- [4.52] D. Fröse, D. Kollewe, and W. von Münch, "Investigations of Carbon Implanted Silicon," in: *Application of Accelerators in Research and Industry '92*, edited by J. L. Duggan and I. L. Morgan, *Nuclear Instruments and Methods in Physics Research B*, vol. 79, 668–671 (1993).
- [4.53] N. Akiyama, Y. Yatsurugi, Y. Endo, Z. Imayoshi, and T. Nozaki, "Lowering of Breakdown Voltage of Semiconductor Silicon Due to the Precipitation of Impurity Carbon," *Appl. Phys. Lett.*, vol. 22, no. 12, 630–631 (1973).
- [4.54] M. J. Hill and P. M. Van Iseghem, "Influence of Carbon Concentration on Gold Diffusion in Silicon," in: *Semiconductor Silicon 1977*, edited by H. R. Huff and E. Sirtl, *Electrochem. Soc. Proc.*, vol. 77-2, 715–725 (1977).
- [4.55] T. Abe, K. Kikuchi, S. Shirai, and S. Muraoka, "Impurities in Silicon Single Crystals," in: *Semiconductor Silicon 1981*, edited by H. R. Huff, R. J. Kriegler, and Y. Takeishi, *Electrochem. Soc. Proc.*, vol. 81-5, 54–71 (1981).
- [4.56] B. O. Kolbesen and A. Mühlbauer, "Carbon in Silicon: Properties and Impact on Devices," *Solid-State Electronics*, vol. 25, no. 8, 759–775 (1982).
- [4.57] H. Wong, N. W. Cheung, and S. S. Wong, "Electronic Defects in Silicon Induced by MeV Carbon and Oxygen Implantations," in: *Ion Implantation Technology*, edited by T. Takagi, *Nuclear Instruments and Methods in Physics Research B*, vol. 37/38, 970–974 (1989).
- [4.58] I. Ban, M. Öztürk, K. Christensen, and D. Maher, "Effects of Carbon Implantation on Generation Lifetime in Silicon," *Appl. Phys. Lett.*, vol. 68, 499–501 (1996).
- [4.59] S. Lombardo, A. Cacciato, K. K. Larsen, V. Rainieri, F. LaVia, V. Privitera, and S. U. Campisano, "High Temperature Annealing Effects on the Electrical Characteristics of C Implanted Si," *J. Appl. Phys.*, vol. 79, no. 7, 3464–3469 (1996).
- [4.60] M. Craig, A. Sultan, and S. Banerjee, "Carbon Co-Implantation for Ultra-Shallow p⁺-n Junction Formation," in: *Ion Implantation Technology—96*, edited by E. Ishidida, S. Banerjee, S. Mehta, T. C. Smith, M. Current, L. Larson, A. Tasch, and T. Romig, Piscataway: IEEE, 665–667 (1997).

- [4.61] H. J. Osten, G. Lippert, P. Gaworzewski, and R. Sorge, "Impact of Low Carbon Concentrations on the Electrical Properties of Highly Boron Doped SiGe Layers," *Appl. Phys. Lett.*, vol. 71, no. 11, 1522–1524 (1997).
- [4.62] B. O. Kolbesen, "Carbon in Silicon," in: *Aggregation Phenomena of Point Defects in Silicon*, edited by E. Sirtl and J. Goorissen, *Electrochem. Soc. Proc.*, vol. 83-4, 155–175 (1983).
- [4.63] U. Gösele, "The Role of Carbon and Point Defects in Silicon," in: *Oxygen, Carbon, Hydrogen and Nitrogen in Crystalline Silicon*, edited by J. C. Mikkelsen, Jr., S. J. Pearson, J. W. Corbett, and S. J. Pennycook, *Mat. Res. Soc. Symp. Proc.*, vol. 59, 419–431 (1986).
- [4.64] G. Davies and R. C. Newman, "Carbon in Monocrystalline Silicon," in: *Materials, Properties and Preparation*, edited by T. S. Moss and S. Mahajan, *Handbook on Semiconductors*, vol. 3b, Amsterdam: North-Holland, 1557–1635 (1994).
- [4.65] R. C. Newman and J. Wakefield, "The Diffusivity of Carbon in Silicon," *J. Phys. Chem. Solids*, vol. 19, no. 3/4, 230–234 (1961).
- [4.66] R. C. Newman and J. Wakefield, "Diffusion and Precipitation of Carbon in Silicon," in: *Metallurgy of Semiconductor Materials*, edited by J. B. Schroeder, *Metallurgical Society Conferences*, vol. 15, New York: Interscience, 201–208 (1962).
- [4.67] R. C. Newman and J. B. Willis, "Vibrational Absorption of Carbon in Silicon," *J. Phys. Chem. Solids*, vol. 26, 373–379 (1965).
- [4.68] P. G. Dawber and J. R. Elliott, "The Vibrations of an Atom of Different Mass in a Cubic Crystal," *Proc. Roy. Soc. Lond. A*, vol. 273, 222–236 (1963).
- [4.69] P. G. Dawber and R. J. Elliott, "Theory of Optical Absorption by Vibrations of Defects in Silicon," *Proc. Phys. Soc. (London)*, vol. 81, 453–460 (1963).
- [4.70] J. A. Baker, T. N. Tucker, N. E. Moyer, and R. C. Buschert, "Effect of Carbon on the Lattice Parameter in Silicon," *J. Appl. Phys.*, vol. 39, no. 9, 4365–4368 (1968).
- [4.71] D. Windisch and P. Becker, "Lattice Distortions Induced by Carbon in Silicon," *Phil. Mag. A*, vol. 58, no. 2, 435–443 (1988).
- [4.72] G. G. DeLeo, W. B. Fowler, and G. D. Watkins, "Theory of Off-Center Impurities in Silicon: Substitutional Nitrogen and Oxygen," *Phys. Rev. B*, vol. 29, no. 6, 3193–3207 (1984).
- [4.73] R. Jones, "Local Density Functional Calculations of the Structure and Vibratory Modes of the Substitutional Carbon Impurity in Silicon," *J. Phys. C*, vol. 20, L713–L716 (1987).
- [4.74] J. Zhu, "Ab Initio Pseudopotential Calculations of Dopant Diffusion in Si," *Comput. Mater. Sci.*, vol. 12, 309–318 (1998).
- [4.75] H. P. Hjalmarson, P. Vogl, D. J. Wolford, and J. D. Dow, "Theory of Substitutional Deep Traps in Covalent Semiconductors," *Phys. Rev. Lett.*, vol. 44, no. 12, 810–813 (1980).
- [4.76] A. A. Demkov and O. F. Sankey, "Theoretical Investigation of Random Si-C Alloys," *Phys. Rev. B*, vol. 48, no. 4, 2207–2214 (1993).
- [4.77] W. Windl, O. F. Sankey, and J. Menéndez, "Theory of Strain and Electronic Structure of $\text{Si}_{1-x}\text{C}_x$ and $\text{Si}_{1-x-y}\text{Ge}_x\text{C}_y$ Alloys," *Phys. Rev. B*, vol. 57, no. 4, 2431–2442 (1998).
- [4.78] J. Xie, K. Zhang, and X. Xie, "Electronic Structure of $\text{Si}_{1-x}\text{C}_x$ and $\text{Si}_{1-x-y}\text{C}_x\text{Ge}_y$ Alloys," *J. Appl. Phys.*, vol. 77, no. 8, 3868–3871 (1995).
- [4.79] R. C. Newman and A. R. Bean, "Irradiated Damage in Carbon-Doped Silicon Irradiated at Low Temperatures by 2 MeV Electrons," *Radiation Effects*, vol. 8, 189–193 (1971).
- [4.80] F. A. Abou-el-Fotouh and R. C. Newman, "Electron Irradiation Damage in Silicon Containing Carbon and Diffused ^{18}O ," *Solid State Communications*, vol. 15, 1409–1411 (1974).
- [4.81] G. D. Watkins and K. L. Brower, "EPR Observation of the Isolated Interstitial Carbon Atom in Silicon," *Phys. Rev. Lett.*, vol. 36, no. 22, 1329–1332 (1976).
- [4.82] J. Weber, R. J. Davis, H.-U. Habermeier, W. D. Sawyer, and M. Singh, "Photoluminescence Detection of Impurities Induced in Silicon by Dry Etching Processes," *Appl. Phys. A*, vol. 41, 175–178 (1986).
- [4.83] H. J. Stein and F. L. Vook, "Infrared Studies of Oxygen and Carbon Associated Defects in Electron-Irradiated Silicon," *Radiation Effects*, vol. 1, 41–46 (1969).

- [4.84] Y. H. Lee, L. J. Cheng, J. D. Gerson, P. M. Mooney, and J. W. Corbett, “Carbon Interstitial in Electron-Irradiated Silicon,” *Solid State Communications*, vol. 21, 109–111 (1977).
- [4.85] L. C. Kimerling, P. Blood, and W. M. Gibson, “Defect States in Proton-Bombarded Silicon at T<300 K,” in: *Defects and Radiation Effects in Semiconductors, 1978*, edited by J. H. Albany, *Inst. Phys. Conf. Ser.*, no. 46, 273–280 (1979).
- [4.86] A. G. Litvinko, L. F. Makarenko, L. I. Murin, and V. D. Tkachev, “Electrically Active Interstitial Defects in Irradiated n-Type Silicon,” *Sov. Phys. Semicond.*, vol. 14, no. 4, 455–457 (1980).
- [4.87] Y. H. Lee, K. L. Wang, A. Jaworoski, P. M. Mooney, L. J. Cheng, and J. W. Corbett, “A Transient Capacitance Study of Radiation-Induced Defects in Aluminum-Doped Silicon,” *phys. stat. sol. (a)*, vol. 57, 697–704 (1980).
- [4.88] H. Lefèvre, “Annealing Behavior of Trap-Centers in Silicon Containing A-Swirl Defects,” *Applied Physics A*, vol. 29, 105–111 (1982).
- [4.89] R. D. Harris and G. D. Watkins, “Interstitial Related Defects in n-Type Silicon,” in: *Thirteenth International Conference on Defects in Semiconductors*, edited by L. C. Kimerling and J. M. Parsey, Jr., The Metallurgical Society of AIME, 799–805 (1985).
- [4.90] L. W. Song and G. D. Watkins, “EPR Identification of the Single-Acceptor State of Interstitial Carbon in Silicon,” *Phys. Rev. B*, vol. 42, no. 9, 5759–5764 (1990).
- [4.91] J. F. Zheng, M. Stavola, and G. D. Watkins, “Structure of the Neutral Charge State of Interstitial Carbon in Silicon,” in: *The Physics of Semiconductors*, edited by D. J. Lockwood, Singapore: World Scientific, 2363–2366 (1994).
- [4.92] R. Woolley, E. C. Lightowers, A. K. Tipping, M. Claybourn, and R. C. Newman, “Electronic and Vibrational Absorption of Interstitial Carbon in Silicon,” in: *Defects in Semiconductors 14*, edited by H. J. von Bardeleben, *Materials Science Forum*, vol. 10-12, 929–934 (1986).
- [4.93] K. Thonke, A. Teschner, and R. Sauer, “New Photoluminescence Defect Spectra in Silicon Irradiated at 100 K: Observation of Interstitial Carbon,” *Solid State Communications*, vol. 61, no. 4, 241–244 (1987).
- [4.94] L. C. Kimerling, M. T. Asom, J. L. Benton, P. J. Drebinsky, and C. E. Caefer, “Interstitial Defect Reaction in Silicon,” in: *Defects in Semiconductors 15*, edited by G. Ferenczi, *Materials Science Forum*, vol. 38-41, 141–150 (1989).
- [4.95] R. B. Capaz, A. Dal Pino, Jr., and J. D. Joannopoulos, “Identification of the Migration Path of Interstitial Carbon in Silicon,” *Phys. Rev. B*, vol. 50, no. 11, 7439–7442 (1994).
- [4.96] P. Leary, R. Jones, S. Öberg, and V. J. B. Torres, “Dynamic Properties of Interstitial Carbon and Carbon-Carbon Pair Defects in Silicon,” *Phys. Rev. B*, vol. 55, no. 4, 2188–2194 (1997).
- [4.97] C.-L. Liu, W. Windl, L. Borucki, S. Lu, and X.-Y. Liu, “*Ab Initio* Modeling and Experimental Study of C-B Interactions in Si,” *Appl. Phys. Lett.*, vol. 80, no. 1, 52–54 (2002).
- [4.98] A. Mattoni, F. Bernardini, and L. Colombo, “Self-Interstitial Trapping by Carbon Complexes in Crystalline Silicon,” *Phys. Rev. B*, vol. 66, 195214 (2002).
- [4.99] M. E. Law, M. D. Griglione, and M. Northridge, “Influence of Carbon on the Diffusion of Interstitials and Boron in Silicon,” in: *Si Front-End Processing — Physics and Technology of Dopant-Defect Interactions II*, edited by A. Agarwal, L. Pelaz, H.-H. Vuong, P. Packan, and M. Kase, *Mat. Res. Soc. Symp. Proc.*, vol. 610, B7.4.1–B7.4.5 (2000).
- [4.100] G. D. Watkins and J. W. Corbett, “Electron Paramagnetic Resonance of Defects in Irradiated Silicon,” in: *Radiation Effects in Inorganic Solids, Discussions of the Faraday Society*, no. 31, 86–95 (1961).
- [4.101] A. V. Dvurechenskii, A. A. Karanovich, and B. P. Kashnikov, “Vacancy-Impurity Defect with Spatially Separated Components in Electron-Irradiated Silicon,” *Sov. Phys. Semicond.*, vol. 21, no. 1, 29–33 (1987).
- [4.102] K. A. Abdullin and B. N. Mukashev, “Vacancy Defect in Silicon Single Crystals Bombarded at 77 K,” *Semiconductors*, vol. 29, no. 2, 169–174 (1995).
- [4.103] A. Dal Pino, Jr., A. M. Rappe, and J. D. Joannopoulos, “*Ab Initio* Investigation of Carbon-Related Defects in Silicon,” *Phys. Rev. B*, vol. 47, no. 19, 12554–12557 (1993).

- [4.104] R. W. Olesinski and G. J. Abbaschian, "The C-Si (Carbon-Silicon) System," *Bull. Alloy Phase Diagrams*, vol. 5, no. 5, 486–489 (1984).
- [4.105] H. A. Papazian and S. P. Wolsky, "Volatile Impurities in Silicon and Germanium," *J. Appl. Phys.*, vol. 27, no. 12, 1561 (1956).
- [4.106] T. Nozaki, Y. Yatsurugi, and N. Akiyama, "Concentration and Behavior of Carbon in Semiconductor Silicon," *J. Electrochem. Soc.*, vol. 117, no. 12, 1566–1568 (1970).
- [4.107] Y. Endo, Y. Yatsurugi, N. Akiyama, and T. Nozaki, "Infrared Spectrophotometry for Carbon in Silicon As Calibrated by Charged Particle Activation," *Anal. Chem.*, vol. 44, no. 14, 2258–2262 (1972).
- [4.108] F. Rollert, N. A. Stolwijk, and H. Mehrer, "Diffusion of Carbon-14 in Silicon," in: *Defects in Semiconductors 15*, edited by G. Ferenczi, *Materials Science Forum*, vol. 38-41, 753–758 (1989).
- [4.109] L. A. Ladd and J. P. Kalejs, "Self-Interstitial Injection Effects on Carbon Diffusion in Silicon at High Temperatures," in: *Oxygen, Carbon, Hydrogen and Nitrogen in Crystalline Silicon*, edited by J. C. Mikkelsen, Jr., S. J. Pearton, J. W. Corbett, and S. J. Pennycook, *Mat. Res. Soc. Symp. Proc.*, vol. 59, 445–450 (1986).
- [4.110] V. D. Akhmetov and V. V. Bolotov, "The Effect of Carbon and Boron on the Accumulation of Vacancy-Oxygen Complexes in Silicon," *Radiation Effects*, vol. 52, 149–152 (1980).
- [4.111] J. P. Kalejs, L. A. Ladd, and U. Gösele, "Self-Interstitial Enhanced Carbon Diffusion in Silicon," *Appl. Phys. Lett.*, vol. 45, no. 3, 268–269 (1984).
- [4.112] G. D. Watkins, Private communication (2001).
- [4.113] A. K. Tipping and R. C. Newman, "The Diffusion Coefficient of Interstitial Carbon in Silicon," *Semicond. Sci. Technol.*, vol. 2, 315–317 (1987).
- [4.114] G. E. Davies, E. C. Lightowers, M. F. Thomaz, and J. G. Wilkes, "A Metastable Precursor to the Production of the Two-Carbon-Atom 'G' Centre in Irradiated Crystalline Silicon," *Semicond. Sci. Technol.*, vol. 3, 608–611 (1988).
- [4.115] S. P. Chappell, G. Davies, E. C. Lightowers, and R. C. Newman, "A Metastable Precursor to the Di-Carbon Centre in Crystalline Silicon," in: *Defects in Semiconductors 15*, edited by G. Ferenczi, *Materials Science Forum*, vol. 38-41, 481–485 (1989).
- [4.116] J. Lalita, N. Keskitalo, A. Hallén, C. Jagadish, and B. G. Svensson, "Defect Evolution in MeV Ion-Implanted Silicon," in: *New Trends in Ion Beam Processing of Materials*, edited by F. Priolo, J. K. N. Lindner, A. Nylandsted Larsen, and J. M. Poate, *Nuclear Instruments and Methods in Physics Research B*, vol. 120, 27–32 (1996).
- [4.117] J. L. Benton, M. T. Asom, R. Sauer, and L. C. Kimerling, "Identification of Interstitial Carbon Related Defects in Silicon," in: *Defects in Electronic Materials*, edited by M. Stavola, S. J. Pearton, and G. Davies, *Mat. Res. Soc. Symp. Proc.*, vol. 104, 85–91 (1988).
- [4.118] R. Pinacho, M. Jaraíz, H. J. Gossmann, G. H. Gilmer, J. L. Benton, and P. Werner, "The Effect of Carbon/Self-Interstitial Clusters on Carbon Diffusion in Silicon Modeled by Kinetic Monte Carlo Simulations," in: *Si Front-End Processing — Physics and Technology of Dopant-Defect Interactions II*, edited by A. Agarwal, L. Pelaz, H.-H. Vuong, P. Packan, and M. Kase, *Mat. Res. Soc. Symp. Proc.*, vol. 610, B7.2.1–B7.2.6 (2000).
- [4.119] N. E. B. Cowern, B. Colombeau, F. Roozeboom, M. Hopstaken, H. Snijders, P. Meunier-Beillard, and W. Lerch, "Experimental Study on the Mechanism of Carbon Diffusion in Silicon," in: *Silicon Front-End Junction Formation Technologies*, edited by D. F. Downey, M. E. Law, A. P. Claverie, and M. J. Rendon, *Mat. Res. Soc. Symp. Proc.*, vol. 717, C5.10.1–C5.10.6 (2002).
- [4.120] N. Cowern, B. Colombeau, F. Roozeboom, M. Hopstaken, H. Snijders, P. Meunier-Beillard, and W. Lerch, "Diffusion Suppression in Silicon by Substitutional C Doping," in: *ESSDERC 2002*, edited by G. Baccarani, E. Gnani, and M. Rudan, Bologna: University of Bologna, 203–206 (2002).
- [4.121] M. T. Asom, J. L. Benton, R. Sauer, and L. C. Kimerling, "Interstitial Defect Reactions in Silicon," *Appl. Phys. Lett.*, vol. 51, no. 4, 256–258 (1987).

- [4.122] A. R. Frederickson, A. S. Karakashian, P. J. Drevinsky, and C. E. Caefter, “Radiation-Induced Carbon-Related Defects in p-Type Silicon,” *J. Appl. Phys.*, vol. 65, no. 8, 3272–3274 (1989).
- [4.123] J. L. Benton, J. Michel, L. C. Kimerling, B. E. Weir, and R. A. Gottscho, “Carbon Reactions in Reactive Ion Etched Silicon,” *J. Electronic Materials*, vol. 20, no. 9, 643–647 (1991).
- [4.124] A. R. Frederickson and A. S. Karakashian, “Recombination-Induced Random-Walk Diffusion of Interstitial Carbon in Silicon,” *J. Electronic Materials*, vol. 21, no. 7, 745–752 (1992).
- [4.125] H. Rücker, B. Heinemann, W. Röpke, R. Kurps, D. Krüger, G. Lippert, and H. J. Osten, “Suppressed Diffusion of Boron and Carbon in Carbon-Rich Silicon,” *Appl. Phys. Lett.*, vol. 73, no. 12, 1682–1684 (1998).
- [4.126] P. Werner, U. Gösele, H.-J. Gossman, and D. C. Jacobson, “Carbon Diffusion in Silicon,” *Appl. Phys. Lett.*, vol. 73, no. 17, 2465–2467 (1998).
- [4.127] R. F. Scholz, P. Werner, U. Gösele, and T. Y. Tan, “The Contribution of Vacancies to Carbon Out-Diffusion in Silicon,” *Appl. Phys. Lett.*, vol. 74, no. 3, 392–394 (1999).
- [4.128] H. Rücker, B. Heinemann, D. Bolze, D. Knoll, D. Krüger, R. Kurps, H. J. Osten, P. Schley, B. Tillack, and P. Zaumseil, “Dopant Diffusion in C-Doped Si and SiGe: Physical Model and Experimental Verification,” in: *Technical Digest of the 1999 International Electron Devices Meeting (IEDM)*, Piscataway: IEEE, 345–348 (1999).
- [4.129] R. Pinacho, P. Castrillo, M. Jaraiz, I. Martin-Bragado, J. Barbolla, H.-J. Gossman, G.-H. Gilmer, and J.-L. Benton, “Carbon in Silicon: Modeling of Diffusion and Clustering Mechanisms,” *J. Appl. Phys.*, vol. 92, no. 3, 1582–1587 (2002).
- [4.130] H. Rücker, B. Heinemann, W. Röpke, R. Krups, D. Krüger, G. Lippert, and H. J. Osten, “Erratum: ‘Suppressed Diffusion of Boron and Carbon in Carbon-Rich Silicon’ [Appl. Phys. Lett. 73, 1682 (1998)],” *Appl. Phys. Lett.*, vol. 75, no. 1, 147 (1999).
- [4.131] B. Colombeau and N. E. B. Cowern, Private communication (2003).
- [4.132] G. Davies, E. C. Lightowers, R. C. Newman, and A. S. Oates, “A Model for Radiation Damage Effects in Carbon-Doped Crystalline Silicon,” *Semicond. Sci. Technol.*, vol. 2, 524–532 (1987).
- [4.133] V. P. Chappell and R. C. Newman, “The Selective Trapping of Self-Interstitials by Interstitial Carbon Impurities in Electron Irradiated Silicon,” *Semicond. Sci. Technol.*, vol. 2, 691 (1987).
- [4.134] G. Davies, “Carbon-Related Processes in Crystalline Silicon,” in: *Defects in Semiconductors 15*, edited by G. Ferenczi, *Materials Science Forum*, vol. 38-41, 151–158 (1989).
- [4.135] J. Guldberg, “Electron Traps in Silicon Doped by Neutron Transmutation,” *J. Phys. D*, vol. 11, 2043–2057 (1978).
- [4.136] H. Rücker, H. Methfessel, B. Dietrich, K. Pressel, and H. J. Osten, “Phonons As a Probe of Short-Range Order in $\text{Si}_{1-x}\text{C}_x$ Alloys,” *Phys. Rev. B*, vol. 53, no. 3, 1302–1309 (1996).
- [4.137] M. A. Meléndez-Lira, J. D. Lorentzen, J. Menéndez, W. Windl, N. G. Cave, R. Liu, J. W. Christiansen, N. D. Theodore, and J. J. Candelaria, “Microscopic Carbon Distribution in $\text{Si}_{1-y}\text{C}_y$ Alloys: A Raman Scattering Study,” *Phys. Rev. B*, vol. 56, no. 7, 3648–3650 (1997).
- [4.138] W. Windl, J. D. Kress, A. F. Voter, J. Menéndez, and O. F. Sankey, “Influence of the Local Microstructure on the Macroscopic Properties of $\text{Si}_{1-x-y}\text{Ge}_x\text{C}_y$ Alloys,” in: *Defects and Diffusion in Silicon Processing*, edited by T. Diaz de la Rubia, S. Coffa, P. A. Stolk, and C. S. Rafferty, *Mat. Res. Soc. Symp. Proc.*, vol. 469, 443–448 (1997).
- [4.139] J. R. Byberg, B. Bech Nielsen, M. Fanciulli, S. K. Estreicher, and P. A. Fedders, “Dimer of Substitutional Carbon in Silicon Studied by EPR and Ab Initio Methods,” *Phys. Rev. B*, vol. 61, no. 19, 12939–12945 (2000).
- [4.140] H. Horiye and E. G. Wikner, “Three New Electron Spin Resonance Centers in Electron-Irradiated Silicon,” *J. Appl. Phys.*, vol. 40, no. 9, 3879–3880 (1969).
- [4.141] E. V. Lavrov, B. Bech Nielsen, J. R. Byberg, B. Hourahine, R. Jones, S. Öberg, and P. R. Briddon, “Local Vibrational Modes of Two Neighboring Substitutional Carbon Atoms in Silicon,” *Phys. Rev. B*, vol. 62, no. 1, 158–165 (2000).

- [4.142] V. P. Markevich, O. Andersen, I. F. Medvedeva, J. H. Evans-Freeman, I. D. Hawkins, L. I. Murin, L. Dobaczewski, and A. R. Peaker, "Defect Reactions Associated with the Dissociation of the Phosphorus-Vacancy Pair in Silicon," *Physica B*, vol. 308-310, 513–516 (2001).
- [4.143] K. L. Brower, "EPR of a Jahn-Teller Distorted (111) Carbon Interstitialcy in Irradiated Silicon," *Phys. Rev. B*, vol. 9, no. 6, 2607–2617 (1974).
- [4.144] K. L. Brower, "Erratum: EPR of a Jahn-Teller Distorted ⟨111⟩ Carbon Interstitialcy in Irradiated Silicon [Phys. Rev. B 9, 2607 (1974)]," *Phys. Rev. B*, vol. 17, no. 10, 4130 (1978).
- [4.145] K. M. Lee, K. P. O'Donnell, J. Weber, B. C. Cavenett, and G. D. Watkins, "Optical Detection of Magnetic Resonance for a Deep-Level Defect in Silicon," *Phys. Rev. Lett.*, vol. 48, no. 1, 37–40 (1982).
- [4.146] K. P. O'Donnell, K. M. Lee, and G. D. Watkins, "Origin of the 0.97 eV Luminescence in Irradiated Silicon," in: *Proceedings of the 12th International Conference on Defects in Semiconductors*, edited by C. A. J. Ammerlaan, *Physica*, vol. 116B, 258–263 (1983).
- [4.147] G. Davies, E. C. Lightowers, and M. do Carmo, "Carbon-Related Vibronic Bands in Electron-Irradiated Silicon," *J. Phys. C*, vol. 16, 5503–5515 (1983).
- [4.148] G. E. Jellison, Jr., "Transient Capacitance Studies of an Electron Trap at $E_c - E_T = 0.105$ eV in Phosphorus-Doped Silicon," *J. Appl. Phys.*, vol. 53, no. 8, 5715–5719 (1982).
- [4.149] J. L. Benton and M. Levinson, "Metastable Defect Configurations in Semiconductors," in: *Defects in Semiconductors II*, edited by S. Mahajan and J. W. Corbett, *Mat. Res. Soc. Symp. Proc.*, vol. 14, 95–100 (1983).
- [4.150] A. Chantre and D. Bois, "Metastable-Defect Behavior in Silicon: Charge-State-Controlled Re-orientation of Iron-Aluminum Pairs," *Phys. Rev. B*, vol. 31, no. 12, 7979–7988 (1985).
- [4.151] L. W. Song, B. W. Benson, and G. D. Watkins, "New Vacancy-Related Defects in n-Type Silicon," *Phys. Rev. B*, vol. 33, no. 2, 1452–1455 (1986).
- [4.152] L. W. Song, X. D. Zhan, B. W. Benson, and G. D. Watkins, "Bistable Interstitial-Carbon-Substitutional-Carbon Pair in Silicon," *Phys. Rev. B*, vol. 42, no. 9, 5765–5783 (1990).
- [4.153] L. S. Vlasenko, Y. V. Martynov, T. Gregorkiewicz, and C. A. J. Ammerlaan, "Electron Paramagnetic Resonance versus Spin-Dependent Recombination: Excited Triplet States of Structural Defects in Irradiated Silicon," *Phys. Rev. B*, vol. 52, no. 2, 1144–1151 (1995).
- [4.154] R. La وهو, L. S. Vlasenko, P. M. Vlasenko, V. A. Kozlov, and V. V. Kozlovski, "Electron Paramagnetic Resonance of Radiation Defects in Hydrogen-Implanted Silicon Detected by Spin-Dependent Microwave Photoconductivity," *Appl. Phys. Lett.*, vol. 74, no. 26, 3948–3950 (1999).
- [4.155] G. Ferenczi, C. A. Londos, T. Pavelka, M. Somogyi, and A. Mertens, "Correlation of the Concentration of the Carbon-Associated Radiation Damage Levels with the Total Carbon Concentration in Silicon," *J. Appl. Phys.*, vol. 63, no. 1, 183–189 (1988).
- [4.156] M.-A. Trauwaert, J. Vanhellemont, H. E. Maes, A.-M. Van Bavel, G. Langouche, A. Stesmans, and P. Clauws, "Influence of Oxygen and Carbon on the Generation and Annihilation of Radiation Defects in Silicon," *Materials Science and Engineering B*, vol. 36, 196–199 (1996).
- [4.157] E. V. Lavrov, L. Hoffmann, and B. Bech Nielsen, "Local Vibrational Modes of the Metastable Dicarbon Center ($C_5\text{-}C_1$) in Silicon," *Phys. Rev. B*, vol. 60, no. 11, 8081–8086 (1999).
- [4.158] C. A. Londos, M. S. Potsidi, and E. Stakakis, "Carbon-Related Complexes in Neutron-Irradiated Silicon," in: *Proceedings of the 22nd International Conference on Defects in Semiconductors*, edited by K. Bonde Nielsen, A. Nylandsted Larsen, and G. Weyer, *Physica B*, vol. 340-342, 551–555 (2003).
- [4.159] A. Cacciato, J. G. E. Klappe, N. E. B. Cowern, W. Vandervost, L. P. Biró, J. S. Custer, and F. W. Saris, "Dislocation Formation and B Transient Diffusion in C Coimplanted Si," *J. Appl. Phys.*, vol. 79, no. 5, 2314–2325 (1996).
- [4.160] V. D. Tkachev and A. V. Mudryi, "Radiative Recombination Centres in Silicon Irradiated by Fast Neutrons and Ions," in: *Radiation Effects in Semiconductors, 1976*, edited by N. B. Urli and J. W. Corbett, *Inst. Phys. Conf. Ser.*, no. 31, 231–243 (1977).

- [4.161] E. H. Wong and B. G. Streetman, "Isothermal Annealing of the 0.97-eV Luminescence in Electron-Irradiated Si," *J. Appl. Phys.*, vol. 42, no. 13, 5882–5883 (1971).
- [4.162] G. Davies and T. K. Kwok, "Annealing the Di-Carbon Radiation Damage Centre in Silicon," *Semicond. Sci. Technol.*, vol. 4, 327–330 (1989).
- [4.163] G. Davies, K. T. Kun, and T. Reade, "Annealing Kinetics of the Dicarbon Radiation-Damage Center in Crystalline Silicon," *Phys. Rev. B*, vol. 44, no. 22, 12146–12157 (1991).
- [4.164] N. I. Boyarkina, S. A. Smagulova, and A. A. Artem'ev, "Dissociation Energies of a C₂C₅ Complex and the A Center in Silicon," *Semiconductors*, vol. 35, no. 8, 845–847 (2002).
- [4.165] R. B. Capaz, A. Dal Pino, Jr., and J. D. Joannopoulos, "Theory of Carbon-Carbon Pairs in Silicon," *Phys. Rev. B*, vol. 58, no. 15, 9845–9850 (1998).
- [4.166] S. Chakravarthi and S. T. Dunham, "Point Defect Properties from Metal Diffusion Experiments — What Does the Data Really Tell Us?" in: *Defects and Diffusion in Silicon Processing*, edited by T. Diaz de la Rubia, S. Coffa, P. A. Stolk, and C. S. Rafferty, *Mat. Res. Soc. Symp. Proc.*, vol. 469, 47–52 (1997).
- [4.167] J. L. Ngau, P. B. Griffin, and J. D. Plummer, "Modeling the Suppression of Boron Transient Enhanced Diffusion in Silicon by Substitutional Carbon Incorporation," *J. Appl. Phys.*, vol. 90, no. 4, 1768–1778 (2001).
- [4.168] D. De Salvador, A. Mattoni, E. Napolitani, A. V. Drigo, S. Mirabella, and F. Priolo, "Modeling of Self-Interstitial Diffusion in Implanted Molecular Beam Epitaxy Silicon," in: *Silicon Front-End Junction Formation Technologies*, edited by D. F. Downey, M. E. Law, A. P. Claverie, and M. J. Rendon, *Mat. Res. Soc. Symp. Proc.*, vol. 717, C5.6.1–C5.6.6 (2002).
- [4.169] S. Mirabella, A. Coati, D. De Salvador, E. Napolitani, A. Mattoni, G. Bisognin, M. Berti, A. Carnera, A. V. Drigo, S. Scalese, S. Pulvirenti, A. Terrasi, and F. Priolo, "Interaction between Self-Interstitials and Substitutional C in Silicon: Interstitial Trapping and C Clustering Mechanism," *Phys. Rev. B*, vol. 65, 045209 (2002).
- [4.170] G. Davies, A. S. Oates, R. C. Newman, R. A. Woolley, E. C. Lightowers, M. H. Binns, and J. G. Wilkes, "Carbon-Related Radiation Damage Centres in Czochralski Silicon," *J. Phys. C*, vol. 19, 841–855 (1986).
- [4.171] A. S. Oates, R. C. Newman, J. M. Tucker, G. Davies, and E. C. Lightowers, "The Role of Vacancies in Enhancing Oxygen Diffusion in Silicon," in: *Oxygen, Carbon, Hydrogen, and Nitrogen in Crystalline Silicon*, edited by J. C. Mikkelsen, Jr., S. J. Pearton, J. W. Corbett, and S. J. Pennycook, *Mat. Res. Soc. Symp. Proc.*, vol. 59, 59–65 (1986).
- [4.172] B. C. MacEvoy, G. Hall, and K. Gill, "Defect Evolution in Irradiated Silicon Detector Material," *Nuclear Instruments and Methods in Physics Research A*, vol. 374, 12–26 (1996).
- [4.173] W. Wijaranakula and J. H. Matlock, "A Formation Mechanism of the Thermal Donors Related to Carbon in Silicon after an Extended Isochronal Anneal," *J. Electrochem. Soc.*, vol. 137, no. 6, 1964–1969 (1990).
- [4.174] C. Kaneta, T. Sasaki, and H. Katayama-Yoshida, "Atomic Configuration, Stabilizing Mechanism, and Impurity Vibrations of Carbon-Oxygen Complexes in Crystalline Silicon," *Phys. Rev. B*, vol. 46, no. 20, 13179–13185 (1992).
- [4.175] Y. Shirakawa, H. Yamada-Kaneta, and H. Mori, "Annealing Behavior of Carbon-Oxygen Complexes in Silicon Crystals Observed by Low-Temperature Infrared Absorption," *J. Appl. Phys.*, vol. 77, no. 1, 41–46 (1995).
- [4.176] H. Yamada-Kaneta, Y. Shirakawa, and C. Kaneta, "Atomic Composition, Structure and Vibrational Excitation of Substitutional Carbon-Oxygen Complexes in Silicon," in: *Early Stages of Oxygen Precipitation in Silicon*, edited by R. Jones, *NATO ASI Series 3*, vol. 17, Dordrecht: Kluwer, 389–396 (1996).
- [4.177] Y. M. Babitskii, P. M. Grinshtein, and M. G. Mil'vidskii, "Interaction of Oxygen and Carbon Atoms in Silicon," *Inorganic Materials*, vol. 21, no. 5, 641–644 (1985).
- [4.178] G. Davies, E. C. Lightowers, M. Savola, K. Bergmann, and B. Svensson, "The 3942-cm⁻¹ Optical Band in Irradiated Silicon," *Phys. Rev. B*, vol. 35, no. 6, 2755–2766 (1987).

- [4.179] J. L. Lindström, T. Hallberg, J. Hermansson, L. I. Murin, V. P. Markevich, M. Kleverman, and B. G. Svensson, "Oxygen and Carbon Clustering in Cz-Si during Electron Irradiation at Elevated Temperatures," in: *Gettering and Defect Engineering in Semiconductor Technology GADEST'99*, edited by H. G. Grimmeiss, L. Ask, M. Kleverman, M. Kittler, and H. Richter, *Solid State Phenomena*, vol. 69-70, 297–302 (1999).
- [4.180] C. P. Foy, "Uniaxial Stress Analysis of the 0.79 eV Vibronic Band in Irradiated Silicon," *J. Phys. C*, vol. 15, 2059–2067 (1982).
- [4.181] K. Thonke, A. Hangleiter, J. Wagner, and R. Sauer, "0.79 eV (C Line) Defect in Irradiated Oxygen-Rich Silicon: Excited State Structure, Internal Strain and Luminescence Decay Time," *J. Phys. C*, vol. 18, L795–L801 (1985).
- [4.182] G. Davies, E. C. Lightowers, R. Woolley, R. C. Newman, and A. S. Oates, "Carbon in Radiation Damage Centres in Czochralski Silicon," *J. Phys. C*, vol. 17, L499–L503 (1984).
- [4.183] K. Thonke, G. D. Watkins, and R. Sauer, "Carbon and Oxygen Isotope Effects in the 0.79 eV Defect Photoluminescence Spectrum in Irradiated Silicon," *Solid State Communications*, vol. 51, no. 3, 127–130 (1984).
- [4.184] J. J. Hopfield, D. G. Thomas, and R. T. Lynch, "Isoelectronic Donors and Acceptors," *Phys. Rev. Lett.*, vol. 17, no. 6, 312–315 (1966).
- [4.185] C. E. Jones and W. D. Compton, "Recombination Luminescence in Irradiated Silicon — Effects of Uniaxial Stress and Temperature Variations," *Radiation Effects*, vol. 9, 83–88 (1971).
- [4.186] E. S. Johnson and W. D. Compton, "Recombination Luminescence in Irradiated Silicon — Effects of Thermal Annealing and Lithium Impurity," *Radiation Effects*, vol. 9, 89–92 (1971).
- [4.187] J. M. Trombetta and G. D. Watkins, "Identification of an Interstitial Carbon-Interstitial Oxygen Complex in Silicon," *Appl. Phys. Lett.*, vol. 51, no. 14, 1103–1105 (1987).
- [4.188] G. D. Watkins, "A Review of EPR Studies in Irradiated Silicon," in: *Radiation Damage in Semiconductors*, Paris: Dunod, 97–113 (1964).
- [4.189] N. Almeleh and B. Goldstein, "Electron Paramagnetic Resonance and Electrical Properties of the Dominant Paramagnetic Defect in Electron-Irradiated p-Type Silicon," *Phys. Rev.*, vol. 149, no. 2, 687–692 (1966).
- [4.190] Y. H. Lee, J. C. Corelli, and J. W. Corbett, "Oxygen-Vibrational Bands in Irradiated Silicon," *Physics Letters*, vol. 60A, no. 1, 55–57 (1977).
- [4.191] Y. H. Lee, J. W. Corbett, and K. L. Brower, "EPR of a Carbon-Oxygen-Divacancy Complex in Irradiated Silicon," *phys. stat. sol. (a)*, vol. 41, 637–647 (1977).
- [4.192] B. N. Mukashev, K. A. Abdullin, and Y. V. Gorelkinskii, "Metastable and Bistable Defects in Silicon," *Physics-Uspekhi*, vol. 43, no. 2, 139–150 (2000).
- [4.193] R. Jones and S. Öberg, "Oxygen Frustration and the Interstitial Carbon-Oxygen Complex in Si," *Phys. Rev. Lett.*, vol. 68, no. 1, 86–89 (1992).
- [4.194] J. Coutinho, R. Jones, P. R. Briddon, S. Öberg, L. I. Murin, V. P. Markevich, and J. L. Lindström, "Interstitial Carbon-Oxygen Center and Hydrogen Related Shallow Thermal Donors in Si," *Phys. Rev. B*, vol. 65, no. 1, 014109 (2002).
- [4.195] M. Roux, J. Bernard, R. Reulet, and R. L. Crabb, "Photon Effect on Electron-Irradiated Boron-Doped Silicon Solar Cell," *J. Appl. Phys.*, vol. 56, no. 2, 531–537 (1984).
- [4.196] V. I. Gubskaya, P. V. Kuchinskii, and V. M. Lomako, "Formation and Thermal Stability of Radiation Defects in p-Type Silicon Irradiated with Alpha Particles," *Sov. Phys. Semicond.*, vol. 20, no. 6, 664–667 (1986).
- [4.197] A. Khan, M. Yamaguchi, Y. Ohshita, N. Dharmarasu, K. Araki, T. Abe, Hisayoshi Itoh, T. Ohshima, M. Imaizumi, and S. Matsuda, "Role of the Impurities in Production Rates of Radiation-Induced Defects in Silicon Materials and Solar Cells," *J. Appl. Phys.*, vol. 90, no. 3, 1170–1178 (2001).
- [4.198] P. M. Mooney, L. J. Cheng, M. Süli, J. D. Gerson, and J. W. Corbett, "Defect Energy Levels in Boron-Doped Silicon Irradiated with 1-MeV Electrons," *Phys. Rev. B*, vol. 15, no. 8, 3836–3843 (1977).

- [4.199] B. N. Mukashev, A. V. Spitsyn, N. Fukuoka, and H. Saito, “Defects in Carbon-Implanted Silicon,” *Jpn. J. Appl. Phys.*, vol. 21, no. 2, 399–400 (1982).
- [4.200] C. A. Londos, “Carbon-Related Radiation Damage Centres and Processes in p-Type Si,” *Semicond. Sci. Technol.*, vol. 5, 645–648 (1990).
- [4.201] M. Yamaguchi, A. Khan, S. J. Taylor, K. Ando, T. Yamaguchi, S. Matsuda, and T. Aburaya, “Deep Level Analysis of Radiation-Induced Defects in Si Crystals and Solar Cells,” *J. Appl. Phys.*, vol. 86, no. 1, 217–223 (1999).
- [4.202] B. G. Svensson, K. H. Rydén, and B. M. S. Lewerentz, “Overlapping Electron Traps in n-Type Silicon Studied by Capacitance Transient Spectroscopy,” *J. Appl. Phys.*, vol. 66, no. 4, 1699–1704 (1989).
- [4.203] F. Shimura, T. Higuchi, and R. S. Hockett, “Outdiffusion of Oxygen and Carbon in Czochralski Silicon,” *Appl. Phys. Lett.*, vol. 53, no. 1, 69–71 (1988).
- [4.204] W. Wijaranakula, “Oxygen Diffusion in Carbon-Doped Silicon,” *J. Appl. Phys.*, vol. 68, no. 12, 6538–6540 (1990).
- [4.205] B. G. Svensson and J. L. Lindström, “Annealing Studies of the 862 cm^{-1} Infrared Band in Silicon,” *phys. stat. sol. (a)*, vol. 95, 537–542 (1986).
- [4.206] K. A. Abdullin, B. N. Mukashev, M. F. Tamendarov, and T. B. Tashenov, “New Defect States in Irradiated p-Type Silicon,” *Phys. Lett. A*, vol. 144, no. 3, 198–200 (1990).
- [4.207] K. Shinoda and E. Ohta, “Interstitial Carbon-Oxygen Complex in Near Threshold Electron-Irradiated Silicon,” *Appl. Phys. Lett.*, vol. 61, no. 22, 2691–2693 (1992).
- [4.208] L. I. Khirunenko, L. I. Murin, J. L. Lindström, M. G. Sosnin, and Y. V. Pomozov, “Self-Interstitial-Oxygen Related Defects in Low-Temperature Irradiated Si,” *Physica B*, vol. 308–310, 458–461 (2001).
- [4.209] M. R. Brozel, R. C. Newman, and D. H. J. Totterdell, “Interstitial Defects Involving Carbon in Irradiated Silicon,” *J. Phys. C*, vol. 8, 243–248 (1975).
- [4.210] N. Magnea, A. Lazrak, and J. L. Pautrat, “Luminescence of Carbon and Oxygen Related Complexes in Annealed Silicon,” *Appl. Phys. Lett.*, vol. 45, no. 1, 60–62 (1984).
- [4.211] G. Davies, E. C. Lightowers, R. Woolley, R. C. Newman, and A. S. Oates, “Carbon, Oxygen and Silicon Isotope Effects in the Optical Spectra of Electron-Irradiated Czochralski Silicon,” in: *Thirteenth International Conference on Defects in Semiconductors*, edited by L. C. Kimerling and J. M. Parsey, Jr., The Metallurgical Society of AIME, 725–731 (1985).
- [4.212] A. Dörnen, R. Sauer, and J. Weber, “Annealing and Stress Study of Oxygen-Related Thermally Induced Defect Luminescence in Silicon,” in: *Thirteenth International Conference on Defects in Semiconductors*, edited by L. C. Kimerling and J. M. Parsey, Jr., The Metallurgical Society of AIME, 653–660 (1985).
- [4.213] J. Wagner, A. Dörnen, and R. Sauer, “Donorlike Excited States of the Thermally Induced 0.767-eV (P Line) Defect in Oxygen-Rich Silicon,” *Phys. Rev. B*, vol. 31, no. 8, 5561–5564 (1985).
- [4.214] W. Kürner, R. Sauer, A. Dörnen, and K. Thonke, “Structure of the 0.767-eV Oxygen-Carbon Luminescence Defect in 450 °C Thermally Annealed Czochralski-Grown Silicon,” *Phys. Rev. B*, vol. 39, no. 18, 13327–13337 (1989).
- [4.215] N. Fukuoka, K. Atobe, and M. Honda, “Effects of Carbon Atoms on the Defects in Czochralski-Grown Silicon Formed by Annealing,” *Jpn. J. Appl. Phys.*, vol. 29, no. 9, 1625–1629 (1990).
- [4.216] C. P. Ewels, R. Jones, and S. Öberg, “Oxygen-Carbon, Oxygen-Nitrogen and Oxygen-Dimer Defects in Silicon,” in: *Early Stages of Oxygen Precipitation in Silicon*, edited by R. Jones, *NATO ASI Series 3*, vol. 17, Dordrecht: Kluwer, 141–162 (1996).
- [4.217] N. S. Minaev and A. V. Mudryi, “Thermally-Induced Defects in Silicon Containing Oxygen and Carbon,” *phys. stat. sol. (a)*, vol. 68, 561–565 (1981).
- [4.218] M. Tajima, P. Stallhofer, and D. Huber, “Deep Level Luminescence Related to Thermal Donors in Silicon,” *Jpn. J. Appl. Phys.*, vol. 22, no. 9, L586–L588 (1983).
- [4.219] J. L. Lindström, H. Weman, and G. S. Oehrlein, “Thermal Donors and Carbon-Oxygen Defects in Silicon,” *phys. stat. sol. (a)*, vol. 99, 581–591 (1987).

- [4.220] Y. M. Dobrovinskii, S. Makhamov, A. Mirzaev, V. I. Mitin, and N. A. Tursunov, "Influence of Heat-Radiation Treatment on the Process of Formation of Defect Centers in Silicon by Electron Irradiation," *Sov. Phys. Semicond.*, vol. 25, no. 3, 316–319 (1991).
- [4.221] W. Kürner, K. Thonke, R. Sauer, M. T. Asom, and W. Zulehner, "Oxygen-Carbon Interactions in Silicon: Photoluminescence Defect Spectrum at 1.06 eV Emission Energy," in: *Defects in Semiconductors 15*, edited by G. Ferenczi, *Materials Science Forum*, vol. 38-41, 159–163 (1989).
- [4.222] A. Chantre and L. C. Kimerling, "Configurational Multistable Defect in Silicon," *Appl. Phys. Lett.*, vol. 48, no. 15, 1000–1002 (1986).
- [4.223] L. W. Song, B. W. Benson, and G. D. Watkins, "Identification of a Bistable Defect in Silicon: The Carbon Interstitial-Carbon Substitutional Pair," *Appl. Phys. Lett.*, vol. 51, no. 15, 1155–1157 (1987).
- [4.224] Z. Su, P. G. Wald, and J. W. Farmer, "Role of Boron in the Multistable Carbon-Related Defect in Silicon," *J. Appl. Phys.*, vol. 67, no. 9, 4249–4252 (1990).
- [4.225] E. Gürer, B. W. Benson, and G. D. Watkins, "Configurational Metastability of Carbon-Phosphorus Pair Defects in Silicon," in: *Defects in Semiconductors 16*, edited by G. Davies, G. G. DeLeo, and M. Stavola, *Materials Science Forum*, vol. 83-87, 339–344 (1992).
- [4.226] Y. Kamiura, T. Maeda, Y. Yamashita, and M. Nakamura, "Formation of Carbon-Related Defects during the Carbon-Enhanced Annihilation of Thermal Donors in Silicon," *Jpn. J. Appl. Phys., Part 2*, vol. 37, no. 2A, L101–L104 (1998).
- [4.227] X. D. Zhan and G. D. Watkins, "Electron Paramagnetic Resonance of a Multistable Interstitial-Carbon-Substitutional-Phosphorus Pair in Silicon," *Appl. Phys. Lett.*, vol. 58, no. 19, 2144–2146 (1991).
- [4.228] X. D. Zhan and G. D. Watkins, "Electron Paramagnetic Resonance of Multistable Interstitial-Carbon-Substitutional-Group-V-Atom Pairs in Silicon," *Phys. Rev. B*, vol. 47, no. 11, 6363–6380 (1993).
- [4.229] E. Gürer and B. W. Benson, "Multiconfigurational Carbon-Group V Pair Defect in Silicon," in: *Impurities, Defects and Diffusion in Semiconductors: Bulk and Layered Structures*, edited by D. J. Wolford, J. Bernholc, and E. E. Haller, *Mat. Res. Soc. Symp. Proc.*, vol. 163, 295–298 (1990).
- [4.230] B. W. Benson, E. Gurer, and G. D. Watkins, "The Multiconfigurational Carbon-Antimony Pair in Silicon," in: *Defects in Semiconductors 15*, edited by G. Ferenczi, *Materials Science Forum*, vol. 38-41, 391–395 (1989).
- [4.231] M. Y. Pines and R. Baron, "Characteristics of Indium Doped Silicon Infrared Detectors," in: *Technical Digest of the 1974 International Electron Devices Meeting (IEDM)*, New York: IEEE, 446–450 (1974).
- [4.232] E. L. Kern, R. Baron, R. H. Walker, D. J. O'Connor, and O. J. Marsh, "Growth Characteristics of Si:In Crystals," *J. Electronic Materials*, vol. 4, no. 6, 1249 (1975).
- [4.233] R. Baron, M. H. Young, J. K. Neeland, and O. J. Marsh, "A New Acceptor Level in Indium-Doped Silicon," *Appl. Phys. Lett.*, vol. 30, no. 11, 594–596 (1977).
- [4.234] W. Scott, "Infrared Spectra of New Acceptor Levels in Indium- or Aluminum-Doped Silicon," *Appl. Phys. Lett.*, vol. 32, no. 9, 540–542 (1978).
- [4.235] R. D. Larrabee, "Interpretation of Hall Measurements," in: *Semiconductor Characterization Techniques*, edited by P. A. Barnes and G. A. Rozgonyi, *Electrochem. Soc. Proc.*, vol. 78-3, 71–80 (1978).
- [4.236] R. N. Thomas, T. T. Braggins, H. M. Hobgood, and W. J. Takei, "Compensation of Residual Boron Impurities in Extrinsic Indium-Doped Silicon by Neutron Transmutation of Silicon," *J. Appl. Phys.*, vol. 49, no. 5, 2811–2820 (1978).
- [4.237] W. Scott and R. J. Hager, "Solution Growth of Indium-Doped Silicon," *J. Electronic Materials*, vol. 8, 581–602 (1979).
- [4.238] C. E. Jones and G. E. Johnson, "Deep Level Transient Spectroscopy Studies of Trapping Parameters for Centers in Indium-Doped Silicon," *J. Appl. Phys.*, vol. 52, no. 8, 5159–5163 (1981).

- [4.239] H. Boudinov, J. P. de Souza, and C. K. Saul, “Enhanced Electrical Activation of Indium Coimplanted with Carbon in a Silicon Substrate,” *J. Appl. Phys.*, vol. 86, no. 10, 5909–5911 (1999).
- [4.240] S. Scalese, M. Italia, A. La Magna, V. Privitera, M. Bersani, D. Giubertoni, M. Barozzi, S. Solmi, and P. Pichler, “Diffusion and Electrical Activation of Indium in Silicon,” *J. Appl. Phys.*, vol. 93, no. 12, 9773–9782 (2003).
- [4.241] R. Baron, J. P. Baukus, S. D. Allen, T. C. McGill, M. H. Young, H. Kimura, H. V. Winston, and O. J. Marsh, “Nature of the 0.111-eV Acceptor Level in Indium-Doped Silicon,” *Appl. Phys. Lett.*, vol. 34, no. 4, 257–259 (1979).
- [4.242] V. Swaminathan, J. E. Lang, P. M. Hemenger, and S. R. Smith, “The Effect of Electron Irradiation on the In-X Acceptor in In-Doped Silicon,” *Appl. Phys. Lett.*, vol. 35, no. 2, 184–187 (1979).
- [4.243] C. E. Jones, D. Schafer, W. Scott, and R. J. Hager, “Carbon-Acceptor Pair Centers (X Centers) in Silicon,” *J. Appl. Phys.*, vol. 52, no. 8, 5148–5158 (1981).
- [4.244] A. C. T. Drakeford and E. C. Lightowers, “Complex Defect Formation in Heat Treated Aluminium Doped CZ Silicon,” in: *Defects in Electronic Materials*, edited by M. Stavola, S. J. Pearton, and G. Davies, *Mat. Res. Soc. Symp. Proc.*, vol. 104, 209–213 (1988).
- [4.245] N. Yarykin, O. V. Feklisova, and J. Weber, “Dominant Boron-Related Radiation Defect in Silicon Revealed by Hydrogenation,” in: *Proceedings of the 22nd International Conference on Defects in Semiconductors*, edited by K. Bonde Nielsen, A. Nylandsted Larsen, and G. Weyer, *Physica B*, vol. 340-342, 528–531 (2003).
- [4.246] P. J. Drevinsky, C. E. Caefer, S. P. Tobin, J. C. Mikkelsen, Jr., and L. C. Kimerling, “Influence of Oxygen and Boron on Defect Production in Irradiated Silicon,” in: *Defects in Electronic Materials*, edited by M. Stavola, S. J. Pearton, and G. Davies, *Mat. Res. Soc. Symp. Proc.*, vol. 104, 167–172 (1988).
- [4.247] J. Adey, R. Jones, and P. R. Briddon, “Formation of $\text{Bi}_\text{O}_\text{i}$, $\text{Bi}_\text{C}_\text{s}$, and $\text{Bi}_\text{B}_\text{s}\text{H}_\text{i}$ Defects in *e*-Irradiated or Ion-Implanted Silicon Containing Boron,” *Appl. Phys. Lett.*, vol. 83, no. 4, 665–667 (2003).
- [4.248] J. P. de Souza and H. Boudinov, “Electrical Activation of Boron Coimplanted with Carbon in a Silicon Substrate,” *J. Appl. Phys.*, vol. 74, no. 11, 6599–6602 (1993).
- [4.249] I. Ban, M. C. Öztürk, and E. K. Demirlioglu, “Suppression of Oxidation-Enhanced Boron Diffusion in Silicon by Carbon Implantation in Silicon by Carbon Implantation and Characterization of MOSFET’s with Carbon-Implanted Channels,” *IEEE Trans. Electron Devices*, vol. 44, no. 9, 1544–1551 (1997).
- [4.250] E. Irion, N. Bürger, K. Thonke, and R. Sauer, “The Defect Luminescence Spectrum at 0.9351 eV in Carbon-Doped Heat-Treated or Irradiated Silicon,” *J. Phys. C*, vol. 18, 5069–5082 (1985).
- [4.251] J. Peters, T. Markvart, and A. Willoughby, “A Study of Radiation Induced Defects in Silicon Solar Cells Showing Improved Radiation Resistance,” in: *Defects in Semiconductors 16*, edited by G. Davies, G. G. DeLeo, and M. Stavola, *Materials Science Forum*, vol. 83-87, 1539–1544 (1992).
- [4.252] L. D. Lanzerotti, J. C. Sturm, E. Stach, R. Hull, T. Buyuklimanli, and C. Magee, “Suppression of Boron Transient Enhanced Diffusion in SiGe HBTs by Carbon Incorporation,” in: *Defects and Diffusion in Silicon Processing*, edited by T. Diaz de la Rubia, S. Coffa, P. A. Stolk, and C. S. Rafferty, *Mat. Res. Soc. Symp. Proc.*, vol. 469, 297–302 (1997).
- [4.253] H. Rücker, B. Heinemann, and R. Kurps, “Nonequilibrium Point Defects and Dopant Diffusion in Carbon-Rich Silicon,” *Phys. Rev. B*, vol. 64, 073202 (2001).
- [4.254] P. Zaumseil and H. Rücker, “X-Ray Diffraction Studies of the Influence of Substitutional Carbon on Si/Ge Interdiffusion in SiGe/Si Superlattices,” in: *Gettering and Defect Engineering in Semiconductor Technology GADEST’99*, edited by H. G. Grimmeiss, L. Ask, M. Kleverman, M. Kittler, and H. Richter, *Solid State Phenomena*, vol. 69-70, 203–208 (1999).
- [4.255] R. Scholz, U. Gösele, J.-Y. Huh, and T. Y. Tan, “Carbon-Induced Undersaturation of Silicon Self-Interstitials,” *Appl. Phys. Lett.*, vol. 72, no. 2, 200–202 (1998).

- [4.256] P. Lavéant, P. Werner, N. Engler, and U. Gösele, "Engineering the Diffusion Behavior of Dopants (B, Sb) in Silicon by Incorporation of Carbon," *Nuclear Instruments and Methods in Physics Research B*, vol. 186, 292–297 (2002).
- [4.257] D. K. Sadana, W. Maszara, J. J. Wortmann, G. A. Rozgonyi, and W. K. Chu, "Germanium Implantation into Silicon," *J. Electrochem. Soc.*, vol. 131, no. 4, 943–945 (1984).
- [4.258] T. E. Seidel, D. M. Maher, and R. Knoell, "Defect and Impurity Behavior from the Recrystallization of Amorphous Silicon Layers," in: *Thirteenth International Conference on Defects in Semiconductors*, edited by L. C. Kimerling and J. M. Parsey, Jr., New York: The Metallurgical Society of AIME, 523–529 (1985).
- [4.259] T. Sands, J. Washburn, R. Gronsky, W. Maszara, D. K. Sadana, and G. A. Rozgonyi, "Influence of the Amorphous-Crystalline Interface Morphology on Dislocation Nucleation in Pre-Amorphized Silicon," in: *Thirteenth International Conference on Defects in Semiconductors*, edited by L. C. Kimerling and J. M. Parsey, Jr., The Metallurgical Society of AIME, 531–537 (1985).
- [4.260] E. Kasper, "Silicon Germanium-Heterostructures on Silicon Substrates," *Festkörperprobleme*, vol. 27, 265–277 (1987).
- [4.261] B. S. Meyerson, "Silicon and Silicon-Germanium Alloy Growth; Means and Applications," in: *Crucial Issues in Semiconductor Materials and Processing Technologies*, edited by S. Coffa, F. Priolo, E. Rimini, and J. M. Poate, *Nato ASI Series E: Applied Sciences*, vol. 222, Dordrecht: Kluwer, 33–47 (1991).
- [4.262] F. Schäffler, "High-Mobility Si and Ge Structures," *Semicond. Sci. Technol.*, vol. 12, 1515–1549 (1997).
- [4.263] D. J. Paul, "Silicon Germanium Heterostructures in Electronics: The Present and the Future," *Thin Solid Films*, vol. 321, 172–180 (1998).
- [4.264] D. J. Paul, "Silicon-Germanium Strained Layer Materials in Microelectronics," *Advanced Materials*, vol. 11, no. 3, 191–204 (1999).
- [4.265] M. C. Öztürk, N. Pesovic, J. Liu, H. Mo, I. Kang, and S. Gannavaram, "Selective Silicon-Germanium Source/Drain Technology for Nanoscale CMOS," in: *Silicon Front-End Junction Formation Technologies*, edited by D. F. Downey, M. E. Law, A. P. Claverie, and M. J. Rendon, *Mat. Res. Soc. Symp. Proc.*, vol. 717, C4.1.1–C4.1.12 (2002).
- [4.266] J. L. Martins and A. Zunger, "Bond Lengths around Isovalent Impurities and in Semiconductor Solid Solutions," *Phys. Rev. B*, vol. 30, no. 10, 6217–6220 (1984).
- [4.267] E. A. Kraut and W. A. Harrison, "Lattice Distortions and Energies of Atomic Substitution," *J. Vac. Sci. Technol. B*, vol. 3, no. 4, 1267–1273 (1985).
- [4.268] R. A. Logan, J. M. Rowell, and F. A. Trumbore, "Phonon Spectra of Ge-Si Alloys," *Phys. Rev.*, vol. 136, no. 6A, A1751–A1755 (1964).
- [4.269] G. D. Watkins, "A Microscopic View of Radiation Damage in Semiconductors Using EPR As a Probe," *IEEE Trans. Nuclear Science*, vol. NS-16, no. 6, 13–18 (1969).
- [4.270] G. D. Watkins, "EPR Studies of the Lattice Vacancy and Low-Temperature Damage Processes in Silicon," in: *Lattice Defects in Semiconductors, 1974, Inst. Phys. Conf. Ser.*, no. 23, 1–22 (1975).
- [4.271] V. V. Emtsev, P. M. Klinger, V. I. Fistul', and Y. V. Shmartsev, "Characteristics of the Interaction of Isovalent Germanium Impurities with Intrinsic Defects in Silicon," *Sov. Phys. Semicond.*, vol. 25, no. 6, 602–606 (1991).
- [4.272] C. V. Budtz-Jørgensen, P. Kringshøj, A. Nylandsted Larsen, and N. V. Abrosimov, "Deep-Level Transient Spectroscopy of the Ge-Vacancy Pair in Ge-Doped n-Type Silicon," *Phys. Rev. B*, vol. 58, no. 3, 1110–1113 (1998).
- [4.273] A. Brelot and J. Charlemagne, "Infrared Studies of Low Temperature Electron Irradiated Silicon Containing Germanium Oxygen and Carbon," *Radiation Effects*, vol. 9, 65–73 (1971).
- [4.274] A. Brelot, "Selective Trapping of Vacancies," in: *Radiation Damage and Defects in Semiconductors, Inst. Phys. Conf. Ser.*, no. 16, 191–201 (1973).

- [4.275] L. I. Khirunenko, V. I. Shakhovtsov, V. K. Shinkarenko, L. I. Shpinar, and I. I. Yaskovets, “Characteristics of Radiation Defect Formation Processes in Si:Ge Crystals,” *Sov. Phys. Semicond.*, vol. 21, no. 3, 345–347 (1987).
- [4.276] N. A. Sobolev and M. H. Nazaré, “Defects Incorporating Ge Atoms in Irradiated Si:Ge,” in: *20th International Conference on Defects in Semiconductors*, edited by C. Van de Walle and W. Walukiewicz, *Physica B*, vol. 273-274, 271–274 (1999).
- [4.277] R. W. Olesinski and G. J. Abbaschian, “The Ge-Si (Germanium-Silicon) System,” *Bull. Alloy Phase Diagrams*, vol. 5, no. 2, 180–183 (1984).
- [4.278] G. L. McVay and A. R. DuCharme, “The Diffusion of Germanium in Silicon,” *J. Appl. Phys.*, vol. 44, no. 3, 1409–1410 (1973).
- [4.279] G. Hettich, H. Mehrer, and K. Maier, “Tracer Diffusion of ^{71}Ge and ^{31}Si in Intrinsic and Doped Silicon,” in: *Defects and Radiation Effects in Semiconductors, 1978*, edited by J. H. Albany, *Inst. Phys. Conf. Ser.*, no. 46, 500–507 (1979).
- [4.280] P. Dorner, W. Gust, B. Predel, and U. Roll, “Investigations by SIMS of the Bulk Impurity Diffusion of Ge in Si,” *Phil. Mag. A*, vol. 49, no. 4, 557–571 (1984).
- [4.281] A. L. Bouchetout, N. Tabet, and C. Monty, “Germanium Impurity Diffusion in Boron Doped Silicon,” in: *Defects in Semiconductors 14*, edited by H. J. von Bardeleben, *Materials Science Forum*, vol. 10-12, 127–132 (1986).
- [4.282] U. Södervall, A. Lodding, and W. Gust, “Activation Volumes of Impurity Diffusion in Silicon,” in: *Diffusion in Metals and Alloys DIMETA 88*, edited by F. J. Kedves and D. L. Beke, *Defect and Diffusion Forum*, vol. 66-69, 415–420 (1989).
- [4.283] P. Fahey, S. S. Iyer, and G. J. Scilla, “Experimental Evidence of Both Interstitial- and Vacancy-Assisted Diffusion of Ge in Si,” *Appl. Phys. Lett.*, vol. 54, no. 9, 843 (1989).
- [4.284] G. F. A. Van de Walle, L. J. Van IJzendoorn, A. A. Van Gorkum, R. A. Van den Heuvel, A. M. L. Theunissen, and D. J. Gravesteijn, “Germanium Diffusion and Strain Relaxation in $\text{Si}/\text{Si}_{1-x}\text{Ge}_x/\text{Si}$ Structures,” *Thin Solid Films*, vol. 183, 183–190 (1989).
- [4.285] P. Fahey, S. Iyer, and G. Scilla, “Diffusion in Silicon,” in: *14th Nordic Semiconductor Meeting*, edited by O. Hansen, Stockholm: Royal Swedish Academy of Sciences, 55–59 (1990).
- [4.286] N. R. Zangenberg, J. Lundsgaard Hansen, J. Fage-Pedersen, and A. Nylandsted Larsen, “Ge Self-Diffusion in Epitaxial $\text{Si}_{1-x}\text{Ge}_x$ Layers,” *Phys. Rev. Lett.*, vol. 87, 125901 (2001).
- [4.287] M. Ogino, Y. Oana, and M. Watanabe, “The Diffusion Coefficient of Germanium in Silicon,” *phys. stat. sol. (a)*, vol. 72, 535–541 (1982).
- [4.288] A. Strohm, T. Voss, W. Frank, P. Laitinen, and J. Räisänen, “Self-Diffusion of ^{71}Ge and ^{31}Si in Si-Ge Alloys,” *Z. Metallkd.*, vol. 93, no. 7, 737–744 (2002).
- [4.289] N. E. B. Cowern, W. J. Kersten, R. C. M. de Kruif, J. G. M. v. B. W. B. de Boer, D. J. Gravesteijn, and C. W. T. Bulle-Liewma, “Interdiffusion Mechanisms in Coherently Strained SiGe Multilayers,” in: *Process Physics and Modeling in Semiconductor Technology*, edited by G. R. Srinivasan, C. S. Murthy, and S. T. Dunham, *Electrochem. Soc. Proc.*, vol. 96-4, 195–209 (1996).
- [4.290] E. A. Perozziello, P. B. Griffin, and J. D. Plummer, “Evidence for a Kickout Mechanism for Ge Diffusion in Si,” in: *Process Physics and Modeling in Semiconductor Technology*, edited by G. R. Srinivasan, K. Taniguchi, and C. S. Murthy, *Electrochem. Soc. Proc.*, vol. 93-6, 167–175 (1993).
- [4.291] N. E. B. Cowern, P. C. Zalm, P. van der Sluis, D. J. Gravesteijn, and W. B. de Boer, “Diffusion in Strained Si(Ge),” *Phys. Rev. Lett.*, vol. 72, no. 16, 2585–2588 (1994).
- [4.292] G. L. McVay and A. R. DuCharme, “The Diffusion of ^{71}Ge in Si and Si-Ge Alloys: A Study of Self-Diffusion Mechanisms,” in: *Lattice Defects in Semiconductors, 1974, Inst. Phys. Conf. Ser.*, no. 23, 91–102 (1975).
- [4.293] A. Nylandsted Larsen, K. Kyllesbech Larsen, P. E. Andersen, and B. G. Svensson, “Heavy Doping Effects in the Diffusion of Group IV and V Impurities in Silicon,” *J. Appl. Phys.*, vol. 73, no. 2, 691–698 (1993).

- [4.294] K. Kyllesbech Larsen, P. Gaiduk, and A. Nylandsted Larsen, "A Comparison of the Diffusivity of As and Ge in Si at High Donor Concentrations," in: *Impurities, Defects and Diffusion in Semiconductors: Bulk and Layered Structures*, edited by D. J. Wolford, J. Bernholc, and E. E. Haller, *Mat. Res. Soc. Symp. Proc.*, vol. 163, 601–604 (1990).
- [4.295] A. Strohm, T. Voss, W. Frank, J. Räisänen, and M. Dietrich, "Self-Diffusion of ^{71}Ge in Si-Ge," *Physica B*, vol. 308–310, 542–545 (2001).
- [4.296] J. Hattendorf, W.-D. Zeitz, N. V. Abrosimov, and W. Schröder, "The Interstitial Boron and the Boron-Germanium Complex in Silicon-Germanium Crystals," *Physica B*, vol. 308–310, 535–538 (2001).
- [4.297] N. Moriya, L. C. Feldman, H. S. Luftman, C. A. King, J. Bevk, and B. Freer, "Boron Diffusion in Strained $\text{Si}_{1-x}\text{Ge}_x$ Epitaxial Layers," *Phys. Rev. Lett.*, vol. 71, no. 6, 883–886 (1993).
- [4.298] G. H. Loechelt, G. Tam, J. W. Steele, L. K. Knoch, K. M. Klein, J. K. Watanabe, and J. W. Christiansen, "Measurement and Modeling of Boron Diffusion in Si and Strained $\text{Si}_{1-x}\text{Ge}_x$ Epitaxial Layers during Rapid Thermal Annealing," *J. Appl. Phys.*, vol. 74, no. 9, 5520–5526 (1993).
- [4.299] P. Kuo, J. L. Hoyt, J. F. Gibons, J. E. Turner, and D. Lefforge, "Boron Diffusion in Si and $\text{Si}_{1-x}\text{Ge}_x$," in: *Strained Layer Epitaxy — Materials, Processing, and Device Applications*, edited by E. A. Fitzgerald, J. Hoyt, K.-Y. Cheng, and J. Bean, *Mat. Res. Soc. Symp. Proc.*, vol. 379, 373–378 (1995).
- [4.300] W. T. C. Fang, P. B. Griffin, and J. D. Plummer, "Implant Enhanced Diffusion of Boron in Silicon Germanium," in: *Strained Layer Epitaxy — Materials, Processing, and Device Applications*, edited by E. A. Fitzgerald, J. Hoyt, K.-Y. Cheng, and J. Bean, *Mat. Res. Soc. Symp. Proc.*, vol. 379, 379–384 (1995).
- [4.301] T. T. Fang, W. T. C. Fang, P. B. Griffin, and J. D. Plummer, "Calculation of the Fractional Interstitial Component of Boron Diffusion and Segregation Coefficient of Boron in $\text{Si}(0.8)\text{Ge}(0.2)$," *Appl. Phys. Lett.*, vol. 68, no. 6, 791–793 (1996).
- [4.302] R. F. Lever, J. M. Bonar, and A. F. W. Willoughby, "Boron Diffusion across Silicon-Silicon Germanium Boundaries," *J. Appl. Phys.*, vol. 83, no. 4, 1988–1994 (1998).
- [4.303] N. R. Zangenberg, J. Fage-Pedersen, J. Lundsgaard Hansen, and A. Nylandsted Larsen, "Boron Diffusion in Strained and Relaxed $\text{Si}_{1-x}\text{Ge}_x$," in: *Diffusion in Materials DIMAT-2000*, edited by Y. Limoge and J. L. Bocquet, *Defect and Diffusion Forum*, vol. 194–199, 703–708 (2001).
- [4.304] N. R. Zangenberg, J. Fage-Pedersen, J. Lundgaard Hansen, and A. Nylandsted Larsen, "Boron and Phosphorus Diffusion in Strained and Relaxed Si and SiGe," *J. Appl. Phys.*, vol. 94, no. 6, 3883–3890 (2003).
- [4.305] K. Rajendran, D. Villaneuve, P. Moens, and W. Schoenmaker, "Modeling of Clustering Reaction and Diffusion of Boron in Strained $\text{Si}_{1-x}\text{Ge}_x$ Epitaxial Layers," *Solid-State Electronics*, vol. 47, 835–839 (2003).
- [4.306] T. H. Yeh and M. L. Joshi, "Strain Compensation in Silicon by Diffused Impurities," *J. Electrochem. Soc.*, vol. 116, no. 1, 73–77 (1969).
- [4.307] K. Yagi, N. Miyamoto, and J.-i. Nishizawa, "Anomalous Diffusion of Phosphorus into Silicon," *Jpn. J. Appl. Phys.*, vol. 9, no. 3, 246–254 (1970).
- [4.308] Y. Yukimoto, G. Nakamura, Y. Watari, K. Horie, and Y. Akasaka, "Effect of Tin on the Diffusion of Impurities in Transistor Structure," in: *Semiconductor Silicon 1973*, edited by H. R. Huff and R. R. Burgess, *Electrochem. Soc. Proc.*, vol. 73-1, 692–700 (1973).
- [4.309] A. Brelo, "Tin As a Vacancy Trap in Silicon at Room Temperature," *IEEE Trans. Nuclear Science*, vol. 19, no. 6, 220–223 (1972).
- [4.310] F. Lemeilleur, G. Lindström, and S. Watts, "2nd RD48 Status Report," *CERN/LHCC Reports*, vol. 98-39, 1–20 (1998).
- [4.311] A. Ruzin, G. Casse, M. Glaser, F. Lemeilleur, R. Talamonti, S. Watts, and A. Zanet, "Radiation Hardness of Silicon Detectors Manufactured on Epitaxial Material and FZ Bulk Enriched with Oxygen, Carbon, Tin and Platinum," *Nuclear Physics B (Proc. Suppl.)*, vol. 78, 645–649 (1999).

- [4.312] G. Lindström, M. Moll, and E. Fretwurst, “Radiation Hardness of Silicon Detectors — A Challenge from High-Energy Physics,” *Nuclear Instruments and Methods in Physics Research A*, vol. 426, 1–15 (1999).
- [4.313] E. Simoen and C. Claeys, “Tin Doping Effects in Silicon,” in: *High Purity Silicon VI*, edited by C. L. Claeys, P. Rai-Choudhury, M. Watanabe, P. Stallhofer, and H. J. Dawson, *Electrochem. Soc. Proc.*, vol. 2000-17, 223–235 (2000).
- [4.314] M. Delfino, D. K. Sadana, and A. E. Morgan, “Shallow Junction Formation by Preamorphization with Tin Implantation,” *Appl. Phys. Lett.*, vol. 49, no. 10, 575–577 (1986).
- [4.315] F. A. Trumbore, C. R. Isenberg, and E. M. Porbansky, “On the Temperature-Dependence of the Distribution Coefficient,” *J. Phys. Chem. Solids*, vol. 9, 60–69 (1958).
- [4.316] Y. Akasaka, K. Horie, G. Nakamura, K. Tsukamoto, and Y. Yukimoto, “Study of Tin Diffusion into Silicon by Backscattering Analysis,” *Jpn. J. Appl. Phys.*, vol. 13, no. 10, 1533–1540 (1974).
- [4.317] G. Weyer, B. I. Deutch, A. Nylandsted-Larsen, J. U. Andersen, and H. L. Nielsen, “Mössbauer and Channeling Studies on ^{119}Te , ^{119}Sb and ^{119}Sn Implants in Group-IV Elements,” in: *Exposés et communications présentés à la Conférence Internationale sur les Applications de l'Effet Mössbauer*, Colloque C6 in *Journal de Physique*, vol. 35, no. 12, 297 (1974).
- [4.318] I. V. Nistiryuk and P. P. Seregin, “State of Tin Impurity Atoms in Silicon,” *Sov. Phys. Solid State*, vol. 17, no. 4, 768–769 (1975).
- [4.319] P. P. Seregin, I. V. Nistiryuk, and F. S. Nasredinov, “Tin As an Isotopic Impurity in Silicon and Germanium,” *Sov. Phys. Solid State*, vol. 17, no. 8, 1540–1542 (1975).
- [4.320] S. R. Bakhchieva, M. G. Kekua, and P. P. Seregin, “A Study of Tin Impurity Atoms in Silicon, Germanium, and Silicon-Germanium Solid Solutions by Means of Mössbauer Spectroscopy,” *phys. stat. sol. (a)*, vol. 63, 23–30 (1981).
- [4.321] H. de Waard and G. J. Kemerink, “Hyperfine Interaction and Channeling Studies of Impurities Implanted in Silicon,” in: *Proceedings of the 12th International Conference on Defects in Semiconductors*, edited by C. A. J. Ammerlaan, *Physica*, vol. 116B, 210–218 (1983).
- [4.322] V. B. Neimash, M. G. Sosnin, B. M. Turovskii, V. I. Shakhovtsov, and V. L. Shindich, “Formation of Defects As a Result of Electron Irradiation of Tin-Doped *p*-Type Silicon,” *Semiconductors*, vol. 16, no. 5, 577–579 (1982).
- [4.323] B. G. Svensson, J. Svensson, J. L. Lindström, G. Davies, and J. W. Corbett, “Generation of Divacancies in Tin-Doped Silicon,” *Appl. Phys. Lett.*, vol. 51, no. 26, 2257–2259 (1987).
- [4.324] Y. M. Dobrovinskii, M. G. Sosnin, V. M. Tsmots’, V. I. Shakhovtsov, and V. L. Shindich, “Influence of the Tin Impurity on the Accumulation of Radiation Defects in *n*-Type Si,” *Sov. Phys. Semicond.*, vol. 22, no. 6, 727–728 (1988).
- [4.325] B. G. Svensson and J. L. Lindström, “Generation of Divacancies in Silicon by MeV Electrons: Dose Rate Dependence and Influence of Sn and P,” *J. Appl. Phys.*, vol. 72, no. 12, 5616–5621 (1992).
- [4.326] K. Matsui, R. R. Hasiguti, T. Shoji, and A. Ohkawa, “Tin-Vacancy Interaction in Silicon Monitored by ^{119}Sn Mössbauer Probe,” in: *Lattice Defects in Semiconductors, 1974, Inst. Phys. Conf. Ser.*, no. 23, 572–578 (1975).
- [4.327] G. D. Watkins, “Defects in Irradiated Silicon: EPR of the Tin-Vacancy Pair,” *Phys. Rev. B*, vol. 12, no. 10, 4383–4390 (1975).
- [4.328] M. Fanciulli and J. R. Byberg, “Tin-Vacancy Complexes in e-Irradiated *n*-Type Silicon,” in: *20th International Conference on Defects in Semiconductors*, edited by C. Van de Walle and W. Walukiewicz, *Physica B*, vol. 273-274, 524–527 (1999).
- [4.329] S. Damgaard, J. W. Petersen, and G. Weyer, “The Tin-Vacancy Pair Defect in Silicon,” *Hyperfine Interactions*, vol. 10, 751–758 (1981).
- [4.330] E. Müller, A. Nylandsted Larsen, and G. Weyer, “Evidence for Vacancy Percolation in Highly-Doped Silicon,” *Hyperfine Interactions*, vol. 93, 1395–1400 (1994).

- [4.331] A. Nylandsted Larsen, J. J. Goubet, P. Mejhlholm, J. Sherman Christensen, M. Fanciulli, H. P. Gunnlaughsson, G. Weyer, J. Wulff Petersen, A. Resende, M. Kaukonen, R. Jones, S. Öberg, P. R. Briddon, B. G. Svensson, J. L. Lindström, and S. Dannefaer, "Tin-Vacancy Acceptor Levels in Electron-Irradiated n-Type Silicon," *Phys. Rev. B*, vol. 62, no. 7, 4535–4544 (2000).
- [4.332] M. Kaukonen, R. Jones, S. Öberg, and P. R. Briddon, "Tin-Vacancy Complexes in Silicon," *Phys. Rev. B*, vol. 64, 245213 (2001).
- [4.333] G. D. Watkins and J. R. Troxell, "Negative-U Properties for Point Defects in Silicon," *Phys. Rev. Lett.*, vol. 44, no. 9, 593–596 (1980).
- [4.334] R. W. Olesinski and G. J. Abbaschian, "The Si-Sn (Silicon-Tin) System," *Bull. Alloy Phase Diagrams*, vol. 5, no. 3, 273–276 (1984).
- [4.335] T. H. Yeh, S. M. Hu, and R. H. Kastl, "Diffusion of Tin into Silicon," *J. Appl. Phys.*, vol. 39, no. 9, 4266–4271 (1968).
- [4.336] M. F. Millea, "The Effect of Heavy Doping on the Diffusion of Impurities in Silicon," *J. Phys. Chem. Solids*, vol. 27, 315–325 (1966).
- [4.337] P. Kringhøj and A. Nylandsted Larsen, "Anomalous Diffusion of Tin in Silicon," *Phys. Rev. B*, vol. 56, no. 11, 6396–6399 (1997).
- [4.338] P. Kringhøj and R. G. Elliman, "Diffusion of Ion Implanted Sn in Si, $\text{Si}_{1-x}\text{Ge}_x$, and Ge," *Appl. Phys. Lett.*, vol. 65, no. 3, 324–326 (1994).
- [4.339] A. Nylandsted Larsen, P. E. Andersen, P. Gaiduk, and K. Kyllesbech Larsen, "The Effect of Phosphorus Background Concentration on the Diffusion of Tin, Arsenic and Antimony in Silicon," *Materials Science and Engineering B*, vol. 4, 107–112 (1989).
- [4.340] M. Fanciulli and J. R. Byberg, "Divacancy-Tin Complexes in Electron-Irradiated Silicon Studied by EPR," *Phys. Rev. B*, vol. 61, no. 4, 2657–2671 (2000).
- [4.341] L. I. Khirunenko, O. O. Kobzar, Y. V. Pomozov, M. G. Sosnin, and M. O. Tripachko, "Peculiarities of Vacancy-Related Defects Formation in Si Doped with Tin," in: *Proceedings of the 22nd International Conference on Defects in Semiconductors*, edited by K. Bonde Nielsen, A. Nylandsted Larsen, and G. Weyer, *Physica B*, vol. 340-342, 541–545 (2003).
- [4.342] E. V. Lavrov, M. Fanciulli, M. Kaukonen, R. Jones, and P. R. Briddon, "Carbon-Tin Defects in Silicon," *Phys. Rev. B*, vol. 64, 125212 (2001).
- [4.343] L. I. Khirunenko, O. O. Kobzar, Y. V. Pomozov, M. G. Sosnin, M. O. Tripachko, N. V. Abrosimov, and H. Riemann, "Interstitial-Related Reactions in Silicon Doped with Isovalent Impurities," in: *Proceedings of the 22nd International Conference on Defects in Semiconductors*, edited by K. Bonde Nielsen, A. Nylandsted Larsen, and G. Weyer, *Physica B*, vol. 340-342, 546–550 (2003).

Chapter 5

Dopants

Atoms of the groups III and V of the periodic system are the heart and soul of silicon technology. Atoms from group V have one positive charge too many for their share of the four valence bonds. Therefore, they form a positive charge in the lattice. The defect is accompanied by an extra electron which neutralizes the positive charge but which cannot be a part of the valence-bond structure. The energy states of this extra electron are described by wave functions in the conduction band and, there, behave much like an electron in free space in presence of a positive charge. Group III acceptor impurities represent negative charges since their atomic cores are insufficiently charged to neutralize the four electrons in their share of the valence bonds. Consequently, they can attract a positive charge. To describe the behavior of this positive charge, the concept of holes in the valence-bond band has been introduced.

Before discussing the properties of donors and acceptors, the concepts of dopant clusters and ion pairs are introduced in Sections 5.1 and 5.2. These complexes may affect seriously the diffusion and activation of dopants.

The basic atomic configurations, solubility, diffusion, and complex formation of the acceptors will be reviewed in Sections 5.3 to 5.6 for boron, aluminum, gallium and indium, respectively. Of these, boron is by far the most important acceptor for microelectronics. Aluminum is used predominantly for the fabrication of power semiconductors since its high diffusion coefficient allows to reduce process times significantly in comparison to other acceptors. Gallium has had its summit at the dawn of silicon technology but is not likely to play an important role except probably for CZ-based solar cells. Indium finally was investigated for infrared detectors. However, there is renewed interest since its diffusion into oxides allows to deplete it in the channel of MOS devices which increases the mobility there.

The first element of Group V of the periodic system, nitrogen, is an exception in this group. As outlined in Section 5.7, it is a rather ineffective dopant which is present predominantly in the form of N₂ complexes. On the other hand, there are various technical applications associated with nitrogen, from influences on crystal growth to the engineering of gate dielectrics. The properties of the other donors will be discussed in Sections 5.8 to 5.10 for phosphorus, arsenic, and antimony. Of these, each element has its own niche with arsenic preferred for source/drain formation in *n*-channel MOS transistors because of its high solubility and low diffusion coefficient. Antimony has a similarly small diffusion coefficient but a significantly smaller solubility. Phosphorus was intensively used in the past. Today, because of its rather high diffusion coefficient, its importance for microelectronics is significantly reduced but it is still used for power semiconductors and for gettering of impurities.

5.1 Dopant Clusters

Studying dopant diffusion at high concentrations, various authors found only a fraction of the total concentration to be electrically active. To explain this discrepancy, the formation of “clusters” was invoked in many publications. Clusters are generally assumed to be energetically favored, small agglomerates of impurities. Typical cluster sizes considered in the literature range from 2 to 6 atoms in one cluster and, in general, one type of cluster is assumed to dominate within a certain range of temperatures.

Ignoring, at first, interactions with intrinsic point defects, all cluster models proposed so far can be generalized in the form of a macroscopic reaction involving substitutional, ionized impurities and charge carriers. For clusters of donor atoms, electrons may be involved and a reaction of m substitutional impurities M_s^+ with j electrons e^- can be written formally as



where Cl_m^{j-m} stands for the clusters in charge state $j - m$, consisting of m impurity atoms. The concentrations of substitutional impurities, electrons and clusters will be denoted by C_{M_s} , n , and C_{Cl} , respectively. The symbols k_{\rightarrow} and k_{\leftarrow} denote the forward and backward reaction constants. For the sake of simplicity, and because arsenic is the dopant for which most cluster models were proposed, the following discussion will be carried out for clusters of donor impurities. For clusters of negatively charged acceptor impurities, holes will appear in the reaction equation instead of the electrons, and positive charge states have to be replaced by negative ones and *vice versa*. The equations derived below remain valid in analogy, with the electron concentration n replaced by the concentration p of holes.

From the reaction (5.1), ignoring the detailed atomistic process, the changes of the concentrations of clusters C_{Cl} and substitutional atoms C_{M_s} with time follow formally as

$$\frac{dC_{Cl}}{dt} = -\frac{1}{m} \cdot \frac{dC_{M_s}}{dt} = k_{\rightarrow} \cdot C_{M_s}^m \cdot n^j - k_{\leftarrow} \cdot C_{Cl}. \quad (5.2)$$

In equilibrium, the time derivative in (5.2) vanishes and the equation reduces to the law of mass action

$$C_{Cl} = \frac{k_{\rightarrow}}{k_{\leftarrow}} \cdot C_{M_s}^m \cdot n^j = K_{Cl} \cdot C_{M_s}^m \cdot n^j \quad (5.3)$$

with the equilibrium constant K_{Cl} introduced for the ratio of the reaction constants. When the total concentration C_M constitutes predominantly of the impurities on substitutional sites and the impurities in the clusters, it can be expressed via

$$C_M = C_{M_s} + m \cdot C_{Cl} = C_{M_s} + m \cdot K_{Cl} \cdot C_{M_s}^m \cdot n^j. \quad (5.4)$$

The electron concentration needed in (5.3) is obtained from a solution of the Poisson equation (cf. Section 1.2). In regions doped with high donor concentrations, the space charge and the concentration of holes can be neglected, and the electron concentration at process temperatures follows as

$$n = C_{M_s} + (m - j) \cdot C_{Cl} = C_M - j \cdot C_{Cl}. \quad (5.5)$$

Special cases are electrically neutral clusters ($m = j$) and totally ionized clusters ($j = 0$) with an electron concentration equal to the concentration of substitutional atoms and the total concentration, respectively. The resulting system of equations can be solved analytically only for some limiting assumptions and, in general, has to be solved numerically.

The qualitative relation between total concentration C_M and the substitutional concentration C_{M_s} in equilibrium depends strongly on the number of atoms and electrons needed to form a cluster. In Figure 5.1, the constant K_{Cl} was adjusted so that the substitutional concentration was equal to $C_{M_s} = C^*$ at a total concentration of $C_M = 2 \cdot C^*$. For total concentrations well below C^* , the influence of clustering decreases rapidly and $C_{M_s} \sim C_M$. Neutral clusters ($m=j$) and totally ionized clusters ($j=0$) are equivalent when the number of atoms in the totally ionized cluster is twice as high as that in the neutral one. For such clusters, for concentrations above C^* , the slope of the curve of the substitutional concentration versus total concentration decreases with increasing number of atoms in the cluster. In any case, the substitutional concentration C_{M_s} increases monotonic with the total concentration C_M . For clusters composing of one electron and, at least, two atoms, Tsai et al. [5.1] and Guerrero et al. [5.2] could show that the substitutional concentration saturates at

$$\hat{C}_s = \sqrt[m]{\frac{1}{K_{Cl} \cdot (m-1)}}. \quad (5.6)$$

For more than two electrons and, at least one atom more in the cluster, Guerrero et al. [5.2] found that the substitutional concentration reaches a maximum and decreases again for higher total concentrations. Neither the saturation of the substitutional concentration nor the decrease would be important since the electron concentration increases in both cases continuously with the total concentration. But a model popularized by Tsai et al. [5.1] postulates that clusters may be ionized at diffusion temperatures and electrically neutral at room temperature. This paradigm has no apparent physical justification, but influenced many studies on cluster models since then.

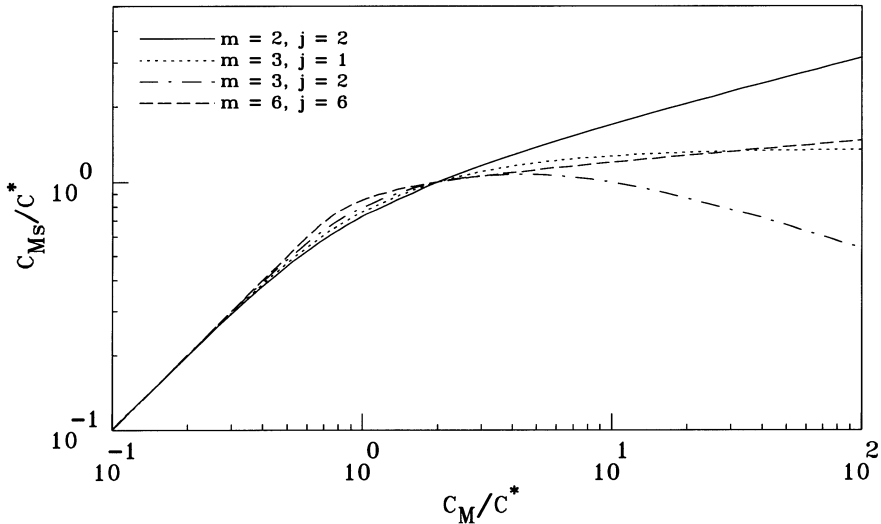


Figure 5.1: Normalized substitutional concentration versus normalized total dopant concentration for clustering.

It is clear that clusters cannot account for the establishment of solid solubility as it was the intention of early cluster models. Solid solubility, as outlined in Section 1.6, is defined only in a two-phase system. But especially for arsenic, gross differences between the solubility and the charge-carrier concentration were reported which can be explained by clusters.

5.2 Ion Pairing

Ion pairs are close complexes of impurities with opposite charge state. The impurities do not necessarily have to be different. Remarkable examples are the $\text{Al}_s^- \text{Al}_i^{++}$ and $\text{Ga}_s^- \text{Ga}_i^{++}$ pairs of negatively charged substitutional atoms and doubly positively charged interstitial atoms discussed in more detail in Sections 5.4.4 and 5.5.4. In the classical sense, the term ion pair refers to an immobile complex of a substitutional donor next to a substitutional acceptor impurity. This concept has been used to explain various phenomena occurring in areas where donors and acceptors are present and where, at least, one of the species is present in high concentrations [5.3]. Among these phenomena are the retarded diffusion and the increased solubility of the impurities involved.

The first experimental evidence for ion pairs came from IR absorption measurements after electron irradiation. In such studies, Newman and Smith [5.4], Tsvetov et al. [5.5], and Bean et al. [5.6] found various lines in samples co-doped with boron and arsenic, phosphorus, or antimony which were not found in samples doped with either impurities. For pairs with indium, informations about their structure were obtained from perturbed angular correlation measurements. These investigations, as discussed in Section 5.6.4, showed that pairs of indium with arsenic, phosphorus, and antimony are C_{3v} -symmetric about a $\langle 111 \rangle$ direction and corroborated that the pairs consist of substitutional impurities on neighboring sites. It has to be mentioned, however, that impurities on neighboring sites are just the usually most stable configuration of a pair attracted mainly by Coulombic interactions. There may be many metastable configurations characterized by larger separations between the dopants. Convincing evidence for ion pairs came also from diffusion studies of samples co-doped with acceptors and donors. In such a study, Culbertson and Pennycook [5.7] found antimony atoms by an ion-beam analysis to stay on substitutional sites although the peak concentration exceeded with 10^{21} cm^{-3} significantly the solid solubility of antimony in silicon and although electrical measurements showed that only a small fraction of these atoms could be electrically active. The properties of boron-donor and indium-donor pairs will be discussed in more detail in Sections 5.3.4 and 5.6.4. In addition, as will be mentioned in Section 6.3.4, evidence for the formation of selenium-acceptor pairs was given in the literature.

A major point of ion pairing is the influence on dopant diffusion. Dynamically, ion pairing can be described by reactions between substitutional donor or acceptor impurities with mobile pairs of intrinsic point defects and respectively acceptor or donor impurities. In equilibrium, the concentration of the pairs can be calculated from statistical thermodynamics and from the law of mass action of the reaction



where D_s , A_s , and P denote unassociated (substitutional), ionized donors, unassociated ionized acceptors, and pairs, respectively. When the total concentrations C_D and C_A of the donor and acceptor impurities constitute predominantly of the unassociated impurities and the impurities in the pairs, an ion pairing coefficient Ω is usually introduced in the form

$$\Omega = \frac{C_P}{(C_D - C_P) \cdot (C_A - C_P)} = \frac{4}{C_{Si}} \cdot \exp\left(\frac{G^B}{k \cdot T}\right) \quad (5.8)$$

to describe the state of local equilibrium. The factor four on the right-hand side comes from the fact that the concentration of sites for pairs of inequivalent, substitutional impurities is four times the concentration of lattice sites. Other phenomena like pair formation, incomplete ionization, clustering, or precipitation are ignored here, but have to be included also in the denominator terms when their contribution to the total concentration is not negligible. In the state of

local equilibrium, the concentration of unassociated acceptor impurities can be computed from (5.8) as

$$C_A - C_P = \frac{1}{2} \cdot \left(C_A - C_D - \frac{1}{\Omega} \right) + \sqrt{\frac{1}{4} \cdot \left(C_A - C_D - \frac{1}{\Omega} \right)^2 + \frac{C_A}{\Omega}}. \quad (5.9)$$

Since the ion pairs are assumed to be immobile, the effective diffusion coefficient D_A^{eff} of the acceptor impurities within macroscopic models can be defined in the form [5.3]

$$D_A^{eff} = D_A \cdot \frac{d(C_A - C_P)}{dC_A} = \frac{D_A}{2} \cdot \left(1 + \frac{\frac{1}{2} \cdot (C_A - C_D + \frac{1}{\Omega})}{\sqrt{\frac{1}{4} \cdot (C_A - C_D - \frac{1}{\Omega})^2 + \frac{C_A}{\Omega}}} \right) \quad (5.10)$$

with D_A denoting the diffusion coefficient of acceptor impurities without ion pairing. For donors, a similar relation is obtained with C_A and C_D exchanged, and D_A replaced by D_D . When both acceptor and donor concentrations are smaller than $1/\Omega$, the effective diffusion coefficient of the acceptors approaches D_A . D_A is also approached when the concentration of donor atoms exceeds the concentration of acceptor atoms as well as $1/\Omega$. When the concentration of the acceptor impurities is much lower than that of the donor impurities, (5.10) simplifies to

$$D_A^{eff} = \frac{D_A}{1 + \Omega \cdot C_D}. \quad (5.11)$$

For a donor concentration C_D exceeding the intrinsic concentration, the Fermi-level-dependent diffusion coefficient of acceptors (3.51) approaches a constant value. However, with ion pairing, the diffusion coefficient continues to decrease indirectly proportional to the increasing counter-doping concentration C_D .

In Figure 5.2, the effective diffusivity of impurities in highly doped background concentrations is shown for the example of boron at 1000 °C. It has to be noted, however, that the interpretation of such experiments [5.8–5.12] may be problematic. The diffusion coefficient

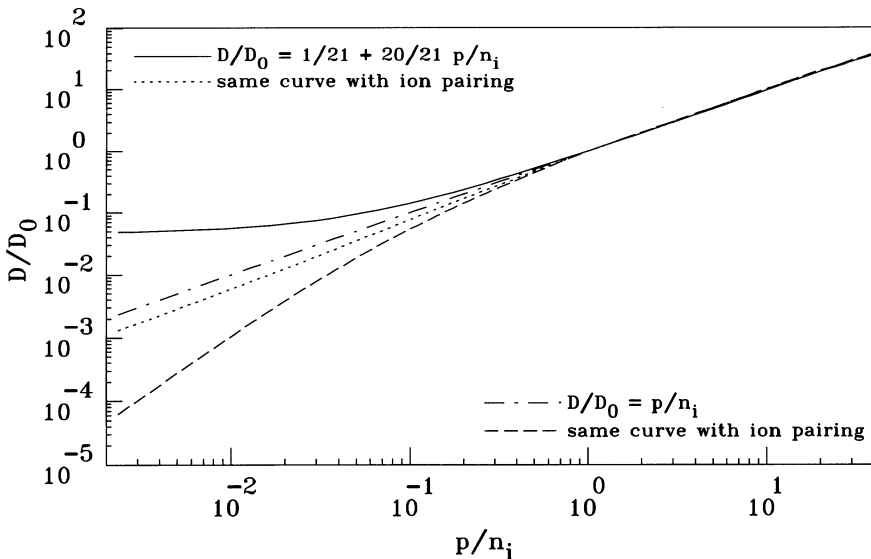


Figure 5.2: Effects of ion pairing on the diffusivity of boron at 1000 °C.

contains already a dependence on the Fermi level which is often only insufficiently known from high-concentration experiments or iso-concentration studies in a background of dopants with the same polarity. The extrapolation of this dependence to counter-doped materials may introduce uncertainties which cannot be verified because of the competing influence of ion pairing. To illustrate this argument, Figure 5.2 contains curves resulting from two assumptions about the dependence of the diffusion coefficient on the Fermi level. For $p/n_i > 1$ both are practically indistinguishable while there are significant differences for $p/n_i < 1$. In addition, ion pairing is just one of the effects to be considered in such iso-concentration experiments. Especially the effects of extrinsic concentrations on the band structure, as discussed in Section 1.2, leads to a deviation of the product of $n \cdot p$ from the value of n_i^2 for low dopant concentrations.

The effects of ion pairing on diffusion can be seen also in the simulation of co-diffusion of arsenic and boron at 950 °C for 100 h shown in Figure 5.3. In agreement with (5.11), a reduction of the boron diffusivity by ion pairing can be observed. The high-concentration arsenic profile shows marginally reduced diffusion in the bulk. At the surface, a hump can be seen which originates from the nearly immobile, paired atoms. The integrated arsenic concentration in this hump corresponds to $\approx 70\%$ of the implanted boron dose.

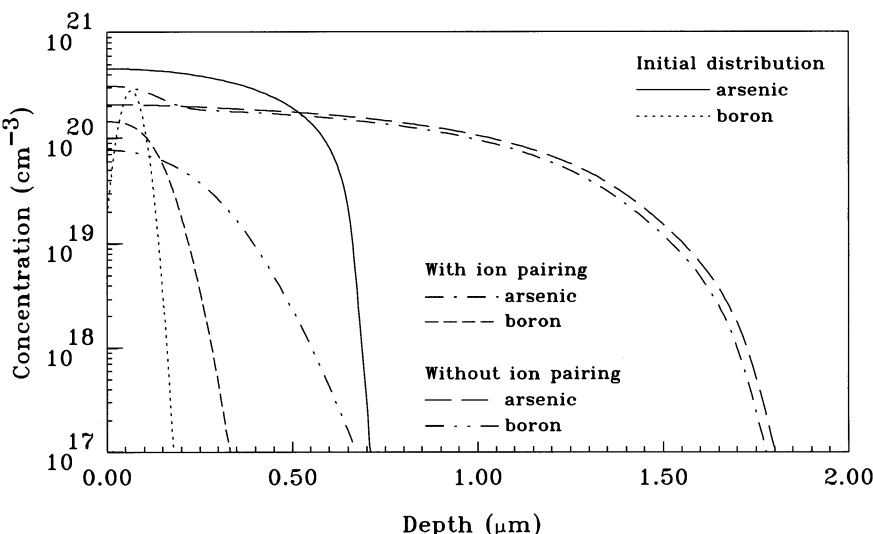


Figure 5.3: Effects of ion pairing on the co-diffusion of arsenic and boron at 950 °C for 100 h.

When only Coulombic interactions are considered, the binding energy is equivalent to the work needed to separate the dipole consisting of the two dopant atoms completely. For a crude estimate, one can assume that the atoms reside initially in the same distance of $a_{Si} \cdot \sqrt{3}/4$ as two silicon atoms in an undistorted lattice. One then arrives at

$$G^B = \frac{q^2}{4 \cdot \pi \cdot \epsilon_0 \cdot \epsilon_r \cdot (a_{Si} \cdot \sqrt{3}/4)} = 0.523 \text{ eV}. \quad (5.12)$$

In (5.12) the value of 11.7 from Table 1.5 was assumed for the relative permittivity. But it has to be kept in mind that the microscopic value of the relative permittivity needed here might deviate from this number since the macroscopic value applies only for distances well above the inter-

atomic spacing. In addition, the experiments discussed in the following sections indicate that stress compensation increases the binding energy while size mismatches of the ions involved reduce the binding energy.

Interaction of donor interstitials and acceptor interstitials was investigated experimentally and theoretically by Aronowitz and coworkers [5.13, 5.14]. The theoretical work, based on extended-Hückel-theory cluster calculations, indicated that the formation of some pairs is energetically favored while the formation of others is associated with an energy increase. The experiments performed indicated that co-implantation of dopants influences their diffusion even at intrinsic concentrations. However, it has to be remarked that an enhancement of the diffusivity of the dopants due to the generation of implantation damage was not taken into considerations and may be the reason for most of the phenomena reported.

5.3 Boron

Boron with its highest solid solubility of all group IIIa elements in silicon has an exceptional importance for the silicon technology and a variety of studies were carried out to characterize and understand its properties. Most important now is its redistribution and activation during post-implantation annealing steps during which it shows remarkably complex transient phenomena. In the following sections, the basic atomic configurations of boron in silicon, its solubility, the diffusion behavior, and the formation of complexes are discussed in detail.

5.3.1 Basic Atomic Configurations

Substitutional Boron

Already the first measurements of the lattice constant as a function of the boron concentration indicated that boron occupies predominantly substitutional sites in the silicon lattice [5.15, 5.16]. They have then one positive charge too few for the valence-bond structure of silicon. In analogy to donors, a hole is assumed to be introduced in the valence band. The ionization energy of substitutional boron was determined by electrical and optical measurements. Hall-effect measurements resulted in values of 0.045 eV [5.17], and 0.044 eV [5.18]. From infrared absorption, values of 0.046 eV [5.19], 0.04385 eV [5.20], and 0.0443 eV [5.21] were deduced, and a determination via measurements of dielectric loss resulted in an estimate of 0.047 eV [5.22].

Negatively charged, substitutional boron atoms were studied by IR measurements [5.6, 5.23, 5.24] where vibration bands at 646/644 (77 K/RT) and 623/620 cm⁻¹ (77 K/RT) were associated with substitutional ¹⁰B and ¹¹B, respectively. These frequencies were found to be in agreement with the theory of substitutional impurities of Dawber and Elliott [5.25, 5.26]. Similar bands were found in Raman measurements [5.27, 5.28]. Their appearance at slightly lower frequencies is usually explained by the presence of free carriers. In samples doped with boron atoms in concentrations up to 10¹⁶ cm⁻³, various photoluminescence lines were found to arise from the decay of excitons bound to neutral boron atoms. The zero-phonon line can be found at 1.1507 eV [5.29], the transverse-acoustic and transverse-optic phonon sidebands have 18.7 and 58.0 eV lower energies.

From diffuse X-ray scattering measurements and lattice-parameter measurements, Mayer et al. [5.30] concluded that substitutional boron contracts the lattice by one atomic volume. This would mean that substitutional boron in silicon occupies no volume. Theoretical studies of substitutional boron in silicon indicated a smaller volume contraction of 32% [5.31, 5.32]. It is interesting to note that the predicted contractions around a boron atom still exceed those around a vacancy.

Boron Interstitials

The first experimental indication of a boron interstitial was obtained by IR spectroscopy. Newman and Smith [5.33] found two lines at 733 and 760 cm⁻¹ (77 K) after electron irradiation which they labeled *Q*-center and which they associated tentatively with interstitial boron. Further studies by Newman and Totterdell [5.34] and Laithwaite et al. [5.35] corroborated this assignment. It was later revised by Tipping and Newman [5.36] who associated two near-by lines at 730 and 757 cm⁻¹ (77K), labeled *R*-center, with interstitial boron. The *Q* lines were later reassigned by Yamauchi et al. [5.37] to a pair of boron atoms in a ⟨100⟩-oriented split configuration (see Section 5.3.4). By photoconductivity measurements on electron-irradiated boron-doped silicon, Cherki and Kalma [5.38] found a defect which introduces a level at $E_v + 0.43$ eV which they tentatively identified as boron interstitial. Its C_{3v} symmetry determined by studies of stress effects was assumed to result from Jahn-Teller distortions. In internal-friction measurements, Tan et al. [5.39] observed four peaks two of which were associated with boron interstitials. For the neutral and negatively charged boron interstitials, a configuration in the form of a ⟨100⟩-oriented split interstitial was suggested. However, as discussed in Section 2.5.1, the identity of the friction peaks is ambiguous. After electron irradiation of boron-doped silicon, an EPR center labeled Si-G28 was observed by Watkins [5.40] and attributed to the neutral charge state of interstitial boron. From the low C_{1h} symmetry of the EPR spectrum, Watkins concluded that the boron atom would be in a distorted position around a bond-centered, tetrahedral, or hexagonal lattice site. Although the positive charge state of the boron interstitial was not observable by EPR, it was concluded from stress-alignment experiment that it has trigonal symmetry about a ⟨111⟩ direction. In a series of studies, Watkins and Troxell [5.41], Troxell and Watkins [5.42], and Harris et al. [5.43, 5.44] found that interstitial boron has a donor level at $E_c - 0.13$ eV which is located above the acceptor level at $E_c - 0.37 \pm 0.08$ eV¹, thus forming an Anderson “negative-U” system. Based also on the observation of athermal diffusion [5.42], the boron interstitial in its neutral charge state was suggested to take a configurationally intermediate position between the atomic arrangements of the positive and negative charge states. For the latter two, based on the results of the stress-alignment studies cited above and early theoretical investigations, bond-centered or hexagonal positions were suggested for B_i⁺, and a configuration in the form of a ⟨100⟩-oriented split interstitial for B_i⁻ [5.42]. From an ion-beam analysis after electron irradiation, Swanson [5.45] suggested a configuration in the form of a ⟨100⟩-oriented split interstitial with a distance of 1.6 Å between the boron and silicon atoms as the dominant atomic arrangement for a boron-interstitial complex. Finally, it remains to note that boron interstitials were tentatively associated in the β-NMR studies of Seelinger et al. [5.46] with a defect having an electric field gradient parallel to a ⟨111⟩ direction. Quoting otherwise unpublished results of Drevinsky et al., Kimerling et al. [5.47] estimated the capture of self-interstitials at substitutional boron to be seven times as effective as the capture at substitutional carbon. Davies and Newman [5.48] even estimated this ratio to be 50.

Values for the binding energy of boron-self-interstitial complexes were obtained from the fitting of diffusion models to experimental data. From the maximum diffusivity of boron determined by Packan [5.49] for post-implantation annealing processes, Law et al. [5.50] estimated a binding energy of 1.7 eV. Later, Park and Law [5.51] used an effective value of 1.52 eV to simulate a variety of intrinsic diffusion experiments under non-equilibrium situations. Studying boron diffusion at high concentrations, a binding energy of 1.4 eV was reported by Hane and Matsumoto [5.52] for positively charged boron-self-interstitial pairs. From their investigations of boron diffusion at high concentrations and in non-equilibrium situations, Baccus et

¹In the first studies, the acceptor level was reported at $E_c - 0.45$ eV. It was corrected by Harris et al. [5.44] taking the effect of electric fields on the electron emission rate into account.

al. [5.53] suggested a binding energy of 1.5 eV for positively charged boron-self-interstitial complexes. For the same parameter, Baccus and Vandebossche [5.54] reported a binding energy of 1.78 eV from high-concentration diffusion experiments. Based on similar simulations, Baccus et al. [5.55] obtained binding energies of 1.4, 1.6, and 1.6 eV for boron-self-interstitial complexes in the negative, neutral, and positive charge state, respectively. The ambiguities of such estimates were demonstrated by Bork and Matsumoto [5.56] who reported that the binding energies have negligible influence on the simulation of boron diffusion at high concentrations as long as the diffusion coefficient of the boron interstitials is adjusted accordingly. In a study of implantation-enhanced diffusion, Hane and Matsumoto [5.52] found a binding energy of 1.4 eV appropriate to explain the experiments. Later, to reproduce the reverse-short-channel characteristics measured, the estimate for the binding energy of boron-self-interstitial complexes was reduced by Hane and his coworkers to about 1.0 eV [5.57] and 0.8 eV [5.58]. To explain the reduced electrical activation after annealing of implanted boron, Kinoshita et al. [5.59] suggested a binding energy of 2.1 eV for boron-self-interstitial pairs. It has to be remarked, though, that the phenomenon is caused by the formation of larger boron-self-interstitial clusters discussed below in Section 5.3.4 rather than by the formation of boron-self-interstitial pairs. Simulating the transient-enhanced diffusion of boron, Uematsu [5.60] concluded that a binding energy of about 0.8 eV might be an upper limit. In addition, they argued that the determination of binding energies would hardly be unambiguous since they depend on the choice of the equilibrium concentration of self-interstitials for which, as shown in Section 2.5.2, the assumptions vary in a wide range. Instead, they suggested that the ratio of the concentration of pairs and the concentration of substitutional boron atoms is of greater physical significance.

The first theoretical investigations of pairs between boron atoms and self-interstitials were performed by Tarnow [5.61]. For the positive charge state of such a defect, he found a doubly positively charged silicon self-interstitial on a tetrahedral interstitial site next to a negatively charged substitutional boron atom to be energetically most stable. This atomic arrangement, as the bond-centered interstitial suggested before, is consistent with the trigonal symmetry found for the positive charge state by Watkins [5.40]. For the neutral and negative charge state, a configuration of lower symmetry was found to be more stable. The self-interstitial moves in and displaces the boron atom from its substitutional site towards a bond-centered interstitial site. Considering only neutral charge states of the defects involved, Zhu et al. [5.31] found Tarnow's D_{3d} -symmetric arrangement with the self-interstitial at a tetrahedral site next to a substitutional boron atom and a self-interstitial at a tetrahedral site near to a silicon neighbor of the boron atom as the most stable configurations. The binding energies estimated were 1.0 and 1.1 eV, respectively. For neutral boron interstitials on hexagonal and tetrahedral sites, Zhu et al. estimated formation energies which are by 0.4 and 0.7 eV, respectively, higher than that of the energetically most favorable B_sI configuration. Later, including charge states, Zhu [5.62] confirmed Tarnow's structure for the positively charged boron-interstitial defect. The binding energy with respect to well-separated B_s^- and I^{++} was calculated to be 0.22 eV. For the negative charge state, a minimum-energy configuration was found as interstitial boron on a hexagonal site associated with an energy gain of 0.16 eV in comparison to a negatively charged substitutional boron atom and a neutral self-interstitial. For the neutral charge state, a configuration similar to that of the positive charge state was suggested. But it was also found that this configuration is not stable, confirming the negative-U properties found experimentally. The *ab-initio* calculations of Windl et al. [5.63] confirmed again a self-interstitial on a tetrahedral interstitial site next to a substitutional boron atom as the energetically most favorable configuration for the neutral and positive charge states of such a pair. In comparison to a negatively charged substitutional boron atom and a tetrahedral silicon self-interstitial in the appropriate charge state,

binding energies of 0.8 and 1.0 eV were calculated in the generalized gradient approximation for the neutral and positive charge states, respectively. In the local-density approximation, the binding energies are, with values of 0.5 and 0.8 eV, somewhat smaller. For the negative charge state of a boron-interstitial complex, Windl et al. found a configuration in the form of a $\langle 110 \rangle$ -oriented split interstitial to be lowest in energy. Its binding energy with respect to a negatively charged substitutional boron atom and a well-separated neutral self-interstitial in form of a $\langle 110 \rangle$ -oriented split interstitial was calculated to be 0.5 and 0.3 eV in the generalized gradient and local-density approximations. Similar investigations by Sadigh et al. [5.64] reproduced the minimum-energy configurations suggested by Windl et al. For a negatively charged substitutional boron atom with a doubly positively charged silicon self-interstitial at a nearest tetrahedral interstitial site, they obtained a binding energy of 1.03 eV from the generalized gradient approximation and 0.9 eV within the local-density approximation. As in all previous investigations, Tarnow's structure with the doubly positively charged self-interstitial on a tetrahedral interstitial site next to a negatively charged substitutional boron atom was found by Hakala et al. [5.32] to be the energetically most favorable configuration by far for a positively charged boron-interstitial complex. It also turned out to be the minimum-energy configuration for the neutral charge state. But an alternative structure was found only 0.21 eV higher in energy. In this C_{1h} -symmetric arrangement, the self-interstitial moves in and displaces the boron atom about 0.8 Å towards a tetrahedral interstitial site. Then, for the negative charge state of the boron-interstitial complex, the C_{1h} -symmetric arrangement with a stronger displacement of the boron atom from its substitutional site was found to be the minimum-energy configuration, but just by 0.13 eV. For the positive and negative charge states of the boron-interstitial complex, the binding energies were calculated to be 0.24 and 0.27 eV, respectively. The experimental observation of a negative-U system was confirmed again. In the theoretical investigations of Jeong and Oshiyama [5.65], the previously suggested tetrahedral self-interstitial next to a substitutional boron atom was found energetically most favorable for the positive charge state, too. Similarly, it was found to be the minimum-energy configuration for the neutral charge state. But a configuration in the form of a $\langle 110 \rangle$ -oriented split interstitial was found to be nearly as favorable energetically with a formation energy higher only by 0.07 eV. This structure is probably identical to that found by Hakala et al. [5.32] and, as in their study, it turned out to be the energetically most favorable configuration for the negative charge state. In any case, the configurations for the neutral charge state were only metastable, confirming the experimentally found negative-U properties for interstitial boron. The minimum-energy configurations found were confirmed by Adey et al. [5.66]. In their work, the $\langle 110 \rangle$ -oriented split interstitial was found to be 0.17 eV higher in energy for the neutral charge state than in comparison to the structure with the silicon atom at a tetrahedral site near the substitutional boron atom. Adey et al. also found the vibrational modes calculated for the latter structure to be in agreement with the IR R lines discussed above. Finally, it remains to mention that Hattendorf et al. [5.67] concluded from their *ab-initio* calculations and β -NMR measurements that Tarnow's structure is more likely than Watkins' bond-centered configuration.

Combining *ab-initio* simulations and kinetic Monte-Carlo simulations, Beardmore et al. [5.68] estimated a capture radius of 4.6 Å for the interaction of self-interstitials and substitutional boron atoms at 900 °C which decreases slightly with increasing temperature.

Boron-Vacancy Pairs

In addition to self-interstitials, boron was found to interact with vacancies. After electron irradiation, Watkins [5.69] found an EPR center labeled Si-G10 which he tentatively identified as a vacancy at the second-nearest neighboring site of a substitutional boron atom. This assign-

ment was corroborated by the ENDOR investigations of Sprenger et al. [5.70] who moreover suggested the boron atom to be in a negative charge state and the vacancy to be in a positive one. After quenching of boron-doped samples by laser annealing, Chantre [5.71] found a bistable defect which he labeled *C*-center. It introduces two hole traps at $E_v + 0.5$ eV and $E_v + 0.36$ eV. Based on a comparison to similar experiments, the defect was tentatively identified as boron-vacancy pair with the vacancy at the nearest and second nearest neighboring site of the substitutional boron atom, respectively. This identification was also found to be consistent with Watkins' investigations of the Si-*G*10 EPR center. From the conversion between the two configurations, a barrier of 0.92 and 0.74 eV were deduced for the jump of the vacancy from the nearest to the second nearest neighboring site when the center is in the neutral and positive charge state, respectively. In DLTS studies after electron irradiation, Bains and Banbury [5.72] likewise found a bistable defect which, from a correlation to the concentration of boron and the kinetics of vacancies, was attributed to a boron-vacancy pair. One of its configurations was associated with levels at $E_v + 0.31$ eV and $E_v + 0.37$ eV. For the second configuration, a level between E_v and $E_v + 0.13$ eV was found. These assignments were supported by the investigations of Londos [5.73] and Zangenberg et al. [5.74]. In the positron-annihilation study of Polity et al. [5.75], the boron-vacancy pair was associated with a positron lifetime of 285 ps.

Binding energies were determined especially from fitting diffusion models to experimental data. From the diffusion of boron at high concentrations, Mathiot and Pfister [5.76] estimated 1.06 and 1.36 eV for the binding energy of the neutral and singly positively charged boron-vacancy pairs, respectively. Reviewing boron diffusion under non-equilibrium conditions, Park and Law [5.51] found an effective binding energy of 0.8 eV for intrinsic conditions. In their theoretical investigations, Nichols et al. [5.77] found the binding energy of a neutral pair of a vacancy at a next nearest neighboring site of a substitutional boron atom to be 0.5 eV. In a later study, Nelson et al. [5.78] estimated a value of 0.17 eV for the binding energy and a barrier of 2.49 eV for the barrier against exchange of sites between the vacancy and the substitutional boron atom.

5.3.2 Solubility

The phase diagram of the boron-silicon system was compiled by Olesinski and Abbaschian [5.79]. Accordingly, below the eutectic temperature of 1385 °C, the boron in the silicon phase is in equilibrium with an orthorhombic SiB_6 phase, and with a rhombohedral SiB_3 phase below about 1270 °C. There are indications, however, that the SiB_3 phase is only metastable [5.80].

Solubility values for boron were obtained from various experiments. Values deduced from the diffusion of boron from the gas phase [5.81–5.84] can be assumed to correspond to binary solubilities only when the binary equilibrium phase forms at the surface. Otherwise, smaller as well as slightly higher values are possible. In some experimental set-ups, boron agglomerates are likely to form or were shown to form. These are supersaturated solutions [5.85, 5.86], ion implantation [5.87–5.101], or diffusion from heavily doped polysilicon [5.102, 5.103]. In each case, annealing with a sufficient thermal budget is mandatory. Of the measurement techniques applied, profiling by the $^{10}\text{B}(\text{n},\alpha)^7\text{Li}$ reaction [5.89] gives chemical profiles without need for calibration. Similarly, properly calibrated SIMS measurements [5.87, 5.90, 5.91, 5.93–5.95, 5.97, 5.98, 5.100–5.103] should be quite reliable for measuring chemical concentrations. In both cases, solubilities are associated with the concentration below which significant redistribution is observed. Methods like sheet resistance measurements [5.81–5.84, 5.86, 5.88] or sheet resistance measurements combined with Hall-effect measurements [5.85, 5.92, 5.101], on the other hand, are sensitive to the electrically active concentration. A summary of the solubility values reported or extracted from the measurements reported can be found in Figure 5.4.

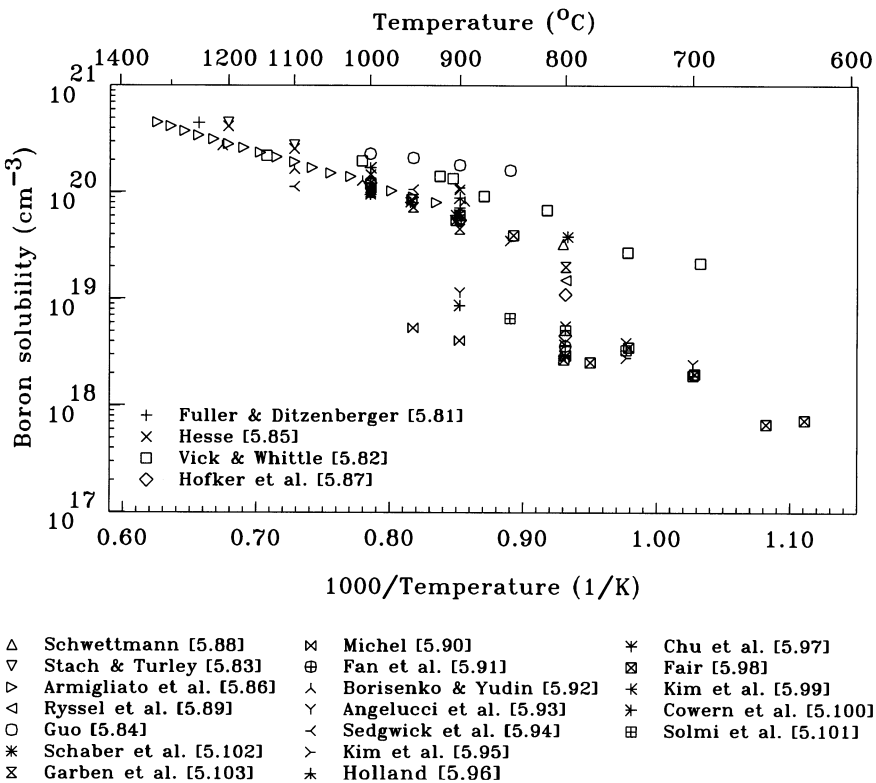


Figure 5.4: Solubility of boron in silicon.

While agreement between the various investigations is fair at 1000 °C and above, discrepancies of more than one order of magnitude are apparent at 900 °C and below. They are related to the transient formation of boron-interstitial complexes. This phenomenon, discussed in Section 5.3.4, has a marked influence on the diffusion and activation of boron after ion implantation and annealing. Hence, only the values for temperatures of 1000 °C and above can be assumed to correspond to solid solubility.

It remains to be mentioned that the *ab-initio* calculations of Sadigh et al. [5.104] indicated that compressive stress increases the solid solubility of boron while tensile stress decreases it.

5.3.3 Diffusion

Intrinsic Diffusion

A determination of the diffusion coefficient of boron under nominally inert and intrinsic conditions was the goal of numerous investigations. Introduction of boron occurred from the gas phase during diffusion [5.105–5.108], from a doped oxide [5.109–5.112], by ion implantation [5.10, 5.113–5.125], or by the epitaxial deposition of boron-doped layers [5.126–5.132]. For the characterization of the diffusion profile several methods were used. In a number of publications, delineation of p-n junctions was used and eventually combined with electrical measurements of the surface concentration [5.105, 5.107, 5.110, 5.116]. Potentially more reliable re-

sult were obtained by electrical depth profiling [5.106, 5.108, 5.109, 5.113–5.115, 5.117, 5.120], radiochemical depth profiling [5.111], and SIMS [5.10, 5.112, 5.118, 5.119, 5.121–5.132]. A summary of the diffusion coefficients reported can be found in Figure 5.5.

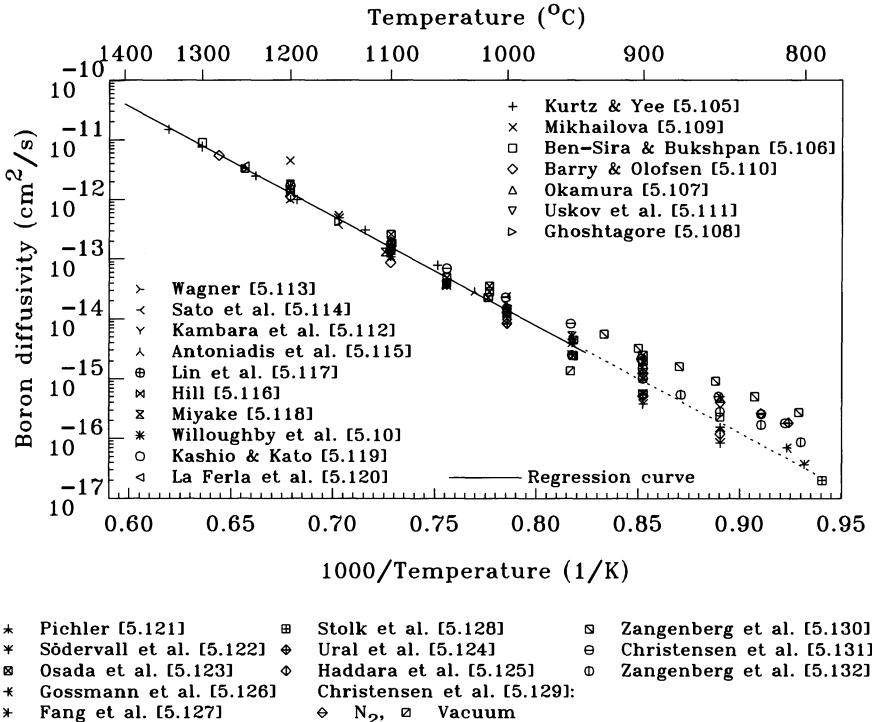


Figure 5.5: Diffusion coefficient of boron under intrinsic and inert conditions in silicon.

At temperatures of 1000 °C and above, the experimental data reported agree sufficiently well. Including the data at 950 °C, the regression curve is given by

$$D_B^i = 3.79 \cdot \exp\left(-\frac{3.645 \text{ eV}}{k \cdot T}\right) \text{ cm}^2/\text{s}. \quad (5.13)$$

with a 90% confidence interval for the activation energy from 3.55 to 3.74 eV. The 90% confidence interval for the diffusion coefficient is about +6.3/-5.9% of the regression curve at 1085 °C and increases to +19/-16% at the melting point and +12/-10% at 950 °C. Additional measurements are expected with 90% confidence within a range of +66/-40% of the regression curve at 1085 °C which increases slightly to +70/-41% at the melting point and +67/-40% at 950 °C.

At temperatures of 950 °C and below, the situation becomes increasingly confused. The experiments of Pichler [5.121], Södervall et al. [5.122], Gossmann et al. [5.126], Stolk et al. [5.128], and Haddara et al. [5.125] agree closely to the extrapolation of the regression curve while the investigations of Fang et al. [5.127], Christensen et al. [5.129] in nitrogen ambient, Zangenberg et al. [5.130], and Christensen et al. [5.131] form a group with consistently higher diffusion coefficients. The latter are characterized by an activation energy of 2.98 eV with a 90% confidence interval from 2.76 to 3.21 eV, and values which are, e. g. at 850 °C, by a factor of about 4 higher than the extrapolated values of the regression curve. For the investigation of

Zangenberg et al. [5.130] a reason for a diffusion enhancement is ready on hand. A first-order estimate based on the oxide thicknesses measured before and after annealing at 900 °C indicates a mean oxygen partial pressures of 0.026 bar during the first hour and $2.2 \cdot 10^{-3}$ bar during the next three hours. A look into Figure 3.3 shows that such partial pressures are well suited to result in the observed OED effect and confirms the corresponding tentative explanation of the authors. The most recent experiments of Zangenberg et al. [5.132] resulted in considerably smaller diffusion coefficients, but there is still a clear trend to a smaller activation energy than in the regression curve in Figure 5.5. For the investigations of Fang et al. [5.127] and Christensen et al. [5.129, 5.131], the reason for the observed discrepancies is not clear but it seems appropriate to comment on some observations. Both groups have in common that they used samples grown by chemical vapor deposition in ASM Epsilon reactors and reported that the apparent diffusion increased at temperatures from 850 to 950 °C within some hours to a final value. These transients were argued to be indicative of the establishment of equilibrium conditions. However, in the work of Haddara et al. [5.125], considerably longer diffusion times were used at 850 and 900 °C after ion implantation and defect removal at 1000 °C. Still, as mentioned above, their values are significantly smaller than those of Fang et al. and Christensen et al. If a simple OED effect would be involved, one would expect the apparent diffusion coefficient to decrease rather than to increase. Ambient effects, on the other hand, are apparent in the work of Christensen et al. [5.129] who reported different diffusion coefficients for annealing in N₂ and in vacuum. In addition, a formation of oxygen complexes in the Czochralski-grown substrates used and possible influences on the concentrations of the intrinsic point defects can at least not be excluded definitely for the work of Christensen et al. [5.129, 5.131]. Ambient and substrate effects, on the other hand, are probably not an explanation for the phenomena observed by Fang et al. [5.127]. To minimize such influences, unstably strained SiGe layers were grown between the boron spikes. In these layers, dislocations were expected to form during heat treatment and to maintain the concentrations of the intrinsic point defects near their equilibrium values.

In addition to data obtained from diffusion at intrinsic concentrations, intrinsic diffusivities were obtained from the analysis of extrinsic diffusion profiles by the Boltzmann-Matano method [5.82]. These results are not considered reliable and were not included because boron diffusion at high concentrations is known to cause a non-negligible influence on the concentrations of the intrinsic point defects which, in turn, may cause deviations of the diffusion coefficient at low concentrations from the intrinsic diffusivity. Similarly, some other methods assuming a concentration-dependent diffusion coefficient [5.84, 5.133] were not considered to give reliable diffusion coefficients at intrinsic concentrations.

Pressure Dependence

Diffusion studies performed by Södervall et al. [5.134] under hydrostatic pressure at 1050, 1170, and 1230 °C resulted in estimates of the activation volume of $(0.29 \pm 0.3) \cdot V_{Si}$, $(0.31 \pm 0.3) \cdot V_{Si}$, and $(-0.12 \pm 0.2) \cdot V_{Si}$, respectively. In a later study, Södervall et al. [5.122] reported a mean activation volume of $(0.27 \pm 0.13) \cdot V_{Si}$ for the temperature range from 1050 to 1230 °C which means a diffusion retarded by compressive stress. Diffusion enhancement under hydrostatic, compressive pressure was found by Zhao et al. [5.135, 5.136]. For 810 and 850 °C, activation volumes of $(-0.17 \pm 0.01) \cdot V_{Si}$ [5.136] and $(-0.125 \pm 0.02) \cdot V_{Si}$ [5.135] were reported.

In a study of diffusion in biaxially strained Si and SiGe layers, Zangenberg et al. [5.132] found an enhanced diffusion of boron under tensile strain while the diffusion was retarded in compressively strained layers. A numerical evaluation indicated that the apparent activation energy of boron diffusion changes by $-(3-63) \cdot s$ eV with s denoting the strain in the layer.

Diffusion Mechanism

Quantitative estimates of the contributions of self-interstitials and vacancies to the diffusion of boron under intrinsic conditions were obtained from experiments involving non-equilibrium conditions as discussed in Section 3.4.3. The values reported are listed in Table 5.1. Especially the recent experiments involving enhanced and retarded dopant diffusion established quite unambiguously that boron diffuses predominantly via self-interstitials. Comparative studies indicated that f_I^B might be somewhat smaller than the fractional diffusivity of phosphorus via self-interstitials. This point is still in debate and it might be that, e. g. a small but non-negligible contribution of the Frank-Turnbull mechanism to boron diffusion causes the discrepancies.

Table 5.1: Fractional diffusivity of boron via self-interstitials. The abbreviations OSF, DifModel, RD, and DifComp for the experimental method refer to estimates from oxidation-enhanced diffusion with self-interstitial oversaturations estimated from OSF growth, from fitting dopant diffusion at high concentrations or under other non-equilibrium conditions, from the observation of retarded diffusion under non-equilibrium conditions, and from the comparison with the diffusivities of other dopants under non-equilibrium conditions, respectively. A description of the methods can be found in Section 3.4.3.

	f_I	Temperature range (°C)	Experimental method	Ref.
Fair	0.17	1000–1200	OSF	[5.137]
Antoniadis & Moskowitz	0.3	1000	OSF	[5.138]
Matsumoto et al.	$7.42 \cdot \exp(-0.263 \text{ eV}/kT)$	950–1150	OSF	[5.139]
Matsumoto et al.	$860 \cdot \exp(-0.829 \text{ eV}/kT)$	950–1100	OSF	[5.140]
Tan et al.	> 0.5	1100–1200	OSF	[5.141]
Gösele & Tan	> 0.83	1200	RD	[5.142]
Guerrero	$1/(1+1.3 \cdot 10^{-5} \cdot \exp(1.2867 \text{ eV}/kT))$	850–1100	OSF	[5.143]
Mathiot & Pfister	$0.96 \cdot \exp(-0.193 \text{ eV}/kT)$	850–1100	DifModel	[5.76]
Morehead & Lever	0.7	800–1100	DifModel	[5.144]
Tsoukalas & Chenevier	0.21 - 0.43	1000	OSF	[5.145]
Hu	0.24 - 0.64	950	DifComp	[5.146]
Mulvaney et al.	$0.0834 \cdot \exp(0.21 \text{ eV}/kT)$	900–1200	DifModel	[5.147]
Giles	0.3	1000	OSF	[5.148]
Moynagh & Rosser	0.88	1100	DifComp	[5.149]
Packan & Plummer	$0.8 \cdot f_I^P$	900–1100	OSF	[5.150]
Tsoukalas	0.4	1000	OSF	[5.151]
Ghaderi et al.	0.67	900–1100	DifComp	[5.152]
Fang et al.	0.8–0.99	850	RD	[5.153]
Gossmann et al.	$\geq 0.94 \pm 0.01$	810	DifComp	[5.154]
	$\geq 0.98 \pm 0.01$	860		
Ural et al.	≥ 0.97	1000	DifComp	[5.124]
	≥ 0.94	1100		
Okino & Shimozaki	0.35	1100	OSF	[5.155]

Extrinsic Diffusion

Information about the diffusion of boron at extrinsic concentrations is available from the isoconcentration diffusion studies of Crowder et al. [5.156], Miyake [5.118], Tsoukalas and Chenevier [5.9], Willoughby et al. [5.10], and Kashio and Kato [5.119]. These results are shown in Fig-

ure 5.6. The full lines were obtained by a numerical optimization using all data points in Figure 5.5 with temperatures of 950 °C and above in addition to the data points shown in Figure 5.6. They are described by

$$\begin{aligned}
 D_B &= 0.123 \cdot \exp\left(-\frac{3.566\text{eV}}{k \cdot T}\right) \text{cm}^2/\text{s} \\
 &+ \frac{p}{n_i} \cdot 4.21 \cdot \exp\left(-\frac{3.671\text{eV}}{k \cdot T}\right) \text{cm}^2/\text{s} \\
 &+ \left(\frac{p}{n_i}\right)^2 \cdot 39.8 \cdot \exp\left(-\frac{4.373\text{eV}}{k \cdot T}\right) \text{cm}^2/\text{s}.
 \end{aligned} \quad (5.14)$$

Results from Boltzmann-Matano analyses [5.82, 5.107, 5.133, 5.157–5.160] were not included since boron is known to cause a non-local influence on the concentration of the intrinsic point defects which does not allow a reliable reduction to isoconcentration conditions. Within the temperature range of the experimental investigations, intrinsic diffusion is dominated by far by the linear term in p/n_i . With increasing temperature and increasing p/n_i , the quadratic term in p/n_i becomes important. The contribution of the hole-concentration-independent term is about 3% at intrinsic concentrations and decreases with increasing p/n_i .

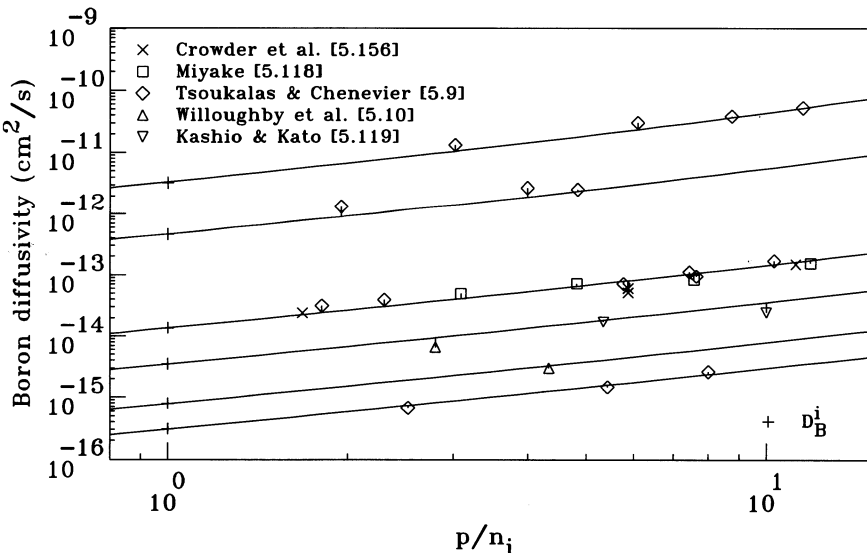


Figure 5.6: Dependence of the normalized diffusion coefficient of boron in silicon on p/n_i for moderate dopant concentrations with $p/n_i \leq 20$. The full lines correspond, from top to bottom, to temperatures of 1250, 1150, 1000, 950, 900, and 870 °C.

As an alternative to a pure Fermi-level effect, Hwang and Goddard III [5.161] suggested that the formation of mobile boron pairs has a significant influence on the diffusion of boron. Since the concentration of such pairs increases quadratically with the boron concentration and linearly with the self-interstitial concentration, their contribution to the total diffusion would be expected to increase proportional to the boron concentration and to the self-interstitial oversaturation. An independent verification is problematic since the solubilities of the other acceptors are rather

low and not really suited for isoconcentration experiments. It has to be remarked, though, that this model offers an explanation for the dominating p/n_i dependence of the diffusion coefficient which would not have been straight-forwardly expected from a Fermi-level effect since the neutral boron interstitial which would give rise to such a dependence was found to be unstable at low temperatures.

Tail Formation and Non-Local Diffusion Enhancement

The formation of kink and tail is one of the most prominent features of the diffusion of phosphorus (see Section 5.8.3). Although less pronounced, such kinks and tails were also seen in boron profiles [5.162–5.164]. In addition, it was observed that the diffusion of other dopants is enhanced below regions of high boron concentrations [5.165]. Although there may be additional effects involved in the case of deposited boron profiles, the main reason for the observed phenomena is that the transport capacity of boron exceeds that of the intrinsic point defects at high concentrations. As a consequence, as discussed in Section 3.4.7, the concentration of self-interstitials is increased in the bulk and causes the enhanced diffusion of other dopants observed below high-concentration boron profiles.

Boron-Vacancy Pairs

From the diffusion of boron at high concentrations, Mathiot and Pfister [5.76] estimated the migration enthalpies of neutral and positively charged boron-vacancy pairs to be 1.28 and 1.58 eV. It has to be mentioned, though, that an unambiguous determination of parameters in such studies is problematic. The *ab-initio* calculations of Zhu [5.62] indicated that a diffusion via vacancies is energetically unfavorable and should not play a role.

Boron Interstitials

From his EPR studies in *p*-type silicon, Watkins [5.40] found that the reorientation of boron interstitials in stress experiments is governed in the temperature range from 176 to 195 K by a time constant with a prefactor of $2 \cdot 10^{-13}$ s and an activation energy of 0.6 ± 0.05 eV. Taking the reorientation-time constant of Watkins' experiment as jump frequency and assuming the jump length to be similar to the distance between two neighboring lattice atoms, the diffusion coefficient of the positively charged boron-interstitial complex was estimated by Tipping and Newman [5.36] to be on the order of

$$D_{B_i} \approx 4 \cdot 10^{-4} \cdot \exp\left(-\frac{0.6 \text{eV}}{k \cdot T}\right) \text{cm}^2/\text{s}. \quad (5.15)$$

Watkins also found that the concentration of boron interstitials decays in annealing experiments around 300 K with a time constant characterized again by an activation energy of 0.6 eV. An analysis of the pre-exponential factors indicated that the annealing experiments are consistent with long-range diffusion of the boron interstitial to traps. Modeling the loss of boron interstitials by a diffusion-limited second-order reaction, Tipping and Newman [5.36] estimated the diffusion coefficient of boron interstitials in the temperature range from 205 to 225 K to be

$$D_{B_i} = 0.04 \cdot \exp\left(-\frac{0.58 \text{eV}}{k \cdot T}\right) \text{cm}^2/\text{s} \quad (5.16)$$

and estimated the uncertainty to be up to a factor of two. This value, as noticed already by the authors, is roughly two orders of magnitude larger than the estimate based on Watkins' measurements of reorientation times. Two theories were offered to explain the discrepancy. The one

is that the diffusion coefficient relates to negatively charged boron-interstitial complexes rather than to positively charged ones as in the reorientation measurements. The other explanation would be that the immobilizing reaction $2 B_i \rightarrow B_{2i}$ occurs predominantly between oppositely charged boron interstitials. Then, the capture radius would be significantly larger because of Coulombic interaction and the increased reaction rate would be interpreted as increased diffusion. Reorientation times in *p*-type silicon were also obtained from β -NMR investigations. Such measurements performed by Seelinger et al. [5.46] were shown to be compatible to the results of Watkins. Using a more sophisticated analysis method, Ittermann et al. [5.166] could determine the reorientation time of the boron interstitial in a temperature range from about 200 to 400 K. Its prefactor of $1.9 \cdot 10^{-12}$ s and the activation energy of 0.53 eV agreed well with the respective values reported by Watkins. Adopting the procedure of Tipping and Newman [5.36], one obtains a diffusion coefficient on the order of

$$D_{B_i} \approx 2.3 \cdot 10^{-5} \cdot \exp\left(-\frac{0.53 \text{eV}}{k \cdot T}\right) \text{cm}^2/\text{s}. \quad (5.17)$$

Analyzing the radiation-enhanced diffusion of boron at temperatures from 500 to 800 °C, Lucas et al. [5.167] extracted a prefactor of $4 \cdot 10^{-3}$ cm²/s and an activation energy of 1.2 eV for the diffusion of boron interstitials. It has to be remarked, though, that the analysis contains a veritable number of *a-priori* assumptions and fitting parameters. The high diffusivity of boron interstitials is documented also by the observation of boron diffusion at room temperature [5.168–5.171]. However, an unambiguous proof that athermal diffusion is not involved is missing. At elevated temperatures, boron diffusion coefficients as high as $2 \cdot 10^{-13}$ cm²/s at 700 °C [5.172] and 10^{-12} cm²/s at 800 °C [5.173] were measured under non-equilibrium conditions. These values are lower bounds of the diffusivity of boron interstitials, but orders of magnitude below the diffusion coefficients given above. Diffusion coefficients of boron interstitials with activation energies of 2.3 to 3.0 eV [5.53–5.55, 5.76] as they were reported from fitting diffusion models to experiments reflect most likely only the ambiguities in such studies.

Studying the short-time diffusion behavior of boron delta-layers at low temperatures, Cowern et al. [5.174] concluded that only a fraction of the boron atoms migrate and that they perform some hundred to some thousand diffusive jumps before they return to an immobile state. The mean projected path length λ_B a boron atom migrates while it is mobile (see Section 1.5.4) was found to be approximately 10 nm at 600 °C. In a subsequent study, Cowern et al. [5.175] found λ_B to be independent of the annealing ambient which means that an immobilization by a reaction with a vacancy is unlikely in comparison to a simple break-up of the mobile boron-interstitial complex. Other estimates for λ_B were obtained from studies of implantation-enhanced diffusion [5.176–5.178] and irradiation-enhanced diffusion [5.179] of boron delta-layers. The values for the mean path length obtained from the experiments are shown in Figure 5.7² together with the regression curve

$$\lambda = 8.7 \cdot 10^{-3} \cdot \exp\left(\frac{0.589 \text{eV}}{k \cdot T}\right) \text{nm} \quad (5.18)$$

for the various values given by Cowern. The activation energy of the curve can be found with 90% confidence between -0.68 and -0.5 eV.

Also shown are estimates of the mean path lengths obtained by Mannino et al. [5.178] from reproducing diffusion profiles after a shallow implantation on the basis of the kick-out mechanism. The values are notably larger than the values reported by Cowern et al. It is not straight-forward to see whether the discrepancies are related to insufficiencies of the model used or to a physical effect. In the latter case, the experiments would mean a higher boron diffusivity

²A factor of $\sqrt{3}$ was used to convert projected mean path lengths to mean path lengths.

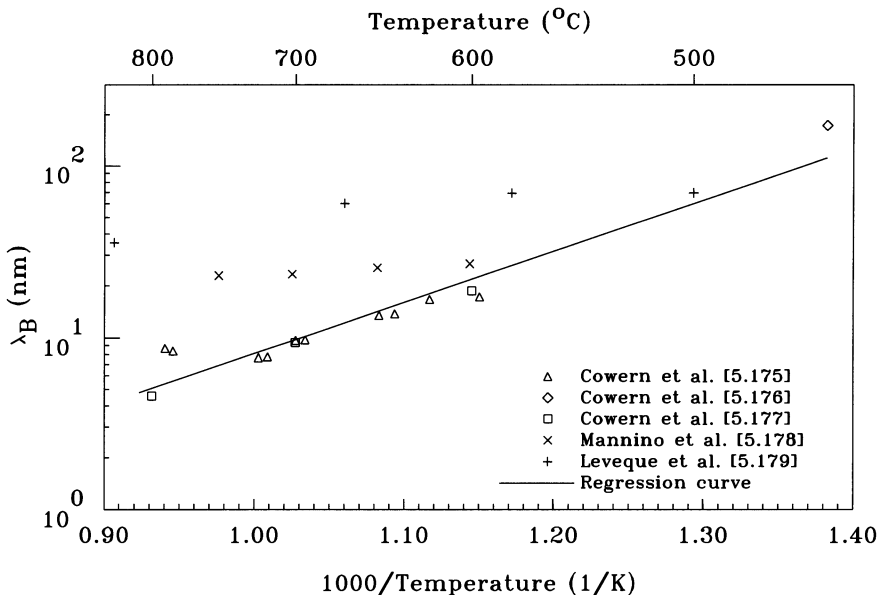


Figure 5.7: Mean path length λ_B a boron atom migrates while it is mobile.

or an increased time a boron interstitial remains in the mobile state. One possibility for an explanation would be that the results refer to a different charge state of boron interstitials than the work of Cowern et al. In the experiment of Mannino et al., the samples were extrinsically doped while those of Cowern et al. were intrinsic.

In comparison to the work of Cowern et al., the values determined by Léveque et al. [5.179] from electron-irradiated samples are significantly larger at higher temperatures and characterized by an activation energy of about -0.148 eV. Léveque et al. also reported that values for λ_B determined from oxidation studies are in perfect agreement with the values of Cowern. As a consequence, it was concluded that the increased values for λ_B due to electron irradiation are related to athermal migration of boron interstitials. From the rate with which substitutional boron atoms are mobilized, Cowern et al. [5.175] concluded on a reaction between substitutional boron atoms and silicon self-interstitials with a barrier smaller than 0.3 eV. A subsequent analysis of Cowern et al. [5.177] leads to a barrier of less than 0.05 eV and a dissociation energy of the boron-interstitial pair of 1.0 ± 0.1 eV. The basic results of the model were reproduced in the Monte-Carlo study of de Souza and Amaralunga [5.180].

Based on educated guesses, various diffusion mechanisms were suggested for boron. From studies of self-diffusion and boron diffusion at high concentrations, Sharp et al. [5.181] concluded that the diffusion of boron does not involve the transport of silicon. This excludes the diffusion via bound boron-self-interstitial pairs.

An elucidation of the diffusion mechanism of boron interstitials was also the goal of various theoretical investigations. The calculations of Nichols et al. [5.77] indicated that electrically neutral boron interstitials diffuse via the kick-out mechanism with a virtually negligible migration barrier. Studying also only neutral defects, Zhu et al. [5.31] suggested that a pair of a self-interstitial at a tetrahedral site next to a substitutional boron atom transforms with an activation energy of 1.0 eV to a boron interstitial on a hexagon site. For its migration, an activation energy of 0.3 eV was given while 0.6 eV would be needed for the return to the initial B_3I con-

figuration. Taking charge states into account, Zhu [5.62] confirmed his results for positively charged boron-interstitial complexes with barriers of 1.1, 0.2, and 0.4 eV for the initial kick-out reaction, diffusion, and final return to the stable configuration. In contrast to the work of Zhu, a completely different mechanism was suggested by Windl et al. [5.63]. They found that the energetically most stable interstitial complex reforms again after each diffusive step of the boron atom. Depending on the charge state, the migration path may include a metastable configuration in the form of a $\langle 100 \rangle$ -oriented split interstitial. The migration enthalpies computed from the generalized gradient approximation were 0.6, 0.2, and 0.8 eV for the negative, neutral, and positive charge states, respectively. Within the local-density approximation, values of respectively 0.5, 0.4, and 1.2 eV were reported. Similar to Windl et al., Sadigh et al. [5.64] concluded from their *ab-initio* calculations that the energetically most stable configuration of a negatively charged substitutional boron atom and a doubly positively charged self-interstitial on a tetrahedral site is assumed again after each diffusive jump of the boron atom. Within the local-density approximation, the authors found a migration enthalpy of 0.68 eV. Parts of the concept of Zhu were taken up by Kohli et al. [5.182]. They suggested on the basis of their *ab-initio* calculations that the boron atom may go from the metastable split-interstitial configuration found already by Windl et al. and Sadigh et al. to a tetragonal site. There, it was assumed to diffuse via hexagonal and tetragonal sites with an activation energy of 0.3 eV until it assumes a substitutional site again. Zhu's suggested path for the diffusion of boron interstitials was rejected again by Jeong and Oshiyama [5.65]. They found for all charge states that the energetically most favorable configuration is assumed again after each diffusive jump of the boron atom. Within the generalized gradient approximation, diffusion barriers of 0.95, 0.4, and 0.32 eV for the positive, neutral, and negative charge states, respectively, were reported. Within the local-density approximation, the respective numbers calculated were 1.08, 0.7, and 0.41 eV.

Based on theoretical investigations, Li et al. [5.183] could show that the presence of other impurities influences the migration of boron interstitials. However, the influence of such effects on the long-range diffusion of boron remains unclear.

Besides thermal diffusion, evidence was given in the literature that boron interstitials may diffuse athermally. Watkins [5.40] found that the reorientation of boron interstitials in stress experiments can be induced by light. Similarly, it was reported by Troxell and Watkins [5.42] that an injection of electrons enhances significantly the migration of boron interstitials. From a quadratic dependence of the annealing rate on the injected current density it was concluded that the athermal migration is a Bourgoin-Corbett mechanism and involves alternations of the charge state between B_i^- and B_i^+ . Years later, the detailed experimental studies of Harris et al. [5.184] allowed them to exclude the Bourgoin-Corbett mechanism as correct interpretation and they suggested an energy-release mechanism instead.

5.3.4 Complexes

B_iI and B_iI_n

From IR spectroscopic investigations after electron irradiation, Laithwaite et al. [5.35] concluded that interstitial boron can react at room temperature with silicon self-interstitials. The first reaction product would be B_iI but it eluded the observation by IR spectroscopy. As an explanation, the authors assumed that various complexes of the composition B_iI_n may form so that the absorption is spread throughout a wide spectral range. A similar chain of B_iI_n clusters was included in the work of Akhmetov and Bolotov [5.185] to explain the dependence of the formation of radiation defects on the boron background concentration.

Complementary information about the energetics of clusters comprising a boron interstitial and self-interstitials came from *ab-initio* calculations. Lenosky et al. [5.186] reported that the reaction of a negatively charged substitutional boron atom and two well-separated positively charged self-interstitials to a complex in the singly negative, neutral, and singly positive charge state is associated with energy gains of respectively 1.89, 2.24, and 2.35 eV when the Fermi level is at mid-gap. In the work of Liu et al. [5.187, 5.188], taking a negative substitutional boron atom and neutral self-interstitials as reference points, the formation of such a complex in the neutral charge state was found to imply an energy gain of 2.3 to 2.5 eV at mid-gap. This compares well to energy gains of 2.14 to 2.3 eV computed by Deák et al. [5.189] for the same charge state and reference points. For the formation of a complex comprising one self-interstitial more, Liu et al. reported an energy gain of 4.5 to 4.8 eV under intrinsic conditions for its positive charge state.

B_{2s}

After electron irradiation, Newman and Smith [5.4, 5.33] observed absorption bands at 552.5, 560.0, and 570.0 cm⁻¹ (77 K) which were labeled *P1* to *P3*. The concentrations were found to reflect the abundances of boron isotopes in substitutional B₂ pairs. Pairs of boron atoms with equal masses are D_{3d}-symmetric with respect to the ⟨111⟩-oriented bond between the boron atoms. For pairs composing of different boron isotopes, the symmetry reduces to C_{3v}. Various other absorption lines were explained by pairs of boron with phosphorus, arsenic, and antimony. Similar conclusions were presented by Tsvetov et al. [5.5] and Bean et al. [5.6].

It is interesting to note that basically all *ab-initio* simulations agree that two substitutional boron atoms at neighboring sites should not be stable in any charge state. For the binding energy of neutral, substitutional boron atoms in a B_{2s}⁰ cluster, Zhu et al. [5.31] calculated a value of -0.6 eV. For charged substitutional boron atoms in a B_{2s}[±] complex, Zhu [5.62] reported a binding energy of likewise -0.6 eV. Okamoto et al. [5.190] obtained a binding energy of -0.405 eV for two neutral boron atoms in a B_{2s}⁰ cluster. In the work of Lenosky et al. [5.186], the energy decrease upon the formation of B_{2s} in the doubly negative, singly negative, and neutral charge state from negatively charged, isolated substitutional boron atoms was calculated to be -0.93, -0.96, and -1.38 eV, respectively, under intrinsic conditions. A comparable binding energy of -0.9 eV was reported also by Liu et al. [5.187, 5.188] for two negatively charged substitutional boron atoms on neighboring sites. For the same complex, Yamauchi et al. [5.37] calculated a somewhat smaller value of -0.73 eV while Deák et al. [5.189] reported values from -0.76 to -0.88 eV, depending on problem size. Finally, Luo et al. [5.191] gave a binding energy of -0.7 eV for electrically neutral boron atoms on neighboring substitutional sites while Adey et al. [5.66] reported B_{2s}⁰ to be 0.6 eV less stable than isolated impurities. The work of Adey et al. indicated also that B_{2s} has an acceptor level at approximately E_v + 0.17 eV.

The unanimous rejection of stable pairs of nearest-neighboring boron atoms is in seeming contrast to the apparently straightforward experimental identification. An other explanation for the experimentally observed D_{3d} symmetry about a ⟨111⟩ axis would be possible only at a fifth-nearest neighbor configuration of the two substitutional boron atoms. The investigations of Yamauchi et al. [5.37] and Windl [5.192] indicated that all these configurations of two substitutional boron atoms are energetically unfavorable, although significantly less than two substitutional boron atoms on adjacent lattice sites. In the work of Yamauchi et al., a local minimum was observed for pairs at fourth coordination sites while Windl observed such a minimum for pairs at third coordination sites on opposite vertices in a hexagonal ring.

Yamauchi et al. [5.37] computed also the vibrational frequencies of B_{2s} . Agreement with the IR P lines of Newman and Smith [5.4, 5.33] was only within about 23 cm^{-1} but a tentative assignment was made on the basis of the isotope shifts. Similar work of Deák et al. [5.189] and Adey et al. [5.66] corroborated the identification.

B_iB_s , $[B-B]_s$, and B_s-I-B_s

From its quadratic dependence on the boron concentration, Drevinsky et al. [5.168] assigned a hole trap at $E_v + 0.30\text{ eV}$ to a B_iB_s complex. The same level was observed by Khan et al. [5.193] to correlate in irradiation studies with the dissolution of B_iO_i complexes as well as with the concentration of substitutional boron atoms. The tentative identification as B_iB_s complex was supported by the absence of this level in gallium-doped samples and by the independence on oxygen. Based on an ion-beam analysis after electron irradiation and annealing, Swanson [5.45] suggested two boron atoms to assume a configuration in the form of a $\langle 100 \rangle$ -oriented $[B-B]_s$ pair about a lattice site in which they are separated by a distance of 1.6 \AA . Near-edge X-ray absorption fine-structure-spectroscopy investigations carried out by Vailionis et al. [5.194] were also consistent with a $\langle 100 \rangle$ -oriented boron pair around a substitutional site. Under the assumption of pairs randomly aligned along equivalent directions, the authors concluded that the length between one of the boron atoms and its neighboring silicon atoms is $2.01 \pm 0.04\text{ \AA}$.

An entirely different configuration was suggested by Thonke et al. [5.195] to explain their PL investigations of the $1.080\text{ eV } I_2$ line. The complex appears after electron irradiation or ion implantation of boron. Isotope experiments resulted in the conclusion that the defect contains two not entirely equivalent boron atoms. On the other hand, there was no indication for an other impurity to be involved so that an intrinsic defect is likely to be required to explain why the spectrum is never observed in unirradiated samples. Measurements under uniaxial stress finally indicated a C_{1h} -symmetric structure and the atomic arrangement suggested to explain all experimental observations consists of two substitutional boron atoms with a silicon self-interstitial in between which is in the (110) plane through the two boron atoms, but distorted out of the bond-centered position. It has to be mentioned, though, that an alternative defect was suggested by Adey et al. [5.66] to be responsible for the I_2 PL line. Their *ab-initio* calculations indicated that a metastable $B_{2i}I$ cluster was found to have all properties required. Based also on *ab-initio* calculations of its vibration frequencies, the B_s-I-B_s complex was suggested by Deák et al. [5.189] and Adey et al. [5.66] to be a viable candidate for the S bands at $903, 917, 928, 599$, and 603 cm^{-1} (77K) reported first by Tipping and Newman [5.36] and ascribed originally to B_{2i} (see below).

The first theoretical investigations of possible atomic arrangements of a defect in which two boron atoms share one lattice site were presented by Tarnow [5.196]. They considered a boron interstitial on a tetrahedral site near to a substitutional atom as well as two boron atoms arranged in a D_{2d} -symmetric $\langle 100 \rangle$ -oriented $[B-B]_s$ split configuration around a lattice site. In the following *ab-initio* investigations, the latter configuration was unanimously found to be the energetically most stable one. With respect to the formation energy, Zhu et al. [5.31] reported an energy gain of 2.9 eV in comparison to two well-separated, neutral substitutional boron atoms and a neutral self-interstitial. Including charge states, Zhu [5.62] computed an energy gain of 1.1 eV with respect to a doubly positively charged silicon self-interstitial and two negatively charged substitutional boron atoms. Somewhat in contrast, Okamoto et al. [5.190] calculated an energy gain of 5.72 eV for a neutral complex and neutral constituents. Taking negatively charged substitutional boron atoms and a doubly charged self-interstitial as reference points, Lenosky et al. [5.186] reported energy gains of $1.6, 2.12$, and 1.43 eV for the formation of $[B-B]_s$ in the singly negative, neutral, and singly positive charge states with the Fermi level at

mid-gap. Using neutral self-interstitials instead as reference point, Liu et al. [5.187, 5.188] estimated energy gains of 1.2 to 2.0 eV for neutral complexes and intrinsic conditions. For neutral complexes and their constituents, Alippi et al. [5.197] obtained an energy gain of 2.11 eV. In the work of Adey et al. [5.66], B_s^- and B_i^+ were calculated to bind in $[B-B]_s^0$ with 1.3 eV.

In the *ab-initio* calculations of Adey et al. [5.66], the B_s -I- B_s complex was found to be 0.4 eV less stable than $[B-B]_s$ and to have an acceptor level at $E_c - 0.2$ eV. In the negative charge state, the silicon atom was found to move out of the bond-centered interstitial site, causing the symmetry to drop from D_{3d} to C_2 or C_{1h} .

Ab-initio simulations by Hwang and Goddard III [5.198] confirmed $[B-B]_s$ to be the most stable configuration. It was also found to be mobile with an activation energy of 1.81 eV. On its migration path, the boron pair has to rearrange from its energetically most favorable configuration in the form of a $\langle 100 \rangle$ -oriented split interstitial to a $\langle 111 \rangle$ -oriented split interstitial, the B_iB_s configuration, and the B_s -I- B_s complex. These intermediate configurations were found to be respectively 0.27, 0.47, and 0.69 eV energetically less favorable than the $\langle 100 \rangle$ -oriented split interstitial. Based on this result, Hwang and Goddard III [5.161] suggested that mobile boron pairs might contribute significantly to the apparent Fermi-level dependence of the boron diffusion coefficient discussed above.

Based on *ab-initio* calculations, Yamauchi et al. [5.37] associated tentatively the two IR Q lines at 733 and 760 cm^{-1} (77 K) reported by Newman and Smith [5.33] and originally assigned to interstitial boron (see Section 5.3.1) with a $[B-B]_s$ cluster in a $\langle 100 \rangle$ -oriented split configuration. This assignment was confirmed by similar calculations of Deák et al. [5.189] and Adey et al. [5.66].

B_iB_s complexes or equivalent clusters were also an important part of several diffusion models. To reproduce boron profiles at high concentrations, Mathiot and Pfister [5.76] introduced an immobile and electrically inert B_iB_s complex. The equilibrium constant, including a binding energy of 1.61 eV, was extracted by fitting the experiments. Simulating similar experiments, Baccus and Vandebossche [5.54] suggested B_iB_s to be electrically neutral, to bind with 2.235 eV, and to be mobile with a diffusion coefficient characterized by an activation energy of 3.756 eV. From measurements of ^{11}B profiles after room-temperature ion implantation into samples with varying ^{10}B background concentration, Collart et al. [5.170] concluded that an energy barrier of 0.06 eV opposes the trapping of boron interstitials at substitutional boron atoms. Quoting otherwise unpublished results of Drevinsky et al., Kimerling et al. [5.47] reported that the reaction probability of interstitial boron is twelve times higher with substitutional boron than with interstitial oxygen.

B_{2i}

In their IR investigations on electron-irradiated, boron-doped samples, Tipping and Newman [5.36] observed the formation of absorption bands at 903, 917, 928, 599, and 603 cm^{-1} (77K). These lines were labeled S1 to S5 and shown to reflect the different isotopes and vibration modes of a defect which involves two equivalent boron atoms. The defect itself was suggested to be a B_iB_i pair of two boron interstitials. Break-up of the defects was observed around 270 K. In addition, the existence of a metastable precursor was surmised since the concentration of B_iB_i pairs increased quadratically with time during the initial annealing stage while the concentration of boron-interstitial complexes decreased linearly. It has to be mentioned, though, that the S lines, as noted above, were suggested later to arise from a B_s -I- B_s complex with a self-interstitial between two substitutional boron atoms.

Structural suggestions for B_{2i} complexes came especially from *ab-initio* calculations. The structure proposed in the work of Liu et al. [5.187, 5.188] arose from relaxation of an $\langle 100 \rangle$ -oriented [B-B]_s complex to which a self-interstitial was added. For a neutral complex, they estimated energy gains of 2.4 and 3.0 eV upon formation from neutral self-interstitials and ionized substitutional boron atoms within the local-density approximation and the generalized gradient approximation, respectively. In comparison to this structure, Shishkin and De Souza [5.199] found a $\langle 110 \rangle$ -oriented boron pair in the {112} planes of parallel bonds to be 0.2 eV energetically more favorable in its neutral charge state. Probably more important, they found that this complex is mobile with a total barrier of about 0.6 eV within the local-density approximation and 0.77 eV in the generalized gradient approximation.

$B_{2i}I$

Based on *ab-initio* calculations of its properties, Adey et al. [5.66] suggested a complex comprising two boron interstitials and a self-interstitial to give rise to a photoluminescence line at 1.080 eV labelled I_2 . This line was associated before by Thonke et al. [5.195] with a B_s -I- B_s complex. The $B_{2i}I$ defect suggested by Adey et al. is similar to the I_3 defect in Figure 2.16 b) with two of the inserted self-interstitials replaced by boron interstitials. In this form, $B_{2i}I$ is only metastable and 0.7 eV higher in energy than the most stable configuration which has no apparent symmetry.

B_{12}

After implantation of boron with doses up to 10^{17} cm^{-2} , Mizushima et al. [5.200] observed by Hall-effect measurements that the number of holes increased approximately by one for about six implanted boron atoms. Complementary XPS and FTIR measurements revealed spectra known from icosahedral B_{12} clusters. From size considerations it was tentatively suggested that the icosahedral boron cluster replaces a tetrahedral structure of five silicon atoms and bonds to the surrounding silicon atoms without dangling bonds. Taking the known properties of icosahedral B_{12} into account, it was further suggested that this structure acts as a double acceptor, explaining the observed increase of holes with the total number of boron atoms. Contrary to the experimental evidence, the *ab-initio* simulations of Yamauchi et al. [5.201] indicated no acceptor levels in the band gap for icosahedral B_{12} . Instead, the generation of holes was ascribed to an unoccupied level generated near the edge of the valence band. Yamauchi et al. [5.201] also confirmed the icosahedron to be more stable than a cubo-octahedron B_{12} cluster. Later, Yamauchi et al. [5.202] showed that the computed oscillation frequencies for an icosahedral B_{12} cluster are compatible to the measured ones.

Boron-Interstitial Clusters

Complexes involving boron atoms and self-interstitials play an important role for the simulation of diffusion and activation of boron during post-implantation annealing [5.187, 5.203–5.211]. They are usually referred to as boron-interstitial clusters or, shorter, BICs. Instead of giving a full structural information, it is customary to denote their composition in the form B_mI_n , referring to m boron atoms and n silicon atoms occupying m regular lattice sites. In addition to information obtained from reproducing experiments, structure and properties of BICs were obtained from tight-binding molecular-dynamics simulations [5.197, 5.212, 5.213] and *ab-initio* studies [5.186–5.190, 5.197, 5.204]. For an overview of the properties of BICs, the interested reader is referred to a recent review article [5.214].

Ion Pairs

After electron irradiation, Newman and Smith [5.4], Tsvetov et al. [5.5], and Bean et al. [5.6] observed various absorption bands in samples co-doped with boron and donor impurities which were explained by pairs of boron with phosphorus, arsenic, and antimony. The participation of boron was shown via its isotope shift.

Important information about boron-donor pairs resulted from diffusion studies. Based on diffusion of boron in a phosphorus background, Fair and Pappas [5.8] determined the ion-pairing coefficient for boron-phosphorus pairs to be $\Omega = 1.25 \cdot 10^{-20} \text{ cm}^3$ at 1050°C . This would correspond to a binding energy of 0.58 eV. However, it has to be remarked that the extrapolation of the Fermi-level dependence of the diffusion coefficient of boron to the range of $p < n_i$ is associated with considerable uncertainties. Studying the diffusion of phosphorus in a boron background as well as boron diffusion in a phosphorus background, Cowern and Godfrey [5.215] and Cowern [5.216] found from their data that the pairing coefficient can be expressed empirically in the form $\Omega = (0.14 - 0.2)/n_i$ and has an apparent activation energy of $0.7 \pm 0.2 \text{ eV}$. Similar studies of phosphorus diffusion in a boron background were performed by Wittel and Dunham [5.217]. Based on their own data in intrinsic and arsenic-doped silicon, they estimated that the formation of a pair is associated with decreases in enthalpy and entropy of 2.51 eV and $16.8 \cdot k$. Including also other data for the intrinsic diffusion coefficient of phosphorus in silicon, a second parameter set was obtained. Pair formation therein was characterized more reasonably with a decrease of the system enthalpy by 0.44 eV and an increase of the system entropy by $2 \cdot k$. In absolute numbers, their value is about twice that of Cowern and Godfrey. Investigating phosphorus diffusion in a boron background, Tishkovskii et al. [5.218] found binding energies of 0.6 eV at 1150°C and 0.7 eV at 1075°C , corresponding to ion pairing coefficients of 10^{-20} and $3 \cdot 10^{-20}$. At a temperature of 1000°C , no diffusive broadening was observed and a lower limit of 0.8 eV was extracted for the pair-binding energy. From the diffusion of boron in a phosphorus background, a binding energy of 0.8 eV was estimated at 1075°C . In the work of Kim et al. [5.219], the diffusion of boron in a phosphorus background at 1020°C was found to be retarded already at phosphorus concentrations less than 10^{19} cm^{-3} . Interpreted in terms of ion pairing, this would require an ion-pairing coefficient which exceeds previous estimates by more than an order of magnitude. Complementary information about boron-phosphorus pairs came from theoretical work. The *ab-initio* calculations of Moon et al. [5.220] indicated that the energetically most stable configuration would be a substitutional boron atom on a second-nearest neighboring site to a substitutional phosphorus atom. In this configuration, the two impurities were calculated to bind with 0.284 eV. At first and third-nearest neighboring sites, the binding energy was found to be 0.051 and 0.006 eV less. Extending the work to boron-self-interstitial pairs and substitutional phosphorus atoms, their complexes were found to be energetically favored in comparison to separated constituents only for *n*-type silicon with Fermi levels above $E_v + 0.62 \text{ eV}$. The most stable pair was then reported to be neutral and to involve a substitutional phosphorus atom on a second-nearest neighboring site of a boron-self-interstitial pair.

Pair formation of boron and arsenic was invoked already by Ziegler et al. [5.221] and Fair [5.222] to explain diffusion profiles found in *n-p-n* bipolar transistors. Studies of boron diffusion in an arsenic background led Fair and Pappas [5.8] to suggest a value of $1.1 \cdot 10^{-20} \text{ cm}^3$ for the ion-pairing coefficient of arsenic-boron pairs. Interpreted in terms of a binding energy, one would obtain a value of 0.56 eV. From data of boron diffusion in an arsenic background and similar experiments from the literature, Cowern [5.216] proposed that the temperature dependence of the ion-pairing coefficient for arsenic-boron pairs can be expressed in form of the empirical relation $\Omega = 0.17/n_i$. All these estimates have to be taken *cum grano salis* since the extrapolation of the Fermi-level dependence of the diffusion coefficient of boron to the range

of $p < n_i$ is associated with considerable uncertainties. In samples doped extrinsically with boron and arsenic, Yokota et al. [5.223] found that the electron concentration in n -type regions could be represented approximately by $n = C_{As} - 3 \cdot C_B$ while the hole concentration in p -type regions corresponded approximately to the boron profile. From these observations, the authors concluded that negatively charged $(BAs_2)^-$ complexes form in the co-doped regions. From the evolution of the profiles during thermal treatments, it was concluded that the complexes are mobile and have a diffusion coefficient of about $9 \cdot 10^{-16} \text{ cm}^2/\text{s}$ at 950°C . The formation of BAs_2 complexes was corroborated by subsequent XPS investigations [5.224]. Later, Yokota et al. [5.225] reported that the effective diffusion coefficient decreases at 950°C with process time from about $3.5 \cdot 10^{-15} \text{ cm}^2/\text{s}$ for a diffusion step of 30 min to the previously reported value for a process time of 1000 min. In contrast, Solmi et al. [5.226] suggested that the redistribution of boron and arsenic in extrinsically doped samples can be reproduced quantitatively when neutral, mobile AsB complexes are assumed to form. For the temperature range of the experiments from 900 to 1000°C , a value of $\Omega = 5 \cdot 10^{-20} \text{ cm}^3$ was suggested for the ion-pairing coefficient. This corresponds to an enthalpy reduction of 0.65 to 0.71 eV or an entropy increase of $6.4 \cdot k$ associated with the formation of a pair. In the notation of Cowern, the ion-pairing coefficient of Solmi et al. corresponds to values of Ω ranging from $0.25/n_i$ to $0.47/n_i$. As in the work of Yokota et al., the pairs were found to be mobile with a diffusion coefficient of $17 \cdot \exp(-4.0 \text{ eV}/kT) \text{ cm}^2/\text{s}$.

From their experimental data of antimony diffusion in a boron background, Fair et al. [5.11] estimated the temperature dependence of the ion-pairing coefficient to be $\Omega = 1.25 \cdot 10^{-30} \cdot (T/\text{°C})^{3.84} \text{ cm}^3$. This would correspond to a binding energy which increases from 0.94 eV at 1000°C to 1.17 eV at 1200°C . However, according to a private communication by Fair cited as reference 9 in an article of Cowern [5.216], the ion-pairing coefficient should correctly read $\Omega = (T/\text{°C})^{-3.84}/1.25 \cdot 10^8 \text{ cm}^3$. This would correspond to a binding energy of about 0.63 eV. Alternatively, Cowern suggested the empirical relation $\Omega = 0.17/n_i$ for the ion-pairing coefficient. Studying the diffusion in samples heavily doped with boron and antimony, Margesin et al. [5.227] showed that the results could be reproduced quantitatively when neutral, mobile SbB complexes are assumed to form. For the temperature range of the experiments from 900 to 1000°C , a value of $\Omega = 2.5 \cdot 10^{-20} \text{ cm}^3$ was suggested for the ion-pairing coefficient. This corresponds to an enthalpy reduction of 0.58 to 0.63 eV or an entropy increase of $5.7 \cdot k$ associated with the formation of a pair. In the notation of Cowern, the ion-pairing coefficient of Margesin et al. corresponds to values of Ω ranging from $0.22/n_i$ to $0.24/n_i$. To obtain a close fit, the pairs had to be assumed to be mobile with a diffusion coefficient of $1.1 \cdot \exp(-4.0 \text{ eV}/kT) \text{ cm}^2/\text{s}$. Studying the formation of shallow junctions by co-implantation of antimony and BF_2 , Solmi [5.228] used an ion-pairing coefficient of $\Omega = 7 \cdot 10^{-22} \cdot \exp(0.5 \text{ eV}/kT) \text{ cm}^3$ to reproduce the experiments. In samples co-implanted with boron and antimony, Allain et al. [5.229] observed that the presence of boron suppresses the formation of antimony precipitates. From EXAFS measurements, they concluded that the complexes formed instead should be $SbBV$ or SbB_2 .

Complexes with Carbon and Nitrogen

The formation of pairs of substitutional boron with substitutional or interstitial carbon atoms was discussed already in Section 4.1.6. Complexes of boron with nitrogen and boron-indium-nitrogen complexes will be discussed below in Section 5.7.4.

B_iO_i

After electron irradiation, Mooney et al. [5.230] found a double-donor level at $E_c - 0.27$ eV which correlated with the boron concentration and transformed upon annealing at 170 °C into an acceptor level at $E_v + 0.3$ eV. They associated the level at $E_c - 0.27$ eV tentatively with a B_iO_i pair. For the level at $E_v + 0.3$ eV, a vacancy-oxygen-boron complex was suggested. This mechanism was supported by Roux et al. [5.231] and Londos [5.232] who both reported the level of the vacancy-oxygen-boron-related hole trap at $E_v + 0.27$ eV, by Asghar et al. [5.233] who associated the B_iO_i pair with an electron trap at $E_c - 0.25$ eV, and by Vanhellemont et al. [5.234] and Trauwaert et al. [5.235] who reported the B_iO_i pair to have an electron trap at $E_c - 0.24$ eV. The assignment of an electron trap found by Drevinsky et al. [5.168] at $E_c - 0.26$ eV to a B_iO_i complex was corroborated by them also via a linear correlation of its introduction rate with the concentrations of oxygen and boron. But Drevinsky et al. [5.168] found the level at $E_v + 0.29$ eV associated usually with a vacancy-oxygen-boron complex to be independent of the oxygen concentration. As an alternative, they assumed it to arise from a B_iC_s complex. This assignment was substantiated by the *ab-initio* calculations of Adey et al. [5.236]. The investigations of Yarykin et al. [5.237], on the other hand, indicated that B_iC_s has no levels detectable by DLTS in *p*-type silicon.

Quoting otherwise unpublished results of Drevinsky et al., Kimerling et al. [5.47] reported that the reaction probability of oxygen with interstitial boron is seven times as large as with interstitial carbon while the reaction probability of interstitial boron is twelve times higher with substitutional boron than with interstitial oxygen.

Ab-initio simulations performed by Ohshita et al. [5.238] indicated a stable configuration in which the oxygen atom occupies a bond-centered position between two neighboring silicon atoms with the boron interstitial along this axis, on the other side of one of the silicon atoms. The calculations also indicated that the defect has a deep level in the band gap and that an energy barrier of 0.7 eV opposes the dissociation of the boron interstitial. In contrast, Adey et al. [5.236] found the most stable structure to be similar to that of the C_iO_i complex shown in Figure 4.7 b). Its binding energy was calculated to be 0.6 eV. The donor level found near to $E_c - 0.23$ eV would be in agreement with the experiments except that Mooney et al. [5.230] had suggested that it is a double-donor level.

Degradation of Boron-Doped CZ Solar Cells

Various irradiation studies were performed to understand the degradation of solar cells in space. Studying electron-irradiated, boron-doped CZ solar cells, Weinberg and Swartz [5.239] found an additional performance drop upon annealing at temperatures from 200 to 400 °C. DLTS measurements and calculations of the recombination behavior led to the identification of a defect with an energy level at $E_v + 0.3$ eV which grows on the expense of a defect with a level at $E_c - 0.27$ eV. Following the work of Mooney et al. [5.230], the level was associated, as discussed above, with a vacancy-oxygen-boron complex. Combining electron irradiation and illumination, Roux et al. [5.231] found that FZ-based solar cells are more prone to degradation than CZ-based ones. They suggested that a main contribution to the degradation comes from a hole trap at $E_v + 0.27$ eV which appears only after post-irradiation illumination. This level was associated again with the vacancy-oxygen-boron complex identified tentatively by Mooney et al. [5.230]. Additional evidence in favor of vacancy-oxygen-boron complexes came from positron-annihilation studies to be discussed at the end of this section.

In the work of Yamaguchi et al. [5.240], part of the degradation seen in solar cells operated in space was explained by a compensation and even type conversion of the doping in the base region. This effect was correlated with an electron trap at $E_c - 0.18$ eV which was suggested to act as a deep donor and which was associated tentatively with B_iO_i . Additional evidence for an association with boron comes from the observation of Khan et al. [5.193] that the level does not appear when gallium is used as dopant instead of boron. In addition to type conversion, the reduction of the minority-carrier lifetime by a hole trap at $E_v + 0.36$ eV was discussed by Yamaguchi et al. [5.240] as the origin of radiation-induced degradation effects. The effect responsible was associated with C_iO_i but, in part, tentatively also with B_iO_i . The association of the level with C_iO_i was corroborated by the experiments of Khan et al. [5.193] who reported that its concentration actually decreases with an increasing boron concentration.

An other degradation phenomenon of solar cells, known since the work of Fischer and Pschunder [5.241], concerns only solar cells made from boron-doped CZ silicon. In such cells, illumination or electron injection may reduce the cell efficiency by 1 to 2% absolute. This effect can be reversed completely by annealing at around 200 °C which indicates that the defect responsible is metastable. Despite its long history, no complete consolidation has been achieved and the path until now was quite warped. It appears to be established, though, that the defect responsible composes only of boron, oxygen, and intrinsic point defects. Based on extensive reasoning, the effects were initially associated by Schmidt et al. [5.242] with the formation of B_iO_i complexes. The work of Glunz et al. [5.243] showed that the increase in inverse carrier lifetime, which is proportional to the number of defects introduced, increases linearly with the boron concentration and with approximately the fifth power of the oxygen concentration. Later work by Schmidt and Cuevas [5.244] based on the Shockley-Read-Hall recombination theory showed that the defect responsible for the minority-lifetime degradation has an energy level between $E_v + 0.35$ eV and $E_c - 0.45$ eV. Based on this finding, they excluded the B_iO_i complex with its level at about $E_c - 0.26$ eV, suggested originally by Schmidt et al. [5.242], from the list of candidates. Instead, following the work of Glunz et al. [5.243], the defect responsible was suggested to be BO_n with $n \approx 5$. In its inactive state, it was found by Glunz et al. [5.245] to be very shallow with an ionization energy of about 0.08 eV. In the atomic model of Bourgoin et al. [5.246], a substitutional boron atom was suggested to be surrounded by oxygen interstitials near three of its four neighboring bond-centered interstitial sites. When an electron is trapped at the otherwise ionized defect, it may undergo a Jahn-Teller distortion and the occupied level moves to the observed mid-gap position. To quantitatively distinguish between models proposed, Rein et al. [5.247] investigated the kinetics of defect formation in dependence of the boron background concentration. From these experiments, a quadratic dependence was found. They also showed that the generation rate shows a negligible dependence on the injected carrier concentration. From both observations, it was concluded that the physical mechanism is not associated with recombination-enhanced defect reactions. Studies of the annealing kinetics indicated a thermally activated process with a barrier of 1.32 eV. An improved experimental technique finally allowed to limit possible values for the level of the defect to within 0.41 eV from either band edge. A reinvestigation of the dependence of the defect concentration on the concentration of boron by Schmidt and Bothe [5.248] confirmed the linear relationship found by Glunz et al. [5.243]. However, only a quadratic dependence on the oxygen concentration was found in contrast to the fifth-power dependence in the earlier work. The investigation confirmed that the annihilation process is thermally activated. It was found to correlate linearly with the boron concentration, characterized by an activation energy of 1.3 eV in excellent agreement with that found by Rein et al. [5.247]. In addition, the generation process was found to be thermally activated with an activation energy of 0.4 eV. Based on the experimental evidence, the

defect responsible for the degradation effects was suggested to form by the reaction of a substitutional boron atom with an oxygen dimer. Under illumination, the formation reaction was suggested to be promoted by recombination-enhanced diffusion of the oxygen dimer. The latest development in the assignment of levels was the work of Rein and Glunz [5.249]. Combining injection-dependent and temperature-dependent lifetime spectroscopy, they found that the defect responsible has a level at $E_c - 0.41$ eV.

Complementary Evidence for Complexes with Oxygen

The existence of boron-oxygen complexes can be inferred also from the observations of Ono et al. [5.250] who reported that oxygen diffusion is retarded at 800 °C when the boron background concentration exceeds 10^{18} cm⁻³. In addition, they reported that the solubility was found to be enhanced by more than a factor of 5 for a boron concentration of $1.2 \cdot 10^{19}$ cm⁻³. Similar observations were reported by Takeno et al. [5.251], although a quantitative disagreement between the investigations remains.

In positron-annihilation studies of annealed boron-doped CZ samples [5.252], boron-implanted CZ samples [5.253, 5.254], or boron-doped CZ samples irradiated with electrons [5.75], the line-shape parameter S (sharpness) was found to decrease upon annealing around 500 to 950 K even below the respective value for undamaged bulk silicon. This somewhat unexpected behavior was explained tentatively by Puff et al. [5.252] by the dissociation of substitutional boron atoms into a vacancy and a boron interstitial staying in its vicinity. The involvement of oxygen was mentioned as a possibility. Oxygen was also taken into considerations by Polity et al. [5.75] who associated the effect on the S parameter with $V_xO_yB_z$ complexes “containing one or two vacancies, oxygen atoms, and boron atoms.” A similar effect was observed by Hori et al. [5.255] already after proton irradiation at room temperature and explained likewise by the formation of vacancy-oxygen-boron complexes. Isochronal annealing studies revealed an annealing stage at about 530 to 550 K which was associated with the formation of larger vacancy complexes.

Studying the lifetime of positrons in electron-irradiated, boron-doped CZ samples, Tamano et al. [5.256] found that the lifetime in such samples decreases below that of bulk silicon. They concluded that this effect is associated with a defect giving rise to a positron lifetime of about 100 ps. Since ordinary vacancy defects like vacancy-dopant pairs, divacancies, and V_mO_n complexes have significantly longer lifetimes, the authors tentatively ascribed the short lifetime component to a complex comprising oxygen, boron, and vacancies generated by the electron irradiation. An association with degradation effects in solar cells was indicated.

5.4 Aluminum

Aluminum is the fastest diffusing acceptor element in silicon. As such, it is used predominantly for the fabrication of power semiconductors having deep p-n junctions with depths of 100 μm and more. The main problem for the application of aluminum is its high reactivity with oxygen which leads to drastic out-diffusion of aluminum during drive-in steps and which makes ion implantation problematic. In the following sections, the basic atomic configurations of aluminum in silicon, its solubility, the diffusion behavior, and the formation of complexes are discussed in detail.

5.4.1 Basic Atomic Configurations

Substitutional Aluminum

Aluminum atoms on substitutional sites have one positive charge too few for the valence-bond structure of silicon. In analogy to donors, a hole is assumed to be introduced in the valence band. The ionization energy of substitutional aluminum was determined by electrical and optical measurements. Hall-effect measurements resulted in estimates of 0.057 to 0.07 eV [5.17,5.257]. An ionization energy of 0.057 eV was obtained from the temperature dependence of resistivity measurements [5.258]. Infrared absorption resulted in values of 0.067 to 0.689 eV [5.19–5.21]. In theoretical investigations, an ionization energy of 0.07 eV [5.259] was calculated.

In samples doped with aluminum atoms in concentrations up to 10^{16} cm^{-3} , various photoluminescence lines were found to arise from the decay of excitons bound to neutral aluminum atoms. The zero-phonon line can be found at 1.1496 eV [5.260], the transverse-acoustic and transverse-optic phonon sidebands have 18.7 and 58.0 eV lower energies.

Theoretical investigations led to the conclusion that aluminum on substitutional sites occupies nearly the same volume as a silicon atom [5.261].

Interstitial Aluminum

After electron irradiation, an EPR defect labeled Si-G18 was observed and attributed to the doubly ionized donor state of the aluminum atom at a tetrahedral interstitial site [5.262,5.263]. A similar result was found by ENDOR investigations [5.264]. By a photoconductivity characterization of electron-irradiated aluminum-doped silicon, Cherki and Kalma [5.38] found a defect which introduces a level at $E_v + 0.395$ eV which they tentatively associated with aluminum interstitials. Its C_{3v} symmetry determined by studies of stress effects was assumed to result from Jahn-Teller distortions. From DLTS measurements, Kimerling [5.265] suggested a double-donor level of the aluminum interstitial at $E_v + 0.25$ eV. Corrected for the temperature dependences of the various parameters involved in the analysis, Troxell et al. [5.266] estimated the true position of the level to be at $E_v + 0.17 \pm 0.04$ eV. The theoretical investigations of Car et al. [5.267] indicated that aluminum atoms on tetrahedral sites are energetically favored in comparison to aluminum atoms on hexagonal or bond-centered interstitial sites as well as in comparison to a self-interstitial on a tetrahedral site adjacent to a substitutional aluminum atom. From a combination with self-interstitial formation energies taken from Car et al. [5.268], one obtains that the formation of neutral and positively charged aluminum atoms on tetrahedral interstitial sites from a substitutional, negatively charged aluminum atom and a correspondingly charged self-interstitial in its minimum-energy configuration is associated with energy gains of respectively 1.97 and 2.37 eV which could be seen formally as binding energies. Calculations by Overhof and Corradi [5.269] indicated that the reaction of a doubly positively charged self-interstitial with a negatively charged substitutional aluminum atom to a doubly positively charged aluminum interstitial and an electron is associated with a reduction of the energy of the system by 2.0 eV in *p*-doped silicon.

Aluminum-Vacancy Pairs

The negative charge state of a substitutional aluminum atom adjacent to a lattice vacancy was identified by Watkins [5.262,5.270] using EPR and ENDOR techniques and labelled Si-G9. From a correlation of DLTS and EPR measurements, an acceptor level at $E_v + 0.48$ eV was assigned to aluminum-vacancy pairs by Kimerling [5.265]. According to the review of Watkins [5.271], Troxell found that Al-V pairs introduce an acceptor level at $E_v + 0.52$ eV. This value was

also suggested by Chantre [5.272] from his DLTS measurements. The theoretical investigations of Car et al. [5.267] with vacancy formation energies taken from Car et al. [5.268] indicate binding energies of 1.3, 1.74, and 1.78 eV for the negative, neutral, and positive charge states of the vacancy-aluminum pair at mid-gap, respectively. In a later study, Nelson et al. [5.78] calculated a binding energy of 1.42 eV for a pair of neutral constituents. But these calculations indicated also that an intermediate position between two semi-vacancies would be 0.3 eV lower in energy. However, such an atomic arrangement is at least not the defect giving rise to the Si-G9 EPR center.

5.4.2 Solubility

The phase diagram of the aluminum-silicon system was compiled by Murray and McAlister [5.273]. Below the eutectic temperature of 577 °C, the aluminum in the silicon phase is in equilibrium with a pure aluminum phase.

Various experimental methods were used to obtain solubility values for aluminum in silicon. Introduction of dopants occurred from the gas phase [5.274, 5.275], via zone melting with a temperature gradient [5.276–5.278], from an aluminum layer on the surface [5.279], or by forming aluminum-silicon alloys by melting followed by long-time annealing and quenching [5.280–5.282]. Concentration values were deduced from spectroscopic analyses [5.277], X-ray analyses [5.278, 5.282], microindentation measurements [5.281, 5.282], the observation of the formation of defects [5.280], resistivity measurements [5.276], Hall-effect measurements [5.278, 5.279, 5.282], or diffusion profiles characterized by sheet-resistivity measurements combined with junction staining [5.274, 5.275]. The solubility values reported³ are shown in Figure 5.8. A further study by Bailey and Mills [5.283] was based on alloying aluminum with silicon. After quenching the alloys from 750 to 1100 °C, the authors found aluminum concentrations of $3 \cdot 10^{20} \text{ cm}^{-3}$ by energy-dispersive X-ray spectroscopy. It is interesting to note that in all studies based on alloy formation by melting [5.280–5.282], consistently higher values, even electrically active, were found than in studies based on zone melting or diffusion.

In various cases, an interaction with oxygen cannot be avoided. Aluminum will then react rapidly with the oxygen to Al_2O_3 . Already the first investigations [5.284, 5.285] indicated that the concentration of aluminum in silicon in equilibrium with Al_2O_3 is several orders of magnitude smaller than the binary solubility of aluminum in silicon.

5.4.3 Diffusion

Intrinsic Diffusion

A determination of the diffusion coefficient of aluminum under nominally inert and intrinsic conditions was the objective of various investigations. Introduction of aluminum occurred from the gas phase during diffusion [5.274, 5.275, 5.284, 5.286–5.291], from an aluminum-containing film at the surface [5.276, 5.292, 5.293], or by ion implantation [5.294–5.298]. For the characterization of the diffusion profile, electrical methods [5.274, 5.275, 5.284, 5.286–5.289, 5.292, 5.293, 5.295, 5.296] as well as SIMS [5.290, 5.291, 5.294–5.298] were used. A summary of the diffusion coefficients reported⁴ can be found in Figure 5.9. Whenever only an Arrhenius

³It has also to be noted that the values ascribed to Kao [5.275] are somewhat ambiguous since the $10000/T$ and T axes in their Figure 2 are incompatible and there is also disagreement between some values in the figure and in their Table II.

⁴It has also to be noted that the values ascribed to Kao [5.275] are somewhat ambiguous since the $10000/T$ and T axes in their Figure 1 are incompatible and there is also disagreement between some values in the figure and in their Table II.

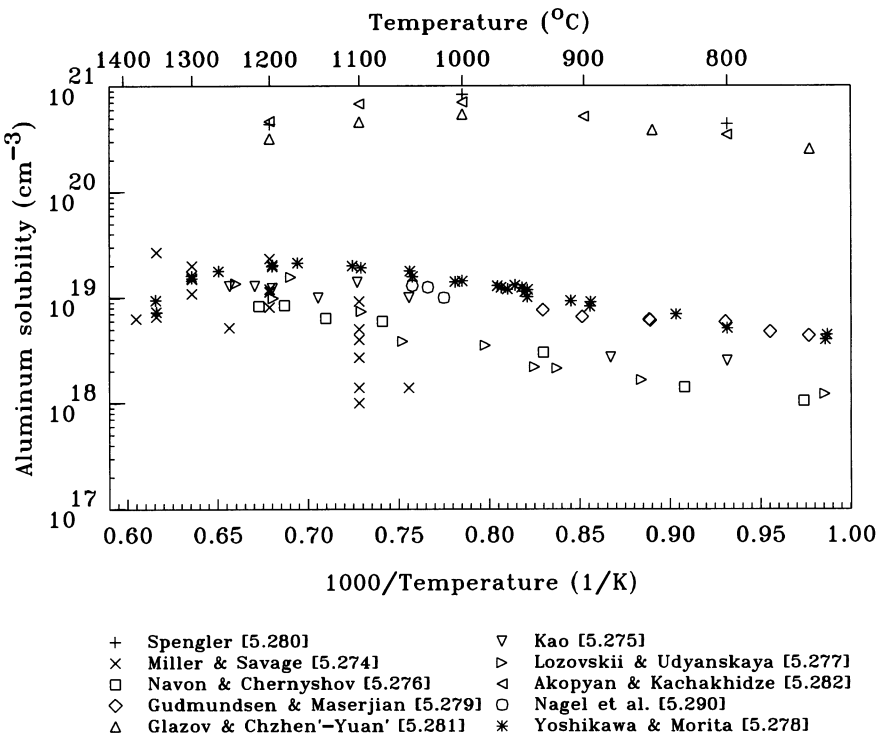


Figure 5.8: Solubility of aluminum in silicon.

expression was given instead of experimental data [5.286, 5.293], the points shown in Figure 5.9 were computed from this Arrhenius expression for the temperatures mentioned in the text. The investigations of Goldstein [5.299] and Ghoshtagore [5.300] were not used since their data are systematically at variance with the data shown in Figure 5.9. Also shown is the regression curve

$$D_{Al}^i = 0.317 \cdot \exp\left(-\frac{3.023 \text{ eV}}{k \cdot T}\right) \text{ cm}^2/\text{s} \quad (5.19)$$

derived from these measurements. The activation energy ranges with a confidence level of 90% from 2.92 to 3.13 eV. The 90% confidence interval for the diffusion coefficient is about +9.4/-8.6% of the regression curve at 1156 °C and increases to +17/-15% at the melting point and +35/-26% at 800 °C. Additional measurements are expected with 90% confidence within a range of +160/-62% of the regression curve at 1020 °C which increases slightly to +163/-62% at the melting point and +172/-63% at 800 °C.

Various diffusion coefficients were determined from aluminum profiles in power semiconductors. In their fabrication, the addition of a small percentage of oxygen is customary to avoid the formation of volatile SiO. As a result, the extracted diffusion coefficients might deviate from intrinsic values. While oxidation-enhanced diffusion is expected for low temperatures and/or (100)-oriented wafers, oxidation-retarded diffusion is expected for the high temperatures and the (111)-oriented wafers typically used for power-semiconductors processes. But at temperatures used for processing of power semiconductors, even nitrogen atmospheres cannot be considered inert. A typical example is the work of Sobolev [5.301] who invoked an interaction of interstitial aluminum and vacancies to explain non-Gaussian diffusion profiles.

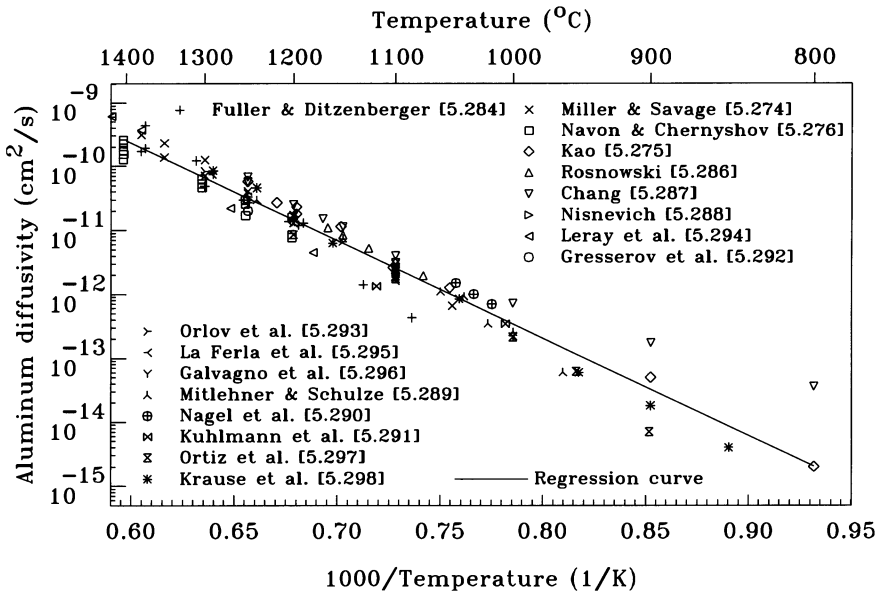


Figure 5.9: Diffusion coefficient of aluminum under intrinsic and inert conditions in silicon.

Diffusion Mechanism

Quantitative estimates for the contributions of self-interstitials and vacancies to the diffusion of aluminum under intrinsic conditions were obtained from experiments involving non-equilibrium conditions as discussed in Section 3.4.3. The values reported are listed in Table 5.2. All estimates agree that aluminum diffuses predominantly via self-interstitials, characterized by an f_I which is probably even larger than that of phosphorus at low temperatures.

Table 5.2: Fractional diffusivity of aluminum via self-interstitials. The abbreviations OSF, RD, and DifComp for the experimental method refer to estimates from oxidation-enhanced diffusion with self-interstitial oversaturations estimated from OSF growth, from the observation of retarded diffusion under non-equilibrium conditions, and from the comparison with the diffusivities of other dopants under non-equilibrium conditions, respectively. A description of the methods can be found in Section 3.4.3.

	f_I	Temperature range (°C)	Experimental method	Ref.
Tan et al.	≥ 0.5	1100	OSF	[5.141]
Gösele & Tan	> 0.85	1150	RD	[5.142]
Gresserov et al.	> 0.95	1250	OSF	[5.292]
Krause et al.	0.92–1.00 0.89–1.00 0.84–0.98 0.75–1.00	900 1044 1100 1290	DifComp	[5.298]

Extrinsic Diffusion

Information about the diffusion of aluminum at extrinsic concentrations is available from the isoconcentration diffusion studies of Kuhlmann et al. [5.291] and Krause et al. [5.298]. These results are shown in Figure 5.10. The full lines were obtained by a numerical optimization using all data points in Figure 5.9 in addition to those in Figure 5.10. They are described by

$$D_{Al} = \frac{p}{n_i} \cdot 0.81 \cdot \exp\left(-\frac{3.14\text{eV}}{k \cdot T}\right) \text{cm}^2/\text{s} \quad (5.20)$$

but it is evident that the small and largely incompatible experimental data basis is insufficient to allow any conclusive statement.

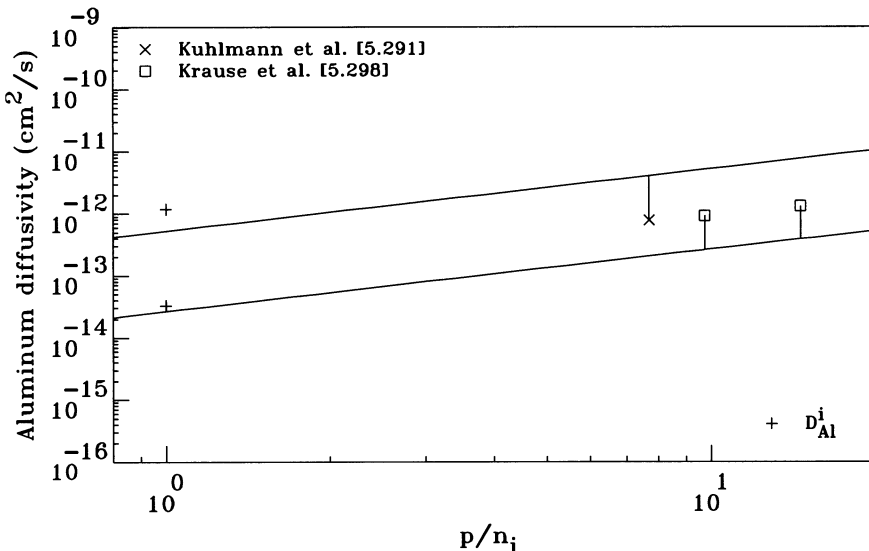


Figure 5.10: Dependence of the normalized diffusion coefficient of aluminum in silicon on p/n_i . The full lines correspond, from top to bottom, to temperatures of 1250, 1150, 1000, 950, 900, and 870 °C.

Although the solubility of aluminum is rather low, the conditions for an influence of aluminum diffusion on the concentrations of the intrinsic point defects as discussed in Section 4.1.7 are fulfilled because of the high diffusion coefficient of aluminum. This explains also the observation of Kuhlmann et al. [5.291] that the diffusion coefficient of aluminum is higher during predeposition than during drive-in since the surface concentration is larger during the former process than during the latter.

Aluminum Interstitials

From EPR measurements of the temperature dependence of the formation of $\text{Al}_s\text{-Al}_i^{++}$ pairs, Devine and Newman [5.302] concluded that Al_i^{++} interstitials have a migration enthalpy of about 1.25 eV. This result is in agreement with the DLTS investigations of Troxell et al. [5.266] who found that aluminum atoms generated by electron irradiation anneal with an activation energy of 1.2 ± 0.1 eV. This value should again correspond to the diffusion enthalpy of the aluminum atom in its doubly positive charge state.

In addition to normal diffusion, athermal diffusion was reported for interstitial aluminum by Troxell et al. [5.266]. Based on the characteristics of the process, the authors concluded that recombination-enhanced diffusion is responsible for the observed reduction of the migration barrier of interstitial aluminum from 1.2 to 0.27 eV. From an *ab-initio* calculation of the energy of the system when the aluminum atom in its various charge states is at a tetrahedral or hexagonal site, Baraff et al. [5.303] suggested a possible path for athermal migration caused by electron injection. They argued that a doubly positively charged aluminum interstitial at a tetrahedral site would transform first to a singly positive charge state, but that this process would not change the migration barrier. Athermal migration was then associated with the capture of two electrons in succession which effectively reduces the diffusion barrier. These arguments were opposed by Pantelides et al. [5.304] who claimed that the energy calculations have to be completed by rate calculations and that interactions with holes have to be taken into considerations also.

5.4.4 Complexes

After annealing of electron-irradiated aluminum-doped samples at 200 °C, Watkins [5.262] observed that the EPR spectrum associated with interstitial aluminum disappeared and new spectra formed. The EPR centers Si-G19 and Si-G20 were both found to arise from a doubly positively charged aluminum atom on a tetrahedral interstitial site paired with a negatively charged substitutional aluminum atom. This structure was confirmed also by ENDOR investigations [5.264] for Si-G19. From DLTS measurements, Kimerling [5.265] suggested a hole trap at $E_v + 0.23$ eV to be associated with the Al_iAl_s pair. The *ab-initio* investigations of Overhof and Corradi [5.269] indicated that a C_{3v} -symmetric pair of an interstitial aluminum atom next to a substitutional aluminum in the [111] direction is a primary candidate for the Si-G19 center. From the energies given in their Figure 2, an energy reduction of about 0.48 eV can be found for the formation of a positively charged pair from well-separated Al_s^- and Al_i^{++} . For the formation of a neutral pair and a hole, the energy reduction is about 0.59 eV for the Fermi level at mid-gap. Later, Hagen and Overhof [5.305] suggested that a C_{2v} -symmetric configuration with the aluminum interstitial in about $\frac{1}{2}[00\bar{1}]$ distance from the substitutional aluminum atom should be of comparable if not higher stability than the previously identified arrangement. The binding energy of 0.8 eV estimated experimentally by Devine and Newman [5.302] was explained predominantly by a Coulombic interaction.

In EPR investigations of hydrogen-implanted, aluminum-doped samples, Gorelkinskii et al. [5.306] observed a center which they labeled Si-AA15 and which was shown to contain two nearly equivalent aluminum atoms. In the model suggested, the two aluminum atoms arrange as $\langle 110 \rangle$ -oriented split interstitial around a substitutional lattice site. The lowering of the symmetry from C_{2v} for such a structure to the observed symmetry C_{1h} was explained by Jahn-Teller relaxations or by the presence of a hydrogen atom.

The formation of substitutional aluminum-carbon pairs, sometimes referred to as Si-X centers, was mentioned already in Section 4.1.6.

When implantation of aluminum with high doses was investigated for a replacement of diffusion from the gas phase, it became soon apparent that only a small fraction of the aluminum atoms implanted with high doses could be activated [5.307–5.314]. A major reason is certainly the diffusion of aluminum into covering oxides. But aluminum was also found to readily form complexes with the implantation damage. Aluminum precipitation during post-implantation anneals is particularly severe when oxygen is involved. This occurs for implants into CZ silicon with its oxygen concentration of typically $6 \cdot 10^{17}$ to 10^{18} cm^{-3} [5.310, 5.315, 5.316], but also in layers with a significantly lower oxygen concentration after crystal growth when the oxygen is

introduced by an oxidation process [5.317, 5.318]. Since no such effects were observed when aluminum was introduced from the gas phase, it was concluded that the damage caused by the implantation catalyzes the precipitation process [5.315]. Tentatively, La Ferla et al. [5.318] suggested that some Al-V complexes serve as precursor for the formation of Al_xO_y precipitates.

5.5 Gallium

Because of its high diffusion coefficient and low eutectic temperature, gallium was used at the beginning of the semiconductor era for the formation of alloy junctions. Since then, it led a shadowy existence at the side of the other acceptors. As a possible application, gallium was suggested as a replacement for boron in CZ-based solar cells since it does not show the degradation effects associated with boron-oxygen complexes [5.193, 5.242, 5.319], see also Section 5.3.4. Remarkable is especially the diffusivity of gallium in silicon dioxide which exceeds that of other dopants by orders of magnitude [5.320]. In the following sections, the basic atomic configurations of gallium in silicon, its solubility, the diffusion behavior, and the formation of complexes are discussed in detail.

5.5.1 Basic Atomic Configurations

Substitutional Gallium

Gallium atoms on substitutional sites have one positive charge too few for the valence-bond structure of silicon. In analogy to donors, a hole is assumed to be introduced in the valence band. The ionization energy of substitutional gallium was determined by electrical and optical measurements. Hall-effect measurements resulted in a value of 0.065 eV [5.17]. From infrared absorption, values of 0.071 eV [5.19], 0.0723 eV [5.20], and 0.0727 eV [5.21] were deduced. In theoretical investigations, an ionization energy of 0.058 eV [5.259] was calculated.

In samples doped with gallium atoms in concentrations up to 10^{16} cm^{-3} , various photoluminescence lines were found to arise from the decay of excitons bound to neutral gallium atoms. The zero-phonon line can be found at 1.1490 eV [5.260], the transverse-acoustic and transverse-optic phonon sidebands have 18.7 and 58.0 eV lower energies.

Theoretical investigations led to the estimates of 3.6% [5.261] for the volume expansion $\Delta V/V_{Si}$ associated with a substitutional gallium atom.

Gallium-Vacancy Pairs

Estimates for the binding energy of gallium-vacancy pairs were obtained indirectly from the comparison of self-diffusion and gallium diffusion under inert and intrinsic conditions. Based on such an analysis, Shaw [5.321] suggested a binding energy of 0.95 to 0.97 eV for negatively charged pairs, and 1.27 to 1.28 for neutral ones. The reliability of these values is limited because of the fallacious assumption that gallium diffusion and self-diffusion proceed entirely via vacancies.

5.5.2 Solubility

The phase diagram of the gallium-silicon system was compiled by Olesinski et al. [5.322]. Below the eutectic temperature of 29.77 °C, the gallium in the silicon phase is in equilibrium with a pure gallium phase.

Solubility values for gallium were obtained from various experiments. Values obtained from the diffusion of gallium from the gas phase [5.323, 5.324] can be assumed to correspond to binary solubilities only when the binary equilibrium phase forms at the surface. Otherwise, smaller as well as slightly higher values are possible. In addition, alloy systems were formed by melting [5.282]. Of the measurement techniques applied, profiling by isotope counting [5.323] and neutron activation [5.324] gives chemical profiles without need for calibration. In the work of Akopyan and Kachakhidze [5.282], microindentation, Hall-effect measurements, and X-ray analyses were combined for the determination of the solid solubility. A summary of the solubility values reported can be found in Figure 5.11. Reasons for the discrepancies between the analyses are not apparent but may be associated with the method by which the dopants were introduced into the silicon.

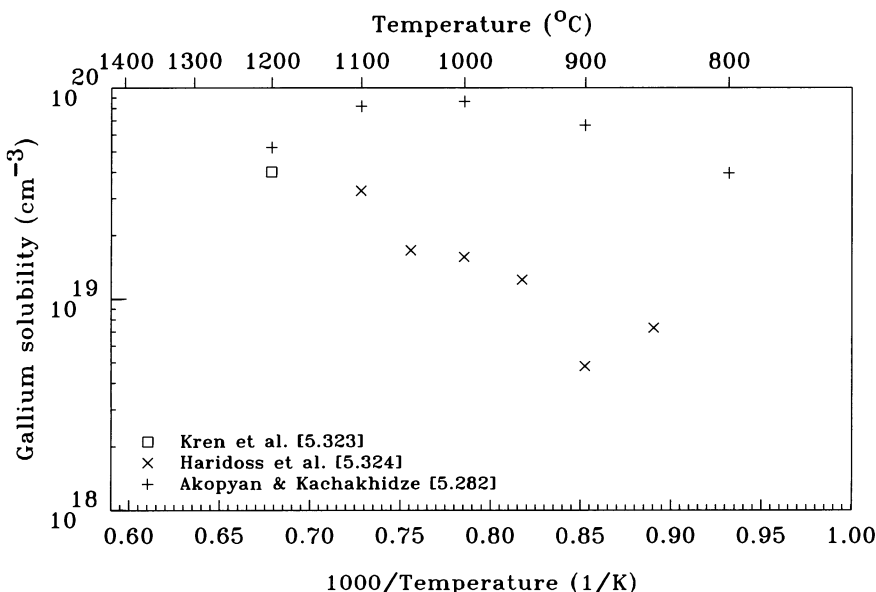


Figure 5.11: Solubility of gallium in silicon.

5.5.3 Diffusion

Intrinsic Diffusion

A determination of the diffusion coefficient of gallium under nominally inert and intrinsic conditions was the objective of various investigations. Introduction of gallium occurred from the gas phase during diffusion [5.284, 5.323, 5.325–5.330], from a gallium-doped oxide [5.331, 5.332], or from a deposited gallium layer [5.122, 5.134]. For the characterization of the diffusion profile, radioactive gallium isotopes [5.323, 5.326, 5.328], electrical techniques [5.284, 5.325, 5.329, 5.331, 5.332], or SIMS [5.122, 5.134, 5.330] were used. A summary of the diffusion coefficients reported can be found in Figure 5.12 together with the regression curve

$$D_{Ga}^i = 3.81 \cdot \exp\left(-\frac{3.552\text{eV}}{k \cdot T}\right) \text{cm}^2/\text{s} \quad (5.21)$$

derived from these measurements. The activation energy ranges with a confidence level of 90% from 3.46 to 3.64 eV. The 90% confidence interval for the diffusion coefficient is about +8.4/-7.7% of the regression curve at 1165 °C and increases to +15/-13% at the melting point and +30/-23% at 800 °C. Additional measurements are expected with 90% confidence within a range of +84/-46% of the regression curve at 1165 °C which increases slightly to +85/-46% at the melting point and +93/-48% at 800 °C.

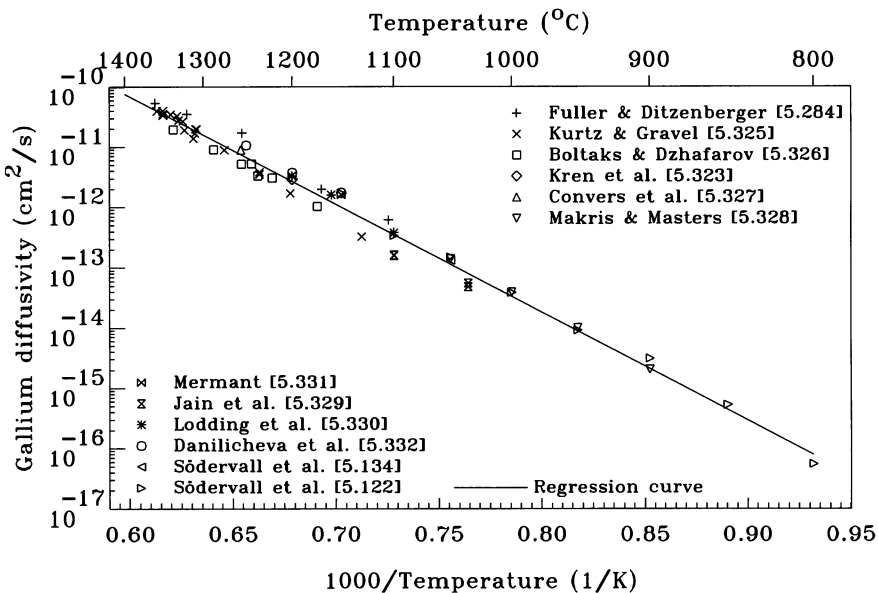


Figure 5.12: Diffusion coefficient of gallium under intrinsic and inert conditions in silicon.

In some investigations in which gallium was introduced from the gas phase it was found that its diffusion in regions covered by an oxide layer was enhanced in comparison to regions with bare surfaces [5.329, 5.333]. The effect is probably related to surface reactions.

Pressure Dependence

Pressure-dependent diffusion studies performed by Södervall et al. [5.134] resulted in an estimate for the activation volume of about $-0.85 \cdot V_{Si}$. In a later publication, Södervall et al. [5.122] reported an activation volume of about $-0.7 \cdot V_{Si}$.

Diffusion Mechanism

Quantitative estimates for the contributions of self-interstitials and vacancies to the diffusion of gallium under intrinsic conditions were obtained from experiments involving non-equilibrium conditions as discussed in Section 3.4.3. The values reported are summarized in Table 5.3. They agree that gallium diffuses predominantly via self-interstitials.

Table 5.3: Fractional diffusivity of gallium via self-interstitials. The abbreviations OSF, RD, and DifComp for the experimental method refer to estimates from oxidation-enhanced diffusion with self-interstitial oversaturations estimated from OSF growth, from the observation of retarded diffusion under non-equilibrium conditions, and from the comparison with the diffusivities of other dopants under non-equilibrium conditions, respectively. A description of the methods can be found in Section 3.4.3.

	f_I	Temperature range (°C)	Experimental method	Ref.
Mizuo & Higuchi	> 0.5	950–1150	DifComp	[5.334]
Tan et al.	0.65	1100	OSF	[5.141]
Gösele & Tan	> 0.88	1150	RD	[5.142]
Fahey	> 0.5	1050	RD	[5.335]
Fahey et al.	≥ 0.95	1050	DifComp	[5.336]

Extrinsic Diffusion

Information about the diffusion of gallium at extrinsic concentrations is available only from the isoconcentration diffusion studies of Makris and Masters [5.328]. These results are shown in Figure 5.13. The full lines were obtained by a numerical optimization using all data points in Figure 5.12 in addition to those in Figure 5.13, and are described by

$$\begin{aligned}
 D_{Ga} = & 1.8 \cdot \exp\left(-\frac{3.489\text{eV}}{k \cdot T}\right) \text{cm}^2/\text{s} \\
 & + \frac{p}{n_i} \cdot 1.59 \cdot \exp\left(-\frac{3.634\text{eV}}{k \cdot T}\right) \text{cm}^2/\text{s} \\
 & + \left(\frac{p}{n_i}\right)^2 \cdot 2.14 \cdot \exp\left(-\frac{3.974\text{eV}}{k \cdot T}\right) \text{cm}^2/\text{s}. \quad (5.22)
 \end{aligned}$$

For intrinsic concentrations, diffusion is dominated by the Fermi-level-independent part while the quadratic term in p/n_i dominates at the highest concentrations.

5.5.4 Complexes

After annealing of electron-irradiated gallium-doped samples at 300 °C, Watkins [5.262] observed the formation of an EPR spectrum labelled Si-G22 which was identified to arise from a doubly positively charged gallium interstitial paired with a negatively charged substitutional gallium atom. A Ga_iGa_s complex was also considered by Khan et al. [5.193] to be a likely candidate for the level at $E_V + 0.18$ eV observed after annealing of electron-irradiated, gallium-doped samples around 300 °C. The other possibility suggested for the defect would be a Ga_iO_i complex.

The formation of substitutional gallium-carbon pairs, sometimes referred to as Si-X centers, was mentioned already in Section 4.1.6.

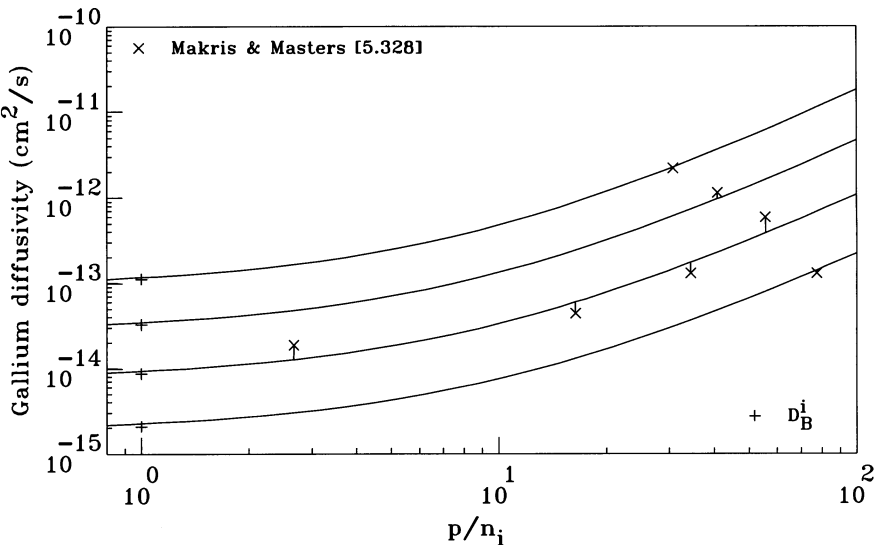


Figure 5.13: Dependence of the normalized diffusion coefficient of gallium in silicon on p/n_i . The full lines correspond, from top to bottom, to temperatures of 1250, 1215, and 1150 °C.

5.6 Indium

Because of its high ionization energy, doping with indium was investigated for the fabrication of infrared detectors [5.257, 5.337]. Interest in indium was revived after Shahidi et al. [5.338] reported improved short-channel characteristics of n -channel MOSFETs associated with steep retrograde channel profiles which can be achieved with indium. In the following sections, the basic atomic configurations of indium in silicon, its solubility, the diffusion behavior, and the formation of complexes are discussed in detail.

5.6.1 Basic Atomic Configurations

Substitutional Indium

Experimental indications for the predominant lattice location of indium were obtained by Forkel et al. [5.339] from a perturbed angular correlation study. In samples implanted with ^{111}In and annealed at 800 °C, all indium atoms were found to be located in an environment with cubic symmetry. This finding is in agreement with the expected substitutional position.

Indium atoms on substitutional sites have one positive charge too few for the valence-bond structure of silicon. In analogy to donors, a hole is assumed to be introduced in the valence band. In contrast to most other dopants, indium is a relatively deep acceptor. Its ionization energy was determined by electrical and optical measurements. Hall-effect measurements resulted in values of 0.153 to 0.165 eV [5.17, 5.257, 5.340–5.344]. The values around 0.164 eV were found from Hall-effect measurements at temperatures above 100 K and were explained by a temperature-dependent relation between Hall mobility and drift mobility which was, owing to lack of better knowledge, assumed unity in most analyses. A value of 0.16 eV was also obtained from the temperature dependence of resistivity measurements [5.258]. From infrared absorption, values of 0.154 to 0.1569 eV were deduced [5.19–5.21, 5.345]. Finally, Newman [5.346] found the ionization energy of indium by photoconductivity measurements to be about

0.15 eV while Jones and Johnson [5.347] used DLTS and reported the acceptor level of indium at $E_v + 0.173$ eV. In theoretical investigations, an ionization energy of 0.134 to 0.164 eV [5.259] was calculated.

Basically all these ionization energies were determined at rather low temperatures. For room temperature, Tardella and Pajot [5.345] suggested that the ionization energy reduces to 0.14 eV. Cerofolini et al. [5.348] even found a level with an ionization energy of 18 meV to dominate in implanted and annealed samples without precipitates. Following the work of Cerofolini [5.349], this was interpreted as the activation energy for thermal ionization to a relaxed ionized state plus a free hole. Values reported around 0.155 eV, on the other hand, were interpreted as activation energies for ionization to an unrelaxed excited state plus a hole localized around the impurity. A more detailed discussion of such and related topics can be found in Section 5.6.2.

In samples doped with indium atoms in concentrations up to 10^{16} cm^{-3} , various photoluminescence lines were found to arise from the decay of excitons bound to neutral indium atoms. The zero-phonon line can be found at 1.1413 eV [5.350], the transverse-acoustic and transverse-optic phonon sidebands have 18.7 and 58.0 eV lower energies.

Theoretical investigations led to the conclusion that substitutional indium occupies a volume which is by $\Delta V/V_{Si} = 21.5\%$ larger than that of silicon atoms [5.261].

Indium-Self-Interstitial Complexes

Although diffusion of indium, as discussed in Section 5.6.3, is dominated by an interaction with self-interstitials, no direct experimental evidence about such complexes is available. The *ab-initio* study of Alippi et al. [5.351] indicated that a C_{1h} -symmetric configuration of a substitutional indium atom and a self-interstitial at a nearest tetrahedral interstitial site should be energetically favored for such a pair in all charge states. For the neutral pair, a formation energy of 2.6 eV was calculated. This resulted in a binding energy of 1.2 eV with respect to an ionized substitutional indium atom and a well-separated, positively charged self-interstitial. Below $E_v + 0.74$ eV, the positive charge state of the pair was found to be more stable.

Indium-Vacancy Pairs

In perturbed angular correlation measurements with radioactive ^{111}In as a probe atom, Kemerink and Pleiter [5.352] found three $\langle 111 \rangle$ -symmetric defects after indium implantation and laser-annealing which they identified tentatively to arise from different charge states of indium-vacancy pairs. Thermal annealing at 400 K was found to lead to an annealing of the defects. In similar experiments, Deicher et al. [5.353] concluded that indium-vacancy pairs form during annealing of indium-doped samples implanted with phosphorus or silicon at temperatures of 230 K and above. Above 300 K, the indium-vacancy pairs were suggested to convert to some larger defects so that the signal was no longer visible after isochronal annealing at 450 K for 5 min.

The *ab-initio* simulations of Alippi et al. [5.351] indicated that indium assumes in all charge states a D_{3d} -symmetric position halfway between two vacant, neighboring lattice sites, similar to the configuration discussed in Section 4.3.1 for the tin-vacancy pair. For the neutral charge state of the pair, a formation energy of 1.48 eV was reported which resulted in a binding energy of 2.4 eV with respect to an ionized substitutional indium atom and a positively charged vacancy. For Fermi levels above $E_v + 0.3$ eV, the negative charge state of the indium-vacancy pair was found to become energetically more favorable.

5.6.2 Solubility

The phase diagram of the indium-silicon system was compiled by Olesinski et al. [5.354]. Below the eutectic temperature around the melting point of indium at 156.6 °C, the indium in the silicon phase is in equilibrium with a pure indium phase.

Values for the solid solubility of indium in silicon were derived by the thermal-gradient crystallization technique [5.355], ion implantation and annealing [5.356–5.359], or molecular-beam epitaxy at elevated temperatures [5.344]. The concentration values reported in these investigations were obtained by combined resistivity and Hall-effect measurements [5.344, 5.355–5.357, 5.359] or capacitance-voltage profiling [5.358]. The solubility values reported are summarized in Figure 5.14.

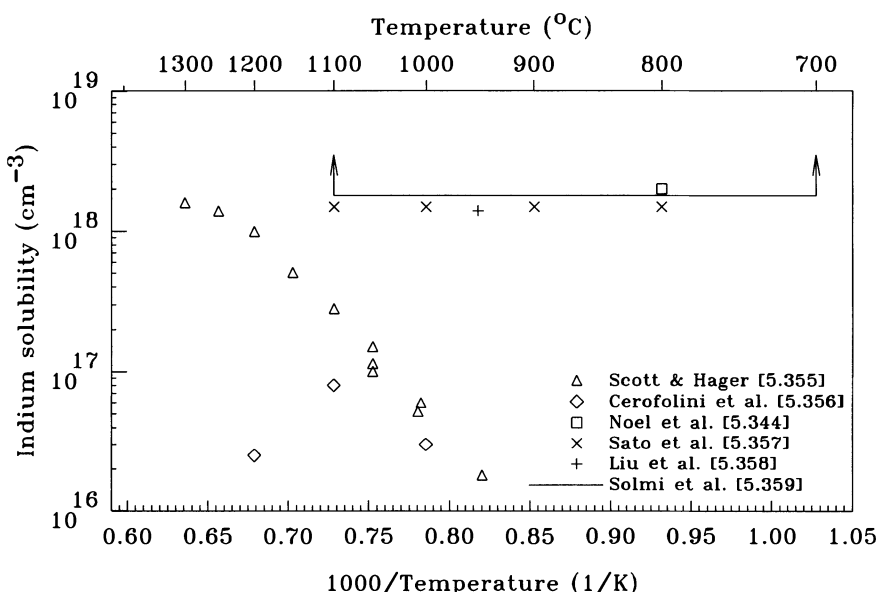


Figure 5.14: Solubility of indium in silicon.

To understand the relevance of the data, it is necessary to discuss the various reports in more detail with respect to the experimental method used for sample preparation as well as with respect to the characterization technique. Of all the preparation techniques used, the thermal-gradient crystallization method should be nearest to equilibrium conditions at a specific temperature. For the implanted and annealed samples, the establishment of the liquid equilibrium phase is uncertain. This is even more true when the thermal budget is as low as 30 s at 950 °C as in the investigation of Liu et al. [5.358]. In the work of Backenstoss [5.360], indium precipitation was reported for concentrations above $4 \cdot 10^{17} \text{ cm}^{-3}$. But it is not clear at what temperature the phase formation took place. Later, the formation of indium precipitates was invoked by Cerofolini et al. [5.356] to explain the marked decrease in activation when the dose of implanted indium was increased from 10^{13} to 10^{14} cm^{-2} . Finally, indium precipitation was mentioned by Noël et al. [5.344] when indium concentrations exceeding $2 \cdot 10^{18} \text{ cm}^{-3}$ were incorporated into MBE films grown at 800 °C.

A serious problem for the comparison of the data is also that different authors mean different things with “solid solubility.” Some use it for the hole concentration, some for the concentration of substitutional indium atoms. Unlike for other dopants, there is a gross difference between the two because of the rather deep ionization level of indium of about 0.16 eV above the valence band. Figure 5.15 shows the relationship between the hole concentration and the substitutional indium concentration for 300 K, derived from the application of Fermi statistics (see Section 1.2). As an example, substitutional indium atoms with a concentration of $5 \cdot 10^{18} \text{ cm}^{-3}$ result in a hole concentration of less than $4 \cdot 10^{17} \text{ cm}^{-3}$ ($\approx 8\%$). For the numerical evaluation, the effective mass of holes was taken from the work of Lang et al. [5.361]. The reduction of the ionization energy was included via the model of Lanyon and Tuft [5.362] and leads to an increase of the hole concentration of about 30% at a concentration of $5 \cdot 10^{18} \text{ cm}^{-3}$.

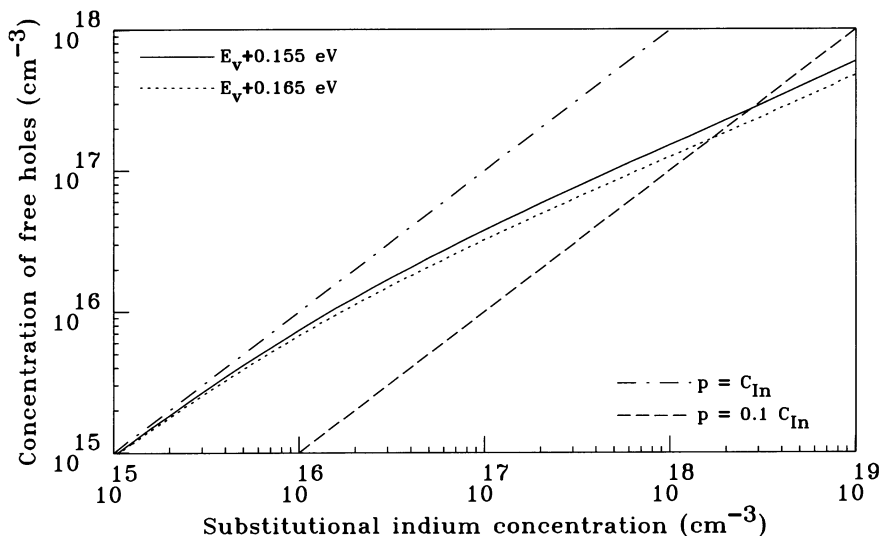


Figure 5.15: Dependence of the concentration of free holes at 300 K on the concentration of substitutional indium atoms for indium levels assumed at $E_v + 0.155 \text{ eV}$ to $E_v + 0.165 \text{ eV}$.

The final problem is the interpretation of the measurement data. Schroder et al. [5.363] could show by an elaborate investigation that the ionization of the indium atoms is enhanced by the depletion of the space-charge region during capacitance-voltage measurements and breakdown measurements and that both methods give consistent results for the total concentration of substitutional indium atoms as long as no other ionizable impurities or complexes are present in significant concentrations. Similarly, Parker et al. [5.364] found capacitance-voltage measurements to give consistent results with atomic absorption measurements. Unfortunately, only the work of Liu et al. [5.358] used capacitance-voltage measurements for the characterization of solid-solubility values. The other investigations were based on Hall-effect measurements. However, the work of Schroder et al. [5.363] and Parker et al. [5.364] showed that such measurements, corrected straightforwardly for the indium donor level, overestimate the substitutional indium concentration considerably. This is of significance especially for the investigations of Scott and Hager [5.355] and Solmi et al. [5.359] although the latter gave only conservative estimates of the solubility concentration.

Although Hall-effect measurements have the reputation of being able to give directly the concentration of substitutional impurity atoms, there are various parameters involved which have to be assumed *a priori* or determined independently. The first one is the Hall-scattering factor. It appears in the relation between the hole concentration and the measured Hall coefficient and is close to unity for very low temperatures and very high magnetic fields. For usual measurement conditions at room temperature it is expected between 0.5 and 1.5 but, without known calibration, often set to unity. When the hole concentration is determined, it is still necessary to calculate the concentration of ionizable indium atoms. This can be done as outlined in Section 1.2.3. A main parameter therein is the ionization level of indium which was determined independently by several methods. However, they were all determined at temperatures significantly below room temperature so that there is still room for speculations. A third parameter influencing the calculation of the position of the Fermi level is the effective mass of holes in the valence band which determines, via (1.13), the effective density of states in the valence band. The values suggested in the literature for undoped silicon vary at 300 K roughly from $0.5 \cdot m_0$ [5.365] to $1.13 \cdot m_0$ [5.361] with m_0 being the mass of a free electron. For indium-doped silicon, as discussed below, even significantly larger values were suggested.

In the work of Schroder et al. [5.363], the discrepancies found between capacitance-voltage measurements and Hall-effect measurements were tentatively related to the Hall-scattering factor. While the authors did not try to bring the measurements into agreement, Parker et al. [5.364] reported that this would be possible assuming a Hall-scattering factor of 0.77 and a reasonable effective mass of holes. In addition, they included a small contribution of indium-carbon pairs (see 4.1.6). Similar values for the Hall-scattering factor and the effective mass of holes were used by Noël et al. [5.344]. Tardella and Pajot [5.345] used likewise a Hall-scattering factor of 0.8 but suggested that the ionization energy reduces to 0.14 eV at room temperature. Unfortunately, they did not mention the effective hole mass used to calculate the number of states in the valence band.

A real exception to all previous investigations is the work of Cerofolini et al. [5.356]. They reported almost full electrical activation below a concentration of 10^{17} cm^{-3} where less than 40% would be expected from Figure 5.15. To explain this unexpected phenomenon as well as differences in the mobility between boron-doped and indium-doped silicon, Cappelletti et al. [5.366] suggested that the effective mass of holes depends on the doping and may be as high as 2.73 times the mass of a free electron in indium-doped samples. It was not sufficient, though, to explain the high electrical activity found experimentally in full. Hall-effect measurements in the temperature range from 80 to 290 K by Cerofolini et al. [5.348] gave an indication of the existence of an indium-related acceptor state with an ionization energy of about 18 meV. The shallow acceptor level was found to dominate in implanted samples without precipitates while in samples with precipitates, a level with an ionization energy of about 160 meV was found to prevail. Both levels were associated with substitutional indium for which two coexisting configurations were postulated.

Finally, analyzing the data reported by Sato et al. [5.357], one has to note that the implanted indium, homogeneously distributed, should be present in a concentration of less than $8.6 \cdot 10^{18} \text{ cm}^{-3}$. According to Figure 5.15, such a total indium concentration would lead to a concentration of free holes of approximately $5.4 \cdot 10^{17} \text{ cm}^{-3}$. Including a Hall-scattering factor of 0.77, the apparent hole concentration should be $7 \cdot 10^{17} \text{ cm}^{-3}$ or less. Since the carrier concentrations reported were twice as high, it may be speculated whether this may be due to non-negligible contributions of indium-carbon pairs, of the shallow indium-related level found by Cerofolini et al., or due to other yet unknown reasons.

5.6.3 Diffusion

Intrinsic Diffusion

The best-studied property of indium is the diffusion coefficient under intrinsic and inert conditions. Introduction of the dopants occurred from the vapor phase [5.284, 5.367] or by ion implantation [5.356, 5.368–5.370]. For the characterization of the diffusion profiles, radiochemical techniques [5.367], electrical measurements [5.284, 5.356, 5.368], or SIMS [5.369, 5.370] were used. A summary of the diffusion coefficients reported can be found in Figure 5.16 together with the regression curve

$$D_{In}^i = 3.13 \cdot \exp\left(-\frac{3.668\text{eV}}{k \cdot T}\right) \text{cm}^2/\text{s} \quad (5.23)$$

derived from these measurements. The activation energy ranges with a confidence level of 90% from 3.47 to 3.87 eV. The 90% confidence interval for the diffusion coefficient is about +21/-17% of the regression curve at 1080 °C and increases to +49/-33% at the melting point and 850 °C. Additional measurements are expected with 90% confidence within a range of +171/-63% of the regression curve at 1080 °C which increases slightly to +188/-65% at the melting point and 850 °C.

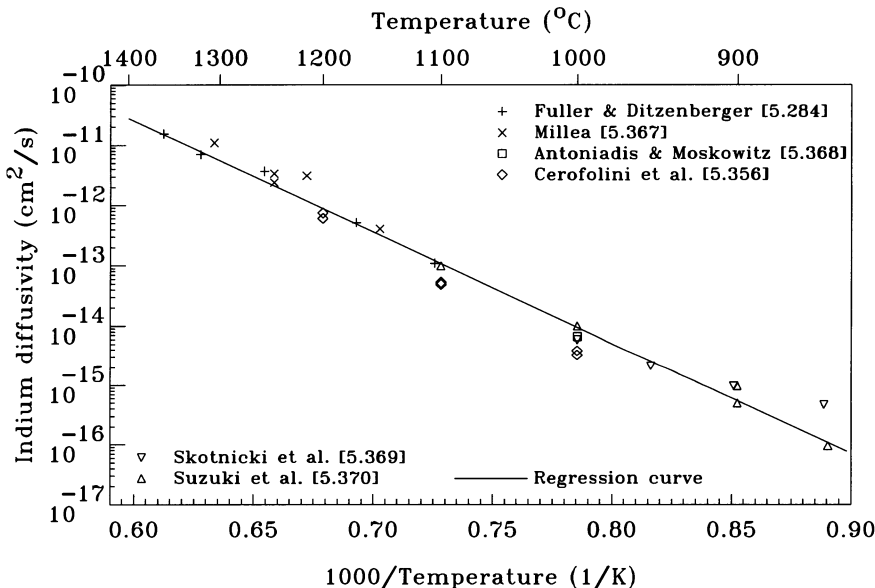


Figure 5.16: Diffusion coefficient of indium under intrinsic and inert conditions in silicon.

Diffusion Mechanism

For indium, Antoniadis and Moskowitz [5.368] estimated the fractional diffusivity via self-interstitials f_I to be about 0.35 at 1000 °C. However, this value has to be taken *cum grano salis*. Antoniadis and Moskowitz estimated it by a comparison with boron and phosphorus for which they had obtained f_I values of 0.3 and 0.38, respectively [5.138]. Taking into account that boron and phosphorus were found thereafter to diffuse nearly entirely via self-interstitials,

one can expect the same for indium. Studies of the oxidation enhancement of indium and boron by Kizilyalli et al. [5.371] indicated that indium is more enhanced at temperatures of 950 °C and above, but probably somewhat less below 900 °C. A diffusion predominantly via self-interstitials was also concluded by Griffin et al. [5.372] from the similarity of the transient-enhanced diffusion of indium and boron.

Extrinsic Diffusion

Information about the diffusion of indium at extrinsic concentrations with $p > n_i$ is available only from the isoconcentration diffusion studies of Millea [5.367]. These results are shown in Figure 5.17. The full lines were obtained by a numerical optimization using all data points in Figure 5.16 in addition to those in Figure 5.17, and are described by

$$D_{In} = \frac{p}{n_i} \cdot 6.45 \cdot \exp\left(-\frac{3.752\text{eV}}{k \cdot T}\right) \text{cm}^2/\text{s}. \quad (5.24)$$

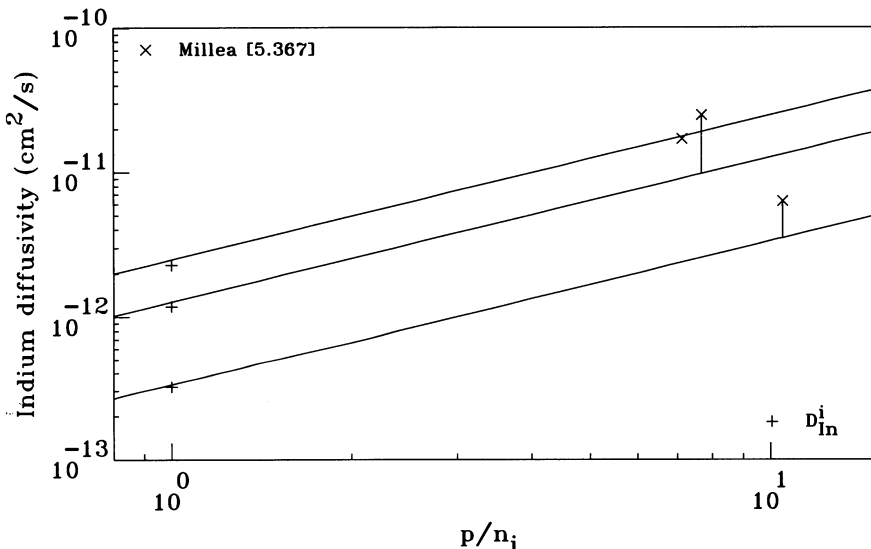


Figure 5.17: Dependence of the normalized diffusion coefficient of indium in silicon on p/n_i . The full lines correspond, from top to bottom, to temperatures of 1250, 1215, and 1150 °C.

There was no indication for a significant Fermi-level-independent contribution. However, it is evident that the experimental basis is insufficient to allow any conclusive statement. Moreover, the investigation of Suzuki et al. [5.370] indicated that indium diffusion is not retarded in heavily n -doped samples. This would either mean that the diffusion via neutral point defects dominates or that one has to assume highly mobile ion pairs which seems rather unlikely.

Indium-Self-Interstitial Complexes

In the work of Alippi et al. [5.351], the diffusion of indium-self-interstitial complexes was investigated by *ab-initio* methods. They obtained a minimum migration enthalpy of 0.5 eV for a path of the indium atom via the tetrahedral interstitial site, independent of the charge state of the complex.

Indium-Vacancy Pairs

The *ab-initio* investigations of Alippi et al. [5.351] indicated a rather erratic interaction of indium with vacancies. Vacancies at second-nearest neighboring site to a substitutional indium atom were found to be unstable while vacancies at the third-nearest neighboring sites are bound again to the indium atom. The total energy barrier for long-range migration as a pair was estimated to be about 2.1 eV.

5.6.4 Complexes

In_{2s}

From their *ab-initio* calculations, Zubkov et al. [5.373] concluded that pairs of substitutional indium would be stable. The energy decrease upon formation with respect to two unassociated substitutional indium atoms was calculated to be 0.72 eV. Similarly, the formation of a pair of a substitutional and an interstitial indium atom from unassociated components was calculated to involve an energy decrease of 2.04 eV.

Ion Pairs

As expected from an acceptor, indium was found experimentally to form substitutional pairs with donors. Perturbed angular correlation measurements performed by Swanson, Wichert, and coworkers [5.374, 5.375] with radioactive ^{111}In as probe atoms revealed indium-arsenic pairs with C_{3v} symmetry about a $\langle 111 \rangle$ direction. The binding energy of the complex was estimated by Swanson et al. [5.374] to be 0.5 eV. In a later report, Wichert and Swanson [5.375] corrected the value to 0.54 ± 0.1 eV. Based on the same data, Cowern [5.216] suggested that the ion-pairing coefficient can be written in the form $\Omega = 0.03/n_i$. A second complex found was interpreted from its concentration dependence as an InAs_2 complex of an indium atom with two arsenic atoms at nearest neighboring sites [5.374, 5.375].

Similar to pairs of indium with arsenic, such with phosphorus were found by Wichert and Swanson [5.375] by perturbed angular correlation measurements. As expected, their symmetry was C_{3v} about a $\langle 111 \rangle$ direction which is consistent with donor and acceptor atoms on neighboring substitutional sites. For the binding energy of the pair, Wichert and Swanson [5.375] suggested a value of 0.69 ± 0.1 eV. The high binding energy reflects most likely strain compensation by the combination of the large indium atom and the small phosphorus atom. Reinterpreting the data, Cowern [5.216] suggested the ion-pairing coefficient in the form of the empirical relation $\Omega = 0.03/n_i$.

Ion pairs of indium and antimony were detected in the perturbed angular correlation investigations of Wichert and Swanson [5.375] and Forkel et al. [5.376]. Their symmetry was determined to be C_{3v} about a $\langle 111 \rangle$ direction, consistent with a pair of substitutional ions on nearest-neighboring sites. The binding energy of 0.32 ± 0.1 eV estimated by Wichert and Swanson [5.375] is considerably smaller than the estimates for the other indium-donor pairs and can be explained by stress from the two atoms which both take up larger volumes than the silicon host atoms. Alternatively, Cowern [5.216] expressed the ion-pairing coefficient empirically in the form $\Omega = 0.015/n_i$.

Pairs of substitutional indium and tellurium atoms were investigated in the perturbed angular correlation investigations of Tessema and Vianden [5.377]. From the symmetry of the electric field gradient, it was concluded that the tellurium atom assumes an interstitial site in the $\langle 100 \rangle$ direction of a substitutional indium atom. Pairing of indium with sulfur and selenium, on the other hand, was not observed.

Pairs with Carbon and Nitrogen

The formation of substitutional indium-carbon pairs, sometimes called Si-X centers, was discussed already in Section 4.1.6. Indium-nitrogen and indium-boron-nitrogen complexes will be discussed below in Section 5.7.4.

The *P,Q,R* Photoluminescence System

The fingerprint of a prominent indium-related defect was reported first by Vouk and Lighowlers [5.378] and Mitchard et al. [5.379]. They found three PL lines in indium-doped samples with the main line at 1.1176 eV and two other lines at 1.1086 and 1.1159 eV, labeled *P,Q,R* by Mitchard et al. [5.379]. These lines were not found in samples not doped with indium and weaker in CZ than in FZ. All three lines were found to be characterized by a binding energy of 30 ± 2 meV and suggested to arise from an iso-electronic center. Uniaxial stress measurements and magnetic-field measurements performed by Weber et al. [5.380] indicated a $\langle 100 \rangle$ axial symmetry and that the center involves at least two different atoms. Based on such findings, they associated the *P,Q,R* system with an iron-indium pair. This suggestion was corroborated by Schlesinger and McGill [5.381] who found that the intensity of the three PL lines increases when iron is introduced intentionally. However, Schlesinger et al. [5.382] found no shift of the *R* line associated with different iron isotopes and Watkins et al. [5.383] reported that they found no correlation with iron at all. Thus, a final identification of the defect giving rise to the *P,Q,R* lines is still missing.

5.7 Nitrogen

From its position in the periodic system, one might have expected nitrogen to act as an efficient donor. It became soon clear that this is not the case. N₂ as an ambient gas is commonly used as quasi-inert atmosphere during devices fabrication. However, there are various other applications associated with nitrogen which will be summarized in the following.

Addition of nitrogen to FZ crystals to suppress the formation of voids was a well-guarded company secret of Wacker [5.384], reinvented finally by Abe et al. [5.385]. The mechanism behind is based on the formation of vacancy-nitrogen complexes which immobilizes the vacancies and suppresses the formation of voids during the cooling phase after crystal growth. Abe et al. also reported that nitrogen leads to a shrinkage of self-interstitial-rich regions when they coexist with balanced and/or vacancy-rich regions on a wafer. However, as shown by Voronkov and Falster [5.386], this effect is not the result of a direct interaction between nitrogen and self-interstitials. It is rather based on a lowering of the critical value of the ratio of crystal growth velocity and thermal gradient at the interface (see Section 2.9) which causes regions which would be self-interstitial-rich in undoped crystals to become vacancy-rich in nitrogen-doped crystals. At the same time, the agglomeration of the vacancies in these regions is suppressed by the formation of vacancy-nitrogen complexes. In CZ crystals, the suppression of void formation was reported at first to work as well, albeit maybe less effective [5.387–5.392]. However, there is evidence now that the main effect of nitrogen doping is just a retardation of the formation of void defects which results in significantly more of them of smaller sizes [5.393–5.395] which may adversely influence the reliability of gate oxides [5.396]. Nitrogen was also added intentionally to FZ crystals because of its ability to improve the mechanical properties of silicon [5.397–5.404], preventing slippage more effectively than oxygen.

Nitrogen, when incorporated into gate oxides, was reported to be able to improve their properties such as leakage current, concentration of interface states, radiation hardness, and especially hardness against degradation induced by high-energetic charge carriers. Due to the sheer wealth of publications, a comprehensive review would exceed the scope of this book by far. As a consequence, only some typical reports will be cited below as examples.

One possibility to introduce nitrogen is by processing in some reactive, nitrogen-containing ambient. Direct nitridation of gate oxides in NH_3 was investigated first [5.405–5.407] but the reliability of the nitroxides, if characterized, was often found to be decreased due to an inadmissibly high concentration of hydrogen-related electron traps. However, it was also found that these properties can be improved considerably by an additional reoxidation step in O_2 [5.408–5.410] or N_2O [5.411]. Equally successful were combinations of thermal processes in O_2 and N_2O [5.412–5.414], although detrimental effect like increased leakage currents were reported for devices with N_2O -grown oxynitrides [5.415,5.416]. Other strategies, sometimes with the intention to lower the thermal budget, were based on combinations of thermal processes in O_2 and NO [5.417,5.418] or mixtures of NO and N_2O [5.419], as well as nitridation of nitroxides in NH_3 [5.420,5.421]. It was also reported that nitridation of the polysilicon layer on top of the gate oxide leads to the incorporation of nitrogen at the interface in between [5.422]. Alternatives to thermal processes are plasma-assisted processes [5.423–5.425]. In addition, nitrogen has been introduced by implantation into the polysilicon before gate definition [5.426,5.427], into gate and source/drain regions after gate definition [5.426,5.428,5.429], and into silicon substrates prior to oxidation [5.430–5.432]. Improved properties are usually found when nitrogen is present at the interface between bulk silicon and the gate oxide. Theoretical investigations combined with spectroscopic measurements confirmed the often expressed suggestion that the observed improvement of electrical properties is the result of a structural improvement of the interface and a reduction of strain [5.433,5.434]. Nitrogen in the bulk of gate oxides or at the interface to the gate polysilicon was often found to degrade the reliability of gate oxides. Because of their higher permittivity constant, oxynitrides are electrically equivalent to much thinner silicon dioxides. A further advantage of nitrogen in gate oxides is its retarding effect on boron penetration [5.413,5.428,5.435,5.436]. Especially nitrogen near the interface between gate oxides and polysilicon gates is here advantageous. A major disadvantage associated with nitrogen is a reduced low-field carrier mobility associated with Coulomb scattering due to fixed charges introduced [5.437]. In general, recipes for nitrogen incorporation have to aim at a compromise between various target parameters.

Although they never became real competitors for oxide-based dielectrics up to now, silicon nitride films were investigated and found useful for dielectrics or barriers against diffusion and oxidation [5.438,5.439]. A potential problem was often the poor quality of the interface to silicon. To improve it, a wet oxidation step [5.440,5.441] or processing in an N_2O or $\text{N}_2\text{O}/\text{NH}_3$ atmosphere [5.442,5.443] following the nitridation or nitride deposition were suggested. Alternatively, gate nitrides grown by plasma processes were shown to have excellent properties [5.444,5.445].

Oxidation of nitrogen-implanted silicon was found soon to proceed with a significantly reduced rate [5.446–5.449]. This effect can be used to either grow thinner gate oxides or to grow gate oxides with different thicknesses in one oxidation step. At high doses, a replacement of the usual nitride deposition for local oxidation was intended. After the synthesis of nitride layers by nitrogen implantation has been demonstrated [5.450–5.452], implantation of nitrogen with very high doses and energies was investigated for the formation of buried insulating Si_3N_4 layers. A catch-phrase for such materials is SIMNI — separation by implanted nitrogen.

Nitrogen was found to be involved in the formation of a family of shallow thermal donors [5.453–5.455], although it is not entirely clear whether nitrogen is part of the defect core or whether the effect is indirect only. The presence of nitrogen was also found to enhance the nucleation of oxygen precipitates [5.456–5.458]. The mechanism behind is clearly that nitrogen preserves vacancies from agglomerating by forming vacancy-nitrogen complexes. These complexes in turn provide the free volume for the nucleation of oxygen precipitates [5.459].

In the following sections, the basic atomic configurations of nitrogen in silicon, its solubility, the diffusion behavior, and the formation of complexes will be discussed in detail.

5.7.1 Basic Atomic Configurations

Substitutional Nitrogen

Electrically active nitrogen atoms were reported first by Pavlov et al. [5.460] after ion implantation and annealing at temperatures of 700 °C and above. But they made only 1% or less of the implanted dose. Similar results indicated that less than 5% of the nitrogen atoms in nitrogen-doped crystals [5.461] and less than 1% of nitrogen introduced by ion implantation and annealing [5.18, 5.462–5.465] are electrically active. As an exception to this rule, Kleinfelder et al. [5.466] reported nearly fully activated profiles after implantation and annealing for 10 min, both at 625 °C. Similarly, Pronko et al. [5.467] reported nearly full activation after implantation at 28 K and solid-phase epitaxy at 700 °C. An excellent review on implantation and annealing of nitrogen, covering especially the early experiments, was given by Pavlov et al. [5.468]. In silicon doped with nitrogen during silicon growth, Yatsurugi et al. [5.461] reported less than 5%, and Tajima [5.469] about 0.5% to 2.5% of the nitrogen concentration to act as shallow donors. After silicon deposition on GaN, Chen et al. [5.470] found an incredibly high electron concentration of $1.4 \cdot 10^{18}$ (0.056%) which they associated with nitrogen. The total concentration of nitrogen was speculated to be about $2.5 \cdot 10^{21} \text{ cm}^{-3}$.

To estimate the ionization energy of substitutional nitrogen, Zorin et al. [5.471] used Hall-effect measurements at temperatures from 100 to 300 K and obtained a value of 0.045 eV. Values from 0.033 to 0.044 eV, depending on the annealing history, were also reported by Clark et al. [5.472]. Extending the temperature range down to 20 K, Mitchell et al. [5.18] corrected the value to 0.017 ± 0.002 eV. A study of Stein [5.473] indicated ionization energies ≤ 0.035 and 0.05 eV, but Stein also suggested that they arise from nitrogen aggregates rather than from substitutional nitrogen. From the doping dependence of EPR investigations, Ito et al. [5.474] suggested an acceptor level at $E_c - 0.08$ eV and a donor level at $E_c - 0.31$ eV. Later, combining EPR and DLTS, Murakami et al. [5.475] suggested a donor level at $E_c - 0.33$ eV to arise from substitutional nitrogen. Calculations of Pantelides and Sah [5.476] indicated that nitrogen introduces an acceptor level at $E_c - 0.0525$ eV in addition to the actual donor level at $E_c - 0.3359$ eV. They also suggested that the value of 0.045 eV found by Zorin et al. [5.471] corresponds to the energy required for double ionization of negatively charged, substitutional nitrogen atoms. This assignment was rejected by Pavlov et al. [5.468] who noted that it would not agree to the temperature dependence of the charge-carrier mobility observed experimentally.

A structural identification of substitutional nitrogen was made first by Brower [5.477] by EPR measurements on nitrogen-implanted, laser-annealed specimen. Instead of the T_d symmetry expected for a substitutional Group V atom, only C_{3v} along the $\langle 111 \rangle$ axis was found for Si-SL5. This symmetry lowering was ascribed to Jahn-Teller distortions as indicated by arrows in Figure 5.18. The distortion was reproduced also by numerous theoretical investigations [5.478–5.481] although it was later interpreted to arise rather from a pseudo-Jahn-Teller effect since the system is not electronically degenerate. From isotope shifts and the forma-

tion and annealing kinetics, Stein [5.482] identified the localized vibrational mode at 653 cm^{-1} (300K) to arise from a substitutional ^{14}N isotope. From theoretical investigations, a substitutional nitrogen atom was estimated to be 3.88 eV energetically more stable than an interstitial nitrogen atom well-separated from a vacancy [5.480].

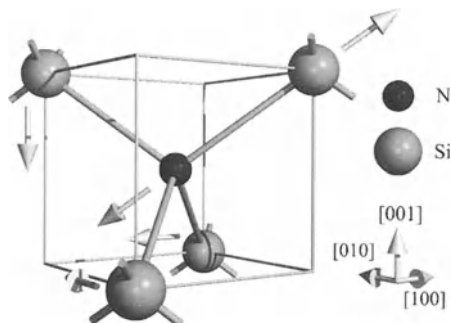


Figure 5.18: Atomic arrangement of substitutional nitrogen. Jahn-Teller distortions around the $\langle 111 \rangle$ axis are indicated by arrows.

EPR measurements performed by Murakami et al. [5.483] indicated also the possibility of a metastable on-center substitutional configuration of nitrogen. They estimated that the T_d -symmetric configuration would be 0.073 eV higher in energy than the $\langle 111 \rangle$ -distorted configuration. Such a small energy barrier was also estimated in theoretical investigations [5.479–5.481].

Nitrogen Pairs

Crystals doped with ^{14}N during growth [5.397], grown from a silicon nitride crucible [5.484], or implanted with ^{14}N [5.485] were found to have dominant IR vibration modes at 764 and 962 cm^{-1} (RT). From isotope shifts, Stein [5.486] and Abe et al. [5.400] concluded that these vibration modes are associated with a nitrogen pair. In electron irradiation studies, Suezawa and Sumino [5.487] found that two additional lines appeared with similar wave numbers on the expense of the N_{2i} -related absorption lines. Since the effects of irradiation were different for the latter, the authors suggested that they are not different vibration modes of the same defect but from different structures of the nitrogen pair. Based on channeling studies, IR measurements, and theoretical investigations, Jones et al. [5.478] and Berg Rasmussen and Bech Nielsen [5.465] suggested the atomic arrangement shown schematically in Figure 5.19. Other configurations were rejected on the basis of the channeling studies or of the theoretical investiga-

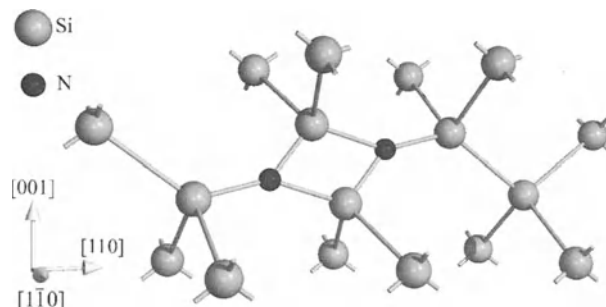


Figure 5.19: Schematic representation of the atomic configuration of the nitrogen pair in silicon.

tions. Further evidence in favor of the proposed structure was obtained by Berg Rasmussen and Bech Nielsen [5.488] from studies of uniaxial stresses on the absorption bands. Complementary theoretical investigations resulted in binding energies from 1.73 eV [5.489] via 3.67 eV [5.481], 3.86 eV [5.490], and 4.1 eV [5.491] to 4.3 eV [5.480] for the N_{2i} pair in comparison to two well-separated nitrogen interstitials. The *ab-initio* calculations of Goss et al. [5.481] also indicated that N_{2i} has neither donor nor acceptor states in the band gap.

Nitrogen Interstitials

Break-up of the nitrogen pair due to electron irradiation was found by Sprenger et al. [5.492] to give rise to the EPR Si-NL26 spectrum which they tentatively attributed to the neutral charge state of a nitrogen interstitial. From its annealing behavior around 40 K, the authors suggested a very high diffusivity even at very low temperatures. The nitrogen interstitial was also associated⁵ with a localized vibrational mode at 691 cm⁻¹ (80 K).

The *ab-initio* calculations of Sawada and Kawakami [5.480], Schultz and Nelson [5.495], Kageshima et al. [5.496], and Goss et al. [5.481] indicated that a configuration close to a ⟨100⟩-oriented split interstitial is the energetically most stable form of a neutral nitrogen-self-interstitial complex in silicon. For the energy gain in comparison to a substitutional nitrogen atom and a well-separated silicon self-interstitial, values of 3.19 [5.480] and 3.5 eV [5.495] were calculated. Diffusion of the nitrogen interstitial was found to be governed by a small activation energy for which values of 0.11 eV [5.480] and 0.5 eV [5.481,5.495] were obtained from *ab-initio* calculations. The work of Sawada and Kawakami [5.480] also showed that interstitial nitrogen may exist in various charge states. For the positive charge state, the ⟨100⟩-oriented split interstitial was found lowest in energy while nitrogen interstitials in the negative charge state were reported to prefer the bond-centered interstitial site. Goss et al. [5.481] confirmed the ⟨100⟩-oriented split interstitial to be the lowest-energy configuration for the positive charge state but found this configuration also to be energetically favored for the negative one.

Within their kinetic model used to reproduce post-implantation diffusion of nitrogen, Adam et al. [5.497] used a binding energy of 4.55 eV for nitrogen interstitials.

Nitrogen-Vacancy Pairs

The vacancy-counterpart of the nitrogen interstitial would be a pair of a substitutional nitrogen atom and a vacancy. An identification of such a complex by positron annihilation was reported by Adam et al. [5.497,5.498] although it is not apparent how other vacancy-nitrogen complexes were excluded as explanation for the measurements. The *ab-initio* simulations of Nelson et al. [5.78] indicated a binding energy of 1.73 eV and a barrier of 4.44 eV against an exchange of sites. The work of Goss et al. [5.481] resulted in a similar binding energy of 1.6 eV which reduces to 0.3 eV when the vacancy is at a second coordination site of the substitutional nitrogen atom.

Within their kinetic model used to reproduce post-implantation diffusion of nitrogen, Adam et al. [5.497] used a binding energy of 3.1 eV for nitrogen-vacancy pairs.

⁵It remains unclear who actually made the suggestion. Berg Rasmussen et al. [5.493] apparently refers to an already made assignment, but in the only cited reference, Stein [5.494] explicitly stated that no configurational assignment has been made.

5.7.2 Solubility

Attempts reported by Kaiser and Thurmond [5.499] to dope crystals with nitrogen resulted in high-resistivity material with a donor concentration of 10^{12} cm^{-3} . Under similar conditions, Yatsurugi et al. [5.461] estimated a donor concentration of $1.4 \cdot 10^{14} \text{ cm}^{-3}$. But, as outlined above, substitutional nitrogen atoms are clearly the minority. Therefore, Yatsurugi et al. [5.461], Nozaki et al. [5.500], and Watanabe et al. [5.484] determined the concentration of nitrogen by nuclear reactions with a proton beam which converts nitrogen to instable ^{11}C . In these measurements, the total concentration of dissolved nitrogen was obtained and values of $4.5 \cdot 10^{15}$, $4.5 \cdot 10^{15}$, and $4.2 \cdot 10^{15} \text{ cm}^{-3}$ were reported, respectively. However, there is neither evidence that the values correspond really to solid solubility, nor is it clear to what temperature they relate.

5.7.3 Diffusion

Intrinsic Diffusion

The first investigations of the diffusion of implanted nitrogen were reported by Clark et al. [5.472, 5.501] from measurements of the junction depth. His diffusion coefficient with a pre-factor of $0.87 \text{ cm}^2/\text{s}$ and an activation energy of 3.29 eV was in agreement with the expected behavior of a substitutional impurity. Considering the very complex diffusion behavior of implanted nitrogen found later with its preferential diffusion to the surface and its trend to decorate strain regions (see below), it is clear that these experiments were not able to characterize the diffusion coefficient of nitrogen in silicon. In a subsequent investigation, Denisova et al. [5.502] obtained a prefactor of $3 \cdot 10^{-2} \text{ cm}^2/\text{s}$ and a considerably smaller activation energy of 2.63 eV . It was based on diffusion of nitrogen from an N_2 ambient. For a determination of the penetration depth, the nitrogen was activated by an amorphizing implantation of neon and recrystallization at 800°C . Since later investigations indicated that nitrogen is highly mobile under such conditions, profile redistribution was probably underestimated.

In contrast to the early studies, much higher diffusivities were found by Itoh and Abe [5.503] from SIMS measurements of out-diffusion profiles of nitrogen. They explained their results by a rapid diffusion of N_{2i} and speculated that nitrogen introduced from a silicon nitride layer is monoatomic and diffuses with much lower diffusion coefficients as do other substitutional impurities. But similar diffusivities were also reported by Hara et al. [5.504] from the depth profiles of electrically active defects, by Willems and Maes [5.505] from SIMS profiles of nitrogen incorporated by laser melting, and by Fuma et al. [5.506, 5.507]⁶ from the depth profiles of a DLTS peak at $E_c - 0.44 \text{ eV}$, both after in-diffusion of nitrogen from the ambient. A summary of the diffusivities is shown in Figure 5.20 together with the regression curve

$$D_N = 79.4 \cdot \exp\left(-\frac{2.444 \text{ eV}}{k \cdot T}\right) \quad (5.25)$$

derived from the measurements. The activation energy ranges with a confidence level of 90% from 2.16 to 2.73 eV . The 90% confidence interval for the diffusion coefficient is about +53/-35% of the regression curve at 950°C and increases to +133/-57% at the melting point and +99/-50% at 750°C . Additional measurements are expected with 90% confidence within a range of +390/-80% of the regression curve at 1165°C which increases to +480/-83% at the melting point and +440/-81% at 750°C .

⁶The values of Fuma et al. [5.506] appear somewhat inconsistent. The text gives a diffusion coefficient of $2.5 \cdot 10^{-10} \text{ cm}^2/\text{s}$ for 850°C while from their Figure 2, a value in excess of $10^{-9} \text{ cm}^2/\text{s}$ is apparent. It should be noted also that the data point labeled SIMS at 750°C is at 800°C in the original work of Itoh and Abe [5.503]

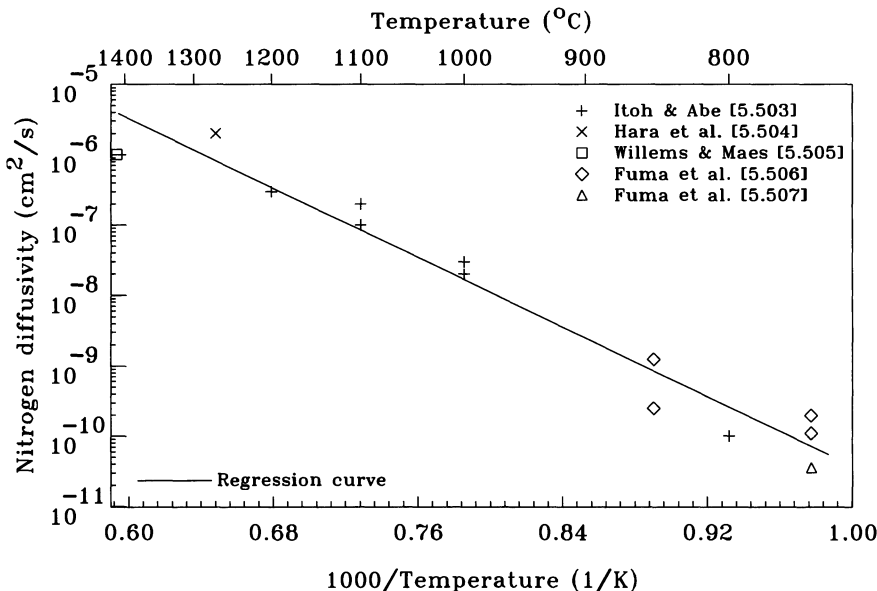


Figure 5.20: Diffusivity of nitrogen in silicon.

Diffusion Mechanism

It was already mentioned above that the dominating nitrogen defect is the nitrogen pair. Direct diffusion of nitrogen pairs was investigated theoretically by Sawada et al. [5.508]. Their *ab-initio* calculations indicated that the energetically most favorable diffusion path involves the separation and re-association of the pair during which both nitrogen atoms remain in the (110) plane. The smallest activation energy was found to be 2.8 eV for the nitrogen pair in the negative charge state. A second conceivable mechanism for the diffusion of N_{2i} would be the dissociation into monomers followed by their diffusion and eventual reunification to nitrogen pairs. However, no conclusive evidence is available yet which would allow to determine the contributions of the two mechanisms to the overall redistribution of nitrogen.

Diffusion during Post-Implantation Annealing

After ion implantation and laser activation, the concentration of substitutional nitrogen was found to decrease during further heat treatment. For this process, activation energies of 1.3 ± 0.2 eV and 1.5 ± 0.2 eV were estimated from EPR [5.509] and IR measurements [5.482], respectively. However, it is not clear to what mechanism these activation energies are related.

The macroscopic diffusion behavior of implanted nitrogen is quite complex. For temperatures of up to 750 °C, Adam et al. [5.510] reported profiles which can be explained qualitatively by a dissociation of stable defects into mobile ones followed by their rapid diffusion towards the surface. Probably in analogy to the diffusion of dopants, Adam and Law [5.511] and Adam et al. [5.497, 5.512] considered nitrogen interstitials, nitrogen-vacancy pairs, substitutional nitrogen and nitrogen-vacancy pairs in addition to self-interstitials, di-interstitials, vacancies, and divacancies in their simulations. Assuming nitrogen interstitials as the only mobile species, they were able to reproduce their experiments excellently. Strangely though, the formation of the otherwise dominating nitrogen pairs was neither included nor apparently required.

In the work of Hockett [5.513], nitrogen-implanted samples were annealed at temperatures of 800 to 1050 °C for 10 s. The profiles thereafter are characterized by profile broadening and diffusion towards the surface. Co-implantation with carbon and/or oxygen was reported to lead to a strong retardation of the redistribution of nitrogen.

Nitrogen implanted into silicon with doses of up to 10^{15} cm^{-2} or deposited during epitaxial growth turned out to accumulate during heat treatments at temperatures of 800 °C and above at the SiO₂ side of the interface to covering oxide layers [5.510, 5.514–5.517]. At the interface, based on XPS measurements, they were suggested to form Si₃N₄ islands [5.517]. Similar observations of a preferential diffusion towards the surface were reported for nitrogen incorporated by laser melting [5.518]. For higher doses, Josquin [5.514] observed a saturation of the surface peak at $2\text{--}3 \cdot 10^{15}$ nitrogen atoms trapped at the interface per cm². Increasing the dose of 40 keV N₂⁺ implants from $5 \cdot 10^{13}$ to $5 \cdot 10^{14}$ and $2 \cdot 10^{15} \text{ cm}^{-2}$, Adam et al. [5.519] observed a continuous reduction in the nitrogen redistribution upon annealing at 750 °C. A similar effect was reported by Dokumaci et al. [5.520] for nitrogen implanted at 11 keV and annealed from 750 to 900 °C for 2 min when the dose was increased from $7 \cdot 10^{14}$ to $2 \cdot 10^{15} \text{ cm}^{-2}$. It was associated with a saturation of the silicon/silicon dioxide interface with nitrogen atoms.

Another important aspect of nitrogen diffusion was reported by Itoh et al. [5.402]. They annealed wafers with oxygen precipitates and residual defects from a boron implantation in a nitrogen ambient and found by SIMS that nitrogen agglomerated at these defects. As an explanation, the authors suggested that reduction of strain fields around the lattice imperfections as driving force. Since the nitrogen aggregates could be dissolved easily by appropriate heat treatments, it was also suggested that the nitrogen pairs do not transform to Si_nN_m complexes. The decoration of oxygen precipitates was reported also by Hockett et al. [5.521]. After implantation of N₂⁺ with 40 keV and a dose of $2 \cdot 10^{15} \text{ cm}^{-2}$, and annealing at 750 °C, Adam et al. [5.519] observed the accumulation of nitrogen in the depth up to which the silicon was amorphized after the implantation. A similar behavior was found by Dokumaci et al. [5.520] after an N₂⁺ implant at 11 keV and a dose of $7 \cdot 10^{14} \text{ cm}^{-2}$ annealed at 900 °C for 2 min. This indicates again that the nitrogen decorates extended defects formed during post-implantation annealing.

5.7.4 Complexes

[N-N]_s

Among the configurations rejected as majority defect by Jones et al. [5.478] and Berg Rasmussen and Bech Nielsen [5.465] is the ⟨100⟩-oriented [N-N]_s pair suggested originally by Stein [5.522]. The theoretical investigations indicated a stable configuration in which the nitrogen atoms are separated within the vacancy by only 1.4 Å. To explain the channeling studies, a separation of 2.2 Å would have been required. Vacancy-nitrogen complexes were suggested as explanation for various experimental observations. Among them is the suppression of the formation of voids mentioned above which implies that nitrogen is able to immobilize vacancies, preventing them from agglomerating. The most simple vacancy-nitrogen complex which should be able to do this is the substitutional nitrogen mentioned above. On the other hand, most researchers favored complexes between nitrogen pairs and vacancies. Abe et al. [5.400] observed that deep-level defects formed homogeneously during heat treatments from 700 to 1000 °C and were lost to the surface for prolonged annealing times. These defects were found to have deep levels at $E_c - 0.44 \text{ eV}$ and $E_v + 0.66 \text{ eV}$ and their maximum concentration was about 1% of the nitrogen concentration. The identification of the defects as N₂V₂ complexes may be disputed but Fuma et al. [5.506, 5.507] observed the same deep level at $E_c - 0.44 \text{ eV}$ after in-diffusion of nitrogen. Based on an injection of self-interstitials, it was shown that the

complex involves indeed vacancies and Fuma et al. ascribed it tentatively to an $[N-N]_s$ complex. In electron-irradiation experiments, Suezawa and Sumino [5.487] observed that new IR absorption spectra appear on the expense of the absorption lines associated with the N_{2i} pair. These new lines at 783 and 960 cm^{-1} (4.2 K) were tentatively ascribed to $[N-N]_s$ complexes. Complementary theoretical investigations indicated that the energy of the system may be lowered by about 0.82 eV [5.490, 5.496] to 1.29 eV [5.480] and 1.3 eV [5.481] by forming an $[N-N]_s$ complex from a well-separated N_{2i} complex and a vacancy. In contrast, Karoui et al. [5.491] found the reaction to be associated with an energy increase of 2.0 eV .

$N_{2i}V_2$

Complexes comprising two vacancies and two nitrogen interstitials can be considered to arise from the reaction of an $N_{2i}V$ complex and a vacancy. Calculations of the reduction in the energy of the system upon such a reaction range from 3.7 eV [5.481] via 4.07 eV [5.490, 5.496] and 4.54 eV [5.480] to 5.2 eV [5.491]. For the alternative reaction of V_2 with N_{2i} , a binding energy of 1.0 eV was reported [5.491]. From such high binding energies it was concluded that $N_{2i}V_2$ complexes might be the dominating vacancy-nitrogen complex at high temperatures. A first-order estimate based on the respective energies of formation, on the other hand, shows that their concentration has to be much lower than that of substitutional nitrogen atoms [5.386].

It should be mentioned also that Goss et al. [5.481] suggested $N_{2i}V_2$ complexes as candidates for the *A,B,C* photoluminescence center discussed in more detail below.

$N_{2i}V_n$

Further attachment of a vacancy to $N_{2i}V_2$ leads to $N_{2i}V_3$. This reaction was calculated by Kageshima et al. [5.496] to lead to an energy reduction of only 0.4 eV . They also found an other configuration of $N_{2i}V_3$ in which the last vacancy binds with 1.68 eV but it was claimed that the transformation requires to overcome an energy barrier of 1.3 eV . This energy barrier was suggested to prevent $N_{2i}V_n$ complexes from further growth. In the work of Goss et al. [5.481], the binding energy of the last vacancy in a $N_{2i}V_3$ complex was calculated to be 1.5 eV .

For larger complexes, energy gains of 1.5 and 2.16 eV were computed by Kageshima et al. [5.496] for the attachment of further vacancies to $N_{2i}V_3$ and $N_{2i}V_4$, respectively. A similar value of 1.6 eV was given by Goss et al. [5.481] for the binding energy of an additional vacancy to $N_{2i}V_3$. They suggested that the attachment of further vacancies may lead to vacancy chains.

$N_{2i}I$

In addition to complexes of N_{2i} with vacancies, such with self-interstitials were found energetically favorable. The reaction of a self-interstitial with an N_{2i} complex was found by Kageshima et al. [5.496] to lead to an energy gain of 0.82 eV . They also found a more stable configuration the formation of which would mean an energy gain of 1.36 eV . In the work of Goss et al. [5.481], a binding energy of 1.0 eV was calculated. These calculations also indicated a donor level at $E_v + 0.2\text{ eV}$ but no acceptor level.

The *A,B,C* Photoluminescence System

A fingerprint of a nitrogen-related complex was found first by Tajima and coworkers [5.469, 5.523]. They reported a PL line at $1.1223 \pm 0.0001\text{ eV}$ in as-grown nitrogen-doped FZ wafers which correlated with nitrogen. Sauer et al. [5.524] confirmed the observation for nitrogen-doped CZ and FZ wafers and could show that the emission corresponds to the *A* line of the

A,B,C PL system investigated intensively by Weber et al. [5.525], Wagner and Sauer [5.526], Davies [5.527], and Davies et al. [5.528]. Alt and Tapfer [5.529] reported the PL line after nitrogen implantation and annealing. At 700 °C, the center was observed after minutes and annealed after about 100 min. In contrast, at 600 °C more than 100 min were required for an observation while the line vanished at 800 °C after some minutes. Further studies by Alt and Tapfer [5.464] indicated the involvement of another impurity which should not be B, P, O, or C.

Based on the results of their *ab-initio* simulations, Goss et al. [5.481] suggested $N_{2i}V_2$ complexes as a candidate for the *A,B,C* PL center.

Complexes with Carbon

Using silicon implanted with nitrogen and carbon, Dörnen et al. [5.530] studied the formation of a PL line at 0.7456 eV. This line, together with a line at 0.767 eV, was reported before by Murakami et al. [5.531] to be correlated with electrically neutral substitutional nitrogen. Based on isotope shifts, the 0.7456 eV PL line was found to contain a single nitrogen and a single carbon atom. In the structure proposed, a carbon-nitrogen pair substitutes for a silicon atom. The nitrogen atom is bonded nearly planarly to three nearest silicon atoms with the carbon atom bridging to the fourth silicon atom. Later studies showed that other PL lines at 0.758, 0.7615, 0.7674, and 0.7724 eV contain also nitrogen and carbon and have similar properties [5.532]. Dörnen et al. suggested that they arise from a CNV complex modified by the presence of a loosely bonded impurity like oxygen.

Complexes with Oxygen

To establish a calibration standard for IR measurements, Itoh et al. [5.533] compared them with measurements based on the nuclear reaction of nitrogen with a proton beam which converts it to instable ^{11}C . They found that the concentration of IR-active N_2 pairs in CZ samples was significantly lower than expected from a calibration in FZ samples. The difference was attributed to the formation of unidentified nitrogen-related complexes.

After implantation of oxygen and nitrogen and annealing, Stein [5.534] found various absorption spectra which were not observed in samples implanted with only one of the impurities. In silicon doped with nitrogen and oxygen, Wagner et al. [5.535] found absorption bands at 802 and 996 cm^{-1} (RT). From a correlation to the concentrations of oxygen and nitrogen, the authors suggested an N_{2i}O_i complex. These conclusions were supported by Qi et al. [5.536] who found a close correlation of a third absorption band at 1026 cm^{-1} (RT) to the other two. Isotope experiments performed by Berg Rasmussen et al. [5.537] confirmed that nitrogen and oxygen are involved in the complex. Their theoretical investigations indicated that the vibration modes result from an N_{2i}O_i complex as shown in Figure 5.21. The binding energy of the interstitial oxygen atom to the N_2 complex was calculated to be 1.2 eV and no deep level was found in the band gap.

Complementary theoretical investigations of Gali et al. [5.489] indicated the alternative structure depicted schematically in Figure 5.22. According to their calculations, the first configuration is more stable in the neutral charge state whereas the second one is more stable in the positive charge state. As a consequence, the N_{2i}O_i complex was predicted to be bistable. In the far-infrared range, Yang et al. [5.538] identified lines at 240, 242, and 249 cm^{-1} (8 K) to arise from nitrogen-oxygen complexes. They were shown later by Yang et al. [5.539] to correlate to the lines at 802, 996, and 1026 cm^{-1} (8 K) in the mid-infrared range associated with N_{2i}O_i . Finally, it has to be mentioned that Yamanaka et al. [5.540] attributed the band at 1026 cm^{-1} to $\text{N}_{2i}\text{O}_{2i}$ rather than to N_{2i}O_i .

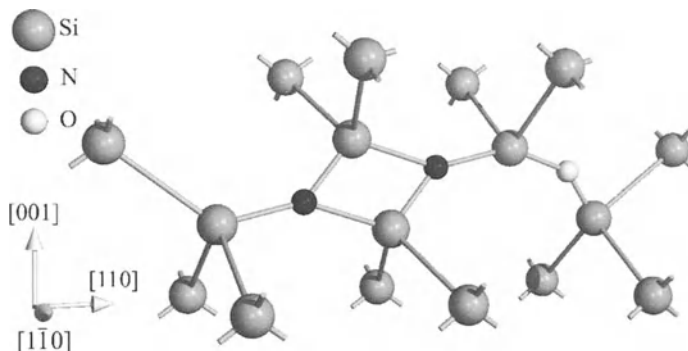


Figure 5.21: Schematic representation of the atomic configuration of the $(N_iN_i)O_i$ complex in silicon.

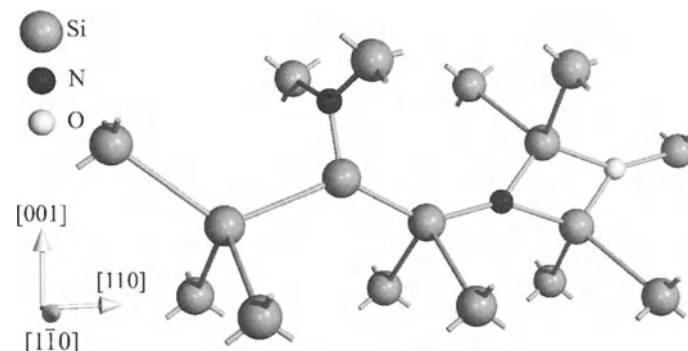


Figure 5.22: Schematic representation of the atomic configuration of the $(N_iO_i)N_i$ complex in silicon.

An annealing study performed by Wagner et al. [5.535] indicated that the concentration of N_{2i} pairs in nitrogen-doped CZ silicon increases during a 770 °C anneal for 10 min on the expense of $N_{2i}O_i$ complexes. They concluded from this observation that the oxygen atom is more loosely bound to the N_{2i} complex than the two nitrogen atoms therein. Similar observations were reported by Libbert et al. [5.541] at or above 700 °C. After an initial period of rapid transformation, the dynamics of this process was found to decrease indicating that a new equilibrium is established between the nitrogen-related complexes.

The core of the $N_{2i}O_i$ complex in Figure 5.22 is an NO ring similar to the N_{2i} ring shown schematically in Figure 5.19 with one of the nitrogen atoms replaced by an oxygen atom. According to the *ab-initio* calculations of Ewels et al. [5.542], such an NO structure has C_{1h} symmetry and acts as a deep donor. Subsequent work of Gali et al. [5.489] resulted in the identification of a defect which introduces a shallow single-donor level and has a binding energy only slightly smaller than that of an N_{2i} complex. Both investigations considered the NO complex as a possible precursors of the nitrogen-related family of “shallow thermal donors.” Adding one oxygen atom to the complex, stable structures with symmetries of C_s and C_{2v} were found. The energetically more stable C_{2v} -symmetric configuration, consisting of a trivalently bonded nitrogen interstitial between two oxygen interstitials, was considered as a possible core of one family of “shallow thermal donors.”

Investigating silicon doped with nitrogen and oxygen, Suezawa et al. [5.453] found several absorption lines in the wavenumber range from 190 to 270 cm⁻¹ (4.2 K). Based on a set of reactions fitted to the concentrations, they suggested that the dominant spectra resulted from ON₄ and ON₆ complexes.

In the work of Kageshima et al. [5.543], the attachment of interstitial oxygen atoms to N_{2i}V₂ complexes was investigated by *ab-initio* calculations. It was found that this reaction involves an energy gain of about 0.95 eV. It was indicated that the complex could serve as nucleation site for the capture of further oxygen atoms.

Electrical measurements performed by Hara et al. [5.504] indicated that nitrogen-oxygen complexes generated by indiffusion of nitrogen into CZ wafers may act as donors. During heat treatments at 700 °C and above, Yang et al. [5.544] found that the resistivity of *n*-type silicon increased. At first, this was suggested to arise from a nitrogen-oxygen complex acting as acceptor. But later investigations demonstrated that the resistivity increase was caused by a decreasing concentration of nitrogen-oxygen-related donor complexes [5.538].

Complexes with Dopants

To explain the effects of nitrogen implantation on the penetration of boron through gate oxides, Chao et al. [5.545] suggested that boron-nitrogen complexes form in the poly-silicon and give rise to an absorption frequency found at 670 cm⁻¹. Studying nitrogen-doped cast multicrystalline silicon, Yang et al. [5.546] found an absorption band at 1206 cm⁻¹ (RT) which appeared only in oxygen-lean samples with high concentrations of boron and nitrogen. Since carbon was not found to play a role, the absorption band was associated tentatively with boron-nitrogen complexes.

In the study of Aronowitz et al. [5.547], co-doping with boron and nitrogen was found to reduce the electrical activity of boron. Theoretical investigations reported by Zubkov et al. [5.373] and Aronowitz et al. [5.547] supported a stable pair of a substitutional boron atom and a nitrogen atom on an adjacent hexagonal interstitial site. The binding energy was calculated to be 2.34 eV. Configurations in which the interstitial nitrogen is further separated from the boron atom were found to be less stable. Pairs of boron and nitrogen atoms on neighboring substitutional sites and substitutional nitrogen with boron on a neighboring hexagonal site were found to be unstable. However, for a substitutional nitrogen separated by four or five bonds from a boron interstitial on a hexagonal site, the binding energy was found to increase up to 2.32 eV. In contrast, Zavodinsky et al. [5.548] found that substitutional boron and nitrogen bind with 1.6 eV. Boron-nitrogen interactions were also invoked by Ahmed et al. [5.549] to explain the depletion of electrically active boron in polysilicon layers at the interface to oxynitrides.

In a study of Aronowitz et al. [5.547], co-doping of silicon with indium and nitrogen was found to reduce the electrical activity of indium significantly. From their *ab-initio* calculations, Zubkov et al. [5.373] and Aronowitz et al. [5.547] found several stable complexes of indium and nitrogen atoms. Pairs of a substitutional indium atom and a substitutional nitrogen atom at nearest neighboring sites were reported to have a binding energy of about 1.54 eV. Further separation between the atoms reduces the binding energy to about 0.13 eV. For substitutional indium atoms with a nitrogen atom on a neighboring hexagonal interstitial site, a binding energy of 2.62 eV was given which even increases to 3.45 eV upon further separation. Pairs of an indium atom on a hexagonal interstitial site next to a substitutional nitrogen atom were found to be characterized by a binding energy of 4.36 eV which reduces to 2.91 eV upon separation by four or five bonds.

In the work of Aronowitz et al. [5.547], co-doping of silicon with gallium and nitrogen was found to reduce the electrical activity of gallium significantly. Based on *ab-initio* studies, Aronowitz et al. [5.547] reported that a complex of a substitutional gallium and a substitutional nitrogen atom is unstable. Pairs comprising a substitutional gallium atom and an interstitial nitrogen atom were found to be characterized by a binding energy of 1.73 eV at nearest neighboring distance which even increases to 1.82 eV upon separation by four or five bonds. Pairs of a gallium atom on a hexagonal interstitial site next to a substitutional nitrogen atoms were found to be characterized by a binding energy of 2.58 eV which reduces to 0.15 eV upon separation by four or five bonds.

Introducing a nitrogen implant in the fabrication of *n*-channel MOSFETs, an unanticipated change in the threshold voltage was observed by Zubkov et al. [5.373]. Further investigations, including *ab-initio* simulations, indicated that this effect was related to the formation of boron-indium-nitrogen complexes which reduced the electrically active dopant concentration in the channel. In a later study, Aronowitz et al. [5.547] confirmed that co-doping with boron, indium and nitrogen leads to a significant reduction of the electrical activity in comparison to doping with boron and indium. In addition, it was found that indium diffusion is suppressed in this combination while no such effect was observed when nitrogen or boron was omitted.

Extending their work on indium to gallium, Aronowitz et al. [5.547] found that co-doping with boron, gallium and nitrogen leads to a significant reduction of the electrical activity in comparison to doping with gallium and boron. *Ab-initio* simulations confirmed that gallium-boron-nitrogen complexes may be stable although the binding energy was significantly smaller than in the indium-boron-nitrogen case.

In a theoretical study of phosphorus-nitrogen interactions, Zavodinsky et al. [5.548] found that substitutional phosphorus and nitrogen bind with 2.4 eV.

5.8 Phosphorus

Phosphorus is by far the fastest-diffusing donor impurity. As such, its importance for the microelectronics decreased but it is still very important for power semiconductors. An additional feature of phosphorus being present in high concentrations is its ability to getter detrimental impurities.

In the following sections, the basic atomic configurations of phosphorus in silicon, its solubility, the diffusion behavior, and the formation of complexes are discussed in detail.

5.8.1 Basic Atomic Configurations

Substitutional Phosphorus

Already the first measurements of the lattice constant as a function of the concentration of phosphorus indicated that it occupies predominantly substitutional sites in the silicon lattice [5.15]. Phosphorus atoms on substitutional sites have one positive charge too many for the valence-bond structure of silicon. The electrons compensating the additional charge are expected to populate the conduction band. From Hall-effect measurements, a donor level at $E_c - 0.045$ eV was reported by Pearson and Bardeen [5.15] while Morin et al. [5.17] deduced a somewhat smaller ionization energy of 0.039 eV. From optical measurements, values of 0.045 [5.20], 0.0453 [5.550, 5.551], 0.04558 [5.552], 0.04559 [5.553], and 0.0503 eV [5.554] were deduced. In theoretical investigations, ionization energies of 0.0425 eV [5.555] and 0.0443 eV were estimated [5.476].

Studying samples with a high concentration of phosphorus by IR spectroscopy, an absorption band was found at 441 cm^{-1} (77K) [5.6, 5.23]. It was tentatively associated with substitutional, positively charged phosphorus although agreement with the theory of substitutional impurities of Dawber and Elliott [5.25, 5.26] was not perfect. In samples doped with phosphorus atoms in concentrations up to 10^{16} cm^{-3} , various photoluminescence lines were found to arise from the decay of excitons bound to neutral phosphorus atoms. The zero-phonon line can be found at 1.1499 eV [5.29], the transverse-acoustic and transverse-optic phonon sidebands have 18.7 and 58.0 eV lower energies.

From differences between experimentally determined line spacings in the spectrum of silicon doped with phosphorus and the corresponding line spacings computed from the effective-mass theory, Pajot and Stoneham [5.556] estimated that substitutional phosphorus is associated with a volume contraction of $\Delta V/V_{Si} = -8\%$. In contrast, similar investigations by Sasireka and Palaniyandi [5.555] indicated a volume expansion of $\Delta V/V_{Si} = 2.3\%$. Considering that X-ray measurements indicated unambiguously that phosphorus causes a contraction of the lattice [5.15, 5.557], a volume expansion would not really be expected. Theoretical investigations led to estimates of $\Delta V/V_{Si}$ between -2.5% and 4.9% [5.261, 5.558].

Phosphorus Interstitials

After quenching of samples into which gold or platinum was diffused at 1200 to 1300 °C, Scheerer et al. [5.559] found by EPR that the phosphorus atoms formed complexes which were tentatively identified as two different configurations of phosphorus-self-interstitial pairs. The EPR spectrum labeled SIR-1P(a) was suggested to arise from a substitutional phosphorus atom with a self-interstitial at a nearest site in a <111> direction. For the spectrum SIR-1P(b), a somewhat more remote position of the self-interstitial in a <100> or <110> direction from the substitutional phosphorus atom was suggested. In contrast, Chelyadinskii and Burenkov [5.560] concluded from their X-ray diffraction studies that phosphorus and self-interstitials do not form stable complexes and that they would form split interstitials bound solely by grid relaxation. Further direct experimental evidence for phosphorus interstitials is probably missing. Therefore, binding energies of phosphorus-self-interstitial complexes were obtained especially from fitting diffusion models to experimental data.

Reviewing phosphorus diffusion under non-equilibrium conditions, Park and Law [5.51] estimated an effective binding energy of 1.49 eV for intrinsic conditions. From simulating the diffusion of phosphorus at extrinsic concentrations, Baccus et al. [5.53] suggested a binding energy of 1.53 eV for neutral phosphorus-self-interstitial complexes.

The theoretical investigations of Car et al. [5.267] indicated that phosphorus atoms on hexagonal interstitial sites are energetically favored in comparison to phosphorus atoms on tetrahedral or bond-centered interstitial sites as well as in comparison to a self-interstitial on a tetrahedral site adjacent to a substitutional phosphorus atom. From a combination with self-interstitial formation energies taken from Car et al. [5.268], one obtains that the formation of a positively charged phosphorus atom on a tetrahedral interstitial site from a substitutional, positively charged phosphorus atom and a neutral self-interstitial in its minimum-energy configuration is associated with an energy gain of 3.0 eV which could be seen formally as a binding energy. Sugino and Oshiyama [5.561] concluded from their theoretical investigations that the most stable interstitial configuration for a neutral phosphorus interstitial has no symmetry and is located between the bond-centered site and the hexagonal site. Its formation energy was calculated to be 3.5 eV. In a later study, Liu et al. [5.562] found two energetically degenerate minimum-energy configurations for neutral phosphorus-self-interstitial pairs. The first one was a <110>-oriented split interstitial, the second one an approximately C_2 -symmetric inter-

stitial configuration in which the phosphorus atom forms four-fold bonds with nearby silicon atoms. The binding energy was calculated to be 1.5 eV with respect to a positively charged substitutional phosphorus atom and a negatively charged self-interstitial, 1.2 eV with respect to a neutral substitutional phosphorus atom and a neutral self-interstitial, and 0.8 eV at mid-gap with respect to a positively charged substitutional phosphorus atom and a neutral self-interstitial. For the positive charge state of the phosphorus interstitial, the hexagonal interstitial site and a $\langle 100 \rangle$ -oriented split interstitial were found to be characterized by energy reductions of 0.6 and 0.5 eV, respectively, with a positively charged substitutional phosphorus atoms and a neutral self-interstitial as reference point. For the negative charge state, the C_2 -symmetric configuration was found again to be energetically most favorable with a binding energy of 2.0 eV with respect to a negatively charged self-interstitial and a neutral substitutional phosphorus atom or 0.8 eV at mid-gap with respect to a positively charged substitutional phosphorus atom and a neutral self-interstitial.

Phosphorus-Vacancy Pairs

A further prominent configuration of phosphorus is the phosphorus-vacancy pair. Its EPR spectrum was reported first by Watkins et al. [5.563] in an electron-irradiation study and labelled Si-*E*. EPR and ENDOR investigations were finally used to identify it as to arise from a vacancy adjacent to a substitutional phosphorus atom in the neutral charge state of the defect [5.564]. The EPR center was later relabelled to Si-*G*8, but the name Si-*E* center remained in use and was even extended to other pairs of substitutional group-V impurities with adjacent vacancies.

The electronic levels assigned to the phosphorus-vacancy pair vary significantly. From Hall-effect measurements after irradiation experiments, ionization energies of 0.38 [5.565, 5.566] and 0.47 eV [5.567] were ascribed to the phosphorus-vacancy pair. It has to be remarked, though, that the ionization energy of 0.38 eV corresponds closely to levels of the carbon-phosphorus pairs discussed in Section 4.1.6. Watkins et al. [5.563] and Watkins and Corbett [5.564] deduced acceptor levels at respectively E_c - 0.44 eV and E_c - 0.43 eV from their EPR investigations. Thermally stimulated capacitance measurements reported by Walker and Sah [5.568] indicated again an acceptor level at E_c - 0.471 eV. From DLTS measurements, Kimerling et al. [5.569] estimated an ionization energy of 0.44 eV, Chantre et al. [5.570] 0.45 eV, and Bortherton and Bradly [5.571] 0.456 eV. Such ionization energies are very close to the suggested acceptor level of the divacancy at E_c - 0.43 eV. Using Laplace DLTS, Evans-Freeman et al. [5.572] could show that there are indeed two centers with similar emission rates associated in electron irradiated silicon with this level. Studying the annealing of Si-*E* centers, Boyarkina [5.573] suggested that their neutral charge state has a 16-fold degeneracy compared to that of the negative charge state. In positron-annihilation studies, the neutral and negative charge states of the phosphorus-vacancy pair were associated with positron lifetimes of 268 ps and 248 to 255 ps, respectively [5.75, 5.574–5.578]. From these lifetimes, Mäkinen et al. [5.576] concluded that the transition from the negative charge state to the neutral charge state is associated with an outward relaxation of the atoms surrounding the vacancy. A similar conclusion was derived before by Samara [5.579] from DLTS measurements.

Important parameters for the formation and migration of phosphorus-vacancy pairs are the binding energies of vacancies at the first and third coordination sites of a phosphorus atom. Estimates of the binding energy at the first coordination site were obtained from the kinetics of phosphorus-vacancy pairs after electron irradiation and from the diffusion behavior of phosphorus at high concentrations. From a comparison of the time constants of reorientation and decay of the Si-*E* center observed by EPR, Watkins and Corbett [5.564] estimated the binding energy of the vacancy at the first coordination site of the phosphorus atom to be $\gtrsim 0.85$ eV. Al-

ternatively, from the data of Saito et al. [5.580], they estimated a binding energy of $\gtrsim 1.05$ eV at the first coordination site. By a similar analysis, Hirata et al. [5.581] obtained a binding energy of 1.04 eV. Alternative estimates of the binding energy were obtained indirectly from measurements of the diffusion coefficient of phosphorus under inert and intrinsic conditions, the migration enthalpy of the phosphorus-vacancy pair, and an estimate for the formation enthalpy of vacancies. Based on such an analysis, Yoshida [5.582] suggested a binding energy of 1.42 eV. A similar analysis of Yoshida and Hasiguti [5.583] led to an estimate of 1.87 eV, and Fair and Tsai [5.584] determined values of 0.25, 0.55, and 0.81 eV for positively charged, neutral, and negatively charged phosphorus-vacancy pairs. The reliability of these values is limited because these early analyses were based on limited experimental data, the fallacious assumption that phosphorus diffuses entirely via vacancies, and unreliable values for the formation enthalpy of vacancies which is still in debate. In a similar way, Shaw [5.321] estimated a binding energy of 0.69 to 0.71 eV for positively charged phosphorus-vacancy pairs and 0.86 to 0.89 eV for neutral ones from a comparison of self-diffusion and phosphorus diffusion. The reliability of these values is likewise limited because of the fallacious assumption that phosphorus diffusion and self-diffusion proceed entirely via vacancies. Binding energies were also obtained by fitting diffusion models to experimental data. From the diffusion of phosphorus at high concentrations, Mathiot and Pfister [5.76] estimated 1.86 and 2.16 eV for the binding energies of the neutral and singly negatively charged phosphorus-vacancy pairs, respectively. Reviewing phosphorus diffusion under non-equilibrium conditions, Park and Law [5.51] estimated an effective binding energy of 0.6 eV under intrinsic conditions. From the study of phosphorus redistribution at extrinsic concentrations, Baccus et al. [5.53] suggested binding energies of 1.51 and 1.52 eV for the neutral and negative charge states of phosphorus-vacancy pairs, respectively. The theoretical investigations of Car et al. [5.267] with vacancy formation energies taken from Car et al. [5.268] resulted in binding energies of 2.21 and 1.7 eV for the neutral and positive charge states of the phosphorus-vacancy pair at mid-gap, respectively. In similar work, Nichols et al. [5.77] found the binding energy of a neutral pair of a vacancy at a next nearest neighboring site of a substitutional phosphorus atom to be 1.0 eV. In good agreement, Sugino and Oshiyama [5.561] calculated a binding energy of 1.1 eV for the same configuration. In a subsequent study, Nelson et al. [5.78] estimated a value of 1.05 eV for the binding energy and a barrier of also 1.05 eV for the exchange of sites between the vacancy and the substitutional phosphorus atom. Finally, Liu et al. [5.562] calculated binding energies of 1.19 and 1.49 eV at mid-gap for neutral and negatively charged phosphorus-vacancy pairs with respect to positively charged substitutional phosphorus and neutral vacancies.

For the binding energy at the third coordination site, Watkins and Corbett [5.564] suggested a value of 0.28 eV estimated from the Coulomb attraction of two opposite charges. This value agrees well with the 0.3 eV calculated by Sugino and Oshiyama [5.561].

Combining *ab-initio* simulations and kinetic Monte-Carlo simulations, Beardmore et al. [5.68] estimated a capture radius of 7.4 Å for the interaction of vacancies and substitutional phosphorus atoms at 900 °C which decreases slightly with increasing temperature.

5.8.2 Solubility

The phase diagram of the phosphorus-silicon system was compiled by Olesinski et al. [5.585]. Below the eutectic temperature of 1131 °C, the phosphorus in the silicon phase is in equilibrium with an SiP phase.

Solubility values for phosphorus were deduced from various experiments. Investigations based on deposition from the gas phase [5.81, 5.586–5.596] result in the formation of a phosphorus glass at the surface. The total concentration of phosphorus introduced under such con-

ditions into the silicon may be significantly higher since the solubility of phosphorus in silicon in equilibrium with P_2O_5 exceeds the binary solubility of phosphorus in silicon. In some of these investigations, evidence for the formation of an SiP phase was given [5.588, 5.594–5.596]. The formation of precipitates with compositions near to the equilibrium phase can also be expected after annealing of diffused samples at lower temperatures [5.592], in doped polysilicon [5.597], and after high-dose ion implantation and annealing with a sufficient thermal budget [5.92, 5.596, 5.598–5.603]. To obtain the concentration of electrically active atoms in equilibrium with an SiP phase, methods like resistivity measurements [5.596, 5.598], differential sheet-resistivity measurements [5.81, 5.586, 5.589–5.593, 5.599, 5.600], and combinations of resistivity and Hall-effect measurements [5.92, 5.594, 5.595, 5.597, 5.601–5.603] were used. Total concentrations were obtained by neutron activation [5.588], channeling RBS [5.595], and SNMS [5.603]. In addition, microindentation measurements were used [5.587]. It has to be noted, however, that only concentrations in precipitate-free regions adjacent to layers with SiP precipitates are characteristic for the total phosphorus concentration in equilibrium with an SiP phase. Otherwise, contributions from the precipitates being present would add to the total concentration measured. A summary of the solubility values reported can be found in Figure 5.23.

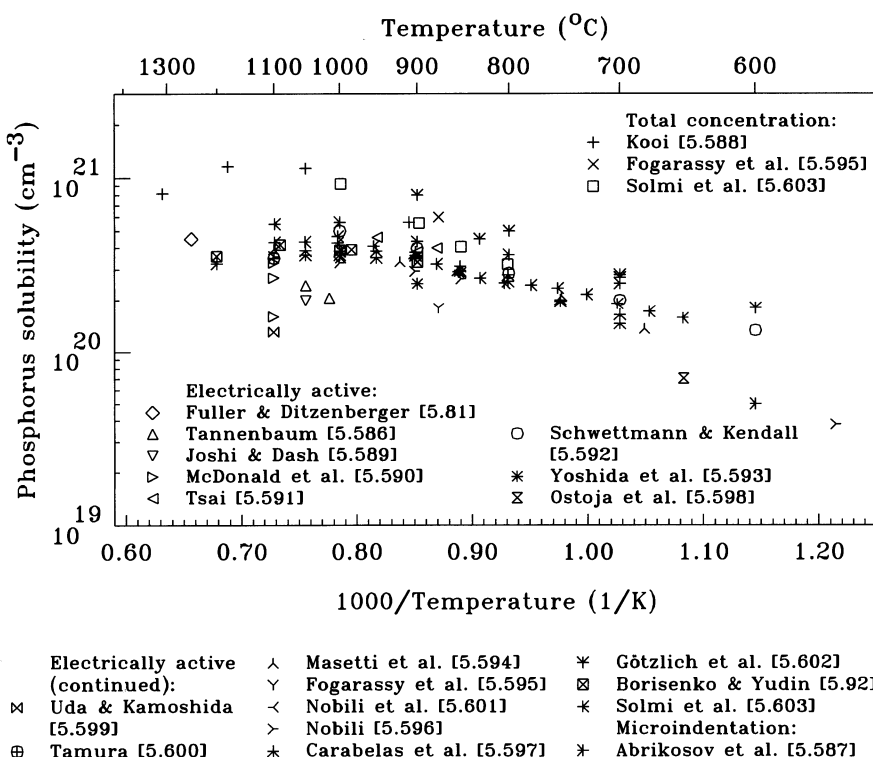


Figure 5.23: Solubility of phosphorus in silicon.

At this point, it seems appropriate to comment on the difference between total and electrically active phosphorus profiles measured especially after predeposition from the gas phase, and on potential differences between values for the total and electrically active concentration in equilibrium with an SiP phase. It was mentioned already above that the presence of a P_2O_5

phase can introduce more phosphorus atoms into the silicon than expected from the solid solubility. As a consequence, SiP precipitates will form at sufficiently high supersaturations of phosphorus. During the predeposition process, the growth of these precipitates is fed by a continuous supply of phosphorus from the gas phase via the phosphorus glass into the silicon. The rather flat carrier profiles in the high-concentration regime measured in several investigations are taken as a clear indication that they correspond closely to the concentration of electrically active phosphorus atoms in steady state with an SiP phase. The total concentrations, on the other hand, may exceed these values significantly since they include also the phosphorus in the SiP precipitates. Values for the total concentration of phosphorus atoms in steady state with SiP precipitates can, therefore, only be determined from precipitate-free regions or by subtracting the concentration of phosphorus in the precipitates. The chemical concentration values reported by Kooi [5.588] are likely to correspond to solubility values since they were measured after an annealing step following predeposition and in depths exceeding the extent of the surface layer with the precipitates. His values agree well with the solubility values of Mackintosh cited by Trumbore [5.604]. Unfortunately, no details of this work were given which makes it impossible to assess the significance of the results. In the work of Fogarassy et al. [5.595], channeling RBS was used to determine the lattice sites and phosphorus atoms found on interstitial sites were assumed to be in precipitates. Clear evidence for differences between total and electrically active concentrations in equilibrium with SiP precipitates was given by Solmi et al. [5.603] who used ion implantation to introduce the phosphorus and who found by SNMS measurements that the concentration of mobile phosphorus exceeds the electrical solubility. However, such differences were found only for temperatures exceeding about 750 °C.

5.8.3 Diffusion

Intrinsic Diffusion

A determination of the diffusion coefficient under nominally inert and intrinsic conditions was the goal of various investigations. Introduction of phosphorus occurred from the gas phase during diffusion [5.108, 5.605], from a doped oxide layer [5.111, 5.606], by epitaxial deposition of a phosphorus-doped layer [5.129, 5.131, 5.132, 5.607], by a predeposition step [5.608, 5.609], or by ion implantation [5.114, 5.116, 5.117, 5.124, 5.125, 5.217, 5.610–5.615]. For the characterization of the diffusion profile, junction delineation [5.116, 5.606, 5.608], electrical depth profiling [5.108, 5.114, 5.117, 5.607, 5.609, 5.610, 5.614], radiochemical depth profiling [5.111], neutron activation [5.605], and SIMS [5.124, 5.125, 5.129, 5.131, 5.132, 5.217, 5.611–5.613, 5.615] were used. A summary of the diffusion coefficients reported can be found in Figure 5.24.

At temperatures between about 900 and 1200 °C, the experimental data obtained in the numerous investigations agree well. The regression curve is given by

$$D_P^i = 1.03 \cdot \exp\left(-\frac{3.507 \text{ eV}}{k \cdot T}\right) \text{ cm}^2/\text{s} \quad (5.26)$$

with a 90% confidence interval for the activation energy from 3.42 to 3.6 eV. The 90% confidence interval for the diffusion coefficient is about +6.1/-5.8% of the regression curve at 1030 °C and increases to +12/-10% at 900 and 1200 °C. Additional measurements are expected with 90% confidence within a range of +74/-42% from 900 to 1200 °C.

For temperatures below 900 °C, especially the experiments of Christensen et al. [5.129, 5.131] and Zangenberg et al. [5.132], but also one of the data points of Haddara et al. [5.125] were significantly above the extrapolation of the regression curve. Similar phenomena were discussed already in Section 5.3.3 for the diffusion of boron. However, it is remarkable that

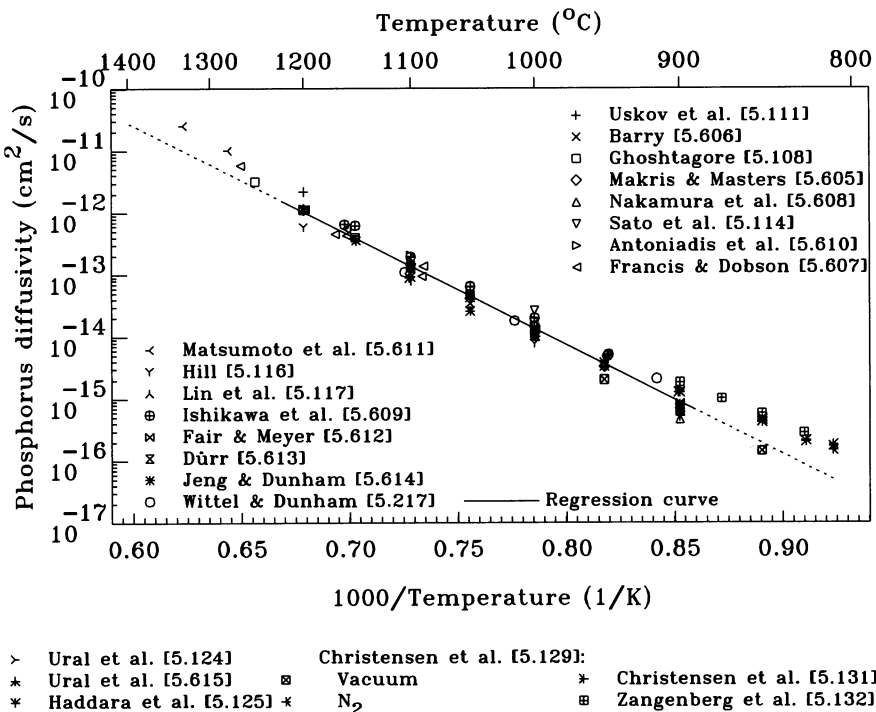


Figure 5.24: Diffusion coefficient of phosphorus under intrinsic and inert conditions in silicon.

the work of Haddara et al. and Christensen et al. agree for phosphorus and it remains to be decided whether the leveling-off is indicative of a change in the diffusion mechanism below about 920 °C which would be characterized by an activation energy of about 2.61 eV. Also remarkable is that the diffusion coefficients above 1250 °C exceed the extrapolated regression line by a factor of two. The same trend is obvious from the investigation of Kunz et al. [5.616] at 1306 °C although for their conditions an oxidation-retarded diffusion would be expected. However, the few data points available do not allow to conclude whether the increased diffusivities are due to experimental artifacts or due to physical effects.

Diffusion Mechanism

Quantitative estimates for the contributions of self-interstitials and vacancies to the diffusion of phosphorus under intrinsic conditions were obtained from experiments involving non-equilibrium conditions as discussed in Section 3.4.3. The values reported are listed in Table 5.4. Especially the recent experiments involving enhanced and retarded dopant diffusion established quite clearly that phosphorus diffuses at least at low concentrations predominantly via self-interstitials. Comparative studies indicated that phosphorus and aluminum have the largest f_I values of all dopants.

The situation might be different at high phosphorus concentrations as discussed further below in this section. Although essential features of high-concentration profiles can be reproduced assuming diffusion via self-interstitials only or with a Fermi-level-independent fractional diffusivity via self-interstitials, arguments were presented in several publications in favor of a significant increase of the diffusion via vacancies at high electron concentrations [5.53, 5.617–5.620].

This effect is likely to arise from the proximity of phosphorus atoms at high concentrations which reduces the enthalpies of formation and migration of vacancies. Similar effects have been observed experimentally for germanium, tin, arsenic, and antimony.

Table 5.4: Fractional diffusivity of phosphorus via self-interstitials. The abbreviations OSF, DifModel, RD, and DifComp for the experimental method refer to estimates from oxidation-enhanced diffusion with self-interstitial oversaturations estimated from OSF growth, from fitting dopant diffusion at high concentrations or under other non-equilibrium conditions, from the observation of retarded diffusion under non-equilibrium conditions, and from the comparison with the diffusivities of other dopants under non-equilibrium conditions, respectively. A description of the methods can be found in Section 3.4.3.

	f_I	Temperature range (°C)	Experimental method	Ref.
Fair	0.12	900–1200	OSF	[5.137]
Antoniadis & Moskowitz	0.38	1000	OSF	[5.138]
Antoniadis	0.37 - 0.38	1000	OSF	[5.621]
	0.53 - 0.57	1100		
	0.64 - 0.74	1200		
Matsumoto et al.	$12.9 \cdot \exp(-0.33 \text{ eV}/kT)$	950–1150	OSF	[5.139]
Matsumoto et al.	$156 \cdot \exp(-0.666 \text{ eV}/kT)$	950–1100	OSF	[5.140]
Tan et al.	0.7 - 0.8	1100–1200	OSF	[5.141]
Gösele & Tan	> 0.75	1150	RD	[5.142]
	> 0.95	1267		
Guerrero	$1/(1+3.2347 \cdot 10^{-4} \cdot \exp(0.9439 \text{ eV}/kT))$	900–1200	OSF	[5.143]
Mathiot & Pfister	$17.1 \cdot \exp(-0.51 \text{ eV}/kT)$	900–1250	DifModel	[5.76]
Fahey et al.	> 0.94	1100	DifComp	[5.622]
Collard & Taniguchi	$1/(1+5.8 \cdot 10^{-8} \cdot \exp(1.77 \text{ eV}/kT))$	900–1200	OSF	[5.623]
Yoshida et al.	0.585	1100	OSF	[5.624]
Morehead & Lever	0.9	700–1100	DifModel	[5.144]
Yoshida	0.236–0.681	1100	OSF	[5.625]
Mulvaney et al.	$0.0147 \cdot \exp(0.4 \text{ eV}/kT)$	900–1200	DifModel	[5.147]
Moynagh & Rosser	≥ 0.92	1100	DifComp	[5.149]
Okino & Yoshida	0.527	1100	DifComp	[5.626]
Packan & Plummer	$f_I^P \cdot 1.25$	900–1100	OSF	[5.150]
Park & Law	$1.45 \cdot \exp(-0.05 \text{ eV}/kT)$	800–1100	DifModel	[5.51]
Okino	0.92	1100	DifComp	[5.627]
Okino	0.93	1100	DifComp	[5.628]
Shimizu et al.	0.96	900 (-1100)	RD	[5.629]
Ural et al.	≥ 0.9	1000	DifComp	[5.630]
	≥ 0.88	1100		
Ural et al.	≥ 0.96	1000	DifComp	[5.124]
	≥ 0.96	1100		
Okino & Shimozaki	0.45	1100	OSF	[5.155]
Krause et al.	0.94–0.96	900	DifComp	[5.298]
	0.81–0.96	1044		
	0.83–1.00	1100		
	0.77–1.00	1290		

From an analysis in which parallel reactions were included in addition to the usual pair formation reactions, Vandenbossche and Baccus [5.631] estimated the partition constant for pairs with self-interstitials to be $\alpha_{PI} = 0.3$.

Extrinsic Diffusion

Information about the diffusion of phosphorus at extrinsic concentrations is available from the isoconcentration diffusion studies of Millea [5.367], Makris and Masters [5.605], Fair and Meyer [5.612], John and Law [5.632], and Wittel and Dunham [5.217]. In addition, diffusion coefficients were extracted from the phosphorus-arsenic-co-diffusion study of Solmi et al. [5.633]. These results are shown in Figure 5.25.

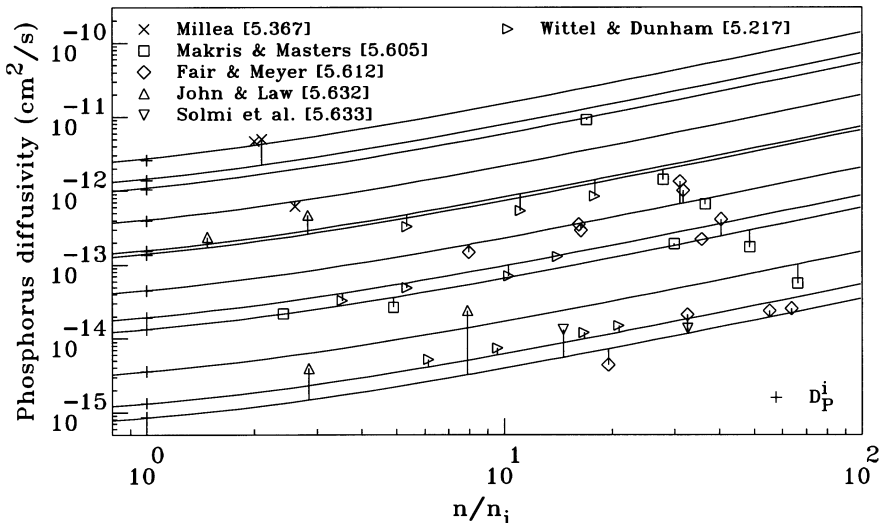


Figure 5.25: Dependence of the normalized diffusion coefficient of phosphorus in silicon on n/n_i for moderate dopant concentrations with $n/n_i \leq 20$. The full lines correspond, from top to bottom, to temperatures of 1250, 1215, 1200, 1150, 1105, 1100, 1050, 1015, 1000, 950, 915, and 900 °C.

To account for systematic differences between the reported diffusivities, the data sets were multiplied each by a constant so that the scaled values corresponded for intrinsic conditions to (5.26). The full lines were obtained by a numerical optimization using the data points in Figure 5.24 in addition to those in Figure 5.25, and are described by

$$D_P = 0.453 \cdot \exp\left(-\frac{3.482 \text{ eV}}{k \cdot T}\right) \text{ cm}^2/\text{s}$$

$$+ \frac{n}{n_i} \cdot 1.61 \cdot \exp\left(-\frac{3.647 \text{ eV}}{k \cdot T}\right) \text{ cm}^2/\text{s}. \quad (5.27)$$

Results from Boltzmann-Matano analyses [5.584, 5.586, 5.593, 5.634] were not included since phosphorus is known to cause a non-local influence on the concentration of the intrinsic point defects which does not allow a reliable reduction to isoconcentration conditions.

Within the temperature range of the experimental investigations, intrinsic diffusion is dominated by the Fermi-level-independent term while extrinsic diffusion is dominated by the linear term in n/n_i . Indication for a significant contribution of a quadratic term in n/n_i were not found within the concentration range covered by the investigations but cannot be excluded conclusively, on the other hand. A quadratic dependence of the diffusion coefficient on n/n_i has already been suggested by Fair and Tsai [5.584]. However, this dependence was called into question by Dutton et al. [5.635] who noted that it is a direct consequence of Fair and Tsai's

particular choice of a relationship between electron mobility and concentration to convert resistivity data to electron concentrations. They also pointed out that a much flatter increase of diffusivity with electron concentration would have been obtained with more recent mobility data. But various other models contained also a quadratic dependence of the diffusion coefficient on the electron concentration as an indispensable component to reproduce phosphorus diffusion at high concentrations. Although there is no direct experimental evidence available, one would expect from the existence of bound phosphorus-vacancy pairs that the proximity of phosphorus atoms at high concentrations causes a reduction of the enthalpies of formation and migration of vacancies. This should lead to an increase of the diffusion of phosphorus impurities at high electron concentrations in analogy to the effects observed for germanium, tin, arsenic, and antimony.

Tail Formation and Emitter-Push Effect

One of the most remarkable diffusion effects at high concentrations is the formation of a kink in phosphorus profiles separating the high-concentration region from a tail region with much higher diffusivity [5.162, 5.591, 5.636–5.638]. In these studies, the phosphorus was introduced from an oxygen-containing gas phase (POCl_3 , P_2O_5 , or $\text{PH}_3 + \text{O}_2$), associated with the formation of a phosphorus glass at the surface of the wafers. However, similar effects were observed when the phosphorus was introduced from a doped oxide [5.639] or by ion implantation [5.601]. The example in Figure 5.26 was reported by Masetti et al. [5.594] and shows the depth profile after a predeposition step at 920°C for 7 min from a POCl_3 source. It has all typical features like the tail region separated from the high-concentration region in which large parts of the profile are electrically inactive. Closely related to the formation of kink and tail is the enhanced diffusion of dopants below regions with high phosphorus concentrations [5.165, 5.640–5.644]. This effect leads to a broadening of the base region of bipolar transistors and, therefore, was named emitter-dip effect or emitter-push effect. It was observed even in depths of up to $12\text{ }\mu\text{m}$ [5.645] which excludes any direct interaction between the dopants.

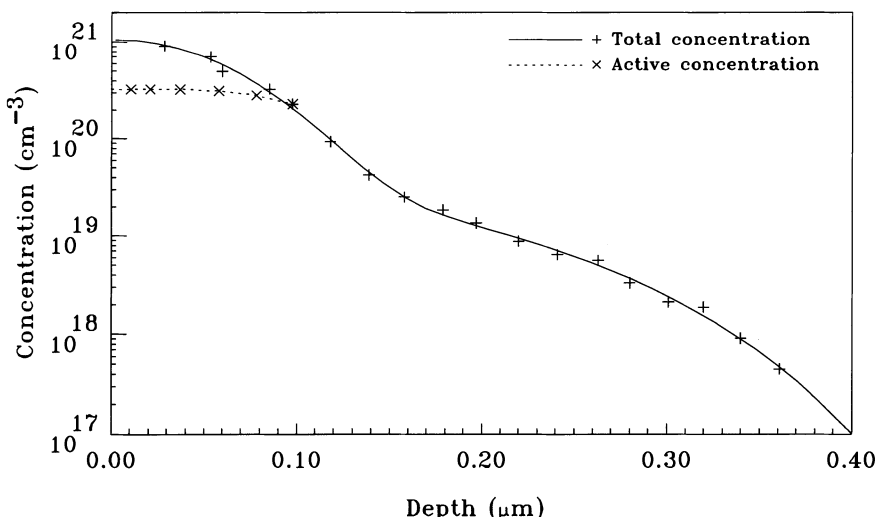


Figure 5.26: Total and electrically active concentrations of phosphorus after a predeposition step at 920°C for 7 min from a POCl_3 source [5.594] (symbols). The lines are only to guide the eyes.

The main reason for such effects is that the transport capacity of phosphorus exceeds that of the intrinsic point defects at high concentrations. In consequence, as discussed in Section 3.4.7, the concentrations of the intrinsic point defects will deviate from their equilibrium concentration and cause the observed phenomena. However, other phenomena like the formation of a phosphorus glass during deposition and the formation of phosphorus precipitates at high concentrations contribute in parallel to the diffusion phenomena and are extremely tedious to separate. As a consequence, also because of the technical relevance of high-concentration phosphorus diffusion from the 1970s up to at least the 1990s, there exists a vast body of experiments and controversial models.

Especially in the first years, a vacancy supersaturation caused by the climb of dislocations was made responsible for the observed diffusion effects. Such concepts became untenable after several reports made clear that the formation of kink and tail in phosphorus profiles and the emitter-push effect can be observed even when no extended defects are present [5.592, 5.593, 5.608, 5.646]. Several other models suggested at that time were discussed and refuted in a review of Hu [5.647]. The first models featuring phosphorus-vacancy pairs appeared after 1972 [5.592, 5.646]. They have not been brought to a quantitative stage but can be considered as predecessors of more elaborate models. One of them, a model developed by Fair and Tsai [5.584] became most popular. It was based on an experimentally determined relationship between the electrically active concentration and the total concentration of phosphorus and a functional dependence of the diffusion coefficient on the concentration derived from a Boltzmann-Matano analysis. Although the physical motivation of these relationships was questioned, e.g. in a review of Hu et al. [5.648], the model retained its usefulness for predicting one-dimensional profile shapes due to its empirical nature and simple structure.

Already before the work of Fair and Tsai, the methodology of diffusion-reaction equations discussed in Section 1.5.4 was developed by Yoshida et al. [5.593] and applied to the diffusion of phosphorus via the formation of phosphorus-vacancy pairs. A first numerical implementation was presented by Yoshida [5.649] who found that the model reproduces essential features of high-concentration phosphorus profiles but not the kink and tail observed experimentally. Yoshida [5.650] then revised his model and assumed that the vacancy-formation energy decreases with the second power of the phosphorus concentration. Like Yoshida, Mathiot and Pfister [5.651] concluded that diffusion via phosphorus-vacancy pairs cannot explain the features of measured phosphorus profiles. To reproduce plateau, kink, and tail they assumed that a percolation cluster forms in the high-concentration region due to the proximity of the phosphorus atoms [5.652]. Within this percolation cluster, the enthalpies of formation and migration of vacancies are reduced which leads to considerably enhanced redistribution of phosphorus. This explanation was adopted later also by Yoshida [5.653] as a physical motivation for the decrease of the vacancy-formation energy at high phosphorus concentrations in his model.

The core assumption of vacancy-based models for the diffusion of phosphorus at high concentration is that phosphorus-vacancy pairs form in regions of high phosphorus concentration. Their diffusion and dissociation in regions of lower phosphorus concentration leads to an oversaturation of vacancies in the bulk which explains the formation of the tail region as well as the emitter-push effect. This concept became doubtful after electron-microscopy investigations showed that extrinsic extended defects, i.e. agglomerates of self-interstitials, grow below regions with high phosphorus concentration [5.654–5.657]. In complementary diffusion experiments, high-concentration phosphorus diffusion was found to result in an enhanced diffusion of phosphorus [5.658] and boron [5.659], and a retarded diffusion of antimony [5.658–5.660] below but spatially separated from the phosphorus-doped region. These results confirmed that phosphorus diffusion causes an oversaturation of self-interstitials rather than of vacancies. But

there exists also controversial evidence from investigations in which it was found that phosphorus diffusion induces a shrinkage of preexisting stacking faults [5.661–5.663]. In addition, Fair [5.664] found that the junction depth obtained from phosphorus predeposition increases with concentration below about the solubility concentration, and decreases for higher concentrations. These experiments were taken up by Mathiot and Pfister [5.665] who suggested that the observed self-interstitial supersaturation originates from the precipitation of phosphorus above solid solubility while phosphorus diffusion would lead to an oversaturation of vacancies. A quantitative implementation of this concept, on the other hand, was not presented.

After phosphorus diffusion was found experimentally to induce an oversaturation of self-interstitials in the bulk rather than an oversaturation of vacancies, many models were developed based either entirely on the diffusion of phosphorus via self-interstitials [5.144, 5.666–5.668] or on a predominant diffusion via self-interstitials with a smaller vacancy contribution which eventually increases at high dopant concentrations [5.53, 5.617–5.620, 5.648, 5.669–5.672]. In the respective publications, important individual aspects of phosphorus diffusion were discussed but competing groups usually considered different aspects most important. On the other hand, points like the generation of point defects by the formation of the phosphorus glass during deposition, the precipitation of phosphorus at concentrations above solid solubility, or the formation of extended defects in ion-implanted samples were largely ignored. Some models also ignored that intrinsic point defects and the mobile phosphorus complexes may exist in several charge states. This alone reduces them to studies without real relevance to technological problems. It has to be remarked also that most studies used only very limited sets of experimental data for validation. Since at least qualitative agreement was claimed in all studies in which models were implemented numerically, one has to conclude that basic features of phosphorus profiles like the formation of kink and tail can be reproduced without problems even by largely incompatible models. This is substantiated by the investigation of Yoshida et al. [5.673] who reported that experimental profiles could be reproduced equally well by substantially different models. Considering the high number of parameters, it is generally problematic to assess the physical relevance of individual ones. On the other hand, for the application to technology-relevant problems, the most important aspect of models is their ability to reproduce experiments within a wide range of experimental conditions. This applies probably best to the models of Dunham [5.618], Ghaderi and Hobler [5.674], and Uematsu [5.620].

A major point excluded from most discussions in the literature is the electrically inactive part in the high-concentration region. In careful studies, Masetti et al. [5.594] found that the electrically active concentration depends only on temperature and not on predeposition conditions. Nobili et al. [5.601] complemented these investigations and reported the same electrical solubility limits after post-implantation annealing. But Masetti et al. also reported that the total concentration increases monotonically with time and POCl_3 partial pressure during predeposition processes. Solubility, as discussed in Section 1.6, is defined in a two-phase system. In the case of predeposition processes, the concentration of phosphorus in silicon in the system phosphorus-glass/silicon apparently exceeds that in the system SiP/silicon. Consequently, phosphorus precipitates will form and the flux of phosphorus atoms from the phosphorus glass into the silicon is fed to a large part into these SiP precipitates. This leads to the observed increase in the total concentration since it constitutes of the phosphorus atoms in the growing precipitates in addition to those on substitutional sites. In general, the assumption of a constant total concentration of phosphorus atoms at the interface often found often in the literature is simply inadmissible for modeling predeposition processes.

Phosphorus Interstitials

The diffusion of phosphorus interstitials was never characterized directly. Diffusion coefficients of phosphorus-self-interstitial complexes with activation energies of 2.7 eV [5.53] as they were reported from fitting diffusion models to experimental data reflect most likely only the ambiguities in such studies. The *ab-initio* calculations of Liu et al. [5.562] resulted in activation energies of 0.6 and 0.3 eV for the migration of phosphorus interstitials in the neutral and positive charge states. Allowing charge variations during the diffusion, the migration barrier for neutral phosphorus interstitials may be lowered to 0.2 to 0.3 eV. For phosphorus interstitials in the negative charge state, a significantly higher migration barrier of 1.4 eV was found.

Phosphorus-Vacancy Pairs

In their EPR measurements, Watkins and Corbett [5.564] found the reorientation of the electrically neutral vacancy-phosphorus pair to be governed by an activation energy of 0.93 eV. Reorientation requires already that the vacancy passes a third coordination site which is one of the rate-limiting steps for long-range diffusion. Thus, if the barrier against an exchange of sites between the vacancy and the phosphorus atom is smaller, the activation energy of reorientation should also be characteristic for long-range diffusion. Following the derivation of Yoshida [5.582], the reorientation time measured by Watkins and Corbett can be converted to the diffusion coefficient

$$D_{PV^0} = 9.7 \cdot 10^{-4} \cdot \exp\left(-\frac{0.93\text{eV}}{k \cdot T}\right) \text{cm}^2/\text{s} \quad (5.28)$$

of the neutral Si-*E* centers. In annealing studies after irradiation, Saito and Hirata [5.566] and Hirata et al. [5.675, 5.676] found that the deep level associated with phosphorus-vacancy pairs anneals out in the temperature range from 120 to 180 °C with an activation energy of 0.94 eV. Hirata et al. associated the annealing stage with the diffusion of the Si-*E* center. Later, another annealing stage was found by Hirata et al. [5.677] for temperatures above 200 °C, characterized also by an activation energy of 0.94 eV. Hirata et al. [5.581] finally associated this annealing stage with the diffusion of the Si-*E* center. There were also indications that the diffusivity of phosphorus-vacancy pairs depends on the donor concentration. Kimerling et al. [5.678] explained this effect by a much lower diffusivity of phosphorus-vacancy pairs in the negative charge state. From a later experimental study, Kimerling et al. [5.569] obtained activation energies of 0.95 and 1.25 eV for the neutral and the negative charge states of the phosphorus-vacancy pair, respectively. A quantitative explanation for the different activation energies was given on the basis of a doubled Coulomb attraction between the positively charged phosphorus atom and the doubly negatively charged vacancy which increases the diffusion barrier. When it can be assumed that the different time constants for the annealing out of the two charge states of the VP pair reflect just the different diffusion coefficients, it is possible to estimate that of the pairs in the negative charge state. It follows from the diffusion coefficient (5.28) of the neutral VP pairs and the ratio 0.015 of the inverse time constants of annealing out of negatively charged and neutral pairs around 150 °C in the form

$$D_{PV^-} = 0.096 \cdot \exp\left(-\frac{1.25\text{eV}}{k \cdot T}\right) \text{cm}^2/\text{s}. \quad (5.29)$$

Diffusion coefficients of phosphorus-vacancy pairs with activation energies of 2.5 to 3.0 eV [5.53, 5.76] as they were reported from fitting diffusion models to experimental data reflect most likely only the ambiguities in such studies.

In a theoretical study, Liu et al. [5.562] found that the reorientation of neutral phosphorus-vacancy pairs is characterized by an activation energy of 0.8 eV while the exchange of the vacancy and the phosphorus atom in the pair involves an energy barrier of 1.29 eV. For negatively charged pairs, the respective barriers calculated are 0.9 and 1.16 eV, respectively.

5.8.4 Complexes

Phosphorus Clusters and Phosphorus-Vacancy Complexes

Irradiation of phosphorus-doped samples was found by Wada et al. [5.679] to give rise to a level at $E_c - 0.3$ eV which correlated with the concentration of phosphorus and was tentatively associated with PV_2 . From measurements of the annealing behavior of electron-irradiated samples, Lugakov and Luk'yanitsa [5.680] postulated likewise that complexes of two or three vacancies bound to a phosphorus atom form by the reaction of phosphorus-vacancy pairs with divacancies. After electron irradiation of phosphorus-doped FZ and CZ samples, Suezawa et al. [5.681] observed several absorption lines between 800 and 1600 cm^{-1} which were not observed in undoped samples. The largest peak at 1156.6 cm^{-1} (7 K) was shown to reflect the concentration of phosphorus. Its kinetics was found to be identical to that of lines at 1316.2 cm^{-1} and 1563.3 cm^{-1} . All three lines as well as lines at 1150.6, 1309.2, and 1312.5 cm^{-1} were shown to have the same ground state and were suggested to arise from the same defect. From the differences between CZ and FZ samples, it was concluded that the defect is vacancy-related, and from the dependence of their intensities on the electron dose, the spectra were tentatively associated with PV_2 .

In EPR investigations of phosphorus-doped, electron-irradiated samples, Sieverts and Ammerlaan [5.682] found several spectra which they labeled Si-NL1 to Si-NL3 and which were shown to arise from defects containing two phosphorus atoms. From a detailed analysis of the EPR spectrum, Si-NL1 was suggested to arise from the positive charge state of a C_{2v} -symmetric defect formed by a vacancy with two phosphorus atoms at nearest neighboring sites. The likewise C_{2v} -symmetric Si-NL2 EPR spectrum was suggested to arise from the positive charge state of two substitutional phosphorus atoms with a silicon lattice atom in between. From theoretical considerations and the occurrence as a function of the Fermi level which changed during irradiation, its donor and double donor level were estimated to be about 0.4 and 0.1–0.2 eV below the conduction band. Annealing of vacancy-phosphorus pairs was found by Nylandsted Larsen et al. [5.683] to occur around 425 K, accompanied by the formation of a new defect with a donor character and a level at $E_c - 0.15$ eV. This defect was tentatively associated with a P_2V complex.

Based on the similarities of phosphorus and arsenic deactivation after ion implantation and laser annealing, Takamura et al. [5.684, 5.685] suggested that phosphorus deactivates by the formation of phosphorus-vacancy complexes accompanied by the ejection of self-interstitials. Investigating P_nV complexes theoretically, Chadi et al. [5.686] concluded that such complexes with $n > 2$ have exothermic formation energies. But they suggested the DP(2) and DP(4) structures of not connected phosphorus atoms (similar to the structures discussed in Section 5.10.4) to be energetically most stable and responsible for deactivation at high phosphorus concentrations. As an alternative, Kim et al. [5.687] suggested from *ab-initio* studies that two configurations of a neutral pair of substitutional phosphorus atoms on neighboring sites are energetically more favorable than the DP(2) and DP(4) complexes.

Phosphorus-Self-Interstitial Complexes

To reproduce the redistribution of phosphorus during post-implantation anneals, Schroer and Uematsu [5.688] invoked the formation of P_iI clusters in analogy to the boron-interstitial clus-

ters discussed in Section 5.3.4. The necessity to include such and probably larger phosphorus-interstitial clusters in simulations of post-implantation annealing was corroborated also in subsequent publications of Uematsu [5.689] and the work of Keys et al. [5.690].

Pairs with Acceptors, Carbon, Nitrogen, and Oxygen

As expected from a donor, experimental evidence for pair formation with boron and indium was reported in the literature. These studies were discussed in Sections 5.3.4 and 5.6.4, respectively.

The remarkable properties of phosphorus-carbon pairs, which form multi-configurational defects in silicon, were discussed already in Section 4.1.6. Complexes of phosphorus with nitrogen were discussed in Section 5.7.4.

After annealing of phosphorus-doped, electron-irradiated samples, the appearance of a vibration band at $910/916 \text{ cm}^{-1}$ (RT/10 K) was observed by Svensson and Lindström [5.691], accompanied by a decrease of the intensities of the VO-related spectra. Subsequently, Lindström et al. [5.692] found an other band at $859/864 \text{ cm}^{-1}$ (RT/10 K) which was shown to originate from a different charge state of the same defect. The level associated with the change was tentatively associated with a DLTS peak at $E_c - 0.27 \text{ eV}$. Complementary ODMR investigations indicated a perturbed VO defect involving two phosphorus atoms. The structure suggested comprises a VO-like core in which the oxygen atom is bonded to two phosphorus atoms.

5.9 Arsenic

Arsenic as an impurity is characterized by a rather high solubility and a rather low diffusivity. These properties make it ideally suited for applications in microelectronics with its trend towards shallower and shallower profiles. In the following sections, the basic atomic configurations of arsenic in silicon, its solubility, the diffusion behavior, and the formation of complexes are discussed in detail.

5.9.1 Basic Atomic Configurations

Substitutional Arsenic

Arsenic atoms on substitutional sites have one positive charge too many for the valence-bond structure of silicon. The electrons compensating the additional charge are expected to populate the conduction band. From Hall-effect measurements, a donor level at $E_c - 0.049 \text{ eV}$ was deduced by Morin et al. [5.17]. The same ionization energy was derived by Holland and Paul [5.258] from the temperature dependence of resistivity measurements. Optical measurements resulted in ionization energies of 0.0533 [5.554], 0.0534 eV [5.693], 0.0535 [5.550, 5.551], 0.0537 [5.20], and 0.5376 eV [5.553], and a determination via measurements of dielectric loss resulted in an estimate of 0.0496 eV [5.22]. In theoretical investigations, ionization energies of 0.043 [5.259], 0.0493 eV [5.555], and 0.0531 eV [5.476] were calculated.

In samples doped with arsenic atoms in concentrations up to 10^{16} cm^{-3} , various photoluminescence lines were found to arise from the decay of excitons bound to neutral arsenic atoms. The zero-phonon line can be found at 1.1492 eV [5.694], the transverse-acoustic and transverse-optic phonon sidebands have 18.7 and 58.0 eV lower energies.

From differences between line spacings in the spectrum of arsenic-doped silicon and the corresponding values computed from the effective-mass theory, Pajot and Stoneham [5.556] estimated that substitutional arsenic is associated with a volume expansion of $\Delta V/V_{Si} = 4\%$. Similar investigations by Sasireka and Palaniyandi [5.555] based on *ab-initio* calculations and

a comparison to the experimentally determined ionization energy indicated a volume expansion of $\Delta V/V_{Si} = 1.7\%$ associated with substitutional arsenic. EXAFS measurements resulted in estimates for the distance between substitutional arsenic atoms and their silicon neighbors of $2.41 \pm 0.01 \text{ \AA}$ [5.695–5.699]. These values correspond to volume expansions $\Delta V/V_{Si}$ of 6.2% to 7.6% in comparison to the volume associated with silicon atoms. Theoretical investigations led to estimate of $\Delta V/V_{Si}$ of 2.6% [5.558] and 8.9% [5.261]. As an apparent contradiction, a lattice contraction perpendicular to the surface was measured by X-ray diffractometry [5.697, 5.700]. This discrepancy was explained by Cargill III et al. [5.700] and Parisini et al. [5.697] on the basis of a model of Yokota [5.701] which predicts that the lattice strain in a semiconducting material results both from a size effect and from an electronic effect. For the deformation-potential constant for the conduction-band edge, which has a prominent role in this theory, values of $3.3 \pm 0.7 \text{ eV}$ [5.700] and $3.5 \pm 0.9 \text{ eV}$ [5.697] were estimated from the experiments.

An important parameter for diffusion and activation is the fraction of arsenic dopants incorporated at substitutional sites. While this parameter is nearly unity for most other dopants, there are indications that this is not necessarily the case for arsenic. A first indication came from backscattering experiments which showed that only about 50% to 75% of the arsenic atoms after implantation and annealing or after implantation at elevated temperatures were on substitutional sites [5.702, 5.703]. However, Rimini et al. [5.704] and Haskell et al. [5.705] soon found that the analysis beam caused 20% to 40% of the arsenic atom to move to off-substitutional lattice sites during the analysis. Their own measurements indicated that more than 90% would be substitutional. A physical explanation for this effect was given by Swanson et al. [5.706] who suggested that the displacement of arsenic from substitutional sites is caused by the trapping of vacancies generated by the irradiation. Nylandsted Larsen and Borisenko [5.707] finally reported substitutional fractions between 95% and 99% after annealing even for arsenic doses of 10^{16} cm^{-2} . Non-negligible concentrations of pairs with intrinsic point defects were also assumed by Borucki [5.708] to explain a reduced electron concentration observed already at low arsenic concentrations. Later, they were postulated by Heinrich et al. [5.709] and Novell and Law [5.710] to explain the experiments of Fahey et al. [5.622] which led to inconsistent estimates for f_I of arsenic and to interpret the much less pronounced diffusion enhancement of arsenic observed after ion implantation. However, it has to be noted that the inconsistent estimates for f_I were explained equally well by Cowern [5.711] and Vandebosse and Baccus [5.631] by alternative reactions in parallel to the usual pair-formation reactions.

Arsenic Interstitials

Arsenic interstitials were probably never identified experimentally. From fitting a diffusion model to experimental data, Novell and Law [5.710] estimated the binding energy of a positively charged pair of an arsenic atom and a self-interstitial to be 1.9 eV. Simulating arsenic redistribution at high concentrations, Baccus et al. [5.53] found a binding energy of 1.53 eV for neutral arsenic-self-interstitial pairs. To reproduce the diffusion of arsenic during post-implantation annealing, Hane et al. [5.58] used a binding energy of 1.0 eV for such pairs. Finally, to interpret the effects of a homogeneous arsenic background concentration on the formation of {113} defects induced by a low-dose silicon implantation, Brindos et al. [5.712] invoked the formation of arsenic-self-interstitial pairs for which a binding energy of 0.95 eV was determined from the experiment. From theoretical investigations, Sugino and Oshiyama [5.561], concluded that the most stable interstitial configuration for a neutral arsenic interstitial has no symmetry and is located between the bond-center site and the hexagonal site. Its formation energy was calculated to be 3.4 eV.

Arsenic-Vacancy Pairs

The neutral charge state of a substitutional arsenic atom adjacent to a lattice vacancy was identified by Elkin and Watkins [5.713] using EPR and ENDOR techniques and labelled Si-*G*23. In arsenic-doped silicon, Sonder and Templeton [5.567] observed by Hall-effect measurements a level at $E_c - 0.46$ eV after irradiation which they did not discuss further but which, from similarities to the other dopants investigated, should be associated with arsenic-vacancy pairs. According to the review of Watkins [5.271], Troxell found that As-V introduces an acceptor level at $E_c - 0.47$ eV. Based on DLTS investigations after electron irradiation, the arsenic-vacancy pair was suggested to act as an electron trap with a level at $E_c - 0.42$ eV [5.714] or $E_c - 0.34$ eV [5.715]. It has to be mentioned, though, that both levels are close to levels reported for the arsenic-carbon complexes discussed in Section 4.1.6. In the positron-annihilation studies of Polity et al. [5.75], Saarinen et al. [5.578], and Ranki et al. [5.716], arsenic-vacancy pairs were associated with positron lifetimes of 248, 248, and 240 ps, respectively.

An important parameter for the formation of arsenic-vacancy pairs is the binding energy of a vacancy at the first coordination site of the substitutional arsenic atom. Combining their own data with those of Elkin and Watkins [5.713], Hirata et al. [5.581] estimated a lower limit of 1.23 eV for the neutral arsenic-vacancy pair. From DLTS studies, Evvaray [5.714] concluded that the dissociation energy of neutral and negatively charged arsenic-vacancy pairs is 1.4 and 1.7 eV, respectively. Alternative estimates for the binding energy were obtained indirectly from measurements of the diffusion coefficient of arsenic under inert and intrinsic conditions, the migration enthalpy of the arsenic-vacancy pair, and an estimate for the formation enthalpy of vacancies. Based on such an analysis, Yoshida [5.582] suggested a binding energy of 1.68 eV for the arsenic-vacancy pair. A similar analysis by Yoshida and Hasiguti [5.583] led to an estimate of 1.87 eV. The reliability of these values is limited because these early analyses were based on limited experimental data, the fallacious assumption that arsenic diffuses entirely via vacancies, and unreliable values for the formation enthalpy of vacancies which is still in debate. In a similar way, Shaw [5.321] estimated a binding energy of 0.69 to 0.71 eV for neutral arsenic-vacancy pairs from a comparison of self-diffusion and arsenic diffusion. The reliability of this value is likewise limited because of the fallacious assumption that arsenic diffusion and self-diffusion proceed entirely via vacancies. Other estimates were obtained from fitting diffusion models to experiments. This way, Novell and Law [5.710] estimated the binding energy of a neutral arsenic-vacancy pair to be 1.4 eV. From the study of arsenic redistribution at extrinsic concentrations, Baccus et al. [5.53] suggested binding energies of 1.51 and 1.52 eV for the neutral and negative charge states of arsenic-vacancy pairs. To reproduce the diffusion of arsenic during post-implantation annealing, Hane et al. [5.58] used binding energies of 1.0 and 1.6 eV for neutral and negatively charged arsenic-vacancy pairs. In theoretical investigations, binding energies of 1.17 eV [5.717], 1.2 eV [5.77], 1.21 eV [5.718], 1.31 eV [5.719], 1.4 eV [5.720], and 1.6 eV [5.561] were calculated for neutral pairs with respect to a neutral vacancy well-separated from a neutral substitutional arsenic atom. For vacancies at a third-nearest neighboring site, binding energies of 0.25 eV [5.718], 0.36 eV [5.717], and 0.7 eV [5.561] were reported. Exchanges of sites between the vacancy and the substitutional arsenic atoms were found to require surmounting an energy barrier for which heights of 0.55 eV [5.718] and 0.58 eV [5.717] were calculated.

Combining *ab-initio* simulations and kinetic Monte-Carlo simulations, Beardmore et al. [5.68] estimated a capture radius of 6.9 Å for the interaction of vacancies and substitutional arsenic atoms at 900 °C which decreases slightly with increasing temperature. From *ab-initio* calculations of the electronic structure, Mueller et al. [5.720] found a double acceptor level, an acceptor level, and a donor level 0.63, 0.47, and 0.33 eV above the valence band, respectively.

5.9.2 Solubility

The phase diagram of the arsenic-silicon system was compiled by Olesinski and Abbaschian [5.721]. Below the eutectic temperature of 1097 °C, the arsenic in the silicon phase is in equilibrium with an orthorhombic SiAs phase.

Solubility values for arsenic in silicon were deduced from various experiments. Most reliable seem studies in which the formation of the SiAs equilibrium phase was actually observed after ion implantation and annealing with a sufficient thermal budget [5.722, 5.723]. In similar studies [5.1, 5.92, 5.596, 5.602, 5.724–5.727] as well as in highly doped polysilicon layers [5.597], the formation of arsenic precipitates can at least be assumed. In these investigations, carrier-concentration profiles were obtained by sheet resistance and Hall-effect measurements [5.92, 5.596, 5.597, 5.602, 5.722, 5.722, 5.725–5.727] or spreading-resistance profiling [5.1, 5.724] while the concentration of chemical arsenic concentrations was characterized by secondary neutral-mass spectroscopy [5.723]. The solubility values obtained are shown in Figure 5.27.

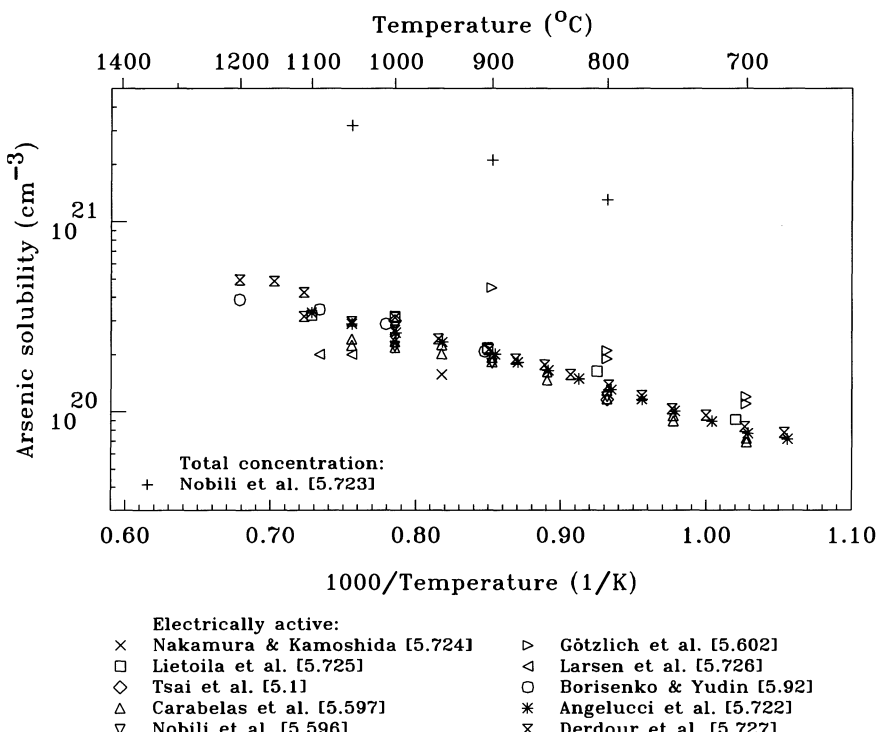


Figure 5.27: Solubility of arsenic in silicon.

Comparing electrical and chemical solubilities, a gross difference is apparent. This difference is usually associated with small, electrically inactive clusters which coexist with the electrically active substitutional arsenic atoms and which cannot be observed by TEM. However, there is some uncertainty associated with the question when the formation of these small clusters actually takes place.

The critical stage is cooling-down at the end of the thermal process. During this phase, the solid solubility is continuously lowered. However, inactivation of arsenic atoms requires

the formation of complexes. This process is limited by the diffusion coefficient of the arsenic atoms which rapidly decreases during cooling-down. An infinitely fast quench would guarantee that the electrically active concentration does not change. In the case of slow cooling rates as during the furnace processes typically used for the majority of the electrical measurements, on the other hand, the arsenic atoms have more time to agglomerate and the electrically active concentration measured will be lower than the electrical solubility concentration at the nominal process temperature. This was shown convincingly by Nylandsted Larsen et al. [5.728] and Ranki et al. [5.729] who investigated the effects of different cooling rates on the final electrical activity. However, in their investigations, it is not sure that steady-state conditions were present at the onset of fast cooling.

5.9.3 Diffusion

Intrinsic Diffusion

Diffusion coefficients of arsenic under nominally inert and intrinsic conditions were determined in various investigations. Introduction of the arsenic occurred from the gas phase during diffusion [5.284, 5.730–5.734], by a predeposition step [5.609], or by ion implantation [5.116, 5.124, 5.610, 5.611, 5.735, 5.736]. For the characterization of the diffusion profiles, several methods were used. In a number of publications, delineation of p-n junctions was used and eventually combined with electrical measurements of the surface concentration [5.116, 5.284, 5.730–5.732, 5.735]. Potentially more reliable result were obtained by differential sheet-resistivity measurements [5.609], spreading-resistance profiling [5.610], depth profiling of a radioactive tracer [5.733], neutron activation analysis [5.734], or depth profiling by SIMS [5.124, 5.611, 5.736]. A summary of the diffusion coefficients reported can be found in Figure 5.28 together with the regression curve

$$D_{As}^i = 8.85 \cdot \exp\left(-\frac{3.971 \text{ eV}}{k \cdot T}\right) \text{ cm}^2/\text{s} \quad (5.30)$$

derived from these measurements. In addition to the low-concentration data, intrinsic diffusion coefficients from a Boltzmann-Matano analysis have been included in which the profiles were obtained by diffusion from the gas phase and measured by radioactivation techniques [5.737]. Also included are the results from a quasi-Boltzmann-Matano analysis after ion implantation [5.738] although some of the experimental conditions have to be taken *cum grano salis*. Whenever only an Arrhenius expression was given instead of experimental data [5.734], the points shown in Figure 5.28 were computed from this Arrhenius expression for the temperatures mentioned in the text.

The activation energy ranges with a confidence level of 90% from 3.9 to 4.04 eV. The 90% confidence interval for the diffusion coefficient is about +5.4/-5.2% of the regression curve at 1100 °C and increases to +12/-11% at the melting point and +15/-13% at 850 °C. Additional measurements are expected with 90% confidence within a range of +65/-39% of the regression curve at 1100 °C which increases slightly to +66/-40% at the melting point and +68/-40% at 850 °C.

Pressure Dependence

Pressure-dependent diffusion studies at high arsenic concentrations performed by Nygren et al. [5.739] resulted in an estimate of the activation volume of about $(-0.47 \pm 0.07) \cdot V_{Si}$. According to the theoretical investigations of Sugino and Oshiyama [5.740], this would be consistent with a vacancy mechanism but not with an interstitial mechanism.

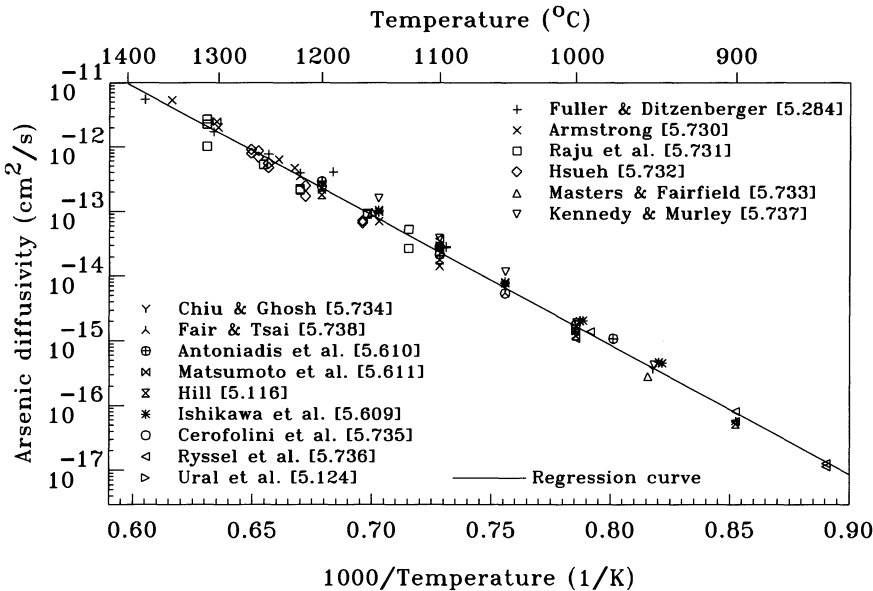


Figure 5.28: Diffusion coefficient of arsenic under intrinsic and inert conditions in silicon.

Diffusion Mechanism

An important parameter for diffusion simulation is the fractional diffusivity via self-interstitials. The values reported in the literature are compiled in Table 5.5. The more reliable estimates obtained from comparisons with the diffusivities of other dopants under non-equilibrium conditions indicate that arsenic is one of the few impurities which diffuse in a considerable degree via self-interstitials as well as via vacancies. Remarkably, the analysis of Fahey et al. [5.622] resulted in two incompatible estimates for the lower and upper limits. The reasons discussed in the literature include parallel reactions to the usual pair-formation reactions [5.631, 5.711] and non-negligible concentrations of pairs [5.709, 5.710]. An experimental verification is still missing. Interpreting their own experiments, Ural et al. [5.124] estimated that concerted exchange might contribute up to 36% to the diffusion of arsenic at 1000 °C, and up to 61% at 1100 °C.

Table 5.5: Fractional diffusivity of arsenic via self-interstitials. The abbreviations OSF, DifModel, and DifComp for the experimental method refer to estimates from oxidation-enhanced diffusion with self-interstitial oversaturations estimated from OSF growth, from fitting dopant diffusion at high concentrations or under other non-equilibrium conditions, and from the comparison with the diffusivities of other dopants under non-equilibrium conditions, respectively. A description of the methods can be found in Section 3.4.3.

	f_I	Temperature range (°C)	Experimental method	Ref.
Fair	0.09	975–1200	OSF	[5.137]
Antoniadis & Moskowitz	0.35	1090	OSF	[5.138]
Matsumoto et al.	$2.47 \cdot \exp(-0.184 \text{ eV}/kT)$	950–1150	OSF	[5.139]
Matsumoto et al.	$42 \cdot \exp(-0.542 \text{ eV}/kT)$	950–1100	OSF	[5.140]
Tan et al.	0.5	1160	OSF	[5.141]
Guerrero	$1/(1+4.081 \cdot 10^{-3} \cdot \exp(0.7189 \text{ eV}/kT))$	950–1100	OSF	[5.143]

	f_I	Temperature range (°C)	Experimental method	Ref.
Mathiot & Pfister	$29.5 \cdot \exp(-0.6 \text{ eV}/kT)$	900–1250	DifModel	[5.76]
Fahey et al.	< 0.22	1100	DifComp	[5.622]
	> 0.44			
Cowern	0.4	1100	DifComp	[5.711]
Mulvaney et al.	0.35	950–1200	DifModel	[5.147]
Moynagh & Rosser	0.43 - 0.56	1100	DifComp	[5.149]
Vandenbossche & Baccus	0.21	1100	DifComp	[5.631]
Ghaderi et al.	0.27–0.3	900–1100	DifComp	[5.152]
Ural et al.	0.35–0.55	1000	DifComp	[5.124]
	$\leq 0.17\text{--}0.47$	1100		

From an analysis in which parallel reactions were included in addition to the usual pair-formation reactions, Cowern [5.711] estimated the partition constant α_{AsI} to be in the range $3 \lesssim \alpha_{AsI} \lesssim 10$. A similar analysis by Vandenbossche and Baccus [5.631] led to the estimates $0.01 \leq \alpha_{AsV} \leq 0.02$ and $5 \leq \alpha_{AsI} \leq 7$.

Extrinsic Diffusion

Information about the diffusion of arsenic at extrinsic concentrations is available from the isoconcentration diffusion studies of Masters and Fairfield [5.733] and Nylandsted Larsen et al. [5.741, 5.742], the Boltzmann-Matano analyses of Fair and Weber [5.743] and Murota et al. [5.744, 5.745], and a quasi-Boltzmann-Matano analysis of Fair and Tsai [5.738]. In case of the Boltzmann-Matano analyses and the quasi-Boltzmann-Matano analysis, the field enhancement (3.82) was subtracted from the data reported. The results are shown in Figure 5.29. The full lines were obtained by a numerical optimization using all data points in Figure 5.28 in addition to those in Figure 5.29, and are described by

$$\begin{aligned} D_{As} = & \frac{n}{n_i} \cdot 8.0 \cdot \exp\left(-\frac{3.964 \text{ eV}}{k \cdot T}\right) \text{ cm}^2/\text{s} \\ & + \left(\frac{n}{n_i}\right)^2 \cdot 4.82 \cdot \exp\left(-\frac{4.823 \text{ eV}}{k \cdot T}\right) \text{ cm}^2/\text{s}. \end{aligned} \quad (5.31)$$

No indication was found for a significant Fermi-level independent contribution to the diffusion coefficient. For intrinsic concentrations, the term with the quadratic dependence in n/n_i is on the order of one percent of the term with the linear dependence. The existence of a quadratic term is in agreement with the results of Hoyt and Gibbons [5.746], Nylandsted Larsen et al. [5.726], and Shiryaev et al. [5.747] who reported that modeling of arsenic redistribution during RTA requires at least a quadratic term in n/n_i to describe the profile form for concentrations above about $2 \cdot 10^{20} \text{ cm}^{-3}$ correctly.

Diffusion of arsenic at concentrations exceeding about $2 \cdot 10^{20} \text{ cm}^{-3}$ led to quite inconsistent experimental as well as theoretical results. For total concentrations $C_T \lesssim 20 \cdot n_i$, as discussed above, an approximately linear increase of the diffusion coefficient with the total dopant concentration can be expected. At higher concentrations, as shown in Figure 5.30, the normalized diffusion coefficient D/D^i was found in the early Boltzmann-Matano analyses to level off and even to decrease [5.737, 5.743–5.745]. This retardation of the diffusion at high total concentrations was attributed to the formation of immobile clusters. In striking contrast, Nylandsted Larsen and his coworkers [5.741, 5.742] reported that the diffusion coefficient increases sharply

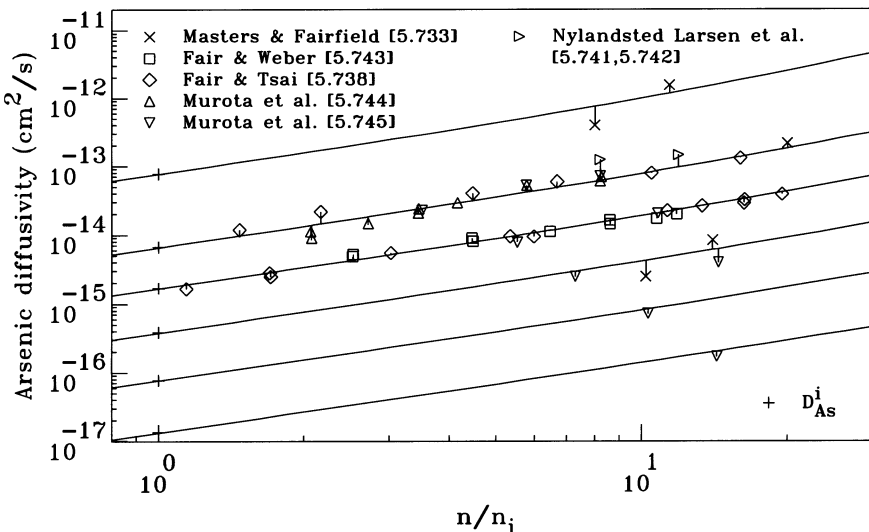


Figure 5.29: Dependence of the normalized diffusion coefficient of arsenic in silicon on n/n_i for moderate dopant concentrations with $n/n_i \leq 20$. The full lines correspond, from top to bottom, to temperatures of 1150, 1050, 1000, 950, 900, and 850 °C.

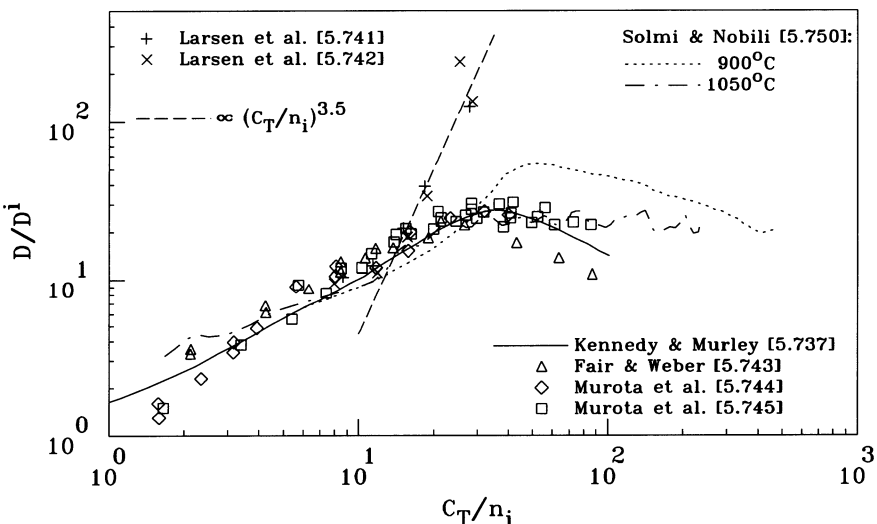


Figure 5.30: Dependence of the normalized diffusion coefficient of arsenic in silicon on the normalized total concentration C_T for high dopant concentrations.

for total concentration of $C_T \gtrsim 20 \cdot n_i$. At the same time, the activation energy for arsenic diffusion decreases to about 1.7 eV. Following the earlier suggestion of Mathiot and Pfister [5.748], based on the percolation theory of Stauffer [5.749], this increase was interpreted to arise from the proximity of the dopant atoms which reduces the formation and migration enthalpies of vacancies in their vicinity and which leads to an enhanced diffusion. The recent Boltzmann-Matano analyses of Solmi and Nobili [5.750] show differences to the early Boltzmann-Matano

analyses and disagree again totally with the work of Nylandsted Larsen and his coworkers.

Equally controversial were theoretical contributions. The Lattice Monte-Carlo simulations of Dunham and Wu [5.751] reproduced the rapid increase in the diffusivity of arsenic at concentrations above $2 \cdot 10^{20} \text{ cm}^{-3}$ observed by Nylandsted Larsen and coworkers and confirmed the percolation model. In contrast, Ramamoorthy and Pantelides [5.719] rejected the idea of a percolation cluster and argued that a percolation cluster would dissolve rapidly due to dopant agglomeration. Instead, they proposed that mobile As_2V clusters would be responsible for the observed diffusion enhancement. The probabilistic diffusion simulations of List and Ryssel [5.752] based on an attractive interaction between vacancies and impurities confirmed the formation of dopant agglomerates postulated by Ramamoorthy and Pantelides. List and Ryssel criticized the work of Dunham and Wu for too short simulation times which, they argued, did not create a physically meaningful statistical ensemble. Instead, they showed that a non-attractive interaction between dopants and vacancies would lead to the observed dopant dependence. Using dopant-impurity binding energies from *ab-initio* simulations, Bunea and Dunham [5.753] revised the original work of Dunham and Wu. They confirmed the diffusivity enhancement at very high impurity concentrations observed experimentally for short simulation times but confirmed also that the diffusivity enhancement would reduce drastically for long simulation times due to the formation of impurity clusters. As_2V complexes were suggested to be mobile and to contribute substantially to arsenic diffusion at high concentrations. But they were found not to be responsible for the high diffusivity enhancement found experimentally. Xie and Chen [5.754] came to the same conclusion and noted that the strongly enhanced diffusion is found in experiments as well as in simulations only for short-time annealings. Formation of dopant clusters, beginning with As_2V , leads to a break-up of the percolation cluster and to the retarded diffusion observed experimentally and found also in theoretical investigations. Although this picture explains the diffusion experiments, it is, at first glance, not consistent with recent experimental evidence from the activation kinetics of arsenic doped layers. Ranki et al. [5.729] found that pre-existing arsenic complexes (mainly As_3V) in *in-situ* ion-implantation-doped MBE-grown layers with arsenic concentrations from $1.5 \cdot 10^{20}$ to $3.5 \cdot 10^{20} \text{ cm}^{-3}$ dissolve nearly completely during annealing at 800 to 900 °C. The formation of arsenic-vacancy complexes, on the other hand, was found to occur during cooling-down with the final activation determined by the ramping rate.

Arsenic-Vacancy Pairs

By EPR measurements, Elkin and Watkins [5.713] found the reorientation of electrically neutral arsenic-vacancy pairs to be governed by an activation energy of 1.07 eV. Reorientation requires already that the vacancy passes a third coordination site which is one of the rate-limiting steps for long-range diffusion. Thus, if the barrier against an exchange of sites between the vacancy and the phosphorus atom is smaller, the activation energy of reorientation should also be characteristic for long-range diffusion. Following the derivation of Yoshida [5.582], the reorientation time measured by Elkin and Watkins can then be converted to an estimate

$$D_{\text{AsV}^0} = 6.1 \cdot 10^{-4} \cdot \exp\left(-\frac{1.07 \text{ eV}}{k \cdot T}\right) \text{ cm}^2/\text{s} \quad (5.32)$$

for the diffusion coefficient of the neutral arsenic-vacancy pairs. In annealing studies after irradiation of arsenic-doped samples, Hirata et al. [5.675, 5.676] found the a deep level associated with AsV pairs to anneal out below 200 °C. For this process, activation energies of 1.5 eV [5.676] and 1.27 eV [5.675] were reported. Hirata et al. associated the annealing stage with the diffusion of the arsenic-vacancy pair. Later, another annealing stage was found by

Hirata et al. [5.677] for temperatures above 200 °C. Hirata et al. [5.581] finally associated this annealing state with the diffusion of the arsenic-vacancy pair. Its activation energy of 1.07 eV is identical to that obtained by Elkin and Watkins from EPR investigations. Studies of the formation of As₂V complexes in highly arsenic-doped, electron-irradiated samples allowed Ranki et al. [5.716] to estimate an activation energy of 1.3 eV for the diffusion of AsV.

From their theoretical investigations, Pankratov et al. [5.717] obtained an activation energy of 0.76 eV. They also found that diffusion of arsenic via vacancies proceeds nearly entirely via a pair-diffusion mechanism. In contrast, a somewhat higher value of 1.19 eV was calculated for the migration enthalpy of the AsV pair by Xie and Chen [5.718]. Diffusion coefficients of arsenic-vacancy pairs with activation energies of more than 3.0 eV [5.53], as they were reported from fitting diffusion models to experimental data, reflect most likely only the ambiguities in such studies.

In agreement with the concept of diffusion in a percolation cluster, Xie and Chen [5.718] calculated that the presence of another arsenic atom at a fifth neighboring site reduces the barrier for the migration of the vacancy in this direction from 1.3 eV to 0.45 eV.

5.9.4 Complexes

Arsenic Clusters and Arsenic-Vacancy Complexes

It was mentioned already above that the formation of SiAs precipitates can account only for a fraction of the arsenic atoms found electrically inactive at high concentrations. For the difference, the formation of small clusters is usually considered to be responsible. Several such models have been presented to explain diffusion and activation measurements with clusters comprising two [5.58, 5.697, 5.743, 5.748, 5.755–5.758], three [5.1, 5.2, 5.58, 5.758], or four [5.647, 5.750, 5.758–5.762] arsenic atoms, or with coexisting clusters of different sizes [5.763]. In some publications, a specific atomic structure was postulated. Prominent examples are the As₂V clusters which were assumed to exist in an electrically neutral form [5.58, 5.743, 5.748, 5.756, 5.757] or positively charged [5.697] at process temperature, and the As₄ cluster in which the arsenic atoms occupy the four inner sites of the unit cell shown in Figure 1.4 [5.647].

Based on EXAFS measurements and theoretical investigations, Pandey et al. [5.764] suggested an As₄V complex with four arsenic atoms surrounding a vacancy. Considering also second-nearest neighboring sites, Allain et al. [5.765] concluded from their EXAFS measurements that the clusters formed below 750 °C consist of 7 ± 4 arsenic atoms around a vacancy. An ion-channelling analysis reported by Chu and Masters [5.766] indicated that deactivation of arsenic atoms is associated with a displacement of the arsenic atoms by approximately 0.15 Å from regular lattice sites. These results were interpreted tentatively in terms of an As⁺V=As⁺ complex but it was emphasized that the data cannot be used as evidence to support any models. In similar studies, Erbil et al. [5.695] and Brizard et al. [5.767] found average displacements of 0.13 and 0.23 Å, respectively. Combining their ion-channelling data with their previous EXAFS measurements, Brizard et al. [5.767] concluded that large As_mV_n complexes, with m up to 12 and n up to 5, may form. An X-ray standing-wave spectroscopy study performed by Herrera-Gomez et al. [5.768] confirmed that the arsenic atoms remain basically at substitutional sites which was interpreted in terms of complexes forming coherently in the lattice. An involvement of vacancies in the formation of arsenic clusters was inferred also from the experiments of Rousseau et al. [5.769]. These authors reported that deactivation in a surface-near arsenic-

doped layer induced an enhanced diffusivity of a boron marker layer below. This enhanced diffusion was argued to be caused by self-interstitials generated by the reaction



Already before, it was found by Osvenskii et al. [5.770] and Hirota et al. [5.771] that the annealing of a supersaturated solution of arsenic atoms at low temperatures causes the formation of extrinsic dislocation loops correlated with the deactivation of arsenic. These experiments were interpreted in favor of a precipitation of arsenic at the loops but it may be speculated that the loops are rather remnants of the self-interstitials generated by the deactivation. On the other hand, in the subsequent analysis of Brindos et al. [5.772], no dependence on the dose of the implanted arsenic atoms was found and the observed diffusion enhancement was associated with the presence of implantation-induced extended defects. Annealing studies based on the implantation of arsenic into samples preamorphized by the implantation of germanium indicated that high concentrations of arsenic may even lead to a reduction of the concentration of self-interstitials. Complementary positron-annihilation studies performed by Lawther et al. [5.773] confirmed the presence of vacancies in the arsenic-doped layer. Correlating the concentration of vacancies measured with the concentration of deactivated arsenic atoms led to the estimate that the average number of arsenic atoms per complex is larger than two. In a subsequent investigation, Myler et al. [5.774] concluded from a comparison of positron annihilation in arsenic and arsenic-doped silicon that the vacancies found have arsenic atoms in their immediate vicinity. Combining measurements of positron lifetime and electron-momentum distribution, Saarinen et al. [5.578] found As_3V complexes in a concentration of about 10^{17} cm^{-3} in CZ bulk crystals doped with arsenic to a concentration of 10^{20} cm^{-3} . In a later study, Ranki et al. [5.729] found that the majority of the arsenic atoms in *in-situ* ion-implantation-doped MBE-grown layers with arsenic concentrations from $1.5 \cdot 10^{20}$ to $3.5 \cdot 10^{20} \text{ cm}^{-3}$ are in As_3V and As_5V_2 complexes. These complexes were found to dissolve during heat treatment even at temperatures of 800 to 900 °C. They reform eventually during the cooling-down period with the final arsenic activation determined by the ramping rate. Positron-annihilation measurements in highly-doped, electron-irradiated samples allowed Ranki et al. [5.716] to follow the formation of As_2V at about 450 K which in turn convert to As_3V around 700 K. The investigations allowed also to estimate a value of 2.0 eV for the migration energy of As_2V . An injection of self-interstitials driving the diffusion of arsenic was invoked by Chakravarthi et al. [5.762] to reproduce their diffusion experiments. From the suggested involvement of vacancies in arsenic complexes, one would have expected a marked influence of excess vacancies or self-interstitials on the kinetics of the formation of such complexes. However, the experiment of Solmi et al. [5.775] gave no indication that either excess has a measurable influence on the deactivation kinetics of arsenic. In a subsequent experiment, Solmi et al. [5.776] investigated the time dependence of transient-enhanced diffusion of arsenic at 800 °C. To separate the contributions of implantation damage and arsenic clustering, implantation damage was annealed in one sample by an RTP step at 1030 °C for 5 s. The results gave clear evidence of a generation of self-interstitials by the arsenic deactivation.

Because of their technological importance, theoretical investigations were performed to elucidate the energetics of arsenic complexes. Based on theoretical investigations and EXAFS measurements, Pandey et al. [5.764] suggested an As_4V complex with four neutral arsenic atoms surrounding a vacancy to be energetically stable with an energy gain of 1.4 eV in comparison to four well-separated, neutral substitutional arsenic atoms. This is already remarkable since it means that substitutional arsenic might not be the most stable configuration. In the study of Ramamoorthy and Pantelides [5.719], a variety of complexes of arsenic atoms and intrinsic point defects were considered. They found that arsenic atoms show in thermal equilibrium only

negligible tendency to cluster without intrinsic point defects. On the other hand, arsenic atoms were found to bind strongly to vacancies. For As_nV complexes, the binding energy per arsenic atom was calculated to vary from 1.31 eV for AsV to 1.54 eV for As_4V . Similarly, for complexes with divacancies, the binding energy per arsenic atom was found to vary from 1.69 eV for As_2V_2 to 1.57 eV for As_6V_2 . As a consequence, As_nV_m complexes with $n > 2 \cdot m$ were found to have negative formation energies. This would, as Ramamoorthy and Pantelides expressed it, mean that “As-doped silicon is metastable at any doping level and the preparation of electrically active samples is possible only because of kinetic limitations.” Chadi et al. [5.686] confirmed As_nV complexes with $n > 2$ to have exothermic formation energies. But they suggested the DP(2) and DP(4) structures of not connected arsenic atoms (similar to the structures discussed in Section 5.10.4) to be energetically most stable and responsible for deactivation at high arsenic concentrations. Berding and Sher [5.777] also found negative formation energies for As_3V and As_4V complexes with the zero of energy defined by electrically neutral, substitutional arsenic atoms in an otherwise undisturbed lattice. In addition, they took ionization and entropy contributions into account. Of all the arsenic complexes, As_4V was found to have the most important influence on deactivation. Neither the DP(2) complexes nor V_2As_6 complexes were found to have significant contributions in equilibrium. Considering complexes of neutral arsenic atoms and vacancies, Xie and Chen [5.718] calculated that a pair of two substitutional arsenic atoms would have a negative binding energy of -0.13 eV so that such clusters are unlikely to form. For an As_2V cluster, the most stable configuration with a binding energy of 2.55 eV was found for two arsenic atoms at next neighboring sites of a vacancy. The migration energy of the vacancy in a hexagonal ring with two arsenic atoms at nearest neighboring sites of each other or of the vacancy was calculated to be 2.0 eV [5.718, 5.754]. For As_3V and As_4V , Xie and Chen [5.778] obtained binding energies of 4.08 and 5.34 eV, respectively. Both have negative formation energies in agreement with the work of Pandey et al. and Ramamoorthy and Pantelides. Xie and Chen [5.718, 5.778] also investigated AsV_2 complexes, the most stable of which was found to comprise an arsenic atom at a next neighboring site to one of the vacancies of a divacancy. However, its binding energy of 1.82 eV was very close to that of a divacancy. Concentrating on the formation of an As_4V complex by the reaction (5.33), Fastenko et al. [5.761] calculated from first principles a barrier of 1.4 eV for the process which is significantly less than the barrier for the Frenkel-pair process which is at least as large as the sum of the formation energies of vacancies and self-interstitials. Continuum simulations based on this reaction showed good agreement with experimental data. In the work of Mueller et al. [5.720], the energetics of As_nV_m complexes were investigated by similar *ab-initio* methods. Neutral arsenic dimers and trimers were found to bind only weakly with 0.035 and 0.017 eV per neutral arsenic atom. When vacancies are involved in the clusters, the arsenic atoms were found to bind with about 1.5 eV per arsenic atoms to the vacancy or divacancy. All these complexes were found to have levels in the band gap. As_2V was found to be mobile with a migration barrier of 2.0 eV. As an alternative, Kim et al. [5.687] suggested from *ab-initio* studies that two configurations of a neutral pair of substitutional arsenic atoms on neighboring sites are energetically even more favorable than the DP(2) and DP(4) complexes.

Arsenic-Self-Interstitial Complexes

The ability of arsenic to form complexes with silicon self-interstitials was demonstrated by the experiments of Brindos et al. [5.779] based on the kinetics of {113} defects during annealing of silicon-implanted samples at 750 °C. It was found that the number of self-interstitials trapped in the {113} defects reduces when the arsenic background concentration increases. From a correlation, the formation of As_2I complexes was suggested. In the theoretical investigation

of Ramamoorthy and Pantelides [5.719], arsenic atoms were found to bind with 0.19 eV per arsenic atom in As_2I and with 0.49 eV in As_4I . In a later experiment, Brindos et al. [5.780] compared the effects of high-dose arsenic implants on the supersaturation of self-interstitials in the bulk with the effects of silicon implants and arsenic/silicon co-implants. It was found that the additional silicon implants lead during annealing at 750 °C to a reduction of the oversaturation of self-interstitials in comparison to the arsenic-only implants and, for annealing times of 10 min and less, also in comparison to the silicon-only implants. In addition, it was found that the arsenic/silicon co-implants lead to a reduction of the density of extended defects. Both effects were explained by the authors by a formation of arsenic-self-interstitial complexes which reduce the initial oversaturation of self-interstitials and which eventually break up at longer process times. The existence of immobile arsenic-self-interstitial complexes was also invoked by Kim et al. [5.781] to explain the suppression of arsenic diffusion during the initial stage of post-implantation annealing. From the suggested involvement of self-interstitials in arsenic complexes, one would have expected a marked influence of excess vacancies or self-interstitials on the kinetics of the formation of such complexes. However, the experiment of Solmi et al. [5.775] gave no indication that either excess has a measurable influence on the deactivation kinetics of arsenic.

Ion Pairs and Complexes with Carbon and Oxygen

As expected from a donor, the formation of substitutional pairs with acceptors was observed experimentally. Complexes with boron and indium atoms were discussed in Sections 5.3.4 and 5.6.4, respectively.

The remarkable properties of arsenic-carbon pairs which form multi-configurational defects in silicon were discussed already in Section 4.1.6.

After annealing of arsenic-doped, electron-irradiated samples, Hallberg et al. [5.782] observed that a band at $908/915 \text{ cm}^{-1}$ (RT/10 K) appears at the expense of VO-related spectra. In analogy to a similar defect observed before in phosphorus-doped silicon, the bands were attributed to a VO-like defect in which the oxygen atom is bonded to two arsenic atoms. The existence of arsenic-oxygen complexes, although most likely with other configurations, can be inferred also from the observations of Ono et al. [5.250] who reported retarded diffusion and enhanced solubility of oxygen at 800 °C in samples with an arsenic background concentration of $1.1 \cdot 10^{19} \text{ cm}^{-3}$. Similar observations were reported by Takeno et al. [5.251] who estimated a binding energy of about 1.0 eV from their experiments.

5.10 Antimony

Antimony has a low diffusivity, comparable to arsenic, albeit a significantly smaller solubility. Besides tin, it is the only impurity which is known to diffuse nearly entirely via a vacancy mechanism. As such, antimony is used intensively for diffusion studies. Despite its smaller equilibrium solubility in comparison to arsenic, there are indications (e.g. [5.783–5.785]) that significantly higher electrically active concentrations can be achieved at least in non-equilibrium situations. This makes antimony a viable candidate for source/drain engineering in VLSI applications. In the following sections, the basic atomic configurations of antimony in silicon, its solubility, the diffusion behavior, and the formation of complexes are discussed in detail.

5.10.1 Basic Atomic Configurations

Substitutional Antimony

Antimony atoms on substitutional sites have one positive charge too many for the valence-bond structure of silicon. The electrons compensating the additional charge are expected to populate the conduction band. From Hall-effect measurements, a donor level at $E_c - 0.039$ eV was deduced by Morin et al. [5.17]. From optical measurements, values of 0.426 eV [5.554], 0.043 eV [5.20], and 0.04251 eV [5.551] were deduced. In theoretical investigations, ionization energies of 0.031 eV [5.555], 0.0317 eV [5.476], and 0.44 eV [5.259] were calculated.

In samples doped with antimony atoms in concentrations up to 10^{16} cm⁻³, various photoluminescence lines were found to arise from the decay of excitons bound to neutral antimony atoms. The zero-phonon line can be found at 1.1501 eV [5.694], the transverse-acoustic and transverse-optic phonon sidebands have 18.7 and 58.0 eV lower energies.

Antimony is generally assumed to occupy predominantly substitutional sites. Backscattering experiments performed by Chou et al. [5.703] indicated a substitutional fraction of 88% to 94% after a heat treatment at 1250 °C. A high substitutional fraction of implanted and annealed antimony atoms was also confirmed by the Mössbauer spectroscopy investigations of Weyer et al. [5.786].

Because of the larger covalent radius of antimony in comparison to silicon, an expansion of the lattice around an antimony atom can be expected. From differences between experimentally determined line spacings in the spectrum of antimony-doped silicon and the corresponding line spacings computed from the effective-mass theory, Pajot and Stoneham [5.556] estimated that substitutional antimony is associated with a volume expansion of $\Delta V/V_{Si} = 17\%$. Similar investigations by Sasireka and Palaniyandi [5.555] based on *ab-initio* calculations and a comparison to the experimentally determined ionization energy indicated a volume expansion of $\Delta V/V_{Si} = 23.3\%$ associated with substitutional antimony. EXAFS measurements resulted in estimates for the distance between substitutional antimony atoms and their silicon neighbors of 2.528 to 2.54 Å [5.787–5.790]. These values correspond to volume expansions $\Delta V/V_{Si}$ of 24.2% to 25.9% in comparison to the volume associated with silicon atoms. Theoretical investigations led to the conclusion that substitutional antimony occupies a volume which is by $\Delta V/V_{Si} = 23\%$ larger than that of silicon atoms [5.261].

Antimony Interstitials

Antimony interstitials were probably never observed directly. However, ¹¹⁹Sn atoms on interstitial sites were observed in the Mössbauer-spectroscopy investigations of Weyer et al. [5.786]. They originated from the decay of radioactive ¹¹⁹Sb atoms and are expected to inherit their environment. From theoretical investigations, Sugino and Oshiyama [5.561] concluded that the most stable interstitial configuration for a neutral antimony interstitial is close to a ⟨100⟩-oriented split interstitial. Its formation energy was calculated to be 3.9 eV.

Antimony-Vacancy Pairs

The neutral charge state of a substitutional antimony atom adjacent to a lattice vacancy was identified by Elkin and Watkins [5.713] using EPR and ENDOR techniques and labelled Si-G24. This structure was supported by the Mössbauer spectroscopy investigations of Damgaard et al. [5.791], too.

Antimony-vacancy pairs were also associated with electronic levels. After irradiation of samples doped with antimony, Sonder and Templeton [5.567] found a level at $E_c - 0.43$ eV by Hall-effect measurements which they associated with antimony-vacancy pairs. According to the review of Watkins [5.271], Troxell found that Sb-V introduces an acceptor level at $E_c - 0.44$ eV. From DLTS investigations, Evwaraye [5.792] suggested that antimony-vacancy pairs act as electron traps with a level at $E_c - 0.39$ eV while Awadelkarim et al. [5.715] tentatively associated an electron trap at $E_c - 0.51$ eV with them. In the work of Kringsjø and Nylandsted Larsen [5.793], an acceptor state was found after proton irradiation of $\text{Si}_{1-x}\text{Ge}_x$ samples which was identified to originate from antimony-vacancy pairs. It had an activation energy which varied from $E_c - 0.41$ eV in pure silicon to $E_c - 0.51$ eV in $\text{Si}_{0.75}\text{Ge}_{0.25}$. A detailed analysis of the data resulted in the conclusion that the free-energy change associated with the ionization of the state remained 0.41 eV, independent of the germanium content. It has to be mentioned, however, that the carbon-antimony pairs discussed in Section 4.1.6 introduce levels similar to those suggested here for arsenic-vacancy pairs.

In the positron-annihilation studies of Kawasuso et al. [5.794] and Polity et al. [5.75], antimony-vacancy pairs were associated with positron lifetimes of 240 and 252 ps, respectively. Antimony-vacancy pairs were also found by Szpala et al. [5.795] in their study of core-electron contributions to positron annihilation and made responsible for antimony deactivation at high concentrations.

An important parameter for the formation of antimony-vacancy pairs is the binding energy of a vacancy at the first coordination site of the substitutional antimony atom. Combining their own data with those of Elkin and Watkins [5.713], Hirata et al. [5.581] estimated a lower limit of 1.44 eV for the neutral antimony-vacancy pair. In samples highly doped with phosphorus, pairs of radioactive antimony probe atoms with vacancies were detected by Weyer et al. [5.796] in their Mössbauer-spectroscopy experiments. From these, an upper limit of 1.9 eV was deduced for their binding energy in the negative charge state. From similar studies, Kobayashi et al. [5.797] estimated the binding energy of the antimony-vacancy pair to be in the range from 1.5 to 2.1 eV. Alternative estimates of the binding energy were obtained indirectly from measurements of the diffusion coefficient of antimony under inert and intrinsic conditions, the migration enthalpy of the antimony-vacancy pair, and an estimate for the formation enthalpy of vacancies. Based on such an analysis, Yoshida [5.582] suggested a binding energy of 1.47 to 1.5 eV. A similar analysis of Yoshida and Hasiguti [5.583] led to an estimate of 1.88 eV. The reliability of these values is limited because these early analyses were based on limited experimental data and unreliable values for the formation enthalpy of vacancies which is still in debate. In a quantitative analysis of a Mössbauer-spectroscopy investigation, Nylandsted Larsen and Weyer [5.798] found a value of 1.1 eV for the formation energy of a negatively charged vacancy next to a positively charged antimony atom. In a theoretical investigation, Nichols et al. [5.77] found the binding energy of a neutral pair of a vacancy at a next nearest neighboring site of a substitutional antimony atom to be 1.2 eV. Sugino and Oshiyama [5.561] calculated a value of 1.6 eV for the same configuration which reduces to 0.7 eV at a third-nearest neighboring site. In a later study, Nelson et al. [5.78] found a binding energy of 1.45 eV for a neutral pair. The calculations indicated also that the barrier against exchange of sites between the vacancy and the substitutional antimony atom is negligible.

5.10.2 Solubility

The phase diagram of the antimony-silicon system was compiled by Olesinski and Abbaschian [5.799]. Below the eutectic temperature of 629.7 °C, the antimony in the silicon phase is in equilibrium with a pure antimony phase.

Solubility values for antimony in silicon were deduced from various experiments. Values obtained from the diffusion of antimony from the gas phase [5.800] can be assumed to correspond to binary solubilities only when an antimony phase forms at the surface. Otherwise, smaller as well as slightly higher values are possible. The establishment of a binary system is expected in zone melting experiments with a thermal gradient [5.604] and after forming antimony-silicon alloys by melting followed by long-time annealing and quenching [5.281]. Agglomeration of antimony is expected during annealing of supersaturated solutions, e. g. after ion implantation [5.92, 5.357, 5.722, 5.783, 5.801, 5.802] and annealing with a sufficient thermal budget. The most reliable of them should be those in which the formation of large antimony precipitates was actually observed [5.604, 5.802]. For a characterization of the solubility, techniques like electrical measurements and chemical profiling techniques were applied. When charge-carrier concentrations were measured, resistivity measurements [5.604] or a combination of resistivity and Hall-effect measurements [5.92, 5.357, 5.722, 5.783] were used. Profiles of the total concentration of antimony atoms were obtained from depth profiling of radioactive tracer atoms [5.800], RBS [5.783, 5.801], or SIMS [5.802]. In addition, microindentation measurements were performed [5.281]. The solubility values obtained are shown in Figure 5.31. It is obvious that the agreement is not overly good. A reason might be that in some of the investigations antimony atoms stayed on substitutional sites even at concentrations above solid solubility because the establishment of a phase equilibrium was not completed. On the other hand, it might be that small antimony-related defects form during cooling-down so that slow cooling-rate experiments result in smaller electrical activity than solid solubility at the nominal process temperature

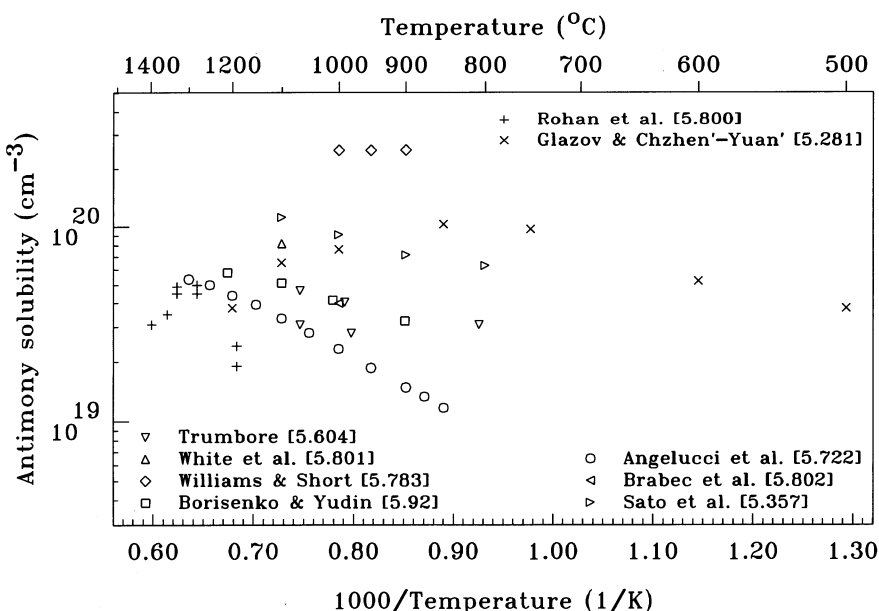


Figure 5.31: Solubility of antimony in silicon.

5.10.3 Diffusion

Intrinsic Diffusion

The diffusion coefficient of antimony under intrinsic and inert conditions is one of its best-studied properties. Introduction of the dopants occurred either from the gas phase [5.111, 5.284, 5.800, 5.803, 5.804] or from a dopant-containing layer. Dopant-containing silicon layers were formed by a predeposition step [5.805], by ion implantation [5.12, 5.121, 5.124, 5.615, 5.629, 5.806–5.808], or epitaxial deposition of antimony-doped layers [5.336, 5.809]. Alternatively, doped oxides [5.810, 5.811] or other dopant-containing layers [5.367, 5.812, 5.813] were deposited prior to the diffusion process. For the characterization of the diffusion profiles, radioactive antimony isotopes [5.111, 5.367, 5.800, 5.812], electrical measurements [5.284, 5.803, 5.805, 5.810, 5.811, 5.813], or SIMS [5.12, 5.121, 5.124, 5.336, 5.615, 5.629, 5.806–5.809] were used. For the data of Adda published in the work of Fair et al. [5.11], the experimental conditions are unknown. A summary of the diffusion coefficients reported can be found in Figure 5.32 together with the regression curve

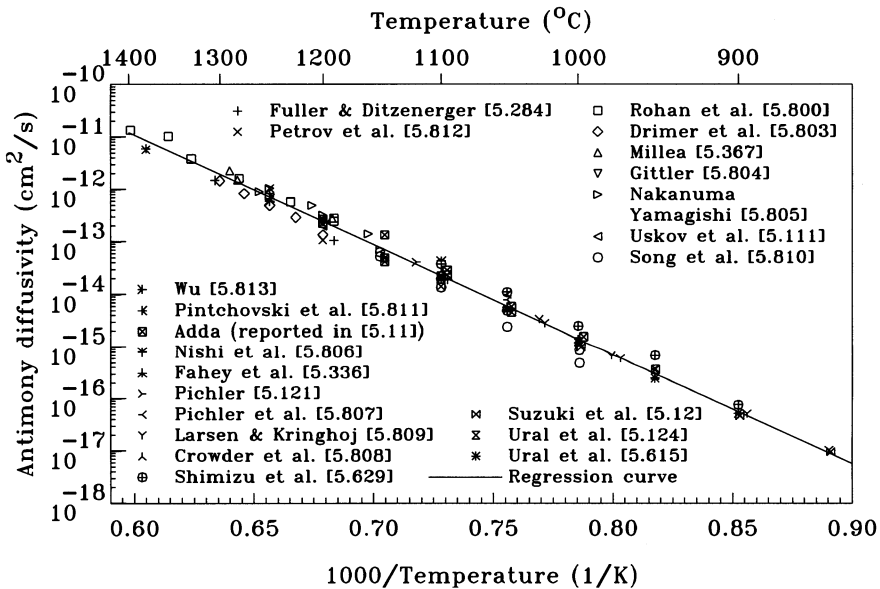


Figure 5.32: Diffusion coefficient of antimony under intrinsic and inert conditions in silicon.

$$D_{Sb}^i = 40.9 \cdot \exp\left(-\frac{4.158 \text{ eV}}{k \cdot T}\right) \text{ cm}^2/\text{s} \quad (5.34)$$

derived from these measurements. Whenever only an Arrhenius expression was given instead of experimental data [5.808], the points shown in Figure 5.32 were computed from this Arrhenius expression for the temperatures mentioned in the text. The activation energy ranges with a confidence level of 90% from 4.08 to 4.24 eV. The 90% confidence interval for the diffusion coefficient is about +6.6/-6.2% of the regression curve at 1115 °C and increases to +14/-13% at the melting point and +18/-16% at 850 °C. Additional measurements are expected with 90% confidence within a range of +86/-46% of the regression curve at 1115 °C which increases slightly to +89/-47% at the melting point and at 850 °C.

Pressure Dependence

Pressure-dependent diffusion studies performed by Zhao et al. [5.814] resulted in an estimate for the activation volume of $0.07 \cdot V_{Si}$.

Diffusion Mechanism

In the case of antimony there is general agreement that it diffuses predominantly via vacancies. Estimates for the values for the fractional diffusivity via self-interstitials reported in the literature are listed in Table 5.6.

From an analysis in which parallel reactions were included in addition to the usual pair-formation reactions, Vandebossche and Baccus [5.631] estimated the partition constant for pairs with vacancies to be $\alpha_{SbV} = 0.01$.

Table 5.6: Fractional diffusivity of antimony via self-interstitials. The abbreviations OSF, DifModel, RD, and DifComp for the experimental method refer to estimates from oxidation-enhanced diffusion with self-interstitial oversaturations estimated from OSF growth, from fitting dopant diffusion at high concentrations or under other non-equilibrium conditions, from the observation of retarded diffusion under non-equilibrium conditions, and from the comparison with the diffusivities of other dopants under non-equilibrium conditions, respectively. A description of the methods can be found in Section 3.4.3.

	f_I	Temperature range (°C)	Experimental method	Ref.
Antoniadis & Moskowitz	0.015	1100	OSF	[5.138]
Tan & Ginsberg	0.02	1100–1200	OSF	[5.815]
Fahey et al.	< 0.15	1100	DifComp	[5.622]
Yoshida et al.	0.0246	1100	OSF	[5.624]
Yoshida	0.00026–0.066	1100	OSF	[5.625]
Fahey et al.	≤ 0.02	1050	DifComp	[5.336]
Moynagh & Rosser	≤ 0.16	1100	DifComp	[5.149]
Okino & Yoshida	0.0676	1100	DifComp	[5.626]
Okino	0.029	1100	DifComp	[5.627]
Perozziello et al.	≤ 0.0035	850	DifModel	[5.816]
	≤ 0.01	950		
	≤ 0.03	1050		
Okino	0.03	1100	DifComp	[5.628]
Ghaderi et al.	0.01	900–1100	DifComp	[5.152]
Pichler et al.	≤ 0.027	950	RD	[5.807]
	≤ 0.043	1050		
Gossmann et al.	≤ 0.01 ± 0.01	790	DifComp	[5.154]
Ural et al.	≤ 0.02	1000	DifComp	[5.124]
	≤ 0.03	1100		
Ural et al.	≤ 0.08	1000	DifComp	[5.630]
	≤ 0.17	1100		

Extrinsic Diffusion

Information about the diffusion of antimony at extrinsic concentrations is available from the iso-concentration diffusion studies of Millea [5.367], Nishi et al. [5.806], Fair et al. [5.11], Kashio and Kato [5.119], Nylandsted Larsen et al. [5.742, 5.817], and Suzuki et al. [5.12]. These results are shown in Figure 5.33. The full lines were obtained by a numerical optimization using all

data points in Figure 5.32 in addition to those in Figure 5.33, and are described by

$$\begin{aligned}
 D_{Sb} = & 17.6 \cdot \exp\left(-\frac{4.111\text{eV}}{k \cdot T}\right) \text{cm}^2/\text{s} \\
 & + \frac{n}{n_i} \cdot 17.3 \cdot \exp\left(-\frac{4.186\text{eV}}{k \cdot T}\right) \text{cm}^2/\text{s} \\
 & + \left(\frac{n}{n_i}\right)^2 \cdot 49.8 \cdot \exp\left(-\frac{4.554\text{eV}}{k \cdot T}\right) \text{cm}^2/\text{s}.
 \end{aligned} \quad (5.35)$$

For intrinsic concentrations, the diffusion is dominated by the electron-concentration-independent term. For n/n_i on the order of 10, the quadratic term in n/n_i dominates. This was noted already by Fair et al. [5.11]. Within the ranges of temperature and n/n_i shown in Figure 5.33, all three components contribute with more than 10% to the total diffusion coefficient.

In the isoconcentration experiments of Petrov et al. [5.812], a pronounced dependence on the resistivity of the wafers was observed for resistivities of 0.1 to 10 Ωcm . The respective impurity concentrations were orders of magnitude below the intrinsic concentration at diffusion temperature so that another explanation than a Fermi-level effect has to be sought for the observed effects. It has to be mentioned also that Nylandsted Larsen et al. [5.817] found that the diffusivity increases at a temperature 1019 °C significantly with concentration even when the concentration is below the intrinsic carrier concentration. This effect was explained tentatively by the formation and diffusion of Sb_2V complexes.

For concentrations in excess of about $2 \cdot 10^{20} \text{ cm}^{-3}$, Nylandsted Larsen and his coworkers [5.741, 5.742, 5.818] found that the diffusion coefficient of antimony increases sharply with $(n/n_i)^n$. For the apparent exponent n , values of about 3.6 and 4.6 were reported for

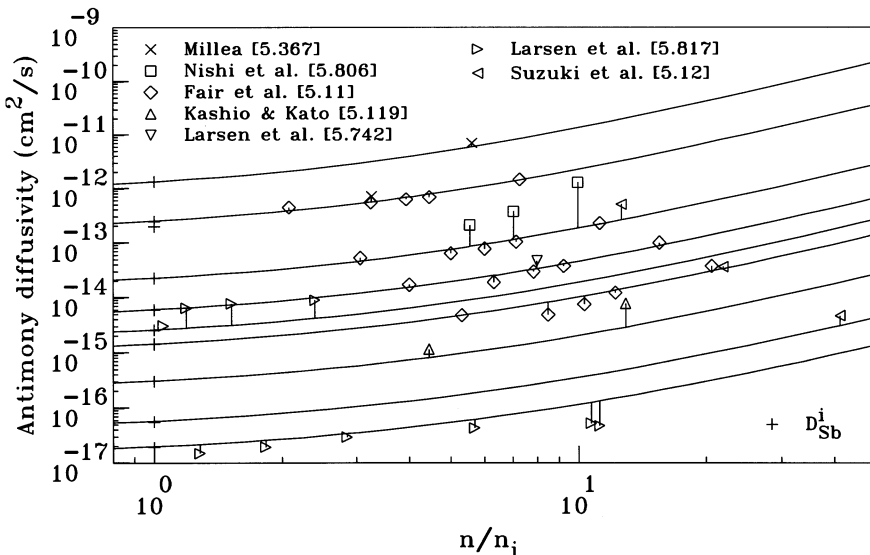


Figure 5.33: Dependence of the normalized diffusion coefficient of antimony in silicon on n/n_i for moderate dopant concentrations with $n/n_i < 20$. The full lines correspond, from top to bottom, to temperatures of 1280, 1200, 1100, 1050, 1000, and 950 °C.

temperatures of 1050 and 1000 °C, respectively. For such concentrations, the activation energy for antimony diffusion was found to reduce to about 1.7 eV. Similar results were reported from the precipitation of antimony in delta-doped layers [5.819]. Complementary Mössbauer-spectroscopy investigations [5.798, 5.818] of samples with phosphorus and arsenic as background impurities showed that the enhanced diffusion is correlated with the change of antimony from substitutional sites to a complex which was tentatively assigned to neutral antimony-phosphorus-vacancy and antimony-arsenic-vacancy complexes. Following the suggestion of Mathiot and Pfister [5.820], Nylandsted Larsen and his coworkers [5.741, 5.742] and van Oordorp et al. [5.819] interpreted the increased diffusivity within the percolation theory of Stauffer [5.749] to arise from the proximity of the dopant atoms which reduces the formation and migration enthalpies of vacancies in their vicinity and which leads to an enhanced diffusion of dopants within the percolation cluster.

Antimony Interstitials

Antimony interstitials are unanimously considered to play only a minor role for the diffusion of antimony under conditions where the intrinsic point defects are in equilibrium. They can be important, though, under conditions in which self-interstitials are present in large supersaturations. In such a situation, induced by amorphizing implants of antimony and low-temperature annealing, Pennycook et al. [5.821] found a greatly enhanced diffusion of antimony into precipitates, accompanied by the formation of extrinsic extended defects. From the growth of the antimony precipitates, a diffusion coefficient with a prefactor of 0.04 cm²/s and an activation energy of 1.8 eV was estimated and attributed to interstitial antimony.

Antimony-Vacancy Pairs

In their EPR measurements, Elkin and Watkins [5.713] found the reorientation of electrically neutral antimony-vacancy pairs to be governed by an activation energy of 1.29 eV. Reorientation requires already that the vacancy passes a third coordination site which is one of the rate-limiting steps for long-range diffusion. Thus if the barrier against an exchange of sites between the vacancy and the phosphorus atom is smaller, the activation energy of reorientation should also be characteristic for long-range diffusion. Following the derivation of Yoshida [5.582], the reorientation time measured by Elkin and Watkins can then be interpreted in terms of a diffusion coefficient

$$D_{SbV^0} = 5.5 \cdot 10^{-2} \cdot \exp\left(-\frac{1.29 \text{ eV}}{k \cdot T}\right) \text{ cm}^2/\text{s} \quad (5.36)$$

of the neutral antimony-vacancy pairs. In annealing studies after irradiation of arsenic-doped samples, Hirata et al. [5.675] found that the deep level associated with SbV pairs anneals below 200 °C with an activation energy of 1.84 to 1.86 eV. Later, another annealing stage was found by Hirata et al. [5.677] for temperatures above 190 °C. Hirata et al. [5.581] then associated this annealing stage with the diffusion of the antimony-vacancy pair. Its activation energy of 1.28 eV is nearly identical to that obtained by Elkin and Watkins from EPR investigations. Similarly, Evvaraye [5.792] obtained a migration enthalpy of 1.29 eV from DLTS studies of the annealing kinetics of neutral antimony-vacancy pairs after electron irradiation. Finally, a value of 1.27 eV was deduced from positron-annihilation measurements [5.794]. In contrast, a significantly larger migration enthalpy of 1.62 eV was estimated from DLTS studies of the annealing kinetics after electron irradiation for negatively charged antimony-vacancy pairs [5.792]. As in the case of phosphorus-vacancy pairs, an increased migration enthalpy could be explained by

the doubled Coulomb attraction between a positively charged arsenic atom and a doubly negatively charged vacancy. Finally, it has to be noted that an extraction of migration enthalpies from the annealing kinetics is possible only when the disappearance of the respective signal occurs by thermal diffusion. An alternative which cannot be excluded completely is that the pairs break up. In this case, the extracted activation energies would correspond to their dissociation energy.

5.10.4 Complexes

From a combination of characterization techniques, including Mössbauer spectroscopy, Nylandsted Larsen et al. [5.822] concluded that a significant fraction of antimony implanted at doses of $2 \cdot 10^{15} \text{ cm}^{-2}$ and above forms complexes with vacancies during annealing. From EXAFS measurements, Allain et al. [5.229] found that each antimony atom in such defects is surrounded by two silicon atoms so that the complex should be SbV_2 .

From theoretical investigations, Chadi et al. [5.686] concluded that Sb_nV complexes with $n > 2$ have exothermic formation energies. But they suggested the DP(2) and DP(4) structures of not connected antimony atoms shown in Figure 5.34 are energetically most stable and responsible for deactivation at high concentrations. It was also concluded that the structure of these complexes are compatible to EXAFS measurements. Sb_2V complexes were invoked by Nylandsted Larsen et al. [5.817] to explain the increase of the diffusion of antimony with concentration for concentrations below the intrinsic carrier concentration. Atomic-scale imaging of antimony atoms with a concentration of 10^{21} cm^{-3} allowed Voyles et al. [5.823] to conclude that the primary deactivating defect contains two antimony atoms. Unfortunately, their technique did not allow to distinguish between Sb_2V , DP(2) or DP(4) configurations. As an alternative, Kim et al. [5.687] suggested from *ab-initio* studies that a neutral pair of two three-fold coordinated, substitutional arsenic atoms on neighboring sites is similar in energy to the DP(4) complex and energetically more favorable than the DP(2) complex. Using a combination of atomic-scale imaging and *ab-initio* calculations, Voyles et al. [5.824] concluded that neither Sb_2V , DP(2), nor DP(4) complexes would be important for deactivation in highly antimony-doped layers. Instead, a neutral complex was suggested which composes of a vacancy around which two substitutional antimony atoms and a silicon self-interstitial are arranged.

In their Mössbauer-spectroscopy investigations, Nylandsted Larsen and Weyer [5.798] associated lines tentatively with antimony-vacancy-phosphorus pairs and antimony-vacancy-arsenic pairs. The measurements also allowed to estimate formation energies of 0.8 eV for $\text{Sb}_s^+\text{V=P}_s^+$ and $\text{Sb}^+\text{V=As}^+$ pairs.

Donors like antimony, as discussed in Section 5.2, are expected to form pairs with acceptors. Pairs with boron, as discussed in Section 5.3.4, have higher binding energies than the indium-antimony complexes mentioned in Section 5.6.4. This can be related consistently to stress effects associated with the covalent radii of the ions involved.

The remarkable properties of antimony-carbon pairs which form multi-configurational defects in silicon were discussed already in Section 4.1.6.

After annealing of antimony-doped, electron-irradiated samples, Hallberg et al. [5.782] observed that bands at $861/867$ and $906/913 \text{ cm}^{-1}$ (RT/10 K) appear at the expense of VO-related spectra. In analogy to a similar defect observed in phosphorus-doped silicon, the bands were attributed to a VO-like defect in which the oxygen atom is bonded to two antimony atoms. The existence of antimony-oxygen complexes, although probably with other configurations, can be inferred from the observations of Takeno et al. [5.251] who reported retarded diffusion of oxygen at 700°C and below in samples with an antimony background concentration of $1.3 \cdot 10^{18} \text{ cm}^{-3}$. From these experiments, they extracted a binding energy of about 1.4 eV.

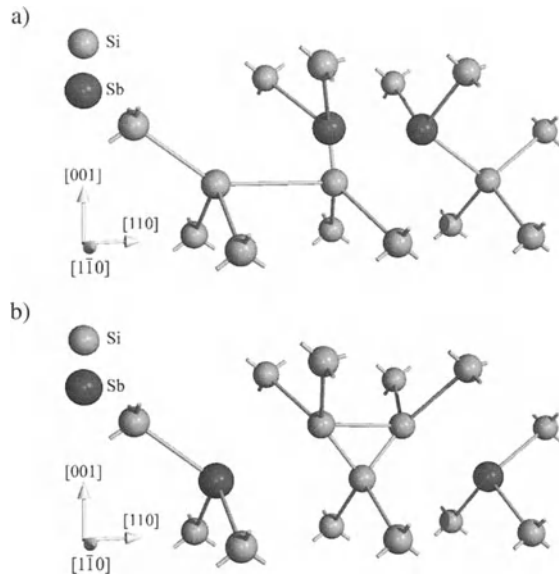


Figure 5.34: Schematic representation of a) DP(2) and b) DP(4) complexes of non-connected antimony atoms at second and fourth neighboring sites as suggested by Chadi et al. [5.686].

Bibliography

- [5.1] M. Y. Tsai, F. F. Morehead, J. E. E. Baglin, and A. E. Michel, “Shallow Junctions by High-Dose As Implants in Si: Experiments and Modeling,” *J. Appl. Phys.*, vol. 51, no. 6, 3230–3235 (1980).
- [5.2] E. Guerrero, H. Pötzl, R. Tielert, M. Grasserbauer, and G. Stingedter, “Generalized Model for the Clustering of As Dopants in Si,” *J. Electrochem. Soc.*, vol. 129, no. 8, 1826–1831 (1982).
- [5.3] H. Reiss, C. S. Fuller, and F. J. Morin, “Chemical Interactions among Defects in Germanium and Silicon,” *Bell Syst. Techn. J.*, vol. 35, no. 3, 535–636 (1956).
- [5.4] R. C. Newman and R. S. Smith, “Local Mode Absorption from Boron Complexes in Silicon,” in: *Localized Excitations in Solids*, edited by R. F. Wallis, New York: Plenum Press, 177–184 (1968).
- [5.5] V. Tsvetov, W. Allred, and W. G. Spitzer, “Localized Vibrational Modes of Defect Pairs in Silicon,” in: *Localized Excitations in Solids*, edited by R. F. Wallis, New York: Plenum Press, 185–192 (1968).
- [5.6] A. R. Bean, S. R. Morrison, R. C. Newman, and R. S. Smith, “Electron Irradiation Damage in Silicon Containing High Concentrations of Boron,” *J. Phys. C*, vol. 5, 379–400 (1972).
- [5.7] R. J. Culbertson and S. J. Pennycook, “Formation of Stable Point Defects in Ion-Implanted Si,” in: *Beam-Solid Interactions and Transient Processes*, edited by M. O. Thompson, S. T. Picraux, and J. S. Williams, *Mat. Res. Soc. Symp. Proc.*, vol. 74, 391–396 (1987).
- [5.8] R. B. Fair and P. N. Pappas, “Diffusion of Ion-Implanted B in High Concentration P- and As-Doped Silicon,” *J. Electrochem. Soc.*, vol. 122, no. 9, 1241–1244 (1975).
- [5.9] D. Tsoukalas and P. Chenevier, “Boron Diffusion in Silicon by a Vacancy Mechanism,” *phys. stat. sol. (a)*, vol. 92, 495–501 (1985).
- [5.10] A. F. W. Willoughby, A. G. R. Evans, P. C. K. J. Yallup, D. J. Godfrey, and M. G. Dowsett, “Diffusion of Boron in Heavily Doped N- and P-Type Silicon,” *J. Appl. Phys.*, vol. 59, no. 7, 2392–2397 (1986).

- [5.11] R. B. Fair, M. L. Manda, and J. J. Wortman, “The Diffusion of Antimony in Heavily Doped and n- and p-Type Silicon,” *J. Mater. Res.*, vol. 1, no. 5, 705–711 (1986).
- [5.12] K. Suzuki, H. Tashiro, and T. Aoyama, “Sb Diffusion in Heavily Doped Si Substrates,” *J. Electrochem. Soc.*, vol. 146, no. 1, 336–338 (1999).
- [5.13] S. Aronowitz and G. Riga, “Arsenic-Aluminium, Phosphorus-Aluminium Push Effect,” *J. Electrochem. Soc.*, vol. 134, no. 3, 702–707 (1987).
- [5.14] S. Aronowitz, “Dopant Diffusion in Silicon in the Presence of Other Dopants: A New Predictive Approach Based on Modelling Boron and Phosphorus Diffusion in Germanium-Rich Regions of Silicon,” *J. Appl. Phys.*, vol. 69, no. 7, 3901–3906 (1991).
- [5.15] G. L. Pearson and J. Bardeen, “Electrical Properties of Pure Silicon and Silicon Alloys Containing Boron and Phosphorus,” *Phys. Rev.*, vol. 75, no. 5, 865–883 (1949).
- [5.16] F. H. Horn, “Densitometric and Electrical Investigation of Boron in Silicon,” *Phys. Rev.*, vol. 97, no. 6, 1521–1525 (1955).
- [5.17] F. J. Morin, J. P. Maita, R. G. Shulman, and N. B. Hannay, “Impurity Levels in Silicon,” *Phys. Rev.*, vol. 96, no. 3, 833 (1954).
- [5.18] J. B. Mitchell, J. Shewchun, D. A. Thompson, and J. A. Davies, “Nitrogen-Implanted Silicon. II. Electric Properties,” *J. Appl. Phys.*, vol. 46, no. 1, 335–343 (1975).
- [5.19] E. Burstein, G. Picus, B. Henvis, and R. Wallis, “Absorption Spectra of Impurities in Silicon — I,” *J. Phys. Chem. Solids*, vol. 1, 65–74 (1956).
- [5.20] H. J. Hrostowski, “Infrared Absorption of Semiconductors,” in: *Semiconductors*, edited by N. B. Hannay, New York: Reihold Publishing Corp., 437–481 (1959).
- [5.21] A. Onton, P. Fisher, and A. K. Ramdas, “Spectroscopic Investigation of Group-III Acceptor States in Silicon,” *Phys. Rev.*, vol. 163, no. 3, 686–703 (1967).
- [5.22] G. A. Samara and C. E. Barnes, “Pressure Dependence of Impurity Levels in Semiconductors: The Deep Gold Acceptor Level and Shallow Donor and Acceptor Levels in Silicon,” *Phys. Rev. B*, vol. 35, no. 14, 7575–7584 (1987).
- [5.23] J. F. Angress, A. R. Goodwin, and S. D. Smith, “A Study of the Vibrations of Boron and Phosphorus in Silicon by Infra-Red Absorption,” *Proc. Roy. Soc. Lond. A*, vol. 287, 64–88 (1965).
- [5.24] M. Balkanski and W. J. Nazarewicz, “Infrared Study of Localized Vibrations in Silicon Due to Boron and Lithium,” *J. Phys. Chem. Solids*, vol. 27, 671–684 (1966).
- [5.25] P. G. Dawber and J. R. Elliot, “The Vibrations of an Atom of Different Mass in a Cubic Crystal,” *Proc. Roy. Soc. Lond. A*, vol. 273, 222–236 (1963).
- [5.26] P. G. Dawber and R. J. Elliott, “Theory of Optical Absorption by Vibrations of Defects in Silicon,” *Proc. Phys. Soc. (London)*, vol. 81, 453–460 (1963).
- [5.27] F. Cerdeira, T. A. Fjeldly, and M. Cardona, “Raman Study of the Interaction between Localized Vibrations and Electronic Excitations in Boron-Doped Silicon,” *Phys. Rev. B*, vol. 9, no. 10, 4344–4350 (1974).
- [5.28] M. Chandrasekhar, H. R. Chandrasekhar, M. Grimsditch, and M. Cardona, “Study of the Localized Vibrations of Boron in Heavily Doped Si,” *Phys. Rev. B*, vol. 22, no. 10, 4825–4833 (1980).
- [5.29] K. Kosai and M. Gershenson, “New Photoluminescence Line-Series Spectra Attributed to Decay of Multiexciton Complexes Bound to Li, B, and P Centers in Si,” *Phys. Rev. B*, vol. 9, no. 2, 723–736 (1974).
- [5.30] W. Mayer, D. Grasse, and J. Peisl, “Diffuse X-Ray Scattering from Neutron-Irradiated Silicon Doped with Boron,” *phys. stat. sol. (a)*, vol. 87, 583–588 (1985).
- [5.31] J. Zhu, T. Diaz de la Rubia, L. H. Yang, C. Maillhot, and G. H. Gilmer, “Ab Initio Pseudopotential Calculations of B Diffusion and Pairing in Si,” *Phys. Rev. B*, vol. 54, no. 7, 4741–4747 (1996).
- [5.32] M. Hakala, M. J. Puska, and R. M. Nieminen, “First-Principles Calculations of Interstitial Boron in Silicon,” *Phys. Rev. B*, vol. 61, no. 12, 8155–8161 (2000).

- [5.33] R. C. Newman and R. S. Smith, "Local Mode Absorption from Boron Pairs in Silicon," *Physics Letters*, vol. 29A, no. 12, 671–672 (1967).
- [5.34] R. C. Newman and D. H. J. Totterdell, "Electron Irradiation Damage in Silicon Containing High Concentrations of Boron," *J. Phys. C*, vol. 7, 3418–3426 (1974).
- [5.35] K. Laithwaite, R. C. Newman, and D. H. J. Totterdell, "Interstitial Defects Involving Boron in Irradiated Silicon," *J. Phys. C*, vol. 8, 236–242 (1975).
- [5.36] A. K. Tipping and R. C. Newman, "An Infrared Study of the Production, Diffusion and Complexing of Interstitial Boron in Electron-Irradiated Silicon," *Semicond. Sci. Technol.*, vol. 2, 389–398 (1987).
- [5.37] J. Yamauchi, N. Aoki, and I. Mizushima, "Vibrational Properties of Two Boron Atoms in Silicon," *Phys. Rev. B*, vol. 63, 073202 (2001).
- [5.38] M. Cherki and A. H. Kalma, "Photoconductivity Studies of Defects in p-Type Silicon: Boron Interstitial and Aluminum Interstitial Defects," *Phys. Rev. B*, vol. 1, no. 2, 647–657 (1970).
- [5.39] S. I. Tan, B. S. Berry, and W. F. J. Frank, "Internal Friction Study of Point Defects in Boron-Implanted Silicon," in: *Ion Implantation in Semiconductors and Other Materials*, edited by B. Crowder, New York: Plenum Press, 19–30 (1973).
- [5.40] G. D. Watkins, "Defects in Irradiated Silicon: EPR and Electron-Nuclear Double Resonance of Interstitial Boron," *Phys. Rev. B*, vol. 12, no. 12, 5824–5839 (1975).
- [5.41] G. D. Watkins and J. R. Troxell, "Negative-U Properties for Point Defects in Silicon," *Phys. Rev. Lett.*, vol. 44, no. 9, 593–596 (1980).
- [5.42] J. R. Troxell and G. D. Watkins, "Interstitial Boron in Silicon: a Negative-U System," *Phys. Rev. B*, vol. 22, no. 2, 921–931 (1980).
- [5.43] R. D. Harris, J. L. Newton, and G. D. Watkins, "Negative-U Properties for Interstitial Boron in Silicon," *Phys. Rev. Lett.*, vol. 48, no. 18, 1271–1274 (1982).
- [5.44] R. D. Harris, J. L. Newton, and G. D. Watkins, "Negative-U Defect: Interstitial Boron in Silicon," *Phys. Rev. B*, vol. 36, no. 2, 1094–1104 (1987).
- [5.45] M. L. Swanson, "Lattice Location of Solute Atoms by Channeling," *Vacuum*, vol. 39, no. 2-4, 87–90 (1989).
- [5.46] W. Seelinger, B. Fischer, E. Diehl, K.-H. Ergezinger, H.-P. Frank, B. Ittermann, and F. Mai, " β -NMR Study on the Lattice Location of Boron Implanted into Silicon," in: *Nuclear Methods in Semiconductor Physics*, edited by G. Langouche, J. C. Soares, and J. P. Stoquert, *Nuclear Instruments and Methods in Physics Research B*, vol. 63, 173–178 (1992).
- [5.47] L. C. Kimerling, M. T. Asom, J. L. Benton, P. J. Drevinsky, and C. E. Caefer, "Interstitial Defect Reaction in Silicon," in: *Defects in Semiconductors 15*, edited by G. Ferenczi, *Materials Science Forum*, vol. 38-41, 141–150 (1989).
- [5.48] G. Davies and R. C. Newman, "Carbon in Monocrystalline Silicon," in: *Materials, Properties and Preparation*, edited by T. S. Moss and S. Mahajan, *Handbook on Semiconductors*, vol. 3b, Amsterdam: North-Holland, 1557–1635 (1994).
- [5.49] P. A. Packan, *Physical Modeling of Transient Diffusion Effects in Silicon Due to Surface Oxidation and Ion-Implantation*, Ph.D. thesis, Integrated Circuits Laboratory, Department of Electrical Engineering, Stanford University (1991).
- [5.50] M. E. Law, H. Park, and P. Novell, "Theory of Dopant Diffusion Assuming Nondilute Concentrations of Dopant-Defect Pairs," *Appl. Phys. Lett.*, vol. 59, no. 26, 3488–3489 (1991).
- [5.51] H. Park and M. E. Law, "Point Defect Based Modeling of Low Dose Silicon Implant Damage and Oxidation Effects on Phosphorus and Boron Diffusion in Silicon," *J. Appl. Phys.*, vol. 72, no. 8, 3431–3439 (1992).
- [5.52] M. Hane and H. Matsumoto, "A Model for Boron Short Time Annealing after Ion Implantation," *IEEE Trans. Electron Devices*, vol. 40, no. 7, 1215–1222 (1993).
- [5.53] B. Baccus, T. Wada, N. Shigyo, M. Norishima, H. Nakajima, K. Inoue, T. Iinuma, and H. Iwai, "A Study of Nonequilibrium Diffusion Modeling — Applications to Rapid Thermal Annealing

- and Advanced Bipolar Technologies," *IEEE Trans. Electron Devices*, vol. 39, no. 3, 648–661 (1992).
- [5.54] B. Baccus and E. Vandenbossche, "Boron Diffusion at High Concentrations during Predeposition Processes," in: *Process Physics and Modeling in Semiconductor Technology*, edited by G. R. Srinivasan, K. Taniguchi, and C. S. Murthy, *Electrochem. Soc. Proc.*, vol. 93-6, 75–87 (1993).
 - [5.55] B. Baccus, E. Vandenbossche, and M. Lannoo, "Modeling High-Concentration Boron Diffusion under Amorphization Conditions," *J. Appl. Phys.*, vol. 77, no. 11, 5630–5641 (1995).
 - [5.56] I. Bork and H. Matsumoto, "On the Determination of Boron Diffusivities and Boron Interstitial Pair Binding Energies in Silicon," in: *1996 International Conference on Simulation of Semiconductor Processes and Devices (SISPAD'96)*, Tokyo: Japan Society of Applied Physics, 91–92 (1996).
 - [5.57] M. Hane, C. S. Rafferty, T. Ikezawa, and H. Matsumoto, "Boron Diffusion Model Refinement and Its Effect on the Calculation of Reverse Short Channel Effect," in: *1996 International Conference on Simulation of Semiconductor Processes and Devices (SISPAD'96)*, Tokyo: Japan Society of Applied Physics, 15–16 (1996).
 - [5.58] M. Hane, T. Ikezawa, M. Hiroi, and M. Matsumoto, "Dopant Diffusion Model Refinement and Its Impact on the Calculation of Reverse Short Channel Effect," in: *Technical Digest of the 1996 International Electron Devices Meeting (IEDM)*, Piscataway: IEEE, 803–806 (1996).
 - [5.59] H. Kinoshita, T. H. Huang, and D. L. Kwong, "Modeling of Suppressed Dopant Activation in Boron- and BF₂-Implanted Silicon," *J. Appl. Phys.*, vol. 75, no. 12, 8213–8215 (1994).
 - [5.60] M. Uematsu, "Reduction of the Number of Parameters for the Simulation of Impurity Diffusion," *Jpn. J. Appl. Phys., Part 1*, vol. 36, no. 12A, 7100–7103 (1997).
 - [5.61] E. Tarnow, "Theory of the B Interstitial Related Defect in Si," *Europhysics Letters*, vol. 16, no. 5, 449–454 (1991).
 - [5.62] J. Zhu, "Ab Initio Pseudopotential Calculations of Dopant Diffusion in Si," *Comput. Mater. Sci.*, vol. 12, 309–318 (1998).
 - [5.63] W. Windl, M. M. Bunea, R. Stumpf, S. T. Dunham, and M. P. Masquelier, "First-Principles Study of Boron Diffusion in Silicon," *Phys. Rev. Lett.*, vol. 83, no. 21, 4345–4348 (1999).
 - [5.64] B. Sadigh, T. J. Lenosky, S. K. Theiss, M.-J. Caturla, T. Diaz de la Rubia, and M. A. Foad, "Mechanism of Boron Diffusion in Silicon: An Ab Initio and Kinetic Monte Carlo Study," *Phys. Rev. Lett.*, vol. 83, no. 21, 4341–4344 (1999).
 - [5.65] J.-W. Jeong and A. Oshiyama, "Atomic and Electronic Structures of a Boron Impurity and Its Diffusion Pathways in Crystalline Si," *Phys. Rev. B*, vol. 64, 235204 (2001).
 - [5.66] J. Adey, J. P. Goss, R. Jones, and P. R. Briddon, "Identification of Boron Clusters and Boron-Interstitial Clusters in Silicon," *Phys. Rev. B*, vol. 67, 245325 (2003).
 - [5.67] J. Hattendorf, W.-D. Zeitz, N. V. Abrosimov, and W. Schröder, "The Interstitial Boron and the Boron-Germanium Complex in Silicon-Germanium Crystals," *Physica B*, vol. 308–310, 535–538 (2001).
 - [5.68] K. M. Beardmore, W. Windl, B. P. Haley, and N. Grønbech-Jensen, "Diffusion Mechanisms and Capture Radii in Silicon," in: *Computational Nanoscience and Nanotechnology 2002*, Cambridge: Applied Computational Research Society, 251–254 (2002).
 - [5.69] G. D. Watkins, "EPR of a Trapped Vacancy in Boron-Doped Silicon," *Phys. Rev. B*, vol. 13, no. 6, 2511–2518 (1976).
 - [5.70] M. Sprenger, R. van Kemp, E. G. Sieverts, and C. A. J. Ammerlaan, "Electronic and Atomic Structure of the Boron-Vacancy Complex in Silicon," *Phys. Rev. B*, vol. 35, no. 4, 1582–1592 (1987).
 - [5.71] A. Chantre, "Configurationally Bistable C Center in Quenched Si:B: Possibility of a Boron-Vacancy Pair," *Phys. Rev. B*, vol. 32, no. 6, 3687–3694 (1985).
 - [5.72] S. K. Bains and P. C. Banbury, "A Bistable Defect in Electron-Irradiated Boron-Doped Silicon," *J. Phys. C*, vol. 18, L109–L116 (1985).

- [5.73] C. A. Londos, "Capacitance Transient Studies of a Metastable Defect in Silicon," *Phys. Rev. B*, vol. 34, no. 2, 1310–1313 (1986).
- [5.74] N. Zangenberg, J.-J. Goubet, and A. Nylandsted Larsen, "On-Line DLTS Investigations of the Mono- and Di-Vacancy in p-Type Silicon after Low Temperature Electron Irradiation," *Nuclear Instruments and Methods in Physics Research B*, vol. 186, 71–77 (2002).
- [5.75] A. Polity, F. Börner, S. Huth, S. Eichler, and R. Krause-Rehberg, "Defects in Electron-Irradiated Si Studied by Positron-Lifetime Spectroscopy," *Phys. Rev. B*, vol. 58, no. 16, 10363–10377 (1998).
- [5.76] D. Mathiot and J. C. Pfister, "Dopant Diffusion in Silicon: A Consistent View Involving Nonequilibrium Defects," *J. Appl. Phys.*, vol. 55, no. 10, 3518–3530 (1984).
- [5.77] C. S. Nichols, C. G. van de Walle, and S. T. Pantelides, "Mechanisms of Dopant Impurity Diffusion in Silicon," *Phys. Rev. B*, vol. 40, no. 8, 5484–5496 (1989).
- [5.78] J. S. Nelson, P. A. Schultz, and A. F. Wright, "Valence and Atomic Size Dependent Exchange Barriers in Vacancy-Mediated Dopant Diffusion," *Appl. Phys. Lett.*, vol. 73, no. 2, 247–249 (1998).
- [5.79] R. W. Olesinski and G. J. Abbaschian, "The B-Si (Boron-Silicon) System," *Bull. Alloy Phase Diagrams*, vol. 5, no. 5, 478–484 (1984).
- [5.80] T. L. Aselage, "The Coexistence of Silicon Borides with Boron-Saturated Silicon: Metastability of SiB_3 ," *J. Mater. Res.*, vol. 13, no. 7, 1786–1794 (1998).
- [5.81] C. S. Fuller and J. A. Ditzenberger, "Diffusion of Boron and Phosphorus into Silicon," *J. Appl. Phys.*, vol. 25, no. 11, 1439–1440 (1954).
- [5.82] G. L. Vick and K. M. Whittle, "Solid Solubility and Diffusion Coefficients of Boron in Silicon," *J. Electrochem. Soc.*, vol. 116, no. 8, 1142–1144 (1969).
- [5.83] J. Stach and A. Turley, "Anomalous Boron Diffusion in Silicon from Planar Boron Nitride Sources," *J. Electrochem. Soc.*, vol. 121, no. 5, 722–725 (1974).
- [5.84] S. F. Guo, "A Simple Model for the Deposition of Boron in Silicon by Using a BN Diffusion Source," *J. Electrochem. Soc.*, vol. 127, no. 11, 2506–2509 (1980).
- [5.85] J. Hesse, "Löslichkeit und Ausscheidungskinetik von Bor in polykristallinem Silizium," *Z. Metallkd.*, vol. 59, no. 6, 499–502 (1968).
- [5.86] A. Armigliato, D. Nobili, P. Ostoja, M. Servidori, and S. Solmi, "Solubility and Precipitation of Boron in Silicon and Supersaturation Resulting by Thermal Predeposition," in: *Semiconductor Silicon 1977*, edited by H. R. Huff and E. Sirtl, *Electrochem. Soc. Proc.*, vol. 77-2, 638–647 (1977).
- [5.87] W. K. Hofker, H. W. Werner, D. P. Oosthoek, and H. A. M. de Grefte, "Influence of Annealing on the Concentration Profiles of Boron Implantations in Silicon," *Appl. Phys.*, vol. 2, 265–278 (1973).
- [5.88] F. N. Schwettmann, "Characterization of Incomplete Activation of High-Dose Boron Implants in Silicon," *J. Appl. Phys.*, vol. 45, no. 4, 1918–1920 (1974).
- [5.89] H. Ryssel, K. Müller, K. Haberger, R. Henkelmann, and F. Jahnel, "High Concentration Effects of Ion Implanted Boron in Silicon," *Appl. Phys.*, vol. 22, 35–38 (1980).
- [5.90] A. E. Michel, W. Rausch, P. A. Ronsheim, and R. H. Kastl, "Rapid Annealing and the Anomalous Diffusion of Ion Implanted Boron into Silicon," *Appl. Phys. Lett.*, vol. 50, no. 7, 416–418 (1987).
- [5.91] D. Fan, J. Huang, R. J. Jaccodine, P. Kahora, and F. Stevie, "Enhanced Tail Diffusion of Ion Implanted Boron in Silicon," *Appl. Phys. Lett.*, vol. 50, no. 24, 1745–1747 (1987).
- [5.92] V. E. Borisenko and S. G. Yudin, "Steady-State Solubility of Substitutional Impurities in Silicon," *phys. stat. sol. (a)*, vol. 101, 123–127 (1987).
- [5.93] R. Angelucci, R. Cembali, P. Negri, M. Servidori, and S. Solmi, "Temperature and Time Dependence of Dopant Enhanced Diffusion in Self-Ion Implanted Silicon," *J. Electrochem. Soc.*, vol. 134, no. 12, 3130–3134 (1987).

- [5.94] T. O. Sedgwick, A. E. Michel, V. R. Deline, S. A. Cohen, and J. B. Lasky, "Transient Boron Diffusion in Ion-Implanted Crystalline and Amorphous Silicon," *J. Appl. Phys.*, vol. 63, no. 5, 1452–1463 (1988).
- [5.95] Y. Kim, H. Z. Massoud, and R. B. Fair, "The Effect of Ion-Implantation Damage on Dopant Diffusion in Silicon during Shallow-Junction Formation," *J. Electronic Materials*, vol. 18, no. 2, 143–150 (1989).
- [5.96] O. W. Holland, "New Mechanism for Diffusion of Ion-Implanted Boron in Si at High Concentration," *Appl. Phys. Lett.*, vol. 54, no. 9, 798–800 (1989).
- [5.97] W. K. Chu, M. Z. Numan, J. Z. Zhang, and G. S. Sandhu, "Transient Diffusion of Boron Implanted in Si along Random and Channeling Directions," in: *Ion Implantation Technology*, edited by T. Takagi, *Nuclear Instruments and Methods in Physics Research B*, vol. 37/38, 365–370 (1989).
- [5.98] R. B. Fair, "Point Defect Charge-State Effects on Transient Diffusion of Dopants in Si," *J. Electrochem. Soc.*, vol. 137, no. 2, 667–671 (1990).
- [5.99] Y. M. Kim, G. Q. Lo, D. L. Kwong, A. F. Tasch, and S. Novak, "Extended Defect Evolution in Boron-Implanted Si during Rapid Thermal Annealing and Its Effects on the Anomalous Boron Diffusion," *Appl. Phys. Lett.*, vol. 56, no. 13, 1254–1256 (1990).
- [5.100] N. E. B. Cowern, K. T. F. Janssen, and H. F. F. Jos, "Transient Diffusion of Ion-Implanted B in Si: Dose, Time, and Matrix Dependence of Atomic and Electrical Profiles," *J. Appl. Phys.*, vol. 68, no. 12, 6191–6198 (1990).
- [5.101] S. Solmi, F. Baruffaldi, and R. Canteri, "Diffusion of Boron in Silicon during Post-Implantation Annealing," *J. Appl. Phys.*, vol. 69, no. 4, 2135–2142 (1991).
- [5.102] H. Schaber, R. von Criegern, and I. Weitzel, "Analysis of Polycrystalline Silicon Diffusion Sources by Secondary Ion Mass Spectrometry," *J. Appl. Phys.*, vol. 58, no. 11, 4036–4042 (1985).
- [5.103] B. Garben, W. A. Orr-Arienzo, and R. F. Lever, "Investigation of Boron Diffusion from Polycrystalline Silicon," *J. Electrochem. Soc.*, vol. 133, no. 10, 2152–2156 (1986).
- [5.104] B. Sadigh, T. J. Lenosky, M.-J. Caturla, A. A. Quong, L. X. Benedict, T. Diaz de la Rubia, M. M. Giles, M. Foad, C. D. Spataru, and S. G. Louie, "Large Enhancement of Boron Solubility in Silicon Due to Biaxial Stress," *Appl. Phys. Lett.*, vol. 80, no. 25, 4738–4740 (2000).
- [5.105] A. D. Kurtz and R. Yee, "Diffusion of Boron into Silicon," *J. Appl. Phys.*, vol. 31, no. 2, 303–305 (1960).
- [5.106] M. Y. Ben-Sira and S. Bukshpan, "Deep Diffusion of Boron into Silicon Single Crystals," *Solid State Communications*, vol. 3, 15–17 (1965).
- [5.107] M. Okamura, "Boron Diffusion into Silicon Using Elemental Boron," *Jpn. J. Appl. Phys.*, vol. 8, no. 12, 1440–1448 (1969).
- [5.108] R. N. Ghoshtagore, "Low Concentration Diffusion in Silicon under Sealed Tube Conditions," *Solid-State Electronics*, vol. 15, 1113–1120 (1972).
- [5.109] D. N. Mikhailova, "The Diffusion Distribution of Boron in Silicon," *Sov. Phys. Solid State*, vol. 4, no. 10, 2195–2196 (1963).
- [5.110] M. L. Barry and P. Olofson, "Doped Oxides As Diffusion Sources," *J. Electrochem. Soc.*, vol. 116, no. 6, 854–860 (1969).
- [5.111] V. A. Uskov, P. V. Pavlov, E. V. Kuril'chik, and V. I. Pashkov, "Diffusion of Antimony, Phosphorus, and Boron in Silicon with Various Surface Concentrations of the Diffusant," *Sov. Phys. Solid State*, vol. 12, no. 5, 1181–1185 (1970).
- [5.112] G. Kambara, S. Koike, T. Matsuda, and M. Inoue, "A New Technique for Low Concentration Diffusion of Boron into Silicon," *Jpn. J. Appl. Phys.*, vol. 16, no. 16-1, 37–41 (1977).
- [5.113] S. Wagner, "Diffusion of Boron from Shallow Ion Implants in Silicon," *J. Electrochem. Soc.*, vol. 119, no. 11, 1570–1576 (1972).
- [5.114] T. Sato, H. Nishi, and T. Furuya, "Redistribution of Implanted Boron and Phosphorus during Thermal Diffusion," *Fujitsu Scientific & Technical Journal*, vol. 12, 115–124 (1976).

- [5.115] D. A. Antoniadis, A. G. Gonzales, and R. W. Dutton, "Boron in Near-Intrinsic ⟨100⟩ and ⟨111⟩ Silicon under Inert and Oxidizing Ambients -Diffusion and Segregation," *J. Electrochem. Soc.*, vol. 125, no. 5, 813–819 (1978).
- [5.116] C. Hill, "Measurements of Local Diffusion Coefficients in Planar Device Structures," in: *Semiconductor Silicon*, edited by H. R. Huff, R. J. Kriegler, and Y. Takeishi, *Electrochem. Soc. Proc.*, vol. 81-5, 988–1006 (1981).
- [5.117] A. M.-R. Lin, D. A. Antoniadis, and R. W. Dutton, "The Oxidation Rate Dependence of Oxidation-Enhanced Diffusion of Boron and Phosphorus in Silicon," *J. Electrochem. Soc.*, vol. 128, no. 5, 1131–1137 (1981).
- [5.118] M. Miyake, "Oxidation-Enhanced Diffusion of Ion-Implanted Boron in Silicon in Extrinsic Conditions," *J. Appl. Phys.*, vol. 57, no. 6, 1861–1868 (1985).
- [5.119] T. Kashio and K. Kato, "A New Dopant Diffusion Modeling Based on Point Defect Kinetics," in: *Extended Abstracts of the 20th Conference on Solid State Devices and Materials*, Tokyo: Business Center for Academic Societies, 121–124 (1988).
- [5.120] A. La Ferla, A. Di Franco, E. Rimini, G. Ciavola, and G. Ferla, "Implants of 15–50 MeV Boron Ions into Silicon," *Materials Science and Engineering B*, vol. 2, 69–73 (1989).
- [5.121] P. Pichler, Unpublished (1990).
- [5.122] U. Södervall, M. Friesel, and A. Lodding, "Atomic Transport of Trivalent Impurities in Silicon: Diffusion, Isotope Effects, Activation Volumes," *J. Chem. Soc. Faraday Trans.*, vol. 86, no. 8, 1293–1298 (1990).
- [5.123] K. Osada, Y. Zaitsu, S. Matsumoto, M. Yoshida, E. Arai, and T. Abe, "Effect of Stress in the Deposited Silicon Nitride Films on Boron Diffusion of Silicon," *J. Electrochem. Soc.*, vol. 142, no. 1, 202–206 (1995).
- [5.124] A. Ural, P. B. Griffin, and J. D. Plummer, "Fractional Contributions of Microscopic Diffusion Mechanisms for Common Dopants and Self-Diffusion in Silicon," *J. Appl. Phys.*, vol. 85, no. 9, 6440–6446 (1999).
- [5.125] Y. M. Haddara, B. T. Folmer, M. E. Law, and T. Buyuklimanli, "Accurate Measurements of the Intrinsic Diffusivities of Boron and Phosphorus in Silicon," *Appl. Phys. Lett.*, vol. 77, no. 13, 1976–1978 (2000).
- [5.126] H.-J. Goossen, G. H. Gilmer, C. S. Rafferty, F. C. Unterwald, T. Boone, J. M. Poate, H. S. Luftman, and W. Frank, "Determination of Si Self-Interstitial Diffusivities from the Oxidation-Enhanced Diffusion in B Doping-Superlattices: The Influence of the Marker Layers," *J. Appl. Phys.*, vol. 77, no. 5, 1948–1951 (1995).
- [5.127] W. T. C. Fang, T. T. Fang, P. B. Griffin, and J. D. Plummer, "Surface and Bulk Point Defect Generation in Czochralski and Float Zone Type Silicon Wafers," *Appl. Phys. Lett.*, vol. 68, no. 15, 2085–2087 (1996).
- [5.128] P. A. Stolk, H.-J. Goossen, D. J. Eaglesham, and J. M. Poate, "The Effect of Carbon on Diffusion in Silicon," *Materials Science and Engineering B*, vol. 36, 275–281 (1996).
- [5.129] J. S. Christensen, A. Y. Kuznetsov, H. H. Radamson, and B. G. Svensson, "Phosphorus Diffusion in Silicon; Influence of Annealing Conditions," in: *Si Front-End Processing — Physics and Technology of Dopant-Defect Interactions III*, edited by K. S. Jones, M. D. Giles, P. Stolk, J. Matsuo, and E. C. Jones, *Mat. Res. Soc. Symp. Proc.*, vol. 669, J3.9.1–J3.9.6 (2001).
- [5.130] N. R. Zangenberg, J. Fage-Pedersen, J. Lundsgaard Hansen, and A. Nylandsted Larsen, "Boron Diffusion in Strained and Relaxed $\text{Si}_{1-x}\text{Ge}_x$," in: *Diffusion in Materials DIMAT-2000*, edited by Y. Limoge and J. L. Bocquet, *Defect and Diffusion Forum*, vol. 194–199, 703–708 (2001).
- [5.131] J. S. Christensen, H. H. Radamson, A. Y. Kuznetsov, and B. G. Svensson, "Phosphorus and Boron Diffusion in Silicon under Equilibrium Conditions," *Appl. Phys. Lett.*, vol. 82, no. 14, 2254–2256 (2003).
- [5.132] N. R. Zangenberg, J. Fage-Pedersen, J. Lundgaard Hansen, and A. Nylandsted Larsen, "Boron and Phosphorus Diffusion in Strained and Relaxed Si and SiGe," *J. Appl. Phys.*, vol. 94, no. 6, 3883–3890 (2003).

- [5.133] K. P. Frohmader and L. Baumbauer, “Comparison of Thai’s Theory with Experimental Boron Doping Profiles in Silicon, Diffused from Boron Nitride Sources,” *Solid-State Electronics*, vol. 23, 1263–1265 (1980).
- [5.134] U. Södervall, A. Lodding, and W. Gust, “Activation Volumes of Impurity Diffusion in Silicon,” in: *Diffusion in Metals and Alloys DIMETA 88*, edited by F. J. Kedves and D. L. Beke, *Defect and Diffusion Forum*, vol. 66-69, 415–420 (1989).
- [5.135] Y. Zhao, M. J. Aziz, S. Mitha, and D. Schiferl, “Effect of Pressure on Boron Diffusion in Silicon,” in: *Defects in Electronic Materials II*, edited by J. Michel, T. Kennedy, K. Wada, and K. Thonke, *Mat. Res. Soc. Symp. Proc.*, vol. 442, 305–310 (1997).
- [5.136] Y. Zhao, M. J. Aziz, H.-J. Gossmann, S. Mitha, and D. Schiferl, “Activation Volume for Boron Diffusion in Silicon and Implications for Strained Films,” *Appl. Phys. Lett.*, vol. 74, no. 1, 31–33 (1999).
- [5.137] R. B. Fair, “On the Role of Self-Interstitials in Impurity Diffusion in Silicon,” *J. Appl. Phys.*, vol. 51, no. 11, 5828–5832 (1980).
- [5.138] D. A. Antoniadis and I. Moskowitz, “Diffusion of Substitutional Impurities in Silicon at Short Oxidation Times: An Insight into Point Defect Kinetics,” *J. Appl. Phys.*, vol. 53, no. 10, 6788–6796 (1982).
- [5.139] S. Matsumoto, Y. Ishikawa, and T. Niimi, “Fraction of Interstitialcy Mechanism in Impurity Diffusion in Silicon,” in: *Extended Abstracts of the 15th Conference on Solid State Devices and Materials*, Tokyo: Business Center for Academic Societies, 19–22 (1983).
- [5.140] S. Matsumoto, Y. Ishikawa, and T. Niimi, “Oxidation Enhanced and Concentration Dependent Diffusions of Dopants in Silicon,” *J. Appl. Phys.*, vol. 54, no. 9, 5049–5054 (1983).
- [5.141] T. Y. Tan, U. Gösele, and F. F. Morehead, “On the Nature of Point Defects and the Effect of Oxidation on Substitutional Dopant Diffusion in Silicon,” *Appl. Phys. A*, vol. 31, 97–108 (1983).
- [5.142] U. Gösele and T. Y. Tan, “The Nature of Point Defects and Their Influence on Diffusion Processes in Silicon at High Temperatures,” in: *Defects in Semiconductors II*, edited by S. Mahajan and J. W. Corbett, *Mat. Res. Soc. Symp. Proc.*, vol. 14, 45–59 (1983).
- [5.143] E. Guerrero, *Verteilung von Dotierungsatomen in Silicium-Einkristallen*, Ph.D. thesis, Technical University of Vienna (1984).
- [5.144] F. F. Morehead and R. F. Lever, “Enhanced “Tail” Diffusion of Phosphorus and Boron in Silicon: Self-Interstitial Phenomena,” *Appl. Phys. Lett.*, vol. 48, no. 2, 151–153 (1986).
- [5.145] D. Tsoukalas and P. Chenevier, “Boron Diffusion in Silicon in Inert and Oxidizing Ambient and Extrinsic Conditions,” *phys. stat. sol. (a)*, vol. 100, 461–465 (1987).
- [5.146] S. M. Hu, “Point Defect Generation and Enhanced Diffusion in Silicon Due to Tantalum Sili-cide Overlay,” *Appl. Phys. Lett.*, vol. 51, no. 5, 308–310 (1987).
- [5.147] B. J. Mulvaney, W. B. Richardson, and T. L. Crandle, “PEPPER — A Process Simulator for VLSI,” *IEEE Trans. Computer-Aided Design*, vol. 8, no. 4, 336–349 (1989).
- [5.148] M. D. Giles, “Defect-Coupled Diffusion at High Concentrations,” *IEEE Trans. Computer-Aided Design*, vol. 8, no. 5, 460–467 (1989).
- [5.149] P. B. Moynagh and P. J. Rosser, “Quantification of Diffusion Mechanisms of Boron, Phospho-rus, Arsenic, and Antimony in Silicon,” in: *ESSDERC’89*, edited by A. Heuberger, H. Ryssel, and P. Lange, Berlin: Springer-Verlag, 291–296 (1989).
- [5.150] P. A. Packan and J. D. Plummer, “Temperature and Time Dependence of B and P Diffusion in Si during Surface Oxidation,” *J. Appl. Phys.*, vol. 68, no. 8, 4327–4329 (1990).
- [5.151] D. Tsoukalas, “Transient Behavior of Boron Diffusion Coefficient in Silicon in Oxidizing Am-bient and Extrinsic Conditions: Influence of Point Defect Recombination,” *J. Appl. Phys.*, vol. 70, no. 12, 7309–7314 (1991).
- [5.152] K. Ghaderi, G. Hobler, M. Budil, H. Pötzl, P. Pichler, H. Ryssel, W. Hansch, I. Eisele, C. Tian, and G. Stingededer, “Simulation of Buried Layer Experiments Containing All Four Dopant Species,” in: *Semiconductor Silicon*, edited by H. R. Huff, W. Bergholz, and K. Sumino, *Elec-trochem. Soc. Proc.*, vol. 94-10, 613–624 (1994).

- [5.153] T. T. Fang, W. T. C. Fang, P. B. Griffin, and J. D. Plummer, "Calculation of the Fractional Interstitial Component of Boron Diffusion and Segregation Coefficient of Boron in Si(0.8)Ge(0.2)," *Appl. Phys. Lett.*, vol. 68, no. 6, 791–793 (1996).
- [5.154] H.-J. Gossmann, T. E. Haynes, P. A. Stolk, D. C. Jacobson, G. H. Gilmer, J. M. Poate, H. S. Luftman, T. K. Mogi, and M. O. Thompson, "The Interstitial Fraction of Diffusivity of Common Dopants in Si," *Appl. Phys. Lett.*, vol. 71, no. 26, 3862–3864 (1997).
- [5.155] T. Okino and T. Shimozaki, "Analysis of Dopant Diffusion in Si with Stacking Faults," *Materials Transactions, JIM*, vol. 40, no. 6, 474–478 (1999).
- [5.156] B. L. Crowder, J. F. Ziegler, F. F. Morehead, and G. W. Cole, "The Application of Ion Implantation to the Study of Diffusion of Boron in Silicon," in: *Ion Implantation in Semiconductors and Other Materials*, edited by B. L. Crowder, New York: Plenum Press, 267–274 (1973).
- [5.157] R. B. Fair, "Boron Diffusion in Silicon-Concentration and Orientation Dependence, Background Effects, and Profile Estimation," *J. Electrochem. Soc.*, vol. 122, no. 6, 800–805 (1975).
- [5.158] D. K. An, L. H. Mai, and P. Hoi, "Concentration Dependence of the Boron Diffusion Coefficient in Silicon," *phys. stat. sol. (a)*, vol. 76, K85–K88 (1983).
- [5.159] C. Kim, Z.-Y. Zhu, R.-I. Kang, and K. Shono, "Boltzmann-Matano Analysis of Boron Profiles in Silicon," *J. Electrochem. Soc.*, vol. 131, no. 12, 2962–2964 (1984).
- [5.160] F. Găseanu, "Boron Diffusion Profile in Silicon and Data Analysis," *J. Electrochem. Soc.*, vol. 132, no. 9, 2287–2289 (1985).
- [5.161] G. S. Hwang and W. A. Goddard III, "Shouldering in B Diffusion Profiles in Si: Role of Di-Boron Diffusion," *Appl. Phys. Lett.*, vol. 83, no. 17, 3501–3503 (2003).
- [5.162] K. H. Nicholas, "Studies of Anomalous Diffusion of Impurities," *Solid-State Electronics*, vol. 9, 35–47 (1966).
- [5.163] H. Rupprecht and G. H. Schwuttke, "Distribution of Boron-Induced Defects in Shallow Difused Surface Layers of Silicon," *J. Appl. Phys.*, vol. 37, no. 7, 2862–2866 (1966).
- [5.164] S. Matsumoto, Y. Ishikawa, Y. Shirai, S. Sekine, and T. Niimi, "Concentration Dependence of the Diffusion Coefficient of Boron in Silicon," *Jpn. J. Appl. Phys.*, vol. 19, no. 1, 217–218 (1980).
- [5.165] J. E. Lawrence, "The Cooperative Diffusion Effect," *J. Appl. Phys.*, vol. 37, no. 11, 4106–4112 (1966).
- [5.166] B. Ittermann, D. Peters, M. Füllgrabe, F. Kroll, H. Ackermann, and H.-J. Stöckmann, "Mobility of Interstitial B in Si Analyzed by a Stochastic Reorientation Model," *Physica B*, vol. 308–310, 236–239 (2001).
- [5.167] C. Lucas, J. P. Gailliard, S. Loualiche, P. Baruch, J. C. Pfister, and R. Truche, "Study of the Diffusion of Boron in High-Temperature Proton-Irradiated Silicon," in: *Defects and Radiation Effects in Semiconductors, 1978*, edited by J. H. Albany, *Inst. Phys. Conf. Ser.*, no. 46, 551–558 (1979).
- [5.168] P. J. Drevinsky, C. E. Caefer, S. P. Tobin, J. C. Mikkelsen, Jr., and L. C. Kimerling, "Influence of Oxygen and Boron on Defect Production in Irradiated Silicon," in: *Defects in Electronic Materials*, edited by M. Stavola, S. J. Pearton, and G. Davies, *Mat. Res. Soc. Symp. Proc.*, vol. 104, 167–172 (1988).
- [5.169] S. Libertino, J. L. Benton, D. C. Jacobson, D. J. Eaglesham, J. M. Poate, S. Coffa, P. G. Fuochi, and M. Lavalle, "The Effect of Impurity Content on Point Defect Evolution in Ion Implanted and Electron Irradiated Si," *Appl. Phys. Lett.*, vol. 70, no. 22, 3002–3004 (1997).
- [5.170] E. J. H. Collart, K. Weemers, D. J. Gravenstein, J. G. M. van Berkum, and N. E. B. Cowern, "Room-Temperature Migration of Ion-Implanted Boron in Silicon," in: *Defects and Diffusion in Silicon Processing*, edited by T. Diaz de la Rubia, S. Coffa, P. A. Stolk, and C. S. Rafferty, *Mat. Res. Soc. Symp. Proc.*, vol. 469, 53–58 (1997).
- [5.171] N. E. B. Cowern, E. J. H. Collart, J. Politiek, P. H. L. Bancken, J. G. M. van Berkum, K. Kyllonen Larsen, P. A. Stolk, H. G. A. Huitzing, P. Pichler, A. Burenkov, and D. J. Gravenstein, "Low Energy Implantation and Transient Enhanced Diffusion: Physical Mechanisms and Technology Implications," in: *Defects and Diffusion in Silicon Processing*, edited by T. Diaz de la

- Rubia, S. Coffa, P. A. Stolk, and C. S. Rafferty, *Mat. Res. Soc. Symp. Proc.*, vol. 469, 265–276 (1997).
- [5.172] H. G. A. Huizing, C. C. G. Visser, N. E. B. Cowern, P. A. Stolk, and R. C. M. de Kruif, “Ultrafast Interstitial Injection during Transient Enhanced Diffusion of Boron in Silicon,” *Appl. Phys. Lett.*, vol. 69, no. 9, 1211–1213 (1996).
- [5.173] R. Schork, P. Pichler, A. Kluge, and H. Ryssel, “Radiation-Enhanced Diffusion during High-Temperature Ion Implantation,” in: *Ion Beam Modification of Materials*, edited by S. P. Withrow and D. B. Poker, *Nuclear Instruments and Methods in Physics Research B*, vol. 59/60, 499–503 (1991).
- [5.174] N. E. B. Cowern, K. T. F. Janssen, G. F. A. van de Walle, and K. J. Gravesteijn, “Impurity Diffusion via an Intermediate Species: The B-Si System,” *Phys. Rev. Lett.*, vol. 65, no. 19, 2434–2437 (1990).
- [5.175] N. E. B. Cowern, G. F. A. van de Walle, D. J. Gravesteijn, and C. J. Vriezema, “Experiments on Atomic-Scale Mechanisms of Diffusion,” *Phys. Rev. Lett.*, vol. 67, no. 2, 212–215 (1991).
- [5.176] N. E. B. Cowern, G. F. A. van de Walle, P. C. Zalm, and D. J. Oostra, “Reactions of Point Defects and Dopant Atoms in Silicon,” *Phys. Rev. Lett.*, vol. 69, no. 1, 116–119 (1992).
- [5.177] N. E. B. Cowern, G. Mannino, P. A. Stolk, F. Roozeboom, H. G. A. Huizing, J. G. M. van Berkum, F. Cristiano, A. Claverie, and M. Jaraiz, “Cluster Ripening and Transient Enhanced Diffusion in Silicon,” *Materials Science in Semiconductor Processing*, vol. 2, 369–376 (1999).
- [5.178] G. Mannino, S. Whelan, E. Schroer, V. Privitera, P. Leveque, B. G. Svensson, and E. Napolitani, “An Investigation of the Modelling of Transient Enhanced Diffusion of Ultralow Energy Implanted Boron in Silicon,” *J. Appl. Phys.*, vol. 89, no. 10, 5381–5385 (2001).
- [5.179] P. Lévéque, A. Y. Kuznetsov, J. S. Christensen, B. G. Svensson, and A. Nylandsted Larsen, “Irradiation Enhanced Diffusion of Boron in Delta-Doped Silicon,” *J. Appl. Phys.*, vol. 89, no. 10, 5400–5405 (2001).
- [5.180] M. M. de Souza and G. A. J. Amaralunga, “A Monte Carlo Study of the Kickout Mechanism of Boron Diffusion in Silicon,” *J. Appl. Phys.*, vol. 79, no. 5, 2418–2425 (1996).
- [5.181] I. D. Sharp, H. A. Bracht, H. H. Silvestri, S. P. Nicols, J. W. Beeman, J. L. Hansen, A. Nylandsted Larsen, and E. E. Haller, “Self- and Dopant Diffusion in Extrinsic Boron Doped Isotopically Controlled Silicon Multilayer Structures,” in: *Defect and Impurity Engineered Semiconductors and Devices III*, edited by S. Ashok, J. Chevallier, N. M. Johnson, B. L. Sopori, and H. Okushi, *Mat. Res. Soc. Symp. Proc.*, vol. 719, F13.11.1–F13.11.6 (2002).
- [5.182] P. Kohli, H.-J. Li, S. Ganguly, T. Kirichenko, B. Murto, E. Graetz, P. Zeitzoff, M. Pawlik, P. B. Merrill, and S. Banerjee, “High Ramp Rate Rapid Thermal Annealing for Ultra-Shallow Junctions,” in: *Rapid Thermal and Other Short-Time Processing Technologies*, edited by F. Roozeboom, M. C. Öztürk, J. C. Gelpay, K. G. Reid, and D.-L. Kwong, *Electrochem. Soc. Proc.*, vol. 2000-9, 3–14 (2000).
- [5.183] H.-J. Li, P. Kohli, S. Ganguly, T. A. Kirichenko, P. Zeitzoff, K. Torres, and S. Banerjee, “Boron Diffusion and Activation in the Presence of Other Species,” in: *Technical Digest of the 2000 International Electron Devices Meeting (IEDM)*, Piscataway: IEEE, 515–518 (2000).
- [5.184] R. D. Harris, G. D. Watkins, and L. C. Kimerling, “Migration of Interstitial Boron in Silicon,” in: *Defects in Semiconductors 14*, edited by H. J. von Bardeleben, *Materials Science Forum*, vol. 10-12, 163–168 (1986).
- [5.185] V. D. Akhmetov and V. V. Bolotov, “The Effect of Carbon and Boron on the Accumulation of Vacancy-Oxygen Complexes in Silicon,” *Radiation Effects*, vol. 52, 149–152 (1980).
- [5.186] T. J. Lenosky, B. Sadigh, S. K. Theiss, M. J. Caturla, and T. Diaz de la Rubia, “Ab Initio Energetics of Boron-Interstitial Clusters in Crystalline Si,” *Appl. Phys. Lett.*, vol. 77, no. 12, 1834–1836 (2000).
- [5.187] X.-Y. Liu, W. Windl, and M. P. Masquelier, “Ab Initio Modeling of Boron Clustering in Silicon,” *Appl. Phys. Lett.*, vol. 77, no. 13, 2018–2020 (2000).
- [5.188] X.-Y. Liu, W. Windl, and M. P. Masquelier, “Erratum: ‘Ab Initio Modeling of Boron Clustering in Silicon’ [Appl. Phys. Lett. 77, 2018 (2000)],” *Appl. Phys. Lett.*, vol. 77, no. 24, 4064 (2000).

- [5.189] P. Deák, A. Gali, A. Sólyom, P. Ordejón, K. Kamarás, and G. Battistig, "Studies of Boron-Interstitial Clusters in Si," *J. Phys.: Condens. Matter*, vol. 15, 4967–4977 (2003).
- [5.190] M. Okamoto, K. Takayanagi, and S. Takeda, "Boron Clusters in a Complex Defect in Silicon," in: *Defect and Impurity Engineered Semiconductors II*, edited by S. Ashok, J. Chevalier, K. Sumino, B. L. Sopori, and W. Götz, *Mat. Res. Soc. Symp. Proc.*, vol. 510, 343–348 (1998).
- [5.191] X. Luo, S. B. Zhang, and S.-H. Wei, "Understanding Ultrahigh Doping: The Case of Boron in Silicon," *Phys. Rev. Lett.*, vol. 90, 026103 (2003).
- [5.192] W. Windl, "Multiscale Simulation of Diffusion, Deactivation and Segregation of Boron in Silicon," *IEICE Trans. Electron.*, vol. E86-C, no. 3, 269–275 (2003).
- [5.193] A. Khan, M. Yamaguchi, Y. Ohshita, N. Dharmarasu, K. Araki, T. Abe, Hisayoshi Itoh, T. Ohshima, M. Imaizumi, and S. Matsuda, "Role of the Impurities in Production Rates of Radiation-Induced Defects in Silicon Materials and Solar Cells," *J. Appl. Phys.*, vol. 90, no. 3, 1170–1178 (2001).
- [5.194] A. Vailionis, G. Glass, P. Desjardins, D. G. Cahill, and J. E. Greene, "Electrically Active and Inactive B Lattice Sites in Ultrahighly B Doped Si(001): An X-Ray Near-Edge Absorption Fine-Structure and High-Resolution Diffraction Study," *Phys. Rev. Lett.*, vol. 82, no. 22, 4464–4467 (1999).
- [5.195] K. Thonke, J. Weber, J. Wagner, and R. Sauer, "Origin of the 1.080 eV (I2) Photoluminescence Line in Irradiated Silicon," in: *Proceedings of the 12th International Conference on Defects in Semiconductors*, edited by C. A. J. Ammerlaan, *Physica*, vol. 116B, 252–257 (1983).
- [5.196] E. Tarnow, "Theory of Two Boron Neutral Pair Defects in Silicon," *J. Phys.: Condens. Matter*, vol. 4, 5405–5410 (1992).
- [5.197] P. Alippi, P. Ruggerone, and L. Colombo, "Atomistic Study of Boron Clustering in Silicon," in: *Gettering and Defect Engineering in Semiconductor Technology GADEST 2001*, edited by V. Rainieri, F. Priolo, M. Kittler, and H. Richter, *Solid State Phenomena*, vol. 82–84, 163–170 (2002).
- [5.198] G. S. Hwang and W. A. Goddard III, "Diffusion of the Diboron Pair in Silicon," *Phys. Rev. Lett.*, vol. 89, no. 5, 055901 (2002).
- [5.199] M. P. Shishkin and M. M. De Souza, "Structure and Diffusion of Interstitial Boron Pairs in Silicon," *Phys. Rev. B*, vol. 69, 033201 (2004).
- [5.200] I. Mizushima, A. Murakoshi, M. Watanabe, M. Yoshiki, M. Hotta, and M. Kashiwagi, "Hole Generation without Annealing in High Dose Boron Implanted Silicon: Heavy Doping by B₁₂ Icosahedron As a Double Acceptor," *Jpn. J. Appl. Phys., Part 1*, vol. 33, no. 1B, 404–407 (1994).
- [5.201] J. Yamauchi, N. Aoki, and I. Mizushima, "First-Principles Study on B₁₂ Clusters in Si," *Phys. Rev. B*, vol. 55, no. 16, R10245–R10252 (1997).
- [5.202] J. Yamauchi, N. Aoki, and I. Mizushima, "Dynamical Properties of Impurity Clusters in Silicon," *phys. stat. sol. (b)*, vol. 210, 273–276 (1998).
- [5.203] L. Pelaz, M. Jaraiz, G. H. Gilmer, H.-J. Gossmann, C. S. Rafferty, D. J. Eaglesham, and J. M. Poate, "B Diffusion and Clustering in Ion Implanted Si: The Role of B Cluster Precursors," *Appl. Phys. Lett.*, vol. 70, no. 17, 2285–2287 (1997).
- [5.204] M.-J. Caturla, T. Diaz de la Rubia, J. Zhu, and M. Johnson, "Monte Carlo Simulation of Boron Diffusion during Low Energy Implantation and High Temperature Annealing," in: *Defects and Diffusion in Silicon Processing*, edited by T. Diaz de la Rubia, S. Coffa, P. A. Stolk, and C. S. Rafferty, *Mat. Res. Soc. Symp. Proc.*, vol. 469, 335–340 (1997).
- [5.205] A. D. Lilak, S. K. Earles, K. S. Jones, M. E. Law, and M. D. Giles, "A Physics-Based Modeling Approach for the Simulation of Anomalous Boron Diffusion and Clustering Behaviors," in: *Technical Digest of the 1997 International Electron Devices Meeting (IEDM)*, Piscataway: IEEE, 493–496 (1997).
- [5.206] M. J. Caturla, M. D. Johnson, and T. Diaz de la Rubia, "The Fraction of Substitutional Boron in Silicon during Ion Implantation and Thermal Annealing," *Appl. Phys. Lett.*, vol. 72, no. 21, 2736–2738 (1998).

- [5.207] L. Pelaz, G. H. Gilmer, H.-J. Gossmann, C. S. Rafferty, M. Jaraiz, and J. Barbolla, “B Cluster Formation and Dissolution in Si: A Scenario Based on Atomistic Modeling,” *Appl. Phys. Lett.*, vol. 74, no. 24, 3657–3659 (1999).
- [5.208] D. Stiebel, P. Pichler, and H. Ryssel, “On the Influence of Boron-Interstitial Complexes on Transient Enhanced Diffusion,” in: *Si Front-End Processing — Physics and Technology of Dopant-Defect Interactions*, edited by H.-J. L. Gossmann, T. E. Haynes, M. E. Law, A. Nylandsted Larsen, and S. Odanaka, *Mat. Res. Soc. Symp. Proc.*, vol. 568, 141–146 (1999).
- [5.209] S. K. Theiss, J. M. Caturla, M. D. Johnson, J. Zhu, T. Lenosky, B. Sadigh, and T. Diaz de la Rubia, “Atomic Scale Models of Ion Implantation and Dopant Diffusion in Silicon,” *Thin Solid Films*, vol. 365, 219–230 (2000).
- [5.210] S. Chakravarthi and S. T. Dunham, “A Simple Continuum Model for Boron Clustering Based on Atomistic Calculations,” *J. Appl. Phys.*, vol. 89, no. 7, 3650–3655 (2001).
- [5.211] F. Boucard, D. Mathiot, E. Guichard, and P. Rivallin, “A Model for Boron TED in Silicon: Full Couplings of Dopant with Free and Clustered Interstitials,” in: *Silicon Front-End Junction Formation Technologies*, edited by D. F. Downey, M. E. Law, A. P. Claverie, and M. J. Rendon, *Mat. Res. Soc. Symp. Proc.*, vol. 717, C5.2.1–C5.2.6 (2002).
- [5.212] W. Luo, P. B. Rasband, P. Clancy, and B. W. Roberts, “Tight-Binding Studies of the Tendency for Boron to Cluster in c-Si. II. Interaction of Dopants and Defects in Boron-Doped Si,” *J. Appl. Phys.*, vol. 84, no. 5, 2476–2486 (1998).
- [5.213] W. Luo and P. Clancy, “Identification of Stable Boron Clusters in c-Si Using Tight-Binding Statics,” *J. Appl. Phys.*, vol. 89, no. 3, 1596–1604 (2001).
- [5.214] P. Pichler, “Current Understanding and Modeling of Boron-Interstitial Clusters,” in: *Silicon Front-End Junction Formation Technologies*, edited by D. F. Downey, M. E. Law, A. P. Claverie, and M. J. Rendon, *Mat. Res. Soc. Symp. Proc.*, vol. 717, C3.1.1–C3.1.12 (2002).
- [5.215] N. E. B. Cowern and D. J. Godfrey, “A Model for Coupled Dopant Diffusion in Silicon,” *COMPEL*, vol. 6, no. 1, 59–63 (1987).
- [5.216] N. E. B. Cowern, “Ion Pairing Effects on Substitutional Impurity Diffusion in Silicon,” *Appl. Phys. Lett.*, vol. 54, no. 8, 703–705 (1989).
- [5.217] F. Wittel and S. Dunham, “Diffusion of Phosphorus in Arsenic and Boron-Doped Silicon,” *Appl. Phys. Lett.*, vol. 66, no. 11, 1415–1417 (1995).
- [5.218] E. G. Tishkovskii, V. I. Obodnikov, A. A. Taskin, K. V. Feklistov, and V. G. Seryapin, “Redistribution of Phosphorus Implanted into Silicon Doped Heavily with Boron,” *Semiconductors*, vol. 34, no. 6, 629–633 (2000).
- [5.219] R. Kim, T. Aoki, T. Hirose, Y. Furuta, S. Hayashi, T. Shano, and K. Taniguchi, “Modeling of Arsenic Transient Enhanced Diffusion and Background Boron Segregation in Low-Energy As⁺ Implanted Si,” in: *Technical Digest of the 2000 International Electron Devices Meeting (IEDM)*, Piscataway: IEEE, 523–526 (2000).
- [5.220] C.-Y. Moon, Y.-S. Kim, and K. J. Chang, “Atomic Structure of B-Related and B Diffusion in Si Predoped with P Impurities,” *Phys. Rev. B*, vol. 69, 085208 (2004).
- [5.221] J. F. Ziegler, G. W. Cole, and J. E. E. Baglin, “Discovery of Anomalous Base Regions in Transistors,” *Appl. Phys. Lett.*, vol. 21, no. 4, 177–179 (1972).
- [5.222] R. B. Fair, “Quantitative Theory of Retarded Base Diffusion in Silicon N-P-N Structures with Arsenic Emitters,” *J. Appl. Phys.*, vol. 44, no. 1, 283–291 (1973).
- [5.223] K. Yokota, M. Ochi, T. Hirao, Y. Horino, M. Satho, Y. Ando, and K. Matsuda, “Interactions between Arsenic and Boron Implanted in Silicon during Annealing,” *J. Appl. Phys.*, vol. 69, no. 5, 2975–2980 (1991).
- [5.224] K. Yokota, Y. Sunagawa, T. Hirao, Y. Ando, and K. Matsuda, “Chemical Interactions between Arsenic and Boron Implanted in Silicon during Annealing,” *Jpn. J. Appl. Phys., Part 2*, vol. 31, no. 8A, L1100–L1102 (1992).
- [5.225] K. Yokota, Y. Okamoto, F. Miyashita, T. Hirao, M. Watanabe, K. Sekine, Y. Ando, and K. Matsuda, “Dual Arsenic and Boron Ion Implantation in Silicon,” *J. Appl. Phys.*, vol. 75, no. 11, 7247–7251 (1994).

- [5.226] S. Solmi, S. Valmorri, and R. Canteri, "Codiffusion of Arsenic and Boron Implanted in Silicon," *J. Appl. Phys.*, vol. 77, no. 6, 2400–2406 (1995).
- [5.227] B. Margesin, R. Canteri, S. Solmi, A. Armigliato, and F. Baruffaldi, "Boron and Antimony Codiffusion in Silicon," *J. Mater. Res.*, vol. 6, no. 11, 2353–2361 (1991).
- [5.228] S. Solmi, "Counterdoped Very Shallow p⁺/n Junctions Obtained by B and Sb Implantation and Codiffusion in Si," *J. Appl. Phys.*, vol. 83, no. 3, 1742–1747 (1998).
- [5.229] J. L. Allain, A. Bourret, J. R. Regnard, and A. Armigliato, "X-Ray Absorption Study of the Atomic Environment of Sb⁺ and Sb^{+/B⁺} Implanted Silicon," *Appl. Phys. Lett.*, vol. 61, 264–266 (1992).
- [5.230] P. M. Mooney, L. J. Cheng, M. Süli, J. D. Gerson, and J. W. Corbett, "Defect Energy Levels in Boron-Doped Silicon Irradiated with 1-MeV Electrons," *Phys. Rev. B*, vol. 15, no. 8, 3836–3843 (1977).
- [5.231] M. Roux, J. Bernard, R. Reulet, and R. L. Crabb, "Photon Effect on Electron-Irradiated Boron-Doped Silicon Solar Cell," *J. Appl. Phys.*, vol. 56, no. 2, 531–537 (1984).
- [5.232] C. A. Londos, "Annealing Study of Defects Pertinent to Radiation Damage in Si:B," *phys. stat. sol. (a)*, vol. 102, 639–644 (1987).
- [5.233] M. Asghar, M. Zafar Iqbal, and N. Zafar, "Study of Alpha-Radiation-Induced Deep Levels in p-Type Silicon," *J. Appl. Phys.*, vol. 73, no. 9, 4240–4247 (1993).
- [5.234] J. Vanhellemont, A. Kaniava, E. Simoen, M.-A. Trauwaert, C. Claeys, B. Johlander, R. Harboe-Sörensen, L. Adams, and P. Clauws, "Generation and Annealing Behaviour of MeV Proton and ²⁵²Cf Irradiation Induced Deep Levels in Silicon Diodes," *IEEE Trans. Nuclear Science*, vol. NS-41, no. 3, 479–486 (1994).
- [5.235] M.-A. Trauwaert, J. Vanhellemont, H. E. Maes, A.-M. Van Bavel, G. Langouche, A. Stesmans, and P. Clauws, "Influence of Oxygen and Carbon on the Generation and Annihilation of Radiation Defects in Silicon," *Materials Science and Engineering B*, vol. 36, 196–199 (1996).
- [5.236] J. Adey, R. Jones, and P. R. Briddon, "Formation of Bi_iO_i, Bi_iC_s, and Bi_iB_sH_i Defects in e-Irradiated or Ion-Implanted Silicon Containing Boron," *Appl. Phys. Lett.*, vol. 83, no. 4, 665–667 (2003).
- [5.237] N. Yarykin, O. V. Feklisova, and J. Weber, "Dominant Boron-Related Radiation Defect in Silicon Revealed by Hydrogenation," in: *Proceedings of the 22nd International Conference on Defects in Semiconductors*, edited by K. Bonde Nielsen, A. Nylandsted Larsen, and G. Weyer, *Physica B*, vol. 340–342, 528–531 (2003).
- [5.238] Y. Ohshita, T. K. Vu, and M. Yamaguchi, "Interstitial Boron and Oxygen Related Defects As the Origin of the Deep Energy Level in Czochralski-Grown Silicon," *J. Appl. Phys.*, vol. 91, no. 6, 3741–3744 (2002).
- [5.239] I. Weinberg and C. K. Swartz, "Origin of Reverse Annealing in Radiation-Damaged Silicon Solar Cells," *Appl. Phys. Lett.*, vol. 36, no. 8, 693–695 (1980).
- [5.240] M. Yamaguchi, A. Khan, S. J. Taylor, K. Ando, T. Yamaguchi, S. Matsuda, and T. Aburaya, "Deep Level Analysis of Radiation-Induced Defects in Si Crystals and Solar Cells," *J. Appl. Phys.*, vol. 86, no. 1, 217–223 (1999).
- [5.241] H. Fischer and W. Pschunder, "Investigation of Photon and Thermal Induced Changes in Silicon Solar Cells," in: *10th IEEE Photovoltaic Specialists Conference*, New York: IEEE, 404–411 (1973).
- [5.242] J. Schmidt, A. G. Aberle, and R. Hezel, "Investigation of Carrier Lifetime Instabilities in CZ-Grown Silicon," in: *26th IEEE Photovoltaic Specialists Conference*, Piscataway: IEEE, 13–18 (1997).
- [5.243] S. W. Glunz, S. Rein, W. Warta, J. Knobloch, and W. Wetling, "On the Degradation of CZ-Silicon Solar Cells," in: *2nd World Conference on Photovoltaic Solar Energy Conversion*, edited by J. Schmid, H. A. Ossenbrink, P. Helm, H. Ehmann, and E. D. Dunlop, Luxembourg: Office for Official Publications of the European Communities, 1343–1346 (1998).
- [5.244] J. Schmidt and A. Cuevas, "Electronic Properties of Light-Induced Recombination Centers in Boron-Doped Czochralski Silicon," *J. Appl. Phys.*, vol. 86, no. 6, 3175–3180 (1999).

- [5.245] S. W. Glunz, S. Rein, J. Y. Lee, and W. Warta, "Minority Carrier Lifetime Degradation in Boron-Doped Czochralski Silicon," *J. Appl. Phys.*, vol. 90, no. 5, 2397–2404 (2001).
- [5.246] J. C. Bourgoin, N. de Angelis, and G. Strobl, "Light Induced Degradation of Si Cells. Model of a Metastable Defect," in: *Proceedings of the 16th European Photovoltaic Solar Energy Conference*, edited by H. Scheer, B. McNelis, W. Palz, H. A. Ossenbrink, and P. Helm, London: James & James, 1356–1358 (2000).
- [5.247] S. Rein, T. Rehrl, W. Warta, S. W. Glunz, and G. Willeke, "Electrical and Thermal Properties of the Metastable Defect in Boron-Doped Czochralski Silicon (CZ-Si)," in: *Proceedings of the 17th European Photovoltaic Solar Energy Conference*, Munich: WIP-Renewable Energies, 1555–1560 (2001).
- [5.248] J. Schmidt and K. Bothe, "Structure and Transformation of the Metastable Boron- and Oxygen-Related Defect Center in Crystalline Silicon," *Phys. Rev. B*, vol. 69, 024107 (2004).
- [5.249] S. Rein and S. W. Glunz, "Electronic Properties of the Metastable Defect in Boron-Doped Czochralski Silicon: Unambiguous Determination by Advanced Lifetime Spectroscopy," *Appl. Phys. Lett.*, vol. 82, no. 7, 1054–1056 (2003).
- [5.250] T. Ono, G. A. Rozgonyi, E. Asayama, H. Horie, H. Tsuya, and K. Sueoka, "Oxygen Diffusion in Heavily Antimony-, Arsenic-, and Boron-Doped Czochralski Silicon Wafers," *Appl. Phys. Lett.*, vol. 74, no. 24, 3648–3650 (1999).
- [5.251] H. Takeno, K. Sunakawa, and M. Suezawa, "Temperature-Dependent Retardation Effect of Dopants on Oxygen Diffusion in Heavily Doped Czochralski Silicon," *Appl. Phys. Lett.*, vol. 77, no. 3, 376–378 (2000).
- [5.252] W. Puff, P. Mascher, D. Kerr, and S. Dannefaer, "Effects of Boron Doping on the Annealing Characteristics of Cz-Silicon," in: *Defects in Semiconductors 15*, edited by G. Ferenczi, *Materials Science Forum*, vol. 38-41, 225–229 (1989).
- [5.253] M. Fujinami and S. Hayashi, "Study of Defect Behavior in Ion-Implanted Si Wafers by Slow Positron Annihilation Spectroscopy," in: *Defects in Semiconductors 18*, edited by M. Suezawa and H. Katayama-Yoshida, *Materials Science Forum*, vol. 196-201, 1165–1169 (1995).
- [5.254] S. Eichler, J. Gebauer, F. Börner, A. Polity, R. Krause-Rehberg, E. Wendler, B. Weber, W. Wesch, and H. Börner, "Defects in Silicon after B⁺ Implantation: A Study Using a Positron-Beam Technique, Rutherford Backscattering, Secondary Neutral Mass Spectroscopy, and Infrared Absorption Spectroscopy," *Phys. Rev. B*, vol. 56, no. 3, 1393–1403 (1997).
- [5.255] F. Hori, T. Chijiwa, R. Oshima, and T. Hisamatsu, "Positron Annihilation Study of Dopant Effects on Proton-Irradiated Defect in Silicon," in: *20th International Conference on Defects in Semiconductors*, edited by C. Van de Walle and W. Walukiewicz, *Physica B*, vol. 273-274, 480–484 (1999).
- [5.256] T. Tamano, F. Hori, R. Oshima, and T. Hisamatsu, "Study of Behavior of Electron Irradiation Defects and Impurities in Czochralski Silicon with Annealing by Positron Annihilation," *Jpn. J. Appl. Phys., Part 1*, vol. 40, no. 2A, 452–456 (2001).
- [5.257] T. T. Braggins, H. M. Hobgood, J. C. Swartz, and R. N. Thomas, "High Infrared Responsivity Indium-Doped Silicon Detector Material Compensated by Neutron Transmutation," *IEEE Trans. Electron Devices*, vol. ED-27, no. 1, 2–10 (1980).
- [5.258] M. G. Holland and W. Paul, "Effect of Pressure on the Energy Levels of Impurities in Semiconductors. I. Arsenic, Indium, and Aluminum in Silicon," *Phys. Rev.*, vol. 128, no. 1, 30–38 (1962).
- [5.259] A. Rockett, D. D. Johnson, S. V. Khare, and B. R. Tuttle, "Prediction of Dopant Ionization Energies in Silicon: The Importance of Strain," *Phys. Rev. B*, vol. 68, 233208 (2003).
- [5.260] M. L. W. Thewalt, "Details of the Structure of Bound Excitons and Bound Multiexciton Complexes in Si," *Can. J. Phys.*, vol. 55, no. 17, 1463–1480 (1977).
- [5.261] F. Bechstedt and W. A. Harrison, "Lattice Relaxation around Substitutional Defects in Semiconductors," *Phys. Rev. B*, vol. 39, no. 8, 5041–5050 (1989).
- [5.262] G. D. Watkins, "A Review of EPR Studies in Irradiated Silicon," in: *Radiation Damage in Semiconductors*, Paris: Dunod, 97–113 (1964).

- [5.263] K. L. Brower, "Electron Paramagnetic Resonance of the Aluminum Interstitial in Silicon," *Phys. Rev. B*, vol. 1, no. 5, 1908–1917 (1970).
- [5.264] J. R. Niklas, J.-M. Spaeth, and G. D. Watkins, "ENDOR-Investigations of Al⁺⁺ and Al⁺⁺⁺-Al[−] Pairs in Silicon," in: *Microscopic Identification of Electronic Defects in Semiconductors*, edited by N. M. Johnson, S. G. Bishop, and G. D. Watkins, *Mat. Res. Soc. Symp. Proc.*, vol. 46, 237–242 (1985).
- [5.265] L. C. Kimerling, "Defect States in Electron-Bombarded Silicon: Capacitance Transient Analyses," in: *Radiation Effects in Semiconductors, 1976*, edited by N. B. Urli and J. W. Corbett, *Inst. Phys. Conf. Ser.*, no. 31, 221–230 (1977).
- [5.266] J. R. Troxell, A. P. Chatterjee, G. D. Watkins, and L. C. Kimmerling, "Recombination-Enhanced Migration of Interstitial Aluminum in Silicon," *Phys. Rev. B*, vol. 19, no. 10, 5336–5348 (1979).
- [5.267] R. Car, P. J. Kelly, A. Oshiyama, and S. T. Pantelides, "Microscopic Theory of Impurity-Defect Reactions and Impurity Diffusion in Silicon," *Phys. Rev. Lett.*, vol. 54, no. 4, 360–363 (1985).
- [5.268] R. Car, P. J. Kelly, A. Oshiyama, and S. T. Pantelides, "Microscopic Theory of Self-Diffusion and Impurity Diffusion in Silicon," in: *Thirteenth International Conference on Defects in Semiconductors*, edited by L. C. Kimerling and J. M. Parsey, Jr., The Metallurgical Society of AIME, 269–275 (1985).
- [5.269] H. Overhof and G. Corradi, "Electronic Structure of Isolated Aluminium Point Defects and Defect Pairs in Silicon," in: *Defects in Semiconductors I6*, edited by G. Davies, G. G. DeLeo, and M. Stavola, *Materials Science Forum*, vol. 83-87, 279–284 (1992).
- [5.270] G. D. Watkins, "Defects in Irradiated Silicon: Electron Paramagnetic Resonance and Electron-Nuclear Double Resonance of the Aluminium-Vacancy Pair," *Phys. Rev.*, vol. 155, no. 3, 802–815 (1967).
- [5.271] G. D. Watkins, "Intrinsic Point Defects in Semiconductors," in: *Electronic Structure and Properties of Semiconductors*, edited by W. Schröter, *Materials Science and Technology: A Comprehensive Treatment*, vol. 4, Weinheim: VCH, 105–141 (1991).
- [5.272] A. Chantre, "Defects in Ultrafast Quenched Aluminum-Doped Silicon," *Appl. Phys. Lett.*, vol. 46, no. 3, 263–265 (1985).
- [5.273] J. L. Murray and A. J. McAlister, "The Al-Si (Aluminum-Silicon) System," *Bulletin of Alloy Phase Diagrams*, vol. 5, no. 1, 74–84 (1984).
- [5.274] R. C. Miller and A. Savage, "Diffusion of Aluminum in Single Crystal Silicon," *J. Appl. Phys.*, vol. 27, no. 12, 1430–1432 (1956).
- [5.275] Y. C. Kao, "On the Diffusion of Aluminum into Silicon," *Electrochemical Technology*, vol. 5, no. 3-4, 90–94 (1967).
- [5.276] D. Navon and V. Chernyshov, "Retrograde Solubility of Aluminum in Silicon," *J. Appl. Phys.*, vol. 28, no. 7, 823–824 (1957).
- [5.277] V. N. Lozovskii and A. I. Udyanskaya, "Solubility of Aluminum in Silicon Single Crystals," *Inorganic Materials*, vol. 4, no. 7, 1030–1031 (1968).
- [5.278] T. Yoshikawa and K. Morita, "Solid Solubilities and Thermodynamic Properties of Aluminum in Solid Silicon," *J. Electrochem. Soc.*, vol. 150, no. 8, G465–G468 (2003).
- [5.279] R. A. Gudmundsen and J. Maserjian, Jr., "Semiconductor Properties of Recrystallized Silicon in Aluminium Alloy Junction Diodes," *J. Appl. Phys.*, vol. 28, no. 11, 1308–1316 (1957).
- [5.280] H. Spengler, "Über das System Aluminium-Silizium," *Metall*, vol. 9, no. 5/6, 181–186 (1955).
- [5.281] V. M. Glazov and L. Chzhen'-Yuan', *Investigation of Separate and Joint Solubilities of Aluminum and Antimony in Silicon*, Russian Metallurgy and Fuels, London: Scientific Information Consultants (1960).
- [5.282] R. A. Akopyan and V. V. Kachakhidze, "Refinement of the Boundaries of Silicon-Based Regions of Homogeneity in the Si-Al and Si-Ga Systems," *Inorg. Mater.*, vol. 17, no. 10, 1326–1328 (1982).

- [5.283] R. F. Bailey and T. G. Mills, "Solid Solubility of Aluminum in Silicon by Electron Beam Microprobe Analysis," *Electrochem. Soc. Extended Abstracts*, vol. 71-1, 159–160 (1971).
- [5.284] C. S. Fuller and J. A. Ditzenberger, "Diffusion of Donor and Acceptor Elements in Silicon," *J. Appl. Phys.*, vol. 27, no. 5, 544–553 (1956).
- [5.285] R. Bullough, R. C. Newman, and J. Wakefield, "Diffusion of Aluminium to the Surface and to Dislocations in Silicon," *Proc. IEE*, vol. 106B (supp.15), 277–281 (1959).
- [5.286] W. Rosnowski, "Aluminum Diffusion into Silicon in an Open Tube High Vacuum System," *J. Electrochem. Soc.*, vol. 125, no. 6, 957–962 (1978).
- [5.287] M. Chang, "Open-Tube Diffusion," *J. Electrochem. Soc.*, vol. 128, no. 9, 1987–1992 (1981).
- [5.288] Y. D. Nisnevich, "Aluminum Distribution for Diffusion into Silicon from Doped SiO₂," *Izv. Akad. Nauk SSSR, Neorg. Mater.*, vol. 19, no. 6, 853–856 (1983).
- [5.289] H. Mitlehner and H.-J. Schulze, "Current Developments in High-Power Thyristors," *EPE Journal*, vol. 4, no. 1, 36–42 (1994).
- [5.290] D. Nagel, U. Kuhlmann, and R. Sittig, "Rapid Thermal Processes for Power Devices," in: *3rd International Rapid Thermal Processing Conference RTP'95*, edited by R. B. Fair and B. Lojek, 109–114 (1995).
- [5.291] U. Kuhlmann, D. Nagel, and R. Sittig, "Short-Time Diffusion of Aluminium in Silicon and Co-Diffusion with Phosphorus and Boron," in: *Diffusion in Materials*, edited by H. Mehrer, C. Herzog, N. A. Stolwijk, and H. Bracht, *Defect and Diffusion Forum*, vol. 143–147, 1009–1014 (1997).
- [5.292] B. N. Gresserov, N. A. Sobolev, Y. V. Vyzhigin, V. V. Eliseev, and V. M. Likunova, "Influence of the Ambient Atmosphere on the Diffusion of Aluminum in Silicon," *Sov. Phys. Semicond.*, vol. 25, no. 5, 488–491 (1991).
- [5.293] A. M. Orlov, M. M. Lagun, T. M. Levkina, and A. I. Somov, "High-Temperature Transport Processes in Joint Diffusion of Al and P in Si," *Inorganic Materials*, vol. 28, no. 3, 357–360 (1992).
- [5.294] C. Leray, J. E. Bouree, and M. Rodot, "Diffusion de l'aluminium dans le silicium cristallin par recuit laser semi-continu," in: *Interactions Laser-Solides, Recuits par Faisceaux d'Energie*, Colloque C5 in *Journal de Physique*, vol. 44, no. 10, 235–240 (1983).
- [5.295] A. La Ferla, L. Torrisi, G. Galvagno, E. Rimini, G. Ciavola, A. Carnera, and A. Gasparotto, "Implants of Aluminum in the 50–120 MeV Energy Range into Silicon," *Nuclear Instruments and Methods in Physics Research B*, vol. 73, 9–13 (1993).
- [5.296] G. Galvagno, F. La Via, F. Priolo, and E. Rimini, "Diffusion and Outdiffusion of Aluminum Implanted into Silicon," *Semicond. Sci. Technol.*, vol. 8, 488–494 (1993).
- [5.297] C. Ortiz, D. Mathiot, C. Dubois, and R. Jérison, "Diffusion of Low-Dose Implanted Aluminum in Silicon in Inert and Dry O₂ Ambient," *J. Appl. Phys.*, vol. 87, no. 5, 2661–2663 (2000).
- [5.298] O. Krause, H. Ryssel, and P. Pichler, "Determination of Aluminum Diffusion Parameters in Silicon," *J. Appl. Phys.*, vol. 91, no. 9, 5645–5649 (2002).
- [5.299] B. Goldstein, "Diffusion of Aluminum in Silicon," *Bull. Am. Phys. Soc., Series II*, vol. 1, no. 3, 145 (1956).
- [5.300] R. N. Ghoshagore, "Dopant Diffusion in Silicon. III. Acceptors," *Phys. Rev. B*, vol. 3, no. 8, 2507–2514 (1971).
- [5.301] N. A. Sobolev, "Intrinsic Point Defect Engineering in Silicon High-Voltage Power Device Technology," in: *Defects in Semiconductors 19*, edited by G. Davies and M. H. Nazaré, *Materials Science Forum*, vol. 258–263, 1801–1806 (1997).
- [5.302] S. D. Devine and R. C. Newman, "One Phonon Absorption from Aluminium Complexes in Silicon Compensated by Lithium or Electron Irradiation," *J. Phys. Chem. Solids*, vol. 31, 685–700 (1970).
- [5.303] G. A. Baraff, M. Schlüter, and G. Allan, "Theory of Enhanced Migration of Interstitial Aluminum in Silicon," *Phys. Rev. Lett.*, vol. 50, no. 10, 739–742 (1983).

- [5.304] S. T. Pantelides, A. Oshiyama, R. Car, and P. J. Kelly, "Theory of Electronically Stimulated Defect Migration in Semiconductors," *Phys. Rev. B*, vol. 30, no. 4, 2260–2262 (1984).
- [5.305] M. Hagen and H. Overhof, "Metastability of the Al(i)-Al(Si) Pair in Silicon?" in: *Defects in Semiconductors 17*, edited by H. Heinrich and W. Jantsch, *Materials Science Forum*, vol. 143-147, 1197–1201 (1994).
- [5.306] Y. V. Gorelkinskii, B. N. Mukashev, and K. A. Abdullin, "Observation of Low-Temperature Diffusion of Aluminum Impurity Atoms in Hydrogen-Implanted Silicon," *Semiconductors*, vol. 32, no. 4, 375–381 (1998).
- [5.307] R. Baron, G. A. Shifrin, O. J. Marsh, and J. W. Mayer, "Electrical Behavior of Group III and V Implanted Dopants in Silicon," *J. Appl. Phys.*, vol. 40, no. 9, 3702–3719 (1969).
- [5.308] B. L. Crowder, "The Influence of the Amorphous Phase on Ion Distributions and Annealing Behavior of Group III and Group V Ions Implanted into Silicon," *J. Electrochem. Soc.*, vol. 118, no. 6, 943–952 (1971).
- [5.309] M. Tamura, K. Ohya, K. Yagi, and N. Natsuaki, "Electrical Activation and Deep Diffusion of Ion-Implanted Al and Ga in Si," in: *Proceedings of the 14th Conference (1982 International) on Solid State Devices, Jpn. J. Appl. Phys.*, vol. 22, Supplement 22-1, 153–156 (1983).
- [5.310] D. K. Sadana, M. H. Norcott, R. G. Wilson, and U. Dahmen, "Transmission Electron Microscopy of Aluminum Implanted and Annealed (100) Si: Direct Evidence of Aluminum Precipitate Formation," *Appl. Phys. Lett.*, vol. 49, no. 18, 1169–1171 (1986).
- [5.311] R. G. Wilson, "Characterization of Depth Profiles and Redistribution during Thermal Processing of Aluminium Implanted into Silicon," *J. Appl. Phys.*, vol. 61, no. 3, 933–939 (1987).
- [5.312] H. R. Chang, N. Lewis, G. A. Smith, E. L. Hall, and V. A. K. Temple, "Incorporation of Ion-Implanted Aluminum in Silicon Annealed at High Temperatures," *J. Electrochem. Soc.*, vol. 135, no. 1, 252–257 (1988).
- [5.313] P. Brüesch, E. Halder, P. Kluge, J. Rhyner, P. Roggwiller, T. Stockmeier, F. Stucki, and H. J. Wiesmann, "Electrical Activity of Aluminum Implanted in Silicon: An Interface Problem in High-Power Devices," *J. Appl. Phys.*, vol. 68, no. 5, 2226–2234 (1990).
- [5.314] A. Scandurra, G. Galvagno, V. Raineri, F. Frisina, and A. Torrisi, "Diffusion and Electrical Behavior of Al Implanted into Capped Si," *J. Electrochem. Soc.*, vol. 140, no. 7, 2057–2062 (1993).
- [5.315] A. La Ferla, L. Torrisi, G. Galvagno, E. Rimini, G. Ciavola, A. Carnera, and A. Gasparotto, "Al-O Complex Formation in Ion Implanted Czochralski and Floating-Zone Si Substrates," *Appl. Phys. Lett.*, vol. 62, no. 4, 393–395 (1993).
- [5.316] A. La Ferla, G. Galvagno, V. Raineri, F. Priolo, A. Carnera, A. Gasparotto, and E. Rimini, "Dopant, Defects and Oxygen Interaction in MeV Implanted Czochralski Silicon," in: *Ion Implantation Technology—94*, edited by S. Coffa, G. Ferla, F. Priolo, and E. Rimini, *Nuclear Instruments and Methods in Physics Research B*, vol. 96, Amsterdam: Elsevier, 232–235 (1995).
- [5.317] E. Rimini, G. Galvagno, A. La Ferla, V. Raineri, G. Franco, M. Camalleri, A. Gasparotto, and A. Carnera, "Al Precipitate Evolution in Epitaxial Silicon Layers Induced by Thermal Oxidation," in: *Ion Implantation Technology—96*, edited by E. Ishidida, S. Banerjee, S. Mehta, T. C. Smith, M. Current, L. Larson, A. Tasch, and T. Romig, Piscataway: IEEE, 654–657 (1997).
- [5.318] A. La Ferla, G. Galvagno, P. K. Giri, G. Franzò, E. Rimini, V. Raineri, A. Gasparotto, and D. Cali, "Oxidation Induced Precipitation in Al Implanted Epitaxial Silicon," *J. Appl. Phys.*, vol. 88, no. 7, 3988–3992 (2000).
- [5.319] S. W. Glunz, S. Rein, J. Knobloch, W. Wetling, and T. Abe, "Comparison of Boron- and Gallium-Doped p-Type Czochralski Silicon for Photovoltaic Application," *Progress in Photovoltaics: Research and Applications*, vol. 7, 463–469 (1999).
- [5.320] A. H. Van Ommeren, "Diffusion of Group III and V Elements in SiO₂," *Applied Surface Science*, vol. 30, 244–264 (1987).
- [5.321] D. Shaw, "Self- and Impurity Diffusion in Ge and Si," *phys. stat. sol. (b)*, vol. 72, 11–39 (1975).

- [5.322] R. W. Olesinski, N. Kanani, and G. J. Abbaschian, "The Ga-Si (Gallium-Silicon) System," *Bull. Alloy Phase Diagrams*, vol. 6, no. 4, 362–364 (1985).
- [5.323] J. G. Kren, B. J. Masters, and E. S. Wajda, "Effect of Surface Imperfections on Gallium Diffusion in Silicon," *Appl. Phys. Lett.*, vol. 5, no. 3, 49–50 (1964).
- [5.324] S. Haridoss, F. Bénière, M. Gauneau, and A. Ruper, "Diffusion of Gallium in Silicon," *J. Appl. Phys.*, vol. 51, no. 11, 5833–5837 (1980).
- [5.325] A. D. Kurtz and C. L. Gravel, "Diffusion of Gallium in Silicon," *J. Appl. Phys.*, vol. 29, no. 10, 1456–1459 (1958).
- [5.326] B. I. Boltaks and T. D. Dzhafarov, "Diffusion of Gallium in Inhomogeneous Silicon," *Sov. Phys. Solid State*, vol. 5, no. 12, 2649–2651 (1964).
- [5.327] D. Convers, J. Dupraz, R. Mascotto, and A. Vanazia, "Rétrodiffusion du gallium dans le silicium," *Helvetica Physica Acta*, vol. 43, 765–767 (1970).
- [5.328] J. S. Makris and B. J. Masters, "Gallium Diffusions into Silicon and Boron-Doped Silicon," *J. Appl. Phys.*, vol. 42, no. 10, 3750–3754 (1971).
- [5.329] G. C. Jain, A. Prasad, and B. C. Chakravarty, "Diffusion of Ga into Si through SiO_2 ," *phys. stat. sol. (a)*, vol. 46, K151–K155 (1978).
- [5.330] A. Lodding, H. Odellius, and U. Södervall, "Application of SIMS in Studies of Slow Diffusion and Isotope Diffusion," in: *Secondary Ion Mass Spectrometry SIMS III*, edited by A. Benninghoven, J. Giber, J. László, M. Riedel, and H. W. Werner, *Springer Series in Chemical Physics*, vol. 19, 351–356 (1982).
- [5.331] G. Mermant, "Diffusion solide-solide du gallium dans le silicium à partir de couches minces déposées sous vide," in: *3me Colloque international sur les applications des techniques du vide à l'industrie des semiconducteurs, des composants électroniques et de la microélectronique*, Paris: Société Française des ingénieurs et techniciens du vide, 72–78 (1971).
- [5.332] T. A. Danilicheva, V. S. Markvicheva, and Y. D. Nisnevich, "Gallium Diffusion from Doped Oxide Films into Silicon," *Inorg. Mater.*, vol. 21, 450–454 (1985).
- [5.333] Y. Nakajima and S. Ohkawa, "The Effect of the Oxide Layer on the Diffusion of Ga in Si," *Jpn. J. Appl. Phys.*, vol. 11, 1742 (1972).
- [5.334] S. Mizuo and H. Higuchi, "Oxidation Effects on Gallium Diffusion in Silicon," *Denki Kagaku*, vol. 50, no. 4, 338–343 (1982).
- [5.335] P. Fahey, "Diffusion of Shallow Impurities in Silicon," in: *Shallow Impurities in Semiconductors, 1988*, edited by B. Monemar, *Inst. Phys. Conf. Ser.*, no. 95, 483–492 (1989).
- [5.336] P. Fahey, S. S. Iyer, and G. J. Scilla, "Experimental Evidence of Both Interstitial- and Vacancy-Assisted Diffusion of Ge in Si," *Appl. Phys. Lett.*, vol. 54, no. 9, 843 (1989).
- [5.337] M. Y. Pines and R. Baron, "Characteristics of Indium Doped Silicon Infrared Detectors," in: *Technical Digest of the 1974 International Electron Devices Meeting (IEDM)*, New York: IEEE, 446–450 (1974).
- [5.338] G. G. Shahidi, B. Davari, T. J. Bucelot, P. A. Ronsheim, P. J. Coane, S. Pollack, C. R. Blair, B. Clark, and H. H. Hansen, "Indium Channel Implant for Improved Short-Channel Behaviour of Submicrometer NMOSFETs," *IEEE Electron Device Letters*, vol. 14, no. 8, 409–411 (1993).
- [5.339] D. Forkel, F. Meyer, W. Withuhn, H. Wolf, M. Deicher, and M. Uhrmacher, "PAC Studies of Ion Implanted Silicon," *Hyperfine Interactions*, vol. 35, 715–718 (1987).
- [5.340] R. D. Pashley, "Electrical Properties of Indium Implanted Silicon," *Radiation Effects*, vol. 11, 1–8 (1971).
- [5.341] R. Baron, M. H. Young, J. K. Neeland, and O. J. Marsh, "A New Acceptor Level in Indium-Doped Silicon," *Appl. Phys. Lett.*, vol. 30, no. 11, 594–596 (1977).
- [5.342] R. D. Larrabee, "Interpretation of Hall Measurements," in: *Semiconductor Characterization Techniques*, edited by P. A. Barnes and G. A. Rozgonyi, *Electrochem. Soc. Proc.*, vol. 78-3, 71–80 (1978).

- [5.343] R. N. Thomas, T. T. Braggins, H. M. Hobgood, and W. J. Takei, "Compensation of Residual Boron Impurities in Extrinsic Indium-Doped Silicon by Neutron Transmutation of Silicon," *J. Appl. Phys.*, vol. 49, no. 5, 2811–2820 (1978).
- [5.344] J.-P. Noël, N. Hirashita, L. C. Markert, Y.-W. Kim, J. E. Greene, J. Knall, W.-X. Ni, M. A. Hasan, and J.-E. Sundgren, "Electrical Properties of Si Films Doped with 200-eV In⁺ Ions during Growth by Molecular-Beam Epitaxy," *J. Appl. Phys.*, vol. 65, no. 3, 1189–1197 (1989).
- [5.345] A. Tardella and B. Pajot, "The Infrared Spectrum of Indium in Silicon Revisited," *J. Phys.*, vol. 43, 1789–1795 (1982).
- [5.346] R. Newman, "Optical Properties of Indium-Doped Silicon," *Phys. Rev.*, vol. 99, no. 2, 465–467 (1955).
- [5.347] C. E. Jones and G. E. Johnson, "Deep Level Transient Spectroscopy Studies of Trapping Parameters for Centers in Indium-Doped Silicon," *J. Appl. Phys.*, vol. 52, no. 8, 5159–5163 (1981).
- [5.348] G. F. Cerofolini, G. U. Pignatello, E. Mazzega, and G. Ottaviani, "Supershallow Levels in Indium-Doped Silicon," *J. Appl. Phys.*, vol. 58, no. 6, 2204–2207 (1985).
- [5.349] G. Cerofolini, "A Deep-Impurity Model for Acceptors in Silicon," *Phil. Mag. B*, vol. 47, no. 4, 393–405 (1983).
- [5.350] P. J. Dean, J. R. Haynes, and W. F. Flood, "New Radiative Recombination Processes Involving Neutral Donors and Acceptors in Silicon and Germanium," *Phys. Rev.*, vol. 161, no. 3, 711–729 (1967).
- [5.351] P. Alippi, A. La Magna, S. Scalese, and V. Privitera, "Energetics and Diffusivity of Indium-Related Defects in Silicon," *Phys. Rev. B*, vol. 69, 085213 (2004).
- [5.352] G. J. Kemerink and F. Pleiter, "Indium-Vacancy Interaction in Laser-Annealed Silicon," *Hyperfine Interactions*, vol. 35, 711–713 (1987).
- [5.353] M. Deicher, G. Grübel, E. Recknagel, H. Skudlik, and T. Wichert, "Structural Lattice Defects in Silicon Observed at ¹¹¹In by Perturbed Angular Correlation," *Hyperfine Interactions*, vol. 35, 719–722 (1987).
- [5.354] R. W. Olesinski, N. Kanani, and G. J. Abbaschian, "The In-Si (Indium-Silicon) System," *Bull. Alloy Phase Diagrams*, vol. 6, no. 2, 128 (1985).
- [5.355] W. Scott and R. J. Hager, "Solution Growth of Indium-Doped Silicon," *J. Electronic Materials*, vol. 8, 581–602 (1979).
- [5.356] G. F. Cerofolini, G. Ferla, G. U. Pignatello, and F. Riva, "Thermodynamic and Kinetic Properties of Indium-Implanted Silicon II: High Temperature Diffusion in an Inert Atmosphere," *Thin Solid Films*, vol. 101, 275–283 (1983).
- [5.357] A. Sato, K. Suzuki, H. Horie, and T. Sugii, "Determination of Solid Solubility Limit of In and Sb in Si Using Bonded Silicon-on-Insulator (SOI) Substrate," in: *Proceedings of the 8th International Conference on Microelectronic Test Structures*, Piscataway: IEEE, 259–263 (1995).
- [5.358] J. Liu, U. Jeong, S. Mehta, J. Sherbondy, A. Lo, K. H. Shim, and J. E. Lim, "Investigation of Indium Activation by C-V Measurement," in: *Ion Implantation Technology — 2000*, edited by H. Ryssel, L. Frey, J. Gyulai, and H. Glawischnig, Piscataway: IEEE, 66–69 (2000).
- [5.359] S. Solmi, A. Parisini, M. Bersani, D. Giubertoni, V. Soncini, G. Carnevale, A. Benvenuti, and A. Marmiroli, "Investigation of Indium Diffusion in Silicon," *J. Appl. Phys.*, vol. 92, no. 3, 1361–1366 (2002).
- [5.360] G. Backenstoss, "Conductivity Mobilities of Electrons and Holes in Heavily Doped Silicon," *Phys. Rev.*, vol. 108, no. 6, 1416–1419 (1957).
- [5.361] J. E. Lang, F. L. Madrasz, and P. M. Hemenger, "Temperature Dependent Density of States Effective Mass in Nonparabolic *p*-Type Silicon," *J. Appl. Phys.*, vol. 54, no. 6, 3612 (1983).
- [5.362] H. P. D. Lanyon and R. A. Tuft, "Bandgap Narrowing in Moderately to Heavily Doped Silicon," *IEEE Trans. Electron Devices*, vol. ED-26, no. 7, 1014–1018 (1979).
- [5.363] D. K. Schroder, T. T. Braggins, and H. M. Hobgood, "The Doping Concentrations of Indium-Doped Silicon Measured by Hall, C-V, and Junction-Breakdown Techniques," *J. Appl. Phys.*, vol. 49, no. 10, 5256–5259 (1978).

- [5.364] G. D. Parker, S. D. Brotherton, I. Gate, and A. Gill, "Measurement of Concentration and Photoionization Cross Section of Indium in Silicon," *J. Appl. Phys.*, vol. 54, no. 7, 3926–3929 (1983).
- [5.365] S. Selberherr, *Analysis and Simulation of Semiconductor Devices*, Vienna: Springer (1984).
- [5.366] P. Cappelletti, G. F. Cerofolini, and G. U. Pignatelli, "Effective Mass Considered As a Local Property," *J. Appl. Phys.*, vol. 54, no. 2, 853–856 (1983).
- [5.367] M. F. Millea, "The Effect of Heavy Doping on the Diffusion of Impurities in Silicon," *J. Phys. Chem. Solids*, vol. 27, 315–325 (1966).
- [5.368] D. A. Antoniadis and I. Moskowitz, "Diffusion of Indium in Silicon Inert and Oxidizing Ambients," *J. Appl. Phys.*, vol. 53, no. 12, 9214–9216 (1982).
- [5.369] T. Skotnicki, L. Guerin, D. Mathiot, M. Gauneau, A. Grouillet, C. D'Anterroches, E. Andre, P. Bouillon, and M. Haond, "Channel Engineering by Heavy Ion Implants," in: *ESSDERC'94*, edited by C. Hill and A. Ashburn, Gif-sur-Yvette: Editions Frontières, 671–674 (1994).
- [5.370] K. Suzuki, H. Tashiro, and T. Aoyama, "Diffusion Coefficient of Indium on Si Substrates and Analytical Redistribution Profile Model," *Solid-State Electronics*, vol. 43, 27–31 (1998).
- [5.371] I. C. Kizilyalli, T. L. Rich, F. A. Stevie, and C. S. Rafferty, "Diffusion Parameters of Indium for Silicon Process Modeling," *J. Appl. Phys.*, vol. 80, no. 9, 4944–4947 (1996).
- [5.372] P. B. Griffin, M. Cao, P. Van de Voorde, Y.-L. Chang, and W. M. Greene, "Indium Transient Enhanced Diffusion," *Appl. Phys. Lett.*, vol. 73, no. 20, 2986–2988 (1998).
- [5.373] V. Zubkov, S. Aronowitz, H. Puchner, and J. P. Senoslain, "Modeling Boron and Indium Electrical Activities in Silicon in the Presence of Nitrogen," in: *Si Front-End Processing — Physics and Technology of Dopant-Defect Interactions III*, edited by K. S. Jones, M. D. Giles, P. Stolk, J. Matsuo, and E. C. Jones, *Mat. Res. Soc. Symp. Proc.*, vol. 669, J6.5.1–J6.5.6 (2001).
- [5.374] M. L. Swanson, N. R. Parikh, E. C. Frey, and T. Wichert, "Ion Channeling and Perturbed Angular Correlation (PAC) Studies of In-As Atom Pairs in Silicon," *Nuclear Instruments and Methods in Physics Research B*, vol. 33, 591–594 (1988).
- [5.375] T. Wichert and M. L. Swanson, "Perturbed Angular Correlation Studies of Dopant Atom Interactions in Silicon," *J. Appl. Phys.*, vol. 66, no. 7, 3026–3037 (1989).
- [5.376] D. Forkel, H. Foettinger, M. Iwatschenko-Borho, S. Malzer, F. Meyer, W. Witthuhn, and H. Wolf, "Acceptor-Donor-Interactions in Silicon Studied by the PAC Method," in: *Defects in Semiconductors 14*, edited by H. J. von Bardeleben, *Materials Science Forum*, vol. 10-12, 557–562 (1986).
- [5.377] G. Tessema and R. Vianden, "Formation and Properties of In-Te Pairs in Si," in: *Proceedings of the 22nd International Conference on Defects in Semiconductors*, edited by K. Bonde Nielsen, A. Nylandsted Larsen, and G. Weyer, *Physica B*, vol. 340–342, 613–616 (2003).
- [5.378] M. A. Vouk and E. C. Lighowers, "A High Resolution Investigation of the Recombination Radiation from Si Containing the Acceptors B, Al, Ga, In and Tl," *Journal of Luminescence*, vol. 15, 357–384 (1977).
- [5.379] G. S. Mitchard, S. A. Lyon, K. R. Elliot, and T. C. McGill, "Observation of Long Lifetime Lines in Photoluminescence from Si:In," *Solid State Communications*, vol. 29, 425–429 (1979).
- [5.380] J. Weber, R. Sauer, and P. Wagner, "Photoluminescence from a Thermally Induced Indium Complex in Silicon," *Journal of Luminescence*, vol. 24/25, 155–158 (1981).
- [5.381] T. E. Schlesinger and T. C. McGill, "Role of Fe in New Luminescence Lines in Si:Tl and Si:In," *Phys. Rev. B*, vol. 25, no. 12, 7850–7851 (1982).
- [5.382] T. E. Schlesinger, R. J. Hauenstein, R. M. Feenstra, and T. C. McGill, "Isotope Shifts for the *P,Q,R* Lines in Indium-Doped Silicon," *Solid State Communications*, vol. 46, no. 4, 321–324 (1983).
- [5.383] S. P. Watkins, M. L. W. Thewalt, and T. Steiner, "Isoelectronic Bound Excitons in In- and Tl-Doped Si: A Novel Semiconductor Defect," *Phys. Rev. B*, vol. 29, no. 10, 5727–5738 (1984).
- [5.384] W. von Ammon, Private communication (1998).

- [5.385] T. Abe, H. Harada, and J.-i. Chikawa, "Microdefects and Impurities in Dislocation-Free Silicon Crystals," in: *Defects in Semiconductors II*, edited by S. Mahajan and J. W. Corbett, *Mat. Res. Soc. Symp. Proc.*, vol. 14, 1–17 (1983).
- [5.386] V. V. Voronkov and R. Falster, "Intrinsic Growth and Impurities in Silicon Crystal Growth," *J. Electrochem. Soc.*, vol. 149, no. 3, G167–G174 (2002).
- [5.387] T. Abe and H. Takeno, "Dynamic Behavior of Intrinsic Point Defects in FZ and CZ Silicon Crystals," in: *Defect Engineering in Semiconductor Growth, Processing and Device Technology*, edited by S. Ashok, J. Chevallier, K. Sumino, and E. Weber, *Mat. Res. Soc. Symp. Proc.*, vol. 262, 3–13 (1992).
- [5.388] D. Gräf, M. Suhren, U. Lambert, R. Schmolke, E. Ehlert, W. von Ammon, and P. Wagner, "Characterization of Crystal Quality by Crystal Originated Particle Delineation and the Impact on the Silicon Wafer Surface," *J. Electrochem. Soc.*, vol. 145, no. 1, 275–284 (1998).
- [5.389] M. Tamatsuka, N. Kobayashi, S. Tobe, and T. Masui, "High Performance Silicon Wafer with Wide Grown-in Void-Free Zone and High Density Internal Gettering Site Achieved via Rapid Crystal Growth with Nitrogen Doping and High Temperature Hydrogen and/or Argon Annealing," *Electrochem. Soc. Extended Abstracts*, vol. 99-1, no. 353 (1999).
- [5.390] M. Iida, W. Kusaki, M. Tamatsuka, E. Iino, M. Kimura, and S. Muraoka, "Effects of Light Element Impurities on the Formation of Grown-in Defects Free Region of Czochralski Silicon Single Crystal," *Electrochem. Soc. Extended Abstracts*, vol. 99-1, no. 357 (1999).
- [5.391] M. Tamatsuka, N. Kobayashi, S. Tobe, and T. Masui, "High Performance Silicon Wafer with Wide Grown-in Void Free Zone and High Density Internal Gettering Site Achieved via Rapid Crystal Growth with Nitrogen Doping and High Temperature Hydrogen and/or Argon Annealing," in: *Defects in Silicon III*, edited by T. Abe, W. M. Bullis, S. Kobayashi, W. Lin, and P. Wagner, *Electrochem. Soc. Proc.*, vol. 99-1, 456–467 (1999).
- [5.392] B. M. Park, G. H. Seo, and G. Kim, "Nitrogen-Doping Effect in a Fast-Pulled Cz-Si Single Crystal," *J. Crystal Growth*, vol. 222, 74–81 (2001).
- [5.393] K. Nakai, Y. Inoue, H. Yokota, A. Ikari, J. Takahashi, A. Tachikawa, K. Kitahara, Y. Ohta, and W. Ohashi, "Oxygen Precipitation in Nitrogen-Doped Czochralski-Grown Silicon Crystals," *J. Appl. Phys.*, vol. 89, no. 8, 4301–4309 (2001).
- [5.394] M. Hourai, T. Ono, S. Umeno, and T. Tanaka, "Control of Grown-in Defects in Nitrogen-Doped CZ Silicon Crystals for New Generation Devices," in: *Crystalline Defects and Contamination: Their Impact and Control in Device Manufacturing III – DECON 2001*, edited by B. O. Kolbesen, C. Claeys, P. Stallhofer, and F. Tardif, *Electrochem. Soc. Proc.*, vol. 2001-29, 19–34 (2001).
- [5.395] X. Yu, D. Yang, X. Ma, J. Yang, L. Li, and D. Que, "Grown-in Defects in Nitrogen-Doped Czochralski Silicon," *J. Appl. Phys.*, vol. 92, no. 1, 188–194 (2002).
- [5.396] A. Huber, M. Kapser, J. Grabmeier, U. Lambert, W. von Ammon, and R. Pech, "Impact of Nitrogen Doping in Silicon onto Gate Oxide Integrity," in: *Semiconductor Silicon 2002*, edited by H. R. Huff, L. Fabry, and S. Kishino, *Electrochem. Soc. Proc.*, vol. 2002-2, 280–286 (2002).
- [5.397] T. Abe, K. Kikuchi, S. Shirai, and S. Muraoka, "Impurities in Silicon Single Crystals," in: *Semiconductor Silicon 1981*, edited by H. R. Huff, R. J. Kriegler, and Y. Takeishi, *Electrochem. Soc. Proc.*, vol. 81-5, 54–71 (1981).
- [5.398] K. Sumino, I. Yonenaga, M. Imai, and T. Abe, "Effects of Nitrogen on Dislocation Behavior and Mechanical Strength in Silicon Crystals," *J. Appl. Phys.*, vol. 54, no. 9, 5016–5020 (1983).
- [5.399] H.-D. Chiou, J. Moody, R. Sandfort, and F. Shimura, "Effects of Oxygen and Nitrogen on Slip in CZ Silicon Wafers," in: *VLSI Science and Technology/1984*, edited by K. E. Bean and G. A. Rozgonyi, *Electrochem. Soc. Proc.*, vol. 84-7, 59–65 (1984).
- [5.400] T. Abe, H. Harada, N. Ozawa, and K. Adomi, "Deep Level Generation-Annihilation in Nitrogen Doped FZ Crystals," in: *Oxygen, Carbon, Hydrogen, and Nitrogen in Crystalline Silicon*, edited by J. C. Mikkelsen, Jr., S. J. Pearson, J. W. Corbett, and S. J. Pennycook, *Mat. Res. Soc. Symp. Proc.*, vol. 59, 537–544 (1986).

- [5.401] L. Jastrzebski, G. W. Cullen, R. Soydan, G. Harbeke, J. Lagowski, S. Vecrumba, and W. N. Henry, "The Effect of Nitrogen on the Mechanical Properties of Float Zone Silicon and on CCD Device Performance," *J. Electrochem. Soc.*, vol. 134, no. 2, 466–470 (1987).
- [5.402] T. Itoh, Y. Hayamizu, and T. Abe, "In-Diffusion of Nitrogen from N₂ Ambient and Its Aggregation at Lattice Imperfections in Silicon Crystals," *Materials Science and Engineering B*, vol. 4, 309–313 (1989).
- [5.403] M. Akatsuka and K. Sueoka, "Pinning Effect of Punched-Out Dislocations in Carbon-, Nitrogen- or Boron-Doped Silicon Wafers," *Jpn. J. Appl. Phys., Part 1*, vol. 40, no. 3A, 1240–1241 (2001).
- [5.404] G. Wang, D. Yang, D. Li, Q. Shui, J. Yang, and D. Que, "Mechanical Strength of Nitrogen-Doped Silicon Single Crystal Investigated by Three-Point Bending Method," *Physica B*, vol. 308-310, 450–453 (2001).
- [5.405] T. Ito, H. Arakawa, T. Nozaki, and H. Ishikawa, "Retardation of Destructive Breakdown of SiO₂ Films Annealed in Ammonia Gas," *J. Electrochem. Soc.*, vol. 127, no. 10, 2248–2251 (1980).
- [5.406] M. L. Naiman, F. L. Terry, J. A. Burns, J. I. Raffel, and R. Aucoin, "Properties of Thin Oxynitride Gate Dielectrics Produced by Thermal Nitridation of Silicon Dioxide," in: *Technical Digest of the 1980 International Electron Devices Meeting (IEDM)*, New York: IEEE, 562–564 (1980).
- [5.407] I. Kato, T. Ito, S.-i. Inoue, T. Nakamura, and H. Ishikawa, "Ammonia-Annealed SiO₂ Films for Thin-Gate Insulator," in: *Proceedings of the 13th Conference on Solid State Devices, Jpn. J. Appl. Phys.*, vol. 21, Supplement 21-1, 153–158 (1982).
- [5.408] T. T. L. Chang, H. S. Jones, C. S. Jenq, W. S. Johnson, J. Lee, S. K. Lai, and V. Dham, "Oxidized-Nitrided Oxide (ONO) for High Performance EEPROMS," in: *Technical Digest of the 1982 International Electron Devices Meeting (IEDM)*, New York: IEEE, 810 (1982).
- [5.409] S. S. Wong, S. H. Kwan, H. R. Grinolds, and W. G. Oldham, "Composition and Electrical Properties of Nitrided-Oxide and Re-Oxidized Nitrided-Oxide," in: *Silicon Nitride Thin Insulating Films*, edited by V. J. Kapoor and H. J. Stein, *Electrochem. Soc. Proc.*, vol. 83-8, 346–354 (1983).
- [5.410] T. Hori, H. Iwasaki, and K. Tsuji, "Electrical and Physical Properties of Ultrathin Reoxidized Nitrided Oxides Prepared by Rapid Thermal Processing," *IEEE Trans. Electron Devices*, vol. 36, no. 2, 340–350 (1989).
- [5.411] L. K. Han, J. Kim, G. W. Yoon, J. Yan, and D. L. Kwong, "High Quality Oxynitride Gate Dielectrics Prepared by Reoxidation of NH₃-Nitrided SiO₂ in N₂O Ambient," *Electronics Letters*, vol. 31, no. 14, 1196–1198 (1995).
- [5.412] H. Fukuda, T. Arakawa, and S. Ohno, "Electrical Properties of Thin Oxynitrided SiO₂ Films Formed by Rapid Thermal Processing in an N₂O Ambient," *Electronics Letters*, vol. 26, no. 18, 1505–1506 (1990).
- [5.413] H. Hwang, W. Ting, D.-L. Kwong, and J. Lee, "Electrical and Reliability Characteristics of Ultrathin Oxynitride Gate Dielectric Prepared by Rapid Thermal Processing in N₂O," in: *Technical Digest of the 1990 International Electron Devices Meeting (IEDM)*, New York: IEEE, 421–424 (1990).
- [5.414] H. Fukuda, T. Arakawa, and S. Ohno, "Highly Reliable Thin Nitrided SiO₂ Films Formed by Rapid Thermal Processing in an N₂O Ambient," *Jpn. J. Appl. Phys.*, vol. 29, no. 12, L2333–L2336 (1990).
- [5.415] V. K. Matews, R. L. Maddox, P. C. Fazan, J. Rosato, H. Hwang, and J. Lee, "Degradation of Junction Leakage in Devices Subjected to Gate Oxidation in Nitrous Oxide," *IEEE Electron Device Letters*, vol. 13, no. 12, 648–650 (1992).
- [5.416] X. Zeng, P. T. Lai, and W. T. Ng, "Enhanced Off-State Leakage Currents in n-Channel MOS-FET's with N₂O-Grown Gate Dielectric," *IEEE Electron Device Letters*, vol. 16, no. 10, 436–438 (1995).

- [5.417] Y. Okada, P. J. Tobin, K. G. Reid, R. I. Hedge, B. Maiti, and S. A. Ajuria, "Furnace Grown Gate Oxynitride Using Nitric Oxide (NO)," *IEEE Trans. Electron Devices*, vol. 41, no. 9, 1608–1613 (1994).
- [5.418] M. Bhat, D. Wristers, J. Yan, L. K. Han, J. Fulford, and D. L. Kwong, "Performance and Hot-Carrier Reliability of N- and P-MOSFETs with Rapid Thermally NO-Nitrided SiO₂ Gate Dielectrics," in: *Technical Digest of the 1994 International Electron Devices Meeting (IEDM)*, Piscataway: IEEE, 329–332 (1994).
- [5.419] G. D. Leonardiuzzi and D.-L. Kwong, "Improving Performance with Oxynitride Gate Dielectrics," *Semiconductor International*, vol. 21, no. 8, 225–230 (1998).
- [5.420] G. W. Yoon, A. B. Joshi, J. Kim, and D.-L. Kwong, "MOS Characteristics of NH₃-Nitrided N₂O-Grown Oxides," *IEEE Electron Device Letters*, vol. 14, no. 4, 179–181 (1993).
- [5.421] M. Bhat, G. W. Yoon, J. Kim, D. L. Kwong, M. Arendt, and J. M. White, "Effects of NH₃ Nitridation on Oxides Grown in Pure N₂O Ambient," *Appl. Phys. Lett.*, vol. 64, no. 16, 2116–2118 (1994).
- [5.422] Y. Suizu, M. Fukumoto, and Y. Ozawa, "A Method of Making Oxynitrides by Interface Nitridation through Silicon," *J. Electrochem. Soc.*, vol. 148, no. 4, F51–F55 (2001).
- [5.423] S. S. Wong, C. G. Sodini, T. W. Ekstedt, H. R. Grinolds, K. H. Jackson, S. H. Kwan, and W. G. Oldham, "Low Pressure Nitrided-Oxide As a Thin Gate Dielectric for MOSFET's," *J. Electrochem. Soc.*, vol. 130, no. 5, 1139–1144 (1983).
- [5.424] D. R. Lee, C. R. Parker, J. R. Hauser, and G. Lucovsky, "Reliability of Nitrided Si SiO₂ Interfaces Formed by a New, Low-Temperature, Remote-Plasma Process," *J. Vac. Sci. Technol. B*, vol. 13, no. 4, 1788–1793 (1995).
- [5.425] S. R. Kaluri and D. W. Hess, "Nitrogen Incorporation in Thin Silicon Oxides in a N₂O Plasma," *J. Electrochem. Soc.*, vol. 145, no. 2, 662–668 (1998).
- [5.426] S. Haddad and M.-S. Liang, "Improvement of Thin-Gate Oxide Integrity Using through-Silicon-Gate Nitrogen Ion Implantation," *IEEE Electron Device Letters*, vol. EDL-8, no. 2, 58–60 (1987).
- [5.427] S. Strobel, A. J. Bauer, M. Beichele, and H. Ryssel, "Suppression of Boron Penetration through Thin Gate Oxides by Nitrogen Implantation into the Gate Electrode in PMOS Devices," *Microelectronics Reliability*, vol. 41, 1085–1088 (2001).
- [5.428] T. Kuroi, T. Yamaguchi, M. Shirahata, Y. Okumura, Y. Kawasaki, M. Inuishi, and N. Tsubouchi, "Novel NICE (Nitrogen Implantation into CMOS Gate Electrode and Source-Drain) Structure for High Reliability and High Performance 0.25 μm Dual Gate CMOS," in: *Technical Digest of the 1993 International Electron Devices Meeting (IEDM)*, Piscataway: IEEE, 325–328 (1993).
- [5.429] S. Shimizu, T. Kuroi, Y. Kawasaki, S. Kusunoki, Y. Okumura, M. Inuishi, and H. Miyoshi, "Impact of Surface Proximity Gettering and Nitrided Oxide Side-Wall Spacer by Nitrogen Implantation on Sub-Quarter Micron CMOS LDD FETs," in: *Technical Digest of the 1995 International Electron Devices Meeting (IEDM)*, Piscataway: IEEE, 859–862 (1995).
- [5.430] C. Lin, A. Chou, P. Choudhury, J. C. Lee, K. Kumar, B. Doyle, and H. R. Soleimani, "Reliability of Gate Oxide Grown on Nitrogen-Implanted Si Substrates," *Appl. Phys. Lett.*, vol. 69, no. 24, 3701–3703 (1996).
- [5.431] Y. Y. Chen, I. M. Liu, M. Gardner, J. Fulford, and D. L. Kwong, "Performance and Reliability of Dual-Gate CMOS Devices with Gate Oxide Grown on Nitrogen Implanted Si Substrates," in: *Technical Digest of the 1997 International Electron Devices Meeting (IEDM)*, Piscataway: IEEE, 639–642 (1997).
- [5.432] L. K. Han, S. Crowder, M. Hargrove, E. Wu, S. H. Lo, F. Guarin, E. Crabbé, and L. Su, "Electrical Characteristics and Reliability of Sub-3 nm Gate Oxides Grown on Nitrogen Implanted Silicon Substrates," in: *Technical Digest of the 1997 International Electron Devices Meeting (IEDM)*, Piscataway: IEEE, 643–646 (1997).
- [5.433] K.-S. Chang-Liao and H.-C. Lai, "Correlation between Nitrogen Concentration Profile and Infrared Spectroscopy in Silicon Dioxide," *Appl. Phys. Lett.*, vol. 72, no. 18, 2280–2282 (1998).

- [5.434] A. A. Demkov, R. Liu, X. Zhang, and H. Loechelt, “Theoretical and Experimental Investigation of Ultrathin Oxynitrides and the Role of Nitrogen at the Si-SiO₂ Interface,” *J. Vac. Sci. Technol. B*, vol. 18, no. 5, 2388–2394 (2000).
- [5.435] D. Mathiot, A. Straboni, E. Andre, and P. Debenest, “Boron Diffusion through Thin Gate Oxides: Influence of Nitridation and Effect on the Si/SiO₂ Interface Electrical Characteristics,” *J. Appl. Phys.*, vol. 73, no. 12, 8215–8220 (1993).
- [5.436] T. Aoyama, K. Suzuki, H. Tashiro, Y. Toda, T. Yamazaki, Y. Arimoto, and T. Ito, “Boron Diffusion through Pure Silicon Oxide and Oxynitride Used for Metal-Oxide-Semiconductor Devices,” *J. Electrochem. Soc.*, vol. 140, no. 12, 3624–3627 (1993).
- [5.437] T. Ishihara, S.-i. Takagi, and M. Kondo, “Quantitative Understanding of Electron Mobility Limited by Coulomb Scattering in Metal Oxide Semiconductor Field Effect Transistors with N₂O and NO Oxynitrides,” *Jpn. J. Appl. Phys., Part 1*, vol. 40, no. 4B, 2597–2602 (2001).
- [5.438] T. Ito, S. Hijiya, T. Nozaki, H. Arakawa, M. Shinoda, and Y. Fukukawa, “Very Thin Silicon Nitride Films Grown by Direct Thermal Reaction with Nitrogen,” *J. Electrochem. Soc.*, vol. 125, no. 3, 448–452 (1978).
- [5.439] J. A. Nemetz and R. E. Tressler, “Thermal Nitridation of Silicon and Silicon Dioxide for Thin Gate Insulators,” *Solid State Technology*, vol. 26, no. 2, 79–85 (1983).
- [5.440] X. Wang, M. Khare, and T. P. Ma, “Effects of Water Vapor Anneal on MIS Devices Made of Nitrided Gate Dielectrics,” in: *1996 Symposium on VLSI Technology*, IEEE Electron Devices Society & Japan Society of Applied Physics, 226–227 (1996).
- [5.441] T. Yamamoto, T. Ogura, Y. Saito, K. Uwasawa, T. Tatsumi, and T. Mogami, “An Advanced 2.5 nm Oxidized Nitride Gate Dielectric for Highly Reliable 0.25 μm MOSFET’s,” in: *1997 Symposium on VLSI Technology*, Japan Society of Applied Physics & IEEE Electron Devices Society, 45–46 (1997).
- [5.442] T. M. Pan, T. F. Lei, H. C. Wen, and T. S. Chao, “Characterization of Ultrathin Oxynitride (18–21 Å) Gate Dielectrics by NH₃ Nitridation and N₂O RTA Treatment,” *IEEE Trans. Electron Devices*, vol. 48, no. 5, 907–912 (2001).
- [5.443] S. C. Song, B. Y. Kim, H. F. Luan, D. L. Kwong, M. Gardner, J. Fulford, D. Wristers, J. Gelpey, and S. Marcus, “Recent Developments in Ultrathin Nitride Gate Stack Prepared by In-Situ RTP Multiprocessing for CMOS ULSI,” in: *Advances in Rapid Thermal Processing*, edited by F. Roozeboom, J. C. Gelpey, M. C. Ozturk, and J. Nakos, *Electrochem. Soc. Proc.*, vol. 99-10, 45–56 (1999).
- [5.444] K. Sekine, Y. Saito, M. Hirayama, and T. Ohmi, “Highly Robust Ultrathin Silicon Nitride Films Grown at Low-Temperature by Microwave-Excitation High-Density Plasma for Giga Scale Integration,” *IEEE Trans. Electron Devices*, vol. 47, no. 7, 1370–1374 (2000).
- [5.445] S. Sugawa, I. Ohshima, H. Ishino, Y. Saito, M. Hirayama, and T. Ohmi, “Advantage of Silicon Nitride Gate Insulator Transistor by Using Microwave-Excited High-Density Plasma for Applying 100nm Technology Node,” in: *Technical Digest of the 2001 International Electron Devices Meeting (IEDM)*, Piscataway: IEEE, 817–820 (2001).
- [5.446] C. R. Fritzsche and W. Rothmund, “Thermal Oxidation of Silicon after Ion Implantation,” *J. Electrochem. Soc.*, vol. 120, no. 11, 1603–1605 (1973).
- [5.447] Y. Wada and M. Ashikawa, “Oxidation Characteristics of Nitrogen Implanted Silicon,” *Jpn. J. Appl. Phys.*, vol. 15, no. 2, 389–390 (1976).
- [5.448] T.-Y. Chiu, H. Bernt, and I. Ruge, “Low Energy Nitrogen Implantation into Silicon: Its Material Composition, Oxidation Resistance, and Electrical Characteristics,” *J. Electrochem. Soc.*, vol. 129, no. 2, 408–412 (1982).
- [5.449] W. J. M. J. Josquin and Y. Tamminga, “The Oxidation Inhibition in Nitrogen-Implanted Silicon,” *J. Electrochem. Soc.*, vol. 129, no. 8, 1803–1811 (1982).
- [5.450] J. H. Freeman, “The Use of an Isotope Separator for Ion Implantation in Semi-Conductors,” in: *International Conference on Applications of Ion Beams to Semiconductor Technology*, edited by P. Glotin, Grenoble: Edition OPHRYS, 75–90 (1967).

- [5.451] N.-G. Blamires, D.-N. Osborne, R.-B. Owen, and J. Stephen, "A Preliminary Study of Semiconductor Structures Produced by Ion-Implantation," in: *International Conference on Applications of Ion Beams to Semiconductor Technology*, edited by P. Glotin, Grenoble: Edition OPHRYS, 669–684 (1967).
- [5.452] V. P. Astakhov, T. B. Karashev, and R. M. Aranovich, "Mechanism of the Current Flow in and the Properties of Ion-Implanted Layers of Si₃N₄ on Silicon," *Sov. Phys. Semicond.*, vol. 4, no. 11, 1826–1830 (1971).
- [5.453] M. Suezawa, K. Sumino, H. Harada, and T. Abe, "The Nature of Nitrogen-Oxygen Complexes in Silicon," *Jpn. J. Appl. Phys.*, vol. 27, no. 1, 62–67 (1988).
- [5.454] A. Hara, T. Fukuda, T. Miyabo, and I. Hirai, "Electron Spin Resonance of Oxygen-Nitrogen Complex in Silicon," *Jpn. J. Appl. Phys.*, vol. 28, no. 1, 142–143 (1989).
- [5.455] A. G. Steele, I. C. Lenchyshyn, and M. L. W. Thewalt, "Photoluminescence Study of Nitrogen-Oxygen Donors in Silicon," *Appl. Phys. Lett.*, vol. 56, no. 2, 148–150 (1990).
- [5.456] F. Shimura and R. S. Hockett, "Nitrogen Effect on Oxygen Precipitation in Czochralski Silicon," *Appl. Phys. Lett.*, vol. 48, no. 3, 224–226 (1986).
- [5.457] X. Zhou, A. R. Preston, and C. J. Humphreys, "TEM Study of Nitrogen Enhanced Oxygen Precipitation in Nitrogen-Doped Czochralski-Grown Silicon," in: *Microscopy of Semiconducting Materials 1991*, edited by A. G. Cullis and N. J. Long, *Inst. Phys. Conf. Ser.*, no. 117, 211–216 (1991).
- [5.458] Q. Sun, K. H. Yao, H. C. Gatos, and J. Lagowski, "Effects of Nitrogen on Oxygen Precipitation in Silicon," *J. Appl. Phys.*, vol. 71, no. 8, 3760–3765 (1992).
- [5.459] R. Falster, M. Pagani, D. Gambaro, M. Cornara, M. Olmo, G. Ferrero, P. Pichler, and M. Jacob, "Vacancy-Assisted Oxygen Precipitation Phenomena in Si," in: *Gettering and Defect Engineering in Semiconductor Technology GADEST'97*, edited by C. Claeys, J. Vanhellemont, H. Richter, and M. Kittler, *Solid State Phenomena*, vol. 57–58, 129–136 (1997).
- [5.460] P. V. Pavlov, E. I. Zorin, D. I. Tetl'baum, and Y. S. Popov, "Donor Properties of Nitrogen Introduced into Silicon and Germanium by Ion Bombardment," *Soviet Physics-Doklady*, vol. 10, no. 8, 786–787 (1966).
- [5.461] Y. Yatsurugi, N. Akiyama, Y. Endo, and T. Nozaki, "Concentration, Solubility, and Equilibrium Distribution Coefficient of Nitrogen and Oxygen in Semiconductor Silicon," *J. Electrochem. Soc.*, vol. 120, no. 7, 975–979 (1973).
- [5.462] J. Stephen, B. J. Smith, G. W. Hinder, D. C. Marshall, and E. M. Wittam, "Some Observations on High Energy Nitrogen Implantations in Silicon," in: *Ion Implantation in Semiconductors*, edited by I. Ruge and J. Graul, Berlin: Springer, 489–494 (1971).
- [5.463] J. B. Mitchell, P. P. Pronko, J. Shewchun, D. A. Thompson, and J. A. Davies, "Nitrogen-Implanted Silicon. I. Damage Annealing and Lattice Location," *J. Appl. Phys.*, vol. 46, no. 1, 332–334 (1975).
- [5.464] H. C. Alt and L. Tapfer, "Photoluminescence Observation of the A, B, C Exciton," in: *Thirteenth International Conference on Defects in Semiconductors*, edited by L. C. Kimerling and J. M. Parsey, Jr., The Metallurgical Society of AIME, 833–838 (1985).
- [5.465] F. Berg Rasmussen and B. Bech Nielsen, "Microstructure of the Nitrogen Pair in Crystalline Silicon Studied by Ion Channeling," *Phys. Rev. B*, vol. 49, no. 23, 16353–16360 (1994).
- [5.466] W. J. Kleinfelder, W. S. Johnson, and J. F. Gibbons, "Impurity Distribution Profiles in Ion-Implanted Silicon," *Can. J. Phys.*, vol. 46, 597–606 (1968).
- [5.467] P. P. Pronko, J. B. Mitchell, and J. Shewchun, "Nitrogen Implantation of p-Silicon at Cryogenic Temperatures," in: *Ion Implantation in Semiconductors*, edited by I. Ruge and J. Graul, Berlin: Springer, 495–498 (1971).
- [5.468] P. V. Pavlov, E. I. Zorin, D. I. Tel'tbaum, and A. F. Khokhlov, "Nitrogen As Dopant in Silicon and Germanium," *phys. stat. sol. (a)*, vol. 35, 11–36 (1976).
- [5.469] M. Tajima, "Recent Advances in Photoluminescence Analysis of Si: Application to an Epitaxial Layer and Nitrogen in Si," in: *Proceedings of the 13th Conference on Solid State Devices, Jpn. J. Appl. Phys.*, vol. 21, Supplement 21-1, 113 (1982).

- [5.470] P. Chen, Y. D. Zheng, S. M. Zhu, D. J. Xi, Z. M. Zhao, S. L. Gu, P. Han, and R. Zhang, “Nitrogen Diffusion in the Si Growth on GaN by Low-Pressure Chemical Vapor Deposition,” *J. Mater. Res.*, vol. 17, no. 8, 1881–1883 (2002).
- [5.471] E. I. Zorin, P. V. Pavlov, and E. I. Tetel’baum, “Donor Properties of Nitrogen in Silicon,” *Sov. Phys. Semicond.*, vol. 2, no. 1, 111–113 (1968).
- [5.472] A. H. Clark, J. D. Macdougall, K. E. Manchester, P. E. Roughan, and F. W. Anderson, “Nitrogen Donor Level in Silicon,” *Bull. Am. Phys. Soc., Series II*, vol. 13, no. 3, 376 (1968).
- [5.473] H. J. Stein, “Nitrogen Related Donors in Silicon,” *J. Electrochem. Soc.*, vol. 134, no. 10, 2592–2596 (1987).
- [5.474] H. Ito, K. Murakami, K. Takita, and K. Masuda, “Charge-State Changes of Substitutional Nitrogen Impurities in Silicon Induced by Additional Impurities and Defects,” *J. Appl. Phys.*, vol. 61, no. 10, 4862–4868 (1987).
- [5.475] K. Murakami, H. Kuribayashi, and K. Masuda, “Electronic Energy Level of Off-Center Substitutional Nitrogen in Silicon: Determination by Electron Spin Resonance Measurements,” *Jpn. J. Appl. Phys.*, vol. 27, no. 8, L1414–L1416 (1988).
- [5.476] S. T. Pantelides and C. T. Sah, “Theory of Localized States in Semiconductors. II. The Pseudo Impurity Theory Application to Shallow and Deep Donors in Silicon,” *Phys. Rev. B*, vol. 10, no. 2, 638–658 (1974).
- [5.477] K. L. Brower, “Deep-Level Nitrogen Centers in Laser-Annealed Ion-Implanted Silicon,” *Phys. Rev. B*, vol. 26, no. 11, 6040–6052 (1982).
- [5.478] R. Jones, S. Öberg, F. Berg Rasmussen, and B. Bech Nielsen, “Identification of the Dominant Nitrogen Defect in Silicon,” *Phys. Rev. Lett.*, vol. 72, no. 12, 1882–1885 (1994).
- [5.479] M. Saito and Y. Miyamoto, “Atomic and Electronic Structures of the N Substitutional Impurity in Si,” *Phys. Rev. B*, vol. 56, no. 15, 9193–9196 (1997).
- [5.480] H. Sawada and K. Kawakami, “First-Principles Calculation of the Interaction between Nitrogen Atoms and Vacancies in Silicon,” *Phys. Rev. B*, vol. 62, no. 3, 1851–1858 (2000).
- [5.481] J. P. Goss, I. Hahn, and R. Jones, “Vibrational Modes and Electronic Properties of Nitrogen Defects in Silicon,” *Phys. Rev. B*, vol. 67, 045206 (2003).
- [5.482] H. J. Stein, “Infrared Absorption Band for Substitutional Nitrogen in Silicon,” *Appl. Phys. Lett.*, vol. 47, no. 12, 1339–1341 (1985).
- [5.483] K. Murakami, H. Kuribayashi, and K. Masuda, “Motional Effects between On-Center and Off-Center Substitutional Nitrogen in Silicon,” *Phys. Rev. B*, vol. 38, no. 2, 1589–1592 (1988).
- [5.484] M. Watanabe, T. Usami, H. Muraoka, S. Matsuo, Y. Imanishi, and H. Nagashima, “Oxygen-Free Silicon Single Crystal Grown from Silicon Nitride Crucible,” in: *Semiconductor Silicon 1981*, edited by H. R. Huff, R. J. Krieger, and Y. Takeishi, *Electrochem. Soc. Proc.*, vol. 81-5, 126–137 (1981).
- [5.485] H. J. Stein, “Vibrational Absorption Bands for Implanted Nitrogen in Crystalline Silicon,” *Appl. Phys. Lett.*, vol. 43, no. 3, 296–298 (1983).
- [5.486] H. J. Stein, “Evidence for Pairing of Implanted Nitrogen in Silicon,” in: *Thirteenth International Conference on Defects in Semiconductors*, edited by L. C. Kimerling and J. M. Parsey, Jr., The Metallurgical Society of AIME, 839–845 (1985).
- [5.487] M. Suezawa and K. Sumino, “Complexes of Nitrogen and Point Defects in Silicon,” *Jpn. J. Appl. Phys.*, vol. 26, no. 6, L997–L999 (1987).
- [5.488] F. Berg Rasmussen and B. Bech Nielsen, “Uniaxial Stress Studies on the Dominant Nitrogen Defect in Silicon and Germanium,” *Materials Science and Engineering B*, vol. 36, 241–245 (1996).
- [5.489] A. Gali, J. Miro, P. Deak, C. P. Ewels, and R. Jones, “Theoretical Studies on Nitrogen-Oxygen Complexes in Silicon,” *J. Phys.: Condens. Matter*, vol. 8, 7711–7722 (1996).
- [5.490] H. Kageshima, A. Taguchi, and K. Wada, “Theoretical Investigation of Nitrogen-Doping Effect on Vacancy Aggregation Processes in Si,” *Appl. Phys. Lett.*, vol. 76, no. 26, 3718–3720 (2000).

- [5.491] A. Karoui, F. Sahtout Karoui, G. A. Rozgonyi, M. Hourai, and K. Sueoka, "First Principle Calculations for Nitrogen-Vacancy Related Defects in Nitrogen Doped Silicon: Structure, En-ergetics and Thermal Stability," in: *Semiconductor Silicon 2002*, edited by H. R. Huff, L. Fabry, and S. Kishino, *Electrochem. Soc. Proc.*, vol. 2002-2, 670–681 (2002).
- [5.492] M. Sprenger, E. G. Sieverts, S. H. Muller, and C. A. J. Ammerlaan, "Electron Paramagnetic Resonance of a Nitrogen-Related Centre in Electron Irradiated Silicon," *Solid State Communications*, vol. 51, no. 12, 951–955 (1984).
- [5.493] F. Berg Rasmussen, R. Jones, and S. Öberg, "Nitrogen in Germanium: Identification of the Pair Defect," *Phys. Rev. B*, vol. 50, no. 7, 4378–4384 (1994).
- [5.494] H. J. Stein, "Implanted Nitrogen in Germanium," *Appl. Phys. Lett.*, vol. 52, no. 2, 153–154 (1988).
- [5.495] P. A. Schultz and J. S. Nelson, "Fast through-Bond Diffusion of Nitrogen in Silicon," *Appl. Phys. Lett.*, vol. 78, no. 6, 736–738 (2001).
- [5.496] H. Kageshima, A. Taguchi, and K. Wada, "Theoretical Investigation of Nitrogen-Doping Effect on Native Defect Aggregation Processes in Silicon," in: *Defect and Impurity Engineered Semiconductors and Devices III*, edited by S. Ashok, J. Chevallier, N. M. Johnson, B. L. Sopori, and H. Okushi, *Mat. Res. Soc. Symp. Proc.*, vol. 719, F3.3.1–F3.3.7 (2002).
- [5.497] L. S. Adam, M. E. Law, S. Hegde, and O. Dokumaci, "Comprehensive Model for Nitrogen Diffusion in Silicon," in: *Technical Digest of the 2001 International Electron Devices Meeting (IEDM)*, Piscataway: IEEE, 847–850 (2001).
- [5.498] L. S. Adam, M. E. Law, S. Szpala, P. J. Simpson, D. Lawther, O. Dokumaci, and S. Hegde, "Experimental Identification of Nitrogen-Vacancy Complexes in Nitrogen Implanted Silicon," *Appl. Phys. Lett.*, vol. 79, no. 5, 623–625 (2001).
- [5.499] W. Kaiser and C. D. Thurmond, "Nitrogen in Silicon," *J. Appl. Phys.*, vol. 30, no. 3, 427–431 (1959).
- [5.500] T. Nozaki, Y. Yatsurugi, N. Akiyama, Y. Endo, and Y. Makide, "Behaviour of Light Impurity Elements in the Production of Semiconductor Silicon," *Journal of Radioanalytical Chemistry*, vol. 19, 109–128 (1974).
- [5.501] P. E. Roughan, A. H. Clark, J. D. Macdougall, K. E. Manchester, and F. W. Anderson, *Introduction of Diffusion Sources by Implantation*, *Electrochem. Soc. Extended Abstracts*, vol. 6-1, no. 130, New York: Electrochemical Society (1968).
- [5.502] N. V. Denisova, E. I. Zorin, P. V. Pavlov, D. I. Tetel'baum, and A. F. Khokholov, "Diffusion of Nitrogen in Silicon," *Inorganic Materials*, vol. 11, no. 12, 1920–1921 (1975).
- [5.503] T. Itoh and T. Abe, "Diffusion Coefficient of a Pair of Nitrogen Atoms in Float-Zone Silicon," *Appl. Phys. Lett.*, vol. 53, no. 1, 39–41 (1988).
- [5.504] A. Hara, T. Fukuda, T. Miyabo, and I. Hirai, "Oxygen-Nitrogen Complexes in Silicon Formed by Annealing in Nitrogen," *Appl. Phys. Lett.*, vol. 54, no. 7, 626–628 (1989).
- [5.505] G. J. Willems and H. E. Maes, "Analytical Model for the Out-Diffusion of an Exponentially Decaying Impurity Profile. Application to Nitrogen in Silicon," *J. Appl. Phys.*, vol. 73, no. 7, 3256–3260 (1993).
- [5.506] N. Fuma, K. Tashiro, K. Kakimoto, and Y. Takano, "Generation of Deep Level by Nitrogen Diffusion in Si," in: *Defects in Semiconductors 18*, edited by M. Suezawa and H. Katayama-Yoshida, *Materials Science Forum*, vol. 196-201, 797–802 (1995).
- [5.507] N. Fuma, K. Tashiro, K. Kakimoto, and Y. Takano, "Diffused Nitrogen-Related Deep Level in n-Type Silicon," *Jpn. J. Appl. Phys., Part 1*, vol. 35, no. 4A, 1993–1999 (1996).
- [5.508] H. Sawada, K. Kawakami, A. Ikari, and W. Ohashi, "Atomistic Model of Nitrogen-Pair Diffusion in Silicon," *Phys. Rev. B*, vol. 65, 075201 (2002).
- [5.509] H. Itoh, K. Murakami, K. Takita, and K. Musada, "Thermal Stability and Electronic States of Substitutional Nitrogen Impurity in Pulsed Laser Annealed Si," in: *Proceedings of the 15th Symposium on Ion Implantation and Submicron Fabrication*, Wako: Institute of Physical and Chemical Research, 85–92 (1984).

- [5.510] L. S. Adam, M. E. Law, K. S. Jones, O. Dokumaci, C. S. Murthy, and S. Hegde, “Diffusion of Implanted Nitrogen in Silicon,” *J. Appl. Phys.*, vol. 87, no. 5, 2282–2284 (2000).
- [5.511] L. S. Adam and M. E. Law, “A Physical Model for Implanted Nitrogen Diffusion and Its Effect on Oxide Growth,” in: *Technical Digest of the 2000 International Electron Devices Meeting (IEDM)*, Piscataway: IEEE, 507–510 (2000).
- [5.512] L. S. Adam, M. E. Law, O. Dokumaci, and S. Hegde, “Physical Integrated Diffusion-Oxidation Model for Implanted Nitrogen in Silicon,” *J. Appl. Phys.*, vol. 91, no. 4, 1894–1900 (2002).
- [5.513] R. S. Hockett, “Anomalous Diffusion of Nitrogen-Implanted Silicon,” *Appl. Phys. Lett.*, vol. 54, no. 18, 1793–1795 (1989).
- [5.514] W. J. M. J. Josquin, “The Application of Nitrogen Ion Implantation in Silicon Technology,” *Nuclear Instruments and Methods*, vol. 209/210, 581–587 (1983).
- [5.515] C. T. Liu, Y. Ma, K. P. Cheung, C. P. Chang, L. Fritzinger, J. Becerro, H. Luftman, H. M. Vaidya, J. I. Colonell, A. Kamgar, J. F. Minor, R. G. Murray, W. Y. C. Lai, C. S. Pai, and S. J. Hillenius, “25Å Gate Oxide without Boron Penetration for 0.25 and 0.3- μ m PMOSFETs,” in: *1996 Symposium on VLSI Technology*, IEEE Electron Devices Society & Japan Society of Applied Physics, 18–19 (1996).
- [5.516] P. S. Lysaght, B. Nguyen, J. Bennett, G. Williamson, K. Torres, M. Gilmer, T.-Y. Luo, D. Brady, J. Guan, G. A. Brown, P. Zeitzoff, G. Bersuker, J. Mucha, F. Geyling, G. Gebara, L. Vishnubhotla, M. D. Jackson, and H. R. Huff, “Experimental Observations of the Redistribution of Implanted Nitrogen at the Si-SiO₂ Interface during RTA Processing,” in: *Si Front-End Processing — Physics and Technology of Dopant-Defect Interactions*, edited by H.-J. L. Gossmann, T. E. Haynes, M. E. Law, A. Nylandsted Larsen, and S. Odanaka, *Mat. Res. Soc. Symp. Proc.*, vol. 568, 283–288 (1999).
- [5.517] Y. Jeong, M. Sakuraba, T. Matsuura, and J. Murota, “Atomic-Layer Doping of N in Si Epitaxial Growth on Si(100) and Its Thermal Stability,” in: *Semiconductor Silicon 2002*, edited by H. R. Huff, L. Fabry, and S. Kishino, *Electrochem. Soc. Proc.*, vol. 2002-2, 287–296 (2002).
- [5.518] C. I. Drowley and T. I. Kamins, “Oxygen and Nitrogen Incorporation during CW Laser Recrystallization of Polysilicon,” in: *Laser-Solid Interactions and Transient Thermal Processing of Materials*, edited by J. Narayan, W. L. Brown, and R. A. Lemons, *Mat. Res. Soc. Symp. Proc.*, vol. 13, 511–516 (1983).
- [5.519] L. S. Adam, L. Robertson, M. E. Law, K. Jones, K. Gable, S. Hegde, and O. Dokumaci, “Diffusion of Implanted Nitrogen in Silicon at High Doses,” in: *Si Front-End Processing — Physics and Technology of Dopant-Defect Interactions III*, edited by K. S. Jones, M. D. Giles, P. Stolk, J. Matsuo, and E. C. Jones, *Mat. Res. Soc. Symp. Proc.*, vol. 669, J3.10.1–J3.10.6 (2001).
- [5.520] O. Dokumaci, R. Kaplan, M. Khare, P. Ronshem, J. Burnham, A. Domenicucci, J. Li, R. Flemming, L. S. Adam, and M. E. Law, “Diffusion and Defect Structure in Nitrogen Implanted Silicon,” in: *Si Front-End Processing — Physics and Technology of Dopant-Defect Interactions III*, edited by K. S. Jones, M. D. Giles, P. Stolk, J. Matsuo, and E. C. Jones, *Mat. Res. Soc. Symp. Proc.*, vol. 669, J6.4.1–J6.4.6 (2001).
- [5.521] R. S. Hockett, C. A. Evans, Jr., and P. K. Chu, “The SIMS Measurement of Nitrogen in Nitrogen-Doped CZ Silicon,” in: *Secondary Ion Mass Spectrometry: SIMS VI*, edited by A. Benninghoven, A. M. Huber, and H. W. Werner, New York: Wiley, 441–444 (1988).
- [5.522] H. J. Stein, “Nitrogen in Crystalline Si,” in: *Oxygen, Carbon, Hydrogen, and Nitrogen in Crystalline Silicon*, edited by J. C. Mikkelsen, Jr., S. J. Pearton, J. W. Corbett, and S. J. Pennycook, *Mat. Res. Soc. Symp. Proc.*, vol. 59, 523–534 (1986).
- [5.523] M. Tajima, T. Masui, T. Abe, and T. Nozaki, “Photoluminescence Associated with Nitrogen in Silicon,” *Jpn. J. Appl. Phys.*, vol. 20, no. 6, L423–L425 (1981).
- [5.524] R. Sauer, J. Weber, and W. Zulehner, “Nitrogen in Silicon: Towards the Identification of the 1.1223-eV (A,B,C) Photoluminescence Lines,” *Appl. Phys. Lett.*, vol. 44, no. 4, 440–442 (1984).
- [5.525] J. Weber, W. Schmid, and R. Sauer, “Localized Exciton Bound to an Isoelectronic Trap in Silicon,” *Phys. Rev. B*, vol. 21, no. 6, 2401–2414 (1980).

- [5.526] J. Wagner and R. Sauer, "Acceptorlike Excited States of the Isoelectronic A,B,C Exciton System in Silicon," *Phys. Rev. B*, vol. 26, no. 6, 3502–3505 (1982).
- [5.527] G. Davies, "A Simple Model for Excitons Bound to Axial Isoelectronic Defects in Silicon," *J. Phys. C*, vol. 17, 6331–6348 (1984).
- [5.528] G. Davies, M. Zafar Iqbal, and E. C. Lightowers, "Exciton Self-Trapping at an Isoelectronic Center in Silicon," *Phys. Rev. B*, vol. 50, no. 16, 11520–11530 (1994).
- [5.529] H. C. Alt and L. Tapfer, "Photoluminescence Study of Nitrogen Implanted Silicon," *Appl. Phys. Lett.*, vol. 45, no. 4, 426–428 (1984).
- [5.530] A. Dörnen, G. Pensl, and R. Sauer, "Nitrogen-Carbon Radiative Defect at 0.746 eV in Silicon," *Phys. Rev. B*, vol. 33, no. 2, 1495–1498 (1986).
- [5.531] K. Murakami, H. Itoh, K. Takita, K. Masuda, and T. Nishino, "Supersaturated Substitutional-Nitrogen Impurities in Nanosecond-Pulsed Laser Annealed Silicon," in: *17th International Conference on the Physics of Semiconductors*, edited by J. D. Chadi and W. A. Harrison, New York: Springer-Verlag, 1493–1496 (1985).
- [5.532] A. Dörnen, G. Pensl, and R. Sauer, "Set of Five Related Photoluminescence Defects in Silicon Formed through Nitrogen-Carbon Interactions," *Phys. Rev. B*, vol. 35, no. 17, 9318–9321 (1987).
- [5.533] Y. Itoh, T. Nozaki, T. Masui, and T. Abe, "Calibration Curve for Infrared Spectrophotometry of Nitrogen in Silicon," *Appl. Phys. Lett.*, vol. 47, no. 5, 488–489 (1985).
- [5.534] H. J. Stein, "Oxygen-Nitrogen Interactions in Ion-Implanted Silicon," in: *Microscopic Identification of Electronic Defects in Semiconductors*, edited by N. M. Johnson, S. G. Bishop, and G. D. Watkins, *Mat. Res. Soc. Symp. Proc.*, vol. 46, 287–290 (1985).
- [5.535] P. Wagner, R. Oeder, and W. Zulehner, "Nitrogen-Oxygen Complexes in Czochralski-Silicon," *Appl. Phys. A*, vol. 46, 73–76 (1988).
- [5.536] M. W. Qi, S. S. Tan, B. Zhu, P. X. Cai, W. F. Gu, X. M. Xu, T. S. Shi, D. L. Que, and L. B. Li, "The Evidence for Interaction of the N-N Pair with Oxygen in Czochralski Silicon," *J. Appl. Phys.*, vol. 69, no. 6, 3775–3777 (1991).
- [5.537] F. Berg Rasmussen, S. Öberg, R. Jones, C. Ewels, J. Goss, J. Miro, and P. Deák, "The Nitrogen-Pair Oxygen Defect in Silicon," *Materials Science and Engineering B*, vol. 36, 91–95 (1996).
- [5.538] D. Yang, R. Fan, L. Li, D. Que, and K. Sumino, "Effect of Nitrogen-Oxygen Complex on Electrical Properties of Czochralski Silicon," *Appl. Phys. Lett.*, vol. 68, no. 4, 487–489 (1996).
- [5.539] D. Yang, X. Ma, R. Fan, D. Li, J. Zhang, L. Li, D. Que, and K. Sumino, "Infrared Absorption of Nitrogen-Oxygen Complex in Silicon," *Materials Science and Engineering B*, vol. 72, 121–123 (2000).
- [5.540] Y. Yamanaka, H. Harada, K. Tanahashi, T. Mikayama, and N. Inoue, "Infrared Absorption Analysis of Nitrogen in Czochralski Silicon," in: *Gettering and Defect Engineering in Semiconductor Technology GADEST 2001*, edited by V. Raineri, F. Priolo, M. Kittler, and H. Richter, *Solid State Phenomena*, vol. 82-84, 63–68 (2002).
- [5.541] J. L. Libbert, L. Mule'Stagno, and M. Banan, "Dissociation of Nitrogen-Oxygen Complexes by Rapid Thermal Anneal Heat Treatments," *J. Appl. Phys.*, vol. 92, no. 3, 1238–1241 (2002).
- [5.542] C. P. Ewels, R. Jones, S. Öberg, J. Miro, and P. Deák, "Shallow Thermal Donor Defects in Silicon," *Phys. Rev. Lett.*, vol. 77, no. 5, 865–868 (1996).
- [5.543] H. Kageshima, A. Taguchi, and K. Wada, "Formation of Stable N-V-O Complexes in Si," in: *Proceedings of the 22nd International Conference on Defects in Semiconductors*, edited by K. Bonde Nielsen, A. Nylandsted Larsen, and G. Weyer, *Physica B*, vol. 340-342, 626–629 (2003).
- [5.544] D. Yang, L. Jun, L. Liben, Y. Hongnian, and Q. Duanling, "Thermal Acceptor Formation in Nitrogen-Doped Silicon," *Appl. Phys. Lett.*, vol. 59, no. 10, 1227–1229 (1991).
- [5.545] T. S. Chao, M. C. Liaw, C. H. Chu, C. Y. Chang, C. H. Chien, C. P. Hao, and T. F. Lei, "Mechanism of Nitrogen Coimplant for Suppressing Boron Penetration in P⁺-Polycrystalline Silicon Gate of p Metal-Oxide Semiconductor Field Effect Transistor," *Appl. Phys. Lett.*, vol. 69, no. 12, 1781–1782 (1996).

- [5.546] D. Yang, D. Li, M. Ghosh, and H. J. Möller, “Defects in Nitrogen-Doped Multicrystalline Silicon,” *Physica B*, vol. 344, 1–4 (2004).
- [5.547] S. Aronowitz, V. Zubkov, H. Puchner, and J. Kimball, “Activation of Group III Combinations in Silicon and Modifications Introduced by Nitrogen,” *J. Vac. Sci. Technol. B*, vol. 20, no. 1, 230–237 (2002).
- [5.548] V. G. Zavodinsky, A. V. Visikovski, I. A. Kuyanov, and J. Dabrowski, “Nitrogen Trapping of Boron and Phosphorus in Silicon,” *Physics of Low-Dimensional Structures*, vol. 3/4, 13–18 (2000).
- [5.549] K. Z. Ahmed, P. A. Kraus, C. Olsen, S. Hung, and F. Nouri, “Observation of Nitrogen-Enhanced Doping Deactivation at the Polysilicon-Oxynitride Interface of pMOSFETs with 12-AA Gate Dielectrics,” *IEEE Electron Device Letters*, vol. 24, no. 7, 445–447 (2003).
- [5.550] J. W. Bichard and J. C. Giles, “Optical Absorption Spectra of Arsenic and Phosphorus in Silicon,” *Can. J. Phys.*, vol. 40, 1480–1489 (1962).
- [5.551] R. L. Aggarwal and A. K. Ramdas, “Optical Determination of the Symmetry of the Ground State of Group-V Donors in Silicon,” *Phys. Rev.*, vol. 140, no. 4A, A1246–A1253 (1965).
- [5.552] B. Pajot, J. Kauppinen, and R. Anttila, “High-Resolution Study of the Group V Impurities Absorption in Silicon,” *Solid State Communications*, vol. 31, 759–763 (1979).
- [5.553] C. Jagannath, Z. W. Grabowski, and A. K. Ramdas, “Linewidths of the Electronic Excitation Spectra of Donors in Silicon,” *Phys. Rev. B*, vol. 23, no. 5, 2082–2098 (1981).
- [5.554] G. Picus, E. Burstein, and B. Henvis, “Absorption Spectra of Impurities in Silicon — II,” *J. Phys. Chem. Solids*, vol. 1, 75–81 (1956).
- [5.555] D. Sasireka and E. Palaniyandi, “Effect of Local Relaxation on the Binding Energy of Group-V Donors in Silicon,” *Phys. Rev. B*, vol. 46, no. 4, 2047–2049 (1992).
- [5.556] B. Pajot and A. M. Stoneham, “A Spectroscopic Investigation of the Lattice Distortion at Substitutional Sites for Groups V and VI Donors in Silicon,” *J. Phys. C*, vol. 20, 5241–5252 (1987).
- [5.557] B. G. Cohen, “X-Ray Measurement of Elastic Strain and Lattice Constant of Diffused Silicon,” *Solid-State Electronics*, vol. 10, 33–37 (1967).
- [5.558] M. Scheffler, “Lattice Relaxations at Substitutional Impurities in Semiconductors,” *Physica*, vol. 146B, 176–186 (1987).
- [5.559] O. Scheerer, U. Juda, and M. Höhne, “Self-Interstitial Shallow-Donor Complexes in Silicon: An Electron-Paramagnetic-Resonance Study,” *Phys. Rev. B*, vol. 57, no. 16, 9657–9662 (1998).
- [5.560] A. R. Chelyadinskii and V. A. Burenkov, “Model of the Pair Phosphorus Atom-Interstitial Silicon Atom,” *Physics of the Solid State*, vol. 40, no. 11, 1806–1808 (1998).
- [5.561] O. Sugino and A. Oshiyama, “Microscopic Mechanism of Atomic Diffusion in Si under Pressure,” *Phys. Rev. B*, vol. 46, no. 19, 12335–12341 (1992).
- [5.562] X.-Y. Liu, W. Windl, K. M. Beardmore, and M. P. Masquelier, “First-Principles Study of Phosphorus Diffusion in Silicon: Interstitial and Vacancy-Mediated Diffusion Mechanisms,” *Appl. Phys. Lett.*, vol. 82, no. 12, 1839–1841 (2003).
- [5.563] G. D. Watkins, J. W. Corbett, and R. M. Walker, “Spin Resonance in Electron Irradiated Silicon,” *J. Appl. Phys.*, vol. 30, no. 8, 1198–1203 (1959).
- [5.564] G. D. Watkins and J. W. Corbett, “Defects in Irradiated Silicon: Electron Paramagnetic Resonance and Electron-Nuclear Double Resonance of the Si-E Center,” *Phys. Rev.*, vol. 134, no. 5A, A1359–A1377 (1964).
- [5.565] G. K. Wertheim and D. N. E. Buchanan, “Electron-Bombardment Damage in Oxygen-Free Silicon,” *J. Appl. Phys.*, vol. 30, no. 8, 1232–1234 (1959).
- [5.566] H. Saito and M. Hirata, “Nature of Radiation Defects in Silicon Single Crystals,” *Japan. J. Appl. Phys.*, vol. 2, 678–687 (1963).
- [5.567] E. Sonder and L. C. Templeton, “Gamma Irradiation of Silicon. II. Levels in n-Type Float-Zone Material,” *J. Appl. Phys.*, vol. 34, no. 11, 3295–3301 (1963).
- [5.568] J. W. Walker and C. T. Sah, “Properties of 1.0-MeV-Electron-Irradiated Defect Centers in Silicon,” *Phys. Rev. B*, vol. 7, no. 10, 4587–4605 (1973).

- [5.569] L. C. Kimerling, H. M. De Angelis, and J. W. Diebold, “On the Role of Defect Charge State in the Stability of Point Defects in Silicon,” *Solid State Communications*, vol. 16, 171–174 (1975).
- [5.570] A. Chantre, M. Kechouane, and D. Bois, “Vacancy-Diffusion Model for Quenched-in E-Centers in CW Laser Annealed Virgin Silicon,” in: *Proceedings of the 12th International Conference on Defects in Semiconductors*, edited by C. A. J. Ammerlaan, *Physica*, vol. 116B, 547–552 (1983).
- [5.571] S. D. Brotherton and P. Bradley, “Defect Production and Lifetime Control in Electron and gamma-Irradiated Silicon,” *J. Appl. Phys.*, vol. 53, no. 8, 5720–5732 (1982).
- [5.572] J. H. Evans-Freeman, A. R. Peaker, I. D. Hawkins, P. Y. Y. Kan, J. Terry, L. Rubaldo, M. Ahmed, S. Watts, and L. Dobaczewski, “High-Resolution DLTS Studies of Vacancy-Related Defects in Irradiated and in Ion-Implanted n-Type Silicon,” *Materials Science in Semiconductor Processing*, vol. 3, 237–241 (2000).
- [5.573] N. I. Boyarkina, “Participation of the Electron Subsystem of a Crystal in the Reactions of Defect-Complex Decomposition in Semiconductors,” *Semiconductors*, vol. 34, no. 4, 410–414 (2000).
- [5.574] J. Mäkinen, C. Corbel, P. Hautojärvi, P. Moser, and F. Pierre, “Positron Trapping at Vacancies in Electron-Irradiated Si at Low Temperatures,” *Phys. Rev. B*, vol. 39, no. 14, 10162–10173 (1989).
- [5.575] R. Würschum, W. Bauer, K. Maier, A. Seeger, and H.-E. Schaefer, “Defects in Semiconductors after Electron Irradiation or in High-Temperature Thermal Equilibrium, As Studied by Positron Annihilation,” *J. Phys.: Condens. Matter*, vol. 1, SA33–SA48 (1989).
- [5.576] J. Mäkinen, P. Hautojärvi, and C. Corbel, “Positron Annihilation and the Charge States of the Phosphorus-Vacancy Pair in Silicon,” *J. Phys.: Condens. Matter*, vol. 4, 5137–5154 (1992).
- [5.577] A. Kawasuso, M. Hasegawa, M. Suezawa, S. Yamaguchi, and K. Sumino, “Annealing Processes of Vacancies in Silicon Induced by Electron Irradiation: Analysis Using Positron Lifetime,” in: *Positron Annihilation*, edited by Y.-J. He, B.-S. Cao, and Y. C. Jean, *Materials Science Forum*, vol. 175–178, 423–426 (1995).
- [5.578] K. Saarinen, J. Nissilä, H. Kauppinen, M. Hakala, M. J. Puska, P. Hautojärvi, and C. Corbel, “Identification of Vacancy-Impurity Complexes in Highly n-Type Si,” *Phys. Rev. Lett.*, vol. 82, no. 9, 1883–1886 (1999).
- [5.579] G. A. Samara, “Pressure Dependence of Deep Electronic Levels in Semiconductors: Phosphorus-Vacancy Pair (or Si E Center) and Divacancy in Silicon,” *Phys. Rev. B*, vol. 39, no. 17, 12764–12774 (1989).
- [5.580] H. Saito, M. Hirata, and T. Horiuchi, “Annealing of Radiation Defects in Silicon Single Crystals,” in: *Proceedings of the International Conference on Crystal Lattice Defects, 1962*, *J. Phys. Soc. Japan*, vol. 18, Supplement III, 246–250 (1963).
- [5.581] M. Hirata, M. Hirata, and H. Saito, “The Interaction of Point Defects with Impurities in Silicon,” *J. Phys. Soc. Japan*, vol. 27, no. 2, 405–414 (1969).
- [5.582] M. Yoshida, “Diffusion of Group V Impurity in Silicon,” *Jpn. J. Appl. Phys.*, vol. 10, no. 6, 702–713 (1971).
- [5.583] M. Yoshida and R. R. Hasiguti, “The Binding Energy between a Group 5 Impurity Atom and a Vacancy in Silicon,” in: *Radiation Damage and Defects in Semiconductors, Inst. Phys. Conf. Ser.*, no. 16, 223–227 (1973).
- [5.584] R. B. Fair and J. C. C. Tsai, “A Quantitative Model for the Diffusion of Phosphorus in Silicon and the Emitter Dip Effect,” *J. Electrochem. Soc.*, vol. 124, no. 7, 1107–1117 (1977).
- [5.585] R. W. Olesinski, N. Kanani, and G. J. Abbaschian, “The P-Si (Phosphorus-Silicon) System,” *Bull. Alloy Phase Diagrams*, vol. 6, no. 2, 130–133 (1985).
- [5.586] E. Tannenbaum, “Detailed Analysis of Thin Phosphorus-Diffused Layers in P-Type Silicon,” *Solid-State Electronics*, vol. 2, 123–132 (1961).
- [5.587] N. K. Abrikosov, V. M. Glazov, and L. Chén-yüan, “Individual and Joint Solubilities of Aluminium and Phosphorus in Germanium and Silicon,” *Russian Journal of Inorganic Chemistry*, vol. 7, 429–431 (1962).

- [5.588] E. Kooi, "Formation and Comparison of Surface Layers and Solubility Limits of Phosphorus during Diffusion in Silicon," *J. Electrochem. Soc.*, vol. 111, no. 12, 1383–1387 (1964).
- [5.589] M. L. Joshi and S. Dash, "Dislocation-Induced Deviation of Phosphorus-Diffusion Profiles in Silicon," *IBM J. Res. Develop.*, vol. 10, 446–454 (1966).
- [5.590] R. A. McDonald, G. G. Ehlenberger, and T. R. Huffman, "Control of Diffusion Induced Dislocations in Phosphorus Diffused Silicon," *Solid-State Electronics*, vol. 9, 807–812 (1966).
- [5.591] J. C. C. Tsai, "Shallow Phosphorus Diffusion Profiles in Silicon," *Proc. IEEE*, vol. 57, no. 9, 1499–1506 (1969).
- [5.592] F. N. Schwettmann and D. L. Kendall, "On the Nature of the Kink in the Carrier Profile for Phosphorus-Diffused Layers in Silicon," *Appl. Phys. Lett.*, vol. 21, no. 1, 2–4 (1972).
- [5.593] M. Yoshida, E. Arai, H. Nakamura, and Y. Terunuma, "Excess Vacancy Generation Mechanisms at Phosphorus Diffusion into Silicon," *J. Appl. Phys.*, vol. 45, no. 4, 1498–1506 (1974).
- [5.594] G. Masetti, D. Nobili, and S. Solmi, "Profiles of Phosphorus Predeposited in Silicon and Carrier Concentration in Equilibrium with SiP Precipitates," in: *Semiconductor Silicon 1977*, edited by H. R. Huff and E. Sirtl, *Electrochem. Soc. Proc.*, vol. 77-2, 648–657 (1977).
- [5.595] E. Fogarassy, R. Stuck, J. C. Muller, A. Grob, J. J. Grob, and P. Siffert, "Effects of Laser Irradiation on Phosphorus Diffused Layers in Silicon," *J. Electronic Materials*, vol. 9, no. 1, 197–209 (1980).
- [5.596] D. Nobili, "Coherent Precipitation and Solubility of Phosphorus and Arsenic in Silicon," in: *Aggregation Phenomena of Point Defects in Silicon*, edited by E. Sirtl and J. Goorissen, *Electrochem. Soc. Proc.*, vol. 83-4, 189–208 (1983).
- [5.597] A. Carabelas, D. Nobili, and S. Solmi, "Grain Boundary Segregation in Silicon Heavily Doped with Phosphorus and Arsenic," Colloque C1 in *Journal de Physique*, vol. 43, no. 10, 187–192 (1982).
- [5.598] P. Ostoja, D. Nobili, A. Armigliato, and R. Angelucci, "Isochronal Annealing of Silicon-Phosphorus Solid Solutions," *J. Electrochem. Soc.*, vol. 123, no. 1, 124–129 (1976).
- [5.599] K. Uda and M. Kamoshida, "Annealing Characteristics of Highly P⁺-Ion-Implanted Silicon Crystal — Two-Step Anneal," *J. Appl. Phys.*, vol. 48, no. 1, 18–21 (1977).
- [5.600] M. Tamura, "Dislocation Networks in Phosphorus-Implanted Silicon," *Phil. Mag.*, vol. 35, no. 3, 663–691 (1977).
- [5.601] D. Nobili, A. Armigliato, M. Finetti, and S. Solmi, "Precipitation As the Phenomenon Responsible for the Electrically Inactive Phosphorus in Silicon," *J. Appl. Phys.*, vol. 53, no. 3, 1484–1491 (1982).
- [5.602] J. Götzlich, P. H. Tsien, and H. Ryssel, "Relaxation Behavior of Metastable As and P Concentrations in Si after Pulsed and CW Laser Annealing," in: *Energy Beam-Solid Interactions and Transient Thermal Processing*, edited by J. C. C. Fan and N. M. Johnson, *Mat. Res. Soc. Symp. Proc.*, vol. 23, 235–240 (1984).
- [5.603] S. Solmi, A. Parisini, R. Angelucci, A. Armigliato, D. Nobili, and L. Moro, "Dopant and Carrier Concentration in Si in Equilibrium with Monoclinic SiP Precipitates," *Phys. Rev. B*, vol. 53, no. 12, 7836–7841 (1996).
- [5.604] F. A. Trumbore, "Solid Solubilities of Impurity Elements in Germanium and Silicon," *Bell Syst. Techn. J.*, vol. 39, no. 1, 205–233 (1960).
- [5.605] J. S. Makris and B. J. Masters, "Phosphorus Isoconcentration Diffusion Studies in Silicon," *J. Electrochem. Soc.*, vol. 120, no. 9, 1252–1255 (1973).
- [5.606] M. L. Barry, "Doped Oxides As Diffusion Sources. II. Phosphorus into Silicon," *J. Electrochem. Soc.*, vol. 117, no. 11, 1405–1410 (1970).
- [5.607] R. Francis and P. S. Dobson, "The Effect of Oxidation on the Diffusion of Phosphorus in Silicon," *J. Appl. Phys.*, vol. 50, no. 1, 280–284 (1979).
- [5.608] H. Nakamura, S. Ohyama, and C. Tadachi, "Boron Diffusion Coefficient Increased by Phosphorus Diffusion," *J. Electrochem. Soc.*, vol. 121, no. 10, 1377–1381 (1974).

- [5.609] Y. Ishikawa, Y. Sakina, H. Tanaka, S. Matsumoto, and T. Niimi, "The Enhanced Diffusion of Arsenic and Phosphorus in Silicon by Thermal Oxidation," *J. Electrochem. Soc.*, vol. 129, no. 3, 644–648 (1982).
- [5.610] D. A. Antoniadis, A. M. Lin, and R. W. Dutton, "Oxidation-Enhanced Diffusion of Arsenic and Phosphorus in Near-Intrinsic ⟨100⟩ Silicon," *Appl. Phys. Lett.*, vol. 33, no. 12, 1030–1033 (1978).
- [5.611] S. Matsumoto, J. F. Gibbons, V. Deline, and C. A. Evans, Jr., "High-Temperature Scanning CW Laser-Induced Diffusion of Arsenic and Phosphorus in Silicon," *Appl. Phys. Lett.*, vol. 37, no. 9, 821–824 (1980).
- [5.612] R. B. Fair and W. G. Meyer, "Modeling Anomalous Junction Formation in Silicon by the Codiffusion of Implanted Arsenic with Phosphorus," in: *Silicon Processing*, edited by D. C. Gupta, *ASTM Special Technical Publication*, vol. 804, 290–305 (1982).
- [5.613] R. Dürr, *Beschreibung der dualen Diffusion von Dotieratomen in Silicium für die Anwendung in der Prozeßsimulation*, Ph.D. thesis, Universität Erlangen-Nürnberg (1991).
- [5.614] N. Jeng and S. T. Dunham, "Interstitial Supersaturation during Oxidation of Silicon in Steam Ambients," *J. Appl. Phys.*, vol. 72, no. 5, 2049–2053 (1992).
- [5.615] A. Ural, P. B. Griffin, and J. D. Plummer, "Self-Diffusion in Silicon: Similarity between the Properties of Native Point Defects," *Phys. Rev. Lett.*, vol. 83, no. 17, 3454–3457 (1999).
- [5.616] H. Kunz, D. Clerc, and D. Jahn, "Diffusion aus dotierten Oxydhäuten als Verfahren zur Herstellung von Halbleiter-Bauelementen," *Brown Borveri Mitteilungen*, vol. 53, no. 1/2, 31–34 (1966).
- [5.617] M. Budil, H. Pötzl, G. Stingededer, M. Grasserbauer, and K. Goser, "A New Model of Anomalous Phosphorus Diffusion in Silicon," in: *Defects in Semiconductors 15*, edited by G. Ferenczi, *Materials Science Forum*, vol. 38-41, 719–724 (1989).
- [5.618] S. T. Dunham, "A Quantitative Model for the Coupled Diffusion of Phosphorus and Point Defects in Silicon," *J. Electrochem. Soc.*, vol. 139, no. 9, 2628–2636 (1992).
- [5.619] A. O. Konstantinov, "Non-Equilibrium Phenomena during Impurity Diffusion in Heavily Doped Silicon," in: *Defects in Semiconductors NCDS-1*, edited by N. T. Bagraev, *Defect and Diffusion Forum*, vol. 103-105, 215–220 (1993).
- [5.620] M. Uematsu, "Simulation of Boron, Phosphorus, and Arsenic Diffusion in Silicon Based on an Integrated Diffusion Model, and the Anomalous Phosphorus Diffusion Mechanism," *J. Appl. Phys.*, vol. 82, no. 5, 2228–2246 (1997).
- [5.621] D. A. Antoniadis, "Oxidation-Induced Point Defects in Silicon," *J. Electrochem. Soc.*, vol. 129, no. 5, 1093–1097 (1982).
- [5.622] P. Fahey, G. Barbuscia, M. Moslehi, and R. W. Dutton, "Kinetics of Thermal Nitridation Processes in the Study of Dopant Diffusion Mechanisms in Silicon," *Appl. Phys. Lett.*, vol. 46, no. 8, 784–786 (1985).
- [5.623] D. Collard and K. Taniguchi, "IMPACT — A Point-Defect-Based Two-Dimensional Process Simulator: Modeling the Lateral Oxidation-Enhanced Diffusion of Dopants in Silicon," *IEEE Trans. Electron Devices*, vol. ED-33, no. 10, 1454–1462 (1986).
- [5.624] M. Yoshida, S. Matsumoto, and Y. Ishikawa, "Solutions of Simultaneous Equations for Oxidation Enhanced and Retarded Diffusions and Oxidation Stacking Fault in Silicon," *Jpn. J. Appl. Phys.*, vol. 25, no. 7, 1031–1035 (1986).
- [5.625] M. Yoshida, "Analysis of Oxidation Enhanced and Retarded Diffusions and Growth of Oxidation Stacking Fault in Silicon," *Jpn. J. Appl. Phys.*, vol. 27, no. 6, 967–971 (1988).
- [5.626] T. Okino and M. Yoshida, "Two-Time Three-Equation Method for Analysis of Oxidation-Enhanced and -Retarded Diffusions and Growth of Oxidation Stacking Faults in Silicon," *Jpn. J. Appl. Phys.*, vol. 29, no. 1, 5–7 (1990).
- [5.627] T. Okino, "Analysis of Oxidation-Enhanced/Retarded Diffusions of Substitutional Impurities in Silicon," *Jpn. J. Appl. Phys., Part 1*, vol. 31, no. 4, 965–968 (1992).

- [5.628] T. Okino, "Behavior of Self-Interstitials and Vacancies in Silicon," in: *Diffusion in Materials DIMAT-92*, edited by M. Koiba, K. Hirano, H. Nakajima, and T. Okada, *Defect and Diffusion Forum*, vol. 95-98, 961–966 (1993).
- [5.629] T. Shimizu, T. Takagi, S. Matsumoto, Y. Sato, E. Arai, and T. Abe, "Fraction of Interstitial Component of Phosphorus and Antimony Diffusion in Silicon," *Jpn. J. Appl. Phys., Part 1*, vol. 37, no. 3B, 1184–1187 (1998).
- [5.630] A. Ural, P. B. Griffin, and J. D. Plummer, "Experimental Evidence for a Dual Vacancy-Interstitial Mechanism of Self-Diffusion in Silicon," *Appl. Phys. Lett.*, vol. 73, no. 12, 1706–1708 (1998).
- [5.631] E. Vandebossche and B. Baccus, "Interactions between Dopants and Point Defects during Nitridation Processes," *J. Appl. Phys.*, vol. 72, no. 2, 447–453 (1992).
- [5.632] J. P. John and M. E. Law, "Phosphorus Diffusion in Isoconcentration Backgrounds under Inert Conditions in Silicon," *Appl. Phys. Lett.*, vol. 62, no. 12, 1388–1389 (1993).
- [5.633] S. Solmi, P. Maccagnani, and R. Canteri, "Codiffusion of Arsenic and Phosphorus Implanted Silicon," *J. Appl. Phys.*, vol. 74, no. 8, 5005–5012 (1993).
- [5.634] S. Matsumoto, M. Yoshida, and T. Niimi, "The Confirmation of the Surface Effect upon Phosphorus Diffusion into Silicon," *Jpn. J. Appl. Phys.*, vol. 13, no. 11, 1899 (1974).
- [5.635] R. W. Dutton, P. Fahey, K. Doganis, L. Mei, and H. G. Lee, "Computer-Aided Process Modeling for Design and Process Control," in: *Silicon Processing*, edited by D. C. Gupta, *ASTM Special Technical Publication*, vol. 804, 407–421 (1983).
- [5.636] M. C. Duffy, F. Barson, J. M. Fairfield, and G. H. Schwuttke, "Effects of High Phosphorus Concentration on Diffusion into Silicon," *J. Electrochem. Soc.*, vol. 115, no. 1, 84–88 (1968).
- [5.637] E. Biedermann and A. Bogh, "Pre-Precipitation of Phosphorus in Heavily Doped Silicon," *Appl. Phys. Lett.*, vol. 17, no. 10, 457–459 (1970).
- [5.638] J. Makris, A. Ferris-Prahbu, and M. L. Joshi, "Effects of Extremely Thin Nitrogenous Surface Films on Phosphorus-Impurity Profiles in Silicon," *IBM J. Res. Develop.*, vol. 15, no. 2, 132–139 (1971).
- [5.639] R. Francis and P. S. Dobson, "The Diffusion Mechanism of Phosphorus in Silicon," in: *Lattice Defects in Semiconductors, 1974, Inst. Phys. Conf. Ser.*, no. 23, 545–549 (1975).
- [5.640] L. E. Miller, "Uniformity of Junctions in Diffused Silicon Devices," in: *Properties of Elemental and Compound Semiconductors*, edited by H. C. Gatos, *Metall. Soc. Conf. Proc.*, vol. 5, New York: Interscience Publishers, 303–322 (1960).
- [5.641] T. H. Yeh, "Diffusion of Phosphorus in Silicon," *Bull. Am. Phys. Soc., Series II*, vol. 7, no. 4, 332 (1962).
- [5.642] G. E. Moore, "Semiconductor Integrated Circuits," in: *Microelectronics*, edited by E. Keonjian, New York: McGraw-Hill, 282–283 (1963).
- [5.643] Y. Sato and H. Arata, "Distribution of Dislocations near the Junction Formed by Diffusion of Phosphorus in Silicon," *Jpn. J. Appl. Phys.*, vol. 3, no. 9, 511–515 (1964).
- [5.644] R. Gereth, P. G. G. van Loon, and V. Williams, "Localized Enhanced Diffusion in NPN Silicon Structures," *J. Electrochem. Soc.*, vol. 112, no. 3, 323–329 (1965).
- [5.645] D. B. Lee and A. F. W. Willoughby, "A New Observation of Enhanced Diffusion," *J. Appl. Phys.*, vol. 43, no. 1, 245–247 (1972).
- [5.646] R. F. Peart and R. C. Newman, "The Role of Defects in Diffusion," in: *Radiation Damage and Defects in Semiconductors, Inst. Phys. Conf. Ser.*, no. 16, 170–181 (1973).
- [5.647] S. M. Hu, "Diffusion in Silicon and Germanium," in: *Atomic Diffusion in Semiconductors*, edited by D. Shaw, London: Plenum Press, 217–350 (1973).
- [5.648] S. M. Hu, P. Fahey, and R. W. Dutton, "On Models of Phosphorus Diffusion in Silicon," *J. Appl. Phys.*, vol. 54, no. 12, 6912–6922 (1983).
- [5.649] M. Yoshida, "Excess Vacancy Generation by E-Center Dissociation in the Case of Phosphorus Diffusion in Silicon," *J. Appl. Phys.*, vol. 48, no. 6, 2169–2174 (1977).

- [5.650] M. Yoshida, "Numerical Solution of Phosphorus Diffusion Equation in Silicon," *Jpn. J. Appl. Phys.*, vol. 18, no. 3, 479–489 (1979).
- [5.651] D. Mathiot and J. C. Pfister, "Influence of the Nonequilibrium Vacancies on the Diffusion of Phosphorus into Silicon," *J. Appl. Phys.*, vol. 53, no. 4, 3053–3058 (1982).
- [5.652] D. Mathiot and J. C. Pfister, "High Concentration Diffusion of P in Si: a Percolation Problem?" *J. Physique Lettres*, vol. 43, 453–459 (1982).
- [5.653] M. Yoshida, "Diffusion of Phosphorus in Silicon," *Jpn. J. Appl. Phys.*, vol. 22, no. 9, 1404–1413 (1983).
- [5.654] A. Armigliato, M. Servidori, S. Solmi, and I. Vecchi, "On the Growth of Stacking Faults and Dislocations Induced in Silicon by Phosphorus Predeposition," *J. Appl. Phys.*, vol. 48, no. 5, 1806–1812 (1977).
- [5.655] C. L. Claeys, G. J. Declerck, and R. J. Van Overstraeten, "Influence of Phosphorus Diffusion on the Growth Kinetics of Oxidation-Induced Stacking Faults in Silicon," in: *Semiconductor Characterization Techniques*, edited by P. A. Barnes and G. A. Rozgonyi, *Electrochem. Soc. Proc.*, vol. 78-3, 366–375 (1978).
- [5.656] W. F. Tseng, S. S. Lau, and J. W. Mayer, "Formation of Stacking Faults and Dislocations in Phosphorus Diffused Silicon," *Phys. Lett.*, vol. 68A, no. 1, 93–94 (1978).
- [5.657] H. Strunk, U. Gösele, and B. O. Kolbesen, "Interstitial Supersaturation near Phosphorus-Diffused Emitter Zones in Silicon," *Appl. Phys. Lett.*, vol. 34, no. 8, 530–532 (1979).
- [5.658] P. Fahey, R. W. Dutton, and S. M. Hu, "Supersaturation of Self-Interstitials and Undersaturation of Vacancies during Phosphorus Diffusion in Silicon," *Appl. Phys. Lett.*, vol. 44, no. 8, 777–779 (1984).
- [5.659] R. M. Harris and D. A. Antoniadis, "Silicon Self-Interstitial Supersaturation during Phosphorus Diffusion," *Appl. Phys. Lett.*, vol. 43, no. 10, 937–939 (1983).
- [5.660] J. C. C. Tsai, D. B. Schimmel, R. B. Fair, and W. Maszara, "Point Defect Generation during Phosphorus Diffusion in Silicon," *J. Electrochem. Soc.*, vol. 134, no. 6, 1508–1518 (1987).
- [5.661] H. Hashimoto, H. Shibayama, H. Masaki, and H. Ishikawa, "Annihilation of Stacking Faults in Silicon by Impurity Diffusion," *J. Electrochem. Soc.*, vol. 123, no. 12, 1899–1902 (1976).
- [5.662] R. B. Fair and A. Carim, "On the Doping Dependence of Oxidation-Induced Stacking Fault Shrinkage in Silicon," *J. Electrochem. Soc.*, vol. 129, no. 10, 2319–2321 (1982).
- [5.663] S. Matsumoto and T. Niimi, "Effect of Phosphorus Diffusion on Oxidation-Induced Stacking Faults," *Electrochem. Soc. Extended Abstracts*, vol. 83-1, 440–441 (1983).
- [5.664] R. B. Fair, "The Effect of Strain-Induced Band-Gap Narrowing on High Concentration Phosphorus Diffusion in Silicon," *J. Appl. Phys.*, vol. 50, no. 2, 860–868 (1979).
- [5.665] D. Mathiot and J. C. Pfister, "Evidences That P Diffusion in Si Is Assisted Mainly by Vacancies," *Appl. Phys. Lett.*, vol. 47, no. 9, 962–964 (1985).
- [5.666] H. F. Schaake, "The Diffusion of Phosphorus in Silicon from High Surface Concentrations," *J. Appl. Phys.*, vol. 55, no. 4, 1208–1211 (1984).
- [5.667] B. J. Mulvaney and W. B. Richardson, "Model for Defect-Impurity Pair Diffusion in Silicon," *Appl. Phys. Lett.*, vol. 51, no. 18, 1439–1441 (1987).
- [5.668] A. O. Konstantinov, "Cause of the Appearance of a Surface Plateau of the Phosphorus Diffusion Profile in Silicon," *Sov. Phys. Semicond.*, vol. 26, no. 2, 191–198 (1992).
- [5.669] F. F. Morehead and R. F. Lever, "The Steady-State Model for Coupled Defect-Impurity Diffusion in Silicon," *J. Appl. Phys.*, vol. 66, no. 11, 5349–5352 (1989).
- [5.670] M. Orlowski, "Unified Model for Impurity Diffusion in Silicon," *Appl. Phys. Lett.*, vol. 53, no. 14, 1323–1325 (1988).
- [5.671] W. B. Richardson and B. J. Mulvaney, "Nonequilibrium Behaviour of Charged Point Defects during Phosphorus Diffusion in Silicon," *J. Appl. Phys.*, vol. 65, no. 6, 2243–2247 (1989).
- [5.672] S. Dunham and R. A. Meade, "Point Defect Models for High Concentration Phosphorus Diffusion," in: *Process Physics and Modeling in Semiconductor Technology*, edited by G. R. Srinivasan, J. D. Plummer, and S. T. Pantelides, *Electrochem. Soc. Proc.*, vol. 91-4, 287–303 (1991).

- [5.673] M. Yoshida, M. Morooka, M. Takahashi, and H. Tomokage, “Effective Diffusion Coefficient and Controlling Process of P Diffusion in Si Based on the Pair Diffusion Models of Vacancy and Interstitial Mechanisms,” *Jpn. J. Appl. Phys., Part 1*, vol. 39, no. 5A, 2483–2491 (2000).
- [5.674] K. Ghaderi and G. Hobler, “Simulation of Phosphorus Diffusion in Silicon Using a Pair Diffusion Model with a Reduced Number of Parameters,” *J. Electrochem. Soc.*, vol. 142, no. 5, 1654–1658 (1995).
- [5.675] M. Hirata, M. Hirata, and H. Saito, “Annealing of E Center in Irradiated Silicon,” *Jpn. J. Appl. Phys.*, vol. 5, 252 (1966).
- [5.676] M. Hirata, M. Hirata, and H. Saito, “Recombination Centers in Gamma-Irradiated Silicon,” *J. Appl. Phys.*, vol. 37, no. 4, 1867–1872 (1966).
- [5.677] M. Hirata, M. Hirata, H. Saito, and J. H. Crawford, “Annealing of Irradiated Silicon Containing Phosphorus Atoms,” *J. Phys. Soc. Japan*, vol. 22, no. 3, 1301 (1967).
- [5.678] L. C. Kimerling, H. M. De Angelis, and C. P. Carnes, “Annealing of Electron-Irradiated n-Type Silicon. I. Donor Concentration Dependence,” *Phys. Rev.*, vol. 3, no. 2, 427–433 (1971).
- [5.679] T. Wada, K. Yasuda, S. Ikuta, M. Takeda, and H. Masuda, “Complex Defects Introduced into Si by High-Energy Electron Irradiation: Production Rates of Defects in *n*-Si,” *J. Appl. Phys.*, vol. 48, no. 6, 2145–2152 (1977).
- [5.680] P. F. Lugakov and V. V. Luk’yanitsa, “Interaction of Vacancy- and Interstitial-Type Defects during Annealing of Irradiated *n*-Type Si,” *Sov. Phys. Semicond.*, vol. 17, no. 1, 106–107 (1983).
- [5.681] M. Suezawa, N. Fukata, T. Mchedlidze, and A. Kasuya, “Many Optical Absorption Peaks Observed in Electron-Irradiated *n*-Type Si,” *J. Appl. Phys.*, vol. 92, no. 11, 6561–6566 (2002).
- [5.682] E. G. Sieverts and C. A. J. Ammerlaan, “Electron Paramagnetic Resonance of New Defects in Heavily Phosphorus-Doped Silicon after Electron Irradiation,” in: *Radiation Effects in Semiconductors, 1976*, edited by N. B. Urli and J. W. Corbett, *Inst. Phys. Conf. Ser.*, no. 31, 213–220 (1977).
- [5.683] A. Nylandsted Larsen, C. Christensen, and J. Wulff Petersen, “Room-Temperature Vacancy Migration in Crystalline Si from an Ion-Implanted Surface Layer,” *J. Appl. Phys.*, vol. 86, no. 9, 4861–4864 (1999).
- [5.684] Y. Takamura, S. H. Jain, P. B. Griffin, and J. D. Plummer, “Thermal Stability of Dopants in Laser Annealed Silicon,” *J. Appl. Phys.*, vol. 92, no. 1, 230–234 (2002).
- [5.685] Y. Takamura, P. B. Griffin, and J. D. Plummer, “Physical Processes Associated with the Deactivation of Dopants in Laser Annealed Silicon,” *J. Appl. Phys.*, vol. 92, no. 1, 235–244 (2002).
- [5.686] D. J. Chadi, P. H. Citrin, C. H. Park, D. L. Adler, M. A. Marcus, and H.-J. Gossmann, “Fermi-Level-Pinning Defects in Highly *n*-Doped Silicon,” *Phys. Rev. Lett.*, vol. 79, no. 24, 4834–4837 (1997).
- [5.687] Y.-S. Kim, E.-C. Lee, and K. J. Chang, “Electrically Deactivating Nearest-Neighbor Donor Pair Defects in Si,” *Phys. Rev. Lett.*, vol. 91, 125503 (2003).
- [5.688] E. Schroer and M. Uematsu, “Simulation of Clustering and Pile-Up during Post-Implantation Annealing of Phosphorus in Silicon,” *Jpn. J. Appl. Phys., Part 1*, vol. 38, no. 1A, 7–11 (1999).
- [5.689] M. Uematsu, “Simulation of High-Concentration Phosphorus Diffusion in Silicon Taking into Account Phosphorus Clustering and Pile-Up,” *Jpn. J. Appl. Phys., Part 1*, vol. 38, no. 11, 6188–6192 (1999).
- [5.690] P. H. Keys, K. S. Jones, M. E. Law, M. Puga-Lambers, and S. M. Cea, “Dopant-Defect Clustering in Phosphorus Implanted Silicon: Experimentation and Modeling,” in: *Abstracts of the 2001 MRS Spring Meeting*, J5.5, 195–196 (2001).
- [5.691] B. G. Svensson and J. L. Lindström, “Annealing of Irradiated Highly Phosphorus-Doped Czochralski Silicon,” in: *Defects in Semiconductors 14*, edited by H. J. von Bardeleben, *Materials Science Forum*, vol. 10-12, 1087–1092 (1986).
- [5.692] J. L. Lindström, B. G. Svensson, and W. M. Chen, “A New Defect Observed in Annealed Phosphorus-Doped Electron-Irradiated Silicon,” in: *Defects in Semiconductors 16*, edited by G. Davies, G. G. DeLeo, and M. Stavola, *Materials Science Forum*, vol. 83-87, 333–338 (1992).

- [5.693] H. J. Hrostowski and R. H. Kaiser, "Absorption Spectrum of Arsenic Doped Silicon," *J. Phys. Chem. Solids*, vol. 7, 236–239 (1958).
- [5.694] A. S. Kaminskii, L. I. Kolesnik, B. M. Leiferov, and Y. E. Pokrovski, "Luminescence Analysis of Group III and V Impurities in Silicon," *J. Appl. Spektrosc.*, vol. 36, no. 5, 516–520 (1982).
- [5.695] A. Erbil, G. S. Cargill III, and R. F. Boehme, "Local Atomic Structure and Electrical Activity of Arsenic Implanted in Silicon," in: *Advanced Photon and Particle Techniques for the Characterization of Defects in Solids*, edited by J. B. Roberto, R. W. Carpenter, and M. C. Wittels, *Mat. Res. Soc. Symp. Proc.*, vol. 41, 275–280 (1985).
- [5.696] E. Canova, Y. H. Kao, and T. M. E. Arnold, "Local Environment of Arsenic Impurities in Semi-Insulating Polycrystalline Silicon," *Phys. Rev. B*, vol. 39, no. 5, 3131–3137 (1989).
- [5.697] A. Parisini, A. Bourret, A. Armigliato, M. Servidori, S. Solmi, R. Fabbri, J. R. Regnard, and J. L. Allain, "Electrical Activity and Structural Evolution Correlations in Laser and Thermally Annealed As-Implanted Si Specimens," *J. Appl. Phys.*, vol. 67, no. 5, 2320–2332 (1990).
- [5.698] Y. Horii, Y. Kikuchi, M. Kase, and S. Komiya, "Local Structure Analysis around Arsenic Implanted into Silicon by XAFS Technique," in: *Defects in Semiconductors 18*, edited by M. Suezawa and H. Katayama-Yoshida, *Materials Science Forum*, vol. 196-201, 1887–1890 (1995).
- [5.699] M. A. Sahiner, S. W. Novak, J. C. Woicik, J. Liu, and V. Krishnamoorthy, "Determining the Ratio of the Precipitated Versus Substituted Arsenic by XAFS and SIMS in Heavy Dose Arsenic Implants in Silicon," in: *Si Front-End Processing — Physics and Technology of Dopant-Defect Interactions III*, edited by K. S. Jones, M. D. Giles, P. Stolk, J. Matsuo, and E. C. Jones, *Mat. Res. Soc. Symp. Proc.*, vol. 669, J5.8.1–J5.8.7 (2001).
- [5.700] G. S. Cargill III, J. Angilello, and K. L. Kavanagh, "Lattice Compression from Conduction Electrons in Heavily Doped Si:As," *Phys. Rev. Lett.*, vol. 61, no. 15, 1748–1751 (1988).
- [5.701] I. Yokota, "Lattice Distortion around Charged Impurity in Semiconductors," *J. Phys. Soc. Japan*, vol. 19, 1487 (1964).
- [5.702] L. Eriksson, J. A. Davies, J. G. E. Johansson, and J. W. Mayer, "Implantation and Annealing Behavior of Group III and V Dopants in Silicon As Studied by the Channeling Technique," *J. Appl. Phys.*, vol. 40, no. 2, 842–854 (1969).
- [5.703] S. Chou, L. A. Davidson, and J. F. Gibbons, "A Study of Diffused Layers of Arsenic and Antimony in Silicon Using the Ion-Scattering Technique," *Appl. Phys. Lett.*, vol. 17, no. 1, 23–26 (1970).
- [5.704] E. Rimini, J. Haskell, and J. W. Mayer, "Beam Effects in the Analysis of As-Doped Silicon by Channeling Measurements," *Appl. Phys. Lett.*, vol. 20, no. 7, 237–239 (1972).
- [5.705] J. Haskell, E. Rimini, and J. W. Mayer, "Channeling Measurements in As-Doped Si," *J. Appl. Phys.*, vol. 43, no. 8, 3425–3431 (1972).
- [5.706] M. L. Swanson, J. A. Davies, A. F. Quenneville, F. W. Saris, and L. W. Wiggers, "Backscattering Measurement of the Temperature Dependence of Irradiation-Induced Displacement of As and Sb Atoms in Si Crystals," *Radiation Effects*, vol. 35, 51–59 (1978).
- [5.707] A. Nylandsted Larsen and V. E. Borisenko, "Behaviour of Implanted Arsenic in Silicon Single Crystals Subjected to Transient Heating with Incoherent Light," *Appl. Phys. A*, vol. 33, 51–58 (1984).
- [5.708] L. J. Borucki, "Evidence and Modeling of Anomalous Low Concentration Arsenic Inactivation," in: *Technical Digest of the 1990 International Electron Devices Meeting (IEDM)*, New York: IEEE, 753–756 (1990).
- [5.709] M. Heinrich, M. Budil, and H. W. Pötzl, "Determination of Diffusion Parameters for Arsenic," in: *Impurities, Defects and Diffusion in Semiconductors: Bulk and Layered Structures*, edited by D. J. Wolford, J. Bernholc, and E. E. Haller, *Mat. Res. Soc. Symp. Proc.*, vol. 163, 535–541 (1990).
- [5.710] P. Novell and M. E. Law, "The Effect of Nondilute Dopant-Defect Pair Concentrations on Arsenic Diffusion," in: *Proceedings NUPAD IV*, New York: IEEE, 41–44 (1992).

- [5.711] N. E. B. Cowern, “General Model for Intrinsic Dopant Diffusion in Silicon under Nonequilibrium Point-Defect Conditions,” *J. Appl. Phys.*, vol. 64, no. 9, 4484–4490 (1988).
- [5.712] R. Brindos, K. S. Jones, and M. E. Law, “Effect of Arsenic on Extended Defect Evolution in Silicon,” in: *Si Front-End Processing — Physics and Technology of Dopant-Defect Interactions III*, edited by K. S. Jones, M. D. Giles, P. Stolk, J. Matsuo, and E. C. Jones, *Mat. Res. Soc. Symp. Proc.*, vol. 669, J5.2.1–J5.2.6 (2001).
- [5.713] E. L. Elkin and G. D. Watkins, “Defects in Irradiated Silicon: Electron Paramagnetic Resonance and Electron-Nuclear Double Resonance of the Arsenic- and Antimony-Vacancy Pairs,” *Phys. Rev.*, vol. 174, no. 3, 881–897 (1968).
- [5.714] A. O. Evwaraye, “Annealing of Irradiation-Induced Defects in Arsenic-Doped Silicon,” *J. Appl. Phys.*, vol. 48, no. 5, 1840–1843 (1977).
- [5.715] O. O. Awadelkarim, A. Henry, B. Monemar, and J. L. Lindström, “The Role of Group-V Impurities in Defect Formation in Irradiated Silicon,” *phys. stat. sol. (a)*, vol. 120, 539–546 (1990).
- [5.716] V. Ranki, J. Nissilä, and K. Saarinen, “Formation of Vacancy-Impurity Complexes by Kinetic Processes in Highly As-Doped Si,” *Phys. Rev. Lett.*, vol. 88, no. 10, 105506 (2002).
- [5.717] O. Pankratov, H. Huang, T. Diaz de la Rubia, and C. Mailhot, “As-Vacancy Interaction and Ring Mechanism of Diffusion in Si,” *Phys. Rev. B*, vol. 56, no. 20, 13172–13176 (1997).
- [5.718] J. Xie and S. P. Chen, “Interaction Potentials for Vacancy-Assisted As Diffusion in Silicon,” *J. Phys.: Condens. Matter*, vol. 11, no. 38, 7219–7226 (1999).
- [5.719] M. Ramamoorthy and S. T. Pantelides, “Complex Dynamical Phenomena in Heavily Arsenic Doped Silicon,” *Phys. Rev. Lett.*, vol. 76, no. 25, 4753–4756 (1996).
- [5.720] D. C. Mueller, E. Alonso, and W. Fichtner, “Arsenic Deactivation in Si: Electronic Structure and Charge States of Vacancy-Impurity Clusters,” *Phys. Rev. B*, vol. 68, 045208 (2003).
- [5.721] R. W. Olesinski and G. J. Abbaschian, “The As-Si (Arsenic-Silicon) System,” *Bull. Alloy Phase Diagrams*, vol. 6, no. 3, 254–258 (1985).
- [5.722] R. Angelucci, A. Armigliato, E. Landi, D. Nobili, and S. Solmi, “Equilibrium Solubility of Arsenic and Antimony in Silicon,” in: *ESSDERC 87*, Bologna: Tecnoprint, 461–464 (1987).
- [5.723] D. Nobili, S. Solmi, A. Parisini, M. Derdour, A. Armigliato, and L. Moro, “Precipitation, Aggregation, and Diffusion in Heavily Arsenic-Doped Silicon,” *Phys. Rev. B*, vol. 49, no. 4, 2477–2483 (1994).
- [5.724] K. Nakamura and M. Kamoshida, “Implanted As Redistribution during Annealing in Oxidizing Ambient,” *J. Electrochem. Soc.*, vol. 125, no. 9, 1518–1521 (1978).
- [5.725] A. Lietoila, J. F. Gibbons, and T. W. Sigmon, “The Solid Solubility and Thermal Behavior of Metastable Concentration of As in Si,” *Appl. Phys. Lett.*, vol. 36, no. 9, 765–768 (1980).
- [5.726] A. Nylandsted Larsen, S. Y. Shiryaev, E. Schwartz Sørensen, and P. Tidemand-Petersson, “Rapid Thermal Annealing of High Concentration, Arsenic Implanted Silicon Single Crystals,” *Appl. Phys. Lett.*, vol. 48, no. 26, 1805–1807 (1986).
- [5.727] M. Derdour, D. Nobili, and S. Solmi, “High-Temperature Equilibrium Carrier Density of Arsenic-Doped Silicon,” *J. Electrochem. Soc.*, vol. 138, no. 3, 857–860 (1991).
- [5.728] A. Nylandsted Larsen, B. Christensen, and S. Y. Shiryaev, “Deactivation of Electrically Active Arsenic in Silicon during Cooling-Down from Elevated Temperatures,” *J. Appl. Phys.*, vol. 71, no. 10, 4854–4858 (1992).
- [5.729] V. Ranki, K. Saarinen, J. Fage-Pedersen, J. Lundsgaard Hansen, and A. Nylandsted Larsen, “Electrical Deactivation by Vacancy-Impurity Complexes in Highly As-Doped Si,” *Phys. Rev. B*, vol. 67, 041201 (2003).
- [5.730] W. J. Armstrong, “The Diffusivity of Arsenic in Silicon,” *J. Electrochem. Soc.*, vol. 109, no. 11, 1065–1067 (1962).
- [5.731] P. S. Raju, N. R. K. Rao, and E. V. K. Rao, “Diffusion of Arsenic in Silicon,” *Indian J. Pure Appl. Phys.*, vol. 2, 353–355 (1964).
- [5.732] Y. W. Hsueh, “Arsenic Diffusion in Silicon Using Arsine,” *Electrochemical Technology*, vol. 6, no. 9–10, 361–365 (1968).

- [5.733] B. J. Masters and J. M. Fairfield, "Arsenic Isoconcentration Diffusion Studies in Silicon," *J. Appl. Phys.*, vol. 40, no. 6, 2390–2394 (1969).
- [5.734] T. L. Chiu and H. N. Ghosh, "A Diffusion Model for Arsenic in Silicon," *IBM J. Res. Develop.*, vol. 15, no. 6, 472–476 (1971).
- [5.735] G. F. Cerofolini, P. Manini, L. Meda, M. L. Polignano, G. Queirolo, F. Nava, G. Ottaviani, and M. Gallorini, "Thermodynamic and Kinetic Properties of Arsenic-Implanted Silicon," *Thin Solid Films*, vol. 135, 59–72 (1986).
- [5.736] H. Ryssel, H. Betz, J. Lorenz, J. Pelka, A. Barthel, L. M. Buchmann, W. Krüger, H. Mader, D. Mewes, K. O. Müller, G. Neumayer, P. Pichler, A. Sachs, A. Seidl, and M. Svoboda, "Zweidimensionale Prozeßsimulation vollständiger technologischer Prozeßabläufe," *Forschungsbericht NT 2686 I3*, Fraunhofer-Arbeitsgruppe für Integrierte Schaltungen, Abteilung für Bauelementetechnologie, Erlangen, Germany (1986).
- [5.737] D. P. Kennedy and P. C. Murley, "Concentration Dependent Diffusion of Arsenic in Silicon," *Proc. IEEE*, vol. 59, 335–336 (1971).
- [5.738] R. B. Fair and J. C. C. Tsai, "The Diffusion of Ion-Implanted Arsenic in Silicon," *J. Electrochem. Soc.*, vol. 122, no. 12, 1689–1696 (1975).
- [5.739] E. Nygren, M. J. Aziz, D. Turnbull, J. M. Poate, D. C. Jacobson, and R. Hull, "Pressure Dependence of Arsenic Diffusivity in Silicon," *Appl. Phys. Lett.*, vol. 47, no. 2, 105–107 (1985).
- [5.740] O. Sugino and A. Oshiyama, "Pressure Dependence of Formation and Migration Enthalpies for Atomic Diffusion in Si: Conjugate Gradient Minimization of Total Energy," in: *Defects in Semiconductors 16*, edited by G. Davies, G. G. DeLeo, and M. Stavola, *Materials Science Forum*, vol. 83–87, 469–474 (1992).
- [5.741] A. Nylandsted Larsen, P. E. Andersen, P. Gaiduk, and K. Kylliesbech Larsen, "The Effect of Phosphorus Background Concentration on the Diffusion of Tin, Arsenic and Antimony in Silicon," *Materials Science and Engineering B*, vol. 4, 107–112 (1989).
- [5.742] A. Nylandsted Larsen, K. Kylliesbech Larsen, P. E. Andersen, and B. G. Svensson, "Heavy Doping Effects in the Diffusion of Group IV and V Impurities in Silicon," *J. Appl. Phys.*, vol. 73, no. 2, 691–698 (1993).
- [5.743] R. B. Fair and G. R. Weber, "Effect of Complex Formation on Diffusion of Arsenic in Silicon," *J. Appl. Phys.*, vol. 44, no. 1, 273–279 (1973).
- [5.744] J. Murota, E. Arai, K. Kobayashi, and K. Kudo, "Arsenic Diffusion in Silicon from Doped Polycrystalline Silicon," *Jpn. J. Appl. Phys.*, vol. 17, no. 2, 457–458 (1978).
- [5.745] J. Murota, E. Arai, K. Kobayashi, and K. Kudo, "Relationship between Total Arsenic and Electrically Active Arsenic Concentrations in Silicon Produced by the Diffusion Process," *J. Appl. Phys.*, vol. 50, no. 2, 804–808 (1979).
- [5.746] J. L. Hoyt and J. F. Gibbons, "Rapid Thermal Annealing of As in Si," in: *Rapid Thermal Processing*, edited by T. O. Sedgwick, T. E. Seidel, and B.-Y. Tsaur, *Mat. Res. Soc. Symp. Proc.*, vol. 52, 15–22 (1986).
- [5.747] S. Y. Shiryaev, A. Nylandsted Larsen, E. Schwartz Sørensen, and P. Tidemand-Petersson, "Redistribution and Activation of Ion Implanted As in Si during RTA for Concentrations around Solid Solubility," *Nuclear Instruments and Methods in Physics Research B*, vol. 19/20, 507–511 (1987).
- [5.748] D. Mathiot and J. C. Pfister, "Diffusion of Arsenic in Silicon: Validity of the Percolation Model," *Appl. Phys. Lett.*, vol. 42, no. 12, 1043–1044 (1983).
- [5.749] D. Stauffer, "Scaling Theory of Percolation Clusters," *Physics Reports*, vol. 54, 1–74 (1979).
- [5.750] S. Solmi and D. Nobili, "High Concentration Diffusivity and Clustering of Arsenic and Phosphorus in Silicon," *J. Appl. Phys.*, vol. 83, no. 5, 2484–2490 (1998).
- [5.751] S. T. Dunham and C. D. Wu, "Atomistic Models of Vacancy-Mediated Diffusion in Silicon," *J. Appl. Phys.*, vol. 78, no. 4, 2362–2366 (1995).
- [5.752] S. List and H. Ryssel, "Atomistic Modeling of High-Concentration Effects of Impurity Diffusion in Silicon," *J. Appl. Phys.*, vol. 83, no. 12, 7595–7607 (1998).

- [5.753] M. M. Bunea and S. T. Dunham, “Lattice Monte Carlo Simulations of Vacancy-Mediated Diffusion and Aggregation Using Ab-Initio Parameters,” in: *Defects and Diffusion in Silicon Processing*, edited by T. Diaz de la Rubia, S. Coffa, P. A. Stolk, and C. S. Rafferty, *Mat. Res. Soc. Symp. Proc.*, vol. 469, 353–358 (1997).
- [5.754] J. Xie and S. P. Chen, “Diffusion and Clustering in Heavily Arsenic-Doped Silicon: Discrepancies and Explanation,” *Phys. Rev. Lett.*, vol. 83, no. 9, 1795–1798 (1999).
- [5.755] R. O. Schwenker, E. S. Pan, and R. F. Lever, “Arsenic Clustering in Silicon,” *J. Appl. Phys.*, vol. 42, no. 8, 3195–3200 (1971).
- [5.756] M. Yoshida, “General Theory of Phosphorus and Arsenic Diffusions in Silicon,” *Jpn. J. Appl. Phys.*, vol. 19, no. 12, 2427–2440 (1980).
- [5.757] D. Mathiot and P. Scheiblin, “Modelling of Low Thermal Budget Redistribution of Arsenic in Silicon: Dynamic Clustering,” in: *ULSI Science and Technology/1995*, edited by E. M. Middlesworth and H. Massoud, *Electrochem. Soc. Proc.*, vol. 95-5, 13–20 (1995).
- [5.758] H. Bauer, P. Pichler, and H. Ryssel, “Modeling Dynamic Clustering of Arsenic Including Non-Negligible Concentrations of Arsenic-Point Defect Pairs,” *IEEE Trans. Semiconductor Manufacturing*, vol. 8, no. 4, 414–418 (1995).
- [5.759] V. I. Fistul’, *Heavily Doped Semiconductors*, New York: Plenum Press (1969).
- [5.760] D. Nobili, S. Solmi, and J. Shao, “Clustering Equilibrium and Deactivation Kinetics in Arsenic Doped Silicon,” *J. Appl. Phys.*, vol. 90, no. 1, 101–107 (2001).
- [5.761] P. Fastenko, S. T. Dunham, and G. Henkelman, “Modeling of Annealing of High Concentration Arsenic Profiles,” in: *Si Front-End Processing — Physics and Technology of Dopant-Defect Interactions III*, edited by K. S. Jones, M. D. Giles, P. Stolk, J. Matsuo, and E. C. Jones, *Mat. Res. Soc. Symp. Proc.*, vol. 669, J5.10.1–J5.10.6 (2001).
- [5.762] S. Chakravarthi, P. R. Chidambaram, C. Machala, A. Jain, and X. Zhang, “Modeling of Diffusion and Activation of Low Energy Arsenic Implants in Silicon,” in: *Silicon Front-End Junction Formation Technologies*, edited by D. F. Downey, M. E. Law, A. P. Claverie, and M. J. Rendon, *Mat. Res. Soc. Symp. Proc.*, vol. 717, C3.7.1–C3.7.6 (2002).
- [5.763] P. Shah, “Computer Aided Process Design and Optimization for Semiconductor Device Fabrication,” in: *Semiconductor Silicon 1977*, edited by H. R. Huff and E. Sirtl, *Electrochem. Soc. Proc.*, vol. 77-2, 923–931 (1977).
- [5.764] K. C. Pandey, A. Erbil, G. S. Cargill III, R. F. Boehme, and D. Vanderbilt, “Annealing of Heavily Arsenic-Doped Silicon: Electrical Deactivation and a New Defect Complex,” *Phys. Rev. Lett.*, vol. 61, no. 11, 1282–1285 (1988).
- [5.765] J. L. Allain, J. R. Regnard, A. Bourret, A. Parisini, A. Armigliato, G. Tourillon, and S. Pizzini, “Extended X-Ray-Absorption Fine-Structure Study of the Local Atomic Structure in As⁺ Heavily Implanted Silicon,” *Phys. Rev. B*, vol. 46, no. 15, 9434–9445 (1992).
- [5.766] W. K. Chu and B. J. Masters, “Channeling Study of the Formation of Arsenic Clusters in Silicon,” in: *Laser-Solid Interactions and Laser Processing — 1978*, edited by S. D. Ferris, H. J. Leamy, and J. M. Poate, *AIP Conference Proceedings*, no. 50, 305–309 (1979).
- [5.767] C. Brizard, J. R. Regnard, J. L. Allain, A. Bourret, M. Dubus, A. Armigliato, and A. Parisini, “Backscattering Spectrometry and Ion Channeling Studies of Heavily Implanted As⁺ in Silicon,” *J. Appl. Phys.*, vol. 75, no. 1, 126–133 (1994).
- [5.768] A. Herrera-Gomez, P. M. Rousseau, G. Materlik, T. Kendelewicz, J. C. Woicik, P. B. Griffin, J. Plummer, and W. E. Spicer, “Evolution of the Crystallographic Position of As Impurities in Heavily Doped Si Crystals As Their Electrical Activity Changes,” *Appl. Phys. Lett.*, vol. 68, no. 22, 3090–3092 (1996).
- [5.769] P. M. Rousseau, P. B. Griffin, and J. D. Plummer, “Electrical Deactivation of Arsenic As a Source of Point Defects,” *Appl. Phys. Lett.*, vol. 65, no. 5, 578–580 (1994).
- [5.770] V. B. Osvenskii, L. M. Morgulis, S. P. Gishina, and N. M. Klimova, “An Electron Microscope Investigation of Strongly Doped n-Type Silicon,” *Sov. Phys. Solid State*, vol. 11, no. 5, 1064–1067 (1969).

- [5.771] S. Hirota, M. Miyake, S. Nakayama, E. Arai, and J. Murota, "Cross-Sectional TEM Observations of Process-Induced Defects in Heavily Arsenic-Diffused Silicon Layers," *J. Electrochem. Soc.*, vol. 137, no. 1, 318–322 (1990).
- [5.772] R. Brindos, M. H. Clark, K. S. Jones, M. Griglione, H.-J. Gossman, A. Agarwal, B. Murto, and E. Andideh, "Influence of Arsenic Clustering and Precipitation on the Interstitial and Vacancy Concentration in Silicon," in: *Si Front-End Processing — Physics and Technology of Dopant-Defect Interactions III*, edited by K. S. Jones, M. D. Giles, P. Stolk, J. Matsuo, and E. C. Jones, *Mat. Res. Soc. Symp. Proc.*, vol. 669, J5.7.1–J5.7.6 (2001).
- [5.773] D. W. Lawther, U. Myler, P. J. Simpson, P. M. Rousseau, P. B. Griffin, and J. D. Plummer, "Vacancy Generation Resulting from Electrical Deactivation of Arsenic," *Appl. Phys. Lett.*, vol. 67, no. 24, 3575–3577 (1995).
- [5.774] U. Myler, P. J. Simpson, D. W. Lawther, and P. M. Rousseau, "On the Electrical Deactivation of Arsenic in Silicon," *J. Vac. Sci. Technol. B*, vol. 15, no. 3, 757–759 (1997).
- [5.775] S. Solmi, M. Attari, and D. Nobili, "Effect of Vacancy and Interstitial Excess on the Deactivation Kinetics of As in Si," *Appl. Phys. Lett.*, vol. 80, no. 25, 4774–4776 (2002).
- [5.776] S. Solmi, M. Ferri, M. Bersani, D. Giubertoni, and V. Soncini, "Transient Enhanced Diffusion of Arsenic in Silicon," *J. Appl. Phys.*, vol. 94, no. 8, 4950 (2003).
- [5.777] M. A. Berding and A. Sher, "Electronic Quasichemical Formalism: Application to Arsenic Deactivation in Silicon," *Phys. Rev. B*, vol. 58, no. 7, 3853–3864 (1998).
- [5.778] J. Xie and S. P. Chen, "Generation of Frenkel Defects in Heavily Arsenic Doped Silicon: A First-Principles Study," *J. Appl. Phys.*, vol. 87, no. 9, 4160–4163 (2000).
- [5.779] R. Brindos, P. Keys, K. S. Jones, and M. E. Law, "Effect of Arsenic Doping on {311} Defect Dissolution in Silicon," *Appl. Phys. Lett.*, vol. 75, no. 2, 229–231 (1999).
- [5.780] R. Brindos, P. H. Keys, M. Griglione, K. S. Jones, M. E. Law, A. Agarwal, and E. Andideh, "Reaction of Excess Silicon Interstitials in the Presence of Arsenic and Germanium," in: *Si Front-End Processing — Physics and Technology of Dopant-Defect Interactions II*, edited by A. Agarwal, L. Pelaz, H.-H. Vuong, P. Packan, and M. Kase, *Mat. Res. Soc. Symp. Proc.*, vol. 610, B8.4.1–B8.4.6 (2000).
- [5.781] R. Kim, T. Aoki, Y. Furuta, H. Kobyashi, J. Xia, T. Saito, Y. Kamakura, and K. Taniguchi, "Transient Enhanced Diffusion of Arsenic by Self-Implantation: The Role of As-I Clusters," in: *Si Front-End Processing — Physics and Technology of Dopant-Defect Interactions II*, edited by A. Agarwal, L. Pelaz, H.-H. Vuong, P. Packan, and M. Kase, *Mat. Res. Soc. Symp. Proc.*, vol. 610, B8.2.1–B8.2.6 (2000).
- [5.782] T. Hallberg, J. L. Lindström, B. G. Svensson, and K. Swiatek, "Annealing of Electron Irradiated P-, As-, Sb- and Bi-Doped Czochralski Silicon," in: *Defects in Semiconductors 17*, edited by H. Heinrich and W. Jantsch, *Materials Science Forum*, vol. 143–147, 1239–1243 (1994).
- [5.783] J. S. Williams and K. T. Short, "Metastable Doping Behavior in Antimony-Implanted (100) Silicon," *J. Appl. Phys.*, vol. 53, no. 12, 8663–8667 (1982).
- [5.784] P. H. Citrin, D. A. Muller, H.-J. Gossman, R. Vanfleet, and P. A. Northrup, "Geometric Frustration of 2D Dopants in Silicon: Surpassing Electrical Saturation," *Phys. Rev. Lett.*, vol. 83, no. 16, 3234–3237 (1999).
- [5.785] K. Suzuki and H. Tashiro, "High Activation of Sb during Solid-Phase Epitaxy and Deactivation during Subsequent Thermal Process," *IEEE Trans. Electron Devices*, vol. 50, no. 8, 1753–1757 (2003).
- [5.786] G. Weyer, A. Nylandsted Larsen, N. E. Holm, and H. L. Nielsen, "Radiation Defects in Ion-Implanted Silicon. I. Mössbauer Spectroscopy of ^{119}Sn Defect Structures from Implantations of Radioactive Antimony," *Phys. Rev. B*, vol. 21, no. 11, 4939–4950 (1980).
- [5.787] J. R. Dennis and E. B. Hale, "Model Correction for the Formation of Amorphous Silicon by Ion Implantation," *Radiation Effects*, vol. 19, 67–68 (1973).
- [5.788] J. L. Allain, A. Bourret, J. R. Regnard, and A. Armigliato, "Local Atomic Structure in Sb^+ and Sb^+/B^+ Heavily Implanted Silicon from Fluorescence EXAFS," in: *Proceedings of the*

- 7th International Conference on X-Ray Absorption Fine Structure, *Jpn. J. Appl. Phys.*, vol. 32, Supplement 32-2, 616–618 (1993).
- [5.789] C. Revenant-Brizard, J. R. Regnard, S. Solmi, A. Armigliato, S. Valmorri, C. Cellini, and F. Romanato, “High-Temperature Annealings of Sb and Sb/B Heavily Implanted Silicon Wafers Studied by Near Grazing Incidence Fluorescence Extended X-Ray Absorption Fine Structure,” *J. Appl. Phys.*, vol. 79, no. 12, 9037–9042 (1996).
- [5.790] M. A. Sahiner, S. W. Novak, J. C. Woicik, Y. Takamura, P. B. Griffin, and J. D. Plummer, “The Local Structure of Antimony in High Dose Antimony Implants in Silicon by XAFS and SIMS,” in: *Silicon Front-End Junction Formation Technologies*, edited by D. F. Downey, M. E. Law, A. P. Claverie, and M. J. Rendon, *Mat. Res. Soc. Symp. Proc.*, vol. 717, C3.6.1–C3.6.7 (2002).
- [5.791] S. Damgaard, J. W. Petersen, and G. Weyer, “The Tin-Vacancy Pair Defect in Silicon,” *Hyperfine Interactions*, vol. 10, 751–758 (1981).
- [5.792] A. O. Evvaraye, “Electron-Irradiation Damage in Antimony-Doped Silicon,” *J. Appl. Phys.*, vol. 48, no. 2, 734–738 (1977).
- [5.793] P. Kringshøj and A. Nylandsted Larsen, “Irradiation-Induced Defect States in Epitaxial *n*-Type Si_{1-x}Ge_x Alloys,” *Phys. Rev. B*, vol. 52, no. 23, 16333–16336 (1995).
- [5.794] A. Kawasuso, M. Hawegawa, M. Suezawa, S. Yamauchi, and K. Sumino, “An Annealing Study of Defects Induced by Electron Irradiation of Czochralski-Grown Si Using a Positron Lifetime Technique,” *Applied Surface Science*, vol. 85, 280–286 (1995).
- [5.795] S. Szpala, P. Asoka-Kumar, B. Nielsen, J. P. Peng, S. Hayakawa, K. G. Lynn, and H.-J. Gossmann, “Defect Identification Using the Core-Electron Contribution in Doppler-Broadening Spectroscopy of Positron-Annihilation Radiation,” *Phys. Rev. B*, vol. 54, no. 7, 4722–4731 (1996).
- [5.796] G. Weyer, M. Fanciulli, K. Freitag, A. Nylandsted Larsen, M. Lindroos, E. Müller, H. C. Verstergaard, and ISOLDE Collaboration, “Evidence for High Vacancy Concentrations in Heavily Doped *n*-Type Silicon from Mossbauer Experiments,” in: *Defects in Semiconductors 18*, edited by M. Suezawa and H. Katayama-Yoshida, *Materials Science Forum*, vol. 196–201, 1117–1121 (1995).
- [5.797] T. Kobayashi, C. F. McConville, J. Nakamura, G. Dorenbos, H. Sone, T. Katayama, and M. Aono, “Study of Diffusion and Defects by Medium-Energy Coaxial Impact-Collision Ion Scattering Spectroscopy,” *Defect and Diffusion Forum*, vol. 183–185, 207–214 (2000).
- [5.798] A. Nylandsted Larsen and G. Weyer, “Defect Impurity Complex Formation at High Donor Concentration in Silicon,” in: *Defects in Semiconductors 16*, edited by G. Davies, G. G. DeLeo, and M. Stavola, *Materials Science Forum*, vol. 83–87, 273–278 (1992).
- [5.799] R. W. Olesinski and G. J. Abbaschian, “The Sb-Si (Antimony-Silicon) System,” *Bull. Alloy Phase Diagrams*, vol. 6, no. 5, 445–448 (1985).
- [5.800] J. J. Rohan, N. E. Pickering, and J. Kennedy, “Diffusivity of Radioactive Antimony in Silicon,” *J. Electrochem. Soc.*, vol. 106, no. 8, 705–709 (1959).
- [5.801] C. W. White, S. R. Wilson, B. R. Appleton, F. W. Young, Jr., and J. Narayan, “Supersaturated Substitutional Alloys in Silicon Formed by Ion Implantation and Laser Annealing,” in: *Laser and Electron Beam Processing of Materials*, edited by C. W. White and P. S. Peercy, New York: Academic Press, 111–116 (1980).
- [5.802] T. Brabec, M. Schrems, M. Budil, H. W. Pötzl, W. Kuhnert, P. Pongratz, G. Stingereder, and M. Grasserbauer, “Modeling of Antimony Precipitation in Silicon,” *J. Electrochem. Soc.*, vol. 136, no. 5, 1542–1545 (1989).
- [5.803] D. Drimer, P. Taranu, A. Hafner, L. Vescan, and L. Nemoda, “Contribution to the Study of the Diffusion of Antimony in Silicon,” *Acad. Rep. Populare Romine, Filiala Iasi, Studii si Cercetari Stiintifice: Fizica si Stiinte Tehnice*, vol. 13, 39–50 (1960).
- [5.804] F. L. Gittler, “A Liquid Antimony Diffusion System,” *Electrochem. Soc. Extended Abstracts*, vol. 67-1, no. 94, 56–57 (1967).
- [5.805] S. Nakanuma and S. Yamagishi, “Diffusion of Antimony into Silicon Epitaxial Layers from Buried Layers,” *J. Electrochem. Soc. Japan*, vol. 36, no. 1, 310 (1968).

- [5.806] K. Nishi, K. Sakamoto, and J. Ueda, "Enhanced Diffusion of Antimony within a Heavily Phosphorus-Doped Layer," *J. Appl. Phys.*, vol. 59, no. 12, 4177–4179 (1986).
- [5.807] P. Pichler, H. Ryssel, R. Ploss, C. Bonafos, and A. Claverie, "Phosphorus-Enhanced Diffusivity of Antimony Due to Generation of Self-Interstitials," *J. Appl. Phys.*, vol. 78, no. 3, 1623–1629 (1995).
- [5.808] S. W. Crowder, P. B. Griffin, and J. D. Plummer, "Nitridation Enhanced Diffusion of Antimony in Bulk and Silicon-on-Insulator Material," in: *Process Physics and Modeling in Semiconductor Technology*, edited by G. R. Srinivasan, C. S. Murthy, and S. T. Dunham, *Electrochem. Soc. Proc.*, vol. 96-4, 54–63 (1996).
- [5.809] A. Nylandsted Larsen and P. Kringhøj, "Diffusion of Sb in Relaxed $\text{Si}_{1-x}\text{Ge}_x$," *Appl. Phys. Lett.*, vol. 68, no. 19, 2684–2686 (1996).
- [5.810] S. H. Song, S. Matsumoto, and T. Niimi, "Antimony Diffusion into Silicon by the Doped Oxide Method," *Jpn. J. Appl. Phys.*, vol. 18, no. 11, 2181–2182 (1979).
- [5.811] F. Pintchovski, P. J. Tobin, M. Kottke, and J. B. Price, "Antimony Diffusion in Silicon: Effects of Ambient Gas and Time," *J. Electrochem. Soc.*, vol. 131, no. 8, 1875–1883 (1984).
- [5.812] D. A. Petrov, J. M. Schaschkow, and A. S. Belanovski, "Die Diffusion der Beimengungen im Silizium," in: *Halbleiter und Phosphore*, edited by M. Schön and H. Welker, Braunschweig: Vieweg, 652–655 (1958).
- [5.813] S.-y. Wu, "Antimony Diffusion from Spin-on Doped Oxide," *J. Electrochem. Soc.*, vol. 128, no. 8, 1804–1808 (1981).
- [5.814] Y. Zhao, M. J. Aziz, H.-J. Gossman, S. Mitha, and D. Schiferl, "Activation Volume for Antimony Diffusion in Silicon and Implications for Strained Films," *Appl. Phys. Lett.*, vol. 75, no. 7, 941–943 (1999).
- [5.815] T. Y. Tan and B. J. Ginsberg, "Observation of Oxidation-Enhanced and Oxidation-Retarded Diffusion of Antimony in Silicon," *Appl. Phys. Lett.*, vol. 42, no. 5, 448–450 (1983).
- [5.816] E. A. Perozziello, P. B. Griffin, and J. D. Plummer, "Retarded Diffusion of Sb in a High Concentration As Background during Silicon Oxidation," *Appl. Phys. Lett.*, vol. 61, no. 3, 303–305 (1992).
- [5.817] A. Nylandsted Larsen, P. Kringhøj, J. Lundsgaard Hansen, and S. Y. Shiryaev, "Isoconcentration Studies of Antimony Diffusion in Silicon," *J. Appl. Phys.*, vol. 81, no. 5, 2173–2184 (1997).
- [5.818] A. Nylandsted Larsen, P. Tidemand-Petersson, P. E. Andersen, and G. Weyer, "The Effect of Heavy Doping on Complex-Formation and Diffusivity of Sb in Si," in: *Shallow Impurities in Semiconductors, 1988*, edited by B. Monemar, *Inst. Phys. Conf. Ser.*, no. 95, 499–504 (1989).
- [5.819] C. van Opdorp, L. J. van IJzedoorn, C. W. Fredriksz, and D. J. Gravesteijn, "A Model for the Diffusion and Precipitation of Antimony in Highly Doped Delta Layers in Silicon," *J. Appl. Phys.*, vol. 72, no. 9, 4047–4062 (1992).
- [5.820] D. Mathiot and J. C. Pfister, "Dopant Redistribution in Heavily Doped Silicon: Confirmation of the Validity of the Vacancy-Percolation Model," *J. Appl. Phys.*, vol. 66, no. 2, 970–972 (1989).
- [5.821] S. J. Pennycook, J. Narayan, and O. W. Holland, "Point Defect Trapping in Solid-Phase Epitaxially Grown Silicon-Antimony Alloys," *J. Appl. Phys.*, vol. 55, no. 4, 837–840 (1984).
- [5.822] A. Nylandsted Larsen, F. T. Pedersen, G. Weyer, R. Galloni, R. Rizzoli, and A. Armigliato, "The Nature of Electrically Inactive Antimony in Silicon," *J. Appl. Phys.*, vol. 59, no. 6, 1908–1917 (1986).
- [5.823] P. M. Voyles, D. A. Muller, J. L. Grazul, P. H. Citrin, and H.-J. L. Gossmann, "Atomic-Scale Imaging of Individual Dopant Atoms and Clusters in Highly *n*-Type Bulk Si," *Nature*, vol. 416, 826–829 (2002).
- [5.824] P. M. Voyles, D. J. Chadi, P. H. Citrin, D. A. Muller, J. L. Grazul, P. A. Northrup, and H.-J. L. Gossmann, "Evidence for a New Class of Defects in Highly *n*-Doped Si: Donor-Pair-Vacancy-Interstitial Complexes," *Phys. Rev. Lett.*, vol. 91, 125505 (2003).

Chapter 6

Chalcogens

Considering the free valences of group VIA elements, one might expect them to act as double donors on substitutional sites. Oxygen, the most prominent of them, does not fit into this scheme. It assumes predominantly bond-centered interstitial sites. Three other members of the group, sulfur, selenium, and tellurium, were found to show the expected double-donor properties. They were also found to be very similar, showing a tendency to form pairs which also act as double donors. A comprehensive review of their properties was given by Grimmeiss and Janzén [6.1]. For the sake of space, only the most important facts can be recapitulated here.

6.1 Oxygen

During crystal growth by the Czochralski (CZ) method [6.2,6.3], the melt is contained in a silica crucible from which oxygen diffuses into the melt. From there, the oxygen is incorporated into the growing crystal. Typical oxygen concentrations in CZ wafers range from about $6 \cdot 10^{17}$ to 10^{18} cm^{-3} .

Such concentrations correspond to the solubility of oxygen in silicon at temperatures of about 1210 and 1270 °C, respectively. For temperatures below, which are rather typical for VLSI processing, the oxygen atoms are in a metastable state and will tend to agglomerate. A typical phenomenon associated with oxygen agglomeration is the formation of donor states during heat treatments [6.4–6.6]. At sufficiently high temperatures, macroscopic oxygen precipitates form by phase transitions [6.7–6.10]. Both phenomena are not desired *per se*. Thermal donors may influence the electrical properties of devices, and precipitates in the active area of devices can deteriorate seriously their performance. The technological importance of oxygen, first suggested by Tice, Tan, and Gardner [6.11,6.12] and Rozgonyi et al. [6.13], arises from the ability of oxygen precipitates to directly or indirectly provide getter centers for metallic impurities, the so-called “intrinsic gettering.”

In addition to intrinsic gettering, oxygen is known to have a beneficial effect on the mechanical properties of silicon [6.14–6.19]. For such a purpose, oxygen precipitation is less desired since it reduces also the concentration of oxygen atoms which might segregate to dislocations to lock them.

After the synthesis of oxide layers by oxygen implantation has been demonstrated [6.20–6.23], implantation of oxygen with very high doses and energies was investigated for the formation of buried insulating oxide layers. A catch-phrase for such materials is SIMOX — separation by implanted oxygen [6.24].

Oxygen is known to give rise to a variety of complexes with intrinsic point defects. Especially complexes with silicon self-interstitials might be responsible for the reduction of transient effects during post-implantation annealing observed experimentally [6.25–6.28].

In the following sections, the basic atomic configurations of oxygen in silicon, its solubility, the diffusion behavior, and the formation of complexes are discussed in detail. For a comprehensive review of the various effects associated with oxygen in silicon, the interested reader is referred especially to two recent publications in this field [6.29, 6.30].

6.1.1 Basic Atomic Configurations

The X-ray investigations of Bond and Kaiser [6.31] gave direct evidence of the interstitial nature of the majority of the oxygen atoms by showing that the lattice parameter of silicon increases with increasing oxygen concentration. Infrared-absorption measurements [6.32–6.38] led likewise to the conclusion that oxygen occupies interstitial positions between two neighboring silicon atoms which are, as shown in Figure 6.1, slightly displaced perpendicular to the {111}-oriented connecting line between the two silicon atoms. Transitions between the six equivalent positions around the {111} axis are considered to occur more frequently than a jump from one bond-center sites to one of the six nearest bond-center sites. This structure was reproduced also in numerous theoretical investigations. Calculations by Yamada-Kaneta et al. [6.39], Artacho et al. [6.40], Ramírez et al. [6.41], and Coutinho et al. [6.42], on the other hand, indicated that the probability to meet the oxygen atom has its maximum in the middle between the two neighboring silicon atoms despite the small local maximum of the potential energy there. It was also shown that the vibration modes observed experimentally can be explained more consistently on the basis of such a D_{3d} -symmetric configuration. The vibrational frequencies associated usually with oxygen are around 30, 517, 1136, 1205, and 1749 cm^{-1} (4.2 K) [6.43].

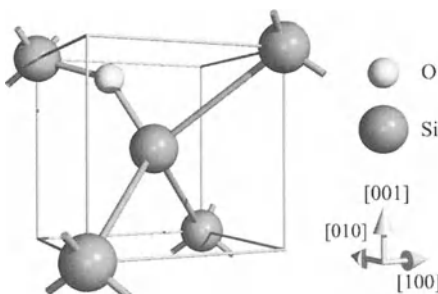


Figure 6.1: Atomic configuration of interstitial oxygen in silicon.

As an alternative to the bond-centered oxygen interstitial, Doremus [6.44] suggested that oxygen is dissolved predominantly in the form of {111}-oriented Si-O quasi-molecules. It was suggested to be consistent with spectroscopic investigations, although a verification by *ab-initio* calculations is missing.

Another possible configuration would be an oxygen atom on a substitutional site. This possibility has been promoted especially by O'Mara [6.45] who associated it with an oxygen-related absorption band at 517 cm^{-1} . However, it was rejected unanimously by the other researchers. Theoretical investigations indicated that the oxygen atom moves in a vacancy strongly off-center along the [001] C_{2v} symmetry axis of the defect. This configuration was found after electron irradiation to give rise to the prominent Si-A center and will be discussed in more detail together with other complexes of oxygen and intrinsic point defects in Section 6.1.5.

6.1.2 Solubility

A major parameter determining the formation of oxygen agglomerates is the solubility of interstitial oxygen in silicon. The experimental data in Figure 6.2 shows considerable scatter related to systematic errors in the experimental set-ups or in the interpretation of measurements.

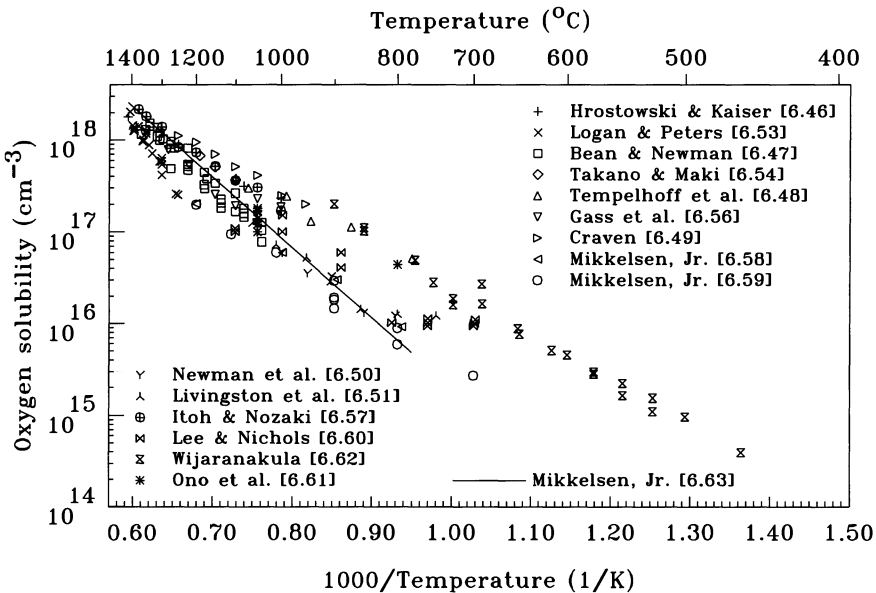


Figure 6.2: Solubility of interstitial oxygen in silicon.

Infrared-absorption measurements of the interstitial oxygen concentration in samples which were heat-treated to allow oxygen precipitates to grow and which were quenched afterwards [6.46–6.51] may be influenced by the presence of the precipitates since they show absorption in the same spectral region as the O_i band. Even when such problems are avoided, the concentration of interstitial oxygen is not the concentration in stress-free silicon being in equilibrium with a flat phase boundary. The concentration measured is rather that in steady state with oxygen precipitates of mean size. Stress effects or intrinsic point defects in concentrations deviating from their equilibrium value may additionally alter the measurements. A clear indication for such effects can be found in the work of Livingston et al. [6.51] and Messoloras et al. [6.52] who reported that the solubility of oxygen in silicon levels off below 800 °C and even increases again for temperatures below about 650 °C. It has also to be remarked that the data points shown in Figure 6.2 were not corrected for the calibration constants which varied by a factor of two in the past.

A second frequently used method is based on the diffusion of oxygen into silicon with a low initial concentration or out of silicon with a high oxygen concentration. Profiles and especially the surface concentration were measured via the formation of thermal donors in a second process step at 450 °C [6.53], by X-ray diffraction [6.54], by a nuclear reaction with a proton or helium beam which converts oxygen to instable ¹⁸F [6.55–6.57], or by SIMS [6.58–6.61]. Such measurements led to the conclusion that the surface concentration in silicon depends strongly on the processing conditions [6.58–6.60]. Profiles after oxidation, especially after steam oxidation, show considerably higher surface concentrations than after an additional annealing in an inert

ambient. This effect is most likely caused primarily by an incomplete reaction at the interface between silicon and silicon dioxide with stress and disturbed concentrations of the intrinsic point defects in the silicon being of secondary importance. Of the experiments cited above, those of Takano and Maki [6.54] were derived after processing in a steam ambient, and Logan and Peters [6.53] and Itoh and Nozaki [6.57] based their experimental set-up on processing in an O₂ ambient. The reported solubility values, especially those of Takano and Maki, might be somewhat higher than the respective equilibrium solubility. For the experiments of Logan and Peters, one has to take into account also that the relation between the concentrations of thermal donors and interstitial oxygen used for a conversion of their measurements is certainly less reliable than the experimental techniques used more than 20 years afterwards.

An indirect determination of the oxygen solubility from measurements of the precipitation rate [6.62] relies on various assumption. Considering that nucleation is still not completely understood, it is not astonishing that the data derived this way are among the highest reported.

From a compilation of published data, Mikkelsen [6.63] estimated the temperature dependence of the solubility of oxygen in silicon in the form

$$C_{O_i}^{sol} = 9 \cdot 10^{22} \cdot \exp\left(-\frac{1.52\text{eV}}{k \cdot T}\right) \text{ cm}^{-3} \quad (6.1)$$

shown also in Figure 6.2.

6.1.3 Normal Diffusion

Certainly one of the key parameters for the kinetics of oxygen precipitation is the diffusion coefficient of oxygen in silicon. For the sake of space only the most important experimental results and theories can be mentioned here. For a full account, the interested reader is referred especially to the reviews of Mikkelsen [6.63] and Newman and Jones [6.64].

The experimental data reported in the literature was determined by various methods. At high temperatures, diffusion coefficients were determined from diffusion profiles of oxygen measured via the formation of thermal donors in a second process step at 450 °C [6.53, 6.65], by X-ray diffraction [6.54, 6.66], by a nuclear reaction with a proton or helium beam which converts oxygen to unstable ¹⁸F [6.56, 6.57, 6.66–6.68], or by SIMS [6.60, 6.61, 6.69–6.74]. Alternatively, the required information was extracted [6.75] from internal-friction measurements [6.76]. Diffusion coefficients were also obtained indirectly from the locking of dislocations [6.77], or from the growth kinetics of precipitates via fitting the loss of oxygen from solution with time with Ham's theory for diffusion-limited growth [6.78], the increase in precipitate size observed by small angle neutron scattering (SANS), or a combination of the methods [6.50, 6.51, 6.79–6.81]. At low temperatures, diffusion coefficients were determined from the recovery kinetics of a stress-induced dichroism in the 9 μm infrared-absorption band [6.36, 6.82–6.84]. The respective experimental data are shown in Figure 6.3 together with the regression curve

$$D_{O_i} = 0.16 \cdot \exp\left(-\frac{2.529\text{eV}}{k \cdot T}\right). \quad (6.2)$$

which corresponds closely to the estimate of Mikkelsen, Jr. [6.63] from a compilation of the available experimental data. The activation energy ranges with a confidence level of 90% from 2.5 to 2.56 eV. The 90% confidence interval for the diffusion coefficient is about +7.1/-6.6% of the regression curve at 920 °C and increases to +11/-10% at the melting point and +29/-23% at 330 °C. Additional measurements are expected with 90% confidence within a range of +138/-58% of the regression curve at 920 °C which increases slightly to +139/-58% at the melting point and +146/-59% at 330 °C.

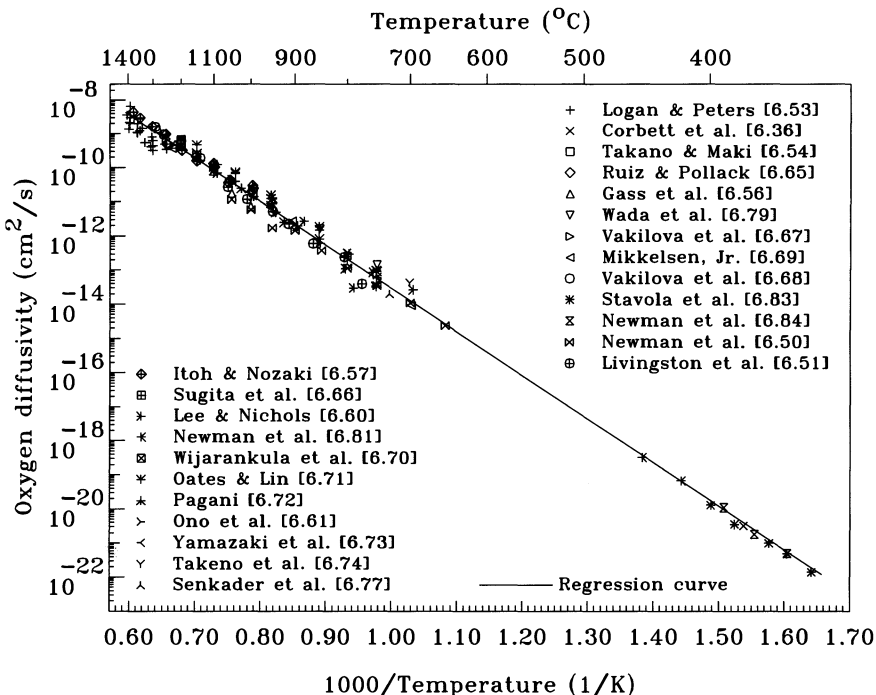


Figure 6.3: Diffusion coefficient of interstitial oxygen in silicon.

Corroborated by numerous theoretical investigations which indicated activation energies in the range from 1.8 to 2.8 eV, (6.2) is generally accepted to characterize the intrinsic diffusion coefficient for oxygen jumping from one bond-center site to another.

Experimental conditions like the concentration of oxygen, process conditions, or the concentrations of intrinsic point defects were found in the vast majority of the investigations to be of little influence and considered evidence for the interstitial nature of the diffusion mechanism. As always in real life, also the opposite behavior was reported. The experiments of Heck et al. [6.85] performed at 1100 °C clearly show a dependence of the oxygen diffusion on process conditions with a significant retardation for oxidizing conditions. Similarly, Shimura et al. [6.86] observed that oxygen precipitation is accompanied by a retardation of oxygen diffusion. An alternative to the intuitive explanation of a non-negligible diffusion component via vacancies would be the formation of complexes between oxygen and silicon self-interstitials which could also retard the effective diffusivity of oxygen. In the work of Maddalon-Vinante et al. [6.87], oxygen diffusion during an RTA step for 5 s at 1200 °C in N₂ was found to be increased by more than two orders of magnitude. This enhancement was associated tentatively with ultraviolet light absorbed within some microns from the surface.

When the impurity background concentration in the samples increases, non-negligible concentrations of oxygen-dopant complexes will form as outlined in Section 5. As a consequence, only a fraction of the oxygen atoms will be mobile and the effective diffusivity of oxygen reduces. Such effects were observed for boron [6.61,6.67,6.74], arsenic [6.74], phosphorus [6.67], and antimony [6.74] for high dopant concentrations and sufficiently low temperatures.

6.1.4 Enhanced Diffusion

The situation changes for temperatures between about 400 and 700 °C. For such temperatures, various investigations based on different experimental set-ups suggested an enhanced diffusion of oxygen in comparison to the normal diffusion characterized by (6.2).

Direct experimental evidence for an enhanced oxygen diffusion comes from profiles of oxygen measured by SIMS [6.74, 6.88–6.90] after diffusion processes. Most other methods outlined in the following rely on models or assumptions which were controversially discussed in the literature.

A first indication of an enhanced diffusion resulted from stress-induced dichroism measurements [6.82, 6.83, 6.91, 6.92]. It was noted that the occurrence of enhanced diffusion depends on the thermal history of the samples and is only a transient effect. In any case, the method is based on the detection of single diffusion jumps and it was argued that the observation of the local effect of an enhanced hopping rate would not allow to infer that long-range macroscopic diffusion occurs [6.93].

Bergholz et al. [6.94] observed rod-like defects after heat treatment at 485 °C and interpreted them as coesite. From the growth kinetics, they obtained an oxygen diffusion coefficient nearly 4 orders of magnitude higher than the intrinsic oxygen diffusion coefficient. But beginning with the work of Bourret [6.95], the rod-like defects were reassigned to agglomerates of silicon self-interstitials.

Evidence for enhanced diffusion of oxygen was suggested to arise also from the formation of thermal donors. The conclusion follows straightforwardly from reaction kinetics when thermal donors are assumed to contain more than three oxygen atoms and when the interstitial oxygen is assumed to be initially distributed homogeneously and the only mobile species [6.96–6.101]. An additional indication for an enhanced diffusion is that the rate of formation of thermal donors is governed by an activation energy of 1.7 to 1.85 eV rather than the 2.53 eV characterizing the intrinsic diffusion of oxygen [6.102–6.106]. But the requirement for a fast diffusion of oxygen does not arise in models in which the various kinds of thermal donors are assumed to form by a successive attachment of intrinsic point defects at a common defect core. A fast diffusion of oxygen is also not stringently required when the assumption of an initially homogeneous distribution of oxygen atoms is dropped or when the oxygen chains forming the thermal donors are assumed to be mobile. It should be mentioned also that Oehrlein et al. [6.107] found from the application of the theory of homogeneous nucleation to the initial rate of thermal-donor formation that it is governed by the intrinsic oxygen diffusion coefficient.

Experimental evidence for an enhanced diffusion of oxygen was also reported from the reduction of the concentration of thermal donors near surfaces [6.89, 6.108, 6.109]. But this conclusion is based on the assumption that the profiles of the thermal donors resulted from an out-diffusion of oxygen to the surface. Alternatively, in other models for the formation of thermal donors, this role is attributed to intrinsic point defects or highly mobile thermal donors. Similarly, evidence for an enhanced diffusion of oxygen was obtained from precipitation experiments which included a nucleation step in the temperature range from 400 to 750 °C [6.110]. Possible points of criticism might address here that the nucleation process and especially its interaction with thermal donors is not sufficiently understood to exclude all other possibilities. Finally, Senkader et al. [6.111] showed that the locking of dislocations in the temperature range from 350 to 700 °C requires oxygen diffusion coefficients which exceed the normal diffusion coefficient by up to three orders of magnitude.

Although a fast-diffusion mode of oxygen was, as noted above, demonstrated unambiguously by SIMS measurements, the mechanism is still not clear. Oxygen is known to form various complexes with other point defects and any of them might be able to have a higher diffusivity than interstitial oxygen. The most popular mechanisms suggested in the literature will be outlined in the following.

Various experiments made clear that hydrogen may directly or indirectly enhance oxygen diffusion [6.106, 6.112–6.115]. Such an enhanced diffusion of oxygen may then explain the rapid denudation of oxygen near surfaces [6.116], the enhanced formation of thermal donors [6.6, 6.105, 6.112, 6.117–6.120], the enhanced consumption of interstitial oxygen [6.106, 6.112, 6.121, 6.122], and the enhanced formation of oxygen dimers and small oxygen complexes [6.115, 6.123] observed under process conditions involving hydrogen. Most of the phenomena were observed at low temperatures. At a temperature of 1200 °C, on the other hand, Yamazaki et al. [6.73] found no indication of enhanced oxygen diffusion in a hydrogen atmosphere. In several publications it was speculated that hydrogen-enhanced diffusion might be sufficient to explain all phenomena since even the small hydrogen concentration in as-grown wafers was suggested to have noticeable effects on oxygen diffusion [6.124, 6.125]. Possible explanations for the mechanism causing the enhanced oxygen diffusion were proposed on the basis of *ab-initio* calculations [6.126–6.128] and indicate a catalytic effect of hydrogen which lowers the migration barrier for the diffusional jump of oxygen interstitials. But also evidence for an oxygen-hydrogen complex was found experimentally [6.129].

Enhanced diffusion of oxygen was also reported in carbon-rich silicon [6.86, 6.130]. Of the various complexes of carbon with oxygen discussed in Section 4.1, the C_iO_i complex is considered a primary candidate to cause an enhanced diffusion of oxygen.

In situations in which hydrogen or other impurities are not likely to be present in sufficient concentrations, rapid diffusion via oxygen-vacancy pairs, oxygen-self-interstitial pairs or oxygen dimers is usually postulated. These defects will be discussed in more detail in Sections 6.1.5 and 6.1.6.

Based on the exclusion of other possibilities rather than on a precise atomistic concept, Voronkov [6.131] suggested that the thermal donors themselves should be able to diffuse with a much higher diffusion coefficient than interstitial oxygen. A similar conclusion was suggested by Murin and Markevich [6.132]. Recently, the *ab-initio* and kinetic simulations of Coutinho et al. [6.133] and Lee et al. [6.134] confirmed that small chains of oxygen atoms have significantly smaller migration energies than oxygen interstitials and that mobile oxygen chains acting as thermal donors grow by capturing slow oxygen atoms.

To explain enhanced diffusion without the interaction with another agent, Fuller and Logan [6.6], Markevich et al. [6.104], and Chen et al. [6.135] suggested that oxygen may exist in an unbound state with a high diffusivity in addition to its usual location at bond-center sites.

6.1.5 Complexes with Intrinsic Point Defects

In irradiation experiments, various oxygen-vacancy defects were found to form. Some of them were suggested to diffuse more rapidly than interstitial oxygen. Vacancy-oxygen complexes play also an important role in some theories of the formation of thermal donors and of precipitation of oxygen. Similarly, oxygen-self-interstitial complexes were suggested to enhance the redistribution of interstitial oxygen. An excellent review on complexes of oxygen with intrinsic point defects was written by Londos et al. [6.136].

VO

After electron irradiation of silicon, various well-resolved spectra were observed spectroscopically. The primary EPR defect in Czochralski-pulled silicon, reported first by Bemski et al. [6.137], was labelled Si-*A* by Watkins et al. [6.138] and relabelled later Si-*B1* [6.139]. The original investigations were complemented by electrical measurements [6.140–6.144], EPR and ENDOR investigations [6.138,6.145–6.150], and IR studies [6.151–6.153], as well as characterization of the ionization level via photoconductivity [6.154], thermally-stimulated capacitance measurements [6.155], and DLTS [6.156–6.158]. They made clear that the Si-*B1* EPR center arises from the negative charge state of a C_{2v} -symmetric defect formed by an oxygen atom occupying an off-center position in a vacancy between two silicon atoms, and helped to establish its properties. This configuration, sometimes called substitutional oxygen, is shown schematically in Figure 6.4. In its neutral charge state, the vacancy-oxygen complex was found to give rise to the Si-*S1* EPR spectrum [6.159]. VO complexes were found to act as acceptors with a level situated about 0.16 to 0.18 eV below the conduction band. In addition to this well-known and extensively studied level, Frens [6.160] showed by his EPR study that the VO complex is amphoteric and has a donor level near to $E_c - 0.76$ eV. This assignment was questioned by Makarenko [6.161] who reviewed the experiments published and who concluded also on the basis of his gamma-ray irradiation experiments that the Si-*A* center has an acceptor level at $E_c - (0.15\text{--}0.16)$ eV and a donor level at $E_c - (0.19\text{--}0.20)$ eV. Associated with the neutral and the negative charge states of $V^{16}O$ are localized vibrational modes at 835 and 884 cm^{-1} at 77 K which shift to respectively 830 and 877 cm^{-1} at room temperature. Lindström et al. [6.162] and Murin et al. [6.163] showed that these vibrational modes correlate to lines at 1370 and 1430 cm^{-1} (10 K), respectively. Measurements of the pressure dependence of the emission rate for electrons indicated that electron emission is associated with a volume contraction of $\Delta V/V \approx 30\%$ [6.164]. In positron-annihilation studies, VO pairs were suggested to be associated with positron lifetimes of 225 ps [6.165] and 270 to 275 ps [6.166–6.168]. The positron lifetime of 270 ps means that the off-center oxygen atom does not influence the positron lifetime which is then close to that of a vacancy. This assignment was corroborated also by theoretical investigations [6.166]. Since oxygen is an efficient trap for vacancies, VO pairs were also found after ion implantation of oxygen [6.169].

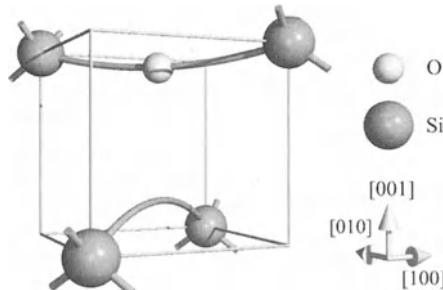


Figure 6.4: Schematic representation of the atomic configuration of the vacancy-oxygen complex in silicon.

Theoretical investigations confirmed the C_{2v} symmetry of the VO defect and indicated that the oxygen atom moves strongly off-center along the [001]-oriented symmetry axis with the position depending slightly on the charge state [6.42,6.170–6.173]. In contrast, the theoretical work of Van Oosten [6.174] suggested that the Si-*A* center has only the lower C_{1h} symmetry which appears, time-averaged, as C_{2v} -symmetric. A similar result was reported before already by Kelly [6.175] who observed a minimum-energy configuration along the [111] direction.

In the work of Boyarkina et al. [6.176], values of 2.27 and 1.94 eV were estimated for the dissociation energy and the binding energy of VO, respectively. From theoretical calculations, Pesola et al. [6.177] estimated a binding energy of 0.8 eV for neutral VO. In comparison, Coutinho et al. [6.42] obtained a value of 1.6 eV, and Casali et al. [6.178] 1.7 eV. As an explanation for the inconsistent results, Casali attributed the lower value of Pesola et al. to an inconsistent combination of energies from simulations of interstitial oxygen and VO complexes with different supercell sizes and different methods for Brillouin-zone integration.

Oxygen-vacancy pairs, generated by particle irradiation or low-mass MeV ion implantation, were found to determine the Shockley-Read-Hall carrier lifetime at high injection levels [6.179–6.181]. An application is life-time control in power semiconductors [6.182, 6.183].

With a C_{2v} -symmetric configuration as shown in Figure 6.4, the VO complex may assume four equivalent positions in the vacancy. Reorientations between them were found experimentally by Watkins and Corbett [6.146], Corbett et al. [6.151], and Meese et al. [6.158] to be characterized by an activation energy of 0.37 to 0.38 eV. In theoretical investigations with various levels of sophistication, activation energies from 0.26 [6.42] via 0.3 [6.177] and 0.47 [6.184] to 0.5 eV [6.173] were calculated. Several of them favored a C_{3v} -symmetric configuration for the saddle point. This was confirmed by the piezospectroscopic analysis of Dobaczewski et al. [6.185].

From the annealing behavior of Si-A centers around 300 °C, a migration enthalpy of 1.86 eV was extracted by Svensson et al. [6.186] while Londos et al. [6.187] reported a migration enthalpy of 1.46 eV. In later studies, Londos et al. reported tentatively activation energies of 1.95 eV [6.188] and 1.8 eV [6.189] to govern the reaction kinetics of VO. They should correspond to the migration enthalpy of VO when no reaction barriers have to be considered. In a simulation of the kinetics of defects after electron irradiation, Svensson and Lindström [6.190] used a value of $5 \cdot 10^{-16} \text{ cm}^2/\text{s}$ for the diffusion coefficient of VO at 350 °C. Annealing of VO complexes formed during the implantation of silicon was found by Pellegrino et al. [6.191] to display a complicated behavior which was explained by an interaction with hydrogen. For the diffusion of VO, a diffusion coefficient with a prefactor of $6 \text{ cm}^2/\text{s}$ and an activation energy of 1.8 eV was used. A value of 1.84 eV was also estimated for the activation energy of VO diffusion by Grönberg et al. [6.192] from molecular-dynamics simulations using an empirical potential.

Vacancy-assisted processes involving the continuous formation and dissociation of Si-A centers were suggested to explain enhanced oxygen diffusion under electron-irradiation conditions [6.84, 6.186, 6.193]. But it is not clear whether such a mechanism may be responsible for enhanced diffusion of oxygen without electron irradiation. Oxygen-vacancy interactions were invoked by Newman et al. [6.91] to explain the enhanced recovery kinetics of a stress-induced dichroism in samples contaminated with copper. Indirect evidence for a vacancy-assisted diffusion of oxygen comes also from the observations of a retarded diffusion of oxygen under conditions in which the self-interstitial concentration is enhanced due to oxidation [6.85] or oxygen precipitation [6.86].

After electron irradiation at cryogenic temperatures, Watkins [6.194] found two EPR centers labelled Si-G3 and Si-G4 which finally convert to Si-A centers. From this conversion and the structural information obtained by EPR, the defects were identified as a negatively charged vacancy paired with an oxygen atom in the $\langle 100 \rangle$ and $\langle 111 \rangle$ directions, respectively. Depending on the Fermi level of the material, conversion from Si-G4 to Si-A was observed at 45 and 120 K. To explain this discrepancy, Watkins assumed the conversion around 120 K to be thermally activated and the conversion around 45 K to be catalyzed by the capture of an electron. A similar observation was made by Abdullin and Mukashev [6.195]. After irradiation of CZ samples with

alpha particles, they found a level $E1$ at $E_c - 0.22$ eV which transformed into a level $E2$ at $E_c - 0.25$ eV which finally transformed into VO defects. While $E1$ was suggested to be a primarily defect of vacancy nature, $E2$ was associated with the Si-G4 center.

VO_2

Above 300 °C, the infrared-absorption bands associated with the Si-A center were found to anneal out, accompanied by the formation of a band at about 887 cm⁻¹ at room temperature [6.196, 6.197] and 895 cm⁻¹ at 10 K [6.152, 6.162]. The vibration mode at 887 cm⁻¹ was assumed to arise from a VO_2 complex shown in Figure 6.5 which forms by a reaction of mobile VO complexes with interstitial oxygen. However, it has to be mentioned that the 887 cm⁻¹ band was also associated with the V_3O complex and that it was suggested to contain contributions of a band at 884 cm⁻¹ (RT) arising from a vacancy trapped near a VO_2 complex. The assignment of the absorption line at 887 cm⁻¹ to VO_2 was corroborated by Lindström and Svensson [6.198] and Lindström et al. [6.162] based on studies of its kinetics of formation and annealing. In isotope experiments, on the other hand, neither Abou-el-Fotouh and Newman [6.199] nor Stein [6.200] found an indication of two interacting oxygen atoms as one might expect from VO_2 . In positron-annihilation studies, Li et al. [6.167] and Ikari et al. [6.168] assumed VO_2 complexes to be associated with a positron lifetime of 270 ps, close to that of a vacancy. With two equivalent oxygen atoms, the complex has D_{2d} symmetry. The structure was reproduced by theoretical investigations which also indicated a large separation of the oxygen atoms [6.172, 6.173, 6.175, 6.201]. From such theoretical investigations, the energy gain associated with the formation of VO_2 from a neutral vacancy well-separated from two interstitial oxygen atoms was estimated to be 1.6 eV [6.177], 3.3 eV [6.42], and 2.7 eV [6.178]. Combining their estimate for vacancy properties with an estimate for the temperature at which VO_2 complexes form during cooling-down of grown crystals, Voronkov and Falster [6.202] estimated a binding energy of 3.76 eV. Alternatively, from measurements of vacancy profiles in CZ wafers after RTP treatment at 1150 to 1280 °C, Falster et al. [6.203] estimated the binding energy of VO_2 complexes to be about 5.0 eV. Some investigations indicated that the structure would not have energy levels in the band gap and all of them agreed that the relaxed structure would not give rise to a donor state. Similarly, Svensson et al. [6.204] concluded from electrical measurements that the VO_2 complex is electrically neutral. A donor state was suggested by Chadi [6.172] to arise from a VO_2 in which, as a modification of the configuration shown in Figure 6.5, the oxygen atoms are trivalently bonded and share one bond. Based on the annealing characteristics, Corbett et al. [6.196] suggested that the VO_2 pair might diffuse faster than interstitial oxygen.

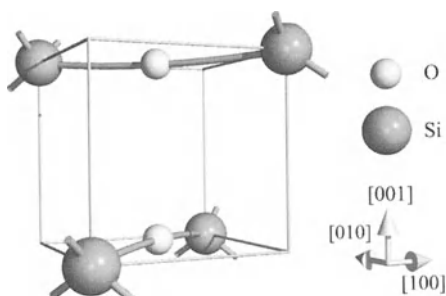


Figure 6.5: Schematic representation of the atomic configuration of the VO_2 complex in silicon.

Simultaneously, with the VO₂ bands, Pomozov et al. [6.205] and Londos et al. [6.206,6.207] observed after neutron irradiation the formation of other bands around 914 and 1000 cm⁻¹ (RT). They were interpreted as an intermediate configuration of an interstitial oxygen atom next to a VO pair. After electron irradiation, Lindström et al. [6.208] found similar absorption bands at 928/923 cm⁻¹ (15 K/RT) and 1003.8/1000 cm⁻¹ (15 K/RT) to be correlated to VO₂. They were suggested to arise from a metastable configuration of VO₂ for which they introduced the symbol VO₂^{*}. The formation energy of VO₂^{*} was shown to be 0.25 eV higher than that of VO₂ and the reversible transformations between the two configurations were found to be characterized by an energy barrier of 1.95 eV. Interpreted in terms of an activation energy for long-term diffusion, VO₂ would migrate faster than interstitial oxygen as suggested before by Corbett et al. [6.196]. The observed shifts of the vibration frequencies in low-dose-irradiated *n*-type silicon to 967 cm⁻¹ (15 K) and 1023 cm⁻¹ (15 K) were taken as an indication that VO₂^{*} may exist in a neutral and a negative charge states, similar to VO.

VO₃

When the VO₂ pair anneals out at temperatures above 450 °C, new absorption bands appear around 904, 968, and 1000 cm⁻¹ (RT) which all show the same kinetic behavior. They were attributed by Corbett et al. [6.196] and Stein [6.209] to local vibration modes of three inequivalent oxygen atoms in a VO₂O_i complex composing of a VO₂ structure with an oxygen interstitial attached. This structure was also supported by Deák et al. [6.210] who found it more stable than a C_{2v}-symmetric VO₃ complex. Based on its kinetics, a hole trap at about E_v + 0.35 eV [6.211] and an electron trap at about E_c - 0.12 eV [6.212] were suggested to be associated with the VO₃ complex. Electrical measurements performed by Svensson et al. [6.204], on the other hand, indicated that the VO₂O_i complex is electrically inactive. In positron-annihilation studies, Li et al. [6.167] assumed VO₃ complexes to be associated with a positron lifetime of 270 ps, close to that of a vacancy.

VO₄

During annealing for 15 minutes at temperatures of 550 to 600 °C, but also by prolonged heat treatment around 500 °C, the VO₃ complex was found to anneal out again [6.196, 6.198]. At such temperatures, Stein [6.209] found absorption bands at 983 and 1004 cm⁻¹ to appear in oxygen-implanted samples. He attributed them to a VO₄ complex in which interstitial oxygen atoms attach to each of the two oxygen atoms of the VO₂ core. In contrast, Londos et al. [6.206] associated this defect tentatively with absorption bands at 1032 and 1043 cm⁻¹ (RT). This assignment was reconsidered by Londos and Fytros [6.213] and their theoretical work indicated that Stein's original assignment is correct and that the bands at 1032 and 1043 cm⁻¹ (RT) are likely to arise from larger oxygen-vacancy complexes.

Multi-Vacancy-Oxygen Complexes

Not all of the oxygen atoms generated by irradiation experiments follow the reaction chain outlined above. Using EPR, Lee and Corbett [6.214] found that complexes like V₂O, V₂O₂, V₃O, V₃O₂, and V₃O₃ form in succession. Structural data extracted from the EPR measurement suggested that the defects form along chains in the ⟨110⟩ direction. The existence of V_mO_n complexes was also inferred from positron-annihilation studies [6.167, 6.215].

V₂O

Based on photo-EPR investigations, Lee et al. [6.216] suggested a level at $E_c - 0.5$ eV to be associated with the V₂O defect identified in its neutral charge state as Si-A14 EPR center [6.214]. From correlations of their kinetics of formation and annealing to the EPR measurements, DLTS levels at $E_c - 0.3$ eV [6.156, 6.217] and $E_v + 0.44$ eV [6.218] were proposed tentatively for the V₂O complex. The formation of V₂O was also studied by Trauwaert et al. [6.219] who observed a conversion from divacancies to a donor level at $E_v + 0.24$ which they ascribed to it. Of the various levels measured after neutron irradiation of high-resistivity silicon detectors, Watts [6.220] associated V₂O tentatively with an electron trap at $E_c - 0.52$ eV. To be able to describe the apparent type conversion of silicon detectors upon gamma irradiation, Gill et al. [6.221] looked for a deep acceptor defect. The most promising candidate was V₂O with its level assumed to be at $E_c - 0.5$ eV from the work of Lee et al. [6.216]. Later, MacEvoy and Hall [6.222] located the acceptor level of V₂O at $E_c - 0.54$ eV to achieve quantitative agreement between simulations and experiments. More recently, two conflicting identifications were reported. Pintilie et al. [6.223] found a level at $E_c - 0.545$ eV in high-dose-irradiated FZ wafers which was shown to explain 90% of the type-conversion effect mentioned above. Based again primarily on the similarity to the photo-EPR identification of Lee et al. [6.216], the defect associated was tentatively identified as V₂O. In a subsequent publication, Pintilie et al. [6.224] showed that the defect has a second-order generation rate as a function of the irradiation dose. The indirectly proportional variation with the oxygen concentration was explained by competing mechanisms in which the more effective reaction of vacancies with interstitial oxygen in oxygen-rich materials suppresses the reaction of vacancies with VO complexes. Additional arguments in favor of an identification as V₂O were presented in the course of the discussion by Pintilie et al. [6.225]. An opposite identification arose from the work of Monakhov et al. [6.226]. After proton irradiation of high-purity oxygenated FZ samples, they found the annealing of V₂ to be correlated with the formation of a defect with similar levels as the divacancy. Based on this evidence, the newly formed defect was tentatively identified as V₂O. The ionization enthalpies for its acceptor and double acceptor level were determined to be 0.47-0.49 and 0.23 eV, respectively. An identical conclusion and a very similar assignment of levels was reported by Markevich et al. [6.227]. The identification was further substantiated by the work of Alfieri et al. [6.228] who reported the levels at $E_c - 0.46$ eV and $E_c - 0.23$ eV, respectively and who found that the conversion rate from V₂ to V₂O correlates with the oxygen concentration in the samples.

Comparing the kinetics of IR absorption bands and EPR, Lee et al. [6.229] suggested the V₂O complex to have a localized vibrational mode at 835 cm⁻¹, very close to that of VO. Similarly, based on annealing kinetics and theoretical investigations, Sarlis et al. [6.230] assigned a local vibrational mode observed at 839 cm⁻¹ (RT) to V₂O. A careful investigation of the 836 cm⁻¹ VO band by Lindström et al. [6.162] revealed contributions of a band at about 833 cm⁻¹ (10 K) which was found to increase in strength on the costs of the divacancies. Based on this evidence, it was associated with V₂O.

In positron-annihilation studies, positron lifetimes of 270 [6.165], 295 [6.231], and 325 ps [6.167] were suggested to be associated with V₂O. These numbers reflect the question whether the off-center oxygen makes the positrons “see” V₂O rather as a vacancy or as a divacancy.

From theoretical investigations, Pesola et al. [6.177] estimated a binding energy of 0.5 eV for an interstitial oxygen atom and a neutral divacancy. From similar *ab-initio* calculations, Coutinho et al. [6.232] suggested that an interstitial oxygen binds with 1.34 eV to a neutral divacancy while a vacancy binds with 1.3 eV to VO. Combining their calculations with known levels of other defects, they supported the level scheme suggested by Monakhov et al. [6.226], Markevich et al. [6.227], and Alfieri et al. [6.228].

V₂O₂

From photo-EPR investigations, Lee et al. [6.216] suggested the V₂O₂ complex, identified in its neutral charge state as Si-*P2* EPR center [6.214], to have a level at $E_c - 0.4$ eV or $E_v + 0.4$ eV. Based on its growth after neutron irradiation, Meese et al. [6.233] tentatively assigned an electron trap at $E_c - 0.27$ eV to V₂O₂. Correlating the kinetics of IR and EPR measurements, Lee et al. [6.229] suggested V₂O₂ to give rise to an absorption band at 1000 cm⁻¹. Based on annealing kinetics and theoretical investigations, Sarlis et al. [6.230] assigned the local vibrational mode at 824 cm⁻¹ (RT) to V₂O₂. In similar work reported by Londos et al. [6.234], a band at 884 cm⁻¹ (RT) was assigned to a vacancy near to a VO₂ complex. In positron-annihilation studies, positron lifetimes of 240 ps [6.231] and 325 ps [6.167] were associated with V₂O₂.

From theoretical investigations, Pesola et al. [6.177] estimated that a neutral V₂O₂ complex is by 1.4 eV energetically more stable than a neutral divacancy well-separated from two oxygen interstitials. Combining similar *ab-initio* calculations with known levels of other defects, Coutinho et al. [6.232] suggested an acceptor state of V₂O₂ to be around $E_c - 0.42$ eV, a double acceptor state to be 0.2-0.3 eV nearer to the conduction band, and a donor state to be around $E_v + 0.22$ eV.

V₃O

For the V₃O complex, identified in its neutral charge state as Si-*P4* EPR center [6.214], Lee et al. [6.229] proposed a level at $E_v + 0.4$ eV. From similarities in the kinetics of a DLTS level at $E_c - 0.2$ eV¹ to the EPR measurements of Lee and Corbett, Kimerling [6.156] tentatively assigned this level to the V₃O complex. However, this assignment was discussed and rejected later by Awadelkarim et al. [6.217]. Also based on a correlation to the growth of the Si-*P4* EPR center, Meese et al. [6.233] suggested V₃O to act as a hole trap with a level at $E_v + 0.35$ eV. From a correlation of their kinetics, Lee et al. [6.229] suggested the V₃O complex to give rise to an absorption band at 887 cm⁻¹ associated also with VO₂. This assignment was corroborated by Londos et al. [6.234] who tentatively associated with V₃O a localized vibrational mode at 884 cm⁻¹ (RT) which he found as a shoulder of the 887 cm⁻¹ peak. In positron-annihilation studies, a positron lifetime of 325 ps was associated with V₃O [6.231]. The theoretical investigations of Akiyama and Oshiyama [6.235] indicated a binding energy of 0.88 eV for the oxygen atom.

V₃O₂

For the V₃O₂ complex, identified in its neutral charge state as Si-*P5* EPR center [6.214], a level at $E_c - 0.4$ eV or $E_v + 0.4$ eV was inferred by Lee et al. [6.216] from photo-EPR measurements. The assignment is problematic, though, since Lee et al. [6.216] associated V₃O₂ and its levels with the Si-A15 EPR spectrum which, according to Lee and Corbett [6.214], arises from V₃O₃. Correlating the kinetics of IR and EPR measurements, Lee et al. [6.229] associated V₃O₂ tentatively with bands at 904 and 968 cm⁻¹. Based on annealing kinetics and theoretical investigations, Sarlis et al. [6.230] assigned the local vibrational mode observed at 833 cm⁻¹ (RT) to V₃O₂. The theoretical investigations of Akiyama and Oshiyama [6.235] indicated a binding energy of 1.12 eV for the last oxygen atom.

¹In Figure 8 of the publication of Kimerling [6.156], the ionization level is positioned at $E_c - 0.27$ eV, in the text at $E_c - 0.20$ eV

V_mO_n

Binding energies for oxygen atoms in V_mO_n complexes with *n* and *m* up to 6 were reported by Akiyama and Oshiyama [6.235] from theoretical calculations.

IO_i

The other possibility for a complex of oxygen with an intrinsic point defect would be with a self-interstitial. To such a silicon-oxygen complex, infrared-absorption bands at 935, 944, and 956 cm⁻¹ (77 K) were assigned [6.236, 6.237], although especially the assignment of the 935 cm⁻¹ band was not undisputed [6.238–6.240]. For all of them, the presence of oxygen was demonstrated by Khirunenko et al. [6.241] via isotope experiments with samples doped with ¹⁸O. In such an environment, the absorption bands were found to shift to 895, 903, and 915 cm⁻¹, respectively. The formation of oxygen-self-interstitial complexes was also found by Oehrlein et al. [6.242] to explain the dependence of the divacancy production during electron irradiation on the oxygen concentration reported by Lindström et al. [6.243]. Comparing samples with different oxygen content, Harris and Watkins [6.244] suggested that oxygen atoms are competing with substitutional carbon for silicon self-interstitials. At 245 K, the silicon self-interstitials were found to be released from the complexes with oxygen. EPR investigations performed by Abdullin et al. [6.245] indicated that IO_i defects may assume different atomic configurations. For the atomic arrangement of the A configuration, associated with the EPR center labeled Si-A18, a donor level was found at E_v + 0.4 eV. The EPR centers Si-AA13 and Si-AA14 were suggested to arise from different charge states of the same atomic arrangement B with ionization levels at E_v + 0.13 eV and E_c - 0.19 eV. Similar levels were found by DLTS [6.246]. *Ab-initio* calculations reported by Pinho et al. [6.247] supported the assignment of the EPR Si-A18 center to IO_i in the positive charge state. In the atomic arrangement suggested, the self-interstitial assumes a tetrahedral position near to the oxygen atom on a bond-centered site. This configuration, in its neutral charge state, was suggested to be responsible also for the absorption band at 944 cm⁻¹. The energetically most stable configuration for the neutral and negative charge states, on the other hand, was found to be C_{1h}-symmetric with the oxygen atom near to and in the symmetry plane of a [110]-oriented split interstitial.

Pajot et al. [6.248] suggested that oxygen-self-interstitial pairs might diffuse rapidly in silicon. This model was supported as a possibility, e. g. by Newman and coworkers [6.84, 6.249], Ourmazd et al. [6.99], and Voronkov [6.131] on the basis of indirect evidence. In addition, the possibility of a rapidly diffusing complex of an oxygen atom and a silicon self-interstitial was corroborated by the theoretical investigations of Deák et al. [6.171, 6.210]. Evidence against the possibility that oxygen diffusion is enhanced by the interaction with self-interstitials was summarized later by Newman [6.250].

I₂O_i, IO_{2i}, and I₂O_{2i}

Reviewing the properties associated with IO_i complexes, Murin et al. [6.239] and Hermansson et al. [6.240] argued that the band at 935 cm⁻¹ attributed commonly to such defects arises rather from an I₂O_i complex.

Based on their generation kinetics during electron irradiation, Lindström et al. [6.251] associated vibration bands at 911/922 and 1034/1037 cm⁻¹ (RT/10 K) to IO_{2i} complexes and vibration bands at 916/918 and 1031/1034 cm⁻¹ (RT/10 K) to I₂O_{2i} defects. For both, the presence of oxygen in the defects was confirmed by the observation of isotope shifts. From a comparison of the annealing kinetics, it was also concluded that an electron trap at E_c - 0.11 eV arises from the same defect as the 922 cm⁻¹ band, i. e. the IO_{2i} complex.

6.1.6 Oxygen Dimers and Trimmers

To explain the kinetics of the formation of SiO_4 complexes acting as thermal donors, Gösele and Tan [6.98] suggested that gas-like O_2 molecules may form and diffuse rapidly through the silicon crystal. This mechanism was invoked also in other theories to explain certain experimental results [6.101, 6.122, 6.252]. Although in the first spectroscopy investigations no vibrational modes were observed to accompany the formation of oxygen dimers [6.253], several absorption bands were later interpreted in favor of a complex of two interstitial oxygen atoms [6.101, 6.132, 6.254–6.258]. Especially bands at 556, 690, 1012, 1060, and 1105 cm^{-1} (10 K) were associated with O_{2i} . Using such spectroscopic data, Murin et al. [6.256] estimated the binding energy of O_{2i} to be in the range from 0.16 to 0.3 eV. They also suggested the diffusion coefficient of O_{2i} to be several orders of magnitude higher than that of interstitial oxygen, characterized by activation energies around 1.6 eV. Within the kinetic model of Åberg et al. [6.101], an activation energy of 1.3 eV was estimated to characterize the diffusion of O_2 . Assuming the binding energy of O_2 to be in the range from 0.2 to 0.4 eV, Senkader et al. [6.111] estimated the migration enthalpy of O_2 to be about 1.7 to 1.9 eV.

Theoretical studies have shown that an oxygen molecule is not stable in the lattice whereas other structures shown schematically in Figure 6.6 may be. The first configuration, shown in Figure 6.6 a) with the two interstitial oxygen atoms sharing a common silicon neighbor is usually referred to as “staggered” dimer. Calculations of its energetics by *ab-initio* methods range from a classification as unstable [6.175] to binding energies from 0.1 eV [6.259], 0.2 [6.177], ≤ 0.4 eV [6.173], 0.53 eV [6.260], and 0.54 eV [6.42] to 1.0 eV [6.261]. The stability of the structure was also mentioned in other reports [6.257, 6.258, 6.262–6.264] without giving full details of the energetics. It should be noted, however, that the calculated geometries for the minimum-energy configuration do not always agree, especially with respect to the directions of relaxation of the two oxygen atoms. For the diffusion of the oxygen dimer, activation energies of 0.95 eV [6.134], 1.1–1.5 eV [6.264], 1.36 eV [6.259], and 1.4 eV [6.42] were calculated for the energetically most favorable path.

A second structure, depicted schematically in Figure 6.6 b) considered as alternative contains two trivalently bonded oxygen atoms and two silicon atoms in a four-membered ring. Calculations of its formation energetics range from slightly endothermal [6.261] to exothermal with a binding energy of 0.05 eV [6.259]. It is generally found to be less stable than the first structure and represents often an intermediate position for the diffusion of the oxygen dimer.

The third configuration, shown in Figure 6.6 c), is often referred to as “skewed” oxygen dimer. It comprises two oxygen atoms which assume interstitial positions in a hexagonal ring, separated by two silicon atoms. The calculated binding energies for this defect range from 0.1 eV [6.177] to 0.35 eV [6.42]. Its stability was mentioned also in other reports [6.257, 6.258, 6.264] without giving full details of the energetics. Although energetically stable, the third configuration was found to give less satisfactory explanations for the vibrational modes observed experimentally.

Theoretical investigations indicated also that a configuration of three interstitial oxygen atoms arranged approximately in {110} direction might be energetically stable [6.173, 6.177, 6.261] with the estimated binding energies scattering from 0.7 to 2.0 eV. In a somewhat less stable configuration, the middle oxygen interstitial is replaced by a so-called “ylid”, a trivalently bonded oxygen atom suggested as a possible candidate for the core of thermally induced oxygen-related donors by Stavola and Snyder [6.93]. The *ab-initio* calculations of Lee et al. [6.134] and Coutinho et al. [6.133] confirmed that O_3 and larger oxygen chains are more mobile than interstitial oxygen.

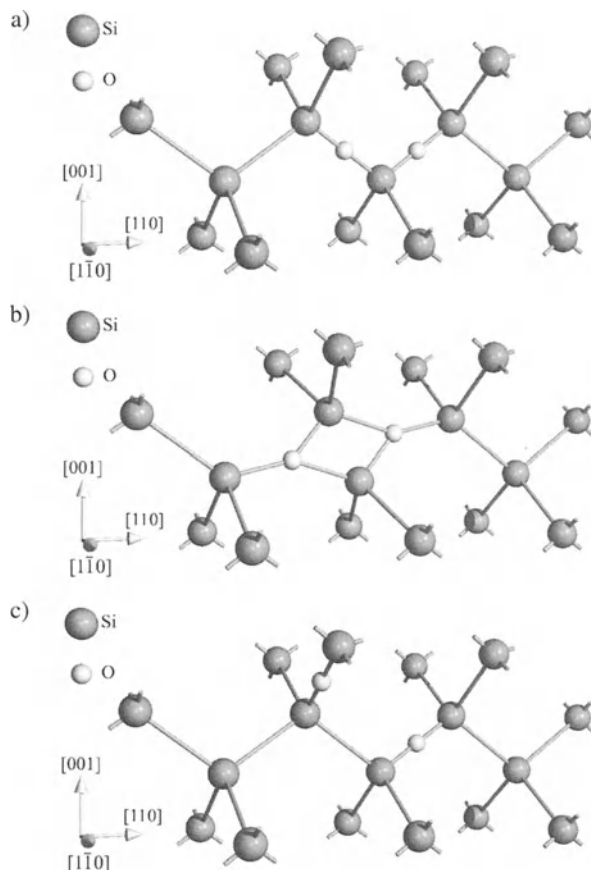


Figure 6.6: Atomic configurations suggested for stable oxygen dimers: a) Di-oxygen complex with common silicon neighbor, b) Two trivalently bonded oxygen atoms in a ring with two silicon atoms, c) Two oxygen interstitials in a hexagon ring, separated by two neighboring silicon atoms.

6.2 Sulfur

Sulfur, like selenium and tellurium, was investigated predominantly because of its properties as deep double donor in silicon. However, sulfur-doped devices were also investigated for infrared detectors. In the following sections, the basic atomic configurations of sulfur in silicon, its solubility, the diffusion behavior, and the formation of complexes will be discussed.

6.2.1 Basic Atomic Configurations

Beginning with the work of Carlson et al. [6.265], various levels were reported in sulfur-doped silicon. Four of them were finally attributed to substitutional sulfur atoms and sulfur pairs, both acting as double donors. For the others, no definite assignment is known up to now.

The quest for substitutional sulfur atoms started with the EPR and ENDOR measurements of Ludwig [6.266]. They revealed a positively charged sulfur atom on a T_d -symmetric site but could not associate it unambiguously with a substitutional or a tetrahedral interstitial site. Similar conclusions were drawn by Greulich-Weber et al. [6.267] from ENDOR investigations.

Ludwig [6.266] also cited unpublished work of Kravitz and Paul which indicated an ionization energy of 0.59 eV² for the double ionization of positively charged sulfur ions. This value is compatible to the ionization energies of 0.61 to 0.614 eV found by infrared-absorption measurements [6.269–6.274], 0.55 to 0.59 eV obtained from photocapacitance measurements [6.275, 6.276], 0.512 to 0.526 eV derived from isothermal transient-capacitance measurements [6.277, 6.278], 0.53 eV deduced from dark-capacitance and current-transient measurements [6.279], 0.64 eV estimated from photocurrent measurements [6.280], 0.526 eV found using the isothermal transient-capacitance technique [6.281], as well as 0.527 to 0.587 eV deduced from DLTS investigations [6.282–6.284]. Studies of the effects of uniaxial stress on the respective infrared-absorption spectra conducted by Krag et al. [6.274] confirmed the T_d symmetry for the defect associated.

Neutral substitutional sulfur was finally found to have an energy for positive ionization compatible with values of 0.3 eV estimated from Hall-effect investigations [6.283], 0.318 to 0.3184 eV obtained from infrared-absorption studies [6.271–6.273, 6.285, 6.286], 0.3 to 0.32 eV derived from photocapacitance measurements [6.275, 6.276, 6.287], 0.36 eV estimated from photocurrent measurements [6.280], 0.268 eV derived from isothermal transient-capacitance measurements [6.277], 0.275 eV deduced from dark-capacitance and current-transient measurements [6.279], 0.3 eV derived from Fourier photo-admittance spectroscopy [6.288], as well as 0.267 to 0.325 eV measured by DLTS [6.282–6.284].

In agreement with a substitutional site, the respective photoconductivity spectra were found by Janzén et al. [6.286] to be consistent with a tetragonal symmetry. From a comparison of experimental line spacings and the predictions of the effective-mass theory for group V and VI elements, Pajot and Stoneham [6.289] suggested sulfur to occupy substitutional sites. Similarly, substitutional sites were found in theoretical investigations to be energetically favored in comparison to interstitial sites [6.290]. A strong indication that both levels relate to different charge states of the same defect was given by Brotherton et al. [6.283] and Pensl et al. [6.284] who found that the respective concentrations always had similar concentrations, independent of sample preparation. Final evidence was obtained by Kleverman et al. [6.291] from their study of hole-capture processes at sulfur double donors.

Ionization energies were calculated also in various theoretical investigations. They led to estimates of 0.26 to 0.35 eV for the ionization of neutral substitutional sulfur atoms [6.292–6.296] and 0.61 to 0.798 eV for positively charged substitutional sulfur atoms [6.292–6.295].

In various reports, energy levels were reported for additional sulfur-related defects. One of them, denoted S_c⁰(X₁) in the review of Grimmeiss and Janzén [6.1], is characterized by a shallow level with ionization energies of 0.105 eV determined by Hall-effect investigations [6.268], 0.109 to 0.10952 eV measured by infrared-absorption measurements [6.269, 6.274, 6.285, 6.286], as well as 0.102 eV obtained from photoconductivity measurements [6.297]. Based on its response to uniaxial stress, Camphausen et al. [6.268] speculated that it might be a neutral sulfur atom on a D_{3d}-symmetric bond-centered interstitial position. Similar studies of the effects of uniaxial stress on infrared absorption conducted by Krag et al. [6.274] confirmed that the symmetry of the defect associated is C_{3v} or D_{3d}.

²Ludwig [6.266] originally reported a value of 0.52 eV. According to reference 11 of the work of Camphausen et al. [6.268], a value near to 0.59 eV was suggested by Kravitz and Paul for the ionization energy of singly ionized sulfur.

6.2.2 Solubility

The only study of the solubility of sulfur in silicon was reported by Carlson et al. [6.265] from electrical measurements after diffusion of sulfur from the gas phase. Since their energy levels were found later to be associated with sulfur pairs, solid solubility is probably up to twice as high as reported. The experimentally determined values are shown in Figure 6.7.

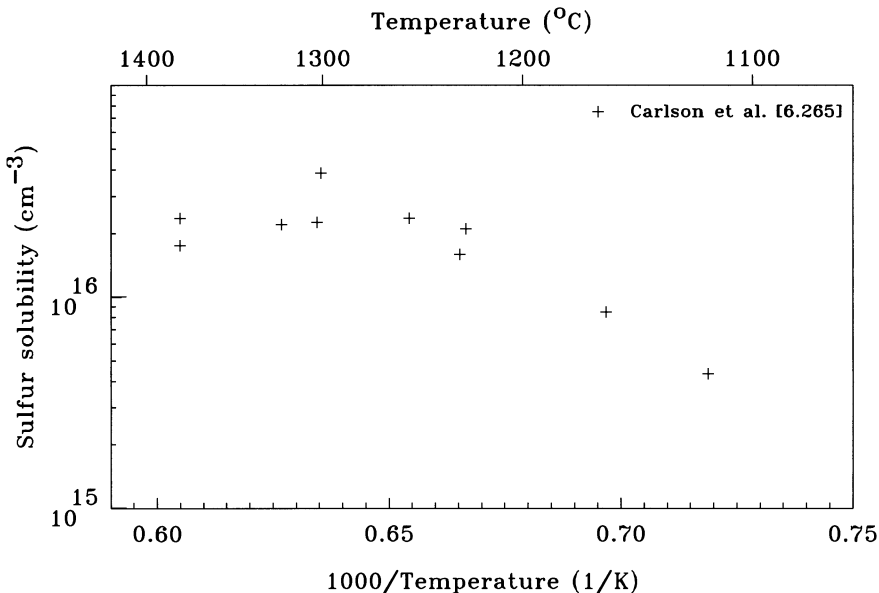


Figure 6.7: Solubility of sulfur in silicon.

6.2.3 Diffusion

A first study of the diffusivity of sulfur in silicon was reported by Carlson et al. [6.265] from electrical measurements. In the following, Gruzin et al. [6.298] based his experiments on a radiometric analysis of ^{35}S . Their values turned out to be about one magnitude smaller than the respective values reported by Carlson et al. which indicates a systematic error in one of the two analyses. To avoid problems from sulfur complexes in electrical measurements, Rollert et al. [6.299] based their investigations also on the radioactive ^{35}S isotope. Their results confirmed the data of Carlson et al. The experimentally determined diffusion coefficients are shown in Figure 6.8 together with the regression curve

$$D_S^i = 0.255 \cdot \exp\left(-\frac{2.024\text{eV}}{k \cdot T}\right) \text{cm}^2/\text{s} \quad (6.3)$$

derived from the measurements of Carlson et al. [6.265] and Rollert et al. [6.299].

The activation energy ranges with a confidence level of 90% from 1.86 to 2.19 eV. The 90% confidence interval for the diffusion coefficient is about +10/-9.2% of the regression curve at 1230 °C and increases to +18/-16% at the melting point and +22/-18% at 1050 °C. Additional measurements are expected with 90% confidence within a range of +59/-37% of the regression curve at 1230 °C which increases slightly to +62/-38% at the melting point and +64/-39% at 1050 °C.

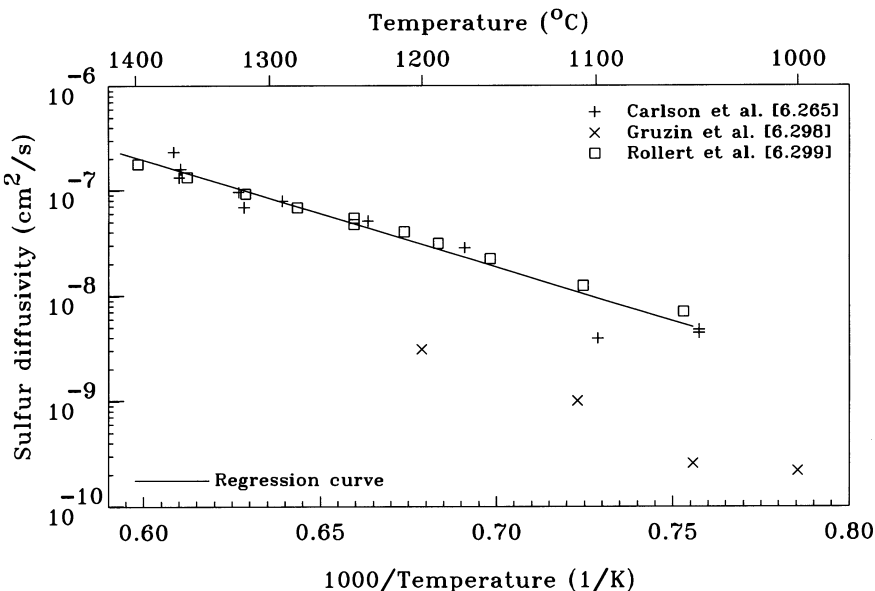


Figure 6.8: Diffusion coefficient of sulfur in silicon.

Since the transport capacity of sulfur is close to that of self-diffusion, an influence of sulfur diffusion on the concentrations of the intrinsic point defects can be expected according to the discussion in Section 3.4.7. Evidence for such an influence was indeed found by Stolwijk et al. [6.300] who explained deviations of sulfur profiles from error-function profiles by a kick-out mechanism.

6.2.4 Complexes

In addition to sulfur on tetrahedral sites, Ludwig [6.266] found sulfur-sulfur pairs in his EPR investigations. He also cited unpublished work of Kravitz and Paul which indicated an energy of 0.37 eV for the double ionization of singly positively charged sulfur pairs. This value agrees well to ionization energies of 0.36 to 0.38 eV found by Hall-effect measurements [6.265, 6.268, 6.283, 6.284, 6.301], 0.3655 to 0.3711 eV deduced from infrared-absorption measurements [6.269, 6.273, 6.274, 6.286], 0.28 to 0.38 eV derived from photoconductivity measurements [6.302, 6.303], as well as 0.353 eV obtained by DLTS investigations [6.284].

In many of these investigations, a shallower level was noted with ionization energies of 0.177 to 0.19 eV estimated from Hall-effect measurements [6.265, 6.268, 6.283, 6.284], 0.1859 to 0.1877 eV measured by infrared-absorption measurements [6.269, 6.273, 6.274, 6.285, 6.286], 0.174 to 0.18 eV obtained from photoconductivity measurements [6.297, 6.303], as well as 0.17 to 0.2 eV found by DLTS investigations [6.282–6.284]. It is generally associated with the ionization of neutral sulfur pairs.

A strong indication that both levels relate to different charge states of the same defect was given by Brotherton et al. [6.283] and Pensl et al. [6.284] who found that the respective concentrations always had similar concentrations, independent of sample preparation.

An association with sulfur pairs rather than with substitutional sulfur was corroborated by the uniaxial-stress investigations of Krag et al. [6.269, 6.274] who found the defects associated to have trigonal symmetry around a $\langle 111 \rangle$ -oriented axis rather than T_d as expected for a substitutional sulfur atom. Similar evidences for a D_{3d} -symmetric center were reported by Camphausen et al. [6.268] and Janzen et al. [6.286]. Finally, the ENDOR investigations of van Oosten and Ammerlaan [6.304] and Greulich-Weber et al. [6.305] confirmed the sulfur pair to be D_{3d} -symmetric around a $\langle 111 \rangle$ -oriented axis and corroborated the evidence that the sulfur atoms occupy neighboring substitutional sites.

From a study of the dissolution of sulfur pairs during isochronal annealing with a subsequent quenching, Pensl et al. [6.284] estimated a value of 0.58 eV for their dissociation energy.

Ionization energies of sulfur pairs on nearest neighboring sites were estimated also in theoretical investigations. Binding energies of electrons so obtained are in the range of 0.27 to 0.3 eV for single ionization [6.294, 6.295, 6.306] as well as 0.42 to 0.61 eV for double ionization [6.294, 6.295, 6.306]. These estimates reproduce the experimental finding that the levels of sulfur pairs are shallower than those of substitutional sulfur atoms. Theoretical investigations performed by Weinert and Scheffler [6.307] indicated that pairs of sulfur atoms on neighboring substitutional sites should be favorable energetically in comparison to interstitial-interstitial or substitutional-interstitial sulfur pairs. For the binding energy of a pair of neutral substitutional sulfur atoms, they estimated a value of 0.3 eV. Complementary calculations by Taskin [6.308] gave a binding energy of 2.4 eV.

In material co-doped with sulfur, selenium, and tellurium, Wagner et al. [6.273] reported the formation of mixed chalcogen pairs and of a sulfur-selenium-tellurium complex.

Various energy levels were correlated with sulfur but could not be identified up to now. The theoretical investigations of Jansen and Sankey [6.294] indicated that the ionization energies of neutral as well as positively charged sulfur complexes become shallower when the number of sulfur atoms in the complex increases. Based on these results, the authors suggested that the unidentified energy levels might be associated with large sulfur complexes.

6.3 Selenium

Selenium, like sulfur and tellurium, was investigated predominantly because of its properties as deep double donor in silicon. However, selenium-doped devices were also investigated for infrared detectors [6.297, 6.309]. In the following sections, the basic atomic configurations of selenium in silicon, its solubility, the diffusion behavior, and the formation of complexes will be discussed.

6.3.1 Basic Atomic Configurations

EPR and ENDOR Investigations performed by Grimmeiss et al. [6.310] resulted in spectra compatible with substitutional, singly ionized selenium atoms, although a selenium interstitial on a T_d -symmetric would also be possible. Similar conclusions were drawn by Greulich-Weber et al. [6.267] from ENDOR investigations. Theoretical investigations [6.290, 6.295] unambiguously indicated that the substitutional site is energetically favored in comparison to the interstitial site and corroborated the assignment of Grimmeiss et al. Further evidence for a substitutional character of selenium atoms was given by Pajot and Stoneham [6.289] on the basis of a comparison of experimental line spacings and the predictions of the effective-mass theory for group V and VI elements.

The EPR investigations of Grimmeiss et al. [6.310] further indicated that positively charged selenium can be further ionized by photons with energies of about 0.6 eV. This value is compatible with ionization energies of 0.5 to 0.66 eV [6.311, 6.312] derived from Hall-effect measurements, 0.5894 to 0.593 eV obtained from infrared-absorption investigations [6.271, 6.273, 6.286, 6.313], 0.57 eV found from photocapacitance measurements [6.276], as well as 0.524 to 0.589 eV obtained from DLTS studies [6.284, 6.314].

Neutral substitutional selenium was finally suggested to be associated with ionization energies of 0.26 to 0.3 eV estimated from Hall-effect investigations [6.311, 6.312, 6.315, 6.316], 0.3065 to 0.307 eV determined from infrared-absorption studies [6.271, 6.273, 6.286, 6.313, 6.317], 0.301 eV found from photocapacitance measurements [6.276], 0.3 eV derived from photoresistance investigations [6.297], as well as 0.3 to 0.315 eV [6.284, 6.314] obtained from DLTS studies.

A strong indication that both levels relate to different charge states of the same defect was given by Grimmeiss et al. [6.318] and Pensl et al. [6.284] who found that the respective concentrations in measured profiles always had comparable concentrations. Final evidence was obtained by Kleverman et al. [6.291] from their study of hole-capture processes at selenium double donors.

Various theoretical investigations aimed at reproducing the ionization levels of substitutional selenium. For neutral selenium atoms, values of 0.31 to 0.38 eV were reported [6.293–6.296]. Ionization of positively charged selenium atoms was estimated to require energies of 0.59 to 0.921 eV [6.293–6.295].

Lattice positions of selenium after ion implantation and annealing were investigated by channeling RBS measurements by Meyer et al. [6.319] and Gyulai et al. [6.320, 6.321]. They noted that about 30% to 40% of the implanted atoms may be substitutional. But Gyulai et al. reported also unexpected features which might be caused by selenium residing on tetrahedral interstitial sites.

6.3.2 Solubility

The phase diagram of the selenium-silicon system was compiled by Okamoto [6.322]. Accordingly, below 870 °C, the selenium in the silicon phase is in equilibrium with a Se₂Si phase. For temperatures above 870 °C and below 1190 °C, the equilibrium phase is SeSi.

In the investigations of Zhdanovich and Kozlow [6.323], Vydyanath et al. [6.315], and Kim and Sakata [6.312], solubility values were estimated from the surface concentration after diffusion of selenium from the gas phase. The value attributed to Grimmeiss et al. [6.318] was taken from their Figure 5 showing a diffusion profile after selenium diffusion from the gas phase characterized via junction-space-charge methods and SIMS. Taskin et al. [6.324] obtained their values by ion implantation and annealing. They may be influenced by transient effects associated with an oversaturation of self-interstitials as well as the presence of selenium clusters rather than a homogeneous binary phase. The values determined experimentally are shown in Figure 6.9.

6.3.3 Diffusion

In the diffusion studies of Zhdanovich and Kozlow [6.323], Vydyanath et al. [6.315], Kim and Sakata [6.312], and Stümpel et al. [6.316], diffusion of selenium from the gas phase was combined with electrical measurements to obtain diffusion profiles. After a similar diffusion procedure, Grimmeiss et al. [6.318] used DLTS, constant-capacitance spectroscopy, and SIMS to characterize the diffusion profiles. The diffusion coefficient reported by Richou et al. [6.325]

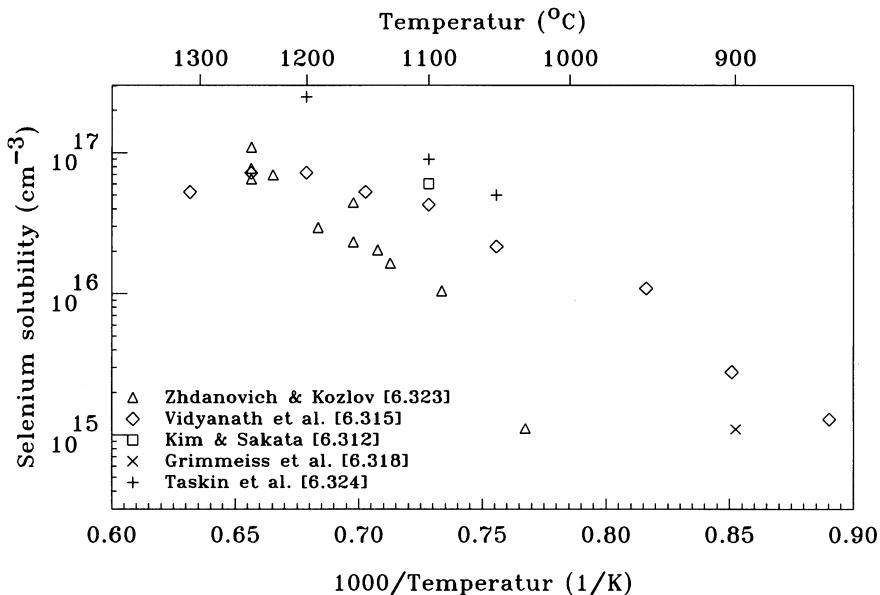


Figure 6.9: Solubility of selenium in silicon.

was obtained by DLTS measurements of the selenium distribution after ion implantation and diffusion. It is significantly higher than expected from an extrapolation of diffusion coefficients reported at higher temperatures and most probably influenced by transient-enhanced diffusion during the post-implantation annealing. A summary of the diffusion coefficients determined experimentally together with the regression curve

$$D_{Se} = 0.123 \cdot \exp\left(-\frac{2.457 \text{ eV}}{k \cdot T}\right) \text{ cm}^2/\text{s} \quad (6.4)$$

from the data points at 900 °C and above is shown in Figure 6.10. The activation energy ranges with a confidence level of 90% from 2.36 to 2.55 eV. The 90% confidence interval for the diffusion coefficient is about +6.1/-5.8% of the regression curve at 1100 °C and increases to +17/-14% at the melting point and +16/-14% at 900 °C. Additional measurements are expected with 90% confidence within a range of +73/-42% of the regression curve at 1100 °C which increases slightly to +76/-43% at the melting point and at 900 °C.

6.3.4 Complexes

The most prominent complexes are pairs of substitutional selenium atoms. Neutral selenium pairs can be correlated with energies for positive ionization of 0.206 to 0.23 eV estimated from Hall-effect measurements [6.284, 6.323], 0.2064 to 0.2065 eV measured by infrared-absorption measurements [6.273, 6.286, 6.313], 0.2 eV derived from photoresistance investigations [6.297], as well as 0.204 to 0.225 eV found by DLTS investigations [6.284, 6.325]. Energies for the double ionization of positively charged selenium pairs are associated with values of 0.38 eV deduced from Hall-effect measurements [6.284], 0.3879 to 0.3895 eV from infrared-absorption measurements [6.273, 6.286, 6.313], 0.4 eV obtained from capacitance-voltage curves [6.326], as well as 0.485 eV derived from DLTS investigations [6.325]. A strong indication that both

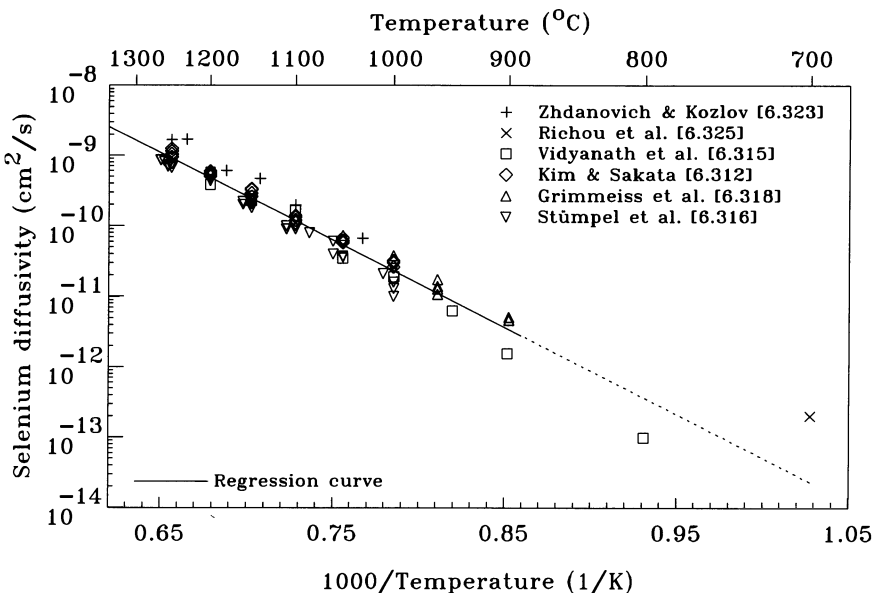


Figure 6.10: Diffusion coefficient of selenium in silicon.

levels relate to the same defect was given by Richou et al. [6.325] and Pensl et al. [6.284] who found the respective concentrations to be equal within the measurement error. The EPR measurements of Wörner and Schirmer [6.327] and the ENDOR investigations of Greulich-Weber et al. [6.305] suggested the selenium pair to be D_{3d}-symmetric around a ⟨111⟩-oriented axis and corroborated the evidence that the sulfur atoms occupy neighboring substitutional sites.

Estimates of the ionization level of neutral selenium pairs on nearest neighboring sites on the basis of theoretical investigations led to positions 0.27 to 0.36 eV below the conduction band [6.294, 6.295, 6.306]. For positively charged selenium pairs, energy levels of 0.39 to 0.6 eV were calculated [6.294, 6.295, 6.306]. These estimates reproduce the experimental finding that the levels of selenium pairs are shallower than those of substitutional selenium atoms.

From a kinetic study of the formation of selenium complexes, Taskin and Tishkovskii [6.328] estimated a value of 1.35 eV for the binding energy of a pair of substitutional selenium atoms. In a subsequent publication, Taskin and Tishkovskii [6.329] reported a binding energy of 1.4 eV.

Theoretical investigations performed by Weinert and Scheffler [6.307] indicated that pairs of selenium atoms on neighboring substitutional sites should be favorable energetically in comparison to interstitial-interstitial or substitutional-interstitial selenium pairs. For the binding energy of a pair of neutral substitutional selenium atoms, they estimated a value of 0.1 eV. Complementary calculations by Taskin [6.308] gave a binding energy of 1.9 eV. The smaller binding energies in comparison to sulfur compare well to the reduced tendency to form complexes noted by Wagner et al. [6.273].

Various energy levels were correlated with selenium but could not be identified up to now. The theoretical investigations of Jansen and Sankey [6.294] indicated that the ionization energies of neutral as well as of positively charged selenium complexes become shallower when the number of selenium atoms in the complex increases. Based on these results, the authors suggested that the unidentified energy levels might be associated with large selenium

complexes. Studying the formation of complexes in selenium-implanted samples, Taskin and Tishkovskii [6.328] suggested a defect with an ionization energy of 0.13 eV to comprise three selenium atoms. In a subsequent publication, Taskin and Tishkovskii [6.329] estimated a binding energy of 1.15 eV for the third selenium atom to Se_2 . They further estimated a binding energy of about 1.0 eV for the attachment of further selenium atoms up to Se_5 . For the completion of an Se_6 ring structure, the binding energy of the last selenium atom was estimated to be about 2.0 eV.

In material co-doped with sulfur, selenium, and tellurium, Wagner et al. [6.273] reported the formation of mixed chalcogen pairs and of a sulfur-selenium-tellurium complex.

From the formation of a donor level at $E_c - 0.2$ eV when selenium was diffused into silicon doped with boron, gallium, aluminum, or indium to a concentration of 10^{15} cm^{-3} , Vydyanath et al. [6.315] concluded that selenium forms ion pairs with the acceptors.

6.4 Tellurium

Like sulfur and selenium, tellurium was investigated primarily because of its double-donor properties. In the following sections, the basic atomic configurations of tellurium in silicon, its solubility, the diffusion behavior, and the formation of complexes will be discussed.

6.4.1 Basic Atomic Configurations

The EPR and ENDOR investigations of Grimmeiss et al. [6.310] resulted in spectra compatible with a substitutional, singly ionized tellurium atom, although a tellurium interstitial on a T_d -symmetric site could not be ruled out. Similar conclusions were drawn by Niklas and Spaeth [6.330] and Greulich-Weber et al. [6.267] from ENDOR investigations. The substitutional character of isolated tellurium atoms was corroborated by theoretical investigations [6.290, 6.295] which unambiguously indicated that the substitutional site is energetically favored in comparison to the interstitial site. Similarly, from a comparison of experimental line spacings and the predictions of the effective-mass theory for group V and VI elements, Pajot and Stonerham [6.289] suggested tellurium to occupy substitutional sites.

The EPR investigations of Grimmeiss et al. [6.310] further indicated that positively charged tellurium can be ionized further by photons with energies of 0.4 eV. This value correlates to ionization energies of 0.42 to 0.44 eV derived from Hall-effect measurements [6.284, 6.331], 0.4108 to 0.411 eV obtained from infrared-absorption measurements [6.271, 6.273, 6.310], 0.411 eV from photocapacitance investigations [6.310], as well as 0.364 to 0.445 eV determined by DLTS measurements [6.284, 6.310, 6.332, 6.333].

Positive ionization of neutral, substitutional tellurium was associated with energies of about 0.19 to 0.2 eV estimated from Hall-effect investigations [6.284, 6.316, 6.331, 6.334, 6.335], 0.1987 to 0.199 eV from infrared-absorption studies [6.271, 6.273, 6.334], as well as 0.196 to 0.207 eV obtained from DLTS measurements [6.284, 6.310, 6.333]. A strong indication that both levels relate to the same defect came from the work of Pensl et al. [6.284] who found the respective concentrations to be equal within the measurement error. Final evidence that both levels correspond to different charge states of the same defect was obtained by Kleverman et al. [6.291] from their study of hole-capture processes.

Estimates for the ionization energies of substitutional tellurium atoms were obtained also from theoretical investigations. They resulted in values of 0.1368 to 0.28 eV for neutral tellurium atoms [6.293–6.296]. Ionization of positively charged tellurium atoms was estimated to require energies of 0.41 to 0.4569 eV [6.293–6.295].

Already in the first investigations of the lattice position of tellurium after ion implantation and annealing by channeling RBS measurements, Picraux et al. [6.336], Meyer et al. [6.319], and Gyulai et al. [6.321] noted a high substitutional fraction of tellurium atoms. After ion implantation and annealing, Lee et al. [6.337] found by channeling RBS measurements that up to 80% of the implanted tellurium atoms can reside on substitutional sites. With increasing dose, it was found that the fraction of tellurium atoms on substitutional sites decreases.

Using Mössbauer spectroscopy, Weyer et al. [6.338] and Nylandsted Larsen et al. [6.339] confirmed that a large fraction of the implanted tellurium atoms are substitutional, especially when the target was heated during implantation. But Nylandsted Larsen et al. found also complexes related to vacancies and self-interstitials which showed a remarkable stability. Other Mössbauer studies were not completely consistent with a T_d symmetry of the substitutional tellurium atom [6.340, 6.341]. Depending on the annealing conditions, also spectra from defects with lower symmetry were found. As a tentative explanation, Dézsi et al. [6.341] suggested that the shift from the regular substitutional position is caused by a vacancy in the nearest neighborhood.

6.4.2 Solubility

The phase diagram of the tellurium-silicon system was compiled by Davey and Baker [6.342]. Accordingly, below about 890 °C, the tellurium in the silicon is in equilibrium with a Si_2Te_3 phase. The solubility of tellurium in silicon was obtained by Janzén et al. [6.343] from SIMS measurements after diffusion with tellurium in a quartz ampoule. These values are shown in Figure 6.11.

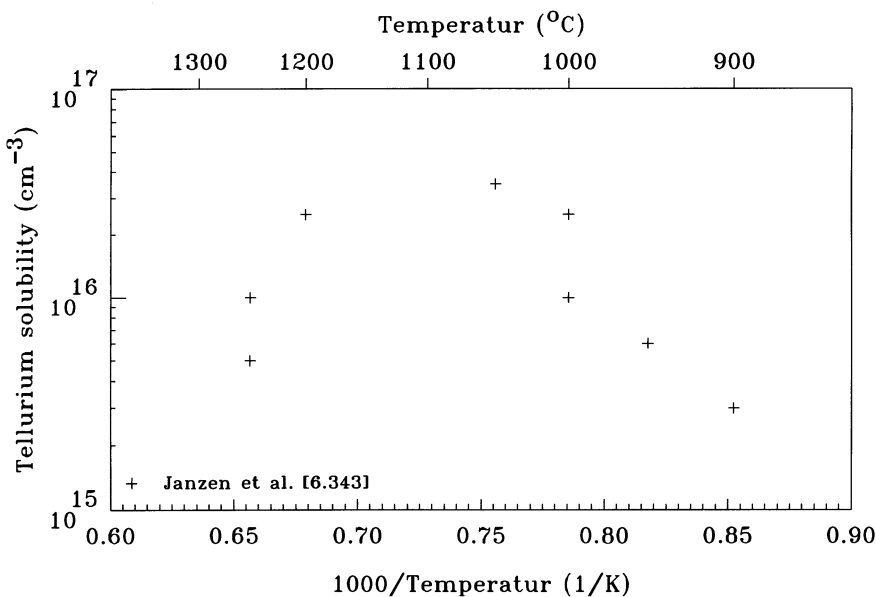


Figure 6.11: Solubility of tellurium in silicon.

6.4.3 Diffusion

The diffusivity of tellurium was investigated first by Janzén et al. [6.343] using SIMS measurements after diffusion in a quartz ampoule in the presence of tellurium. A similar diffusion set-up combined with electrical measurements was used by Stolwijk et al. [6.344] and Stümpel et al. [6.316]. As an alternative to diffusion of tellurium contained in the ambient, Stolwijk et al. [6.344] and Rollert et al. [6.345] implanted the radioactive isotope ^{121}Te into silicon and characterized the depth profiles via lapping and radioactive counting. The experimentally determined diffusion coefficients together with the regression curve

$$D_{\text{Te}} = 2.58 \cdot \exp\left(-\frac{3.47 \text{ eV}}{k \cdot T}\right) \text{ cm}^2/\text{s} \quad (6.5)$$

determined from them are shown in Figure 6.12. The activation energy ranges with a confidence level of 90% from 3.34 to 3.6 eV. The 90% confidence interval for the diffusion coefficient is about +10/-9.4% of the regression curve at 1150 °C and increases to +21/-17% at the melting point and +34/-25% at 850 °C. Additional measurements are expected with 90% confidence within a range of +110/-52% of the regression curve at 1150 °C which increases slightly to +113/-53% at the melting point and +119/-54% at 850 °C.

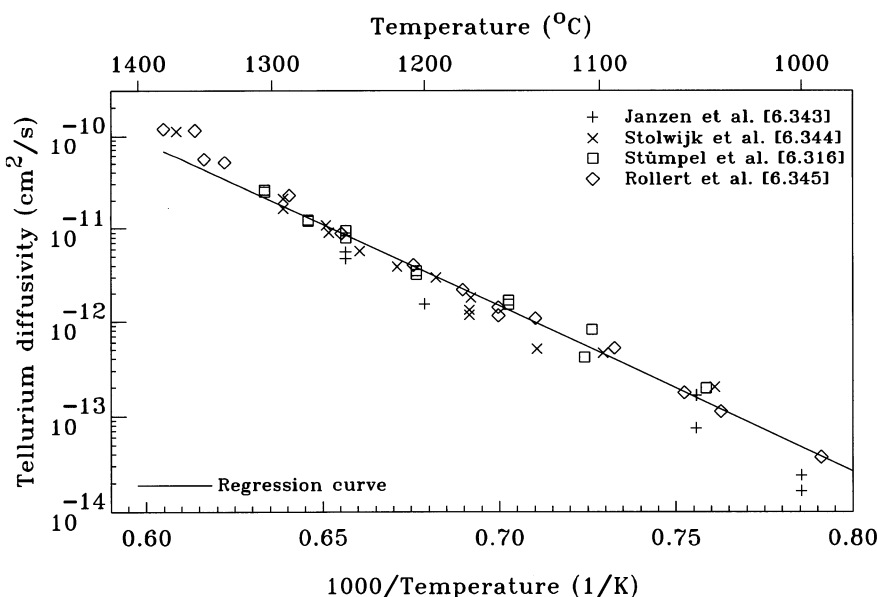


Figure 6.12: Diffusion coefficient of tellurium in silicon.

Based on the wide temperature range of their experiments, Stolwijk et al. [6.344] and Rollert et al. [6.345] argued that the temperature dependence would be better explained by a sum of two Arrhenius functions which represent diffusion via self-interstitials and via vacancies.

6.4.4 Complexes

Similar to the case of sulfur and selenium, pairs of substitutional atoms are the most prominent tellurium complexes. Tellurium pairs were reported first by Sirtl [6.346] in reference to the then unpublished work of Wagner et al. [6.273]. Therein, Wagner et al. presented infrared-absorption measurement which indicated an ionization energy of 0.158 eV for neutral tellurium pairs. Levels for the double ionization were probably not reported up to now.

Theoretical investigations resulted in estimates of 0.19 to 0.27 eV for the energy required to remove an electron from a neutral tellurium pair on nearest neighboring sites [6.294, 6.295, 6.306], and of 0.28 to 0.54 eV to remove a second electron from such a tellurium pair in a singly ionized state [6.294, 6.295, 6.306]. Theoretical investigations performed by Weinert and Scheffler [6.307] indicated that tellurium pairs are energetically less stable than two well-separated substitutional tellurium atoms. Complementary calculations by Taskin [6.308] gave a binding energy of approximately 1.5 eV. These findings reproduce the trend noted by Wagner et al. [6.273] that the tendency of chalcogen atoms to form complexes reduces from sulfur via selenium to tellurium.

In material co-doped with sulfur, selenium, and tellurium, Wagner et al. [6.273] reported the formation of mixed chalcogen pairs and of a sulfur-selenium-tellurium complex.

Various energy levels were correlated with tellurium but could not be identified up to now. The theoretical investigations of Jansen and Sankey [6.294] indicated that the ionization energies of neutral as well as positively charged tellurium complexes become shallower when the number of tellurium atoms in the complex increases. Based on these results, the authors suggested that the unidentified energy levels might be associated with large tellurium complexes.

Bibliography

- [6.1] H. G. Grimmeiss and E. Janzén, "Chalcogen-Related Defects in Silicon," in: *Materials, Properties and Preparation*, edited by T. S. Moss and S. Mahajan, *Handbook on Semiconductors*, vol. 3b, Amsterdam: North-Holland, 1755–1888 (1994).
- [6.2] W. Zulehner and D. Huber, *Czochralski-Grown Silicon, Crystals*, vol. 8, Berlin: Springer-Verlag (1982).
- [6.3] T. Abe, "Silicon Crystals for Giga-Bit Scale Integration," in: *Materials, Properties and Preparation*, edited by T. S. Moss and S. Mahajan, *Handbook on Semiconductors*, vol. 3b, Amsterdam: North-Holland, 1889–1911 (1994).
- [6.4] C. S. Fuller, N. B. Ditzenberger, N. B. Hannay, and E. Buehler, "Resistivity Changes in Silicon Induced by Heat Treatment," *Phys. Rev.*, vol. 96, no. 3, 833 (1954).
- [6.5] W. Kaiser, "Electrical and Optical Properties of Heat-Treated Silicon," *Phys. Rev.*, vol. 105, no. 6, 1751–1756 (1957).
- [6.6] C. S. Fuller and R. A. Logan, "Effect of Heat Treatment upon the Electrical Properties of Silicon Crystals," *J. Appl. Phys.*, vol. 28, no. 12, 1427–1436 (1957).
- [6.7] A. Bourret, "Oxygen Aggregation in Silicon," in: *Thirteenth International Conference on Defects in Semiconductors*, edited by L. C. Kimerling and J. M. Parsey, Jr., New York: The Metallurgical Society of AIME, 129–146 (1985).
- [6.8] H. Bender and J. Vanhellemont, "Oxygen in Silicon," in: *Materials, Properties and Preparation*, edited by T. S. Moss and S. Mahajan, *Handbook on Semiconductors*, vol. 3b, Amsterdam: North-Holland, 1637–1753 (1994).
- [6.9] A. Borghesi, B. Pivac, A. Sassella, and A. Stella, "Oxygen Precipitation in Silicon," *J. Appl. Phys.*, vol. 77, no. 9, 4169–4244 (1995).

- [6.10] K. F. Kelton, R. Falster, D. Gambaro, M. Olmo, M. Cornara, and P. F. Wei, “Oxygen Precipitation in Silicon: Experimental Studies and Theoretical Investigations within the Classical Theory of Nucleation,” *J. Appl. Phys.*, vol. 85, no. 12, 8097–8111 (1999).
- [6.11] W. K. Tice and T. Y. Tan, “Nucleation of CuSi Precipitate Colonies in Oxygen-Rich Silicon,” *Appl. Phys. Lett.*, vol. 28, no. 9, 564–565 (1976).
- [6.12] T. Y. Tan, E. E. Gardner, and W. K. Tice, “Intrinsic Gettering by Oxide Precipitate Induced Dislocations in Czochralski Si,” *Appl. Phys. Lett.*, vol. 30, no. 4, 175–176 (1977).
- [6.13] G. A. Rozgonyi, R. P. Deysher, and C. W. Pearce, “The Identification, Annihilation, and Suppression of Nucleation Sites Responsible for Silicon Epitaxial Stacking Faults,” *J. Electrochem. Soc.*, vol. 123, no. 12, 1910–1915 (1976).
- [6.14] W. D. Sylwestrowicz, “Mechanical Properties of Single Crystals of Silicon,” *Phil. Mag.*, vol. 7, no. 83, 1825–1845 (1962).
- [6.15] S. M. Hu, “Dislocation Pinning Effect of Oxygen Atoms in Silicon,” *Appl. Phys. Lett.*, vol. 31, no. 2, 53–55 (1977).
- [6.16] K. Sumino, H. Harada, and I. Yonenaga, “The Origin of the Difference in the Mechanical Strengths of Czochralski-Grown Silicon and Float-Zone-Grown Silicon,” *Jpn. J. Appl. Phys.*, vol. 19, no. 1, L49–L52 (1980).
- [6.17] D. Thebault and L. Jastrzebski, “Review of Factors Affecting Warpage of Silicon Wafers,” *RCA Review*, vol. 41, 592–611 (1980).
- [6.18] I. Yonenaga and K. Sumino, “Mechanical Strength of Silicon Crystals As a Function of the Oxygen Concentration,” *J. Appl. Phys.*, vol. 56, no. 8, 2346–2350 (1984).
- [6.19] M. Akatsuka, K. Sueoka, H. Katahama, N. Morimoto, and N. Adachi, “Pinning Effect on Punched-Out Dislocations in Silicon Wafers Investigated Using Indentation Method,” *Jpn. J. Appl. Phys., Part 2*, vol. 36, no. 11A, L1422–L1425 (1997).
- [6.20] M. Watanabe and A. Too, “Formation of SiO₂ Films by Oxygen-Ion Bombardment,” *Jpn. J. Appl. Phys.*, vol. 5, 737–738 (1966).
- [6.21] P. V. Pavlov and E. V. Shitova, “The Structure of Oxide Films Obtained by Oxygen Ion Bombardment of a Silicon Surface,” *Soviet Physics-Doklady*, vol. 12, no. 1, 11–13 (1967).
- [6.22] J. H. Freeman, “The Use of an Isotope Separator for Ion Implantation in Semi-Conductors,” in: *International Conference on Applications of Ion Beams to Semiconductor Technology*, edited by P. Glotin, Grenoble: Edition OPHRYS, 75–90 (1967).
- [6.23] N.-G. Blamires, D.-N. Osborne, R.-B. Owen, and J. Stephen, “A Preliminary Study of Semiconductor Structures Produced by Ion-Implantation,” in: *International Conference on Applications of Ion Beams to Semiconductor Technology*, edited by P. Glotin, Grenoble: Edition OPHRYS, 669–684 (1967).
- [6.24] K. Izumi, M. Doken, and H. Ariyoshi, “C.M.O.S. Devices Fabricated on Buried SiO₂ Layers Formed by Oxygen Implantation into Silicon,” *Electronics Letters*, vol. 14, no. 18, 593–594 (1978).
- [6.25] D. Fan and R. J. Jaccodine, “Role of Recoil Implanted Oxygen in Determining Boron Diffusion in Silicon,” *J. Appl. Phys.*, vol. 67, no. 10, 6135–6140 (1990).
- [6.26] L. Kaabi, C. Gontrand, M. Lemiti, and B. Balland, “Implantation Damage and Anomalous Diffusion of Implanted Boron in Silicon through SiO₂ Films,” *phys. stat. sol. (a)*, vol. 138, 99–109 (1993).
- [6.27] S. Chaudhry and M. E. Law, “Effects of Low Dose Silicon, Carbon, and Oxygen Implantation Damage on Diffusion of Phosphorus in Silicon,” *J. Electrochem. Soc.*, vol. 141, no. 12, 3516–3521 (1994).
- [6.28] K. Kyllesbech Larsen, P. A. Stolk, V. Privitera, J. G. M. van Berkum, W. B. de Boer, G. Mannino, N. E. B. Cowern, and H. G. A. Huizing, “The Effect of Oxygen on the Electrical Activation and Diffusion of Ion-Implanted Boron,” in: *Defects and Diffusion in Silicon Processing*, edited by T. Diaz de la Rubia, S. Coffa, P. A. Stolk, and C. S. Rafferty, *Mat. Res. Soc. Symp. Proc.*, vol. 469, 291–296 (1997).

- [6.29] F. Shimura (Ed.), *Oxygen in Silicon, Semiconductors and Semimetals*, vol. 42, Boston: Academic Press (1994).
- [6.30] R. Jones (Ed.), *Early Stages of Oxygen Precipitation in Silicon, NATO ASI Series 3*, vol. 17, Dordrecht: Kluwer (1996).
- [6.31] W. L. Bond and W. Kaiser, "Interstitial versus Substitutional Oxygen in Silicon," *J. Phys. Chem. Solids*, vol. 16, 44–45 (1960).
- [6.32] W. Kaiser, P. H. Keck, and C. F. Lange, "Infrared Absorption and Oxygen Content in Silicon and Germanium," *Phys. Rev.*, vol. 101, no. 4, 1264–1268 (1956).
- [6.33] H. J. Hrostowski and R. H. Kaiser, "Infrared Absorption of Oxygen in Silicon," *Phys. Rev.*, vol. 107, no. 4, 966–972 (1957).
- [6.34] H. J. Hrostowski and B. J. Alder, "Evidence for Internal Rotation in the Fine Structure of the Infrared Absorption of Oxygen in Silicon," *J. Chem. Phys.*, vol. 33, no. 4, 980–990 (1960).
- [6.35] D. R. Bosomworth, W. Hayes, A. R. L. Spray, and G. D. Watkins, "Absorption of Oxygen in Silicon in the Near and the Far Infrared," *Proc. Roy. Soc. Lond. A*, vol. 317, 133–152 (1970).
- [6.36] J. W. Corbett, R. S. McDonald, and G. D. Watkins, "The Configuration and Diffusion of Isolated Oxygen in Silicon and Germanium," *J. Phys. Chem. Solids*, vol. 25, 873–879 (1964).
- [6.37] M. Stavola, "Infrared Spectrum of Interstitial Oxygen in Silicon," *Appl. Phys. Lett.*, vol. 44, no. 5, 514–516 (1984).
- [6.38] B. Pajot and B. Cales, "Infrared Spectroscopy of Interstitial Oxygen in Silicon," in: *Oxygen, Carbon, Hydrogen and Nitrogen in Crystalline Silicon*, edited by J. C. Mikkelsen, Jr., S. J. Pearton, J. W. Corbett, and S. J. Pennycook, *Mat. Res. Soc. Symp. Proc.*, vol. 59, 39–44 (1986).
- [6.39] H. Yamada-Kaneta, C. Kaneta, and T. Ogawa, "Theory of Local-Phonon-Coupled Low-Energy Anharmonic Excitation of the Interstitial Oxygen in Silicon," *Phys. Rev. B*, vol. 42, no. 15, 9650–9656 (1990).
- [6.40] E. Artacho, A. Lizón-Nordström, and F. Ynduráin, "Geometry and Quantum Delocalization of Interstitial Oxygen in Silicon," *Phys. Rev. B*, vol. 51, no. 12, 7862–7865 (1995).
- [6.41] R. Ramírez, C. P. Herrero, E. Artacho, and F. Ynduráin, "Low-Energy Quantum Dynamics of Atoms at Defects; Interstitial Oxygen in Silicon," *J. Phys.: Condens. Matter*, vol. 9, 3107–3116 (1997).
- [6.42] J. Coutinho, R. Jones, P. R. Briddon, and S. Öberg, "Oxygen and Dioxygen Centers in Si and Ge: Density-Functional Calculations," *Phys. Rev. B*, vol. 62, no. 16, 10824–10840 (2000).
- [6.43] B. Pajot, E. Artacho, C. A. J. Ammerlaan, and J. M. Spaeth, "Interstitial O Isotope Effects in Silicon," *J. Phys.: Condens. Matter*, vol. 7, 7077–7085 (1995).
- [6.44] R. H. Doremus, "Diffusion of Oxygen and Silicon in Silicon: Silicon Monoxide Model," *J. Mater. Res.*, vol. 16, no. 1, 185–191 (2001).
- [6.45] W. C. O'Mara, "Oxygen, Carbon and Nitrogen in Silicon," in: *Handbook of Semiconductor Silicon Technology*, edited by W. C. O'Mara, R. B. Herring, and L. P. Hunt, Park Ridge: Noyes Publications, 451–549 (1992).
- [6.46] H. J. Hrostowski and R. H. Kaiser, "The Solubility of Oxygen in Silicon," *J. Phys. Chem. Solids*, vol. 9, 214–216 (1959).
- [6.47] A. R. Bean and R. C. Newman, "The Solubility of Carbon in Pulled Silicon Crystals," *J. Phys. Chem. Solids*, vol. 32, 1211–1219 (1971).
- [6.48] K. Tempelhoff, F. Spiegelberg, and R. Gleichmann, "Precipitation of Oxygen in Dislocation-Free Silicon," in: *Semiconductor Silicon 1977*, edited by H. R. Huff and E. Sirtl, *Electrochem. Soc. Proc.*, vol. 77-2, 585–595 (1977).
- [6.49] R. A. Craven, "Oxygen Precipitation in Czochralski Silicon," in: *Semiconductor Silicon 1981*, edited by H. R. Huff, R. J. Kriegler, and Y. Takeishi, *Electrochem. Soc. Proc.*, vol. 81-5, 254–271 (1981).

- [6.50] R. C. Newman, M. J. Binns, W. P. Brown, F. M. Livingstone, S. Messoloras, R. J. Stewart, and J. G. Wilkes, "Precipitation of Oxygen in Silicon. Kinetics, Solubility, Diffusivity and Particle Size," in: *Proceedings of the 12th International Conference on Defects in Semiconductors*, edited by C. A. J. Ammerlaan, *Physica*, vol. 116B, 264–270 (1983).
- [6.51] F. M. Livingstone, S. Messoloras, R. C. Newman, B. C. Pike, R. J. Stewart, M. J. Binns, W. P. Brown, and J. G. Wilkes, "An Infrared and Neutron Scattering Analysis of the Precipitation of Oxygen in Dislocation-Free Silicon," *J. Phys. C*, vol. 17, 6253–6276 (1984).
- [6.52] S. Messoloras, R. C. Newman, R. J. Stewart, and J. H. Tucker, "Is Enhanced Interstitial Oxygen Diffusion Necessary to Explain the Kinetics of Precipitation in Silicon at Temperatures below 650 °C," *Semicond. Sci. Technol.*, vol. 2, 14–19 (1987).
- [6.53] R. A. Logan and A. J. Peters, "Diffusion of Oxygen in Silicon," *J. Appl. Phys.*, vol. 30, no. 11, 1627–1630 (1959).
- [6.54] Y. Takano and M. Maki, "Diffusion of Oxygen in Silicon," in: *Semiconductor Silicon 1973*, edited by H. R. Huff and R. R. Burgess, *Electrochem. Soc. Proc.*, vol. 73-1, 469–481 (1973).
- [6.55] Y. Yatsurugi, N. Akiyama, Y. Endo, and T. Nozaki, "Concentration, Solubility, and Equilibrium Distribution Coefficient of Nitrogen and Oxygen in Semiconductor Silicon," *J. Electrochem. Soc.*, vol. 120, no. 7, 975–979 (1973).
- [6.56] J. Gass, H. H. Müller, H. Stüssi, and S. Schweitzer, "Oxygen Diffusion in Silicon and the Influence of Different Dopants," *J. Appl. Phys.*, vol. 51, no. 4, 2030–2037 (1980).
- [6.57] Y. Itoh and T. Nozaki, "Solubility and Diffusion Coefficient of Oxygen in Silicon," *Jpn. J. Appl. Phys.*, vol. 24, no. 3, 279–284 (1985).
- [6.58] J. C. Mikkelsen, Jr., "Excess Solubility of Oxygen in Silicon during Steam Oxidation," *Appl. Phys. Lett.*, vol. 41, no. 9, 871–873 (1982).
- [6.59] J. C. Mikkelsen, Jr., "Oxygen Solubility in Silicon As a Function of Oxidizing Temperature, Ambient, and Wafer Orientation," in: *Defects in Silicon*, edited by W. M. Bullis and L. C. Kimerling, *Electrochem. Soc. Proc.*, vol. 83-9, 95–104 (1983).
- [6.60] S. T. Lee and D. Nichols, "Outdiffusion and Diffusion Mechanism of Oxygen in Silicon," *Appl. Phys. Lett.*, vol. 47, no. 9, 1001–1003 (1985).
- [6.61] T. Ono, G. A. Rozgonyi, E. Asayama, H. Horie, H. Tsuya, and K. Sueoka, "Oxygen Diffusion in Heavily Antimony-, Arsenic-, and Boron-Doped Czochralski Silicon Wafers," *Appl. Phys. Lett.*, vol. 74, no. 24, 3648–3650 (1999).
- [6.62] W. Wijaranakula, "Solubility of Interstitial Oxygen in Silicon," *Appl. Phys. Lett.*, vol. 59, no. 10, 1185–1187 (1991).
- [6.63] J. C. Mikkelsen, Jr., "The Diffusivity and Solubility of Oxygen in Silicon," in: *Oxygen, Carbon, Hydrogen and Nitrogen in Crystalline Silicon*, edited by J. C. Mikkelsen, Jr., S. J. Pearton, J. W. Corbett, and S. J. Pennycook, *Mat. Res. Soc. Symp. Proc.*, vol. 59, 19–30 (1986).
- [6.64] R. C. Newman and R. Jones, "Diffusion of Oxygen in Silicon," in: *Oxygen in Silicon*, edited by F. Shimura, *Semiconductors and Semimetals*, vol. 42, Boston: Academic Press, 289–352 (1994).
- [6.65] H. J. Ruiz and G. P. Pollack, "High Temperature Annealing Behavior of Oxygen in Silicon," *J. Electrochem. Soc.*, vol. 125, no. 1, 128–130 (1978).
- [6.66] Y. Sugita, H. Kawata, S. Nakamichi, T. Okabe, T. Watanabe, S. Yoshikawa, Y. Itoh, and T. Nozaki, "Measurement of the Out-Diffusion Profile of Oxygen in Silicon," *Jpn. J. Appl. Phys.*, vol. 24, no. 10, 1302–1306 (1985).
- [6.67] G. Vakilova, R. F. Vitman, V. B. Voronkov, A. A. Lebedev, and S. Mukhammedov, "Influence of Diffusants on the Distribution of Oxygen in Silicon Containing Dislocations," *Sov. Phys. Semicond.*, vol. 15, no. 7, 830–831 (1981).
- [6.68] G. Vakilova, R. F. Vitman, A. A. Lebedev, and S. Mukhammedov, "Problem of Behavior of Oxygen in Si," *Sov. Phys. Semicond.*, vol. 16, no. 12, 1426–1427 (1982).
- [6.69] J. C. Mikkelsen, Jr., "Diffusivity of Oxygen in Silicon during Steam Oxidation," *Appl. Phys. Lett.*, vol. 40, no. 4, 336–337 (1982).

- [6.70] W. Wijarankula, J. H. Matlock, and H. Mollenkopf, "Oxygen Diffusion in Antimony-Doped Silicon," *Appl. Phys. Lett.*, vol. 53, no. 12, 1068–1070 (1988).
- [6.71] A. S. Oates and W. Lin, "Temperature Dependence of Interstitial Oxygen Diffusion in Antimony-Doped Czochralski Silicon," *Appl. Phys. Lett.*, vol. 53, no. 26, 2659–2660 (1988).
- [6.72] M. Pagani, "Secondary Ion Mass Spectroscopy Determination of Oxygen Diffusion Coefficient in Heavily Sb Doped Si," *J. Appl. Phys.*, vol. 68, no. 7, 3726–3728 (1990).
- [6.73] H. Yamazaki, H. Matsushita, J. Sugamoto, and N. Tsuchiya, "Influence of Annealing Ambient on Oxygen Out-Diffusion in Czochralski Silicon," *J. Appl. Phys.*, vol. 87, no. 9, 4194–4197 (2000).
- [6.74] H. Takeno, K. Sunakawa, and M. Suezawa, "Temperature-Dependent Retardation Effect of Dopants on Oxygen Diffusion in Heavily Doped Czochralski Silicon," *Appl. Phys. Lett.*, vol. 77, no. 3, 376–378 (2000).
- [6.75] C. Haas, "The Diffusion of Oxygen in Silicon and Germanium," *J. Phys. Chem. Solids*, vol. 15, 108–111 (1960).
- [6.76] P. D. Southgate, "Internal Friction in Germanium and Silicon II: Oxygen Movement and Dislocation Damping," *Proc. Phys. Soc. (London)*, vol. 76, 398–408 (1960).
- [6.77] S. Senkader, K. Jurkschat, D. Gambaro, R. J. Falster, and P. R. Wilshaw, "On the Locking of Dislocations by Oxygen in Silicon," *Phil. Mag. A*, vol. 81, no. 3, 759–775 (2001).
- [6.78] F. S. Ham, "Theory of Diffusion-Limited Precipitation," *J. Phys. Chem. Solids*, vol. 6, 335–351 (1958).
- [6.79] K. Wada, N. Inoue, and K. Kohara, "Diffusion-Limited Growth of Oxide Precipitates in Czochralski Silicon," *J. Crystal Growth*, vol. 49, 749–752 (1980).
- [6.80] M. J. Binns, W. P. Brown, J. G. Wilkes, R. C. Newman, F. M. Livingston, S. Messoloras, and R. J. Stewart, "Diffusion Limited Precipitation of Oxygen in Dislocation-Free Silicon," *Appl. Phys. Lett.*, vol. 42, no. 6, 525–527 (1983).
- [6.81] R. C. Newman, M. Claybourn, S. H. Kinder, S. Messoloras, A. S. Oates, and R. J. Stewart, "Precipitation of Oxygen at Low Temperatures," in: *Semiconductor Silicon*, edited by H. R. Huff, T. Abe, and B. Kolbesen, *Electrochem. Soc. Proc.*, vol. 86-4, 766–777 (1986).
- [6.82] J. L. Benton, L. C. Kimerling, and M. Stavola, "The Oxygen Related Donor Effect in Silicon," in: *Proceedings of the 12th International Conference on Defects in Semiconductors*, edited by C. A. J. Ammerlaan, *Physica*, vol. 116B, 271–275 (1983).
- [6.83] M. Stavola, J. R. Patel, L. C. Kimerling, and P. E. Freeland, "Diffusivity of Oxygen in Silicon at the Donor Formation Temperature," *Appl. Phys. Lett.*, vol. 42, no. 1, 73–75 (1983).
- [6.84] R. C. Newman, H. H. Tucker, and F. M. Livingston, "Radiation-Enhanced Diffusion of Oxygen in Silicon at Room Temperature," *J. Phys. C*, vol. 16, L151–L156 (1983).
- [6.85] D. Heck, R. E. Tressler, and J. Monkowski, "The Effects of Processing Conditions on the Out-Diffusion of Oxygen from Czochralski Silicon," *J. Appl. Phys.*, vol. 54, no. 10, 5739–5743 (1983).
- [6.86] F. Shimura, T. Higuchi, and R. S. Hockett, "Outdiffusion of Oxygen and Carbon in Czochralski Silicon," *Appl. Phys. Lett.*, vol. 53, no. 1, 69–71 (1988).
- [6.87] C. Maddalon-Vinante, D. Barbier, H. Erramli, and G. Blondiaux, "Charged Particle Activation Analysis Study of the Oxygen Outdiffusion from Czochralski-Grown Silicon during Classical and Rapid Thermal Annealing in Various Gas Ambients," *J. Appl. Phys.*, vol. 74, no. 10, 6115–6119 (1993).
- [6.88] S. T. Lee, P. Fellinger, and S. Chen, "Enhanced and Wafer-Dependent Oxygen Diffusion in CZ-Si at 500–700 °C," *J. Appl. Phys.*, vol. 63, no. 6, 1924–1927 (1988).
- [6.89] Y. Tokuda, M. Katayama, and T. Hattori, "Depth Profiles of Thermal Donors Formed at 450 °C in Oxygen-Rich n-Type Silicon," *Semicond. Sci. Technol.*, vol. 8, 163–166 (1993).
- [6.90] S. A. McQuaid, B. K. Johnson, D. Gambaro, R. Falster, M. J. Ashwin, and J. H. Tucker, "The Conversion of Isolated Oxygen Atoms to a Fast Diffusing Species in Czochralski Silicon at Low Temperatures," *J. Appl. Phys.*, vol. 86, no. 4, 1878–1887 (1999).

- [6.91] R. C. Newman, A. K. Tipping, and J. H. Tucker, "The Effect of Metallic Contamination on Enhanced Oxygen Diffusion in Silicon at Low Temperatures," *J. Phys. C*, vol. 18, L861–L866 (1985).
- [6.92] A. K. Tipping, R. C. Newman, D. C. Newton, and J. H. Tucker, "Enhanced Oxygen Diffusion in Silicon at Low Temperatures," in: *Defects in Semiconductors 14*, edited by H. J. von Bardeleben, *Materials Science Forum*, vol. 10-12, 887–892 (1986).
- [6.93] M. Stavola and L. C. Snyder, "Oxygen Aggregation and Diffusivity in Silicon," in: *Defects in Silicon*, edited by W. M. Bullis and L. C. Kimerling, *Electrochem. Soc. Proc.*, vol. 83-9, 61–75 (1983).
- [6.94] W. Bergholz, J. L. Hutchison, and P. Pirouz, "Precipitation of Oxygen at 485 °C: Direct Evidence for Accelerated Diffusion of Oxygen in Silicon?" *J. Appl. Phys.*, vol. 58, no. 9, 3419–3424 (1985).
- [6.95] A. Bourret, "Defects Induced by Oxygen Precipitation in Silicon: A New Hypothesis Involving Hexagonal Silicon," in: *Microscopy of Semiconducting Materials, 1987*, edited by A. G. Cullis and P. D. Augustus, *Inst. Phys. Conf. Ser.*, no. 87, 39–48 (1987).
- [6.96] W. Kaiser, H. L. Frisch, and H. Reiss, "Mechanism of the Formation of Donor States in Heat-Treated Silicon," *Phys. Rev.*, vol. 112, no. 5, 1546–1554 (1958).
- [6.97] C. S. Fuller, F. H. Doleiden, and K. Wolfstirn, "Reactions of Group III Acceptors with Oxygen in Silicon Crystals," *J. Phys. Chem. Solids*, vol. 13, 187–203 (1960).
- [6.98] U. Gösele and T. Y. Tan, "Oxygen Diffusion and Thermal Donor Formation in Silicon," *Appl. Phys. A*, vol. 28, 79–92 (1982).
- [6.99] A. Ourmazd, W. Schröter, and A. Bourret, "Oxygen-Related Thermal Donors in Silicon: A New Structural and Kinetic Model," *J. Appl. Phys.*, vol. 56, no. 6, 1670–1681 (1984).
- [6.100] Y. Kamiura, F. Hashimoto, and K. Endo, "Initial Generation Kinetics of Oxygen-Related Thermal Donors at 430 °C in Silicon," *J. Appl. Phys.*, vol. 61, no. 7, 2478–2485 (1987).
- [6.101] D. Åberg, B. G. Svensson, T. Hallberg, and J. L. Lindström, "Kinetic Study of Oxygen Dimer and Thermal Donor Formation in Silicon," *Phys. Rev. B*, vol. 58, no. 19, 12944–12951 (1998).
- [6.102] H. J. Stein, S. K. Hahn, and S. C. Shatas, "Rapid Thermal Annealing and Regrowth of Thermal Donors in Silicon," *J. Appl. Phys.*, vol. 59, no. 10, 3495–3502 (1986).
- [6.103] M. Claybourn and R. C. Newman, "Activation Energy for Thermal Donor Formation in Silicon," *Appl. Phys. Lett.*, vol. 51, no. 26, 2197–2199 (1987).
- [6.104] V. P. Markevich, L. F. Makarenko, and L. L. Murin, "Thermal Donor Formation and Mechanism of Enhanced Oxygen Diffusion in Silicon," in: *Defects in Semiconductors 15*, edited by G. Ferenczi, *Materials Science Forum*, vol. 38-41, 589–594 (1989).
- [6.105] R. C. Newman and M. Claybourn, "The Kinetics of Thermal Donor Formation in Silicon," in: *Shallow Impurities in Semiconductors, 1988*, edited by B. Monemar, *Inst. Phys. Conf. Ser.*, no. 95, 211–220 (1989).
- [6.106] A. R. Brown, R. Murray, R. C. Newman, and J. H. Tucker, "Measurement of Enhanced Oxygen Diffusion in Silicon during Thermal Donor Formation: New Evidence for Possible Mechanisms," in: *Impurities, Defects and Diffusion in Semiconductors: Bulk and Layered Structures*, edited by D. J. Wolford, J. Bernholc, and E. E. Haller, *Mat. Res. Soc. Symp. Proc.*, vol. 163, 555–560 (1990).
- [6.107] G. S. Oehrlein, J. L. Lindström, and S. A. Cohen, "A Kinetic Study of Oxygen-Related Thermal Donor Formation," in: *Thirteenth International Conference on Defects in Semiconductors*, edited by L. C. Kimerling and J. M. Parsey, Jr., The Metallurgical Society of AIME, 701–708 (1985).
- [6.108] P. Gaworzewski and G. Ritter, "On the Out-Diffusion of Oxygen from Silicon," *phys. stat. sol. (a)*, vol. 67, 511–516 (1981).
- [6.109] S. Hahn, "Formation of a Low Thermal Donor Concentration Layer in Cz Si Wafer during 450°C/64h Annealing," in: *Oxygen, Carbon, Hydrogen, and Nitrogen in Crystalline Silicon*, edited by J. C. Mikkelsen, Jr., S. J. Pearton, J. W. Corbett, and S. J. Pennycook, *Mat. Res. Soc. Symp. Proc.*, vol. 59, 181–186 (1986).

- [6.110] H. Takeno, Y. Hayamizu, and K. Miki, "Diffusivity of Oxygen in Czochralski Silicon at 400–750 °C," *J. Appl. Phys.*, vol. 84, no. 6, 3113–3117 (1998).
- [6.111] S. Senkader, P. R. Wilshaw, and R. J. Falster, "Oxygen-Dislocation Interactions in Silicon at Temperatures below 700 °C: Dislocation Locking and Oxygen Diffusion," *J. Appl. Phys.*, vol. 89, no. 9, 4803–4808 (2001).
- [6.112] R. C. Newman, A. R. Brown, R. Murray, A. K. Tipping, and J. H. Tucker, "Enhanced Thermal Donor Formation and Oxygen Diffusion in Silicon Exposed to Atomic Hydrogen," in: *Semiconductor Silicon 1990*, edited by H. R. Huff, K. G. Barraclough, and J.-i. Chikawa, *Electrochem. Soc. Proc.*, vol. 90-7, 734–745 (1990).
- [6.113] R. C. Newman, J. H. Tucker, A. R. Brown, and S. A. McQuaid, "Hydrogen Diffusion and the Catalysis of Enhanced Oxygen Diffusion in Silicon at Temperatures below 500 °C," *J. Appl. Phys.*, vol. 70, no. 6, 3061–3070 (1991).
- [6.114] L. Zhong and F. Shimura, "Hydrogen Enhanced Out-Diffusion of Oxygen in Czochralski Silicon," *J. Appl. Phys.*, vol. 73, no. 2, 707–710 (1993).
- [6.115] L. I. Murin, V. P. Markevich, M. Suezawa, J. L. Lindström, M. Kleverman, and T. Hallberg, "Early Stages of Oxygen Clustering in Hydrogenated Cz-Si: Infrared Absorption Studies," *Physica B*, vol. 302-303, 180–187 (2001).
- [6.116] N. M. Johnson, S. K. Hahn, and H. J. Stein, "Selective Hydrogen Passivation of Oxygen-Related Thermal-Donor Clusters in Silicon," in: *Defects in Semiconductors 14*, edited by H. J. von Bardeleben, *Materials Science Forum*, vol. 10-12, 585–590 (1986).
- [6.117] A. R. Brown, M. Claybourn, R. Murray, P. S. Nandhra, R. C. Newman, and J. H. Tucker, "Enhanced Thermal Donor Formation in Silicon Exposed to a Hydrogen Plasma," *Semicond. Sci. Technol.*, vol. 3, 591–593 (1988).
- [6.118] V. P. Markevich, L. I. Murin, and A. G. Litvinko, "Accelerated Formation of Thermal Donors in Hydrogen-Saturated Si(O) Crystals," *Tech. Phys. Lett.*, vol. 19, 617–618 (1993).
- [6.119] H. J. Stein and S. Hahn, "Hydrogen Introduction and Hydrogen-Enhanced Thermal Donor Formation in Silicon," *J. Appl. Phys.*, vol. 75, no. 7, 3477–3484 (1994).
- [6.120] H. Takeno, K. Aihara, Y. Hayamizu, T. Masui, and M. Suezawa, "Influence of Rapid Thermal Annealing on Thermal Donor Formation and Oxygen Precipitation in Czochralski Silicon," in: *Defects in Silicon III*, edited by T. Abe, W. M. Bullis, S. Kobayashi, W. Lin, and P. Wagner, *Electrochem. Soc. Proc.*, vol. 99-1, 150–161 (1999).
- [6.121] R. Murray, A. R. Brown, and R. C. Newman, "Enhanced Thermal Donor Formation and Oxygen Diffusion in Silicon Exposed to a Hydrogen Plasma," *Materials Science and Engineering B*, vol. 4, 299–302 (1989).
- [6.122] S. A. McQuaid, M. J. Binns, C. A. Londos, J. H. Tucker, A. R. Brown, and R. C. Newman, "Oxygen Loss during Thermal Donor Formation in Czochralski Silicon: New Insights into Oxygen Diffusion Mechanisms," *J. Appl. Phys.*, vol. 77, no. 4, 1427–1442 (1995).
- [6.123] V. P. Markevich, L. I. Murin, J. L. Lindström, and M. Suezawa, "Early Stages of Oxygen Precipitation in Silicon: The Effect of Hydrogen," *Semiconductors*, vol. 34, no. 9, 998–1003 (2000).
- [6.124] A. Hara, M. Koizuka, M. Aoki, T. Fukuda, H. Yamada-Kaneta, and H. Mori, "Influence of Grown-in Hydrogen on Thermal Donor Formation and Oxygen Precipitation in Czochralski Silicon Crystals," *Jpn. J. Appl. Phys., Part 1*, vol. 33, no. 10, 5577–5584 (1994).
- [6.125] M. Koizuka, A. Hara, and H. Yamada-Kaneta, "A New Method of Measuring Hydrogen Concentrations of As-Grown Czochralski Si Crystals," *Electrochem. Soc. Extended Abstracts*, vol. 95-2, no. 515, 821–822 (1995).
- [6.126] S. K. Estreicher, "Interstitial O in Si and Its Interactions with H," *Phys. Rev. B*, vol. 41, no. 14, 9886–9891 (1990).
- [6.127] M. Ramamoorthy and S. T. Pantelides, "Enhanced Modes of Oxygen Diffusion in Silicon," *Solid State Communications*, vol. 106, no. 5, 243–248 (1998).

- [6.128] R. B. Capaz, L. V. C. Assali, L. C. Kimerling, K. Cho, and J. D. Joannopoulos, “Mechanism for Hydrogen-Enhanced Oxygen Diffusion in Silicon,” *Phys. Rev. B*, vol. 59, no. 7, 4898–4900 (1999).
- [6.129] V. P. Markevich, I. F. Medvedeva, and L. I. Murin, “Effect of Hydrogen on Oxygen-Related Defect Reactions in Silicon at Elevated Temperatures,” in: *Early Stages of Oxygen Precipitation in Silicon*, edited by R. Jones, *NATO ASI Series 3*, vol. 17, Dordrecht: Kluwer, 103–122 (1996).
- [6.130] W. Wijaranakula, “Oxygen Diffusion in Carbon-Doped Silicon,” *J. Appl. Phys.*, vol. 68, no. 12, 6538–6540 (1990).
- [6.131] V. V. Voronkov, “Generation of Thermal Donors in Silicon: Oxygen Aggregation Controlled by Self-Interstitials,” *Semicond. Sci. Technol.*, vol. 8, 2037–2047 (1993).
- [6.132] L. I. Murin and V. P. Markevich, “Thermal Double Donors in Silicon: A New Insight into the Problem,” in: *Early Stages of Oxygen Precipitation in Silicon*, edited by R. Jones, *NATO ASI Series 3*, vol. 17, Dordrecht: Kluwer, 329–336 (1996).
- [6.133] J. Coutinho, R. Jones, L. I. Murin, V. P. Markevich, J. L. Lindström, S. Öberg, and P. R. Briddon, “Thermal Double Donors and Quantum Dots,” *Phys. Rev. Lett.*, vol. 87, no. 23, 235501 (2001).
- [6.134] Y. J. Lee, J. von Boehm, M. Pesola, and R. M. Nieminen, “First-Principles Study of Migration, Restructuring, and Dissociation Energies of Oxygen Complexes in Silicon,” *Phys. Rev. B*, vol. 65, 085205 (2002).
- [6.135] C. S. Chen, F. Q. Zeng, Y. X. Huang, H. J. Ye, C. M. Hu, and D. K. Schroder, “Thermal Configuration of Oxygen in Silicon,” *Appl. Phys. A*, vol. 55, 317–323 (1992).
- [6.136] C. A. Londos, L. G. Fytros, and G. J. Georgiou, “IR Studies of Oxygen-Vacancy Related Defects in Irradiated Silicon,” in: *Defects and Diffusion in Semiconductors: An Annual Retrospective II*, edited by D. J. Fisher, *Defect and Diffusion Forum*, vol. 171–172, 1–31 (1999).
- [6.137] G. Bemski, G. Feher, and E. Gere, “Spin Resonance in Electron Irradiated Silicon,” *Bull. Am. Phys. Soc., Series II*, vol. 3, 135 (1958).
- [6.138] G. D. Watkins, J. W. Corbett, and R. M. Walker, “Spin Resonance in Electron Irradiated Silicon,” *J. Appl. Phys.*, vol. 30, no. 8, 1198–1203 (1959).
- [6.139] G. D. Watkins, “A Review of EPR Studies in Irradiated Silicon,” in: *Radiation Damage in Semiconductors*, Paris: Dunod, 97–113 (1964).
- [6.140] G. K. Wertheim, “Energy Levels in Electron-Bombarded Silicon,” *Phys. Rev.*, vol. 105, no. 6, 1730–1735 (1957).
- [6.141] G. K. Wertheim, “Electron-Bombardment Damage in Silicon,” *Phys. Rev.*, vol. 110, no. 6, 1272–1279 (1958).
- [6.142] D. E. Hill, “Electron Bombardment of Silicon,” *Phys. Rev.*, vol. 114, no. 6, 1414–1420 (1959).
- [6.143] E. Sonder and L. C. Templeton, “Gamma Irradiation of Silicon. I. Levels in n-Type Materials Containing Oxygen,” *J. Appl. Phys.*, vol. 31, no. 7, 1279–1286 (1960).
- [6.144] E. Sonder and L. C. Templeton, “Gamma Irradiation of Silicon. II. Levels in n-Type Float-Zone Material,” *J. Appl. Phys.*, vol. 34, no. 11, 3295–3301 (1963).
- [6.145] G. Bemski, “Paramagnetic Resonance in Electron Irradiated Silicon,” *J. Appl. Phys.*, vol. 30, no. 8, 1195–1198 (1959).
- [6.146] G. D. Watkins and J. W. Corbett, “Defects in Irradiated Silicon. I. Electron Spin Resonance of the Si-A Center,” *Phys. Rev.*, vol. 121, no. 4, 1001–1014 (1961).
- [6.147] K. L. Brower, “Electron Paramagnetic Resonance of the Neutral (S=1) One-Vacancy-Oxygen Center in Irradiated Silicon,” *Phys. Rev. B*, vol. 4, no. 6, 1968–1982 (1971).
- [6.148] K. L. Brower, “¹⁷O Hyperfine Structure of the Neutral (S=1) Vacancy-Oxygen Center in Ion-Implanted Silicon,” *Phys. Rev. B*, vol. 5, no. 11, 4274–4280 (1972).
- [6.149] P. R. Brosious, “EPR Evidence for a Positively Charged Vacancy-Oxygen Defect in Silicon,” *Appl. Phys. Lett.*, vol. 29, no. 4, 265–267 (1976).

- [6.150] R. van Kemp, E. G. Sieverts, and C. A. J. Ammerlaan, "The Electronic Structure of the Oxygen-Vacancy Complex in Silicon," in: *Defects in Semiconductors 14*, edited by H. J. von Bardeleben, *Materials Science Forum*, vol. 10-12, 875–880 (1986).
- [6.151] J. W. Corbett, G. D. Watkins, R. M. Chrenko, and R. S. McDonald, "Defects in Irradiated Silicon. II. Infrared Absorption of the Si-A Center," *Phys. Rev.*, vol. 121, no. 4, 1015–1022 (1961).
- [6.152] A. K. Ramdas and M. G. Rao, "Infrared Absorption Spectra of Oxygen-Defect Complexes in Irradiated Silicon," *Phys. Rev.*, vol. 142, no. 2, 451–456 (1966).
- [6.153] A. R. Bean and R. C. Newman, "An Infra-Red Study of Defects Produced in n-Type Silicon by Electron Irradiation at Low Temperatures," *Solid State Communications*, vol. 9, 271–274 (1971).
- [6.154] R. C. Young and J. C. Corelli, "Photoconductivity Studies of Radiation-Induced Defects in Silicon," *Phys. Rev. B*, vol. 5, no. 4, 1455–1467 (1972).
- [6.155] J. W. Walker and C. T. Sah, "Properties of 1.0-MeV-Electron-Irradiated Defect Centers in Silicon," *Phys. Rev. B*, vol. 7, no. 10, 4587–4605 (1973).
- [6.156] L. C. Kimerling, "Defect States in Electron-Bombarded Silicon: Capacitance Transient Analyses," in: *Radiation Effects in Semiconductors, 1976*, edited by N. B. Urli and J. W. Corbett, *Inst. Phys. Conf. Ser.*, no. 31, 221–230 (1977).
- [6.157] S. D. Brotherton and P. Bradley, "Defect Production and Lifetime Control in Electron and gamma-Irradiated Silicon," *J. Appl. Phys.*, vol. 53, no. 8, 5720–5732 (1982).
- [6.158] J. M. Meese, J. W. Farmer, and C. D. Lamp, "Defect Symmetry from Stress Transient Spectroscopy," *Phys. Rev. Lett.*, vol. 51, no. 14, 1286–1289 (1983).
- [6.159] K. L. Brower, "Structure of Multiple-Vacancy (Oxygen) Centers in Irradiated Silicon," in: *Radiation Effects in Semiconductors*, edited by J. W. Corbett and G. D. Watkins, New York: Gordon and Breach, 189–195 (1971).
- [6.160] A. M. Frens, "Observation of Rapid Direct Charge Transfer between Deep Defects in Silicon," *Phys. Rev. Lett.*, vol. 72, no. 18, 2939–2942 (1994).
- [6.161] L. F. Makarenko, "Re-Evaluation of Energy Levels of Oxygen-Vacancy Complex in n-Type Silicon Crystals: I. Weak Compensation," *Semicond. Sci. Technol.*, vol. 16, 619–630 (2001).
- [6.162] J. L. Lindström, L. I. Murin, V. P. Markevich, T. Hallberg, and B. G. Svensson, "Vibrational Absorption from Vacancy-Oxygen-Related Complexes (VO, V₂O, VO₂) in Irradiated Silicon," in: *20th International Conference on Defects in Semiconductors*, edited by C. Van de Walle and W. Walukiewicz, *Physica B*, vol. 273-274, 291–295 (1999).
- [6.163] L. I. Murin, V. P. Markevich, T. Hallberg, and J. L. Lindström, "New Infrared Vibrational Bands Related to Interstitial and Substitutional Oxygen in Silicon," in: *Gettering and Defect Engineering in Semiconductor Technology GADEST'99*, edited by H. G. Grimmeiss, L. Ask, M. Kleverman, M. Kittler, and H. Richter, *Solid State Phenomena*, vol. 69–70, 309–314 (1999).
- [6.164] G. A. Samara and C. E. Barnes, "Lattice Relaxation Accompanying Carrier Capture and Emission by Deep Electronic Levels in Semiconductors," *Phys. Rev. Lett.*, vol. 57, no. 16, 2069–2072 (1986).
- [6.165] P. Mascher, S. Dannefaer, and D. Kerr, "Positron Trapping Rates and Their Temperature Dependencies in Electron-Irradiated Silicon," *Phys. Rev. B*, vol. 40, no. 17, 11764–11771 (1989).
- [6.166] S. Mäkinen, H. Rajainmäki, and S. Linderoth, "Low-Temperature Positron-Lifetime Studies of Proton-Irradiated Silicon," *Phys. Rev. B*, vol. 42, no. 17, 11166–11173 (1990).
- [6.167] A. Li, H. Huang, D. Li, S. Zheng, H. Du, S. Zhu, and T. Iwata, "A Positron Lifetime Study of Defects in Neutron-Irradiated Si," *Jpn. J. Appl. Phys., Part 1*, vol. 32, no. 3A, 1033–1038 (1993).
- [6.168] A. Ikari, H. Haga, A. Oedono, Y. Ujihira, and O. Yoda, "Oxygen Clusters in Quenched Czochralski-Si Studied by Infrared Spectroscopy and Positron Annihilation," *Jpn. J. Appl. Phys., Part 1*, vol. 33, no. 4A, 1723–1727 (1994).

- [6.169] H. J. Stein, "Interactions of Implanted Carbon with Oxygen and Nitrogen in Silicon," in: *Defects in Electronic Materials*, edited by M. Stavola, S. J. Pearton, and G. Davies, *Mat. Res. Soc. Symp. Proc.*, vol. 104, 173–178 (1988).
- [6.170] H. P. Hjalmarson and D. R. Jennison, "Investigation of Off-Center Substitutional N in Si," *Phys. Rev. B*, vol. 31, no. 2, 1208–1211 (1985).
- [6.171] D. Deak, L. C. Snyder, J. W. Corbett, R. Z. Wu, and A. Solyom, "One- and Two-Oxygen Defects in Silicon — A Theoretical Study," in: *Defects in Semiconductors 15*, edited by G. Ferenczi, *Materials Science Forum*, vol. 38-41, 281–286 (1989).
- [6.172] D. J. Chadi, "Oxygen-Oxygen Complexes and Thermal Donors in Silicon," *Phys. Rev. B*, vol. 41, no. 15, 10595–10603 (1990).
- [6.173] D. J. Chadi, "Core Structure of Thermal Donors in Silicon," *Phys. Rev. Lett.*, vol. 77, no. 5, 861–864 (1996).
- [6.174] A. B. Van Oosten, "Ab Initio Cluster Theory of Substitutional Oxygen in Silicon," in: *Defects in Semiconductors 17*, edited by H. Heinrich and W. Jantsch, *Materials Science Forum*, vol. 143-147, 1299–1304 (1994).
- [6.175] P. J. Kelly, "Equilibrium Geometries and Electronic Structure of Oxygen Related Defects in Silicon," in: *Defects in Semiconductors 15*, edited by G. Ferenczi, *Materials Science Forum*, vol. 38-41, 269–274 (1989).
- [6.176] N. I. Boyarkina, S. A. Smagulova, and A. A. Artem'ev, "Dissociation Energies of a C_1C_s Complex and the A Center in Silicon," *Semiconductors*, vol. 35, no. 8, 845–847 (2002).
- [6.177] M. Pesola, J. von Boehm, T. Mattila, and R. M. Nieminen, "Computational Study of Interstitial Oxygen and Vacancy-Oxygen Complexes in Silicon," *Phys. Rev. B*, vol. 60, no. 16, 11449–11463 (1999).
- [6.178] R. A. Casali, H. Rücker, and M. Methfessel, "Interaction of Vacancies with Interstitial Oxygen in Silicon," *Appl. Phys. Lett.*, vol. 78, no. 7, 913–915 (2001).
- [6.179] A. Hallén, N. Keskitalo, F. Masszi, and V. Nágli, "Lifetime in Proton Irradiated Silicon," *J. Appl. Phys.*, vol. 79, no. 8, 3906–3014 (1996).
- [6.180] H. Bleichner, P. Jonsson, N. Keskitalo, and E. Nordlander, "Temperature and Injection Dependence of the Shockley-Read-Hall Lifetime in Electron Irradiated n-Type Silicon," *J. Appl. Phys.*, vol. 79, no. 12, 9142–9148 (1996).
- [6.181] A. M. Ivanov, N. B. Strokan, and V. B. Shuman, "Properties of p^+ -n Structures with a Buried Layer of Radiation-Induced Defects," *Semiconductors*, vol. 32, no. 3, 325–331 (1998).
- [6.182] D. C. Sawko and J. Bartko, "Production of Fast Switching Power Thyristors by Proton Irradiation," *IEEE Trans. Nuclear Science*, vol. NS-30, no. 2, 1756–1758 (1983).
- [6.183] A. Mogro-Campero, R. P. Love, M. F. Chang, and R. Dyer, "Localized Lifetime Control in Insulated-Gate Transistors by Proton Implantation," *IEEE Trans. Electron Devices*, vol. ED-33, no. 11, 1667–1671 (1986).
- [6.184] G. G. DeLeo, W. B. Fowler, and G. D. Watkins, "Theory of Off-Center Impurities in Silicon: Substitutional Nitrogen and Oxygen," *Phys. Rev. B*, vol. 29, no. 6, 3193–3207 (1984).
- [6.185] L. Dobaczewski, O. Andersen, L. Rubaldo, K. Gościński, V. P. Markevich, A. R. Peaker, and K. Bonde Nielsen, "Saddle Point for Oxygen Reorientation in the Vicinity of a Silicon Vacancy," *Phys. Rev. B*, vol. 19, 195204 (2003).
- [6.186] B. G. Svensson, J. L. Lindström, and J. W. Corbett, "Growth of the 889 cm^{-1} Infrared Band in Annealed Electron-Irradiated Silicon," *Appl. Phys. Lett.*, vol. 47, no. 8, 841–843 (1985).
- [6.187] C. Londos, N. V. Sarlis, and L. Fytros, "Isochronal Annealing Studies of the Oxygen-Vacancy Centres in Neutron-Irradiated Si," *phys. stat. sol. (a)*, vol. 163, 325–335 (1997).
- [6.188] C. A. Londos, N. V. Sarlis, and L. G. Fytros, "An IR Study of the Annealing Behaviour of A-Center in Silicon," in: *Gettering and Defect Engineering in Semiconductor Technology GADEST'97*, edited by C. Claeys, J. Vanhellemont, H. Richter, and M. Kittler, *Solid State Phenomena*, vol. 57-58, 245–250 (1997).

- [6.189] C. A. Londos, N. V. Sarlis, and L. G. Fytros, "Infrared Studies of Defects Formed during Postirradiation Anneals of Czochralski Silicon," *J. Appl. Phys.*, vol. 84, no. 7, 3569 (1998).
- [6.190] B. G. Svensson and J. L. Lindström, "Kinetic Study of the 830- and 889-cm⁻¹ Infrared Bands during Annealing of Irradiated Silicon," *Phys. Rev. B*, vol. 34, no. 12, 8709–8717 (1986).
- [6.191] P. Pellegrino, P. Lévéque, J. Lalita, A. Hallén, C. Jagadish, and B. G. Svensson, "Annealing Kinetics of Vacancy-Related Defects in Low-Dose MeV Self-Ion-Implanted *n*-Type Silicon," *Phys. Rev. B*, vol. 64, 195211 (2001).
- [6.192] P. J. Grönberg, J. von Boehm, and R. M. Nieminen, "Molecular Dynamics Study of Oxygen Defects in Silicon," in: *Early Stages of Oxygen Precipitation in Silicon*, edited by R. Jones, *NATO ASI Series 3*, vol. 17, Dordrecht: Kluwer, 441–446 (1996).
- [6.193] A. S. Oates and R. C. Newman, "Involvement of Oxygen-Vacancy Defects in Enhancing Oxygen Diffusion in Silicon," *Appl. Phys. Lett.*, vol. 49, no. 5, 262–264 (1986).
- [6.194] G. D. Watkins, "EPR Studies of the Lattice Vacancy and Low-Temperature Damage Processes in Silicon," in: *Lattice Defects in Semiconductors, 1974, Inst. Phys. Conf. Ser.*, no. 23, 1–22 (1975).
- [6.195] K. A. Abdullin and B. N. Mukashev, "Vacancy Defect in Silicon Single Crystals Bombarded at 77 K," *Semiconductors*, vol. 29, no. 2, 169–174 (1995).
- [6.196] J. W. Corbett, G. D. Watkins, and R. S. McDonald, "New Oxygen Infrared Bands in Annealed Irradiated Silicon," *Phys. Rev.*, vol. 135, no. 5A, A1381–A1385 (1964).
- [6.197] J. L. Lindström, G. S. Oehrlein, and J. W. Corbett, "A Study of the Annealing of the 830 cm⁻¹ IR Band Observed in Electron-Irradiated Silicon," *phys. stat. sol. (a)*, vol. 95, 179–184 (1986).
- [6.198] J. L. Lindström and B. G. Svensson, "Oxygen-Related Defects in Silicon," in: *Oxygen, Carbon, Hydrogen, and Nitrogen in Crystalline Silicon*, edited by J. C. Mikkelsen, Jr., S. J. Pearton, J. W. Corbett, and S. J. Pennycook, *Mat. Res. Soc. Symp. Proc.*, vol. 59, 45–58 (1986).
- [6.199] F. A. Abou-el-Fotouh and R. C. Newman, "Electron Irradiation Damage in Silicon Containing Carbon and Diffused ¹⁸O," *Solid State Communications*, vol. 15, 1409–1411 (1974).
- [6.200] H. J. Stein, "Oxygen Isotope Effect on the 889 cm⁻¹ Band in Silicon," *Appl. Phys. Lett.*, vol. 48, no. 22, 1540–1541 (1986).
- [6.201] G. G. DeLeo, C. S. Milsted, Jr., and J. C. Kralik, "Substitutional Oxygen-Oxygen Pair in Silicon," *Phys. Rev. B*, vol. 31, no. 6, 3588–3592 (1985).
- [6.202] V. V. Voronkov and R. Falster, "Grown-in Microdefects, Residual Vacancies and Oxygen Precipitation Bands in Czochralski Silicon," *Journal of Crystal Growth*, vol. 204, 462–474 (1999).
- [6.203] R. Falster, V. V. Voronkov, and F. Quast, "On the Properties of the Intrinsic Point Defects in Silicon: A Perspective from Crystal Growth and Wafer Processing," *phys. stat. sol. (b)*, vol. 222, 219–244 (2000).
- [6.204] J. Svensson, B. G. Svensson, and J. L. Lindström, "Thermal Donor Formation in Electron-Irradiated Czochralski Silicon," *Appl. Phys. Lett.*, vol. 49, no. 21, 1435–1437 (1986).
- [6.205] Y. V. Pomozov, L. I. Khirunenko, V. I. Shakhovtsov, and V. I. Yashnik, "Transformation of Point Defects by Annealing Neutron-Irradiated Si and Si:Ge," *Sov. Phys. Semicond.*, vol. 24, no. 6, 624–626 (1990).
- [6.206] C. A. Londos, G. I. Georgiou, L. G. Fytros, and K. Papastergiou, "Interpretation of Infrared Data in Neutron-Irradiated Silicon," *Phys. Rev. B*, vol. 50, no. 16, 11531–11534 (1994).
- [6.207] C. A. Londos, N. Sarlis, L. G. Fytros, and K. Papastergiou, "Precursor Defect to the Vacancy-Dioxygen Center in Si," *Phys. Rev. B*, vol. 53, no. 11, 6900–6903 (1996).
- [6.208] J. L. Lindström, L. I. Murin, B. G. Svensson, V. P. Markevich, and T. Hallberg, "The VO₂* Defect in Silicon," in: *Proceedings of the 22nd International Conference on Defects in Semiconductors*, edited by K. Bonde Nielsen, A. Nylandsted Larsen, and G. Weyer, *Physica B*, vol. 340-342, 509–513 (2003).
- [6.209] H. J. Stein, "Ion-Implanted Oxygen Isotopes in Silicon," in: *Defects in Semiconductors 14*, edited by H. J. von Bardeleben, *Materials Science Forum*, vol. 10-12, 935–940 (1986).

- [6.210] P. Deák, L. C. Snyder, and J. W. Corbett, “Theoretical Studies on the Core Structure of the 450 °C Oxygen Thermal Donors in Silicon,” *Phys. Rev. B*, vol. 45, no. 20, 11612–11626 (1992).
- [6.211] T. Maekawa, S. Inone, and A. Usami, “Hole Trap Annealing in Neutron-Transmutation-Doped Silicon with Different Initial Resistivities,” *Semicond. Sci. Technol.*, vol. 5, 663–668 (1990).
- [6.212] Y. M. Dobrovinskii, S. Makhamov, A. Mirzaev, V. I. Mitin, and N. A. Tursunov, “Influence of Heat-Radiation Treatment on the Process of Formation of Defect Centers in Silicon by Electron Irradiation,” *Sov. Phys. Semicond.*, vol. 25, no. 3, 316–319 (1991).
- [6.213] C. A. Londos and L. G. Fytros, “Investigation of Two Infrared Bands at 1032 and 1043 cm⁻¹ in Neutron Irradiated Silicon,” *J. Appl. Phys.*, vol. 89, no. 2, 928–932 (2001).
- [6.214] Y.-H. Lee and J. W. Corbett, “EPR Studies of Defects in Electron-Irradiated Silicon: A Triplet State of Vacancy-Oxygen Complexes,” *Phys. Rev. B*, vol. 13, no. 6, 2653–2666 (1976).
- [6.215] A. Uedono, Y.-K. Cho, S. Tanigawa, and A. Ikari, “Positron Annihilation in Proton Irradiated Czochralski-Grown Si,” *Jpn. J. Appl. Phys., Part 1*, vol. 33, no. 1A, 1–5 (1994).
- [6.216] Y. H. Lee, T. D. Bilash, and J. W. Corbett, “Photo-EPR Experiments on Defects in Irradiated Silicon,” *Radiation Effects*, vol. 29, 7–12 (1976).
- [6.217] O. O. Awadelkarim, H. Weman, B. G. Svensson, and J. L. Lindström, “Deep-Level Transient Spectroscopy and Photoluminescence Studies of Electron-Irradiated Czochralski Silicon,” *J. Appl. Phys.*, vol. 60, no. 6, 1974–1979 (1986).
- [6.218] Y. H. Lee, K. L. Wang, A. Jaworoski, P. M. Mooney, L. J. Cheng, and J. W. Corbett, “A Transient Capacitance Study of Radiation-Induced Defects in Aluminum-Doped Silicon,” *phys. stat. sol. (a)*, vol. 57, 697–704 (1980).
- [6.219] M.-A. Trauwaert, J. Vanhellemont, H. E. Maes, A.-M. Van Bavel, G. Langouche, A. Stesmans, and P. Clauws, “Influence of Oxygen and Carbon on the Generation and Annihilation of Radiation Defects in Silicon,” *Materials Science and Engineering B*, vol. 36, 196–199 (1996).
- [6.220] S. J. Watts, “Overview of Radiation Damage in Silicon Detectors — Models and Defect Engineering,” *Nuclear Instruments and Methods in Physics Research A*, vol. 386, 149–155 (1997).
- [6.221] K. Gill, G. Hall, and B. MacEvoy, “Bulk Damage Effects in Irradiated Silicon Detectors Due to Clustered Divacancies,” *J. Appl. Phys.*, vol. 82, no. 1, 126–136 (1997).
- [6.222] B. C. MacEvoy and G. Hall, “Defect Kinetics in Novel Detector Materials,” *Materials Science in Semiconductor Processing*, vol. 3, 243–249 (2000).
- [6.223] I. Pintilie, E. Fretwurst, G. Lindström, and J. Stahl, “Close to Midgap Trapping Level in ⁶⁰Co Gamma Irradiated Silicon Detectors,” *Appl. Phys. Lett.*, vol. 81, no. 1, 165–167 (2002).
- [6.224] I. Pintilie, E. Fretwurst, G. Lindström, and J. Stahl, “Second-Order Generation of Point Defects in Gamma-Irradiated Float-Zone Silicon, an Explanation for “Type Inversion”,” *Appl. Phys. Lett.*, vol. 82, no. 13, 2169–2171 (2003).
- [6.225] I. Pintilie, E. Fretwurst, G. Kramberger, G. Lindstroem, Z. Li, and J. Stahl, “Second-Order Generation of Point Defects in Highly Irradiated Float Zone Silicon-Annealing Studies,” in: *Proceedings of the 22nd International Conference on Defects in Semiconductors*, edited by K. Bonde Nielsen, A. Nylandsted Larsen, and G. Weyer, *Physica B*, vol. 340-342, 578–582 (2003).
- [6.226] E. V. Monakhov, B. S. Avset, A. Hallén, and B. G. Svensson, “Formation of a Double Acceptor Center during Divacancy Annealing in Low-Doped High-Purity Oxygenated Si,” *Phys. Rev. B*, vol. 65, 233207 (2002).
- [6.227] V. P. Markevich, A. R. Peaker, S. B. Lastovskii, L. I. Murin, and J. L. Lindström, “Defect Reactions Associated with Divacancy Elimination in Silicon,” *J. Phys.: Condens. Matter*, vol. 15, S2779–S2789 (2003).
- [6.228] G. Alfieri, E. V. Monakhov, B. S. Avset, and B. G. Svensson, “Evidence for Identification of the Divacancy-Oxygen Center in Si,” *Phys. Rev. B*, vol. 68, 233202 (2003).
- [6.229] Y. H. Lee, J. C. Corelli, and J. W. Corbett, “Oxygen-Vibrational Bands in Irradiated Silicon,” *Physics Letters*, vol. 60A, no. 1, 55–57 (1977).

- [6.230] N. V. Sarlis, C. A. Londos, and L. G. Fytros, "Origin of Infrared Bands in Neutron-Irradiated Silicon," *J. Appl. Phys.*, vol. 81, no. 4, 1645–1650 (1997).
- [6.231] A. Kawasuso, M. Hawegawa, M. Suezawa, S. Yamauchi, and K. Sumino, "An Annealing Study of Defects Induced by Electron Irradiation of Czochralski-Grown Si Using a Positron Lifetime Technique," *Applied Surface Science*, vol. 85, 280–286 (1995).
- [6.232] J. Coutinho, R. Jones, S. Öberg, and P. R. Briddon, "The Formation, Dissociation and Electrical Activity of Divacancy-Oxygen Complexes in Si," in: *Proceedings of the 22nd International Conference on Defects in Semiconductors*, edited by K. Bonde Nielsen, A. Nylandsted Larsen, and G. Weyer, *Physica B*, vol. 340-342, 523–527 (2003).
- [6.233] J. M. Meese, M. Chandrasekhar, D. L. Cowan, S. L. Chang, H. Yousif, H. R. Chandrasekhar, and P. McGrail, "Defect Production during Neutron Doping of Si," in: *Neutron-Transmutation-Doped Silicon*, edited by J. M. Meese, New York: Plenum Press, 101–140 (1981).
- [6.234] C. A. Londos, N. V. Sarlis, and L. G. Fytros, "Shoulder at the 887 cm⁻¹ Infrared Band in Neutron Irradiated Si," *J. Appl. Phys.*, vol. 85, no. 12, 8074–8078 (1999).
- [6.235] T. Akiyama and A. Oshiyama, "Stability and Vibrational Properties of Multivacancy-Oxygen Complexes in Crystalline Silicon," in: *Proceedings of the 25th International Conference on the Physics of Semiconductors*, edited by N. Miura and T. Ando, Berlin: Springer, 1425–1426 (2001).
- [6.236] A. Brelo, "Selective Trapping of Vacancies," in: *Radiation Damage and Defects in Semiconductors, Inst. Phys. Conf. Ser.*, no. 16, 191–201 (1973).
- [6.237] H. J. Stein, "Self-Interstitials and the 935 cm⁻¹ Band in Silicon," *Appl. Phys. Lett.*, vol. 55, no. 9, 870–872 (1989).
- [6.238] J. L. Lindström, B. G. Svensson, J. W. Corbett, and G. S. Oehrlein, "On the Complex of the Oxygen Interstitial and the Silicon Interstitial in Silicon," *phys. stat. sol. (a)*, vol. 85, K109–K111 (1984).
- [6.239] L. I. Murin, V. P. Markevich, T. Hallberg, J. L. Lindström, M. Kleverman, J. Hermansson, and B. G. Svensson, "Interaction of Silicon Self-Interstitials with Interstitial Oxygen: An Infrared Absorption Study," in: *Proceedings of the 2nd ENDEASD Workshop*, edited by C. Claeyns, 248–253 (2000).
- [6.240] J. Hermansson, L. I. Murin, T. Hallberg, V. P. Markevich, J. L. Lindström, M. Kleverman, and B. G. Svensson, "Complexes of the Self-Interstitial with Oxygen in Irradiated Silicon: A New Assignment of the 936 cm⁻¹ Band," *Physica B*, vol. 302-303, 188–192 (2001).
- [6.241] L. I. Khirunenko, L. I. Murin, J. L. Lindström, M. G. Sosnin, and Y. V. Pomozov, "Self-Interstitial-Oxygen Related Defects in Low-Temperature Irradiated Si," *Physica B*, vol. 308-310, 458–461 (2001).
- [6.242] G. S. Oehrlein, I. Krafcsik, J. L. Lindström, A. E. Jaworowski, and J. W. Corbett, "The Mechanism of the Enhancement of Divacancy Production by Oxygen during Electron Irradiation of Silicon. II. Computer Modeling," *J. Appl. Phys.*, vol. 54, no. 1, 179–183 (1983).
- [6.243] J. L. Lindström, G. S. Oehrlein, A. E. Jaworowski, and J. W. Corbett, "The Mechanism of the Enhancement in Divacancy Production by Oxygen during Electron Irradiation of Silicon. I. Experimental," *J. Appl. Phys.*, vol. 53, no. 12, 8686–8690 (1982).
- [6.244] R. D. Harris and G. D. Watkins, "Interstitial Related Defects in n-Type Silicon," in: *Thirteenth International Conference on Defects in Semiconductors*, edited by L. C. Kimerling and J. M. Parsey, Jr., The Metallurgical Society of AIME, 799–805 (1985).
- [6.245] K. A. Abdullin, B. N. Mukashev, and Y. V. Gorelkinskii, "Metastable Oxygen-Silicon Interstitial Complex in Crystalline Silicon," *Semicond. Sci. Technol.*, vol. 11, 1696–1703 (1996).
- [6.246] K. A. Abdullin and B. N. Mukashev, "Defects in p-Si Bombarded at 77 K: Energy Spectrum and Annealing Kinetics," *Semiconductors*, vol. 28, no. 10, 1012–1017 (1994).
- [6.247] N. Pinho, J. Coutinho, R. Jones, and P. R. Briddon, "Interaction between Oxygen and Single Self-Interstitials in Silicon," in: *Proceedings of the 22nd International Conference on Defects in Semiconductors*, edited by K. Bonde Nielsen, A. Nylandsted Larsen, and G. Weyer, *Physica B*, vol. 340-342, 575–577 (2003).

- [6.248] B. Pajot, H. Compain, J. Lerouille, and B. Clerjaud, “Spectroscopic Studies of 450 °C Thermal Donors in Silicon,” in: *16th International Conference on the Physics of Semiconductors*, edited by M. Averous, *Physica*, vol. 117B&118B, 110–112 (1983).
- [6.249] R. C. Newman, A. S. Oates, and F. M. Livingston, “Self-Interstitials and Thermal Donor Formation in Silicon: New Measurements and a Model for the Defects,” *J. Phys. C*, vol. 16, L667–L674 (1983).
- [6.250] R. C. Newman, “Thermal Donors in Silicon: Oxygen Clusters or Self-Interstitial Aggregates,” *J. Phys. C*, vol. 18, L967–L972 (1985).
- [6.251] J. L. Lindström, T. Hallberg, J. Hermansson, L. I. Murin, B. A. Komarov, V. P. Markevich, M. Kleverman, and B. G. Svensson, “Interaction between Self-Interstitials and the Oxygen Dimer in Silicon,” *Physica B*, vol. 308–310, 284–289 (2001).
- [6.252] J. Schmidt, K. Bothe, and R. Hezel, “Formation and Annihilation of the Metastable Defect in Boron-Doped Czochralski Silicon,” in: *29th IEEE Photovoltaic Specialists Conference*, New York: IEEE, 178–181 (2002).
- [6.253] L. C. Kimerling, “Structure and Properties of the Oxygen Donor,” in: *Oxygen, Carbon, Hydrogen, and Nitrogen in Crystalline Silicon*, edited by J. C. Mikkelsen, Jr., S. J. Pearton, J. W. Corbett, and S. J. Pennycook, *Mat. Res. Soc. Symp. Proc.*, vol. 59, 83–92 (1986).
- [6.254] E. Dittrich, W. Scheitler, and W. Eisenmenger, “Satellite Phonon Absorption Lines above the 875 GHz Resonance of Interstitial Oxygen in Silicon,” in: *18th International Conference on Low Temperature Physics, Jpn. J. Appl. Phys.*, vol. 26, Supplement 26-3, 873–874 (1987).
- [6.255] H. J. Stein and J. W. Medernach, “Oxygen-Related Vibrational Modes Produced in Czochralski Silicon by Hydrogen Plasma Exposure,” *J. Appl. Phys.*, vol. 79, no. 5, 2337–2342 (1996).
- [6.256] L. I. Murin, T. Hallberg, V. P. Markevich, and J. L. Lindström, “Experimental Evidence of the Oxygen Dimer in Silicon,” *Phys. Rev. Lett.*, vol. 80, no. 1, 93–96 (1998).
- [6.257] S. Öberg, C. P. Ewels, R. Jones, T. Hallberg, J. L. Lindström, L. I. Murin, and P. B. Briddon, “First Stage of Oxygen Aggregation in Silicon: The Oxygen Dimer,” *Phys. Rev. Lett.*, vol. 81, no. 14, 2930–2933 (1998).
- [6.258] M. Pesola, J. von Boehm, and R. M. Nieminen, “Vibrations of the Interstitial Oxygen Pairs in Silicon,” *Phys. Rev. Lett.*, vol. 82, no. 20, 4022–4025 (1999).
- [6.259] L. C. Snyder, J. W. Corbett, P. Deák, and R. Wu, “On the Diffusion of Oxygen Dimer in a Silicon Crystal,” in: *Defects in Electronic Materials*, edited by M. Stavola, S. J. Pearton, and G. Davies, *Mat. Res. Soc. Symp. Proc.*, vol. 104, 179–184 (1988).
- [6.260] A. Gali, J. Miro, P. Deák, C. P. Ewels, and R. Jones, “Theoretical Studies on Nitrogen-Oxygen Complexes in Silicon,” *J. Phys.: Condens. Matter*, vol. 8, 7711–7722 (1996).
- [6.261] M. Needels, J. D. Joannopoulos, Y. Bar-Yam, and S. T. Pantelides, “Oxygen Complexes in Silicon,” *Phys. Rev. B*, vol. 43, no. 5, 4208–4215 (1991).
- [6.262] R. Jones, “Ab Initio Calculations on Thermal Donors in Si: An Over-Coordinated O Atom Model for the NL10 and NL8 Centres,” *Semicond. Sci. Technol.*, vol. 5, 255–260 (1990).
- [6.263] A. Umerski and R. Jones, “The Interaction of Oxygen with Dislocation Cores in Silicon,” *Phil. Mag. A*, vol. 67, no. 4, 905–915 (1993).
- [6.264] C. P. Ewels, R. Jones, and S. Öberg, “Oxygen-Carbon, Oxygen-Nitrogen and Oxygen-Dimer Defects in Silicon,” in: *Early Stages of Oxygen Precipitation in Silicon*, edited by R. Jones, *NATO ASI Series 3*, vol. 17, Dordrecht: Kluwer, 141–162 (1996).
- [6.265] R. O. Carlson, R. N. Hall, and E. M. Pell, “Sulfur in Silicon,” *J. Phys. Chem. Solids*, vol. 8, 81–83 (1959).
- [6.266] G. W. Ludwig, “Paramagnetic Resonance Study of a Deep Donor in Silicon,” *Phys. Rev.*, vol. 137, no. 5A, A1520–A1530 (1965).
- [6.267] S. Greulich-Weber, J. R. Niklas, and J.-M. Spaeth, “ENDOR Investigations of Se⁺ in Silicon,” *J. Phys. C*, vol. 17, L911–L914 (1984).

- [6.268] D. L. Camphausen, H. M. James, and R. J. Sladek, "Influence of Hydrostatic Pressure and Temperature on the Deep Donor Levels of Sulfur in Silicon," *Phys. Rev. B*, vol. 2, no. 6, 1899–1917 (1970).
- [6.269] W. E. Krag, W. H. Kleiner, H. J. Zeiger, and S. Fischler, "Sulfur Donors in Silicon: Infrared Transitions and Effects of Calibrated Uniaxial Stress," in: *The Physics of Semiconductors, J. Phys. Soc. Jap.*, vol. 21, Supplement, 230–233 (1966).
- [6.270] R. A. Forman, "Optical Study of Isotopic Effects in Sulfur Deep Level in Silicon," *Appl. Phys. Lett.*, vol. 37, no. 9, 776–778 (1980).
- [6.271] H. G. Grimmeiss, E. Janzén, and K. Larsson, "Multivalley Spin Splitting of 1s States for Sulfur, Selenium, and Tellurium Donors in Silicon," *Phys. Rev. B*, vol. 25, no. 4, 2627–2632 (1982).
- [6.272] B. Pajot and C. Naud, "Spectroscopy of the Neutral Sulphur-Related Centres in Silicon," *Journal de Physique*, vol. 45, 539–543 (1984).
- [6.273] P. Wagner, C. Holm, E. Sirtl, R. Oeder, and W. Zulehner, "Chalcogens As Point Defects in Silicon," *Festkörperprobleme*, vol. 24, 191–228 (1984).
- [6.274] W. E. Krag, W. H. Kleiner, and H. J. Zeiger, "Electronic Structure of Deep-Lying Sulfur Centers in Si," *Phys. Rev. B*, vol. 33, no. 12, 8304–8320 (1986).
- [6.275] C. T. Sah, L. L. Rosier, and L. Forbes, "Direct Observation of the Multiplicity of Impurity Charge States in Semiconductors from Low-Temperature High-Frequency Photocapacitance," *Appl. Phys. Lett.*, vol. 15, no. 10, 316–318 (1969).
- [6.276] H. G. Grimmeiss and B. Skarstam, "Excited States at Deep Centers in Si:S and Si:Se," *Phys. Rev. B*, vol. 23, no. 4, 1947–1960 (1981).
- [6.277] R. Y. Koyama, W. E. Phillips, D. R. Myers, Y. M. Liu, and H. B. Dietrich, "The Energy Levels and the Defect Signature of Sulfur-Implanted Silicon by Thermally Stimulated Measurements," *Solid-State Electronics*, vol. 21, 953–955 (1978).
- [6.278] D. R. Myers and W. E. Phillips, "Existence of an Isotope Shift for the Sulfur Deep Level in Silicon," *Appl. Phys. Lett.*, vol. 32, no. 11, 756–758 (1978).
- [6.279] L. L. Rosier and C. T. Sah, "Thermal Emission and Capture of Electrons at Sulfur Centers in Silicon," *Solid-State Electronics*, vol. 14, 41–54 (1971).
- [6.280] O. Engström and H. G. Grimmeiss, "Optical Properties of Sulfur-Doped Silicon," *J. Appl. Phys.*, vol. 47, no. 9, 4090–4097 (1976).
- [6.281] D. R. Myers, R. Y. Koyama, and W. E. Phillips, "An Implantation Predeposition Technique for the Introduction of Deep-Level Chemical Impurities," *Radiation Effects*, vol. 48, 145–150 (1980).
- [6.282] H. G. Grimmeiss, E. Janzén, and B. Skarstam, "Deep Sulfur-Related Centers in Silicon," *J. Appl. Phys.*, vol. 51, no. 8, 4212–4217 (1980).
- [6.283] S. D. Brotherton, M. J. King, and G. J. Parker, "The Electrical Properties of Sulphur in Silicon," *J. Appl. Phys.*, vol. 52, no. 7, 4649–4658 (1981).
- [6.284] G. Pensl, G. Roos, and C. H. P. Wagner, "Chalcogen Double Donors in Silicon," in: *Defects in Semiconductors 14*, edited by H. J. von Bardeleben, *Materials Science Forum*, vol. 10-12, 911–916 (1986).
- [6.285] R. G. Humphreys and P. Migliorato, "Sharp Line Photoconductivity in Si:S," *Solid State Communications*, vol. 40, 819–823 (1981).
- [6.286] E. Janzén, R. Stedman, G. Grossmann, and H. G. Grimmeis, "High-Resolution Studies of Sulfur- and Selenium-Related Donor Centers in Silicon," *Phys. Rev. B*, vol. 29, no. 4, 1907–1918 (1984).
- [6.287] T. H. Ning and C. T. Sah, "Photoionization Cross Sections of a Two-Electron Donor Center in Silicon," *Phys. Rev. B*, vol. 14, no. 6, 2528–2533 (1976).
- [6.288] E. Janzén, K. Larsson, R. Stedman, and H. G. Grimmeiss, "Fourier Photo-Admittance Spectroscopy," *J. Appl. Phys.*, vol. 53, no. 11, 7520–7525 (1982).
- [6.289] B. Pajot and A. M. Stoneham, "A Spectroscopic Investigation of the Lattice Distortion at Substitutional Sites for Groups V and VI Donors in Silicon," *J. Phys. C*, vol. 20, 5241–5252 (1987).

- [6.290] F. Beeler, M. Scheffler, O. Jepsen, and O. Gunnarsson, “Identification of Chalcogen Point-Defect Sites in Silicon by Total-Energy Calculations,” *Phys. Rev. Lett.*, vol. 54, no. 23, 2525–2528 (1985).
- [6.291] M. Kleverman, H. G. Grimmeiss, A. Litwin, and E. Janzén, “Capture Processes at Double Donors in Silicon,” *Phys. Rev. B*, vol. 31, no. 6, 3659–3666 (1985).
- [6.292] S. T. Pantelides and C. T. Sah, “Theory of Localized States in Semiconductors. I. New Results Using an Old Method,” *Phys. Rev. B*, vol. 10, no. 2, 621–637 (1974).
- [6.293] S. T. Pantelides and C. T. Sah, “Theory of Localized States in Semiconductors. II. The Pseudo Impurity Theory Application to Shallow and Deep Donors in Silicon,” *Phys. Rev. B*, vol. 10, no. 2, 638–658 (1974).
- [6.294] R. W. Jansen and O. F. Sankey, “Theory of Deep Electronic Levels of Large Chalcogen (S, Se, and Te) Complexes in Si,” *Phys. Rev. B*, vol. 33, no. 6, 3994–4001 (1986).
- [6.295] H. Overhof, M. Scheffler, and C. M. Weinert, “Formation Energies, Electronic Structure, and Hyperfine Fields of Chalcogen Point Defects and Defect Pairs in Silicon,” *Phys. Rev. B*, vol. 43, no. 15, 12494–12506 (1991).
- [6.296] M. Thiagarajan, K. Iyakutti, and E. Palaniyandi, “Electronic Structure of Chalcogen Impurities in Silicon,” *phys. stat. sol. (b)*, vol. 205, 553–558 (1998).
- [6.297] N. Sclar, “The Effect of Dopant Diffusion Vapor Pressure on the Properties of Sulfur and Selenium Doped Silicon Infrared Detectors,” *J. Appl. Phys.*, vol. 52, no. 8, 5207–5217 (1981).
- [6.298] P. L. Gruzin, S. V. Zemskii, A. D. Bulkin, and N. M. Makarov, “Diffusion of Carbon and Sulfur in Phosphorus-Doped Silicon,” *Sov. Phys. Semicond.*, vol. 7, no. 9, 1241 (1974).
- [6.299] F. Rollert, N. A. Stolwijk, and H. Mehrer, “Diffusion of Sulfur-35 into Silicon Using an Elementary Vapor Source,” *Appl. Phys. Lett.*, vol. 63, no. 4, 506–508 (1993).
- [6.300] N. A. Stolwijk, D. Grünebaum, M. Perret, and M. Brohl, “Zinc and Sulphur in Silicon: Experimental Evidence for Kick-Out Diffusion Behaviour,” in: *Defects in Semiconductors 15*, edited by G. Ferenczi, *Materials Science Forum*, vol. 38-41, 701–706 (1989).
- [6.301] A. A. Lebedev, A. T. Mamadalimov, and N. A. Sultanov, “Investigation of Sulfur-Doped Silicon Diodes Exhibiting S-Type Negative Resistance,” *Sov. Phys. Semicond.*, vol. 5, no. 1, 17–24 (1971).
- [6.302] A. A. Lebedev, A. T. Mamadalimov, and S. Makhkamov, “Investigation of the Photoconductivity and Infrared Quenching in Si:S,” *Sov. Phys. Semicond.*, vol. 8, no. 2, 169–171 (1974).
- [6.303] N. S. Zhdanovich and Y. I. Kozlov, “Infrared Absorption and Photoconductivity of Silicon Doped with Sulfur or Selenium,” *Sov. Phys. Semicond.*, vol. 10, no. 10, 1102–1104 (1976).
- [6.304] A. B. van Oosten and C. A. J. Ammerlaan, “Sulfur Pair in Silicon: ^{33}S Electron-Nuclear Double Resonance,” *Phys. Rev. B*, vol. 38, no. 18, 13291–13296 (1988).
- [6.305] S. Greulich-Weber, J. R. Niklas, and J.-M. Spaeth, “The Structure of Chalcogen Pairs in Silicon,” *J. Phys.: Condens. Matter*, vol. 1, 35–45 (1989).
- [6.306] O. F. Sankey and J. D. Dow, “Theory of Electron Spin Resonance Measurements of Chalcogen Pairs in Si,” *Solid State Communications*, vol. 51, no. 9, 705–708 (1984).
- [6.307] C. Weinert and M. Scheffler, “Chalcogen and Vacancy Pairs in Silicon: Electronic Structure and Stabilities,” in: *Defects in Semiconductors 14*, edited by H. J. von Bardeleben, *Materials Science Forum*, vol. 10-12, 25–30 (1986).
- [6.308] A. A. Taskin, “Chalcogen Dimers in Silicon,” *Semiconductors*, vol. 35, no. 10, 1083–1090 (2002).
- [6.309] H. R. Vydyanath, W. J. Helm, H. S. Lorenzo, and S. T. Hoelke, “Development of Selenium-Doped Silicon for 3–5 μm Applications,” *Infrared Physics*, vol. 19, 93–102 (1979).
- [6.310] H. G. Grimmeiss, E. Janzén, H. Ennen, O. Schirmer, J. Schneider, R. Wörner, C. Holm, E. Sirtl, and P. Wagner, “Tellurium Donors in Silicon,” *Phys. Rev. B*, vol. 24, no. 8, 4571–4586 (1981).
- [6.311] N. A. Sultanov, “Photoelectric Properties of Selenium-Doped Silicon,” *Sov. Phys. Semicond.*, vol. 8, no. 9, 1148–1149 (1975).

- [6.312] C.-S. Kim and M. Sakata, "Diffusion Coefficient of Selenium in Silicon by Sheet Hall Coefficient Measurements," *Jpn. J. Appl. Phys.*, vol. 18, no. 2, 247–254 (1979).
- [6.313] J. C. Swartz, D. H. Lemmon, and R. N. Thomas, "Optical Excitation Spectra of Selenium-Doped Silicon," *Solid State Communications*, vol. 36, 331–334 (1980).
- [6.314] H. G. Grimmeiss, E. Janzén, and B. Skarstam, "Electronic Properties of Selenium-Doped Silicon," *J. Appl. Phys.*, vol. 51, no. 7, 3740–3745 (1980).
- [6.315] H. R. Vydyanath, J. S. Lorenzo, and F. A. Kröger, "Defect Pairing Diffusion, and Solubility Studies in Selenium-Doped Silicon," *J. Appl. Phys.*, vol. 49, no. 12, 5928–5937 (1978).
- [6.316] H. Stümpel, M. Vorderwülbecke, and J. Mimkes, "Diffusion of Selenium and Tellurium in Silicon," *Appl. Phys. A*, vol. 46, 159–163 (1988).
- [6.317] B. Skarstam and J. L. Lindström, "A Comparison between Selenium Mass-Transported and Selenium-Diffused Silicon," *Appl. Phys. Lett.*, vol. 39, no. 6, 488–490 (1981).
- [6.318] H. G. Grimmeiss, E. Janzén, B. Skarstam, and A. Lodding, "Chemical Identification of Deep Energy Levels in Si:Se," *J. Appl. Phys.*, vol. 51, no. 12, 6238–6242 (1980).
- [6.319] O. Meyer, N. G. E. Johansson, S. T. Picraux, and J. W. Mayer, "Lattice Location and Dopant Behavior of Group II and VI Elements Implanted in Silicon," *Solid State Communications*, vol. 8, 529–531 (1970).
- [6.320] J. Gyulai, O. Meyer, R. D. Pashley, and J. W. Mayer, "Lattice Location and Dopant Behavior of Group II and VI Elements Implanted in Silicon," in: *1st International Conference on Ion Implantation*, edited by L. Chadderton and F. H. Eisen, New York: Gordon and Breach, 297–304 (1971).
- [6.321] J. Gyulai, O. Meyer, R. D. Pashley, and J. W. Mayer, "Lattice Location and Dopant Behavior of Group II and VI Elements Implanted in Silicon," *Radiation Effects*, vol. 7, 17–24 (1971).
- [6.322] H. Okamoto, "Se-Si (Selenium-Silicon)," *Journal of Phase Equilibria*, vol. 21, no. 5, 499 (2000).
- [6.323] N. S. Zhdanovich and Y. I. Kozlow, "Diffusion of Selenium and Tellurium in Silicon," *Sov. Phys. Semicond.*, vol. 9, no. 8, 1049 (1976).
- [6.324] A. A. Taskin, B. A. Zaitsev, V. I. Obodnikov, and E. G. Tishkovskii, "Special Features of Spatial Redistribution of Selenium Atoms Implanted in Silicon," *Semiconductors*, vol. 34, no. 3, 312–318 (2000).
- [6.325] F. Richou, G. Pelous, and D. Lecrosnier, "Selenium Implantation into Silicon Studied by DLTS Technique," *Appl. Phys. Lett.*, vol. 31, no. 8, 525–527 (1977).
- [6.326] W. Fahrner and A. Goetzberger, "Determination of Deep Energy Levels in Si by MOS Techniques," *Appl. Phys. Lett.*, vol. 21, no. 7, 329–331 (1972).
- [6.327] R. Wörner and O. F. Schirmer, "ESR of Selenium Pairs (Se_2^+) in Silicon," *Solid State Communications*, vol. 51, no. 9, 665–669 (1984).
- [6.328] A. A. Taskin and E. G. Tishkovskii, "Formation of Se_2 Quasimolecules in Selenium-Doped Silicon," *Semiconductors*, vol. 32, no. 11, 1162–1167 (1998).
- [6.329] A. A. Taskin and E. G. Tishkovskii, "Formation of Selenium-Containing Complexes in Silicon," *Semiconductors*, vol. 35, no. 6, 605–614 (2002).
- [6.330] J. R. Niklas and J. M. Spaeth, "ENDOR Investigation of Tellurium Donors in Silicon," *Solid State Communications*, vol. 46, no. 2, 121–126 (1983).
- [6.331] R. Schaub, G. Pensl, M. Schulz, and C. Holm, "Donor States in Tellurium-Doped Silicon," *Appl. Phys. A*, vol. 34, 215–222 (1984).
- [6.332] C. Hofmann and M. Schulz, "Tellurium-Related Trap Levels in Silicon," *Appl. Phys. A*, vol. 33, 19–24 (1984).
- [6.333] I. D. Desnica and U. V. Desnica, "Tellurium Related Deep Traps in Silicon," in: *Properties of Crystalline Silicon*, edited by R. Hull, *EMIS Datareviews Series*, no. 20, London: INSPEC, 153–158 (1999).
- [6.334] A. L. Lin, A. G. Crouse, J. Wendt, A. G. Campbell, and R. Newman, "Electrical and Optical Properties of Tellurium-Doped Silicon," *Appl. Phys. Lett.*, vol. 38, no. 8, 683–685 (1981).

- [6.335] G. J. Kemerink, H. de Waard, L. Niesen, and D. O. Boerma, “Tellurium and Iodine in Silicon Part II: Hall Effect and Resistivity Measurements on Ion Implanted Silicon,” *Radiation Effects*, vol. 69, 101–112 (1983).
- [6.336] S. T. Picraux, N. G. E. Johansson, and J. W. Mayer, “Analysis of Cd and Te Implantations in Silicon by Channeling and Hall Measurements,” in: *Semiconductor Silicon 1969*, edited by R. R. Haberecht and E. L. Kern, *Electrochem. Soc. Proc.*, vol. 69-4, 422–432 (1969).
- [6.337] T. F. Lee, R. D. Pashley, T. C. McGill, and J. W. Mayer, “Investigation of Tellurium-Implanted Silicon,” *J. Appl. Phys.*, vol. 46, no. 1, 381–388 (1975).
- [6.338] G. Weyer, B. I. Deutch, A. Nylandsted-Larsen, J. U. Andersen, and H. L. Nielsen, “Mössbauer and Channeling Studies on ^{119}Te , ^{119}Sb and ^{119}Sn Implants in Group-IV Elements,” in: *Exposés et communications présentés à la Conférence Internationale sur les Applications de l'Effet Mössbauer*, Colloque C6 in *Journal de Physique*, vol. 35, no. 12, 297 (1974).
- [6.339] A. Nylandsted Larsen, G. Weyer, and L. Nanver, “Radiation Defects in Ion-Implanted Silicon. II. Mössbauer Spectroscopy of ^{119}Sn Defect Structures from Implantations of Radioactive Tellurium,” *Phys. Rev. B*, vol. 21, no. 11, 4951–4966 (1980).
- [6.340] G. J. Kemerink, D. O. Boerma, H. de Waard, J. C. de Wit, and S. A. Drentje, “Mössbauer and Channeling Experiments on TeSi and SmSi,” in: *International Conference on Mössbauer Spectroscopy*, Colloque C1 in *Journal de Physique*, vol. 41, 435–438 (1980).
- [6.341] I. Dézsi, M. Van Rossum, G. Langouche, R. Coussement, D. Schroyen, and M. F. Wu, “Location of Te in Epitaxially Regrown Si Layers,” *Appl. Phys. Lett.*, vol. 44, no. 5, 505–507 (1984).
- [6.342] T. G. Davey and E. H. Baker, “A Note on the Si-Te Phase Diagram,” *Journal of Materials Science*, vol. 15, 1601–1602 (1980).
- [6.343] E. Janzén, H. Grimmeiss, A. Lodding, and C. Deline, “Diffusion of Tellurium Dopant in Silicon,” *J. Appl. Phys.*, vol. 53, no. 11, 7367–7371 (1982).
- [6.344] N. A. Stolwijk, F. Rollert, D. Grünebaum, H. Mehrer, and G. Weyer, “Diffusion of Tellurium in Silicon,” in: *Defects in Semiconductors 14*, edited by H. J. von Bardeleben, *Materials Science Forum*, vol. 10-12, 133–138 (1986).
- [6.345] F. Rollert, N. A. Stolwijk, and H. Mehrer, “Diffusion of Tellurium in Silicon Studied by the Redistribution of an Implanted Source of Radioactive ^{121}Te ,” *Materials Science and Engineering B*, vol. 18, 107–114 (1993).
- [6.346] E. Sirtl, “Point Defect Complexing in Silicon,” in: *Defects in Silicon*, edited by W. M. Bullis and L. C. Kimerling, *Electrochem. Soc. Proc.*, vol. 83-9, 45–58 (1983).

Chapter 7

Halogens

Fluorine as the probably most important halogen element was introduced initially to reduce the effective implantation energy of boron by using molecules like BF_2 instead. It shows, as discussed in Section 7.1, a very complex diffusion behavior and has a marked influence on the diffusion of dopants during post-implantation annealing. In general, shallower profiles with a higher degree of electrical activation are expected although some adverse effects were also mentioned in the literature. In addition, fluorine was found to enhance oxide growth and to reduce the associated generation of self-interstitials. Its presence at silicon/silicon dioxide interfaces was associated with a variety of advantages while fluorine in the bulk of oxides may have detrimental effects.

The properties of chlorine and its major applications in the silicon technology are reviewed in Section 7.2. In silicon, chlorine has only limited significance and only few experimental and theoretical investigations were devoted to this system. The major applications are associated with its influence on oxidation, oxide properties, and especially the gettering of undesired impurities like sodium. As for fluorine, an increased oxide growth but reduced generation of self-interstitials were found when chlorine is present in the system.

Bromine, the last of the halogen elements considered, leads a shadowy existence in silicon. The few experiments related to it are outlined in Section 7.3 only for the sake of completeness.

7.1 Fluorine

Fabrication of modern devices requires the implantation of boron with energies in the keV range and below. In conventional implanters, deceleration of the ions can be used to achieve such energies. A disadvantage of this method, on the other hand, is a usually low beam current which implies prolonged implantation times. In addition, the implantation profiles are expected to reflect a certain mixture of implantation energies since not entirely decelerated ions may collide after scanning with gas molecules being still present in the vacuum which neutralizes them and prevents them from further deceleration. An alternative suggested already in the early 1970s by Müller et al. [7.1] is to implant BF_2 molecules by which the effective implantation energy of boron is reduced in proportion to the masses by a factor of 11/49 for ^{11}B . But fluorine may also be introduced by a separate implantation into bulk silicon or polysilicon gates, via an HF dip without rinse in de-ionized water prior to an oxidation [7.2–7.4], from tungsten silicides deposited using WF_6 [7.5–7.7], from processing in an atmosphere containing NF_3 [7.8–7.12], or from using F_2 for wafer cleaning prior to the deposition of an SiO_2 film [7.13].

Especially in *n*-channel MOSFETs but also in *p*-channel MOSFETs, low doses of fluorine (typically up to 10^{15} cm^{-2}) were reported to have an advantageous influence on the properties of gate oxides. In 1985, Deal et al. [7.5] reported a significantly reduced fixed-charge density in silicide/polysilicon structures in comparison to polysilicon gates. They explained the effect tentatively by the fluorine introduced by the silicide deposition. Fluorine introduced by the last HF dip before oxidation was most likely also the reason for the improved interface-trap density and dielectric breakdown strength reported also in 1985 by Bhattacharyya et al. [7.14]. Later, in particular a reduced interface trap density [7.2, 7.15–7.18], a reduced leakage current associated with a reduced surface recombination velocity [7.16], and an increased immunity of gate oxides against degradation induced by high-energetic charge carriers [7.2, 7.9, 7.15, 7.16, 7.19] and radiation damage [7.9, 7.11, 7.20–7.22] were reported. They were associated with the termination of dangling bonds and the replacement of weak silicon-hydrogen bonds in the oxide near the silicon/silicon dioxide interface [7.15, 7.16], as well as with the relaxation of locally strained SiO_2 regions [7.16, 7.23–7.25]. Stress relaxation in fluorinated oxides was also observed experimentally by Kouvatsof et al. [7.26, 7.27]. In comparison to an optimum fluorine dosage, higher doses (usually above $5 \cdot 10^{15} \text{ cm}^{-2}$, sometimes already at doses down to 10^{15} cm^{-2}) were found to lead again to increasing leakage currents [7.16, 7.28] and to reduce again the immunity of gate oxides against hardness against degradation induced by high-energetic charge carriers [7.10, 7.16, 7.17, 7.24, 7.29] and radiation damage [7.11, 7.12, 7.20, 7.23]. Such detrimental effects were explained by the break-up of silicon-oxide bonds in the bulk of the oxide and the replacement of the oxygen by non-bridging fluorine [7.24, 7.25, 7.30]. Since, as reasoned by Chowdhury et al. [7.31], fluorine atoms are likely to improve the interface even at higher concentrations while they degrade bulk oxides, ultra-thin oxides should be less susceptible to degradation by high fluorine doses. This effect is likely to explain some discrepancies with respect to the question at what dose improvement changes to degradation. High doses of fluorine were also reported to cause threshold instabilities in *p*-channel MOSFETs associated with an enhanced diffusion of boron through the gate oxide [7.17, 7.32–7.35]. With respect to the breakdown voltage of fluorinated gate oxides, reports range from improved [7.3] via slightly degraded [7.15] to severely degraded [7.6] in comparison to non-fluorinated gate oxides. The breakdown-voltage degradation observed by Shioya et al. [7.6] is probably related to the very high fluorine concentration (on the order of 10^{20} cm^{-3}) in the oxide but it was also argued by Wright and Saraswat [7.15] that the mechanism responsible might have other reasons than fluorine. In the work of Deal et al. [7.5], as mentioned above, fluorine was associated with a reduction of the fixed-charge density. On the other hand, fluorine incorporation at the interface was later also made responsible for an increase in fixed charge [7.36].

In the following sections, the basic atomic configurations of fluorine in silicon, its diffusion behavior, the formation of complexes, as well as its influences on transient diffusion and activation of dopants and on oxide growth are discussed in detail.

7.1.1 Basic Atomic Configurations

Direct implantation of fluorine was investigated with controversial results. Greeuw and Verwey [7.37] reported that implanted and annealed fluorine led to the formation of donors. In contrast, Zaima et al. [7.38] found that implantation and annealing of fluorine generates deep acceptors the nature of which depended significantly on processing. A similar observation by Chu et al. [7.39] was interpreted in terms of band-bending which was suggested to lead to a generation of holes. The creation of holes, associated with acceptor-type defects was reported also by Wang et al. [7.22] after fluorine implantation and annealing. Omel'yanovskaya et al. [7.40]

finally observed a complex annealing behavior from which they concluded that acceptor-like and donor-like defects may form, depending on the particular implantation and annealing conditions.

In an *ab-initio* study, Chadi [7.41] found that substitutional fluorine acts as a single shallow donor. A similar study by Hirose et al. [7.42] indicated that the substitutional fluorine atom moves strongly off-center towards one of the neighboring silicon atoms. They found two energetically nearly equally favored configurations in each of which the fluorine is negatively charged and in a distance of 1.5 Å from the nearest silicon atom. Judging from the figures shown, the energetically slightly less favorable configuration is characterized by a trigonal symmetry while the fluorine in the energetically slightly more favorable structure moves towards one of the {111} planes defined by three of the four silicon atoms at nearest neighboring sites to the vacancy. From complementary *ab-initio* calculations, van de Walle et al. [7.43] concluded that the lowest-energy state for fluorine is the tetrahedral interstitial site in the negative charge state. The hexagonal and bond-centered interstitial sites were found to be respectively less than 0.5 and 1.5 eV higher in energy for the negatively charged fluorine atom. Later, Van de Walle et al. [7.44] estimated that the formation energy of a negatively charged fluorine at the hexagonal site is less than 0.7 eV higher than at the tetrahedral interstitial site. The former configuration was suggested to be the saddle point for the diffusion of fluorine interstitials. In a similar study, Chadi [7.41] confirmed the tetrahedral interstitial site to be stable in *n*-type silicon. In this configuration, fluorine was found to act as an acceptor. Taguchi and Hirayama [7.45] confirmed likewise the tetrahedral interstitial site to be energetically most favorable for the negative charge state of a fluorine interstitial and to dominate for *n*-type silicon. For the neutral and positive charge states, the bond-centered interstitial site was found to be energetically most favorable with the positive charge state dominating for neutral and *p*-type silicon.

To study the lattice location of fluorine atoms, Bonde Nielsen et al. [7.46] measured the time-differential perturbed-angular distribution (TDPAD) of samples in which the fluorine atoms were introduced by recoil implantation from a CaF₂ layer or a shallow BF₂-implanted layer. These measurements led to the identification of two different sites. One site, observed in amorphous and crystalline silicon, was characterized by a randomly-oriented electric-field gradient. The second site, observed in crystalline silicon only, had an electric-field gradient parallel to a ⟨111⟩ direction. In a later study, Nunes et al. [7.47] combined the results of similar experiments with theoretical investigations of sites along a ⟨111⟩ direction through a silicon atom. From the comparison of the computed nuclear quadrupole coupling constants to the experimentally determined values, they concluded that fluorine occupies bond-centered sites rather than anti-bond sites.

Using XPS and IR spectroscopy, Kinoshita et al. [7.48] concluded that fluorine forms predominantly B-F bonds directly after BF₂ implantation (60 to 130 keV/10¹⁶ cm⁻²). These bonds were found to decompose during annealing at 900 °C.

7.1.2 Diffusion

Diffusion of fluorine after implantation of low doses was investigated by Jeng et al. [7.49]. They found a preferential diffusion of implanted fluorine (30 keV/10¹² and 10¹³ cm⁻²) above 500 °C towards the surface with profiles becoming steeper rather than broader. Investigations using differently doped substrates gave no indication of an influence on fluorine diffusion. Including also positron-annihilation experiments in their reasoning, Szeles et al. [7.50] concluded tentatively that fluorine atoms assume substitutional sites after implantation (30 keV/10¹³ cm⁻²). The diffusion profiles observed were explained qualitatively by a slow dissociation of the substitutional fluorine into a fluorine interstitial and a vacancy followed by a rapid diffusion of the fluorine

interstitial towards the surface. To investigate the interactions of fluorine with vacancies and vacancy clusters, Shano et al. [7.51] combined fluorine implants ($100 \text{ keV}/10^{14} \text{ cm}^{-2}$) with much deeper silicon implants ($500\text{--}1000 \text{ keV}/2\cdot10^{14} \text{ cm}^{-2}$). It was found from the measured depth profiles that fluorine accumulates during annealing at 820°C for 1 min in regions in which a surplus of vacancies was generated by the implants. From positron-annihilation spectroscopy, Pi et al. [7.52] concluded that fluorine implanted at high energies forms at 400°C preferentially complexes with vacancies in the peak region which hamper bulk recombination. These FV pairs were suggested to agglomerate and an activation energy of $2.12 \pm 0.08 \text{ eV}$ was estimated from this process for their migration enthalpy. This value was confirmed by a diffusion experiment at 700°C .

From *ab-initio* studies, van de Walle et al. [7.43] concluded that negatively charged fluorine atoms can diffuse in the lattice with an energy barrier of less than 0.5 eV. Later, Van de Walle et al. [7.44] estimated it to be less than 0.7 eV. These results were confirmed by Taguchi and Hirayama [7.45] who estimated an energy barrier of 0.6 eV. For neutral and positively charged fluorine interstitials, the energy barriers were calculated to be 1.3 and 1.6 eV, respectively. Combining *ab-initio* and continuum simulations, Diebel and Dunham [7.53] assumed that rapidly diffusing fluorine interstitials react with vacancies to form strongly bound F_nV_m complexes after implantation. Annealing at elevated temperatures will lead to their annihilation by self-interstitials and to the liberation of fluorine atoms. Based on these assumptions, the model was able to predict the experiments of Jeng et al. [7.49] qualitatively. Later, Diebel et al. [7.54] showed that it also reproduces the influence of fluorine on the diffusion of boron and phosphorus under amorphizing and non-amorphizing conditions.

The steepening of fluorine profiles found by Jeng et al. [7.49], was observed also after BF_2 implantation and annealing albeit the mechanism may be different. In one of the first investigations of this kind, Wilson [7.55] implanted BF_2 with varying energies (36 to 45 keV) and doses ($5\cdot10^{14}$ to $2\cdot10^{15} \text{ cm}^{-2}$). The fluorine profiles measured by SIMS moved seemingly back towards the surface during post-implantation annealing at 925°C for 20 min and the fluorine was also found to pile up at the end-of-range defects which remained after heat treatment. Similar observations were reported by Kim et al. [7.56] (40 keV, $2\cdot10^{14} \text{ cm}^{-2}$, annealing at 650 to 850°C for 30 min) and Walker [7.57] (30 keV $7\cdot10^{14} \text{ cm}^{-2}$, annealing at 1000 to 1150°C for 10 s). In the work of Sands et al. [7.58], an apparent steepening of the fluorine profile was observed after RTA at 1100°C . The fluorine was introduced in these experiment into preamorphized samples either by implantation as BF_2 ($42 \text{ keV}/2\cdot10^{15} \text{ cm}^{-2}$) or by an equivalent implant of elemental fluorine. In both cases, the peak of the profile could be associated with fluorine-related clusters.

Segregation of implanted fluorine to regions of high lattice damage and to extended defects was observed in various investigations [7.59–7.71], and fluorine decoration of extended defects was even used as diagnostic tool [7.60].

Some of the fluorine redistribution at high implant doses was found to be associated with the recrystallization of the amorphous layer resulting from the BF_2 implantation. In the work of Tsai et al. [7.59], BF_2 was implanted with 150 keV and a dose of 10^{15} cm^{-2} and annealed at 550°C for times from 10 to 100 min. The fluorine depth profiles clearly showed peaks corresponding to the positions up to which recrystallization occurred. This effect is known as snow-plowing and can be observed when an impurity segregates preferentially to the amorphous layer in front of the recrystallization front. The effect was also described by Queirolo et al. [7.72]. They found that fluorine redistribution towards the surface after BF_2 implants with 60 keV and doses of $5\cdot10^{15} \text{ cm}^{-2}$ and above occurs already during an annealing step of 600°C for 20 min. In contrast, no fluorine redistribution was found for doses of $3\cdot10^{15} \text{ cm}^{-2}$ and below.

When the concentration of fluorine atoms pushed ahead of the recrystallization front exceeds a certain limit, they may eventually coalesce into extended defects. In particular, the occurrence of fluorine-filled bubbles was reported in several investigations [7.69, 7.73–7.76]. Injection of self-interstitials by annealing in oxidizing atmospheres was found to reduce their formation considerably [7.75]. XPS investigations of samples containing fluorine bubbles performed by Kinoshita et al. [7.48] indicated that fluorine forms SiF_2 and SiF_3 bonds in the silicon matrix during annealing after BF_2 implantation. Such bonding configurations mean that the respective silicon atoms have only one or two bonds to other silicon atoms and may exist at lattice defects like micro-voids or dislocations only.

Various investigations indicated that fluorine segregates preferentially into silicon dioxide [7.6, 7.15, 7.18, 7.25, 7.30, 7.32, 7.77, 7.78] where it was suggested to be mobile at least in part even at room temperature [7.79]. It was also found that fluorine segregates preferentially to the oxide sides of oxide/silicon interfaces [7.3, 7.10, 7.12, 7.25, 7.30, 7.77, 7.80, 7.81]. From a correlation between a reduction of the concentration of EPR P_b centers and the fluorine concentration at the interface, Ono et al. [7.81] concluded that fluorine terminates dangling bonds at the interface and that this mechanism is the origin of the observed fluorine segregation to the interface. However, it has to be remarked that segregation to interfaces was not observed under all conditions and that the distribution in the oxide depends on the way the fluorine is incorporated [7.18, 7.29, 7.32, 7.77, 7.82] which even gave rise to a discussion of whether interface segregation is reality or just a measurement artifact (see, e.g., [7.29, 7.83, 7.84]).

7.1.3 Complexes

Using positron annihilation to study vacancy defects in fluorine-implanted silicon ($30 \text{ keV}/10^{13} \text{ cm}^{-2}$), Szeles et al. [7.50] found that the vacancy defects anneal already at temperatures below 550°C where the fluorine was found to be immobile. From the absence of positron annihilation at vacancy defects thereafter, they concluded that only an insignificant fraction of the fluorine atoms can be associated with open-volume defects. On the other hand, Uedono et al. [7.76] found small vacancy clusters in their positron-annihilation studies even after BF_2 implantation ($30 \text{ keV}/2 \cdot 10^{15} \text{ cm}^{-2}$) and annealing at 1100°C for 20 s. They concluded that fluorine has a stabilizing effect on vacancy clusters and that the latter may act as precursors for the bubbles discussed above. It should be noted that this finding contrasts also with the work of Fujinami and Chilton [7.85] who found no indications of implantation-induced vacancies after fluorine implantation ($120 \text{ keV}/2 \cdot 10^{14} \text{ cm}^{-2}$) and annealing at 600°C for 30 min.

Using *ab-initio* simulations, Shano et al. [7.51] calculated that fluorine binds with an energy of 2.36 eV to a V_6 vacancy cluster. Similar work by Diebel and Dunham [7.53] indicated also large binding energies for F_nV and F_nV_2 complexes. For complexes with single vacancies, fluorine atoms were found to bind with energy gains from 2.38 eV for the first fluorine atom to 0.54 eV for the fourth fluorine atom. For F_nV_2 complexes, a non-monotonous behavior was found with mean energy gains of about 2.0 eV per fluorine atom from FV_2 to F_6V_2 .

In several investigations, as discussed below, fluorine was postulated to form complexes with self-interstitials to effectively reduce the oversaturation of the latter during post-implantation anneals. It has to be mentioned, though, that direct evidence as well as evidence from *ab-initio* calculations are missing.

To explain fluorine effects on boron diffusion during post-implantation anneals, boron-fluorine complexes were often postulated. The *ab-initio* calculations of Hirose et al. [7.42] indicated that the fluorine atom moves into the bond between the substitutional boron atom and one of its silicon neighbors, pushing the two apart. In this configuration, the complex is electrically inactive since the fluorine terminates a dangling bond of the silicon atom next to it.

7.1.4 Influence on Transient Diffusion and Dopant Activation

In a variety of experiments, it was established that fluorine is able to reduce the oversaturation of self-interstitials during post-implantation anneals. In probably the first report, Ohyu et al. [7.67] described that the diffusion of boron implanted with a dose of $2 \cdot 10^{15} \text{ cm}^{-2}$ can be reduced significantly by additional implants of fluorine with doses ranging from 10^{14} to $2 \cdot 10^{16} \text{ cm}^{-2}$. In a further experiment, Ohyu et al. [7.28] compared the diffusion of a deep boron implant ($0.8 \text{ MeV}/10^{14} \text{ cm}^{-2}$) with and without a shallow fluorine implant ($100 \text{ keV}/10^{15} \text{ cm}^{-2}$). In case of the fluorine implant, a reduced broadening was observed especially towards the surface. Similarly, Kato [7.86] reported that additional fluorine implants may reduce transient-enhanced diffusion and defect production during annealing of high-concentration arsenic and phosphorus implants. For boron diffusion, Ando et al. [7.87] noted a retardation when the substrate was preamorphized with fluorine prior to the BF_2 implantation. In the investigation of Current et al. [7.69], the post-implantation diffusion of a boron implant ($10 \text{ keV}/3 \cdot 10^{15} \text{ cm}^{-2}$) was compared to boron with an additional pre-implant of fluorine ($39 \text{ keV}/10^{15} \text{ cm}^{-2}$) and a BF_2 implant comparable to the boron implant ($50 \text{ keV}/3 \cdot 10^{15} \text{ cm}^{-2}$). The resulting profiles gave clear evidence of a reduction in junction depth with increasing fluorine dose. A similar experiment was reported by Huang et al. [7.70]. They compared the diffusion of boron implants ($5 \text{ keV}/5 \cdot 10^{14} \text{ cm}^{-2}$) with and without a preamorphization by fluorine ($40 \text{ keV}/2 \cdot 10^{15} \text{ cm}^{-2}$) and a BF_2 implant comparable to the boron implant ($23 \text{ keV}/5 \cdot 10^{14} \text{ cm}^{-2}$). Again, it was found that the diffusion of boron decreases with increasing fluorine concentration. For the fluorine dose of $2 \cdot 10^{15}$, no enhanced diffusion was observed. Studying the diffusion of phosphorus, Lin and Rost [7.88] found a retardation for fluorine implants from $8 \cdot 10^{13}$ to $2 \cdot 10^{15} \text{ cm}^{-2}$. While the effects of fluorine on transient diffusion were obvious in all these experiments, a clear-cut separation of effects was not possible.

To be able to distinguish between chemical effects and other possible influences, Krasnobaev et al. [7.89] compared the effects of fluorine implants on the diffusion of boron with those of neon implants. Because of the similar masses of fluorine and neon, both implants were suggested to result in nearly identical implantation damage. After annealing at 900°C , they found that fluorine leads consistently to a reduced broadening of the boron profile with the difference increasing with increasing fluorine and neon doses. Annealing at 1000°C for 60 min, on the other hand, showed no comparable effects. This was probably related to the out-diffusion of fluorine observed also experimentally. Comparing nominally equivalent shallow implants of fluorine and boron, and neon and boron, Liu et al. [7.90] found that junction depth and sheet resistivity after annealing from 950 to 1050°C for 10 s were significantly larger in the latter case. Using boron spikes to monitor the supersaturation of self-interstitials, Vuong et al. [7.91] compared the effects of silicon, neon, and fluorine implants with a dose of $3.5 \cdot 10^{13} \text{ cm}^{-2}$. Of these, the fluorine-implanted samples caused the least transient diffusion of the boron spikes.

To exclude possible influences from the fact that BF_2 implants create significantly more implantation damage than boron implants, Downey et al. [7.92] implanted boron and BF_2 with a dose of 10^{15} cm^{-2} into a layer preamorphized by the implantation of silicon which extended well beyond the penetration depth of the boron profile. After spike annealing, the BF_2 -implanted samples showed consistently smaller diffusion than the boron-implanted samples. Similar conclusions were drawn by Robertson et al. [7.93]. They used silicon-preamorphized samples and co-implanted boron ($1.12 \text{ keV}/10^{15} \text{ cm}^{-2}$) and fluorine (2 to $36 \text{ keV}/2 \cdot 10^{15} \text{ cm}^{-2}$). For all fluorine implant energies, a reduction of the boron diffusion was observed in comparison to samples not implanted with fluorine. The minimum penetration depth was achieved with a fluorine implant energy of 12 keV at which it was noted that the projected range of the fluorine profile coincides with that of the boron profile. A retarding effect of fluorine was also ob-

served by Dusch et al. [7.94] who used germanium pre-amorphization prior to the implantation of boron ($3 \text{ keV}/10^{14} \text{ cm}^{-2}$) or BF_2 ($15 \text{ keV}/3 \cdot 10^{14} \text{ cm}^{-2}$). In a similar experiment, Shano et al. [7.51] implanted boron ($2 \text{ keV}/5 \cdot 10^{15} \text{ cm}^{-2}$) and fluorine ($4 \text{ keV}/2 \cdot 10^{13} \text{--} 2 \cdot 10^{15} \text{ cm}^{-2}$) with overlapping ranges into samples preamorphized by silicon implants. The presence of fluorine was found to reduce the broadening of the chemical boron profile during post-implantation annealing at 820°C . But the electrical junction depth was found to decrease even more. From this, the authors concluded that fluorine reduces the boron activation in the tail region. Later, Dusch et al. [7.95] found that the diffusion of boron, implanted as BF_2 ($15 \text{ keV}/4 \cdot 10^{14} \text{ cm}^{-2}$), drops at 1000°C even below the intrinsic diffusion coefficient. A similar result was reported by El Mubarek and Ashburn [7.96] who compared the diffusion of a grown boron spike at 1000°C without and with a fluorine implant ($185 \text{ keV}/2.3 \cdot 10^{15} \text{ cm}^{-2}$) which extended well beyond the boron spike. The experiment of Downey et al. [7.92] discussed above was improved by Mokhberi et al. [7.97] by introducing a boron marker layer in the bulk to monitor the oversaturation of self-interstitials in a depth in which a direct influence by the implants can be excluded. Varying the fluorine implant dose, it was found that the fluorine retards the diffusion of the boron implanted with a dose of 10^{15} cm^{-2} but has no effect on the diffusion of the marker layer. Comparing boron implants with arsenic implants, it was found that much more fluorine was retained in the samples when boron was present. In summary, a retarding effect of fluorine was found in all in these experiments. On the other hand, using a significantly smaller boron dose of $5 \cdot 10^{13} \text{ cm}^{-2}$, Ishida et al. [7.98] found only a small retardation of the boron diffusion due to fluorine when they repeated the experiment of Downey et al. [7.92]. As before, no effect of fluorine on the end-of-range damage was observed.

Finally, it has to be mentioned that a retarding effect of fluorine was also found by Kasnavi et al. [7.99] from a numerical analysis of the diffusion profiles of boron implanted either as atoms or in the form of BF_2 . In this investigations, the doses were kept low ($2 \cdot 10^{13} \text{ cm}^{-2}$) in order to avoid the formation of extended defects.

Although the retardation of transient diffusion effects by fluorine is well established, the physical mechanism is not entirely clear. At high fluorine or BF_2 doses which amorphize the silicon, a considerable part of the retarding effect can be associated with the different extended defects forming during annealing. Annealing of boron implants results typically in the formation of small self-interstitial clusters and $\{113\}$ defects. On the other hand, after amorphizing implants, end-of-range disorder is typically observed. The dislocation loops, the end-of-range disorder composes of, are significantly more stable than small self-interstitial clusters and $\{113\}$ defects [7.100] and the oversaturation of self-interstitials will be significantly smaller. It has to be mentioned, though, that retardation of transient diffusion effects was also apparent in some investigations in which none of the compared samples or both had amorphized surface layers prior to annealing. This indicates that an additional effect is operative.

A possible explanation, suggested in the work of Huang et al. [7.70], might be that the segregation of fluorine to extended defects increases their stability, e. g. by saturating dangling bonds. An indication of such an interaction is the preferential segregation of fluorine to extended defects discussed above. Extending a previously established model for boron diffusion during post-implantation annealing, Uematsu [7.101] assumed that the interaction of fluorine with the end-of-range disorder renders them incapable of maintaining an oversaturation of self-interstitials. It has to be noted, though, that the investigations of Downey et al. [7.92], Ishida et al. [7.98], and Robertson et al. [7.93] indicated no influence of fluorine on the evolution of the extended defects. In addition, the experiments of Mokhberi et al. [7.97] made clear that the oversaturation of self-interstitials caused by the Ostwald ripening of the extended defects is not influenced by the fluorine.

As an alternative, proposed already by Ohyu et al. [7.28] and Huang et al. [7.70], the trapping of self-interstitials in the fluorine-implanted region was proposed in the literature. To simulate the effects observed, Vuong et al. [7.91] assumed that the fluorine causes a homogeneous, time-independent increase of the concentration of traps for self-interstitials within the epi-layer. Although the model was purely empirical, it was shown to reproduce the depth dependence of the transient diffusion of the boron spikes. Motivated by the accumulation of fluorine atoms at end-of-range defects, Höfler et al. [7.102] modeled their effects on point defects during post-implantation annealing after BF_2 implantation via a Gaussian-shaped distribution of interstitial traps at the position of the a/c interface after implantation. In the work of Park and Kim [7.103], the formation of mobile fluorine-self-interstitial complexes was hypothesized to reduce the concentration of self-interstitials during post-implantation annealing. Based on a qualitative analysis of own experiments, Hirose et al. [7.42] postulated that mobile complexes of fluorine atoms and silicon self-interstitials form in ion-implanted layers, thus reducing the oversaturation of the latter. To quantitatively simulate the diffusion of implanted fluorine, Robinson and Law [7.104] invoked the formation of F_mI_n clusters of fluorine atoms and silicon self-interstitials.

A third possibility is the direct interaction of fluorine with boron. Such an effect was postulated by Robertson et al. [7.93] who observed that the smallest penetration depth after annealing of boron implanted into silicon-preamorphized samples can be achieved by a fluorine implant with an energy at which the projected ranges of the boron and fluorine profiles coincide. The formation of complexes between boron interstitials and fluorine was also invoked by Dusch et al. [7.95] to explain why the diffusion of boron in germanium-preamorphized, BF_2 -implanted silicon is even less than the intrinsic diffusion. On the other hand, a direct interaction between fluorine and boron was ruled out by Kim et al. [7.56] on the basis of their observation that the presence of fluorine did not influence the segregation coefficient of boron. Evidence for direct fluorine-boron interactions came again from the work of Mokhberi et al. [7.97]. Using a buried boron marker layer, they showed that implanted fluorine has no effects on the intrinsic point defects while it retarded the diffusion of implanted boron atoms. Additional evidence for boron-fluorine-complex formation came from the observation that the presence of boron led to a significant retainment of fluorine while strong out-diffusion of fluorine was observed for comparable arsenic implants. Evidence against a formation of boron-fluorine complexes came also from the work of Impellizzeri et al. [7.105]. They used a preamorphized structure in which a grown boron marker layer was used to investigate the effects of fluorine implants. For a doses of $7 \cdot 10^{13}$, a significant reduction of the boron diffusivity was observed after annealing at 750°C for 60 min while the fluorine concentration at the position of the boron marker layer was two orders of magnitude below its peak concentration.

Already in the initial publications of Müller et al. [7.1] it was shown that the electrical activity after BF_2 implantation and annealing is significantly higher than after boron implantation under equivalent conditions. Various subsequent reports confirmed that fluorine may, under certain conditions, increase the concentration of electrically active boron atoms [7.67, 7.70, 7.106–7.108]. In these experiments, the higher electrical activity of BF_2 -implanted samples can be associated in part with the fact that BF_2 implantation leads to an amorphization while implantation of boron does not. Upon recrystallization, which occurs already at relatively low temperatures, the majority of the boron atoms in BF_2 -implanted samples will be incorporated in substitutional sites while boron-interstitial clusters will form in the boron-implanted samples (see Section 5.3.4).

Although the total electrical activity of implanted and annealed boron was usually found to increase due to the presence of fluorine, there were reports that the electrical activity may be reduced locally. Comparing electrical and chemical depth profiles after BF_2 implantation (150

$\text{keV}/10^{15} \text{ cm}^{-2}$) and annealing at 550°C for times from 10 to 100 min, Tsai and Streetman [7.109] concluded that the tail region did not become electrically activated. Using a similar method, Queirolo et al. [7.66] confirmed that the boron in the tail region of the diffusion profile after BF_2 implantation ($60 \text{ keV}/5 \cdot 10^{15} \text{ cm}^{-2}$) and annealing at 900°C for 20 min was not electrically active. Comparable results, mentioned already above, were reported later by Shano et al. [7.51] for annealed boron and fluorine implants into preamorphized samples.

In silicon implanted with boron and fluorine, a significantly reduced concentration of boron atoms or a significantly increased sheet resistivity were found in several studies after annealing in comparison to samples not containing fluorine [7.28, 7.69, 7.99, 7.107, 7.110, 7.111]. This effect is caused by a fluorine-enhanced out-diffusion of boron from silicon. The fluorine-enhanced diffusion of boron into bulk silicon was mentioned above already as the reason for threshold instabilities in *p*-channel MOSFETs.

7.1.5 Fluorine and Silicon Oxidation

In a variety of studies it was shown that the addition of fluorine compounds like NF_3 [7.12, 7.18, 7.26, 7.82, 7.112, 7.113], F_2 [7.114], SiF_4 [7.115], or $\text{C}_2\text{H}_3\text{Cl}_2\text{F}$ [7.18, 7.116] during oxidation leads to an increased oxide-growth rate. Detailed analyses of Morita et al. [7.112] and Kazor et al. [7.114] indicated that the growth rate does not increase monotonically with the fluorine partial pressure but decreases again after a temperature-dependent maximum. The oxidation enhancement was attributed to the high reactivity of fluorine which enhances the oxidation reaction at the interface [7.18, 7.112] but also to the incorporation of fluorine into the SiO_2 network which reduces its density and leads to a higher diffusivity of oxygen, a reduced viscosity, and reduced stress [7.18, 7.26, 7.113]. The decreasing oxide thicknesses for high fluorine pressures was explained by an etching mechanism enhanced also by the presence of fluorine [7.112]. Fluorine introduced by ion implantation was found by Greeuw and Verwey [7.37] to enhance the oxidation rate while Virdi et al. [7.117] reported the opposite. In the work of Kuper et al. [7.80], fluorine implants into oxides were shown to enhance the rate of further oxidation.

A side-effect of the introduction of fluorine into gate oxides is an increase in oxide thickness [7.7, 7.15, 7.25, 7.118]. This effect was explained by oxide atoms being liberated by the incorporation of fluorine into the silicon dioxide network. These oxygen atoms will in turn oxidize silicon layers on top or below the oxide.

From the enhanced oxidation rate of dry oxidation processes, one might have expected an enhanced generation of self-interstitials due to the addition of fluorine compounds, too. But already Kim and Jaccodine [7.8] found that the shrinkage rate of oxidation stacking faults is significantly increased by oxidation in an O_2/NF_3 ambient even in comparison to literature data from annealing in an inert atmosphere. From this observation, an injection of vacancies rather than of self-interstitials was deduced. Using implanted boron as a marker and junction staining for characterization, Kim et al. [7.119] concluded that oxidation in an O_2/NF_3 ambient leads to a retarded diffusion of boron, indicative of a vacancy oversaturation. However, it has to be remarked that the conclusiveness of this investigation was limited since a possible diffusion of boron into the oxide was not taken into consideration. Kim and Jaccodine [7.18] eliminated this problem by growing an epitaxial layer on top of the implanted samples and confirmed their previous results of a vacancy oversaturation. Finally, using stacking faults and the diffusion of phosphorus, boron, and antimony as monitors, Jaccodine and Kim [7.120] confirmed that the addition of small amounts of NF_3 during dry oxidation results indeed in an oversaturation of vacancies instead of an oversaturation of self-interstitials as it is usually observed for dry oxidation without NF_3 .

7.2 Chlorine

Chlorine has only limited significance in crystalline silicon. Its main applications in silicon technology are associated with the addition of chlorine during oxidation processing. The main features summarized below are increasing oxidation rate, decreasing generation of self-interstitials, improved oxide properties, and especially the ability to getter undesired impurities like sodium.

7.2.1 Chlorine in Silicon

Early investigations of Meyer [7.121] indicated that chlorine implanted with a high dose into silicon may act as a donor. A similar conclusion was drawn by Greeuw and Verwey [7.37]. Runge [7.122] investigated chlorine implants with significantly lower doses. In these samples, after annealing in hydrogen, an acceptor level 0.85 eV below the conduction band was found which correlated in dose to the implanted chlorine atoms. Krasnobaev and Omelyanovskaya [7.123] finally observed a complex annealing behavior from which they concluded that acceptor-like and donor-like defects may form, depending on the particular annealing conditions.

An *ab-initio* study of Chadi [7.41] indicated that substitutional chlorine and chlorine on bond-centered interstitial sites would be shallow donors. In the energetically much less favorable tetrahedral interstitial configuration, on the other hand, it was found to act as an acceptor. From the energetics of Cl_n clusters, such complexes were suggested to be the main reason for deactivation. Because of the low mobility of chlorine, Chadi suggested that cluster formation would be impeded so that chlorine doping might be a candidate to achieve very high donor concentrations.

Proposed first by Müller et al. [7.1], BCl molecules can be used instead of boron to reduce the effective implantation energy of boron in proportion to the masses by a factor of 11/46 for ^{11}B . It probably became never popular since it was reported that chlorine inhibits boron activation and leads to enhanced diffusion in comparison to BF_2 -implanted samples [7.63, 7.106, 7.107]. It was also reported that BCl_2 implantation for ultrashallow junctions leads to a drastically increased leakage current in comparison to BF_2 [7.124].

Searching for means to reduce transient diffusion during post-implantation annealing processes, Roberts et al. [7.125] co-implanted preamorphized structures with boron and chlorine. This led to a slight decrease in the transient diffusion of the boron and an increased electrical activation.

Diffusion of implanted chlorine was investigated by Datar et al. [7.126]. For a dose of 10^{13} cm^{-2} , profile evolution during annealing at 1100°C from two to eight hours was characterized by a continuous reduction of the concentration, especially at the surface-near side, without apparent broadening. This behavior is typical for a process in which the main barrier is the liberation of mobile species from some immobile complexes followed by a rapid diffusion of the mobile species to the surface and to interfaces. For a dose of $5 \cdot 10^{14} \text{ cm}^{-2}$, the chlorine remained virtually immobile even after annealing for eight hours at 1100°C and a reduction of the chlorine concentration was observed only near the surface.

7.2.2 Addition of Chlorine Compounds during Oxidation

The first major application of chlorine was driven in the 1970s by the discovery that the addition of chlorine or chlorine compounds during oxidation may improve the properties of oxides. A comprehensive review of such effects was given by Monkowski [7.127, 7.128]. Phenomena associated were in particular the gettering of mobile ions like sodium [7.129–7.133], improvements in the minority-carrier lifetime [7.134–7.138], and the dielectric breakdown strength

[7.139–7.143], as well as a reduction of noise in MOSFETs [7.144]. At least for low chlorine contents, an improvement of the hardness of gate oxides against degradation induced by high-energetic charge carriers and radiation [7.2, 7.145], and a reduction of the interface-trap density [7.146] were reported. Because of safety reasons and the corrosiveness of Cl₂ and HCl, compounds like CCl₄ [7.147], trichloroethylene (TCE, CHCl=CCl₂, turned out to be carcinogen) [7.129, 7.147], 1,1,1-trichloroethane (TCA, CH₃-CCl₃, turned out to be an ozone killer) [7.141], and eventually trans-1,2 dichloroethylene (t-DCE, CHCl=CHCl) [7.148] were soon investigated as replacements. Typically, beneficial effects of, e. g. HCl oxidation requires temperatures of 1150 °C and above for a 30 min oxidation. With TCE and TCA, the process temperature could be lowered towards 900 °C while keeping some of the beneficial effects. Major problems associated with the addition of chlorine compounds during oxidation were etching of the silicon and the eventual delamination of the oxide observed upon prolonged oxidation or annealing in inert ambient [7.149–7.152]. Despite the trend to ever thinner oxides, the addition of chlorine compounds is still wide-spread in VLSI technology although, maybe, not in the leading-edge technologies.

In several investigations it was found that an effective passivation can be achieved only when the partial pressure of the chlorine compound used during dry oxidation exceeds a certain threshold [7.130, 7.131, 7.153]. This threshold, which has to be understood as a “steep portion of a continuous, smooth curve, rather than a sharp discontinuity” [7.154], reduces for higher temperatures or longer process times. When exceeding the threshold, a roughening of the interface was frequently noted [7.151, 7.155–7.158] and associated with the formation of a chlorine-rich phase at the interface. Later, Claeys et al. [7.152] showed that the roughening results from the formation of gas bubbles near the silicon/silicon dioxide interface. Their growth and coalescence would finally lead to the lift-off of the oxide mentioned above.

Various characterization methods resulted in the conclusion that the chlorine piles up at the oxide side of the interface between silicon and silicon dioxide [7.132, 7.155, 7.159–7.161]. This corresponds to the site where the sodium passivation was found to occur [7.155]. Increases in temperature, oxidation time, and partial pressure led to a continuous increase in the chlorine concentration. Measurements by Rohatgi et al. [7.156] showed that the chlorine content in the oxide increases rapidly within a certain range of chlorine partial pressures. Below and above this range, chlorine incorporation occurs at a significantly lower rate. The work of Rohatgi et al. [7.153] further showed that the lower limit corresponds to the threshold for passivation of mobile ions while the upper limit correlates approximately to the lowest partial pressure at which complete passivation can be achieved.

Investigations of oxides grown in H₂O/HCl ambients either by bubbling N₂ through H₂O [7.160] or by a pyrogenic process [7.162] showed that they contained significantly less chlorine at the interface than oxides grown in H₂O/HCl ambients by bubbling O₂ through H₂O, or in O₂/HCl ambients. It was thus concluded that the presence of uncomplexed oxygen plays some role in the chlorine-incorporation process and that chlorine incorporation is not associated with the simple replacement of oxygen in the silicon dioxide by chlorine. The latter point is also in agreement with the observation that no significant sodium passivation can be achieved by annealing of oxides in a chlorine-compound-containing ambient in which the oxygen is replaced by an inert gas [7.163].

An explanation for the mechanism of passivation of sodium was the goal of several investigations. Measurements of the activation energy by Kriegler and Devenyi [7.164] resulted in a value of 0.8 eV. They concluded from their experiments that the time constant for passivation is much longer than the time required by sodium atoms to reach the interface and assumed that the rate-limiting step is the reaction between the sodium and the chlorine. Later, Stagg

and Boudry [7.157] reported an activation energy of 0.87 eV. In their explanation, the rate-limiting step is the lateral diffusion of the sodium atoms at the silicon/silicon dioxide interface to chlorine-containing islands discussed above. For this process, the activation energy was found to be 0.8 eV [7.165].

The beneficial effect of the addition of chlorine compounds during oxidation on the lifetime of minority charge carriers was usually associated with the gettering of undesired metallic impurities in the oxide. In contrast, the investigation of Janssens and Declerck [7.166] indicated that the effect is associated primarily with the suppression of stacking faults.

Investigations of the oxidation kinetics indicated that oxide growth in dry O₂ is enhanced significantly by the addition of some percent of HCl [7.130, 7.136, 7.167–7.169], Cl₂ [7.130, 7.168, 7.170], CCl₄ [7.171], TCE [7.133, 7.140, 7.141, 7.172, 7.173], and TCA [7.141, 7.174–7.176]. Some quantitative estimates on the basis of the model of Deal and Grove [7.177] indicated that especially the parabolic rate constant increases with increasing chlorine concentration. In other investigations, also an increase in the linear growth rate was found, reflecting probably the known difficulties in differentiating between the two experimentally. Addition of chlorine compounds during wet oxidation, on the other hand leads to a slightly decreased oxide growth associated with the reduced partial pressure of water vapor [7.178, 7.179]. Even for oxidation in dry O₂, qualitative differences were found in the effects of different chlorine compounds on oxidation kinetics. As an example, about the same oxide thickness results from adding 1.5% Cl₂ or TCE, or from more than 10% HCl. To explain such phenomena, Ritchey et al. [7.180] and Tressler et al. [7.181] considered the formation of various gaseous Cl-O-H compounds in the oxidation furnace. They then found a correlation between the parabolic rate constant of oxide growth and the partial pressure of Cl₂ (and possibly ClO), regardless of whether Cl₂ or HCl was used as additive. A similar correlation was found between the passivation of mobile ions and the Cl₂ partial pressure, explaining the observation of Kriegler [7.149] that trace amounts of water vapor may significantly reduce the beneficial effects of adding HCl during dry oxidation. In the analysis of Ehara et al. [7.182], oxide growth in the O₂-H₂-HCl system was entirely explained by the partial pressures of O₂ and H₂O established by chemical reactions in the gas phase. Similar to the addition of chlorine compounds, implantation of chlorine prior to the oxidation was found to increase the oxidation rate [7.37, 7.183]. This effect was observed for oxidation in dry O₂ but also in H₂O ambients. It was speculated that the implanted chlorine might pile up at the interface in both ambients, thus leading to the observed phenomenon. However, it is also known that even the implantation of noble-gas ions causes oxidation enhancement.

From the enhanced oxidation rate of dry oxidation processes, one might have expected an enhanced generation of self-interstitials due to the addition of chlorine compounds, too. In contrast, the addition of HCl [7.184–7.186] or TCE [7.187] during dry oxidation and the implantation of chlorine prior to oxidation [7.183, 7.188, 7.189] were found to reduce the growth of stacking faults and even cause their shrinkage for sufficiently high chlorine-compound concentrations. In agreement with such observations, Nabeta et al. [7.190] reported that the addition of HCl during dry oxidation causes a reduction of the diffusion of boron and phosphorus. For certain HCl concentrations and temperatures, the diffusion of phosphorus was even found to be retarded with respect to annealing in inert ambients but artifacts from high surface concentrations and the simple measurement technique via sheet resistivity and junction depth cannot be excluded. A reduction of the oxidation-enhanced diffusion of phosphorus and boron was also observed by Solmi and Negrini [7.183] who introduced the chlorine by ion implantation prior to dry or wet oxidation. In the experiments of Oh et al. [7.191], a buried antimony marker layer was used to monitor the effects of HCl additions to dry O₂. It was found that the HCl does not

lead to a generation of vacancies but rather reduces the generation of self-interstitials. Retarded diffusion of boron and arsenic upon addition of HCl during dry oxidation was also observed by Subrahmanyam et al. [7.192] and modeled by an empirical relation. In an investigation of the effects of HCl on the kinetics of stacking faults during wet oxidation, Shibayama et al. [7.160] found that the growth of stacking faults decreased when N₂ was bubbled through H₂O. On the other hand, when O₂ was bubbled through H₂O, the stacking faults shrunk after an initial growth and finally disappeared. Similar results were obtained by Hattori [7.179] bubbling O₂ independently through H₂O and liquid TCE.

Initially, it was often speculated that the chlorine may lead to a generation of vacancies at the silicon/silicon dioxide interface. An alternative explanation for the effects of chlorine on the generation of self-interstitials during oxidation was given by Oh et al. [7.191], following the suggestion of Kriegler [7.163] that such oxides contain Si-O-Cl complexes which form during oxide growth. The Cl atom is thought to replace an oxygen atom which leads to a non-bridging bond and makes the SiO₂ network less rigid. As a consequence, self-interstitials may diffuse more easily into the oxide so that less will be injected into the silicon.

7.3 Bromine

In comparison to fluorine and chlorine, only very few experimental and theoretical investigations were concerned with bromine.

Because of its higher molecular weight, implantation of BBr₂ seems a logical extension of BF₂ and BCl₂. Comparing BF₂, BCl₂, and BBr₂ implants, Ganguly et al. [7.124] concluded that the latter might indeed be a superior replacement of BF₂ for ultra-small devices. Searching for means to reduce transient diffusion during post-implantation processes, Roberts et al. [7.125] co-implanted preamorphized structures with boron and bromine. The result was a degradation of the electrical properties in comparison to the boron implant.

An *ab-initio* study of Chadi [7.41] indicated that substitutional bromine would be a shallow donor. In the energetically much less favorable tetrahedral interstitial configuration, on the other hand, it was found to act as an acceptor. In analogy to his work on lithium-saturated vacancies, Tarnow [7.193] investigated a defect configuration in which a vacancy is surrounded by four bromine atoms on tetrahedral interstitial sites. This T_d-symmetric configuration was found to be 8.0 eV more stable than a similar configuration in which one of the bromine atoms occupies the site of the vacancy.

Addition of HBr during dry oxidation as a substitute for chlorine compounds led to detrimental effects on the minority-carrier lifetime [7.147] while the dielectric breakdown strength of the oxides was found to be improved [7.139]. Also reported was a drastic increase in the density of interface states with a pronounced peak at about $E_v + 0.15$ eV [7.194].

Similar to the other halogens, bromine was found in an initial investigation by Poon and Card [7.194] to enhance dry oxidation. Later, Susa et al. [7.195] reported that bromine causes a reduction of the linear oxidation rate while the parabolic rate was enhanced. From a correlation to the depth distribution of bromine it was concluded that the accumulation of bromine at the interface retards oxidation while an incorporation in the bulk of the silicon dioxide enhances it.

Bibliography

- [7.1] H. Müller, H. Ryssel, and K. Schmid, “Electrical Properties of Silicon Layers Implanted with BF₂ Molecules,” *J. Appl. Phys.*, vol. 43, no. 4, 2006–2008 (1972).
- [7.2] Y. Nishioka, E. F. Da Silva, Jr., Y. Wang, and T.-P. Ma, “Dramatic Improvement of Hot-Electron-Induced Interface Degradation in MOS Structures Containing F or Cl in SiO₂,” *IEEE Electron Device Letters*, vol. 9, no. 1, 38–40 (1988).
- [7.3] Y. Nishioka, Y. Ohji, K. Mukai, T. Sugano, Y. Wang, and T. P. Ma, “Dielectric Characteristics of Fluorinated Ultradry SiO₂,” *Appl. Phys. Lett.*, vol. 54, no. 12, 1127–1129 (1989).
- [7.4] B.-g. Yu, E. Arai, and T. P. Ma, “Investigation of Fluorine in SiO₂ and on Si Surface by the ¹⁹F(p, α y)¹⁶O Reaction, Secondary-Ion Mass Spectrometry, and X-Ray Photoelectron Spectroscopy,” *Appl. Phys. Lett.*, vol. 56, no. 15, 1430–1432 (1990).
- [7.5] M. D. Deal, D. Pramanik, A. N. Saxena, and K. C. Saraswat, “Tungsten Silicide/n⁺ Polysilicon Technology for VLSI,” in: *Proceedings of the 2nd International IEEE VLSI Multilevel Interconnection Conference*, New York: IEEE, 324–334 (1985).
- [7.6] Y. Shioya, S. Wawamura, I. Kobayashi, M. Maeda, and K. Yanagida, “Effect of Fluorine in Chemical-Vapor-Deposited Tungsten Silicide Film on Electrical Breakdown of SiO₂ Film,” *J. Appl. Phys.*, vol. 61, no. 11, 5102–5109 (1987).
- [7.7] V. Jain, D. Pramanik, K. Y. Chang, and C. Hu, “Improved Sub-Micron CMOS Device Performance Due to Fluorine in CVD Tungsten Silicide,” in: *1991 Symposium on VLSI Technology*, Japan Society of Applied Physics & IEEE Electron Devices Society, 91–92 (1991).
- [7.8] U. S. Kim and R. J. Jaccodine, “Fast Shrinkage of Oxidation Stacking Faults during O₂/NF₃ Oxidation of Silicon,” *Appl. Phys. Lett.*, vol. 49, no. 18, 1201–1203 (1986).
- [7.9] E. F. da Silva, Jr., Y. Nishioka, and T.-P. Ma, “Radiation and Hot-Electron Hardened MOS Structures Based on SiO₂ Grown in O₂ + NF₃,” in: *Technical Digest of the 1987 International Electron Devices Meeting (IEDM)*, New York: IEEE, 848–849 (1987).
- [7.10] W. Ting, G. Q. Lo, T. Y. Hsieh, D. L. Kwong, J. Kuehne, and C. Magee, “Fluorinated Thin SiO₂ Grown by Rapid Thermal Processing,” *Appl. Phys. Lett.*, vol. 56, no. 22, 2255–2257 (1990).
- [7.11] J. Ahn, G. Q. Lo, W. Ting, D. L. Kwong, J. Kuehne, and C. W. Magee, “Radiation Hardened Metal-Oxide-Semiconductor Devices with Gate Dielectrics Grown by Rapid Thermal Processing in O₂ with Diluted NF₃,” *Appl. Phys. Lett.*, vol. 58, no. 4, 425–427 (1991).
- [7.12] G. Q. Lo, W. Ting, J. H. Ahn, D. Kwong, and J. Kuehne, “Thin Fluorinated Gate Dielectrics Grown by Rapid Thermal Processing in O₂ with Diluted NF₃,” *IEEE Trans. Electron Devices*, vol. 39, no. 1, 148–153 (1992).
- [7.13] K. Inoue, M. Nakamura, M. Okuyama, and Y. Hamakawa, “Reduction of Interface-State Density by F₂ Treatment in a Metal-Oxide Semiconductor Diode Prepared from a Photochemical Vapor Deposited SiO₂ Film,” *Appl. Phys. Lett.*, vol. 55, no. 23, 2402–2404 (1989).
- [7.14] A. Bhattacharyya, C. Vorst, and A. H. Carim, “A Two-Step Oxidation Process to Improve the Electrical Breakdown Properties of Thin Oxides,” *J. Electrochem. Soc.*, vol. 132, no. 8, 1900–1903 (1985).
- [7.15] P. J. Wright and K. C. Saraswat, “The Effect of Fluorine in Silicon Dioxide Gate Dielectrics,” *IEEE Trans. Electron Devices*, vol. 36, no. 5, 879–889 (1989).
- [7.16] K. Ohyu, T. Itoga, Y. Hishioka, and N. Natsuaki, “Improvement of SiO₂/Si Interface Properties Utilising Fluorine Ion Implantation and Drive-in Diffusion,” *Jpn. J. Appl. Phys.*, vol. 28, no. 6, 1041–1045 (1989).
- [7.17] J. R. Pfeister, F. K. Baker, T. C. Mele, H.-H. Tseng, P. J. Tobin, J. D. Hayden, J. W. Miller, C. D. Gunderson, and L. C. Parrillo, “The Effects of Boron Penetration on p⁺ Polysilicon Gated PMOS Devices,” *IEEE Trans. Electron Devices*, vol. 37, no. 8, 1842–1851 (1990).
- [7.18] U. S. Kim and R. J. Jaccodine, “Fluorine Enhanced Oxidation of Silicon and Related Phenomena,” in: *Semiconductor Silicon 1990*, edited by H. R. Huff, K. G. Barracough, and J.-i. Chikawa, *Electrochem. Soc. Proc.*, vol. 90-7, 376–387 (1990).

- [7.19] K. P. MacWilliams, L. F. Halle, and T. C. Zietlow, "Improved Hot-Carrier Resistance with Fluorinated Gate Oxides," *IEEE Electron Device Letters*, vol. 11, no. 1, 3–5 (1990).
- [7.20] Y. Nishioka, K. Ohyu, N. Natuaki, K. Mukai, and T. P. Ma, "The Effect of Fluorine Implantation on the Interface Radiation Hardness of Si-Gate Metal-Oxide-Semiconductor Transistors," *J. Appl. Phys.*, vol. 66, no. 8, 3909–3912 (1989).
- [7.21] L. Vishnubhotla, T. P. Ma, H.-H. Tseng, and P. J. Tobin, "Interface Trap Generation and Electronic Trapping in Fluorinated SiO_2 ," *Appl. Phys. Lett.*, vol. 59, no. 27, 3595–3597 (1991).
- [7.22] X.-W. Wang, A. Balasinski, T. P. Ma, and Y. Nishioka, "Pre-Oxidation Fluorine Implantation into Si," *J. Electrochem. Soc.*, vol. 139, no. 1, 238–241 (1992).
- [7.23] E. F. da Silva, Jr., Y. Nishioka, and T.-P. Ma, "Radiation Response of MOS Capacitors Containing Fluorinated Oxides," *IEEE Trans. Nuclear Science*, vol. NS-34, no. 6, 1190–1195 (1987).
- [7.24] Y. Nishioka, K. Ohyu, Y. Ohji, N. Natuaki, K. Mukai, and T.-P. Ma, "Hot-Electron Hardened Si-Gate MOSFET Utilizing F Implantation," *IEEE Electron Device Letters*, vol. 10, no. 4, 141–143 (1989).
- [7.25] Y. Mitani, H. Satake, Y. Nakasaki, and Y. Toriumi, "Reexamination of Fluorine Incorporation into SiO_2 — Significant Improvement of Charge-to-Breakdown Distribution Tail," in: *Proceedings of the 37th International Reliability Physics Symposium*, Piscataway: IEEE, 93–98 (1999).
- [7.26] D. Kouvatsos, J. G. Huang, and R. J. Jaccodine, "Fluorine-Enhanced Oxidation of Silicon — Effects of Fluorine on Oxide Stress and Growth Kinetics," *J. Electrochem. Soc.*, vol. 138, no. 6, 1752–1755 (1991).
- [7.27] D. Kouvatsos, J. G. Huang, V. Saikumar, P. J. Macfarlane, R. J. Jaccodine, and F. A. Stevie, " SiO_2 Film Stress — Thickness Dependence, Non-Planar Oxidation, and Fluorine-Related Effects," *J. Electrochem. Soc.*, vol. 139, no. 8, 2322–2326 (1992).
- [7.28] K. Ohyu, T. Itoga, and N. Natuaki, "Advantages of Fluorine Introduction in Boron Implanted Shallow p⁺/n-Junction Formation," *Jpn. J. Appl. Phys.*, vol. 29, no. 3, 457–462 (1990).
- [7.29] P. J. Wright, N. Kasai, S. Inoue, and K. C. Saraswat, "Hot-Electron Immunity of SiO_2 Dielectrics with Fluorine Incorporation," *IEEE Electron Device Letters*, vol. 10, no. 8, 347–348 (1989).
- [7.30] D. Krüger, J. Dabrowski, P. Gaworzewski, R. Kurps, and K. Pomplun, "Fluorine Incorporation into Gate Stacks of Advanced Silicon Memory Technologies: Simulation, Depth Distribution, and Reliability," *J. Appl. Phys.*, vol. 90, no. 7, 3578–3584 (2001).
- [7.31] P. Chowdhury, A. I. Chou, K. Kumar, C. Lin, and J. C. Lee, "Improvement of Ultrathin Gate Oxide and Oxynitride Integrity Using Fluorine Implantation Technique," *Appl. Phys. Lett.*, vol. 70, no. 1, 37–39 (1997).
- [7.32] J. J. Sung and C.-Y. Lu, "A Comprehensive Study on p⁺ Polysilicon-Gate MOSFET's Instability with Fluorine Incorporation," *IEEE Trans. Electron Devices*, vol. 37, no. 11, 2312–2321 (1990).
- [7.33] T. Mogami, L. E. G. Johansson, I. Sakai, and M. Fukuma, "Hot-Carrier Effects in Surface-Channel PMOSFETs with BF₂- or Boron-Implanted Gates," in: *Technical Digest of the 1991 International Electron Devices Meeting (IEDM)*, New York: IEEE, 533–536 (1991).
- [7.34] H.-H. Tseng, P. J. Tobin, F. K. Baker, J. R. Pfeister, K. Evans, and P. L. Fejes, "The Effect of Silicon Gate Microstructure and Gate Oxide Process on Threshold Voltage Instabilities in p⁺-Gate p-Channel MOSFET's with Fluorine Incorporation," *IEEE Trans. Electron Devices*, vol. 39, no. 7, 1687–1693 (1992).
- [7.35] C.-C. Chen, H.-C. Lin, C.-Y. Chang, T.-Y. Huang, C.-H. Chien, and M.-S. Liang, "Improved Ultrathin Gate Oxide Integrity in p⁺-Polysilicon-Gate p-Channel Metal Oxide Semiconductor with Medium-Dose Fluorine Implantation," *Electrochemical and Solid State Letters*, vol. 3, no. 6, 290–292 (2000).
- [7.36] Y. Suizu, "Reexamination of the Role of Nitrogen in Oxynitrides — Fixed Charge Reduction in the p⁺-Polysilicon Gate MOS," *IEEE Trans. Electron Devices*, vol. 48, no. 12, 2777–2784 (2001).

- [7.37] G. Greeuw and J. F. Verwey, “Donor Generation in Monocrystalline Silicon by Halogen Implantation,” *Solid-State Electronics*, vol. 26, no. 3, 241–246 (1983).
- [7.38] S. Zaima, Y. Yasuda, M. Ito, and T. Nakamura, “Effects of Fluorine Ion Implantation on Metal-Oxide-Semiconductor Devices of Silicon-on-Sapphire,” *Appl. Phys. Lett.*, vol. 52, no. 6, 459–461 (1988).
- [7.39] C. H. Chu, L. J. Chen, and H. L. Hwang, “Formation of Surface Inversion Layer in F⁺-Implanted n-Type Silicon,” *J. Crystal Growth*, vol. 103, 188–196 (1990).
- [7.40] N. M. Omel’yanovskaya, L. Y. Krasnobaev, and V. V. Fedorov, “Influence of Postimplantation Annealing on Electrical Properties of Fluorine-Implanted Silicon Layers,” *Semiconductors*, vol. 27, no. 4, 308–310 (1993).
- [7.41] D. J. Chadi, “Halogen Impurities in Silicon: Shallow Single Donors,” *Appl. Phys. Lett.*, vol. 71, no. 6, 806–808 (1997).
- [7.42] T. Hirose, T. Shano, R. Kim, H. Tsuji, Y. Kamakura, and K. Taniguchi, “Atomic Configuration Study of Implanted F in Si Based on Experimental Evidence and Ab Initio Calculations,” *Materials Science and Engineering B*, vol. 91–92, 148–151 (2002).
- [7.43] C. G. van de Walle, Y. Bar-Yam, F. R. McFeely, and S. T. Pantelides, “Summary Abstract: Theoretical Investigations of Fluorine-Silicon Systems,” *J. Vac. Sci. Technol. A*, vol. 6, no. 3, 1973–1974 (1988).
- [7.44] C. G. Van de Walle, F. R. McFeely, and S. T. Pantelides, “Fluorine-Silicon Reactions and the Etching of Crystalline Silicon,” *Phys. Rev. Lett.*, vol. 61, no. 16, 1867–1870 (1988).
- [7.45] A. Taguchi and Y. Hirayama, “Stable Site and Stable Charge State of Fluorine Atom in Si,” *Solid State Communications*, vol. 116, 595–597 (2000).
- [7.46] K. Bonde Nielsen, H. K. Schou, T. Lauritsen, G. Weyer, I. Steensgard, J. W. Petersen, and S. Damgaard, “The Electric Quadrupole Hyperfine Interaction at Sites of Ion-Implanted Fluorine in Amorphous and Crystalline Silicon,” *J. Phys. C*, vol. 17, 3519–3530 (1984).
- [7.47] S. S. Nunes, S. Sulaiman, N. Sahoo, T. P. Das, M. Frank, W. Kreische, and K. B. Nielsen, “Study of the Location of Implanted Fluorine Atoms in Silicon and Germanium through Their Nuclear Quadrupole Interactions,” *Z. Naturforsch.*, vol. 51a, 560–564 (1996).
- [7.48] T. Kinoshita, M. Takakura, S. Miyazaki, S. Yokoyama, M. Koyanagi, and M. Hirose, “Chemical Bonding Features of Fluorine and Boron in BF₂⁺-Ion-Implanted Si,” *Jpn. J. Appl. Phys.*, vol. 29, no. 12, L2349–L2352 (1990).
- [7.49] S.-P. Jeng, T.-P. Ma, R. Canteri, M. Anderle, and G. W. Rubloff, “Anomalous Diffusion of Fluorine in Silicon,” *Appl. Phys. Lett.*, vol. 61, no. 11, 1310–1312 (1992).
- [7.50] C. Szentes, B. Nielsen, P. Asoka-Kumar, K. G. Lynn, M. Anderle, T. P. Ma, and G. W. Rubloff, “Role of Implantation-Induced Defects in Surface-Oriented Diffusion of Fluorine in Silicon,” *J. Appl. Phys.*, vol. 76, no. 6, 3403–3409 (1994).
- [7.51] T. Shano, R. Kim, T. Hirose, Y. Furuta, H. Tsuji, M. Furuhashi, and K. Taniguchi, “Realization of Ultra-Shallow Junction: Suppressed Boron Diffusion and Activation by Optimized Fluorine Co-implantation,” in: *Technical Digest of the 2001 International Electron Devices Meeting (IEDM)*, Piscataway: IEEE, 821–824 (2001).
- [7.52] X. D. Pi, C. P. Burrows, and P. G. Coleman, “Fluorine in Silicon: Diffusion, Trapping, and Precipitation,” *Phys. Rev. Lett.*, vol. 90, 155901 (2003).
- [7.53] M. Diebel and S. T. Dunham, “Ab-Initio Calculations to Model Anomalous Fluorine Behavior,” in: *Silicon Front-End Junction Formation Technologies*, edited by D. F. Downey, M. E. Law, A. P. Claverie, and M. J. Rendon, *Mat. Res. Soc. Symp. Proc.*, vol. 717, C4.5.1–C4.5.6 (2002).
- [7.54] M. Diebel, S. Chakravarthi, S. T. Dunham, C. F. Machala, S. Ekbote, and A. Jain, “Investigation and Modeling of Fluorine Co-Implantation Effects on Dopant Redistribution,” in: *CMOS Front-End Materials and Process Technology*, edited by T.-J. King, B. Yu, R. J. P. Lander, and S. Saito, *Mat. Res. Soc. Symp. Proc.*, vol. 765, D6.15.1–D6.15.6 (2003).
- [7.55] R. G. Wilson, “Boron, Fluorine, and Carrier Profiles for B and BF₂ Implants into Crystalline and Amorphous Si,” *J. Appl. Phys.*, vol. 54, no. 12, 6879–6889 (1983).

- [7.56] Y. Kim, H. Z. Massoud, and R. B. Fair, "Boron Profile Changes during Low-Temperature Annealing of BF₂-Implanted Silicon," *Appl. Phys. Lett.*, vol. 53, no. 22, 2197–2199 (1988).
- [7.57] A. J. Walker, "Rapid Thermal Diffusion of Boron Implanted As Boron Difluoride in Preamorphized Silicon," *J. Appl. Phys.*, vol. 71, no. 4, 2033–2035 (1992).
- [7.58] T. Sands, J. Wahsburn, E. Myers, and D. K. Sadana, "On the Origins of Structural Defects in BF₂ -Implanted and Rapid Thermally-Annealed Silicon: Conditions for Defect-Free Regrowth," *Nuclear Instruments and Methods in Physics Research B*, vol. 7/8, 337–341 (1985).
- [7.59] M. Y. Tsai, D. S. Day, B. G. Streetman, P. Williams, and C. A. Evans, Jr., "Recrystallization of Implanted Amorphous Silicon Layers. II. Migration of Fluorine in BF₂⁺-Implanted Silicon," *J. Appl. Phys.*, vol. 50, no. 1, 188–192 (1979).
- [7.60] S. Prussin, D. I. Margolese, R. N. Tauber, and W. B. Hewitt, "Detection of Defect Structures in Arsenic Ion-Implanted Silicon by Fluorine Decoration," *J. Appl. Phys.*, vol. 56, no. 4, 915–923 (1984).
- [7.61] W. Maszara, C. Carter, D. K. Sadana, J. Liu, V. Ozguz, J. Ozguz, J. Wortman, and G. A. Rozgonyi, "Influence of Rapid Thermal Annealing on Shallow BF₂ Implantation into Pre-Amorphized Silicon," in: *Energy Beam-Solid Interactions and Transient Thermal Processing*, edited by J. C. C. Fan and N. M. Johnson, *Mat. Res. Soc. Symp. Proc.*, vol. 23, 285–291 (1984).
- [7.62] M. E. Lunnon, J. T. Chen, and J. E. Baker, "Structural and Electrical Properties of BF₂⁺ Implanted, Rapid Annealed Silicon," *Appl. Phys. Lett.*, vol. 45, no. 10, 1056–1058 (1984).
- [7.63] M. Delfino and M. E. Lunnon, "A Structural and Electrical Comparison of BCl and BF₂ Ion-Implanted Silicon," *J. Electrochem. Soc.*, vol. 132, no. 2, 435–440 (1985).
- [7.64] J. Narayan, O. W. Holland, W. H. Christie, and J. J. Wortman, "Rapid Thermal and Pulsed Laser Annealing of Boron Fluoride-Implanted Silicon," *J. Appl. Phys.*, vol. 57, no. 8, 2709–2716 (1985).
- [7.65] I.-W. Wu, R. T. Fulks, and J. C. Mikkelsen, Jr., "Optimization of BF₂⁺ Implanted and Rapidly Annealed Junctions in Silicon," *J. Appl. Phys.*, vol. 60, no. 7, 2422–2438 (1986).
- [7.66] G. Queirolo, P. Caprara, L. Meda, C. Guareschi, M. Anderle, G. Ottaviani, and A. Armigliato, "Lattice Damage, Boron Diffusion, and Dopant Activation in BF₂ Implanted Layers," *J. Electrochem. Soc.*, vol. 134, no. 11, 2905–2911 (1987).
- [7.67] K. Ohyu, T. Itoga, and N. Natsuaki, "Retardation of Boron Diffusion by Fluorine Implantation," in: *Proceedings of the 20th Symposium on Ion Implantation and Submicron Fabrication*, Wako: Institute of Physical and Chemical Research, 149–152 (1989).
- [7.68] L. Y. Krasnobaev, A. A. Malnin, V. V. Makarov, and I. B. Sayapin, "Interaction of Implanted into Silicon Fluorine with Radiation Effects," in: *Gettering and Defect Engineering in Semiconductor Technology GADEST'91*, edited by M. Kittler and H. Richter, *Solid State Phenomena*, vol. 19/20, 411–416 (1991).
- [7.69] M. I. Current, M. Inoue, S. Nakashima, N. Ohno, M. Kuribara, Y. Matsunaga, T. Hara, D. Wagner, S. Leung, B. Adibi, G. Lecouras, L. A. Larson, and S. Prussin, "Defect Engineering of p⁺-Junctions by Multiple-Species Ion Implantation," in: *Ion Implantation Technology*, edited by D. F. Downey, M. Farley, K. S. Jones, and G. Ryding, *Nuclear Instruments and Methods in Physics Research B*, vol. 74, 175–180 (1993).
- [7.70] T. H. Huang, H. Kinoshita, and D. L. Kwong, "Influence of Fluorine Preamorphization on the Diffusion and Activation of Low-Energy Implanted Boron during Rapid Thermal Annealing," *Appl. Phys. Lett.*, vol. 65, no. 14, 1829–1831 (1994).
- [7.71] N. Ohno, T. Hara, Y. Matsunaga, M. I. Current, and M. Inoue, "Diffusion of Ion-Implanted Boron Impurities into Pre-Amorphized Silicon," *Materials Science in Semiconductor Processing*, vol. 3, 221–225 (2000).
- [7.72] G. Queirolo, C. Bresolin, D. Robba, M. Anderle, R. Canteri, A. Armigliato, G. Ottaviani, and S. Frabboni, "Low Temperature Dopant Activation of BF₂ Implanted Silicon," *J. Electronic Materials*, vol. 20, no. 5, 373–378 (1991).

- [7.73] L. J. Chen, C. W. Nieh, and C. H. Chu, “Cross-Sectional Transmission Electron Microscope Study of BF_2^+ -Implanted (001) and (111) Silicon,” in: *Ion Implantation in Semiconductors*, edited by D. Stievenard and J. C. Bourgoin, *Solid State Phenomena*, vol. 1-2, 45–58 (1988).
- [7.74] G. E. Pike, M. J. Carr, W. K. Shubert, C. R. Hills, G. C. Nelson, and P. J. McWhorter, “Dislocations and Bubbles in BF_2 Implanted Silicon,” in: *Characterization of the Structure and Chemistry of Defects in Materials*, edited by B. C. Larson, M. Ruhle, and D. N. Seidman, *Mat. Res. Soc. Symp. Proc.*, vol. 138, 227–232 (1989).
- [7.75] C. H. Chu, J. J. Yang, and L. J. Chen, “Influence of Point Defects on Formation of Fluorine Bubbles and Characterization of Defects in BF_2^+ Implanted Silicon,” in: *Ion Implantation Technology*, edited by D. F. Downey, M. Farley, K. S. Jones, and G. Ryding, *Nuclear Instruments and Methods in Physics Research B*, vol. 74, 138–141 (1993).
- [7.76] A. Uedono, T. Kitano, M. Watanabe, T. Moriya, N. Komuro, T. Kawano, S. Tanigawa, R. Suzuki, T. Ohdaira, and T. Mikado, “Fluorine-Related Defects in BF_2^+ -Implanted Si Probed by Monoenergetic Positron Beams,” *Jpn. J. Appl. Phys., Part 1*, vol. 36, no. 3A, 969–974 (1997).
- [7.77] D. Kouvatsos, F. P. McCluskey, R. J. Jaccodine, and F. A. Stevie, “Silicon-Fluorine Bonding and Fluorine Profiling in SiO_2 Films Grown by NF_3 -Enhanced Oxidation,” *Appl. Phys. Lett.*, vol. 61, no. 7, 780–782 (1992).
- [7.78] C.-Y. Lin, F.-M. Pan, P.-F. Chou, and C.-Y. Chang, “Effect of Oxygen Impurity on Microstructure and Boron Penetration in a BF_2^+ Implanted LPCVD Stacked Amorphous Silicon p^+ Gated PMOS Capacitor,” *J. Electrochem. Soc.*, vol. 142, no. 7, 2434–2437 (1995).
- [7.79] R. Williams and M. H. Woods, “Mobile Fluorine Ions in SiO_2 ,” *J. Appl. Phys.*, vol. 46, no. 2, 695–698 (1975).
- [7.80] F. G. Kuper, J. T. M. De Hosson, and J. F. Verwey, “Effects of Fluorine Implantation on the Kinetics of Dry Oxidation of Silicon,” *J. Appl. Phys.*, vol. 60, no. 3, 985–990 (1986).
- [7.81] Y. Ono, M. Tabe, and Y. Sakakibara, “Segregation and Defect Termination of Fluorine at SiO_2/Si Interfaces,” *Appl. Phys. Lett.*, vol. 62, no. 4, 375–377 (1993).
- [7.82] M. Morita, S. Aritome, M. Tsukude, and M. Hirose, “A New SiO_2 Growth by Fluorine-Enhanced Thermal Oxidation,” in: *Technical Digest of the 1984 International Electron Devices Meeting (IEDM)*, New York: IEEE, 144–147 (1984).
- [7.83] P. J. Wright and K. C. Saraswat, “Comment on ‘Hot-Electron Hardened Si-Gate MOSFET Utilizing F Implantation’,” *IEEE Electron Device Letters*, vol. 10, no. 8, 397 (1989).
- [7.84] Y. Nishioka, K. Ohyu, Y. Ohji, N. Natsuaki, K. Mukai, and T.-P. Ma, “Reply to ‘Comment on ‘Hot-Electron Hardened Si-Gate MOSFET Utilizing F Implantation’’,” *IEEE Electron Device Letters*, vol. 10, no. 8, 397–399 (1989).
- [7.85] M. Fujinami and N. B. Chilton, “A Slow Positron Beam Study of Vacancy Formation in Fluorine-Implanted Silicon,” *J. Appl. Phys.*, vol. 73, no. 7, 3242–3245 (1993).
- [7.86] J. Kato, “The Effects of Fluorine Atoms in High-Dose Arsenic or Phosphorus Ion Implanted Silicon,” *J. Electrochem. Soc.*, vol. 137, no. 6, 1918–1924 (1990).
- [7.87] S. Ando, H. Horie, M. Imai, K. Oikawa, H. Kato, H. Ishiwari, and S. Hijiya, “Very Shallow p^+-n Junctions and Subquarter Micron Gate p -Channel MOSFETs,” in: *1990 Symposium on VLSI Technology*, IEEE Electron Devices Society & Japan Society of Applied Physics, 65–66 (1990).
- [7.88] D. Lin and T. A. Rost, “The Impact of Fluorine on CMOS Channel Length and Shallow Junction Formation,” in: *Technical Digest of the 1993 International Electron Devices Meeting (IEDM)*, Piscataway: IEEE, 843–846 (1993).
- [7.89] L. Y. Krasnobaev, N. M. Omelyanovskaya, and V. V. Makarov, “The Effect of Fluorine on the Redistribution of Boron in Ion-Implanted Silicon,” *J. Appl. Phys.*, vol. 74, no. 10, 6020–6022 (1993).
- [7.90] J. Liu, D. F. Downey, K. S. Jones, and E. Ishida, “Fluorine Effect on Boron Diffusion: Chemical or Damage?” in: *Ion Implantation Technology—98*, edited by J. Matsuo, G. Takaoka, and I. Yamada, Piscataway: IEEE, 951–954 (1999).

- [7.91] H.-H. Vuong, H.-J. Gossman, C. S. Rafferty, H. S. Luftman, F. C. Unterwald, D. C. Jacobson, R. E. Ahrens, T. Boone, and P. M. Zeitzoff, "Influence of Fluorine Implant on Boron Diffusion: Determination of Process Modeling Parameters," *J. Appl. Phys.*, vol. 77, no. 7, 3056–3060 (1995).
- [7.92] D. F. Downey, J. W. Chow, E. Ishida, and K. S. Jones, "Effect of Fluorine on the Diffusion of Boron in Ion Implanted Si," *Appl. Phys. Lett.*, vol. 73, no. 9, 1263–1265 (1998).
- [7.93] L. S. Robertson, P. N. Warnes, K. S. Jones, S. K. Earles, M. E. Law, D. F. Downey, S. Falk, and J. Liu, "Junction Depth Reduction of Ion Implanted Boron in Silicon through Fluorine Ion Implantation," in: *Si Front-End Processing — Physics and Technology of Dopant-Defect Interactions II*, edited by A. Agarwal, L. Pelaz, H.-H. Vuong, P. Packan, and M. Kase, *Mat. Res. Soc. Symp. Proc.*, vol. 610, B4.2.1–B4.2.6 (2000).
- [7.94] A. Dusch, J. Marcon, K. Masmoudi, F. Olivie, M. Benzohra, K. Ketata, and M. Ketata, "Modeling of the Transient Enhanced Diffusion of Boron Implanted into Preamorphized Silicon: The Case of BF₂ Implantation," *Materials Science and Engineering B*, vol. 80, 65–67 (2001).
- [7.95] A. Dusch, J. Marcon, K. Masmoudi, K. Ketata, F. Olivie, M. Benzohra, and M. Ketata, "Influence of Fluorine on the Simulation of the Transient Enhanced Diffusion of 15 keV BF₂⁺ Ion Implantation into Silicon," *Nuclear Instruments and Methods in Physics Research B*, vol. 186, 360–365 (2002).
- [7.96] H. A. W. El Mubarek and P. Ashburn, "Reduction of Boron Thermal Diffusion in Silicon by High Energy Fluorine Implantation," *Appl. Phys. Lett.*, vol. 83, no. 20, 4134–4136 (2003).
- [7.97] A. Mokhberi, R. Kasnavi, P. B. Griffin, and J. D. Plummer, "Fluorine Interaction with Point Defects, Boron, and Arsenic in Ion-Implanted Si," *Appl. Phys. Lett.*, vol. 80, no. 19, 3530–3532 (2002).
- [7.98] E. Ishida, D. F. Downey, K. S. Jones, and J. Liu, "The Chemical Effect of Fluorine on Boron Transient Enhanced Diffusion," in: *Ion Implantation Technology—98*, edited by J. Matsuo, G. Takaoka, and I. Yamada, Piscataway: IEEE, 909–912 (1999).
- [7.99] R. Kasnavi, P. B. Griffin, and J. D. Plummer, "A Comparative Study of Dose Loss and Diffusion for B¹¹ and BF₂ Implants," in: *Si Front-End Processing — Physics and Technology of Dopant-Defect Interactions II*, edited by A. Agarwal, L. Pelaz, H.-H. Vuong, P. Packan, and M. Kase, *Mat. Res. Soc. Symp. Proc.*, vol. 610, B4.3.1–B4.3.6 (2000).
- [7.100] B. Colombeau, F. Cristiano, G. Ben Assayag, A. Altibelli, and A. Claverie, "Energetics of Interstitial Defects and TED in Ultra Low Energy Implants," in: *Ion Implantation Technology — 2000*, edited by H. Ryssel, L. Frey, J. Gyulai, and H. Glawischnig, Piscataway: IEEE, 107–110 (2000).
- [7.101] M. Uematsu, "Simulation of Boron Diffusion in High-Dose BF₂ Implanted Silicon," *Jpn. J. Appl. Phys., Part 1*, vol. 39, no. 4A, 1608–1611 (2000).
- [7.102] A. Höfler, T. Feudel, N. Strecker, W. Fichtner, K. Suzuki, Y. Kataoka, N. Sasaki, and K.-H. Stegemann, "Modeling of Boron Diffusion after Shallow Implants Using BF₂," in: *Process Physics and Modeling in Semiconductor Technology*, edited by G. R. Srinivasan, C. S. Murthy, and S. T. Dunham, *Electrochem. Soc. Proc.*, vol. 96-4, 75–84 (1996).
- [7.103] Y.-J. Park and J.-J. Kim, "Fluorine Implantation Effect on Boron Diffusion in Si," *J. Appl. Phys.*, vol. 85, no. 2, 803–806 (1999).
- [7.104] R. R. Robinson and M. E. Law, "Fluorine Diffusion: Models and Experiments," in: *Technical Digest of the 2002 International Electron Devices Meeting (IEDM)*, Piscataway: IEEE, 883–886 (2002).
- [7.105] G. Impellizzeri, J. H. R. dos Santos, S. Mirabella, F. Priolo, E. Napolitani, and A. Carnera, "Role of Fluorine in Suppressing Boron Transient Enhanced Diffusion in Preamorphized Si," *Appl. Phys. Lett.*, vol. 84, no. 11, 1862–1864 (2004).
- [7.106] D. G. Beanland, "The Behaviour of Boron Molecular Ion Implants into Silicon," *Solid-State Electronics*, vol. 21, 537–547 (1978).
- [7.107] G. Fuse, T. Hirao, K. Inoue, S. Takayanagi, and Y. Yaegashi, "Electrical Properties of Si Heavily Implanted with Boron Molecular Ions," *J. Appl. Phys.*, vol. 53, no. 5, 3650–3653 (1982).

- [7.108] J. Kato, "The Annealing Time and Temperature Dependence of Electrical Dopant Activation in High-Dose BF₂ Ion Implanted Silicon," *J. Electrochem. Soc.*, vol. 141, no. 11, 3158–3161 (1994).
- [7.109] M. Y. Tsai and B. G. Streetman, "Recrystallization of Implanted Amorphous Silicon Layers. I. Electrical Properties of Silicon Implanted with BF₂⁺ or Si⁺+B⁺," *J. Appl. Phys.*, vol. 50, no. 1, 183–187 (1979).
- [7.110] Y. Sato and I. Kawashima, "Fluorine-Enhanced Boron Migration into Oxide from Underlying Silicon," *J. Electrochem. Soc.*, vol. 141, no. 5, 1381–1386 (1994).
- [7.111] H.-H. Vuong, C. S. Rafferty, W. Mansfield, H. Luftman, D. Jacobson, M. R. Pinto, S. A. Eshragi, J. R. McMacken, and R. E. Ham, "Modeling C-V Shifts in Boron/BF₂-Implanted Capacitors," in: *Technical Digest of the 1996 International Electron Devices Meeting (IEDM)*, Piscataway: IEEE, 807–810 (1996).
- [7.112] M. Morita, T. Kubo, T. Ishihara, and M. Hirose, "Fluorine-Enhanced Thermal Oxidation of Silicon in the Presence of NF₃," *Appl. Phys. Lett.*, vol. 45, no. 12, 1312–1314 (1984).
- [7.113] K. Imai and K. Yamabe, "Nonplanar Silicon Oxidation in Dry O₂ + NF₃," *Appl. Phys. Lett.*, vol. 56, no. 3, 280–282 (1990).
- [7.114] A. Kazor, C. Jeynes, and I. W. Boyd, "Fluorine Enhanced Oxidation of Silicon at Low-Temperatures," *Appl. Phys. Lett.*, vol. 65, no. 12, 1572–1574 (1994).
- [7.115] G. Peev, T. Racheva, E. Dacheva, and N. Nedev, "Thermal Oxidation of Silicon in O₂-SiF₄ Mixtures," *Thin Solid Films*, vol. 169, 173–178 (1989).
- [7.116] P. F. Schmidt, R. J. Jaccodine, C. H. Wolowodiuk, and T. Kook, "Chemically Enhanced Thermal Oxidation of Silicon," *Materials Letters*, vol. 3, no. 5-6, 235–238 (1985).
- [7.117] G. S. Virdi, C. M. S. Rauthan, B. C. Pathak, and W. S. Khokle, "Properties of the Fluorine-Implanted Si-SiO₂ System," *Solid-State Electronics*, vol. 34, no. 8, 889–892 (1991).
- [7.118] J.-Y. Tsai, Y. Shi, S. Prasad, S. W.-C. Yeh, and R. Rakshit, "Slight Gate Oxide Thickness Increase in PMOS Devices with BF₂ Implanted Polysilicon Gate," *IEEE Electron Device Letters*, vol. 19, no. 9, 348–350 (1998).
- [7.119] U. S. Kim, T. Kook, and R. J. Jaccodine, "Diffusion of Boron in Silicon during O₂/NF₃ Oxidation," *J. Electrochem. Soc.*, vol. 135, no. 1, 270–271 (1988).
- [7.120] R. J. Jaccodine and U. S. Kim, "Study of Point Defect Concentrations during the Fluorinated Oxidation of Silicon," in: *Defects and Diffusion in Silicon Processing*, edited by T. Diaz de la Rubia, S. Coffa, P. A. Stolk, and C. S. Rafferty, *Mat. Res. Soc. Symp. Proc.*, vol. 469, 71–76 (1997).
- [7.121] O. Meyer, "Semiconductor Counters with Thin Window n⁺ and p⁺-Contacts Produced by Ion-Implantation," *IEEE Trans. Nuclear Science*, vol. NS-15, no. 3, 232–238 (1968).
- [7.122] H. Runge, "Spatial Position of Deep Levels near the Si-SiO₂ Interface of Ion Implanted MOS Structures," *IEEE Trans. Electron Devices*, vol. ED-23, no. 11, 1233–1236 (1976).
- [7.123] L. Y. Krasnobaev and N. M. Omelyanovskaya, "Electrical Activity of Halogen-Silicon Complexes," in: *Gettering and Defect Engineering in Semiconductor Technology GADEST'91*, edited by M. Kittler and H. Richter, *Solid State Phenomena*, vol. 19/20, 417 (1991).
- [7.124] S. Ganguly, L. Lin, P. Kohli, H.-J. Li, T. Kirichenko, R. Srinivasa, V. Agarwal, and S. Banerjee, "Comparison of Low Energy BF₂⁺, BC₁⁺, and BBr₂⁺ Implants for the Fabrication of Ultrashallow P⁺-N Junctions," *J. Appl. Phys.*, vol. 91, no. 4, 2023–2027 (2002).
- [7.125] L. S. Roberts, R. Brindos, K. S. Jones, M. E. Law, D. F. Downey, S. Falk, and J. Liu, "The Effect of Impurities on Diffusion and Activation of Ion Implanted Boron in Silicon," in: *Si Front-End Processing — Physics and Technology of Dopant-Defect Interactions II*, edited by A. Agarwal, L. Pelaz, H.-H. Vuong, P. Packan, and M. Kase, *Mat. Res. Soc. Symp. Proc.*, vol. 610, B5.8.1–B5.8.6 (2000).
- [7.126] S. A. Datar, H. E. Gove, R. T. D. Teng, and J. P. Lavine, "AMS Studies of the Diffusion of Chlorine in Silicon Wafers," *Nuclear Instruments and Methods in Physics Research B*, vol. 99, 549–552 (1995).

- [7.127] J. Monkowski, "Role of Chlorine in Silicon Oxidation. Part I," *Solid State Technology*, vol. 22, no. 7, 58–61 (1979).
- [7.128] J. Monkowski, "Role of Chlorine in Silicon Oxidation. Part II," *Solid State Technology*, vol. 22, no. 8, 113–119 (1979).
- [7.129] M.-C. Chen and J. W. Hile, "Oxide Charge Reduction by Chemical Gettering with Trichloroethylene during Thermal Oxidation of Silicon," *J. Electrochem. Soc.*, vol. 119, no. 2, 223–225 (1972).
- [7.130] R. J. Kriegler, Y. C. Cheng, and D. R. Colton, "The Effect of HCl and Cl₂ on the Thermal Oxidation of Silicon," *J. Electrochem. Soc.*, vol. 119, no. 3, 388–392 (1972).
- [7.131] K. Kobayashi, K. Tanabashi, K. Ohta, and T. Kubota, "Electrical Properties of HCl-Passivated MOS Structure," *Denki Kagaku*, vol. 42, no. 6, 294–299 (1974).
- [7.132] Y. J. van der Meulen, C. M. Osburn, and J. F. Ziegler, "Properties of SiO₂ Grown in the Presence of HCl or Cl₂," *J. Electrochem. Soc.*, vol. 122, no. 2, 284–290 (1975).
- [7.133] G. J. Declerck, T. Hattori, G. A. May, J. Beaudouin, and J. D. Meindl, "Some Effects of "Trichloroethylene Oxidation" on the Characteristics of MOS Devices," *J. Electrochem. Soc.*, vol. 122, no. 3, 436–439 (1975).
- [7.134] M. Waldner and L. Sivo, "Lifetime Preservation in Diffused Silicon," *J. Electrochem. Soc.*, vol. 107, no. 4, 298–301 (1960).
- [7.135] P. H. Robinson and F. P. Heiman, "Use of HCl Gettering in Silicon Device Processing," *J. Electrochem. Soc.*, vol. 118, no. 1, 141–143 (1971).
- [7.136] S. Brojdo, J. V. Dalton, W. J. Palito, and H. A. Waggener, "Growth, Properties and Applications of High Temperature HCl-O₂ Oxides," *Electrochem. Soc. Extended Abstracts*, vol. 72-2, no. 244, 604–606 (1972).
- [7.137] R. S. Ronen and P. H. Robinson, "Hydrogen Chloride and Chlorine Gettering: An Effective Technique for Improving Performance of Silicon Devices," *J. Electrochem. Soc.*, vol. 119, no. 6, 747–752 (1972).
- [7.138] G. Baccarani, M. Severi, and G. Soncini, "Electrical Characteristics of MOS Structures on ⟨111⟩ and ⟨100⟩ Oriented *n*-Type Silicon As Influenced by Use of Hydrogen Chloride during Thermal Oxidation," *J. Electrochem. Soc.*, vol. 120, no. 10, 1436–1438 (1973).
- [7.139] C. M. Osburn, "Dielectric Breakdown Properties of SiO₂ Films Grown in Halogen and Hydrogen-Containing Environments," *J. Electrochem. Soc.*, vol. 121, no. 6, 809–815 (1974).
- [7.140] T. Hattori, "Effects of Trichloroethylene Addition on the Thermal Oxidation of Silicon at 1200 °C," *Jpn. J. Appl. Phys.*, vol. 17, no. 1, 69–72 (1978).
- [7.141] E. J. Janssens and G. J. Declerck, "The Use of 1, 1, 1-Trichloroethane As an Optimized Additive to Improve the Silicon Thermal Oxidation Technology," *J. Electrochem. Soc.*, vol. 125, no. 10, 1696–1703 (1978).
- [7.142] Y. C. Cheng and B. Y. Liu, "Oxidation Characteristics and Electrical Properties of Low Pressure Dual TCE Oxides," *J. Electrochem. Soc.*, vol. 131, no. 2, 354–359 (1984).
- [7.143] B. Y. Liu and Y. C. Cheng, "Growth and Characterization of Thin Gate Oxides by Dual TCE Process," *J. Electrochem. Soc.*, vol. 131, no. 3, 683–686 (1984).
- [7.144] Y. C. Cheng, J. W. Haslett, E. J. M. Kendall, R. J. Kriegler, and F. J. Scholz, "Low-Frequency Noise in HCl Processed IGFET's," *Proc. IEEE*, vol. 62, no. 6, 294–295 (1974).
- [7.145] Y. Wang, Y. Nishioka, T.-P. Ma, and C. R. Barker, "Radiation and Hot-Electron Effects on SiO₂/Si Interfaces with Oxides Grown in O₂ Containing Small Amounts of Trichloroethane," *Appl. Phys. Lett.*, vol. 52, no. 7, 573–575 (1988).
- [7.146] R. K. Bhan, S. K. Lomash, P. K. Basu, and K. C. Cahabra, "Interface Properties of Thermal SiO₂ Using 1,1,1, Trichloroethane (TCA)," *J. Electrochem. Soc.*, vol. 134, no. 11, 2826–2828 (1987).
- [7.147] D. R. Young and C. M. Osburn, "Minority Carrier Generation Studies in MOS Capacitors on N-Type Silicon," *J. Electrochem. Soc.*, vol. 120, no. 11, 1578–1581 (1973).

- [7.148] D. DeBusk, S. Ruby, and A. Legendijk, “Thermal Oxidation without TCA: Is t-DCE the Answer?” *Semiconductor International*, vol. 18, no. 6, 167–172 (1995).
- [7.149] R. J. Kriegler, “The Passivating Effect of Chlorine in SiO₂,” *Denki Kagaku*, vol. 41, no. 7, 466–475 (1973).
- [7.150] D. W. Hess and R. C. McDonald, “Investigation of Silicon Etching and Silicon Dioxide Bubbler Formation during Silicon Oxidation in HCl-Oxygen Atmospheres,” *Thin Solid Films*, vol. 42, 127–131 (1977).
- [7.151] J. Monkowski, R. E. Tressler, and J. Stach, “The Structure and Composition of Silicon Oxides Grown in HCl/O₂ Ambients,” *J. Electrochem. Soc.*, vol. 125, no. 11, 1867–1873 (1978).
- [7.152] C. Claeys, J. Vanhellemont, G. Declerck, J. Van Landuyt, R. Van Overstraeten, and S. Amelinckx, “Ambient Effects on the Si-SiO₂ Interface Morphology of Chlorinated Oxides,” in: *VLSI Science and Technology/1985*, edited by W. M. Bullis and S. Broydo, *Electrochem. Soc. Proc.*, vol. 85-5, 329–338 (1985).
- [7.153] A. Rohatgi, S. R. Butler, and F. J. Feigl, “Mobile Sodium Ion Passivation in HCl Oxides,” *J. Electrochem. Soc.*, vol. 126, no. 1, 149–154 (1979).
- [7.154] J. Monkowski, J. Stach, and R. E. Tressler, “Phase Separation and Sodium Passivation in Silicon Oxides Grown in HCl/O₂ Ambients,” *J. Electrochem. Soc.*, vol. 126, no. 7, 1129–1134 (1979).
- [7.155] R. J. Kriegler, A. Aitken, and J. D. Morris, “The Use of HCl Passivation in the Processing Technology of MOSFET Devices,” in: *Proceedings of the 5th Conference (1973 International) on Solid State Devices, Tokyo, 1973, Journal of the Japan Society of Applied Physics / Supplement*, vol. 43, 341–347 (1974).
- [7.156] A. Rohatgi, S. R. Butler, F. J. Feigl, H. W. Kraner, and K. W. Jones, “Chlorine Incorporation in HCl Oxides,” *J. Electrochem. Soc.*, vol. 126, no. 1, 143–149 (1979).
- [7.157] J. P. Stagg and M. R. Boudry, “Sodium Passivation in Al-SiO₂-Si Structures Containing Chlorine,” *J. Appl. Phys.*, vol. 52, no. 2, 885–899 (1981).
- [7.158] H. L. Tsai, S. R. Butler, D. B. Williams, H. W. Kraner, and K. W. Jones, “Cl Incorporation at the Si/SiO₂ Interface during the Oxidation of Si in HCl/O₂ Ambients,” *J. Electrochem. Soc.*, vol. 131, no. 2, 411–418 (1984).
- [7.159] R. L. Meek, “Residual Chlorine in O₂:HCl Grown SiO₂,” *J. Electrochem. Soc.*, vol. 120, no. 2, 308–310 (1973).
- [7.160] M. Shibayama, H. Masaki, H. Ishikawa, and H. Hashimoto, “Shrinkage Effect of Stacking Faults during HCl Oxidation,” *Appl. Phys. Lett.*, vol. 29, no. 3, 136–138 (1976).
- [7.161] S. R. Butler, J. F. Feigl, A. Rohatgi, H. W. Kraner, and K. W. Jones, “Cl Incorporation in SiO₂ Prepared by Oxidation of Si in O₂-HCl Ambients,” *Electrochem. Soc. Extended Abstracts*, vol. 77-1, no. 77, 217–218 (1977).
- [7.162] B. E. Deal, A. Hurle, and M. J. Schulz, “Chlorine Concentration Profiles in O₂/HCl and H₂O/HCl Thermal Silicon Oxides Using SIMS Measurements,” *J. Electrochem. Soc.*, vol. 125, no. 12, 2024–2027 (1978).
- [7.163] R. J. Kriegler, “The Role of HCl in the Passivation of MOS Structures,” *Thin Solid Films*, vol. 13, 11–14 (1972).
- [7.164] R. J. Kriegler and T. F. Devenyi, “Temperature-Bias Aging of (HCl) MOS Structures,” in: *Proceedings of the 11th International Reliability Physics Symposium*, New York: IEEE, 153–158 (1973).
- [7.165] J. P. Stagg and M. R. Boudry, “Lateral Diffusion of Na⁺ Ions at the Si-SiO₂ Interface and Na⁺ Neutralisation in the Presence of Chlorine,” in: *Insulating Films on Semiconductors INFOS 79*, edited by G. G. Roberts and J. Morant, *Inst. Phys. Conf. Ser.*, no. 50, 75–80 (1980).
- [7.166] E. J. Janssens and G. J. Declerck, “The Mechanism of Lifetime Improvement by “HCl-Oxidation”,” *Electrochem. Soc. Extended Abstracts*, vol. 78-1, no. 263, 654–656 (1978).
- [7.167] K. Hirabayashi and J. Iwamura, “Kinetics of Thermal Growth of HCl-O₂ Oxides on Silicon,” *J. Electrochem. Soc.*, vol. 120, no. 11, 1595–1601 (1973).

- [7.168] Y. J. van der Meulen and J. G. Cahill, "Effects of HCl and Cl₂ Additions on Silicon Oxidation Kinetics," *J. Electronic Materials*, vol. 3, no. 2, 371–389 (1974).
- [7.169] D. W. Hess and B. E. Deal, "Kinetics of the Thermal Oxidation of Silicon in O₂/HCl Mixtures," *J. Electrochem. Soc.*, vol. 124, no. 5, 735–739 (1977).
- [7.170] B. E. Deal, D. W. Hess, J. D. Plummer, and C. P. Ho, "Kinetics of the Thermal Oxidation of Silicon in O₂/H₂O and O₂/Cl₂ Mixtures," *J. Electrochem. Soc.*, vol. 125, no. 2, 339–346 (1978).
- [7.171] B. R. Singh and P. Balk, "Thermal Oxidation of Silicon in O₂-Trichloroethane," *J. Electrochem. Soc.*, vol. 126, no. 7, 1288–1294 (1979).
- [7.172] W. H. Grubbs, M. B. Das, J. Stach, and R. E. Tressler, "A Comparison of HCl and Trichloroethylene (TCE) Grown Oxides on Silicon," (1976).
- [7.173] D. L. Heald, R. M. Das, and R. O. Khosla, "Influence of Trichloroethylene on Room Temperature Flatband Voltages of MOS Capacitors," *J. Electrochem. Soc.*, vol. 123, no. 2, 302–303 (1976).
- [7.174] J. R. Flemish, R. E. Tressler, and J. R. Monkowski, "Enhancement of the Kinetics of Thermal Oxidation of Silicon Using 1,1,1-Trichloroethane," *J. Electrochem. Soc.*, vol. 135, no. 5, 1192–1194 (1988).
- [7.175] Z.-M. Ling, L. H. Dupas, and K. De Meyer, "Modeling of the Oxide Growth in a Chlorine Ambient," in: *The Physics and Chemistry of SiO₂ and the Si-SiO₂ Interface*, edited by C. R. Helms and B. E. Deal, New York: Plenum Press, 53–59 (1988).
- [7.176] W. Ahmed and E. Ahmed, "The Effects of Trichloroethane HCl and Ion-Implantation on the Oxidation Rate of Silicon," *Journal of Materials Science*, vol. 29, 184–188 (1994).
- [7.177] B. E. Deal and A. S. Grove, "General Relationship for the Thermal Oxidation of Silicon," *J. Appl. Phys.*, vol. 36, no. 12, 3770–3778 (1965).
- [7.178] B. E. Deal, "Thermal Oxidation Kinetics of Silicon in Pyrogenic H₂O and 5% HCl/H₂O Mixtures," *J. Electrochem. Soc.*, vol. 125, no. 4, 576–579 (1978).
- [7.179] T. Hattori, "Thermal Oxidation of Silicon in Wet O₂/TCE Mixtures at 1200 °C," *J. Electrochem. Soc.*, vol. 126, no. 10, 1789–1792 (1979).
- [7.180] P. M. Ritchey, J. Stach, and R. E. Tressler, "Thermally Grown HCl-O₂ Oxides and the Effects of Trace Amounts of Water Vapor in the Oxidizing Ambient," *Electrochem. Soc. Extended Abstracts*, vol. 76-2, no. 324, 832–835 (1976).
- [7.181] R. E. Tressler, J. Stach, and D. M. Metz, "Gas Phase Composition Consideration in the Thermal Oxidation of Silicon in Cl-H₂O Ambients," *J. Electrochem. Soc.*, vol. 124, no. 4, 607–609 (1977).
- [7.182] K. Ehara, K. Sakuma, and K. Ohwada, "Kinetics and Oxide Properties of Silicon Oxidation in O₂-H₂-HCl Mixtures," *J. Electrochem. Soc.*, vol. 126, no. 12, 2249–2254 (1979).
- [7.183] S. Solmi and P. Negrini, "Effect of Chlorine Implantation on Oxidation Enhanced Diffusion of Phosphorus in Silicon," *Appl. Phys. Lett.*, vol. 45, no. 2, 157–159 (1984).
- [7.184] H. Shiraki, "Silicon Device Consideration on Grown-in and Process Induced Defect and Fault Annihilation," in: *Semiconductor Silicon 1977*, edited by H. R. Huff and E. Sirtl, *Electrochem. Soc. Proc.*, vol. 77-2, 546–558 (1977).
- [7.185] T. Hattori, "HCl Oxidation Conditions for Stacking-Fault Nuclei Getting and for Silicon Etching," *J. Appl. Phys.*, vol. 49, no. 5, 2994–2995 (1978).
- [7.186] Y. Hokari, "Secondary Defect Generation Suppression and Diffusivity Restraint in Heavily Phosphorus Implanted Silicon by HCl Oxidation," *Jpn. J. Appl. Phys.*, vol. 18, no. 5, 873–880 (1979).
- [7.187] T. Hattori, "Elimination of Stacking Faults in Silicon by Trichloroethylene Oxidation," *J. Electrochem. Soc.*, vol. 123, no. 6, 945–946 (1976).
- [7.188] S. Kawado, "Control of Oxidation-Induced Stacking Faults in Silicon by Chlorine Implantation," *Jpn. J. Appl. Phys.*, vol. 18, no. 2, 225–232 (1979).

- [7.189] A. Armigliato, S. Solmi, C. Donolato, P. Negrini, E. Gabilli, A. Garulli, and M. Kittler, "Influence of Chlorine Implantation on Phosphorus Diffusivity and Oxidation-Induced Defects in Silicon," *phys. stat. sol. (a)*, vol. 87, 207–216 (1985).
- [7.190] Y. Nabeta, T. Uno, S. Kubo, and H. Tsukamoto, "Restrained Diffusion of Boron and Phosphorus in Silicon under HCl-Added Oxygen Atmosphere," *J. Electrochem. Soc.*, vol. 123, no. 9, 1416–1417 (1976).
- [7.191] S. Oh, W. A. Tiller, and S. Hahn, "Effect of HCl on Silicon Point Defect Formation during Thermal Oxidation of (100) Float Zone Silicon Wafers," *Appl. Phys. Lett.*, vol. 48, no. 17, 1125–1126 (1986).
- [7.192] R. Subrahmanyam, H. Z. Massoud, and R. B. Fair, "The Influence of HCl on the Oxidation-Enhanced Diffusion of Boron and Arsenic in Silicon," *J. Appl. Phys.*, vol. 61, no. 10, 4804–4807 (1987).
- [7.193] E. Tarnow, "Theory of Li- and Br-Saturated Vacancies in Radiation Damaged Silicon," *J. Phys.: Condens. Matter*, vol. 4, 1459–1464 (1992).
- [7.194] T. C. Poon and H. C. Card, "Incorporation of Bromine into Si-SiO₂ Interfaces and Effects on Interface State Distributions," *Electronics Letters*, vol. 15, 756–758 (1979).
- [7.195] M. Susa, H. Shinohara, K. Nagata, and K. S. Goto, "Influence of Bromine on Thermal Oxidation of Silicon Substrates," *Journal of the Japan Institute of Metals*, vol. 53, no. 10, 1054–1061 (1989).

List of Tables

1.1	Rotation and rotoinversion symmetry operations.	8
1.2	Definition of symmetry groups.	9
1.3	Point groups possible in silicon.	10
1.4	Schoenflies notation of point symmetries relevant for the cubic system.	10
1.5	Relative permittivity constants.	24
1.6	Distribution probability from random walk	31
2.1	Tracer diffusion coefficients.	93
2.2	Parameters for self-diffusion via vacancies.	97
2.3	Parameters for self-diffusion via self-interstitials.	98
2.4	Energy levels proposed for vacancies.	105
2.5	Equilibrium concentration of vacancies under intrinsic conditions.	110
2.6	Formation enthalpies and entropies of vacancies obtained from <i>ab-initio</i> calculations.	113
2.7	Diffusion coefficient of vacancies under intrinsic conditions.	116
2.8	Migration enthalpies of vacancies obtained from <i>ab-initio</i> calculations.	120
2.9	Energy levels proposed for divacancies.	123
2.10	Positron lifetimes associated with vacancy clusters.	129
2.11	Binding energy of a vacancy in a vacancy agglomerate as obtained from theoretical investigations.	130
2.12	Energy levels proposed for self-interstitials.	134
2.13	Equilibrium concentration of self-interstitials under intrinsic conditions.	137
2.14	Formation enthalpies and entropies of self-interstitials obtained from <i>ab-initio</i> calculations.	140
2.15	Diffusion coefficient of self-interstitials under intrinsic conditions.	142
2.16	Migration enthalpies of self-interstitials obtained from <i>ab-initio</i> calculations.	147
2.17	Binding energy of a self-interstitial in a self-interstitial agglomerate as obtained from experimental and theoretical investigations.	157
2.18	Parameters for the recombination of vacancies at surfaces and interfaces.	180
2.19	Parameters for the recombination of self-interstitials at surfaces and interfaces.	180
4.1	Ionization levels of the C _i P _s pair.	297
5.1	Fractional diffusivity of boron via self-interstitials.	345
5.2	Fractional diffusivity of aluminum via self-interstitials.	363
5.3	Fractional diffusivity of gallium via self-interstitials.	369
5.4	Fractional diffusivity of phosphorus via self-interstitials.	397
5.5	Fractional diffusivity of arsenic via self-interstitials.	409
5.6	Fractional diffusivity of antimony via self-interstitials.	421

List of Figures

1.1	Definition of a crystal plane via Miller indices.	3
1.2	Miller indices for typical planes in cubic crystals.	3
1.3	Definition of parallel crystals planes via Miller indices.	4
1.4	Atomic structure of silicon.	5
1.5	Schematic representation of point defects in silicon.	7
1.6	Atomic arrangement of atoms around a vacancy.	11
1.7	Atomic arrangement of atoms around a substitutional impurity atom.	11
1.8	Tetrahedral interstitial site in the diamond lattice.	11
1.9	Hexagonal interstitial site in the diamond lattice.	11
1.10	Bond-centered interstitial site in the diamond lattice.	11
1.11	Anti-bond interstitial site in the diamond lattice.	11
1.12	$\langle 001 \rangle$ -oriented split interstitial of equivalent atoms.	12
1.13	$\langle 110 \rangle$ -oriented split interstitial of equivalent atoms.	12
1.14	$\langle 001 \rangle$ -oriented split interstitial of inequivalent atoms.	12
1.15	$\langle 110 \rangle$ -oriented split interstitial of inequivalent atoms.	12
1.16	Pair of inequivalent substitutional atoms.	13
1.17	Pair of equivalent substitutional atoms.	13
1.18	Electron and hole concentration as a function of net doping and temperature.	21
1.19	Intrinsic carrier concentration after Morin and Maita.	23
1.20	Width of the forbidden band gap.	24
1.21	Summary of diffusivities in silicon.	28
1.22	Error function profiles.	29
1.23	Gaussian profiles.	30
1.24	Binomial distribution and its approximation.	33
1.25	Schematic representation of fluxes between adjacent planes.	34
1.26	Schematic energy-barrier diagram without driving forces.	35
1.27	Schematic energy-barrier diagram with a driving force.	36
1.28	Reactions in a ternary system.	53
1.29	Schematic energy-barrier diagram for a reaction according to the transition-state theory.	54
1.30	Transient effects in diffusion-reaction equations.	61
2.1	Tracer diffusion coefficient in silicon.	93
2.2	Concentration dependence of the tracer diffusion coefficient.	95
2.3	Self-diffusion coefficients via vacancies.	100
2.4	Self-diffusion coefficients via self-interstitials.	101
2.5	Fractional contribution of self-interstitials to self-diffusion.	102
2.6	Equilibrium concentration of vacancies under intrinsic condition.	112

2.7	Intrinsic diffusion coefficient of vacancies.	118
2.8	Intrinsic diffusion coefficient of vacancies at elevated temperatures.	119
2.9	Schematic atomic representation of the divacancy.	121
2.10	Binding energy of a vacancy in a vacancy agglomerate as obtained from theoretical investigations.	131
2.11	Equilibrium concentration of self-interstitials under intrinsic conditions.	139
2.12	Intrinsic diffusion coefficient of self-interstitials.	145
2.13	Intrinsic diffusion coefficient of self-interstitials at elevated temperatures.	146
2.14	Atomic configurations of di-interstitials suggested from EPR investigations.	148
2.15	Atomic configurations of di-interstitials suggested from theoretical work.	150
2.16	Atomic configurations of the tri-interstitial.	152
2.17	Atomic configuration of the tetra-interstitial.	153
2.18	Binding energy of a self-interstitial in a self-interstitial agglomerate as obtained from experimental and theoretical investigations.	158
2.19	Energy-barrier diagram for a self-interstitial in the vicinity of a vacancy.	159
2.20	Atomic configuration of the bond defect.	160
2.21	Relaxation time constant for bulk recombination.	167
2.22	Recombination constant k_V for vacancies at interfaces.	182
2.23	k_V/D_V for vacancies at interfaces.	182
2.24	Recombination constant k_I for self-interstitials at interfaces.	183
2.25	k_I/D_I for self-interstitials at interfaces.	184
3.1	Energy-barrier diagram of an impurity-vacancy pair.	235
3.2	Energy-barrier diagram for a non-attractive interaction between impurity and vacancy.	235
3.3	Oxygen partial pressure required for a certain oversaturation of self-interstitials.	254
3.4	Relative diffusion enhancement as a function of the self-interstitial oversaturation.	256
3.5	Dependence of arsenic diffusion parameters on the self-interstitial oversaturation.	259
3.6	Diffusion coupling via the electrostatic field.	261
3.7	Point-defect generation by dopant diffusion.	263
3.8	Relative transport capacity of dopants.	266
3.9	Relative transport capacity of isovalent impurities and chalcogens.	266
3.10	Platinum diffusion profiles resulting from the Frank-Turnbull mechanism.	271
3.11	Comparison of Frank-Turnbull and Kick-Out diffusion profiles.	271
4.1	Atomic configuration of carbon interstitials.	283
4.2	Solubility of carbon in silicon.	285
4.3	Diffusion coefficient of carbon in silicon.	286
4.4	Diffusion coefficient of carbon interstitials.	287
4.5	Mean path length λ_C a carbon atom migrates while it is mobile.	288
4.6	Atomic configuration of the C_iC_s pair.	290
4.7	Atomic configuration of the C_iO_i complex.	294
4.8	Atomic configuration suggested for the C_iVO_2 complex.	295
4.9	Atomic configurations suggested for C_iO_{12} complexes.	296
4.10	Intrinsic diffusion coefficient of germanium.	302
4.11	Concentration dependence of the diffusion coefficient of germanium.	304
4.12	Retardation factor for the diffusion of boron in SiGe.	306
4.13	Solubility of tin in silicon.	308
4.14	Intrinsic diffusion coefficient of tin.	309

4.15 Concentration dependence of the diffusion coefficient of tin.	310
5.1 Concentration dependence of the formation of impurity clusters.	333
5.2 Effects of ion pairing on the diffusivity of dopants in iso-concentration experiments.	335
5.3 Effects of ion pairing on the co-diffusion of dopants.	336
5.4 Solubility of boron in silicon.	342
5.5 Intrinsic diffusion coefficient of boron.	343
5.6 Concentration dependence of the diffusion coefficient of boron.	346
5.7 Mean path length λ_B a boron atom migrates while it is mobile.	349
5.8 Solubility of aluminum in silicon.	362
5.9 Intrinsic diffusion coefficient of aluminum.	363
5.10 Concentration dependence of the diffusion coefficient of aluminum.	364
5.11 Solubility of gallium in silicon.	367
5.12 Intrinsic diffusion coefficient of gallium.	368
5.13 Concentration dependence of the diffusion coefficient of gallium.	370
5.14 Solubility of indium in silicon.	372
5.15 Electrical activation of indium atoms.	373
5.16 Intrinsic diffusion coefficient of indium.	375
5.17 Concentration dependence of the diffusion coefficient of indium.	376
5.18 Atomic configuration of substitutional nitrogen.	381
5.19 Atomic configuration of the nitrogen pair.	381
5.20 Diffusivity of nitrogen in silicon.	384
5.21 Atomic configuration of the $(N_i N_i)O_i$ complex.	388
5.22 Atomic configuration of the $(N_i O_i)N_i$ complex.	388
5.23 Solubility of phosphorus in silicon.	394
5.24 Intrinsic diffusion coefficient of phosphorus.	396
5.25 Concentration dependence of the diffusion coefficient of phosphorus.	398
5.26 High-concentration phosphorus-diffusion profile.	399
5.27 Solubility of arsenic in silicon.	407
5.28 Intrinsic diffusion coefficient of arsenic.	409
5.29 Concentration dependence of the diffusion coefficient of arsenic in silicon for moderate doping levels.	411
5.30 Concentration dependence of the diffusion coefficient of arsenic in silicon for high doping levels.	411
5.31 Solubility of antimony in silicon.	419
5.32 Intrinsic diffusion coefficient of antimony.	420
5.33 Concentration dependence of the diffusion coefficient of antimony.	422
5.34 Atomic configuration of DP(2) and DP(4) complexes.	425
6.1 Atomic configuration of interstitial oxygen in silicon.	470
6.2 Solubility of interstitial oxygen in silicon.	471
6.3 Diffusion coefficient of interstitial oxygen in silicon.	473
6.4 Atomic configuration of the vacancy-oxygen complex.	476
6.5 Atomic configuration of the VO_2 complex.	478
6.6 Atomic configurations of oxygen dimers.	484
6.7 Solubility of sulfur in silicon.	486
6.8 Diffusion coefficient of sulfur in silicon.	487
6.9 Solubility of selenium in silicon.	490

6.10 Diffusion coefficient of selenium in silicon.	491
6.11 Solubility of tellurium in silicon.	493
6.12 Diffusion coefficient of tellurium in silicon.	494

Index

- (...), 3
- {...}, 4
- $\langle 001 \rangle$ split interstitial configuration, 12
- $\langle 110 \rangle$ split interstitial configuration, 12
- $\langle 111 \rangle$ split interstitial configuration, 12
- [...], 4
- {...}, 4
- Abundances, 5
- Acceptors, 7, 14–15
- Activated complex, 54
- Activation volume, 45
- Activity coefficient, 41, 42
 - of electrons and holes, 42
- Affinity, *see also* Reactions, 43
- Aluminum, 359–366
 - precipitation, *see* Precipitation
- Amphoteric defects, 15
- Anderson negative-U system, 15, 104, 133, 136, 156, 338–340
- Anti-bond interstitial site, 11
- Antimony, 416–424
 - precipitation, *see* Precipitation
- Arrhenius law, 27
- Arsenic, 404–416
 - precipitation, *see* Precipitation
- Athermal diffusion, 38
 - aluminum interstitials, 364–365
 - boron interstitials, 338, 348–350
 - carbon interstitials, 287
 - Frenkel pairs, 160
 - self-interstitials, 133, 135, 141
 - vacancies, 120
- Atomic and molar quantities, 39
- Atomic arrangement of silicon atoms, 4–5
- Atomic fraction, 42
- Band gap, 14, 18, 23–24, 83–84, 283, 305
- Binding energy, 49–51
- Bloch functions, 13
- Boltzmann statistics, 17–18
- Boltzmann-Matano analysis, 261–262, 344, 346, 398, 408, 410, 411
- Bond defect, *see* Frenkel pairs
- Bond-centered interstitial site, 11
- Boron, 337–359
- Boundary conditions
 - Dirichlet boundary condition, 27, 177, 178
 - for mobile impurity complexes, 247
 - generalized boundary condition, 178
 - Neumann boundary condition, 27, 177, 178
- Breathing-mode relaxations, 106
- Bromine, 525
- Brownian movement, *see* Random walk
- Bulk recombination of self-interstitials and vacancies, 161–167
 - indirect recombination via extended defects, 171
 - indirect recombination via impurities, 167–168, 251
- C_{1h} symmetry, 10
- C_{2h} symmetry, 10
- C_{2v} symmetry, 10
- C_{3v} symmetry, 10
- Capture radius, *see* Reactions
- Car-Parinello method, *see* Diffusion
- Carbon, 281–300
 - precipitation, *see* Precipitation
- Charge carriers, *see* Electron and Hole
- Charge-neutrality condition, 15, 20, 21
- Chemical potential, 41
 - dependence on concentration, 41–42
 - dependence on pressure, 41
 - dependence on temperature, 41
 - of electrons, 15
- Chemical pump effect, 232
- Chlorine, 522–525
- Coarsening of extended defects, *see* Ostwald ripening

- Complexion number, 39, 40, 80, 81, 238–240
- Concentration, 26
- Concerted exchange mechanism, *see* Diffusion mechanisms
- Conduction band, 14–19
- effective density of states, 16
- Configuration entropy, *see* Entropy
- Continuity equation, 26
- Crystal defects, *see* Defects
- C_s symmetry, 10
- Cubic symmetry, 9
- D_{2d} symmetry, 10
- D_{3d} symmetry, 10
- Debye length, 21
- Debye temperature, 23, 35
- Defect symmetries, 8–12
- Defects, 5–8
- extended defects, *see* Extended defects
 - extrinsic, 5
 - intrinsic, 5
 - point defects, *see* Point defects
 - symmetries, *see* Defect symmetries
- Detailed balance, *see* Principle of detailed balance
- Detailed equilibrium, *see* Principle of detailed balance
- Di-interstitial, *see* Self-interstitial complexes
- Diffusion, 25
- activation energy, 27
 - analytical solutions, 27–30
 - athermal, *see* Athermal diffusion
 - attempt frequency, 35, 54, 56, 87
 - Car-Parinello method, 25
 - continuity equation, 26
 - diffusion coefficient, *see* Diffusion coefficient
 - diffusion-segregation equation, 66
 - driving forces, 36–38
 - electrostatic fields, 37–38
 - stress gradients, 45–46
 - thermal gradients, 46–47
 - effects from the proximity of impurities, 95, 240, 304, 310, 397, 399, 400, 411, 423
 - enhanced
 - nitridation, 187
 - oxidation, 60, 175, 186, 255, 362, 524–525 - enthalpy of diffusion, *see* Enthalpy/of migration
 - enthalpy of migration, *see* Enthalpy
 - entropy of diffusion, *see* Entropy/of migration
 - entropy of migration, *see* Entropy
 - extrinsic diffusion, *see* Extrinsic diffusion
 - Gibbs free energy of migration, 35
 - in a percolation cluster, *see* Percolation
 - intrinsic diffusion, *see* Intrinsic diffusion
 - intrinsic point defects, *see* Intrinsic point defects
 - irreversible thermodynamics, 43–44
 - isoconcentration experiments, *see* Isoconcentration diffusion experiments
 - jump frequency, 32, 33, 35
 - mean square distance from origin, 31
 - mechanisms, *see* Diffusion mechanisms
 - molecular-dynamics methods, 25, 33, 35, 107, 120, 132, 135, 147, 160, 161, 185
 - Monte-Carlo approaches, 25, 151, 171, 185, 232, 234, 288, 349, 412
 - proximity effects, *see* Diffusion/effects from the proximity of impurities
 - random walk, *see* Random walk retarded
 - nitridation, 187
 - oxidation, 164, 186, 362, 521
 - stress effects, 45 - transport capacity, *see* Transport capacity
 - transport coefficient, *see* Transport coefficient
- Diffusion coefficient
- atomistic interpretation, 32–34
 - macroscopic definition, 26
- Diffusion current, 26

- Diffusion mechanisms
- concerted exchange, 91–92, 103, 161, 230–231, 244, 251, 258, 409
 - direct exchange, 230–231, 244, 251, 258
 - dissociative mechanism, 58, 233
 - Frank-Turnbull mechanism, 58, 96, 233, 267–272, 273, 274, 345
 - interstitial mechanism, 91, 132, 229–230, 233, 285, 303, 408
 - interstitialcy mechanism, 91, 132, 233, 236
 - kick-out mechanism, 58, 96, 233–234, 270, 272–275, 288, 349–350, 487
 - non-fickian diffusion mechanism, 232
 - pair diffusion mechanism, 58, 232–234, 240, 251–265, 413
 - vacancy mechanism, 90, 96, 231–232, 233, 303, 309, 408
 - Watkins replacement mechanism, 58, 233
- Diffusion-reaction equations, methodology of, 58–62
- Direct exchange mechanism, *see* Diffusion mechanisms
- Dirichlet boundary conditions, *see* Boundary conditions
- Dissipation function, 43, 53
- Dissociation energy, 57
- Dissociative mechanism, *see* Diffusion mechanisms
- Distribution coefficient, *see* Segregation
- Divacancy, *see* Vacancy complexes
- Donors, 7, 14–15
- Dopant clusters, 62, 332–333
- Dopants, *see* Acceptors and Donors
- Double acceptors, 15
- Double donors, 15
- DP(2) and DP(4) dopant complexes, 403, 415, 424
- Driving forces, *see* Diffusion
- Dual-diffusion model, 252
- Effective intrinsic concentration of charge carriers, 19, 84
- Einstein relation, *see* Nernst-Einstein relation
- Electric displacement vector, 20
- Electric field vector, 20
- Electron, 13–22
- effective mass, 14, 16, 22
- Electron concentration, 21
- Boltzmann statistics, 18
 - Fermi statistics, 16
 - gradient, 18
- Electronic levels (experimentally well established ones only)
- E_c - 0.043 eV: Sb_s (+/0), 417
 - E_c - (0.045–0.05) eV: P_s (+/0), 390
 - E_c - 0.054 eV: As_s (+/0), 404
 - E_c - 0.07 eV C_iP_s(IB) (0/-), 297
 - E_v + 0.30 eV: B_iB_s, 352
 - E_c - 0.11 eV: C_s-I-C_s (0/-), 291
 - E_c - 0.12 eV: C_i (0/-), 283
 - E_c - 0.12 eV: C_iAs_s(IIB) (0/-), 298
 - E_c - 0.13 eV: B_i (+/0), 338
 - E_c - 0.13 eV: C_iSb_s(IIB) (0/-), 298
 - E_c - 0.16 eV: C_iSb_s(III) (0/-), 298
 - E_c - 0.16 eV: Te₂ (+/0), 495
 - E_c - (0.16–0.18) eV: VO (0/-), 476
 - E_c - 0.17 eV: C_iC_s (0/-), 290
 - E_c - 0.19 eV: S₂ (+/0), 487
 - E_c - 0.2 eV: Te_s (+/0), 492
 - E_c - 0.21 eV: Se₂ (+/0), 490
 - E_c - 0.214 eV: SnV (-/=), 308
 - E_c - (0.21–0.23) eV: V₂ (-/=), 122
 - E_c - 0.23 eV C_iP_s(III) (+/0), 297
 - E_c - 0.23 eV: V₂O (-/=), 480
 - E_c - (0.24–0.27) eV: B_iO_i, 357
 - E_c - 0.26 eV C_iP_s(IIA) (0/-), 297
 - E_c - 0.27 eV: C_iAs_s(IIA) (0/-), 298
 - E_c - 0.27 eV: C_iSb_s(IIA) (0/-), 298
 - E_c - 0.31 eV: Se_s (+/0), 489
 - E_c - 0.32 eV C_iP_s(IIB) (+/0), 297
 - E_c - 0.32 eV: S_s (+/0), 485
 - E_c - 0.34 eV: C_iAs_s(III) (+/0), 298
 - E_c - 0.37 eV: B_i (0/-), 338
 - E_c - 0.37 eV: S₂ (++/), 487
 - E_c - 0.38 eV C_iP_s(IA) (0/-), 297
 - E_c - 0.39 eV C_iP_s(IB) (+/0), 297
 - E_c - 0.39 eV: C_iSb_s(I) (0/-), 298
 - E_c - 0.39 eV: Se₂ (++/), 490
 - E_c - (0.39–0.43) eV: V₂ (0/-), 122
 - E_c - 0.41 eV: Oxygen-boron complex responsible for the degradation of solar cells, 359
 - E_c - 0.41 eV: Te_s (++/), 492

- E_c - 0.42 eV: $\text{C}_i\text{Sb}_s(\text{III})$ (+/0), 298
 E_c - 0.43 eV: $\text{C}_i\text{As}_s(\text{I})$ (0/-), 298
 E_c - (0.39–0.51) eV: SbV (0/-), 418
 E_c - (0.43–0.47) eV: PV (0/-), 392
 E_c - 0.45 eV: $\text{C}_i\text{As}_s(\text{IIB})$ (+/0), 298
 E_c - 0.46 eV: $\text{C}_i\text{Sb}_s(\text{IIB})$ (+/0), 298
 E_c - (0.46–0.47) eV: AsV (0/-), 406
 E_c - 0.501 eV: SnV (0/-), 308
 E_c - (0.46–0.54) eV: V_2O (0/-), 480
 $E_v + 0.57$ eV $\text{C}_i\text{P}_s(\text{IIA})$ (+/0), 297
 E_c - 0.59 eV: Se_s (+/+/), 489
 E_c - 0.61 eV: S_s (++/+/), 485
 $E_v + (0.48–0.52)$ eV: AlV (-/0), 360
 $E_v + 0.48$ eV $\text{C}_i\text{P}_s(\text{IA})$ (+/0), 297
 $E_v + (0.37–0.4)$ eV: Fe_i , 108
 $E_v + (0.36–0.37)$ eV: C_iC_s , 291
 $E_v + (0.3–0.4)$ eV: C_iO_i (+/0), 294
 $E_v + (0.32–0.35)$ eV: SnV (+/0), 307–308
 $E_v + 0.395$ eV: Al_i , 360
 $E_v + 0.28$ eV: C_i (+/0), 283
 $E_v + 0.24$ eV: V_2O (+/0), 480
 $E_v + 0.19$ eV: V_2 (+/0), 123
 $E_v + 0.17$ eV: Al_i (++/+/), 360
 $E_v + (0.154–0.157)$ eV: In_s (0/-), 370
 $E_v + 0.111$ eV: In_sC_s (0/-), 298
 $E_v + (0.11–0.13)$ eV: V (++/+/), 103–104
 $E_v + 0.09$ eV: C_iC_s (+/0), 290
 $E_v + (0.071–0.073)$ eV: Ga_s (0/-), 366
 $E_v + 0.07$ eV: SnV (++/+/), 308
 $E_v + (0.067–0.069)$ eV: Al_s (0/-), 360
 $E_v + 0.057$ eV: Ga_sC_s (0/-), 300
 $E_v + 0.056$ eV: Al_sC_s (0/-), 299
 $E_v + (0.044–0.047)$ eV: B_s (0/-), 337
 $E_v + 0.037$ eV: B_sC_s (0/-), 299
 $E_v + (0.028–0.057)$ eV: V (+/0), 103–104
- Electrostatic potential, 18–21
Emitter-push effect, 399–401
Enthalpy, 39
of diffusion, *see* Enthalpy/of migration
of formation, 40, 79
of migration, 35, 87
- Entropy, 39
of configuration, 40, 80
of diffusion, *see* Entropy/of migration
of formation, 40, 80, 94
- of migration, 35, 94
partial atomic, 41
- Entropy dilemma, 94
- EPR spectra
on-center N_s , 381
selenium, 488
selenium pairs, 491
Si-*A*: $(\text{V}-\text{O})^-$, 476
Si-*A3*: V_4^- (non-planar), 127
Si-*A4*: V_3^- , 127, 128
Si-*A5*: I_2^0 , 148
Si-*A14*: $(\text{V}_2\text{O})^0$, 480
Si-*A15*: $(\text{V}_3\text{O}_3)^0$, 481
Si-*A18*: IO_i , 482
Si-*AA12*: I^+ , 133
Si-*AA13*: IO_i , 482
Si-*AA14*: IO_i , 482
Si-*AA15*: $(\text{Al}_2)_i$, 365
Si-*AA19*: Frenkel pair, 160
Si-*B*: C-V complex, 284
Si-*B1*: $(\text{V}-\text{O})^-$, 476
Si-*B3*: I_2^+ or I_4^+ , 148–149, 154
Si-*C*: $(\text{V}_2)^-$, 121
Si-*DK1*: $(\text{SnV}_2)^-$, 311
Si-*DK2*: $(\text{Sn}_2\text{V}_2)^-$, 311
Si-*DK3*: $(\text{Sn}_2\text{V}_2)^-$, 311
Si-*DK4*: $(\text{Sn}-\text{V})^-$, 307
Si-*E*: $(\text{P}-\text{V})^0$, 392
Si-*G1*: V^+ , 103
Si-*G2*: V^- , 103
Si-*G3*: $(\text{V}-\text{O})^-$, 477
Si-*G4*: $(\text{V}-\text{O})^-$, 477
Si-*G6*: $(\text{V}_2)^+$, 121, 125
Si-*G7*: $(\text{V}_2)^-$, 121–122, 125
Si-*G8*: $(\text{P}-\text{V})^0$, 392
Si-*G9*: $(\text{Al}-\text{V})^-$, 360
Si-*G10*: BV^0 , 340
Si-*G11*: $(\text{C}_i\text{C}_s)^+$, 290
Si-*G12*: C_i^+ , 283, 286
Si-*G15*: $(\text{C}_i\text{O}_i)^+$, 293–295
Si-*G16*: C-V complex, 284
Si-*G17*: $(\text{C}_i\text{C}_s)^-$, 290
Si-*G18*: Al_i^{++} , 360
Si-*G19*: $\text{Al}_i^{++}\text{Al}_s^-$, 365
Si-*G22*: $\text{Ga}_i^{++}\text{Ga}_s^-$, 369
Si-*G23*: $(\text{As}-\text{V})^0$, 406
Si-*G24*: $(\text{Sb}-\text{V})^0$, 417

- Si-*G*25: self-interstitial related, 133, 141
 Si-*G*26: (Ge-V)⁺, 301
 Si-*G*27: (Ge-V)⁻, 301
 Si-*G*28: B_i⁰, 338
 Si-*G*29: (Sn-V)⁰, 307
 Si-*GGA*2: C_{2s}⁻, 289
 Si-*I*1: (V₂)⁰ or (V₂O)⁰, 121
 Si-*J*: (V₂)⁺, 121
 Si-*K*: (C_iC_s)⁺, 293
 Si-*L*1: self-interstitial related, 133
 Si-*L*6: C_i⁻, 283, 286
 Si-*L*7: (C_s-I-C_s)⁻, 290
 Si-*L*8: C_iP_s, 297
 Si-*L*9: C_iP_s, 298
 Si-*L*10: C_iP_s, 298
 Si-*L*11: C_iAs_s, 298
 Si-*L*12: C_iSb_s, 298
 Si-*N*: V₅⁻, 128
 Si-*NL*1: (P_{2s}-V)⁺, 403
 Si-*NL*2: P_{2s}⁺, 403
 Si-*NL*11: V₂⁰ sponge, 121
 Si-*NL*26: N_i⁰, 382
 Si-*NL*51: I₂⁰ or I₄⁰, 149, 154
 Si-*O*2: interstitial-related, 149
 Si-*P*1: V₅⁻, 128
 Si-*P*2: (V₂O₂)⁰, 481
 Si-*P*3: V₄⁰ (planar), 127
 Si-*P*4: (V₃O)⁰, 481
 Si-*P*5: (V₃O₂)⁰, 481
 Si-*P*6: I₂⁺, 148–150
 Si-*PT*1: (C_s-I-C_s)⁰, 290
 Si-*S*1: (V-O)⁰, 476
 Si-*SL*5: N_s, 380
 SIR-1P(a): P_sI, 391
 SIR-1P(b): P_sI, 391
 sulfur, 484
 sulfur pairs, 487
 tellurium, 492
 Equilibrium concentration, *see* Intrinsic point defects
 Equilibrium thermodynamics, *see* Thermodynamics
 Error function, 27
 Eutectic temperature, 63
 Extended defects, 6
 - decoration by fluorine, 516
 - decoration by nitrogen, 385
 formation by stress, 44
 grain boundaries, 6
 influence of fluorine, 519
 line defects, 6
 Ostwald ripening, 170
 reactions with intrinsic point defects, 168–171
 small clusters of self-interstitials, 151–158
 small clusters of vacancies, 127–131
 sponge defect, 121
 stacking faults, 6
 - extrinsic, 6
 - intrinsic, 6
 swirl defects, 136, 189, 282
 volume defects, 6
 Extrinsic
 - defects, *see* Defects
 - stacking faults, *see* Extended defects/stacking faults
 Extrinsic conditions, 21
 Extrinsic diffusion, 260
 - aluminum, 364
 - antimony, 421–423
 - arsenic, 410–412
 - boron, 345–347
 - gallium, 369
 - germanium, 303–304
 - indium, 376
 - phosphorus, 398–399
 - tin, 310
 Fermi distribution, 16
 Fermi integral, 16
 Fermi level, 16, 80
 Fermi statistics, 15–17
 Fick's first law of diffusion, 26
 Fick's second law of diffusion, 26
 Five-stream diffusion model, 247
 Fluorine, 513–521
 Flux, 26
 Formation energy, 40, 49–50
 Fractional diffusivity via self-interstitials, 252, 255–260
 - aluminum, 363
 - antimony, 421
 - arsenic, 409–410
 - boron, 345
 - gallium, 368–369

- germanium, 303
- indium, 375–376
- phosphorus, 396–397
- tin, 309
- tracer diffusion, 102–103
- Frank-Turnbull mechanism, *see* Diffusion mechanisms
- Frenkel pairs, 158–161
 - bond defect, 160
 - I-V complex, 160
- Fusion
 - atomic enthalpy of, 64
 - atomic entropy of, 64
- Gallium, 366–369
- Gaussian distribution, 30
- Generalized forces, 43
- Generation rate in continuity equations, 26
- Germanium, 300–305
- Gettering, 189, 230, 282, 390, 469, 522, 524
- Gibbs free energy, 39
 - of formation, 40
 - of migration, 35
- Gibbs fundamental equation, 43, 48
- Gibbs-Duhem equation, 43, 64
- Heat of transfer, 46
- Hermann-Mauguin notation of point symmetries, 9
- Hexagonal interstitial site, 11
- Hexagonal symmetry, 9
- Hole, 15–22
 - effective mass, 17, 22
- Hole concentration, 21
 - Boltzmann statistics, 18
 - Fermi statistics, 17
 - gradient, 18
- Hydrostatic pressure, 45
- I-V complex, *see* Frenkel pairs
- Impurity band, 19
- Impurity-self-interstitial pairs, *see also*
 - Interstitial impurity atoms, 7–8
 - formation, *see* Diffusion mechanisms/pair-diffusion mechanism
- Impurity-vacancy pairs, 7
 - formation, *see* Diffusion mechanisms/pair-diffusion mechanism
- Indium, 370–378
 - precipitation, *see* Precipitation
- Interface segregation, 66
- Interstitial impurity atoms, 7–8
 - possible atomic arrangements, *see* Interstitials — possible sites and atomic arrangements
- Interstitial mechanism, *see* Diffusion mechanisms
- Interstitial wind, 234
- Interstitialcy mechanism, *see* Diffusion mechanisms
- Interstitials — possible sites and atomic arrangements
 - $\langle 001 \rangle$ split interstitial configuration, 12
 - $\langle 110 \rangle$ split interstitial configuration, 12
 - $\langle 111 \rangle$ split interstitial configuration, 12
 - anti-bond interstitial site, 11
 - bond-centered interstitial site, 11
 - hexagonal interstitial site, 11
 - tetrahedral interstitial site, 11
- Intrinsic
 - defects, *see* Defects
 - stacking faults, *see* Extended defects/stacking faults
- Intrinsic concentration of charge carriers, 18, 21–22
- Intrinsic conditions, 21
- Intrinsic diffusion, 260
 - aluminum, 361–362
 - antimony, 420
 - arsenic, 408
 - boron, 342–344
 - carbon, 285
 - gallium, 367–368
 - germanium, 302–303
 - indium, 375
 - nitrogen, 383
 - phosphorus, 395–396
 - selenium, 489–490
 - sulfur, 486
 - tellurium, 494
 - tin, 309
- Intrinsic diffusion coefficient, 253–255

- Intrinsic point defects, 6–7, 77–190
attempt frequency, 87
bond defect, *see also* Frenkel pairs
bulk recombination with
self-interstitials, *see* Bulk
recombination of self-interstitials
and vacancies
di-interstitial, *see* Self-interstitial
complexes
diffusion, 87–90
divacancy, *see* Vacancy complexes
effective charge state, 89
effective diffusion coefficient, 89
enthalpy of formation, 79
entropy of configuration, 80
entropy of formation, 80
equilibrium concentration, 79–87
of neutral intrinsic point defects, 81
pressure dependence, 86–87
total concentration, 85
Frenkel pairs, *see* Frenkel pairs
generation by bulk processes, 176
generation by interface processes,
186–188
I-V complex, *see also* Frenkel pairs
initial conditions, 188–190
ionization energies, 81–84
temperature dependence, 84
self-interstitial, *see* Self-interstitial
surface recombination, *see* Surface
recombination
traps, *see* Traps for intrinsic point
defects
vacancy, *see* Vacancy
Ion pairs, 62, 65, 334–337
boron-antimony, 355–356
boron-arsenic, 355–356
boron-phosphorus, 355
indium-antimony, 377
indium-arsenic, 377
indium-phosphorus, 377
indium-tellurium, 377
selenium-acceptors, 492
Isoconcentration diffusion experiments, 94,
262, 303, 310, 345, 364, 369, 376,
398, 410, 421
Jahn-Teller effect, 15, 103, 106, 121, 122,
126, 338, 358, 360, 365, 380, 381
Kick-out mechanism, *see* Diffusion
mechanisms
Kinetic law of mass action, 52
Law of mass action, 49
Liquidus curve, 64
Loss rate in continuity equations, 26
Ludwig-Soret effect, *see* Thermodiffusion
Mass of a silicon atom, 5
Miller indices, 2–4
Mixing entropy, *see* Entropy/of
configuration
Molar and atomic quantities, 39
Mole, 39
Mole fraction, 41, 42, 49
Molecular-dynamics methods, *see*
Diffusion
Monoclinic symmetry, 9
Monte-Carlo approaches to diffusion, *see*
Diffusion
Mössbauer spectroscopy
antimony interstitial, 417
antimony-arsenic-vacancy complex,
423, 424
antimony-phosphorus-vacancy
complex, 423, 424
antimony-vacancy complexes, 424
antimony-vacancy pair, 417–418
substitutional antimony, 417
substitutional tellurium, 493
substitutional tin, 307
tin-phosphorus-vacancy complex, 311
tin-vacancy pair, 307
Natural abundances, 5
Negative-U system, *see* Anderson
negative-U system
Nernst theorem, 5
Nernst-Einstein relation, 38, 44, 261
Neumann boundary conditions, *see*
Boundary conditions
New donors, *see* Thermal donors
Nitridation-enhanced diffusion, *see*
Diffusion/enhanced/nitridation
Nitridation-retarded diffusion, *see*
Diffusion/retarded/nitridation
Nitrogen, 378–390
Non-Fickian diffusion mechanism, *see*
Diffusion mechanisms

- Onsager's reciprocity law, 43, 46, 53
 Order of a reaction, *see* Reactions
 Orientations in crystals, 2–4
 Ostwald ripening, 170
 Oxidation-enhanced diffusion, *see*
 Diffusion/enhanced/oxidation
 Oxidation-retarded diffusion, *see*
 Diffusion/retarded/oxidation
 Oxygen, 469–483
 precipitation, *see* Precipitation
- Pair diffusion mechanism, *see* Diffusion mechanisms
 Partial atomic quantities, 41
 Partition constant, 249
 antimony-vacancy pairs, 421
 arsenic-self-interstitial pairs, 410
 arsenic-vacancy pairs, 410
 phosphorus-self-interstitial pairs, 397
 Pauli exclusion principle, 14
 Percolation, 62, 400, 411–413, 423
 Permittivity, 20, 24
 Perturbed angular correlation
 measurements
 indium-donor ion pairs, 377
 indium-tellurium ion pairs, 377
 indium-vacancy pairs, 371
 substitutional indium, 370
 Phase, 62
 Phenomenological coefficients, 43
 Phosphorus, 390–404
 precipitation, *see* Precipitation
 Photoluminescence lines
 0.7456 eV: C-N pair, 387
 0.758 eV: carbon and nitrogen related, 387
 0.7615 eV: carbon and nitrogen related, 387
 0.7673 eV *P*-line: C_iO_{2i} , 295, 296
 0.7674 eV: carbon and nitrogen related, 387
 0.7724 eV: carbon and nitrogen related, 387
 0.7894 eV *C*-line: C_iO_i , 293–295
 0.812–1.0 eV *D*1 to *D*4 lines:
 dislocation-related, 128
 0.856 eV: C_i , 284
 0.885 eV self-interstitial-cluster related, 156
 0.922 eV: aluminum and carbon related, 299
 0.9351 eV *T*-line: B_iC_s , 299
 0.94 eV self-interstitial-cluster related, 156
 0.969 eV *G*-line: C_s -I-C_s, 290–291
 1.018 eV *I*₁ or *W*-line: intrinsic radiation-induced defect, 127, 128, 151, 154, 155
 1.0398 eV *I*₃ or *X*-line:
 tetra-interstitial, 152, 154
 1.0595 eV: carbon and oxygen related, 297
 1.080 eV *I*₂-line: B_s -I-B_s or $B_{2i}I$, 352, 354
 1.108 eV B_{80}^4 or *J*-line: Hexavacancy, 128
 1.1176 eV *P,Q,R* system:
 indium-related, 378
 1.1223 eV *A,B,C* system:
 nitrogen-related, 386
 1.1413 eV In_s , 371
 1.1491 eV Gas , 366
 1.1492 eV Ass , 404
 1.1496 eV Al_s , 360
 1.1499 eV P_s , 391
 1.1501 eV Sb_s , 417
 1.1507 eV B_s , 337
 Point defects, 6–8
 extrinsic, *see* Defects
 high-symmetry configurations, 10–12
 interstitial impurity atoms, *see*
 Interstitial impurity atoms
 intrinsic, *see* Intrinsic point defects
 self-interstitial, *see* Self-interstitial
 self-interstitial complexes, *see*
 Self-interstitial complexes
 substitutional impurity atoms, *see*
 Substitutional impurity atoms
 vacancy, *see* Vacancy
 vacancy complexes, *see* Vacancy complexes
 Poisson equation, 20
 Positron annihilation
 antimony-vacancy pairs, 418, 423
 arsenic complexes, 414
 arsenic-vacancy pairs, 406
 boron-vacancy pairs, 341

- boron-vacancy-oxygen complexes, 359
chlorine complexes, 517
fluorine-vacancy complexes, 516
nitrogen-vacancy pairs, 382
phosphorus-vacancy pairs, 392
 V_2O complexes, 480
 V_2O_2 complexes, 481
 V_3O complexes, 481
 V_mO_n complexes, 479
vacancies, 104, 106, 108, 190
 VO complexes, 476
 VO_2 complexes, 478
 VO_3 complexes, 479
- Precipitation, 230
aluminum, 365–366
antimony, 356, 419, 423
arsenic, 407, 413
carbon, 282
indium, 372
oxygen, 79, 109, 171, 176, 188–190, 281, 380, 385, 469, 471–473
phosphorus, 176, 394–395
- Pressure, *see* Stress
- Principle of detailed balance, 53, 162, 168
- Principle of detailed equilibrium, *see* Principle of detailed balance
- Pseudo-donors, 15
- Random walk, 31–34
- Reaction kinetics, 47–62
- Reaction order, *see* Reactions
- Reaction rate, 52
- Reaction variable, *see* Reactions
- Reactions
affinity, 48, 52, 53
capture radius, 55, 56
diffusion-limited, 55–56
diffusion-limited, charged species, 55–56
dynamic theories, 52–54
order of, 52
reaction barrier, 56
reaction variable, 48
relation between concentrations in equilibrium, 49–51
- Rhombic symmetry, 9
- S symmetry (C_{1h}), 10
- S_2 symmetry (C_i), 10
- Schoenflies notation of point symmetries, 9–10
- Schrödinger's wave equation, 13–14
- Segregation
distribution coefficient, 63
models and implementations, 65–66
segregation coefficient, 63
segregation coefficient between Si and SiO_2 , 65
- Selenium, 488–492
- Self-diffusion, 5, 90–103
- Self-interstitial, 6, 131–158
caged interstitial, 135
equilibrium concentration
pressure dependence, 86
formation energy, 49
generation by bulk processes, *see* Intrinsic point defects
generation by interface processes, *see* Intrinsic point defects
initial conditions, *see* Intrinsic point defects
possible atomic arrangements, *see* Interstitials — possible sites and atomic arrangements
- reaction with a substitutional impurity atom, *see* Diffusion mechanisms/kick-out mechanism and Diffusion mechanisms/pair-diffusion mechanism
- segregation into oxide layers, 185–186
- surface recombination, *see* Surface recombination
- traps, *see* Traps for intrinsic point defects
- Self-interstitial complexes
di-interstitial, 6, 148–151
impurity-self-interstitial pairs, *see* Impurity-self-interstitial pairs
- small clusters of self-interstitials, 151–158
- Shallow thermal donors, *see* Thermal donors
- Silicon
atomic arrangement of atoms, 4–5
atomic enthalpy of fusion, 64
atomic entropy of fusion, 64

- concentration of silicon atoms, 4
- mass of a silicon atom, 5
- melting point, 64
- natural abundances, 5
- surface concentration, 5
- unit cell, 4
- SIMNI, 379
- SIMOX, 186, 469
- Site fraction, 42, 49, 50
- Solar cells
 - degradation by illumination and electron injection, 358–359
 - degradation by radiation, 294, 299, 357–358
 - increase of radiation hardness, 306
- Solid solubility, 63–65
 - aluminum, 361
 - antimony, 418–419
 - arsenic, 407–408
 - boron, 341–342
 - carbon, 284
 - gallium, 366–367
 - indium, 372–374
 - nitrogen, 383
 - oxygen, 471–472
 - phosphorus, 393–395
 - selenium, 489
 - sulfur, 486
 - tellurium, 493
 - tin, 308
- Solid-phase epitaxy, 265, 281
- Solubility concentration, *see* Solid solubility
- Soret effect, *see* Thermodiffusion
- Space-charge density, 20
- Steady state, 40
- Sterling's formula, 32
 - simplified, 40
- Strain activation tensor, 45
- Stress effects
 - on diffusion, 45
 - on the equilibrium concentration of intrinsic point defects, 86–87
- Substitutional impurity atoms, 7, 10
 - dissociation into interstitial impurity and vacancy, *see* Diffusion mechanisms/dissociative mechanism
- reaction with a self-interstitial, *see* Diffusion mechanisms/kick-out mechanism and Diffusion mechanisms/ pair-diffusion mechanism
- reaction with a vacancy, *see* Diffusion mechanisms/pair-diffusion mechanism
- Sulfur, 484–488
- Surface recombination, 177–185
- Surface recombination velocity, 178
- Surface reconstruction, 179
- Symmetry of defects, *see* Defect symmetries
- Tail formation in dopant profiles, 265, 347, 399–401
- T_d symmetry, 10
- Tellurium, 492–495
- Tetragonal symmetry, 9
- Tetrahedral interstitial site, 11
- Thermal donors, 469, 475, 483
 - influence of carbon, 281, 296–297
 - influence of hydrogen, 475
 - new donors, 281
 - shallow thermal donors, 380, 388
- Thermal equilibrium, 40
- Thermodiffusion, 46–47
- Thermodynamics
 - equilibrium thermodynamics, 39–42
 - of irreversible processes, 42–44, 52
- Tin, 306–311
- Tracer diffusion, 90–103
- Transition-state theory, 54
- Transport capacity, 26, 96, 108, 189, 233, 265
- Transport coefficient, 26
- Traps for intrinsic point defects, 171–175
- Trigonal symmetry, 9
- Unit cell, 2
 - silicon, 4
- V symmetry (D_2), 10
- Vacancy, 6, 10, 103–131
 - bulk recombination with self-interstitials, *see* Bulk recombination of self-interstitials and vacancies

- charge states, 103–106
 coexisting configurations, 106
 equilibrium concentration
 pressure dependence, 86
 extended state, 106–107
 formation energy, 49
 generation by bulk processes, *see*
 Intrinsic point defects
 generation by interface processes, *see*
 Intrinsic point defects
 initial conditions, *see* Intrinsic point
 defects
 positron annihilation studies, *see*
 Positron annihilation
 reaction with a substitutional impurity
 atom, *see* Diffusion mechanisms/
 pair-diffusion mechanism
 reaction with an interstitial impurity
 atom, *see* Diffusion mechanisms/
 Frank-Turnbull mechanism
 semi-vacancy pair, 107
 structure, 103
 surface recombination, *see* Surface
 recombination
 theoretical investigations
 structure, 106
 traps, *see* Traps for intrinsic point
 defects
 Vacancy complexes
 divacancy, 6, 120–127
 impurity-vacancy pairs, *see*
 Impurity-vacancy pairs
 non-reorientable divacancies, *see* EPR
 spectra/Si-G25
 small clusters of vacancies, 127–131
 Vacancy mechanism, *see* Diffusion
 mechanisms
 Vacancy wind, 232
 Valence-bond band, 14–15, 17–19
 effective density of states, 17
 V_d symmetry (D_{2d}), 10
 Vibration modes
 30 cm^{-1} : O_i , 470
 190–270 cm^{-1} : N_4O , N_6O , 389
 240–249 cm^{-1} : nitrogen-oxygen
 complexes, 387
 441 cm^{-1} : P_s , 391
 517 cm^{-1} : O_i , 470
 527.4 cm^{-1} : C_{2s}^0 , 289
 540.4 cm^{-1} : $\text{C}_s\text{-I-C}_s$, 291
 543.3 cm^{-1} : $\text{C}_s\text{-I-C}_s$, 291
 552.5 cm^{-1} $P1$: B_{2s} , 351
 556 cm^{-1} : O_{2i} , 483
 560 cm^{-1} $P2$: B_{2s} , 351
 570 cm^{-1} $P3$: B_{2s} , 351
 579.8 cm^{-1} : $\text{C}_s\text{-I-C}_s$, 291
 594.6 cm^{-1} : C_iC_s , 291
 596.6 cm^{-1} : C_iC_s , 291
 599 cm^{-1} $S4$: B_{2i} or $\text{B}_s\text{-I-B}_s$, 352, 353
 603 cm^{-1} $S5$: B_{2i} or $\text{B}_s\text{-I-B}_s$, 352, 353
 607 cm^{-1} : $^{12}\text{C}_s$, 283
 620 cm^{-1} : $^{11}\text{B}_s$, 337
 640.6 cm^{-1} : $\text{C}_s\text{-I-C}_s$, 291
 644 cm^{-1} : $^{10}\text{B}_s$, 337
 653 cm^{-1} : $^{14}\text{N}_s$, 381
 670 cm^{-1} : boron-nitrogen complexes,
 389
 690 cm^{-1} : O_{2i} , 483
 691 cm^{-1} : N_i , 382
 722.4 cm^{-1} : C_iC_s , 291
 730 cm^{-1} R : B_i , 338
 730.4 cm^{-1} : $\text{C}_s\text{-I-C}_s$, 291
 733 cm^{-1} Q : $[\text{B-B}]_s$, 338, 353
 748.7 cm^{-1} : C_{2s}^- , 289
 757 cm^{-1} R : B_i , 338
 760 cm^{-1} Q : $[\text{B-B}]_s$, 338, 353
 764 cm^{-1} : N_{2i} , 381
 783 cm^{-1} : $[\text{N-N}]_s$, 386
 802 cm^{-1} : N_{2i}O_i , 387
 802 cm^{-1} : nitrogen-oxygen
 complexes, 387
 807 cm^{-1} : SnVO , 311
 824 cm^{-1} : V_2O_2 , 481
 830 cm^{-1} : VO , 476
 833 cm^{-1} : V_2O , 480
 833 cm^{-1} : V_3O_2 , 481
 835 cm^{-1} : V_2O , 480
 835 cm^{-1} : VO , 476
 839 cm^{-1} : V_2O , 480
 842.4 cm^{-1} : $\text{C}_s\text{-I-C}_s$, 291
 859 cm^{-1} : P_2VO , 404
 861 cm^{-1} : Sb_2VO , 424
 865.2 cm^{-1} $C(3)$: C_iO_i , 293–295
 872.6 cm^{-1} : C_iC_s , 291
 873.5 cm^{-1} : C_iSn_s , 311
 877 cm^{-1} : VO , 476

- 884 cm⁻¹: V₃O, 481
 884 cm⁻¹: V-VO₂, 481
 884 cm⁻¹: VO, 476
 887 cm⁻¹: V₃O, 481
 887 cm⁻¹: VO₂, 478, 481
 888.9 cm⁻¹: (C_iSn_s)^{2N}, 311
 895 cm⁻¹: VO₂, 478
 902 cm⁻¹: VO_{2i}-O_iC_i, 296
 903 cm⁻¹ S1: B_{2i} or B_s-I-B_s, 352, 353
 904 cm⁻¹: V₃O₂, 481
 904 cm⁻¹: VO₃, 479
 905 cm⁻¹: Sb₂VO, 424
 908 cm⁻¹: As₂VO, 416
 910 cm⁻¹: P₂VO, 404
 911 cm⁻¹: IO_{2i}, 482
 916 cm⁻¹: I₂O_{2i}, 482
 917 cm⁻¹ S2: B_{2i} or B_s-I-B_s, 352, 353
 918 cm⁻¹: I₂O_{2i}, 482
 922 cm⁻¹: C_i, 283
 922 cm⁻¹: IO_{2i}, 482
 922 cm⁻¹: precursor of C_iO_i, 295
 928 cm⁻¹ S3: B_{2i} or B_s-I-B_s, 352, 353
 928 cm⁻¹: VO₂^{*0}, 479
 932 cm⁻¹: C_i, 283
 935 cm⁻¹: I₂O_i, 482
 935 cm⁻¹: IO_i, 482
 940 cm⁻¹ C(4): C_iO_iI, 295
 944 cm⁻¹: IO_i, 482
 953 cm⁻¹: C_iC_s, 291
 956 cm⁻¹: IO_i, 482
 956 cm⁻¹: VO_{2i}-O_iC_i, 296
 959 cm⁻¹: C_i-I, 289
 960 cm⁻¹: [N-N]_s, 386
 962 cm⁻¹: N_{2i}, 381
 966 cm⁻¹: C_i-I, 289
 967 cm⁻¹: VO₂^{*-}, 479
 967 cm⁻¹: precursor of C_iO_i, 295
 968 cm⁻¹: V₃O₂, 481
 968 cm⁻¹: VO₃, 479
 983 cm⁻¹: VO₄, 479
 985.3 cm⁻¹: (C_iSn_s)^{2N}, 311
 987 cm⁻¹ C(4): C_iC_sI, 292
 993 cm⁻¹ C(4): C_iC_sI, 292
 996 cm⁻¹: N_{2i}O_i, 387
 996 cm⁻¹: nitrogen-oxygen complexes, 387
 1000 cm⁻¹: V₂O₂, 481
 1000 cm⁻¹: VO₃, 479
 1003.8 cm⁻¹: VO₂^{*0}, 479
 1004 cm⁻¹: VO₄, 479
 1012 cm⁻¹: O_{2i}, 483
 1023 cm⁻¹: VO₂^{*-}, 479
 1024 cm⁻¹ C(4): C_iO_iI, 295
 1025 cm⁻¹: C_iSn_s, 311
 1025 cm⁻¹: VO_{2i}-O_iC_i, 296
 1026 cm⁻¹: N_{2i}O_i, 387
 1026 cm⁻¹: nitrogen-oxygen complexes, 387
 1026–1112 cm⁻¹: C_sO_{ni}, 292–293
 1031 cm⁻¹: I₂O_{2i}, 482
 1034 cm⁻¹: I₂O_{2i}, 482
 1034 cm⁻¹: IO_{2i}, 482
 1037 cm⁻¹: IO_{2i}, 482
 1060 cm⁻¹: O_{2i}, 483
 1105 cm⁻¹: O_{2i}, 483
 1115.5 cm⁻¹ C(3): C_iO_i, 293
 1136 cm⁻¹: O_i, 470
 1150.6 cm⁻¹: V₂P, 403
 1156.6 cm⁻¹: V₂P, 403
 1201 cm⁻¹: boron-nitrogen complexes, 389
 1205 cm⁻¹: O_i, 470
 1309.2 cm⁻¹: V₂P, 403
 1312.5 cm⁻¹: V₂P, 403
 1316.2 cm⁻¹: V₂P, 403
 1370 cm⁻¹: VO, 476
 1430 cm⁻¹: VO, 476
 1563.3 cm⁻¹: V₂P, 403
 1749 cm⁻¹: O_i, 470
 2560 cm⁻¹: (V₂)⁺, 121–122
 3027 cm⁻¹: (V₂)⁻, 121–122
 3942 cm⁻¹: C_iO_iV, 293
 4100 cm⁻¹: Sn₂V₂, 311
 5560 cm⁻¹: (V₂)⁰, 121–122
 6875 cm⁻¹: C_iSn_s, 311
 6915 cm⁻¹: (C_iSn_s)^{2N}, 311
- Volume
 of activation, 45
 partial atomic, 41
- Watkins replacement mechanism, *see*
 Diffusion mechanisms
- Ylid, 483

Vassil Palankovski, Rüdiger Quay

**Analysis and Simulation
of Heterostructure Devices**

2004. XX, 289 pages. 183 figures.

Hardcover EUR 120,-

(Recommended retail price)

Net-price subject to local VAT.

ISBN 3-211-40537-2

Computational Microelectronics

The topic of this monograph is the physical modeling of heterostructure devices. A detailed discussion of physical models and parameters for compound semiconductors is presented including the relevant aspects of modern submicron heterostructure devices. More than 25 simulation examples for different types of Si(Ge)-based, GaAs-based, InP-based, and GaN-based heterostructure bipolar transistors (HBTs) and high electron mobility transistors (HEMTs) are given in comparison with experimental data from state-of-the-art devices.

From the table of contents:

List of Acronyms • List of Symbols • Introduction • State-of-the-Art of Materials, Device Modeling, and RF Devices • Physical Models • RF Parameter Extraction for HEMTs and HBTs • Heterojunction Bipolar Transistors • High Electron Mobility Tranistors • Novel Devices • Appendix: Benchmark Structures • References



SpringerWienNewYork

P.O. Box 89, Sachsenplatz 4–6, 1201 Vienna, Austria, Fax +43.1.330 24 26, e-mail: books@springer.at, springer.at
Haberstraße 7, 69126 Heidelberg, Germany, Fax +49.6221.345-4229, e-mail: orders@springer.de, springeronline.com
P.O. Box 2485, Secaucus, NJ 07096-2485, USA, Fax +1.201.348-4505, e-mail: orders@springer-ny.com
Eastern Book Service, 3-13, Hongo 3-chome, Bunkyo-ku, Tokyo 113, Japan, Fax +81.3.38 18 08 64, e-mail: orders@svt-ebs.co.jp
Prices and other details are subject to change without notice. All errors and omissions excepted.

SpringerEngineering

Christoph Jungemann, Bernd Meinerzhagen

Hierarchical Device Simulation

The Monte-Carlo Perspective

2003. XVI, 254 pages. 147 figures.

Hardcover **EUR 120,-**

(Recommended retail price)

Net-price subject to local VAT.

ISBN 3-211-01361-X

Computational Microelectronics

This monograph is intended for scientists and TCAD engineers who are interested in physics-based simulation of Si and SiGe devices. The common theoretical background of the drift-diffusion, hydrodynamic, and Monte-Carlo models and their synergy are discussed and it is shown how these models form a consistent hierarchy of simulation tools. The basis of this hierarchy is the full-band Monte-Carlo device model which is discussed in detail, including its numerical and stochastic properties. The drift-diffusion and hydrodynamic models for large-signal, small-signal, and noise analysis are derived from the Boltzmann transport equation in such a way that all transport and noise parameters can be obtained by Monte-Carlo simulations. With this hierarchy of simulation tools the device characteristics of strained Si MOSFETs and SiGe HBTs are analysed and the accuracy of the momentum-based models is assessed by comparison with the Monte-Carlo device simulator.



SpringerWienNewYork

P.O. Box 89, Sachsenplatz 4–6, 1201 Vienna, Austria, Fax +43.1.330 24 26, e-mail: books@springer.at, springer.at
Haberstraße 7, 69126 Heidelberg, Germany, Fax +49.6221.345-4229, e-mail: orders@springer.de, springeronline.com
P.O. Box 2485, Secaucus, NJ 07096-2485, USA, Fax +1.201.348-4505, e-mail: orders@springer-ny.com
Eastern Book Service, 3-13, Hongo 3-chome, Bunkyo-ku, Tokyo 113, Japan, Fax +81.3.38 18 08 64, e-mail: orders@svt-ebs.co.jp
Prices and other details are subject to change without notice. All errors and omissions excepted.

SpringerEngineering

Christoph Wasshuber

Computational Single-Electronics

2001. X, 278 pages. 131 figures.

Hardcover EUR 126,-

(Recommended retail price)

Net-price subject to local VAT.

ISBN 3-211-83558-X

Computational Microelectronics

This book brings together for the first time a review of the theory behind single-electronics, a state-of-the-art description of simulation methods for single-electron devices and circuits, and a comprehensive discussion of a wide selection of applications ranging from logic and memory to metrology. The author shares his almost a decade-long experience in single-electronics. Attention is given to open challenges such as the random background charge problem, where old and new ideas are presented to overcome it.

Many simulation methods described in this book are not particular to single-electronics. The efficient calculation of capacitances, tunnel rates, and bound energy states have applications in many other fields. This book is written with the practical side in mind. Simulation methods are described in a manner which makes their implementation straight forward.



SpringerWienNewYork

P.O. Box 89, Sachsenplatz 4–6, 1201 Vienna, Austria, Fax +43.1.330 24 26, e-mail: books@springer.at, springer.at
Haberstraße 7, 69126 Heidelberg, Germany, Fax +49.6221.345-4229, e-mail: orders@springer.de, springeronline.com
P.O. Box 2485, Secaucus, NJ 07096-2485, USA, Fax +1.201.348-4505, e-mail: orders@springer-ny.com
Eastern Book Service, 3-13, Hongo 3-chome, Bunkyo-ku, Tokyo 113, Japan, Fax +81.3.3818 08 64, e-mail: orders@svt-ebs.co.jp
Prices and other details are subject to change without notice. All errors and omissions excepted.

SpringerEngineering

Andreas Schenk

Advanced Physical Models for Silicon Device Simulation

1998. XVIII, 349 pages. 125 figures.

Hardcover **EUR 153,-**

(Recommended retail price)

Net-price subject to local VAT.

ISBN 3-211-83052-9

Computational Microelectronics

The book contains an extensive review on physical models for silicon device simulators. Referencing fundamental experimental and theoretical work, the models are discussed in terms of physical accuracy and application results. The derivation of device models from "first principles" and the fundamental problems therein are then described in detail for the most important examples using some new approaches of "taylored quantum mechanics".

"... this is a well produced book, written in a easy to read style, and will also be a very useful primer for someone starting out in the field who wants to know what can and cannot be done, and a useful source of reference for experienced users ..."

Microelectronics Journal



SpringerWienNewYork

P.O. Box 89, Sachsenplatz 4–6, 1201 Vienna, Austria. Fax +43.1.330 24 26, e-mail: books@springer.at, springer.at
Haberstraße 7, 69128 Heidelberg, Germany. Fax +49.6221.345 4229, e-mail: orders@springer.de, springeronline.com
P.O. Box 2485, Secaucus, NJ 07096-2485, USA. Fax +1.201.348-4505, e-mail: orders@springer-ny.com
Eastern Book Service, 3-13, Hongo 3-chome, Bunkyo-ku, Tokyo 113, Japan. Fax +81.3.38 18 08 64, e-mail: orders@svt-ebs.co.jp
Prices and other details are subject to change without notice. All errors and omissions excepted.

SpringerEngineering

Dietmar Schroeder

Modelling of Interface Carrier Transport for Device Simulation

1994. XI, 221 pages. 69 figures.

Hardcover **EUR 109,-**

(Recommended retail price)

Net-price subject to local VAT.

ISBN 3-211-82539-8

Computational Microelectronics

The book contains a comprehensive review of the physics, modelling and simulation of electron transport at interfaces in semiconductor devices. Particular emphasis is put on the consistent derivation of interface or boundary conditions for semiconductor device simulation. It combines a review of existing interface charge transport models with original developments. A unified representation of charge transport at semiconductor interfaces is introduced. Models for the most important interfaces are derived, classified within the unique modelling framework, and discussed in the context of device simulation. Discretization methods for numerical solution techniques are presented.

From the Table of Contents:

Introduction • Charge Transport in the Volume • General Electronic Model of the Interface • Charge Transport Across the Interface • Semiconductor-Insulator Interface • Metal-Semiconductor Contact • Semiconductor Heterojunction • MOSFET Gate • Discretization • Appendices



SpringerWienNewYork

P.O. Box 89, Sachsenplatz 4–6, 1201 Vienna, Austria, Fax +43.1.330 24 26, e-mail: books@springer.at, springer.at
Haberstraße 7, 69128 Heidelberg, Germany, Fax +49.6221.345 4229, e-mail: orders@springer.de, springeronline.com
P.O. Box 2485, Secaucus, NJ 07096-2485, USA, Fax +1.201.348-4505, e-mail: orders@springer-ny.com
Eastern Book Service, 3–13, Hongo 3-chome, Bunkyo-ku, Tokyo 113, Japan, Fax +81.3.38 18 08 64, e-mail: orders@svt-ebs.co.jp
Prices and other details are subject to change without notice. All errors and omissions excepted.

SpringerEngineering

Carlo Jacoboni, Paolo Lugli

The Monte Carlo Method for Semiconductor Device Simulation

1989. X, 356 pages. 228 figures.

Hardcover **EUR 109,-**

(Recommended retail price)

Net-price subject to local VAT.

ISBN 3-211-82110-4

Computational Microelectronics

The application of the Monte Carlo method to the simulation of semiconductor devices is presented. A review of the physics of transport in semiconductors is given, followed by an introduction to the physics of semiconductor devices. The Monte Carlo algorithm is discussed in great details, and specific applications to the modelling of semiconductor devices are given. A comparison with traditional simulators is also presented.

From the Table of Contents:

Introduction • Charge Transport in Semiconductors • The Monte Carlo Simulation • Review of Semiconductor Devices • Monte Carlo Simulation of Semiconductor Devices • Applications • Appendices



SpringerWienNewYork

P.O. Box 89, Sachsenplatz 4–6, 1201 Vienna, Austria, Fax +43.1.330 24 26, e-mail: books@springer.at, springer.at
Haberstraße 7, 69126 Heidelberg, Germany, Fax +49.621.345-4229, e-mail: orders@springer.de, springeronline.com
P.O. Box 2485, Secaucus, NJ 07096-2485, USA, Fax +1.201.348-4505, e-mail: orders@springer-ny.com
Eastern Book Service, 3-13, Hongo 3-chome, Bunkyo-ku, Tokyo 113, Japan, Fax +81.3.38 18 08 64, e-mail: orders@svt-ebs.co.jp
Prices and other details are subject to change without notice. All errors and omissions excepted.

Peter A. Markowich

The Stationary Semiconductor Device Equations

1986. IX, 193 pages. 40 figures.

Hardcover EUR 64,-

(Recommended retail price)

Net-price subject to local VAT.

ISBN 3-211-81892-8

Computational Microelectronics

The static semiconductor device problem is treated in an “applied mathematics” way. Qualitative properties, e.g. existence and uniqueness of solutions, and quantitative properties, particularly the structure of steady state solutions, are analysed. Physical interpretations of the mathematical results are given. Also, these results serve as a basis for the derivation and convergence analysis of numerical discretisation techniques.

From the Table of Contents:

Introduction • Mathematical Modeling of Semiconductor Devices • Analysis of the Basic Stationary Semiconductor Device Equations • Singular Perturbation Analysis of the Stationary Semiconductor Device Problem • Discretisation of the Stationary Device Problem • Numerical Simulation – A Case Study • Appendix: Notation of Physical Quantities / Mathematical Notation



SpringerWienNew York

P.O. Box 89, Sachsenplatz 4–6, 1201 Vienna, Austria, Fax +43.1.330 24 26, e-mail: books@springer.at, springer.at
Haberstraße 7, 69126 Heidelberg, Germany, Fax +49.6221.345-4229, e-mail: orders@springer.de, springeronline.com
P.O. Box 2485, Secaucus, NJ 07096-2485, USA, Fax +1.201.348-4505, e-mail: orders@springer-ny.com
Eastern Book Service, 3-13, Hongo 3-chome, Bunkyo-ku, Tokyo 113, Japan, Fax +81.3.38 18 08 64, e-mail: orders@svt-ebs.co.jp
Prices and other details are subject to change without notice. All errors and omissions excepted.

*Springer-Verlag
and the Environment*

WE AT SPRINGER-VERLAG FIRMLY BELIEVE THAT AN international science publisher has a special obligation to the environment, and our corporate policies consistently reflect this conviction.

WE ALSO EXPECT OUR BUSINESS PARTNERS – PRINTERS, paper mills, packaging manufacturers, etc. – to commit themselves to using environmentally friendly materials and production processes.

THE PAPER IN THIS BOOK IS MADE FROM NO-CHLORINE pulp and is acid free, in conformance with international standards for paper permanency.